frontiers | Research Topics

Advancing genomics for rare disease diagnosis and therapy development

vol II

Edited by
Weida Tong, Tieliu Shi, Zhichao Liu, Ruth Roberts and Mike Mikailov

Published in
Frontiers in Genetics
Frontiers in Pediatrics



FRONTIERS EBOOK COPYRIGHT STATEMENT

The copyright in the text of individual articles in this ebook is the property of their respective authors or their respective institutions or funders. The copyright in graphics and images within each article may be subject to copyright of other parties. In both cases this is subject to a license granted to Frontiers.

The compilation of articles constituting this ebook is the property of Frontiers.

Each article within this ebook, and the ebook itself, are published under the most recent version of the Creative Commons CC-BY licence. The version current at the date of publication of this ebook is CC-BY 4.0. If the CC-BY licence is updated, the licence granted by Frontiers is automatically updated to the new version.

When exercising any right under the CC-BY licence, Frontiers must be attributed as the original publisher of the article or ebook, as applicable.

Authors have the responsibility of ensuring that any graphics or other materials which are the property of others may be included in the CC-BY licence, but this should be checked before relying on the CC-BY licence to reproduce those materials. Any copyright notices relating to those materials must be complied with.

Copyright and source acknowledgement notices may not be removed and must be displayed in any copy, derivative work or partial copy which includes the elements in question.

All copyright, and all rights therein, are protected by national and international copyright laws. The above represents a summary only. For further information please read Frontiers' Conditions for Website Use and Copyright Statement, and the applicable CC-BY licence.

ISSN 1664-8714
ISBN 978-2-8325-3323-9
DOI 10.3389/978-2-8325-3323-9

About Frontiers

Frontiers is more than just an open access publisher of scholarly articles: it is a pioneering approach to the world of academia, radically improving the way scholarly research is managed. The grand vision of Frontiers is a world where all people have an equal opportunity to seek, share and generate knowledge. Frontiers provides immediate and permanent online open access to all its publications, but this alone is not enough to realize our grand goals.

Frontiers journal series

The Frontiers journal series is a multi-tier and interdisciplinary set of open-access, online journals, promising a paradigm shift from the current review, selection and dissemination processes in academic publishing. All Frontiers journals are driven by researchers for researchers; therefore, they constitute a service to the scholarly community. At the same time, the *Frontiers journal series* operates on a revolutionary invention, the tiered publishing system, initially addressing specific communities of scholars, and gradually climbing up to broader public understanding, thus serving the interests of the lay society, too.

Dedication to quality

Each Frontiers article is a landmark of the highest quality, thanks to genuinely collaborative interactions between authors and review editors, who include some of the world's best academicians. Research must be certified by peers before entering a stream of knowledge that may eventually reach the public - and shape society; therefore, Frontiers only applies the most rigorous and unbiased reviews. Frontiers revolutionizes research publishing by freely delivering the most outstanding research, evaluated with no bias from both the academic and social point of view. By applying the most advanced information technologies, Frontiers is catapulting scholarly publishing into a new generation.

What are Frontiers Research Topics?

Frontiers Research Topics are very popular trademarks of the *Frontiers journals series*: they are collections of at least ten articles, all centered on a particular subject. With their unique mix of varied contributions from Original Research to Review Articles, Frontiers Research Topics unify the most influential researchers, the latest key findings and historical advances in a hot research area.

Find out more on how to host your own Frontiers Research Topic or contribute to one as an author by contacting the Frontiers editorial office: frontiersin.org/about/contact

Advancing genomics for rare disease diagnosis and therapy development vol II

Topic editors

Weida Tong — National Center for Toxicological Research (FDA), United States
Tieliu Shi — Hunan University of Arts and Science, China
Zhichao Liu — Boehringer Ingelheim, United States
Ruth Roberts — ApconiX, United Kingdom
Mike Mikailov — United States Food and Drug Administration, United States

Citation

Tong, W., Shi, T., Liu, Z., Roberts, R., Mikailov, M., eds. (2023). *Advancing genomics for rare disease diagnosis and therapy development vol II*. Lausanne: Frontiers Media SA. doi: 10.3389/978-2-8325-3323-9

Table of contents

08 Case Report: Report of Two Cases of Interstitial Lung Disease Caused by Novel Compound Heterozygous Variants in the *ABCA3* Gene
Fang Chen, Zhiwei Xie, Victor Wei Zhang, Chen Chen, Huifeng Fan, Dongwei Zhang, Wenhui Jiang, Chunli Wang and Peiqiong Wu

15 Case Report: Hereditary Fibrosing Poikiloderma With Tendon Contractures, Myopathy, and Pulmonary Fibrosis (POIKTMP) Presenting With Liver Cirrhosis and Steroid-Responsive Interstitial Pneumonia
Michiko Takimoto-Sato, Toshinari Miyauchi, Masaru Suzuki, Hideyuki Ujiie, Toshifumi Nomura, Tomoo Ikari, Tomohiko Nakamura, Kei Takahashi, Machiko Matsumoto-Sasaki, Hirokazu Kimura, Hiroki Kimura, Yuichiro Matsui, Takashi Kitagataya, Ren Yamada, Kazuharu Suzuki, Akihisa Nakamura, Masato Nakai, Takuya Sho, Koji Ogawa, Naoya Sakamoto, Naoko Yamaguchi, Noriyuki Otsuka, Utano Tomaru and Satoshi Konno

22 Novel Mutations in ACP5 and SAMHD1 in a Patient With Pediatric Systemic Lupus Erythematosus
Soon-Min Hong, Wei Chen, Jiaqi Feng, Dai Dai and Nan Shen

35 Case Report: A Novel Intronic Mutation in *AIFM1* Associated With Fatal Encephalomyopathy and Mitochondrial Disease in Infant
Qi Peng, Keze Ma, Linsheng Wang, Yinghua Zhu, Yaozhong Zhang, Chunbao Rao, Dong Luo, Zaixue Jiang, Wei Lai, Huiling Lu, Chaohui Duan, Zhongjun Zhou and Xiaomei Lu

43 Cardiovascular Abnormalities and Gene Mutations in Children With Noonan Syndrome
Ling Sun, Yu-mei Xie, Shu-shui Wang and Zhi-wei Zhang

53 The *EIF2AK4*/rs4594236 AG/GG Genotype Is a Hazard Factor of Immunoglobulin Therapy Resistance in Southern Chinese Kawasaki Disease Patients
Hongyan Yu, Fucheng Liu, Kaining Chen, Yufen Xu, Yishuai Wang, Lanyan Fu, Huazhong Zhou, Lei Pi, Di Che, Hehong Li and Xiaoqiong Gu

62 ARID2, a Rare Cause of Coffin–Siris Syndrome: A Clinical Description of Two Cases
Xiaoyan Wang, Haiying Wu, Hui Sun, Lili Wang and Linqi Chen

68 Case Report: Whole-Exome Sequencing-Based Copy Number Variation Analysis Identified a Novel *DRC1* Homozygous Exon Deletion in a Patient With Primary Ciliary Dyskinesia
Ying Liu, Cheng Lei, Rongchun Wang, Danhui Yang, Binyi Yang, Yingjie Xu, Chenyang Lu, Lin Wang, Shuizi Ding, Ting Guo, Shaokun Liu and Hong Luo

77 Case Report: Identification of Two Variants of *ALG13* in Families With or Without Seizure and Binocular Strabismus: Phenotypic Spectrum Analysis
Tao Cai, Jieting Huang, Xiuwei Ma, Siqi Hu, Lina Zhu, Jinwen Zhu and Zhichun Feng

84 Case Report: DPM1-CDG: Novel Variant with Severe Phenotype and Literature Review
Hanna Lausmann, Martin Zacharias, Teresa M. Neuhann, Melanie K. Locher and Karl F. Schettler

92 Analysis of characteristic genes and ceRNA regulation mechanism of endometriosis based on full transcriptional sequencing
Chengmao Xie, Ziran Yin and Yong Liu

106 Phenotypes of Cornelia de Lange syndrome caused by non-cohesion genes: Novel variants and literature review
Huakun Shangguan and Ruimin Chen

115 Novel *MEIOB* variants cause primary ovarian insufficiency and non-obstructive azoospermia
Yurong Wang, Ling Liu, Chen Tan, Guiquan Meng, Lanlan Meng, Hongchuan Nie, Juan Du, Guang-Xiu Lu, Ge Lin, Wen-Bin He and Yue-Qiu Tan

122 Cell-based analysis of *CLIC5A* and *SLC12A2* variants associated with hearing impairment in two African families
Samuel Mawuli Adadey, Edmond Wonkam-Tingang, Leonardo Alves de Souza Rios, Elvis Twumasi Aboagye, Kevin Esoh, Noluthando Manyisa, Carmen De Kock, Gordon A. Awandare, Shaheen Mowla and Ambroise Wonkam

134 Case Report: Aarskog-scott syndrome caused by FGD1 gene variation: A family study
Yijia Liang, Honglin Wu, Xiumei He and Xiyu He

141 Case report: Novel compound heterozygous missense mutations in the *DDHD2* gene in a Chinese patient associated with spastic paraplegia type 54
Xin Xu, Fen Lu, Senjie Du, Xiaoke Zhao, Hongying Li, Li Zhang and Jian Tang

148 Detection of a Cryptic 25 bp Deletion and a 269 Kb Microduplication by Nanopore Sequencing in a Seemingly Balanced Translocation Involving the LMLN and LOC105378102 Genes
Yanan Wang, Zhenhua Zhao, Xinyu Fu, Shufang Li, Qiuyan Zhang and Xiangdong Kong

157 Genotypic and phenotypic characteristics of 12 chinese children with glycogen storage diseases
Rui Dong, Xuxia Wei, Kaihui Zhang, Fengling Song, Yuqiang Lv, Min Gao, Dong Wang, Jian Ma, Zhongtao Gai and Yi Liu

168 Systematic analysis of inheritance pattern determination in genes that cause rare neurodevelopmental diseases
Soojin Park, Se Song Jang, Seungbok Lee, Minsoo Kim, Hyungtai Sim, Hyeongseok Jeon, Sung Eun Hong, Jean Lee, Jeongeun Lee, Eun Young Jeon, Jeongha Lee, Cho-Rong Lee, Soo Yeon Kim, Man Jin Kim, Jihoon G. Yoon, Byung Chan Lim, Woo Joong Kim, Ki Joong Kim, Jung Min Ko, Anna Cho, Jin Sook Lee, Murim Choi and Jong-Hee Chae

182 A single-center analysis of genotype–phenotype characteristics of Chinese patients with autosomal dominant polycystic kidney disease by targeted exome sequencing
Ziyan Yan, Yuchen Wang, Wenfeng Deng, Yi Zhou, Yangcheng Hu, Ka Qi, Ding Liu, Renfei Xia, Rumin Liu, Wenli Zeng, Wei Zhang, Jian Xu, Fu Xiong and Yun Miao

190 The development of a novel signature based on the m^{6}A RNA methylation regulator-related ceRNA network to predict prognosis and therapy response in sarcomas
Huling Li, Dandan Lin, Xiaoyan Wang, Zhiwei Feng, Jing Zhang and Kai Wang

211 Characterization of m6A-related lncRNA signature in neuroblastoma
Liming Li, Sisi Chen, Jianhong Li, Guochou Rong, Juchao Yang and Yunquan Li

224 Clinical manifestations and genetic analysis of a newborn with Arboleda–Tham syndrome
Feng Zeng, Yue Yang, Zhaohui Xu, Ziwen Wang, Huan Ke, Jianhong Zhang, Tongtong Dong, Wenming Yang and Jiuxiang Wang

232 Case report: Five-year periodontal management of a patient with two novel mutation sites in *ELANE*-induced cyclic neutropenia
Zhentao Lao, Jiarun Fu, Zhiying Wu, Lihong Zhu, Shiwen Wu, Yongheng Lin, Chaoming Hu, Dingyu Duan and Panpan Wang

241 One potential hotspot *SLC25A20* gene variants in Chinese patients with carnitine-acylcarnitine translocase deficiency
Xiaoli Li and Jian Shen

252 Genotype and phenotype spectrum of 10 children with *STXBP1* gene-related encephalopathy and epilepsy
Meng Dong, Tianyu Zhang, Ruimei Hu, Meng Li, Guan Wang and Xinjie Liu

262 Case report: A novel mutation in *TRPS1* identified in a Chinese family with tricho-rhino-phalangeal syndrome I: A therapeutic challenge
Qi Huang, Cheng Jiang, Jiazhong Sun, Junli Xue and Victor Wei Zhang

268 Integrative analyses of potential biomarkers and pathways for non-obstructive azoospermia
Yucheng Zhong, Xiaoqing Chen, Jun Zhao, Hao Deng, Xiaohang Li, Zhongju Xie, Bingyu Zhou, Zhuojie Xian, Xiaoqin Li, Guoqun Luo and Huan Li

281 Two novel mutations in *VPS33B* gene cause a milder ARC syndrome with prolonged survival in a 12-year-old patient: Case report
Yingjie Zhu and Dongmei Chen

289 Phenotype and genotype analyses of Chinese patients with autosomal dominant mental retardation type 5 caused by *SYNGAP1* gene mutations
Yanxin Wang, Yuqiang Lv, Zilong Li, Min Gao, Xiaomeng Yang, Yue Li, Jianguo Shi, Zaifen Gao, Yi Liu and Zhongtao Gai

299 Clinical, genetic, and experimental research of hyperphenylalaninemia
Anqi Chen, Yukun Pan and Jinzhong Chen

312 Novel variants of *NEK9* associated with neonatal arthrogryposis: Two case reports and a literature review
Fang Liu, Liying Dai, Zhi Li and Xiaowei Yin's

322 Autosomal dominant chronic mucocutaneous candidiasis with STAT1 mutation can be associated with chronic active hepatitis: A case report
Lingling Liu, Yuan Huang, Yi Liao and Sainan Shu

329 Chronic granulomatous disease associated with Duchenne muscular dystrophy caused by Xp21.1 contiguous gene deletion syndrome: Case report and literature review
Shaohua Bi, Liying Dai, Liangliang Jiang, Lili Wang, Mia Teng, Guanghui Liu and Ru-Jeng Teng

337 Case report: Fatal infantile hypertonic myofibrillar myopathy with compound heterozygous mutations in the *CRYAB* gene
Shan-shan Zhang, Li-niu Gu, Teng Zhang, Lu Xu, Xiang Wei, Su-hong Chen, Su-jie Shi, Da-quan Sun, Shao-hong Zhou and Qian-ye Zhao

344 Case Report: Early diagnosis of lethal multiple pterygium syndrome with micrognathia: Two novel mutations in the *CHRND* gene
Caiyuan Chen, Jin Han, Jiaxin Xue, Ru Li, Guilan Chen, Xin Yang, Jiajie Tang, Fucheng Li and Dongzhi Li

351 Case report: The CCDC103 variant causes ultrastructural sperm axonemal defects and total sperm immotility in a professional athlete without primary ciliary diskinesia
Francesca Paola Luongo, Alice Luddi, Rosetta Ponchia, Rossella Ferrante, Sara Di Rado, Eugenio Paccagnini, Mariangela Gentile, Pietro Lupetti, Raffaella Guazzo, Alfredo Orrico, Liborio Stuppia and Paola Piomboni

357 Case Report: Recombinant human growth hormone therapy in a patient with spondyloepiphyseal dysplasia, Kondo-Fu type
Congli Chen, Jin Wu and Ying Liu

363 Case report: Novel TBX5-related pathogenic mechanism of Holt–Oram syndrome
Yuheng Lang, Yue Zheng, Bingcai Qi, Weifeng Zheng, Chengxiu Zhao, Hu Zhai, Gang Wang, Zhiqiang Luo and Tong Li

369 Case report: Sideroblastic anemia with B-cell immunodeficiency, periodic fevers, and developmental delay: Three cases and a literature review
Xiangyuan Chen, Fang Fu, Xiaolan Mo, Suyun Cheng and Huasong Zeng

379 Identification of key pathways, genes and immune cell infiltration in hypoxia of high-altitude acclimatization *via* meta-analysis and integrated bioinformatics analysis
Qiong Li, Zhichao Xu, Fujin Fang, Yan Shen, Huan Lei and Xiaobing Shen

392 Novel compound heterozygous variants of *SLC12A3* gene in a Chinese patient with Gitelman syndrome: a case report
Wenqing Chen, Qin Zhou, Hongjun Chen, Heng Li and Jianghua Chen

frontiers | Frontiers in Genetics

CASE REPORT
published: 06 April 2022
doi: 10.3389/fgene.2022.875015

Case Report: Report of Two Cases of Interstitial Lung Disease Caused by Novel Compound Heterozygous Variants in the *ABCA3* Gene

*Fang Chen[1], Zhiwei Xie[1], Victor Wei Zhang[2,3], Chen Chen[1], Huifeng Fan[1], Dongwei Zhang[1], Wenhui Jiang[1], Chunli Wang[3] and Peiqiong Wu[1]**

[1]Respiratory Department of Guangzhou Women and Children's Medical Center, Guangzhou, China, [2]Department of Human and Molecular Genetics, Baylor College of Medicine, Houston, TX, United States, [3]AmCare Genomics Lab, Guangzhou, China

Interstitial lung disease (ILD) is a heterogeneous group of pulmonary disorders involving the lung interstitium and distal airways, also known as diffuse lung disease. The genetic defects resulting in alveolar surfactant protein dysfunction are a rare cause of ILD in pediatric patients. We report two unrelated pediatric patients with shortness of breath, dyspnea and hypoxemia, and the chest CT findings including patchy ground-glass opacity in both lung fields, suggestive of diffuse ILD. One patient was a full-term male infant who had shortness of breath a few hours after the birth, and then developed into severe respiratory distress syndrome (RDS). Whole exome sequencing revealed novel compound heterozygous variants in the *ABCA3* gene (NM_001,089.3): paternally inherited c.4035+5G > A and c.668T > C (p.M223T), and maternally inherited c.1285+4A > C. The second patient was a 34-month-old boy with onset of chronic repeated cough and hypoxemia at 9 months of age. We unveiled novel compound heterozygous *ABCA3* variants (c.704T > C, p.F235S; c.4037_4040del, p.T1346Nfs*15) in this patient. Surfactant protein dysfunction due to bi-allelic mutations in the *ABCA3* gene was the cause of ILD in two patients. The novel mutations found in this study expanded the spectrum of known mutations in the *ABCA3* gene.

Keywords: ABCA3, interstitial lung disease, ILD, surfactant protein dysfunction, pediatric

OPEN ACCESS

Edited by:
Ruth Roberts,
ApconiX, United Kingdom

Reviewed by:
Dongdong Tang,
First Affiliated Hospital of Anhui Medical University, China
Xiaoqiang Xiao,
Shantou University and the Chinese University of Hong Kong, China

****Correspondence:***
Peiqiong Wu
wupeiqiong@hotmail.com

Specialty section:
This article was submitted to Genetics of Common and Rare Diseases, a section of the journal Frontiers in Genetics

Received: *13 February 2022*
Accepted: *16 March 2022*
Published: *06 April 2022*

Citation:
Chen F, Xie Z, Zhang VW, Chen C, Fan H, Zhang D, Jiang W, Wang C and Wu P (2022) Case Report: Report of Two Cases of Interstitial Lung Disease Caused by Novel Compound Heterozygous Variants in the ABCA3 Gene. Front. Genet. 13:875015. doi: 10.3389/fgene.2022.875015

INTRODUCTION

Pediatric interstitial lung disease (ILD) is a group of rare diseases that occurs in the neonatal or infancy period, which are characterized by varying degrees of inflammation and fibrosis in the lung, and diffuse interstitial changes in imaging examinations. It is being increasingly recognized that ILD affecting newborns, infants and young children usually has an underlying genetic causes, which may be identified through genetic analysis based upon next-generation sequencing methods (Nogee, 2017; Bush et al., 2020; Nathan et al., 2020). Genetic mutations resulting in surfactant protein dysfunction have been regarded as an important etiology of full-term neonates with acute and progressive respiratory distress and chronic respiratory disease in older children. These symptoms are associated with significant morbidity and mortality (Turcu et al., 2013; Nogee, 2019).

Pulmonary surfactant is a complex of phospholipids (90%) and proteins (10%) by mass, which functions to keep alveoli from collapsing at expiration (Carreto-Binaghi et al., 2016). There are four surfactant proteins have been identified, including surfactant proteins A (SP-A), B (SP-B), C (SP-C),

TABLE 1 | Patient characteristics.

Characteristics	Patient 1	Patient 2
Sex	Male	Male
Age at onset	A few hours after birth	9 months
Gestational age	41 weeks	39 weeks
Pulmonary presentation	Severe RDS; ILD; Persistent tachypnea and hypoxemia	ILD; Hypoxemia
Extrapulmonary symptoms	Poor weight gain	Poor weight gain; Developmental delay; Pestle finger
Family history	The elder brother suffered from repeated pneumonia after birth, and died of severe pneumonia when he was 7 months old	None
Age at genetic diagnosis	70 days	34 months
ABCA3 gene mutations	c.4035+5G > A, c.668T > C (p.M223T) c.1285+4A > C	c.704T > C (p.F235S) c.4037_4040del (p.T1346Nfs*15)
ABCA3 deficiency treatment regimen	Azithromycin Hydroxychloroquine Dexamethasone	Azithromycin Budesonide suspension Ipratropium bromide solution
Additional therapies	Ventilator support	Oxygen therapy
Maximal respiratory support	CPAP	Medium flow oxygen supply
Current outcome	Died aged 94 days	Alive, 41-month-old without respiratory support

RDS, respiratory distress syndrome; ILD, interstitial lung disease; CPAP, continuous positive airway pressure.

and D (SP-D). Other proteins such as ATP binding cassette number A3 (ABCA3) and thyroid transcription factor-1 (TTF1) are required for the normal structure and functions of pulmonary surfactants. Research shows that the genetic mutations in the SP-B gene (*SFTPB*), SP-C gene (*SFTPC*), *ABCA3* and *TTF1* genes have been identified as the main causes of surfactant protein dysfunction (Turcu et al., 2013; Nathan et al., 2020). ABCA3 protein is a member of the highly conserved multispan transmembrane ABC superfamily of proteins that hydrolyze ATP to move substrates across biological membranes, which mediates the transport of choline phospholipids and is required for lamellar body biogenesis (Peca et al., 2015). The clinical manifestations of pulmonary diseases caused by *ABCA3* gene mutations vary greatly, ranging from neonatal respiratory failure to childhood or adult diffuse ILD (Panigrahy et al., 2014; Klay et al., 2020; Al-Iede et al., 2021). Here, we report two unrelated pediatric patients with interstitial lung disease caused by compound heterozygous mutations in the *ABCA3* gene.

CASE PRESENTATION

Patients

Two patients were referred to our department of pediatric respiratory for pneumonia without previous clinical diagnosis. This study was approved by the ethical committees of Guangzhou Women and Children's Medical Center. Written informed consent was obtained from the parents. Clinical characteristics of the two patients were summarized in **Table 1**.

Patient 1

Patient 1 was a 46-day-old male infant, who presented with repeated shortness of breath and cough. The infant was born full term at 41 weeks of gestation with a birth weight of 3,660 g. He had shortness of breath without an obvious organic cause on the first day after birth and then he had a single cough 1 week later that developed into paroxysmal continuous cough, accompanied by shortness of breath and sputum. Clinical symptoms of the infant were not alleviated after treatments in local hospitals several times. The patient was admitted to our hospital because of the aggravated cough and shortness of breath. Chest X-ray of the patient revealed multiple patchy shadows in both lung fields (**Figure 1A**). The chest high-resolution computed tomography (HRCT) showed large scattered ground-glass opacity in both lung fields (**Figures 1A, 1a–c**). He was the second child of non-consanguineous parents. In his family history, his older brother had a history of repeated pneumonia after birth, and died of severe pneumonia when he was 7 months old.

On day 70 of life, whole exome sequencing revealed compound heterozygous variants in the *ABCA3* gene (NM_001,089); paternally inherited c.4035+5G > A in intron 26 and c.668T > C (p.M223T) in exon 8, and maternally inherited c.1285+4A > C in intron 11. Sanger sequencing was performed to verity the three variants in the patient and his parents (**Figure 2A**). The three variants of the *ABCA3* gene were all absent from the gnomAD and ExAC databases, and have not been reported in the literature. The intron variants c.4035+5G > A and c.1285+4A > C were predicted to affect RNA splicing by several different splice site algorithms (SpliceSiteFinder-like, MaxEntScan, NNSPLICE, GeneSplicer, and CADD). The predicted tertiary structure of the ABCA3 transporter showed the location of the missense variant p.M223T (**Figure 3**), and the variant was predicted to be deleterious by different algorithms (SIFT: 0.002, Damaging; Polyphen-2: 0.948, Probably_damaging; MutationTaster: 1.000, Disease_causing; FATHMM: 3.83, Damaging; and CADD: 23.4, Damaging).

According to the clinical phenotypes and genetic analysis, the patient was diagnosed as having ILD caused by bi-allelic mutations in the *ABCA3* gene. He was then treated with azithromycin 10 mg/kg/d for 3 days, dexamethasone

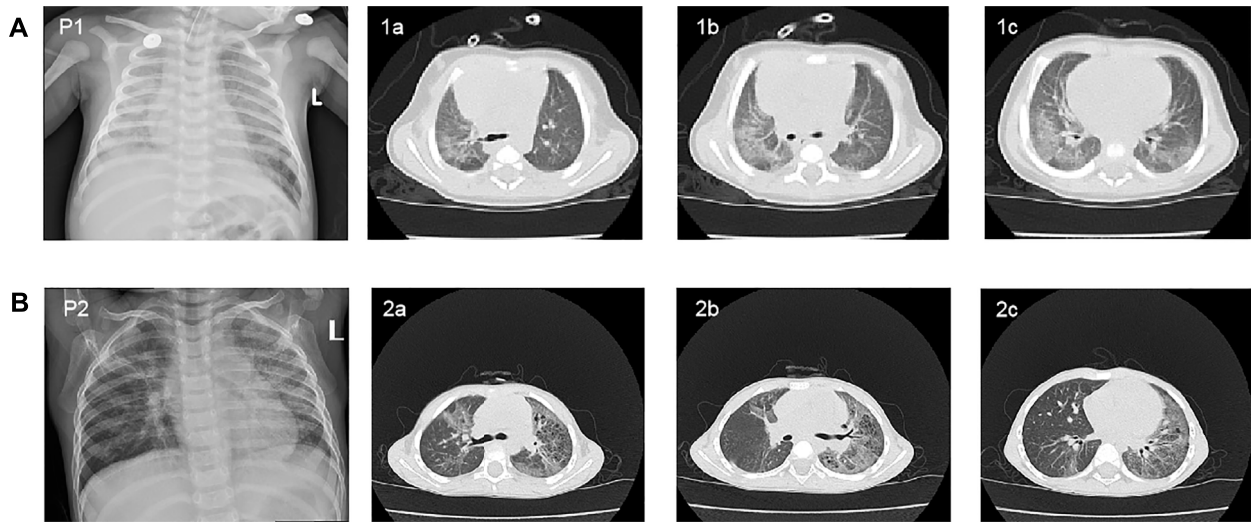


FIGURE 1 | Chest X-ray and high-resolution computed tomography (HRCT) scan findings in two patients. **(A)** Chest X-ray revealed multiple patchy shadows in both lung fields of patient 1 at 60 days of age (P1). The chest HRCT of the patient showed large scattered ground-glass opacity in both lung fields at 46 days of age (1a, 1b, and 1c). **(B)** Chest X-ray of patient2 revealed the bilateral diffuse plaque-like shadows (P2). The chest HRCT scan showed multiple striped fuzzy shadows and ground-glass opacity in both lung fields (2a, 2b, and 2c).

0.2 mg/kg/d for 5 days and 0.1 mg/kg/d for 18 days, and hydroxychloroquine 10 mg/kg/d for 20 days. However, the patient did not respond to these therapies and progressed into severe respiratory distress syndrome (RDS). Unfortunately, the patient died at 94 days of age.

Patient 2

Patient two was a 34-month-old boy who suffered from repeating cough from 9 months of age. The boy was delivered at full term (39 weeks), with a birth weight of 3,000 g. In the beginning the patient's cough was mainly induced by cold temperature, exercise, and crying, which was accompanied by cyanotic complexion and wheezing. The cough still persisted after several outpatient and hospitalized treatments, which alleviated the symptoms after azithromycin treatment. Upon physical examination, the patient had pestle fingers. Chest X-ray revealed bilateral diffuse plaque-like shadows (**Figure 1B**). The chest HRCT scan showed multiple striped fuzzy shadows and ground-glass opacity in both lung fields (**Figure 1B**, **2a-c**). His parents were both asymptomatic, and no family history of genetic disease was reported.

The genetic analysis showed compound heterozygous *ABCA3* variants; paternally inherited c.704T > C (p.F235S) in exon 8, and maternally inherited c.4037_4040del (p.T1346Nfs*15) in exon 27 (**Figure 2B**). The two variants in the *ABCA3* gene were both absent from the gnomAD and ExAC databases, and have not been reported in the literature. The predicted tertiary structure of the ABCA3 transporter showed the location of the missense variant p.M223T (**Figure 3**), and the variant was predicted to be deleterious by different algorithms (SIFT: 0.001, Damaging; Polyphen-2: 0.744, Probably_damaging; MutationTaster: 1.000, Disease_causing; FATHMM: 4.28, Damaging; and CADD: 21.0, Damaging).

Based on the clinical characteristics and genetic analysis, the patient was diagnosed to have ILD caused by *ABCA3* gene mutations. Subsequently, budesonide, ipratropium bromide atomization and acetylcysteine oral symptomatic treatments were given. The patient was slightly short of breath and had no obvious cyanosis. The patient was followed-up in the outpatient clinic after being discharged from hospital, and presented with alleviated clinical features without respiratory support at the age of 41 months.

WHOLE EXOME SEQUENCING

Whole exome sequencing and data analysis for the two patients and their patients were carried out in AmCare Genomic Laboratory (Guangzhou, China). Genomic DNA was extracted using the SolPure Blood DNA kit (Magen) according to manufacturer's instructions and was fragmented by Q800R Sonicator (Qsonica). The paired-end libraries were prepared following Illumina library preparation the protocol. The whole-exomes were captured using the Agilent Sure-Select Human All Exon Kit (Agilent Technologies, Santa Clara, CA). Captured DNA samples were amplified by PCR with indexed primers and then sequenced on an Illumina NovaSeq 6,000 sequencer (Illumina, San Diego, CA). Raw-image data conversion and demultiplexing were performed following Illumina's primary data analysis pipeline using CASAVA version 2.0 (Illumina). Low-quality reads (Phred score < Q20) were removed before demultiplexing. Sequences were aligned to the hg19 reference genome by NextGENe software (SoftGenetics, State College, PA) using the recommended standard settings for single-nucleotide variant and insertion/deletion discovery. The variants with minor allele frequency

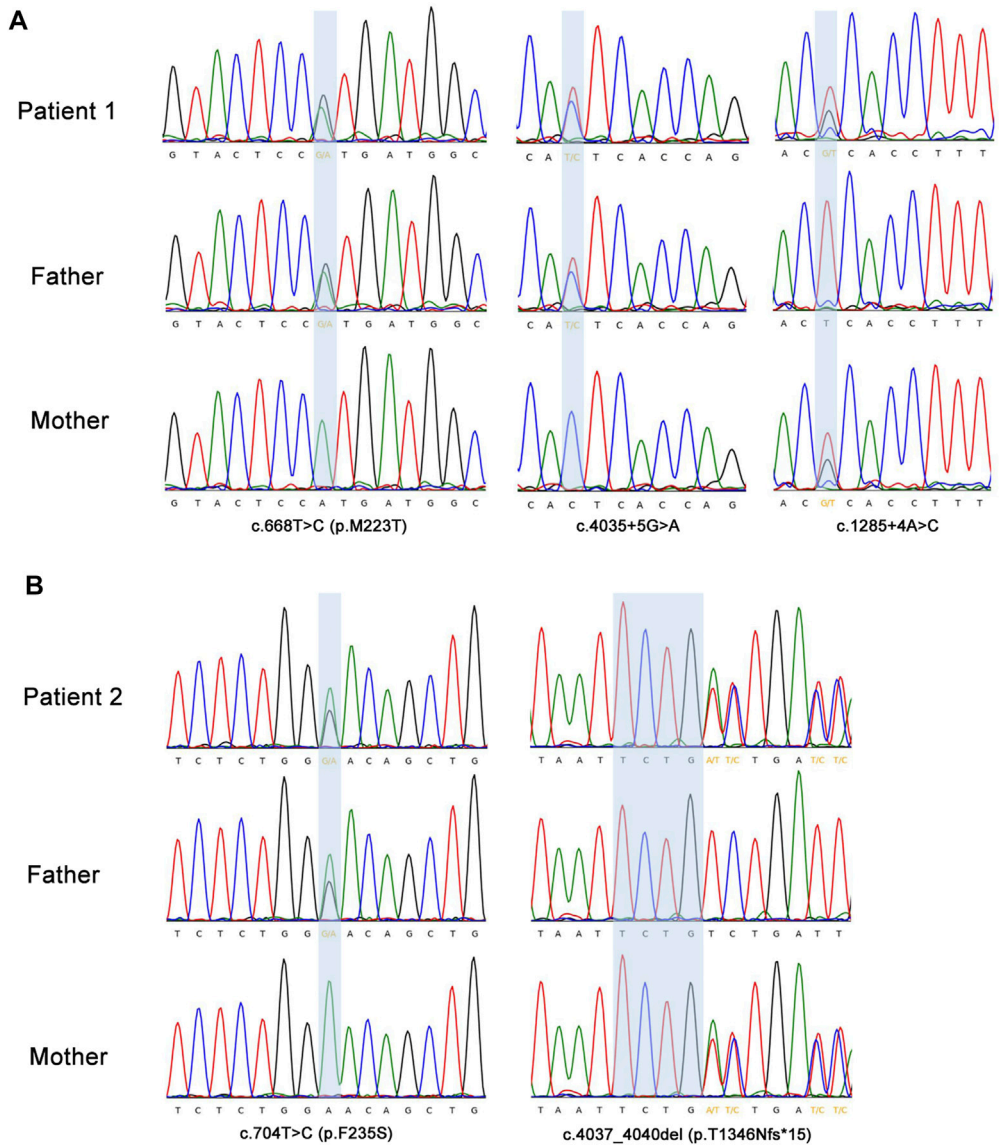


FIGURE 2 | Sanger sequencing confirmation of the *ABCA3* gene variants detected by exome sequencing. **(A)** The highlighting blue background area showed two heterozygous paternally inherited variants (c.4035+5G > A; c.668T > C, p.M223T) and a heterozygous maternally inherited variant (c.1285+4A > C) in *ABCA3* gene in patient 1. **(B)** Patient 2 had a heterozygous missense variant c.704T > C (p.F235S) inherited from the father and a heterozygous frameshift variant c.4037_4040del (p.T1346Nfs*15) from the mother in the *ABCA3* gene. Sanger sequencing showed the antisense sequence alignment of the *ABCA3* gene.

(MAF) > 1% in the Asian population and synonymous variants and were filtered out. Variant annotation was further confirmed through literature and population databases, including GnomAD (https://gnomad.broadinstitute.org/), Clinvar (https://www.ncbi.nlm.nih.gov/clinvar/), HGMD (http://www.hgmd.cf.ac.uk/ac/index.php), and OMIM (https://www.omim.org/). Genetic evaluation of pathogenicity of candidate gene variants was performed using multiple computational algorithms, including SIFT, Polyphen-2, MutationTaster, and CADD. The pathogenicity of the variants was estimated using the American College of Medical Genetics and Genomics (ACMG) guidelines (Richards et al., 2015).

DISCUSSION

Pediatric patients with ILD represent varying degrees of respiratory disorders with different age of onset and clinical manifestations. Chest HRCT scan is the key tool for the ILD diagnosis, while diffuse ground-glass attenuation is the most common feature. Once the diagnosis of ILD is made, the etiological diagnostic approach is required in patients. An underlying genetic causes occurs frequently in early onset ILD, and the genetic diagnosis is important for predicting prognosis and counseling families regarding recurrence risks. ILD manifesting in term newborns or young infants is usually due

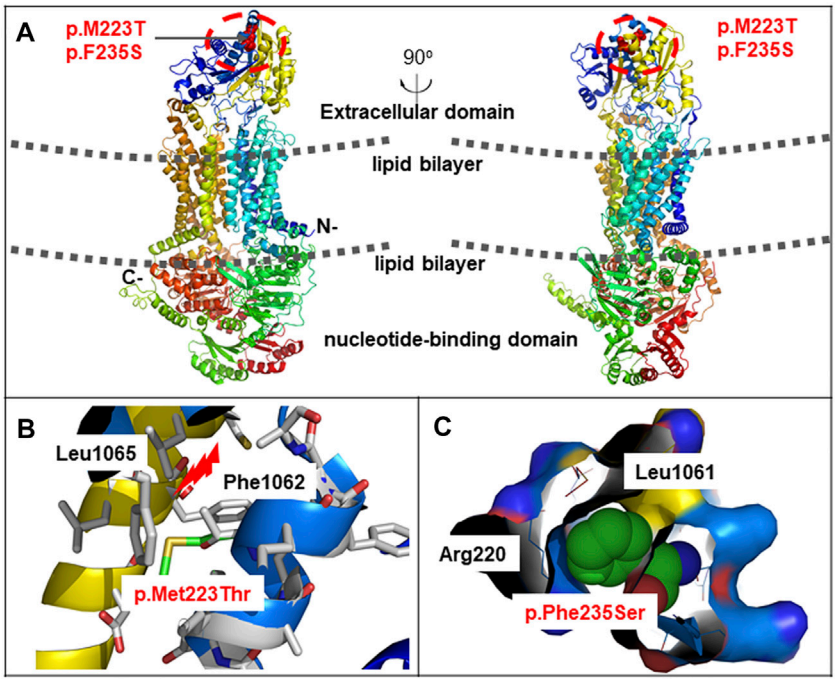


FIGURE 3 | Schematic representation of missense variants p.M223T and p. F235S on the ABCA3 protein. **(A)** Predicted tertiary structure of the ABCA3 transporter by PyMOL. ABCA3 is an integral membrane protein that contains 12 membrane-spanning helices and two cytosolic nucleotide binding domains. The two missense variants were located on the extracellular domain. **(B)** Spatial disposition of the amino acid residues Met223, Leu1065, and Phe1062. **(C)** Spatial disposition of the amino acid residues Phe235, Arg220, and Leu1061.

to mutations in the surfactant protein genes (Gupta and Zheng, 2017), or conditions related to congenital alveolar capillary dysplasia and congenital acinar dysplasia. In this study, we reported two unrelated pediatric patients with shortness of breath, dyspnea and hypoxemia, and chest HRCT findings of patchy ground-glass opacity in both lung fields, suggestive of diffuse ILD. Novel compound heterozygous variants in the *ABCA3* gene were identified using whole exome sequencing in the two patients. Patient one had paternally inherited c.4035+5G > A and c.668T > C (p.M223T), and maternally inherited c.1285+4A > C while patient two had c.704T > C (p.F235S) and c.4037_4040del (p.T1346Nfs*15).

The *ABCA3* gene is located on human chromosome 16p13.3 and contains 33 exons encoding a protein consisting of 1,704 amino acids. Protein Structure prediction algorithms shows that ABCA3 has a typical structure of most ABC transporters, consisting of two six-unit membrane-spanning domains, two nucleotide-binding domains (NBD1 and NBD2) oriented toward the cytosol, and six extracellular domains (ECD1-6) oriented towards the inner compartment of lamellar bodies (Peca et al., 2015). The ABCA3 glycoprotein uses the energy of ATP hydrolysis to translocate substrates across cell membranes. More specifically, ABCA3 transports surfactant phospholipids to lamellar bodies, which play a crucial role in maintaining the homeostasis of lung surfactant phospholipids (Schindlbeck et al., 2018). Bi-allelic mutations in the *ABCA3* gene were first reported in a group of full-term infants with severe neonatal surfactant deficiency occurring shortly after birth (Shulenin et al., 2004). ABCA3-related surfactant protein disorder is an autosomal recessive disease that leads to the dysfunction of phospholipid transporters related to lung surfactants. To date, more than 200 mutations in the *ABCA3* gene have been reported in patients with respiratory diseases, including nonsense, frameshift, spice-site, and missense mutations (Beers and Mulugeta, 2017; Wei et al., 2020; Bozkurt and Sahin, 2021; Zhang et al., 2021). Many deleterious mutations found in human tend to cluster on ECD1, ECD4, and NBD2 (Peca et al., 2015; Beers and Mulugeta, 2017). Experimental studies showed that ABCA3 proteins with ECD1 and ECD4 mutations remained localized in the endoplasmic reticulum and exhibited impaired glycosylation, whereas mutant proteins in NBD1 and NBD2 led to decreased ATP binding and/or hydrolysis (Matsumura et al., 2006; Wambach et al., 2016). In this study, the two novel missense variants c.668T > C (p.M223T) and c.704T > C (p.F235S) were located on ECD1, which were predicted to be deleterious by different algorithms.

Many evidences indicate that the *ABCA3* gene mutation-associated lung diseases are highly heterogeneous, ranging from RDS in term neonates to childhood ILD and fibrosing ILD in adults. A study of genotype-phenotype correlations in 185 infants and children with bi-allelic *ABCA3* mutations showed that all of the infants with frameshift and/or nonsense mutations presented with respiratory failure at birth compared with 75% of infants with other genotypes (non-allelic frameshift and/or nonsense mutations); all of the infants with frameshift and/or

nonsense mutations have died or undergone lung transplantation by 1 year of age compared with 62% of infants/children with other genotypes (Wambach et al., 2014). A number of studies have shown that bi-allelic frameshift or nonsense *ABCA3* mutations are predictive of neonatal presentation and poor outcome, whereas the presentation and outcome for infants and children with other genotypes (missense, splice site, and in-frame mutations) were more variable and less predictable (Cho et al., 2020; Klay et al., 2020; Wang et al., 2021). Of note, many studies showed that monoallelic *ABCA3* mutations are also common in infants with RDS, childhood ILD, and adults with idiopathic pulmonary fibrosis (IPF) and diffuse parenchymal lung disease (DPLD) (Wambach et al., 2012; Coghlan et al., 2014). In this study, patient 1 with missense and intron compound heterozygous variants in the *ABCA3* gene presented with shortness of breath at birth, and then developed into severe RDS with a poor outcome. Moreover, patient 2 with a missense and a frameshift compound heterozygous variants presented with chronic repeated cough and hypoxemia at 9 months of age with a diagnosis of childhood ILD. He was given surface hormone inhalation therapy and is currently under follow-up.

Until now, there have been no specific therapeutic strategies for children with surfactant protein dysfunction caused by *ABCA3* mutations. In the acute setting, patients with increased respiratory effort and hypoxaemia could be provided with respiratory supportive care, ranging from oxygen supplementation to non-invasive or invasive ventilation. Most neonates presenting acute respiratory distress would initially receive surfactant replacement therapy, which may lead to a clinical response initially but not maintained in the longer term. Other drug treatments include corticosteroids, hydroxychloroquine, and azithromycin have been reported to be effective in some cases with *ABCA3* mutations (Hayes et al., 2012; Thouvenin et al., 2013; Nishida et al., 2021; Shaaban et al., 2021). Immunosuppression with corticosteroids are the preferred choice, administered intravenous methylprednisolone or oral prednisolone. Intravenous methylprednisolone is usually given at a dose of 10 mg/kg/day or 500 mg/m^2 for 3 days consecutively at monthly intervals, assessing the clinical response to treatment after 7 days in children who are ventilated or at 28 days in non-ventilated children. Oral prednisolone is most commonly administered at a dose of 1 mg/kg/day, used in between pulses of methylprednisolone. Hydroxychloroquine can be started with a recommended dose of 6–10 mg/kg/day, and clinical response to treatment should be assessed after 3–4 weeks or after 3 months in children who are ventilated or not. Alternatively, azithromycin with a recommended dose of 10 mg/kg 3 days per week can be used as a second-line therapy (Bush et al., 2015). However, it is difficult to evaluate the effects of treatment with the above-mentioned drugs due to the lack of either randomized or controlled studies. Lung transplantation may be the only option for children with end-stage lung disease that is unresponsive to other therapies.

In conclusion, a diagnosis of surfactant protein dysfunction should be suspected in full-term newborns with unexplained respiratory distress and in older children with persistent unexplained respiratory symptoms such as cough, hypoxemia, and shortness of breath. The main HRCT characteristic manifestation is ground-glass opacification. Genetic testing now enables non-invasive diagnosis of surfactant protein dysfunction, negating the need for histology on lung biopsy. Timely genetic diagnosis is important for conducting management, predicting prognosis, and counseling families regarding recurrence risks. In this study, we reported the clinical and genetic features of two children with compound heterozygous variants in the *ABCA3* gene, and the novel mutations have expanded the spectrum of known mutations in the *ABCA3* gene. A deeper understanding of pathogenic mechanisms involved in ABCA3 deficiency may contribute to elucidate the genotype-phenotype correlations and the development of mutation specific drugs in the future.

DATA AVAILABILITY STATEMENT

The datasets for this article are not publicly available due to concerns regarding participant/patient anonymity. Requests to access the datasets should be directed to the corresponding author.

ETHICS STATEMENT

Written informed consent was obtained from the minor(s)' legal guardian/next of kin for the publication of any potentially identifiable images or data included in this article.

AUTHOR CONTRIBUTIONS

FC is responsible for collecting clinical data and writing articles. ZX and others provided modification suggestions for the article. VZ and CW interpreted and analyzed the gene results and assisted in the revision of the article. PW participated in the revision of the article and served as the corresponding author of this article.

REFERENCES

Al-Iede, M., Khanfar, M., Srour, L., Rabah, R., Al-Abbadi, M., Azab, B., et al. (2021). A Homozygous Variant in ABCA3 Is Associated with Severe Respiratory Distress and Early Neonatal Death. *Congenit. Anom.* 61, 231–233. doi:10.1111/cga.12437

Beers, M. F., and Mulugeta, S. (2017). The Biology of the ABCA3 Lipid Transporter in Lung Health and Disease. *Cell Tissue Res* 367, 481–493. doi:10.1007/s00441-016-2554-z

Bozkurt, H. B., and Şahin, Y. (2021). Whole Exome Sequencing Identifies a Novel Variant in ABCA3 in an Individual with Fatal Congenital Surfactant Protein Deficiency. *TurkJPediatr* 63, 703–707. doi:10.24953/turkjped.2021.04.019

Bush, A., Cunningham, S., de Blic, J., Barbato, A., Clement, A., Epaud, R., et al. (2015). European Protocols for the Diagnosis and Initial Treatment of Interstitial Lung Disease in Children. *Thorax* 70, 1078–1084. doi:10.1136/thoraxjnl-2015-207349

Bush, A., Gilbert, C., Gregory., J., Nicholson, A. G., Semple, T., and Pabary, R. (2020). Interstitial Lung Disease in Infancy. *Early Hum. Dev.* 150, 105186. doi:10.1016/j.earlhumdev.2020.105186

Carreto-Binaghi, L. E., Aliouat, E. M., and Taylor, M. L. (2016). Surfactant Proteins, SP-A and SP-D, in Respiratory Fungal Infections: Their Role in the Inflammatory Response. *Respir. Res.* 17, 66. doi:10.1186/s12931-016-0385-9

Cho, J. G., Thakkar, D., Buchanan, P., Graf, N., and Wheatley, J. (2020). ABCA3 Deficiency from Birth to Adulthood Presenting as Paediatric Interstitial Lung Disease. *Respirology Case Rep.* 8, e00633. doi:10.1002/rcr2.633

Coghlan, M. A., Shifren, A., Huang, H. J., Russell, T. D., Mitra, R. D., Zhang, Q., et al. (2014). Sequencing of Idiopathic Pulmonary Fibrosis-Related Genes Reveals Independent Single Gene Associations. *BMJ Open Resp Res.* 1, e000057. doi:10.1136/bmjresp-2014-000057

Gupta, A., and Zheng, S. L. (2017). Genetic Disorders of Surfactant Protein Dysfunction: when to Consider and How to Investigate. *Arch. Dis. Child.* 102, 84–90. doi:10.1136/archdischild-2012-303143

Hayes, D., Jr., Lloyd, E. A., Fitch, J. A., and Bush, A. (2012). ABCA3 Transporter Deficiency. *Am. J. Respir. Crit. Care Med.* 186, 807. doi:10.1164/ajrccm.186.8.807a

Klay, D., Platenburg, M. G. J. P., van Rijswijk, R. H. N. A. J., Grutters, J. C., and van Moorsel, C. H. M. (2020). ABCA3 Mutations in Adult Pulmonary Fibrosis Patients: a Case Series and Review of Literature. *Curr. Opin. Pulm. Med.* 26, 293–301. doi:10.1097/MCP.0000000000000680

Matsumura, Y., Ban, N., Ueda, K., and Inagaki, N. (2006). Characterization and Classification of ATP-Binding Cassette Transporter ABCA3 Mutants in Fatal Surfactant Deficiency. *J. Biol. Chem.* 281, 34503–34514. doi:10.1074/jbc.M600071200

Nathan, N., Berdah, L., Delestrain, C., Sileo, C., and Clement, A. (2020). Interstitial Lung Diseases in Children. *La Presse Médicale* 49, 103909. doi:10.1016/j.lpm.2019.06.007

Nishida, D., Kawabe, S., Iwata, N., and Cho, K. (2021). ABCA3 Deficiency Dramatically Improved by Azithromycin Administration. *Pediatr. Int.* 63, 602–604. doi:10.1111/ped.14487

Nogee, L. M. (2019). Genetic Causes of Surfactant Protein Abnormalities. *Curr. Opin. Pediatr.* 31, 330–339. doi:10.1097/MOP.0000000000000751

Nogee, L. M. (2017). Interstitial Lung Disease in Newborns. *Semin. Fetal Neonatal Med.* 22, 227–233. doi:10.1016/j.siny.2017.03.003

Panigrahy, N., Poddutoor, P. K., and Chirla, D. K. (2014). ATP-binding Cassette Transporter A3 (ABCA3) Mutation in a Late Preterm with Respiratory Distress Syndrome. *Indian Pediatr.* 51, 579–580. doi:10.1007/s13312-014-0454-4

Peca, D., Cutrera, R., Masotti, A., Boldrini, R., and Danhaive, O. (2015). ABCA3, a Key Player in Neonatal Respiratory Transition and Genetic Disorders of the Surfactant System. *Biochem. Soc. Trans.* 43, 913–919. doi:10.1042/BST20150100

Richards, S., Aziz., N., Bale, S., Bick, D., Das, S., Gastier-Foster, J., et al. (2015). Standards and Guidelines for the Interpretation of Sequence Variants: a Joint Consensus Recommendation of the American College of Medical Genetics and Genomics and the Association for Molecular Pathology. *Genet. Med.* 17, 405–424. doi:10.1038/gim.2015.30

Schindlbeck, U., Wittmann., T., Höppner, S., Kinting, S., Liebisch, G., Hegermann, J., et al. (2018). ABCA3 Missense Mutations Causing Surfactant Dysfunction Disorders Have Distinct Cellular Phenotypes. *Hum. Mutat.* 39, 841–850. doi:10.1002/humu.23416

Shaaban, W., Hammoud, M., Abdulraheem, A., Elsayed, Y. Y., and Alkazemi, N. (2021). Hydroxychloroquine, a Successful Treatment for Lung Disease in ABCA3 Deficiency Gene Mutation: a Case Report. *J. Med. Case Rep.* 15, 54. doi:10.1186/s13256-020-02604-5

Shulenin, S., Nogee, L. M., Annilo, T., Wert, S. E., Whitsett, J. A., and Dean, M. (2004). ABCA3Gene Mutations in Newborns with Fatal Surfactant Deficiency. *N. Engl. J. Med.* 350, 1296–1303. doi:10.1056/NEJMoa032178

Thouvenin, G., Nathan., N., Epaud, R., and Clement, A. (2013). Diffuse Parenchymal Lung Disease Caused by Surfactant Deficiency: Dramatic Improvement by Azithromycin. *Case Rep.* 2013, bcr2013009988. doi:10.1136/bcr-2013-009988

Turcu, S., Ashton, E., Jenkins, L., Gupta, A., and Mok, Q. (2013). Genetic Testing in Children with Surfactant Dysfunction. *Arch. Dis. Child.* 98, 490–495. doi:10.1136/archdischild-2012-303166

Wambach, J. A., Casey, A. M., Fishman, M. P., Wegner., D. J., Wert, S. E., Cole, F. S., et al. (2014). Genotype-phenotype Correlations for Infants and Children with ABCA3 Deficiency. *Am. J. Respir. Crit. Care Med.* 189, 1538–1543. doi:10.1164/rccm.201402-0342OC

Wambach, J. A., Wegner, D. J., Depass, K., Heins, H., Druley, T. E., Mitra, R. D., et al. (2012). Single ABCA3 Mutations Increase Risk for Neonatal Respiratory Distress Syndrome. *Pediatrics* 130, e1575–e1582. doi:10.1542/peds.2012-0918

Wambach, J. A., Yang, P., Wegner, D. J., Heins, H. B., Kaliberova, L. N., Kaliberov, S. A., et al. (2016). Functional Characterization of ATP-Binding Cassette Transporter A3 Mutations from Infants with Respiratory Distress Syndrome. *Am. J. Respir. Cel Mol Biol* 55, 716–721. doi:10.1165/rcmb.2016-0008OC

Wang, J., Fan, J., Zhang, Y., Huang, L., and Shi, Y. (2021). ABCA3 Gene Mutations Shape the Clinical Profiles of Severe Unexplained Respiratory Distress Syndrome in Late Preterm and Term Infants. *Transl Pediatr.* 10, 350–358. doi:10.21037/tp-20-283

Wei, M., Fu, H., Han, A., and Ma, L. (2020). A Term Neonatal Case with Lethal Respiratory Failure Associated with a Novel Homozygous Mutation in ABCA3 Gene. *Front. Pediatr.* 8, 138. doi:10.3389/fped.2020.00138

Zhang, W., Liu., Z., Lin., Y., Wang., R., Xu, J., He, Y., et al. (2021). A Novel Synonymous ABCA3 Variant Identified in a Chinese Family with Lethal Neonatal Respiratory Failure. *BMC Med. Genomics* 14, 256. doi:10.1186/s12920-021-01098-4

Conflict of Interest: The authors declare that the research was conducted in the absence of any commercial or financial relationships that could be construed as a potential conflict of interest.

Publisher's Note: All claims expressed in this article are solely those of the authors and do not necessarily represent those of their affiliated organizations, or those of the publisher, the editors and the reviewers. Any product that may be evaluated in this article, or claim that may be made by its manufacturer, is not guaranteed or endorsed by the publisher.

Copyright © 2022 Chen, Xie, Zhang, Chen, Fan, Zhang, Jiang, Wang and Wu. This is an open-access article distributed under the terms of the Creative Commons Attribution License (CC BY). The use, distribution or reproduction in other forums is permitted, provided the original author(s) and the copyright owner(s) are credited and that the original publication in this journal is cited, in accordance with accepted academic practice. No use, distribution or reproduction is permitted which does not comply with these terms.

frontiers | Frontiers in Genetics

CASE REPORT
published: 05 May 2022
doi: 10.3389/fgene.2022.870192

Case Report: Hereditary Fibrosing Poikiloderma With Tendon Contractures, Myopathy, and Pulmonary Fibrosis (POIKTMP) Presenting With Liver Cirrhosis and Steroid-Responsive Interstitial Pneumonia

Michiko Takimoto-Sato[1†], Toshinari Miyauchi[2†], Masaru Suzuki[1], Hideyuki Ujiie[2], Toshifumi Nomura[2,3], Tomoo Ikari[1], Tomohiko Nakamura[1], Kei Takahashi[1], Machiko Matsumoto-Sasaki[1], Hirokazu Kimura[1], Hiroki Kimura[1], Yuichiro Matsui[4], Takashi Kitagataya[5], Ren Yamada[5], Kazuharu Suzuki[5], Akihisa Nakamura[5], Masato Nakai[5], Takuya Sho[5], Koji Ogawa[5], Naoya Sakamoto[5], Naoko Yamaguchi[6], Noriyuki Otsuka[6], Utano Tomaru[6] and Satoshi Konno[1]*

[1]Department of Respiratory Medicine, Faculty of Medicine and Graduate School of Medicine, Hokkaido University, Sapporo, Japan, [2]Department of Dermatology, Faculty of Medicine and Graduate School of Medicine, Hokkaido University, Sapporo, Japan, [3]Department of Dermatology, Faculty of Medicine, University of Tsukuba, Tsukuba, Japan, [4]Department of Orthopaedic Surgery, Faculty of Medicine and Graduate School of Medicine, Hokkaido University, Sapporo, Japan, [5]Department of Gastroenterology and Hepatology, Faculty of Medicine and Graduate School of Medicine, Hokkaido University, Sapporo, Japan, [6]Department of Pathology, Faculty of Medicine and Graduate School of Medicine, Hokkaido University, Sapporo, Japan

Background: Hereditary fibrosing poikiloderma with tendon contractures, myopathy, and pulmonary fibrosis (POIKTMP) is an extremely rare disease caused by mutations in FAM111B, and only approximately 30 cases have been reported worldwide. Some patients develop interstitial pneumonia, which may lead to progressive pulmonary fibrosis and poor prognosis. However, no effective treatment for interstitial pneumonia associated with POIKTMP has been reported. Here, we report an autopsy case of POIKTMP, wherein interstitial pneumonia was improved by corticosteroids.

Case Presentation: A 44-year-old Japanese man was referred to our hospital due to poikiloderma, hypotrichosis, and interstitial pneumonia. He developed progressive poikiloderma and muscle weakness since infancy. He also had tendon contractures, short stature, liver cirrhosis, and interstitial pneumonia. Mutation analysis of FAM111B revealed a novel and *de novo* heterozygous missense mutation, c.1886T > G (p(Phe629Cys)), through which we were able to diagnose the patient with POIKTMP.

Abbreviations: POIKTMP, hereditary fibrosing poikiloderma with tendon contractures, myopathy, and pulmonary fibrosis; CT, computed tomography; PCR, polymerase chain reaction; RTS, Rothmund-Thomson syndrome; VC, vital capacity; DLCO, diffusing capacity for carbon monoxide; KL-6, Krebs Von den Lungen-6; SP-A, surfactant protein A; SP-D, surfactant protein D; BAL, bronchoalveolar lavage; H&E, Hematoxylin and eosin; f-NSIP, fibrotic-nonspecific interstitial pneumonia; UIP, usual interstitial pneumonia.

OPEN ACCESS

Edited by:
Ruth Roberts,
ApconiX, United Kingdom

Reviewed by:
Joshi Stephen,
Baylor College of Medicine, United States
Shreyans Gandhi,
King's College Hospital NHS Foundation Trust, United Kingdom
Sandra Mercier,
Centre Hospitalier Universitaire (CHU) de Nantes, France

***Correspondence:**
Masaru Suzuki
suzumasa@med.hokudai.ac.jp

[†]These authors have equally contributed to this work and share first authorship

Specialty section:
This article was submitted to Genetics of Common and Rare Diseases, a section of the journal Frontiers in Genetics

Received: 06 February 2022
Accepted: 22 April 2022
Published: 05 May 2022

Citation:
Takimoto-Sato M, Miyauchi T, Suzuki M, Ujiie H, Nomura T, Ikari T, Nakamura T, Takahashi K, Matsumoto-Sasaki M, Kimura H, Kimura H, Matsui Y, Kitagataya T, Yamada R, Suzuki K, Nakamura A, Nakai M, Sho T, Ogawa K, Sakamoto N, Yamaguchi N, Otsuka N, Tomaru U and Konno S (2022) Case Report: Hereditary Fibrosing Poikiloderma With Tendon Contractures, Myopathy, and Pulmonary Fibrosis (POIKTMP) Presenting With Liver Cirrhosis and Steroid-Responsive Interstitial Pneumonia. Front. Genet. 13:870192. doi: 10.3389/fgene.2022.870192

3 years after the POIKTMP diagnosis, interstitial pneumonia had worsened. After 2 weeks of administrating 40 mg/day of prednisolone, his symptoms and lung shadows improved. However, he subsequently developed severe hepatic encephalopathy and eventually died of respiratory failure due to bacterial pneumonia and pulmonary edema. Autopsy revealed an unclassifiable pattern of interstitial pneumonia, as well as the presence of fibrosis and fatty degeneration in several organs, including the liver, kidney, skeletal muscle, heart, pancreas, and thyroid.

Conclusions: We report a case of POIKTMP in which interstitial pneumonia was improved by corticosteroids, suggesting that corticosteroids could be an option for the treatment of interstitial pneumonia associated with this disease.

Keywords: POIKTMP, FAM111B, interstitial pneumonia, liver cirrhosis, case report

INTRODUCTION

Hereditary fibrosing poikiloderma with tendon contractures, myopathy, and pulmonary fibrosis (POIKTMP) is a recently described genetic disorder, caused by mutation in FAM111B, which is inherited in an autosomal dominant manner (Mercier et al., 2013). POIKTMP is an extremely rare disease, and only approximately 30 cases have been reported worldwide. Patients with POIKTMP develop poikiloderma during early infancy, predominantly in sun-exposed areas, as well as progressive muscle atrophy, tendon contractures, and sparse hair. Elevation of liver enzymes, cataracts, and exocrine pancreatic insufficiency were also observed. Some patients develop interstitial pneumonia, which may lead to progressive pulmonary fibrosis and poor prognosis due to respiratory failure in their 30–50 s (Khumalo et al., 2006; Mercier et al., 2015; Sanchis-Borja et al., 2018). To date, no effective treatment has been reported for this disease, including interstitial pneumonia.

Here, we report an autopsy case of POIKTMP in which interstitial pneumonia was improved by corticosteroids.

Case Description

A 44-year-old Japanese man was referred to our hospital with various systemic symptoms that had gradually developed since infancy. His parents were non-consanguineous, and there was no family history of similar symptoms. He had a medical history of dysphagia and dysarthria from around the age of 35 years, and hearing loss occurred at approximately 40 years of age.

Dermatological and orthopedic examinations revealed several characteristic manifestations. The patient had a short stature (149 cm) and presented with muscle weakness in all extremities. Poikiloderma with mottled pigmentation and telangiectasia was remarkable on the face (**Figure 1A**). The eyebrows and eyelashes were almost absent, and lagophthalmos due to skin sclerosis was observed (**Figure 1B**). Scalp hairs were also sparse, and the top of the head had been almost hairless since childhood (**Figure 1C**). The trunk and extremities showed dry skin, mild eczema, small pigmented macules, and skin sclerosis (**Figure 1D**). He had mild lymphedema of the lower limbs and a medical history of cellulitis due to this symptom. His left heel could not be placed on the ground due to Achilles tendon contracture, resulting in a constant flexed position of his left knee (**Figures 1E,F**). Mild hypoplasia of the hands and feet, multiple calluses on the soles, and impaired extension of the fingers were noted (**Figures 1G–I**). Histology of the non-sun-exposed skin showed epidermal atrophy and mild dermal fibrosis (**Figure 1J**). Fragmented elastic fibers were clearly observed with Elastica–Masson staining (**Figure 1K**). Muscle magnetic resonance imaging (MRI) findings showed severe fatty infiltration in the bilateral quadriceps muscles (**Figure 1L**), erector spinae muscles, and muscles in the upper extremities.

Further examinations revealed interstitial pneumonia, liver cirrhosis, and chronic kidney disease. A chest computed tomography (CT) scan revealed interstitial lung shadows, predominantly in the upper lobes, indicating the cause of his shortness of breath. His liver cirrhosis was graded as Child–Pugh class B and was accompanied by portal hypertension and esophageal varix. In this case, liver cirrhosis was diagnosed based on the findings of CT and ultrasonography, since a biopsy could not be performed. Ophthalmological examination revealed the presence of retinal rod dysfunction, lacrimal passage obstruction, and ptosis, but not cataract. Otolaryngological examination revealed atrophied vocal cords and mild sensorineural hearing loss.

Diagnostic Assessment

Based on the clinical findings described above, a diagnosis of POIKTMP was highly suspected. To confirm this, mutation analysis of FAM111B was performed. The patient and his parents provided written informed consent to participate in this study, in compliance with the Declaration of Helsinki. The Institutional Review Board at Hokkaido University Graduate School of Medicine approved this study (project no. 14–063). In brief, genomic DNA was extracted from peripheral blood using the QIAamp DNA Blood Maxi Kit (Qiagen, Hilden, Germany), and all exons and exon–intron boundaries of FAM111B were amplified using polymerase chain reaction (PCR). The PCR products were sequenced using an ABI 3130xl Genetic Analyzer (Applied Biosystems, Foster City, CA, United States), which led to the identification of a novel and *de novo* heterozygous missense mutation c.1886T > G (p(Phe629Cys)) (RefSeq accession number NM_198,947.4) in the patient (**Figures 2A,B**). This mutation was absent in 96

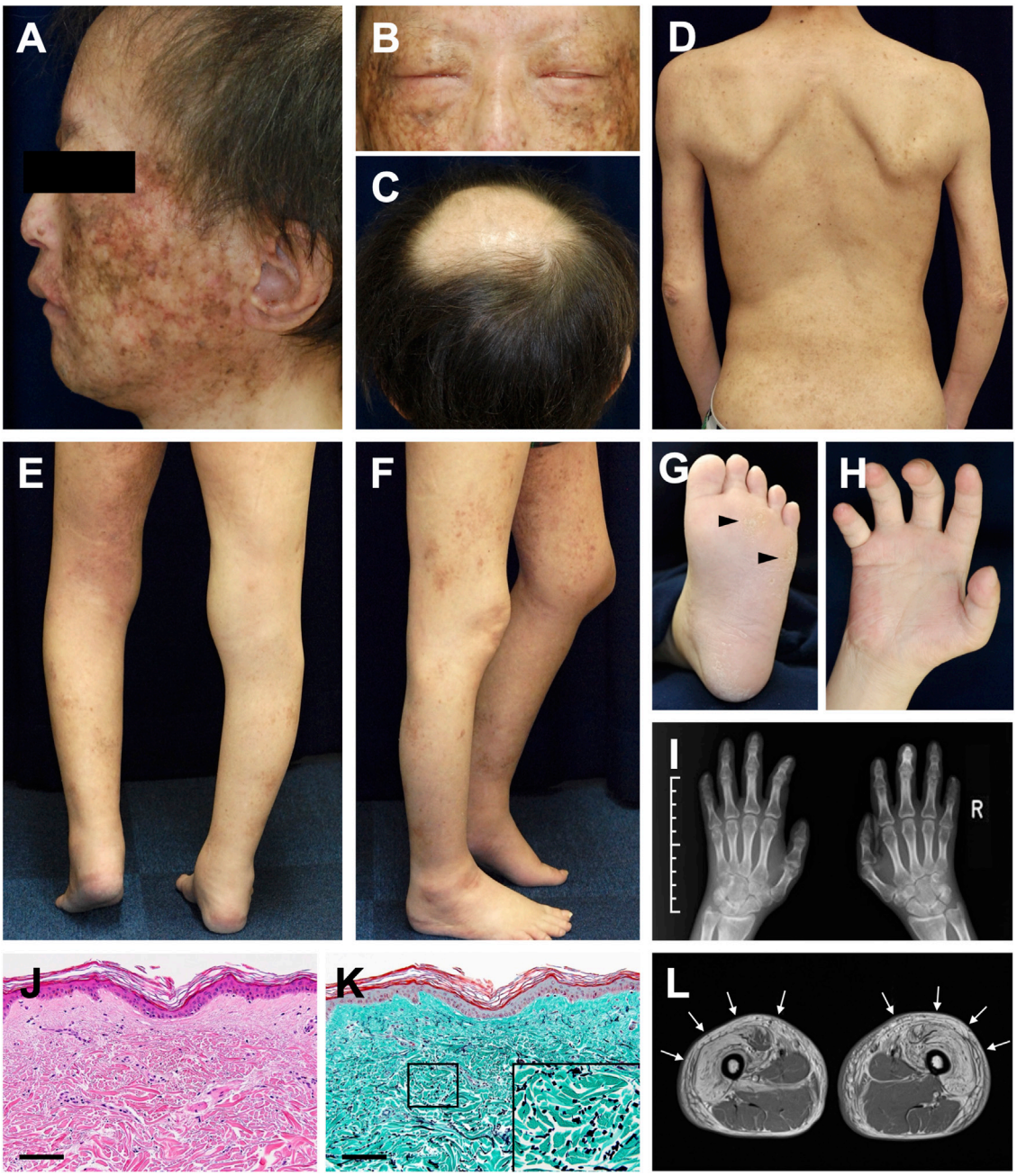


FIGURE 1 | Clinical and histopathological manifestations **(A)** Poikiloderma with mottled pigmentation and telangiectasia on the face **(B)** Sparse eyebrows and eyelashes and lagophthalmos **(C)** Hairless on top of the head **(D)** Dry skin, mild eczema, and small pigmented macules with skin sclerosis **(E,F)** Mild lymphedema of the lower limbs **(E)** and contracture of the left Achilles tendon **(F) (G)** Mild hyperkeratosis with calluses (arrowheads) on the sole **(H)** Impaired extension of the fingers **(I)** Mild hypoplasia of the hands evaluated using X-ray photography **(J)** Pathological features of the non-sun-exposed area of the anterior chest. Hematoxylin and eosin (H&E) stain (scale bar, 100 μm) **(K)** Elastica–Masson staining. The inset shows a high-magnification image of the area indicated in the box (scale bar, 100 μm). **(L)** Diffuse bright appearance (white arrows) of the bilateral quadriceps muscles detected with muscle MRI (T1-weighted sequence).

unrelated Japanese controls and in databases, such as the 1000 Genomes Browser, the Single Nucleotide Polymorphism Database, the Human Genetic Variation Database, and gnomAD. Notably, the position of the mutation was very close to that of other pathogenic mutations previously reported (**Figure 2C**), and the amino acid residue affected by this missense mutation was conserved among mammals (Mercier et al., 2015), suggesting the importance of the residue in the function of FAM111B. The pathogenicity was also estimated using *in silico* algorithms; PolyPhen2 (probably damaging), PROVEAN (deleterious), SIFT (damaging), and CADD score (25.4). Furthermore, it is classified as pathogenic also according to

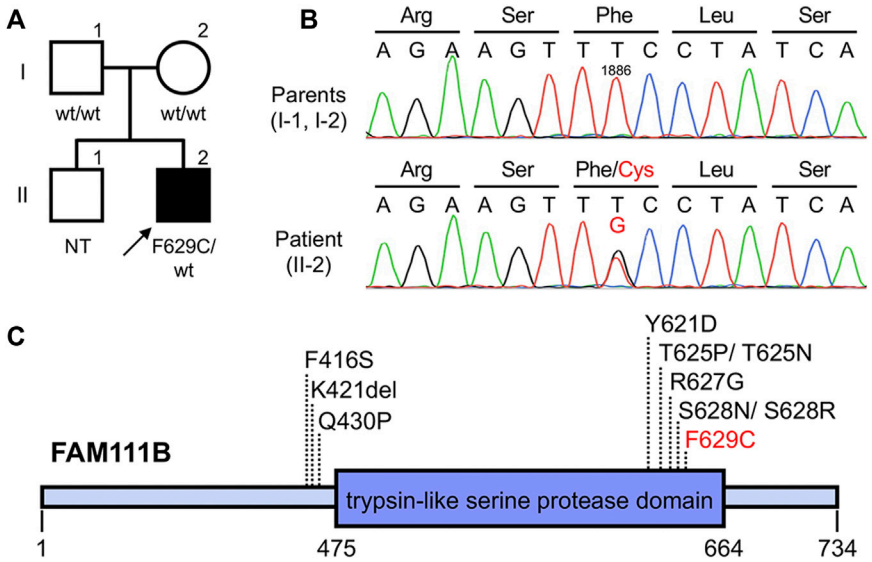


FIGURE 2 | Pedigree and genetic analysis of FAM111B **(A,B)** Pedigree of this case **(A)**. The patient was heterozygous for **(C)**1886T > G (p(Phe629Cys)) in FAM111B, whereas his parents did not harbor this mutation **(B)**. wt, wild-type; NT, not tested **(C)** Overview of POIKTMP-related mutations detected in the present case and previous cases.

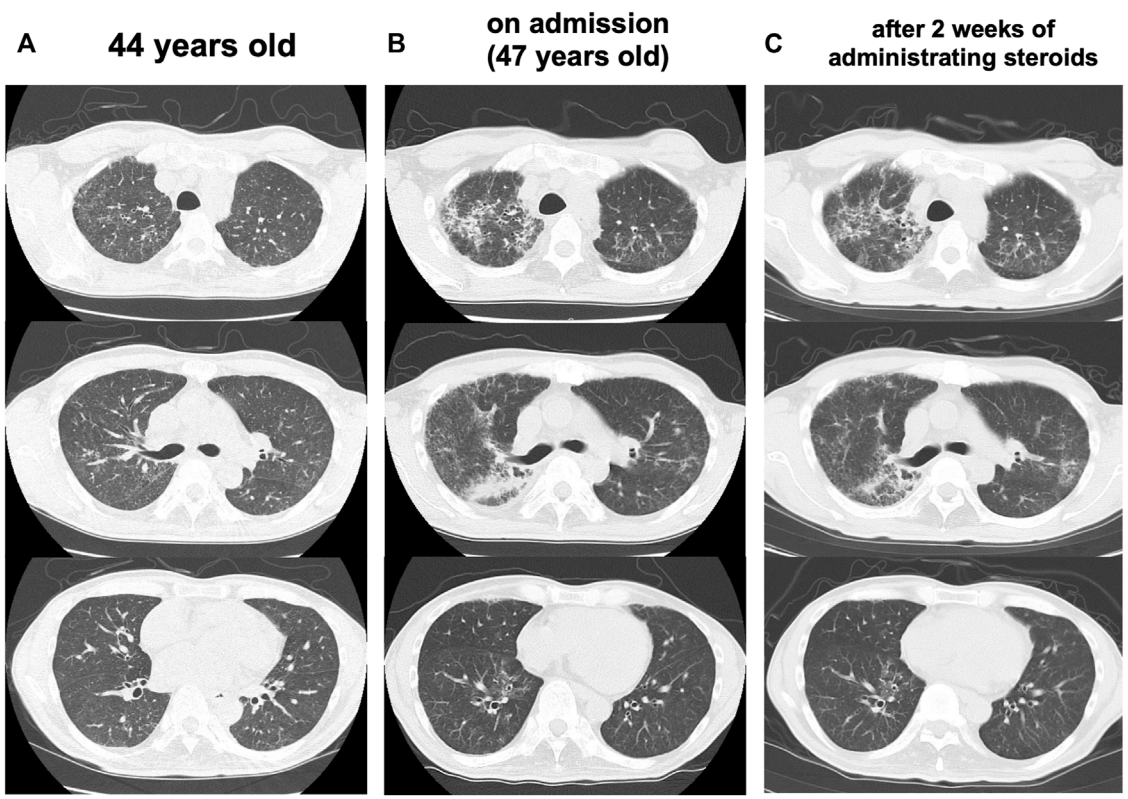


FIGURE 3 | Progress of lung CT scans **(A)** At 44 years old **(B)** On admission (47 years old), the interstitial lung shadows worsened **(C)** 2 weeks after administrating corticosteroids, interstitial shadows were improved.

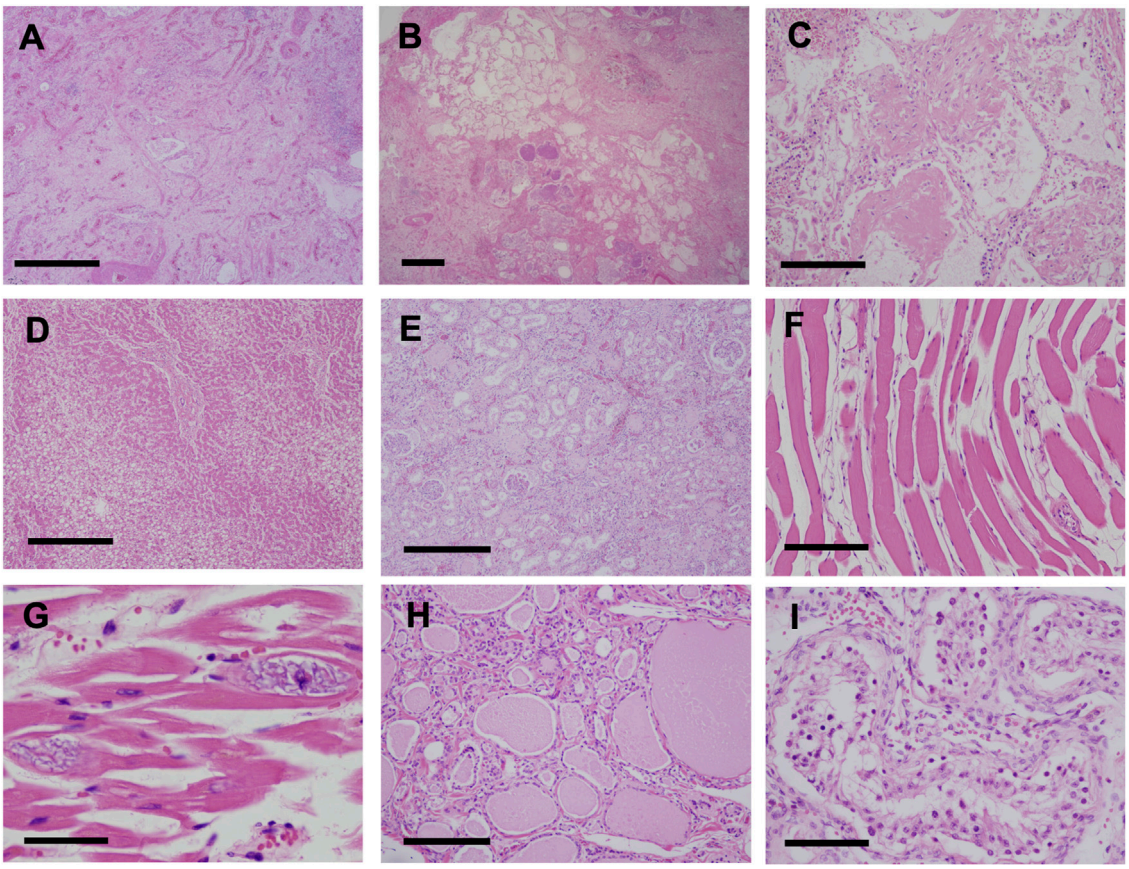


FIGURE 4 | Pathological findings (H&E stain) **(A,B)** Fibrotic changes with unclassifiable pattern predominantly in the right upper lobe of the lung **(A)** Fibrotic-nonspecific interstitial pneumonia (f-NSIP) pattern (scale bar, 1.0 mm) **(B)** Usual interstitial pneumonia (UIP) pattern and bacterial pneumonia with gram-positive cocci (scale bar, 1.0 mm) **(C)** Organizing pneumonia (scale bar, 200 μm) **(D)** Liver tissue showed fibrosis and fatty degeneration (scale bar, 500 μm) **(E)** Interstitial fibrosis, glomerular sclerosis, and tubular atrophy in the kidneys (scale bar, 500 μm). Skeletal muscles (scale bar, 200 μm) **(F)** and the myocardium (scale bar, 100 μm) **(G)** showed atrophy, fatty degeneration, and basophilic degeneration **(H)** Thyroid tissue showed atrophy and interstitial fibrosis (scale bar, 200 μm) **(I)** Testis tissue showed atrophy of the seminiferous tubules, indicating male infertility (scale bar, 100 μm).

the ACMG guideline. Conversely, although RECQL4, the causative gene of Rothmund–Thomson syndrome (RTS) (which is the most common differential diagnosis), was also analyzed, no pathogenic mutations were detected in the patient (data not shown). These findings verified the diagnosis of POIKTMP, making this the first case in Japan.

At the age of 47 years, his shortness of breath and interstitial lung shadows on chest CT worsened compared to those at 44 years of age (**Figures 3A,B**) immediately after recovery from bacterial pneumonia. His oxygen saturation was 94% in ambient air. Bilateral fine crackles were detected predominantly in the right upper fields on chest auscultation. Pulmonary function tests showed a restrictive ventilatory impairment (vital capacity [VC], 1.56 L; VC % predicted, 45.7%) and a decline in diffusing capacity (diffusing capacity for carbon monoxide % predicted [DLCO % predicted], 42.6%). The ratio of residual volume to total lung capacity was elevated (38.1%), indicating the presence of respiratory muscle weakness. Serum levels of Krebs Von den Lungen-6 (KL-6), surfactant protein A (SP-A), and surfactant protein D (SP-D) were elevated to 1,085 U/mL, 98.3 ng/ml, 505.6 ng/ml, respectively. Bronchoalveolar lavage (BAL) from the right upper lobe (B^3b) revealed an increased proportion of neutrophils and eosinophils (macrophages, 82.0%; lymphocytes, 7.0%; neutrophils, 6.7%; eosinophils, 4.3%; CD4/CD8 ratio, 0.66) in the BAL fluid. Echocardiography results were within the normal limits. Based on these findings, an exacerbation of interstitial pneumonia was considered, and 40 mg/day of prednisolone was administered. 2 weeks later, his shortness of breath, interstitial shadows on the chest CT scan (**Figure 3C**), and markers of interstitial pneumonia improved. Serum levels of SP-A and SP-D decreased (62.9 ng/ml and 321.4 ng/ml, respectively), although serum KL-6 unchanged. Pulmonary function tests showed improvements in %VC and % DLCO (49.5 and 54.5%, respectively). However, shortly thereafter, he abruptly developed severe hepatic encephalopathy. Although he temporarily recovered after treatment with amino acid preparation and lactulose, there was no more effective treatment since he was already in a phase of hepatorenal syndrome. He finally developed severe hypoxemia due to worsening of bilateral pneumonia and

pulmonary edema, which led to death within a few days. Subsequently, an autopsy was performed.

Pathological findings in the lungs revealed fibrotic changes with an unclassifiable pattern, predominantly in the right upper lobe (**Figures 4A,B**). Findings of organizing pneumonia and bacterial pneumonia with gram-positive cocci were also noted (**Figures 4B,C**). Pulmonary edema was observed in a large part of the lungs, and alveolar hemorrhage was seen in the right middle lobe and left lung. Liver tissue showed fibrosis and steatosis (**Figure 4D**), but findings indicative of nonalcoholic steatohepatitis were not observed. Kidney tissue showed interstitial fibrosis, glomerular sclerosis, and tubular atrophy (**Figure 4E**). Skeletal muscles and the myocardium showed atrophy, fatty degeneration, and basophilic degeneration (**Figures 4F,G**). Pancreatic tissue showed severe atrophy and fatty infiltration with scarce exocrine glands. Thyroid tissue showed atrophy and interstitial fibrosis (**Figure 4H**). Laryngeal tissue showed atrophy and degeneration in the cricothyroid and thyroarytenoid muscles, which led to vocal cord atrophy. The testis tissue showed atrophy of seminiferous tubules, indicating male infertility (**Figure 4I**).

DISCUSSION

The first family affected by POIKTMP was reported in 2006 (Khumalo et al., 2006). In 2013, Mercier et al. identified FAM111B as a gene responsible for this disease (Mercier et al., 2013). FAM111B is located on chromosome 11 (11q12.1) and encodes a protein with a trypsin-like cysteine/serine peptidase domain. Recently, it was reported that the FAM111B mutation was possibly associated with cancer, including pancreatic cancer and lung adenocarcinoma (Mercier et al., 2019; Sanada et al., 2019; Sun et al., 2019). It is inherited in an autosomal dominant manner, and 50% of cases are sporadic. To the best of our knowledge, there have been only 15 families with 34 patients diagnosed with this disease worldwide, and the present case is the first Japanese patient with POIKTMP. In contrast, several patients with poikiloderma might be misdiagnosed with RTS, which is another genetic disorder that causes poikiloderma (Lessem et al., 1980; Otsu et al., 2008; Meier and Schwarz 2012).

The novel missense mutation was detected in the present case. We evaluated it *in silico*, and the results suggested its pathogenicity. However, the cellular functions of FAM111B and the impact of its genetic mutations have not been fully elucidated. Hoffmann et al. recently discovered that FAM111B harbors intrinsic proteolytic activity and that mutations in FAM111B undermine cellular fitness by eliminating inhibitory constraints on its protease activity, blocking DNA and RNA synthesis, and promoting apoptotic cell death (Hoffmann et al., 2020). In their research, they evaluated two mutations among those reported as pathogenic mutations for POIKTMP. A similar analysis of the present mutation could be useful to confirm its pathogenicity.

Furthermore, an important new insight with implications for genotype-phenotype correlation was recently reported. Arowolo et al. suggested that patients with mutations within the putative protease domain of the FAM111B protein may have higher disease burden and poorer prognoses compared to patients with mutations outside the domain (Arowolo et al., 2022). Among the reported causative mutations in FAM111B, all except three are within this domain (**Figure 2C**), as is the present mutation. That our patient had multiple organ impairment leading to a poor prognosis would seem to support this suggestion.

POIKTMP often causes poikiloderma, muscle weakness, and tendon contracture. Some patients develop pulmonary fibrosis, which has been reported to lead to poor prognosis. In a previous review, only symptomatic therapy was recommended for those with respiratory failure (Arowolo et al., 2022). Only two patients with POIKTMP have been reported to be treated for pulmonary involvement. The first patient was a South African man who experienced dyspnea at 28 years of age (Sanchis-Borja et al., 2018). The percentages of neutrophils and eosinophils were elevated in the BAL fluid. High-dose corticosteroid therapy was ineffective, and respiratory failure progressed rapidly, which led to death 15 months later. Autopsy revealed pulmonary fibrosis with a usual interstitial pneumonia pattern in the lungs (Sanchis-Borja et al., 2018). The second patient was a French man who developed dyspnea at 38 years of age (Mercier et al., 2015; Sanchis-Borja et al., 2018). The levels of eosinophils in BAL fluid were elevated. He died after experiencing several exacerbations and remissions for 2 years. The antifibrotic drug pirfenidone could not be tolerated due to its adverse effects. Pulse steroid therapy and cyclophosphamide were administered; however, these treatments were completely ineffective. To the best of our knowledge, the present case describes the first reported patient with POIKTMP, whose interstitial pneumonia responded to corticosteroid therapy. Worsening of his pulmonary lesions was observed after recovery from bacterial pneumonia, and autopsy revealed the presence of organizing pneumonia with an unclassifiable pattern of interstitial pneumonia; therefore, corticosteroid therapy in the present case might be mainly effective for the lesions of organizing pneumonia among unclassifiable interstitial pneumonia.

Autopsy revealed the presence of atrophy and fatty degeneration in multiple organs, which suggests that the FAM111B mutation systemically impairs organ function through its enhanced proteolytic activity. Of note, the present case showed liver cirrhosis. As far as we know, there has been only 1 patient with POIKTMP who had liver cirrhosis. He had progressive liver impairment and vanishing duct syndrome from infancy, and died due to decompensated liver cirrhosis at 17 years of age (Mercier et al., 2016) (Roversi et al., 2021). The cause of cirrhosis was not described. Our patient had not been infected with hepatitis B or hepatitis C virus, and autopsy findings showed no evidence of nonalcoholic steatohepatitis. Although the pathogenesis of liver cirrhosis in POIKTMP is unclear, fibrosis seems to be one of the key features of this disease.

The present case also had chronic kidney disease with interstitial fibrosis, glomerular sclerosis, and tubular atrophy. There was only one patient with renal failure, which was supposed to be associated with POIKTMP (Meier and Schwarz 2012). The patient was a Dutch woman initially reported as having RTS, although Mercier et al. later pointed out that she had POIKTMP. In addition, testis tissue of the present case showed atrophy of seminiferous tubules that indicated male infertility, which has not been reported as a feature of POIKTMP.

In conclusion, we report the first Japanese case of POIKTMP whose interstitial pneumonia was improved by corticosteroids, suggesting that corticosteroids could be an option for the treatment of interstitial pneumonia associated with this disease.

DATA AVAILABILITY STATEMENT

The datasets for this article are not publicly available due to concerns regarding participant/patient anonymity. Requests to access the datasets should be directed to the corresponding author.

ETHICS STATEMENT

Written informed consent was obtained from the individual(s) for the publication of any potentially identifiable images or data included in this article.

AUTHORS CONTRIBUTIONS

MTS and MS took part in the treatment and wrote the manuscript. TM and TN took part in the treatment, performed the genetic analysis, and wrote the manuscript. TI, TN, KT, MMS, Hirokazu Kimura, Hiroki Kimura, TK, RY, KS, AN, MN, TS, KO, and NS took part in the treatment. HU contributed to the dermatological evaluation, YM to the orthopedic evaluation, and NY, NO, and UT to the pathological diagnosis. SK supervised the treatment and drafted the manuscript.

SUPPLEMENTARY MATERIAL

The Supplementary Material for this article can be found online at: https://www.frontiersin.org/articles/10.3389/fgene.2022.870192/full#supplementary-material

REFERENCES

Arowolo, A., Rhoda, C., and Khumalo, N. (2022). Mutations within the Putative Protease Domain of the Human *FAM111B* Gene May Predict Disease Severity and Poor Prognosis: A Review of POIKTMP Cases. *Exp. Dermatol* Online ahead of print. doi:10.1111/exd.14537

Hoffmann, S., Pentakota, S., Mund, A., Haahr, P., Coscia, F., Gallo, M., et al. (2020). FAM111 Protease Activity Undermines Cellular Fitness and Is Amplified by Gain-Of-Function Mutations in Human Disease. *EMBO Rep.* 21, e50662. doi:10.15252/embr.202050662

Khumalo, N. P., Pillay, K., Beighton, P., Wainwright, H., Walker, B., Saxe, N., et al. (2006). Poikiloderma, Tendon Contracture and Pulmonary Fibrosis: a New Autosomal Dominant Syndrome? *Br. J. Dermatol* 155, 1057–1061. doi:10.1111/j.1365-2133.2006.07473.x

Lessem, J., Bjerre, I., and Forslund, M. (1980). Epilepsy and Myopathy in a Patient with Rothmund-Thomson's Syndrome. *Acta Med. Scand.* 207, 237–239. doi:10.1111/j.0954-6820.1980.tb09713.x

Meier, M., and Schwarz, A. (2012). Rothmund-Thomson Syndrome-Aa Single Case Report with Systemic Muscular Atrophy, Multiple Organ Fibrosis and Pulmonary Cachexia. *Rheumatology* 51, 2109–2111. doi:10.1093/rheumatology/kes143

Mercier, S., Kury, S., Barbarot, S., Adam, M. P., Ardinger, H. H., Pagon, R. A., et al. (2016). Hereditary Fibrosing Poikiloderma with Tendon Contractures, Myopathy, and Pulmonary Fibrosis Genereview. Available at: https://www.ncbi.nlm.nih.gov/books/NBK390610/(Accessed Oct 13, 2016).

Mercier, S., Küry, S., Nahon, S., Salort-Campana, E., Barbarot, S., and Bézieau, S. (2019). FAM111B Mutation Is Associated with Pancreatic Cancer Predisposition. *Pancreas* 48, e41–e42. doi:10.1097/mpa.0000000000001303

Mercier, S., Küry, S., Salort-Campana, E., Magot, A., Agbim, U., Besnard, T., et al. (2015). Expanding the Clinical Spectrum of Hereditary Fibrosing Poikiloderma with Tendon Contractures, Myopathy and Pulmonary Fibrosis Due to FAM111B Mutations. *Orphanet J. Rare Dis.* 10, 135. doi:10.1186/s13023-015-0352-4

Mercier, S., Küry, S., Shaboodien, G., Houniet, D. T., Khumalo, N. P., Bou-Hanna, C., et al. (2013). Mutations in FAM111B Cause Hereditary Fibrosing Poikiloderma with Tendon Contracture, Myopathy, and Pulmonary Fibrosis. *Am. J. Hum. Genet.* 93, 1100–1107. doi:10.1016/j.ajhg.2013.10.013

Otsu, U., Moriwaki, S., Iki, M., Nozaki, K., Horiguchi, Y., and Kiyokane, K. (2008). Early Blistering, Poikiloderma, Hypohidrosis, Alopecia and Exocrine Pancreatic Hypofunction: a Peculiar Variant of Rothmund-Thomson Syndrome? *Eur. J. Dermatol* 18, 632–634. doi:10.1684/ejd.2008.0509

Roversi, G., Colombo, E. A., Magnani, I., Gervasini, C., Maggiore, G., Paradisi, M., et al. (2021). Spontaneous Chromosomal Instability in Peripheral Blood Lymphocytes from Two Molecularly Confirmed Italian Patients with Hereditary Fibrosis Poikiloderma: Insights into Cancer Predisposition. *Genet. Mol. Biol.* 44, e20200332. doi:10.1590/1678-4685-GMB-2020-0332

Sanada, H., Seki, N., Mizuno, K., Misono, S., Uchida, A., Yamada, Y., et al. (2019). Involvement of Dual Strands of miR-143 (miR-143-5p and miR-143-3p) and Their Target Oncogenes in the Molecular Pathogenesis of Lung Adenocarcinoma. *Int. J. Mol. Sci.* 20, 4482. doi:10.3390/ijms20184482

Sanchis-Borja, M., Pastré, J., Mercier, S., Juvin, K., Benattia, A., and Israël-Biet, D. (2018). Fibrose pulmonaire au cours de la poïkilodermie héréditaire sclérosante associée à la mutation du gène FAM111B : à propos d'un cas. *Rev. Des. Mal. Respir.* 35, 968–973. doi:10.1016/j.rmr.2018.09.002

Sun, H., Liu, K., Huang, J., Sun, Q., Shao, C., Luo, J., et al. (2019). FAM111B, a Direct Target of P53, Promotes the Malignant Process of Lung Adenocarcinoma. *Ott* 12, 2829–2842. doi:10.2147/ott.s190934

Conflict of Interest: The authors declare that the research was conducted in the absence of any commercial or financial relationships that could be construed as a potential conflict of interest.

Publisher's Note: All claims expressed in this article are solely those of the authors and do not necessarily represent those of their affiliated organizations, or those of the publisher, the editors and the reviewers. Any product that may be evaluated in this article, or claim that may be made by its manufacturer, is not guaranteed or endorsed by the publisher.

Copyright © 2022 Takimoto-Sato, Miyauchi, Suzuki, Ujiie, Nomura, Ikari, Nakamura, Takahashi, Matsumoto-Sasaki, Kimura, Kimura, Matsui, Kitagataya, Yamada, Suzuki, Nakamura, Nakai, Sho, Ogawa, Sakamoto, Yamaguchi, Otsuka, Tomaru and Konno. This is an open-access article distributed under the terms of the Creative Commons Attribution License (CC BY). The use, distribution or reproduction in other forums is permitted, provided the original author(s) and the copyright owner(s) are credited and that the original publication in this journal is cited, in accordance with accepted academic practice. No use, distribution or reproduction is permitted which does not comply with these terms.

frontiers | Frontiers in Pediatrics

ORIGINAL RESEARCH
published: 13 May 2022
doi: 10.3389/fped.2022.885006

Novel Mutations in ACP5 and SAMHD1 in a Patient With Pediatric Systemic Lupus Erythematosus

Soon-Min Hong[1,2†], *Wei Chen*[3†], *Jiaqi Feng*[2], *Dai Dai*[1,2*] *and Nan Shen*[1,2,4,5,6,7*]

[1] Shanghai Institute of Rheumatology, School of Medicine, Renji Hospital, Shanghai Jiao Tong University, Shanghai, China, [2] Department of Rheumatology, School of Medicine, Renji Hospital, Shanghai Jiao Tong University, Shanghai, China, [3] Department of Pediatrics, School of Medicine, Renji Hospital, Shanghai Jiao Tong University, Shanghai, China, [4] Shenzhen Futian Hospital for Rheumatic Diseases, Shenzhen, China, [5] State Key Laboratory of Oncogenes and Related Genes, Shanghai Cancer Institute, School of Medicine, Renji Hospital, Shanghai Jiao Tong University, Shanghai, China, [6] Center for Autoimmune Genomics and Etiology (CAGE) and Divisions of Rheumatology, Cincinnati Children's Hospital Medical Center, Cincinnati, OH, United States, [7] Joint Research Laboratory for Rheumatology of Shenzhen University Health Science Center and Shenzhen Futian Hospital for Rheumatic Diseases, Shenzhen, China

OPEN ACCESS

Edited by:
Mike Mikailov, United States Food and Drug Administration, United States

Reviewed by:
Mikhail Kostik, Saint Petersburg State Pediatric Medical University, Russia
Sezgin Sahin, Istanbul University-Cerrahpasa, Turkey

***Correspondence:**
Nan Shen
nanshensibs@gmail.com
Dai Dai
daidaisibs@163.com

[†]*These authors have contributed equally to this work and share first authorship*

Specialty section:
This article was submitted to Genetics of Common and Rare Diseases, a section of the journal Frontiers in Pediatrics

Received: *27 February 2022*
Accepted: *18 April 2022*
Published: *13 May 2022*

Citation:
Hong S-M, Chen W, Feng J, Dai D and Shen N (2022) Novel Mutations in ACP5 and SAMHD1 in a Patient With Pediatric Systemic Lupus Erythematosus. Front. Pediatr. 10:885006. doi: 10.3389/fped.2022.885006

Background: The study of genetic predisposition to pediatric systemic lupus erythematosus (pSLE) has brought new insights into the pathophysiology of SLE, as it is hypothesized that genetic predisposition is greater in children. Furthermore, identifying genetic variants and linking disrupted genes to abnormal immune pathways and clinical manifestations can be beneficial for both diagnosis and treatment. Here, we identified genetic alterations in a patient with childhood-onset SLE and analyzed the immunological mechanisms behind them to support future diagnosis, prognosis, and treatment.

Methods: Whole exome sequencing (WES) was adopted for genetic analysis of a patient with childhood-onset SLE. Gene mutations were confirmed by Sanger sequencing. Clinical data of this patient were collected and summarized. Ingenuity Pathway Analysis was used to provide interacting genes of the perturbed genes. Online Enrichr tool and Cytoscape software were used to analysis the related pathways of these genes.

Results: We present a case of a 2-year-old girl who was diagnosed with idiopathic thrombocytopenic purpura (ITP) and SLE. The patient was characterized by cutaneous bleeding spots on both lower extremities, thrombocytopenia, decreased serum complements levels, increased urinary red blood cells, and positive ANA and dsDNA. The patient was treated with methylprednisolone and mycophenolate, but clinical remission could not be achieved. The genomic analysis identified three novel mutations in this pSLE patient, a double-stranded missense mutation in ACP5 (c.1152G>T and c.420G>A) and a single-stranded mutation in SAMHD1 (c.1423G>A). Bioinformatic analysis showed that these two genes and their interacting genes are enriched in the regulation of multiple immune pathways associated with SLE, including cytokine signaling and immune cell activation or function. Analysis of the synergistic regulation of these two genes suggests that abnormalities in the type I interferon pathway caused by genetic variants may contribute to the pathogenesis of SLE.

Conclusion: The combined complexity of polymorphisms in the coding regions of ACP5 and SAMHD1 influences the susceptibility to SLE. Alterations in these genes may lead to abnormalities in the type I interferon pathway. Our study extends the spectrum

of mutations in the ACP5 and SAMHD1 genes. The identification of these mutations could aid in the diagnosis of SLE with genetic counseling and suggest potential precise treatments for specific pathways.

Keywords: novel mutation, ACP5/TRAP, SAMHD1, systemic lupus erythematosus (SLE), whole-exome sequencing (WES), bioinformatics

INTRODUCTION

Systemic lupus erythematosus (SLE) is a chronic multisystem autoimmune disease characterized by the production of autoantibodies and overactivation of the type I interferon (IFN) pathway, with alternating exacerbations and remissions (1). SLE is a heterogeneous disease and the diagnosis of SLE requires the presence of 4 of the 11 defining criteria. Clinical manifestations of SLE patients include arthritis, rash, serositis, various cytopenias, renal disease, psychiatric, neurological, and other manifestations (2, 3). Despite the wide variability, approximately 50% of SLE patients have persistently elevated blood levels of type I IFN over time. In addition, 60–80% of SLE patients have increased expression of interferon-stimulated genes (ISG) in peripheral blood, which is referred to as an IFN signature (1, 4). As with other heterogeneous diseases, the pathogenesis of SLE remains unclear. However, heritability has long been recognized as an important causative factor, affecting approximately 66% in SLE (5). To date, genome-wide association studies (GWAS) have identified more than 80 loci closely associated with lupus, and single-gene susceptibility to SLE has been suggested to be caused by single-nucleotide mutations in the coding regions of nearly 30 genes (6–8). The current view linking many susceptibility genes to key immune pathways is consistent with previous experimental studies including the role of immune complexes, host immune signaling, and interferon pathways in the pathogenesis of SLE (8, 9). Monogenic type I interferon diseases such as spinal chondrodystrophy (SPENCD) and Aicardi-Goutières syndrome (AGS) clinically overlap with SLE, both of which are associated with spontaneous type I IFN responses with no detectable exogenous viral infection (10). SPENCD is driven by an autosomal recessive mutation in ACP5. AGS can have different patterns of inheritance, mostly caused by single mutations in the ADAR, TREX1, RNASEH2A, RNASEH2B, RNASEH2C or SAMHD1 genes (11). These studies, together with laboratory observations, suggest that IFN plays an important role in the pathogenesis of SLE.

Given the complexity and heterogeneity of SLE, identifying genetic alterations and linking them to underlying immunologic pathogenesis could improve individualized diagnostic and therapeutic approaches to SLE. Here, we identified a pediatric-onset SLE patient with germline mutations in both ACP5 and SAMHD1.This patient carried three novel mutations from both father and mother, resulting in a double missense mutation in ACP5 (c.1152G>T in the mother and c.420G>A in the father) and a single missense mutation in SAMHD1 (c.1423G>A in the mother). We found that these two genes and their regulatory networks were enriched in multiple immune pathways associated with SLE, including cytokine signaling and immune cell activation or function. We also analyzed the synergistic regulation of these two genes and demonstrated their combined contribution to type I IFN, which suggests a pathogenic role of this genetic variant in this pSLE patient.

MATERIALS AND METHODS

Human Patients

We collected and summarized the clinical data of a patient who was diagnosed with lupus and carried specific gene mutations. Laboratory results before treatment were recorded for analysis. Written informed consent to participatein this study was provided by the participants' legal guardian/next of kin. Protocol of this study was approved by the Renji Hospital Biobank is funded by the National Human Genetic Resources Sharing Service Platform (2005DKA21300).

DNA Sequencing

DNA from probands and their family members were isolated and purified from blood and prepared for whole-exome sequencing (WES). DNA samples were enriched with Human SureSelect XT2 All Exon V4 Kit and sequenced by Illumina HiSeq 2000 (Illumina, Inc.). WES had 21% low or uncovered exon bases. Bioinformatic analysis was performed at JCSMR, ANU. Raw sequence reads were aligned to the reference genome (Hg19) and single-nucleotide variants and small insertions and deletions called using GATK. All SNVs of interest in ACP5 and SAMHD1 were confirmed by Sanger sequencing. Amplifluor to detect ACP5G290V, ACP5R46Q, and SAMHD1R408H in the APOSLE cohort was performed using the CHEMICON Amplifluor SNPs HT Genotyping System Fam-Joe kit S7909 (Merck-Millipore). The 45 and Up (12, 13) and ASPREE (14) datasets were used as reference healthy controls, accessed through the MGRB Collaborative (http://sgc.garvan.org.au/mgrb/initiatives).

WES Data Processing and Batch Correction

Probes were filtered out if the detection P value was greater than 0.01 for at least 100% of the samples. All data values <10 was set to 10 and then the data were log2 transformed. An additional filter selecting the 75% most variable transcripts was performed, leaving a total 18,004 probes for analysis. Principal variance component analysis (PVCA) was conducted to identify undesirable sources of technical variability within the data and batch correction was applied to correct for this technical variation. Both PVCA and batch correction

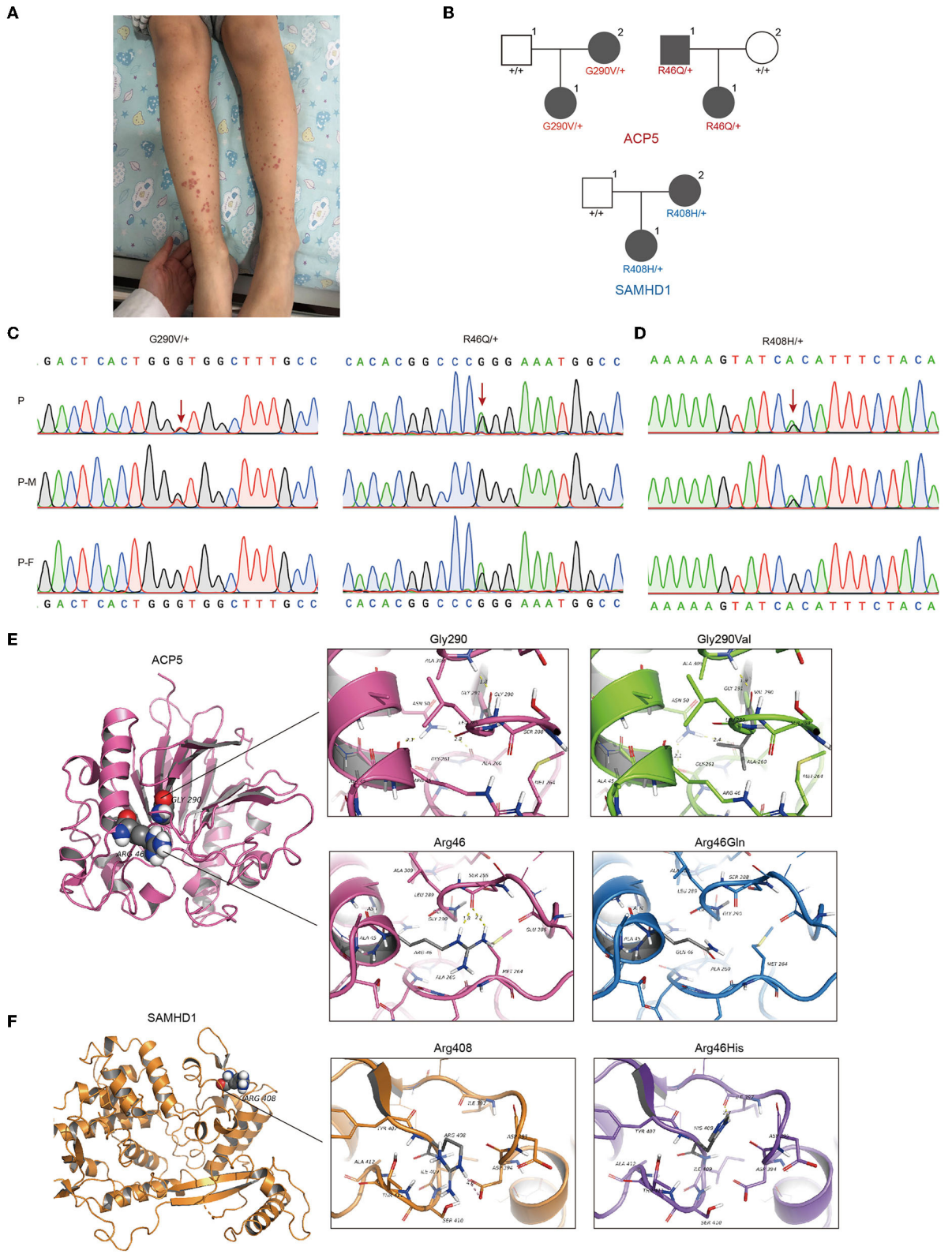


FIGURE 1 | Identification of gene mutations in patient with pSLE. **(A)**The patient initially presented skin bleeding spots in both lower limbs. **(B)** Pedigrees showing affected probands and parents. Sanger sequencing confirmation of the c.1152G>T (p.Gly290Val), c.420G>A (p. Arg46Gln) at ACP5 **(C)** and c.1423G>A (p.Arg408His) at SAMHD1 **(D)** variant identified in our patient using exome sequencing. Chromatograms represent the reference (top) and the mutant sequence. The

(Continued)

FIGURE 1 | variant is indicated by the red arrow. **(E)** Top: Structure modeling of wild type and p.Gly290Val mutation of ACP5. Top left: Gly290 form H-bond with Ala309; Asn50 form H-bonds with Arg46 (Distance: 2.1Å) and Ala 260 (Distance: 2.8 Å). Top right: The mutant model shows the change of H-bonds, Asn50 form H-bonds with Gly261 (Distance: 2.1 Å) and Ala 260 (Distance: 2.4 Å). Bottom: Wild type and p.Arg46Gln mutation of ACP5. Bottom left: Arg46 form H-bonds with Ser288 (Distance: 1.8 Å and 2.3 Å). Bottom right: The mutant shows the loss of two H-bonds, this might lose the ability to form any polar interaction with other residues. **(F)** Wild type and p.Arg408His mutation of SAMHD1. Left: Arg408 form salt bridge with Asp394. Right: The mutant shows the loss of salt bridge with Asp394, and form H-bond with Ile397 (Distance: 2.3 Å). P, patient; P-M, mother; P-F, father.

TABLE 1 | Immune indices of patient.

Items	Patient	Reference
WBC ($\times 10^9$/L)	14.63↑	3.69–9.16
Hb (g/L)	137	113–151
PLT ($\times 10^9$/L)	122	101–320
CRP (mg/L)	3.48	0–8
ESR (mm/h)	5	0–20
PCT(ng/mL)	0.280↑	<0.05
Anti-dsDNA(IU/mL)	31.79↑	0–7.0
ANA	1:640 (+)	0
ANuA	4.702 (+)	<1
C3 (g/L)	0.66↓	0.90–1.80
C4 (g/L)	0.06↓	0.10–0.40
IgG (g/L)	11.5	7.00–16.00
IgA (g/L)	0.31↓	0.70–4.00
IgM (g/L)	1.3	0.40–2.30
IgE (IU/mL)	308.47↑	1.31–165
$CD3^+$ (%)	35.61↓	61.1–77
$CD4^+$ (%)	19.78↓	25.8–41.6
$CD8^+$ (%)	14.73↓	18.1–29.6
$CD16^+$ $CD56^+$ (%)	8.14↓	8.7–38.3
$CD19^+$ (%)	57.46↑	4.7–19.3
NK cytotoxic index (%)	8.5↓	15–25
AST(U/L)	42↑	10–40
ALT(U/L)	22	0–75
Urinary protein (mg/24h)	45.1	31–120
EBV-IgG (INDEX)	6.07↑	<1
EBV-IgM (INDEX)	0.08	<1
CMV-IgG (AU/mL)	79 (+)	0–6
CMV-IgM (INDEX)	0.32	0–1

↑, *Increase;* ↓, *decrease; (+) positive.*

were conducted using JMP Genomics 7.0 (SAS Institute) analysis software.

Protein Preparation and Mutations Interactions Analysis

The X-ray resolved crystal structures of wild type ACP5 (PDB: 2BQ8) and SAMHD1 (PDB: 7A5Y) were download from RCSB PDB database, the mutations' structures were generated by pymol2.2. Water molecules, ions, heteroatoms, and all ligands were eliminated. Finally, the protonation states of the wild and mutated structures were then deliberated using a H++ server. Additionally, all missing hydrogen atoms were inserted by pymol2.2 The interactions analysis was used pymol2.2.

Statistical and Bioinformatics Analysis With IPA, Cytoscape

We used BioProfiler searches the Ingenuity Pathway Analysis (IPA, Qiagen) database to explore associations gene and phenotypes. IPA was used to construct pathways and networks (15, 16), to quickly identify biological relationships, mechanisms, pathways, functions and diseases most relevant to experimental datasets. Then we obtain two comprehensive lists of proteins implicated in either the ACP5 or SAMHD1 by IPA. Detailed information of the expressed proteins and endogenous biochemical compounds that have been associated with genes by using the "Annotation" module in IPA. The protein-protein interaction (PPI) network based on ACP5 and SAMHD1 was obtained via String (V.11.5) to predicting the protein interactions and obtaining protein connection scores, and the interaction scores beyond 0.400 were uploaded to Cytoscape for visualization and analysis of biological networks (17, 18). Protein overlapping network identification by using CentiScaPe to investigate node centrality in both networks, and important module in the protein network related to the hub genes were abstracted by using Molecular Complex Detection (MCODE) (19). The Kyoto Encyclopedia of Genes and Genomes (KEGG) pathway analysis from ClueGO were used to perform biological pathway enrichment analysis for the core cluster identified by MCODE (20).

RESULTS

Case Presentation

The patient was a 2-year-old girl who had recurrent upper respiratory tract infections and oral thrush since birth. She initially presented with cutaneous bleeding spots on both lower extremities, mainly on the calves and dorsum of the feet (**Figure 1A**). There was no fever, cough, sputum, joint pain, or other signs of discomfort. She was seen at a local pediatric outpatient clinic, which showed thrombocytopenia (4×10^9/L) and decreased hemoglobin (98 g/L). The renal function report showed decreased blood creatinine (Bcr) level (19.3 μmol/L), urine red blood cells (373.4/ul) and urine protein (2+). Serum complement levels were decreased (C3 387 mg/L, C4 44 mg/L). No signs of hematological malignancy were found in bone marrow smear and bone marrow biopsy sections. Systemic lupus erythematosus and idiopathic thrombocytopenic purpura (ITP) were diagnosed based on skin symptoms, thrombocytopenia and decreased serum complement levels. She was then started on methylprednisolone (MP). However, the abnormalities in urine red blood cells and serum complement levels persisted.

TABLE 2 | Cases of SPENCD associated with SLE.

Case	Gender	Mutation	Amino-acid alteration	ANA	Anti-dsDNA	Thrombocytopenia	Proteinuria	Hematuria	Autoimmunehaemolytic anemia	LN	Renal involvement	Raynaud's /vasculitis	Hypocomplementemia (C3 and C4)	Drug	References
1	Female	1152G>T/420G>A	G290V Het/R46Q Het	Yes (1:640)	Yes	Yes	No	Yes	No	NA	Yes	Yes	Yes	Prednisolone, HCQ and MMF	
2	Female	369C>A/721G>A	Y123X Het/D241N Het	Yes (1:640)	Yes (1:320)	Yes	Yes	No	No	Class IV	Yes	No	Yes		(20)
3	Female	791 T>A	M264K Hom	Yes (1:1280)	No	Yes	No	No	No	NA	No	No	No		(20)
4	Female	643G>A	G215R Hom	Yes (1:1600)	Yes (>100)	Yes	No	No	Yes	Class V	Yes	No	Yes		(20)
5	Male	325G>A/831 _833delCTA	G109R Het/Y278del Het	Yes	No	Yes	Yes	No	Yes	NA	No	Yes	No	Nivaquin and steroids	(22)
6	Male	791T>A	M264K Hom	Yes	No	No	Yes	No	No	Class V	Yes	No	No		(22)
7	NA	325G>A	G109R Hom	No	No	No	No	No	No	NA	No	No	No		(22)
8	NA	325G>A	G109R Hom	Yes	No	No	Yes	No	No	Class IV	Yes	No	No		(22)
9	NA	155A>C	K52T Hom	Yes	No	Yes	No	No	No	NA	No	No	No		(22)
10	Male	11,543,690-11,548,656 del	Ex5_7 del Hom	Yes (1:640)	Yes (>100)	Yes	Yes	No	No	Class III	Yes	Yes	Yes	Corticosteroids, CQ and CYC	(23)
11	Male	NA	NA	Yes (1:640)	Yes (>100)	No	No	Yes	No	Class IV	Yes	No	Yes	Steroid,CYC,MMF and CQ	(24)
12	Female	NA	NA	Yes (1:320)	Yes (>100)	NA	Yes	No	No	Class V	Yes	Yes	Yes	Steroid,CYC,AZA and CQ	(24)
13	Female	NA	NA	Yes (1:320)	Yes (>100)	No	No	No	No	Class IV	Yes	Yes	Yes	Steroid,CYC and CQ	(24)
14	Male	NA	NA	No	No	No	Yes	Yes	Yes	NA	Yes	Yes	No	Steroid and nivaquine	(25)
15	Female	131C >T/816dupC	T44M Het/K272fs Het	Yes (1:1280)	No	No	Yes	Yes	No	NA	No	Yes	Yes	Steroid,MMF and intravenous Ig	(26)
16	Female	NA	NA	Yes	Yes	No	No	Yes	Yes	NA	No	Yes	Yes	AZA and HCQ	(27)
17	Male	155A >C	K52T Hom	Yes	Yes	No	Yes	No	No	Class II	Yes	Yes	Yes	Prednisolone, AZA, HCQ and rituximab	(27)
18	Male	NA	NA	Yes	Yes	No	Yes	Yes	Yes	Class III	Yes	Yes	NA		(28)
19	Male	449T>A/136C>T	V150E Het/R46W Het	Yes	Yes	No	Yes	No	No	Class IV	Yes	No	Yes	Piroxicam, prednisolone, AZA, gabapentin, topiramate, atenolol and enalapril	(29)
20	Female	449T>A/136C>T	V150E Het/R46W Het	Yes	Yes	No	No	No	No	NA	No	No	Yes	Corticosteroids and infliximab	(29)
]21	Female	550C>T/740T>G	Q184* Het/L247R Het	Yes	Yes	No	No	No	No	IgA nephropathy	Yes	No	No	Amlodipine, enalapril and labetalol	(30)
22	Female	369C >A/721G >A	Y123X Het/D241N Het	Yes (1:640)	Yes (1:320)	No	No	No	Yes	NA	Yes	Yes	No	MMFand prednisolone	(31)
23	Male	266C > T	T89I Hom	Yes (1:640)	Yes (>100)	No	No	No	No	NA	Yes	Yes	No	AZA	(31)
24	Female	791 T>A	M264V Hom	Yes (1:1280)	Yes (>100)	Yes	No	No	Yes	NA	No	No	No		(31)
25	Female	643G>A	G215R Hom	Yes (1:1600)	Yes (>100)	Yes	No	No	Yes	NA	Yes	No	No	Prednisolone, HCQ and MMF	(31)
26	Male	155 A>C/790 A>G	K52T Hom/M264V Het	Yes (1:100)	Yes	No	No	No	Yes	NA	Yes	Yes	No	Prednisolone	(31)
27	Male	359 A>G	Q120R Hom	Yes (1:640)	Yes	No	No	No	Yes	NA	Yes	No	No	Prednisolone	(31)
28	Male	325G>A/712 T>C	G109R Het/C238R Het	Yes (1:640)	Yes	Yes	No	No	Yes	NA	Yes	No	No		(31)
29	Female	131C>T/712 T>C	T44M Het/C238R Het	Yes (1:2560)	Yes	Yes	No	No	Yes	NA	No	No	No		(31)
30	Female	798dupC/716G>A	S267Lfs*20 Het/G239D Het	Yes (1:320)	Yes	Yes	No	No	No	NA	No	No	Yes	Prednisolone and MMF	(32)

All cases had typical radiographic findings of SPENCD with short stature. Cases and 3, 8 and 9, and 13 and 14, were sib couples. NA, Not assessed/reported; ANA, antinuclear antibodies; LN, lupus nephritis; HCQ, Hydroxochloroquine; MMF, Mycophenolate mofetil; CQ, Chloroquine; CYC, Cyclophosphamide; AZA, Azathioprine.

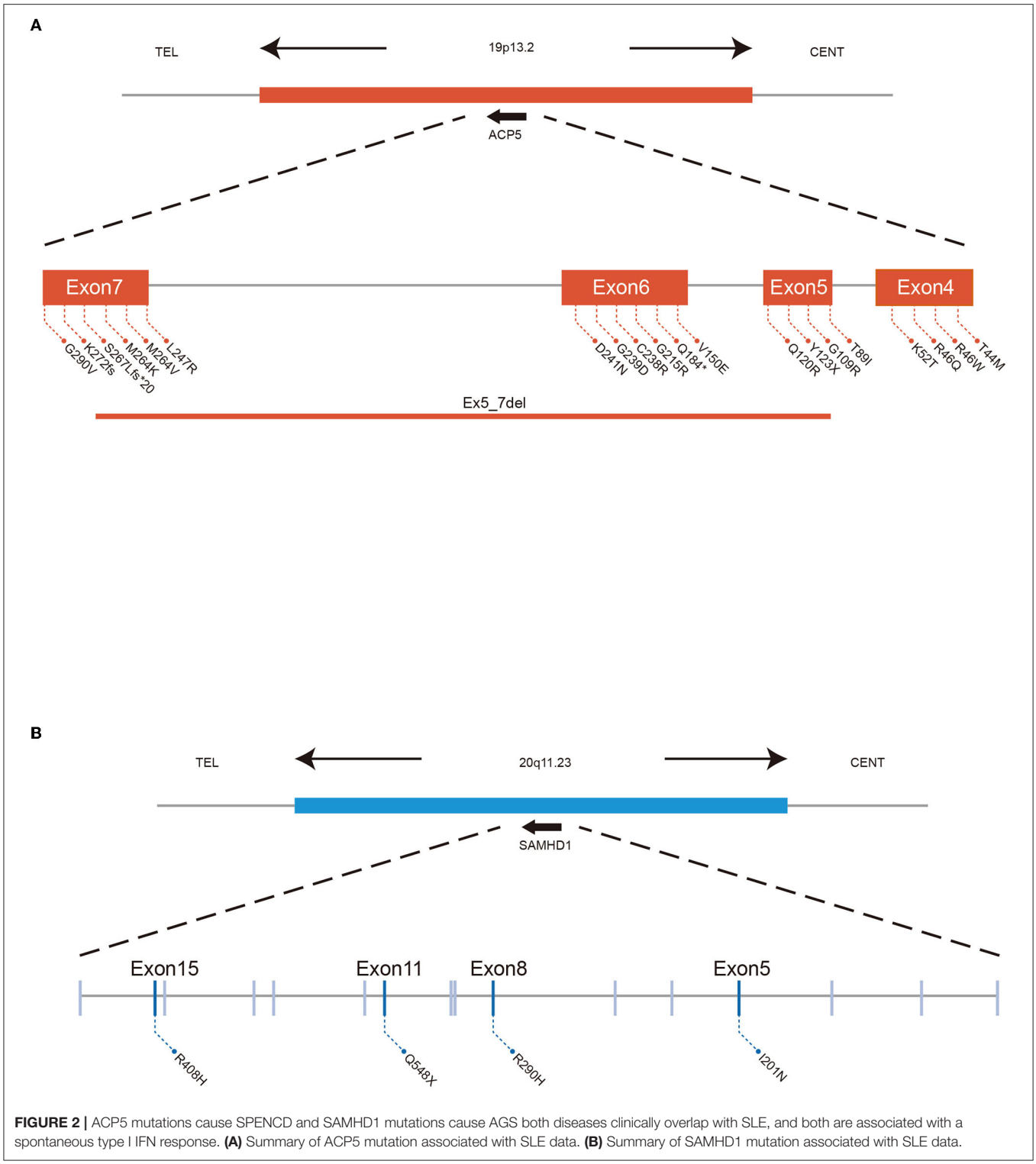


FIGURE 2 | ACP5 mutations cause SPENCD and SAMHD1 mutations cause AGS both diseases clinically overlap with SLE, and both are associated with a spontaneous type I IFN response. **(A)** Summary of ACP5 mutation associated with SLE data. **(B)** Summary of SAMHD1 mutation associated with SLE data.

Three months later, she presented to our pediatric clinic. Laboratory tests showed elevated white blood cell count (14.63×10^9/L), lymphocyte count (6.45×10^9/L), monocyte count (1.6×10^9/L), calcitonin (0.28 ng/ml), and decreased Bcr (16 μmol/L). Anti-nuclear antibody (ANA, >1/80), anti-ribosomal antibody (ANuA, >1) and anti-dsDNA (31.79 IU/ml) were positive. Serum complement (C3 0.66 g/L, C4 0.06 g/L), immunoglobulin (Ig) A (0.31 g/L) was decreased and IgE (308.47 IU/ml) was increased.

The percentage of T lymphocytes ($CD3^+$ 35.61%, $CD4^+$ 19.78%, $CD8^+$ 14.73%) in PBMC was decreased and B lymphocytes were increased ($CD19^+$% 57.46%). Mycoplasma pneumoniae IgM antibodies were positive (1:80). Erythrocyte sedimentation rate (ESR), C-reactive protein (CRP) and renal function were normal. Cytomegalovirus (CMV) and Epstein-Barr virus (EBV) antibodies were negative. Rheumatoid factor, IgG, IgM and urine protein were all negative. Antibodies to chlamydial pneumonia, tuberculosis, TORCH, and anti-streptozotocin O were negative. Her abdominal ultrasound scan, skeletal radiography, EEG and brain MRI were normal. Immune markers such as serum immunoglobulin, complement and lymphocyte subpopulation values are listed in **Table 1**.

Therefore, she met the diagnostic criteria for SLE and growth retardation (weight: 10.5 kg, −1.20 standard deviation (SD); height: 80 cm, −2.20 SD). She was then started on MP and mycophenolate mofetil (MMF) for 1 year and measures associated with SLE activity remained abnormal (increased dsDNA, positive ANA). At the same time, we found that the patient's IFN-α (31.56 pg/ml), IFN-γ (10.92 pg/ml), TNF-α (8.93 pg/ml), and IL-17A (23.78 pg/ml) increased dramatically during the active phase. Therefore, methotrexate (MTX) was given, but she developed leukopenia (2.76×10^9/L). Considering the inhibitory effect of MTX on bone marrow hematopoiesis, MTX was discontinued at that time and the regimen of MP, HCQ and MMF was changed. However, the patient's indicators such as dsDNA, serum complement and Ig remained unstable.

Given the early onset, multi-organ involvement and the refractory nature of alternating episodes and remissions, we should further explore the etiology to improve the clinical diagnosis and treatment of this patient.

The Germline Rare Mutations of ACP5 and SAMHD1 Identified in This Patient

Next-generation sequencing brings great convenience for accurate diagnosis. High-throughput sequencing can detect genetic alterations in an entire genome, an exome, or a group of genes. Patients with early-onset lupus often carry a high frequency of pathogenic variants, highlighting the importance of genetic testing for pSLE (21, 22). We then applied WES and identified three new mutations in this patient, all inherited from her father and mother. This patient carried a bilateral missense mutation in the ACP5 gene (NM_001111034.2) at 2 different loci (c.1152G>T [p. Gly290Val, G290V]; c.420G>A [p. Arg46Gln, R46Q]) and a unilateral missense mutation in the SAMDH1 gene (NM_15474.3) (c.1423G>A [p.ARG408HIS, R408H]). The combined annotation-dependent depletion (CADD) scores representing the deleteriousness of these three mutations were 21 (ACP5, c.1152G>T), 22 (ACP5, c.420G>A) and 6.649 (SAMDH1, c.1423G>A) (**Figures 1B–D**). The sites of these mutations have not been reported previously. Protein structure predictions showed that the G290V mutation resulted in weaker hydrogen bond (H bond) strength, the R46Q mutation in ACP5 resulted in the loss of two H bonds (**Figure 1E**), and the R408H mutation in SAMHD1 resulted in the loss of the salt bridge and the formation of an H bond (**Figure 1F**). We know that protein structure is closely related to function, and changes in protein structure caused by mutations may lead to disruption of biological function. Therefore, in combination with the high CADD score and altered protein structure, mutations in ACP5 may have greater pathogenicity.

Mutations in ACP5 and SAMHD1 are known to drive the pathogenesis of SPENCD and AGS, both of which are monogenic interferon diseases characterized by increased type I IFN signaling leading to vasculopathy, autoinflammation, and SLE-like disease (8, 23, 24). To date, 30 cases of SPENCD with SLE have been reported in the literature (23, 25–35) (**Figure 2A**; **Table 2**), and 9 cases of SLE with SAMHD1 mutations have been reported in the literature (21, 36–41) (**Figure 2B**; **Table 3**), including the patients in this article. Patients with SPENCD or AGS with SLE have a homogeneous clinical presentation, including autoantibody positivity, hematologic involvement, and neurologic symptomatic manifestations. Interestingly, this patient did not show clinical manifestations of epiphyseal lesions of SPENCD and neurological dysfunction of AGS in addition to autoimmune disease, implying that complex protein functional alterations due to polymorphisms in the ACP5 and SAMHD1 genes lead to different clinical symptoms. Here, we used high-throughput sequencing to identify three novel mutations in the coding regions of ACP5 and SAMHD1 in this patient that have not been previously reported to be associated with SLE.

The Potential Regulation Networks of ACP5 and SAMHD1 in SLE

To comprehensively summarize these two genes and their potential roles in disease, we used the IPA BioProfiler to explore the phenotype-gene relationships of ACP5 and SAMHD1 (**Figure 3A**). Indeed, ACP5 is associated with skeletal disorders and other diseases such as neoplastic disorders, including hematological malignancies. The same is true for SAMHD1 with inflammatory, neurological and neoplastic disorders. To further determine the regulatory roles of ACP5 and SAMHD1, we searched the interaction network of these two genes by IPA. We annotated the genome in the network by the online Enrihr tool (**Figure 3B**). Pathway analysis showed that ACP5 and its interacting genes are associated with osteoclast differentiation, associated with bone disorders in SPENCD. Importantly, many immune pathways were enriched, such as the Toll-like receptor signaling pathway and IL-17 signaling pathway, suggesting a potential regulatory role of ACP5 in SLE, except for type I IFN. For SAMHD1, the enriched pathways mainly were associated with viral infections, implying a dominant effect of genetic alterations in SAMHD1 on infectious diseases. SAMHD1 and its interaction network were associated with the production of type I IFN, as multiple nuclease pathways were significantly associated with it. In conclusion, we found that ACP5 and SAMHD1 are associated with multiple immune pathways that have been shown to be critical in the pathogenesis of SLE, suggesting that genetic perturbations in

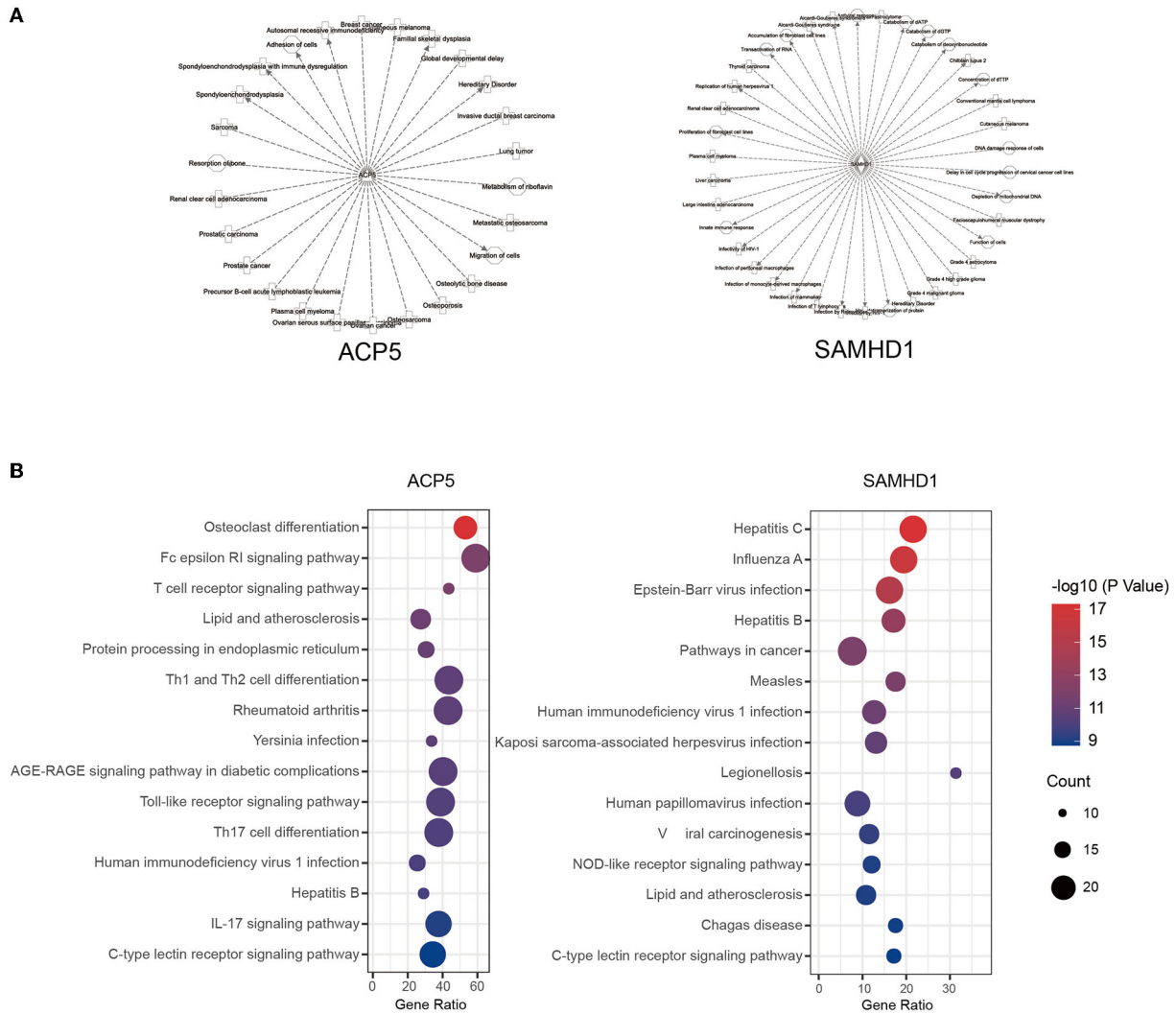


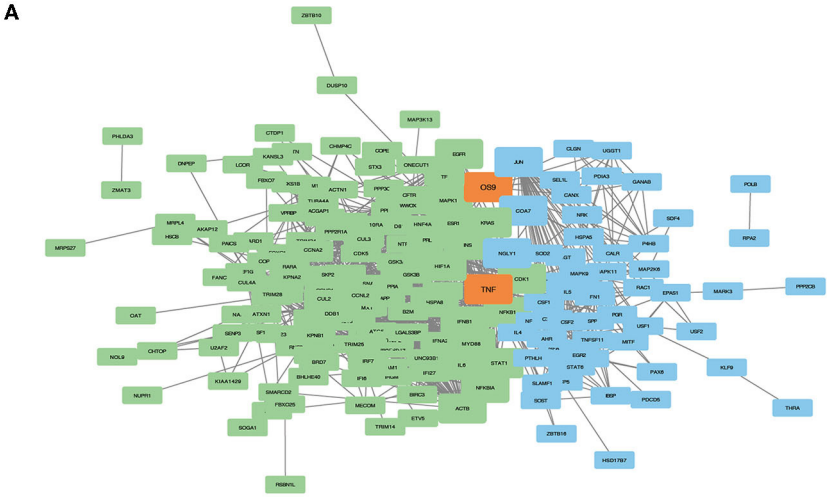
FIGURE 3 | The potential regulation of ACP5 and SAMHD1 in SLE. The phenotype-gene relationship **(A)** and pathway analysis **(B)** were shown to be associated with immunity responses.

these two genes may lead to immunological abnormalities in these pathways.

Interaction of ACP5 and SAMHD1 Is Associated With Interferon Pathway

Since ACP5 and SAMHD1 are associated with the type I IFN pathway, which exhibits abnormalities in both SPENCD and AGS. We interrogated the synergistic regulation of these genes by PPI network and pathway analysis and explored whether there is a link between ACP5 and SAMHD1. We constructed two protein interaction networks in Cytoscape to explore the link between ACP5 and SAMHD1 and the potential connection to the etiology of SLE (**Figure 4A**). The ACP5 protein interaction network included 60 nodes and 277 edges, while the SAMHD1 protein interaction network included 144 nodes and 982 edges. We merged these two networks, with blue representing nodes in the ACP5 protein interaction network and green representing nodes in the SAMHD1 protein interaction network (orange representing nodes in the duplication network). These results demonstrate a significant relationship between these genes (*P*-value for PPI enrichment: <1.0e-16).

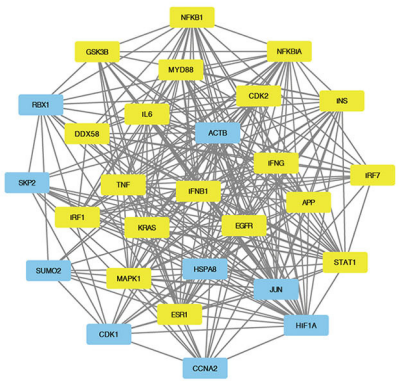
Next, we evaluated the central properties of the nodes in the PPI network. Highly significant nodes (score >25) had more interaction partners than non-central nodes, representing proteins with higher relevance in linking regulatory molecules. A unique protein interaction network for ACP5 and SAMHD1 was extracted by overlapping networks, including 28 nodes and 241 edges (**Figure 4B**). This new network was statistically significant for protein association (PPI-enriched *P*-value: 2.26e-11), showing highly connected edges of both networks, suggesting the possible existence of common pathways involved in the pathogenesis of SLE. To scrutinize the interconnected core clusters of the two protein interaction networks, we identified densely connected



B

Network Parameters

Node	Degree	Neighborhood Connectivity	Closeness Centrality
TNF	82	18.82926829	0.579881657
ACTB	66	22.43939394	0.545961003
STAT1	51	23.78431373	0.510416667
IL6	45	25.48888889	0.494949495
HIF1A	43	26.1627907	0.514435696
NFKBIA	42	27.26190476	0.502564103
EGFR	42	25.23809524	0.502564103
ESR1	42	25.35714286	0.498727735
INS	41	24.04878049	0.49
NFKB1	36	27.61111111	0.485148515
JUN	34	13.55882353	0.412631579
MYD88	33	26.78787879	0.470023981
HSPA8	33	21.06060606	0.4375
KRAS	31	28.87096774	0.480392157
MAPK1	30	28.06666667	0.473429952
CDK1	30	22.5	0.424242424
IFNB1	30	27.66666667	0.462264151
APP	29	26.13793103	0.474576271
DDX58	29	25.62068966	0.451612903
IRF7	29	25.93103448	0.459016393
RBX1	28	22.85714286	0.435555556
IRF1	28	28.14285714	0.463356974
IFNG	27	32.03703704	0.464454976
CDK2	27	29.59259259	0.475728155
SKP2	27	24.37037037	0.42516269
CCNA2	26	24.61538462	0.422413793
GSK3B	25	29.28	0.46778043
SUMO2	25	21.56	0.426086957



C

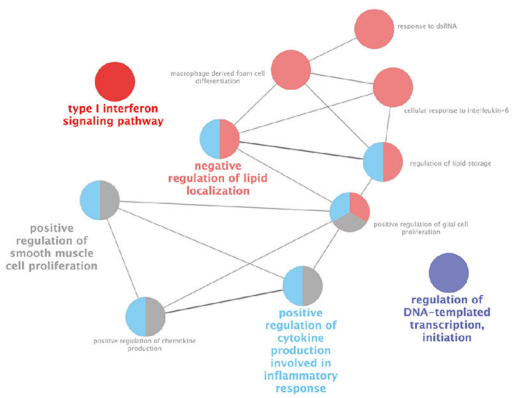


FIGURE 4 | Protein interaction networks of ACP5 and SAMHD1 have connections and a core cluster with significant connections with two networks. **(A)** Merge of ACP5 protein network (green) and SAMHD1 protein network (blue) with overlap nodes in both networks (orange). The size of nodes represents the degree and betweenness of nodes. **(B)** Left: The table outlines the degree, neighborhood connectivity, and closeness centrality values of the core cluster nodes. Right: Networks of core cluster in merge of ACP5 protein network and SAMHD1 protein network. The yellow nodes are the densely connected MCOD clusters, based on their parameters, including connectivity, degree, and centrality. **(C)** ClueGo analysis identifies KEGG pathways and biological processes linked to the essential proteins in the MCOD clusters.

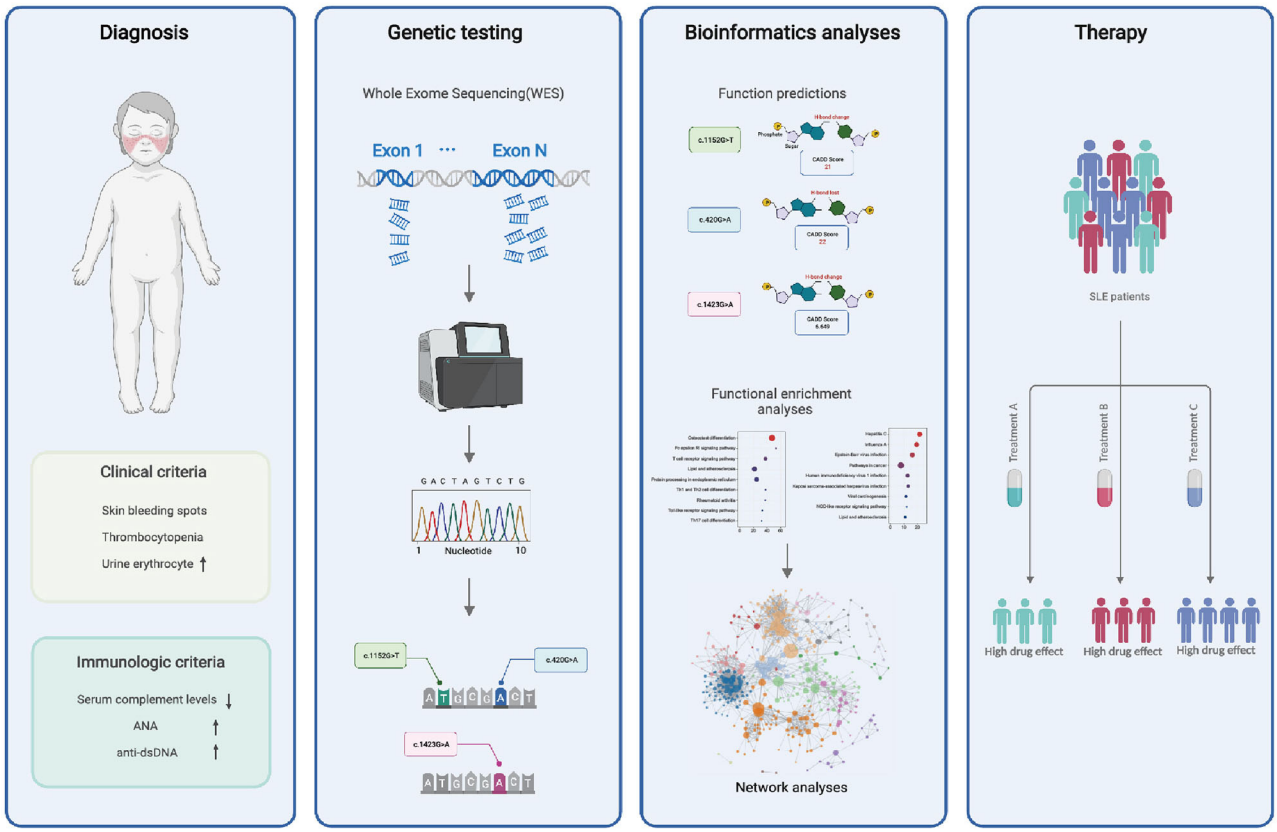


FIGURE 5 | WES may help to analyze the potential pathogenesis of patients. Our findings suggest that the combinatorial complexity of polymorphisms in ACP5 and SAMHD1 coding regions impacts SLE susceptibility, and may contribute to the abnormal immune pathway in SLE. These mutations should be considered for potential precision therapy targeting specific pathways.

MCOD clusters and found an overlap between the ACP5 and SAMHD1 protein networks. The proteins in the core MCOD cluster include IFN-related genes, including MYD88, IRF1, IRF7, and NFKB1. These clusters were also analyzed by KEGG pathway enrichment, including the type I interferon signaling pathway. Collectively, these results further suggest that ACP5 and SAMHD1 can synergistically regulate the type I IFN pathway and that genetic alteration in these two genes accumulate susceptibility to SLE through dysregulation of the IFN pathway (**Figure 4C**).

DISCUSSION

In this study, we describe the clinical manifestations of SLE in childhood, with the involvement of organs mainly affecting the skin, kidneys, and hematological system. However, several indicators of SLE remained abnormal after the patient underwent a thorough examination and treatment. We highly suspected that the patient might have some inherited genetic mutations. Then by genome sequencing, we found that the patient had novel missense mutations c.1152G>T and c.420G>A in ACP5 and c.1423G>A in SAMHD1, which were highly predictive of impaired gene function. The further bioinformatic analysis confirmed the regulatory role of these two genes in the type I IFN pathway and revealed that other immune pathways might be affected by mutations in ACP5 and SAMHD1 genes (**Figure 5**).

Mutations in ACP5 and SAMHD1 genes contribute to the pathogenesis of SPENCD and AGS. Both diseases clinically overlap with SLE and are associated with a spontaneous IFN response (23, 24). However, our patient did not exhibit the typical symptoms of AGS and SPENCD, neither skeletal dysplasia nor neurological dysfunction. Therefore, based on her clinical features, we diagnosed childhood-onset SLE. In addition, we observed a dramatic increase in serum IFN-α during disease flares. The patient presented with refractory SLE, with alternating exacerbations and remissions, and suboptimal treatment outcomes. Identifying genetic defects provides a unique opportunity to apply precise therapies targeting the type I IFN pathway. Unfortunately, our paper has some limitations. We will observe more patients with ACP5 and SAMHD1 mutations

TABLE 3 | Cases of SLE associated with mutation of SAMHD1.

Case	Gender	Mutation	Amino-acid alteration	ANA	Anti-dsDNA	Thrombocytopenia	Proteinuria	Hematuria	Autoimmunehaemolytc anemia	LN	Renal involvement	Raynaud's /vasculitis	Rash	Hypocomplementemia (C3 and C4)	Drug	References
1	Female	1423G>A	R408H Het	Yes (1:640)	Yes	Yes	No	Yes	No	NA	Yes	No	Yes	Yes	Prednisolone,HCQ and MMF	
2	Male	NA		Yes (1:132)	Yes (>100)	Yes	No	Yes	No	NA	Yes	Yes	Yes	Yes	NA	(33, 34)
3	Male	NA		No	Yes (>100)	Yes	No	No	Yes	No	No	Yes	Yes	Yes	NA	(33, 34)
4	Female	NA		Yes (1:2,500)	Yes (1:140)	Yes	No	No	Yes	No	No	Yes	Yes	No	Prednisolone,AZA	(35)
5	Female	NA		NA	NA	Yes	NA	NA	No	NA	NA	No	Yes	No	NA	(36)
6	Female	NA		No	Yes	Yes	No	No	No	No	No	No	Yes	No	NA	(36)
7	Male	1642C>T/869G>A	Q548X Het/R290H Het	Yes (1:160)	Yes (1:40)	Yes	No	No	Yes	No	No	Yes	Yes	No	Topiramate, intrathecal baclofen, naproxen, etanercept, and prednisone.	(37, 38)
8	Female	602T>A	I201N Het	No	No	No	No	No	No	NA	No	Yes	Yes	No	Nifedipine, HCQ	(39)
9	Male	602T>A	I201N Het	No	No	No	No	No	No	NA	No	Yes	Yes	No	Nifedipine, HCQ	(39)

Cases 5 and 6, 8 and 9 were sib couples. NA, Not assessed/reported; ANA, antinuclear antibodies; LN, lupus nephritis; HCQ, Hydroxochloroquine; MMF, Mycophenolate mofetil; AZA, Azathioprine.

by genetic testing and describe the clinical characteristics of these patients.

Through bioinformatic analysis, we found that genetic alterations in ACP5 and SAMHD1 may synergistically enhance the interferon response and participate in the pathogenesis of SLE. However, this patient acquired three germline mutations from her parents. Her mother was normal but carried two mutations in ACP5 and SAMHD1, respectively. Another missense mutation in ACP5 was passed to her by her father. Since these genes are autosomal recessive, the genetic predisposition may come mainly from the double-stranded mutation in ACP5. To clarify whether the pathogenic effect is from a double-copy mutation in ACP5 or a combined defect in ACP5 and SAMHD1 resulting in an enhanced interferon response, we will perform additional functional tests to support our findings directly.

In conclusion, after a comprehensive clinical examination and high-throughput genetic testing, we diagnosed three novel missense mutations in ACP5 and SAMHD1 in a patient with refractory SLE. We analyzed the underlying pathogenesis in this patient, pointing to dysregulated IFN signaling and other indicated immune pathways. These mutations have not been previously reported and should be considered for early and accurate diagnosis of SLE. And the association of dysfunctional APC5 and SAMHD1 with immune abnormalities suggests a potential precise treatment targeting specific pathways.

DATA AVAILABILITY STATEMENT

The datasets for this article are not publicly available due to concerns regarding participant/patient anonymity. Requests to access the datasets should be directed to the corresponding author.

ETHICS STATEMENT

The studies involving human participants were reviewed and approved by Renji Hospital Biobank is funded by the National Human Genetic Resources Sharing Service Platform (2005DKA21300). Written informed consent to participate in this study was provided by the participants' legal guardian/next of kin. Written informed consent was obtained from the individual(s), and minor(s)' legal guardian/next of kin, for the publication of any potentially identifiable images or data included in this article.

AUTHOR CONTRIBUTIONS

S-MH and WC were responsible for article writing, methodology, and genetic interpretation. JF: genetic testing. DD and NS provide writing ideas and guidance. All authors contributed to the article and approved the submitted version.

FUNDING

This study was supported by grants from the National Natural Science Foundation of China (31630021, 31930037,

82071843, and 81901637), Shenzhen Science and Technology Project JCYJ20180504170414637 and JCYJ20180302145033769, Shenzhen Futian Public Welfare Scientific Research Project FTWS2021006 and Sanming Project of Medicine in Shenzhen SZSM201602087, Shanghai Municipal Key Medical Center Construction Project (2017ZZ01024-002).

ACKNOWLEDGMENTS

We gratefully acknowledge the family members for their contribution to this work. We also thank Dr. Qu Bo from Shanghai Jiao Tong University School of Medicine for his critical and insightful suggestions about our work.

REFERENCES

1. Postal M, Vivaldo JF, Fernandez-Ruiz R, Paredes JL, Appenzeller S, Niewold TB. Type I interferon in the pathogenesis of systemic lupus erythematosus. *Curr Opin Immunol.* (2020) 67:87–94. doi: 10.1016/j.coi.2020.10.014
2. Tan EM, Cohen AS, Fries JF, Masi AT, McShane DJ, Rothfield NF, et al. The 1982 revised criteria for the classification of systemic lupus erythematosus. *Arthritis Rheum.* (1982) 25:1271–7. doi: 10.1002/art.1780251101
3. Hochberg MC. Updating the American College of rheumatology revised criteria for the classification of systemic lupus erythematosus. *Arthritis Rheum.* (1997) 40:1725. doi: 10.1002/art.1780400928
4. Psarras A, Alase A, Antanaviciute A, Carr IM, Md Yusof MY, Wittmann M, et al. Functionally impaired plasmacytoid dendritic cells and non-haematopoietic sources of type I interferon characterize human autoimmunity. *Nat Commun.* (2020) 11:6149. doi: 10.1038/s41467-020-19918-z
5. Ha E, Bae SC, Kim K. Recent advances in understanding the genetic basis of systemic lupus erythematosus. *Semin Immunopathol.* (2022) 44:29–46. doi: 10.1007/s00281-021-00900-w
6. Jeong DY, Lee SW, Park YH, Choi JH, Kwon YW, Moon G, et al. Genetic variation and systemic lupus erythematosus: a field synopsis and systematic meta-analysis. *Autoimmun Rev.* (2018) 17:553–66. doi: 10.1016/j.autrev.2017.12.011
7. Manolio TA, Collins FS, Cox NJ, Goldstein DB, Hindorff LA, Hunter DJ, et al. Finding the missing heritability of complex diseases. *Nature.* (2009) 461:747–53. doi: 10.1038/nature08494
8. Demirkaya E, Sahin S, Romano M, Zhou Q, Aksentijevich I. New horizons in the genetic etiology of systemic lupus erythematosus and lupus-like disease: monogenic lupus and beyond. *J Clin Med.* (2020) 9:712. doi: 10.3390/jcm9030712
9. Moser KL, Kelly JA, Lessard CJ, Harley JB. Recent insights into the genetic basis of systemic lupus erythematosus. *Genes Immun.* (2009) 10:373–9. doi: 10.1038/gene.2009.39
10. Eleftheriou D, Brogan PA. Genetic interferonopathies: an overview. *Best Pract Res Clin Rheumatol.* (2017) 31:441–59. doi: 10.1016/j.berh.2017.12.002
11. d'Angelo DM, Di Filippo P, Breda L, Chiarelli F. Type I interferonopathies in children: an overview. *Front Pediatr.* (2021) 9:631329. doi: 10.3389/fped.2021.631329
12. Comino EJ, Harris E, Page J, McDonald J, Harris MF. The 45 and up study: a tool for local population health and health service planning to improve integration of healthcare. *Public Health Res Pract.* (2016) 26:2631629. doi: 10.17061/phrp2631629
13. Banks E, Redman S, Jorm L, Armstrong B, Bauman A, Beard J, et al. Cohort profile: The 45 and up study. *Int J Epidemiol.* (2008) 37:941–7. doi: 10.1093/ije/dym184
14. Lacaze P, Woods R, Zoungas S, McNeil J. The genomic potential of the aspirin in reducing events in the elderly and statins in reducing events in the elderly studies. *Intern Med J.* (2017) 47:461–3. doi: 10.1111/imj.13384
15. Chu Y, Jiang H, Ju J, Li Y, Gong L, Wang X, et al. A metabolomic study using Hplc-Tof/Ms coupled with ingenuity pathway analysis: intervention effects of rhizoma alismatis on spontaneous hypertensive rats. *J Pharm Biomed Anal.* (2016) 117:446–52. doi: 10.1016/j.jpba.2015.09.026
16. Li K, He Z, Wang X, Pineda M, Chen R, Liu H, et al. Apigenin C-Glycosides of microcos paniculata protects lipopolysaccharide induced apoptosis and inflammation in acute lung injury through Tlr4 signaling pathway. *Free Radic Biol Med.* (2018) 124:163–75. doi: 10.1016/j.freeradbiomed.2018.06.009
17. Szklarczyk D, Franceschini A, Wyder S, Forslund K, Heller D, Huerta-Cepas J, et al. String V10: protein-protein interaction networks, integrated over the tree of life. *Nucleic Acids Res.* (2015) 43(Database issue):D447–52. doi: 10.1093/nar/gku1003
18. Shannon P, Markiel A, Ozier O, Baliga NS, Wang JT, Ramage D, et al. Cytoscape: a software environment for integrated models of biomolecular interaction networks. *Genome Res.* (2003) 13:2498–504. doi: 10.1101/gr.1239303
19. Bader GD, Hogue CW. An automated method for finding molecular complexes in large protein interaction networks. *BMC Bioinformatics.* (2003) 4:2. doi: 10.1186/1471-2105-4-2
20. Bindea G, Mlecnik B, Hackl H, Charoentong P, Tosolini M, Kirilovsky A, et al. Cluego: a cytoscape plug-in to decipher functionally grouped gene ontology and pathway annotation networks. *Bioinformatics.* (2009) 25:1091–3. doi: 10.1093/bioinformatics/btp101
21. Ravenscroft JC, Suri M, Rice GI, Szynkiewicz M, Crow YJ. Autosomal dominant inheritance of a heterozygous mutation in Samhd1 causing familial chilblain lupus. *Am J Med Genet A.* (2011) 155a:235–7. doi: 10.1002/ajmg.a.33778
22. Dasdemir S, Yildiz M, Celebi D, Sahin S, Aliyeva N, Haslak F, et al. Genetic screening of early-onset patients with systemic lupus erythematosus by a targeted next-generation sequencing gene panel. *Lupus.* (2022) 31:330–7. doi: 10.1177/09612033221076733
23. Briggs TA, Rice GI, Daly S, Urquhart J, Gornall H, Bader-Meunier B, et al. Tartrate-resistant acid phosphatase deficiency causes a bone dysplasia with autoimmunity and a type I interferon expression signature. *Nat Genet.* (2011) 43:127–31. doi: 10.1038/ng.748
24. Fazzi E, Cattalini M, Orcesi S, Tincani A, Andreoli L, Balottin U, et al. Aicardi-goutieres syndrome, a rare neurological disease in children: a new autoimmune disorder? *Autoimmun Rev.* (2013) 12:506–9. doi: 10.1016/j.autrev.2012.08.012
25. Lausch E, Janecke A, Bros M, Trojandt S, Alanay Y, De Laet C, et al. Genetic deficiency of tartrate-resistant acid phosphatase associated with skeletal dysplasia, cerebral calcifications and autoimmunity. *Nat Genet.* (2011) 43:132–7. doi: 10.1038/ng.749
26. Navarro V, Scott C, Briggs TA, Barete S, Frances C, Lebon P, et al. Two further cases of spondyloenchondrodysplasia (Spencd) with immune dysregulation. *Am J Med Genet A.* (2008) 146a:2810–5. doi: 10.1002/ajmg.a.32518
27. Bilginer Y, Düzova A, Topaloglu R, Batu ED, Boduroglu K, Güçer S, et al. Three cases of spondyloenchondrodysplasia (Spencd) with systemic lupus erythematosus: a case series and review of the literature. *Lupus.* (2016) 25:760–5. doi: 10.1177/0961203316629000
28. Renella R, Schaefer E, LeMerrer M, Alanay Y, Kandemir N, Eich G, et al. Spondyloenchondrodysplasia with spasticity, cerebral calcifications, and immune dysregulation: clinical and radiographic delineation of a pleiotropic disorder. *Am J Med Genet A.* (2006) 140:541–50. doi: 10.1002/ajmg.a.31081
29. Girschick H, Wolf C, Morbach H, Hertzberg C, Lee-Kirsch MA. Severe immune dysregulation with neurological impairment and minor bone changes in a child with spondyloenchondrodysplasia due to two novel mutations in the Acp5 Gene. *Pediatr Rheumatol Online J.* (2015) 13:37. doi: 10.1186/s12969-015-0035-7
30. Kara B, Ekinci Z, Sahin S, Gungor M, Gunes AS, Ozturk K, et al. Monogenic lupus due to spondyloenchondrodysplasia with spastic paraparesis and intracranial calcification: case-based review. *Rheumatol Int.* (2020) 40:1903–10. doi: 10.1007/s00296-020-04653-x
31. Kulkarni ML, Baskar K, Kulkarni PM. A syndrome of immunodeficiency, autoimmunity, and spondylometaphyseal dysplasia. *Am J Med Genet A.* (2007) 143a:69–75. doi: 10.1002/ajmg.a.31526

32. Hong SW, Huh KH, Lee JK, Kang JH. Craniofacial anomalies associated with spondyloenchondrodysplasia: two case reports. *Medicine (Baltimore).* (2018) 97:e13644. doi: 10.1097/MD.0000000000013644
33. Sait H, Gangadharan H, Gupta A, Aggarwal A, Jain M, Phadke SR. Monogenic lupus with iga nephropathy caused by spondyloenchondrodysplasia with immune dysregulation. *Indian J Pediatr.* (2021) 88:819–23. doi: 10.1007/s12098-020-03636-x
34. Briggs TA, Rice GI, Adib N, Ades L, Barete S, Baskar K, et al. Spondyloenchondrodysplasia due to mutations in Acp5: a comprehensive survey. *J Clin Immunol.* (2016) 36:220–34. doi: 10.1007/s10875-016-0252-y
35. Zhong LQ, Wang L, Song HM, Wang W, Wei M, He YY. Spondyloenchondrodysplasia with immune dysregulation: a case report and literature review. *Zhonghua Er Ke Za Zhi.* (2018) 56:611–6. doi: 10.3760/cma.j.issn.0578-1310.2018.08.011
36. Dale RC, Tang SP, Heckmatt JZ, Tatnall FM. Familial systemic lupus erythematosus and congenital infection-like syndrome. *Neuropediatrics.* (2000) 31:155–8. doi: 10.1055/s-2000-7492
37. Aicardi J, Goutières F. Systemic lupus erythematosus or aicardi-goutières syndrome? *Neuropediatrics.* (2000) 31:113. doi: 10.1055/s-2000-7533
38. De Laet C, Goyens P, Christophe C, Ferster A, Mascart F, Dan B. Phenotypic overlap between infantile systemic lupus erythematosus and aicardi-goutières syndrome. *Neuropediatrics.* (2005) 36:399–402. doi: 10.1055/s-2005-873058
39. Rasmussen M, Skullerud K, Bakke SJ, Lebon P, Jahnsen FL. Cerebral thrombotic microangiopathy and antiphospholipid antibodies in aicardi-goutieres syndrome–report of two sisters. *Neuropediatrics.* (2005) 36:40–4. doi: 10.1055/s-2004-830532
40. Ramantani G, Häusler M, Niggemann P, Wessling B, Guttmann H, Mull M, et al. Aicardi-goutières syndrome and systemic lupus erythematosus (Sle) in a 12-year-old boy with Samhd1 mutations. *J Child Neurol.* (2011) 26:1425–8. doi: 10.1177/0883073811408310
41. Ramantani G, Kohlhase J, Hertzberg C, Innes AM, Engel K, Hunger S, et al. Expanding the phenotypic spectrum of lupus erythematosus in aicardi-goutières syndrome. *Arthritis Rheum.* (2010) 62:1469–77. doi: 10.1002/art.27367

Conflict of Interest: The authors declare that the research was conducted in the absence of any commercial or financial relationships that could be construed as a potential conflict of interest.

Publisher's Note: All claims expressed in this article are solely those of the authors and do not necessarily represent those of their affiliated organizations, or those of the publisher, the editors and the reviewers. Any product that may be evaluated in this article, or claim that may be made by its manufacturer, is not guaranteed or endorsed by the publisher.

Copyright © 2022 Hong, Chen, Feng, Dai and Shen. This is an open-access article distributed under the terms of the Creative Commons Attribution License (CC BY). The use, distribution or reproduction in other forums is permitted, provided the original author(s) and the copyright owner(s) are credited and that the original publication in this journal is cited, in accordance with accepted academic practice. No use, distribution or reproduction is permitted which does not comply with these terms.

frontiers | Frontiers in Pediatrics

CASE REPORT
published: 31 May 2022
doi: 10.3389/fped.2022.889089

Case Report: A Novel Intronic Mutation in *AIFM1* Associated With Fatal Encephalomyopathy and Mitochondrial Disease in Infant

Qi Peng[1,2,3†], Keze Ma[4†], Linsheng Wang[5], Yinghua Zhu[1,2,3], Yaozhong Zhang[1,2,3], Chunbao Rao[2,3], Dong Luo[2,3], Zaixue Jiang[2,3], Wei Lai[6], Huiling Lu[4], Chaohui Duan[7], Zhongjun Zhou[5] and Xiaomei Lu[1,2,3]*

[1] Laboratory Department, Dongguan Children's Hospital Affiliated to Guangdong Medical University, Dongguan, China, [2] Department of Medical and Molecular Genetics, Dongguan Institute of Pediatrics, Dongguan, China, [3] Key Laboratory for Children's Genetics and Infectious Diseases of Dongguan, Dongguan, China, [4] Pediatric Intensive Care Unit, Dongguan Children's Hospital Affiliated to Guangdong Medical University, Dongguan, China, [5] School of Biomedical Sciences, Li Ka Shing Faculty of Medicine, The University of Hong Kong, Pokfulam, Hong Kong SAR, China, [6] Department of Radiology, Dongguan Children's Hospital Affiliated to Guangdong Medical University, Dongguan, China, [7] Laboratory of Clinical, The Sun Yat-sen Memorial Hospital, Sun Yat-sen University, Guangzhou, China

OPEN ACCESS

Edited by:
Ruth Roberts,
ApconiX, United Kingdom

Reviewed by:
Vaidutis Kučinskas,
Vilnius University, Lithuania
Lindsey Hawke,
Queen's University, Canada

***Correspondence:**
Xiaomei Lu
lxm020@126.com

† These authors have contributed equally to this work

Specialty section:
This article was submitted to Genetics of Common and Rare Diseases, a section of the journal Frontiers in Pediatrics

Received: 03 March 2022
Accepted: 05 May 2022
Published: 31 May 2022

Citation:
Peng Q, Ma K, Wang L, Zhu Y, Zhang Y, Rao C, Luo D, Jiang Z, Lai W, Lu H, Duan C, Zhou Z and Lu X (2022) Case Report: A Novel Intronic Mutation in AIFM1 Associated With Fatal Encephalomyopathy and Mitochondrial Disease in Infant. Front. Pediatr. 10:889089. doi: 10.3389/fped.2022.889089

Background: The *AIFM1* gene is located on chromosome Xq26.1 and encodes a flavoprotein essential for nuclear disassembly in apoptotic cells. Mutations in this gene can cause variable clinical phenotypes, but genotype-phenotype correlations of *AIFM1*-related disorder have not yet been fully determined because of the clinical scarcity.

Case Presentation: We describe a 4-month-old infant with mitochondrial encephalopathy, carrying a novel intronic variant in *AIFM1* (NM_004208.4: c.1164 + 5G > A). TA cloning of the complementary DNA (cDNA) and Sanger sequencing revealed the simultaneous presence of an aberrant transcript with exon 11 skipping (89 bp) and a normal transcript through analysis of mRNA extracted from the patient's fibroblasts, which is consistent with direct RNA sequencing results.

Conclusion: We verified the pathogenic effect of the *AIFM1* c.1164 + 5G > A splicing variant, which disturbed normal mRNA splicing. Our findings expand the mutation spectrum of *AIFM1* and point out the necessity of intronic sequence analysis and the importance for integrative functional studies in the interpretation of sequence variants.

Keywords: *AIFM1*, whole-exome sequencing, fatal encephalomyopathy, novel intronic mutation, mitochondrial disease

INTRODUCTION

The *AIFM1* (Mitochondria-Associated Apoptosis-Inducing Factor 1) gene (OMIM *300169) is located at Xq26.1 and contains 16 exons, coding for AIF (Apoptosis-Inducing Factor), a 67 kDa mitochondrial flavin adenine dinucleotide (FAD)-dependent oxidoreductase that plays a role in oxidative phosphorylation (OxPhos) and apoptosis pathway (1). This protein is present in the mitochondria and nucleus, where it participates in caspase-independent apoptosis by nuclear

fragmentation (2). When apoptosis is induced, calpains and/or cathepsins cleave this protein into a soluble, proapoptogenic form that translocates to the nucleus and promotes chromosomal condensation and fragmentation (3).

AIFM1 is known to have roles in electron transport, apoptosis, ferredoxin metabolism, reactive oxygen species generation, and immune system regulation (4). Mutations in the *AIFM1* gene have been reported to be associated with Cowchock syndrome, also known as X-linked recessive Charcot-Marie-Tooth disease-4 (CMTX-4) (5, 6), X-linked deafness-5 (DFNX5) (7), hypomyelinating leukodystrophy, and spondylometaphyseal dysplasia (H-SMD) (8). In addition, *AIFM1* mutations can cause oxidative phosphorylation defects, resulting in severe mitochondrial encephalomyopathy, which is characterized by ventriculomegaly, congenital lactic acidosis, intractable seizures, polyneuropathy, and myopathy, including hypotonia and weakness (9).

Here we describe a male infant with severe mitochondrial encephalomyopathy. We demonstrated that the patient's state was caused by the novel hemizygous mutation c.1164 + 5G > A in the *AIFM1* gene. To our knowledge, this is the first report of the novel *AIFM1* mutation (c.1164 + 5G > A). Experiments were carried out to explore the pathogenicity of this mutation, which confirmed that the mutation could destroy the original donor splice site and lead to exon 11 skipping.

MATERIALS AND METHODS

Clinical Presentation

The proband is a 4-month-old male infant, the second affected child of healthy non-consanguineous parents. His elder brother experienced similar symptoms and died 5 years ago at the age of 4 months. The proband was born at term with a birth weight of 2.53 kg following a normal pregnancy. On the second day after birth, the patient presented with frequent apneas and cyanosis, and was transferred to our hospital.

He presented with hypotonia and marked muscle weakness. His blood oxygen level was reduced to 77% (normal range for newborns: 93–100%), and the heart rate dropped to 110–120 beats/min (normal range for newborns:120–140 beats/min). The peripheral blood glucose fluctuated between 4.0 and 6.0 mmol/L (normal range: 3.9–6.1 mmol/L) during this period. Nasal continuous positive airway pressure (NCPAP) was used to maintain airway patency. A CT scan of the brain revealed an existing subarachnoid hemorrhage. Laboratory investigations revealed plasma lactate concentration fluctuated between normal and abnormal. Blood acylcarnitine analysis and urinary organic acid profiling showed no abnormality. Laboratory tests revealed total bilirubin (TBIL) of 170.8 μmol/L (normal range: 0–23 μmol/L) and direct bilirubin (DBIL) of 11.1 μmol/L (normal range: 0–4 μmol/L), and renal functions were basically normal.

After being hospitalized for 5 days in our hospital, the child was transferred to a provincial hospital for more than 2 months. During this period, the child underwent a number of examinations and no clear cause was determined. At said hospital, no pathogenic mutations or copy number variations were found in genes related to the disease.

At roughly 4 months old, the child was sent to the emergency department of our hospital due to spit-up and cyanosis at home. He had gone into a sudden respiratory and cardiac arrest. After rescue, the child's complexion gradually turned rosy, and his spontaneous heartbeat was restored. Considering that the child's breathing was unstable after successful cardiopulmonary resuscitation, advanced life support treatment was still needed, so he was transferred to PICU under the condition of tracheal intubation and resuscitation bag positive pressure ventilation for further monitoring and treatment.

Later, despite the use of non-invasive respiratory support, the child still had repeated apneas, accompanied by mental fatigue, drowsiness, and sudden hypotension. The lactic acid was always high, fluctuating at 5–12.9 mmo/L (normal range: 0.5–2.2 mmol/L), showing a progressive increase.

A brain magnetic resonance imaging (MRI) examination was performed and revealed a bilateral hyperintensity of basal ganglia (**Figure 1A**). Hydrocephalus was suggested by a moderately enlarged ventricle system, centered on each side of the ventricle and a widened extracerebral space in the temporal part of both sides. The patient's lactate peak was distinctly discernible as an inverted doublet at TE = 144 ms by single voxel magnetic resonance spectroscopy (MRS) of the left basal ganglia (**Figure 1B**). Multiple basic symmetrical abnormal signals, combined with MRS can be seen in the bilateral basal ganglia, brainstem, thalamus, frontal lobe, parietal lobe, bilateral limbic lobe, and temporal cortex, suggesting mitochondrial encephalopathy. Finally, the proband died due to respiratory failure after the parents ceased treatment.

Whole Exome Sequencing and Bioinformatic Analyses

The peripheral blood samples were obtained from the patient and his family members after informed consent was obtained. Whole Exome Sequencing (WES) was performed to analyze the coding exons and the exon-intron boundaries of protein-coding genes by the Novogene Bioinformatics Institute (Tianjin, China). The American College of Medical Genetics and Genomics (ACMG) guidelines were also used to classify this variant. The 3D models of the normal and mutant protein are predicted by the I-TASSER server[1] and visualization was carried out by PyMOL.

mRNA Sequencing

RNA sequencing was conducted by the Novogene Bioinformatics Institute (Beijing, China). Preparation of sample is followed by the RNA library preparation. RNA library is formed by polyA capture (or rRNA removal) and reverse transcription of cDNA. Illumina PE150 technology is employed to sequence the sample and the final stage involves the bioinformatics analysis.

Muscle and Skin Biopsy

Quadricep muscle and skin biopsies were obtained from the patient. Age- and gender-matched specimens of normal human

[1]https://zhanglab.dcmb.med.umich.edu/I-TASSER/

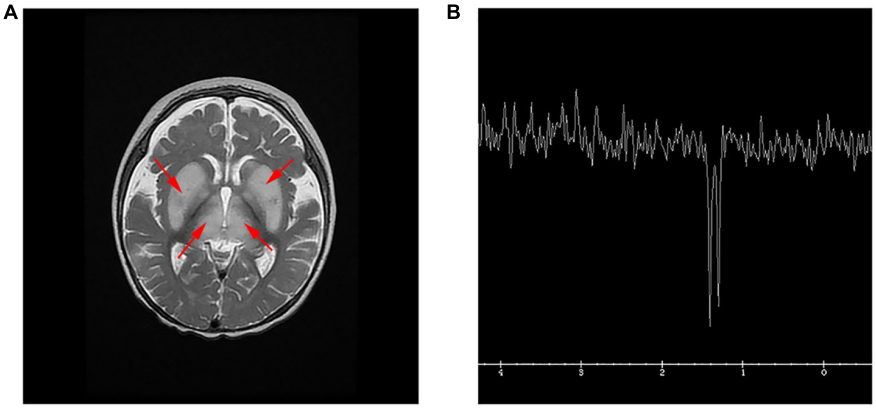


FIGURE 1 | MRI and MRS in the patient. **(A)** T2 weighted image (T2WI) showed symmetrical hyperintensity in the basal ganglia and thalamus, and a small amount of subdural effusion in the forehead. **(B)** Single voxel MRS of the left basal ganglia. The lactate peak, clearly visible as an inverted doublet at TE = 144 ms.

muscle and skin were obtained from a patient during surgery. For the use of biomedical studies, fibroblasts were cultured and harvested from the biopsies.

Reverse Transcription-Polymerase Chain Reaction and TA Clone Sequencing

We preformed reverse transcription-polymerase chain reaction (RT-PCR) on mRNA extracted from the patient's fibroblasts in order to evaluate the potential effect of this variant on splicing. The cDNA obtained was amplified by PCR, using a set of primers: the forward primer aligning on exon 10 (5′-CAGCAACTGGACCATGGAAA-3′) and the reverse primer aligning on exon 12 (5′-GCTCTGCATTTACCCGGAAG-3′) of *AIFM1* gene. The PCR products were gel-purified and ligated into the pMD19-T vector and transformed into *E. coli* DH5α. The colonies were picked and screened by PCR, and the positive clones were sent for sequencing (Sangon Biotech, Shanghai, China).

Real-Time Quantitative Polymerase Chain Reaction

The relative mRNA expression levels of *AIFM1* in the fibroblasts of the patient and control normal individual were compared by real-time quantitative polymerase chain reaction (RT-qPCR). Four pairs of primers were designed to detect the mRNA level of *AIFM1*. Each experiment was performed in triplicate, and expression data were normalized to β-actin as an internal reference gene. The $2^{-\Delta\Delta Ct}$ method was used for quantification by comparing the Ct values.

Western Blot Analysis

Fibroblasts were trypsinied, centrifuged at 1000 *g* for the duration of 5 min, followed by solubilizing in RIPA buffer with protease inhibitors. For muscle tissues, ice-cold lysis buffer was rapidly added to the samples, followed by homogenizing with an electric homogenizer and rinsing the blade twice with another 2 × 300 μL lysis buffer. The samples were then kept at 4°C for 2 h with continual agitation. Immunoblot analysis was performed with the ECL-chemiluminescence kit in accordance with manufacturer's protocol. A mouse monoclonal anti-GAPDH (4A Biotech Co., Ltd., Shanghai, China, Cat. No. 4ab030004) and mouse monoclonal anti-AIFM1 antibody binding to the C-terminus of human AIF (Boster Biological Technology, Wuhan, China, Cat. No. M01571-1) were used. The HRP-conjugated Affinipure Goat Anti- Rabbit IgG (H + L) was used as secondary antibody (Proteintech, Illinois, IL, United States, Cat. No. SA00001-2).

Immunofluorescence

For immunofluorescence, cells were fixed in 4% paraformaldehyde and permeabilized in 0.25% Triton X-100. Subsequently, cells were blocked and immunostained with antibodies in 5% goat serum and treated with 4′,6-Diamidino-2-phenylindole (DAPI) staining solution (Beyotime Biotechnology, Shanghai, China) before mounting. Anti-TOMM20 (Millipore, Bedford, MA, United States) was used at 1/200 dilution for mitochondria localization. Images were visualized using Nikon Eclipse Ti-S Phase Contrast Fluorescence Inverted Microscope (Nikon, Tokyo, Japan).

NAD^+ and Cytochrome C Oxidase Measurement

The level of NAD^+ in fibroblasts was determined using NAD^+ /NADH assay kit (Beyotime, S0175, Shanghai, China) with WST-8 according to the manufacturer's instructions. Human Cytochrome C Oxidase (COX) of cell culture supernatant were measured using the Human COX ELISA kit (RX105095H, Ruixin Biotech, Quanzhou, Fujian, China) according to instruction of the manufacturer.

RESULTS

Whole Exome Sequencing Analysis

In the proband, WES identified a maternally inherited hemizygous variant in intron 11 of the *AIFM1* gene, c.1164 + 5G > A, on the X chromosome. Sanger sequencing

confirmed that this mutation was also present in his elder brother who died 5 years ago due to similar symptoms. His mother is a heterozygous carrier of the mutation, but maternal grandparents don't have this mutation. Therefore, this is a *de novo* mutation that occurred in the mother and passed down to the two sons (**Figures 2A,B**).

c.1164 + 5G > A is absent from dbSNP version 147, 1000 genomes project, ExAC, HGMD, and Clinvar databases and not found in the literature. Computational predictions using SpliceAI, HSF, and MatEntScan did not predict intronic c.1164 + 5G > A to have an impact on splicing.

Functional Analysis

We evaluated the functional significance of the c.1164 + 5G > A mutation because it was missing from databases and co-segregated with disease phenotype in the family. The control fibroblasts produced a single 236 bp product by reverse-transcription PCR targeting exon 10 and exon12 of the *AIFM1* gene, whereas the patient's fibroblasts produced two bands (236 and 147 bp) (**Figure 2C**). In order to clarify the two bands, the PCR products were TA cloned and screened by cPCR, then two sizes of products were clearly seen (**Figure 2D**). Sanger sequencing showed that the shorter product on the patient's fibroblasts lacked exon 11 (89 bp) (**Figure 2E**). The novel splice variant in *AIFM1* led to exon 11 skipping. The effect of this intron mutation on splicing was confirmed through RNA-sequencing (**Figure 2F**).

The RT-qPCR analysis using four pairs of primers targeting the sequence after the mutation site showed that the *AIFM1* mRNA levels were significantly decreased in the patient's fibroblasts (**Figure 3A**). The detrimental effect of the identified variant was also confirmed using western blot analysis, which showed a highly reduced amount of AIF protein in the patient's fibroblasts (**Figure 3B**) and muscle (**Figure 3C**) compared with controls. These findings highlighted the novel variant's potential pathogenic effect, as the intronic mutation leads to reduced AIF1 expression, likely due to incomplete penetrance of the splicing defect, allowing minimal production of wildtype transcript.

Electron microscopy analysis of a muscle biopsy from the patient revealed large mitochondria with insufficient fusion of the inner mitochondrial membrane. The mitochondria were contorted and irregularly shaped, with no inclusions (**Figure 3D**). Mitochondrial fragmentation was also noted in the patient's fibroblast by staining the mitochondrial protein TOMM20 (**Figure 3E**).

The AIF protein contains three major domains: a FAD-binding domain (residues 128–262 and 401–480), a NADH-binding domain (residues 263–400), and a C-terminal domain (residues 481–608) (**Figure 4A**). The non-coding mutation identified in the present study was located at 5 bp of intron 11 which was close to exon 11 (**Figure 4B**). It was located at the 5′ splice site and was verified to cause exon 11 skipping, which competes with the wild-type splicing donor site, resulting in two coexisting transcript populations, the mutant, and the wild-type form. The mutant causes a frameshift resulted in the change of amino acid coding after R358, and the early termination codon was generated at the position of amino acid 362 (the full-length of AIF is 613 amino acids) (**Figure 4B**). Computational modeling for wild-type and mutant AIF were performed using I-TASSER to execute the 3D structure. As shown in **Figure 4C**, part of the NADH domain, the second FAD region and C-terminal are deleted in the mutant *AIFM1*, which might change its protein stability. The NAD^+/NADH ratio is decreased in patient's fibroblasts (**Figure 4D**), while the COX of cell culture supernatant showed no difference between the patient and control (**Figure 4E**).

DISCUSSION

This study describes a patient with fatal encephalomyopathy and mitochondrial disease that carried a novel intronic variant in the *AIFM1* gene (NM_004208.4: c.1164 + 5G > A). *AIFM1* gene has already been linked to mitochondrial encephalomyopathy, while intronic mutations of *AIFM1* have not been reported yet (4). To the best of our knowledge, this study is the first to report the variant, which is not included in the HGMD, 1000 Genomes Project and dbSNP147 databases.

The discovery of an intronic mutation in the AIFM1 gene prompted us to evaluate AIFM1 mRNA splicing in patient fibroblasts using RNASeq. We provided the first experimental characterization of this novel variant and elucidated its impact on RNA splicing. There are two possible outcomes for mRNAs carrying premature termination codons: non-sense-mediated mRNA decay (NMD) (10, 11) or translation to truncated proteins (12). NMD is an evolutionarily conserved quality assurance pathway found in eukaryotic cells. It has the function of examining mRNA for any potential errors, eliminating any error-containing transcripts, and regulating the amount of non-mutated transcript in the transcriptome (13). According to the mammalian non-sense-mediated mRNA decay (NMD) rule that stop codons located > 50–55 nucleotides upstream of the 3′ most splice-generated exon-exon junction usually trigger NMD in mammals (14), this mutation probably results in degradation by non-sense-mediated decay.

Alternative splicing is one of the important mechanisms in regulating gene expression, splice sites (5′ and 3′), the branch site and the polypyrimidine sequence are the key splicing signals that have major roles in the splicing of pre-mRNA (15). Splicing mutations have been identified in a number of different genes and shown to have a variety of consequences, including exon skipping and intron retention (16). Most of these splicing mutations occur within or close to conserved consensus donor (+1/+2) or acceptor (−1/−2) splice sites (17). However, mutations remote from the splice donor or acceptor sites have also been shown to lead to aberrant splicing in a number of reports (18–20). Thus, intronic mutations particularly within the splice sites (∼20 bp) must be considered more readily when evaluating sequence variants, especially when tributary mutation in coding regions or canonical splice sites cannot be found. This mutation was not recognized until this case study despite the subject's brother having the same mutation and dying of the same disease 5 years previous. Unfortunately, due to the lack of regular intronic sequencing, and

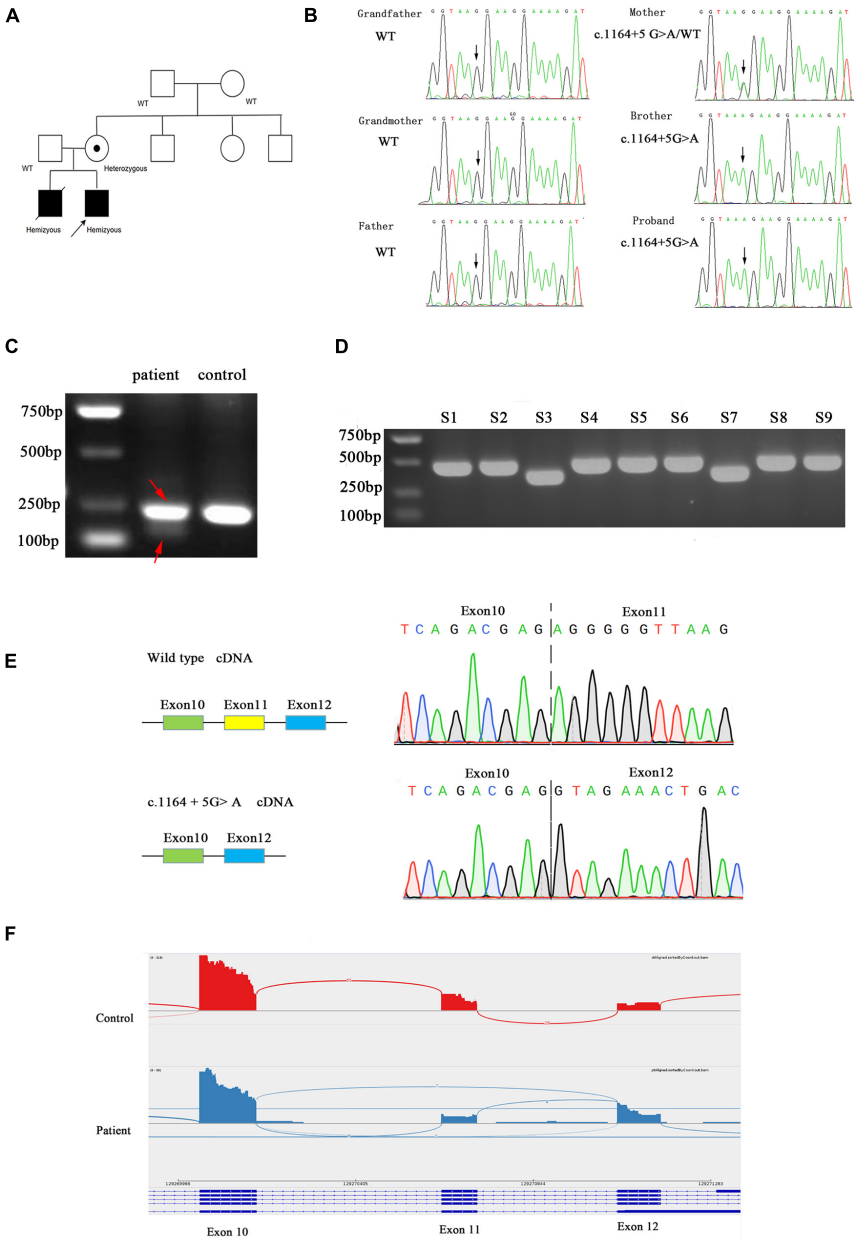


FIGURE 2 | (A) Family pedigree. Black symbols represent affected persons and symbols with a dot, carriers. The proband is indicated by an arrow. **(B)** Chromatograms for the mutations confirmed by Sanger sequencing. **(C)** Agarose gel electrophoresis of the transcripts generated by cDNA amplification of the patient and control, with adjacent schematic representation of the resulting splicing events. The PCR product of patient was marked by red arrow. **(D)** Agarose gel electrophoresis of cloning PCR. S1–S9 represent the different clones picked. **(E)** Sanger sequencing electropherogram of gel-purified fragments for the upper band and lower band from the patient cDNA samples. **(F)** AIFM1 Sashimi plot of RNA extracted from patient's and control's fibroblasts.

atypical mitochondrial encephalopathy presentation in the early stage, with mild changes in lactic acid meant the subjects were not diagnosed until after death.

Pathogenic intronic mutations can be detected by WGS and analyzed by RNA-Seq. This combined strategy makes it possible to unravel cases with more arduous molecular causes and will indisputably improve the mutation identification methods in the future. Due to the limitations of bioinformatic tools such as the splicing predictor, our study suggested that functional analysis is required to determine the pathogenicity of mutations. As a result, our research is the first functional validation report of a novel splicing mutation in *AIFM1* associated with fatal encephalomyopathy and mitochondrial disease.

In conclusion, our findings show that a unique intronic mutation of the *AIFM1* gene affects splicing, expanding the mutation spectrum of *AIFM1* and emphasizing the importance of intronic sequence analysis and integrative functional research in the elucidation of sequence variants.

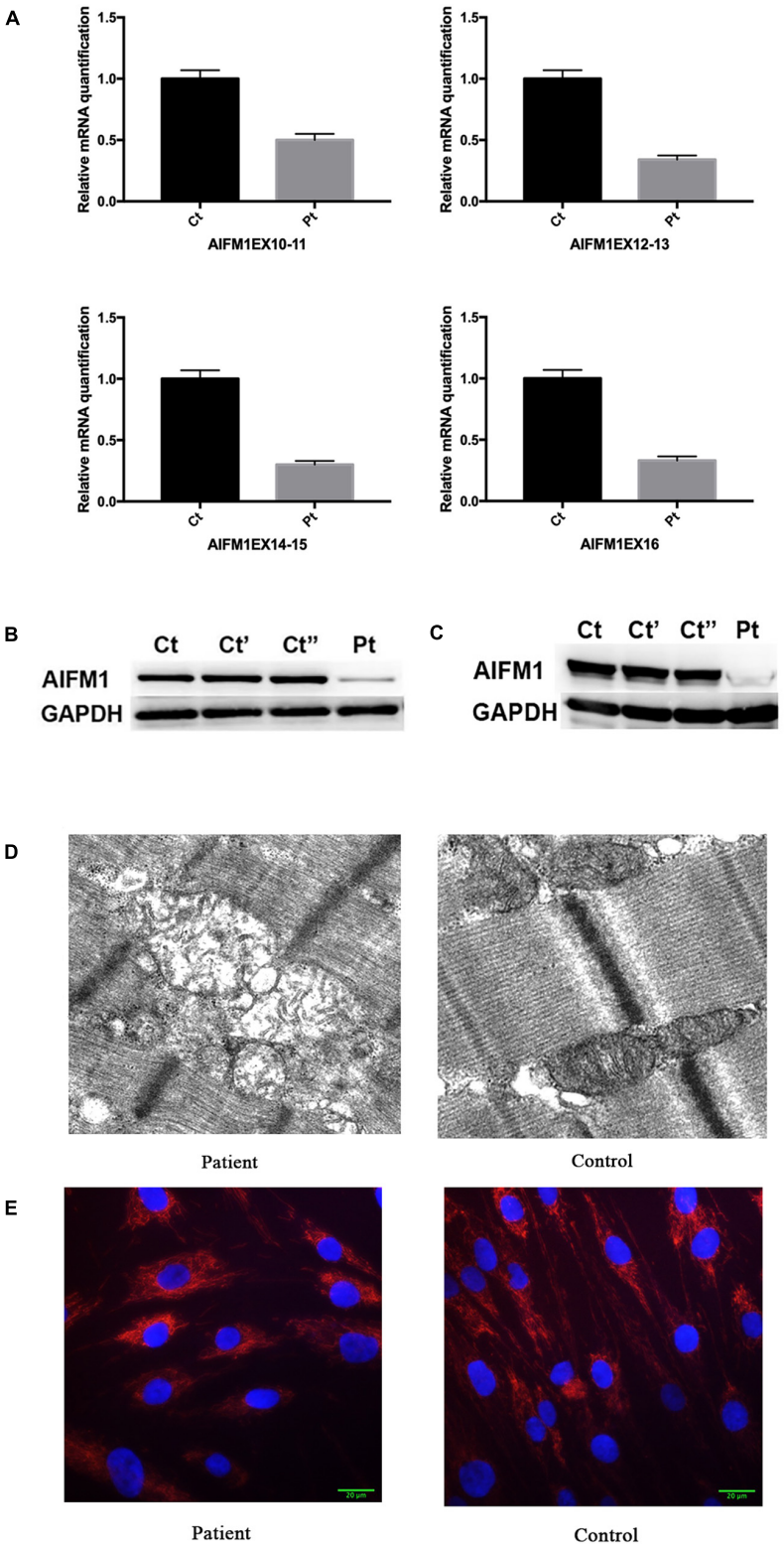


FIGURE 3 | (A) Relative quantification of mRNA levels for AIFM1 in controls and patient's fibroblasts using different primers. The results of mRNA are the average of the values assessed after three reaction tests. **(B)** Western blot analysis in controls and patient's fibroblasts using AIF antibody. GAPDH was used as loading control. The patient's sample shows a clear reduction in the AIF amount compared with the control lines. **(C)** Western blot analysis in controls and patient's muscles using AIF antibody. GAPDH was used as loading control. **(D)** Electron microscopy of quadriceps muscle demonstrating large, irregularly shaped mitochondria, including one with concentric cisternae. **(E)** TOMM20 staining of the patient's and control fibroblast. DAPI was used to mark the nucleus.

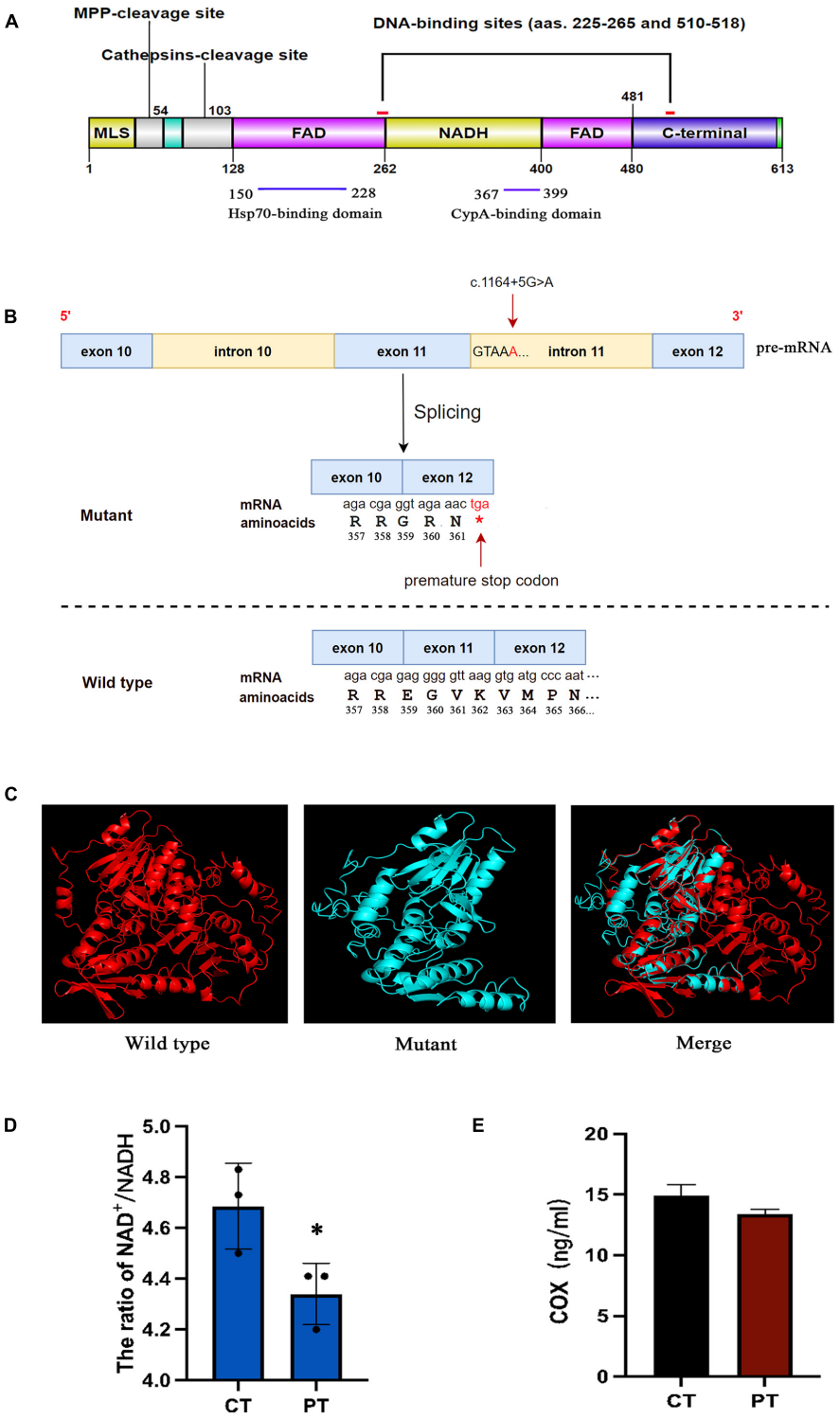


FIGURE 4 | (A) Schematic model representing the AIF protein. AIF is a flavoprotein (with an oxidoreductase enzymatic activity) containing a FAD-bipartite domain (amino-acids 128–262 and 401–480), a NADH-binding motif (amino-acids 263–400), and a C-terminal domain (amino-acids 481–608) where the proapoptotic activity of the protein resides. In addition, it has a Mitochondria Localization Sequence (MLS, amino-acids 1–41) placed in its N-terminal region. AIF also possesses two DNA-binding sites, which are located in amino-acids 255–265 and 510–518, respectively. **(B)** The mutant causes a frameshift resulted in the change of amino acid coding after R358, and the early termination codon was generated at the position of amino acid 362. **(C)** Protein structure modeling of wild-type and mutated AIFM1. A part of the amino acid sequence has been eliminated in the mutated protein compared to the wild type protein. **(D)** The NAD^+/NADH ratios in fibroblasts of patient and control. **(E)** The human COX of cell culture supernatant in patient and control. *Statistically significant difference at $p < 0.05$.

DATA AVAILABILITY STATEMENT

The datasets presented in this study can be found in online repositories. The names of the repository/repositories and accession number(s) can be found below: NCBI (accession: NM_004208.4).

ETHICS STATEMENT

This study was authorized by and carried out in compliance with the protocol of the Institutional Medical and Ethics Committee of Dongguan Children's Hospital Affiliated to Guangdong Medical University. Written informed consent to participate in this study was provided by the participants' legal guardian/next of kin.

AUTHOR CONTRIBUTIONS

XL and ZZ designed the study. KM, LW, YHZ, YZZ, CR, DL, ZJ, and HL carried out experimental work. WL performed the MRI studies. QP and XL prepared the first draft of the manuscript. CD revised the manuscript. All authors approved the final manuscript.

FUNDING

This study was supported by the Medical Scientific Research Foundation of Guangdong Province of China (Project Number: A2020261) and Guangdong Basic and Applied Basic Research Fund (Guangdong-Dongguan Joint Fund) (Project Number: 2020A1515110186). The funders had no role in the design of the study or in the collection, analysis, and interpretation of data or in writing the manuscript.

ACKNOWLEDGMENTS

We thank the patient and his family for participating in this study.

REFERENCES

1. Joza N, Pospisilik JA, Hangen E, Hanada T, Modjtahedi N, Penninger JM, et al. AIF: not just an apoptosis-inducing factor. *Ann N Y Acad Sci.* (2009) 1171:2–11. doi: 10.1111/j.1749-6632.2009.04681.x
2. Susin SA, Lorenzo HK, Zamzami N, Marzo I, Snow BE, Brothers GM, et al. Molecular characterization of mitochodrial apoptosis-inducing factor. *Nature.* (1999) 397:441–6. doi: 10.1038/17135
3. Ferreira P, Villanueva R, Martínez-Júlvez M, Herguedas B, Marcuello C, Fernandez-Silva P, et al. Structural insights into the coenzyme mediated monomer-dimer transition of the pro-apoptotic apoptosis inducing factor. *Biochemistry.* (2014) 53:4204–15. doi: 10.1021/bi500343r
4. Morton SU, Prabhu SP, Lidov HGW, Shi J, Anselm I, Brownstein CA, et al. AIFM1 mutation presenting with fatal encephalomyopathy and mitochondrial disease in an infant. *Mol Case Stud.* (2017) 3:a001560. doi: 10.1101/mcs.a001560
5. Rinaldi C, Grunseich C, Sevrioukova IF, Schindler A, Horkayne-Szakaly I, Lamperti C, et al. Cowchock syndrome is associated with a mutation in apoptosis-inducing factor. *Am J Hum Genet.* (2012) 91:1095–102. doi: 10.1016/j.ajhg.2012.10.008
6. Cowchock FS, Duckett SW, Streletz LJ, Graziani LJ, Jackson LG. X-linked motor-sensory neuropathy type II with deafness and mental retardation: a new disorder. *Am J Med Genet.* (1985) 20:307–15. doi: 10.1002/ajmg.1320200214
7. Zong L, Guan J, Ealy M, Zhang Q, Wang D, Wang H, et al. Mutations in apoptosis-inducing factor cause X-linked recessive auditory neuropathy spectrum disorder. *J Med Genet.* (2015) 52:523–31. doi: 10.1136/jmedgenet-2014-102961
8. Mierzewska H, Rydzanicz M, Biegański T, Kosinska J, Mierzewska-Schmidt M, Ługowska A, et al. Spondyloepimetaphyseal dysplasia with neurodegeneration associated with AIFM1 mutation – a novel phenotype of the mitochondrial disease. *Clin Genet.* (2017) 91:30–7. doi: 10.1111/cge.12792
9. Ghezzi D, Sevrioukova I, Invernizzi F, Lamperti C, Mora M, D'Adamo P, et al. Severe X-Linked Mitochondrial Encephalomyopathy Associated with a Mutation in Apoptosis-Inducing Factor. *Am J Hum Genet.* (2010) 86:639–49. doi: 10.1016/j.ajhg.2010.03.002
10. Brogna S, Wen J. Nonsense-mediated mRNA decay (NMD) mechanisms. *Nat Struct Mol Biol.* (2009) 16:107–13. doi: 10.1038/nsmb.1550
11. Hug N, Longman D, Cáceres JF. Mechanism and regulation of the nonsense-mediated decay pathway. *Nucleic Acids Res.* (2015) 44:1483–95. doi: 10.1093/nar/gkw010
12. Roest PAM, Roberts RG, Sugino S, Van Ommen GJB, Den Dunnen JT. Protein truncation test (PTT) for rapid detection of translation-terminating mutations. *Hum Mol Genet.* (1993) 2:1719–21. doi: 10.1093/hmg/2.10.1719
13. Chang YF, Imam JS, Wilkinson MF. The Nonsense-mediated decay RNA surveillance pathway. *Annu Rev Biochem.* (2007) 76:51–74. doi: 10.1146/annurev.biochem.76.050106.093909
14. Nagy E, Maquat LE. A rule for termination-codon position within intron-containing genes: when nonsense affects RNA abundance. *Trends Biochem Sci.* (1998) 23:198–9. doi: 10.1016/s0968-0004(98)01208-0
15. Wang Y, Liu J, Huang B, Ym Xu, Li J, Huang LF, et al. Mechanism of alternative splicing and its regulation. *Biomed Rep.* (2015) 3:152–8. doi: 10.3892/br.2014.407
16. Mayer K, Ballhausen W, Leistner W, Rott H. Three novel types of splicing aberrations in the tuberous sclerosis TSC2 gene caused by mutations apart from splice consensus sequence. *Biochim Biophys Acta.* (2000) 1502:495–507. doi: 10.1016/s0925-4439(00)00072-7
17. Anna A, Monika G. Splicing mutations in human genetic disorders: examples, detection, and confirmation. *J Appl Genet.* (2018) 59:253–68.
18. Sangermano R, Khan M, Cornelis SS, Richelle V, Albert S, Garanto A, et al. ABCA4 midigenes reveal the full splice spectrum of all reported noncanonical splice site variants in Stargardt disease. *Genome Res.* (2018) 28:100–10. doi: 10.1101/gr.226621.117
19. Parada GE, Munita R, Cerda CA, Gysling K. A comprehensive survey of non-canonical splice sites in the human transcriptome. *Nucleic Acids Res.* (2014) 42:10564–78. doi: 10.1093/nar/gku744
20. Conboy JGA. Deep exon cryptic splice site promotes aberrant intron retention in a von willebrand disease patient. *Int J Mol Sci.* (2021) 22:13248. doi: 10.3390/ijms222413248

Conflict of Interest: The authors declare that the research was conducted in the absence of any commercial or financial relationships that could be construed as a potential conflict of interest.

Publisher's Note: All claims expressed in this article are solely those of the authors and do not necessarily represent those of their affiliated organizations, or those of the publisher, the editors and the reviewers. Any product that may be evaluated in this article, or claim that may be made by its manufacturer, is not guaranteed or endorsed by the publisher.

Copyright © 2022 Peng, Ma, Wang, Zhu, Zhang, Rao, Luo, Jiang, Lai, Lu, Duan, Zhou and Lu. This is an open-access article distributed under the terms of the Creative Commons Attribution License (CC BY). The use, distribution or reproduction in other forums is permitted, provided the original author(s) and the copyright owner(s) are credited and that the original publication in this journal is cited, in accordance with accepted academic practice. No use, distribution or reproduction is permitted which does not comply with these terms.

frontiers | Frontiers in Genetics

ORIGINAL RESEARCH
published: 13 June 2022
doi: 10.3389/fgene.2022.915129

Cardiovascular Abnormalities and Gene Mutations in Children With Noonan Syndrome

Ling Sun, Yu-mei Xie, Shu-shui Wang and Zhi-wei Zhang**

Department of Pediatric Cardiology, Guangdong Cardiovascular Institute, Guangdong Provincial People's Hospital, Guangdong Academy of Medical Sciences, Guangzhou, China

Background: Common cardiac abnormalities in Noonan syndrome (NS) include congenital heart diseases (CHD), pulmonary valve stenosis and hypertrophic cardiomyopathy (HCM). Molecular diagnoses are enabling earlier and more precise diagnosis of patients who have a subtle or atypical presentation. The aims of this study were to investigate genotype-phenotype associations with respect to Noonan syndrome (NS)-associated cardiac abnormalities and catheter or surgery-based interventions conditions.

Methods: From January 2019 to December 2021, 22 children with a confirmed molecular diagnosis of NS combined with cardiovascular abnormalities were consecutively enrolled into the current study. A comprehensive review was carried out of echocardiography and electrocardiogram results, second-generation whole-exome sequencing results and catheter or surgery-based interventions conditions.

Results: The main manifestations of electrocardiogram abnormalities were QTc prolongation, abnormal Q wave in the precordial lead and limb lead, right ventricular hypertrophy and left or right deviation of the electrical axis. The most commonly detected abnormality was pulmonary valve dysplasia with stenosis, seen in 15 (68.2%) patients, followed by atrial septal defect in 11 (50%) patients. Seven genes (*RAF1*, *RIT1*, *SOS1*, *PTPN11*, *BRAF*, *SOS2*, and *LZTR1*) were found to contain disease-associated variants. The most commonly observed genetic mutations were *PTPN11* (27%) and *RAF1* (27%). Each genotype was associated with specific phenotypic findings. *RIT1*, *SOS1*, *PTPN11*, and *SOS2* had common echocardiography features characterized by pulmonary valve stenosis, while *RAF1* was characterized by HCM. Interestingly, patients with *BRAF* mutations were not only characterized by HCM, but also by pulmonary valve stenosis. In the cohort there was only one patient carrying a *LZTR1* mutation characterized by left ventricle globose dilation. Ten cases underwent catheter or surgery-based interventions. All the operations had immediate results and high success rates. However, some of the cases had adverse outcomes during extended follow-up. Based on the genotype-phenotype associations observed during follow-up, *BRAF* and *RAF1* genotypes seem to be poor prognostic factors, and multiple interventions may be required for NS patients with severe pulmonary stenosis or myectomy for HCM.

Conclusions: The identification of causal genes in NS patients has enabled the evaluation of genotype-cardiac phenotype relationships and prognosis of the disease. This may be beneficial for the development of therapeutic approaches.

OPEN ACCESS

Edited by:
Tieliu Shi,
Hunan University of Arts and Science, China

Reviewed by:
Simone Martinelli,
National Institute of Health (ISS), Italy
Sina Zoghi,
Shiraz University of Medical Sciences, Iran

****Correspondence:***
Shu-shui Wang
wsscome@126.com
Zhi-wei Zhang
drzhangzhiwei@sina.com

Specialty section:
This article was submitted to Genetics of Common and Rare Diseases, a section of the journal Frontiers in Genetics

Received: *07 April 2022*
Accepted: *23 May 2022*
Published: *13 June 2022*

Citation:
Sun L, Xie Y-m, Wang S-s and Zhang Z-w (2022) Cardiovascular Abnormalities and Gene Mutations in Children With Noonan Syndrome. Front. Genet. 13:915129. doi: 10.3389/fgene.2022.915129

Keywords: cardiovascular abnormalities, echocardiography, genotype-phenotype, noonan syndrome, pulmonary valve stenosis

INTRODUCTION

Noonan syndrome (NS) is an autosomal dominant disorder that is characterized by facial dysmorphism (hypertelorism, ptosis and low-set ears), short stature, congenital heart defects and other additional extracardiac features (Romano et al., 2010). Although Noonan syndrome is mainly transmitted as a dominant trait, an autosomal recessive form of this condition has recently been associated with biallelic LZTR1 variants (Johnston et al., 2018). The incidence of NS is estimated to be 1 in 1000–2500 live births (Allanson et al., 1985). One of the principal features of NS, which is also the cause of seeking early treatment, is cardiac involvement, most frequently including congenital heart diseases, pulmonary valve stenosis and hypertrophic cardiomyopathy (HCM) (Romano et al., 2010). With the elucidation of the underlying genetic variants causing NS, numerous studies have revealed that NS and NS-like disorders are 'RASopathies' or 'RAS/mitogen-activated protein kinase (MAPK) syndromes' because they share aberrant signaling through the RAS/MAPK pathway that controls cell proliferation, differentiation and survival (Aoki et al., 2008; Tidyman and Rauen, 2009). Recently, some studies have discussed the genotype-phenotype associations together with the prognostic assessment in these patients. A large study was published by Calcagni et al. in 2020. The authors reported the cardiac features in 440 molecularly characterized patients with RASopathies enrolled from seven centers participating in the CArdiac Rasopathy NETwork—CARNET study (Calcagni et al., 2020). Among them, 312 subjects presented a common congenital heart defect or HCM, whereas atypical findings were reported in 45 patients. Leoni et al. assessed genotype-cardiac phenotype correlations in a single-center cohort of 116 patients with a molecularly confirmed RASopathy (Leoni et al., 2022). Yi et al. assessed the therapeutic landscape for the treatment of heart disease in RASopathies (Yi et al., 2022). In addition, the clinical presentation and natural history of RASopathy-related HCM was extensively described in two recent reviews (Calcagni et al., 2018; Lioncino et al., 2022). To evaluate genotype-cardiac phenotype relationships and improve prognoses for patients with NS, it is necessary to look for genotype-phenotype associations with respect to NS-associated congenital heart diseases (CHD), and a personalized targeted therapy approach should be developed according to genotype-phenotype correlations.

In this study, we reviewed the cardiac manifestations of patients with a confirmed molecular diagnosis of NS by evaluating clinical echocardiography and electrocardiogram features and performing molecular analyses of the known causative genes of NS. We also evaluated genotype-cardiac phenotype associations.

METHODS

Study Participants

This retrospective study was approved by the Clinical Research Ethic Committee of Guangdong Provincial People's Hospital (ethical approval number KY-Z-2021-191-01 and KY2020-033-01). From January 2019 to December 2021, 22 children with a confirmed molecular diagnosis of NS combined with cardiovascular abnormalities were consecutively enrolled into the current study after parental written informed consent was obtained. Some of the children underwent corrective cardiac surgery or catheter-based interventions at Guangdong Provincial People's Hospital, the largest tertiary cardiac center in China. We reviewed the clinical phenotypes of cardiac structural anomalies evaluated by electrocardiogram, echocardiography findings and follow-up data.

Data Collection

Transthoracic echocardiographic examination was carried out preoperatively using IE33, IE Epic-7C (Philips, Andover, MA, United States) and Vivid E 9 (GE Healthcare, Horten, Norway) ultrasound systems with a transducer of 5–8 Mhz. The preoperative and postoperative TTE images and electrocardiogram were reviewed by two independent experienced pediatric cardiologists. If there were discrepancies between these two observers, another independent experienced pediatric cardiologist was invited to review the images.

Molecular Genetic Analyses

Molecular diagnosis was performed using second-generation whole-exome sequencing. Genomic DNA was extracted from peripheral blood using the Solpure Blood DNA kit (Magen), then fragmented by Q800R Sonicator (Qsonica) to generate 200–500 bp insert fragments. Custom designed NimbleGen SeqCap probes (Roche NimbleGen, Madison, Wis) were used for in-solution hybridization to enrich target sequences. Enriched DNA samples were indexed and sequenced on a NextSeq500 sequencer (Illumina, San Diego, Calif) with 100 cycles of single end reads, according to the manufacturer's protocols. The target gene capture/NGS assay provides an average read depth of approximately 200×. The insufficiently covered (<20×) target exons were analyzed by using gene-specific amplicon-based Sanger sequencing. Deleterious mutations and novel variants detected by using NGS were confirmed by means of Sanger sequencing. Variants interpretation was manipulated according to the American College of Medical Genetics (ACMG) guidelines (Richards et al., 2015). When an NS molecular diagnosis report was suspected, a clinical geneticist was invited to evaluate the diagnosis. The NS patients and their molecular diagnoses are shown in **Table 1**.

TABLE 1 | NS patients and their clinical characteristics.

Case	Sex (F/M)	Age (m)	Genotype	Nucleotide change	Origin of variant	ACMG	Echo prestation	ECG	Follow-up (y)
Case 1	F	76	*RAF1*	c.770C > T	New mutations	1	Obstructive HCM, PFO, ASD, the right coronary artery arises from the left coronary sinus with intramural course	QTc prolonged, V4-V6 leads abnormal Q wave, electrical axis deviation to the right	2
Case 2	F	10	*RIT1*	c.229G > A	New mutations	1	Pulmonary valve dysplasia with stenosis (moderate to severe); biventricular hypertrophy; PFO	Right ventricular hypertrophy	2.5
Case 3	F	10	*SOS1*	c.508A > G	New mutations	1	Pulmonary valve dysplasia with stenosis (severe); biventricular hypertrophy; ASD; left pulmonary artery slight stenosis	Right ventricular hypertrophy	2
Case 4	M	15	*RIT1*	c.170C > G	New mutations	1	Pulmonary valve dysplasia with stenosis (severe); biventricular hypertrophy; ASD; PFO; slightly dilated opening of the left coronary artery	Atrial hypertrophy, left and right ventricular hypertrophy	1
Case 5	F	16	*SOS1*	c.770C > T	New mutations	1	Pulmonary valve dysplasia with stenosis (moderate); biventricular hypertrophy	Right ventricular hypertrophy	1.5
Case 6	F	11	*PTPN11*	c.174C > G	New mutations	2	Pulmonary valve stenosis (mild); PFO; left pulmonary artery stenosis	Normal	No
Case 7	M	23	*PTPN11*	c.922A > G	New mutations	1	Pulmonary valve stenosis (mild); ASD	Normal	No
Case 8	F	36	*RAF1*	c.770C > T	New mutations	1	Obstructive HCM; mitral regurgitation (moderate-severe)	QTc prolonged, electric axis deviated to the left, T wave changed	1.25
Case 9	M	96	*PTPN11*	c.922A > G	New mutations	1	Pulmonary valve bicuspid with regurgitation; ASD; tricuspid regurgitation; right aortic coronary valve prolapse with regurgitation	Sinus arrhythmia, electric axis deviated to the left, I, avL leads abnormal Q wave	0.5
Case 10	M	20	*PTPN11*	c.188A > G	New mutations	1	Pulmonary valve stenosis (mild); ASD	Normal	1
Case 11	M	0.7	*RAF1*	c.770C > T	New mutations	1	Left ventricular hypertrophy; ASD	Frequent atrial premature beats	No
Case 12	F	7	*RIT1*	c.284G > C	New mutations	1	Pulmonary valve stenosis with regurgitation (mild); ASD; PFO	Right ventricular hypertrophy	3
Case 13	M	23	*BRAF*	c.1502A > G	New mutations	2	Pulmonary valve stenosis (severe); mitral regurgitation (mild-moderate); biventricular hypertrophy; ASD	Atrial hypertrophy, left and right ventricular hypertrophy	1.5
Case 14	F	49	*SOS2*	c.458G > A	New mutations	2	Pulmonary valve stenosis (severe) with regurgitation (mild)	Right ventricular hypertrophy	0.25
Case 15	F	5	*BRAF*	c.1796C > G	New mutations	1	Pulmonary valve stenosis (mild)	Normal	No
Case 16	M	22	*LZTR1*	c.742G > A	New mutations	1	Left ventricle globose dilated	Normal	2
Case 17	F	108	*BRAF*	c.736G > C	New mutations	2	Obstructive HCM; mitral regurgitation (severe); tricuspid regurgitation (mild)	Normal	No
Case 18	M	12	*PTPN11*	c.922A > G	New mutations	1	No obstructive HCM; ASD; PFO	Normal	1
Case 19	M	66	*RAF1*	c.775T > A	New mutations	1	Obstructive HCM; mitral regurgitation (mild)	Normal	1
Case 20	F	168	*RAF1*	c.1082G > C	New mutations	2	Obstructive HCM; mitral regurgitation (mild)	Sinus bradycardia with irregularities,II,III, aVF abnormal Q wave	No
Case 21	M	36	*PTPN11*	c.124A > G	New mutations	1	Pulmonary valve stenosis (severe); VSD, ASD, PDA	Complete right bundle branch block, right ventricular hypertrophy	2
Case 22	M	60	*RAF1*	c.775T > A	New mutations	1	Left ventricular hypertrophy; mitral regurgitation (severe); tricuspid regurgitation (mild)	No	No

Abbreviations: HCM, hypertrophic cardiomyopathy; PFO, patent foramen ovale; ASD, atrial septal defect; PDA, patent ductus arteriosus; VSD, ventricular septal defect; ACMG, american college of medical genetics.

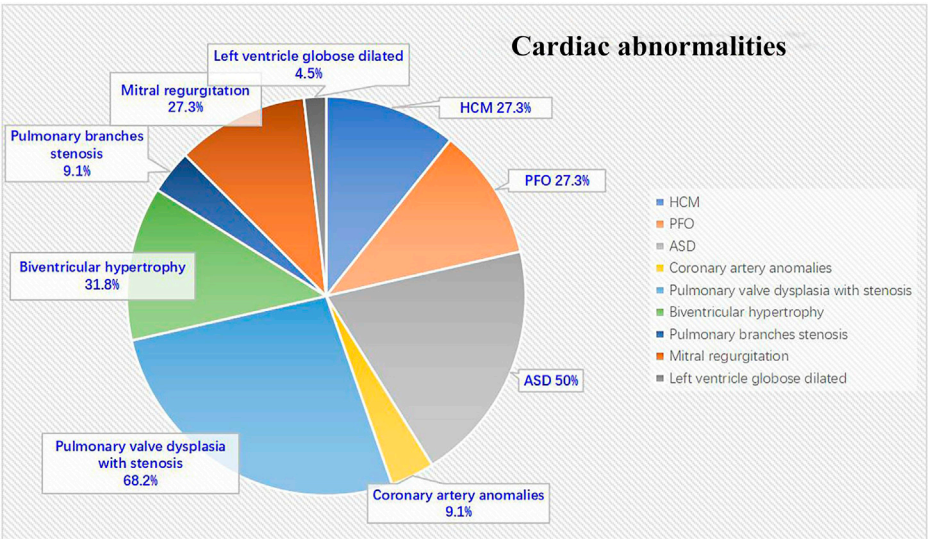


FIGURE 1 | Cardiac abnormalities in NS patients (N = 22).

Statistical Analysis

Continuous variables are presented as mean ± standard deviation if normally distributed, otherwise they are presented as the median (interquartile range). Categorial variables are presented as number and proportion. All analyses were performed using SPSS Statistics 23 software (IBM, Chicago, IL, United States).

RESULTS

Electrocardiographic Findings

A total of 22 children with NS were included in the current analysis. There were 11 female patients and 10 male patients. Their ages ranged from 0.7 to 168 months old (mean age: 39.5 ± 41.6 months). All patients had confirmed diagnoses by molecular analysis. The preoperative echocardiography and electrocardiogram features and genotypes are listed in **Table 1**. Follow-up ranged from 0.5 to 3 years (mean follow-up: 1.02 ± 0.94 years). Case 22 had no follow-up and no electrocardiogram. Thirteen cases (62%) had electrocardiographic abnormalities. The main manifestations of electrocardiogram abnormalities were QTc prolongation, abnormal Q wave in the precordial lead and limb lead, right ventricular hypertrophy and left or right deviation of the electrical axis.

Cardiac Abnormalities

All 22 NS patients had cardiac abnormalities. The most commonly detected abnormality was pulmonary valve dysplasia with stenosis, seen in 15 (68.2%) patients, followed by atrial septal defect (ASD) in 11 (50%) patients, biventricular hypertrophy in seven (31.8%) patients, left HCM in six (27.3%) patients, mitral regurgitation in six (27.3%) patients, patent foramen ovale (PFO) in six (27.3%) patients, both coronary artery anomalies and pulmonary branches stenosis in two (9.1%) patients and left ventricle globose dilated in one (4.5%) patient (**Figure 1**).

Genotype–Cardiac Phenotype Abnormalities

The genotype distribution in the 22 NS patients is listed in **Figure 2**, including mutation of *RAF1* in six patients (27%), *RIT1* in three patients (14%), *SOS1* in two patients (9%), *PTPN11* in six patients (27%), *BRAF* in three patients (14%), *SOS2* in one patient (4.5%) and *LZTR1* in one patient (4.5%). The most commonly observed genetic mutations in patients were in *PTPN11* and *RAF1*. Each genotype had specific echocardiography findings. Patients with *RAF1* mutations were characterized by left ventricular hypertrophy (obstructive or not obstructive), ASD and mitral regurgitation. Patients with *RIT1* mutation were characterized by pulmonary valve dysplasia with stenosis and ASD/PFO. Patients with mutations in *SOS1* had pulmonary valve dysplasia with stenosis, biventricular hypertrophy and ASD. *PTPN11*-mutation carriers had

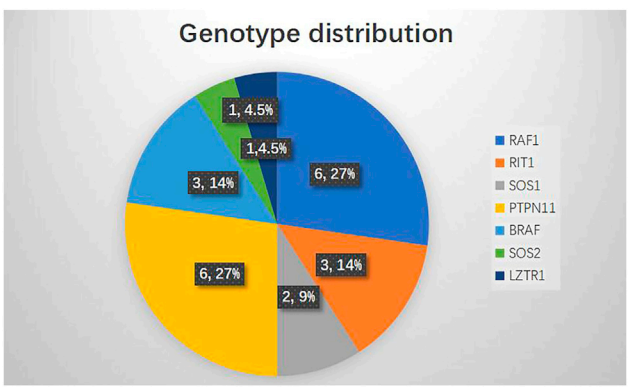


FIGURE 2 | Genotype distribution in NS patients (N = 22).

TABLE 2 | Genotype–cardiac phenotype abnormalities in NS patients (N = 22).

Genotype	Cardiac Echo prestation	N (%)
RAF1	Left ventricular hypertrophy (obstructive or un- obstructive), ASD, mitral regurgitation	6 (27)
RIT1	Pulmonary valve dysplasia with stenosis, ASD/PFO	3 (14)
SOS1	Pulmonary valve dysplasia with stenosis, biventricular hypertrophy, ASD	2 (9)
PTPN11	Pulmonary valve stenosis, ASD	6 (27)
BRAF	Pulmonary valve stenosis, Obstructive HCM, ASD, mitral regurgitation	3 (14)
SOS2	Pulmonary valve stenosis with regurgitation	1 (4.5)
LZTR1	Left ventricle globose dilated	1 (4.5)

Abbreviations: HCM, hypertrophic cardiomyopathy; PFO, patent foramen ovale; ASD, atrial septal defect.

TABLE 3 | Catheter or surgery-based interventions and follow-up clinical data.

Case	Age (m)	Genotype	Procedure type	Follow-up (y)	PV* (mmHg)	PV# (mmHg)	LVOT* (mmHg)	LVOT# (mmHg)	RVOT* (mmHg)	RVOT# (mmHg)
Case 3	10	*SOS1*	PBPV, right ventricular outflow tract dredge + pulmonary valve formation (GOTX bicuspid valve) + atrial septal defect repair	2	99	45	—	—	—	—
Case 4	15	*RIT1*	PBPV, right ventricular outflow tract dredge + pulmonary valve formation (GOTX bicuspid valve) + atrial septal defect repair	1	112	22	—	—	43	19
Case 5	16	*SOS1*	PBPV	1.5	64	42	—	—	—	—
Case 8	36	*RAF1*	Morrow, mitral valvuloplasty, left ventricular + right ventricular outflow tract dredge	1.25	—	—	75	80	33	11
Case 9	96	*PTPN11*	Percutaneous closure of atrial septal defect	0.5	—	—	—	—	—	—
Case 10	20	*PTPN11*	Percutaneous closure of atrial septal defect	1	23	9	—	—	—	—
Case 13	23	*BRAF*	right ventricular outflow tract dredge + pulmonary valve formation (GOTX bicuspid valve) + atrial septal defect repair	1.5	110	62	—	—	83	29
Case 14	49	*SOS2*	PBPV	0.25	95	20	—	—	—	—
Case 17	108	*BRAF*	Left ventricular outflow tract dredge + mitral valve replacement	No	—	—	128	—	—	—
Case 21	36	*PTPN11*	PBPV, pulmonary valve formation + ASD + VSD repair + PDA ligation	2	71	57	—	—	76	64

Abbreviations, preoperative peak pressure; #, the last postoperative follow-up peak pressure; PV, pulmonary valve; —, no pressure or loss to follow-up; RVOT, right ventricular outflow tract; LVOT, left ventricular outflow tract.*

pulmonary valve stenosis and ASD. *BRAF* carriers had pulmonary valve stenosis, obstructive HCM, ASD, and mitral regurgitation. *SOS2*-mutation carriers had pulmonary valve stenosis with regurgitation. Only one patient carrying a LZTR1 mutation had left ventricle globose dilation (**Table 2**). Among all the pathogenic variants, we found that patients with mutations in *RIT1*, *SOS1*, *PTPN11*, and *SOS2* had common echocardiography figures characterized by pulmonary valve stenosis, while *RAF1* patients had HCM. Interestingly, *BRAF* patients were characterized not only by HCM but also by pulmonary valve stenosis, meaning poor prognoses.

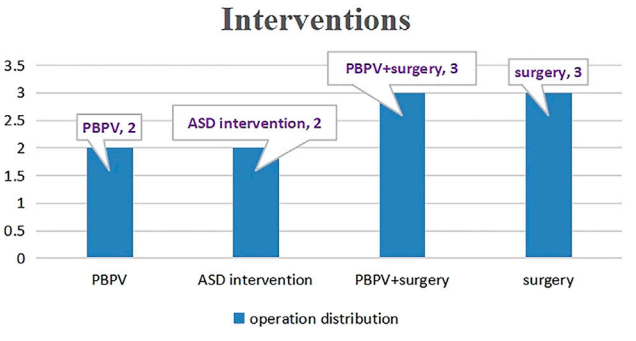


FIGURE 3 | Operation distributions in interventions patients.

Catheter or Surgery-Based Interventions and Follow-Up Data

A total of ten cases underwent catheter or surgery-based interventions (**Table 3**). Percutaneous balloon pulmonary valve dilation (PBPV) was seen in two (20%) patients, percutaneous closure of ASD in two (20%) patients and complex surgery in three (30%) patients. Another three cases

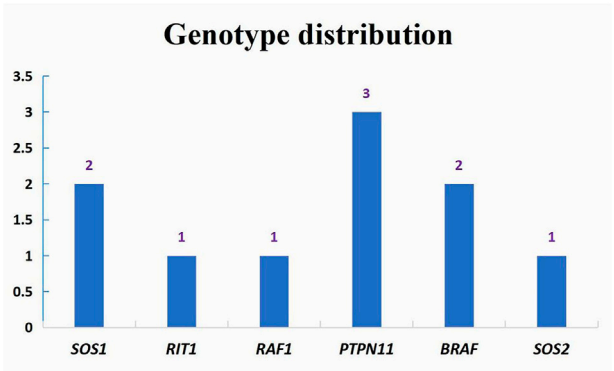


FIGURE 4 | Genotype distribution in interventions patients.

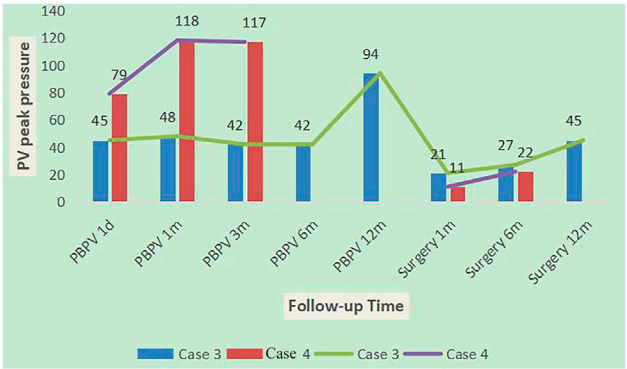


FIGURE 5 | Follow-up results in case 3 and case 4.

underwent not only PBPV, but also complex surgery because of poor outcomes (**Figure 3**). The genotype distribution in 10 NS patients is listed in **Figure 4**, including *SOS1* in two patients (20%), *RIT1* in one patient (10%), *RAF1* in one patient (10%), *PTPN11* in three patients (30%), *BRAF* in two patients (20%) and *SOS2* in one patient (10%). All surgeries had immediate results and high success rates. However, some of the cases had adverse outcomes during extended follow-up. According to the follow-up results of the last echocardiography, the degree of pulmonary valve stenosis and the left ventricular outflow tract severity were determined from measurements of mean and peak gradients across the obstruction, and were quantitatively divided into mild, medium, and severe grades, following the recommendations of ESC guidelines (Baumgartner et al., 20202021) and EAE/ASE (Baumgartner et al., 2009). *SOS1, RIT1, PTPN11*, and *SOS2* mutations seemed to have good prognosis, while *BRAF* mutations and *RAF1* mutations seemed to have poor prognosis because of medium or severe mean and peak gradients across the obstruction of pulmonary valve or the left ventricular outflow tract.

Among ten NS patients, cases 3, 4, and 21 had common features of pulmonary valve dysplasia with stenosis, and each experienced interventions twice. The first interventions for cases 3 and 4 were PBPV, but afterward, the pulmonary valve peak differential pressures increased gradually at 1 year of follow-up, and both patients then experienced a second intervention [right ventricular outflow tract dredge + pulmonary valve (GOTX bicuspid valve) formation]. After 1 year of follow-up, the peak differential pressure of the pulmonary valve increased gradually, but more slowly than PBPV (**Figure 5**). The first intervention of case 21 was pulmonary valve formation, ASD and VSD repair and PDA ligation in another hospital, but 2 years later, the pulmonary valve peak differential pressure was 71 mmHg, so PBPV was performed in our hospital. After 2 years of follow-up, the peak differential pressure of the pulmonary valve was 57 mmHg. From the clinical data, we speculate that PBPV was not a good choice for NS patients. Three patients had only complex surgery. Case 13 and 17 with *BRAF* mutation showed pulmonary valve stenosis or HCM. Case 13 underwent right ventricular outflow tract dredge, pulmonary valve formation (GOTX bicuspid valve) and ASD repair. The pulmonary valve peak differential pressure decreased from 110 to 62 mmHg after 1 and a half years. Case 17 was lost to follow-up. Before the operation, the patient had severe left ventricular outflow tract stenosis and mitral regurgitation. Case 8, with a *RAF1* mutation, showed severe obstructive HCM and mitral regurgitation, then underwent Morrow and mitral valvuloplasty procedures. However, the left ventricular outflow tract peak differential pressure still increased to 80 mmHg after 15 months, which was not a good outcome. Thus, for HCM in NS patients, surgery appears to lead to poor outcomes.

DISCUSSION

NS is the second most common syndromic cause of congenital heart disease, exceeded in prevalence only by trisomy 21 (Marino et al., 1999). Cardiac defects problems are the most common reasons that prompted these patients to see a doctor. There are several cardiovascular phenotypes abnormalities in NS. The most common phenotypes are pulmonary valve dysplasia with stenosis (50–62%), HCM (20%), ASDs (6–10%) and unusual electrocardiographic patterns (50%). Other cardiac abnormalities were also noted, like peripheral pulmonary stenosis, ventricular septal defect, mitral valve abnormalities, atrioventricular canal, aortic valve stenosis, aortic coarctation and coronary artery anomalies (Sanchez-Cascos, 1983; Patton, 1994; Shaw et al., 2007). Rarely, tetralogy of Fallot or patent ductus arteriosus are observed in NS. Often, patients display complex cardiac phenotypes with multiple defects such as pulmonary valve stenosis and aortic valve stenosis or CHD and HCM (Prendiville et al., 2014). This result is not entirely consistent with our clinical data from a single center. In this study, we found that the most commonly detected abnormality was pulmonary valve dysplasia with stenosis (68.2%), followed by ASD (50%), biventricular hypertrophy (31.8%), left HCM (27.3%), mitral regurgitation (27.3%), PFO (27.3%), both coronary artery anomalies and pulmonary branches stenosis (9.1%) and left ventricle globose dilation (4.5%). In particular, the incidence of ASD was significantly higher than that reported in literature, due to the small cohort. Also, we observed left ventricle globose dilation, which has not been reported in previous literature. The presentation was similar to dilated cardiomyopathy.

With the development of whole-exome sequencing, genetic testing is very useful for diagnosis of NS or NS-like disorders. If a patient has a mild or atypical presentation, genotyping could establish the diagnosis. To establish better treatment and management, it is necessary to look for genotype-phenotype associations with respect to NS-associated CHD phenotypes. There are eight known genotypes that cause NS, in the genes *PTPN11*, *SOS1*, *RAF1*, *KRAS*, *NRAS*, *BRAF*, *SHOC2*, and *CBL* (Romano et al., 2010). Recently, however, studies have found several novel genes associated with NS, like *RIT1*, *RASA2*, *A2ML1*, *SOS2* and *LZTR1* (Aoki et al., 2016). In our study, we detected variants in seven genes associated with NS. Mutations in four known genes (*PTPN11*, *RAF1*, *SOS1*, *BRAF*) and three novel genes (*RIT1*, *SOS2*, *LZTR1*) and, overall, *PTPN11* (27%) and *RAF1* (27%) were the most common.

PTPN11 encodes the Src homology-2 domain containing protein tyrosine phosphatase (Tartaglia et al., 2001; Tartaglia et al., 2002; Tartaglia et al., 2010). Studies suggest that 50% of cases of NS are caused by missense, gain-of-function mutations in *PTPN11* (Tartaglia et al., 2001; Maheshwari et al., 2002; Tartaglia et al., 2002). NS in patients with *PTPN11* mutations is more likely be associated with pulmonary valve stenosis or ASD (ostium secundum type) (Yoshida et al., 2004; Sznajer et al., 2007). This is consistent with the findings of our study. Six patients had pulmonary valve stenosis or ASD with *PTPN11* mutations. *RAF1* was another commonly mutated gene, often associated with HCM and negatively associated with pulmonary valve stenosis (Pandit et al., 2007). NS cases with *RAF1* mutations were estimated to comprise 5–15% of the population (Pandit et al., 2007; Razzaque et al., 2007). *RAF1* mutations prevent the phosphorylation of Ser259, causing a gain of function of the kinase, contributing to the autoinhibition of RAF1, affecting the activation loop and reducing the activity of the kinase (Pandit et al., 2007; Tidyman and Rauen, 2009). Our study found that six patients had *RAF1* mutations, and the cardiac abnormalities included not only HCM (obstructive or non-obstructive), but also ASD and mitral regurgitation. *SOS1* mutations most often result in pulmonary valve stenosis, much like *PTPN11* mutations (Lepri et al., 2011). Missense mutations in *SOS1* account for roughly 10% of cases of NS (Tidyman and Rauen, 2009; Tartaglia et al., 2010), close to our study results (9%). The protein product of *SOS1* is a guanine nucleotide exchange factor that activates RAS proteins by displacing GDP, enabling GTP to bind through mass action (Egan and Weinberg, 1993; Takai et al., 2001). Other than pulmonary valve stenosis, *SOS1* was associated with pulmonary valve dysplasia, biventricular hypertrophy and ASD in our study. *BRAF* mutations were rare, but have also been reported in individuals meeting clinical diagnostic criteria for NS. *BRAF* mutation-associated NS is characterized by HCM (Razzaque et al., 2007; Nyström et al., 2008; Sarkozy et al., 2009). However, *BRAF* predisposed patients to both HCM and valve abnormalities and accounted for roughly 14% of cases of NS in our study.

Three novel genotypes were also related to cardiac abnormalities. The mutations in *RIT1* in NS patients are located in its G1 domain (p.S35T) and in the switch I region that is included in its G2 domain (p.A57G) (Aoki et al., 2016). Chen et al. (Chen et al., 2014) identified *RIT1* mutations in five out of 27 (18.5%) individuals with NS. Bertola et al. (Bertola et al., 2014) and Gos et al. (Gos et al., 2014) identified *RIT1* mutations in six out of 70 (8.6%) individuals and four out of 106 individuals (3.8%), respectively. Aoki et al. (Aoki et al., 2016) suggested that the frequency of *RIT1* mutations can be estimated at ~5% in patients with NS. Our study found that 3/22 (14%) NS patients had *RIT1* mutations, significantly higher than the data reported in the literature. This may be related to the ethnicity of the population and the small number of patients, which requires further study. *RIT1* mutations predispose patients to both HCM and valve abnormalities (Gelb et al., 2015), while our findings related to cardiac malformation were pulmonary valve dysplasia with stenosis, ASD and PFO. To date, few studies have reported cardiac abnormalities related to *SOS2* and *LZTR1*. *SOS2* is homologous to *SOS1*, and the identified variants, p.M267K and p.T376S, were located in the DH domain of *SOS2* (Aoki et al., 2016). In our study, we found that pulmonary valve stenosis with regurgitation was related to cardiac malformation, which was similar to *SOS1*. Another novel genotype in *LZTR1* had a unique cardiac phenotype, left ventricle globose dilation, with a presentation similar to dilated cardiomyopathy. *LZTR1* is located within the 3-Mb-long region that is often deleted in 22q11 deletion syndrome patients (Kurahashi et al., 1995). Some studies have found that somatic and germline mutations in *LZTR1* were associated with glioblastoma multiforme (Frattini et al., 2013) and multiple schwannomas (Piotrowski et al., 2014). Our study first reported this unique cardiac malformation related to *LZTR1*. Additional studies should be performed on mutational and cardiac malformation analyses.

A total of ten cases underwent catheter or surgery-based interventions in our study. Major interventions were PBPV, percutaneous closure of ASD and complex surgery. Cardiac malformations that require management were severe pulmonary valve stenosis, obstructive HCM and congenital heart disease of hemodynamic significance. In this group NS patients, we tried to describe the trend of prognosis for the correlations between genotypes and cardiac phenotypes according to the follow-up results of the last echocardiogram after catheter or surgery-based interventions. *SOS1*, *RIT1*, *PTPN11*, and *SOS2* mutations showed common cardiac abnormalities such as pulmonary valve stenosis. For mild pulmonary valve stenosis in NS, stenosis tends to be nonprogressive and unlikely to require intervention. For moderate or severe obstruction, like *BRAF* mutations and *RAF1* mutations, the rates of intervention are higher (~50 and 100%, respectively) (Linglart and Gelb, 2020). McCrindle reported that the standard intervention using PBPV was often not as successful as was typical for pulmonary valve stenosis because of frequent dysplasia with commissural fusion and thickened pulmonary valve leaflets (McCrindle, 1994). We found that some of the cases had good results via PBPV, such as case 5 and case 14 with mutations in *SOS1* and *SOS2*, respectively, but this may be related to our short follow-up period. Cases like case 3 and 4, with mutations in *SOS1* and *RIT1*, respectively, did not show good results after the first PBPV, so they underwent surgical valvotomy again, which appeared to be highly successful. However, case 21 with a mutation in *PTPN11* first underwent surgical valvotomy with poor results at 2 years of follow-up, then underwent PBPV again, which appeared to be successful. Holzmann et al. (Holzmann et al., 2018) reported that the pulmonary gradient remained unfavorably elevated in 80% of patients with NS after the initial PBPV and reintervention was

necessary in up to 65% of cases (Prendiville et al., 2014). The clinical data from our center suggests that multiple interventions may be required for NS patients with severe pulmonary stenosis, whether PBPV or valvulotomy. Additionally, when the first intervention fails, the second intervention appears to be highly successful. Additional follow-up data are needed.

.Obstructive HCM in NS is another complex problem in the clinic. It can lead to severe heart failure and arrhythmias with progression of HCM. Most patients prefer to choose surgery. In our study, two genotypes in *RAF1* and *BRAF* resulted in a common cardiac abnormality, obstructive HCM. These two genotypes seemed to have poor prognosis. While myectomy for HCM in a patient with NS is initially useful, with time, the left ventricular outflow tract may become obstructed again. Wilkinson et al. (Wilkinson et al., 2012) reported that patients with NS with HCM have a worse risk profile at presentation compared with other children with HCM, resulting in significant early mortality (22% at 1 year). Thus, heart transplantation may be a preferrable approach. It is encouraging that much progress has been made in our understanding of the molecular genetic causes of NS, and novel therapeutic drugs have been given to patients. To date, there are some publications describing the use of RAS pathway inhibition as useful for NS (Andelfinger et al., 2019; Mek Inhibitor Reverses Hypertrophic Cardiomyopathy, 2019; Dori et al., 2020; Meisner et al., 2021; Mussa et al., 2021; Kontaridis et al., 2022). Trametinib, a MEK-inhibitor approved for treatment of RAS/MAPK-mutated cancers, is an emerging treatment option for HCM in NS. Trametinib was given to two infants with the severe, rapidly progressive form of HCM with *RIT1* mutations and no adverse effects have been observed as of yet (Andelfinger et al., 2019). However, further study of the effects of trametinib and other pathway inhibitors for pulmonary valve stenosis or HCM in NS is necessary.

STUDY LIMITATIONS

The retrospective design of the study had some limitations. We tried to grade the correlations between genotypes and cardiac phenotypes according to the follow-up results of the last echocardiogram after catheter or surgery-based interventions. However, the relatively small size of the cohort may have biased the results. Since each genotype group consisted of only a few individuals, we limited our analysis to describing prognostic trends for cardiac phenotypes within each group.

CONCLUSION

Molecular diagnoses are enabling earlier and more precise identification of patients with a subtle or atypical presentation of NS. The identification of causal genes in NS patients has enabled the evaluation of genotype-cardiac phenotype relationships and may be beneficial to the development of therapeutic approaches. Although there are many extracardiac malformations, in some cases, progressive cardiac malformations still need to be managed, which will lead to better prognoses for patients with this disorder. In addition, NS-specific therapeutic medications require further research.

DATA AVAILABILITY STATEMENT

The original contributions presented in the study are included in the article/supplementary material, further inquiries can be directed to the corresponding authors.

ETHICS STATEMENT

The studies involving human participants were reviewed and approved by the Clinical Research Ethic Committee of Guangdong Provincial People's Hospital. Written informed consent to participate in this study was provided by the participants' legal guardian/next of kin. Written informed consent was obtained from the individual (s), and minor (s)' legal guardian/next of kin, for the publication of any potentially identifiable images or data included in this article.

AUTHOR CONTRIBUTIONS

LS contributed to conception and manuscript writing. Y-mX contributed to design and formal analysis. S-sW and Zw-Z contributed to editing, supervision and funding acquisition. All authors contributed to manuscript revision, read, and approved the submitted version.

FUNDING

This research was funded by the National Natural Science Foundation of China (grant number 82070321).

REFERENCES

Allanson, J. E., Hall, J. G., Hughes, H. E., Preus, M., Witt, R. D., Opitz, J. M., et al. (1985). Noonan Syndrome: the Changing Phenotype. *Am. J. Med. Genet.* 21 (3), 507–514. doi:10.1002/ajmg.1320210313

Andelfinger, G., Marquis, C., Raboisson, M.-J., Théoret, Y., Waldmüller, S., Wiegand, G., et al. (2019). Hypertrophic Cardiomyopathy in Noonan Syndrome Treated by MEK-Inhibition. *J. Am. Coll. Cardiol.* 73 (17), 2237–2239. doi:10.1016/j.jacc.2019.01.066

Aoki, Y., Niihori, T., Inoue, S.-i., and Matsubara, Y. (2016). Recent Advances in RASopathies. *J. Hum. Genet.* 61 (1), 33–39. doi:10.1038/jhg.2015.114

Aoki, Y., Niihori, T., Narumi, Y., Kure, S., and Matsubara, Y. (2008). The RAS/MAPK Syndromes: Novel Roles of the RAS Pathway in Human Genetic Disorders. *Hum. Mutat.* 29 (8), 992–1006. doi:10.1002/humu.20748

Baumgartner, H., De Backer, J., Babu-Narayan, S. V., Budts, W., Chessa, M., Diller, G. P., et al. (20202021). 2020 ESC Guidelines for the Management of Adult Congenital Heart Disease. *Eur. Heart J.* 42 (6), 563–645. doi:10.1093/eurheartj/ehaa554

Baumgartner, H., Hung, J., Bermejo, J., Chambers, J. B., Evangelista, A., Griffin, B. P., et al. (2009). Echocardiographic Assessment of Valve Stenosis: EAE/ASE

Recommendations for Clinical Practice. *Eur. J. Echocardiogr.* 10 (1), 1–25. quiz 101-2. doi:10.1093/ejechocard/jen303

Bertola, D. R., Yamamoto, G. L., Almeida, T. F., Buscarilli, M., Jorge, A. A. L., Malaquias, A. C., et al. (2014). Further Evidence of the Importance ofRIT1in Noonan Syndrome. *Am. J. Med. Genet.* 164 (11), 2952–2957. doi:10.1002/ajmg.a.36722

Calcagni, G., Adorisio, R., Martinelli, S., Grutter, G., Baban, A., Versacci, P., et al. (2018). Clinical Presentation and Natural History of Hypertrophic Cardiomyopathy in RASopathies. *Heart Fail. Clin.* 14 (2), 225–235. doi:10.1016/j.hfc.2017.12.005

Calcagni, G., Gagliostro, G., Limongelli, G., Unolt, M., De Luca, E., Digilio, M. C., et al. (2020). Atypical Cardiac Defects in Patients with RASopathies: Updated Data on CARNET Study. *Birth Defects Res.* 112 (10), 725–731. doi:10.1002/bdr2.1670

Chen, P.-C., Yin, J., Yu, H.-W., Yuan, T., Fernandez, M., Yung, C. K., et al. (2014). Next-generation Sequencing Identifies Rare Variants Associated with Noonan Syndrome. *Proc. Natl. Acad. Sci. U.S.A.* 111 (31), 11473–11478. doi:10.1073/pnas.1324128111

Dori, Y., Smith, C., Pinto, E., Snyder, K., March, M. E., Hakonarson, H., et al. (2020). Severe Lymphatic Disorder Resolved with MEK Inhibition in a Patient with Noonan Syndrome and SOS1 Mutation. *Pediatrics* 146 (6). doi:10.1542/peds.2020-0167

Egan, S. E., and Weinberg, R. A. (1993). The Pathway to Signal Achievement. *Nature* 365 (6449), 781–783. doi:10.1038/365781a0

Frattini, V., Trifonov, V., Chan, J. M., Castano, A., Lia, M., Abate, F., et al. (2013). The Integrated Landscape of Driver Genomic Alterations in Glioblastoma. *Nat. Genet.* 45 (10), 1141–1149. doi:10.1038/ng.2734

Gelb, B. D., Roberts, A. E., and Tartaglia, M. (2015). Cardiomyopathies in Noonan Syndrome and the Other RASopathies. *Prog. Pediatr. Cardiol.* 39 (1), 13–19. doi:10.1016/j.ppedcard.2015.01.002

Gos, M., Fahiminiya, S., Poznański, J., Klapecki, J., Obersztyn, E., Piotrowicz, M., et al. (2014). Contribution ofRIT1mutations to the Pathogenesis of Noonan Syndrome: Four New Cases and Further Evidence of Heterogeneity. *Am. J. Med. Genet.* 164 (9), 2310–2316. doi:10.1002/ajmg.a.36646

Holzmann, J., Tibby, S. M., Rosenthal, E., Qureshi, S., Morgan, G., and Krasemann, T. (2018). Results of Balloon Pulmonary Valvoplasty in Children with Noonan's Syndrome. *Cardiol. Young* 28 (5), 647–652. doi:10.1017/s1047951117002827

Johnston, J. J., van der Smagt, J. J., Rosenfeld, J. A., Pagnamenta, A. T., Alswaid, A., Baker, E. H., et al. (2018). Autosomal Recessive Noonan Syndrome Associated with Biallelic LZTR1 Variants. *Genet. Med.* 20 (10), 1175–1185. doi:10.1038/gim.2017.249

Kontaridis, M. I., Roberts, A. E., Schill, L., Schoyer, L., Stronach, B., Andelfinger, G., et al. (2022). The Seventh International RASopathies Symposium: Pathways to a Cure-Expanding Knowledge, Enhancing Research, and Therapeutic Discovery. *Am. J. Med. Genet. A* 188 (6), 1915–1927. doi:10.1002/ajmg.a.62716

Kurahashi, H., Akagi, K., Inazawa, J., Ohta, T., Niikawa, N., Kayatani, F., et al. (1995). Isolation and Characterization of a Novel Gene Deleted in DiGeorge Syndrome. *Hum. Mol. Genet.* 4 (4), 541–549. doi:10.1093/hmg/4.4.541

Leoni, C., Blandino, R., Delogu, A. B., De Rosa, G., Onesimo, R., Verusio, V., et al. (2022). Genotype-cardiac Phenotype Correlations in a Large Single-center Cohort of Patients Affected by RASopathies: Clinical Implications and Literature Review. *Am. J Med Genet. Pt A* 188 (2), 431–445. doi:10.1002/ajmg.a.62529

Lepri, F., De Luca, A., Stella, L., Rossi, C., Baldassarre, G., Pantaleoni, F., et al. (2011). SOS1 Mutations in Noonan Syndrome: Molecular Spectrum, Structural Insights on Pathogenic Effects, and Genotype-Phenotype Correlations. *Hum. Mutat.* 32 (7), 760–772. doi:10.1002/humu.21492

Linglart, L., and Gelb, B. D. (2020). Congenital Heart Defects in Noonan Syndrome: Diagnosis, Management, and Treatment. *Am. J. Med. Genet.* 184 (1), 73–80. doi:10.1002/ajmg.c.31765

Lioncino, M., Monda, E., Verrillo, F., Moscarella, E., Calcagni, G., Drago, F., et al. (2022). Hypertrophic Cardiomyopathy in RASopathies. *Heart Fail. Clin.* 18 (1), 19–29. doi:10.1016/j.hfc.2021.07.004

Maheshwari, M., Belmont, J., Fernbach, S., Ho, T., Molinari, L., Yakub, I., et al. (2002). PTPN11 Mutations in Noonan Syndrome Type I: Detection of Recurrent Mutations in Exons 3 and 13. *Hum. Mutat.* 20 (4), 298–304. doi:10.1002/humu.10129

Marino, B., Digilio, M. C., Toscano, A., Giannotti, A., and Dallapiccola, B. (1999). Congenital Heart Diseases in Children with Noonan Syndrome: An Expanded Cardiac Spectrum with High Prevalence of Atrioventricular Canal. *J. Pediatr.* 135 (6), 703–706. doi:10.1016/s0022-3476(99)70088-0

McCrindle, B. W. (1994). Independent Predictors of Long-Term Results after Balloon Pulmonary Valvuloplasty. Valvuloplasty and Angioplasty of Congenital Anomalies (VACA) Registry Investigators. *Circulation* 89 (4), 1751–1759. doi:10.1161/01.cir.89.4.1751

Meisner, J. K., Bradley, D. J., and Russell, M. W. (2021). Molecular Management of Multifocal Atrial Tachycardia in Noonan's Syndrome with MEK1/2 Inhibitor Trametinib. *Circ. Genom Precis. Med.* 14 (5), e003327. doi:10.1161/CIRCGEN.121.003327

Mek Inhibitor Reverses Hypertrophic Cardiomyopathy in RIT1 Mutated Noonan Syndrome: For the First Time, Hypertrophic Cardiomyopathy Was Reversed in Noonan Syndrome Associated with a RIT1 Mutation. *Am. J. Med. Genet. A.* 2019;179(8):1408–1409.doi:10.1002/ajmg.a.40456

Mussa, A., Carli, D., Giorgio, E., Villar, A. M., Cardaropoli, S., Carbonara, C., et al. (2021). MEK Inhibition in a Newborn with RAF1-Associated Noonan Syndrome Ameliorates Hypertrophic Cardiomyopathy but Is Insufficient to Revert Pulmonary Vascular Disease. *Genes. (Basel)* 13 (1). doi:10.3390/genes13010006

Nyström, A.-M., Ekvall, S., Berglund, E., Björkqvist, M., Braathen, G., Duchen, K., et al. (2008). Noonan and Cardio-Facio-Cutaneous Syndromes: Two Clinically and Genetically Overlapping Disorders. *J. Med. Genet.* 45 (8), 500–506. doi:10.1136/jmg.2008.057653

Pandit, B., Sarkozy, A., Pennacchio, L. A., Carta, C., Oishi, K., Martinelli, S., et al. (2007). Gain-of-function RAF1 Mutations Cause Noonan and LEOPARD Syndromes with Hypertrophic Cardiomyopathy. *Nat. Genet.* 39 (8), 1007–1012. doi:10.1038/ng2073

Patton, M. A. Noonan Syndrome: A Review. 1994;33:1–3.

Piotrowski, A., Xie, J., Liu, Y. F., Poplawski, A. B., Gomes, A. R., Madanecki, P., et al. (2014). Germline Loss-Of-Function Mutations in LZTR1 Predispose to an Inherited Disorder of Multiple Schwannomas. *Nat. Genet.* 46 (2), 182–187. doi:10.1038/ng.2855

Prendiville, T. W., Gauvreau, K., Tworog-Dube, E., Patkin, L., Kucherlapati, R. S., Roberts, A. E., et al. (2014). Cardiovascular Disease in Noonan Syndrome. *Archives Dis. Child.* 99 (7), 629–634. doi:10.1136/archdischild-2013-305047

Razzaque, M. A., Nishizawa, T., Komoike, Y., Yagi, H., Furutani, M., Amo, R., et al. (2007). Germline Gain-Of-Function Mutations in RAF1 Cause Noonan Syndrome. *Nat. Genet.* 39 (8), 1013–1017. doi:10.1038/ng2078

Richards, S., Aziz, N., Bale, S., Bick, D., Das, S., Gastier-Foster, J., et al. (2015). Standards and Guidelines for the Interpretation of Sequence Variants: a Joint Consensus Recommendation of the American College of Medical Genetics and Genomics and the Association for Molecular Pathology. *Genet. Med.* 17 (5), 405–424. doi:10.1038/gim.2015.30

Romano, A. A., Allanson, J. E., Dahlgren, J., Gelb, B. D., Hall, B., Pierpont, M. E., et al. (2010). Noonan Syndrome: Clinical Features, Diagnosis, and Management Guidelines. *Pediatrics* 126 (4), 746–759. doi:10.1542/peds.2009-3207

Sanchez-Cascos, A. (1983). The Noonan Syndrome. *Eur. Heart J.* 4 (4), 223–229. doi:10.1093/oxfordjournals.eurheartj.a061452

Sarkozy, A., Carta, C., Moretti, S., Zampino, G., Digilio, M. C., Pantaleoni, F., et al. (2009). GermlineBRAFmutations in Noonan, LEOPARD, and Cardiofaciocutaneous Syndromes: Molecular Diversity and Associated Phenotypic Spectrum. *Hum. Mutat.* 30 (4), 695–702. doi:10.1002/humu.20955

Shaw, A. C., Kalidas, K., Crosby, A. H., Jeffery, S., and Patton, M. A. (2007). The Natural History of Noonan Syndrome: a Long-Term Follow-Up Study. *Arch. Dis. Child.* 92 (2), 128–132. doi:10.1136/adc.2006.104547

Sznajer, Y., Keren, B., Baumann, C., Pereira, S., Alberti, C., Elion, J., et al. (2007). The Spectrum of Cardiac Anomalies in Noonan Syndrome as a Result of Mutations in the PTPN11 Gene. *Pediatrics* 119 (6), e1325–e1331. doi:10.1542/peds.2006-0211

Takai, Y., Sasaki, T., and Matozaki, T. (2001). Small GTP-Binding Proteins. *Physiol. Rev.* 81 (1), 153–208. doi:10.1152/physrev.2001.81.1.153

Tartaglia, M., Kalidas, K., Shaw, A., Song, X., Musat, D. L., van der Burgt, I., et al. (2002). PTPN11 Mutations in Noonan Syndrome: Molecular Spectrum, Genotype-Phenotype Correlation, and Phenotypic Heterogeneity. *Am. J. Hum. Genet.* 70 (6), 1555–1563. doi:10.1086/340847

Tartaglia, M., Mehler, E. L., Goldberg, R., Zampino, G., Brunner, H. G., Kremer, H., et al. (2001). Mutations in PTPN11, Encoding the Protein Tyrosine Phosphatase SHP-2, Cause Noonan Syndrome. *Nat. Genet.* 29 (4), 465–468. doi:10.1038/ng772

Tartaglia, M., Zampino, G., and Gelb, B. D. (2010). Noonan Syndrome: Clinical Aspects and Molecular Pathogenesis. *Mol. Syndromol.* 1 (1), 2–26. doi:10.1159/000276766

Tidyman, W. E., and Rauen, K. A. (2009). The RASopathies: Developmental Syndromes of Ras/MAPK Pathway Dysregulation. *Curr. Opin. Genet. Dev.* 19 (3), 230–236. doi:10.1016/j.gde.2009.04.001

Wilkinson, J. D., Lowe, A. M., Salbert, B. A., Sleeper, L. A., Colan, S. D., Cox, G. F., et al. (2012). Outcomes in Children with Noonan Syndrome and Hypertrophic Cardiomyopathy: a Study from the Pediatric Cardiomyopathy Registry. *Am. Heart J.* 164 (3), 442–448. doi:10.1016/j.ahj.2012.04.018

Yi, J.-S., Perla, S., and Bennett, A. M. (2022). An Assessment of the Therapeutic Landscape for the Treatment of Heart Disease in the RASopathies. *Cardiovasc Drugs Ther.* doi:10.1007/s10557-022-07324-0

Yoshida, R., Hasegawa, T., Hasegawa, Y., Nagai, T., Kinoshita, E., Tanaka, Y., et al. (2004). Protein-tyrosine Phosphatase, Nonreceptor Type 11 Mutation Analysis and Clinical Assessment in 45 Patients with Noonan Syndrome. *J. Clin. Endocrinol. Metab.* 89 (7), 3359–3364. doi:10.1210/jc.2003-032091

Conflict of Interest: The authors declare that the research was conducted in the absence of any commercial or financial relationships that could be construed as a potential conflict of interest.

Publisher's Note: All claims expressed in this article are solely those of the authors and do not necessarily represent those of their affiliated organizations, or those of the publisher, the editors and the reviewers. Any product that may be evaluated in this article, or claim that may be made by its manufacturer, is not guaranteed or endorsed by the publisher.

Copyright © 2022 Sun, Xie, Wang and Zhang. This is an open-access article distributed under the terms of the Creative Commons Attribution License (CC BY). The use, distribution or reproduction in other forums is permitted, provided the original author(s) and the copyright owner(s) are credited and that the original publication in this journal is cited, in accordance with accepted academic practice. No use, distribution or reproduction is permitted which does not comply with these terms.

frontiers | Frontiers in Genetics

ORIGINAL RESEARCH
published: 22 June 2022
doi: 10.3389/fgene.2022.868159

The *EIF2AK4*/rs4594236 AG/GG Genotype Is a Hazard Factor of Immunoglobulin Therapy Resistance in Southern Chinese Kawasaki Disease Patients

Hongyan Yu[1†], Fucheng Liu[2†], Kaining Chen[1], Yufen Xu[1], Yishuai Wang[1], Lanyan Fu[1], Huazhong Zhou[1], Lei Pi[1], Di Che[1], Hehong Li[3] and Xiaoqiong Gu[1,4]**

[1]Department of Clinical Biological Resource Bank, Guangdong Provincial Key Laboratory of Research in Structural Birth Defect Disease, Guangzhou Institute of Pediatrics, Guangzhou Women and Children's Medical Center, Guangzhou Medical University, Guangzhou, China, [2]Department of Cardiology, The First Affiliated Hospital of Jinan University, Guangzhou, China, [3]Department of Radiology, Guangzhou Women and Children's Medical Center, Guangzhou Medical University, Guangzhou, China, [4]Department of Blood Transfusion and Clinical Lab, Guangzhou Institute of Pediatrics, Guangzhou Women and Children's Medical Center, Guangzhou Medical University, Guangzhou, China

OPEN ACCESS

Edited by:
Tieliu Shi,
Hunan University of Arts and Science, China

Reviewed by:
Fatma Savran Oguz,
Istanbul University, Turkey
Hiromichi Hamada,
Chiba University, Japan

***Correspondence:**
Hehong Li
hornc@163.com
Xiaoqiong Gu
guxiaoqiong@gwcmc.org

[†]These authors have contributed equally to this work

Specialty section:
This article was submitted to Genetics of Common and Rare Diseases, a section of the journal Frontiers in Genetics

Received: 02 February 2022
Accepted: 16 May 2022
Published: 22 June 2022

Citation:
Yu H, Liu F, Chen K, Xu Y, Wang Y, Fu L, Zhou H, Pi L, Che D, Li H and Gu X (2022) The EIF2AK4/rs4594236 AG/GG Genotype Is a Hazard Factor of Immunoglobulin Therapy Resistance in Southern Chinese Kawasaki Disease Patients. Front. Genet. 13:868159. doi: 10.3389/fgene.2022.868159

Background: Kawasaki disease (KD) is an acute, self-limited vasculitis disorder of unknown etiology in children. Immunologic abnormalities were detected during the acute phase of KD, which reflected that the effect cells of the activated immune system markedly increased cytokine production. High-dose intravenous immunoglobulin (IVIG) therapy is effective in resolving inflammation from KD and reducing occurrence of coronary artery abnormalities. However, 10%–20% of KD patients have no response to IVIG therapy, who were defined as IVIG resistance. Furthermore, these patients have persistent inflammation and increased risk of developing coronary artery aneurysm (CAA). *EIF2AK4* is a stress sensor gene and can be activated by pathogen infection. In addition, the polymorphisms of *EIF2AK4* were associated with various blood vessel disorders. However, it remains unclear whether the *EIF2AK4* gene polymorphisms were related to IVIG therapy outcome in KD patients.

Methods: *EIF2AK4*/rs4594236 polymorphism was genotyped in 795 IVIG response KD patients and 234 IVIG resistant KD patients through TaqMan, a real-time polymerase chain reaction. The odds ratios (ORs) and 95% confidence intervals (CIs) were calculated to assess the strength of association between *EIF2AK4*/rs4594236 polymorphism and IVIG therapeutic effects.

Results: Our results showed that the *EIF2AK4*/rs4594236 AG/GG genotype was significantly associated with increased risk to IVIG resistance compared to the AA genotype (AG vs. AA: adjusted ORs = 1.71, 95% CIs = 1.17–2.51, and $p = 0.0061$; GG vs. AA: adjusted ORs = 2.09, 95% CIs = 1.36–3.23, and $p = 0.0009$; AG/GG vs. AA: adjusted ORs = 1.82, 95% CIs = 1.27–2.63, and $p = 0.0013$; and GG vs. AA/AG: adjusted ORs = 1.45, 95% CI = 1.04–2.02, and $p = 0.0306$). Furthermore, the stratified analysis of

age and gender in the KD cohort indicated that male patients carrying the rs4594236 AG/GG genotype tends to be more resistant to IVIG therapy than female patients.

Conclusion: These results suggested that *EIF2AK4*/rs4594236 polymorphism might be associated with increased risk of IVIG resistance in southern Chinese KD patients.

Keywords: Kawasaki disease, IVIG resistance, polymorphism, *EIF2AK4*/rs4594236, intravenous immunoglobulin

INTRODUCTION

Kawasaki disease (KD) is an acute, self-limited vasculitis disease in children aged from 6 months to 5 years (Burns and Glodé, 2004). Immunologic abnormalities were detected during the acute phase of KD, which reflected that the effect cells of the activated immune system markedly increased cytokine production (Burns and Glodé, 2004). The etiology of KD is unknown, while several epidemiological and clinical reports have suggested that KD might be triggered by infectious agents or viruses (Sharma et al., 2021). This was evidenced by the fact that proinflammatory cytokines (IL-6, IL-10, TNFα, and IFNγ) were increased significantly in the acute stage of KD (Wang et al., 2013). Since lots of cytokines and activated immune cells attacked medium-sized arteries, especially coronary arteries, 20%–25% of untreated patients will develop coronary artery aneurysm (CAA) (Gersony, 2009), which has made KD the leading cause of acquired heart disease among children in developed countries (Kato et al., 1975).

Intravenous immunoglobulin (IVIG) contains pooled immunoglobulin G (IgG) from the plasma of over thousand blood donors and is widely used in people with weakened immune systems or other diseases to fight off infections (Lünemann et al., 2015). High-dose IVIG therapy is effective in resolving inflammation from KD and reducing occurrence of CAA. However, 10%–20% of KD patients will develop IVIG resistance, defined by recrudescent or persistent fever for over 36 h after the end of the IVIG infusion primary therapy. In addition, these patients have persistent inflammation and increased risk of developing CAA (McCrindle et al., 2017). Therefore, uncovering the mechanism of IVIG resistance in KD is urgently needed. While the mechanism of IVIG action is complicated and how it works on KD is still confused and unknown, at present, several studies have shown that genetic polymorphisms, especially some immune functional genes, are associated with IVIG resistance, such as inositol 1.4.5-trisposhate 3-kinase C (*ITPKC*), Fcγ IgG receptor 2A (*FCGR2A*), *CD40*, and interferon-gamma (*IFN-γ*) (Onouchi et al., 2008; Khor et al., 2011; Lee et al., 2012; Onouchi et al., 2013; Huang et al., 2016). These studies suggested that genetic factors might be involved in IVIG resistance.

Eukaryotic translation initiation factor 2-alpha kinase 4 (*EIF2AK4*, also known as *GCN2*) is a member of the kinase family that phosphorylates the alpha subunit of eukaryotic translation initiation factor-2 (eIF2a)(Wang et al., 2019). EIF2AK4 phosphorylates eIF2a on the serine 51 site and reduces GDP/GTP exchange activity subsequently. In addition, this resulted in mRNA translation changes and subsequently modulated cellular physiological activities (McGaha et al., 2012).

EIF2AK4 mutation was found in patients classified as having idiopathic and heritable pulmonary arterial hypertension (Hadinnapola et al., 2017). Histopathology of *EIF2AK4* mutation carriers in pulmonary veno-occlusive disease (PVOD) patients was distinctive from noncarriers regarding arterial remodeling, with significantly more severe intimal fibrosis and less severe medial hypertrophy (Nossent et al., 2018). Furthermore, under nutrient-deprived conditions, *EIF2AK4* could promote angiogensis of endothelial cells by increasing VEGF expression (Longchamp et al., 2018). These literature studies showed that *EIF2AK4* could modulate vascular remodeling and angiogensis, which are closely associated with coronary arterial lesions (CALs) of KD (Takahashi et al., 2013). What's more, *EIF2AK4* was also found to regulate cytokine production and macrophage function in several infectious diseases. *Eif2ak4* knockout mice challenged with lipopolysaccharide (LPS) showed reduced inflammatory response, including decreased IL-6 and IL-12 expression, as compared to wild-type mice (Liu et al., 2014). Interestingly, IL-6 and IL-10 were at a high level in the IVIG resistant group compared to the IVIG response group after IVIG treatment (Wang et al., 2013). In inflammatory kidney disease, IFN-γ–activated EIF2AK4 could suppress proinflammatory cytokine production in glomeruli and reduce macrophage recruitment to the kidneys (Chaudhary et al., 2015), while Ravindran et al. (2016) showed that EIF2AK4 also controlled intestinal inflammation through inhibiting inflammasome activation and IL-1β production. In conclusion, these studies indicate that *EIF2AK4* may be associated with KD.

Our team has worked on the area of the etiology and therapy effect of KD for many years (Che et al., 2018; Lin et al., 2021; Wang et al., 2021). We found that the single-nucleotide polymorphism (SNP) of immune and/or cardiovascular-related genes were usually related to IVIG therapy outcome of KD, such as *IL-1β* (Fu et al., 2019), *PLA2G7* (Gu et al., 2020), *P2RY12* (Wang et al., 2020), and *MRP4* (Wang et al., 2021). However, evidence regarding the polymorphisms of *EIF2AK4* and IVIG resistance of KD is very scarce. Based on this background, we performed this epidemiology study to investigate whether *EIF2AK4* is related to IVIG resistance of KD by examining the association between *EIF2AK4* polymorphism (rs4594236) and the risk of IVIG resistance of KD.

MATERIALS AND METHODS

Study Subjects

A total of 1,029 KD patients from the Guangzhou Women and Children's Medical Center between January 2014 and December 2019 were enrolled in this study. All individuals with KD were

diagnosed by pediatricians based on the criteria of the American Heart Association (Newburger et al., 2004; McCrindle et al., 2017). IVIG resistance was defined as persistent or recrudescent fever (temperature ≥38.0°C, measured axilla or orally) for over 36 h, but for a period of less than 7 days, after completion of the first IVIG infusion (2 g/kg).

Polymorphism Genotyping and DNA Extraction

Peripheral blood was collected from KD patients after treatment completion. Genomic DNA was extracted with a TIANamp Blood DNA Kit (DP318, TIANGEN Biotech, Beijing) following the guidance of the manufacturer's instructions (Wu et al., 2020). Specific fluorescent allele probes for rs4594236 were purchased from ABI (Thermo Fisher Scientific, United States). PCR was performed in 384-well plates with an ABI-Q6 Sequence Detection System machine (Thermo Fisher Scientific).

The genotyping of the SNP was conducted using a TaqMan SNP genotyping assay (Lin et al., 2021). Laboratory technicians were blind to the sample information, including the identities of the replicate aliquots. 10% of the samples from both groups were arbitrarily chosen to repeat the genotyping results. A concordance rate of 100% was obtained.

Statistical Analysis

Statistical analysis of this study was performed by using SAS software (version 9.4; SAS Institute, Cary, NC). Pearson's chi square test was used to evaluate the significant differences between IVIG response and IVIG resistant cases in the distribution of demographic variables and genotype frequency. Odds ratios (ORs) and 95% confidence intervals (CIs) were calculated by logistic regression analysis for measuring the association between the *EIF2AK4*/rs4594236 polymorphism and the risk of IVIG treatment resistance in KD patients. Furthermore, stratification analysis was performed, classified by age and gender. We also performed the eQTL analysis using the GTEx Portal web site (https://www.gtexportal.org/home/) to predict potential associations between the SNP and gene-expression levels (Consortium, 2013). A p-value of less than 0.05 was regarded as statistically significant.

RESULTS

Population Characteristics

The characteristic distribution of 795 IVIG therapy response KD patients and 234 IVIG therapy resistant KD patients is shown in **Table 1**. The average age of the IVIG response group was 25.14 ± 20.33 months (rang 1–131 months), and it was 26.08 ± 21.80 months (rang 2–132 months) for the IVIG resistant group. 67.17% of the KD patients who were responsive to IVIG therapy were men, and the male ratio was 72.65% in KD patients who were resistant to IVIG therapy. The proportion of women was 32.83% and 27.35%, respectively, while there were no significant difference in age (p = 0.3750) and gender (p = 0.1096) between the IVIG response group and the resistant group.

Analysis of the Association Between *EIF2AK4*/rs4594236 Polymorphism and Intravenous Immunoglobulin Resistance

The genotype frequency distribution of *EIF2AK4*/rs4594236 polymorphism in the KD IVIG resistant group and response group is described in **Table 2**. To explore the association between *EIF2AK4*/rs4594236 polymorphism and the risk to IVIG therapy resistance, we performed χ^2 test analysis. We found that *EIF2AK4*/rs4594236 polymorphism was significantly associated with increased IVIG therapy resistance risk in KD patients (AG vs. AA: adjusted OR = 1.71, 95% confidence interval (CI) = 1.17–2.51, and p = 0.0061; GG vs. AA: adjusted OR = 2.09, 95% confidence interval (CI) = 1.36–3.23, and p = 0.0009; AG/GG vs. AA: adjusted OR = 1.82, 95% CI = 1.27–2.63, and p = 0.0013; GG vs. AG/AA: adjusted OR = 1.45, 95% confidence interval (CI) = 1.04–2.02, and p = 0.0306). The results indicated that patients with a GG/AG genotype had a higher risk of suffering IVIG therapy resistance than patients with an AA genotype, suggesting the resistive effect of this SNP against IVIG therapy.

Analysis of the Association Between *EIF2AK4*/rs4594236 Polymorphism and Coronary Arterial Lesions

It is well known that *EIF2AK4* is involved in vascular remodeling (Nossent et al., 2018), which is the critical step for CAL formation. Therefore, the association between *EIF2AK4*/rs4594236 polymorphism and CAL formation was explored. Patients with KD were then divided into the CAL group and the NCAL group depending on whether they had CAL or not, and *EIF2AK4*/rs4594236 genotyping was performed on the two groups (**Table 3**). As shown in **Table 3**, *EIF2AK4*/rs4594236 was not associated with CAL formation. We then analyzed the relation between *EIF2AK4*/rs4594236 polymorphism and CAA formation (the serious lesions of the coronary artery) of KD. However, there was no significant association observed between *EIF2AK4*/rs4594236 and CAA (**Table 4**).

Stratification Analysis

We further explored the association between *EIF2AK4*/rs4594236 polymorphism and the risk effect of IVIG resistance on certain subgroups classified by age and gender (**Table 5**). Compared with the rs4594236 AA genotype, the risk effect of the rs4594236 GG/AG genotype was more prominent in male patients of all ages (adjust OR = 1.91, 95% CI = 1.23–2.95, and p = 0.0039).

Expression Quantitative Trait Loci Analyses

To assess the putative functional relevance of rs4594236 polymorphism affecting *EIF2AK4* mRNA expression, we used the data released from Genotype-Tissue Expression (GTEx) website. It was found that individuals carrying the rs4594236 G allele displayed significantly higher *EIF2AK4* mRNA levels in the artery of the aorta and tibia, the atrial

TABLE 1 | Characteristic distribution in the IVIG therapy resistant group and the response group of KD patients.

Variables	IVIG resistance (*n* = 234)		IVIG response (*n* = 795)		*p*[a]
	No.	%	No.	%	
Total	234	100	795	100	
Age range, month	2-132		1-131		
Mean ± SD	26.08 ± 21.80		25.14 ± 20.33		
≤60	219	93.59	756	95.09	0.3750
>60	15	6.41	39	4.91	
Gender					
Male	170	72.65	534	67.17	0.1096
Female	64	27.35	261	32.83	

[a]*Two-sided χ^2 test for distributions between KD patients with the IVIG therapy–resistant and –response group.*

TABLE 2 | Genotype distribution frequency of *EIF2AK4*/rs4594236 polymorphism in the IVIG therapy–resistant group and –response group of KD patients.

Genotype	IVIG resistance (*N* = 234)	IVIG response (*N* = 795)	*p*-value[a]	OR (95% CI)	*p*-value	Adjusted OR (95% CI)	*p*-value[b]
AA	43 (18.38)	231 (29.06)	0.0020	1		1	
AG	126 (53.85)	397 (49.94)		1.71 (1.16–2.50)	0.0062	1.71 (1.17–2.51)	0.0061
GG	65 (27.78)	167 (21.01)		2.09 (1.36–3.23)	0.0009	2.09 (1.36–3.23)	0.0009
Additive				1.43 (1.16–1.77)	0.0009	1.43 (1.16–1.77)	0.0009
Dominant	191 (81.62)	564 (70.94)	0.0008	1.82 (1.26–2.63)	0.0013	1.82 (1.27–2.63)	0.0013
Recessive	169 (72.22)	628 (78.99)	0.0322	1.45 (1.04–2.02)	0.0299	1.45 (1.04–2.02)	0.0306

[a]*Two-sided χ^2 test for distributions between the IVIG therapy–resistant group and –response group of KD patients.*
[b]*Adjusted for age and gender status in logistic regression models.*

TABLE 3 | Genotype distribution frequency of *EIF2AK4*/rs4594236 polymorphism in the NCAL group and CAL group of KD patients.

Genotype	CAL (*N* = 408)	NCAL (*N* = 621)	*p*-value[a]	OR (95% CI)	*p*-value	Adjusted OR (95% CI)	*p*-value[b]
AA	107 (26.23)	167 (26.89)	0.8297	1.000		1.000	
AG	212 (51.96)	311 (50.08)		1.064 (0.789–1.435)	0.6846	1.041 (0.767–1.414)	0.7945
GG	89 (21.81)	143 (23.03)		0.971 (0.678–1.391)	0.874	0.941 (0.652–1.358)	0.7447
Additive				0.989 (0.827–1.182)	0.9024	0.973 (0.811–1.168)	0.7686
Dominant	301 (73.77)	454 (73.11)	0.8128	1.035 (0.780–1.373)	0.8132	1.010 (0.756–1.349)	0.9482
Recessive	319 (78.19)	478 (76.97)	0.6481	0.933 (0.691–1.259)	0.65	0.916 (0.674–1.245)	0.5751

[a]*Two-sided χ^2 tests were used to determine differences in genotype distributions between KD with and without CAL.*
[b]*Adjusted for age and gender status in logistic regression models.*

TABLE 4 | Genotype and allele frequencies of *EIF2AK4* in KD Patients with (CAA) or without CAA (NCAA).

Genotype	CAA (*N* = 216)	NCAA (*N* = 813)	*p*-value[a]	OR (95% CI)	*p*-value	Adjusted OR (95% CI)	*p*-value[b]
AA	55 (25.46)	219 (26.94)	0.8108	1.000		1.000	
AG	114 (52.78)	409 (50.31)		1.110 (0.773–1.593)	0.5717	1.088 (0.754–1.571)	0.6506
GG	47 (21.76)	185 (22.76)		1.012 (0.654–1.564)	0.9586	0.983 (0.632–1.530)	0.9389
Additive				1.010 (0.815–1.251)	0.9289	0.995 (0.800–1.237)	0.9648
Dominant	161 (74.54)	594 (73.06)	0.6619	1.079 (0.766–1.521)	0.6631	1.055 (0.745–1.495)	0.7615
Recessive	169 (78.24)	628 (77.24)	0.7548	0.944 (0.657–1.356)	0.7556	0.929 (0.643–1.342)	0.6946

[a]*Two-sided χ^2 tests were used to determine differences in genotype distributions between KD with and without CAA.*
[b]*Adjusted for age and gender status in logistic regression models.*

appendage, and the left ventricle of the heart than those with the rs4594236 A allele (**Figure 1**). Furthermore, we evaluated the impact of the rs4594236 polymorphism on the mRNA level of the neighboring genes in the above-mentioned tissues and found that signal recognition particle 14 (SRP14) (or divergent transcript (SRP14-AS1)) mRNA levels in tissues with the rs4594236 G allele were significantly lower than those with the rs4594236 A allele (**Figure 2**).

TABLE 5 | Stratification analysis of *EIF2AK4*/rs4594236 polymorphism in the IVIG therapy resistant group and response group of KD patients.

Variables	rs4594236 (IVIG resistance/IVIG response)		*p*-value[a]	OR (95%CI)	*p*-value	Adjusted OR (95% CI)	Adjust *p*-value[b]
	AA	AG/GG					
Age, months							
≤60	42/216	177/540	0.0044	1.69 (1.16–2.44)	0.0059	1.67 (1.15–2.43)	0.0068
>60	1/15	14/24	0.012	8.75 (1.04–73.54)	0.0458	9.43 (1.08–82.13)	0.0421
Gender							
Male	30/154	140/380	0.0029	1.89 (1.22–2.93)	0.0042	1.91 (1.23–2.95)	0.0039
Female	13/77	51/184	0.1314	1.64 (0.85–3.19)	0.1437	1.62 (0.83–3.15)	0.1551

[a]*Two-sided* χ^2 *test for distributions between the IVIG therapy resistant group and response group of KD patients.*
[b]*Adjusted for gender/age status in logistic regression models.*

DISCUSSION

IVIG has been the optimal and effective treatment for KD to reduce the prevalence of coronary-artery abnormalities and systemic inflammation until now (Newburger et al., 1986). Although the molecular and cellular basis of IVIG function is complicated and remains unknown, some evidence indicated that genetic factors played an important role in IVIG treatment activities. Taking the fact that several genes were associated with the susceptibility of KD and the rates of IVIG resistant patients differ among different ethnic groups (Kashef et al., 2005; Uehara et al., 2008; Tremoulet et al., 2011), some hot genetic factors, especially immune functional genes, were examined to be associated with IVIG resistance, such as *FcγR2C* and *FcγR3B* (Makowsky et al., 2013). Furthermore, Weng et al. (2010) had found that patients with *IL-1β* (−511 TT) and *IL-1β* (−31 CC) genotypes had increased risk of IVIG resistance and were associated with initial IVIG treatment failure based on a study of 156 KD patients (136 with and 20 without response to IVIG treatment) among Taiwanese children .

Herein, we demonstrated a potentially contributing role of *EIF2AK4*/rs4594236 polymorphism in IVIG resistance in KD and for the first time reported that *EIF2AK4*/rs4594236 polymorphism could predispose to IVIG resistance in southern Chinese KD children.

EIF2AK4 is a high molecular weight protein kinase activated by uncharged tRNA (Wek et al., 1990; Nakamura et al., 2018; Schmidt et al., 2019). Activated *EIF2AK4* can phosphorylate eIF2a to upregulate ATF4 translation, which in turn increases amino acid biosynthetic and activated transport pathways (Harding et al., 2000; Harding et al., 2003). The physiological functions of *EIF2AK4* currently remain poorly understood, but its function in human diseases has recently been emphasized.

Several studies demonstrated that *EIF2AK4* was associated with vascular remodeling (Lu et al., 2014; Nossent et al., 2018; Chen et al., 2021). One possible mechanism was that *EIF2AK4* dysfunction enhanced collagen I gene transcription via the ATF3/p38 pathway, which led to increased collagen deposition in the pulmonary artery (Chen et al., 2021). As vascular remodeling is critical for CAL formation of KD, we also investigated the association between *EIF2AK4*/rs4594236 polymorphism and CAL or CAA formation of KD. However, we found that *EIF2AK4*/rs4594236 polymorphism was not associated with either CAL or CAA formation. The possible reason may be that the *EIF2AK4* expression level was decreased significantly in *EIF2AK4* mutation PVOD patients who had undergone vascular modeling. While the data from GTEx showed that individuals carrying the rs4594236 G allele displayed significantly higher EIF2AK4 mRNA levels in the artery of the aorta and tibia, the atrial appendage, and the left ventricle of the heart than those with the rs4594236 A allele (**Figure 1**), it is indicated that the patients with an rs4594236 G allele have a higher risk of IVIG therapy resistance and the EIF2AK4 expression level. In other words, the patients with higher EIF2AK4 expression tend to have a higher IVIG resistant incidence rate. Hence, different expression levels of EIF2AK4 stimulated diverse downstream signals to regulate cell physiological functions differently.

On the other hand, McGaha et al. found loss of *EIF2AK4*-enhanced inflammatory macrophage transcription with a crowd of proinflammatory cytokine expression and production. In addition, the activated regulatory macrophage was attenuated with a decrease in the Arg1 and CCL22 mRNA expression and IL-10 protein level at the same time. Mechanistically, EIF2AK4 altered the myeloid function by activating the CREB-2/ATF4 signal pathway, which was required for maturation and polarization of macrophages in both mice and humans (Halaby et al., 2019). Interestingly, IVIG treatment promotes tumor-associated macrophages from M2 to M1 polarization, and the IVIG effect was dependent on the activation/polarization state of macrophages (Domínguez-Soto et al., 2014). It is possible that the immunomodulatory effect of IVIG observed in other autoimmune diseases such as KD follows a similar pattern. In addition, our results showed the IVIG resistant risk of KD patients may be linked to the upregulated expression levels of the *EIF2AK4* gene (**Figure 1**); thus, we deduced the hypothesis that IVIG treatment promoted macrophage M1 polarization while the immunomodulatory function of the M1 macrophage was inhibited by upregulated EIF2AK4, which caused persistent inflammation. However, more functional experiments need to be carried out to support the possible mechanism.

To date, studies have been conducted regarding the epidemiologic assessment of *EIF2AK4* gene SNPs. Deng et al.

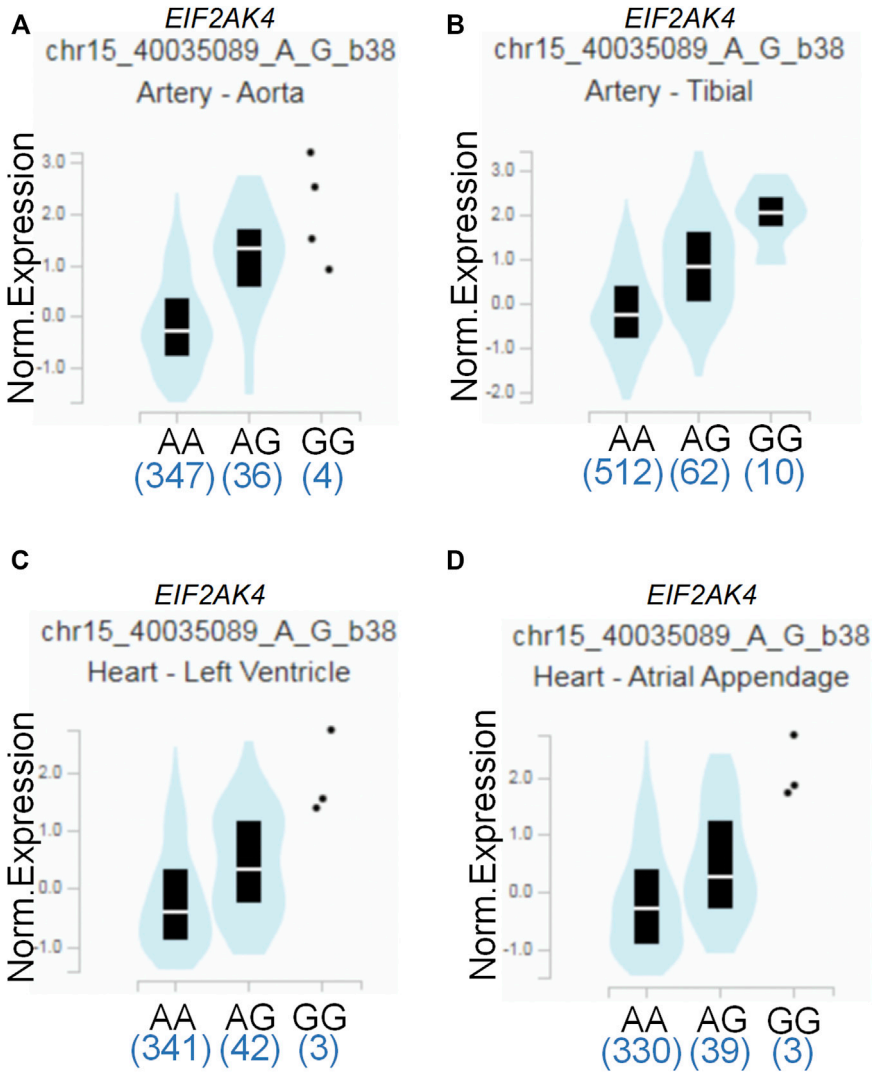


FIGURE 1 | Functional implication of the *EIF2AK4* gene rs4594236 polymorphism in human tissues. **(A)** The genotype of rs4594236 and expression of the *EIF2AK4* gene in the artery of the aorta were searched on the public database GTEx Portal. $p = 2.6 \times 10^{-20}$. **(B)** The genotype of rs4594236 and expression of the *EIF2AK4* gene in the artery of the tibia were searched on the public database GTEx Portal. $p = 2.4 \times 10^{-18}$. **(C)** The genotype of rs4594236 and expression of the *EIF2AK4* gene in the left ventricle of the heart were searched on the public database GTEx Portal. $p = 3.4 \times 10^{-8}$. **(D)** The genotype of rs4594236 and expression of the *EIF2AK4* gene in the atrial appendage of the heart were searched on the public database GTEx Portal. $p = 2.1 \times 10^{-8}$.

carried out a genome-wide association study of body mass index (BMI) from a cohort containing 597 northern Chinese patients and reported 281,533 SNPs. They found that two adjacent SNPs (rs4432245 and rs711906) of *EIF2AK4* were significantly associated with BMI (Yang et al., 2014). Given the critical role of *EIF2AK4* in immunity reactions, it is necessary to investigate the association between *EIF2AK4* gene SNPs and IVIG resistance of KD. The current study revealed that the SNP rs4594236 polymorphism in the *EIF2AK4* gene was associated with increased risk to IVIG resistance of KD in southern Chinese population. Compared with the rs4594236 AA genotype, the AG/GG genotype increased the IVIG resistant risk significantly, especially in male KD patients. We then explored the potential mechanism for the risk role of rs4594236 polymorphism in IVIG resistance. The results from eQTLs analysis indicated that IVIG resistant risk of KD was associated with upregulated expression levels of the *EIF2AK4* gene (**Figure 1**). We also evaluated the impact of rs4594236 polymorphism on the mRNA level of the neighboring genes. We found that the *SRP14* (or *SRP14-AS1*) mRNA level with the rs4594236 G genotype was significantly lower than that in cells with the rs4594236 A genotype (**Figure 2**). *SRP14* is a universal ribonucleoprotein, and combined with SRP9 as a heterodimer, it can recognize the RNA UGUNR motif to regulate target gene translation (Bovia et al., 1995; Hasler and Strub, 2006). Thus, we hypothesized that SRP14 combined with the specific RNA motif of *EIF2AK4* and negatively regulated the *EIF2AK4* mRNA translation level

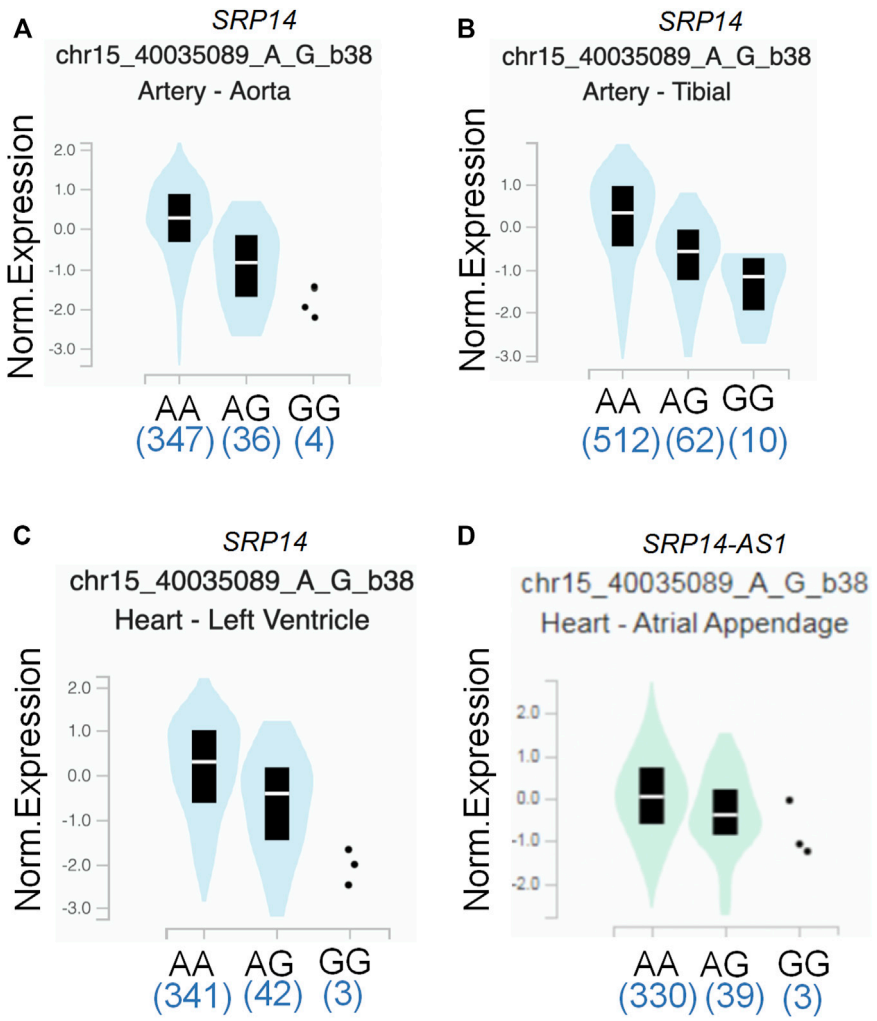


FIGURE 2 | Functional prediction of rs4594236 on a neighboring gene. **(A)** Correlation between rs4594236 and *SRP14* gene expression in the artery of the aorta. $p = 6.9 \times 10^{-10}$. **(B)** Correlation between rs4594236 and *SRP14* gene expression in the artery of the tibia. $p = 2.3 \times 10^{-9}$. **(C)** Correlation between rs4594236 and *SRP14* gene expression in the left ventricle of the heart. $p = 3.4 \times 10^{-8}$. **(D)** Correlation between rs4594236 and *SRP14-AS1* gene expression in the atrial appendage of the heart. $p = 9.8 \times 10^{-9}$.

to trigger downstream physiological reactions to inhibit IVIG therapy response.

The major strength of this study is its novelty; as we know, this is the first study that focuses on the *EIF2AK4* function in IVIG therapy resistance of KD at present. However, our study still has some limitations. First, the enrolled patients of this study were mainly from the southern Chinese population; the study needs multicenter subjects from other geographic populations to support and evaluate the applicability of the findings to other ethnicities. Second, only one functional SNP in the *EIF2AK4* gene was included in this study; more potentially functional SNPs of *EIF2AK4* need to be investigated in the future. Last but not least, the exact biological mechanism of *EIF2AK4* in IVIG resistance of KD is worthy of further investigation.

DATA AVAILABILITY STATEMENT

The raw data supporting the conclusions of this article will be made available by the authors, without undue reservation.

ETHICS STATEMENT

This study was approved by the Ethics Review Committee of the Guangzhou Women and Children's Medical Center (2014073009). All studies had obtained the approval of the local hospital institutional review board, and all the participants were informed of the details of this study and signed the informed consent form.

AUTHOR CONTRIBUTIONS

HY, HL, and XG conceived and designed the study. HY, FL, KC, and YX analyzed and interpreted the data. YW, LF, and HZ provided assistance in performing the study. LP, DC, and HL revised the manuscript. HY, FL, and XG wrote the paper with feedback from all authors. All the authors read and approved the final manuscript.

FUNDING

This study was funded by the Guangdong Natural Science Fund, China (Grant numbers: 2019A1515012061 and 2021A1515011207), the Guangzhou Science and Technology Program Project, China (Grant numbers: 201904010486 and 202102010197), the Guangzhou Institute of Pediatrics/ Guangzhou Women and Children's Medical Center Fund, China (Grant numbers: GCP-2019-003, GCP-2019-006, and YIP-2019-050), and the Postdoctoral Research Initiation Fund from Guangzhou Institute of Pediatrics, Guangzhou Women and Children's Medical Center (Grant number 3001162).

ACKNOWLEDGMENTS

The authors would like to thank the Clinical Biological Resource Bank of the Guangzhou Women and Children's Medical Center for providing all the clinical samples and greatly appreciate all the patients who donated the samples.

SUPPLEMENTARY MATERIAL

The Supplementary Material for this article can be found online at: https://www.frontiersin.org/articles/10.3389/fgene.2022.868159/full#supplementary-material

REFERENCES

Bovia, F., Fornallaz, M., Leffers, H., and Strub, K. (1995). The SRP9/14 Subunit of the Signal Recognition Particle (SRP) Is Present in More Than 20-fold Excess over SRP in Primate Cells and Exists Primarily Free but Also in Complex with Small Cytoplasmic Alu RNAs. *MBoC* 6 (4), 471–484. doi:10.1091/mbc.6.4.471

Burns, J. C., and Glodé, M. P. (2004). Kawasaki Syndrome. *Lancet* 364 (9433), 533–544. doi:10.1016/s0140-6736(04)16814-1

Chaudhary, K., Shinde, R., Liu, H., Gnana-Prakasam, J. P., Veeranan-Karmegam, R., Huang, L., et al. (2015). Amino Acid Metabolism Inhibits Antibody-Driven Kidney Injury by Inducing Autophagy. *J. I.* 194 (12), 5713–5724. doi:10.4049/jimmunol.1500277

Che, D., Pi, L., Fang, Z., Xu, Y., Cai, M., Fu, L., et al. (2018). ABCC4 Variants Modify Susceptibility to Kawasaki Disease in a Southern Chinese Population. *Dis. Markers* 2018, 8638096. doi:10.1155/2018/8638096

Chen, Z., Zhang, J., Wei, D., Chen, J., and Yang, J. (2021). GCN2 Regulates ATF3-P38 MAPK Signaling Transduction in Pulmonary Veno-Occlusive Disease. *J. Cardiovasc Pharmacol. Ther.* 26 (6), 677–689. doi:10.1177/10742484211015535

Consortium, G. T. (2013). The Genotype-Tissue Expression (GTEx) Project. *Nat. Genet.* 45 (6), 580–585. doi:10.1038/ng.2653

Domínguez-Soto, A., de las Casas-Engel, M., Bragado, R., Medina-Echeverz, J., Aragoneses-Fenoll, L., Martín-Gayo, E., et al. (2014). Intravenous Immunoglobulin Promotes Antitumor Responses by Modulating Macrophage Polarization. *J. I.* 193 (10), 5181–5189. doi:10.4049/jimmunol.1303375

Fu, L. Y., Qiu, X., Deng, Q. L., Huang, P., Pi, L., Xu, Y., et al. (2019). The IL-1B Gene Polymorphisms Rs16944 and Rs1143627 Contribute to an Increased Risk of Coronary Artery Lesions in Southern Chinese Children with Kawasaki Disease. *J. Immunol. Res.* 2019, 4730507. doi:10.1155/2019/4730507

Gersony, W. M. (2009). The Adult after Kawasaki Disease. *J. Am. Coll. Cardiol.* 54 (21), 1921–1923. doi:10.1016/j.jacc.2009.06.057

Gu, X., Lin, W., Xu, Y., Che, D., Tan, Y., Lu, Z., et al. (2020). The Rs1051931 G>A Polymorphism in the PLA2G7 Gene Confers Resistance to Immunoglobulin Therapy in Kawasaki Disease in a Southern Chinese Population. *Front. Pediatr.* 8, 338. doi:10.3389/fped.2020.00338

Hadinnapola, C., Bleda, M., Haimel, M., Screaton, N., Swift, A., Dorfmüller, P., et al. (2017). Phenotypic Characterization of EIF2AK4 Mutation Carriers in a Large Cohort of Patients Diagnosed Clinically with Pulmonary Arterial Hypertension. *Circulation* 136 (21), 2022–2033. doi:10.1161/CIRCULATIONAHA.117.028351

Halaby, M. J., Hezaveh, K., Lamorte, S., Ciudad, M. T., Kloetgen, A., MacLeod, B. L., et al. (2019). GCN2 Drives Macrophage and MDSC Function and Immunosuppression in the Tumor Microenvironment. *Sci. Immunol.* 4 (42), 8189. doi:10.1126/sciimmunol.aax8189

Harding, H. P., Novoa, I., Zhang, Y., Zeng, H., Wek, R., Schapira, M., et al. (2000). Regulated Translation Initiation Controls Stress-Induced Gene Expression in Mammalian Cells. *Mol. Cell* 6 (5), 1099–1108. doi:10.1016/s1097-2765(00)00108-8

Harding, H. P., Zhang, Y., Zeng, H., Novoa, I., Lu, P. D., Calfon, M., et al. (2003). An Integrated Stress Response Regulates Amino Acid Metabolism and Resistance to Oxidative Stress. *Mol. Cell* 11 (3), 619–633. doi:10.1016/s1097-2765(03)00105-9

Hasler, J., and Strub, K. (2006). Alu RNP and Alu RNA Regulate Translation Initiation *In Vitro*. *Nucleic Acids Res.* 34 (8), 2374–2385. doi:10.1093/nar/gkl246

Huang, Y.-H., Hsu, Y.-W., Lu, H.-F., Wong, H. S.-C., Yu, H.-R., Kuo, H.-C., et al. (2016). Interferon-gamma Genetic Polymorphism and Expression in Kawasaki Disease. *Med. Baltim.* 95 (17), e3501. doi:10.1097/md.0000000000003501

Kashef, S., Safari, M., and Amin, R. (2005). Initial Intravenous γ-Globulin Treatment Failure in Iranian Children with Kawasaki Disease. *Kaohsiung J. Med. Sci.* 21 (9), 401–404. doi:10.1016/s1607-551x(09)70141-x

Kato, H., Koike, S., Yamamoto, M., Ito, Y., and Yano, E. (1975). Coronary Aneurysms in Infants and Young Children with Acute Febrile Mucocutaneous Lymph Node Syndrome. *J. Pediatr.* 86 (6), 892–898. doi:10.1016/s0022-3476(75)80220-4

Khor, C. C., Davila, S., Davila, S., Breunis, W. B., Lee, Y.-C., Shimizu, C., et al. (2011). Genome-wide Association Study Identifies FCGR2A as a Susceptibility Locus for Kawasaki Disease. *Nat. Genet.* 43 (12), 1241–1246. doi:10.1038/ng.981

Lee, Y.-C., Kuo, H.-C., Chang, J.-S., Chang, L.-Y., Huang, L.-M., Chen, M.-R., et al. (2012). Two New Susceptibility Loci for Kawasaki Disease Identified through Genome-wide Association Analysis. *Nat. Genet.* 44 (5), 522–525. doi:10.1038/ng.2227

Lin, K., Zhang, L., Wang, Y., Li, J., Xu, Y., Che, D., et al. (2021). FNDC1 Polymorphism (Rs3003174 C > T) Increased the Incidence of Coronary Artery Aneurysm in Patients with Kawasaki Disease in a Southern Chinese Population. *Jir* 14, 2633–2640. doi:10.2147/jir.s311956

Liu, H., Huang, L., Bradley, J., Liu, K., Bardhan, K., Ron, D., et al. (2014). GCN2-dependent Metabolic Stress Is Essential for Endotoxemic Cytokine Induction and Pathology. *Mol. Cell Biol.* 34 (3), 428–438. doi:10.1128/mcb.00946-13

Longchamp, A., Mirabella, T., Arduini, A., MacArthur, M. R., Das, A., Treviño-Villarreal, J. H., et al. (2018). Amino Acid Restriction Triggers Angiogenesis via GCN2/ATF4 Regulation of VEGF and H2S Production. *Cell* 173 (1), 117–129. doi:10.1016/j.cell.2018.03.001

Lu, Z., Xu, X., Fassett, J., Kwak, D., Liu, X., Hu, X., et al. (2014). Loss of the Eukaryotic Initiation Factor 2α Kinase General Control Nonderepressible 2 Protects Mice from Pressure Overload-Induced Congestive Heart Failure without Affecting Ventricular Hypertrophy. *Hypertension* 63 (1), 128–135. doi:10.1161/hypertensionaha.113.02313

Lünemann, J. D., Nimmerjahn, F., and Dalakas, M. C. (2015). Intravenous Immunoglobulin in Neurology-Mode of Action and Clinical Efficacy. *Nat. Rev. Neurol.* 11 (2), 80–89. doi:10.1038/nrneurol.2014.253

Makowsky, R., Wiener, H. W., Ptacek, T. S., Silva, M., Shendre, A., Edberg, J. C., et al. (2013). FcγR Gene Copy Number in Kawasaki Disease and Intravenous Immunoglobulin Treatment Response. *Pharmacogenet Genomics* 23 (9), 455–462. doi:10.1097/fpc.0b013e328363686e

McCrindle, B. W., Rowley, A. H., Newburger, J. W., Burns, J. C., Bolger, A. F., Gewitz, M., et al. (2017). Diagnosis, Treatment, and Long-Term Management of Kawasaki Disease: A Scientific Statement for Health Professionals from the American Heart Association. *Circulation* 135 (17), e927–e99. doi:10.1161/CIR.0000000000000484

McGaha, T. L., Huang, L., Lemos, H., Metz, R., Mautino, M., Prendergast, G. C., et al. (2012). Amino Acid Catabolism: a Pivotal Regulator of Innate and Adaptive Immunity. *Immunol. Rev.* 249 (1), 135–157. doi:10.1111/j.1600-065x.2012.01149.x

Nakamura, A., Nambu, T., Ebara, S., Hasegawa, Y., Toyoshima, K., Tsuchiya, Y., et al. (2018). Inhibition of GCN2 Sensitizes ASNS-Low Cancer Cells to Asparaginase by Disrupting the Amino Acid Response. *Proc. Natl. Acad. Sci. U. S. A.* 115 (33), E7776–E85. doi:10.1073/pnas.1805523115

Newburger, J. W., Takahashi, M., Burns, J. C., Beiser, A. S., Chung, K. J., Duffy, C. E., et al. (1986). The Treatment of Kawasaki Syndrome with Intravenous Gamma Globulin. *N. Engl. J. Med.* 315 (6), 341–347. doi:10.1056/nejm198608073150601

Newburger, J. W., Takahashi, M., Gerber, M. A., Gewitz, M. H., Tani, L. Y., Burns, J. C., et al. (2004). Diagnosis, Treatment, and Long-Term Management of Kawasaki Disease. *Circulation* 110 (17), 2747–2771. doi:10.1161/01.cir.0000145143.19711.78

Nossent, E. J., Antigny, F., Montani, D., Bogaard, H. J., Ghigna, M. R., Lambert, M., et al. (2018). Pulmonary Vascular Remodeling Patterns and Expression of General Control Nonderepressible 2 (GCN2) in Pulmonary Veno-Occlusive Disease. *J. Heart Lung Transplant.* 37 (5), 647–655. doi:10.1016/j.healun.2017.09.022

Onouchi, Y., Gunji, T., Burns, J. C., Shimizu, C., Newburger, J. W., Yashiro, M., et al. (2008). ITPKC Functional Polymorphism Associated with Kawasaki Disease Susceptibility and Formation of Coronary Artery Aneurysms. *Nat. Genet.* 40 (1), 35–42. doi:10.1038/ng.2007.59

Onouchi, Y., Suzuki, Y., Suzuki, H., Terai, M., Yasukawa, K., Hamada, H., et al. (2013). ITPKC and CASP3 Polymorphisms and Risks for IVIG Unresponsiveness and Coronary Artery Lesion Formation in Kawasaki Disease. *Pharmacogenomics J.* 13 (1), 52–59. doi:10.1038/tpj.2011.45

Ravindran, R., Loebbermann, J., Nakaya, H. I., Khan, N., Ma, H., Gama, L., et al. (2016). The Amino Acid Sensor GCN2 Controls Gut Inflammation by Inhibiting Inflammasome Activation. *Nature* 531 (7595), 523–527. doi:10.1038/nature17186

Schmidt, S., Gay, D., Uthe, F. W., Denk, S., Paauwe, M., Matthes, N., et al. (2019). A MYC-GCN2-eIF2α Negative Feedback Loop Limits Protein Synthesis to Prevent MYC-dependent Apoptosis in Colorectal Cancer. *Nat. Cell Biol.* 21 (11), 1413–1424. doi:10.1038/s41556-019-0408-0

Sharma, K., Vignesh, P., Srivastava, P., Sharma, J., Chaudhary, H., Mondal, S., et al. (2021). Epigenetics in Kawasaki Disease. *Front. Pediatr.* 9, 673294. doi:10.3389/fped.2021.673294

Takahashi, K., Oharaseki, T., Yokouchi, Y., Naoe, S., and Saji, T. (2013). Kawasaki Disease: Basic and Pathological Findings. *Clin. Exp. Nephrol.* 17 (5), 690–693. doi:10.1007/s10157-012-0734-z

Tremoulet, A. H., Devera, G., Best, B. M., Jimenez-Fernandez, S., Sun, X., Jain, S., et al. (2011). Increased Incidence and Severity of Kawasaki Disease Among Filipino-Americans in San Diego County. *Pediatr. Infect. Dis. J.* 30 (10), 909–911. doi:10.1097/inf.0b013e31821e52c6

Uehara, R., Belay, E. D., Maddox, R. A., Holman, R. C., Nakamura, Y., Yashiro, M., et al. (2008). Analysis of Potential Risk Factors Associated with Nonresponse to Initial Intravenous Immunoglobulin Treatment Among Kawasaki Disease Patients in Japan. *Pediatr. Infect. Dis. J.* 27 (2), 155–160. doi:10.1097/inf.0b013e31815922b5

Wang, K., Cao, Y., Rong, Y., Ning, Q., Jia, P., Huang, Y., et al. (2019). A Novel SNP in EIF2AK4 Gene Is Associated with Thermal Tolerance Traits in Chinese Cattle. *Anim. (Basel)* 9 (6), 375. doi:10.3390/ani9060375

Wang, Y., Wang, W., Gong, F., Fu, S., Zhang, Q., Hu, J., et al. (2013). Evaluation of Intravenous Immunoglobulin Resistance and Coronary Artery Lesions in Relation to Th1/Th2 Cytokine Profiles in Patients with Kawasaki Disease. *Arthritis & Rheumatism* 65 (3), 805–814. doi:10.1002/art.37815

Wang, Y., Xu, Y., Huang, P., Che, D., Wang, Z., Huang, X., et al. (2021). Homozygous of MRP4 Gene Rs1751034 C Allele Is Related to Increased Risk of Intravenous Immunoglobulin Resistance in Kawasaki Disease. *Front. Genet.* 12, 510350. doi:10.3389/fgene.2021.510350

Wang, Z., Xu, Y., Zhou, H., Wang, Y., Li, W., Lu, Z., et al. (2020). Association between P2RY12 Gene Polymorphisms and IVIG Resistance in Kawasaki Patients. *Cardiovasc Ther.* 2020, 3568608. doi:10.1155/2020/3568608

Wek, R. C., Ramirez, M., Jackson, B. M., and Hinnebusch, A. G. (1990). Identification of Positive-Acting Domains in GCN2 Protein Kinase Required for Translational Activation of GCN4 Expression. *Mol. Cell Biol.* 10 (6), 2820–2831. doi:10.1128/mcb.10.6.2820-2831.1990

Weng, K.-P., Hsieh, K.-S., Ho, T.-Y., Huang, S.-H., Lai, C.-R., Chiu, Y.-T., et al. (2010). IL-1B Polymorphism in Association with Initial Intravenous Immunoglobulin Treatment Failure in Taiwanese Children with Kawasaki Disease. *Circ. J.* 74 (3), 544–551. doi:10.1253/circj.cj-09-0664

Wu, Z., Yu, Y., Fu, L., Mai, H., Huang, L., Che, D., et al. (2020). LncRNA SOX2OT Rs9839776 Polymorphism Reduces Sepsis Susceptibility in Southern Chinese Children. *Jir* 13, 1095–1101. doi:10.2147/jir.s281760

Yang, F., Chen, X. D., Tan, L. J., Shen, J., Li, D. Y., Zhang, F., et al. (2014). Genome Wide Association Study: Searching for Genes Underlying Body Mass Index in the Chinese. *Biomed. Environ. Sci.* 27 (5), 360–370. doi:10.3967/bes2014.061

Conflict of Interest: The authors declare that the research was conducted in the absence of any commercial or financial relationships that could be construed as a potential conflict of interest.

Publisher's Note: All claims expressed in this article are solely those of the authors and do not necessarily represent those of their affiliated organizations, or those of the publisher, the editors, and the reviewers. Any product that may be evaluated in this article, or claim that may be made by its manufacturer, is not guaranteed or endorsed by the publisher.

Copyright © 2022 Yu, Liu, Chen, Xu, Wang, Fu, Zhou, Pi, Che, Li and Gu. This is an open-access article distributed under the terms of the Creative Commons Attribution License (CC BY). The use, distribution or reproduction in other forums is permitted, provided the original author(s) and the copyright owner(s) are credited and that the original publication in this journal is cited, in accordance with accepted academic practice. No use, distribution or reproduction is permitted which does not comply with these terms.

frontiers | Frontiers in Pediatrics

CASE REPORT
published: 23 June 2022
doi: 10.3389/fped.2022.911954

ARID2, a Rare Cause of Coffin–Siris Syndrome: A Clinical Description of Two Cases

Xiaoyan Wang†, Haiying Wu†, Hui Sun, Lili Wang and Linqi Chen**

Department of Endocrinology, Children's Hospital of Soochow University, Suzhou, China

Background: Coffin-Siris syndrome (CSS) is a multiple congenital anomaly syndrome characterized by coarse facial features, sparse scalp hair, hypertrichosis, and hypo/aplastic digital nails and phalanges. Mutations in the BAF (SWI/SNF)-complex subunits (SMARCE1, SMARCB1, SMARCA4, SMARCA2, ARID1B, and ARID1A) have been shown to cause CSS. People diagnosed with BAF pathway related diseases are increasing, and *ARID2* (NM_152641.4) is the least common of these genes. Mutations in the ARID2 gene is the cause for Coffin-Siris syndrome 6 (CSS6). By now only 16 individuals with CSS have been reported to have pathogenic variants in *ARID2*.

Case Presentation: In this article, we introduced two individuals with clinical features consistent with CSS6 (Coffin-Siris syndrome 6). This article increases the number of reported cases, provides better phenotypic information for this rare syndrome, and allows everyone to better understand the disease.

Conclusion: Our observations indicate that *ARID2* mutations could have variable phenotypes, even in patients from the same family.

Keywords: Coffin-Siris syndrome, *ARID2*, exome sequenci, short stature, SWI/SNF (BAF) complex

OPEN ACCESS

Edited by:
Weida Tong,
National Center for Toxicological Research (FDA), United States

Reviewed by:
GuangJun Zhang,
Purdue University, United States
Tomoki Kosho,
Shinshu University, Japan

***Correspondence:**
Haiying Wu
hainewhy@163.com
Linqi Chen
xcdxchenlinqi@163.com

†These authors have contributed equally to this work

Specialty section:
This article was submitted to Genetics of Common and Rare Diseases, a section of the journal Frontiers in Pediatrics

Received: *03 April 2022*
Accepted: *01 June 2022*
Published: *23 June 2022*

Citation:
Wang X, Wu H, Sun H, Wang L and Chen L (2022) ARID2, a Rare Cause of Coffin–Siris Syndrome: A Clinical Description of Two Cases. Front. Pediatr. 10:911954. doi: 10.3389/fped.2022.911954

BACKGROUND

Coffin-Siris Syndrome (CSS, OMIM 135900) is a multiple congenital anomaly syndrome. Current studies have proved that the disease is caused by mutations in human BRG- or HRBM-associated factor (BAF) pathway (1). Within this family of genes, pathogenic variants have been found in *ARID1B* (the most common), *ARID1A*, *SMARCB1, SMARCA4*, and *SMARCE1* in individuals with clinical phenotypes consistent with CSS. More recently, pathogenic alterations of the *ARID2* gene were also observed in probands with neurodevelopmental delay and CSS6 characteristics (2). In general, patients with pathogenic variants of *ARID2* tend to share the core features, such as developmental and growth delay, coarsening of the face, intelligence retardation, and abnormal behavior. Intelligence abnormalities are mainly mild to moderate. Atypical facial features primarily involve rough facial features, such as a protruding forehead, short-broad nose with anteverted nostril, low set and posteriorly rotated ear, a large mouth, thick upper lips, and hypoplasia of the nails or phalanges, typically of the 5th digits (3). To date, only 16 individuals with CSS have been reported to have pathogenic variants in *ARID2*. There are no reports of CSS6 cases in China. Herein, we report two cases of *ARID2* gene mutation (2–7). The medical records of two Chinese patients with CSS6 from the inpatient clinics of

the Children's Hospital of Soochow University in May 2019 were analyzed. Clinical data and results of genetic analysis are reported as follows.

MATERIALS AND METHODS

Informed consent was obtained from all individual participants included in the study. This study was approved by the Children's Hospital of Soochow University.

Whole-exome sequencing (WES) analysis were used to analyze the samples from patients. The mean vertical coverage was 325.14X, and the horizontal coverage was 99.99%.

Genomic DNA was extracted from peripheral blood leukocytes following the manufacturer's protocols. DNA samples from the 2 cases were fragmented using a Scientz08-III automated sonicator. Massively parallel sequencing was performed using Illumina MiSeq platform according to the standard manual. The raw data were filtered and aligned against the human reference genome (hg19). The single-nucleotide polymorphisms (SNPs) were called by using the GATK software. Variants were annotated using ANNOVAR 3. Effects of single-nucleotide variants (SNVs) were predicted by SIFT, Polyphen-2, and Mutation Taster programs. The detected pathogenicity variants was evaluated according to the recommendations of the ACMG for variant classification and reporting. The associated phenotypic features of candidate genes were analyzed against the patient's phenotype. Sanger sequencing was used to determine the genotypes of affected and unaffected family members at candidate loci.

Abbreviations: CSS, Coffin-Siris Syndrome; WES, Whole-exome Sequencing; SNVs, single-nucleotide Variants; IQ, Intelligence Quotient; BA, bone age; HCV, hepatitis C virus; GH, growth hormone; NR, no report; ADHD, attention deficit hyperactivity disorder; SGA, small for gestational age.

Case Presentation

Case 1

The proband (P1) was born at term weighing 2.6 kg to a non-consanguineous couple. She had no obvious feeding difficulties in infancy. Developmentally, she exhibited global developmental delay, achieving raising head at 7 months, sitting at 9 months, and walking at 18 months. She attended primary school at 7 years and 8 months old with poor academic performance. At present, she is 115 cm tall (< 2 *SD*), weighs 19.5 kg, and has a special face with dysmorphic features (including thick upper lips, micrognathia, and low-set ears). Furthermore, her toenails were noted to be hyperplastic (**Figure 1** and **Table 1**).

The Chromosome test showed 46 XX, and IQ (Intelligence Quotient) test showed 80. Her bone age (BA) was 6 years old. Magnetic Resonance Imaging (MRI) of pituitary showed no abnormality (approximately 3 mm in height). There was a 2610delT frameshift mutation in the *ARID2* gene, followed by a termination codon. This mutation has not been reported previously, and it has not been recorded in in normal or disease databases. Sanger sequencing was also performed on the parents, and they were found not to carry the same mutation (**Figure 1**). Since this variation is a frameshift mutation (PVS1) and *de novo* variation carried by neither of the parents (PS2). It is also a variation that is absent from controls (PM2). *In silico* programs tested agree on the pathogenic prediction (PP3). It was classified as "pathogenic" according to the ACMG guidelines. Based on the results of gene sequencing and clinical features, the patient was considered as CSS6 caused by *ARID2* gene mutation.

Case 2

The proband (P2) was delivered at full-term *via* cesarean section (birth weight: 5.2 kg). He raised his head at 8 months, sat at 12 months, and walked at 24 months. At present, he is



FIGURE 1 | The patient has coarse facial features, low-set and posteriorly rotated ears **(A)**, a flat, upturned nose **(B)**, sparse bitemporal scalp hair, thick eyebrows, and a wide mouth with thick lips **(C)**.

TABLE 1 | Summary of the features of Coffin-Siris syndrome with *ARID2* mutation reported in the literature.

	Variant	*De novo*	Facial features	Intellectual disability	Behavior abnormality	Short stature	Birth weight	Age acquired walk (months)	Age acquired first word (months)	GERD	Hypotonia	References #
1	Val846Leufs * 3	+	Micrognathia, posteriorly rotated ears, epicanthal folds, down slanting palpebral fissures, highly arched palate	+	ADHD, anxiety	<5%	5%	24	12	–		(3)
2	Leu343*	UR	Micrognathia, posteriorly rotated ears, epicanthal folds, down slanting palpebral fissures, highly arched palate	+	ADHD, aggressive	25%	25–50%	24	NR	–	+	(3)
3	His1481Ilefs * 4	+	Micrognathia, posteriorly rotated ears, epicanthal folds, down slanting palpebral fissures, highly arched palate	+	Affinity water, sensitive	10%	25%	20	18	+	+	(3)
4	Q1440*	+	Micrognathia, posteriorly rotated ears, epicanthal folds, down slanting palpebral fissures, highly arched palate	+	ADHD	< 5%	25–50%	UR	NR	+	+	(3)
5	12q12 Deletion	+	Micrognathia, posteriorly rotated ears, epicanthal folds, down slanting palpebral fissures, highly arched palate, and full lips	+	ADHD, sensitivity	< 1%	10%	27	24	+	+	(2)
6	Y423Afs * 39	+	Down-slanted palpebral fissures with mild ptosis of outer lower lid, telecanthus, small low set ears	+	ADHD	<5%	25–50%	NR	NR	+	+	(4)
7	Deletion exons1-16	+	Thin upper lip, micrognathia and low set ears	+	Sleep disturbance	< 3%	<5%	20	19	+	+	(5)
8	Asn387*	+	Plagiocephaly, protruding ears, thin upper lip vermilion, downturned corners of the mouth	+	Anxiety	< 5%	25–50%	21	24	–	+	(5)
9	Tyr133*	+	High broad forehead with down-slanting palpebral fissures and slightly low-set posteriorly rotated ears	+	"Routine driven"	< 5%	25%	27	60	–	–	(5)
10	Gln1482*	+	Micrognathia, webbed neck	+	Rigid, anxiety	< 10%	50%	27	>60	–	–	(5)
11	Thr1564Lysfs*5	+	Thick eyebrows, ptosis, prominent eyelashes, flat nasal bridge, short nose, anteverted nares, broad philtrum, high and broad forehead and posteriorly rotated ears	+	NR	< 5%	<5%	24	>24	–	+	(5)
12	Val883Leufs*10	+	Coarse face, low anterior hairline, thick eyebrows, broad nasal tip, thick vermilion of the lower lip and micrognathia	+	Quiet	50%	<25%	12	>60	+	+	(5)
13	Deletion exons 4–21	+	Ownslanting palpebral fissures, low-set and posteriorly rotated ears, narrow and high palate, small chin	+	Anxiety	25%	<5%	NR	NR	–	–	(5)
14	Gly1139Ser fs * 20	+	Coarsening of the face, tall forehead, hypertelorism, short nose, prominent and long philtrum, thin upper lip, and full lower lip	+	NR	<3%	<25%	NR	NR	+	+	(6)
15	Arg53Glu fs * 5	+	Midface hypoplasia, horizontal palpebral fissures, and a small, upturned nose. full lower lip	+	ADHD	<3%	90%	19	NR	–	–	(6)
16	Arr 12q12-13.11 (43,005,992_ 46,669,000)	+	Epicanthal folds, down slanting palpebral fissures, webbed neck, thick eyebrows, thick upper lips, large mouth	+	–	3–5%	<3%	NR	NR	+	–	(7)

*NR, no report; ADHD, attention deficit hyperactivity disorder; GERD, Gastroesophageal Reflux Disease. *Termination of translation (English Language Editors: A. Kassem and J. Chapnick).*

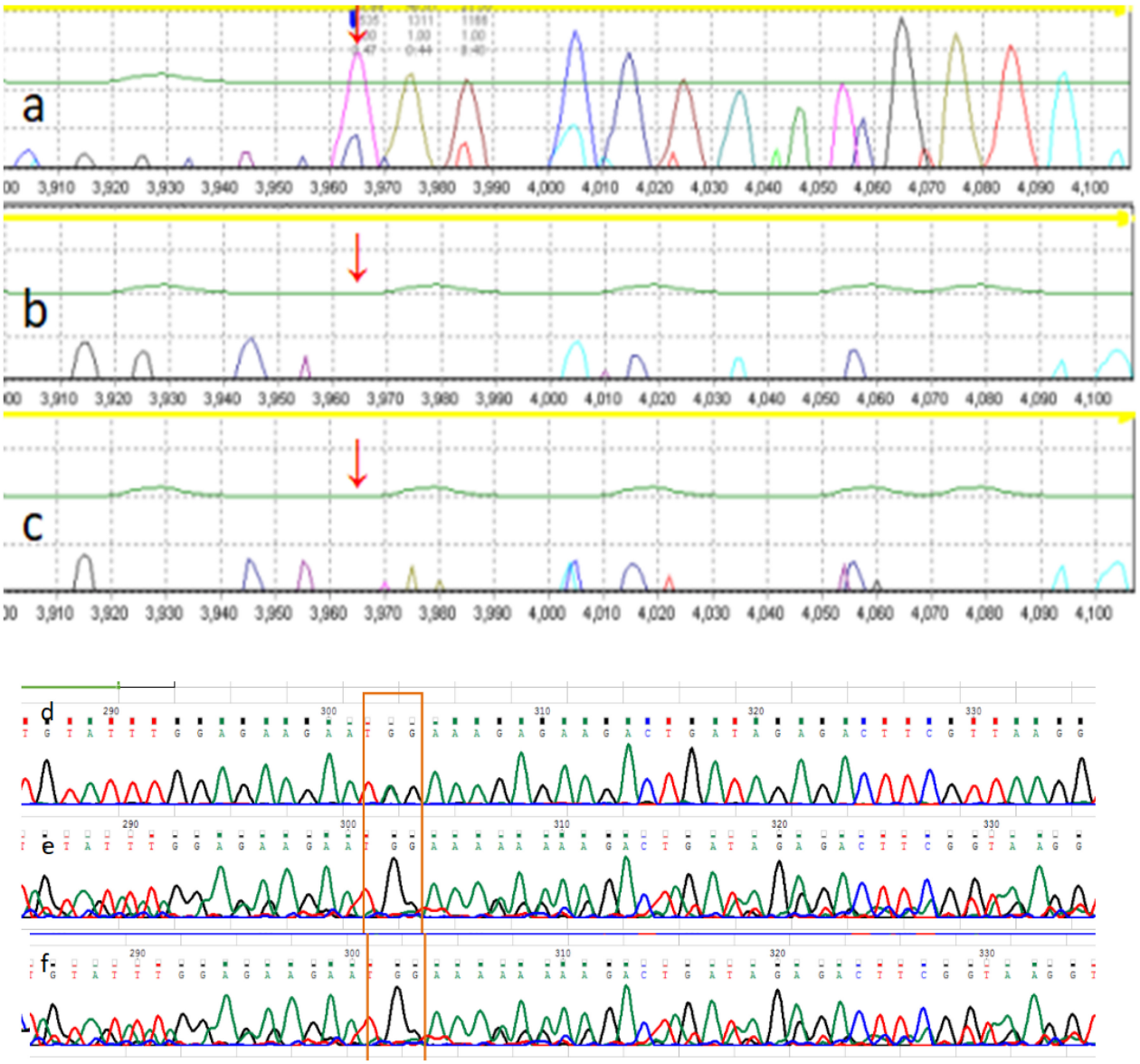


FIGURE 2 | The family pedigree of patient 1. The pedigree of the family with Coffin-Siris syndrome (CSS). **(a)** P1 *ARID2* c.2610delT; **(b)** P1 father *ARID2* gene c.2610T (wild type); **(c)** P1 mother *ARID2* c.2610T (wild type). The mutation is *de novo* in the proband, whereas the parents are wild-type. The family pedigree of patient 2. The pedigree of the family with Coffin-Siris syndrome (CSS). **(d)** P2 father *ARID2* c.674G (wild type); **(e)** P2 *ARID2* c.674G > A; p. Trp225 *; **(f)** P2 mother *ARID2* c.674G > A; p. Trp225 *.

just over 5 years old and cannot speak, but can understand others. He is currently 105.5 cm (< 2 *SD*) in height and has a special face with dysmorphic features (including a prominent forehead, short-broad nose with anteverted nostril, thick upper lips, micrognathia, and low-set ears). Due to sudden occurrence with diabetic ketoacidosis, the patient was diagnosed with type 1 diabetes. The parents of P2 did not agree to make the child's photo public.

The mother also has a similar face, and her development and language were slightly delayed compared to her peers. When she was young, her learning was poor, and she often only achieved a passing grade in exams. Full exon sequencing of P2 showed that the *ARID2* gene had a nonsense mutation c.674G > A; p. Trp225 *, and Sanger sequencing showed that the mutation was inherited form the mother (**Figure 2**). According to the ACMG/AMP guidelines, this mutation can be identified as pathogenic. This variation is a nonsense mutation (PVS1), and it is a variation that is absent from controls (PM2). Multiple lines of evidence from *in silico* prediction indicated that the mutation was potentially deleterious (PP3). Based on the results of gene sequencing and clinical features, the child was considered CSS6 caused by the *ARID2* gene mutation.

DISCUSSION AND CONCLUSION

Clinical Features Associated With Coffin-Siris Syndrome 6

In this article, we reviewed the clinical and molecular aspects of the 16 CSS6 patients, as well as all previously reported individuals, and provided a summary of their clinical findings (**Table 1**). We also summarized the published phenotypes of CSS6 in the literature (**Table 1**, $N = 16$) (2–7). The vast majority of patients reported to date have intelligence retardation (100%) and developmental retardation (100%). These features can only be recognized during the postnatal period.

ARID2 Variants and Coffin-Siris Syndrome 6

Although the phenotypes of patients caused by other genes mutation in in BAF pathway have some overlap, correlation between genotype and phenotype begins to appear with the report of more individuals. ARID1B gene are the most frequently mutated in CSS. The severity of physical abnormalities and intellectual defects varies from person to person (9–12). We described two other patients with *ARID2* gene variation, which is the rarest mutated in CSS.

SWI/SNF is an ATP-dependent chromatin-remodeling complex, which controls the density and position of nucleosomes by remodeling chromatin to control the epigenetic state. It plays an important role in cell proliferation, differentiation, development, and tumor suppression. ATP-dependent chromatin remodeling is a widely used mechanism (12, 13). In mammals, 29 genes are predicted to encode protein complexes similar to yeast SWI2/SNF2. The BAF complex is evolutionarily conserved from yeast to humasns and participates in many biological processes, such as transcriptional regulation, tumorigenesis, and embryonic development. The massively parallel of sequencing technology reveals that an increasing number of somatic mutations may be to compromise in part or whole the functional activity of the SWI/SNF complex in malignant tumors. Sequencing studies have shown that 15 subunits of the BAF complex encoded by 29 genes are mutated in more than 20% of human cancers in multiple types of tumors.

BAF complex subunits vary in different tumors, and specific subunits seem to be mutated in specific cancers, highlighting the tissue-specific protective effect (14). *ARID1A* is the SWI/SNF gene with the highest frequency of tumor mutations, with mutations in more than 10% of tumors. BAF complexes can be oncogenes or tumor suppressors. Studies have shown that *ARID2* gene inactivation mutations exist in HCV (hepatitis C virus)-related liver cancer, melanoma, lung cancer, and colorectal cancer. Additionally, approximately 50% of clear cell carcinomas of the ovary and 40% of endometrial cancers have *ARID1A* mutations.

At present, there are no reports of cancer risk in CSS cases (15). A recent article on *ARID2* described the intelligence retardation and loss-of-function variants of four *ARID2* patients (3). They reported typical deformities, including frontal elevations, epicanthus epidermis, downwardly sloping eyelid fissures, micrognathia, highly arched palate, and low or posterior ears (**Table 1**). All patients exhibited neurodevelopmental delay, short stature, and behavioral abnormalities (including ADHD, anxiety, aggression).

Previously reported *ARID1B* gene knockout (*ARID1B* ±) mice showed neuroanatomy and expression development delays, and abnormal behaviors. Also, the *ARID1B* ± mice's nose to buttocks length and body weight, as well as their growth hormone (GH) stimulation test indicated that *ARID1B* ± sufficient growth hormone could be secreted, but the secretion of insulin-like growth factors -1 (IGF-1) was significantly reduced (16). Celen et al. suggested that *ARID1B* ± may cause shortness due to the reduction of IGF-1 production in the brain, which leads to a decrease in plasma IGF-1. However, the inability to feed back to promote the increase of hypothalamic hormones (GHRH) and GH aggravates growth retardation. Studies have shown that the use of GH can improve growth retardation and muscle strength in mice, and the therapeutic effect has been verified in patients with *ARID1B* variants (17).

P1 exhibits the following manifestations: high forehead, short-broad nose with anteverted nostril, low-set ears, short stature, and mild intellectual disability with attention deficit and hyperactivity disorder (ADHD). GH stimulation suggests no growth hormone deficiency, and no growth hormone treatment has been given thus far. Currently, there is not enough experience in the treatment of GH in patients with short stature CSS, and most patients with CSS were treated with recombinant human growth hormone due to growth hormone deficiency (18). However, currently there is no experience with growth hormone treatment in CSS6; although children with CSS6 have short stature, GH treatment will not be administered temporarily.

As for behavioral abnormalities such as ADHD, corresponding treatment can be given. In addition, P2 did not undergo growth hormone treatment for short stature due to diabetes, and was under intellectual disability with rehabilitation therapy. Insulin was being injected subcutaneously to treat diabetes. As for the mother of P2 who has the same locus variation, intelligence and intellectual disability were not obvious.

CONCLUSION

In this article, we present two cases of novel patients with CSS6 and the pathogenic variant of ARID2 and review the clinical and molecular findings of all previously reported patients. We aimed to provide a comprehensive review of the syndrome in order to help physicians to recognize the syndrome.

Overall, CSS has a spectrum of clinical manifestations. Phenotypic differences within CSS continue to be defined regarding the involved subunit of the BAF-complex or the SOX gene. Parents of P2 had no noticeable developmental or growth delays, which is inconsistent with previous findings. It appears that *ARID2* mutations in P2 are of low penetrance with no genotype-phenotype correlations. Our data challenge the current understanding that pathogenic *ARID2* mutations usually arise *de novo*.

However, considering the small sample size of the present study, further studies are necessary to determine this

phenomenon. As shown in our clinical summary of 16 cases, we confirmed that CSS should be suspected postnatally in cases with global developmental delay or intellectual disability and specific dysmorphic features. The cases we reported indicate that *ARID2* mutations could have variable phenotypes, even in patients from the same family. This work can guide clinicians in performing further testing.

DATA AVAILABILITY STATEMENT

The datasets for this article are not publicly available due to concerns regarding participant/patient anonymity. Requests to access the datasets should be directed to the corresponding author.

ETHICS STATEMENT

The studies involving human participants were reviewed and approved by the Children's Hospital of Soochow University. Written informed consent to participate in this study was provided by the participants' legal guardian/next of kin. Written informed consent was obtained from the individual(s), and minor(s)' legal guardian/next of kin, for the publication of any potentially identifiable images or data included in this article.

AUTHOR CONTRIBUTIONS

XW, HW, and LC made substantial contributions to conception and drafted the final work. LW and HS were involved in following the patients and maintaining integrity in all parts of the work. All authors gave final approval for the article to be published.

FUNDING

This work was funded by Jin Lei Pediatric Endocrinology Growth Research Fund for Young Physicians (PEGRF202011023).

ACKNOWLEDGMENTS

We would like to thank the families for their consent to publish this report.

REFERENCES

1. Cheng SSW, Luk HM, Mok MT, Leung SS, Lo IFM. Genotype and phenotype in 18 Chinese patients with Coffin-Siris syndrome. *Am J Med Genet A.* (2021) 185:2250–61. doi: 10.1002/ajmg.a.62187
2. Van PR, De BP, van der SS, D'hondt M, Fränkel U, Dheedene A, et al. Confirmation of an ARID2 defect in SWI/SNF-related intellectual disability. *Am J Med Genet A.* (2017) 173:3104–8. doi: 10.1002/ajmg.a.38407
3. Shang L, Cho MT, Retterer K, Folk L, Humberson J, Rohena L, et al. Mutations in ARID2 are associated with intellectual disabilities. *Neurogenetics.* (2015) 16:307–14. doi: 10.1007/s10048-015-0454-0
4. Khazanchi R, Ronspies CA, Smith SC, Starr LJ. Patient with anomalous skin pigmentation expands the phenotype of ARID2 loss-of-function disorder, a SWI/SNF-related intellectual disability. *Am J Med Genet A.* (2019) 179:808–12. doi: 10.1002/ajmg.a.61075
5. Gazdagh G, Blyth M, Scurr I, Turnpenny PD, Mehta SG, Armstrong R, et al. Extending the clinical and genetic spectrum of ARID2 related intellectual disability. A case series of 7 patients. *Eur J Med Genet.* (2019) 62:27–34. doi: 10.1016/j.ejmg.2018.04.014
6. Bramswig NC, Caluseriu O, Lüdecke HJ, Bolduc FV, Noel NC, Wieland T, et al. Heterozygosity for ARID2 loss-of-function mutations in individuals with a Coffin-Siris syndrome-like phenotype. *Hum Genet.* (2017) 136:297–305. doi: 10.1007/s00439-017-1757-z
7. Lee Y, Choi Y, Seo GH, Kim GH, Keum C, Kim YM, et al. Phenotypic and molecular spectra of patients with switch/sucrose non-fermenting complex-related intellectual disability disorders in Korea. *BMC Med Genomics.* (2021) 14:254. doi: 10.1186/s12920-021-01104-9
8. Richards S, Aziz N, Bale S, Bick D, Das S, Gastier-Foster J, et al. Standards and guidelines for the interpretation of sequence variants: a joint consensus recommendation of the American college of medical genetics and genomics and the association for molecular pathology. *Genet Med.* (2015) 17:405–24. doi: 10.1038/gim.2015.30
9. Tsurusaki Y, Okamoto N, Ohashi H, Kosho T, Imai Y, Hibi-Ko Y, et al. Mutations affecting components of the SWI/SNF complex cause Coffin-Siris syndrome. *Nat Genet.* (2012) 44:376–8. doi: 10.1038/ng.2219
10. Xu F, Flowers S, Moran E. Essential role of ARID2 protein-containing SWI/SNF complex in tissue-specific gene expression. *J Biol Chem.* (2012) 287:5033–41. doi: 10.1074/jbc.M111.279968
11. Kang E, Kang M, Ju Y, Lee SJ, Lee YS, Woo DC, et al. Association between ARID2 and RAS-MAPK pathway in intellectual disability and short stature. *J Med Genet.* (2021) 58:767–77. doi: 10.1136/jmedgenet-2020-107111
12. Vasko A, Drivas TG, Schrier Vergano SA. Genotype-phenotype correlations in 208 individuals with Coffin-Siris syndrome. *Genes (Basel).* (2021) 12:937. doi: 10.3390/genes12060937
13. Wang Z, Chen K, Jia Y, Chuang JC, Sun X, Lin YH, et al. Dual ARID1A/ARID1B loss leads to rapid carcinogenesis and disruptive redistribution of BAF complexes. *Nat Cancer.* (2020) 1:909–22.
14. Kadoch C, Crabtree GR. Mammalian SWI/SNF chromatin remodeling complexes and cancer: mechanistic insights gained from human genomics. *Sci Adv.* (2015) 1:e1500447. doi: 10.1126/sciadv.1500447
15. Van Houdt JK, Nowakowska BA, Sousa SB, van Schaik BD, Seuntjens E, Avonce N, et al. Heterozygous missense mutations in SMARCA2 cause Nicolaides-Baraitser syndrome. *Nat Genet.* (2012) 44:445–9.
16. Celen C, Chuang JC, Luo X, Nijem N, Walker AK, Chen F, et al. Arid1b haploinsufficient mice reveal neuropsychiatric phenotypes and reversible causes of growth impairment. *Elife.* (2017) 6:e25730. doi: 10.7554/eLife.25730
17. Yu Y, Yao R, Wang L, Fan Y, Huang X, Hirschhorn J, et al. De novo mutations in ARID1B associated with both syndromic and non-syndromic short stature. *BMC Genomics.* (2015) 16:701. doi: 10.1186/s12864-015-1898-1
18. McCague EA, Lamichhane R, Holt N, Schrier Vergano SA. Growth charts for individuals with Coffin-Siris syndrome. *Am J Med Genet A.* (2020) 182:2253–62. doi: 10.1002/ajmg.a.61823

Conflict of Interest: The authors declare that the research was conducted in the absence of any commercial or financial relationships that could be construed as a potential conflict of interest.

Publisher's Note: All claims expressed in this article are solely those of the authors and do not necessarily represent those of their affiliated organizations, or those of the publisher, the editors and the reviewers. Any product that may be evaluated in this article, or claim that may be made by its manufacturer, is not guaranteed or endorsed by the publisher.

Copyright © 2022 Wang, Wu, Sun, Wang and Chen. This is an open-access article distributed under the terms of the Creative Commons Attribution License (CC BY). The use, distribution or reproduction in other forums is permitted, provided the original author(s) and the copyright owner(s) are credited and that the original publication in this journal is cited, in accordance with accepted academic practice. No use, distribution or reproduction is permitted which does not comply with these terms.

frontiers | Frontiers in Genetics

CASE REPORT
published: 06 July 2022
doi: 10.3389/fgene.2022.940292

Case Report: Whole-Exome Sequencing-Based Copy Number Variation Analysis Identified a Novel *DRC1* Homozygous Exon Deletion in a Patient With Primary Ciliary Dyskinesia

Ying Liu[1,2,3†], *Cheng Lei*[1,2,3†], *Rongchun Wang*[1,2,3], *Danhui Yang*[1,2,3], *Binyi Yang*[1,2,3], *Yingjie Xu*[1,2,3], *Chenyang Lu*[1,2,3], *Lin Wang*[1,2,3], *Shuizi Ding*[1,2,3], *Ting Guo*[1,2,3], *Shaokun Liu*[1,2,3*] *and Hong Luo*[1,2,3*]

[1]Department of Pulmonary and Critical Care Medicine, The Second Xiangya Hospital, Central South University, Changsha, China, [2]Research Unit of Respiratory Disease, Central South University, Changsha, China, [3]Hunan Diagnosis and Treatment Center of Respiratory Disease, Changsha, China

Objective: Whole-exome sequencing (WES) based copy number variation (CNV) analysis has been reported to improve the diagnostic rate in rare genetic diseases. In this study, we aim to find the disease-associated variants in a highly suspected primary ciliary dyskinesia (PCD) patient without a genetic diagnosis by routine WES analysis.

Methods: We identified the CNVs using the "Exomedepth" package in an undiagnosed PCD patient with a negative result through routine WES analysis. RNA isolation, PCR amplification, and Sanger sequencing were used to confirm the variant. High-speed video microscopy analysis (HSVA) and immunofluorescence analysis were applied to detect the functional and structural deficiency of nasal cilia and sperm flagella. Papanicolaou staining was employed to characterize the morphology of sperm flagella.

Results: NC_000002.11(NM_145038.5): g.26635488_26641606del, c.156-1724_244-2550del, r.156_243del, p. (Glu53Asnfs*13), a novel *DRC1* homozygous CNV, was identified by WES-based CNV analysis rather than routine variants calling, in a patient from a non-consanguineous family. HSVA results showed no significant change in ciliary beating frequency but with reduced beating amplitude compared with normal control, and his spermatozoa were almost immotile. The diagnosis of multiple morphological abnormalities of the sperm flagella (MMAF) was established through sperm motility and morphology analysis. PCR amplification and Sanger sequencing confirmed the novel variant of *DRC1*. Immunofluorescence showed that both cilia and sperm flagella were deficient in protein expression related to the dynein regulatory complex.

Conclusion: This report identifies a novel *DRC1* disease-associated variant by WES-based CNV analysis from a highly suspected PCD patient with MMAF. Our findings not

OPEN ACCESS

Edited by:
Ruth Roberts,
ApconiX, United Kingdom

Reviewed by:
Tomas Drgon,
United States Food and Drug Administration, United States
Gen Kano,
Kyoto Prefectural University of Medicine, Japan
Weicheng Chen,
Children's Hospital, Fudan University, China
Yanwei Sha,
Xiamen University, China
Chuan Xu,
First Affiliated Hospital of Anhui Medical University, China
Hagar Mor-Shaked,
Hebrew University of Jerusalem, Israel

***Correspondence:**
Shaokun Liu
shaokunliu228@csu.edu.cn
Hong Luo
luohonghuxi@csu.edu.cn

[†]These authors have contributed equally to this work

Specialty section:
This article was submitted to Genetics of Common and Rare Diseases, a section of the journal Frontiers in Genetics

Received: *10 May 2022*
Accepted: *20 June 2022*
Published: *06 July 2022*

Citation:
Liu Y, Lei C, Wang R, Yang D, Yang B, Xu Y, Lu C, Wang L, Ding S, Guo T, Liu S and Luo H (2022) Case Report: Whole-Exome Sequencing-Based Copy Number Variation Analysis Identified a Novel DRC1 Homozygous Exon Deletion in a Patient With Primary Ciliary Dyskinesia. Front. Genet. 13:940292. doi: 10.3389/fgene.2022.940292

only expand the genetic spectrum of PCD with MMAF but suggest that in combination with CNV analysis might improve the efficiency of genetic tests.

Keywords: whole-exome sequencing, CNV, *DRC1*, primary ciliary dykinesia, multiple morphological abnormalities of the sperm flagella

INTRODUCTION

Primary ciliary dyskinesia (PCD, MIM 244400) is a disease mainly inherited in an autosomal recessive manner and primarily caused by variants in genes required for transport, assembly, and function in motile cilia (Lucas et al., 2020). Due to motile cilia distributed mainly in the respiratory and reproductive system, most PCD patients exhibited bronchiectasis, chronic sinusitis, and infertility (Bhatt and Hogg, 2020). With increasing knowledge of the genetic background in PCD, the prevalence of PCD has been estimated up to at least 1:7,500 (Hannah, 2022). According to the guidelines published by the European Respiratory Society (ERS), the diagnosis of PCD requires the use of multiple methods (Lucas et al., 2017). These include the measurement of nasal nitric oxide (nNO), direct analysis of ciliary beat frequency and pattern by high-speed video microscopy analysis (HSVA), followed by the confirmatory method, including transmission electron microscope (TEM) analysis for analyzing the characteristic defects in ciliary ultrastructure, and genetic analysis for identifying biallelic pathogenic variants. However, TEM has some limitations that cannot be ignored when used as a diagnostic tool (Werner and Kouis, 2017). Only three kinds of ciliary ultrastructure defects were regarded to be the diagnostic characteristics for PCD, and the diagnostic rate of TEM is relatively low (Shoemark, 2017). Therefore, genetic analysis plays an indispensable role in PCD diagnosis.

With the continual developments in sequencing techniques and bioinformatic analysis, whole-exome sequencing (WES) provides a powerful tool to confirm the diagnosis of PCD. WES technology can help detect deleterious genetic variants in nearly the entire coding region of the genome. So far, over 50 genes have been reported to cause PCD (Wallmeier et al., 2020), yet the genetic basis of the disease remains unknown in about 30% of suspected PCD patients (Bustamante-Marin et al., 2020). Routine WES analysis in PCD most often focuses on identifying single-nucleotide variations (SNVs) and short insertions and deletions (INDELs), but as another kind of human genetic variation, copy number variations (CNVs), which also play an indispensable role in human Mendelian rare genetic disease (Pös et al., 2021). Meanwhile, the relationship between PCD and CNVs has not been clearly studied.

In this study, we found a patient who presented with highly suspected PCD symptoms but without PCD-associated biallelic pathogenic variants identified by WES-based SNV and INDEL analysis. Then we conducted WES-based CNV analysis and identified a novel dynein regulatory complex subunit 1 (*DRC1*) homozygous CNV. As a central component of the nexin-dynein regulatory complex (N-DRC), *DRC1* can conjugate peripheral A and adjacent B microtubule to sustain regular ciliary motility (Wirschell et al., 2013). *DRC1* variants, detected using routine WES analysis, resulting in DRC1 protein loss of function and consequently PCD with multiple morphological abnormalities of the sperm flagella (MMAF), have been reported in recent studies (Lei et al., 2022). In our study, we identified a novel *DRC1* CNV that can also cause PCD and MMAF, but the PCD-associated biallelic pathogenic variant could not be detected by routine WES analysis initially. Our study showed that the WES-based CNV detecting approach may be an assistant way to improve PCD genetic accuracy.

MATERIALS AND METHODS

Ethical Compliance

The review board of the second Xiangya Hospital of Central South University approved this study. Written informed consent was obtained from the patient and the healthy control.

Routine Whole-Exome Sequencing Analysis

EDTA anti-coagulated venous blood was collected from the patient, the patient's parents, and a healthy control. The genomic DNA was extracted using the QIAamp DNA Blood Mini Kit following the manufacturer's protocol. Whole exome enrichment was performed using xGen Exome Research Panel v2 and sequenced with the Illumina NovaSeq® systems.

The sequenced reads were aligned to the reference genome (hg19) using BWA MEN, and PCR duplicates were marked with PICARD. Variants were called by HaplotypeCaller in GATK4.0 with default parameters, and retained considering DP (reads depth) ≥ 10, MQ (Mapping Quality) ≥ 30, and GQ (Genotyping Quality) ≥ 20. After annotation using ANNOVAR, variants both in coding region and splicing site were kept and synonymous variants were removed. Beyond that, variants were filtered by allele frequencies (AF) in the 1000 genome project, the Genome Aggregation Database (gnomAD v2.1.1), the NHLBI GO Exome Sequencing Project (ESP) and a local AF database with threshold of 1%, and potential damaging effect (predicted to be deleterious by at least 2 predictive tools among SIFT, Polyphen2-HVAR, MutationTaster and CADD for variants in coding region; dbscSNV score > 0.6 for variants in splicing site.

Copy Number Variation Analysis

CNVs were called from the read depth of WES data using the ExomeDepth package according to the developers' guidelines. ExomeDepth is a validated method for exome read-depth analysis, generating normalized read counts of the test sample by using an optimized set of reference samples as a comparison to determine the presence of a CNV at the exon level (Royer-

Bertrand et al., 2021). Each exome was compared with a set of matched, aggregate reference samples for these analyses.

RNA Isolation, PCR and Sanger Sequencing

We collected nasal epithelial biopsy sample from the patient and a healthy control and extracted total RNA using a GeneJET RNA Purification Kit (K0731, Thermo Fisher Scientific, Waltham, MA, United States) according to the manufacturer's instructions. Then, we used TranScript® One-step gDNA Removal and cDNA synthesis SuperMix (AT311, Transgene) to synthesize cDNA. To confirm the deletion identified by CNV analysis, cDNA of *DRC1* were amplified using the GoldenStar® T6 Polymerase (TSE101, Tsingke). Primers were designed using the primer blast of NCBI (https://www.ncbi.nlm.nih.gov/tools/primer-blast/). The sequences of the primers are listed as following: forward primer: 5′-GAGCACTTGTCCACCCAG ATT-3′, reverse primer: 5′-GTATTGAGCATTTCCCACAGC-3′. Meanwhile, according to the manufacturer's instructions, genome DNA was obtained using QIAamp DNA Blood Mini Kit from the patient, patient's parents, and healthy control. PCR and Sanger sequencing were performed to validate the *DRC1* breakpoint. The primer sequences designed are listed as follows: forward primer: 5′- GAGCAGGGTCTTGATGATGTAA-3′, reverse primer: 5′- CACCTTTATGAGATCCAGGGAAA-3′.

High-Speed Video Microscopy Analysis

Nasal brush biopsy samples were imaged using an upright Olympus BX53 microscope (Olympus, Tokyo, Japan) and recorded using a scientific complementary metal oxide semiconductor camera (Prime BSI, Teledyne Photometrics Inc., United States) as previously described (Xu et al., 2022).

Sperm Morphological Analysis

Semen samples were collected from the patient after at least five days of sexual abstinence. According to the World Health Organization guideline to classify sperm flagella morphology (Cooper et al., 2010). Abnormal flagella of the sperm were classified as absent, short, bent, coiled, or irregular using Papanicolaou staining (Auger et al., 2016). Based on the morphology of the sperm flagella, each spermatozoon can only be classified in one morphological category.

Immunofluorescence

Nasal epithelial tissues and sperm were fixed in 4% paraformaldehyde. Immunofluorescence on the slides was performed as described previously (Xu et al., 2022). Briefly, the slides were incubated overnight at 4°C with the primary antibodies DRC4 (HPA041311, 1:50, Sigma-Aldrich, Missouri, United States), and anti-acetylated tubulin (T7451, 1:500, Sigma-Aldrich, Missouri, United States). Then secondary antibodies detected the antibody binding, including Alexa Fluor 488 anti-mouse IgG (A-21121, 1:200, Invitrogen, Carlsbad, CA, United States) and Alexa Fluor 555 anti-rabbit IgG (A31572, 1:400, Invitrogen, Carlsbad, CA, United States). After incubation for 2 h at 37°C, all the slides were stained with 2-(4-aminophenyl)-1H-indole-6-carboxamidine (DAPI) for 5 min at room temperature. Fluorescence signals were recorded using an Olympus BX53 microscope (Olympus, Tokyo, Japan) and scientific complementary metal oxide semiconductor (sCMOS) camera (Prime BSI, Teledyne Photometrics Inc., United States).

RESULTS

Case Presentation

The proband is a 19-year-old unmarried Chinese male with non-consanguineous parents and a healthy sister (**Figure 1A**). He was reported to have coughing, yellowish sputum, and sinusitis when he was three years old, and since then, the symptoms have been recurrent, and combined with exertional dyspnea. High resolution computed tomography revealed chronic sinusitis (**Figure 1B**), and bronchiectasis of both lungs (**Figure 1C**). The lung function test showed mild obstructive ventilatory impairment (predicted forced expiratory volume during the first second (FEV1): 79.3%, FEV1/forced vital capacity: 87.0%). In addition, nNO examination exhibited an abnormal low concentration (10.8 nL/min). HSVA of nasal brush biopsies showed that a normal ciliary beating frequency and a reduced amplitude in ciliary beating pattern (**Figure 1D** and **Supplementary Video S1**) compared with normal control (**Supplementary Video S2**). We also tested the motile function of the patient's sperm, which showed that the patient's spermatozoa were totally immotile (**Table 1**). Subsequent Papanicolaou staining also confirmed that the flagella morphologies of the patient were abnormal, which met the diagnostic criteria of MMAF (**Table 1**; **Figure 1E**).

Whole-Exome Sequencing-Based Copy Number Variation Analysis to Capture Disease-Causing Gene Variations

Combined with the above clinical symptoms of the patient: recurrent cough and sputum expectoration, nasal congestion since early childhood, abnormally low nNO levels, reduced ciliary beating amplitude, and MMAF phenotype, we highly suspected that he had PCD. Later, we performed WES-based SNV and INDEL analysis following PCD diagnostic criteria, and the filtering process was shown in **Supplementary Figure S1**. However, we did not identify any PCD-associated biallelic pathogenic variants (**Supplementary Table S1**). CNV analysis based on WES has been established to broaden the diagnostic rate in genetic disorders, so we further conducted CNV analysis. The results returned a homozygous deletion in exon 2 of *DRC1* in this patient (**Figure 2A**). Further PCR amplification and Sanger sequencing validated the homozygous absence of *DRC1* exon 2 at RNA level (**Figure 2C**). We next verified the breakpoint of the *DRC1* variant at the DNA level. Sanger sequencing of PCR product showed homozygous deletion of 6119 bp and the breakpoints were: NC_000002.11(NM_145038.5): g.26635488_26641606del, c.156-1724_244-2550del, r.156_243del, p. (Glu53Asnfs*13) in this patient (**Figure 2B** and **Supplementary Figure S2**). Yet, the results revealed the patient's parents were all heterozygous carriers (**Supplementary Figure S2**).

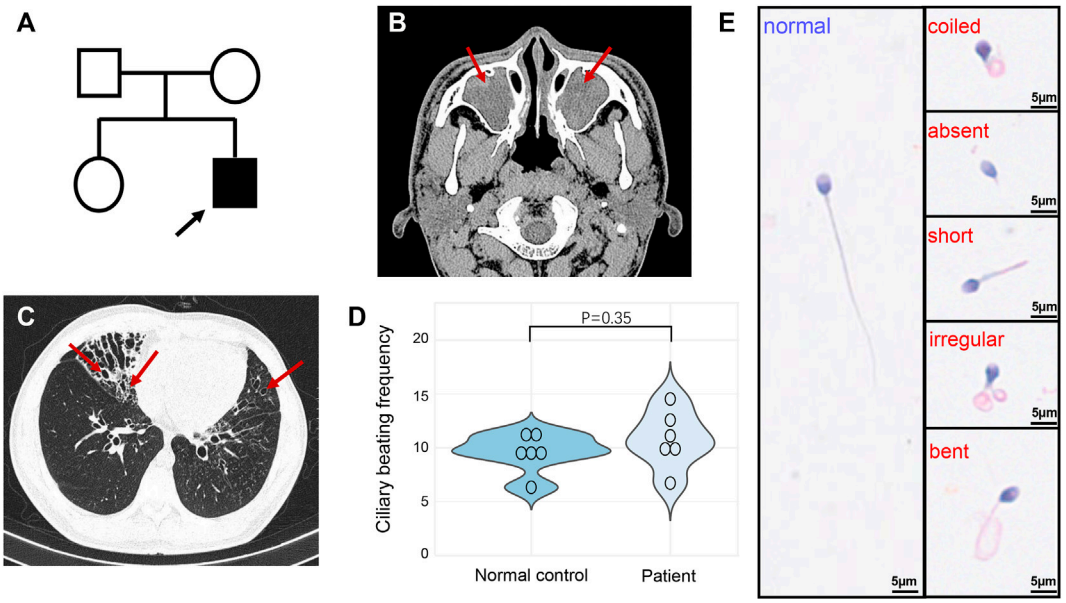


FIGURE 1 | Pedigree and clinical features of the patient. **(A)** The pedigree indicated that the patient was from a non-consanguineous family, and other family members were asymptomatic. The arrow indicates the proband. **(B)** High resolution computed tomography of sinuses exhibited sinusitis (arrows). **(C)** Chest high-resolution computed tomography showed bronchiectasis in both lungs (arrows). **(D)** The ciliary beating frequencies showed no statistically significant difference between normal control and patient. **(E)** Papanicolaou staining revealed the abnormal morphology of sperm flagella compared with the healthy control.

TABLE 1 | Semen parameters and sperm flagella morphology in the patient.

	Patient	References value
Semen parameters		
Semen volume (ml)	3.6	>1.5
Sperm count (10^6/ml)	>2	>15.0
Motility (%)	0	>40.0
Progressive motility (%)	0	>32.0
Sperm morphology		
Normal flagella (%)	3.4	>23.0
Coiled (%)	64.9	<17.0
Short (%)	7.7	<1.0
Absent (%)	7.2	<5.0
Bent (%)	10.6	<13.0
Irregular (%)	6.2	<2.0

At least 200 spermatozoa were observed for morphology analysis.

Analysis of Respiratory Cilia and Sperm Flagella

Previously, it has been reported that the DRC3 or DRC4 protein deletion can confirm the deletion of DRC1 protein through immunofluorescence analysis (Wirschell et al., 2013). Since we do not have a suitable DRC1 antibody, we used the DRC4 antibody (also named *GAS8*, *GAS11*) for immunofluorescence analysis. The results confirmed the absence of DRC4 protein expression in the ciliated tissue of the patient compared with the healthy control (**Figure 3A**); immunofluorescence of the sperm flagellum also confirmed the deficiency of DRC4 expression in the patient (**Figure 3B**). All these results suggested that the patient had DRC1 deficiency.

DISCUSSION

Our study recruited a patient with bronchiectasis, chronic sinusitis, abnormal sperm motility, and abnormal sperm flagellar morphology. The HSVA, nNO, and semen analysis results suggested that the patient has highly clinical suspicion of PCD combined with MMAF. We initially conducted the routine WES analysis to identify the disease-causing variants in this patient, but we got a negative result. Then we performed WES-based CNV analysis, which is less noticed in variants calling and filtering procedures. Finally, a novel homozygous *DRC1* CNV was identified. Subsequent PCR amplification, Sanger sequencing, and immunofluorescence supported the pathogenicity of the CNV in *DRC1*. Although the transmission electron microscopic analysis results were not available, the diagnosis of PCD was made because we identified biallelic pathogenic *DRC1* variants in this patient.

According to PCD diagnostic guidelines, since not all patients have the characteristic abnormal ciliary axonemal ultrastructure and beating pattern in HSVA, it is crucial to identify disease-associated biallelic variants for patients with clinically suspected PCD (Lucas et al., 2017). Currently, among the high-throughput sequencing methods to identify PCD pathogenic variants, the WES analysis is the first-line method in China (Zhao et al., 2021). Though WES analysis covers 1–1.5% of the human genome, it houses approximately all exons of the known protein-coding genes (Ng et al., 2009). Compared with other next-generation sequencing technologies, such as whole-genome sequencing (WGS), WES is a more affordable high-throughput technology that allows the analysis of the coding regions of more than 20,000

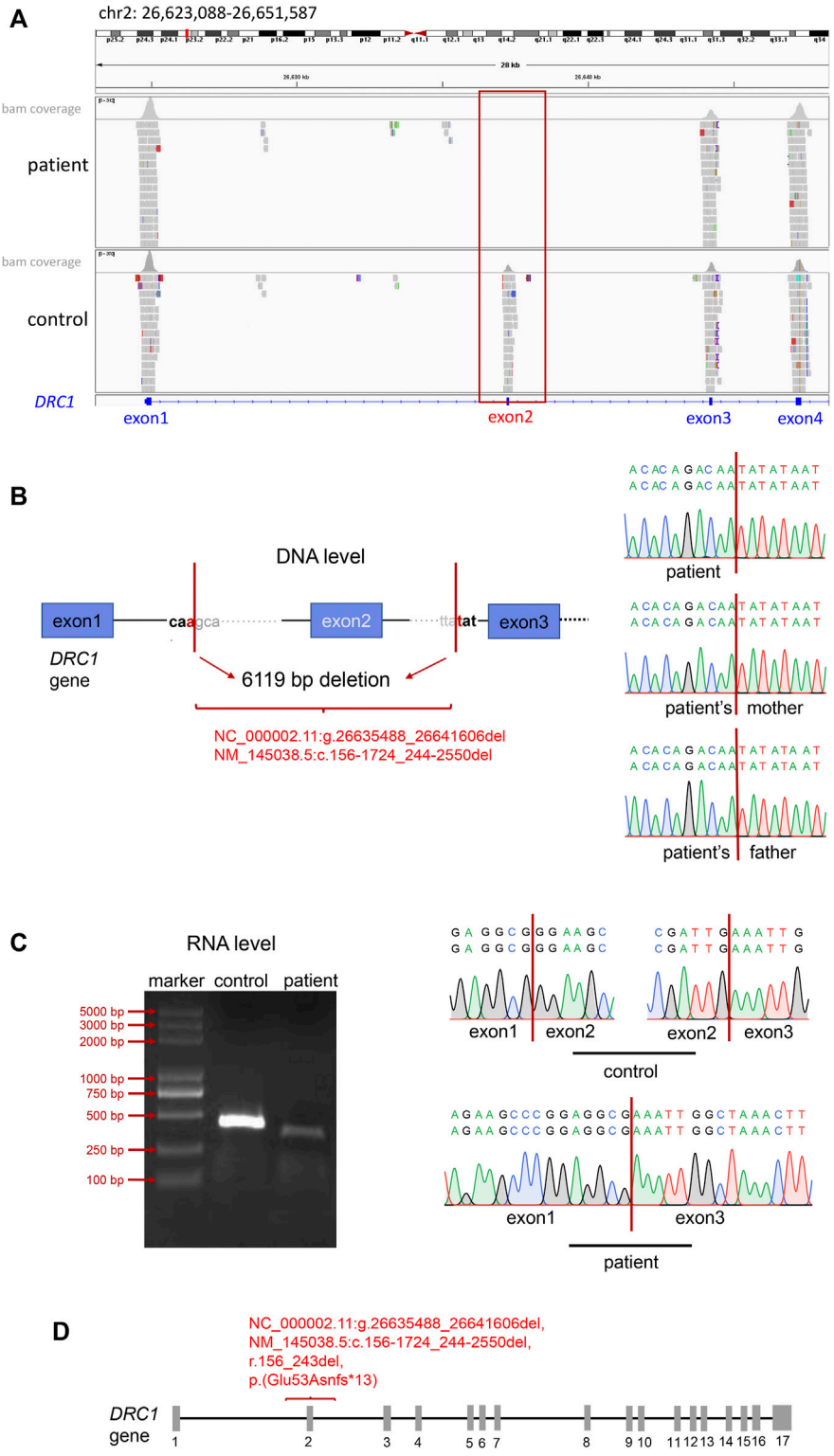


FIGURE 2 | Identification of the *DRC1* variant. **(A)** IGV tools revealed the absence of exon 2 in *DRC1*. **(B)** Sanger sequencing showed the 6119 bp deletion of *DRC1* in the patient and the patient's mother at DNA level. **(C)** Electrophoresis and Sanger sequencing identified the deletion of *DRC1* exon 2 in the patient compared with normal at RNA level. **(D)** The location of the novel *DRC1* homozygous variant in this report.

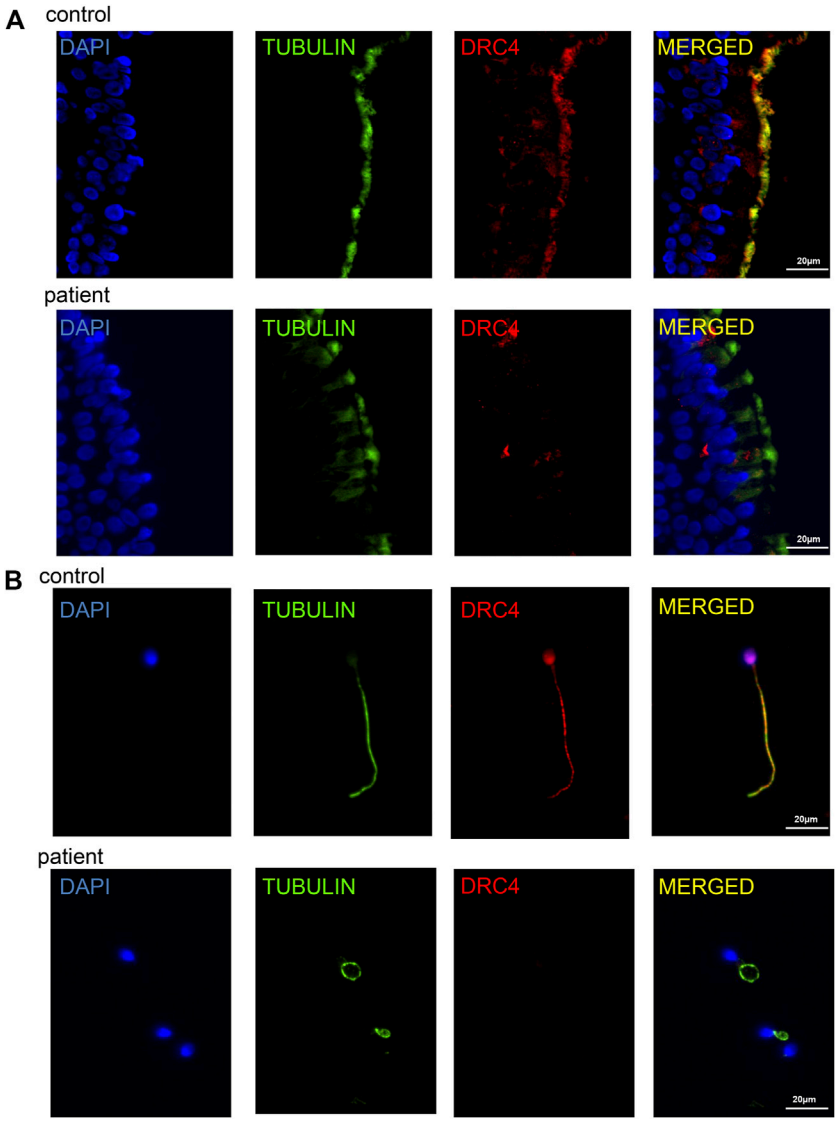


FIGURE 3 | Analysis of ciliary tissue and sperm flagellum. **(A)** immunofluorescence analysis showed the absence of DRC4 protein expression in ciliated tissue of the patient compared with normal control. **(B)** immunofluorescence analysis showed the absence of DRC4 protein expression in sperm flagella of the patient compared to normal control.

genes (Tetreault et al., 2015). Routine WES analysis mainly considered SNVs and INDELs, but the prevalence and clinical significance of CNVs in PCD genes are yet unclear. Until now, only two studies have been conducted to study the relationship between CNVs and PCD. Marshall reported that by combining WES and the targeted CNV method, the genetic diagnosis rate of PCD could increase from 42% to 76% (Marshall et al., 2015). A study from Japan found that CNVs might play an important role in PCD, and CNVs in *DRC1* were the main cause of PCD in the Japanese population (Takeuchi et al., 2020). All the above research indicated that CNVs were significant as PCD disease-causing variants.

Human genetic disorders may arise from genetic variations ranging from the whole chromosome down to SNV. For humans, compared with SNVs and INDELs (smaller than 50 bp), CNVs account for only a tiny fraction (Lappalainen et al., 2019). Traditional CNV assessment mainly contains genome-wide screening technologies such as comparative genomic hybridization-microarray (arrayCGH) or locus CNV detection based on targeted PCR, for instance, multiplex ligation-dependent probe amplification (MLPA) (Zech et al., 2021). However, these two methods are time-consuming and relatively expensive, and each one cannot fully cover all CNV fragments (Falzarano et al., 2015; Roca et al., 2019). In the last decade, WES-based CNV analysis has been used for detecting CNVs, and it can overcome some of these shortcomings. Firstly, it permits concurrently detection of large and small CNVs (as previously detected by array CGH and MLPA, respectively)

(Roca et al., 2019). Secondly, it is practical as it allows to determine SNVs, INDELs, and CNVs simultaneously, thus eliminating the necessity of using multiple different techniques in one patient and helping speed up the diagnostic process (Royer-Bertrand et al., 2021). Among WES-based CNV approaches, the "Exomedepth" package has been corroborated to have higher sensitivity and efficiency in detecting rare CNVs (Roca et al., 2019; Rajagopalan et al., 2020), and it is most used to identify CNVs in neurological diseases and mental disorders (Szatkiewicz et al., 2020; Cheng et al., 2021; Yu et al., 2021). Our study also used the "Exomedepth" package to call CNVs in a patient with a negative routine WES analysis result. The patient was finally confirmed to have a homozygous deletion of 6119 bp in *DRC1*, (NM_145038.5:c.156-1724_244-2550del), which contains exon 2 absence. The results suggested that WES-based CNV may help improve the diagnostic yield in highly suspected PCD.

The N-DRC functions as a linker between neighboring doublet microtubules, stabilizes the axonemal core structure, and serves as a central hub for controlling cilia motility (Gui et al., 2019). In most species, the N-DRC contains at least eleven, mostly well evolutionarily conserved subunits, *DRC1–11* (Osinka et al., 2019). Available data suggested that the 3-subunit core-complex (*DRC1/2/4*) of the N-DRC subunits is a scaffold for the assembly of functional subunits (*DRC3/5* and *DRC8/11*) (Gui et al., 2019). By now, DRC subunits deficiencies have been proved to cause motile ciliopathies. *DRC1*, *DRC2*, and *DRC4* were confirmed to be associated with PCD (Horani et al., 2013; Wirschell et al., 2013; Olbrich et al., 2015), and *DRC5* variants have been linked to asthenospermia and male infertility (Zhou, 2022). Variants in *DRC1* or *DRC2* could cause PCD and result in the loss of DRC4 protein expression, while *DRC4* does not affect the protein expression of DRC1 and DRC2 (Horani et al., 2013; Wirschell et al., 2013; Olbrich et al., 2015). *DRC1*, also known as *CCDC164*, locates on chromosome 2, consisting of 17 exons with 740 amino acids (Lei et al., 2022). A recent study found that *DRC1* variants could lead to PCD and MMAF, which is the same diagnosis as the patient we reported in this study (Lei et al., 2022). So far, only several genes have been covered to be related to PCD with MMAF, including *SPEF2*, *CFAP74*, *BRWD1*, *CCDC39*, *CCDC40*, *ARMC4*, and *DRC1* (Sha et al., 2020; Tu et al., 2020; Chen et al., 2021; Gao et al., 2021; Guo et al., 2021; Lei et al., 2022; Xu et al., 2022). Since the axonemal ultrastructure of respiratory cilia and sperm flagella is highly consistent, it is necessary to consider their sperm motility and morphology when diagnosing a patient with PCD. These findings provide strong evidence to confirm that the *DRC1* novel CNV is associated with PCD and MMAF.

In conclusion, we identified a novel homozygous variant of *DRC1* in a patient with PCD and MMAF by WES-based CNV analysis, while heterozygous in the patient's parents. Moreover, the novel *DRC1* variant (NM_145038.5:c.156-1724_244-2550del), can be found in Esat Asian populations of gnomAD SVs v2.1 database once (https://gnomad.broadinstitute.org/variant/DEL_2_15666?dataset=gnomad_sv_r2_1). Previous studies have always potted the importance of detecting SNVs and INDELs based on WES, often ignoring CNVs. Our study shows that WES-based CNV analysis is a helpful adjunct method for identifying disease-associated variants in highly suspected PCD patients and increases the appropriateness of WES as a first-line genetic diagnostic method for PCD. Further studies could be conducted on the importance of CNVs in PCD, and our results suggest that if routine WES testing cannot detect the PCD-associated pathogenic variants, WES-based CNV analysis can be considered, thus perhaps further improving the PCD diagnostic rate.

DATA AVAILABILITY STATEMENT

The datasets for this article are not publicly available due to concerns regarding participant/patient anonymity. Requests to access the datasets should be directed to the corresponding authors.

ETHICS STATEMENT

The studies involving human participants were reviewed and approved by The review board of the second Xiangya Hospital of Central South University. The patients/participants provided their written informed consent to participate in this study.

AUTHOR CONTRIBUTIONS

YL and CL collected the data and wrote the manuscript. RW, DY, BY, YX, CL, LW, SD, and TG analyzed, interpreted the data, and performed the clinical assessment. SL and HL designed the study and performed the clinical assessment. All authors reviewed, edited, and approved the final manuscript.

FUNDING

This study was supported by National Natural Science Foundation of China (82070003 to HL), Natural Science Foundation of Hunan Province, China (2021JJ30943 to HL), the Science and Technology Program of Changsha, China (kq1901120 to HL), Xiangya Medical Big Data of Central South University (Pulmonary Inflammatory Disease), and the National Key Clinical Specialty Construction Projects of China [(2012) No. 650].

ACKNOWLEDGMENTS

The authors wish to thank the patient and medical staff of the department of Pulmonary and Critical Care Medicine for their help and collaborations.

SUPPLEMENTARY MATERIAL

The Supplementary Material for this article can be found online at: https://www.frontiersin.org/articles/10.3389/fgene.2022.940292/full#supplementary-material

REFERENCES

Auger, J., Jouannet, P., and Eustache, F. (2016). Another Look at Human Sperm Morphology. *Hum. Reprod.* 31 (1), 10–23. doi:10.1093/humrep/dev251

Bhatt, R., and Hogg, C. (2020). Primary Ciliary Dyskinesia: a Major Player in a Bigger Game. *Breathe* 16 (2), 200047. doi:10.1183/20734735.0047-2020

Bustamante-Marin, X. M., Horani, A., Stoyanova, M., Charng, W.-L., Bottier, M., Sears, P. R., et al. (2020). Mutation of CFAP57, a Protein Required for the Asymmetric Targeting of a Subset of Inner Dynein Arms in Chlamydomonas, Causes Primary Ciliary Dyskinesia. *PLoS Genet.* 16 (8), e1008691. doi:10.1371/journal.pgen.1008691

Chen, D., Liang, Y., Li, J., Zhang, X., Zheng, R., Wang, X., et al. (2021). A Novel CCDC39 Mutation Causes Multiple Morphological Abnormalities of the Flagella in a Primary Ciliary Dyskinesia Patient. *Reprod. Biomed. Online* 43 (5), 920–930. doi:10.1016/j.rbmo.2021.07.005

Cheng, H.-L., Shao, Y.-R., Dong, Y., Dong, H.-L., Yang, L., Ma, Y., et al. (2021). Genetic Spectrum and Clinical Features in a Cohort of Chinese Patients with Autosomal Recessive Cerebellar Ataxias. *Transl. Neurodegener.* 10 (1), 40. doi:10.1186/s40035-021-00264-z

Cooper, T. G., Noonan, E., von Eckardstein, S., Auger, J., Baker, H. W. G., Behre, H. M., et al. (2010). World Health Organization Reference Values for Human Semen Characteristics*‡. *Hum. Reprod. Update* 16 (3), 231–245. doi:10.1093/humupd/dmp048

Falzarano, M., Scotton, C., Passarelli, C., and Ferlini, A. (2015). Duchenne Muscular Dystrophy: From Diagnosis to Therapy. *Molecules* 20 (10), 18168–18184. doi:10.3390/molecules201018168

Gao, Y., Xu, C., Tan, Q., Shen, Q., Wu, H., Lv, M., et al. (2021). Case Report: Novel Biallelic Mutations in ARMC4 Cause Primary Ciliary Dyskinesia and Male Infertility in a Chinese Family. *Front. Genet.* 12, 715339. doi:10.3389/fgene.2021.715339

Gui, L., Song, K., Tritschler, D., Bower, R., Yan, S., Dai, A., et al. (2019). Scaffold Subunits Support Associated Subunit Assembly in the Chlamydomonas Ciliary Nexin-Dynein Regulatory Complex. *Proc. Natl. Acad. Sci. U.S.A.* 116 (46), 23152–23162. doi:10.1073/pnas.1910960116

Guo, T., Tu, C.-F., Yang, D.-H., Ding, S.-Z., Lei, C., Wang, R.-C., et al. (2021). Biallelic BRWD1 Variants Cause Male Infertility with Asthenoteratozoospermia and Likely Primary Ciliary Dyskinesia. *Hum. Genet.* 140 (5), 761–773. doi:10.1007/s00439-020-02241-4

Hannah, W. B., Seifert, B. A., Truty, R., Zariwala, M. A., Ameel, K., and Zhao, Y. (2022). The Global Prevalence and Ethnic Heterogeneity of Primary Ciliary Dyskinesia Gene Variants: a Genetic Database Analysis. *Lancet. Respir. Med.* 10, 459–468. doi:10.1016/s2213-2600(21)00453-7

Horani, A., Brody, S. L., Ferkol, T. W., Shoseyov, D., Wasserman, M. G., Ta-shma, A., et al. (2013). CCDC65 Mutation Causes Primary Ciliary Dyskinesia with Normal Ultrastructure and Hyperkinetic Cilia. *PloS One* 8 (8), e72299. doi:10.1371/journal.pone.0072299

Lappalainen, T., Scott, A. J., Brandt, M., and Hall, I. M. (2019). Genomic Analysis in the Age of Human Genome Sequencing. *Cell.* 177 (1), 70–84. doi:10.1016/j.cell.2019.02.032

Lei, C., Yang, D., Wang, R., Ding, S., Wang, L., Guo, T., et al. (2022). DRC1 Deficiency Caused Primary Ciliary Dyskinesia and MMAF in a Chinese Patient. *J. Hum. Genet.* 67 (4), 197–201. doi:10.1038/s10038-021-00985-z

Lucas, J. S., Barbato, A., Collins, S. A., Goutaki, M., Behan, L., Caudri, D., et al. (2017). European Respiratory Society Guidelines for the Diagnosis of Primary Ciliary Dyskinesia. *Eur. Respir. J.* 49 (1), 2016. doi:10.1183/13993003.01090-2016

Lucas, J. S., Davis, S. D., Omran, H., and Shoemark, A. (2020). Primary Ciliary Dyskinesia in the Genomics Age. *Lancet Respir. Med.* 8 (2), 202–216. doi:10.1016/s2213-2600(19)30374-1

Marshall, C. R., Scherer, S. W., Zariwala, M. A., Lau, L., Paton, T. A., Stockley, T., et al. (2015). Whole-Exome Sequencing and Targeted Copy Number Analysis in Primary Ciliary Dyskinesia. *G3* 5 (8), 1775–1781. doi:10.1534/g3.115.019851

Ng, S. B., Turner, E. H., Robertson, P. D., Flygare, S. D., Bigham, A. W., Lee, C., et al. (2009). Targeted Capture and Massively Parallel Sequencing of 12 Human Exomes. *Nature* 461 (7261), 272–276. doi:10.1038/nature08250

Olbrich, H., Cremers, C., Loges, N. T., Werner, C., Nielsen, K. G., Marthin, J. K., et al. (2015). Loss-of-Function GAS8 Mutations Cause Primary Ciliary Dyskinesia and Disrupt the Nexin-Dynein Regulatory Complex. *Am. J. Hum. Genet.* 97 (4), 546–554. doi:10.1016/j.ajhg.2015.08.012

Osinka, A., Poprzeczko, M., Zielinska, M. M., Fabczak, H., Joachimiak, E., and Wloga, D. (2019). Ciliary Proteins: Filling the Gaps. Recent Advances in Deciphering the Protein Composition of Motile Ciliary Complexes. *Cells* 8 (7), 730. doi:10.3390/cells8070730

Pös, O., Radvanszky, J., Buglyó, G., Pös, Z., Rusnakova, D., Nagy, B., et al. (2021). DNA Copy Number Variation: Main Characteristics, Evolutionary Significance, and Pathological Aspects. *Biomed. J.* 44 (5), 548–559. doi:10.1016/j.bj.2021.02.003

Rajagopalan, R., Murrell, J. R., Luo, M., and Conlin, L. K. (2020). A Highly Sensitive and Specific Workflow for Detecting Rare Copy-Number Variants from Exome Sequencing Data. *Genome Med.* 12 (1), 14. doi:10.1186/s13073-020-0712-0

Roca, I., González-Castro, L., Fernández, H., Couce, M. L., and Fernández-Marmiesse, A. (2019). Free-access Copy-Number Variant Detection Tools for Targeted Next-Generation Sequencing Data. *Mutat. Research/Reviews Mutat. Res.* 779, 114–125. doi:10.1016/j.mrrev.2019.02.005

Royer-Bertrand, B., Cisarova, K., Niel-Butschi, F., Mittaz-Crettol, L., Fodstad, H., and Superti-Furga, A. (2021). CNV Detection from Exome Sequencing Data in Routine Diagnostics of Rare Genetic Disorders: Opportunities and Limitations. *Genes (Basel)* 12 (9), 1427. doi:10.3390/genes12091427

Sha, Y., Wei, X., Ding, L., Ji, Z., Mei, L., Huang, X., et al. (2020). Biallelic Mutations of CFAP74 May Cause Human Primary Ciliary Dyskinesia and MMAF Phenotype. *J. Hum. Genet.* 65 (11), 961–969. doi:10.1038/s10038-020-0790-2

Shoemark, A. (2017). Applications of Emerging Transmission Electron Microscopy Technology in PCD Research and Diagnosis. *Ultrastruct. Pathol.* 41 (6), 408–414. doi:10.1080/01913123.2017.1365789

Szatkiewicz, J. P., Fromer, M., Nonneman, R. J., Ancalade, N., Johnson, J. S., Stahl, E. A., et al. (2020). Characterization of Single Gene Copy Number Variants in Schizophrenia. *Biol. Psychiatry* 87 (8), 736–744. doi:10.1016/j.biopsych.2019.09.023

Takeuchi, K., Xu, Y., Kitano, M., Chiyonobu, K., Abo, M., Ikegami, K., et al. (2020). Copy Number Variation in DRC1 Is the Major Cause of Primary Ciliary Dyskinesia in the Japanese Population. *Mol. Genet. Genomic Med.* 8 (3), e1137. doi:10.1002/mgg3.1137

Tetreault, M., Bareke, E., Nadaf, J., Alirezaie, N., and Majewski, J. (2015). Whole-exome Sequencing as a Diagnostic Tool: Current Challenges and Future Opportunities. *Expert Rev. Mol. Diagnostics* 15 (6), 749–760. doi:10.1586/14737159.2015.1039516

Tu, C., Nie, H., Meng, L., Wang, W., Li, H., Yuan, S., et al. (2020). Novel Mutations in SPEF2 Causing Different Defects between Flagella and Cilia Bridge: the Phenotypic Link between MMAF and PCD. *Hum. Genet.* 139 (2), 257–271. doi:10.1007/s00439-020-02110-0

Wallmeier, J., Nielsen, K. G., Kuehni, C. E., Lucas, J. S., Leigh, M. W., Zariwala, M. A., et al. (2020). Motile Ciliopathies. *Nat. Rev. Dis. Prim.* 6 (1), 77. doi:10.1038/s41572-020-0209-6

Werner, C., and Kouis, P. (2017). Should Transmission Electron Microscopy and Ultrastructural Cilia Evaluation Remain Part of the Diagnostic Work-Up for Primary Ciliary Dyskinesia? *Ultrastruct. Pathol.* 41 (6), 386–389. doi:10.1080/01913123.2017.1362089

Wirschell, M., Olbrich, H., Werner, C., Tritschler, D., Bower, R., Sale, W. S., et al. (2013). The Nexin-Dynein Regulatory Complex Subunit DRC1 Is Essential for Motile Cilia Function in Algae and Humans. *Nat. Genet.* 45 (3), 262–268. doi:10.1038/ng.2533

Xu, Y., Yang, B., Lei, C., Yang, D.-h., Ding, S., Lu, C., et al. (2022). Novel Compound Heterozygous Variants in CCDC40 Associated with Primary Ciliary Dyskinesia and Multiple Morphological Abnormalities of the Sperm Flagella. *Pgpm* Vol. 15, 341–350. doi:10.2147/pgpm.s359821

Yu, E., Rudakou, U., Krohn, L., Mufti, K., Ruskey, J. A., Asayesh, F., et al. (2021). Analysis of Heterozygous PRKN Variants and Copy-Number Variations in Parkinson's Disease. *Mov. Disord.* 36 (1), 178–187. doi:10.1002/mds.28299

Zech, M., Boesch, S., Škorvánek, M., Necpál, J., Švantnerová, J., Wagner, M., et al. (2021). Clinically Relevant Copy-Number Variants in Exome Sequencing Data

of Patients with Dystonia. *Park. Relat. Disord.* 84, 129–134. doi:10.1016/j.parkreldis.2021.02.013

Zhao, X., Bian, C., Liu, K., Xu, W., Liu, Y., Tian, X., et al. (2021). Clinical Characteristics and Genetic Spectrum of 26 Individuals of Chinese Origin with Primary Ciliary Dyskinesia. *Orphanet J. Rare Dis.* 16 (1), 293. doi:10.1186/s13023-021-01840-2

Zhou, S. (2022). Bi-allelic Variants in Human TCTE1/DRC5 Cause Asthenospermia and Male Infertility. *Eur. J. Hum. Genet.* 30, 721. doi:10.1038/s41431-022-01095-w

Conflict of Interest: The authors declare that the research was conducted in the absence of any commercial or financial relationships that could be construed as a potential conflict of interest.

Publisher's Note: All claims expressed in this article are solely those of the authors and do not necessarily represent those of their affiliated organizations, or those of the publisher, the editors and the reviewers. Any product that may be evaluated in this article, or claim that may be made by its manufacturer, is not guaranteed or endorsed by the publisher.

Copyright © 2022 Liu, Lei, Wang, Yang, Yang, Xu, Lu, Wang, Ding, Guo, Liu and Luo. This is an open-access article distributed under the terms of the Creative Commons Attribution License (CC BY). The use, distribution or reproduction in other forums is permitted, provided the original author(s) and the copyright owner(s) are credited and that the original publication in this journal is cited, in accordance with accepted academic practice. No use, distribution or reproduction is permitted which does not comply with these terms.

frontiers | Frontiers in Genetics

CASE REPORT
published: 11 July 2022
doi: 10.3389/fgene.2022.892940

Case Report: Identification of Two Variants of *ALG13* in Families With or Without Seizure and Binocular Strabismus: Phenotypic Spectrum Analysis

Tao Cai[1,2]*, *Jieting Huang*[1,3], *Xiuwei Ma*[1], *Siqi Hu*[1,4], *Lina Zhu*[1], *Jinwen Zhu*[5] and *Zhichun Feng*[1,3,4]*

[1]Senior Department of Pediatrics, the Seventh Medical Center of PLA General Hospital, Beijing, China, [2]Experimental Medicine Section, National Institutes of Health/National Institute of Dental and Craniofacial Research, Bethesda, MD, United States, [3]Beijing Key Laboratory of Pediatric Organ Failure, Beijing, China, [4]The National Engineering Laboratory for Birth Defects Prevention and Control of Key Technology, Beijing, China, [5]Angen Gene Medicine Technology, Beijing, China

OPEN ACCESS

Edited by:
Tieliu Shi,
Hunan University of Arts and Science, China

Reviewed by:
Ning Wang,
Jiangnan University, China
Huijun Wang,
Children's Hospital, Fudan University, China

***Correspondence:**
Tao Cai
genfax1@gmail.com
Zhichun Feng
zhjfengzc@126.com

Specialty section:
This article was submitted to Genetics of Common and Rare Diseases, a section of the journal Frontiers in Genetics

Received: 09 March 2022
Accepted: 07 June 2022
Published: 11 July 2022

Citation:
Cai T, Huang J, Ma X, Hu S, Zhu L, Zhu J and Feng Z (2022) Case Report: Identification of Two Variants of ALG13 in Families With or Without Seizure and Binocular Strabismus: Phenotypic Spectrum Analysis. Front. Genet. 13:892940. doi: 10.3389/fgene.2022.892940

Background: Genetic causes in most affected children with intellectual disability and/or development delay remain unknown.

Methods: To identify potential variants responsible for these disorders, we recruited 161 affected families and performed whole-exome sequencing and associated bioinformatics analysis.

Results: In the present study, we report the identification of variants in the *ALG13* gene in two of the families. In family 1, a known pathogenic missense variant (c.23T > C; p.V8A) of *ALG13* was identified in a boy and his mother. In family 2, a novel missense variant (c.862C > G; p.L288V) of the same gene was identified in the affected boy and his phenotypically normal mother. Genotype–phenotype correlation analysis by comparing reported 28 different variants (HGMD) showed that three major phenotypes, including various seizures/epilepsy, intellectual disability, and development delay (such as growth, speech, motor, etc.), are present in most affected individuals. However, other phenotypes, such as strabismus and absence of seizure in our second patient, are not reported if any, which may represent a unique case of X-linked recessive nonsyndromic disorder caused by a mutation in *ALG13*.

Conclusion: We identified two missense variants in *ALG13* in a cohort of 161 families with affected individuals diagnosed as intellectual disability and/or development delay. A novel c.862C > G mutation may represent a case of X-linked recessive.

Keywords: ALG13, mutation, whole-exome sequencing, development delay, X-linked

INTRODUCTION

The *ALG13* gene encodes a subunit of a bipartite UDP-N-acetylglucosamine transferase that regulates protein folding and stability, which is mapped to Xq23 and widely expressed in human tissues, such as brain, liver, and kidney (MIM: 300776). The first *ALG13* mutation with *de novo* origin was identified in a male infant diagnosed with congenital disorders of glycosylation type I with refractory epilepsy, microcephaly, extrapyramidal, and pyramidal symptoms (Timal, et al., 2012).

Many of the affected individuals were diagnosed with developmental and epileptic encephalopathy 36 (DEE36, MIM: 300884), which is caused by heterozygous or hemizygous mutation in *ALG13*. DEE36 is characterized by the onset of seizures at a mean age of 6.5 months. Most patients present with infantile spasms associated with hypsarrhythmia on EEG, consistent with a clinical diagnosis of West syndrome.

To date, a total of 28 different mutations in *ALG13* (HGMD) have been identified in affected individuals or families with epileptic encephalopathies (Epi, et al., 2013; Moller, et al., 2016), intellectual disability (Bissar-Tadmouri, et al., 2014), infantile spasms (Michaud, et al., 2014), West syndrome (Hino-Fukuyo, et al., 2015) or Lennox–Gastaut syndrome (Zhou, et al., 2018; Stranneheim, et al., 2021), congenital disorder of glycosylation (Alsharhan, et al., 2021), and several rare conditions such as left ventricular obstruction (Jin, et al., 2017) and fetal alcohol syndrome (de la Morena-Barrio, et al., 2018).

In the present study, we report the identification of two variants of *ALG13* from two affected males with development delay and seizures or intellectual disability binocular strabismus, including a novel missense variant (c.862C > G; p.L288V) and a previously reported variant (c.23T > C; p.V8A). For a better understanding of this extremely rare disease, we present a detailed phenotype–genotype correlation analysis and a brief literature review.

MATERIALS AND METHODS

Patients and Standard Protocols

Informed consents were obtained from all participants and in the case of minors, from their parents. This study was approved by the Seventh Medical Center of PLA General Hospital Ethics Committee at Beijing (no. 2022-37). A total of 503 individuals in 161 families, including 175 diagnosed as intellectual disability and/or development delay and 328 unaffected individuals, were recruited for genetic analysis. In the current study, three affected individuals with development defects in two families were presented.

WES Analysis and Sanger Sequencing

Genomic DNAs were isolated from peripheral blood leukocytes. The captured exome by a SureSelect Human All Exon Kit (Agilent, Santa Clara, CA) was sequenced by HiSeq2000 sequencer (Illumina, San Diego, CA) and analyzed as previously described (Yu, et al., 2016; Zhu, et al., 2019; Li, et al., 2021). The reads were aligned to hg19, and the variants were identified through the GATK pipeline. An average sequence depth of coverage was 149× for exome sequences. Potential pathogenic variants were selected for further bioinformatics analysis. Primers (forward: TCACAGAAGGCAGTCACT; reverse: CGGAATAATGGGAAGAGGAA) were used for Sanger sequencing confirmation of the c.23T > C variant in the ALG13 gene (NM_001099922). Primer sequences for the confirmation of the second variant (c.862C > G) in *ALG13* include the forward ACCATAATTGTTGAGCTGAGCA and reverse TTGGATTCAACACAGCTGGC.

ALG13 Protein Structure Analysis

The ALG13 protein motif was predicted by the SmartMotif (http://smart.embl-heidelberg.de/). Three-dimensional structure of the AlphaFold ALG13 prediction was obtained from UniProt (https://www.uniprot.org; model ID: AF-Q9NP73-F1). Its associated figures were produced using the program PyMOL (https://pymol.org/2/).

RESULTS

Clinical Manifestations of Three Affected Individuals in Two Unrelated Families

In family 1, the affected boy (**Figure 1A**) was first referred to the clinic when he was 2 years old due to intellectual disability, speech and motor development delay, and seizures. Seizures were first observed when the affected boy was 9 months old, which occurred 1–2 times per week and could be controlled by levetiracetam. He could only call "mom" but no other words at 3 years of age. His walking was unstable and could easily fall down. His height and head circumference were in normal ranges. His mother was also diagnosed with intellectual disability, but with no seizures. She could not read or count. His father was normal. An EEK examination at nearly 2 years of age of the body showed abnormal slow-wave activities in bilateral brain. His MRI showed protruding temporal angle of the left lateral ventricle and slightly wider bilateral frontotemporal extracerebral space.

In family 2, a 3-year-old boy (**Figure 1B**) with intellectual disability and speech and motor development delay was recruited for genetic analysis. His speech was delayed. He could call "mom" and stand up after 2 years of age. His hand movements were not coordinated. His walk was not stable and fell down easily. No seizure was observed. Physical examination showed binocular strabismus and abnormal finger-nose test (FNT). His height and head circumference were in normal ranges. Both of his parents were phenotypically normal. MRI images (**Figure 1C**) showed delayed myelination and widening of bilateral frontotemporal extracerebral space. His EEK report was normal. A combined analysis of DDST, Gesell, and Bayley tests when he was about 3 years old revealed low levels in his language, social behavior, movement, adaptability, and development quotient.

Identification of Mutations in the ALG13 Gene by WES

Trio-WES analysis for family 1 identified a known pathogenic missense variant (c.23T > C; p.V8A) in the *ALG13* gene (NM_001099922.3) and further confirmed by Sanger sequencing (**Figure 2A**) from both the affected boy and his mother. The same

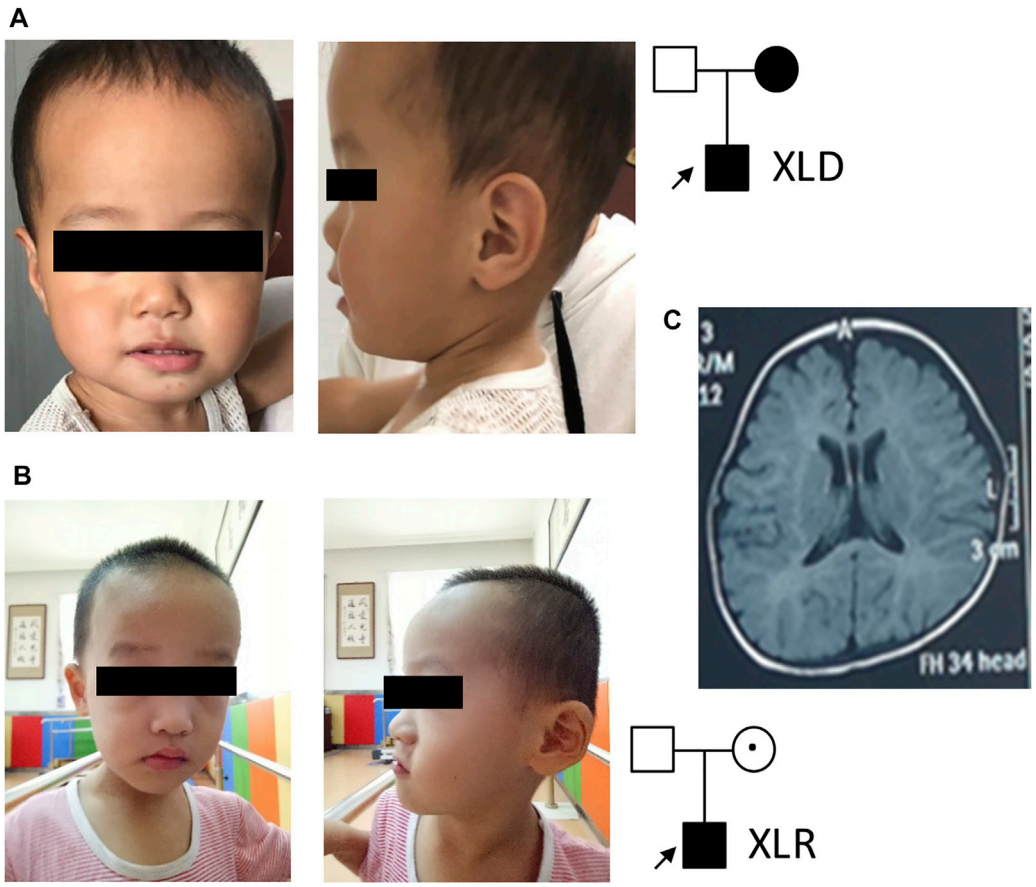


FIGURE 1 | Patient pedigrees and radiographic findings. **(A)** Patient 1 photo and pedigree. **(B)** Patient 2 photo and pedigree. **(C)** Representative MRI image of patient 2.

mutation as a *de novo* allele was previously detected in a female patient (Datta, et al., 2021), who showed mild developmental delay and seizures starting from the second year of life (**Table 1**). The p.V8 residue is located in the Glyco_tran_28_C domain (amino acids 3–133) at the N-terminal region of the encoded protein (**Figures 2C,D**), which involves monogalactosyldiacylglycerol synthase and UDP-N-acetylglucosamine transferase (Pfam, SmartMotif).

Trio-WES analysis for family 2 identified a previously undescribed potentially pathogenic missense variant (c.862C > G) from the affected boy and his phenotypically normal mother. Sanger sequencing further confirmed this variant (**Figure 2B**). Bioinformatics analysis revealed that this variant is not present in ExAC or the in-house database and predicted to be disease-causing by MutationTaster and Polyphen2. Smart Motif analysis revealed that the mutation p.L288 is mapped to the OTU domain (amino acids 237–348) in the ALG13 protein (**Figures 2C,D**), which is OTU-like cysteine protease motif (Makarova, et al., 2000).

Genotype and Phenotype Profile Related to *ALG13* Mutations

As shown in **Table 1**, we summarized 28 different mutations that are listed in HGMD and two mutations identified in the present study. Affected individuals and/or families were either in X-linked dominant (XLD) or X-linked recessive (XLR) pattern or with *de novo* mutation (DNM) origins. Family 1 in our case is in the XLD form, while family 2 is in the XLR pattern. Most of the mutations in **Table 1** are missense variants (27/30); three of them are splicing and deletion mutations (3/30). Three major phenotypes, including various seizures/epilepsy, intellectual disability, and development delay (such as growth, speech, motor, etc.), are observed in most of the cases. Less frequently observed phenotypes include strabismus, optic nerve atrophy, left ventricular obstruction, and ataxia.

DISCUSSION

In the present study, we identified two variants in the *ALG13* gene in patients with either typical phenotypes in family 1 with XLD inheritance form (seizures, intellectual disability, speech, and motor development delay) or atypical phenotypes in family 2 with XLR inheritance pattern (mild intellectual disability, speech and motor development delay, mild ataxia, and binocular strabismus, but no seizures). Previously, only 28 different variants were reported (HGMD). Three of them (c.845G > A; p.G282E,

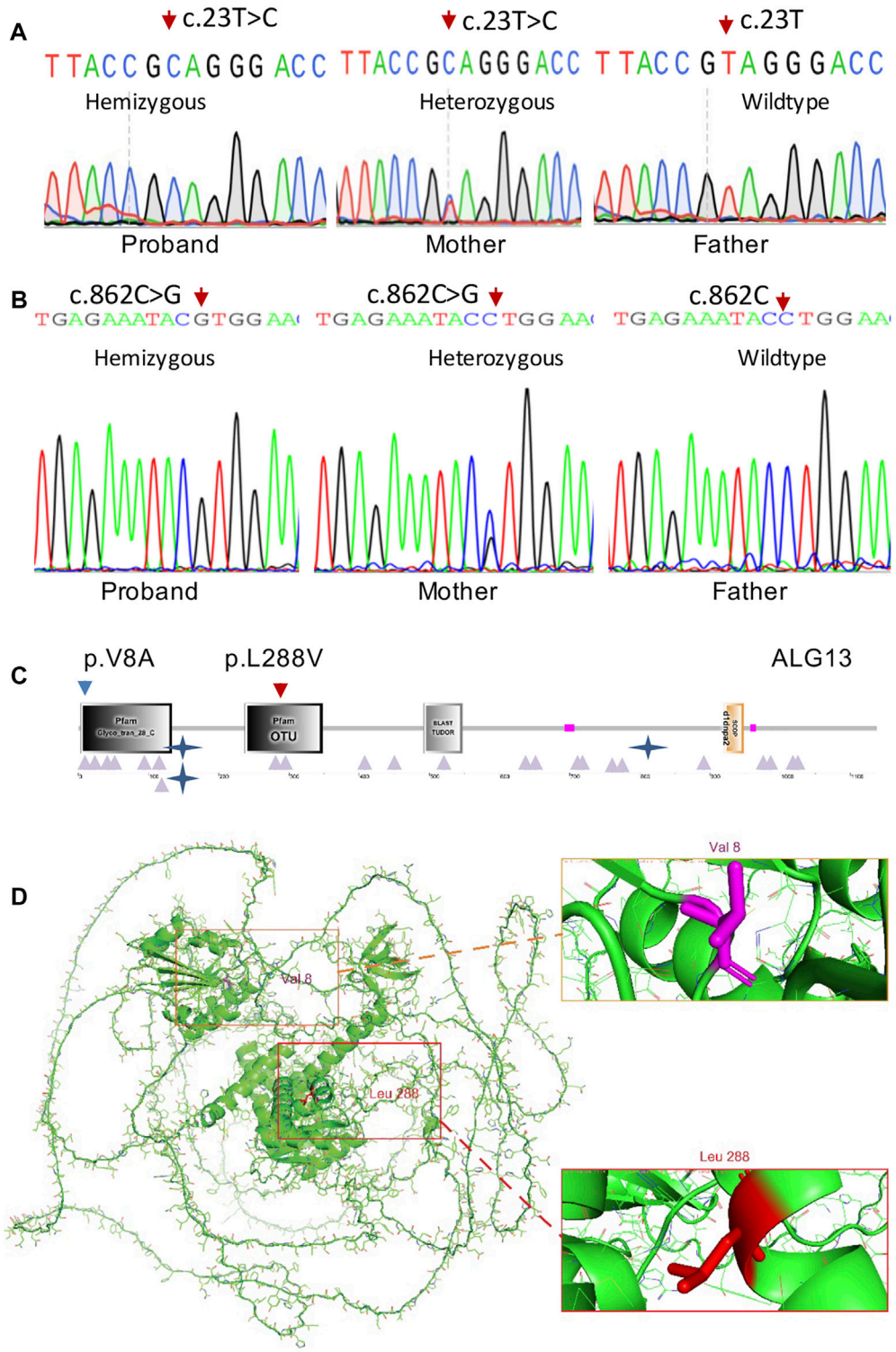


FIGURE 2 | ALG13 mutations and expression. **(A)** Sanger sequencing confirmation of the c.23T > C mutation in case 1 and his mother. **(B)** Sanger sequencing confirmation of the c.862C > G mutation in case 2 and his mother. **(C)** Schematic representations of functional domains of ALG13. The p.V8A mutation of family 1 is located in the Glyco_tans_28 domain at N-terminus (amino acid 3–133). The p.L288V mutation of family 2 is mapped in the OUT domain (amino acid 237–348). **(D)** Residue p.V8 and p.L288 positions are indicated in red in the 3-dimensional structure of the ALG13 protein.

TABLE 1 | Genotype–phenotype correlation analyses for affected individuals with ALG13 variants. The bold presents the phenotype in this study or a special phenotype related to this study.

HGVS	Reported main phenotypes	Brief annotation	References
V8A	Seizures and mild developmental delay (DD)	*De novo* mutation	Datta et al. (2021)
V8A	**Seizures, intellectual disability (ID), speech and motor DD**	**Affected mother and son**	This study
I17N	Lennox-Gastaut syndrome	Epileptic encephalopathy	Ji et al. (2019)
E30Q	Microcephaly, global DD, hypoxic ischemic encephalopathy, and hypotonia	OMIM: 300776	Monies et al. (2019)
Q40H	Epileptic encephalopathy		Datta et al. (2021)
T57P	Epileptic encephalopathy		Datta et al. (2021)
K94E	Congenital disorder of glycosylation 1	OMIM: 300884	Timal et al. (2012)
N107S	Lennox-Gastaut syndrome; **strabismus** in patient 3	Epileptic encephalopathy	Epi et al. (2013) Paprocka et al. (2021)
N107T	Neurodevelopmental disorder		Geisheker et al. (2017)
G282E	Epileptic encephalopathy, infantile		Wei et al. (2018)
L288V	**ID, speech and motor DD; no seizure; finger-nose test (FNT, +); strabismus; MRI: myelination delayed, et al**	EEK (-); the variant-carrier mother is normal	This study
P294S	West syndrome and optic nerve atrophy	Infantile spasms	Hino-Fukuyo et al. (2015)
K411N	Neurological disorder	No detailed info	Jiao et al. (2019)
E463G	Seizures, motor, and speech DD		Gadomski et al. (2017)
Q547H	Epileptic encephalopathy		Moller et al. (2016)
E640K	ID, gross and fine motor DD		Monies et al. (2019)
P658L	Lennox-Gastaut syndrome	Epileptic encephalopathy	Stranneheim et al. (2021)
R701H	Left ventricular obstruction and neurodevelopmental disorder		Jin et al. (2017)
S702R	Seizures and ID		Farwell et al. (2015)
V758F	Congenital disorder of glycosylation	OMIM: 300884	Alsharhan et al. (2021)
R769W	Epilepsy, motor DD, and learning disability		Monies et al. (2019)
S891F	Fetal alcohol syndrome, predisposition to		de la Morena-Barrio et al. (2018)
P963S	Epilepsy and neurodevelopmental abnormalities		Amadori et al. (2020)
G972V	Congenital disorder of glycosylation	OMIM: 300884	Alsharhan et al. (2021)
P1005S	Congenital disorder of glycosylation	OMIM: 300884	Alsharhan et al. (2021)
P1073R	ID, X-linked		Harripaul et al. (2018)
Y1074C	ID, nonsyndromic		Bissar-Tadmouri et al. (2014)
c.384-5C > T	Lennox-Gastaut syndrome	A triad of seizure, EEG findings, and ID	Zhou et al. (2018)
c.384-1G > A	Epilepsy		Hesse et al. (2018)
S820_P862del	Congenital disorder of glycosylation	OMIM: 300884	Alsharhan et al. (2021)
Del 9p24.2	Infantile spasms		Michaud et al. (2014)

**Intellectual disability (ID); development delay (DD).*

c.1233G > C; p.K411N and c.384-5C > T) were identified in Chinese populations (Wei, et al., 2018; Zhou, et al., 2018; Jiao, et al., 2019). Our findings expanded the *ALG-13*-related mutation spectrum and *ALG-13*-associated clinic manifestations.

Genotype–phenotype correlation analysis indicates that the mild clinical manifestations of the patient in family 2 is resulted from a mild pathogenic mutation (c.862C > G; p.L288V). In fact, both leucine and valine in the p.L288V allele are alpha-amino acids, which implies that they contain an alpha-amino group, an alpha-carboxylic acid group, and a side chain isobutyl group/ isopropyl group. Based on the AlphaFold predicted structure model (**Figure 2D**), the Leu288 residue is located in α-helix.

In contrast, alanine in the p.V8A variant in family 1 is a simple amino acid, which has just a methyl as its side chain. Based on the AlphaFold predicted structure model (**Figure 2D**), Val8 residue is located in the loop region involving glycosyltransferase activity (amino acids 1–125), thereby causing more severe clinic phenotypes as we described earlier.

Based on several commonly used gene expression databases, such as BioGPS and human brain transcriptome, the human *ALG13* gene is widely expressed in many tissues, including neurons in developing and adult brain tissues (**Supplementary Figure S1**). Brain-associated clinical manifestations, such as seizures and intellectual disability, are apparently correlated with cortical and central nervous dysfunctions in the affected individuals with *ALG13* variants. Additional rare phenotypes, such as ataxia, nystagmus, and strabismus, are potentially associated with developmental defects or dysfunctions of the cerebellum and brain stem tissues.

In the *Alg13* knockout mouse model, *Alg13* deficiency resulted in an increased seizure and susceptibility in the $Alg13^{-/-}$ mice (Gao, et al., 2019). Previous studies also explored the possible mechanisms of *Alg13*-involved epilepsy by showing hyperactive mTOR signaling pathways in the cortex and hippocampus of $Alg13^{-/-}$ mice (Gao, et al., 2019; Huo, et al., 2020). Further studies using patch-clamp recordings demonstrated that $Alg13^{-/-}$ mice show a marked decrease in the gamma-aminobutyric acid A receptor (GABAAR)–mediated inhibitory synaptic transmission (Huo, et al., 2020). At the human level, a majority of variants are missense, which are linked to either X-linked dominant

phenotypes due to stronger pathogenic variants (such as the variant in family 1) or X-linked recessive phenotypes due to mild pathogenetic variants (such as the variant in family 2).

CONCLUSION

Taken together, we provided clinical and bioinformatics evidences that two *ALG13* variants are pathogenic for the affected individuals with *ALG13*-associated phenotypes. However, the underlying mechanism remains to be explored in further studies.

DATA AVAILABILITY STATEMENT

The original datasets presented in the study are included in the article/**Supplementary Material**, further inquiries can be directed to the corresponding author.

ETHICS STATEMENT

The studies involving human participants were reviewed and approved by the Seventh Medical Center of PLA General Hospital Ethics Committee. Written informed consent to participate in this study was provided by the participants' legal guardian/next of kin. Written informed consent was obtained from the individual(s) and minor(s)' legal guardian/next of kin for the publication of any potentially identifiable images or data included in this article.

AUTHOR CONTRIBUTIONS

TC and ZF conceived and designed the experiment and wrote the manuscript. JH, SH, and JZ provided WES and bioinformatics analysis and performed the experiments. XM and LZ provided clinical information.

ACKNOWLEDGMENTS

The authors are grateful to the patients and family members for their participation in this study.

SUPPLEMENTARY MATERIAL

The Supplementary Material for this article can be found online at: https://www.frontiersin.org/articles/10.3389/fgene.2022.892940/full#supplementary-material

REFERENCES

Alsharhan, H., He, M., Edmondson, A. C., Daniel, E. J. P., Chen, J., Donald, T., et al. (2021). ALG13 X-linked Intellectual Disability: New Variants, Glycosylation Analysis, and Expanded Phenotypes. *J Inher Metab Disea* 44 (4), 1001–1012. doi:10.1002/jimd.12378

Amadori, E., Scala, M., Cereda, G. S., Vari, M. S., Marchese, F., Di Pisa, V., et al. (2020). Targeted Re-sequencing for Early Diagnosis of Genetic Causes of Childhood Epilepsy: the Italian Experience from the 'beyond Epilepsy' Project. *Ital. J. Pediatr.* 46 (1), 92. doi:10.1186/s13052-020-00860-1

Bissar-Tadmouri, N., Donahue, W. L., Al-Gazali, L., Nelson, S. F., Bayrak-Toydemir, P., and Kantarci, S. (2014). X Chromosome Exome Sequencing Reveals a novelALG13mutation in a Nonsyndromic Intellectual Disability Family with Multiple Affected Male Siblings. *Am. J. Med. Genet.* 164 (1), 164–169. doi:10.1002/ajmg.a.36233

Datta, A. N., Bahi-Buisson, N., Bienvenu, T., Buerki, S. E., Gardiner, F., Cross, J. H., et al. (2021). The Phenotypic Spectrum of X-linked, Infantile Onset ALG13 -related Developmental and Epileptic Encephalopathy. *Epilepsia* 62 (2), 325–334. doi:10.1111/epi.16761

de la Morena-Barrio, M. E., Ballesta-Martínez, M. J., López-Gálvez, R., Antón, A. I., López-González, V., Martínez-Ribot, L., et al. (2018). Genetic Predisposition to Fetal Alcohol Syndrome: Association with Congenital Disorders of N-Glycosylation. *Pediatr. Res.* 83 (1-1), 119–127. doi:10.1038/pr.2017.201

Epi, K. C., Epilepsy Phenome/Genome, P., Allen, A. S., Berkovic, S. F., Cossette, P., Delanty, N., et al. (2013). De Novo mutations in Epileptic Encephalopathies. *Nature* 501 (7466), 217–221. doi:10.1038/nature12439

Farwell, K. D., Shahmirzadi, L., El-Khechen, D., Powis, Z., Chao, E. C., Tippin Davis, B., et al. (2015). Enhanced Utility of Family-Centered Diagnostic Exome Sequencing with Inheritance Model-Based Analysis: Results from 500 Unselected Families with Undiagnosed Genetic Conditions. *Genet. Med.* 17 (7), 578–586. doi:10.1038/gim.2014.154

Gadomski, T. E., Bolton, M., Alfadhel, M., Dvorak, C., Ogunsakin, O. A., Nelson, S. L., et al. (2017). ALG13-CDG in a Male with Seizures, Normal Cognitive Development, and Normal Transferrin Isoelectric Focusing. *Am. J. Med. Genet.* 173 (10), 2772–2775. doi:10.1002/ajmg.a.38377

Gao, P., Wang, F., Huo, J., Wan, D., Zhang, J., Niu, J., et al. (2019). ALG13 Deficiency Associated with Increased Seizure Susceptibility and Severity. *Neuroscience* 409, 204–221. doi:10.1016/j.neuroscience.2019.03.009

Geisheker, M. R., Heymann, G., Wang, T., Coe, B. P., Turner, T. N., Stessman, H. A. F., et al. (2017). Hotspots of Missense Mutation Identify Neurodevelopmental Disorder Genes and Functional Domains. *Nat. Neurosci.* 20 (8), 1043–1051. doi:10.1038/nn.4589

Harripaul, R., Vasli, N., Mikhailov, A., Rafiq, M. A., Mittal, K., Windpassinger, C., et al. (2018). Mapping Autosomal Recessive Intellectual Disability: Combined Microarray and Exome Sequencing Identifies 26 Novel Candidate Genes in 192 Consanguineous Families. *Mol. Psychiatry* 23 (4), 973–984. doi:10.1038/mp.2017.60

Hesse, A. N., Bevilacqua, J., Shankar, K., and Reddi, H. V. (2018). Retrospective Genotype-Phenotype Analysis in a 305 Patient Cohort Referred for Testing of a Targeted Epilepsy Panel. *Epilepsy Res.* 144, 53–61. doi:10.1016/j.eplepsyres.2018.05.004

Hino-Fukuyo, N., Kikuchi, A., Arai-Ichinoi, N., Niihori, T., Sato, R., Suzuki, T., et al. (2015). Genomic Analysis Identifies Candidate Pathogenic Variants in 9 of 18 Patients with Unexplained West Syndrome. *Hum. Genet.* 134 (6), 649–658. doi:10.1007/s00439-015-1553-6

Huo, J., Ren, S., Gao, P., Wan, D., Rong, S., Li, X., et al. (2020). ALG13 Participates in Epileptogenesis via Regulation of GABAA Receptors in Mouse Models. *Cell Death Discov.* 6 (1), 87. doi:10.1038/s41420-020-00319-6

Ji, J., Shen, L., Bootwalla, M., Quindipan, C., Tatarinova, T., Maglinte, D. T., et al. (2019). A Semiautomated Whole-Exome Sequencing Workflow Leads to Increased Diagnostic Yield and Identification of Novel Candidate Variants. *Cold Spring Harb. Mol. Case Stud.* 5 (2), a003756. doi:10.1101/mcs.a003756

Jiao, Q., Sun, H., Zhang, H., Wang, R., Li, S., Sun, D., et al. (2019). The Combination of Whole-exome Sequencing and Copy Number Variation Sequencing Enables the Diagnosis of Rare Neurological Disorders. *Clin. Genet.* 96 (2), 140–150. doi:10.1111/cge.13548

Jin, S. C., Homsy, J., Zaidi, S., Lu, Q., Morton, S., DePalma, S. R., et al. (2017). Contribution of Rare Inherited and De Novo Variants in 2,871 Congenital Heart Disease Probands. *Nat. Genet.* 49 (11), 1593–1601. doi:10.1038/ng.3970

Li, Y., Xiong, J., Zhang, Y., Xu, L., Liu, J., and Cai, T. (2021). Case Report: Exome Sequencing Identified Variants in Three Candidate Genes from Two Families

with Hearing Loss, Onychodystrophy, and Epilepsy. *Front. Genet.* 12, 728020. doi:10.3389/fgene.2021.728020

Makarova, K. S., Aravind, L., and Koonin, E. V. (2000). A Novel Superfamily of Predicted Cysteine Proteases from Eukaryotes, Viruses and Chlamydia Pneumoniae. *Trends Biochem. Sci.* 25 (2), 50–52. doi:10.1016/s0968-0004(99)01530-3

Michaud, J. L., Lachance, M., Hamdan, F. F., Carmant, L., Lortie, A., Diadori, P., et al. (2014). The Genetic Landscape of Infantile Spasms. *Hum. Mol. Genet.* 23 (18), 4846–4858. doi:10.1093/hmg/ddu199

Møller, R. S., Larsen, L. H. G., Johannesen, K. M., Talvik, I., Talvik, T., Vaher, U., et al. (2016). Gene Panel Testing in Epileptic Encephalopathies and Familial Epilepsies. *Mol. Syndromol.* 7 (4), 210–219. doi:10.1159/000448369

Monies, D., Abouelhoda, M., Assoum, M., Moghrabi, N., Rafiullah, R., Almontashiri, N., et al. (2019). Lessons Learned from Large-Scale, First-Tier Clinical Exome Sequencing in a Highly Consanguineous Population. *Am. J. Hum. Genet.* 105 (6), 879–201. doi:10.1016/j.ajhg.2019.04.011

Paprocka, J., Jezela-Stanek, A., Boguszewicz, Ł., Sokół, M., Lipiński, P., Jamroz, E., et al. (2021). The First Metabolome Analysis in Children with Epilepsy and ALG13-CDG Resulting from c.320A>G Variant. *Children* 8 (3), 251. doi:10.3390/children8030251

Stranneheim, H., Lagerstedt-Robinson, K., Magnusson, M., Kvarnung, M., Nilsson, D., Lesko, N., et al. (2021). Integration of Whole Genome Sequencing into a Healthcare Setting: High Diagnostic Rates across Multiple Clinical Entities in 3219 Rare Disease Patients. *Genome Med.* 13 (1), 40. doi:10.1186/s13073-021-00855-5

Timal, S., Hoischen, A., Lehle, L., Adamowicz, M., Huijben, K., Sykut-Cegielska, J., et al. (2012). Gene Identification in the Congenital Disorders of Glycosylation Type I by Whole-Exome Sequencing. *Hum. Mol. Genet.* 21 (19), 4151–4161. doi:10.1093/hmg/dds123

Wei, C. M., Xia, G. Z., and Ren, R. N. (2018). Gene Mutations in Unexplained Infantile Epileptic Encephalopathy: an Analysis of 47 Cases. *Zhongguo Dang Dai Er Ke Za Zhi* 20 (2), 125–129.

Yu, P., Yang, W., Han, D., Wang, X., Guo, S., Li, J., et al. (2016). Mutations in WNT10B Are Identified in Individuals with Oligodontia. *Am. J. Hum. Genet.* 99 (1), 195–201. doi:10.1016/j.ajhg.2016.05.012

Zhou, P., He, N., Zhang, J.-W., Lin, Z.-J., Wang, J., Yan, L.-M., et al. (2018). Novel Mutations and Phenotypes of Epilepsy-Associated Genes in Epileptic Encephalopathies. *Genes, Brain Behav.* 17 (8), e12456. doi:10.1111/gbb.12456

Zhu, L., Wu, R., Ye, Z., Gu, R., Wang, Y., Hou, Y., et al. (2019). Identification of Two Novel TPK1 Gene Mutations in a Chinese Patient with Thiamine Pyrophosphokinase Deficiency Undergoing Whole Exome Sequencing. *J. Pediatr. Endocrinol. Metab.* 32 (3), 295–300. doi:10.1515/jpem-2018-0363

Conflict of Interest: Author JZ was employed by Angen Gene Medicine Technology, Beijing, China.

The remaining author declares that the research was conducted in the absence of any commercial or financial relationships that could be construed as a potential conflict of interest.

Publisher's Note: All claims expressed in this article are solely those of the authors and do not necessarily represent those of their affiliated organizations, or those of the publisher, the editors, and the reviewers. Any product that may be evaluated in this article, or claim that may be made by its manufacturer, is not guaranteed or endorsed by the publisher.

Copyright © 2022 Cai, Huang, Ma, Hu, Zhu, Zhu and Feng. This is an open-access article distributed under the terms of the Creative Commons Attribution License (CC BY). The use, distribution or reproduction in other forums is permitted, provided the original author(s) and the copyright owner(s) are credited and that the original publication in this journal is cited, in accordance with accepted academic practice. No use, distribution or reproduction is permitted which does not comply with these terms.

frontiers | Frontiers in Genetics

CASE REPORT
published: 13 July 2022
doi: 10.3389/fgene.2022.889829

Case Report: DPM1-CDG: Novel Variant with Severe Phenotype and Literature Review

Hanna Lausmann[1], Martin Zacharias[2], Teresa M. Neuhann[3], Melanie K. Locher[3] and Karl F. Schettler[1]*

[1]Children's Hospital St. Marien gGmbH, Landshut, Germany, [2]Center of Functional Protein Assemblies, Technical University of Munich, Garching, Germany, [3]Medical Genetics Center, Munich, Germany

Background: Congenital disorders of glycosylation (CDG) type I include variants in the *DPM1* gene leading to DPM1-CDG. The nine previously reported patients showed developmental delay, seizures, electroencephalography abnormalities and dysmorphic features with varying disease onset and severity.

Methods: Clinical features of a new patient are described. Whole exome sequencing using NGS was performed, followed by molecular simulation of the structural changes in the protein.

Results: Our patient with DPM1-CDG presented with more severe symptoms and an earlier onset, specifically non-febrile seizures from the age of 3 weeks, global developmental delay, and severely retarded motor skills. She died at the age of 11 weeks after fulminant sepsis. We identified compound heterozygous variants in the *DPM1* gene, one previously reported point mutation c.1A > C p.? as well as the novel variant c.239_241del p.(Lys80del), resulting in the first in-frame deletion located in exon 2. Loss of Lys80 may lead to an impaired α-helical configuration next to the GDP/GTP binding site.

Conclusion: The presented case extends the spectrum of DPM1-CDG to a very young and severely affected child. The deletion of Lys80 in DPM1 results in an impaired helical configuration. This has implications for further understanding the association of structure and function of DPM1.

Keywords: DPM1, DPM1-CDG, CDG-Ie, CDG, congenital disorder of glycosylation, epilepsy, neuromuscular disorder, neurodevelopment

OPEN ACCESS

Edited by:
Ruth Roberts, ApconiX, United Kingdom

Reviewed by:
Jaeken Jaak, KU Leuven, Belgium
Caterina Marconi, Hôpitaux Universitaires de Genève, Switzerland

****Correspondence:***
Hanna Lausmann
Hanna.Lausmann@st-marien-la.de

Specialty section:
This article was submitted to Genetics of Common and Rare Diseases, a section of the journal Frontiers in Genetics

Received: *04 March 2022*
Accepted: *10 June 2022*
Published: *13 July 2022*

Citation:
Lausmann H, Zacharias M, Neuhann TM, Locher MK and Schettler KF (2022) Case Report: DPM1-CDG: Novel Variant with Severe Phenotype and Literature Review. Front. Genet. 13:889829. doi: 10.3389/fgene.2022.889829

Abbreviations: ACMG, American College of Medical Genetics and Genomics; CDG, congenital disorders of glycosylation; CDT, carbohydrate deficient transferrin; CK, creatine kinase; DD, developmental delay; Dol-P, dolichol-phosphate; Dol-P-Man, dolichol-phosphate mannose; DPM1, dolichol-phosphate mannosyltransferase subunit 1; EEG, electroencephalography; ER, endoplasmic reticulum; FTT, failure to thrive; GDP, guanosine diphosphate; gnomAD, Genome Aggregation Database; Het, heterozygous; Hom, homozygous; MAF, minor allele frequency; MD, Molecular Dynamics; MRI, magnetic resonance imaging; NA, not available; NGS, next-generation sequencing analysis; NICU, neonatal intensive care unit; RMSD, root mean square deviation.

1 INTRODUCTION

Congenital disorders of glycosylation (CDG) are a genetically and clinically heterogeneous group of metabolic disorders caused by defects of the glycoprotein and glycolipid glycan synthesis and modification (Sparks et al., 1993; Jaeken and Matthijs, 2001; Grunewald et al., 2002; Grunewald, 2007; Chang et al., 2018). They typically present with a broad clinical spectrum, including neurological abnormalities, facial dysmorphisms, failure to thrive and other organ involvement. The first-line screening for N-linked glycosylation defects is usually performed by carbohydrate deficient transferrin (CDT) analysis (Lefeber et al., 2011). A type 1 serum transferrin isoelectrofocusing pattern corresponds to a CDG-I characterized by defects of dolichol-linked glycan assembly and transfer localized in the cytoplasm or endoplasmic reticulum (ER), whereas a type 2 pattern is associated with a CDG-II characterized by processing defects of protein-bound glycans in the Golgi apparatus.

The activated mannose used for N-glycosylation, glycosyl phosphatidylinositol membrane anchoring, and O-mannosylation of proteins is provided by the glycolipid intermediate dolichol-phosphate mannose (Dol-P-Man). The synthesis of this molecule is catalyzed by the Dol-P-Man synthase complex from guanosine diphosphate (GDP) mannose and dolichol-phosphate (Dol-P) (Maeda et al., 2000). This enzyme is composed of three subunits: dolichol-phosphate mannosyltransferase subunit 1 (DPM1), DPM2 and DPM3 (Maeda et al., 2000). DPM1 is the cytoplasmic catalytic subunit, which is anchored to the ER membrane by DPM3, whereas DPM2 is also localized to the ER membrane and stabilizes the expression of DPM3 (Maeda et al., 2000; Ashida et al., 2006).

Deficiency of Dol-P-Man synthase, caused by variants in the *DPM1* gene, is defined as DPM1-CDG and were first described in 2000 (Imbach et al., 2000; Kim et al., 2000). Nine patients have been reported; they presented with intellectual disability, seizures, microcephaly, and dysmorphic features (Imbach et al., 2000; Kim et al., 2000; Garcia-Silva et al., 2004; Dancourt et al., 2006; Yan g et al., 2013; Bursle et al., 2017).

Here, we describe a female term newborn who presented with a clinically more severe form of DPM1-CDG and died within 11 weeks. She was found compound heterozygous in the *DMP1* gene for a previously described point mutation (Bursle et al., 2017) and for a novel in-frame deletion in exon 2 potentially affecting an α-helical configuration within the DPM1 protein.

2 CASE PRESENTATION AND METHODS

2.1 Patient Report

We present a female term newborn from a non-consanguineous Caucasian family. She was delivered via Caesarian section at full term after an unremarkable pregnancy. The postnatal course was complicated by apnea and muscular hypotonia, thus she was admitted to neonatal intensive care unit (NICU). She was noted to have dysmorphic signs as rhizomelia, clinodactyly, facial dysmorphia such as high narrow palate, flat nasal bridge, hypertelorism and retrognathia. Her early life was dominated by a global developmental delay with most notably severely impaired motor skills. These were characterized by diffusely reduced muscle tone, incapability of drinking, muted crying and diminished or absent reflexes. She also presented with non-febrile seizures from the age of 3 weeks, characterized by short myoclonic episodes mainly of the limbs, sometimes only seen in electroencephalography (EEG) monitoring without clinical correlate.

An initial laboratory work-up was widely unremarkable, including leucocytes and thrombocytes, basic metabolic panel, infection diagnostics, spinal fluid, creatine kinase (CK) and serum transaminases. Noticeable was merely a mild anemia and a low antithrombin III. A karyotype, testing for Pompe disesase and an extended metabolic work-up (plasma amino acids, urin organic acids, carnitine profile, very long chain fatty acid profile, biotinidase activity) was negative. Ultrasound of the brain revealed pachygyria as well as a dilatation of the left lateral ventricle. An abdominal ultrasound showed enlarged and hyperechogenic kidneys with an enlarged pelvicalyceal system. EEG revealed a burst-suppression pattern with discontinuous background activity, missing sleep-wake cycle and in addition detected multiple short seizures.

2.2 Genetic Testing

Whole exome sequencing was carried out on an Illumina NextSeq 500 system (Illumina, San Diego, CA) as 150 bp paired-end sequencing runs using v2.0 SBS chemistry. Sequencing reads were aligned to the human reference genome (GRCh37/hg19) using BWA (v0.7. 13-r1126) with standard parameters. Statistics on coverage and sequencing depth on the clinically targeted regions (i.e., RefSeq coding exons and ±5 intronic region) was calculated with a custom script. SNV and INDEL calling on the genes were conducted using SAMtools (v1.3.1) with subsequent coverage and quality dependent filter steps. Variant annotation was performed with snpEff (v4.2) and Alamut-Batch (v1.4.4). Variants (SNVs/small INDELs) in the coding and flanking intronic regions (±50 bp) were only evaluated.

2.3 Structural Modeling and Molecular Simulation

Structural models for both human DPM1 wild type and Lys80 deletion were generated using the Alphafold 2 program (Jumper et al., 2021) with high confidence due to the availability of highly homologous structures from other organisms. The structures were further investigated using Molecular Dynamics (MD) simulations with the Amber18 package (Lee et al., 2018). Both wild type and DPM1 without the Lys80 (Lys80del) were solvated in explicit TIP3P water (Jorgensen and Jenson, 1998) and including Na^+ and Cl^- ions to neutralize the system and adjusting to an ion concentration of 0.1 M. After energy minimization (2,500 steps) and a step wise heating and equilibration the systems were simulated for 100 ns at a temperature of 310 K (37°C) and a pressure of 1 bar.

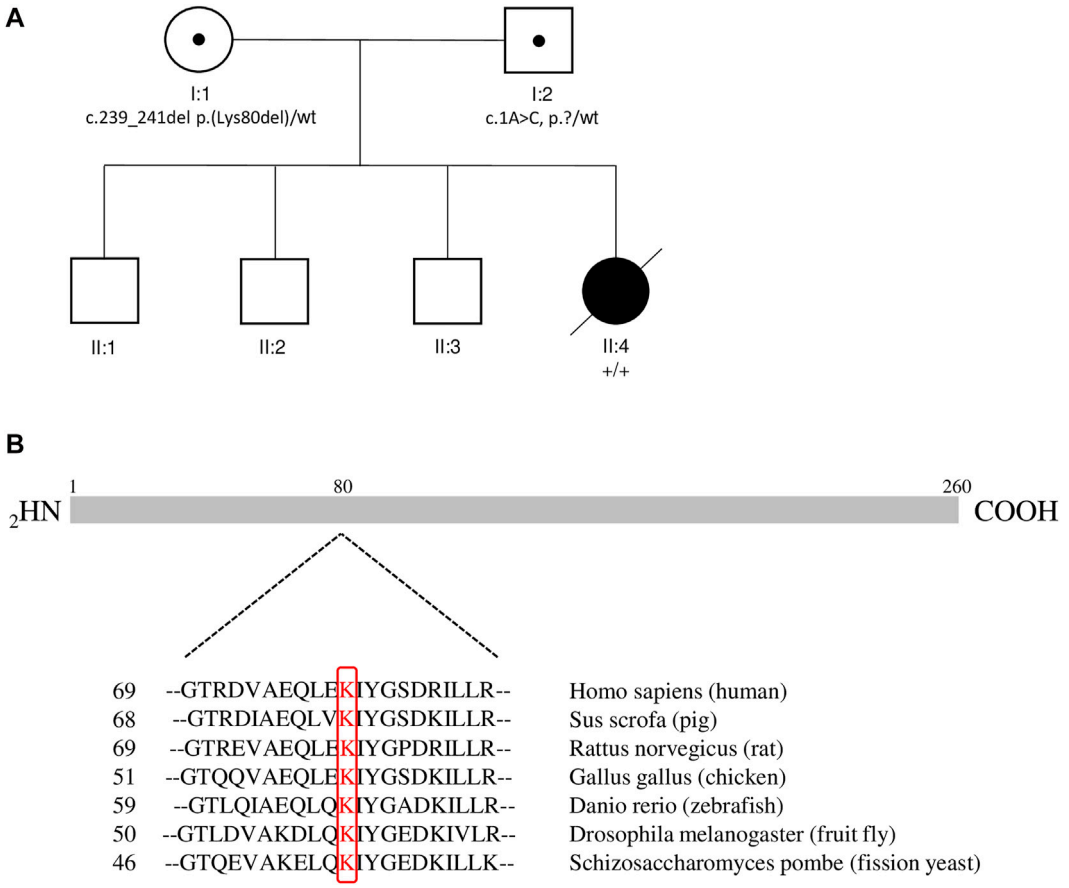


FIGURE 1 | Pedigree and Alignment of Amino Acid Conservation for DPM1. **(A)** The pedigree of the family. Black circle: affected female patient; open squares: unaffected males, open circle: unaffected female; black dots: carrier of the pathogenic variant. **(B)** Alignment of Amino Acid Conservation for DPM1 in Different Species. Sequences are the amino acids for indicated residues of the DPM1 protein in different species. Sequence positions in the respective species are shown on the left. Conserved lysins are highlighted in red. The primary structure of the human DPM1 protein is illustrated in cartoon form above the alignment.

3 RESULTS

Leading symptoms in the clinical presentation were dysmorphic sign, muscular hypotonia as well as non-febrile seizures while the initial laboratory work-up was widely unremarkable. We additionally performed analysis including karyotyping, testing for Pompe disease and extended metabolic work-up in order to rule out the differential diagnosis chromosomal defects, Pompe disease and metabolic disorders, respectively. The clinical features as hypotonia and characteristic dysmorphic signs prompted consideration of a CDG. Isoelectric focusing of serum transferrin and alpha-1 antitrypsin revealed a type 1 pattern. We performed whole exome sequencing of the patient (single exome), and in a further step in a segregation analysis using whole exome sequencing of the parents (trio exome) we identified two compound heterozygous sequence variants in the *DPM1* gene, i.e. NM_003,859.2 c.1A > C p.? which was inherited from her father, and NM_003,859.2 c.239_241del p.(Lys80del) which was inherited from her mother (**Figure 1A**). Variant annotation revealed no other variants compatible with the presented phenotype.

The variant c.1A > C p.? has previously been reported to be linked to DPM1-CDG (CDG-Ie) (Bursle et al., 2017). This variant is predicted to cause a loss of start codon and to interfere with initiation of translation. It is classified as likely pathogenic (Class 4) using the guidelines of the American College of Medical Genetics and Genomics (ACMG, Version 3) (Richards et al., 2015): DPM1 (NM_003,859.2): c.1A > C p.? as Class 4 (PVS1_MOD,PM3,PM2_SUP,PP4).

The variant c.239_241del p.(Lys80del) has not been previously described to be associated with DPM1-CDG. It is reported with a low minor allele frequency (MAF) of 4×10^{-6} using the population references Genome Aggregation Database (gnomAD) (Karczewski et al., 2020). This likely pathogenic variant leads to an in-frame deletion in exon 2, respectively a loss of residue Lys80. This amino acid is highly conserved in eukaryotes (**Figure 1B**), demonstrating its fitness advantage and conservation by natural selection. Potential structural changes in the DPM1 protein by the Lys80 deletion were further investigated by structural modeling with Alphafold2 and MD simulations. In the wild type structure Lys80 is solvent exposed and located at one end of an α-helical segment (**Figure 2**). The structural comparison between the DPM1 wildtype (**Figure 2A**) and variant

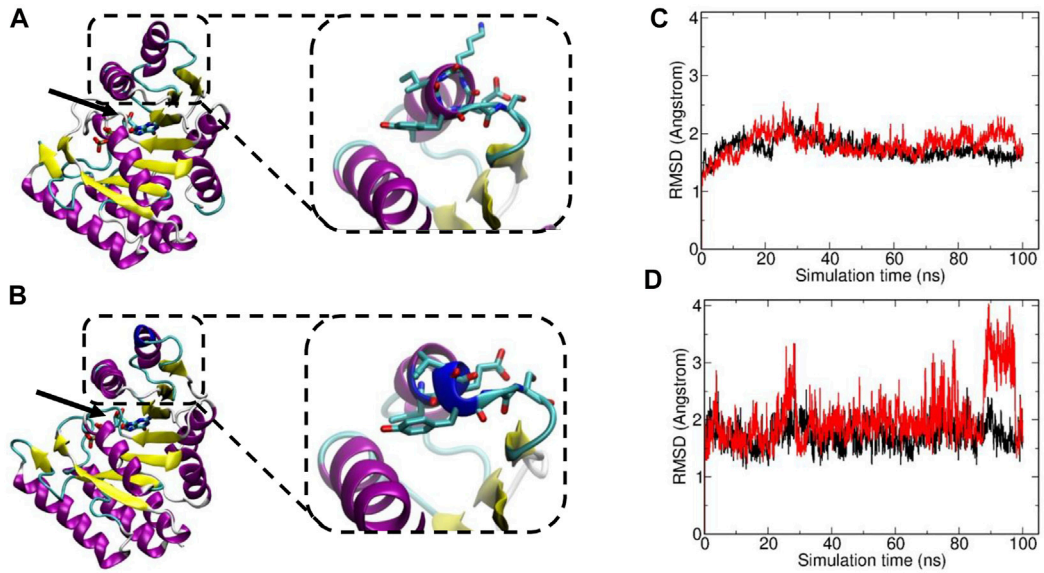


FIGURE 2 | Visualization of Structural Changes of Lys80del in the DPM1 Protein. The DPM1 tertiary structure is shown as color coded cartoon. Alpha helices are colored in pink, beta sheets in yellow, the altered structure near residue 80 in light blue. The location of the GTP/GDP (stick model) is indicated by an arrow. Insets: The location of Lys80 in the one α-helix are highlighted with superimposed amino acids (atom color coded). **(A)** Structure of wildtype DPM1 protein. **(B)** Simulation of DPM1 protein harboring the Lys80 deletion. Dark blue indicates the structural changes in the α-helix. **(C)** Root mean square deviation (RMSD) of the wild type DPM1 (black line) and Lys80 deletion (red line) from the start structure vs. simulation time (ns). **(D)** RMSD vs. simulation time for a segment of ±6 residues around residue 80.

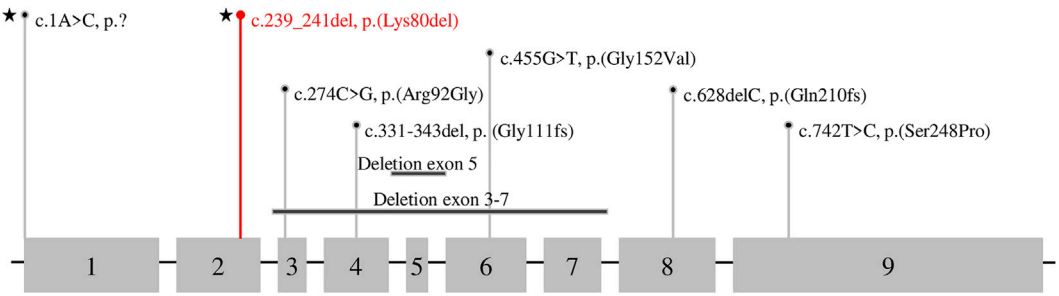


FIGURE 3 | Variant Type and Exon Distribution of Variants in *DPM1*. The *DPM1* (NM_003,859.2, ENST00000371588.5) transcript is shown with numbered exons, grey boxes illustrate the coding sequence. Variants identified in this patient are marked with a star, the novel variant is shown in red and previously reported variants are presented in black.

(**Figure 2B**) indicated an intact overall structure with no tendency of global changes or unfolding due to the Lys80 deletion. The root mean square deviation (RMSD) of both proteins from the start structure remained at a relatively constant small level (~1.8–2 Å, **Figure 2C**) during the whole simulation. However, the MD simulations revealed a local conformational change and local unwinding of the α-helical configuration near residue 80 (**Figure 2B**) and also greater fluctuations of the RMSD of this segment (compare red curve of Lys80 deletion and black curve for wild type in **Figure 2D**). Since this structural element is located in the vicinity of the GDP/GTP binding site in DPM1 the structural changes could potentially affect DPM1 function. In conjunction with the segregation analysis results, this variant can also be classified as likely pathogenic (Class 4) using the guidelines of the American College of Medical Genetics and Genomics (ACMG, Version 3) (Richards et al., 2015): DPM1 (NM_003,859.2): c.239_241del p.(Lys80del) as Class 4 (PM3,PM4,PM2_SUP, PP4).

To date, eight different variants in *DPM1* have been observed to be associated with DPM1-CDG (**Figure 3**; **Tables 1**, **2**). All previously reported variants are either point mutations or larger intragenic deletions, whereas our variant c.239_241del p.(Lys80del) represents the first in-frame deletion described in DPM1-CDG.

At the age of 6 weeks, we were able to make the diagnosis of a DPM1-CDG. However, our patient presented with a progressive neurological and global developmental deterioration including persistent muscular hypotonia, reduced spontaneous movements and seizures. Treatment with multiple anticonvulsants failed to

TABLE 1 | Review of reported DPM1-CDG cases.

Individual	1	2	3	4	5	6	7	8	9	Current Case
age at diagnosis	NA	NA	3 y	19 m	9 y	9 y	7 weeks	9 m	10 y	5 weeks
Gender	female	male	male	female	female	male	female	male	male	female
variant (NM_003,859.2)										
cDNA change	274C>G Hom	1: 274C>G 2: 331-343del	1: 274C>G 2: 628del	1: 274C>G 2: 628del	c.742T>C Hom	373-5T>A Hom	373-5T>A Hom	1: 455G>T 2: (261+1_262–1)_(563+1_564–1)del	1: 1A>C 2: 274C>G	1: 1A>C 2: 239_241del
amino acid change	Arg92Gly	1: Arg92Gly 2: Gly111Leufs*45	1: Arg92Gly 2: Gln210Argfs*4	1: Arg92Gly 2: Gln210Argfs*4	Ser248Pro	p.?	p.?	1: Gly152Val 2: exon3–7 del	1: Met1Leu 2: Arg92Gly	1: p.? 2: Lys80del
Type of mutation	missense	1: missense 2: frameshift	1: missense 2: frameshift	1: missense 2: frameshift	missense	splice site	splice site	1: missense 2: deletion	1: start loss 2: missense	1: start loss 2: in-frame del
inheritance	NA	NA	1: mother 2: father	1: mother 2: father	NA	both parents Het	both parents Het	1: father 2: NA	1: father 2: mother	1: father 2: mother
residual activity of Dol-P-Man synthase	5%	5%	6%	6%	NA	NA	NA	20%	NA	NA
development										
DD (+/-)	+	+	+	+	+	+	+	+	+	+
Speech delay (+/-)	NA	+	+	+	NA	+	+	+	+	NA
Motor delay (+/-)	+	+	+	+	+	+	+	+	NA	+
FTT (+/-)	NA	+	+	+	+	+	+	NA	NA	+
Neurological findings										
Seizures (+/-)	+	+	+	+	+	+	-	+	+	+
age onset of seizures	10 m	11 m	NA	NA	NA	1y	-	NA	NA	3 weeks
hypotension (+/-)	+	+	+	+	-	+	+	+	NA	+
Ataxia (+/-)	NA	NA	NA	NA	+	+	+	NA	NA	+
Dysmorphic features										
facial abnormalities (+/-)	+	-	+	+	+	-	-	NA	+	+
limb abnormalities (+/-)	+	-	+	+	+	-	-	+	+	+
nipple abnormalities (+/-)	-	+	-	-	-	-	-	NA	NA	-
Additional Findings										
Microcephaly (+/-)	+	+	+	-	+	+	+	+	+	-
Brain MRI abnormalities (+/-)	-	+	+	+	+	+	+	+	-	NA
EEG abnormalities (+/-)	+	+	+	+	+	NA	NA	+	+	+
CK elevated (+/-)	+	+	+	+	+	-	-	+	+	-
Eye/Vision abnormalities	+	+	+	+	+	+	+	NA	-	+
Clotting System abnormalities (+/-)	+	+	NA	+	+	+	-	+	NA	+
liver function abnormalities (+/-)	NA	+	+	+	-	-	-	+	NA	-
Gastrointestinal disorders (+/-)	NA	NA	+	+	-	NA	+	-	+	-
recurrend infections	NA	NA	NA	+	NA	NA	NA	+	NA	-
CDG Score	NA	NA	NA	NA	NA	NA	NA	15 p (17m), 26 p (32 m), 28 p (4 years)	NA	43 p (11 weeeeks)
References	Kim et al. (2000)	Kim et al. (2000)	Imbach et al. (2000)	Imbach et al. (2000)	Garcia-Silva et al. (2004)	Dancourt et al. (2006)	Dancourt et al. (2006)	Yang et al. (2013)	Bursle et al. (2017)	Current

Abbreviations: CK, creatine kinase; DD, developmental delay; Dol-P-Man, dolichol-phosphate mannose; EEG, electroencephalography; fs, frameshift; FTT, failure to thrive; Het, heterozygous; Hom, homozygous; MRI, magnetic resonance imaging; NA, not available.

TABLE 2 | Review of reported *DPM1* variants.

Variant (NM_003,859.2)	ACMG Criteria (Richards et al., 2015)	Genotype-Phenotype Correlation (ClinVar database)	Amino Acid Conservation	References
c.274C>G p.(Arg92Gly)	PS4, PS3, PM3, PM2_sup, PP1, PP4	pathogenic	Grantham dist: 125 [0–215]; Comparison between the species: Arg present in 11/13 (total species). Highly conserved amino acid	Kim et al. (2000) Imbach et al. (2000) Bursle et al. (2017)
c.331_343del p.(Gly111Leufs*45)	PVS1, PM3, PM2_sup, PP4	pathogenic		Kim et al. (2000)
c.628del p.(Gln210Argfs*4)	PVS1, PM3, PM2_sup, PP4	pathogenic		Imbach et al. (2000)
c.742T>C p.(Ser248Pro)	PS4, PM3, PM2_sup, PP4	likely-pathogenic	Grantham dist: 74 [0–215]; Comparison between the species: Ser present in 10/13 (total species). Moderately conserved amino acid	Garcia-Silva et al. (2004)
c.373–5T>A p.?	PM4, PM3, PM2_sup, PP4	likely-pathogenic	Predicted change at acceptor site 5 bps downstream: 49.5%	Dancourt et al. (2006)
c.455G>T p.(Gly152Val)	PM1, PM3, PM2_sup, PP4	pathogenic	Grantham dist: 109 [0–215]; Comparison between the species: Gly present in 11/13 (total species). Highly conserved amino acid	Yang et al. (2013)
c.(261+1_262–1) _(563+1_564–1)del	PVS1, PM3, PM2_sup, PP4	unknown		Yang et al. (2013)
c.1A>C p.?	PVS1_MOD, PM3, PM2_SUP, PP4	pathogenic/VUS	Change affects the initiator methionine of the DPM1 mRNA. The next in-frame methionine is located at codon 106	Bursle et al. (2017) Current
c.239_241del p.(Lys80del)	PM4, PM3, PM2_SUP, PP4	unknown	highly conserved amino acid (see **Figure 1B**)	Current

Abbreviations: ClinVar, public database of reports of human variation; VUS, variant of uncertain significance.

achieve satisfactory control of seizures or improvement of the EEG pattern. At the age of 11 weeks, she showed rare spontaneous movements of her extremities, had no head control nor newborn reflexes. She showed no visual fixation and had feeding problems (exclusive nasogastric tube feeding). Using the Nijmegen pediatric CDG rating scale (Achouitar et al., 2011), we assessed the disease severity at the age of 11 weeks with a score of 43, classified into severe category (>26).

The patient developed a pneumonia resulting in a fulminant sepsis and she died at the age of 11 weeks.

4 DISCUSSION

Here we present a child diagnosed with DPM1-CDG, harboring a new variant in the *DPM1* gene resulting in a deletion of Lys80, and showing more severe phenotype than that of previously reported patients.

To date, there are nine cases of DPM1-CDG reported in the literature (Imbach et al., 2000; Kim et al., 2000; Garcia-Silva et al., 2004; Dancourt et al., 2006; Yan g et al., 2013; Bursle et al., 2017), comprising eight different variants in *DPM1* (**Figure 3**; **Tables 1**, **2**). One of the *DPM1* variants we identified in the patient (c.1A > C p.?) has been previously described and is classified as likely pathogenic. The clinical presentation of the previously described patient with this variant was dominated by seizures, developmental delay, and severe gastrointestinal involvement (Bursle et al., 2017). In this case sequencing revealed two compound heterozygous sequence variants, i.e., c.1A > C p.? also found in the current case, and c.274C > G previously described in four other patients (Imbach et al., 2000; Kim et al., 2000; Bursle et al., 2017).

The *DPM1* variant c.239_241del p.(Lys80del) is predicted to lead to an in-frame deletion of the amino acid lysine in position 80 in exon 2. To our knowledge this is the first in-frame deletion described in DPM1-CDG. Due to the high conservation of this position throughout eukaryotes (**Figure 1B**) as well as the absence of this variant in a large reference genome of healthy controls, it is likely to be a causative for the severe phenotype. Moreover, modelling of wildtype and variant DPM1 illustrates that the deletion of Lys80 does not strikingly modify the structure of the whole protein, but leads to changes in an α-helical configuration and increased local conformational fluctuations (**Figure 2**). The affected α-helix is located in the neighborhood of the GDP/GTP binding site, which might indicate a decreased enzyme activity. Note, that the simulations are based on an AlphaFold2-based structural model of DPM1and can only serve to suggest possible explanations for the effect of the mutation. Future experimental studies are required to validate the observed structural changes found in the simulation. Also, substrate binding could be affected, but detailed functional consequences of this single amino acid deletion on the function of DPM1 remains to be analyzed. Thus, we identified the new variant c.239_241del p.(Lys80del) in the *DPM1* gene which appears to be likely pathogenic and possibly causes more severe clinical symptoms in combination with the known likely pathogenic variant.

The clinical features of the reported patient include seizures from infancy, developmental delay, severely retarded motor skills and dysmorphic abnormalities, similar symptoms have been described in previously published DPM1-CDG cases (**Table 1**). She started having medically intractable seizures

from the age of 3 weeks, while onset of seizures in previously described DPM1-CDG patients range from 10 months (Kim et al., 2000) to 1 year or were even absent (Dancourt et al., 2006). However, data availability of seizure onset was limited as only three out of nine previously reported patients state the age of seizure onset. Moreover, she developed severely retarded motor skills including reduced muscle tone and incapability of drinking at the age of 11 weeks. Motor delay as well as muscular hypotension was previously described (Imbach et al., 2000; Kim et al., 2000; Garcia-Silva et al., 2004; Dancourt et al., 2006; Yan g et al., 2013), however not to this extend. As DPM1-CDG has been reported only in nine individuals so far, it is difficult to state an overall prognosis. The clinical course ranges from only mild symptoms (Garcia-Silva et al., 2004; Dancourt et al., 2006) to severely affected individuals with massive physical constraints (Imbach et al., 2000; Kim et al., 2000). The global disease severity can be classified by the previously published Nijmegen pediatric CDG rating scale (Achouitar et al., 2011) into mild (0–14), moderate (15–25) and severe (>26) category. For the reported patient we assessed a score of 43, reflecting a very high level of disease severity. As this rating scale is a recent tool, it was applied only to one previously published DPM1-CDG patient, who scored with 15 points at the age of 17 months and 28 points at the age of 4 years (Yan g et al., 2013). Taken together, the clinical course of our patient seems to be far more severe in comparison to previously reported DPM1-CDG cases.

However, the laboratory workup including serum transaminases and creatine kinase was unremarkable in our patient, other than in previously published DPM1-CDG patients. There are four cases reported to have liver function abnormalities (Imbach et al., 2000; Kim et al., 2000; Yan g et al., 2013). Interestingly, in seven previously published cases creatine kinase was elevated (Imbach et al., 2000; Kim et al., 2000; Garcia-Silva et al., 2004; Yan g et al., 2013; Bursle et al., 2017), while in our case this enzyme was unremarkable. Microcephaly is another clinical feature associated with DPM1-CDG and was observed in eight out of nine cases (Imbach et al., 2000; Kim et al., 2000; Garcia-Silva et al., 2004; Dancourt et al., 2006; Yan g et al., 2013; Bursle et al., 2017), while our patient did not show signs of microcephaly. Yet, her head circumference decreased from birth (35.3 cm, 80th percentile) to the age of 11 weeks (39.0 cm, 60th percentile) and microcephaly might have developed as it is known from one previous case (Imbach et al., 2000).

In conclusion, we present the 10th DPM1-CDG patient, with a severe phenotype and a novel variant, as well as a literature review of this CDG.

DATA AVAILABILITY STATEMENT

The datasets for this article are not publicly available due to concerns regarding participant/patient anonymity. Requests to access the datasets should be directed to the corresponding author.

ETHICS STATEMENT

The studies involving human participants were reviewed and approved by local Institutional Review Board of the Children's Hospital St. Marien in Landshut. Written informed consent to participate in this study was provided by the participants' legal guardian/next of kin. Written informed consent was obtained from the minor(s)' legal guardian/next of kin for the publication of any potentially identifiable images or data included in this article.

AUTHOR CONTRIBUTIONS

HL and KS were involved in acquisition of data and made the concept and design of the study. HL, TN, ML and MZ analyzed and interpretated the data. HL wrote the manuscript and designed the figures with contribution of TN and MZ. KS critically analyzed and edited the manuscript for important intellectual content. All authors reviewed and approved the final draft of this manuscript.

ACKNOWLEDGMENTS

We thank the patient's family for their willingness in agreeing to publish this case report. We thank Theresa Brunet, MD for her input in aspects of human genetic. We thank Edgar Meinl, MD for his thoughtful and helpful comments and input.

REFERENCES

Achouitar, S., Mohamed, M., Gardeitchik, T., Wortmann, S. B., Sykut-Cegielska, J., Ensenauer, R., et al. (2011). Nijmegen paediatric CDG rating scale: A novel tool to assess disease progression. *J. Inherit. Metab. Dis.* 34 (4), 923–927. doi:10.1007/s10545-011-9325-5

Ashida, H., Maeda, Y., and Kinoshita, T. (2006). DPM1, the catalytic subunit of dolichol-phosphate mannose synthase, is tethered to and stabilized on the endoplasmic reticulum membrane by DPM3. *J. Biol. Chem.* 281 (2), 896–904. doi:10.1074/jbc.M511311200

Bursle, C., Brown, D., Cardinal, J., Connor, F., Calvert, S., Coman, D., et al. (2017). DMP1-CDG (CDG1e) with Significant Gastrointestinal Manifestations; Phenotype and Genotype Expansion. *JIMD Rep.* 34, 27–32. doi:10.1007/8904_2016_7

Chang, I. J., He, M., and Lam, C. T. (2018). Congenital disorders of glycosylation. *Ann. Transl. Med.* 6 (24), 477. doi:10.21037/atm.2018.10.45

Dancourt, J., Vuillaumier-Barrot, S., de Baulny, H. O., Sfaello, I., Barnier, A., le Bizec, C., et al. (2006). A new intronic mutation in the DPM1 gene is associated with a milder form of CDG Ie in two French siblings. *Pediatr. Res.* 59 (6), 835–839. doi:10.1203/01.pdr.0000219430.52532.8e

Garcia-Silva, M. T., Matthijs, G., Schollen, E., Cabrera, J. C., Sanchez del Pozo, J., Marti Herreros, M., et al. (2004). Congenital disorder of glycosylation (CDG) type Ie. A new patient. *J. Inherit. Metab. Dis.* 27 (5), 591–600. doi:10.1023/b:boli.0000042984.42433.d8

Grunewald, S. (2007). Congenital disorders of glycosylation: Rapidly enlarging group of (neuro)metabolic disorders. *Early Hum. Dev.* 83 (12), 825–830. doi:10.1016/j.earlhumdev.2007.09.016

Grunewald, S., Matthijs, G., and Jaeken, J. (2002). Congenital disorders of glycosylation: A review. *Pediatr. Res.* 52 (5), 618–624. doi:10.1203/00006450-200211000-00003

Imbach, T., Schenk, B., Schollen, E., Burda, P., Stutz, A., Grunewald, S., et al. (2000). Deficiency of dolichol-phosphate-mannose synthase-1 causes congenital disorder of glycosylation type Ie. *J. Clin. Invest.* 105 (2), 233–239. doi:10.1172/JCI8691

Jaeken, J., and Matthijs, G. (2001). Congenital disorders of glycosylation. *Annu. Rev. Genomics Hum. Genet.* 2, 129–151. doi:10.1146/annurev.genom.2.1.129

Jorgensen, W. L., and Jenson, C. (1998). Temperature dependence of TIP3P, SPC, and TIP4P water from NPT Monte Carlo simulations: Seeking temperatures of maximum density. *J. Comput. Chem.* 19 (10), 1179–1186. doi:10.1002/(sici)1096-987x(19980730)19:10<1179::aid-jcc6>3.0.co;2-j

Jumper, J., Evans, R., Pritzel, A., Green, T., Figurnov, M., Ronneberger, O., et al. (2021). Highly accurate protein structure prediction with AlphaFold. *Nature* 596 (7873), 583–589. doi:10.1038/s41586-021-03819-2

Karczewski, K. J., Francioli, L. C., Tiao, G., Cummings, B. B., Alfoldi, J., Wang, Q., et al. (2020). The mutational constraint spectrum quantified from variation in 141, 456 humans. *Nature* 581 (7809), 434–443. doi:10.1038/s41586-020-2308-7

Kim, S., Westphal, V., Srikrishna, G., Mehta, D. P., Peterson, S., Filiano, J., et al. (2000). Dolichol phosphate mannose synthase (DPM1) mutations define congenital disorder of glycosylation Ie (CDG-Ie). *J. Clin. Invest.* 105 (2), 191–198. doi:10.1172/JCI7302

Lee, T. S., Cerutti, D. S., Mermelstein, D., Lin, C., LeGrand, S., Giese, T. J., et al. (2018). GPU-accelerated molecular Dynamics and free energy methods in Amber18: Performance enhancements and new features. *J. Chem. Inf. Model.* 58 (10), 2043–2050. doi:10.1021/acs.jcim.8b00462

Lefeber, D. J., Morava, E., and Jaeken, J. (2011). How to find and diagnose a CDG due to defective N-glycosylation. *J. Inherit. Metab. Dis.* 34 (4), 849–852. doi:10.1007/s10545-011-9370-0

Maeda, Y., Tanaka, S., Hino, J., Kangawa, K., and Kinoshita, T. (2000). Human dolichol-phosphate-mannose synthase consists of three subunits, DPM1, DPM2 and DPM3. *EMBO J.* 19 (11), 2475–2482. doi:10.1093/emboj/19.11.2475

Richards, S., Aziz, N., Bale, S., Bick, D., Das, S., Gastier-Foster, J., et al. (2015). Standards and guidelines for the interpretation of sequence variants: A joint consensus recommendation of the American College of medical genetics and Genomics and the association for molecular pathology. *Genet. Med.* 17 (5), 405–424. doi:10.1038/gim.2015.30

Sparks, S. E., and Krasnewich, D. M. (1993). "Congenital disorders of N-linked glycosylation and multiple pathway overview," in *GeneReviews((R))*. M. P. Adam, H. H. Ardinger, R. A. Pagon, S. E. Wallace, L. J. H. Bean, G. Mirzaa, et al. Seattle (WA).

Yang, A. C., Ng, B. G., Moore, S. A., Rush, J., Waechter, C. J., Raymond, K. M., et al. (2013). Congenital disorder of glycosylation due to DPM1 mutations presenting with dystroglycanopathy-type congenital muscular dystrophy. *Mol. Genet. Metab.* 110 (3), 345–351. doi:10.1016/j.ymgme.2013.06.016

Conflict of Interest: The authors declare that the research was conducted in the absence of any commercial or financial relationships that could be construed as a potential conflict of interest.

Publisher's Note: All claims expressed in this article are solely those of the authors and do not necessarily represent those of their affiliated organizations, or those of the publisher, the editors and the reviewers. Any product that may be evaluated in this article, or claim that may be made by its manufacturer, is not guaranteed or endorsed by the publisher.

Copyright © 2022 Lausmann, Zacharias, Neuhann, Locher and Schettler. This is an open-access article distributed under the terms of the Creative Commons Attribution License (CC BY). The use, distribution or reproduction in other forums is permitted, provided the original author(s) and the copyright owner(s) are credited and that the original publication in this journal is cited, in accordance with accepted academic practice. No use, distribution or reproduction is permitted which does not comply with these terms.

frontiers | Frontiers in Genetics

TYPE Original Research
PUBLISHED 22 July 2022
DOI 10.3389/fgene.2022.902329

Check for updates

OPEN ACCESS

EDITED BY
Tieliu Shi,
Hunan University of Arts and Science, China

REVIEWED BY
Peter Natesan Pushparaj,
King Abdulaziz University, Saudi Arabia
Shuna Cui,
Yangzhou University, China

*CORRESPONDENCE
Chengmao Xie,
xiechengmao@mail.ccmu.edu.cn
Yong Liu,
youngleu@ccmu.edu.cn

SPECIALTY SECTION
This article was submitted to Genetics of Common and Rare Diseases, a section of the journal Frontiers in Genetics

RECEIVED 23 March 2022
ACCEPTED 01 July 2022
PUBLISHED 22 July 2022

CITATION
Xie C, Yin Z and Liu Y (2022), Analysis of characteristic genes and ceRNA regulation mechanism of endometriosis based on full transcriptional sequencing. *Front. Genet.* 13:902329. doi: 10.3389/fgene.2022.902329

COPYRIGHT
© 2022 Xie, Yin and Liu. This is an open-access article distributed under the terms of the Creative Commons Attribution License (CC BY). The use, distribution or reproduction in other forums is permitted, provided the original author(s) and the copyright owner(s) are credited and that the original publication in this journal is cited, in accordance with accepted academic practice. No use, distribution or reproduction is permitted which does not comply with these terms.

Analysis of characteristic genes and ceRNA regulation mechanism of endometriosis based on full transcriptional sequencing

Chengmao Xie*, Ziran Yin and Yong Liu*

Department of Gynecology, Beijing Obstetrics and Gynecology Hospital, Capital Medical University, Beijing Maternal and Child Health Care Hospital, Beijing, China

Background: Endometriosis is a common gynecological disorder that usually causes infertility, pelvic pain, and ovarian masses. This study aimed to mine the characteristic genes of endometriosis, and explore the regulatory mechanism and potential therapeutic drugs based on whole transcriptome sequencing data and resources from public databases, providing a theoretical basis for the diagnosis and treatment of endometriosis.

Methods: The transcriptome data of the five eutopic (EU) and ectopic (EC) endometrium samples were obtained from Beijing Obstetrics and Gynecology Hospital, Beijing, China, and dinified as the own data set. The expression and clinical data of EC and EU samples in GSE25628 and GSE7305 datasets were obtained from the GEO database (https://www.ncbi.nlm.nih.gov/gds). Differential gene expression analysis and weighted gene co-expression network analysis (WGCNA) were used to identify the endometriosis-related differentially expressed genes. Gene Ontology (GO) and Kyoto Encyclopedia of Genes and Genomes (KEGG) pathway enrichment analyses were conducted by the "clusterProfiler" R package. Then, characteristic genes for endometriosis were identified by the least absolute shrinkage and selection operator (LASSO) and support vector machine recursive feature elimination (SVM-RFE) algorithm. The expression of characteristic genes was verified by quantitative reverse transcription polymerase chain reaction (qRT-PCR) and western-blot. The receiver operating characteristic (ROC) curve was used to evaluate the discriminatory ability of characteristic genes. We assessed the abundance of infiltrating immune cells in each sample using MCP-counter and ImmuCellAI algorithms. The competitive endogenous RNA (ceRNA) regulatory network of characteristic genes was created by Cytoscape and potential targeting drugs were obtained in the CTD database.

Results: 44 endometriosis-related differentially expressed genes were obtained from GSE25628 and the own dataset. Subsequently, LASSO and SVM-RFE algorithms identified four characteristic genes, namely ACLY, PTGFR, ADH1B, and MYOM1. The results of RT-PCR and western-blot were consistent with those of sequencing. The result of ROC curves indicated that the characteristic genes had powerful abilities in distinguishing EC samples from EU samples.

Infiltrating immune cells analysis suggested that there was a certain difference in immune microenvironment between EC and EU samples. The characteristic genes were significantly correlated with specific differential immune cells between EC and EU samples. Then, a ceRNA regulatory network of characteristic genes was constructed and showed a total of 7, 11, 11, and 1 miRNA associated with ACLY, ADH1B, PTGFR, and MYOM1, respectively. Finally, we constructed a gene-compound network and mined 30 drugs targeting ACLY, 33 drugs targeting ADH1B, 13 drugs targeting MYOM1, and 12 drugs targeting PTGFR.

Conclusion: Comprehensive bioinformatic analysis was used to identify characteristic genes, and explore ceRNA regulatory network and potential therapeutic agents for endometriosis. Altogether, these findings provide new insights into the diagnosis and treatment of endometriosis.

KEYWORDS

endometriosis, whole transcriptome, characteristic genes, immune infiltration, ceRNA

Introduction

Endometriosis (EMS) is defined as the presence of ectopic endometrial glands and stroma outside of the uterine cavity and affects 6%–10% of reproductive-aged women. Women with EMS can have symptoms of dyspareunia, dysmenorrhea, irregular uterine bleeding, and chronic pelvic pain (Burney and Giudice, 2012; Johnson et al., 2017; Rogers et al., 2017). Decreased quality of life, increased surgical intervention, and increased use of assisted reproductive technology caused by EMS result in high social costs (Vitagliano et al., 2016). Thus, EMS has become a critical social problem that needs to be addressed. Although medical therapies can relieve symptoms in up to 50%–80% of cases, residual symptoms are still present in at least 20% of patients (Bonocher et al., 2014; Dunselman et al., 2014; Buggio et al., 2017; Parasar et al., 2017). Therefore, exploring new characteristics and potential mechanisms will contribute to the clinical diagnosis of endometriosis and the development of effective treatment methods.

Although there are increasing numbers of studies on EMS immune regulation, its specific mechanism remains unclear. Studies have shown that abnormal immune system function may also be one of the pathogeneses of endometriosis (Seli and Arici, 2003; Symons et al., 2018). The function of almost all types of immune cells in patients with endometriosis is abnormal, that is, the decrease of T cell response activity and NK cytotoxicity, the increase of polyclonal activation and antibody production of B cells, the increase of the number and activation of peritoneal macrophages, the change of inflammatory mediators and so on (Seli and Arici, 2003; Symons et al., 2018). However, so far, there are few studies on the potential genes related to immune cells in endometriosis.

The competitive endogenous RNA (ceRNA) is a novel mode of gene expression regulation, involving lncRNA, microRNA, and mRNA. Through competitive miRNA binding reaction elements (MREs), they form a huge ceRNA regulatory network, enrich the RNA-RNA interaction mechanism and play an important role in the occurrence and development of diseases. LncRNAs are considered to be the main component of ceRNA and regulate the expression level of target genes through competitive binding miRNA. Wang and Chang (2011) reported that lncRNA can regulate gene expression at different levels such as epigenetic, transcriptional, and post transcriptional. Salmena et al. (2011) showed that lncRNAs can act as a natural miRNA "sponge" to competitively bind miRNA through common MREs, inhibit the role of miRNA, and indirectly regulate the expression of target genes. In the ceRNA regulation mode, mRNA and ceRNA have a common MREs binding series, which affects the role of multiple miRNAs, and each ceRNA molecule can be regulated together with multiple different miRNAs to form a huge regulatory network (Chiu et al., 2018). So, exploring the ceRNA regulation mechanism of characteristic genes of endometriosis will provide direction for further study of the molecular mechanism of characteristic genes in the occurrence of endometriosis.

In this study, we screened four characteristic genes of endometriosis (ACLY, PTGFR, ADH1B, and MYOM1) by using the full transcriptome sequencing data of clinical samples and public database resources. Moreover, we further explored the ceRNA regulation mechanism and potential targeted drugs, which provided new insights for exploring the molecular mechanism, clinical diagnosis, and treatment of endometriosis.

Materials and methods

Sample collection and processing

Endometriosis or matched control endometrium from the same patients were obtained from Beijing Obstetrics and Gynecology Hospital, Beijing, China. All donors had not taken drugs and

hormones before surgery. All tissue samples were taken from tissues discarded during surgery after being approved and informed by the ethics review committee of our hospital.

Total RNA extraction and whole transcriptome sequencing

In this study, the whole transcriptome data of the five eutopic (EU) and ectopic (EC) endometrium samples were defined as the own data set. RNA was extracted from snap-frozen tissues, which were placed in precooled TRIzol (Thermo Fisher Scientific, Waltham, MA, United States) reagent. Then, RNA was extracted immediately using chloroform extraction and isopropanol precipitation and quantified using a spectrophotometer. A reverse transcription reaction was carried out according to the manufacturer's instructions in a 20 μl reaction containing 2 μg of total RNA in a gradient cycler (Thermo Fisher Scientific, Waltham, MA, United States). The purity of RNA (OD260/280, OD260/230 ratio) was determined by the NanoDrop ™ One/Onec detection and the RNA integrity (RIN value) was detected by the Agilent 4200 TapeStation system. After the samples passed the test, the library of RNA samples was constructed, and the fragment size of the library was accurately detected by Agilent 4200 tapestation test. After passing the library inspection, different libraries were pooled according to the requirements of effective concentration and target offline data volume, and then Illumina PE150 was sequenced.

Data source from public database

The GSE25628 dataset containing nine EU and seven EC samples was downloaded from the GEO database (https://www.ncbi.nlm.nih.gov/gds) for WGCNA analysis. The GSE7305 dataset including ten EU and ten EC samples was also mined from the GEO database for gene expression validation.

Identification of differentially expressed genes

We performed differential expression analysis on five EC and five EU samples from the own dataset by "limma" R package (Ritchie et al., 2015; Phipson et al., 2016). The screening criteria for differentially expressed genes (DEGs) were $|\log_2$FoldChang (FC)$| > 1$ and p-value < 0.05.

Weighted gene co-expression network analysis

The expression data of GSE25628 cohort was analyzed using the Weighted gene co-expression network analysis ("WGCNA") R package to construct the co-expression network which utilized the EC and EU samples as clinical traits (Langfelder and Horvath, 2008). The "goodSamplesGenes" function was used to conduct sample clustering to identify and remove outliers. For making the co-expression network contented the distribution of scale-free network, a soft-thresholding power was computed with the pickSoftThreshold function. The dynamic tree cutting method was used to identify different modules with the minimum number of genes in each module was 100. Subsequently, a merging threshold of 0.2 was set to merge similar modules. The correlation between these modules and clinical traits was further analyzed. Finally, the module with the |correlation coefficient| > 0.5 and p-value < 0.05 with was chosen as key modules, in which genes with |MM| > 0.8 and |GS| > 0.6 were identified as key module genes, namely endometriosis-related genes. MM represented the correlation of the gene in the module with the module and GS denoted the correlation of the gene with the trait.

Functional enrichment analysis

GO and KEGG enrichment analysis was implemented by the "clusterProfiler" R package (Yu et al., 2012). The threshold for significance was p-value < 0.05. GO enrichment analysis mainly described the biological processes (BP), cellular components (CC), and molecular functions (MF) correlated with genes. KEGG pathway analysis revealed biological pathways associated with genes.

Screening for characteristic genes by machine learning

The "glmnet" R package was employed to screen for characteristic genes using the least absolute shrinkage and selection operator (LASSO) regression (Friedman et al., 2010). The area under the receiver operating characteristic (ROC) curve was used to assess the diagnostic sensitivity and specificity of the LASSO model. Support vector machine-recursive feature elimination (SVM-RFE) is a machine learning method in terms of support vector machine algorithms, which can effectively derive a subset of informative genes and make the classification more reliable (Huang et al., 2014). The characteristic genes were filtered out by the "e1071" R package with the ten-fold cross-validation method. Eventually, characteristic genes, namely, potential biomarkers, were determined by overlapping the genes identified by LASSO and SVM-RFE. The classification performance of these potential biomarkers between EC and EU samples was evaluated using the area under the ROC curve, which was drawn by "pROC" R package (Robin et al., 2011).

Verification of the expression of characteristic genes

EU or EC from the same patients were obtained from Beijing Obstetrics and Gynecology Hospital, Beijing, China. We collected 30 cases were diagnosed as ovarian endometriosis cyst with the inclusion conditions: aged between 20 and 45 years, BMI of 19–25 kg/m^2, non vegetarian patients, no operative contraindication; The exclusion criteria were diabetes and other endocrine diseases, as well as serious gastrointestinal, cardiopulmonary and liver diseases. All donors had not taken drugs and hormones before surgery, and underwent combined uterine and abdominal surgery because of abnormal uterine bleeding at the same time. All tissue samples were taken from tissues excised during surgery after being approved and informed by patients and the ethics review committee of our hospital. Protein preparation, western blotting, RNA isolation, and qRT-PCR were performed as described previously (Chengmao et al., 2017). The PCR reactions contained 3 mM $MgCl_2$, 0.4 μM forward and reverse primers, and 1 μl of LightCycler DNA Master SYBR Green I (10×concentrate, Roche). An initial denaturation step of 95°C for 75 s was performed to activate the FastStart DNA Polymerase and to ensure complete denaturation of the cDNA before amplification. Amplification of ACLY, PTGFR, ADH1B, MYOM1, and GAPDH involved 40 cycles of denaturation at 95°C for 15 s, annealing at 62°C for 10 s, and elongation at 72°C for 25 s. After the last cycle, the amplified products underwent melting curve analysis to check the amplification integrity. Data were analyzed with the Second Derivate Maximum Method using LightCycler Relative Quantification Software. The relative expression level of ACLY, PTGFR, ADH1B, and MYOM1 was normalized to the endogenous control GAPDH. After RT-PCR, we verified the mRNA specificity of ACLY, PTGFR, ADH1B, and MYOM1 with agarose gel electrophoresis. The following primers were used for RT-PCR: ACLY, sense 5′-GAAGGGAGTGAC CATCATCG-3′ and anti-sense 5′-TTAAAGCACCCAGGCTTGAT-3′; PTGFR, sense 5′-GTTTTCCGTCTGGCAGGTTCT -3′ and anti-sense 5′-AGATGACTTGAGTGGT TGGCTTTT-3′; ADH1B, sense 5′-AGGGGGCTGTTTATGGTGG-3′ and anti-sense 5′-GGTACG GATACTTTTCCCAGAGT-3′; MYOM1, sense 5′-CCGAGACATATCA TGCCAAGC-3′ and anti-sense 5′-CGT GTGGGAGCGAGGTTTAAT-3′. Proteins were extracted using the M-PEK kit, following the manufacturer's instructions. The protein concentration in the extracts was determined using the Quick Start Bradford protein assay. SDS-PAGE was conducted with protein samples of approximately 20 μg loaded onto a 7% Tris-acetate gel, run at 120 V for 2 h. To maintain the integrity of the target proteins, samples were not heated prior to electrophoresis. Proteins in the gel were transferred onto an Immobilon-NC transfer membrane at 300 mA for 90 min. The membrane was blocked in 5% nonfat milk powder in Tris-buffered saline with 0.1% Tween 20 (TBST) for 2 h, incubated overnight at 4°C with rabbit monoclonal anti-ATP citrate lyase (*ACLY*) (ab40793; Abcam), mouse monoclonal anti-alcohol dehydrogenase1B (*ADH1B*) (Cat No. 66939-1-Ig; Proteintech), rabbit monoclonal anti-Myomesin1 (*MYOM1*) (ab201228; Abcam) and rabbit monoclonal anti-Prostaglandin F2 alpha Receptor/PTGFR (*PTGFR*) (ab126709; Abcam) antibodies (1:1000 in TBST), and washed with TBST three times for 10 min each. It was then incubated for 45 min at room temperature (RT) with a goat anti-rabbit IgG and a mouse anti-rabbit IgG-horseradish peroxidase (HRP)-conjugated secondary antibody (1:5000 in TBST). After three 10-min washes of the membrane in TBST, the signal was recorded by digital imaging using ChemiDocTM XRS+ with Image Lab™ Software (BIO-RAD, Hercules, California, United States). β-actin served as an internal control.

Immune infiltration analysis

Infiltrating immune cells in the endometrium samples were evaluated by the MCP-counter and ImmuCellAI algorithms. MCP-counter was implemented with the "MCP-counter" R package to compute the content of eight types of immune cells, fibroblasts, and endothelial cells (Becht et al., 2016). ImmuCellAI online website (http://bioinfo.life. hust edu.cn/web/ImmuCellAI) was applied to estimate the proportions of 18 T cells and six other types of immune cells (B cells, NK cells, Monocyte cells, Macrophage cells, Neutrophil cells, and DC cells) (Miao et al., 2020).

Construction of ceRNA network

Aiming to construct the ceRNA regulatory network for the characteristic genes, we first screened the differentially expressed miRNAs (DE-miRNAs) and lncRNAs (DE-lncRNAs) between EU and EC samples using whole transcriptome data from the own dataset, with $|\log_2\text{FoldChange (FC)}| > 1$ and p-value < 0.05 as screening criteria. Then, we predicted the miRNAs targeting the characteristic genes using the miRWalk database (http://mirwalk.umm.uni-heidelberg.de/). The starbase database (http://starbase.sysu.edu.cn/) was exploited to predict the lncRNAs targeting the corresponding miRNAs. Finally, we selected the lncRNA-mRNA pairs with opposite expression trends and miRNA-mRNA pairs with opposite expression trends to establish the ceRNA regulatory network of the characteristic genes. The network was visualized using Cytoscape software (Shannon et al., 2003).

Prediction of potential drugs targeting the characteristic genes

The CTD database (http://ctdbase.org/) was utilized to predict the potential drugs targeting characteristic genes. The

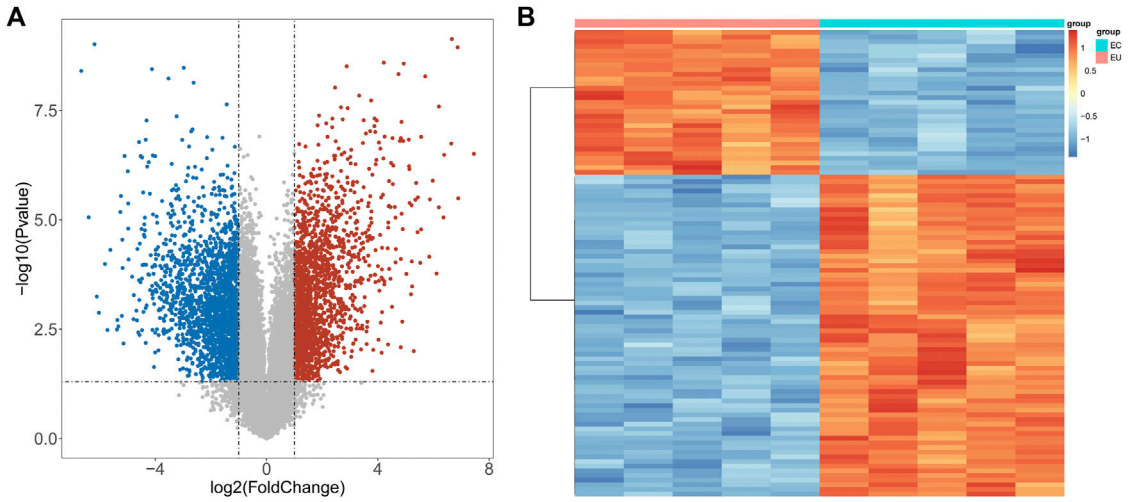


FIGURE 1
DEGs between EU and EC samples. **(A)** Volcano map of DEGs: The red dot indicates that the gene expression is upregulated, the blue dot indicates that the gene expression is down regulated, and the gray dot indicates that there is no significant difference between these genes. **(B)** Heat map of top100 DEGs: Each small square indicates each gene, and its color indicates the expression amount of the gene. The greater the expression amount, the darker the color (red indicates high expression and blue indicates low expression).

network of characteristic gene-compound was visualized using Cytoscape software (Shannon et al., 2003).

Statistical analysis

All bioinformatics analyses were conducted using the R programming language, and the data from different groups were compared by the Wilcoxon test. If not specified above, a *p*-value less than 0.05 was considered statistically significant.

Results

Endometriosis-related differentially expressed genes

To explore the regulatory mechanisms of endometriosis, we conducted whole transcriptome sequencing on five pairs of collected EC and EU samples using high-throughput sequencing technology. Based on the sequencing data, we detected 4057 DEGs in EC samples compared to EU samples using the "limma" package, including 1842 upregulated genes and 2215 downregulated genes (Figure 1A, Supplementary Table S1). Top100 DEGs were displayed in a heatmap (Figure 1B). To further mine the genes associated with endometriosis, we downloaded the data of GSE25628 dataset from the GEO database and performed WGCNA. No obvious outliers were excluded by cluster analysis (Figure 2A). 13 was selected as the optimal soft threshold with an R^2 = 0.85 (Figure 2B). Based on the optimal soft threshold, we divided the genes into different modules according to dynamic tree cutting algorithm. After merging, a total of 18 modules were generated (Figures 2C,D). Correlations between modules and clinical traits (EU samples and EC samples) were calculated (Figure 2E). Three modules (sienna3, darkorange, and midnightblue) was considered as the key modules as the |correlation coefficient| > 0.5 and *p*-value < 0.05 (Figure 2E). According to the criterion of |MM| > 0.8 and |GS| > 0.6, 11 genes in sienna3 module, 69 genes in darkorange module, and 41 genes in midnightblue module were authenticated as key module genes, namely endometriosis-related genes (Figures 2F–H). Hence, 44 endometriosis-related DEGs were obtained by taking the intersection of DEGs and key module genes (Figure 3A, Supplementary Table S2).

Function of endometriosis-related differentially expressed genes

To further understand the biological functions and the pathways involved in the endometriosis-related DEGs, we conducted GO and KEGG functional enrichment analysis. A total of 49 GO entries (including 35 BP entries, 8 CC entries, and 6 MF entries) and one KEGG pathways were enriched (Supplementary Table S3). Top10 GO entries under each category were listed in Figure 3B. We found that these genes were associated with "muscle system process," "muscle contraction," "myofibril assembly," "response to xenobiotic stimulus," "cellular response to drug," "second-messenger-

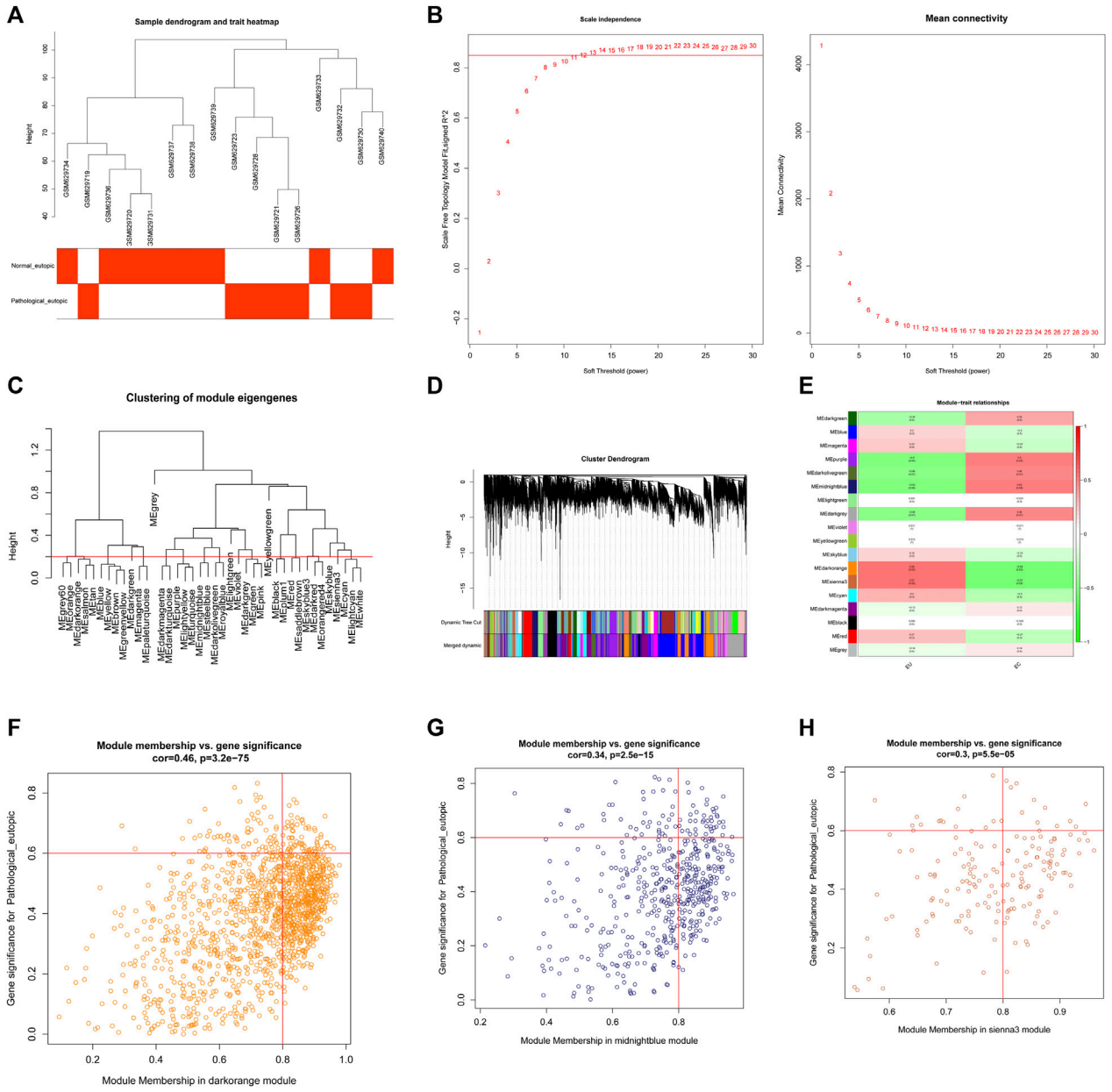


FIGURE 2
Construction and module analysis of weighted gene co-expression network analysis (WGCNA). **(A)** Clustering and phenotypic information of combined data samples, the upper part of the figure is clustering, and the lower part is phenotype. The color represents disease. **(B)** Determination of the soft threshold. **(C)** Merging of the similar modules analyzed by the dynamic cutting tree algorithm. **(D)** Clustering dendrogram of genes with different similarities based on topological overlap and the assigned module color. **(E)** The heat map of correlation between different modules and clinical characters. The ordinate represents different modules and the abscissa represents different traits. Each block represents the correlation coefficient and significance *p* value of a module and a trait. **(F)** Module membership in sienna3 module, the vertical line is |MM| = 0.6 and the horizontal line is |GS| = 0.8. The key gene of the module we selected is in the box of the upper right corner of the figure. **(G)** Module membership in darkorange module, the vertical line is |MM| = 0.6 and the horizontal line is |GS| = 0.8. The key gene of the module we selected is in the box of the upper right corner of the figure. **(H)** Module membership in midnightblue module, the vertical line is |MM| = 0.6 and the horizontal line is |GS| = 0.8. The key gene of the module we selected is in the box of the upper right corner of the figure.

mediated signaling," "positive regulation of inflammatory response," "cyclic-nucleotide-mediated signaling" and so on. In addition, for KEGG pathways, these 55 genes were enriched for "Vascular smooth muscle contraction" (Figure 3C).

Characteristic genes for endometriosis

To dig the characteristic genes from the 44 endometriosis-related DEGs, we adopted LASSO and SVM-RFE algorithms

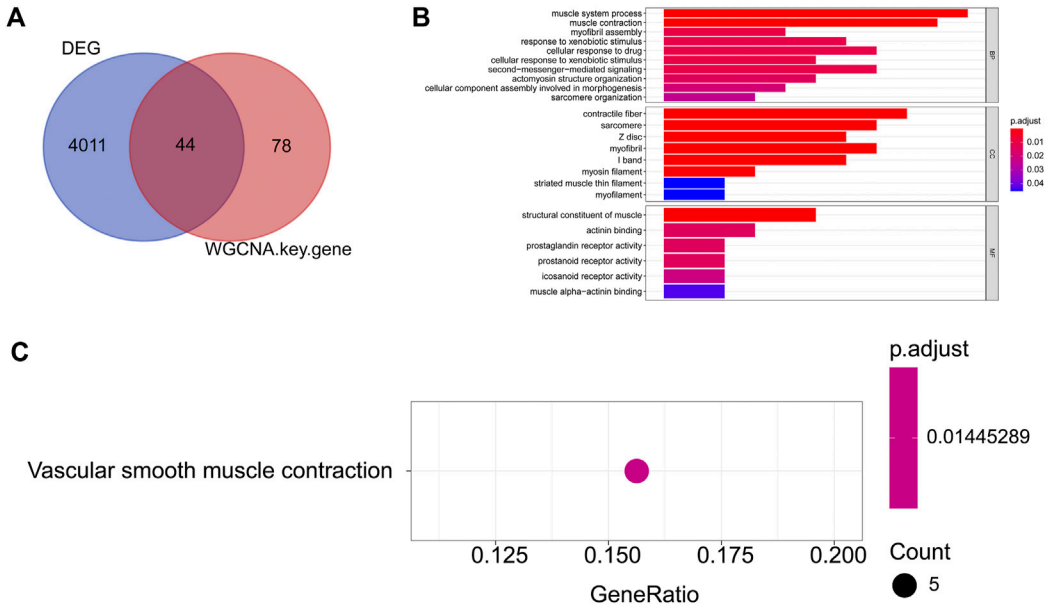


FIGURE 3
GO and KEGG enrichment of endometriosis-related DEGs **(A)** The Venn diagram of the DEGs and key module genes were identified by WGCNA; **(B)** TOP10 GO (BP), GO (CC), and GO (MF) entries. The ordinate represents each GO term, which is sorted according to the *p*-value. The abscissa represents the gene proportion, the color of the column represents the *p*-value, the more reder represents the higher reliability, the length of the column represents the number of genes involved, and the longer the column length represents the greater number of genes involved; **(C)** KEGG enrichment result. The ordinate represents each KEGG term. The abscissa represents the gene proportion.

in the GSE25628 dataset. Four characteristic genes (ACLY, PTGFR, ADH1B, and MYOM1) were discerned using the LASSO algorithm (Figures 4A,B). ROC curve with AUC value was one indicating the LASSO model performed well (Figure 4C). Meanwhile, 40 characteristic genes were selected with the SVM-RFE algorithm, as shown in Figure 4D and Supplementary Table S4. Hence, four genes were defined as characteristic genes for endometriosis by overlapping the genes derived from these two algorithms, including ACLY, PTGFR, ADH1B, and MYOM1 (Figure 4E). In order to investigate the diagnostic ability of each characteristic gene, we plotted the ROC curves for each gene. As shown in Figure 4F, ACLY was down-regulated in EC samples, and ADH1B, MYOM1, and PTGFR were up-regulated in EC samples. The AUC values of these genes were all greater than 0.8, indicating that the characteristic genes could distinguish ECl and EU samples powerfully (Figure 4G). The results were also validated in the own dataset (Figures 4H,I). In addition, we further validated the expression of characteristic genes by external dataset GSE7305. Consistent with the results of GSE25628 dataset and the own dataset, ACLY was down-regulated in EC samples, and ADH1B, MYOM1, and PTGFR were up-regulated in EC samples (Figure 4J). These results indicated that the four characteristic genes have potential diagnostic value in clinical practice.

Verification of characteristic genes expression

We verified the results of the screened characteristic genes at the mRNA and protein level. The verification results revealed that the mRNA levels of ADH1B (Figure 5B), MYOM1 (Figure 5C), and PTGFR (Figure 5D) in EU were higher than those in the control group, while the results of ACLY (Figure 5A) were the opposite, which consistent with the sequencing data. The qRT-PCR graphs (CT curves) of ACLY, ADH1B, MYOM1, and PTGFR were showed in (Figures 5E–H). The verification results revealed that the protein (Figures 6A,B) levels of ADH1B, MYOM1, and PTGFR in EU were higher than those in the control group, while the results of ACLY were the opposite, consistent with the RT-PCR. The samples derive from the same experiment and those gels/blots were processed in parallel.

Characteristic genes and infiltrating immune cells

In order to evaluate the discrepancy of immune microenvironment between the EC and EU samples, we estimated the enrichment of different immune cells using the MCP-counter and ImmuneCellAI algorithm. The results from MCP-counter showed that the EU samples had significantly

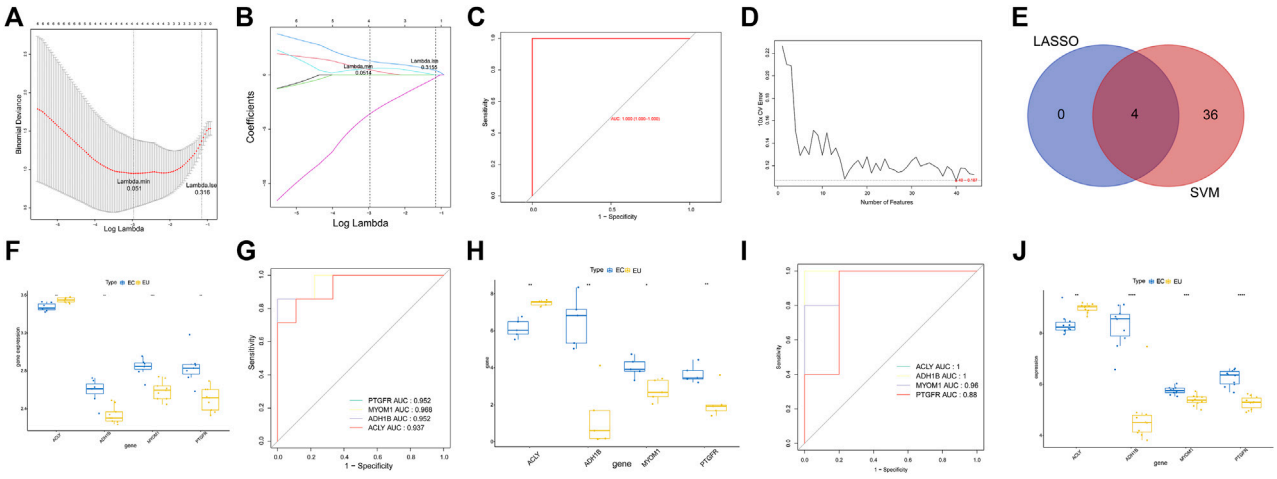


FIGURE 4
The characteristic genes for endometriosis. **(A)** The penalty diagram of lasso logistic regression coefficient. The abscissa deviance represents the proportion of the residual explained by the model, showing the variation relationship between the number of characteristic genes and the proportion of the explained residual (DEV), and the ordinate is the coefficient of genes. The dotted line position on the left is the position where the cross-validation error is the smallest. Determine the corresponding abscissa log (lambda) according to this position (lambda. Min). The number of characteristic genes is displayed on the top. **(B)** The penalty diagram of lasso logic coefficient. The abscissa is log (lambda), and the ordinate represents the error of cross validation. With the change of the penalty coefficient lambda, the coefficients of most variables are compressed to 0. When the 10-fold cross validation error is the smallest, the best lambda value is selected, and the best lambda is obtained in lambda When min = 0.051, select four non-zero coefficient variables. **(C)** The ROC curve of lasso model. **(D)** The relationship between generalization error and characteristic number. The abscissa represents the number of characteristic genes, and the ordinate represents the generalization error under 10-fold cross validation. The trend of broken line graph represents the relationship between the number of characteristic genes and generalization error. **(E)** The Venn diagram of characteristic genes identified by LASSO and SVM-RFP. **(F)** The box diagram of the expression of characteristic genes in the GSE25628 dataset. **(G)** The ROC curve of the characteristic genes in the GSE25628 dataset. **(H)** The box diagram of the expression of characteristic genes in the own dataset gene. **(I)** The ROC curve of characteristic genes in the own dataset. **(J)** The box plot of the expression of characteristic genes in the GEO7305 dataset. *$p < 0.05$, **$p < 0.01$, ***$p < 0.001$.

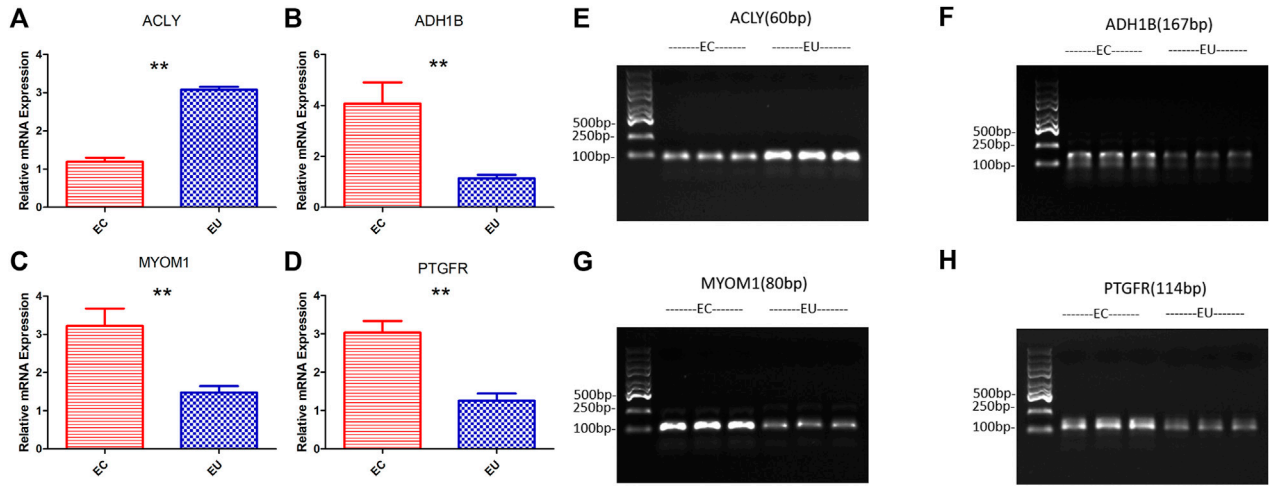


FIGURE 5
The results of RT-PCR and the graphs (CT curves) to verify the expression of characteristic genes at the mRNA level; **(A)**, **(E)** ACLY; **(B)**, **(F)** ADH1B; **(C)**, **(G)** MYOM1; **(D)**, **(H)** PTGFR; **$p < 0.01$.

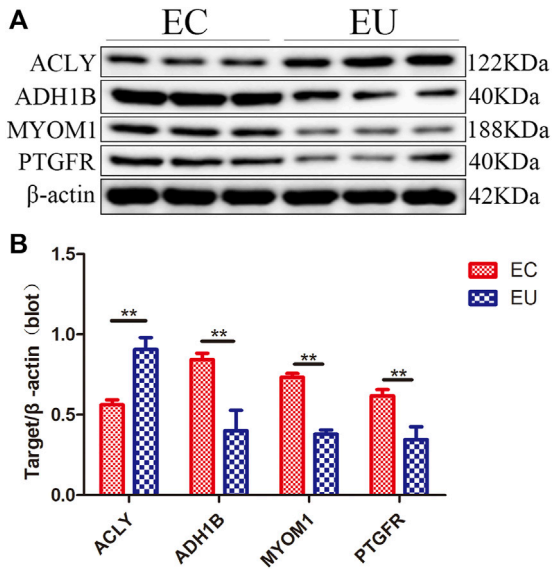


FIGURE 6
The results of western-blot to verify the expression of characteristic genes at the protein level; **(A)** Western blotting results; **(B)** Densitometry of the western blot; $^{**}p < 0.01$.

higher proportions of T cells, Myeloid dendritic cells, endothelial cells, and fibroblasts (Figures 7A,B). The results from ImmuneCellAI algorithm indicated that the EC samples had significantly lower proportions of NKT cells and Tgd cells, and significantly higher proportions of Tc cells and B cells (Figures 7C,D). These findings suggested that there was a certain difference in immune microenvironment between EU and EC samples.

We further analyzed the spearman correlation between the four characteristic genes and differential immune cells. As shown in Figure 7E and Supplementary Table S5, PTGFR was positively correlated with NKT cells and Tgd cells. PTGFR was negatively correlated with endothelial cells and Tc cells. MYOM was negatively correlated with B cells. ADH1B was positively correlated with Tgd cells. ACLY was positively correlated with B cells and Tc cells. ACLY was negatively correlated with Tgd cells.

To further explore the regulatory mechanism of characteristic genes in endometriosis, we proceeded with lncRNA-miRNA-mRNA network construction by utilizing whole transcriptome data from the own dataset. Firstly, we identified 295 differentially expressed miRNAs (DE-miRNAs) between EC and EU samples, including 147 upregulated miRNAs and 148 downregulated miRNAs (Supplementary Figure S1A;

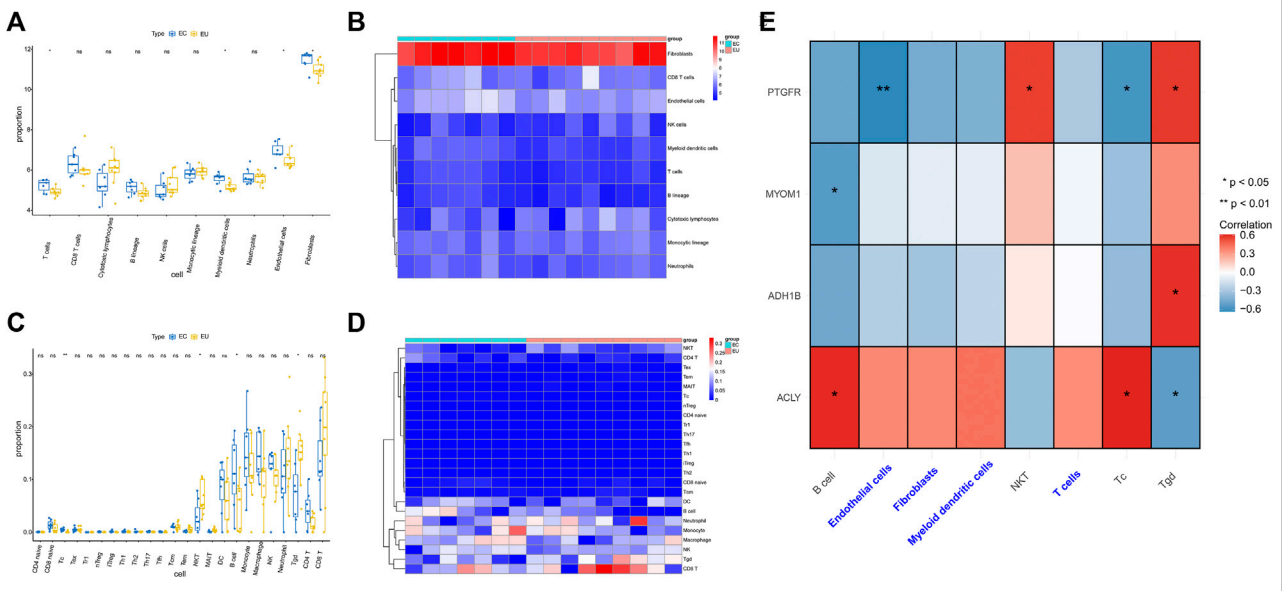


FIGURE 7
The characteristic genes and infiltrating immune cells. **(A)** The box plot of cell content was calculated by MCP-counter between different EU and EC groups. **(B)** The heat map of different cell contents was calculated by MCP-counter. **(C)** The box diagram of immune cell difference between EU group and EC group was calculated by ImmuneCellAI. **(D)** The heat map of different cell contents was calculated by ImmuneCellAI. **(E)** The heat map showed the correlations between immune cells and the characteristic gene. ceRNA regulatory network for characteristic genes.

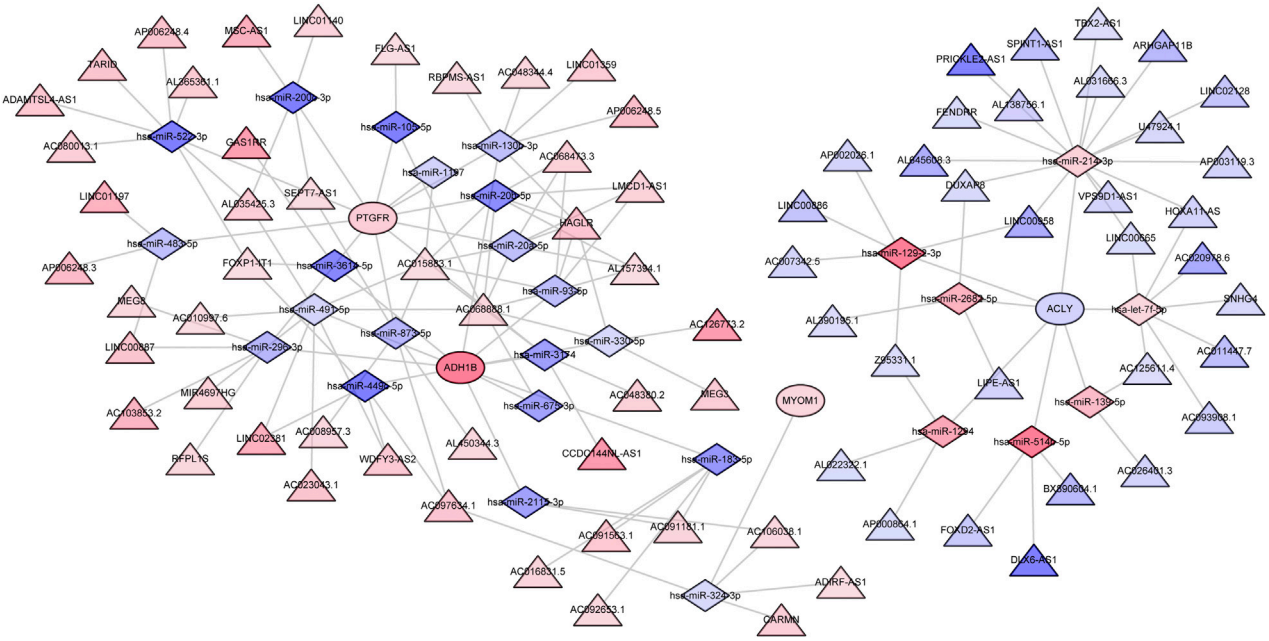


FIGURE 8
The ceRNA regulatory network for characteristic genes. The circle indicates mRNA; the triangle represents lncRNA and the diamond represents miRNA. The color indicates the expression trend, red indicates upregulation, blue indicates downregulation, and the darker the color, the greater the value of |logFC|. Potential drugs targeting the characteristic genes.

Supplementary Table S6). Top100 DE-miRNAs were displayed in the heatmap (Supplementary Figure S1B). Meanwhile, 476 differentially expressed lncRNAs (DE-lncRNAs) were extracted from DEGs between EC and EU samples, including 217 upregulated lncRNAs and 259 downregulated lncRNAs. We took the intersection of DE-miRNAs with miRNAs targeting four characteristic genes predicted at the miRWalk database, and retained miRNA-mRNA relationship pairs with opposite expression trends. Next, we intersected the DE-lncRNAs with the lncRNAs targeting the corresponding miRNAs predicted in the starbase database, and retained the lncRNA-miRNA relationship pairs with opposite expression trends. Ultimately, a lncRNA-miRNA-mRNA regulatory network containing 111 nodes (4 mRNAs, 27 miRNAs, and 80 lncRNAs) and 150 edges was generated (Figure 8, Supplementary Table S7).

To explore the potential drugs for endometriosis therapy, we searched the potential drugs targeting the characteristic genes in the CTD database. As shown in Figure 9 and Supplementary Table S8, 30 drugs targeting ACLY, 33 drugs targeting ADH1B, 13 drugs targeting MYOM1, and 12 drugs targeting PTGFR were mined. Finally, a gene-compound network containing 81 nodes (4 mRNAs and 77 compounds) and 115 edges was generated and exhibited in Figure 9. We noted that fatostatin, abrine, cyclosporine, ganoderic acid A, ivermectin, quercetin, troglitazone, and tunicamycin targeted ACLY. Bosentan, cyclosporine, entinostat, estradiol, fipronil, leflunomide, troglitazone, and resveratrol targeted ADH1B. Doxorubicin, GSK-J4, and incobotulinumtoxin A targeted MYOM1. Fluprostenol, oxidopamine, antirheumatic agents, calcitriol, clothianidin, cyclosporine, dexamethasone, and trichostatin A targeted PTGFR.

Discussion

EMS is a common inflammatory disease, which is caused by the spread or growth of endometrioid tissue in abnormal parts, or by the metaplasia of endometrial tissue outside normal parts, which is characterized by the functional response of glands and stroma to local, endogenous and exogenous hormone stimulation, and its main clinical symptoms are pain, mainly including pelvic pain, infertility Dysmenorrhea and difficult sexual intercourse (Shannon et al., 2003; Acién and Velasco, 2013; Practice Committee of the American Society for Reproductive Medicine, 2014; Peiris et al., 2018; Zondervan et al., 2020). Ectopic endometrium is usually found in pelvic peritoneum and pelvic organs (ovary, fallopian tube, intestine, sigmoid colon and rectum, uterine ligament, rectovaginal septum, and bladder), and can also be planted in tissues and organs outside the pelvic cavity (such as navel, vulva, laparotomy scar, appendix, and lung) (Subramanian and Agarwal, 2010; Rolla, 2019). At present, there are many theories about the

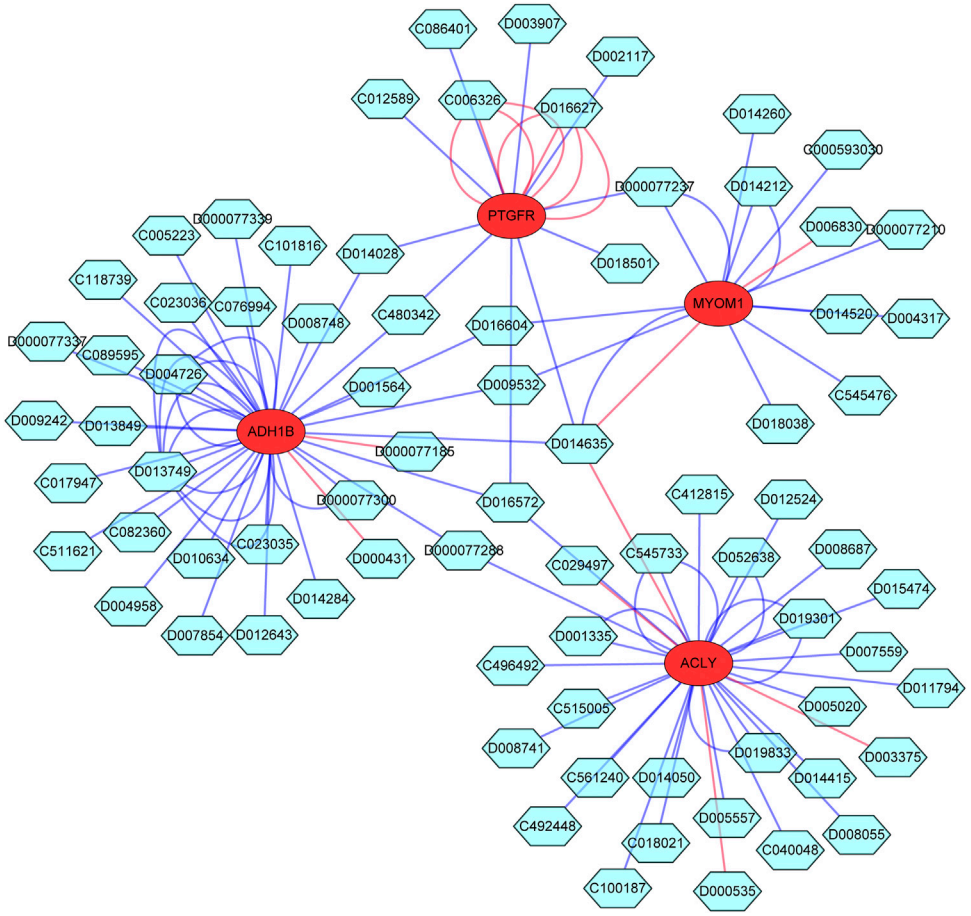


FIGURE 9
The Potential drugs targeting the characteristic genes. The red circle indicates mRNA; The blue green hexagon indicates drugs; The line color indicates different influence effects, red indicates increased expression, and blue indicates decreased expression.

pathogenesis of EMS, among which the most recognized is the menstrual blood retrograde theory proposed by Sampson (1928) in the early 20th century, that is, the disease originates from the retrograde menstruation of endometrial tissue, and the mechanical transfer of endometrial tissue during menstruation progresses to the pelvis, resulting in invasive implantation and ectopic growth of endometrial tissue, which develops into endometriosis (Kobayashi et al., 2014). However, this theory cannot fully explain the origin and other aspects of the disease. Therefore, follow-up studies have put forward a variety of hypotheses for the pathophysiology of EMS, such as coelomic metaplasia, cellular immune changes, metastasis, genetic basis, environmental basis, and multifactor genetic model of the interaction between specific genes and the environment, but the exact pathogenesis of EMS is still unclear (Giudice and Kao, 2004).

As far as we know, our study is the first time to screen the characteristic gene of EMS and explore the ceRNA regulatory mechanism by using our own full transcriptome sequencing data of clinical samples and public database resources. 44 endometriosis-related DEGs were authenticated by differential analysis and WGCNA. Then we analyzed the functional enrichment of these genes, which showed that these genes were mainly involved in biological processes such as muscle contraction, muscle fiber assembly, second messenger mediated signal, positive regulation of inflammatory response, and vascular smooth muscle contraction pathway. Inflammatory response is a defensive response caused by injury and dysfunction caused by external stimulation. After the inflammatory response is activated, it stimulates tissue nerve endings by releasing inflammatory factors, so as to participate in the formation of pain (McKinnon et al., 2015). In recent years, a large number of studies have shown that inflammatory response and emergency response participate in the pathological process of EMS (Samimi et al., 2019; Asally et al., 2020; Wei et al., 2020). A variety of inflammatory factors are differentially expressed in

EMS patients, which can promote the occurrence of EMS, and also play an important role in the generation of pelvic pain in EMS patients (Ayubi and Safiri, 2017). Then we obtained four characteristic genes (ACLY, PTGFR, ADH1B, and MYOM1) of EMS through machine learning, and verified its effective diagnostic ability through ROC curve analysis. Studies have reported that prostaglandin F2a (PTGFR) is a pain causing substance in the body, which is positively correlated with the degree of dysmenorrhea (McAllister et al., 2016). Lysosome's rupture and bleed during menstruation, and a large amount of PTGFR release leads to a significant aggravation of local pain (Yoshino et al., 2018). PTGFR also can significantly improve the activity of aromatase P450, which is a key enzyme in the process of estrogen biosynthesis and can stimulate EMS lesions to increase the synthesized estrogen, and then promote the combination of estrogen and its receptor to accelerate the growth of EMS lesions (Kitawaki et al., 1999). In addition, PTGFR can also reduce the expression of MMPs, scavenger receptor and CD36 in peritoneal macrophages, resulting in the backflow endometrial tissue escaping the clearance of the body, and then the three processes of adhesion, invasion and angiogenesis. PTGFR also stimulates the expression of VEGF, induces the proliferation of epithelial cells, and further promotes the occurrence and development of EMS (Chuang et al., 2009). As far as we know, the relationship between ACLY, ADH1B, MYOM1 and EMS has not been reported. This is the first time to show that those genes are the characteristic gene of EMS, which may play an important role in the occurrence of EMS. However, their role and mechanism in the occurrence and development of EMS are not clear, and further research is needed.

By comparing the infiltrating immune cells of eutopic endometrium samples and ectopic endometrium samples, we found that there were some differences between them, and found that the characteristic gene was related to some immune cells. In fact, the various immune cells in the abdominal cavity environment improve the invasive and adhesive abilities of endometrial cells, including dendritic cells, macrophages, mast cells, NK cells, and T cells, which can lead to ectopic endometrium flowing back into the pelvic and abdominal cavities with menstrual blood (Symons et al., 2018). During the menstrual cycle, endometrial-like tissue can spread outside its endometrial location, and these lesions can attract cytotoxic T cells, macrophages, and NK cells (Sampson, 1927; Dmowski et al., 2001; Christodoulakos et al., 2007; Hansen et al., 2010). Subsequently, the activation of the inflammatory response promotes the secretion of cytokines and chemokines in the abdominal cavity to create a microenvironment and induce the development of ectopic endometrial tissue by promoting local angiogenesis and destroying the process of endometrial apoptosis (Mantovani et al., 2008). The large amount of evidence mentioned above as well as our current results show that several types of invasive immune cells have a crucial role in EMS and should be investigated further in future studies.

Noncoding RNA (ncRNA) transcribed from DNA genome but unable to encode protein plays a role as a general regulator in cell process. Generally, ncRNA can be divided into two categories according to its size: small long-chain noncoding RNA (<200 nucleotides in length) and long-chain noncoding RNA (length ≥200 nucleotides). MiRNA is one of the most concerned small ncRNAs, which has been proved to be abnormally expressed in EMS, but the specific mechanism remains to be clarified (Beermann et al., 2016; Saare et al., 2017). As a new star in the progress of RNA sequencing technology, lncRNA has set off a research upsurge in recent years, and EMS is no exception. It is worth noting that the emerging competitive endogenous RNA (ceRNA) hypothesis shows that lncRNA can be used as a miRNA "sponge" to regulate the target mRNA (Panir et al., 2018). This hypothesis has been confirmed in EMS: lncRNAH19, the first reported in EMS, absorbs mirnalet-7 to regulate its downstream gene IGF1R to affect the proliferation of endometrial stromal cells (Salmena et al., 2011). Exosomes secreted by endometrial stromal cells can transmit information to other cells and promote the occurrence and development of EMS (Bonafede et al., 2016; Sun et al., 2018). However, there are few studies on the comprehensive analysis of EMS related miRNA and lncRNA in ceRNA network environment (Ghazal et al., 2015). In the early stage, after obtaining the expression trend of mRNA, miRNA and lncRNA, we constructed the mRNA-miRNA-lncRNA network of characteristic genes based on the sequencing data of EMS, and finally obtained lots kinds of gene signal axes about EMS, which could provide new ideas and potential targets for us to study the mechanism of EMS in the future.

At present, surgery is the main treatment of endometriosis in clinic, but conservative surgery alone is usually difficult to cure, and drug treatment is an important adjuvant treatment, so EMS patients often need long-term drug management after operation. To explore the potential drugs for endometriosis therapy, we searched the potential drugs targeting the characteristic genes in the CTD database. We noted that fatostatin, abrine, cyclosporine, ganoderic acid A, ivermectin, quercetin, troglitazone, and tunicamycin targeted ACLY. Bosentan, cyclosporine, entinostat, estradiol, fipronil, leflunomide, troglitazone, and resveratrol targeted ADH1B. Doxorubicin, GSK-J4, and incobotulinumtoxin A targeted MYOM1. Fluprostenol, oxidopamine, antirheumatic agents, calcitriol, clothianidin, cyclosporine, dexamethasone, and trichostatin A targeted PTGFR. All the above research results can provide theoretical guidance and potential therapeutic targets for the clinical drug treatment of EMS in the future.

In summary, this study digs the characteristic genes of EMS, which provides a basis for the study of the molecular mechanism, clinical diagnosis, and treatment of EMS. However, our research has not further verified the relevant molecular mechanism, which needs to be further improved in the follow-up research.

Data availability statement

The datasets presented in this study can be found in online repositories. The name of the repository and accession number can be found below: NCBI; PRJNA819530.

Ethics statement

The studies involving human participants were reviewed and approved by the ethics review committee of Beijing Obstetrics and Gynecology Hospital. The patients/participants provided their written informed consent to participate in this study.

Author contributions

All authors have made significant contributions to the work and analysis and interpretation of data. CX and YL conception or design of the work and manuscript writing. CX and ZY acquisition of the data. All authors have approved the submitted version and have agreed on both to be personally accountable for the author's own contributions and to ensure that questions related to the accuracy or integrity of any part of the work.

Conflict of interest

The authors declare that the research was conducted in the absence of any commercial or financial relationships that could be construed as a potential conflict of interest.

Publisher's note

All claims expressed in this article are solely those of the authors and do not necessarily represent those of their affiliated organizations, or those of the publisher, the editors and the reviewers. Any product that may be evaluated in this article, or claim that may be made by its manufacturer, is not guaranteed or endorsed by the publisher.

Supplementary material

The Supplementary Material for this article can be found online at: https://www.frontiersin.org/articles/10.3389/fgene.2022.902329/full#supplementary-material

References

Acién, P., and Velasco, I. (2013). Endometriosis: a disease that remains enigmatic. *ISRN Obstet. Gynecol.* 2013, 242149. doi:10.1155/2013/242149

Asally, R., Markham, R., and Manconi, F. (2020). Mitochondrial DNA haplogroup H association with endometriosis and possible role in inflammation and pain. *J. Endometr. Pelvic Pain Disord.* 12, 158–164. doi:10.1177/2284026520940518

Ayubi, E., and Safiri, S. (2017). Risk factors for uterine rupture with a special interest in uterine fundal pressure: methodological issues. *J. Perinat. Med.* 45, 635–636. doi:10.1515/jpm-2017-0120

Becht, E., Giraldo, N. A., Lacroix, L., Buttard, B., Elarouci, N., Petitprez, F., et al. (2016). Estimating the population abundance of tissue-infiltrating immune and stromal cell populations using gene expression. *Genome Biol.* 17, 218. doi:10.1186/s13059-016-1070-5

Beermann, J., Piccoli, M. T., Viereck, J., and Thum, T. (2016). Non-coding RNAs in development and disease: Background, mechanisms, and therapeutic approaches. *Physiol. Rev.* 96, 1297–1325. doi:10.1152/physrev.00041.2015

Bonafede, , R., Scambi, I., Peroni, D., Potrich, V., Boschi, F., Benati, D., et al. (2016). Exosome derived from murine adipose-derived stromal cells: Neuroprotective effect on *in vitro* model of amyotrophic lateral sclerosis. *Exp. Cell Res.* 340, 150–158. doi:10.1016/j.yexcr.2015.12.009

Bonocher, C. M., Montenegro, M. L., Rosa E Silva, J. C., Ferriani, R. A., and Meola, J. (2014). Endometriosis and physical exercises: A systematic review. *Reprod. Biol. Endocrinol.* 12, 4. doi:10.1186/1477-7827-12-4

Buggio, L., Barbara, G., Facchin, F., Frattaruolo, M. P., Aimi, G., Berlanda, N., et al. (2017). Self-management and psychological-sexological interventions in patients with endometriosis: strategies, outcomes, and integration into clinical care. *Int. J. Womens Health* 9, 281–293. doi:10.2147/IJWH.S119724

Burney, R. O., and Giudice, L. C. (2012). Pathogenesis and pathophysiology of endometriosis. *Fertil. Steril.* 98, 511–519. doi:10.1016/j.fertnstert.2012.06.029

Chengmao, X., Li, L., Yan, L., Jie, Y., Xiaoju, W., Xiaohui, C., et al. (2017). ABCA1 affects placental function via trophoblast and macrophage. *Life Sci.* 191, 150–156. doi:10.1016/j.lfs.2017.10.031

Chiu, H. S., Martínez, M. R., Komissarova, E. V., Llobet-Navas, D., Bansal, M., Paull, E. O., et al. (2018). The number of titrated microRNA species dictates ceRNA regulation. *Nucleic Acids Res.* 46, 4354–4369. doi:10.1093/nar/gky286

Christodoulakos, G., Augoulea, A., Lambrinoudaki, I., Sioulas, V., and Creatsas, G. (2007). Pathogenesis of endometriosis: the role of defective 'immunosurveillance. *Eur. J. Contracept. Reprod. Health Care* 12, 194–202. doi:10.1080/13625180701387266

Chuang, P. C., Wu, M. H., Shoji, Y., and Tsai, S. J. (2009). Downregulation of CD36 results in reduced phagocytic ability of peritoneal macrophages of women with endometriosis. *J. Pathol.* 219, 232–241. doi:10.1002/path.2588

Dmowski, W. P., Ding, J., Shen, J., Rana, N., Fernandez, B. B., Braun, D. P., et al. (2001). Apoptosis in endometrial glandular and stromal cells in women with and without endometriosis. *Hum. Reprod.* 16, 1802–1808. doi:10.1093/humrep/16.9.1802

Dunselman, G. A., Vermeulen, N., Becker, C., Calhaz-Jorge, C., D', Hooghe, T., De Bie, B., et al. (2014). ESHRE guideline: management of women with endometriosis. *Hum. Reprod. Oxf. Engl.* 29, 400–412. doi:10.1093/humrep/det457

Friedman, J., Hastie, T., and Tibshirani, R. (2010). Regularization paths for generalized linear models via coordinate descent. *J. Stat. Softw.* 33, 1–22. doi:10.18637/jss.v033.i01

Ghazal, S., Mckinnon, B., Zhou, J., Mueller, M., Men, Y., Yang, L., et al. (2015). H19 lncRNA alters stromal cell growth via IGF signaling in the endometrium of women with endometriosis. *EMBO Mol. Med.* 7, 996–1003. doi:10.15252/emmm.201505245

Giudice, L. C., and Kao, L. C. (2004). Endometriosis. *Lancet (London, Engl.)* 364, 1789–1799. doi:10.1016/S0140-6736(04)17403-5

Hansen, K. A., Chalpe, A., and Eyster, K. M. (2010). Management of endometriosis-associated pain. *Clin. Obstet. Gynecol.* 53, 439–448. doi:10.1097/GRF.0b013e3181dbda06

Huang, M. L., Hung, Y. H., Lee, W. M., Li, R. K., and Jiang, B. R. (2014). SVM-RFE based feature selection and Taguchi parameters optimization for multiclass SVM classifier. *Sci. World J.* 2014, 795624. doi:10.1155/2014/795624

Johnson, N. P., Hummelshoj, L., Adamson, G. D., Keckstein, J., Taylor, H. S., Abrao, M. S., et al. (2017). World Endometriosis Society consensus on the

classification of endometriosis. *Hum. Reprod.* 32, 315–324. doi:10.1093/humrep/dew293

Kitawaki, J., Kusuki, I., Koshiba, H., Tsukamoto, K., and Honjo, H. (1999). Expression of aromatase cytochrome P450 in eutopic endometrium and its application as a diagnostic test for endometriosis. *Gynecol. Obstet. Invest.* 48 (Suppl. 1), 21–28. doi:10.1159/000052865

Kobayashi, H., Higashiura, Y., Shigetomi, H., and Kajihara, H. (2014). Pathogenesis of endometriosis: the role of initial infection and subsequent sterile inflammation (review). *Mol. Med. Rep.* 9, 9–15. doi:10.3892/mmr.2013.1755

Langfelder, P., and Horvath, S. (2008). WGCNA: an R package for weighted correlation network analysis. *BMC Bioinforma.* 9, 559. doi:10.1186/1471-2105-9-559

Mantovani, A., Allavena, P., Sica, A., and Balkwill, F. (2008). Cancer-related inflammation. *Nature* 454, 436–444. doi:10.1038/nature07205

McAllister, S. L., Giourgas, B. K., Faircloth, E. K., Leishman, E., Bradshaw, H. B., Gross, E. R., et al. (2016). Prostaglandin levels, vaginal innervation, and cyst innervation as peripheral contributors to endometriosis-associated vaginal hyperalgesia in rodents. *Mol. Cell. Endocrinol.* 437, 120–129. doi:10.1016/j.mce.2016.08.017

McKinnon, B. D., Bertschi, D., Bersinger, N. A., and Mueller, M. D. (2015). Inflammation and nerve fiber interaction in endometriotic pain. *Trends Endocrinol. Metab.* 26, 1–10. doi:10.1016/j.tem.2014.10.003

Miao, Y. R., Zhang, Q., Lei, Q., Luo, M., Xie, G. Y., Wang, H., et al. (2020). ImmuCellAI: a unique method for comprehensive T-cell subsets abundance prediction and its application in cancer immunotherapy. *Adv. Sci.* 7, 1902880. doi:10.1002/advs.201902880

Panir, K., Schjenken, J. E., Robertson, S. A., and Hull, M. L. (2018). Non-coding RNAs in endometriosis: A narrative review. *Hum. Reprod. Update* 24, 497–515. doi:10.1093/humupd/dmy014

Parasar, P., Ozcan, P., and Terry, K. L. (2017). Endometriosis: Epidemiology, diagnosis and clinical management. *Curr. Obstet. Gynecol. Rep.* 6, 34–41. doi:10.1007/s13669-017-0187-1

Peiris, A. N., Chaljub, E., and Medlock, D. (2018). Endometriosis. *JAMA* 320, 2608. doi:10.1001/jama.2018.17953

Phipson, B., Lee, S., Majewski, I. J., Alexander, W. S., and Smyth, G. K. (2016). Robust hyperparameter estimation protects against hypervariable genes and improves power to detect differential expression. *Ann. Appl. Stat.* 10, 946–963. doi:10.1214/16-AOAS920

Practice Committee of the American Society for Reproductive Medicine (2014). Treatment of pelvic pain associated with endometriosis: A committee opinion. *Fertil. Steril.* 101, 927–935. doi:10.1016/j.fertnstert.2014.02.012

Ritchie, M. E., Phipson, B., Wu, D., Hu, Y., Law, C. W., Shi, W., et al. (2015). Limma powers differential expression analyses for RNA-sequencing and microarray studies. *Nucleic Acids Res.* 43, e47. doi:10.1093/nar/gkv007

Robin, X., Turck, N., Hainard, A., Tiberti, N., Lisacek, F., Sanchez, J. C., et al. (2011). pROC: an open-source package for R and S+ to analyze and compare ROC curves. *BMC Bioinforma.* 12, 77. doi:10.1186/1471-2105-12-77

Rogers, P. A., Adamson, G. D., Al-Jefout, M., Becker, C. M., D', Hooghe, T. M., Dunselman, G. A., et al. (2017). Research priorities for endometriosis. *Reprod. Sci. (Thousand Oaks, Calif.)* 24, 202–226. doi:10.1177/1933719116654991

Rolla, E. (2019). Endometriosis: Advances and controversies in classification, pathogenesis, diagnosis, and treatment. *F1000Research* 8. doi:10.12688/f1000research.14817.1

Saare, M., Rekker, K., Laisk-Podar, T., Rahmioglu, N., Zondervan, K., Salumets, A., et al. (2017). Challenges in endometriosis miRNA studies - from tissue heterogeneity to disease specific miRNAs. *Biochim. Biophys. Acta. Mol. Basis Dis.* 1863, 2282–2292. doi:10.1016/j.bbadis.2017.06.018

Salmena, L., Poliseno, L., Tay, Y., Kats, L., and Pandolfi, P. P. (2011). A ceRNA hypothesis: the rosetta stone of a hidden RNA language. *Cell* 146, 353–358. doi:10.1016/j.cell.2011.07.014

Samimi, M., Pourhanifeh, M. H., Mehdizadehkashi, A., Eftekhar, T., and Asemi, Z. (2019). The role of inflammation, oxidative stress, angiogenesis, and apoptosis in the pathophysiology of endometriosis: Basic science and new insights based on gene expression. *J. Cell. Physiol.* 234, 19384–19392. doi:10.1002/jcp.28666

Sampson, J. A. (1927). Metastatic or embolic endometriosis, due to the menstrual dissemination of endometrial tissue into the venous circulation. *Am. J. Pathol.* 3, 93–110.43. doi:10.1007/BF01995231

Sampson, J. A. (1928). Peritoneal endometriosis due to premenstrual disseminaton of endometrial tssue into the peritoneal cavity. *Am. J. Obstet. Gynecol.* 15, 101–110. doi:10.1016/s0002-9378(15)30003-x

Seli, E., and Arici, A. (2003). Endometriosis: Interaction of immune and endocrine systems. *Semin. Reprod. Med.* 21, 135–144. doi:10.1055/s-2003-41320

Shannon, P., Markiel, A., Ozier, O., Baliga, N. S., Wang, J. T., Ramage, D., et al. (2003). Cytoscape: A software environment for integrated models of biomolecular interaction networks. *Genome Res.* 13, 2498–2504. doi:10.1101/gr.1239303

Subramanian, A., and Agarwal, N. (2010). Endometriosis – morphology, clinical presentations and molecular pathology. *J. Lab. Physicians* 2, 1–9. doi:10.4103/0974-2727.66699

Sun, H., Li, D., Yuan, M., Li, Q., Zhen, Q., Li, N., et al. (2018). Macrophages alternatively activated by endometriosis-exosomes contribute to the development of lesions in mice. *Mol. Hum. Reprod.* 25, 5–16. doi:10.1093/molehr/gay049

Symons, L. K., Miller, J. E., Kay, V. R., Marks, R. M., Liblik, K., Koti, M., et al. (2018). The immunopathophysiology of endometriosis. *Trends Mol. Med.* 24, 748–762. doi:10.1016/j.molmed.2018.07.004

Vitagliano, A., Noventa, M., Quaranta, M., and Gizzo, S. (2016). Statins as targeted "magical pills" for the conservative treatment of endometriosis: May potential adverse effects on female fertility Represent the "dark side of the same coin"? a systematic Review of literature. *Reprod. Sci.* 23, 415–428. doi:10.1177/1933719115584446

Wang, K. C., and Chang, H. Y. (2011). Molecular mechanisms of long noncoding RNAs. *Mol. Cell* 43, 904–914. doi:10.1016/j.molcel.2011.08.018

Wei, Y., Liang, Y., Lin, H., Dai, Y., and Yao, S. (2020). Autonomic nervous system and inflammation interaction in endometriosis-associated pain. *J. Neuroinflamm.* 17, 80. doi:10.1186/s12974-020-01752-1

Yoshino, O., Yamada-Nomoto, K., Kobayashi, M., Andoh, T., Hongo, M., Ono, Y., et al. (2018). Bradykinin system is involved in endometriosis-related pain through endothelin-1 production. *Eur. J. Pain* 22, 501–510. doi:10.1002/ejp.1133

Yu, G., Wang, L. G., Han, Y., and He, Q. Y. (2012). clusterProfiler: an R package for comparing biological themes among gene clusters. *Omics a J. Integr. Biol.* 16, 284–287. doi:10.1089/omi.2011.0118

Zondervan, K. T., Becker, C. M., and Missmer, S. A. (2020). Endometriosis. *N. Engl. J. Med.* 382, 1244–1256. doi:10.1056/NEJMra1810764

frontiers | Frontiers in Pediatrics

TYPE Original Research
PUBLISHED 22 July 2022
DOI 10.3389/fped.2022.940294

Check for updates

OPEN ACCESS

EDITED BY
Tieliu Shi,
Hunan University of Arts and Science, China

REVIEWED BY
Jian Wang,
Shanghai Children's Medical Center, China
Victor Faundes,
University of Chile, Chile

*CORRESPONDENCE
Ruimin Chen
chenrm321@163.com

SPECIALTY SECTION
This article was submitted to Genetics of Common and Rare Diseases, a section of the journal Frontiers in Pediatrics

RECEIVED 10 May 2022
ACCEPTED 27 June 2022
PUBLISHED 22 July 2022

CITATION
Shangguan H and Chen R (2022) Phenotypes of Cornelia de Lange syndrome caused by non-cohesion genes: Novel variants and literature review.
Front. Pediatr. 10:940294.
doi: 10.3389/fped.2022.940294

COPYRIGHT
© 2022 Shangguan and Chen. This is an open-access article distributed under the terms of the Creative Commons Attribution License (CC BY). The use, distribution or reproduction in other forums is permitted, provided the original author(s) and the copyright owner(s) are credited and that the original publication in this journal is cited, in accordance with accepted academic practice. No use, distribution or reproduction is permitted which does not comply with these terms.

Phenotypes of Cornelia de Lange syndrome caused by non-cohesion genes: Novel variants and literature review

Huakun Shangguan and Ruimin Chen*

Department of Endocrinology, Fuzhou Children's Hospital of Fujian Medical University, Fuzhou, China

Background: Cornelia de Lange syndrome (CdLS) is a genetic disorder caused by variants in cohesion genes including *NIPBL*, *SMC1A*, *SMC3*, *RAD21,* and *HDAC8.* According to the 2018 consensus statement, a patient with clinical scored $\geq$ 11 points could be diagnosed as CdLS. However, some variants in non-cohesion genes rather than cohesion genes can manifest as phenotypes of CdLS.

Objectives: This study describes six variants of non-cohesion genes (*KDM6A*, *KMT2D, KMT2A ANKRD11,* and *UBE2A*), and assesses the reliability of 11-points scale criteria in the clinical diagnosis of CdLS.

Methods: Whole-exome sequencing (WES) was performed on six patients with features of CdLS. Phenotypic and genotypic spectra of 40 previously reported patients with features of CdLS caused by non-cohesion genes variants and 34 previously reported patients with *NIPBL* variants were summarized. Clinical score comparison among patients with *NIPBL* variants versus those with variants in non-cohesin genes was performed.

Results: Variants in non-cohesion genes were found in six patients [*KMT2A* (n = 2), *KMT2D*, *ANKRD11*, *KDM6A,* and *UBE2A*]. Of them, four variants (*KMT2A* c.7789C > T, *ANKRD11* c.1757_1776del, *KDM6A* c.655-1G > A, and *UBE2A* c.439C > T) were novel. Combining with previously reported cases, 46 patients with phenotypes of CdLS caused by variants in 20 non-cohesion genes are now reported. From this total cohort, the average clinical score of patients in *ANKRD11* cohort, *SETD5* cohort, and *AFF4* cohort was statistically lower than those in *NIPBL* cohort (8.92 $\pm$ 1.77 vs. 12.23 $\pm$ 2.58, 7.33 $\pm$ 2.52 vs. 12.23 $\pm$ 2.58, 5.33 $\pm$ 1.53 vs. 12.23 $\pm$ 2.58; $p < 0.05$). The average clinical score of *KMT2A* cohort, *EP300* cohort, and *NIPBL* cohort had not significantly different from (11 $\pm$ 2.19 vs. 12.23 $\pm$ 2.58, 10 $\pm$ 4.58 vs. 12.23 $\pm$ 2.58; $p > 0.05$).

Conclusion: We described 4 novel variants of non-cohesion genes in six Chinese patients with phenotypes of CdLS. Of note, three genes (*KMT2D*, *KDM6A,* and *UBE2A*) causing features of CdLS have never been reported.

The proposed clinical criteria for CdLS needed to be updated and refined, insofar as WES was necessary to confirm the diagnosis of CdLS. Our study expanded the spectra of non-cohesion genetic variations in patients with features of CdLS.

KEYWORDS

Cornelia de Lange syndrome, non-cohesion, clinical diagnosis, whole exome sequencing, CdLS-like phenotypes

Introduction

Cornelia de Lange syndrome (CdLS, OMIM # 122470, #614701, #610759, #300590, and #300882) is a rare genetic disorder caused by variants in cohesion complex genes including *NIPBL* (NM_133433.3), *SMC1A* (NM_006304.4), *SMC3* (NM_005445.3), *HDAC8* (NM_018486.2), and *RAD21* (NM_006265.3) (1). Up to 70% of CdLS patients are diagnosed with *NIPBL* variants. Around 5% of CdLS patients carry *SMC1A* variants, and 5% are *HDAC8* variants, less than 1% of CdLS patients are variants in *SMC3* or *RAD21* genes (2). The mode of inheritance of CdLS in the patient's offspring could be either autosomal dominant (*NIPBL*, *RAD21*, or *SMC3* variants) or X-linked dominant (*SMC1*, or *HDAC8* variants) (2).

CdLS have variable phenotypes, such as microcephaly, minor facial dysmorphisms, intellectual disability, short stature, small hands, and hypertrichosis. In 2018, a diagnostic algorithm for initial evaluation of CdLS patients was proposed (3). Classic CdLS, based on clinical features, scored $\geq$ 11 points according to the consensus statement (3). Adopting this criteria would facilitate bedside diagnosis. However, some patients with features of CdLS were found to carry variants that were associated with other disorders, not with CdLS. Yuan et al. described a pathogenic *KMT2A* (NM_001197104.1) variant in one patient among 32 Turkish patients clinically diagnosed with classic CdLS (4). Cucco et al. also reported pathogenic variants in *EP300* (NM_001429.3) in a patient exhibiting resemblance to the classic CdLS phenotype in 2020 (5). With the development of contemporary genetic technology, it is not surprising that more patients with features of CdLS have been identified to carry variants in non-cohesion genes and, to date, the clinical genetic characteristics of these patients are ill-defined. Adding to the existing knowledge in this field is important in the quest to characterize the extent of heterogeneity of CdLS and Cornelia de Lange syndrome-like (CdLS-like) conditions.

In this study, we analyzed six patients with features of CdLS, and identified six variants in five non-cohesion genes. To date, 40 sporadic patients with features of CdLS caused by non-cohesion variants had been reported (4–17). We also evaluated the clinical features of these patients, and calculate the clinical scores of these patients according to the 2018 consensus statement to assess the reliability of 11-points scale criteria in the diagnosis of CdLS.

Abbreviations: CdLS, Cornelia de Lange syndrome; RAD21, RAD21 cohesin complex component; NIPBL, Nipped-B-like protein; SMC1A, Structural Maintenance of Chromosomes 1A; HDAC8, Histone deacetylases; SMC3, Structural Maintenance of Chromosomes 3; KS, Kabuki syndrome; KMT2D, lysine (K)-specific methyltransferase 2D; KDM6A, lysine (K)-specific methylase 6A; UBE2A, ubiquitin-conjugase E2A; ANKRD11, Ankyrin Repeat Domain 11; KMT2A, lysine (K)-specific methyltransferase 2A; WES, whole-exome sequencing; ACMG/AMP, American College of Medical Genetics and Genomics and the Association for Molecular Pathology; BRD4, Bromodomain containing 4; AFF4, AF4/FMR2 family, member 4; EP300, E1A binding protein p300; SETD5, SET domain containing 5; SMARCB1, SWI/SNF related, matrix associated, actin dependent regulator of chromatin, subfamily b, member 1; TAF1, TAF1 RNA polymerase II, TATA box binding protein (TBP)-associated factor; DDX23, DEAD-box helicase 23; CSNK1G1, casein kinase 1, gamma 1; ZMYND11, zinc finger, MYND-type containing 11; MED13L, Mediator complex subunit 13-like; PHIP, pleckstrin homology domain interacting protein; TAF6, TAF6 RNA polymerase II, TATA box binding protein (TBP)-associated factor; NAA50, N-Terminal Acetyltransferase 50; CREBBP, CREB binding protein.

Subjects and methods

Subjects

All individuals in this study were evaluated by clinical geneticists and found to have clinical signs consistent with CdLS. Clinical details were retrospectively reviewed based on recent clinical criteria (3). This study was approved by the Ethics Committee of Fuzhou Children's Hospital of Fujian Medical University, and written informed consents were obtained from the legal guardians of the patients.

Whole-exome sequencing and variants interpretation

Genomic DNA was extracted from peripheral blood leukocytes of each patient. Blood samples from the parents were also collected. The Whole-exome sequencing (WES) was

performed at Shanghai patient's Medical Center. An adaptor-ligated library was prepared using SureSelect Human All Exon Kit (Agilent Technologies, Santa Clara, CA, America) according to the manufacturer' s protocol. Target regions were sequenced on an Illumina Hiseq X Ten System (Illumina, San Diego, CA, America). Paired end reads were aligned to the GRCh37/hg19 human reference sequence. BAM files were generated by Picard and sequence variants were called by Genome Analysis Toolkit (GATK) Haplotype Caller. Variants were annotated by TGex and putative pathogenic variants detected in the patients by WES were validated by Sanger sequencing. Variants were classified following the American College of Medical Genetics and Genomics/Association for Molecular Pathology (ACMG/AMP) standards and guidelines (18).

Literature review

We first searched the published literature in PUBMED, EMBASE and MEDLINE using the following search keys: ("Cornelia de Lange syndrome" OR "Cornelia de Lange syndrome-like" OR "CdLS" OR CdLS-like), without language restriction, with published data up to March 31, 2022. Then we reviewed the articles, and included the CdLS patients carrying variants in non-cohesion genes. We also used the following keys: ("Cornelia de Lange syndrome" OR "CdLS") AND ("NIPBL") to search the published literature in the same way. The *NIPBL* cases with detail clinical information were included.

Statistics analysis

Statistical analysis for phenotypic among the patients with *NIPBL* variants versus those with variants in non-cohesion genes was performed by (corrected) the Chi-square test or Fisher's exact test using GraphPad prism 8.0.1 software. In addition, the mean of clinical score within each group was analyzed using one way ANOVA test or Kruskal–Wallis test in GraphPad prism 8.0.1 software. $P < 0.05$ was considered statistically significant.

Results

Clinical phenotype of six patients in our study

The six patients exhibited overlapping phenotypes. The main characteristics were as following: facial dysmorphism ($n = 6$), intellectual disability or global developmental delay ($n = 6$), short stature ($n = 6$), small hands ($n = 6$), short 5th finger ($n = 6$), and microcephaly ($n = 4$). Detailed clinical information of the six patients are described in **Table 1** and **Supplementary Table 1**.

Molecular findings of six patients in our study

Whole-exome sequencing of the six individuals with clinically suspected CdLS identified six variants in *KMT2A*, *KMT2D* (NM_003482.3), *ANKRD11* (NM_013275.4), *KDM6A* (NM_021140.2), and *UBE2A* (NM_003336.2) (**Table 1**).

Patient #1 was a carrier of a materal nucleotide substitution in *UBE2A*: c.439C > T, resulting in a premature stop codon (p.Gln147*). Patient #2 showed a *de novo* nucleotide deletion in *KMT2D*: c.5845delC, resulting in a premature stop codon (p.Q1949Sfs*98). Patient #3 had a *de novo* 20 nucleotides deletion in *ANKRD11*: c.1757_1776del, resulting in premature stop codon (p.V586Efs*41). Patient #4 showed a *de novo* nucleotide substitution in *KMT2A*: c.7789C > T, leading to premature stop codon (p.Q2597*). Patient #5 had a *de novo* 2 nucleotide deletion in *KMT2A*: c.2629_2630delGA, resulting in a premature stop codon (p.D877fs*8). Patient #6 was a carrier of a *de novo* splice variant in *KDM6A*: c.655-1G > A. The SpliceTool[1] predicted to delete 2 or 94 bp causing frameshift variants and premature termination, and multiple *in silico* tools predict deleterious outcomes of the splice variant (scored 1 in dbscsnv11_AdaBoost and 0.937 in dbscsnv11_RandomF orest). 4 variants (*UBE2A*: c.439C > T, *ANKRD11*: c.1757_1776del, *KMT2A*: c.7789C > T, and *KDM6A*: c.655-1G > A) were novel, and the *KMT2D* c.5845delC and *KMT2A* c.2629_2630delGA were both reported (19, 20). According to the ACMG/AMP standards and guidelines, these variants could all be classified as pathogenic (For *ANKRD11* c.1757_1776del, *KMT2A* c.7789C > T, and *KDM6A* c.655-1G > A: PVS1 + PS2 + PM2 + PP4; For *UBE2A* c.439C > T: PVS1 + PM2 + PP4; For *KMT2D* c.5845delC and *KMT2A* c.2629_2630delGA: PVS1 + PS2 + PP4).

Phenotypes and genotypes of 46 patients caused by non-cohesion genes variants

To date, 40 patients with features of CdLS caused by variants in non-cohesion genes have been comprehensively described in the literature. Including the six patients in our study, a total of 46 pathogenic/likely pathogenic variants associated with 20 epigenetic genes including *ANKRD11* ($n = 14$), *BRD4* (NM_058243.3) ($n = 2$), *AFF4* (NM_014423.4) ($n = 3$), *KMT2A* ($n = 6$), *EP300* ($n = 3$), *SETD5* (NM_001080517.3) ($n = 3$), *ARID1B* (NM_001374820.1) ($n = 2$), *SMARCB1* (NM_003073.5) ($n = 1$), *TAF1* (NM_4606.5) ($n = 1$), *DDX23* (NM_004818.3) ($n = 1$), *CSNK1G1* (NM_022048.5) ($n = 1$), *ZMYND11*

1 https://rddc.tsinghua-gd.org/tools/split-tool/result?uuid=f8b645a7-9dab-4683-bcc4-00d00711873f

TABLE 1 The genetic variants and clinical features of our six patients.

ID		P1	P2	P3	P4	P5	P6
Gender		Male	Female	Male	Male	Male	Male
Age (years)		5	0.83	3	1	2.5	0.58
Gene		*UBE2A*	*KMT2D*	*KDM6A*	*ANKRD11*	*KMT2A*	*KMT2A*
Variant		c.439C > T, p.Q147*	c.5845delC, p.Q1949Sfs*98	c.655-1G > A	c.1757_1776del, p.V586Efs*41	c.7789C > T, p.Q2597*	c.2629_2630delGA, p.D877fs*8
Inheritance		Materal	*De novo*	*De novo*	*De novo*	*De novo*	*De novo*
Novel or reported		Novel	Reported	Novel	Novel	Novel	Reported
ACMG classifcation		Pathogenic	Pathogenic	Pathogenic	Pathogenic	Pathogenic	Pathogenic
Main features (2 point each if present)	Synophrys and/or thick eyebrows	−	−	−	−	+	−
	Short nose, concave nasal ridge and/or upturned nasal tip	+	−	−	+	+	+
	Long and/or smooth philtrum	−	−	−	−	−	−
	Thin upper lip vermilion and/or downturned corners of mouth	−	+	+	−	+	+
	Hand oligodactyly and/or adactyly	−	−	−	−	−	−
	Congenital diaphragmatic hernia	−	−	−	−	−	−
Suggestive features (1 point each if present)	Small hands and/or feet	+	+	+	+	+	+
	Microcephaly	−	−	+	+	+	+
	Global developmental delay and/or intellectual disability	+	+	+	+	+	+
	Prenatal growth retardation	−	−	−	−	−	−
	Postnatal growth retardation	+	+	+	+	+	+
	Hypertrichosis	−	−	−	−	+	+
	Short fifth finger	+	+	+	+	+	+
Other features		With mouth, hypertelorism, high palate, inguinal hernia, renal cyst	Long palpebral fissures with eversion of the lower lid, ventricular septal defect, single transverse palmar crease, prominent fingertip pads	Long palpebral fissures with eversion of the lower lid, Long eyelashes, defect in the atrial septum, Coarctation of aorta, single transverse palmar crease	Macrodontia of the upper central incisors	Ptosis, long eyelashes, hypertelorism	Ptosis, long eyelashes, hypertelorism, cryptorchidism, patent ductus arteriosus
Clinical scored		6	6	7	7	12	10

(NM_006624.7) ($n = 1$), *MED13L* (NM_015335.5) ($n = 1$), *PHIP* (NM_017934.7) ($n = 1$), *TAF6* (NM_005641.4) ($n = 1$), *NAA50* (NM_025146.4) ($n = 1$), *CREBBP* (NM_004380.3) ($n = 1$), *UBE2A* ($n = 1$), *KMT2D* ($n = 1$), and *KDM6A* ($n = 1$) are described (**Supplementary Table 2**). Of note, although we have reported the patient with *KMT2D* c.5845delC before, his phenotype consistent with CdLS was not recognized (19). Therefore, this case was not included in the literature review.

We divided these patients into six groups: *KMT2A* group, *ANKRD11* group, *EP300* group, *SETD5* group, *AFF4* group and a remaining group consisted of a lower number of patients with features of CdLS caused by non-cohesion genes variants (*BRD4*, *ARID1B, SMARCB1*, *TAF1*, *DDX23*, *CSNK1G1*, *ZMYND11*, *MED13L*, *PHIP*, *TAF6*, *NAA50*, *CREBBP*, *UBE2A*, *KMT2D,* and *KDM6A*). The average clinical score of patients in *KMT2A* group was 11 ± 2.19, 8.92 ± 1.77 in *ANKRD11* group, 10 ± 4.58

TABLE 2 Clinical features of patients in CdLS-like cohort and those in *NIPBL* cohort.

Clinical feature	*NIPBL* cohort ($n = 34$)	*KMT2A* cohort ($n = 6$)	*ANKRD11* cohort ($n = 14$)	*EP300* cohort ($n = 3$)	*SETD5* cohort ($n = 3$)	*AFF4* cohort ($n = 3$)	Remaining genes cohort ($n = 17$)	Chi-square value	*P*-valve
Synophrys	31	5	10	3	2	3	14	5.049	0.45
Thick eyebrows	17	3	11	0	1	2	2[a]	17.772	0.002
Short nose	19	2	0[a]	1	0	1	3[a]	19.015	0.001
Concave nasal ridge	23	4	5	0[a]	2	0[a]	5[a]	14.383	0.011
Upturned nasal tip	22	2	11	2	1	1	7	8.204	0.192
Smooth philtrum	15	3	5	1	2	0	2	8.899	0.139
Long philtrum	28	3	13	1	1	1	10	14.287	0.012
Downturned corners of mouth	18	3	5	1	1	1	7	2.354	0.924
Thin upper lip vermilion	27	4	7	2	2	0	10	10.158	0.08
Adactyly	2	0	0	0	0	0	0	4.945	0.754
Hand oligodactyly	7	0	0	0	0	0	2	2.420	0.944
Small hands	17	3	8	0	0	0	6	8.008	0.205
Small feet	8	0	5	1	0	0	3	4.438	0.594
Microcephaly	24	5	7	2	0	1	11	8.558	0.164
Global developmental delay and/or intellectual disability	28	6	13	3	3	2	17	6.197	0.294
Prenatal growth retardation	23	1[a]	1[a]	1	0[a]	0[a]	4[a]	23.496	0.000
Postnatal growth retardation	23	6	1[a]	3	1	1	10	24.140	0.000
Hypertrichosis	13	4	2	3	0	0	2	16.143	0.005
Short fifth finger	12	5	6	1	0	0	7	8.137	0.194
Average clinical score (mean ± SD)	12.23 ± 2.58	11 ± 2.19[c]	8.92 ± 1.77[b]	10 ± 4.58	7.33 ± 2.52[b]	5.33 ± 1.53[bc]	8.88 ± 2.62[b]		< 0.0001

[a]Indicates that the incidence of phenotype was statistically significant compared with *NIPBL* cohort.
[b]Indicates that the average clinical score was statistically significant compared with *NIPBL* cohort.
[c]Indicates that the average clinical score of the two groups were statistically significant.

in *EP300* group, 7.33 ± 2.52 in *SETD5* group, 5.33 ± 1.53 in *AFF4* group and 8.88 ± 2.62 in the remaining group (Table 2).

Phenotypic and clinical score comparison of the non-cohesion cohort and *NIPBL* cohort

We collected data on a group of 34 cases of CdLS caused by *NIPBL* variants from the literature and summarized the phenotypes and clinical score of the total 34 patients (clinical information and reference are shown in Supplementary Tables 3, 4). This affords us the opportunity to compare the clinical features and score of patients with *NIPBL* variants to those with variants in non-cohesion genes (Table 2 and Figure 1).

The overall clinical characteristics are similar among these groups, however, several differences still can be observed. The patients in *ANKRD11* cohort had lower frequencies of short nose, prenatal growth retardation and postnatal growth retardation than those in *NIPBL* cohort. The features of concave nasal ridge and prenatal growth retardation were more frequent in patients in *AFF4* cohort than those in *NIPBL* cohort. The features of concave nasal ridge and prenatal growth retardation showed significant statistical different from the patients in the *EP300* cohort and those in the *NIPBL* cohort. The frequencies of prenatal growth retardation in patients of *KMT2A* cohort showed lower than those of *NIPBL* cohort. Additionally, the average clinical score of patients in *ANKRD11* cohort, *SETD5* cohort and *AFF4* cohort was statistically lower than those in *NIPBL* cohort, respectively (8.92 ± 1.77 vs. 12.23 ± 2.58, 7.33 ± 2.52 vs. 12.23 ± 2.58, 5.33 ± 1.53 vs. 12.23 ± 2.58; $p < 0.05$). The average clinical score of patients in *KMT2A* cohort and *EP300* cohort both had no significantly difference with those in the *NIPBL* cohort (11 ± 2.19 vs. 12.23 ± 2.58, 10 ± 4.58 vs. 12.23 ± 2.58; $p > 0.05$).

Discussion

In the present study, we provided our findings on the genetic analysis of six patients referred to our clinic for short stature.

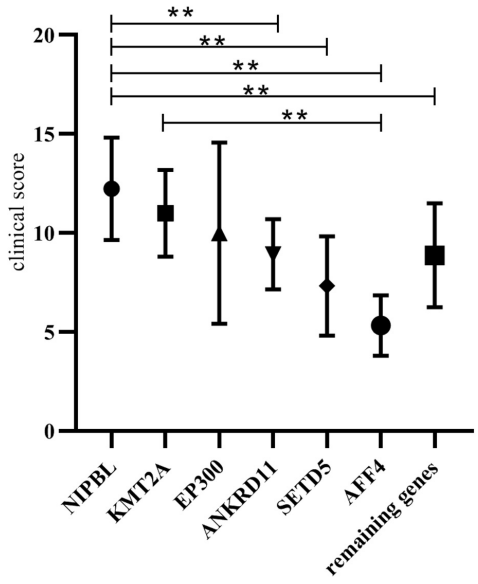


FIGURE 1
Clinical score comparison of the non-cohesion cohort and *NIPBL* cohort. **Indicates that the average clinical score of the two groups were statistically significant ($p < 0.05$).

Short stature can be either a component of known syndromes or occur in undefined manifold complex clinical phenotypes. It was reported that 86% of CdLS presented with short stature, a common finding occurred in other rare genetic disorders, such as Wiedemann-Steiner syndrome (WDSTS, OMIM #605135) (75%), Kabuki syndrome (KS, OMIM #147920, #300867) (57%) and KBG syndrome (KBGS, OMIM #148050) (40–77%) (19, 21–23).

Several common clinical features were observed among the six patients, all of whom had short stature, moderate to severe development delay and/or intellectual disability, small hands and short fifth fingers, partly presenting with microcephaly. Hypertrichosis was also frequent. In addition, some CdLS-specific features including synophrys, concave nasal ridge and long smooth philtrum were observed, which in combination with short stature and intellectual disability resembled CdLS. However, the six patients with clinically suspected CdLS were found to carry 6 variants in *KMT2A*, *KMT2D*, *ANKRD11*, *KDM6A*, and *UBE2A*, which don't function in cohesion protein. These identified variants in the genes (*KMT2A*, *KMT2D*, *KDM6A*, and *ANKRD11*) met the pathogenicity criteria according to ACMG/AMP standards and guidelines, including *de novo* occurrence, absence in general population and predicted LOF effect causing diseases through this pathogenetic mechanism. The *UBE2A* c.439C > T variant was also deemed pathogenic given that the variant causes a premature stop codon and is absent in the general population.

KMT2A variants are associated to the WDSTS, a rare autosomal dominant condition characterized by different debilities, mainly intellectual disability, short stature, hypertrichosis, distinctive facial features (thick eyebrows, long eyelashes, narrow palpebral fissures, hypertelorism, ptosis, broad nasal tip), and skeletal abnormalities (clinodactyly, brachydactyly, advanced bone age) (24). Two patients (P5 and P6) carrying *KMT2A* variants in our study shared a number of clinical features of CdLS including short nose, anteverted nares, concave nasal ridge, short stature, global developmental delay, small hands, short 5th finger and microcephaly. And both had clinical scores of 12 and 10, respectively (**Table 1**). Previously, four patients with features of CdLS found to carry *KMT2A* variants have been reported. With our new two patients, the average clinical score of the six patients was no significantly different from a cohort of *NIPBL* patients (11 ± 2.19 vs. 12.23 ± 2.58), which infers that some patients with *KMT2A* variants may be misdiagnosed as CdLS without molecular test. However, the combination of ptosis and long eyelashes was more frequent in *KMT2A* patients than *NIPBL* patients (24). Four of these six patients (two patients in our study and two patients in literature) had features of ptosis and hypertelorism, which may help to distinguish WDSTS and CdLS (13, 16).

KBG syndrome is a rare condition characterized by intellectual disability, global developmental delay, short stature, skeletal anomalies, distinctive facial features, and macrodontia of the upper central incisors (23). One child (P4) in our study had a frameshift variant in *ANKRD11* gene. He presented with some features of CdLS including anteverted nares, short stature, global developmental delay, microcephaly, small hands and short 5th finger (**Table 1**; scored 7). He also presented with macrodontia of the upper central incisors, which is a component of KBGS (25). Although KBG has clinical features overlapping with CdLS, the average clinical score is lower than the *NIPBL* cohort. Additionally, the features of short nose, prenatal and postnatal growth retardation had a lower frequency in *ANKRD11* cohort than those in the *NIPBL* cohort (**Table 2**). More importantly, a specific combination of a triangular shaped face and a bulbous nasal tip was crucial for the accurate clinical diagnosis of KBGS and CdLS (17).

Additionally, we reported a novel patient (P1) with nonsense variant in *UBE2A,* involved in coding ubiquitin-conjugating enzyme E2A, with CdLS related phenotypes. Haploinsufficiency of *UBE2A* underlies the X-linked intellectual disability type Nascimento (XIDTN, OMIM #300860), also known as UBE2A deficiency syndrome (26). To date, about 40 patients with XIDTN had been reported in literature (26). Nascimento et al. reported that its distinct abnormalities including a myxoedematous appearance and nail dystrophies, yet these features were not observed in P1. Additionally, prominent supraorbital ridge, hypertelorism, and prominent columella/hypoplastic alae nasi and a wide mouth were also common in XIDTN (27). However, except a wide mouth, these features were not found in our patient. Interestingly, the phenotypic features of our patient with *UBE2A* variant shared

similarities with the previously described CdLS individuals including anteverted nares, short stature, intellectual disability, small hands and short 5th finger (**Table 1**, scored 6). These findings suggested that individuals with *UBE2A* variant instead present with specific features that is only minimally overlapping with CdLS.

Our two patients (P2 and P3) found to carry *KTM2D* and *KDM6A* variants, presented with thin upper lip vermilion, downturned corners of mouth, a finding mainly described in CdLS (**Table 1**; score 6 and 7, respectively) (3). Pathogenic variants in the chromatin regulatory methyltransferase gene *KMT2D* and demethyltransferase gene *KDM6A* cause autosomal dominant KS, associated with specific clinical signs including arched eyebrows, long palpebral fissures with eversion of the lower lid, large protuberant ears, and prominent fingertip pads, hypoplastic left heart (28). Corresponding to it, the two patients both had long palpebral fissures with eversion of the lower lid and hypoplastic left heart, features that help to distinguish KS and CdLS. Additionally, P2 had prominent fingertip pads which are considered a distinctive of KS.

A total of 46 patients with feature of CdLS caused by variants in non-cohesion genes were summarized. We collected data on a group of 34 cases of CdLS caused by *NIPBL* variants from the literature and summarized the phenotypes and clinical score of those patients. This affords us the opportunity to compare the clinical features and score of patients with *NIPBL* variants to those with variants in non-cohesion genes. Our results suggested that *KMT2A* and *EP300* can be included within the extended list of CdLS genes that are studied in CdLS panels. In addition, the average clinical score of *ANKRD11* cohort, *SETD5* cohort, and *AFF4* cohort was 8.92 ± 1.77, 7.33 ± 2.52, 5.33 ± 1.53, respectively. Variants in these three genes caused limited phenotypes overlapping with CdLS. Single case with variants in some non-genes causes features of CdLS were reported in literature. The presence of one or two cases made statistical analysis impossible. Additional case accumulation is needed to further explore the relationship between these non-genetic variants and phenotypes of CdLS.

Extensive evidences showed that the cohesion complex functions in sister chromatid cohesion, as well as playing a role in the regulation of transcription. Some reports suggested that the cohesion genes including *NIPBL*, *SMC1A*, *SMC3*, *RAD21*, and *HDAC8* (29–31), are involved in chromatin-mediated transcriptional regulation. Moreover, function experiments showed cell lines of individuals with CdLS displayed global transcriptional disturbances rather than cohesion defects (32). Additionally, the cohesion components and chromatin-remodeling proteins strongly interact (33). These studies provided a new perspective on the distinct roles of epigenetic mechanism of phenotypes of CdLS. As a consequence, identifying the causes of patients with features of CdLS by WES is a requisite for accurate genetic diagnosis.

Conclusion

We describe four novel variants in six Chinese patients with features of CdLS caused by variants in four non-cohesion genes (*ANKRD11*, *KMT2D*, *KDM6A*, and *UBE2A*). In addition, three genes (*KMT2D*, *KDM6A*, and *UBE2A*) causing phenotypes of CdLS have never been reported. Some patients carrying variants in non-cohesion genes could be misdiagnosed as CdLS solely based on the 11-points scale criteria, and WES was necessary to confirm the diagnosis of CdLS. This study expands the spectra of non-cohesion genetic variations in patients with features of CdLS.

Data availability statement

The original contributions presented in this study are included in the article/**Supplementary Material**, further inquiries can be directed to the corresponding author.

Ethics statement

The studies involving human participants were reviewed and approved by the Ethics Committee of Fuzhou Children's Hospital of Fujian Medical University. Written informed consent to participate in this study was provided by the participants' legal guardian/next of kin.

Author contributions

HS conducted the data analysis and interpretation and wrote the manuscript. RC contributed to the study design, helped to analyze data, and revise the first draft. Both authors contributed to the article and approved the submitted version.

Funding

This work was sponsored by the Key Clinical Special Discipline Construction Program of Fuzhou, Fujian, P.R.C (No. 201610191), Clinical Medical Center of Fuzhou, Fujian, P.R.C (No. 201808310), and the Basic and Clinical Research of Rare Disease of Fuzhou, Fujian, P.R.C (ZD-2019-01).

Acknowledgments

We thank to all the participants and their families who participated in the clinical trial. We also thank Wei xia for her tolerance and companionship.

Conflict of interest

The authors declare that the research was conducted in the absence of any commercial or financial relationships that could be construed as a potential conflict of interest.

Publisher's note

All claims expressed in this article are solely those of the authors and do not necessarily represent those of their affiliated organizations, or those of the publisher, the editors and the reviewers. Any product that may be evaluated in this article, or claim that may be made by its manufacturer, is not guaranteed or endorsed by the publisher.

Supplementary material

The Supplementary Material for this article can be found online at: https://www.frontiersin.org/articles/10.3389/fped.2022.940294/full#supplementary-material

References

1. Selicorni A, Mariani M, Lettieri A, Massa VJG. Cornelia de Lange syndrome: from a disease to a broader spectrum. *Genes.* (2021) 12:1075.

2. Avagliano L, Parenti I, Grazioli P, Di Fede E, Parodi C, Mariani M, et al. Chromatinopathies: a focus on Cornelia de Lange syndrome. *Clin Genet.* (2020) 97:3–11. doi: 10.1111/cge.13674

3. Kline A, Moss J, Selicorni A, Bisgaard A, Deardorff M, Gillett P, et al. Diagnosis and management of Cornelia de Lange syndrome: first international consensus statement. *Nat Rev Genet.* (2018) 19:649–66.

4. Yuan B, Pehlivan D, Karaca E, Patel N, Charng W, Gambin T, et al. Global transcriptional disturbances underlie Cornelia de Lange syndrome and related phenotypes. *J Clin Invest.* (2015) 125:636–51.

5. Cucco F, Sarogni P, Rossato S, Alpa M, Patimo A, Latorre A, et al. Pathogenic variants in EP300 and ANKRD11 in patients with phenotypes overlapping Cornelia de Lange syndrome. *Am J Med Genet A.* (2020) 182:1690–6. doi: 10.1002/ajmg.a.61611

6. Burns W, Bird LM, Heron D, Keren B, Ramachandra D, Thiffault I, et al. Syndromic neurodevelopmental disorder associated with de novo variants in DDX23. *Am J Med Genet A.* (2021) 185:2863–72. doi: 10.1002/ajmg.a.62359

7. Gold NB, Li D, Chassevent A, Kaiser FJ, Parenti I, Strom TM, et al. Heterozygous de novo variants in CSNK1G1 are associated with syndromic developmental delay and autism spectrum disorder. *Clin Genet.* (2020) 98:571–6. doi: 10.1111/cge.13851

8. Ansari M, Poke G, Ferry Q, Williamson K, Aldridge R, Meynert AM, et al. Genetic heterogeneity in Cornelia de Lange syndrome (CdLS) and CdLS-like phenotypes with observed and predicted levels of mosaicism. *J Med Genet.* (2014) 51:659–68. doi: 10.1136/jmedgenet-2014-102573

9. Woods SA, Robinson HB, Kohler LJ, Agamanolis D, Sterbenz G, Khalifa M. Exome sequencing identifies a novel EP300 frame shift mutation in a patient with features that overlap cornelia de lange syndrome. *Am J Med Genet A.* (2014) 164A:251–8. doi: 10.1002/ajmg.a.36237

10. O'Rawe JA, Wu Y, Dorfel MJ, Rope AF, Au PY, Parboosingh JS, et al. TAF1 variants are associated with dysmorphic features, intellectual disability, and neurological manifestations. *Am J Hum Genet.* (2015) 97:922–32.

11. Izumi K, Nakato R, Zhang Z, Edmondson AC, Noon S, Dulik MC, et al. Germline gain-of-function mutations in AFF4 cause a developmental syndrome functionally linking the super elongation complex and cohesin. *Nat Genet.* (2015) 47:338–44. doi: 10.1038/ng.3229

12. Parenti I, Gervasini C, Pozojevic J, Graul-Neumann L, Azzollini J, Braunholz D, et al. Broadening of cohesinopathies: exome sequencing identifies mutations in ANKRD11 in two patients with Cornelia de Lange-overlapping phenotype. *Clin Genet.* (2016) 89:74–81. doi: 10.1111/cge.12564

13. Parenti I, Teresa-Rodrigo ME, Pozojevic J, Ruiz Gil S, Bader I, Braunholz D, et al. Mutations in chromatin regulators functionally link Cornelia de Lange syndrome and clinically overlapping phenotypes. *Hum Genet.* (2017) 136:307–20. doi: 10.1007/s00439-017-1758-y

14. Aoi H, Mizuguchi T, Ceroni J, Kim V, Furquim I, Honjo R, et al. Comprehensive genetic analysis of 57 families with clinically suspected Cornelia de Lange syndrome. *J Hum Genet.* (2019) 64:967–78. doi: 10.1038/s10038-019-0643-z

15. Tang H, Guo J, Linpeng S, Wu L. Next generation sequencing identified two novel mutations in NIPBL and a frame shift mutation in CREBBP in three Chinese children. *Orphanet J Rare Dis.* (2019) 14:45. doi: 10.1186/s13023-019-1022-8

16. Demir S, Gürkan H, Oz V, Yalçıntepe S, Atlı E. Wiedemann-Steiner syndrome as a differential diagnosis of cornelia de lange syndrome using targeted next-generation sequencing: a case report. *Mol Syndromol.* (2020) 12:46–51. doi: 10.1159/000511971

17. Parenti I, Mallozzi M, Hüning I, Gervasini C, Kuechler A, Agolini E, et al. ANKRD11 variants: KBG syndrome and beyond. *Clin Genet.* (2021) 100:187–200. doi: 10.1111/cge.13977

18. Richards S, Aziz N, Bale S, Bick D, Das S, Gastier-Foster J, et al. Standards and guidelines for the interpretation of sequence variants: a joint consensus recommendation of the American college of medical genetics and genomics and the association for molecular pathology. *Genet Med.* (2015) 17:405–24.

19. Shangguan H, Su C, Ouyang Q, Cao B, Wang J, Gong C, et al. Kabuki syndrome: novel pathogenic variants, new phenotypes and review of literature. *Orphanet J Rare Dis.* (2019) 14:255. doi: 10.1186/s13023-019-1219-x

20. Jones W, Dafou D, McEntagart M, Woollard W, Elmslie F, Holder-Espinasse M, et al. De novo mutations in MLL cause Wiedemann-Steiner syndrome. *Am J Hum Genet.* (2012) 91:358–64.

21. Huisman S, Mulder PA, Redeker E, Bader I, Bisgaard AM, Brooks A, et al. Phenotypes and genotypes in individuals with SMC1A variants. *Am J Med Genet A.* (2017) 173:2108–25.

22. Li N, Wang Y, Yang Y, Wang P, Huang H, Xiong S, et al. Description of the molecular and phenotypic spectrum of Wiedemann-Steiner syndrome in Chinese patients. *Orphanet J Rare Dis.* (2018) 13:178. doi: 10.1186/s13023-018-0909-0

23. Goldenberg A, Riccardi F, Tessier A, Pfundt R, Busa T, Cacciagli P, et al. Clinical and molecular findings in 39 patients with KBG syndrome caused by deletion or mutation of ANKRD11. *Am J Med Genet A.* (2016) 170:2847–59.

24. Castiglioni S, Di Fede E, Bernardelli C, Lettieri A, Parodi C, Grazioli P, et al. KMT2A: umbrella gene for multiple diseases. *Genes.* (2022) 13:514.

25. Bestetti I, Crippa M, Sironi A, Tumiatti F, Masciadri M, Smeland M, et al. Expanding the molecular spectrum of ANKRD11 gene defects in 33 patients with a clinical presentation of KBG syndrome. *Int. J. Mol. Sci.* (2022) 23:5912. doi: 10.3390/ijms23115912

26. Arslan Satılmış S, Kurt E, Akçay E, Sazci A, Ceylan A. A novel missense mutation in the UBE2A gene causes intellectual disability in the large X-linked family. *J Gene Med.* (2021) 23:e3307. doi: 10.1002/jgm.3307

27. de Oliveira J, do Prado P, da Costa S, Sforça M, Canateli C, Ranzani A, et al. Mechanistic insights revealed by a UBE2A mutation linked to intellectual disability. *Nat Chem Biol.* (2019) 15:62–70. doi: 10.1038/s41589-018-0177-2

28. Adam M, Banka S, Bjornsson H, Bodamer O, Chudley A, Harris J, et al. Kabuki syndrome: international consensus diagnostic criteria. *J Med Genet.* (2019) 56:89–95. doi: 10.1136/jmedgenet-2018-105625

29. Nolen LD, Shelagh B, Morad A, Emily P, Bickmore WA. Regional chromatin decompaction in Cornelia de Lange syndrome associated with NIPBL disruption can be uncoupled from cohesin and CTCF. *Hum Mol Genet.* (2013) 22:4180–93. doi: 10.1093/hmg/ddt265

30. Deardorff M, Wilde J, Albrecht M, Dickinson E, Tennstedt S, Braunholz D, et al. RAD21 mutations cause a human cohesinopathy. *Am J Hum Genet.* (2012) 90:1014–27. doi: 10.1016/j.ajhg.2012.04.019

31. Deardorff M, Bando M, Nakato R, Watrin E, Itoh T, Minamino M, et al. HDAC8 mutations in Cornelia de Lange syndrome provide insight into the cohesin acetylation cycle. *Nature.* (2012) 489:313–7. doi: 10.1038/nature11316

32. Liu J, Zhang Z, Bando M, Itoh T, Deardorff MA, Li JR, et al. Genome-wide DNA methylation analysis in cohesin mutant human cell lines. *Nucleic Acids Res.* (2010) 38:5657–71. doi: 10.1093/nar/gkq346

33. Castronovo P, Gervasini C, Cereda A, Masciadri M, Milani D, Russo S, et al. Premature chromatid separation is not a useful diagnostic marker for Cornelia de Lange syndrome. *Chromosome Res.* (2009) 17:763–71.

frontiers | Frontiers in Genetics

TYPE Original Research
PUBLISHED 05 August 2022
DOI 10.3389/fgene.2022.936264

Check for updates

OPEN ACCESS

EDITED BY
Tieliu Shi,
Hunan University of Arts and Science, China

REVIEWED BY
Zhi-Ping Tan,
Central South University, China
Yang Xiaoyu,
Nanjing Medical University, China

*CORRESPONDENCE
Wen-Bin He,
hewenbin@csu.edu.cn
Yue-Qiu Tan,
tanyueqiu@csu.edu.cn

†These authors have contributed equally to this work

SPECIALTY SECTION
This article was submitted to Genetics of Common and Rare Diseases, a section of the journal Frontiers in Genetics

RECEIVED 05 May 2022
ACCEPTED 28 June 2022
PUBLISHED 05 August 2022

CITATION
Wang Y, Liu L, Tan C, Meng G, Meng L, Nie H, Du J, Lu G-X, Lin G, He W-B and Tan Y-Q (2022), Novel MEIOB variants cause primary ovarian insufficiency and non-obstructive azoospermia. *Front. Genet.* 13:936264. doi: 10.3389/fgene.2022.936264

COPYRIGHT
© 2022 Wang, Liu, Tan, Meng, Meng, Nie, Du, Lu, Lin, He and Tan. This is an open-access article distributed under the terms of the Creative Commons Attribution License (CC BY). The use, distribution or reproduction in other forums is permitted, provided the original author(s) and the copyright owner(s) are credited and that the original publication in this journal is cited, in accordance with accepted academic practice. No use, distribution or reproduction is permitted which does not comply with these terms.

Novel *MEIOB* variants cause primary ovarian insufficiency and non-obstructive azoospermia

Yurong Wang[1†], Ling Liu[2†], Chen Tan[2], Guiquan Meng[2], Lanlan Meng[2,3,4,5], Hongchuan Nie[4], Juan Du[2,4,5], Guang-Xiu Lu[1,2,4,5], Ge Lin[2,3,4,5], Wen-Bin He[1,2,3,4,5]* and Yue-Qiu Tan[1,2,3,4,5]*

[1]Hunan Guangxiu Hospital, Hunan Normal University, Changsha, China, [2]Institute of Reproductive and Stem Cell Engineering, School of Basic Medical Science, Central South University, Changsha, China, [3]National Engineering and Research Center of Human Stem Cells, Changsha, China, [4]Reproductive and Genetic Hospital of CITIC-Xiangya, Changsha, China, [5]Clinical Research Center for Reproduction and Genetics in Hunan Province, Changsha, China

Background: Infertility is a global health concern. *MEIOB* has been found to be associated with premature ovarian insufficiency (POI) and non-obstructive azoospermia (NOA), but its variants have not been reported in Chinese patients. The aim of this study was to identify the genetic aetiology of POI or NOA in three Han Chinese families.

Methods: Whole-exome sequencing (WES) was used to identify candidate pathogenic variants in three consanguineous Chinese infertile families with POI or NOA. Sanger sequencing was performed to validate these variants in the proband of family I and her affected family members. *In vitro* functional analyses were performed to confirm the effects of these variants.

Results: Two novel homozygous frameshift variants (c.258_259del and c.1072_1073del) and one novel homozygous nonsense variant (c.814C > T) in the *MEIOB* gene were identified in three consanguineous Han Chinese families. *In vitro* functional analyses revealed that these variants produced truncated proteins and affected their function.

Conclusion: We identified three novel *MEIOB* loss-of-function variants in local Chinese patients for the first time and confirmed their pathogenicity using *in vitro* functional analyses. These results extend the mutation spectrum of the *MEIOB* gene and have important significance for genetic counselling in these families.

KEYWORDS

primary ovarian insufficiency, non-obstructive azoospermia, MEIOB gene, novel variant, immunofluorescence

Introduction

Infertility is a worldwide health problem, defined as a failure to achieve pregnancy after 12 months of unprotected intercourse (Audibert and Glass, 2015). Infertility can be attributed to female or male factors, or both. The causes of male infertility include oligozoospermia, asthenozoospermia, and azoospermia among others (Agarwal et al., 2021). Non-obstructive azoospermia (NOA) is a serious male infertility disorder that accounts for more than 20% of the male infertility issues (Cioppi et al., 2021). NOA is typically associated with genetic defects, including Y chromosome microdeletions and spermatogenesis related gene mutations (TEX11, HFM1, and MEI1) (Yatsenko et al., 2015; Ben Khelifa et al., 2018; Tang et al., 2021). The causes of female infertility include premature ovarian insufficiency (POI), abnormal ovulation, tubal blockage and endometriosis (Sen et al., 2014). POI is characterized by loss of normal ovarian function in women before 40 years of age (De Vos et al., 2010). It has been reported that a number of genes are responsible for POI, such as DNA damage repair relevant genes (FANCA, DMC1, MCM8, etc) (Desai et al., 2017; He et al., 2018; Yang et al., 2019) and hormone receptor genes (FSHR, LHCGR, etc) (He et al., 2019; Guo et al., 2021; Tang et al., 2021).

Meiosis is an important process in gametogenesis, and defects in several meiosis-related genes have been reported in relation to POI and NOA (*MEI1*, *DMC1*, and *SPO11* (Zhang et al., 2020; Verrilli et al., 2021). *MEIOB* is a meiosis-specific gene mainly involved in double-strand break (DSB) repair, crossover formation, and promotion of complete synapsis (Luo et al., 2013). *MEIOB*-knockout mice presented with meiotic arrest, resulting in female and male infertility (Caburet et al., 2019). However, variants of *MEIOB* associated with human infertility are rare, with only 10 cases reported so far (Table 1), and none of the variants have been reported in the Chinese patients with POI or NOA (Gershoni et al., 2017; Caburet et al., 2019; Gershoni et al., 2019; Krausz et al., 2020; Cannarella et al., 2021; Wu et al., 2021; Kherraf et al., 2022).

In this study, we recruited three consanguineous Chinese infertile families with POI or NOA. Three novel *MEIOB* variants were identified using whole-exome sequencing (WES). These mutations have been confirmed as pathogenic variants using bioinformatics and *in vitro* functional analyses, thereby broadening the MEIOB gene mutation spectrum.

Materials and methods

Study subjects

Three individuals from three consanguineous Han Chinese families were recruited from the Reproductive and Genetic Hospital of CITIC-Xiangya, after providing informed written consent. Two female probands were diagnosed with POI and one male proband was diagnosed with NOA. Diagnostic Criteria of POI refers to the depletion or loss of normal ovarian function in women before 40 years of age, whose clinical characteristics are sparse menstruation or amenorrhea >4 months, and two times of the circulating gonadotropin follicle-stimulating hormone (FSH; >25 mIU/ml) elevated (interval of more than 4 weeks) (De Vos et al., 2010). The Diagnostic Criteria of NOA refers to azoospermia of semen routine examination that after excluding obstruction and hormone factors, and No karyotype abnormality and AZF microdeletion. Subsequently, molecular diagnosis was confirmed through WES (Minhas et al., 2021). This study was reviewed and approved by the ethics committee of the Reproductive and Gxenetic Hospital of CITIC-Xiangya of Central South University, China.

TABLE 1 The currently reported phenotypes and genotypes of *MEIOB* gene in infertility patients.

NO.	cDNA change	Amino acid change (region)	Phenotype of subjects	References
1	c.191A > T (hom)	p.N64I(OBCD1)	NOA	Gershoni et al. (2017)
2	c.1098del (hom)	p.S366fs (OBCD3)	NOA	Gershoni et al. (2019)
3	c.1218G > A (hom)	p.Cys345Trpfs8(OBCD3)	POI	Caburet et al. (2019)
4	c.897_1431del (hom)	p.219del178aa (OBCD2)	NOA	Krausz et al. (2020)
5	c.1140_1143del (hom)	p.Cys345Trpfs8(OBCD3)	NOA	
6	c.318C > A (het)	p.Ser106Arg (OBCD1)	oligozoospermia	Cannarella et al. (2021)
7	c.634G > A (het)	p.Asp212Asn(OBCD2)	oligozoospermia	
	c.643 T > G (het)	p.Ser215Ala (OBCD2)		
8	c.634G > A (het)	p.Asp212Asn(OBCD2)	NOA	
	c.* 4G > A (het)			
9	c.683-1G > A (hom)		NOA and POI	Wu et al. (2021)
10	c.1118-1121del (hom)	p.phe373ser (OBCD3)	NOA	Kherraf et al. (2022)

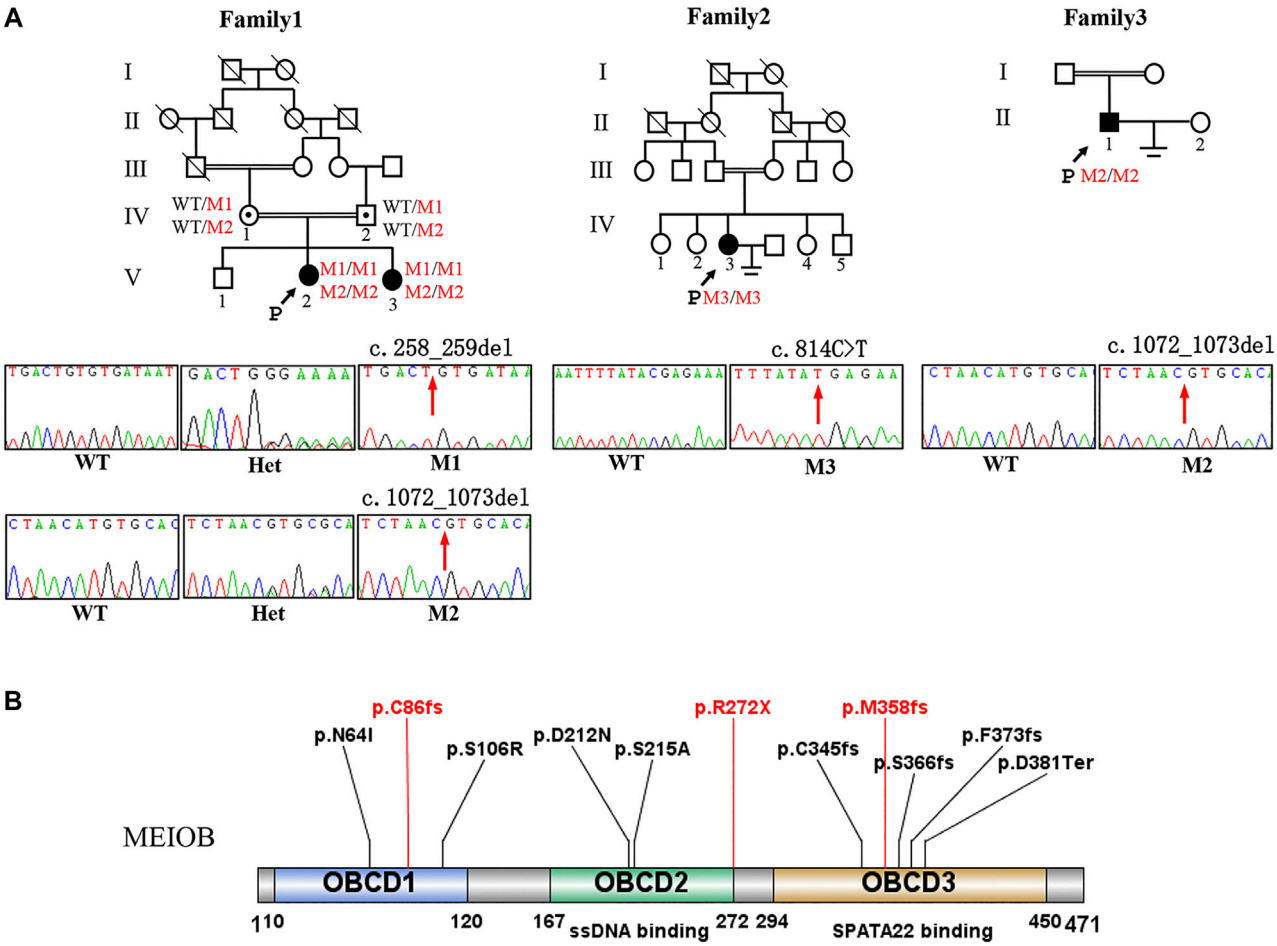


FIGURE 1
Pedigree of three consanguineous Han Chinese family with infertility-related MEIOB variants. **(A)** The black arrow points to the proband. Open symbols indicate the unaffected members. Heterozygous carriers are indicated with a dot in the middle of the symbol. Filled symbols indicate the affected members with POI or NOA. In familyI, two cousins (IV-1 and IV-2) in generation 4 married to each other with two affected individuals (V-2 and V-3 with POI). Sanger sequencing of the c.258_259del and c.1072_1073del (pointed by red arrows) mutation of *MEIOB* in this family. **(B)** The MEIOB protein consists of 471 amino acids, including three OB- domains. Three variants discovered in this study are shown in red font, whereas previously reported variants are displayed in black font.

Genomic DNA extraction and WES

Genomic DNA from peripheral blood samples was extracted using a QIAamp® DNA Blood Midi Kit (Qiagen, Germany), according to the manufacturer's protocol. All probands were subjected to WES, which was performed using the HiSeq2000 sequencing platform (Illumina). The WES raw reads were aligned to NCBI GRCh37 (reference genome Hg19) using Burrows-Wheeler Aligner, while Picard was used to remove and sort the copies of the polymerase chain reaction (PCR; http://broadinstitute. gib. io/picard/). The GATK package was used for mutation identification, including base recalibration variant calling with haplotype caller and variant quality score recalibration, and ANNOVAR software was used for mutation annotation.

We used the following inclusion criteria to identify candidate genes: 1) Frequencies are less than 1% in database of 1,000 Genomes, gnomAD, gnomAD-EAS; 2) Homozygous variants are preferred considered in consanguineous family; 3) The potential pathogenicity of the novel variants were examined by in silico analysis using two different software: Mutation Taster and CADD; 4) Candidate genes which are recorded in OMIM database and responsible for POI or NOA; 5) Candidate genes which are related to POI or NOA in animal models. The suspected variants were validated by Sanger sequencing of the probands

and their family members (Figure 1A), and the primers are listed in Supplementary Table S1.

Plasmid construction

Full-length *MEIOB* was obtained by PCR and inserted into the pcDNA3.1/FLAG expression vector, as described previously, leading to the production of fusion proteins with FLAG at the N-terminus of *MEIOB* (*MEIOB*-WT). The identified mutations (c.258_259del,c.1072_1073del, and c. C814T) were introduced into the *MEIOB*-WT plasmid vector by oligonucleotide-mediated mutagenesis using a MutExpress II Fast Mutagenesis Kit (Vazyme, Guangzhou, China). All expression constructs were sequenced to confirm the presence of the desired mutation and to exclude PCR-induced mutations.

Western blot analysis and immunofluorescence analysis

Cells were harvested 48 h after transfection and homogenised using RIPA lysis buffer (Beyotime Biotechnology, Shanghai, China) supplemented with a protease inhibitor cocktail (Thermo Fisher Scientific, United States). Proteins extracted from the transfected cells were blotted onto a polyvinylidene difluoride membrane and incubated overnight at 4°C with an anti-FLAG antibody (1: 5,000 dilution, Abways, Shanghai, China). The membrane was incubated with secondary antibodies (goat anti-mouse IgG; 1: 5,000 dilution; Abways, Shanghai, China) on the following day. Finally, blots were developed using an ECL western blotting kit (Pierce Biotechnology, Rockford, IL, United States).

Immunofluorescence analysis was performed on transfected Chinese hamster ovary (CHO) cells grown on coverslips using anti-FLAG (1:500 dilution) primary antibodies. Fluorescent images were captured using a confocal microscope (Olympus FV1000, Tokyo, Japan).

Results

Phenotype of the patients with the MEIOB variant

In the first family, the proband (V3, Figure 1A) had started menstruating at the age of 15 years with normal periods. She was infertile for 2 years after marriage and had normal sexual intercourse without contraception. She was diagnosed with primary infertility at the age of 28 years. The clinical manifestations included oligomenorrhea and infertility. Her sex hormone levels showed an elevated FSH level (38.44 IU/L) and a decrease in anti-Mullerian hormone (AMH) levels (0.098 ng/ml). Transvaginal ultrasound revealed that the uterus was of normal size, the left ovary had a small follicle, while no follicles were detected in the right ovary (Supplementary Figure S1). The proband's parents and grandparents were consanguineous. The 29-year-old sister of the proband was also diagnosed with POI, with elevated FSH and decreased AMH (0.4 ng/ml) levels.

The proband (IV3, Figure 1A) of the other family (family II), was a 24-year-old woman, and was diagnosed with POI. She had been infertile for 2 years after marriage following normal sexual intercourse without contraception. Her parents were consanguineous. She had normal pubertal development and a regular menstrual cycle. Transvaginal ultrasound revealed follicles only one follicle in each ovary (Supplementary Figure S1). Basal endocrine testing showed an elevated FSH level of 29.88 IU/L and a low AMH level of 0.092 ng/ml.

The proband (II2) of the third family (family III) was a 29-year-old man and suffering from primary infertility. The patient was diagnosed with non-obstructive azoospermia (NOA) with a normal volume of semen analyses. Endocrine tests revealed normal hormone levels. The proband had a normal 46, XY karyotype, and no abnormalities were observed in the Y chromosome microdeletion detection.

The spouses of our two POI patients have a normal karyotype (46, XY), and have no anomalies in Y chromosomal microdeletion detection or in semen routine examination. The NOA patient's spouse has normal menstrual cycle and sex hormone levels. Transvaginal ultrasound showed she has normal inner reproductive organ (oviduct, ovary and uterine) and she had a good clinical pregnancy after undergoing IVF-ET with donor sperm.

Identification of *MEIOB* variant

WES was performed on the three probands. According to the filtering criteria, two novel homozygous frameshift variants of *MEIOB* (NM_001163560: c.258_259del: p. C86fs; c.1072_1073del: p.M358fs) were identified in the proband of family I. The subsequent Sanger sequencing showed that her affected sister carried the same homozygous variants and her parents both were heterozygous variants carriers. In addition, a novel homozygous nonsense variant and a novel homozygous frameshift variant (NM_001163560: c.C814T:*p*.R272X; c.1072_1073del: *p*.M358fs) were detected in the probands of family II and III, respectively. According to the ACMG standards and guidelines (Richards et al., 2015), all the detected candidate variants were evaluated as pathogenic (c.258_259del: PVS1+PM2+ PM3_Supporting + PP1; c.1072_1073del: PVS1+PM2+PM3_Supporting + PP1; c. C814T: PVS1+PM2+PM3_Supporting).

Impact of MEIOB variant

Western blot analysis showed that the three mutant proteins were expressed in human embryonic kidney (HEK293T) cells

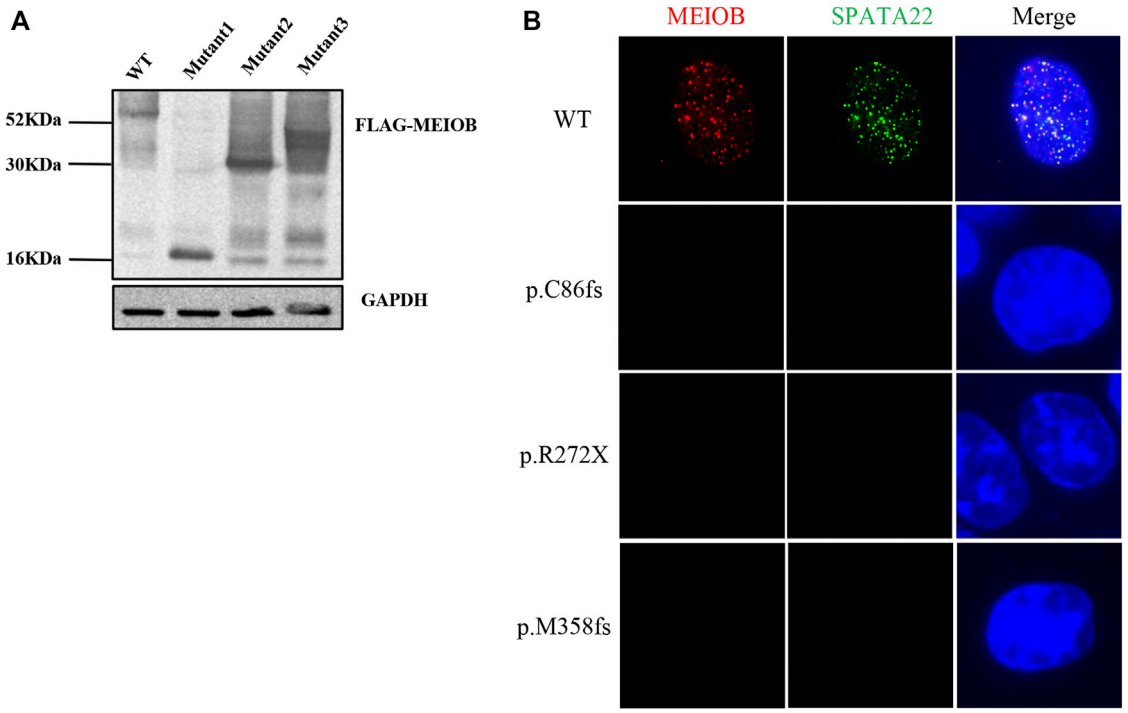


FIGURE 2
In vitro functional analysis of MEIOB variant. **(A)** Western blot analysis showed that the three mutant proteins were expressed in transfected cells, which resulted in the production of truncated proteins. **(B)** Immunofluorescence analysis showed that the wild-type MEIOB colocalised with SPATA22 to ssDNA; the truncated MEIOB was not located in the nucleus.

after transfection with the expression construct and production of truncated proteins. Immunofluorescence analysis showed that the wild-type MEIOB colocalised with SPATA22 to ssDNA; however, MEIOB was not located in the nucleus when cells were transfected with the mutant constructs. *In vitro* functional analyses revealed that all these variants lost the function of MEIOB (Figure 2).

Discussion

In this study, we performed WES to identify two novel homozygous frameshift mutations (c.258_259del and c.1072_1073del) and one novel homozygous nonsense mutation (c.814C > T) in the *MEIOB* gene from three consanguineous Han Chinese families. *In vitro* functional analyses revealed that these mutations produce truncated proteins and affect their function, which might result in the impairment of chromosomal break repair and ultimately lead to male and female infertility. Our study broadens the mutation spectrum of *MEIOB*.

The *MEIOB* gene is located on chromosome 16, consists of 14 exons, and encodes 471 amino acids. It is a meiosis-specific ssDNA-binding protein that participates in homologous recombination and DSB repair (Souquet et al., 2013). *MEIOB* knockout mice (*Meiob*$^{-/-}$) exhibit infertility in both sexes, resulting from meiotic arrest at a zygotene/pachytene-like stage (Luo et al., 2013). Previous studies have reported that mutations in MEIOB may cause infertility in males and females (Gershoni et al., 2017; Caburet et al., 2019). However, only 10 pathogenic MEIOB mutations have been described to date. In our study, three novel MEIOB mutations were identified in patients with POI or NOA. *In vitro* functional analyses showed that these variants lost their functions. Therefore, we suggest that the three *MEIOB* mutations are deleterious and disease-associated mutations in the three families.

The MEIOB protein contains three conserved OB binding domains (OBCD), of which OBCD2 (167-272aa) is responsible for binding the DNA single strand to RPA and OBCD3 (294-450aa) is the interaction domain with SPATA22 (Ribeiro et al., 2016) (Figure 1B). It has been reported that MEIOB first forms the dimerisation core of MEIOB-SPATA22 and subsequently interacts with the preformed RPA complex to participate in meiotic homologous recombination (Ribeiro et al., 2021). Previous studies have shown that the stability of these two proteins (MEIOB and SPATA22) is determined by their interaction (Xu et al., 2017), which is essential for meiosis and gametogenesis. The SPATA22 defect leads to gamete arrest during the pachytene phase of the first meiotic division both in human and mice, consequently the sterile phenotype of POI and NOA (Hays et al., 2017; Yao et al., 2022). In our study, the

three novel mutations of MEIOB were located in each of the three OB-binding domains and the production of truncated proteins without OBCD3. Furthermore, immunofluorescence analysis revealed that mutant MEIOB proteins did not co-localise with SPATA22 in the nucleus. Therefore, we suggest that OBCD3 in MEIOB is important for human fertility.

Different types of variants might have distinguishable impacts on protein function and subsequently lead to different clinical phenotypes (Spillane et al., 2016). In previous studies, it was found that nonsense and frameshift variants of *MEIOB* might both have a greater impact on protein function, resulting in a more severe clinical phenotype. For example, the first homozygous nonsense variant (c.1218G > A) in *MEIOB* causes POI, whereas the compound heterozygous missense variants (c.634G > A and c.643T > G) lead to oligozoospermia instead of NOA (Caburet et al., 2019; Cannarella et al., 2021). In our study, the two novel homozygous frameshift variants (c.258_259del, c.1072_1073del) and one novel homozygous nonsense variant (c.814C > T) in the *MEIOB* gene both caused POI or NOA. Therefore, we suggest that loss-of-function variants of *MEIOB* result in a severe clinical phenotype such as POI or NOA.

It has been reported that mutations in DSB repair-related genes might increase the risk of cancer. For example, mutations in *BRCA1* and *BRCA2* increase the risk of breast cancer, and mutations in *RAD51* increase the risk of rectal cancer (Elstrodt et al., 2006; Osti et al., 2017). *MEIOB* was recently identified as a new cancer testis gene (Wang et al., 2016). Overexpression of the *MEIOB* gene has been observed in triple-negative breast cancer (TNBC) cells, which is confirmed that ectopic expression of *MEIOB* is oncogenic and promotes cancer cell proliferation (Gu et al., 2021). In our study, the patients did not present with any cancer. However, we recommend that patients who have mutations in the *MEIOB* or other DSB repair-related genes, should undergo regular check-up and screening for early detection and timely intervention of cancer.

In conclusion, we identified three novel *MEIOB* loss-of-function mutations in Chinese patients for the first time and confirmed their pathogenicity using *in vitro* functional analyses. These results extend the mutation spectrum of the *MEIOB* gene and have important significance for genetic counselling of families with infertility.

Data availability statement

The raw data supporting the conclusions of this manual will be made available by the authors, without under reservation, to any qualified researcher.

Ethics statement

The studies involving human participants were reviewed and approved by the ethics committee of the Reproductive and Genetic Hospital of CITIC-Xiangya of Central South University, China. The patients/participants provided their written informed consent to participate in this study.

Author contributions

W-BH, Y-QT designed the research; YW analysed the data and wrote the paper; YW, LL, CT, GM, LM performed the research; HN, JD, G-XL, GL performed the clinical work.

Funding

This work was supported by grants from the National Key Research and Developmental Program of China (2018YFC1004901), the National Natural Science Foundation of China (82171608 and 81971447), the Key Grant of Prevention and Treatment of Birth Defect from Hunan Province (2019SK1012), Hunan Provincial Grant for Innovative Province Construction (2019SK4012), Scientific Research Foundation of the Health Committee of Hunan Province (20190862), China Postdoctoral Science Foundation (2022M711119) and the Research Grant of CITIC-Xiangya (YNXM-202002).

Acknowledgments

The authors would like to thank the patients and their family members for their participation in our study.

Conflict of interest

The authors declare that the research was conducted in the absence of any commercial or financial relationships that could be construed as a potential conflict of interest.

Publisher's note

All claims expressed in this article are solely those of the authors and do not necessarily represent those of their affiliated organizations, or those of the publisher, the editors and the reviewers. Any product that may be evaluated in this article, or claim that may be made by its manufacturer, is not guaranteed or endorsed by the publisher.

Supplementary material

The Supplementary Material for this article can be found online at: https://www.frontiersin.org/articles/10.3389/fgene.2022.936264/full#supplementary-material

References

Agarwal, A., Baskaran, S., Parekh, N., Cho, C. L., Henkel, R., Vij, S., et al. (2021). Male infertility. *Lancet* 397 (10271), 319–333. doi:10.1016/s0140-6736(20)32667-2

Audibert, C., and Glass, D. (2015). A global perspective on assisted reproductive technology fertility treatment: an 8-country fertility specialist survey. *Reprod. Biol. Endocrinol.* 13, 133. doi:10.1186/s12958-015-0131-z

Ben Khelifa, M., Ghieh, F., Boudjenah, R., Hue, C., Fauvert, D., Dard, R., et al. (2018). A MEI1 homozygous missense mutation associated with meiotic arrest in a consanguineous family. *Hum. Reprod.* 33 (6), 1034–1037. doi:10.1093/humrep/dey073

Caburet, S., Todeschini, A. L., Petrillo, C., Martini, E., Farran, N. D., Legois, B., et al. (2019). A truncating MEIOB mutation responsible for familial primary ovarian insufficiency abolishes its interaction with its partner SPATA22 and their recruitment to DNA double-strand breaks. *EBioMedicine* 42, 524–531. doi:10.1016/j.ebiom.2019.03.075

Cannarella, R., Condorelli, R. A., Paolacci, S., Barbagallo, F., Guerri, G., Bertelli, M., et al. (2021). Next-generation sequencing: toward an increase in the diagnostic yield in patients with apparently idiopathic spermatogenic failure. *Asian J. Androl.* 23 (1), 24–29. doi:10.4103/aja.aja_25_20

Cioppi, F., Rosta, V., and Krausz, C. (2021). Genetics of azoospermia. *Int. J. Mol. Sci.* 22 (6), 3264. doi:10.3390/ijms22063264

De Vos, M., Devroey, P., and Fauser, B. C. (2010). Primary ovarian insufficiency. *Lancet* 376 (9744), 911–921. doi:10.1016/s0140-6736(10)60355-8

Desai, S., Wood-Trageser, M., Matic, J., Chipkin, J., Jiang, H., Bachelot, A., et al. (2017). MCM8 and MCM9 nucleotide variants in women with primary ovarian insufficiency. *J. Clin. Endocrinol. Metab.* 102 (2), 576–582. doi:10.1210/jc.2016-2565

Elstrodt, F., Hollestelle, A., Nagel, J. H., Gorin, M., Wasielewski, M., van den Ouweland, A., et al. (2006). BRCA1 mutation analysis of 41 human breast cancer cell lines reveals three new deleterious mutants. *Cancer Res.* 66 (1), 41–45. doi:10.1158/0008-5472.Can-05-2853

Gershoni, M., Hauser, R., Yogev, L., Lehavi, O., Azem, F., Yavetz, H., et al. (2017). A familial study of azoospermic men identifies three novel causative mutations in three new human azoospermia genes. *Genet. Med.* 19 (9), 998–1006. doi:10.1038/gim.2016.225

Gershoni, M., Hauser, R., Barda, S., Lehavi, O., Arama, E., Pietrokovski, S., et al. (2019). A new MEIOB mutation is a recurrent cause for azoospermia and testicular meiotic arrest. *Hum. Reprod.* 34 (4), 666–671. doi:10.1093/humrep/dez016

Gu, Y., Wang, C., Zhu, R., Yang, J., Yuan, W., Zhu, Y., et al. (2021). The cancer-testis gene, MEIOB, sensitizes triple-negative breast cancer to PARP1 inhibitors by inducing homologous recombination deficiency. *Cancer Biol. Med.* 18 (1), 74–87. doi:10.20892/j.issn.2095-3941.2020.0071

Guo, C., Yu, H., Feng, G., Lv, Q., Liu, X., Liu, X., et al. (2021). Associations of FSHR and LHCGR gene variants with ovarian reserve and clinical pregnancy rates. *Reprod. Biomed. Online* 43 (3), 561–569. doi:10.1016/j.rbmo.2021.06.016

Hays, E., Majchrzak, N., Daniel, V., Ferguson, Z., Brown, S., Hathorne, K., et al. (2017). Spermatogenesis associated 22 is required for DNA repair and synapsis of homologous chromosomes in mouse germ cells. *Andrology* 5 (2), 299–312. doi:10.1111/andr.12315

He, W. B., Tu, C. F., Liu, Q., Meng, L. L., Yuan, S. M., Luo, A. X., et al. (2018). DMC1 mutation that causes human non-obstructive azoospermia and premature ovarian insufficiency identified by whole-exome sequencing. *J. Med. Genet.* 55 (3), 198–204. doi:10.1136/jmedgenet-2017-104992

He, W. B., Du, J., Yang, X. W., Li, W., Tang, W. L., Dai, C., et al. (2019). Novel inactivating mutations in the FSH receptor cause premature ovarian insufficiency with resistant ovary syndrome. *Reprod. Biomed. Online* 38 (3), 397–406. doi:10.1016/j.rbmo.2018.11.011

Kherraf, Z. E., Cazin, C., Bouker, A., Fourati Ben Mustapha, S., Hennebicq, S., Septier, A., et al. (2022). Whole-exome sequencing improves the diagnosis and care of men with non-obstructive azoospermia. *Am. J. Hum. Genet.* 109 (3), 508–517. doi:10.1016/j.ajhg.2022.01.011

Krausz, C., Riera-Escamilla, A., Moreno-Mendoza, D., Holleman, K., Cioppi, F., Algaba, F., et al. (2020). Genetic dissection of spermatogenic arrest through exome analysis: clinical implications for the management of azoospermic men. *Genet. Med.* 22 (12), 1956–1966. doi:10.1038/s41436-020-0907-1

Luo, M., Yang, F., Leu, N. A., Landaiche, J., Handel, M. A., Benavente, R., et al. (2013). MEIOB exhibits single-stranded DNA-binding and exonuclease activities and is essential for meiotic recombination. *Nat. Commun.* 4, 2788. doi:10.1038/ncomms3788

Minhas, S., Bettocchi, C., Boeri, L., Capogrosso, P., Carvalho, J., Cilesiz, N. C., et al. (2021). European association of urology guidelines on male sexual and reproductive health: 2021 update on male infertility. *Eur. Urol.* 80 (5), 603–620. doi:10.1016/j.eururo.2021.08.014

Osti, M. F., Nicosia, L., Agolli, L., Gentile, G., Falco, T., Bracci, S., et al. (2017). Potential role of single nucleotide polymorphisms of XRCC1, XRCC3, and RAD51 in predicting acute toxicity in rectal cancer patients treated with preoperative radiochemotherapy. *Am. J. Clin. Oncol.* 40 (6), 535–542. doi:10.1097/coc.0000000000000182

Ribeiro, J., Abby, E., Livera, G., and Martini, E. (2016). RPA homologs and ssDNA processing during meiotic recombination. *Chromosoma* 125 (2), 265–276. doi:10.1007/s00412-015-0552-7

Ribeiro, J., Dupaigne, P., Petrillo, C., Ducrot, C., Duquenne, C., Veaute, X., et al. (2021). The meiosis-specific MEIOB-SPATA22 complex cooperates with RPA to form a compacted mixed MEIOB/SPATA22/RPA/ssDNA complex. *DNA Repair (Amst)* 102, 103097. doi:10.1016/j.dnarep.2021.103097

Richards, S., Aziz, N., Bale, S., Bick, D., Das, S., Gastier-Foster, J., et al. (2015). Standards and guidelines for the interpretation of sequence variants: a joint consensus recommendation of the American college of medical genetics and genomics and the association for molecular pathology. *Genet. Med.* 17 (5), 405–424. doi:10.1038/gim.2015.30

Sen, A., Kushnir, V. A., Barad, D. H., and Gleicher, N. (2014). Endocrine autoimmune diseases and female infertility. *Nat. Rev. Endocrinol.* 10 (1), 37–50. doi:10.1038/nrendo.2013.212

Souquet, B., Abby, E., Hervé, R., Finsterbusch, F., Tourpin, S., Le Bouffant, R., et al. (2013). MEIOB targets single-strand DNA and is necessary for meiotic recombination. *PLoS Genet.* 9 (9), e1003784. doi:10.1371/journal.pgen.1003784

Spillane, J., Kullmann, D. M., and Hanna, M. G. (2016). Genetic neurological channelopathies: Molecular genetics and clinical phenotypes. *J. Neurol. Neurosurg. Psychiatry* 87 (1), 37–48. doi:10.1136/jnnp-2015-311233

Tang, D., Lv, M., Gao, Y., Cheng, H., Li, K., Xu, C., et al. (2021). Novel variants in helicase for meiosis 1 lead to male infertility due to non-obstructive azoospermia. *Reprod. Biol. Endocrinol.* 19 (1), 129. doi:10.1186/s12958-021-00815-z

Verrilli, L., Johnstone, E., Allen-Brady, K., and Welt, C. (2021). Shared genetics between nonobstructive azoospermia and primary ovarian insufficiency. *F&S Rev.* 2 (3), 204–213. doi:10.1016/j.xfnr.2021.04.001

Wang, C., Gu, Y., Zhang, K., Xie, K., Zhu, M., Dai, N., et al. (2016). Systematic identification of genes with a cancer-testis expression pattern in 19 cancer types. *Nat. Commun.* 7, 10499. doi:10.1038/ncomms10499

Wu, Y., Li, Y., Murtaza, G., Zhou, J., Jiao, Y., Gong, C., et al. (2021). Whole-exome sequencing of consanguineous families with infertile men and women identifies homologous mutations in SPATA22 and MEIOB. *Hum. Reprod.* 36 (10), 2793–2804. doi:10.1093/humrep/deab185

Xu, Y., Greenberg, R. A., Schonbrunn, E., and Wang, P. J. (2017). Meiosis-specific proteins MEIOB and SPATA22 cooperatively associate with the single-stranded DNA-binding replication protein A complex and DNA double-strand breaks. *Biol. Reprod.* 96 (5), 1096–1104. doi:10.1093/biolre/iox040

Yang, X., Zhang, X., Jiao, J., Zhang, F., Pan, Y., Wang, Q., et al. (2019). Rare variants in FANCA induce premature ovarian insufficiency. *Hum. Genet.* 138 (11-12), 1227–1236. doi:10.1007/s00439-019-02059-9

Yao, C., Hou, D., Ji, Z., Pang, D., Li, P., Tian, R., et al. (2022). Bi-allelic SPATA22 variants cause premature ovarian insufficiency and nonobstructive azoospermia due to meiotic arrest. *Clin. Genet.* 101 (5-6), 507–516. doi:10.1111/cge.14129

Yatsenko, A. N., Georgiadis, A. P., Röpke, A., Berman, A. J., Jaffe, T., Olszewska, M., et al. (2015). X-linked TEX11 mutations, meiotic arrest, and azoospermia in infertile men. *N. Engl. J. Med.* 372 (22), 2097–2107. doi:10.1056/NEJMoa1406192

Zhang, B., Tang, Z., Li, L., and Lu, L. Y. (2020). NBS1 is required for SPO11-linked DNA double-strand break repair in male meiosis. *Cell Death Differ.* 27 (7), 2176–2190. doi:10.1038/s41418-020-0493-4

frontiers | Frontiers in Genetics

TYPE Original Research
PUBLISHED 11 August 2022
DOI 10.3389/fgene.2022.924904

Check for updates

OPEN ACCESS

EDITED BY
Mike Mikailov,
United States Food and Drug Administration, United States

REVIEWED BY
Kevin T. Booth,
Harvard Medical School, United States
Margaret A. Titus,
University of Minnesota Twin Cities, United States

*CORRESPONDENCE
Ambroise Wonkam,
ambroise.wonkam@uct.ac.za,
awonkam1@jhmi.edu

SPECIALTY SECTION
This article was submitted to Genetics of Common and Rare Diseases, a section of the journal Frontiers in Genetics

RECEIVED 20 April 2022
ACCEPTED 18 July 2022
PUBLISHED 11 August 2022

CITATION
Adadey SM, Wonkam-Tingang E, Alves de Souza Rios L, Aboagye ET, Esoh K, Manyisa N, De Kock C, Awandare GA, Mowla S and Wonkam A (2022), Cell-based analysis of CLIC5A and SLC12A2 variants associated with hearing impairment in two African families.
Front. Genet. 13:924904.
doi: 10.3389/fgene.2022.924904

COPYRIGHT
© 2022 Adadey, Wonkam-Tingang, Alves de Souza Rios, Aboagye, Esoh, Manyisa, De Kock, Awandare, Mowla and Wonkam. This is an open-access article distributed under the terms of the Creative Commons Attribution License (CC BY). The use, distribution or reproduction in other forums is permitted, provided the original author(s) and the copyright owner(s) are credited and that the original publication in this journal is cited, in accordance with accepted academic practice. No use, distribution or reproduction is permitted which does not comply with these terms.

Cell-based analysis of *CLIC5A* and *SLC12A2* variants associated with hearing impairment in two African families

Samuel Mawuli Adadey[1,2], Edmond Wonkam-Tingang[1], Leonardo Alves de Souza Rios[3], Elvis Twumasi Aboagye[1,2], Kevin Esoh[1], Noluthando Manyisa[1], Carmen De Kock[1], Gordon A. Awandare[2], Shaheen Mowla[3] and Ambroise Wonkam[1,4]*

[1]Department of Pathology, Division of Human Genetics, Faculty of Health Sciences, University of Cape Town, Cape Town, South Africa, [2]Department of Biochemistry, Cell, and Molecular Biology, West African Centre for Cell Biology of Infectious Pathogens (WACCBIP), University of Ghana, Accra, Ghana, [3]Department of Pathology, Division of Haematology, Faculty of Health Sciences, University of Cape Town, Observatory, Cape Town, South Africa, [4]McKusick-Nathans Institute and Department of Genetic Medicine, Johns Hopkins University School of Medicine, Baltimore, MD, United States

We have previously reported *CLIC5A* and *SLC12A2* variants in two families from Cameroon and Ghana, segregating non-syndromic hearing impairment (NSHI). In this study, biological assays were performed to further functionally investigate the pathogenicity of *CLIC5* [c.224T>C; p.(L75P)] and *SCL12A2* [c.2935G>A: p.(E979K)] variants. Ectopic expression of the proteins in a cell model shows that compared to wild-type, both the *CLIC5A* and *SLC12A2* variants were overexpressed. The mutant CLIC5A protein appears as aggregated perinuclear bodies while the wild-type protein was evenly distributed in the cytoplasm. Furthermore, cells transfected with the wild-type CLIC5A formed thin membrane filopodia-like protrusions which were absent in the CLIC5A mutant expressing and control cells. On the other hand, the wild-type SLC12A2 expressing cells had an axon-like morphology which was not observed in the mutant expressing and control cells. A network analysis revealed that CLIC5A can interact with at least eight proteins at the base of the stereocilia. This study has generated novel biological data associated with the pathogenicity of targeted variants in *CLIC5A* and *SLC12A2,* found in two African families, and therefore expands our understanding of their pathobiology in hearing impairment.

KEYWORDS

CLIC5, SLC12A2, hearing impairment pathobiology, Africa, hearing impairment

Introduction

Hearing impairment can be caused by the malfunction of any part of the auditory system. Disruption of the mechanical transmission of sound through the external and middle ear results in conductive hearing impairment (Nadol, 1978). The mechanical auditory stimulus is converted to an electrical signal by neuro-epithelial hair cells in the inner ear and conducted by spiral-ganglion cells (Nadol, 1978). Failure of this process in the inner ear results in sensorineural hearing impairment which may be due to damage of the cochlear or vestibulocochlear nerve (Brodie et al., 2018). Mixed hearing impairment occurs when the external/middle ear and the inner ear are damaged (Zwartenkot et al., 2014). Over 124 genes have been associated with non-syndromic hearing impairment (NSHI) (Van Camp and Smith, 2020) and many of these genes are known to encode proteins with unique functions in the inner ear which participate in the hearing process (Delmaghani and El-Amraoui, 2020). Among the hearing impairment genes expressed in the inner ear are *CLIC5A* and *SLC12A2* and we have recently identified variants within both genes which were associated with hearing impairment in two families from Cameroon and Ghana, respectively. These variants reside within regions of high evolutionary conservation across species, and we have previously reported, using *in silico* analysis, that these are potentially pathogenic variants (Wonkam-Tingang et al., 2020; Adadey et al., 2021).

The *CLIC5* gene encodes for a protein which belongs to the Chloride Intracellular Ion Channels (CLICs) family of chloride ion channels that are unrelated to the major chloride ion channels (CIC) family. The CLIC family of proteins are particularly interesting for their dimorphism; they exist as either membrane-bound or soluble cytosolic proteins (Harrop et al., 2001; Gururaja Rao et al., 2020). They are characterized by approximately 241 amino acids with two GST-binding domains: one at the N-terminus, and the other at the C-terminus (Gururaja Rao et al., 2020). CLIC5 is an interesting member in that an alternative splicing produces two forms with different molecular masses; CLIC5A (251 amino acids) and CLIC5B (410 amino acids) of which their 238 amino acid C-terminal residues are identical to the core CLIC sequence. CLIC5A has a 13 amino acid N-terminal extension while CLIC5B has a 172 amino acid N-terminal extension. CLIC5A was observed to be present in solution as a dimer (Berryman et al., 2004) and is the predominant form expressed in hair bundles.

SLC12A2 belongs to the solute carriers (SLC) group which are transmembrane proteins that control the transport of molecules across the cell membrane. The SLC group of proteins are the largest group of transport proteins with more than 458 members belonging to over 65 distinctly described families (Cannizzaro et al., 2019; Pizzagalli et al., 2021). Though SLC proteins are mostly known for their membrane activity, some family members are found throughout cellular organelles (Pizzagalli et al., 2021). The SLC12 family, of which SLC12A2 is a member, consist of 9 proteins with a common structure of 12 transmembrane domains and intracellular N and C termini (Gagnon and Delpire, 2013). SLC12A2 is expressed in the inner ear and has been recently associated with hearing impairment in humans (Macnamara et al., 2019; McNeill et al., 2020; Morgan et al., 2020; Adadey et al., 2021).

In this study, we performed cell-based functional assays to pave the way for the understanding of the mechanism(s) by which the *CLIC5A* [c.224T>C; p.(L75P)] and *SCL12A2* [c.2935G>A: p.(E979K)] variants cause hearing impairment.

Methods

Site-directed mutagenesis

Mammalian expression constructs containing human *CLIC5A* (NM_001256023, UniProtKB - Q9NZA1) and *SLC12A2* (NM_001046, UniProtKB - P55011) cDNAs were purchased from ORIGENE (Rockville, Maryland). Both plasmids have GFP, myc, and DDK-FLAG tags as well as ampicillin and neomycin selection markers (Supplementary Figures S1A,B). Site-directed mutagenesis (SDM) primer pairs (Supplementary Figures S1C,D) were designed for both plasmids according to the QuikChange Site-Directed Mutagenesis Kit (Stratagene) guidelines. The *CLIC5A* and *SLC12A2* mutant constructs were created using the KAPA Taq EXtra HotStart® ReadyMix™, amplified in *E. coli* cells and the *SLC12A2*: c.2935G>A and *CLIC5A*: c.224T>C mutations were confirmed using sanger sequencing (Inqaba Biotec, Gauteng, South Africa).

Cell culture and transfection

The mutant or wild-type plasmids were transfected into HEK-293 cells (immortalized human embryonic kidney cells). HEK-293 cells were cultured in Dulbecco's Modified Eagle Medium (DMEM) (Thermo Fisher Scientific, Massachusetts, United States) supplemented with 10% (v/v) fetal bovine serum (Thermo Fisher Scientific, Massachusetts, United States) and 1% (v/v) penicillin/streptomycin (Sigma-Aldrich, Missouri, United States), in a humidified incubator at 37°C and 5% CO_2. Transfections were carried out using the X-tremeGENE™ HP Transfection Reagent (Sigma Aldrich, Missouri, United States) according to manufacturer's instructions. In brief, 250 or 500 ng of the respective plasmid construct was mixed with the transfection reagent following the manufacturer's protocol (pEGFP-N3 control, GFP-tagged wild-type CLIC5A and SLC12A2, or GFP-tagged mutant CLIC5A and SLC12A2) and used to transfect cells at a density of 4×10^4 cells/ml or 8×10^4 cells/ml for confocal microscopy or western blot experiments respectively.

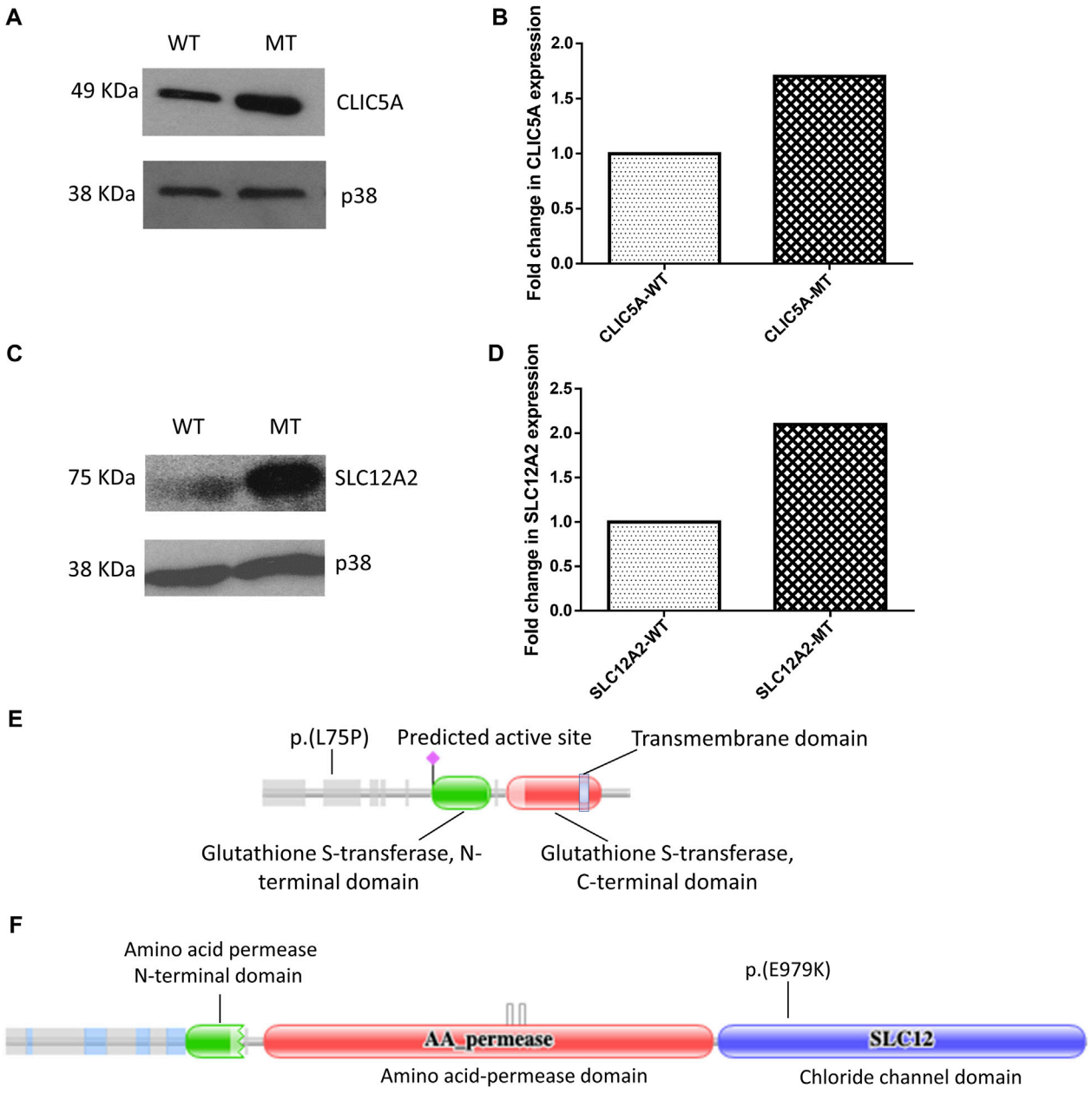


FIGURE 1
Mutant (MT) CLIC5A and SLC12A2 proteins are expressed at higher levels in HEK-293 cells, relative to the wild type proteins (WT). **(A)** Western blot of total proteins from HEK-293 cells transfected with wild-type (WT) or **(C)** 224T>C; p.(L75P) mutant (MT) *CLIC5A* plasmids; using anti-Myc antibody (N-terminal). **(B)** Densitometric analysis of western blot of CLIC5. **(C)** Western blot of total protein isolated from HEK-293 cells transfected with WT and **(C)** 2935G>A:p.(E979K) MT *SLC12A2* plasmids; using anti-flag antibody (N-terminal). **(D)** Densitometric analysis of western blots of SLC12A2 for the WT and MT SLC12A2 treated cells using ImageJ. The uncropped western blot pictures are shown in Supplementary Figure S3. Schematic diagrams showing **(E)** CLIC5 p.(L75P) and **(F)** SLC12A2 p(E979K) variant positions. The protein domains were predicted using the Protein Families Database (Pfam) (https://doi.org/10.1093/nar/gkaa913).

Total protein isolation and western blotting

Total protein was isolated using 2x Laemmli buffer (0.125 mM Tris-HCL pH 6.8, 4% SDS, 10% b-mercaptoethanol, 20% glycerol, and 0.005% of bromophenol blue) and boiled for 5 min at 95°C. Proteins were resolved on 8–12% SDS-PAGE gels and transferred to nitrocellulose membranes (Bio-Rad, Hercules, CA, United States). In addition to total protein quantification using The Bio-Rad QuantiPro BCA Assay kit, and loading equal

concentrations on the SDS-PAGE gel, membranes were stained with Ponceau-S to verify adequate separation and equal loading and transfer of proteins. The membranes incubated in blocking buffer (1×PBS-Tween with5% (w/v) fat-free milk) for 1 h at room temperature followed by overnight incubation at 4°C in primary antibodies diluted in blocking buffer as follows: 1:1000 ANTI-FLAG® M2,(F1804, Sigma-Aldrich, Missouri, United States); 1: 1000 anti c-Myc (9E10) (sc-40, Santa Cruz Biotechnology, Dallas, TX, United States), 1:5000 anti-p38 (M0800, Sigma-Aldrich Missouri, United States) and 1:5000 anti-p-p38 (Bio-Rad, Hercules, CA, United States)]. Secondary antibodies used were Goat Anti Rabbit (H + L) HRP conjugate (170–6515, Bio-Rad, Hercules, CA, United States) and Goat Anti Mouse (H + L) HRP conjugate (170–6516, Bio-Rad, Hercules, CA, United States) at 1: 5000 dilution. In a dark room, the chemiluminescent substrate working solution (ECL Western Blotting Substrate from Thermo Fisher, Waltham, MA United States) was prepared following the manufacturer's instruction and added to the blot and allowed to react for 5 min. The blot was removed and placed between clear plastic protector sheets and all bubbles removed. The blot was overlaid with photographic film and secured in a cassette. The film was developed and fixed in their respective solutions. The developed photographic film was air-dried and scanned for the densitometric analysis of signal intensity of the bands using ImageJ software (NIH, United States).

Confocal microscopy

Live HEK-293 cells transfected with the appropriate plasmids viewed under Zeiss LSM8800 Airyscan confocal microscope (Zeiss, Oberkochen, Germany) 48- and 72-h post transfection. The nucleus was stained with 1:2000 of 10 mg/ml stock Hoechst stain (Invitrogen by Thermo Fisher Scientific, United States). The confocal microscope was equipped with a photomultiplier tube (PMT) detector which was able to detect the green fluorescence signal from a 488 nm Argon laser. The images were acquired and analyzed using ZEN Blue Software from Zeiss.

In silico analysis of protein-protein interactions

A literature search was conducted (Supplementary Material S1) to identify publications on CLIC5A and SLC12A2 protein-protein interactions. Proteins that have biological interaction with CLIC5A or SLC12A2 were used to build protein interaction networks on STRING (Franceschini et al., 2012). The STRING is a web-based tool that predicts protein-protein interactions based on physical and functional associations from computational prediction, knowledge transfer between organisms, and interactions aggregated from other primary databases. The first shell with not more than 10 interacting proteins, with a score of not less than 0.4 (the default score) was considered for further analysis.

Results

The clinical and family history of hearing impaired patients with *CLIC5A*: c.224T>C; p.(L75P) and *SLC12A2*: c.2935G>A: p.(E979K) variants from Cameroon (Wonkam-Tingang et al., 2020) and Ghana (Adadey et al., 2021) was previously reported. The current study provides biological evidence on the pathogenicity of the reported variants using cell models and biological assays.

Mutant CLIC5A and SCL12A2 proteins are more stable than wild-type counterparts

Western blot of total cell lysate of HEK-293 cells revealed differential expression of CLIC5A and SLC12A2 proteins when the mutant proteins were compared to the wild-type. It is worth noting that no statistical difference was observed between the transfection efficiency of the wildtype constructs compared to the mutant constructs (Supplementary Figure S2A). Notably, mutant CLIC5A and SLC12A2 proteins were in high relative abundance compared to wild-type CLIC5A and SLC12A2 proteins (Figures 1A,C). The densitometric analysis of the western blot gave a statistically significant difference (p-values of <0.0001 and 0.0006 for CLIC5 and SLC12A2) in the expression of the mutant and wild-type proteins with respect to the internal control, p38 protein (Figures 1B,C). The fold change in expression of the mutant protein was determined against the wilt-type protein. In brief, the ratio of wild-type densitometric readings against the internal control were set to 1 and used to compare that of mutant proteins. Although cell-based assays do not recapitulate *in vivo* occurrences, it is postulated that the above differences in protein levels possibly contributed to the hearing impairment phenotype by negatively impacting the protein function.

Mutant CLIC5A protein is aggregated into distinct peri-nuclear inclusion bodies

Live cell imaging using confocal microscopy was used to analyze differences in protein localization and cellular morphology of GFP-tagged WT and MT proteins expressed in HEK-293 cells, with a hoechst stain used to stain the nucleus. As expected, control cells (GFP-only) displayed an even distribution of GFP throughout the whole cell (Figure 2). The wild-type CLIC5A protein was found to be evenly distributed throughout the cytoplasm and excluded from the nucleus. This was distinctly different to the mutant CLIC5A protein which appeared to aggregate within inclusion bodies found mostly in the perinuclear space (Figure 2, red arrows). With regards to

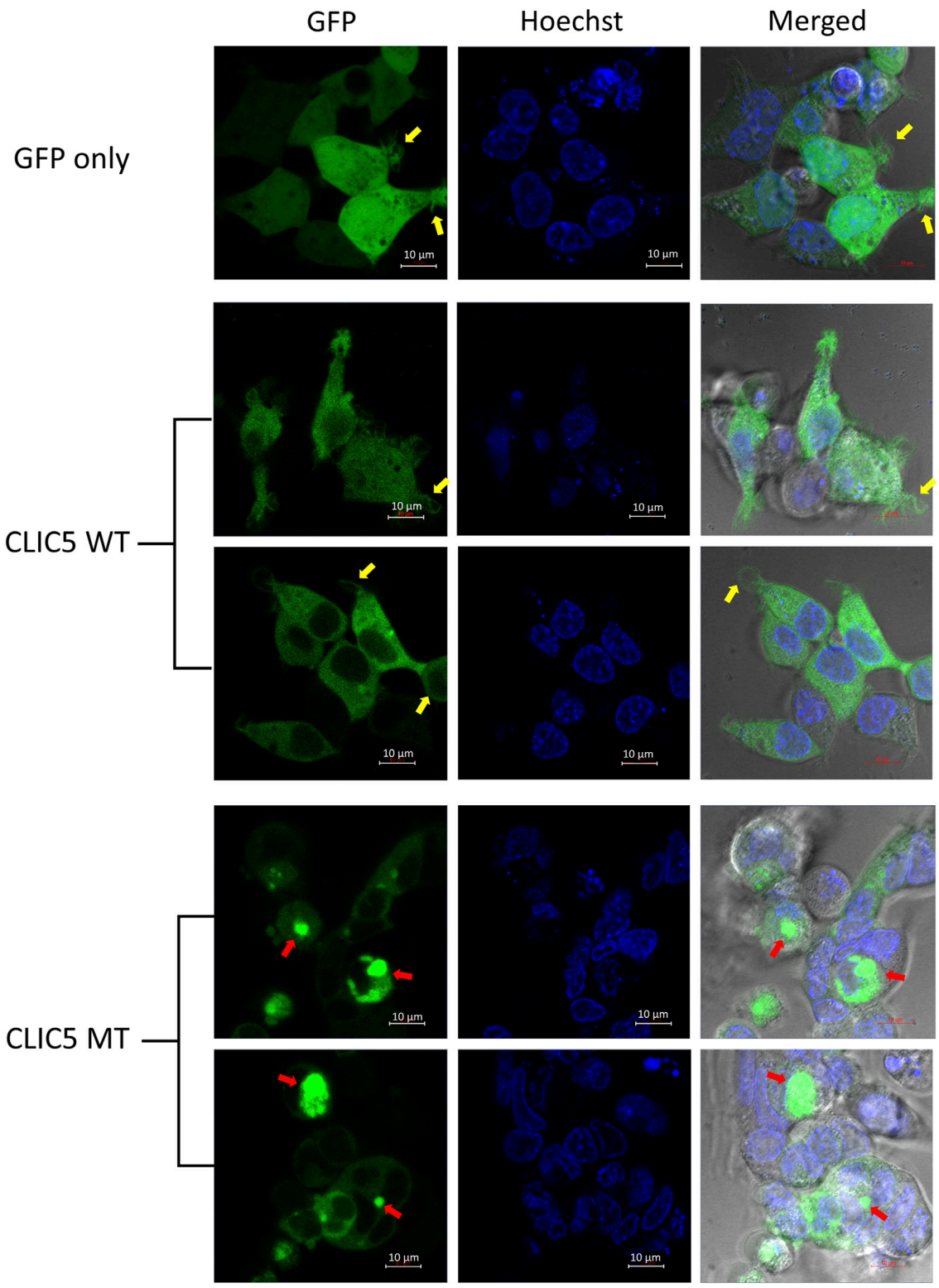


FIGURE 2
CLIC5A MT and not WT are aggregated into sub-cellular compartments. Live HEK293 cells expressing WT or MT GFP-tagged CLIC5A protein and stained with Hoechst were observed using confocal microscopy 48 h post transfection. The yellow arrows point to thin membrane filopodia-like protrusions observed in the WT transfected cells and the red arrows point to CLIC5 MT protein clusters.

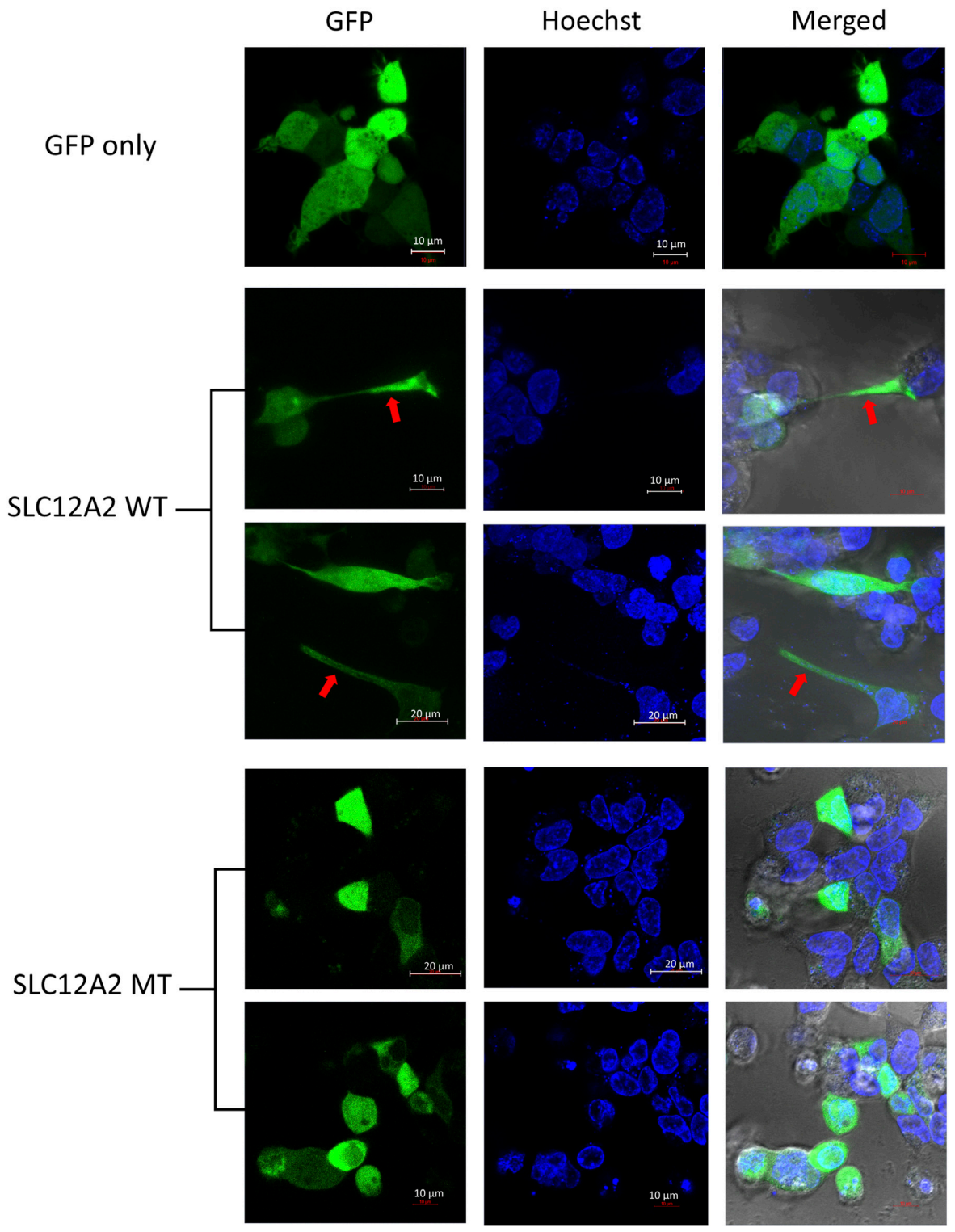


FIGURE 3
SLC12A2 WT HEK293 expressing cells display distinct morphology not observed in mutant-expressing cells. Live HEK293 cells expressing WT or MT GFP-tagged SLC12A2 protein and stained with Hoechst were observed using confocal microscopy 72 h post transfection. The red arrows point to axon-like structures present in the WT- SLC12A2 population of cells.

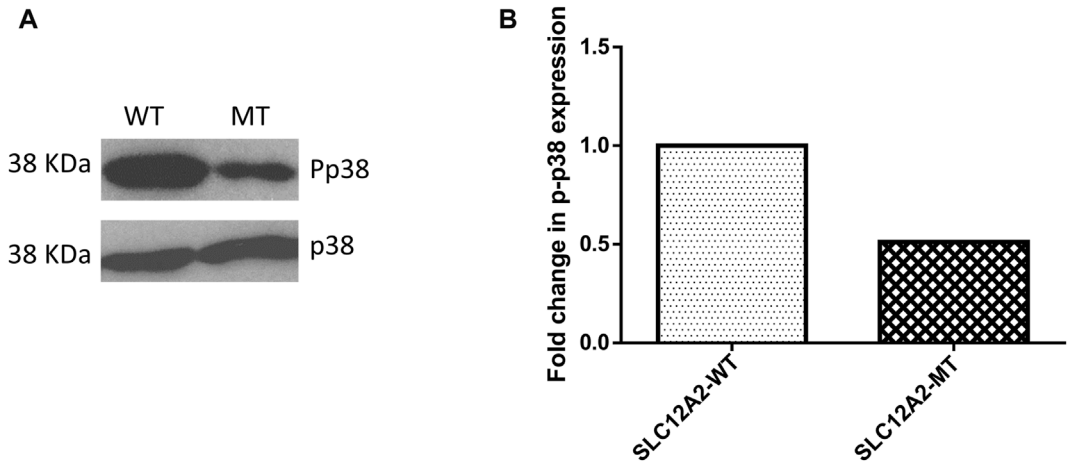


FIGURE 4
Mutant (MT) SLC12A2 expressing cells had relatively less phosphorylated p38 (Pp38) compared to the wild type (WT). **(A)** Western blot showing Pp38 expression in HEK293 cells transfected with WT and (C) 2935G>A: p.(E979K) MT *SLC12A2* plasmids. Total p38 was used for normalization **(B)** Densitometric analysis of western blots of Pp38 the WT and MT SLC12A2 treated cells using ImageJ. The densitometric analysis was conducted 3 times and the mean measurements were recorded. The uncropped western blot pictures are shown in Supplementary Figure S3.

cellular morphology, there were no major changes in cell shape observed between WT and MT CLIC5A, however a notable difference was that cells expressing wild-type CLIC5A had thin membrane filopodia-like protrusions (Figure 2, yellow arrows), which is similar to the control cells expressing GFP only, but this was absent in the cells expressing mutant CLIC5A.

Cells expressing mutant SLC12A2 lose distinct morphological features and express less stress proteins

The main difference observed among HEK-293 cells expressing GFP-tagged wild-type SLC12A2, when compared to mutant SLC12A2 was with regards to cell morphology. The Wild-type SLC12A2 cells displayed an elongated morphology and produced very distinct axon-like structures (Figure 3, red arrows) which were absent in the cells expressing mutant SLC12A2 or GFP only. Both wild-type and mutant SLC12A2 proteins were mostly localized to the cytoplasm of the HEK-293 cells (Figure 3). At 72 h post-transfection, it was observed that SLC12A2-expressing cells (both WT and MT) had detached and moved into suspension indicating stress on the transfected HEK-293 cells. Interestingly, the wild-type had relatively more detached cells than the mutant transfected cells. No cell detachment was observed in the mock-transfected, GFP-only transfected, as well as the CLIC5A-expressing cells at that time point. This prompted an investigation of the induction of cellular stress, which can be assessed via expression of stress pathway proteins (Coulthard et al., 2009). Indeed, expression of the stress phosphorylated $p38^{MAPK}$ protein (p-p38) was significantly higher in WT- SLC12A2 expressing cells compared to those expressing MT-SCL12A2 (Figure 4).

CLIC5A protein-protein interactions in the inner ear

To understand the role of CLIC5A in the inner ear, we investigated CLIC5A protein-protein interactions from published data and on the STRING database. Based on the experimental evidence from published literature, eight (8) proteins were found to interact with CLIC5A at the base of stereocilia (Supplementary Table S1). A protein network was built with these proteins which are known to be involved in the hearing processes or associated with deafness (Figure 5A). The protein network consisted of an additional ten (10) proteins predicted as functional partners (Supplementary Table S2). Most proteins on the network were either connected to EZR or RDX suggesting their major contributions to the formation of a protein complex at the base of stereocilia (Figure 5A). The CLIC5A-interaction network has shown that CLIC5A had physical interactions with only two out of the eight proteins, namely RDX and TPRN (Figure 5A), and an additional protein, CFTR. The physical interaction between CLIC5A and CFTR was from curated databases such as Biomolecular Interaction Network Databank (BIND), NCI-Nature Pathway Interaction Database (PID), Database of Interacting Proteins (DIP), and Biological General Repository for Interaction Datasets (BioGRID) (Figure 5B), however mice inner ear protein expression data suggests that CFTR may not be associated with HI.

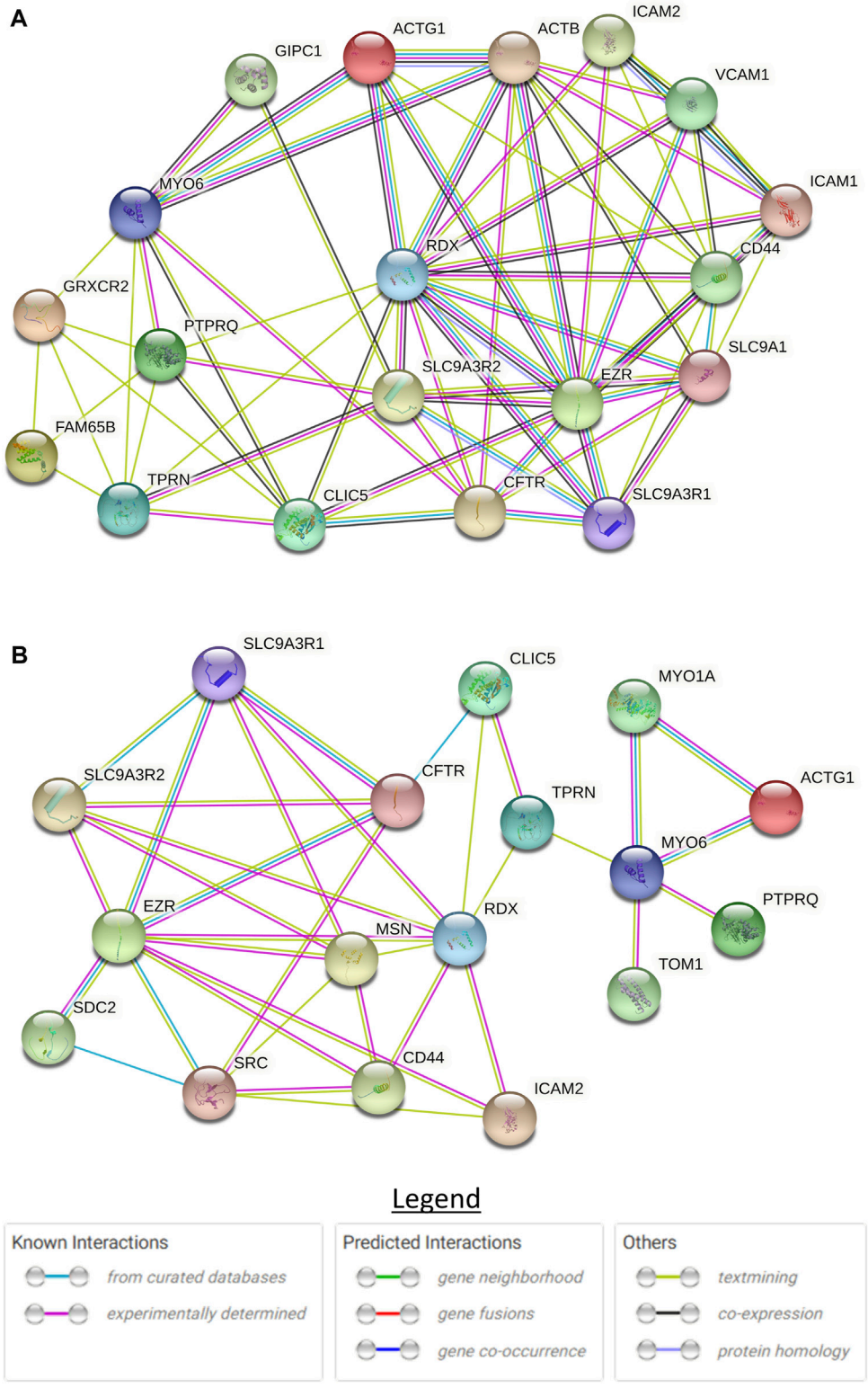


FIGURE 5
STRING protein-protein interaction network of CLIC5. **(A)** Full protein-protein interaction network consisting of both functional and physical protein interactions. **(B)** Subnetwork of physical interactions. The circles with structure in them are proteins with known or predicted structure.

SLC12A2 protein-protein interactions in the inner ear

In the case of SLC12A2, no protein-protein interaction study was identified in the literature. SIX1 and SIX4 proteins were however reported to bind to the promoter of *SLC12A2* and regulate its expression in the inner ear (Ando et al., 2005). Both *Six1* and *Six4* have similar patterns of expression and are expressed in the inner ear of mice. Malformation of different organs including the inner ear was observed in $Six1^{-/-}$ mice and hence showing the importance of these *Slc12a2* regulatory genes in the development of the auditory system (Ando et al., 2005). The three proteins (SLC12A2, SIX1, and SIX4) were analyzed on the STRING database and no protein-protein interaction was observed between the two SIX proteins and SLC12A2.

Discussion

Bioinformatics tools have proven to be effective in predicting the possible pathogenicity of variants, however, their utility is limited in terms of providing definitive evidence for biological pathogenicity (Flanagan et al., 2010). Thus, animal and cell models are critical to elucidate the possible mechanisms of pathogenicity of variants and ascertain their association with human trait and diseases. In this study, investigating protein expression, localization, and morphology of HEK-293 cells, we have provided additional cell-based assays data to support the pathogenic effect of previously reported variants in *CLIC5A* [c.224T>C; p.(L75P)] and *SCL12A2* [c.2935G>A: p.(E979K)].

CLIC5A, the isoform expressed in the inner ear, was initially isolated from placental epithelial cell microvilli as a component of the actin-based cytoskeletal complex, interacting with actin and ezrin at the cell cortex (Berryman and Bretscher, 2000; Berryman et al., 2004). CLIC5A is also expressed in the apical membrane of kidney glomerular endothelial cells (Nyström et al., 2009), podocytes (Tavasoli et al., 2016a), and placental microvilli (Berryman and Bretscher, 2000; Berryman et al., 2004). It was later shown to be highly expressed in the cell stereocilia of the inner ear, and important for sensorineural hearing (Gagnon et al., 2006). Mice deficient of the protein exhibited impaired hearing and vestibular dysfunction (Gagnon et al., 2006). A literature search revealed that the first report of *CLIC5A* variants were in hearing-impaired individuals from Turkey (Seco et al., 2015), with a homozygous nonsense mutation [*CLIC5A*: c.96T>A: p.(C32*)] in two affected individuals with NSHI from the same family. The second report was our previous study from Cameroon where we found compound heterozygous variants [*CLIC5A*: c.224T>C: p.(L75P) and c.63 + 1G>A] in three NSHI patients (Wonkam-Tingang et al., 2020).

In the present study, we found that the mutant CLIC5A protein was proportionally more abundant compared to the wild-type when ectopically expressed in HEK-293 cells and this indicates that the mutant protein likely lost a domain important in cellular turnover. *In silico* analysis of this variant showed that leucine at position 75 of the CLIC5A protein is highly conserved and vital to the protein structure and function (Wonkam-Tingang et al., 2020). The effect of the variant on the protein structure and stability probably resulted in a misfolded and/or non-functional protein which accumulate within autophagosomes or aggresomes when the capacity of the proteosome pathway is exceeded (Johnston et al., 1998). This was supported by the subcellular localization experiment, performed in the present study, which showed that the mutant CLIC5A protein aggregated in perinuclear structures while the wild-type protein was distributed in the cytoplasm of the cell. In the cell, CLIC5A is known to be an integral membrane protein and functions as an ion channel however, it also exists as a soluble cytosolic protein (Dulhunty et al., 2001; Harrop et al., 2001; Gururaja Rao et al., 2020) explaining the cytosolic distribution of the wild-type protein in the HEK-293 cells. During protein synthesis, which takes place in the endoplasmic reticulum (ER), it is possible that the mutation in the CLIC5 protein leads to aggregation, hampering its trafficking outside of the ER, and thus making it unavailable for its normal cellular function.

We observed thin membrane filopodia-like protrusions in the CLIC5A wild-type transfected cells which were absent in the mutant transfected cells as well as control cells. CLIC5A is known to play an important role in the assembly of F-actin-containing complexes, an ATP-dependent process, via the activation of ezrin-radixin-myosin (ERM) proteins in a phosphatidylinositol (4,5)-bisphosphate-dependent manner (Berryman et al., 2004; Tavasoli et al., 2016b). In the inner ear, CLIC5A colocalizes with radixin (RDX), taperin (TPRN) and myosin VI (MYO6) at the base of the stereocilia (Salles et al., 2014). RDX, protein tyrosine phosphatase receptor Q (PTPRQ), and TPRN which are associated with deafness, were mislocalized in fused stereocilia of CLIC5A-deficient mice (Salles et al., 2014). Additionally, CLIC5A was shown to be particularly important for the localization of PTPRQ, RDX, and TPRN in the hair cell rootlet (stereocilia base) and CLIC5A-deficient hair cells showed diffusion of PTPRQ, RDX, and TPRN. Therefore, the absence of thin membrane filopodia-like protrusions in the CLIC5A mutant transfected cells may be attributed to inadequate formation of actin-ERM complexes, known to stabilize the linkage between the plasma membrane and actin cytoskeleton, as a result of the dysfunctional mutant CLIC5A protein (Salles et al., 2014). It is however also possible that the absence of thin membrane filopodia-like protrusions in the mutant CLIC5 expressing cells is as a result of stress response due to the aggregation of the mutant proteins.

The formation of the actin multiprotein complex by CLIC5A, RDX, TPRN, MYO6, and PTPRQ was shown to be critical in membrane-cytoskeletal attachment at the base of the hair bundle, involving the positioning and maintenance of the stereocilia shaft (Salles et al., 2014). Glutaredoxin domain-containing cysteinerich protein 2 (GRXCR2) and RHO family interacting cell polarization regulator 2 (RIPOR2) were reported to interact and localize with CLIC5A, and are essential for normal hearing (Li et al., 2021).

TABLE 1 Association of *CLIC5* and *SLC12A2* variants with hearing impairment in patients.

Gene	Nucleotide change	Protein change	Inh	GT	Condition	Country	References
CLIC5	c.224T>C	p.(L75P)	AR	Het	NSHI	Cameroon	Wonkam-Tingang et al. (2020)
CLIC5	c.63 + 1G>A	-	AR	Het	NSHI	Cameroon	Wonkam-Tingang et al. (2020)
CLIC5	c.96T>A	p.(C32*)	AR	Hom	NSHI	Turkey	Seco et al. (2015)
SLC12A2	c.2935G>A	p.(E979K)	AD	Het	NSHI	Ghana	Adadey et al. (2021)
			AD	Het	congenital, severe HI	Japan	Mutai et al. (2020)
			AD	Het	NSHI with vestibular areflexia syndrome (CANVAS)	-	McNeill et al. (2020)
	c.2939A>T	p.(E980V)	AD	Het	NSHI	Pakistan	Adadey et al. (2021)
SLC12A2	chr5: 127441491–127471419 delins34	-	AR	Hom	HI with Kilquist syndrome	Mixed European ancestry	Macnamara et al. (2019)
SLC12A2	c.3431C>A	p.(T1144N)	AD	Het	NSHI	Italy	Morgan et al. (2020)
SLC12A2	c.2941G>T	p.(D981Y)	AD	Het	NSHI	Japan	Mutai et al. (2020)
SLC12A2	c.2930–2A>G	-	AD	Het	HI with minor motor developmental delay	Japan	Mutai et al. (2020)
SLC12A2	c.2962C>A	p.(P988T)	AD	Het	HI with motor developmental delay	Japan	Mutai et al. (2020)
SLC12A2	c.980C>T	p.(A327V)	AD	Het	HI with multiple congenital anomalies (iris coloboma, ventricular septal defect and tracheo-oesophageal fistula)	United Kingdom	McNeill et al. (2020)
SLC12A2	c.555dupG	p.(H186 Afs*17)	-	-	Spastic quadriparesis and severe global developmental delay	United Kingdom	McNeill et al. (2020)
SLC12A2	c.1127A>T	p.(N376I)	AD	Het	Spastic paraparesis and delay of speech and gross motor development	United Kingdom	McNeill et al. (2020)
SLC12A2	c.1135_1136del GCinsCT	p.(A379L)	-	-	Autism and intellectual disability	United Kingdom	McNeill et al. (2020)
SLC12A2	c.1229G>A	p.(R410Q)	-	-	Autism and intellectual disability	United Kingdom	McNeill et al. (2020)
SLC12A2	c.2675G>A	p.(W892*)	AD	Het	Minor developmental delay. First walked age 3 years	-	McNeill et al. (2020)

Inh, Mode of inheritance, AR, autosomal recessive; AD, autosomal dominant; GT, patient genotype, hom, homozygote, het, heterozygote.

Disruption of the interaction between CLIC5A and GRXCR2 was found to have minimal effects on stereocilia morphogenesis, however, the disruption led to hearing impairment in mice (Li et al., 2021). This underscores the role of GRXCR2 in the formation of the complex and the function of the stereocilia. There are two models to explain the role of CLIC5A at the base of the stereocilia (Salles et al., 2014; Li et al., 2021). Although these models are essential in our understanding of the formation of the protein complex, major proteins were left out in each model. Our literature review and CLIC5A protein interaction network (Figure 4) suggested that at least 8 proteins are involved in the formation of this complex at the base of the stereocilia.

According to the literature search, *SLC12A2* variants were associated with both NSHI and syndromic HI. Our previous report from Ghana and Pakistan (Adadey et al., 2021) and a study from Japan (McNeill et al., 2020) reported variants in NSHI patients (Table 1). The Ghanaian variant (c.2935G>A: p.(E979K) was also found in a Japanese who had NSHI and vestibular areflexia syndrome (CANVAS) (McNeill et al., 2020). The other NSHI variants found were c.3431C>A: p.(T1144N) in Italy (Morgan et al., 2020) and c.2941G>T: p.(D981Y) in Japan. A non-synonymous variant and a splice site variant were reported in unrelated individuals with motor developmental delay (Table 1).

As similarly observed for CLIC5A, the SCL12A2: p.(E979K) mutant protein was found to be relatively expressed in higher proportion when compared to the wild-type (Figure 1C). The p.(E979K) variant is located on exon 21 of *SLC12A2* gene, a region which encodes 17 amino acids critical for the expression and transporter activity in the inner ear (Mutai et al., 2020; Adadey et al., 2021). About 80% of all *SLC12A2* variant associated with hearing impairment are found in the exon 21 of the gene (Adadey et al., 2021). Functional analysis of a splice site variant that results in the skipping of the exon 21 showed a significant reduction of the exon21-skipped variants in the cochlear compared to the wild-type. In fact, the exon21-skipped variant and other variants in exon 21 significantly decreased the chloride transport activity of SLC12A2 protein (Mutai et al., 2020). On the contrary, the SCL12A2: p.(E979K) mutant was proportionally more abundant compared to the wild-type, and this may be due to the variant reducing the protein turnover within the cell.

SLC proteins are predominantly known for their ion transport activities across the cell membrane. This family of proteins are also

found throughout cellular organelles which suggests that they perform other intracellular functions aside their predominant cell membrane activity (Pizzagalli et al., 2021). Both SLC12A2: p.(E979K) mutant and wild-type proteins were expressed predominantly in the cytoplasm of the HEK-293 cells. The wild-type SLC12A2 expressing cells were found to have an axon-like cell morphology, with the cell membrane thrown into extended dendrites, a phenotype which was distinctly absent in the mutant p.(E979K) expressing cells. The SLC12 are a family of SLC proteins that are involved in cell volume regulatory activities. These proteins conduct an electroneutral transport of chloride ions with either sodium or potassium ions which results in the movement of water across the cell membrane. The controlled movement of water across the cell membrane regulates cell volume and movement (Turner and Sontheimer, 2014). Inferring from the cell volume and movement activities of the SLC12 family of proteins, it is possible that the mutant SLC12A2: p.(E979K) protein has lost its function and was not able to influence the change in morphology of the HEK-293 cells.

The current study was limited in the fact that it was unable to examine the membrane transport activity of the CLIC5A and SLC12A2 mutant proteins. However, major differences were observed in the localization and morphology of the mutant and wild-type cells from which the biological effect of the variants could be inferred. We recommend that the interaction of all the eight proteins identified to associate with CLIC5A at the base of the stereocilia should be investigated in mice models to elucidate the role of each protein in the formation of the protein-complex and their importance to the structure and function of the stereocilia.

Conclusion

In this study, we used HEK-293 cell-based experiments to evaluate the pathogenicity of *CLIC5A* [c.224T>C; p.(L75P)] and *SCL12A2* [c.2935G>A: p.(E979K)] variants that were previously reported in the Ghanaian and Cameroonian populations respectively. The protein expression, localization, and cell morphology of the mutant cells were different from their respective wild-type cells showing that the variants likely altered the properties and function of the proteins and thus are pathogenically relevant. Therefore, the study has generated novel biological data associated with the pathogenicity of targeted *CLIC5A* and *SLC12A2* variants, found in two African families, and expands our understanding of their pathobiology in HI.

Data availability statement

The original contributions presented in the study are included in the article/Supplementary Material, further inquiries can be directed to the corresponding author.

Author contributions

Conception of the project: AW and GA; molecular experiments: SA, EW-T, LA, NM, and SM; cellular localization and expression: SA, EW-T, LA, NM, and SM; bioinformatics analysis and Literature review: SA, EW-T, KE, and AW; writing of the first draft: SA; review and editing: all authors; supervision and management of the project: AW, GA, CdK and SM. All authors have agreed to the final version of the manuscript.

Funding

This study was possible because of funding received from the Wellcome Trust, grant number 107755Z/15/Z to GAA and AW; NIH, United States, grant number U01-HG-009716 to AW, the African Academy of Science/Wellcome Trust, grant number H3A/18/001 to AW. The funders were not involved in study design, data collection, and analysis, the decision to publish, or the preparation of the manuscript.

Acknowledgments

We express our profound gratitude to the Confocal and Light Microscope Imaging Facility at the University of Cape Town.

Conflict of interest

The authors declare that the research was conducted in the absence of any commercial or financial relationships that could be construed as a potential conflict of interest.

Publisher's note

All claims expressed in this article are solely those of the authors and do not necessarily represent those of their affiliated organizations, or those of the publisher, the editors and the reviewers. Any product that may be evaluated in this article, or claim that may be made by its manufacturer, is not guaranteed or endorsed by the publisher.

Supplementary material

The Supplementary Material for this article can be found online at: https://www.frontiersin.org/articles/10.3389/fgene.2022.924904/full#supplementary-material

References

Adadey, S. M., Schrauwen, I., Aboagye, E. T., Bharadwaj, T., Esoh, K. K., Basit, S., et al. (2021). Further confirmation of the association of SLC12A2 with non-syndromic autosomal-dominant hearing impairment. *J. Hum. Genet.* 66, 1169–1175. doi:10.1038/s10038-021-00954-6

Ando, Z, Sato, S., Ikeda, K., and Kawakami, K. (2005). Slc12a2 is a direct target of two closely related homeobox proteins, Six1 and Six4. *FEBS J.* 272, 3026–3041. doi:10.1111/j.1742-4658.2005.04716.x

Berryman, M., and Bretscher, A. (2000). Identification of a novel member of the chloride intracellular channel gene family (CLIC5) that associates with the actin cytoskeleton of placental microvilli. *Mol. Biol. Cell* 11, 1509–1521. doi:10.1091/mbc.11.5.1509

Berryman, M., Bruno, J., Price, J., and Edwards, J. C. (2004). CLIC-5A functions as a chloride channel *in vitro* and associates with the cortical actin cytoskeleton *in vitro* and *in vivo*. *J. Biol. Chem.* 279, 34794–34801. doi:10.1074/jbc.M402835200

Brodie, A., Smith, B., and Ray, J. (2018). *The impact of rehabilitation on quality of life after hearing loss: a systematic review*, *Eur. Archives Oto-Rhino-Laryngology*, 275. 2435–2440.

Cannizzaro, M., Jarošová, J., and De Paepe, B. (2019). Relevance of solute carrier family 5 transporter defects to inherited and acquired human disease. *J. Appl. Genet.* 60, 305–317. doi:10.1007/s13353-019-00502-1

Coulthard, L. R., White, D. E., Jones, D. L., McDermott, M. F., and Burchill, S. A. (2009). p38MAPK: stress responses from molecular mechanisms to therapeutics. *Trends Mol. Med.* 15, 369–379. doi:10.1016/j.molmed.2009.06.005

Delmaghani, S., and El-Amraoui, A. (2020). Inner ear gene therapies take off: Current promises and future challenges. *J. Clin. Med.* 9, E2309–E2327. doi:10.3390/jcm9072309

Dulhunty, A., Gage, P., Curtis, S., Chelvanayagam, G., and Board, P. (2001). The glutathione transferase structural family includes a nuclear chloride channel and a ryanodine receptor calcium release channel modulator. *J. Biol. Chem.* 276, 3319–3323. doi:10.1074/jbc.M007874200

Flanagan, S. E., Patch, A-M., and Ellard, S. (2010). Using SIFT and PolyPhen to predict loss-of-function and gain-of-function mutations. *Genet. Test. Mol. Biomarkers* 14, 533–537. doi:10.1089/gtmb.2010.0036

Franceschini, A., Szklarczyk, D., Frankild, S., Kuhn, M., Simonovic, M., Roth, A., et al. (2012). STRING v9. 1: Protein-protein interaction networks, with increased coverage and integration. *Nucleic Acids Res.* 41, D808–D815. doi:10.1093/nar/gks1094

Gagnon, K. B., and Delpire, E. (2013). Physiology of SLC12 transporters: Lessons from inherited human genetic mutations and genetically engineered mouse knockouts. *Am. J. Physiol. Cell Physiol.* 304, C693–C714. doi:10.1152/ajpcell.00350.2012

Gagnon, L. H., Longo-Guess, C. M., Berryman, M., Shin, J-B., Saylor, K. W., Yu, H., et al. (2006). The chloride intracellular channel protein CLIC5 is expressed at high levels in hair cell stereocilia and is essential for normal inner ear function. *J. Neurosci.* 26, 10188–10198. doi:10.1523/JNEUROSCI.2166-06.2006

Gururaja Rao, S., Patel, N. J., and Singh, H. (2020). Intracellular chloride channels: Novel biomarkers in Diseases. *Front. Physiol.* 11, 96–18. doi:10.3389/fphys.2020.00096

Harrop, S. J., DeMaere, M. Z., Fairlie, W. D., Reztsova, T., Valenzuela, S. M., Mazzanti, M., et al. (2001). Crystal structure of a soluble form of the intracellular chloride ion channel CLIC1 (NCC27) at 1.4-Å resolution. *J. Biol. Chem.* 276, 44993–45000. doi:10.1074/jbc.M107804200

Johnston, J. A., Ward, C. L., and Kopito, R. R. (1998). Aggresomes: A cellular response to misfolded proteins. *J. Cell Biol.* 143, 1883–1898. doi:10.1083/jcb.143.7.1883

Li, J., Liu, C., and Zhao, B. (2021). N-terminus of GRXCR2 interacts with CLIC5 and is essential for auditory perception. *Front. Cell Dev. Biol.* 9, 671364–671369. doi:10.3389/fcell.2021.671364

Macnamara, E. F., Koehler, A. E., D'Souza, P., Estwick, T., Lee, P., Vezina, G., et al. (2019). Kilquist syndrome: A novel syndromic hearing loss disorder caused by homozygous deletion of SLC12A2. *Hum. Mutat.* 40, 532–538. doi:10.1002/humu.23722

McNeill, A., Iovino, E., Mansard, L., Vache, C., Baux, D., Bedoukian, E., et al. (2020). SLC12A2 variants cause a neurodevelopmental disorder or cochleovestibular defect. *Brain* 143, 2380–2387. doi:10.1093/brain/awaa176

Morgan, A., Pelliccione, G., Ambrosetti, U., Dell'Orco, D., and Girotto, G. (2020). SLC12A2: A new gene associated with autosomal dominant non-syndromic hearing loss in humans. *Hear. Balance Commun.* 18, 149–151. doi:10.1080/21695717.2020.1726670

Mutai, H., Wasano, K., Momozawa, Y., Kamatani, Y., Miya, F., Masuda, S., et al. (2020). Variants encoding a restricted carboxy-terminal domain of SLC12A2 cause hereditary hearing loss in humans. *PLoS Genet.* 16, e1008643–24. doi:10.1371/journal.pgen.1008643

Nadol, J. B., Jr (1978). Hearing loss as a sequela of meningitis. *Laryngoscope* 88, 739–755. doi:10.1002/lary.1978.88.5.739

Nyström, J., Fierlbeck, W., Granqvist, A., Kulak, S. C., and Ballermann, B. J. (2009). A human glomerular SAGE transcriptome database. *BMC Nephrol.* 10, 13–14. doi:10.1186/1471-2369-10-13

Pizzagalli, M. D., Bensimon, A., and Superti-Furga, G. (2021). A guide to plasma membrane solute carrier proteins. *FEBS J.* 288, 2784–2835. doi:10.1111/febs.15531

Salles, F. T., Andrade, L. R., Tanda, S., Grati, M., Plona, K. L., Gagnon, L. H., et al. (2014). CLIC5 stabilizes membrane-actin filament linkages at the base of hair cell stereocilia in a molecular complex with radixin, taperin, and myosin VI. *Cytoskelet. Hob.* 71, 61–78. doi:10.1002/cm.21159

Seco, C. Z., Oonk, A. M., Domínguez-Ruiz, M., Draaisma, J. M., Gandía, M., Oostrik, J., et al. (2015). Progressive hearing loss and vestibular dysfunction caused by a homozygous nonsense mutation in CLIC5. *Eur. J. Hum. Genet.* 23, 189–194. doi:10.1038/ejhg.2014.83

Tavasoli, M., Al-Momany, A., Wang, X., Li, L., Edwards, J. C., and Ballermann, B. J. (2016). Both CLIC4 and CLIC5A activate ERM proteins in glomerular endothelium. *Am. J. Physiol. Ren. Physiol.* 311, F945–F57. doi:10.1152/ajprenal.00353.2016

Tavasoli, M., Li, L., Al-Momany, A., Zhu, L-F., Adam, B. A., Wang, Z., et al. (2016). The chloride intracellular channel 5A stimulates podocyte Rac1, protecting against hypertension-induced glomerular injury. *Kidney Int.* 89, 833–847. doi:10.1016/j.kint.2016.01.001

Turner, K. L., and Sontheimer, H. (2014). Cl− and K+ channels and their role in primary brain tumour biology. *Philos. Trans. R. Soc. Lond. B Biol. Sci.* 369, 20130095–20130099. doi:10.1098/rstb.2013.0095

Van Camp, G., and Smith, R. (2020). Hereditary hearing loss homepage. Available at: https://hereditaryhearingloss.org/.

Wonkam-Tingang, E., Schrauwen, I., Esoh, K. K., Bharadwaj, T., Nouel-Saied, L. M., Acharya, A., et al. (2020). Bi-allelic novel variants in CLIC5 identified in a Cameroonian multiplex family with non-syndromic hearing impairment. *Genes (Basel)* 11, 1–12. doi:10.3390/genes11111249

Zwartenkot, J. W., Snik, A. F., Mylanus, E. A., and Mulder, J. J. (2014). Amplification options for patients with mixed hearing loss. *Otol. Neurotol.* 35, 221–226. doi:10.1097/MAO.0000000000000258

frontiers | Frontiers in Genetics

TYPE Case Report
PUBLISHED 16 August 2022
DOI 10.3389/fgene.2022.932073

Check for updates

OPEN ACCESS

EDITED BY
Ruth Roberts,
ApconiX, United Kingdom

REVIEWED BY
Ayca Altincik,
Pamukkale University, Turkey
Adib Shafi,
Wayne State University, United States
Antonino Maniaci,
University of Catania, Italy
Piero Pavone,
University of Catania, Italy

*CORRESPONDENCE
Xiyu He,
hxyjs200127@aliyun.com

SPECIALTY SECTION
This article was submitted to Genetics of Common and Rare Diseases, a section of the journal Frontiers in Genetics

RECEIVED 29 April 2022
ACCEPTED 07 July 2022
PUBLISHED 16 August 2022

CITATION
Liang Y, Wu H, He X and He X (2022), Case Report: Aarskog-scott syndrome caused by FGD1 gene variation: A family study.
Front. Genet. 13:932073.
doi: 10.3389/fgene.2022.932073

COPYRIGHT
© 2022 Liang, Wu, He and He. This is an open-access article distributed under the terms of the Creative Commons Attribution License (CC BY). The use, distribution or reproduction in other forums is permitted, provided the original author(s) and the copyright owner(s) are credited and that the original publication in this journal is cited, in accordance with accepted academic practice. No use, distribution or reproduction is permitted which does not comply with these terms.

Case Report: Aarskog-scott syndrome caused by FGD1 gene variation: A family study

Yijia Liang[1,2], Honglin Wu[1], Xiumei He[1] and Xiyu He[1]*

[1]Fifth Medical Center of Chinese PLA General Hospital, Beijing, China, [2]Chinese PLA Medical College, Beijing, China

Aarskog-Scott syndrome is a rare genetic disorder characterized by short stature, abnormal facial features, and digital and genital deformities. FGD1 gene variation is the known cause of this disorder. This paper described a Chinese family study of Aarskog-Scott syndrome in which the main patients were two brothers. Then, the relationship between genotype and phenotype in Aarskog-Scott syndrome was investigated preliminarily. A new FGD1 gene variant was revealed in this study, providing insights into the link between phenotype and genotype variations in Aarskog-Scott syndrome as well as a foundation for its diagnosis and treatment.

KEYWORDS

aarskog-scott syndrome, rare syndromes, FGD1 gene, family study, brother contact

1 Background

Aarskog-Scott syndrome (AAS, MIM number 305400), also known as facio-digital-genital dysplasia, was first described by Aarskog in 1970 (Aarskog, 1971) and later detailed by Scott (Scott and Moyer, 1971). AAS is a rare genetic disorder characterized by short stature, abnormal facial features, and digital and genital deformities. Although FGD1 gene variation is currently the known genetic cause of this disorder and its pathophysiology has been elucidated, any other causes that might be involved need to be yet explored. AAS is an X-linked recessive inherited disease with strong genetic diversity. Aarskog-Scott syndrome most commonly occurs in Europe, the United States, Japan, South Africa, and India, but in China, only a few cases have been reported. Herein, we aimed to present a unique occurrence of Aarskog-Scott syndrome in a Chinese family and analyze the relationship between genotype and phenotype of this disorder. Further, we planned to include relevant literature review.

2 Clinical information

The patients were two brothers. The elder brother was 7 years and 11 months old, and the younger one was 4 years and 9 months old. The cases were admitted to our hospital with the complaints of short stature and multiple deformities, they were born with full-term delivery, and their parents are non-consanguineous. The family reported that the

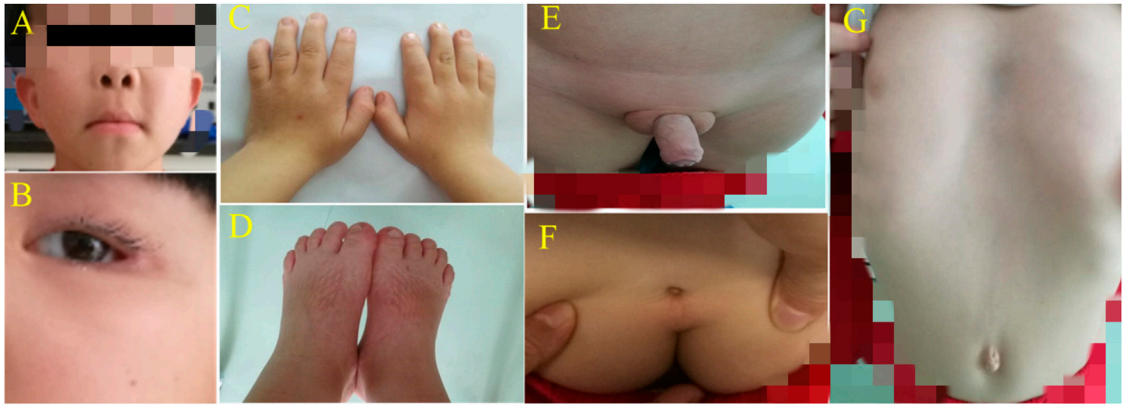


FIGURE 1
(A) + **(B)** High eyebrow arch, wide eye distance, small eye fissure, double eyelid ptosis, flat nose bridge and slightly upturned nostrils; the middle sulcus was wide and long, and the ear was low and backward. **(C)** + **(D)** Hands/soles were small; fingers/toes were short and thick; little fingers on both hands were short and curved with a single finger fold. **(E)** Bilateral oblique inguinal hernia and shapeless scrotum complicated with cryptorchidism (after surgery). **(F)** Sacral tail skin depression. **(G)** Sternum depression, costal margin eversion and a flat navel.

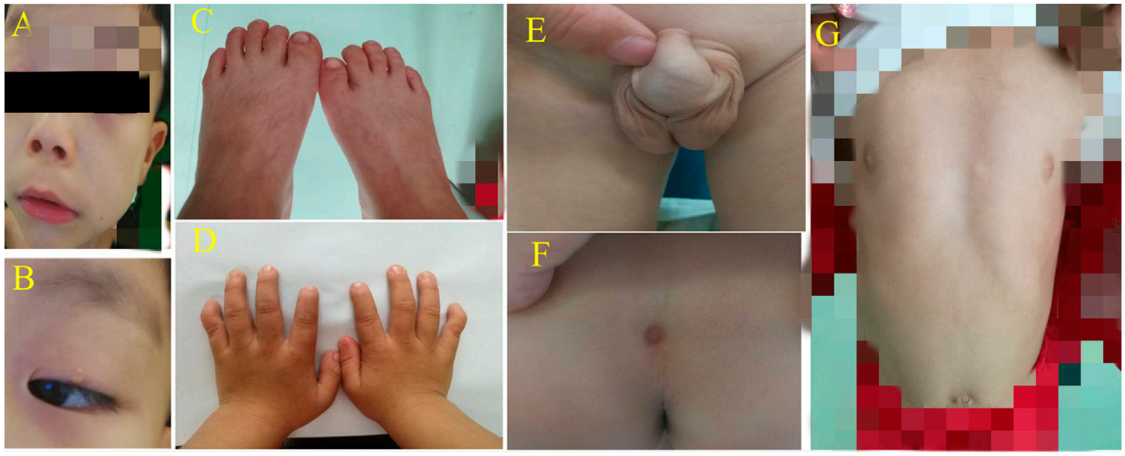


FIGURE 2
(A) + **(B)** High eyebrow arch, widening eye distance, small eye fissure and double eyelid ptosis; the nose bridge was flat, the nostrils were slightly elevated, the middle sulcus was wide and long, and the ear was low and backward. **(C)** + **(D)** Small hands/soles, short fingers/toes, and short little fingers curved with a single finger fold. **(E)** Shapeless scrotum. **(F)** Sacral caudal skin depression. **(G)** Sternal depression, outside costal margin turn and a flat navel.

growth retardation began at the age of one, and the birth weight and length were unknown. Nevertheless, no special attention was paid to these abnormalities and no intervention was performed. The antenatal history, birth event, and perinatal history were unremarkable. But specific growth and developmental milestones were overlooked. At admission to the hospital, the older boy's height and weight were 109.3 cm (−3.7 SD) and 21.5 kg (−1.26 SD) respectively, while the younger boy's height and weight were 100.4 cm (−1.3 SD) and 14.6 kg (−1.3 SD) respectively. Upon physical examination, older boy had a short and uniform body, small hands and soles, short and thick fingers and toes, short and curved little fingers on both hands with single finger pleats, high eyebrow arch, wide eye distance, wide eye cleft, drooping double eyelids, amblyopia, low and flat nose bridge, slightly upturned nostrils, low back and flapping ears, wide and long middle groove, sternal depression, oblique costal margin, inguinal hernia, shapeless scrotum with cryptorchidism (postoperatively), and sacral tail skin depression (Figure 1). The younger boy exhibited a proportionate short stature, small hands and soles, short and thick fingers and toes, short and curved little fingers on both hands with a single finger fold, wide eye distance and small eye cleft, double eyelid drooping, low nose bridge, slightly upturned nostrils, low and backward ear position, wind flapping ear, costal margin

evagination, flat navel, shapeless scrotum, and sacral tail skin depression (Figure 2). Furthermore, the older boy had a long response time, hyperactive response, and inability to concentrate.

The father was 172 cm and the mother is 160 cm in height. The mother had bent little fingers both sides. Their elder sister displayed slight deformities. The patients' cousin, three of their aunts and grandma had bent little fingers. The parents said that their late uncle's height was normal, with facial micro-deformity (specific complaint was unspecified), short and thick digits, and bent little fingers both sides.

Through a battery of laboratory tests on both boys, the older boy had normal liver and kidney functions, as well as normal blood routine parameters and electrolyte levels. Regarding thyroid function, T3:1.28 nmol/L (1.02–2.96 nmol/L), T4: 80.20 nmol/L (55.5–161.3 nmol/L), FT3:6.1 pmol/L (2.8–6.3 pmol/L), FT4: 20.01 pmol/L (11.5–22.7 pmol/L), TSH: 2.31 μIU/ml (0.64–6.27 μIU/L). IGF-1:441 ng/ml (111–551 ng/ml). IGFBP-3: 6.83 μg/mL (2.7–8.9 μg/mL). HbA1c: 4.5% (4.8–5.9%). Fasting insulin:8.12 μU/mL (2.60–24.90 μU/mL). ACTH:18.35 pg/ml (10–52 pg/ml), Cortisol:6.63 μg/dL (2.5–20 μg/dL).17-αhydroxyprogesterone: 0.249 ng/ml (0.07–3.6 ng/ml). The peak of growth hormone exercise screening test:5.167 ng/ml. Echocardiography, abdominal echocardiography and reproductive echocardiography were normal. Bone age assessed by imaging was about 6 years old, and pituitary magnetic resonance examination displayed no abnormalities. Karyotype analysis revealed 46, XY. And the younger boy had normal liver and kidney functions, as well as normal blood routine parameters and electrolyte levels. Regarding thyroid function, T3:2.10 nmol/L (1.02–2.96 nmol/L), T4: 105.4 nmol/L (55.5–161.3 nmol/L), FT3:3.3 pmol/L (2.8–6.3 pmol/L), FT4: 13.5 pmol/L (11.5–22.7 pmol/L), TSH:2.66 μIU/ml (0.64–6.27 μIU/L). IGF-1:127 ng/ml (50–286 ng/ml). IGFBP-3: 4.37 μg/mL (1.8–6.4 μg/mL). HbA1c: 4.5% (4.8–5.9%). Fastinginsulin:7.34 μU/mL (2.60–24.90 μU/mL). ACTH:16.89 pg/ml (10–52 pg/ml), Cortisol:5.34 μg/dL (2.5–20 μg/dL).17-αhydroxyprogesterone:0.179 ng/ml (0.07–3.6 ng/ml). The peak of growth hormone exercise screening test:3.770 ng/ml. Echocardiography, abdominal echocardiography and reproductive echocardiography were normal. Bone age assessed by imaging was about 6 years old, and pituitary magnetic resonance examination displayed no abnormalities. The karyotype was 46, XY.

The trio whole-exome sequencing and Sanger sequencing were performed after informed consent was obtained from parents. Briefly, 2 ml peripheral blood was collected using blood collection tubes coated with EDTA anticoagulant, from the two subjects. Genomic DNA was extracted from peripheral blood using a genomic DNA extraction kit (Kangwei Century Biotechnology Co., Ltd., Beijing, China) and the DNA quality was above the grade D. DNA was fragmented (10–700 bp) by ultrasonic apparatus (Covaris S220 ultrasonicator; Covaris, Woburn, MA, United States). PCR machine was used to amplify the DNA fragments and magnetic beads (Ampure beads: PCR products was 1.5:1) were used to purify the PCR amplicons. Standard library construction kit (independently developed by Mackinac) was used to construct DNA library, and the target region of the library was captured and quantified using GenCap liquid phase capture kit (independently developed by Mackinac) and KAPA qPCR kit (Roche Diagnostics Corporation, Indianapolis, IN, United States) on a PCR instrument. Finally, the high-throughput sequencing system Illumina NextSeq 500 was used for sequencing. After pre-processing and analysis of relevant data, pathogenicity analysis was performed following the American College of Medical Genetics and Genomics (ACMG)guidelines.

The results showed that a *FGD1* gene hemizygous variation was present in both cases, which was derived from their mother and GRCh37/HG19 was used as the reference genome. The *FGD1* gene, located on chrX- 54481880, was screened for variations, and the c.2015 + 1G>A variation was detected in exon 12 (RefSeq: NM_004,463). As a result, nucleotide no. 2015 + 1 in the coding region was changed from guanine to adenine. This was therefore a splicing variation. According to the ACMG guideline, this variant is pathogenic. However, this variant has not yet been reported in Clinvar database and HGMD professional edition database.

In conclusion, both cases were clinically diagnosed as Aarskog-Scott syndrome. Since the patients did not want to do other kinds of growth hormone stimulation experiments and the peak value of the pervious experiment was low, we directly treated the children with growth hormone with the consent of their parents.

Both patients were treated with long-term follow-up. Both boys were given with long-acting growth hormone at 0.2 mg/kg/w on a regular basis with the informed consent from parents. Until now, both cases have been on regular medication for more than 4 years. Throughout the time, periodic monitoring was done on both patients, including fasting blood glucose level, fasting insulin level, glycosylated hemoglobin content, and bone age evaluation. After 1 year, the height and weight of the older boy were 118 cm (−3.00 SD) and 25.6 kg (−0.86 SD) while the height and weight of the younger boy were 111 cm (−0.82 SD) and 20.3 kg (0 SD), respectively, suggesting that the children had catch-up growth in height and weight, which was basically consistent with the research results of Feyza et al. (Darendeliler et al., 2003). At the last follow-up, the height and weight of the older boy were 144 cm (−1.31 SD) and 45 kg (−0.14 SD) while the height and weight of the younger boy were 135 cm (0 SD) and 27 kg (−0.55 SD), respectively.

The presence of *FGD1* gene variation in the family was suspected based on the family history of cases and the nature of X-linked recessive inheritance of *FGD1* gene variation in Aarskog-Scott syndrome. The surviving members of the family were subjected to the genetic tests. The results are shown in Figure 3 and the family diagram is depicted in Figure 4.

Aarskog-Scott syndrome was considered due to the inheritance nature based on clinical reports and genetic test results. We described the clinical phenotypes of two patients

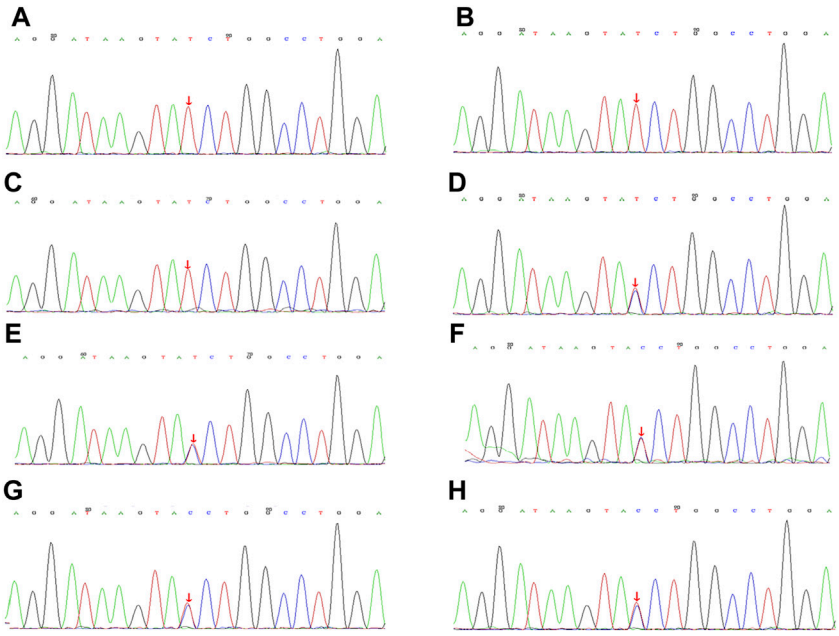


FIGURE 3
Gene sequencing of family members with Aarskog-Scott syndrome, with the variation shown by arrows. **(A)**. Case 1, FGD1 gene with **(C)**.2015 + 1G>A semi-heterozygous variation. **(B)**. Case 2, FGD1 gene with **(C)**.2015 + 1G>A semi-heterozygous variation. **(C)**. The children's cousin FGD1 gene with **(C)**.2015 + 1G>A semi-heterozygous variation. **(D)**. FGD1 gene with **(C)**.2015 + 1G>A heterozygous variation. **(E)** FGD1 gene with **(C)**.2015 + 1G>A heterozygous variation. **(F)**. FGD1 gene with **(C)**.2015 + 1G>A heterozygous variation. **(G)** FGD1 gene with **(C)**.2015 + 1G>A heterozygous variation. **(H)**. FGD1 gene with **(C)**.2015 + 1G>A heterozygous variation.

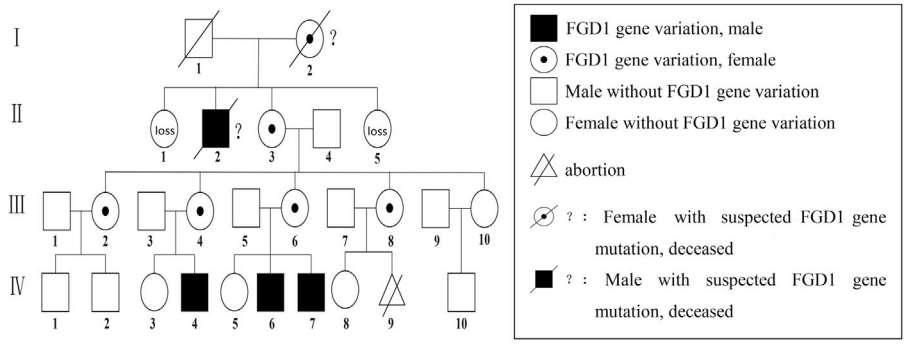


FIGURE 4
Aarskog-Scott syndrome family diagram; IV-4,IV-6, and IV-7 had FGD1 gene C.2015 + 1G>A semi-heterozygous variation, including IV-6 and IV-7 who were our patients. C.2015 + 1G>A heterozygous variation of the FGD1 gene for III-2, III-4, III-6, and III-8; I-2 andI-2 had died, and were speculated to have harbored FGD1 gene variation.

with Aarskog-Scott syndrome in this lineage and identified a new FGD1 gene variant that broadened the spectrum of FGD1 variations causing Aarskog-Scott syndrome. These findings provided a foundation for the diagnosis and correlation between phenotype and genotype in Aarskog-Scott syndrome.

3 Discussion

AAS is a rare disease with genetic heterogeneity, and X-linked recessive inheritance is the most common inheritance mode (Escobar and Weaver, 1978) (Grier et al., 1983); FGD1 gene variation is the only confirmed etiological factor for AAS.

The role of *FGD1* gene variants in the pathogenesis of X-linked AAS was first described in Germany based on a familial translocation breakpoint analysis (Pasteris et al., 1994). The FGD1 gene, located at Xp11.22, about 51 kb in length, contains 18 exons, and encodes a protein containing 961 amino acids, namely guanine nucleotide conversion factor (GEF), which contains five conserved domains (proline rich domain, DH domain, FYVE domain, and 2 PH domains) (Orrico et al., 2000). GEF encoded by the FGDI gene specifically activates the Rho GTPase CDC42, regulating actin morphology and protein kinase/C-Jun N-terminal kinase to control cell proliferation and differentiation through DH and PH domains that catalyze THE release of GDP, as well as binding of GTP. By altering bone development and morphogenesis and regulating extracellular matrix accumulation, GEF acts on the whole-body skeleton, superficial facial structures, eyes, genitals, and nervous system to maintain the normal morphology, development and function of corresponding tissues and organs (Pasteris et al., 1997). Variations in the FGD1 gene lead to the production of dysfunctional proteins that interfere with the CDC42 signaling, resulting in generalized developmental abnormalities. After knocking out the mutant MLK3 allele that is resistant to FGD1/CDC42 activation, mice showed similar skeletal defects, suggesting that FGD1/CDC42-activated MLK3 was critical for bone mineralization (Zou et al., 2011), confirming the influence of FGD1 gene variation on bone development.

FGD1 was also reported to cause cortical malformations through the CDC42 pathway, resulting in attention deficits and impaired intelligence. Fryns et al. showed that at least 30% of patients with AAS displayed intellectual disability, including mild intellectual disability in two-third of the 30% (Fryns, 1992). However, a study on 456 cases in Qinba Mountains with FGD1 gene polymorphisms and intellectual development disorders (IDD) showed that IDD was not significantly associated with the gene frequency, genotype frequency, and haplotype of the five SNP FGD1 loci, suggesting that FGD1 may have not been the single X-linked factor (Li et al., 2014). The specific mechanism by which FGD1 gene/CDC42 pathway induces brain dysplasia and intellectual disability remains to be further explored. The expression of the CDC42 protein was decreased in Xp11, which was predisposed to schizophrenia. A study on four unrelated Chinese male XP11.22 duplicative patients mainly with intellectual disability, language impairment, and motor delay speculated that FGD1 may have been the potential dose-sensitive gene associated with hypogonadism in these patients (Wang et al., 2020). In addition, FGD1 was confirmed as a transforming growth factor-β (TGF-β), regulating guanine nucleotide conversion factor (GEF) that was involved in cytokine-induced nuclear liposome formation, which may have been part of the molecular basis of vascular lesions (Daubon et al., 2011).

The phenotype of Aarskog-Scott syndrome (AAS) is varied. Short stature associated with Aarskog has craniofacial abnormalities such as hyperthyroidism, short nose, ptosis, and genital deformities such as cape scrotum and shawl cryptorchidism (Aarskog, 1971). Scott, on the other hand, described the same features in three different patients (Scott and Moyer, 1971). As time goes on, several other authors reported similar cases, describing the phenotype of these patients as characterized by the presence of various associated signs such as oblique, short, long middle, widow's peak, Camptodactyly, interphalanx webbed, and inguinal/umbilical hernia (P´erez-Coria et al., 2015) (Niida et al., 2014).

Teebi et al. established clear diagnostic criteria by summarizing the features of reported AAS in 1993. Main diagnostic symptoms included short stature, abnormal facial features, short nose with forward slope, maxillary hypoplasia, lower lip wrinkle, mildly crossed fingers, wide and short palms, short and curved little fingers, and shapeless scrotum. Secondary clinical diagnostic symptoms were thick external ear with excessive backward slant, forehead "V" tip, ptosis, downward slant palpebral fissure, hyperextension of joints, wide feet with clubbed toes, inguinal hernia, hypospadias, and navel abnormality. In clinical practice, due to the superposition of clinical phenotypes, it is often necessary to distinguish AAS from other genetic diseases such as Robin syndrome, Optiz syndrome, Bloom syndrome, Noonan syndrome, and pseudo-parathyroidism. Recent studies showed that patients with AAS showed multiple abnormalities, including anatomic abnormalities such as cardiovascular system symptoms (e.g., aortic stenosis and right ventricular hypertrophy) (Fernandez et al., 1994), nerve mental symptoms such as bipolar disorder, ADHD, autism spectrum disorders, epilepsy, Asperger's syndrome, and intellectual disability (Nayak et al., 2012), and musculoskeletal system conditions such as symmetrical distal joint disease, myopathy, hip dislocation, finger and knee jerk before stretching, and flat feet (Zielinski and Pack, 2008), Moreover, Bayat and Calabrese both reported that myopathic involvement should be considered in AAS (Bayat et al., 2022) (Calabrese et al., 2022).

The manifestations of both cases in this family were in line with the main diagnostic indicators mentioned above such as uniformly short stature, small hands and soles, short and thick fingers and toes, short and curved little fingers on both hands with a single finger fold, wide eye distance and small eye cleft, low and flat nose bridge, slightly upturned nostrils, and shawl like scrotum. Secondary indicators such as double eyelid drooping, low and back ear position, and flat navel were also aligned with the stated symptoms. Of note, the older brother had significant neurological symptoms such as hyperactivity, attention deficit, and intellectual disability, but the younger brother did not. The clinical phenotypes of both cases were summarized as short stature, abnormal facial features, and digital and genital deformities. But the elder brother experienced with slight neurological abnormalities, which was in line with current

understanding of abnormal phenotypes in AAS. Further, both patients had semi-heterozygous FGD1 gene variation, which provided strong evidence for the association between FGD1 gene variation and AAS phenotype. By analyzing seven individuals with FGD1 gene variation in three generations of this family, it was considered that AAS displayed the typical X-linked recessive inheritance pattern in this family. There was a FGD1 gene variation in the X chromosome of the grandmother of the children, which was transmitted to their mother and three aunts. Then, the mutated gene was transmitted from mother to both boys. Due to the obvious gender specificity of AAS (Balaton et al., 2018), both boys had typical clinical features of AAS, while their mother, aunt and grandmother only showed slight deformities in fingers.

Drumond et al. conducted a systematic analysis of the correlation between genotype and phenotype in AAS patients, but found no causal relationship between the two (Zanetti et al., 2021). Comparative analysis showed that our patients met the clinical diagnostic criteria of AAS and had a new *FGD1* gene variant, but no significant genotype-phenotype relation was found in the family members.

Recently, a study on AAS syndrome in an Italian family reported the variant C.1828C>T (p. Arg610*) in the FGD1 gene with 16P microdeletion, a genetic variant, but still with unclear phenotypic consequences, which indicated a potential association between AAS and chromosomal disorders (Pavone et al., 2020).

Presently, no studies have clearly confirmed the association between FGD1 genotype and phenotype in Aarskog-Scott syndrome. In the future, more cases combined with new gene testing methods could be used to elucidate the pathological mechanism causing specific genotype and phenotype in Aarskog-Scott syndrome to identify effective intervention measures for this syndrome.

Data availability statement

The datasets for this article are not publicly available due to concerns regarding participant/patient anonymity. Requests to access the datasets should be directed to the corresponding author.

Ethics statement

The study involving human participants were reviewed and approved by the Ethics Committee of Fifth Medical Center of Chinese PLA General Hospital (approval number: KY-2022-3-12-1) and the members and working procedures of the ethics review group comply with GCP principles and relevant national regulations; registration date: 06 April 2022. Written informed consent to participate in this study was provided by the participants' legal guardian/next of kin. Written informed consent was obtained from the individual(s), and minor(s)' legal guardian/next of kin, for the publication of any potentially identifiable images or data included in this article.

Author Contributions

XH and HW have full access to all data from the study and take responsibility for the integrity of the data and the accuracy of the data analysis. YL and XH were involved in the concepts and design of the study. All authors involved in the acquisition, analysis, and interpretation of data. XH and YL supervised the analysis. YL and XH involved in the draft of the manuscript. All authors read, critically revised, and approved the current version of the manuscript.

Funding

The study was supported by study on the key techniques and standard application of early warning and intervention for children with abnormal physical development (19JSZ18).

Conflict of interest

The authors declare that the research was conducted in the absence of any commercial or financial relationships that could be construed as a potential conflict of interest.

Publisher's note

All claims expressed in this article are solely those of the authors and do not necessarily represent those of their affiliated organizations, or those of the publisher, the editors and the reviewers. Any product that may be evaluated in this article, or claim that may be made by its manufacturer, is not guaranteed or endorsed by the publisher.

References

Aarskog, D. (1971). A familial syndrome of short stature associated with facial dysplasia and genital anomalies. *Birth Defects Orig. Artic. Ser.* 7 (6), 235–239.

Balaton, B. P., Dixon-McDougall, T., Peeters, S. B., and Brown, C. J. (2018). The eXceptional nature of the X chromosome. *Hum. Mol. Genet.* 27 (R2), R242–R249. doi:10.1093/hmg/ddy148

Bayat, A., Krett, B., Dunø, M., Torring, P. M., and Vissing, J. (2022). Novel truncating variants in FGD1 detected in two Danish families with Aarskog-Scott syndrome and myopathic features. *Am. J. Med. Genet. A* 188 (7), 2251–2257. doi:10.1002/ajmg.a.62753

Calabrese, G., Licata, G., Buononato, D., Gambardella, A., De Rosa, A., Argenziano, G., et al. (2022). Aarskog-scott syndrome and atopic dermatitis successfully treated with dupilumab: A casual presentation? *Clin. Exp. Dermatol.* 47 (2), 452–453. doi:10.1111/ced.14924

Darendeliler, F., Larsson, P., Neyzi, O., Price, A. D., Hagenas, L., Sipila, I., et al. (2003). Growth hormone treatment in aarskog syndrome: Analysis of the KIGS (pharmacia international growth database) data. *J. Pediatr. Endocrinol. Metab.* 16 (8), 1137–1142. doi:10.1515/jpem.2003.16.8.1137

Daubon, T., Buccione, R., and Génot, E. (2011). The Aarskog-Scott syndrome protein Fgd1 regulates podosome formation and extracellular matrix remodeling in transforming growth factor β-stimulated aortic endothelial cells. *Mol. Cell. Biol.* 31 (22), 4430–4441. doi:10.1128/MCB.05474-11

Escobar, V., and Weaver, D. D. (1978). Aarskog syndrome. New findings and genetic analysis. *Jama* 240 (24), 2638–2641. doi:10.1001/jama.240.24.2638

Fernandez, I., Tsukahara, M., Mito, H., YosHii, H., UchidaM., Matsuo, K., et al. (1994). Congenital heart defects in Aarskog syndrome. *Am. J. Med. Genet.* 50 (4), 318–322. doi:10.1002/ajmg.1320500404

Fryns, J. P. (1992). Aarskog syndrome: The changing phenotype with age. *Am. J. Med. Genet.* 43 (1-2), 420–427. doi:10.1002/ajmg.1320430164

Grier, R. E., Farrington, F. H., Kendig, R., and Mamunes, P. (1983). Autosomal dominant inheritance of the Aarskog syndrome. *Am. J. Med. Genet.* 15 (1), 39–46. doi:10.1002/ajmg.1320150105

Li, J. L., Li, Y. J., Zhang, K. J., Lan, L., Shi, J. G., Yang, X., et al. (2014). No association between FGD1 gene polymorphisms and intellectual developmental disability in the Qinba mountain area. *Genet. Mol. Res.* 13 (1), 127–133. doi:10.4238/2014.January.10.3

Nayak, R. B., Ambika, L., Bhogale, G. S., and Pandurangi, A. (2012). Mania with aarskog-scott syndrome. *Indian Pediatr.* 49 (4), 327–328.

Niida, A., Vonwill, C., and Gillessen-Kaesbach, G., (2014). Two novel mutations confirm FGD1 is responsible for the aarskog syndrome. *Eur. J. HumanGenetics* 8 (11), 869–874.

Orrico, A., Galli, L., Falciani, M., Bracci, M., Cavaliere, M. L., Rinaldi, M. M., et al. (2000). A mutation in the pleckstrin homology (PH) domain of the FGD1 gene in an Italian family with faciogenital dysplasia (Aarskog-Scott syndrome). *FEBS Lett.* 478 (3), 216–220. doi:10.1016/s0014-5793(00)01857-3

Pasteris, N. G., Buckler, J., Cadle, A. B., and Gorski, J. L. (1997). Genomic organization of the faciogenital dysplasia (FGD1; Aarskog syndrome) gene. *Genomics* 43 (3), 390–394. doi:10.1006/geno.1997.4837

Pasteris, N. G., Cadle, A., Logie, L. J., Porteous, M. E., Schwartz, C. E., Stevenson, R. E., et al. (1994). Isolation and characterization of the faciogenital dysplasia (Aarskog-Scott syndrome) gene: A putative rhorac guanine nucleotide exchange factor. *Cell* 79 (4), 669–678. doi:10.1016/0092-8674(94)90552-5

Pavone, P., Marino, S., Maniaci, A., and Cocuzza, S. (2020). Aarskog-scott syndrome: Clinical and molecular characterisation of a family with the coexistence of a novel FGD1 mutation and 16p13.11-p12.3 microduplication. *BMJ Case Rep.* 13 (6), e235183. doi:10.1136/bcr-2020-235183

P´erez-Coria, F., Ozkan, M., Lugo-Trampe, J. J., Rodriguez-Sanchez, I. P., Lugo-Trampe, A., Fuente-Cortez, B., et al. (2015). Identification of novel mutations in Mexican patients with Aarskog–Scott syndrome. *Mol. Genet. Genomic Med.* 3 (3), 197–202. doi:10.1002/mgg3.132

Scott, C. I., and Moyer, F. G. (1971). Focal dermal hypoplasia (goltz syndrome): A follow-up. *Birth Defects Orig. Artic. Ser.* 7 (6), 240–241.

Wang, Q., Chen, P., Liu, J., Lou, J., Liu, Y., Yuan, H., et al. (2020). Xp11.22 duplications in four unrelated Chinese families: Delineating the genotype-phenotype relationship for HSD17B10 and FGD1. *BMC Med. Genomics* 13 (1), 66. doi:10.1186/s12920-020-0728-8

Zanetti, D. V., Sousa, S. L., Sousa, S. C., Oliveira, V. A. L., de Assis, E. M., Campos, R. M., et al. (2021). The prevalence of clinical features in patients with aarskog-scott syndrome and assessment of genotype-phenotype correlation: A systematic review. *Genet. Res.* 2021, 6652957. doi:10.1155/2021/6652957

Zielinski, J. A., and Pack, L. L. (2008). Bilateral anterior hip dislocation in a child with aarskog syndrome: A case report. *J. Pediatr. Orthop.* 28 (7), 729–732. doi:10.1097/BPO.0b013e3181845700

Zou, W., Greenblatt, M. B., Shim, J. H., Kant, S., Zhai, B., Lotinun, S., et al. (2011). MLK3 regulates bone development downstream of the faciogenital dysplasia protein FGD1 in mice. *J. Clin. Invest.* 121 (11), 4383–4392. doi:10.1172/JCI59041

frontiers | Frontiers in Pediatrics

TYPE Case Report
PUBLISHED 26 August 2022
DOI 10.3389/fped.2022.997274

Check for updates

OPEN ACCESS

EDITED BY
Mike Mikailov,
United States Food and Drug Administration, United States

REVIEWED BY
Craig Blackstone,
National Institute of Neurological Disorders and Stroke (NIH), United States
Lingchi Kong,
Shanghai Jiao Tong University, China

*CORRESPONDENCE
Senjie Du
sjdusjn@126.com
Xiaoke Zhao
xiaokezhao@vip.163.com

†These authors have contributed equally to this work

SPECIALTY SECTION
This article was submitted to Genetics of Common and Rare Diseases, a section of the journal Frontiers in Pediatrics

RECEIVED 18 July 2022
ACCEPTED 10 August 2022
PUBLISHED 26 August 2022

CITATION
Xu X, Lu F, Du S, Zhao X, Li H, Zhang L and Tang J (2022) Case report: Novel compound heterozygous missense mutations in the *DDHD2* gene in a Chinese patient associated with spastic paraplegia type 54. *Front. Pediatr.* 10:997274. doi: 10.3389/fped.2022.997274

COPYRIGHT
© 2022 Xu, Lu, Du, Zhao, Li, Zhang and Tang. This is an open-access article distributed under the terms of the Creative Commons Attribution License (CC BY). The use, distribution or reproduction in other forums is permitted, provided the original author(s) and the copyright owner(s) are credited and that the original publication in this journal is cited, in accordance with accepted academic practice. No use, distribution or reproduction is permitted which does not comply with these terms.

Case report: Novel compound heterozygous missense mutations in the *DDHD2* gene in a Chinese patient associated with spastic paraplegia type 54

Xin Xu†, Fen Lu†, Senjie Du*, Xiaoke Zhao*, Hongying Li, Li Zhang and Jian Tang

Department of Rehabilitation, Children's Hospital of Nanjing Medical University, Nanjing, China

Background: Spastic paraplegia type 54 (SPG54) is a rare inherited autosomal recessive disorder, and a complex hereditary spastic paraplegia (HSP) caused by mutations in the phospholipase *DDHD2* gene. SPG54 is characterized by early onset of spastic paraplegia, intellectual disability and dysplasia of corpus callosum.

Case presentation: We report a 9 years and 5 months old Chinese girl with progressive spasm of the lower limbs, muscle weakness and intellectual disability. Brain magnetic resonance imaging (MRI) showed periventricular leukomalacia and thinning of the corpus callosum. According to the Wechsler Intelligence Scale, her IQ is 42. By whole exome sequencing, novel compound heterozygous missense mutations in the *DDHD2* gene [c.168G>C, p.(Trp56Cys) and c.1505T>C, p.(Phe502Ser)] were identified in the proband. Comparative amino acid sequence alignment across different species revealed that Trp56 and Phe502 in the DDHD2 protein were highly conserved during evolution. And multiple *in silico* prediction tools suggested that both mutations were deleterious.

Conclusions: Our study reports a very rare case of complicated HSP caused by two novel compound heterozygous mutations in the *DDHD2* gene. Our findings expand the genetic spectrum of SPG54.

KEYWORDS

spastic paraplegia, DDHD2, compound heterozygous mutations, intellectual disability, children

10.3389/fped.2022.997274

Introduction

Hereditary spastic paraplegia (HSP) is a group of neurodegenerative monogenic diseases characterized by progressive spasticity and weakness of the lower limbs (1, 2). HSP can be divided into pure subtype and complex subtype according to clinical manifestations. The pure subtype presents only with spastic paraplegia, while the complex subtype has additional neurological symptoms, including intellectual disability, ataxia, optic atrophy, peripheral neuropathy and epilepsy. In addition, HSP shows high genetic heterogeneity. At present, more than 80 monogenic causes have been identified, with inheritance patterns including autosomal recessive, autosomal dominant, X-linked and mitochondrial inheritance (3).

Spastic paraplegia type 54 (SPG54, OMIM: 615033) is a complicated HSP characterized by early onset progressive spasm of lower limbs, accompanied with intellectual disability. Other clinical symptoms include short stature, strabismus, ataxia, optic dysplasia, dysphonia and microcephaly (4). Brain magnetic resonance imaging (MRI) often shows corpus callosum dysplasia and non-specific periventricular white matter lesions. SPG54 is caused by mutations in the *DDHD2* gene (OMIM: 615003) on chromosome 8p11.23 (5). *DDHD2* encodes a phospholipase, which is a member of the intracellular phospholipase A_1 ($iPLA_1$) protein family (DDHD1, DDHD2, and SEC23IP). The DDHD2 protein plays a crucial role in organelle biogenesis and membrane trafficking between the endoplastic reticulum and the Golgi body (6, 7). Here, we report a Chinese case with SPG54 who carried novel compound heterozygous missense mutations in the *DDHD2* gene.

Case presentation

Clinical examination

The proband was a 9 years and 5 months old Chinese girl who was admitted to our Department of Rehabilitation due to abnormal walking posture. She was born at term by spontaneous vaginal delivery and was the first child of healthy and non-consanguineous Chinese parents. She weighed 3 kg at birth and had an Apgar score of 10. She was able to sit unsupported around the age of 8 months and crawl at the age of 1. She can walk independently at the age of 2. But at the age of 4, she gradually showed signs of increased muscle tone and gait impairment. Her most obvious clinical symptom was "toe-walking," often falling when walking fast. She can't walk long distances and go upstairs as before. And she also had intellectual disability with poor language expression, slow response, attention deficit and poor grades in school. When the girl was admitted to our department for careful examination at the age of 9 years and 5 months, the physical examination revealed a weight of 35 kg (50th to 75th percentile), a height of 128 cm (10th to 25th percentile) and a head circumference of 51 cm (25th to 50th percentile). The girl was non-dysmorphic, and clinically assessed as increased muscle tension of lower limbs, hyperreflexia of the tendons, limited dorsiflexion of both ankles. The results of her blood counts and thyroid profile were normal, as were liver function tests, renal function tests and blood metabolic screen by mass spectrometry. Electroencephalogram (EEG) result was normal. On ophthalmological assessment, there was no sign of optic atrophy. Brain magnetic resonance imaging showed dysgenesis of the corpus callosum (Figure 1A) and periventricular leukomalacia (Figure 1B). The Wechsler Intelligence Scale for Children-Revised (WISC-R) had an IQ of 42, indicating severe intellectual disability. A detailed study of the family history showed that no family members exhibited HSP phenotypes. And no neurological symptom was observed in the parents. They exhibited normal intelligence and walked without abnormal posture. The proband has a 3-year-old sister with normal intelligence and motor development.

Genetic testing

After approval by the Ethics Committee of Children's Hospital of Nanjing Medical University, 2 mL of peripheral venous blood was extracted from the proband and her family members, including her parents and sister. Genomic DNA was extracted by a DNA extraction kit (Qiagen, Shanghai, China). The DNA library was constructed, and the exomes were captured by xGen® Exome Research Panel v1.0 probe (Integrated Device Technology, USA). The enriched libraries were analyzed on the NovaSeq 6000 Sequencing platform (Illumina, USA). Sequencing reads were mapped to the GRCh37/hg19 reference genome via BWA software. Then candidate genetic variants in exons and

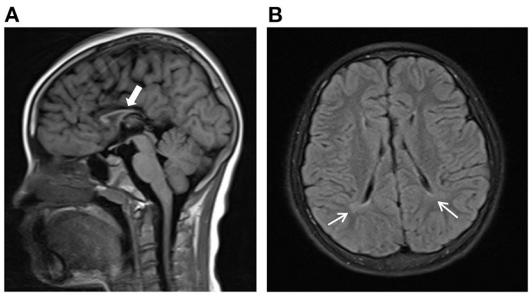


FIGURE 1
Brain magnetic resonance imaging (MRI) findings of the proband. **(A)** Dysgenesis of the corpus callosum from sagittal view shown on axial T1-weighted images. **(B)** Periventricular white matter hyperintense lesions on FLAIR images.

canonical splice sites (±2 bp) were picked up with a minor allele frequency <0.005 using the ExAC database (http://exac.broadinstitute.org/), dbSNP (http:// http://gnomad-sg.org/), and 1000 Genomes Project (http://www.1000genomes.org/). Functional prediction and pathogenicity analysis were performed using bioinformatics software. Potential mutations identified by whole-exome sequencing were validated by Sanger sequencing. Suspicious mutations were assessed according to American College of Medical Genetics and Genomics (ACMG) guidelines. Furthermore, we used the online server, ChimeraX (http://www.cgl.ucsf.edu/chimerax//) for analysis to construct the three-dimensional structure of DDHD2.

Genetic analysis revealed that the proband had two heterozygous missense mutations in the *DDHD2* gene (Genbank association number: NM_015214), exon 2 c.168G>C (p.Trp56Cys) and exon 13 c.1505T>C (p.Phe502Ser). Sanger sequencing confirmed that her mother and sister carried the c.168G>C (p.Trp56Cys) mutation and her father carried the c.1505T>C (p.Phe502Ser) mutation (Figures 2A,B). Comparative amino acid sequence alignment of DDHD2 across different species revealed that the affected amino acids 56 (tryptophan) and 502 (phenylalanine) are highly conserved (Figure 3A). Furthermore, these two *DDHD2* mutations were not found in ExAC, dbSNP and 1000 Genomes Project databases. The altered amino residues 56 (tryptophan) and 502 (phenylalanine) in the proband are located in the WWE and DDHD domains, respectively (Figure 3B). The two missense changes yielded predominantly deleterious prediction scores by multiple *in silico* prediction tools (SIFT, PolyPhen-2, MutationTaster, Provean and REVEL), and the analysis suggested that these two mutations were predicted to be pathogenic (Table 1).

Three-dimensional structural modeling of the DDHD2 protein showed that the mutations did not change the hydrogen bonding in protein, but both mutations resulted in changes in side chain size and space ratio compared with the wild type (Figure 3C), which might lead to changes in the conformation of the DDHD2 protein. Videos of the three-dimensional structure of wild type and mutant DDHD2 can be found in the Supplementary material. Based on the above, these two compound heterozygous mutations could be the molecular basis for SPG54 in this case.

Discussion and conclusion

SPG54 is a rare autosomal recessive neurological disorder characterized by progressive early-onset spasticity, intellectual

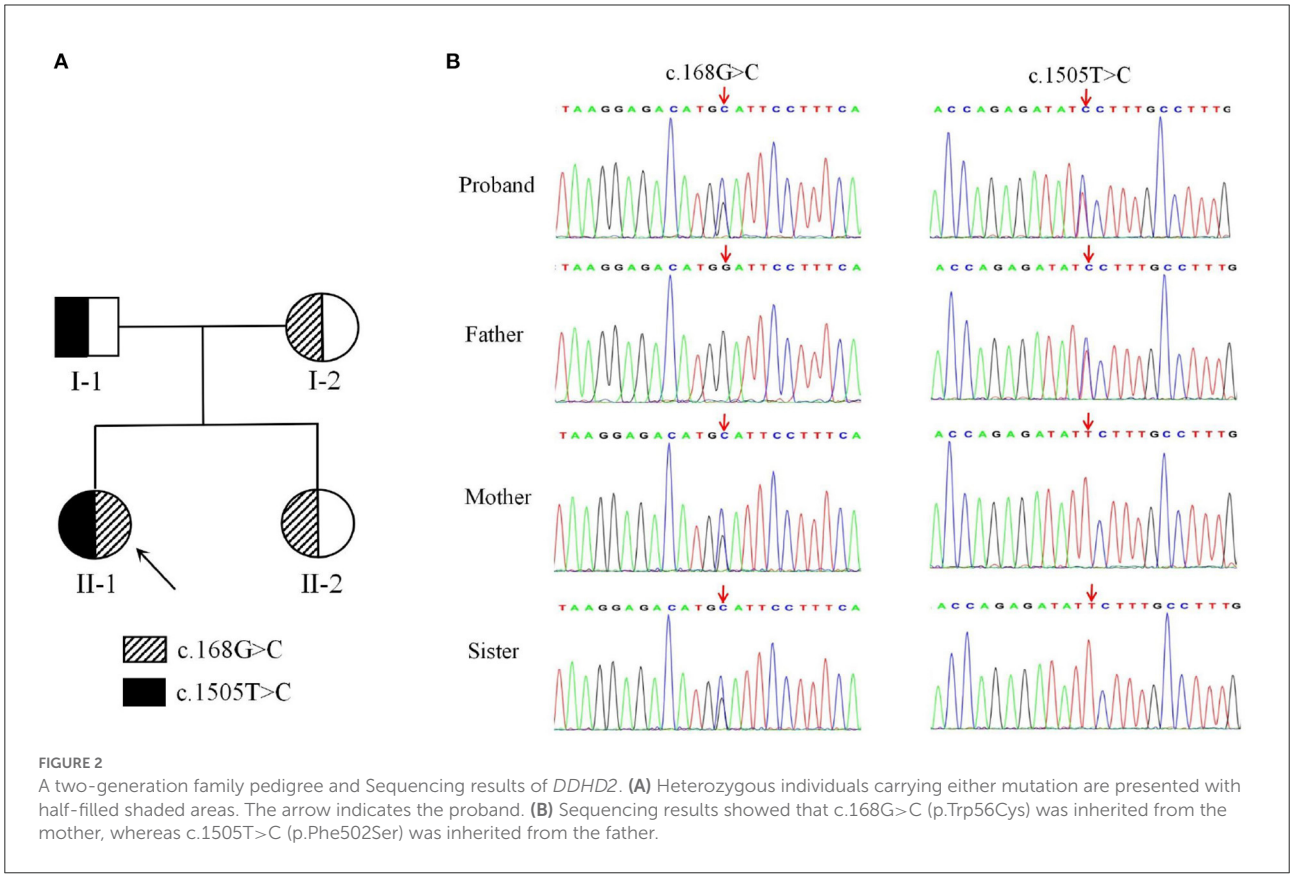


FIGURE 2
A two-generation family pedigree and Sequencing results of *DDHD2*. **(A)** Heterozygous individuals carrying either mutation are presented with half-filled shaded areas. The arrow indicates the proband. **(B)** Sequencing results showed that c.168G>C (p.Trp56Cys) was inherited from the mother, whereas c.1505T>C (p.Phe502Ser) was inherited from the father.

10.3389/fped.2022.997274

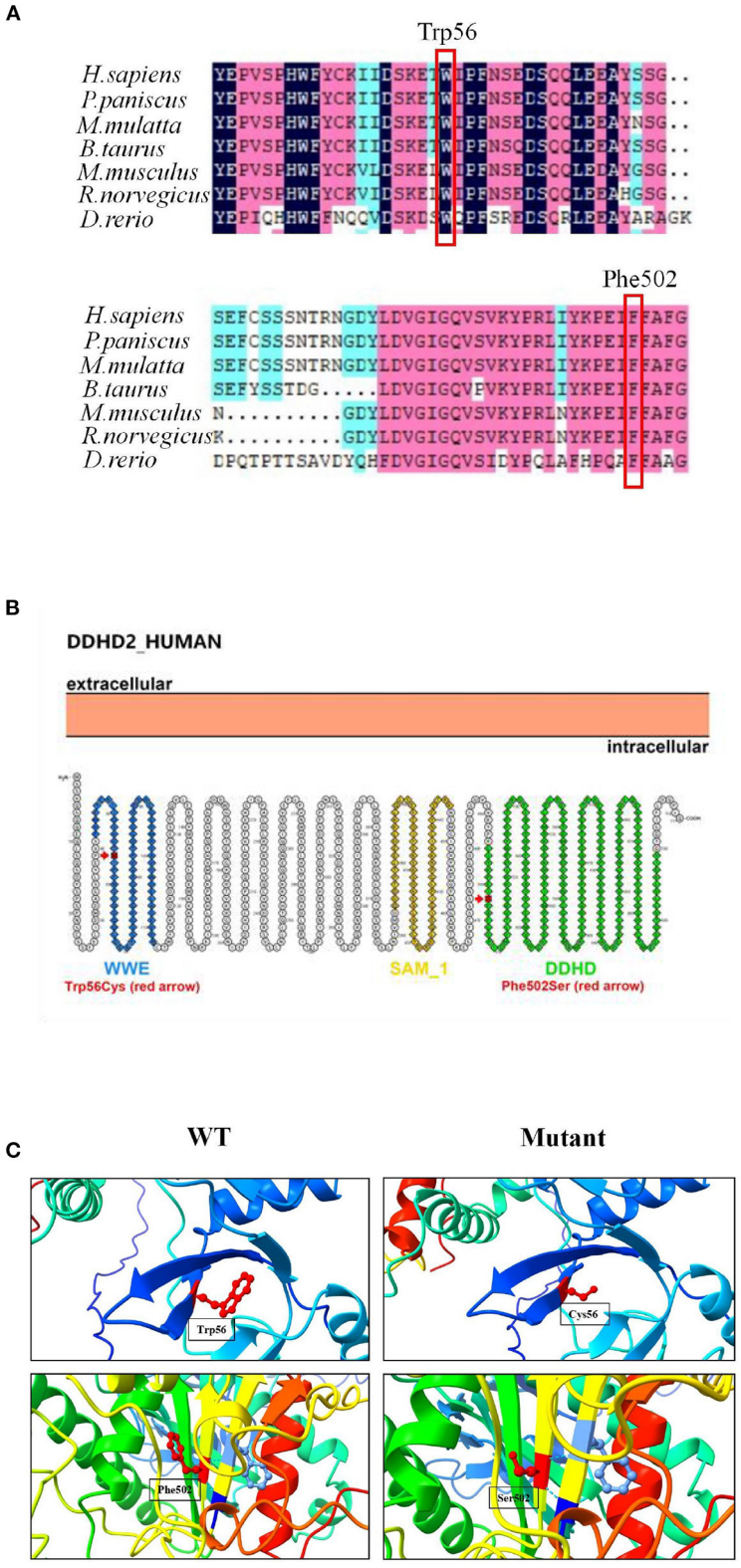


FIGURE 3
Mutation analysis of *DDHD2*. **(A)** Amino acid sequence alignment of DDHD2 from different species. Mutant amino acids 56 (tryptophan) and 502 (phenylalanine) are highly conserved across species. **(B)** Secondary structure diagram of DDHD2 protein. The p.Trp56Cys mutation located in the WWE domain and the p.Phe502Ser mutation located in the DDHD2 domain. **(C)** Protein molecular models of wild type (WT) and mutant DDHD2 protein (Mutant).

TABLE 1 Evaluation of the *DDHD2* mutations identified in this study.

DDHD2 mutation	CytoBand	Position	SIFT score	Polyphen-2	MutationTaster	Provean score	REVEL score	Novel/reported
c.168G>C,	8p11.23	38090680	0	1.0	1	−12.34	0.729	Novel
						(<-1.3)	(>0.5)	
p.Trp56Cys			Damaging	Probably damaging	Disease causing	Deleterious	Deleterious	
c.1505T>C,	8p11.23	38109693	0	0.995	1	−6.88	0.757	Novel
						(<-1.3)	(>0.5)	
p.Phe502Ser			Damaging	Probably damaging	Disease causing	Deleterious	Deleterious	

TABLE 2 *DDHD2* mutations associated with SPG54.

Number	Gene	Clinical phenotypes	Nucleotide change	Amino acid change	Mutation type	References
1	*DDHD2*	SPG54	c.400C>T	p.Gln134*	Nonsense	Travaglini et al. (2)
2	*DDHD2*	SPG54	1125+1G>T	–	Canonical-splice	Kumar et al. (3)
3	*DDHD2*	SPG54	c.2057delA	p.Glu686Glyfs*35	Frameshift	Schuurs-Hoeijmakers et al. (4) Schuurs-Hoeijmakers et al. (14)
4	*DDHD2*	SPG54	c.1803dupT	p.Thr602Ilefs*18	Frameshift	Schuurs-Hoeijmakers et al. (4)
5	*DDHD2*	SPG54	c.1386dupC	p.Ile463Hisfs*6	Frameshift	Schuurs-Hoeijmakers et al. (4)
6	*DDHD2*	SPG54	c.1546C>T	p.Arg516*	Nonsense	Schuurs-Hoeijmakers et al. (4)
7	*DDHD2*	SPG54	c.859C>T	p.Arg287*	Nonsense	Schuurs-Hoeijmakers et al. (4) Alrayes et al. (13)
8	*DDHD2*	SPG54	c.1978G>C	p.Asp660His	Missense	Schuurs-Hoeijmakers et al. (4) Magariello et al. (8) Citterio et al. (9)
9	*DDHD2*	SPG54	c.1982_1983delAT	p.Tyr661Cysfs*8	Frameshift	Gonzalez et al. (5)
10	*DDHD2*	SPG54	c.307T>C	p.Trp103Arg	Missense	Magariello et al. (8)
11	*DDHD2*	SPG54	c.334C>T	p.Arg112*	Nonsense	Nicita et al. (10)
12	*DDHD2*	SPG54	c.589G>A	p.Gly197Arg	Missense	Nicita et al. (10)
13	*DDHD2*	SPG54	c.2096A>G	p.Tyr699Cys	Missense	Nicita et al. (10)
14	*DDHD2*	SPG54	c.806C>T	p.Pro269Leu	Missense	Nicita et al. (10)
15	*DDHD2*	SPG54	c.942delC	p.Thr314*	Frameshift	Nicita et al. (10)
16	*DDHD2*	SPG54	c.340_342dupACG	–	Inframe	Nicita et al. (10)
17	*DDHD2*	SPG54	c.340dupA	p.Thr114Asnfs*11	Frameshift	Nicita et al. (10)
18	*DDHD2*	SPG54	c.658G>T	p.Val220Phe	Missense	Doi et al. (11)
19	*DDHD2*	SPG54	1057+5C>G	–	Canonical-splice	Novarino et al. (12) Thabet et al. (15)
20	*DDHD2*	SPG54	c.297T>A	p.Tyr99*	Nonsense	Dong et al. (16)
21	*DDHD2*	SPG54	c.335G>A	p.Arg112Gln	Missense	Dong et al. (16)
22	*DDHD2*	SPG54	c.292C>T	p.Arg98Trp	Missense	Salinas et al. (17)
23	*DDHD2*	SPG54	c.759delT	p.Phe253Leufs*13	Frameshift	D'Amore et al. (18)
24	*DDHD2*	SPG54	c.38delA	p.Gln13Argfs*16	Frameshift	D'Amore et al. (18)
25	*DDHD2*	SPG54	c.168G>C	p.Trp56Cys	Missense	Our present study
26	*DDHD2*	SPG54	c.1505T>C	p.Phe502Ser	Missense	Our present study

* means termination codon.

disability, short stature and dysplasia of corpus callosum. To date, only about 40 patients have been reported all over the world (2–5, 8–18). The phenotypic of our proband is consistent with the characteristic clinical manifestations of SPG54. About 85% of patients with SPG54 develop relevant symptoms before the age of 5. Typical brain MRI manifestations of SPG54 patients are thin corpus callosum and periventricular white matter lesions. Further examination of brain magnetic resonance spectroscopy (MRS) in patients with SPG54 showed abnormal lipid peaks, with the highest intensity around the basal ganglia and thalamus, indicating abnormal lipid accumulation in the brain (11, 12).

The *DDHD2* gene is the only known pathogenic gene for SPG54. It contains 22 exons and encodes a protein composed of 711 amino acids. DDHD2 protein belongs to the phospholipase A1 family. *In vitro* experiments showed that DDHD2 protein has the catalytic activity of phospholipase A1, which can hydrolyze the ester bond on sn-1 with phospholipid acid as substrate. Studies have showed that DDHD2 was a principal triacylglycerol (TAG) lipase in the nervous system as well (19). *DDHD2* is highly expressed in the human central nervous system (CNS), especially in the occipital cortex, cerebellum, and hippocampus. However, the physiological function of DDHD2, particularly in the brain, is not fully understood. The relationship between DDHD2 protein and synaptic transmission and synaptic plasticity has been discovered in recent years, and it has been reported that the loss of DDHD2 function will affect neurocognitive function (19). Inhibition of *DDHD2* expression in the Drosophila CNS resulted in a decrease in the number of presynaptic active areas and the expression of bruchpilot protein (4). Mutations in the *DDHD2* gene can cause SPG54, with spastic weakness of the lower extremities and intellectual disability. Recent studies showed that *DDHD2* knockout (KO) mice develop motor and cognitive impairments and accumulation of lipid droplets in neurons in the brain (20), which was consistent with the abnormal lipid peak in MRS examination of SPG54 patients. The results indicate that *DDHD2* is involved in lipid pathway and plays an important role in the enzymatic metabolism of lipid droplets. In addition, it has been found that *DDHD2* KO mouse embryonic fibroblasts tend to apoptosis, and the loss of DDHD2 function promotes the production of reactive oxygen species (ROS) in mitochondria, thus accelerating cell apoptosis (21). These results may provide clues to the pathogenesis of SPG54.

Until now, approximately 30 *DDHD2* mutations have been reported in Human Gene Mutation Database (HGMD) and literature, among which truncating mutations and missense mutations are the most common. And the information related to the reported *DDHD2* mutations is shown in Table 2. The DDHD2 protein contains WWE domain, GxSxG lipase motif, sterile-alpha-motif (SAM) domain and DDHD2 domain. And most *DDHD2* mutations reported are located in SAM and DDHD2 domains, and a few are located in WWE domain. The missense mutation of the highly conserved DDHD2 domain, p.Asp660His, was reported in five families, which is a hotspot missense mutation (4, 8, 9). Studies have demonstrated that SAM and DDHD2 domains play a significant role in binding phosphoinositol 4-phosphate and affecting phospholipase activity (7). Three missense mutations (p.Trp103Arg, p.Asp660His and p.Val220Phe) have been previously verified *in vitro* experiments, suggesting that the mutant proteins significantly reduce the phospholipase activity (11, 20). In our study, the mother and sister of the proband carried c.168G>C (p.Trp56Cys) mutation in *DDHD2*, and the father carried c.1505T>C (p.Phe502Ser) mutation in *DDHD2*. Compound heterozygous mutations containing both the maternal and paternal mutations were detected in the proband. And these two missense mutations were predicted to be pathogenic by different bioinformatics softwares and have not been reported previously. In this family, only the proband presented SPG54-related clinical phenotypes. The parents and sister were heterozygous carriers of the *DDHD2* gene, but were healthy. Thus, we concluded that the *DDHD2* compound heterozygous mutations were causative mutations for SPG54. However, further experiments are needed to investigate the function of these two mutations *in vitro* or in animal models.

In conclusion, we describe two novel compound heterozygous missense mutations in the *DDHD2* gene in a Chinese patient associated with SPG54. Through whole-exome sequencing and analysis, the newfound missense mutations enrich the *DDHD2* mutation spectrum and provide a genetic basis for clinical diagnosis.

Data availability statement

The original contributions presented in the study are included in the article/Supplementary material, further inquiries can be directed to the corresponding author/s.

Ethics statement

The studies involving human participants were reviewed and approved by Ethics Committee of Children's Hospital of Nanjing Medical University. Written informed consent to participate in this study was provided by the participants' legal guardian/next of kin. Written informed consent was obtained from the minor(s)' legal guardian/next of kin for the publication of any potentially identifiable images or data included in this article.

Author contributions

XX carried out the molecular genetic studies and drafted the manuscript. FL and LZ performed the clinical data. HL and JT assisted with finding some of the research studies. SD and XZ supervised this research and critically reviewed the

manuscript. All authors contributed to the article and approved the submitted version.

Funding

This work was supported by Science and Technology Development Fund of Nanjing Medical University (No. NMUB2020091).

Acknowledgments

The authors thank the patient who participated in this article.

Conflict of interest

The authors declare that the research was conducted in the absence of any commercial or financial relationships that could be construed as a potential conflict of interest.

Publisher's note

All claims expressed in this article are solely those of the authors and do not necessarily represent those of their affiliated organizations, or those of the publisher, the editors and the reviewers. Any product that may be evaluated in this article, or claim that may be made by its manufacturer, is not guaranteed or endorsed by the publisher.

Supplementary material

The Supplementary Material for this article can be found online at: https://www.frontiersin.org/articles/10.3389/fped.2022.997274/full#supplementary-material

References

1. Lo Giudice T, Lombardi F, Santorelli FM, Kawarai T, Orlacchio A. Hereditary spastic paraplegia: clinical-genetic characteristics and evolving molecular mechanisms. *Exp Neurol.* (2014) 261:518–39. doi: 10.1016/j.expneurol.2014.06.011

2. Travaglini L, Aiello C, Stregapede F, D'Amico A, Alesi V, Ciolfi A, et al. The impact of next-generation sequencing on the diagnosis of pediatric-onset hereditary spastic paraplegias: new genotype–phenotype correlations for rare HSP-related genes. *Neurogenetics.* (2018) 19:111–21. doi: 10.1007/s10048-018-0545-9

3. Kumar KR, Wali GM, Kamate M, Wali G, Minoche AE, Puttick C, et al. Defining the genetic basis of early onset hereditary spastic paraplegia using whole genome sequencing. *Neurogenetics.* (2016) 17:265–70. doi: 10.1007/s10048-016-0495-z

4. Schuurs-Hoeijmakers JH, Geraghty MT, Kamsteeg EJ, Ben-Salem S, de Bot ST, Nijhof B, et al. Mutations in *DDHD2*, encoding an intracellular phospholipase A(1), cause a recessive form of complex hereditary spastic paraplegia. *Am J Hum Genet.* (2012) 91:1073–81. doi: 10.1016/j.ajhg.2012.10.017

5. Gonzalez M, Nampoothiri S, Kornblum C, Oteyza AC, Walter J, Konidari I, et al. Mutations in phospholipase *DDHD2* cause autosomal recessive hereditary spastic paraplegia (SPG54). *Eur J Hum Genet.* (2013) 21:1214–18. doi: 10.1038/ejhg.2013.29

6. Sato S, Inoue H, Kogure T, Tagaya M, Tani K. Golgi-localized KIAA0725p regulates membrane trafficking from the Golgi apparatus to the plasma membrane in mammalian cells. *FEBS Lett.* (2010) 584:4389–95. doi: 10.1016/j.febslet.2010.09.047

7. Inoue H, Baba T, Sato S, Ohtsuki R, Takemori A, Watanabe T, et al. Roles of SAM and DDHD domains in mammalian intracellular phospholipase A1 KIAA0725p. *Biochim Biophys Acta.* (2012) 1823:930–39. doi: 10.1016/j.bbamcr.2012.02.002

8. Magariello A, Citrigno L, Zuchner S, Gonzalez M, Patitucci A, Sofia V, et al. Further evidence that *DDHD2* gene mutations cause autosomal recessive hereditary spastic paraplegia with thin corpus callosum. *Eur J Neurol.* (2014) 21:e25–6. doi: 10.1111/ene.12305

9. Citterio A, Arnoldi A, Panzeri E, D'Angelo MG, Filosto M, Dilena R, et al. Mutations in *CYP2U1*, *DDHD2* and *GBA2* genes are rare causes of complicated forms of hereditary spastic paraparesis. *J Neurol.* (2014) 261:373–81. doi: 10.1007/s00415-013-7206-6

10. Nicita F, Stregapede F, Tessa A, Bassi MT, Jezela-Stanek A, Primiano G, et al. Defining the clinical-genetic and neuroradiological features in SPG54: description of eight additional cases and nine novel *DDHD2* variants. *J Neurol.* (2019) 266:2657–64. doi: 10.1007/s00415-019-09466-y

11. Doi H, Ushiyama M, Baba T, Tani K, Shiina M, Ogata K, et al. Late-onset spastic ataxia phenotype in a patient with a homozygous *DDHD2* mutation. *Sci Rep.* (2014) 4:7132. doi: 10.1038/srep07132

12. Novarino G, Fenstermaker AG, Zaki MS, Hofree M, Silhavy JL, Heiberg AD, et al. Exome sequencing links corticospinal motor neuron disease to common neurodegenerative disorders. *Science.* (2014) 343:506–11. doi: 10.1126/science.1247363

13. Alrayes N, Mohamoud HS, Jelani M, Ahmad S, Vadgama N, Bakur K, et al. Truncating mutation in intracellular phospholipase A1 gene (*DDHD2*) in hereditary spastic paraplegia with intellectual disability (SPG54). *BMC Res Notes.* (2015) 8:271. doi: 10.1186/s13104-015-1227-4

14. Schuurs-Hoeijmakers JH, Vulto-van Silfhout AT, Vissers LE, van de Vondervoort II, van Bon BW, de Ligt J, et al. Identification of pathogenic gene variants in small families with intellectually disabled siblings by exome sequencing. *J Med Genet.* (2013) 50:802–11. doi: 10.1136/jmedgenet-2013-101644

15. Thabet F, Tlili-Graiess K, Tabarki B. Distinct neuroimaging features of *DDHD2* gene-related spastic paraplegia, a mimicker of cerebral palsy. *Arch Dis Child.* (2020) 105:482. doi: 10.1136/archdischild-2018-316484

16. Dong EL, Wang C, Wu S, Lu YQ, Lin XH, Su HZ, et al. Clinical spectrum and genetic landscape for hereditary spastic paraplegias in China. *Mol Neurodegen.* (2018) 13:36. doi: 10.1186/s13024-018-0269-1

17. Salinas V, Vega P, Marsili L, Pérez-Maturo J, Martínez N, Zavala L, et al. The odyssey of complex neurogenetic disorders: from undetermined to positive. *Am J Med Genet C Semin Med Genet.* (2020) 184:876–84. doi: 10.1002/ajmg.c.31848

18. D'Amore A, Tessa A, Casali C, Dotti MT, Filla A, Silvestri G, et al. Next generation molecular diagnosis of hereditary spastic paraplegias: an Italian cross-sectional study. *Front Neurol.* (2018) 9:981. doi: 10.3389/fneur.2018.00981

19. Inloes JM, Hsu KL, Dix MM, Viader A, Masuda K, Takei T, et al. The hereditary spastic paraplegia-related enzyme DDHD2 is a principal brain triglyceride lipase. *Proc Natl Acad Sci USA.* (2014) 111:14924–9. doi: 10.1073/pnas.1413706111

20. Inloes JM, Hsu KL, Dix MM, Viader A, Masuda K, Takei T, et al. Functional contribution of the spastic paraplegia-related triglyceride hydrolase DDHD2 to the formation and content of lipid droplets. *Biochemistry.* (2018) 57:827–38. doi: 10.1021/acs.biochem.7b01028

21. Maruyama T, Baba T, Maemoto Y, Hara-Miyauchi C, Hasegawa-Ogawa M, Okano HJ, et al. Loss of *DDHD2*, whose mutation causes spastic paraplegia, promotes reactive oxygen species generation and apoptosis. *Cell Death Dis.* (2018) 9:797. doi: 10.1038/s41419-018-0815-3

frontiers | Frontiers in Genetics

ORIGINAL RESEARCH
published: 26 August 2022
doi: 10.3389/fgene.2022.883398

Detection of a Cryptic 25 bp Deletion and a 269 Kb Microduplication by Nanopore Sequencing in a Seemingly Balanced Translocation Involving the LMLN and LOC105378102 Genes

*Yanan Wang, Zhenhua Zhao, Xinyu Fu, Shufang Li, Qiuyan Zhang and Xiangdong Kong**

Genetic and Prenatal Diagnosis Center, Department of Obstetrics and Gynecology, the First Affiliated Hospital of Zhengzhou University, Zhengzhou, China

Preimplantation genetic testing plays a critical role in enabling a balanced translocation carrier to obtain the normal embryo. Identifying the precise breakpoints for the carriers with phenotypic abnormity, allows us to reveal disrupted genes. In this study, a seemingly balanced translocation 46, XX, t (3; 6) (q29; q26) was first detected using conventional karyotype analysis. To locate the precise breakpoints, whole genomes of DNA were sequenced based on the nanopore GridION platform, and bioinformatic analyses were further confirmed by polymerase-chain-reaction (PCR) and copy number variation (CNV). Nanopore sequencing results were consistent with the karyotype analysis. Meanwhile, two breakpoints were successfully validated using polymerase-chain-reaction and Sanger Sequencing. LOC105378102 and LMLN genes were disrupted at the breakpoint junctions. Notably, observations found that seemingly balanced translocation was unbalanced due to a cryptic 269 kilobases (Kb) microduplication and a 25 bp deletion at the breakpoints of chromosome (chr) 6 and chr 3, respectively. Furthermore, 269 Kb microduplication was also confirmed by copy number variation analyses. In summary, nanopore sequencing was a rapid and direct method for identifying the precise breakpoints of a balanced translocation despite low coverage (3.8×). In addition, cryptic deletion and duplication were able to be detected at the single-nucleotide level.

Keywords: balanced translocation, nanopore sequencing, cryptic duplication, deletion, karyotype analysis, CNV

OPEN ACCESS

Edited by:
Zhichao Liu,
National Center for Toxicological Research (FDA), United States

Reviewed by:
Enrique Medina-Acosta,
State University of the North Fluminense Darcy Ribeiro, Brazil
Alexej Abyzov,
Mayo Clinic, United States

****Correspondence:***
Xiangdong Kong
kongxd@263.net

Specialty section:
This article was submitted to Genetics of Common and Rare Diseases, a section of the journal Frontiers in Genetics

Received: *25 February 2022*
Accepted: *07 June 2022*
Published: *26 August 2022*

Citation:
Wang Y, Zhao Z, Fu X, Li S, Zhang Q and Kong X (2022) Detection of a Cryptic 25 bp Deletion and a 269 Kb Microduplication by Nanopore Sequencing in a Seemingly Balanced Translocation Involving the LMLN and LOC105378102 Genes. Front. Genet. 13:883398. doi: 10.3389/fgene.2022.883398

INTRODUCTION

Balanced translocation is a kind of common chromosomal rearrangement. After two chromosomes are broken, they exchange genetic materials with each other to form two new derived chromosomes. Most balanced translocations have no serious influences on gene expression and development because the total number of genes does not change. The incidence of balanced translocation in the population is 0.2%, but for patients with a history of recurrent miscarriages, the incidence is increased to 2.2% (Mackie Ogilvie and Scriven, 2002). Generally, carriers have a normal phenotype, but they are at high risk of facing reproductive problems such as infertility, miscarriage, and unbalanced gametes. In the meiosis process, two translocated chromosomes will form quadrivalent, which may produce 18 gamete types depending on the way they are separated. Only one type is perfectly normal, and one is a balanced translocation carrier.

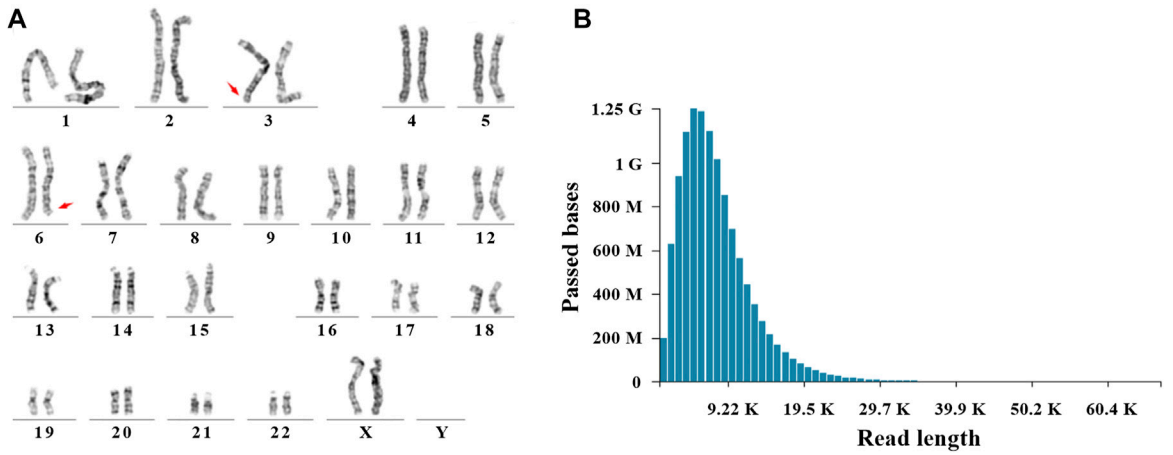


FIGURE 1 | Cytogenetic analysis and Nanopore sequencing. **(A)** A balanced translocation between chr 3 and chr 6 was shown by G-banded karyotype. Red arrows indicated the breakpoints (q29 of chr 3 and q26 of chr 6). **(B)** Read length and passed bases were displayed.

The most common method to detect the balanced translocation is known as the G-banded karyotype analysis, this method can detect the chromosomal structural variation with a resolution of 5–10 megabases (Mb) (Talkowski et al., 2012). Karyotype analysis is the most cost-effective means for balanced translocation, and still cannot be displaced by other technologies (Wilch and Morton, 2018). It is also unable to readily distinguish between similar banding patterns and sizes (Dong et al., 2018a; Dong et al., 2018b). Fluorescence *in situ* hybridization (FISH) is another widely used technology that targets specific genes or locations with a resolution of <1 Mb. The limitation is that probe design is complex and time-consuming (Beyazyurek et al., 2010; Fiorentino et al., 2010). With the development of sequencing technology, low coverage mate-pair whole genome sequencing (WGS) as a complement to conventional karyotype analysis is used for defining precise breakpoints. Talkowski et al. discovered that a breakpoint directly disrupted the CHD7 gene, a causal locus in the CHARGE syndrome (Talkowski et al., 2012). There have been many similar studies in the past decade. Following microdissecting junction region and next-generation sequencing (Jancuskova et al., 2013), Hu et al. combined single-nucleotide polymorphism (SNP) linkage analyses with long-range PCR to identify the carrier and normal embryos, and prenatal diagnosis for fetuses confirmed the feasibility of this strategy (Hu et al., 2016). With the successful application of SNP microarray, several teams have detected embryo biopsy samples for the translocation carrier, this is an indirect and efficient method to distinguish the normal and carrier embryos based on haplotype phasing. However, a translocation carrier's family member or unbalanced embryos are required as a reference to obtain the SNP genotype (Idowu et al., 2015; Treff et al., 2016; Yao et al., 2016; Xu et al., 2017; Zhang et al., 2017; Li et al., 2021). Moreover, the identification of precise breakpoints often requires multiple methods due to technique restrictions. Recently, Wang et al. used a single-molecule optimal mapping technology with the Bionano platform to identify nine balanced reciprocal translocations. Breakpoint regions were finely mapped to small regions of approximately 10 Kb (Wang et al., 2020). Similarly, another study detected a Marfan syndrome caused by the disruption of FBN1 gene due to a reciprocal chromosome translocation with the help of optical genome mapping (Schnause et al., 2021). In recent years, third-generation sequencing technology has developed rapidly due to its long-read length. For structural variations including the balanced translocation, several studies have successfully detected chromosomal rearrangement using Oxford Nanopore or the PacBio SMRT platform (Cretu Stancu et al., 2017; Sedlazeck et al., 2018; Dutta et al., 2019; Hu et al., 2019; Chow et al., 2020; Liu et al., 2021; Cheng et al., 2021; Pei et al., 2021; Wang et al., 2021).

In this study, we aim to locate the precise breakpoints of a balanced translocation carrier with a Nanopore GridION device according to the results of karyotype analysis, provide effective genetic counseling for the patient, help them distinguish between normal and carrier embryos in the following assisted reproduction, and block the transmission of chromosomal translocation to the next generation (Madjunkova et al., 2020).

MATERIALS AND METHODS

Patient Information and Ethics Statement

The use of patient blood was reviewed and approved by the Research and Clinical Trials Ethics Committee of the First Affiliated Hospital of Zhengzhou University, and consent was obtained by the index case. The case patient had two adverse pregnancies. They said that they had conceived a child with a 6q26qter 6.5 MB heterozygous deletion, so the pregnancy had been terminated. Before the assisted reproduction, the ultrasound examination indicated that there were no obvious abnormalities in cardiac structure and function. The electrocardiograph was

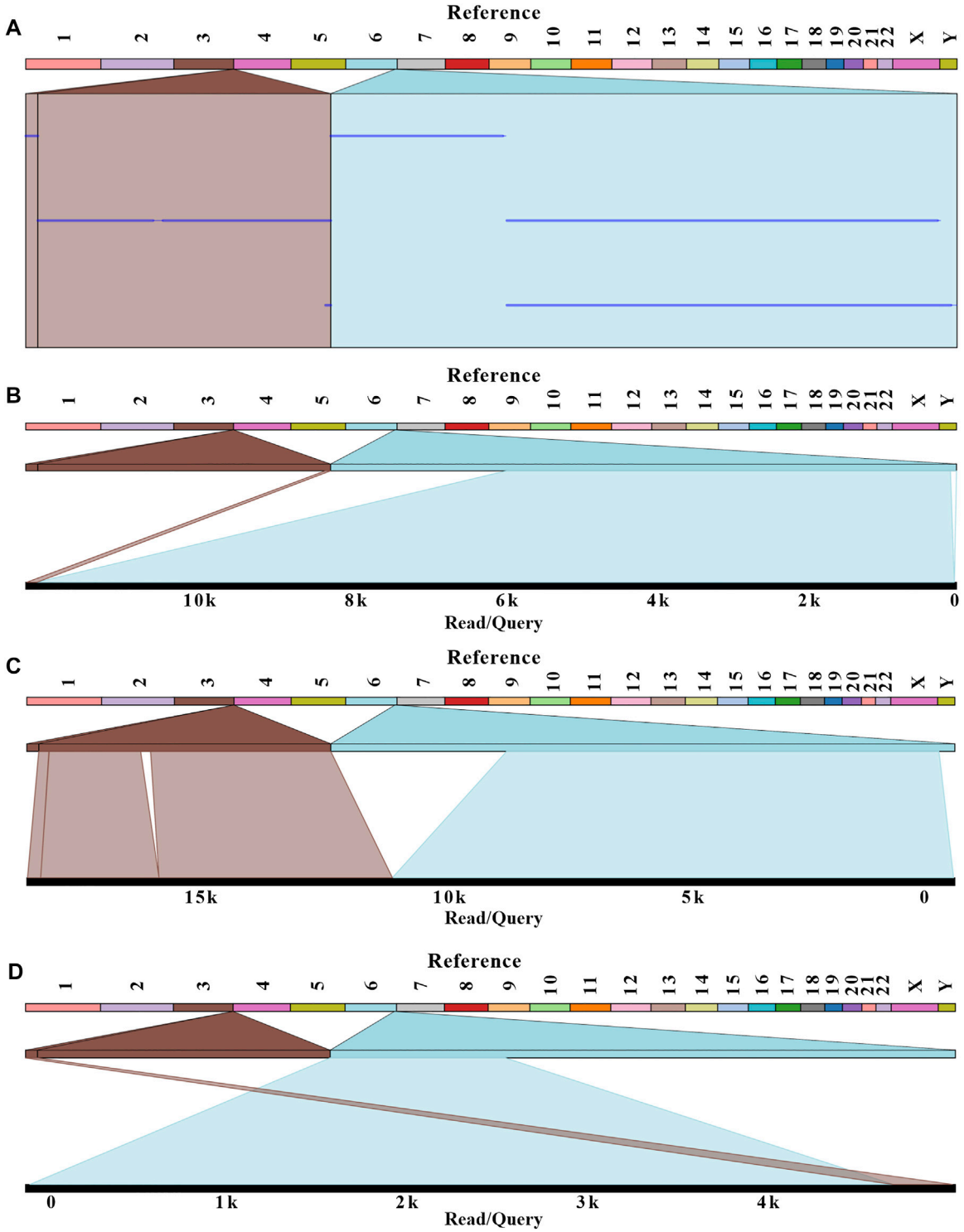


FIGURE 2 | Balanced translocation was visualized with Ribbon. Three reads related to the breakpoints were aligned with a human reference genome (GRCh38/hg38). **(A)** The summary of three reads mapping. **(B–D)** The detailed alignment results for each read were shown. The breakpoints were located at positions: chr 3: 198,009,533; chr 6:164,036,632 for B and C; chr 3:197,740,493; and chr 6:164,036,607 for D.

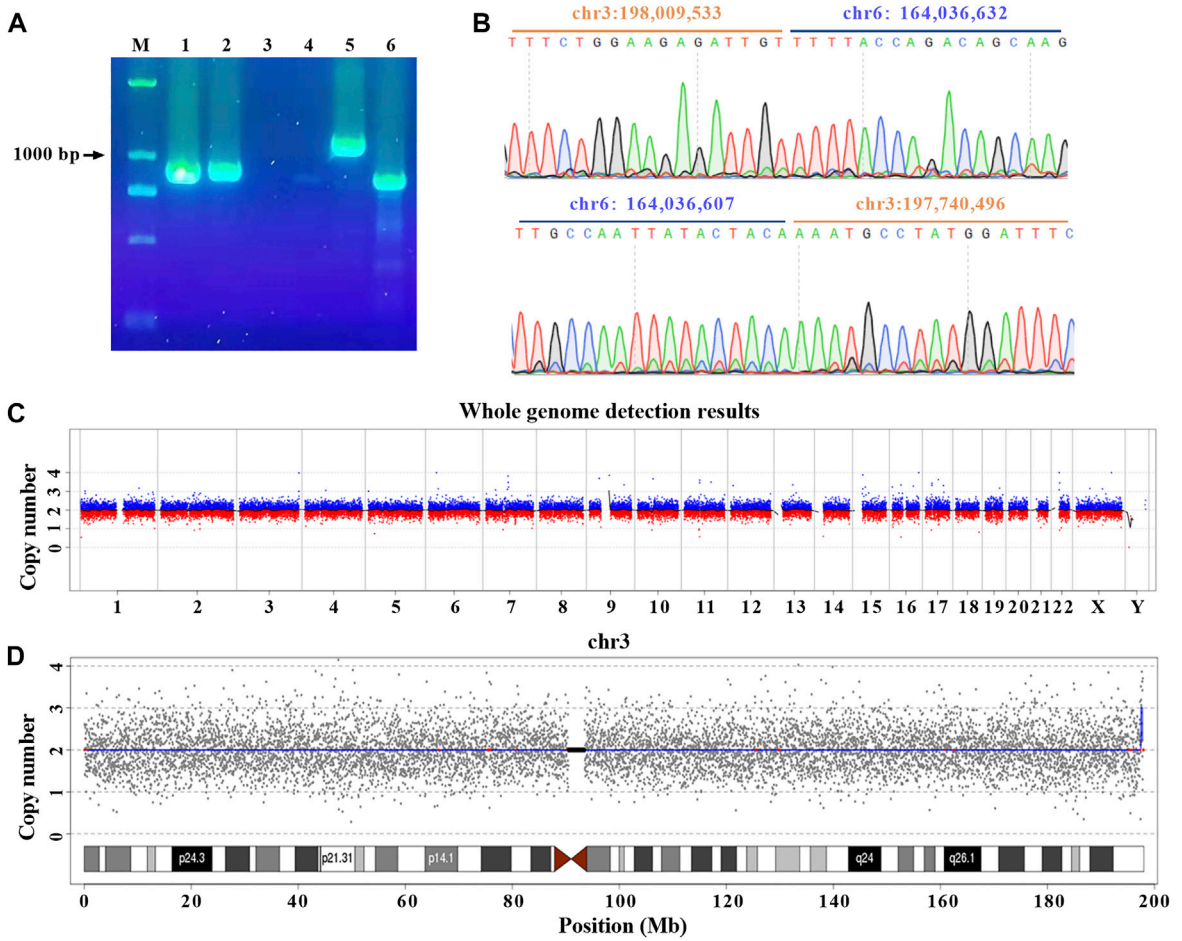


FIGURE 3 | Cryptic deletion and microduplication were confirmed with PCR and CNV. **(A)** gDNA were extracted from 200 μL peripheral blood. PCR was performed with specific primers designed for normal and rearranged chr 3 and chr 6. Amplicons (lanes 1 and 2) were obtained for normal chr 3 (primer pair F1/R1) and chr 6 (primer pair F2/R2) of the patient. Breakpoints of chr 3 (lanes 3 and 5 with primer pair F3/R3) and chr 6 (lanes 4 and 6 with primer pair F4/R4) were amplified for healthy control and the patient, respectively. All primer sequences were shown in materials and methods. M: DNA marker. **(B)** Two breakpoints were validated by Sanger Sequencing. **(C)** Overview of the low-coverage WGS. **(D)** Low-coverage WGS for chr 3. The blue line indicated the abnormal copy number.

also normal. Digital radiography (DR) examination showed no obvious abnormality of the cardiopulmonary diaphragm. After hysteroscopic tubal catheterization, both fallopian tubes were unobstructed and the uterine cavity was normal. They are now continuing to seek assisted reproduction for a healthy pregnancy in our hospital.

Karyotype Analysis

We collected 5 ml of venous blood and incubated the leukocytes at 37°C for 66–72 h. As per the usual procedure, gentle agitation of the culture flask every 24 h promoted cell growth. We added 10 μL of colchicine and culture for an additional 1 h. The cells were then treated with 10 ml of hypotonic KCl and we then fixed the cells twice with freshly prepared fixative. The cells were stained with Giemsa following trypsin treatment. Photograph and identification of specific chromosomes was undertaken using the automatic chromosomal analysis system from Leica.

DNA Extraction

Genomic DNA was extracted from 200 μL of frozen blood. According to the instructions of the Qiaamp blood DNA mini kit, 200 μL of high-quality DNA was obtained. The concentration of DNA was quantified using a Qubit 2.0 fluorometer with a dsDNA HS assay kit (ThermoFisher Scientific). DNA purity and length were measured with Nanodrop 2000 (ThermoFisher Scientific) and the Qseq100 analysis system, respectively.

Library Preparation and Nanopore Sequencing

Based on the pilot experiment, 1.1 μg of gDNA were prepared for library construction according to the manufacturer's instructions using a ligation sequencing kit SQK-LSK109 (Oxford Nanopore Technologies). DNA was cleaned up with Agencourt AMPure XP magnetic beads (Beckman Coulter) following end repair and dA-tailing. Then, 1 μL eluted DNA was quantified to calculate the

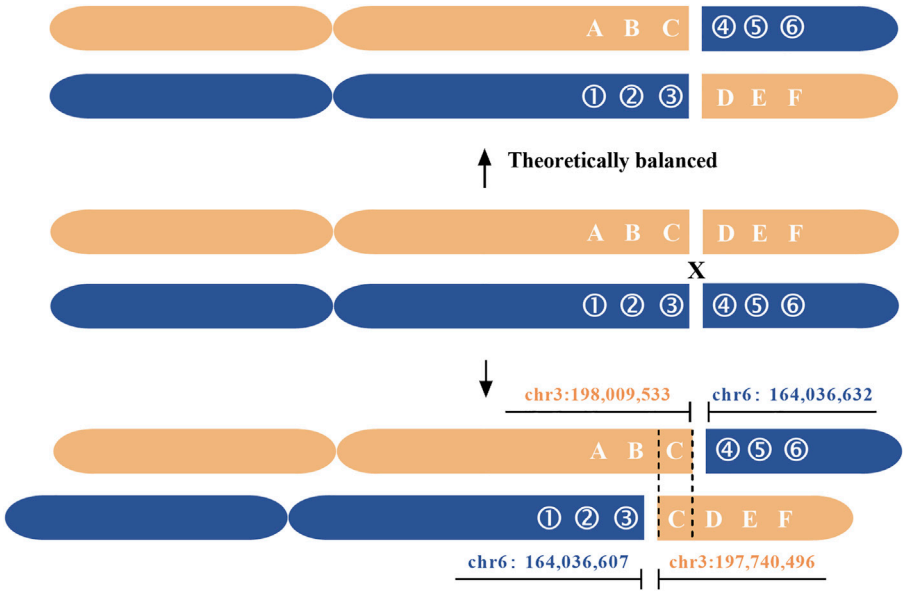


FIGURE 4 | Breakpoint delineation of a seemingly balanced translocation based on nanopore sequencing. Gray and blue represent chr 3 and chr 6, respectively. The arrows point to the breakpoints, and the region between solid lines indicates the 269 Kb microduplication. The dashed line indicates the 25 bp deletion. Nanopore sequencing revealed that the seemingly balanced translocation was unbalanced.

yield. After adapter ligation, all DNA fragments were enriched equally. Generally, 25% of DNA was lost at this step. Different from the standard protocol, we loaded 100 fmol of the final library onto the R9.4.1 flow cell of the nanopore GridION X5 platform.

After running for about 60h, the raw electrical signal (.fast5) was converted to base sequences (.fastq) through superhigh-accuracy basecalling mode. Reads with mean_qscore_template of more than 8 were defined as a "pass". The clean data were aligned to the human reference genome (GRCh38/hg38) using Minimap2 (Li, 2018). The filter parameter mapQ was set up more than 40. Variant calling was performed with Sniffles (Sedlazeck et al., 2018), and the bioinformatics workflow was based on a custom Python script, as shown in the Supplementary Materials of this article. Reads aligned to chr 3 and chr 6 simultaneously were extracted and analyzed manually using the NCBI blast tool (https://blast.ncbi.nlm.nih.gov/Blast.cgi). Finally, reads were visualized by uploading a. Sam or. bam file to the online tool genome Ribbon (Nattestad et al., 2021) (https://genomeribbon.com/).

PCR and Sanger Sequencing

The breakpoints were further confirmed by PCR, and Primer Premier 6 was used for designing primers. For the normal chr 3 and chr 6, 2 Kb bases flanking the potential breakpoints were directly retrieved from NCBI. For the derived chr 3 and chr 6, 2 Kb bases flanking the breakpoints were manually spliced. The primes used in this study were as follows. F1: AATTCAAAACTCTTGTGTCACTTTG, R1: ACATGTTACCACAATTCATGCACT; F2: GGAGAGACAAAGGGAAGTGTCA, R2: CCCCTTTACAATCCCAAATTCAGG; F3: AGTAGTCTGTAGAGTCTGCTA, R3: GTCTTGTCTCACGCTCAG; F4: GCAGCTTTGAAAATGGTTACTTGG, R4: ACAATTTGAGAGAAAGTTGCAGGA. A prepared mix on ice was: gDNA 50 ng, forward primer 1 μL, reverse primer 1 μL, 2×Taq master mix (Tiangen) 10 μL, and add ddH_2O to 20 μL. The cycling conditions were set as follows: 5 min at 95°C, then 32 cycles of 94°C for 30s, 57°C for 30s and 72°C for 30 s, and finally, 5 min at 72°C. Amplicons were visualized on 1% agarose gel and further confirmed by Sanger Sequencing (Sangon Biotech).

CNV Analyses

CNV-seq was performed according to the instructions of the CNV library sequencing kit (Berry Genomics, Beijing). For the CNV, genomic DNA (gDNA) needed to be purified before library preparation. We used the column purification method and the purification efficiency was 60%. gDNA was fragmented by enzyme digestion, followed by the addition of dA-tailing and ligation of barcodes and sequencing adapters. The concentration of each sample was determined by quantitative real-time PCR (qPCR), and different volumes of barcoded gDNA were mixed according to the sample concentration. The sequencing platform was Illumina NextSeq CN500, and the sequencing type was SE45 (single-ended sequencing, read length 45bp). The average sequencing depth was 0.1×. Firstly, the raw sequencing reads were aligned to human genome reference sequence version GRCh37/hg19. Meanwhile, CNVs were obtained based on the following algorithm.

$copyN_{bin} = \frac{obsRC_{bin}}{refRC_{bin}} \times copyN_{chrom}$ ·$copyN_{bin}, obsRC_{bin}, refRC_{bin}$ *and* $copyN_{chrom}$ represents the copy number of bin, the reads number of detected sample and control, and the theoretical copy number of the chromosome at which bin is located, respectively. The genome coordinates between reference versions GRCh37/

hg19 and GRCh38/hg38 were converted with the tool Lift Genome Annotations (https://genome.ucsc.edu/cgi-bin/hgLiftOver). The resolution of CNV was 100 Kb.

Software and Database

Figures were generated with GraphPad Prism 9. In this study, the NCBI blast tool was used for manual alignment. Reads were visualized using the online tool Ribbon. Repetitive sequences were analyzed using RepeatMasker tool (http://repeatmasker.org). Sanger sequencing was visualized using Snapgene, and primers were designed with Primer Premier 6.

RESULTS

Breakpoint Determination by Karyotype Analysis and Nanopore Sequencing

After genetic counseling, conventional cytogenetic analysis was performed for this patient. G-banded results revealed a balanced translocation between chr 3 and chr 6, and the karyotype was 46, XX, t (3; 6) (q29; q26), as shown in **Figure 1**. In order to identify the breakpoints of chr 3 and chr 6, the gDNA library was constructed and sequenced on the nanopore GridION platform. After running for about 60h, we obtained 11.8 gigabases (Gb) of passed bases and the average sequencing coverage was 3.8×. The estimated N50 was 6.57 Kb (**Supplementary Figure S1**). The sequencing coverage was relatively low and unfriendly to bioinformatic analysis. Based on the limited data, a custom Python script was developed for the downstream analysis. The bioinformatic pipeline included two alignment programs (Minimap2 and ngmlr) and a variant calling tool Sniffle. As much data as possible were extracted through two combinations. Considering the resolution of karyotype analysis, all translocations (15 Mb) flanking the q29 of chr 3 and q26 of chr 6 were analyzed. Finally, eight potential breakpoints were discovered. Among them, the physical locations of two breakpoints (chr3:198,009,533 and chr6:164,036,632) were in accordance with karyotype analysis (**Figure 2A**). Two reads supported the above breakpoints. Unexpectedly, another read was located at the breakpoints of chr3: 197,740,493 and chr6:164,036,607 (**Figures 2B–D**). The nucleotide sequences of the abovementioned three reads are provided in the Supplementary Materials. The remaining six breakpoints were located near the target position, and detailed physical locations were shown in **Supplementary Table S1**.

PCR and Sanger Sequencing

To further confirm the precise breakpoints of balanced translocation, PCR and Sanger Sequencing were conducted for each site with specific primers (**Supplementary Figure S2** and **Supplementary Table S2**). The results indicated no expected PCR bands were generated for six potential breakpoints, so we believe the corresponding translocations were false-positive (**Supplementary Figure S3**). Meanwhile, we got the specific amplicons at the breakpoints of chr3: 198,009,533 and chr6:164,036,607 for this translocation carrier. 1,152 bp and 872 bp of PCR products were shown in lanes 5 and 6, respectively. Taking gDNA of a healthy control as a PCR template, no amplicons were generated around the breakpoints of chr 3 and chr 6 (lanes 3 and 4). For the normal chr 3 and chr 6 of this carrier (lanes 1 and 2), 891 bp and 906 bp of PCR products were also obtained (**Figure 3A**). PCR amplicons were further confirmed by Sanger Sequencing (**Figure 3B**).

Deletion and 269 Kb Microduplication occurred at the Breakpoints

Based on the results of nanopore sequencing, we found that the seeming balanced translocation identified by karyotype analysis was actually unbalanced. The q26 of chr 6 was broken and linked to q29 of chr 3. During the process, a 25 bp fragment was deleted (**Figure 3B**). For chr 3, a breakage was at the physical location of 198,009,533, then a 269 Kb microduplication occurred and was translocated to the q26 of chr 6. Different from the karyotype analysis, nanopore sequencing revealed a cryptic deletion and a large microduplication at the single-nucleotide resolution. To further validate the presence of 269 Kb microduplication and the accuracy of bioinformatic analysis, CNV was performed with a resolution of 100 Kb. As listed in **Supplementary Table S2**, eight deletions or duplications were detected throughout the whole genome (**Figure 3C** and **Supplementary Table S3**). We mainly focused on the variations of chr 3 and chr 6. In accordance with nanopore sequencing, a 280 Kb microduplication was identified at the q29 region of chr 3 (**Figure 3D**).

Gene Structure Around the Breakpoints

The genomic regions (5 Kb) flanking the breakpoints were analyzed using an online tool RepeatMasker. We revealed that the breakpoint of chr 3 was located at a long interspersed nuclear element (LINE), furthermore, there were a large number of LINEs and short interspersed nuclear elements (SINEs) around the breakpoint. The highly repetitive elements were also a challenge for PCR confirmation. Different from chr 3, the breakpoint of chr 6 was not located at repetitive regions, and it disrupted the LOC105378102 gene, which encoded long non-coding RNA (lncRNA). The breakpoint of chr 3 disrupted LMLN gene, also known as leishmanolysin like peptidase (**Supplementary Figure S4**). The disruption or fusion of two genes didn't lead to phenotypic abnormity. Additionally, a microduplication from chr3:197,740,496 to 198,009,533 contained five true genes and two pseudogenes (**Figure 4**). Because the patient in this study had a normal phenotype, the effects of chromosomal rearrangement on gene function were not further discussed.

DISCUSSION

As mentioned above, we successfully obtained 11.8 Gb with a sequencing coverage of 3.8×, which was similar to a study by

Chow et al. (2020). Compared to other studies (Hu et al., 2019; Cheng et al., 2021), sequencing coverage was very low, and there was a high risk that breakpoints were not captured by limited reads. After starting the sequencing, we found the number of active nanopores declined sharply, and the duty time was shorter than expected. The actives nanopores seemed to be destroyed by something. We speculated the reason may be impure gDNA. The rapid loss of active pores was the main reason for low sequencing depth. To improve the sequencing coverage, a second sequencing running may be used for one sample with another flow cell. Inevitably, this strategy will increase the cost of sequencing. At present, the relatively low coverage made it challenging for widespread clinical applications of third-generation sequencing because of high-cost consideration. Even so, the throughput in this study was enough for us to finish the downstream bioinformatic analysis. Three reads spanning the breakpoints of chr 3 and chr 6 were extracted. PCR and Sanger sequencing also confirmed the presence of two breakpoints.

In comparison, our bioinformatic analyses were based on chromosomal karyotype. Considering the human error of karyotype analyst, all reads flanking the target position were extracted. This method ensured the accuracy of bioinformatics and increased the workload of subsequent validation. In this study, eight potential breakpoints were identified with nanopore sequencing, but out of eight breakpoints, six cannot be supported by PCR. Therefore, these sites were defined as false-positive. We need to optimize the analysis workflow and improve the sequencing coverage to filter false-positive reads in the next work.

Overall balanced translocation was generally involved in two chromosomes, but some complex chromosomal rearrangements may generate multiple breakpoints (Wang et al., 2014; Li et al., 2020; Tan et al., 2020). For this condition, breakpoint analyses were more complex with other approaches, such as karyotype, FISH, and SNP array. Sequencing was capable of providing a more accurate description of balanced translocation and revising the karyotype results at the single-nucleotide resolution (Talkowski et al., 2012; Dong et al., 2019). In addition to identifying the breakpoints, nanopore sequencing was also able to detect cryptic deletion and duplication directly. Studies have shown that some apparently balanced translocations were prone to gene deletion or disruption (De Gregori et al., 2007), and duplication at the breakpoint junction also occurred but was not common (Howarth et al., 2011). In our study, a 25 bp deletion and a 269 Kb microduplication were at the breakpoint junction. Luckily, they did not have an obvious effect on the patient's health. For the individuals with phenotypic abnormity, the incidence of which was 6.1% in the population with apparently balanced rearrangement (Wapner et al., 2012). Chromosomal rearrangement disrupted the causal gene, and precise breakpoints were especially critical for disease diagnosis (Redin et al., 2017; Aagaard et al., 2020; Bonaglia et al., 2020; Guenzel et al., 2021). As shown in our study, breakage often occurred at highly repetitive regions, and this highlighted another advantage of nanopore sequencing relative to short-read sequencing (Aristidou et al., 2017). Taken together, third-generation sequencing was well suitable for the clinical application and research of balanced translocation.

The limitations of this study include its small sample size, as it was an initial attempt to locate the precise breakpoints of balanced translocation with nanopore sequencing. The findings of this study are useful for genetic counseling and PGT. Hundreds of patients are diagnosed as apparently balanced translocation with chromosomal karyotype at our center every year. Approximately half of the seemingly balanced translocations were in fact unbalanced (De Gregori et al., 2007; Costa et al., 2022). The number of patients facing reproductive difficulty was large. The offspring of a balanced translocation carrier is likely to obtain a derived abnormal chromosome that leads to an increase (partial trisomy) or decrease (partial monosomy) of translocated fragments. The fetus will have an imbalance of genetic material, and the total amount of genetic material will be incorrect, resulting in fetal malformations or spontaneous abortion. In future studies, larger-scale samples will be recruited. At present, this patient is seeking assisted reproduction at the reproduction center of our hospital. By the time our manuscript was submitted, they had not started embryo transfer. By providing the precise breakpoints for them, we hope the patient will readily obtain normal embryos and block the transmission of chromosomal abnormity to offspring. In the future, we will continue to follow up on this patient until they give birth successfully.

DATA AVAILABILITY STATEMENT

The datasets for this article are not publicly available due to concerns regarding participant/patient anonymity. Requests to access the datasets should be directed to the corresponding author.

ETHICS STATEMENT

The studies involving human participants were reviewed and approved by Research and Clinical Trials Ethics Committee of the First Affiliated Hospital of Zhengzhou University. The patients/participants provided their written informed consent to participate in this study.

AUTHOR CONTRIBUTIONS

XK and YW designed the experiment. Nanopore sequencing and bioinformatic analyses were performed by YW and ZZ. Cytogenetic analysis was finished with the help of SL and QZ. Primer design and PCR were completed by XF. YW wrote the manuscript and drew the figures. All authors discussed the results and approved the submission.

FUNDING

This study was supported by Key Scientific Research Projects in Colleges and Universities of Henan Province (22A320075).

ACKNOWLEDGMENTS

This study was completed in the Genetic and Prenatal Diagnosis Center of First Affiliated Hospital of Zhengzhou University.

SUPPLEMENTARY MATERIAL

The Supplementary Material for this article can be found online at: https://www.frontiersin.org/articles/10.3389/fgene.2022.883398/full#supplementary-material

REFERENCES

Aagaard, K. S., Brusgaard, K., Miceikaite, I., Larsen, M. J., Kjeldsen, A. D., Lester, E. B., et al. (2020). Chromosomal Translocation Disrupting the SMAD4 Gene Resulting in the Combined Phenotype of Juvenile Polyposis Syndrome and Hereditary Hemorrhagic Telangiectasia. *Mol. Genet. Genomic Med.* 8 (11), e1498. doi:10.1002/mgg3.1498

Aristidou, C., Koufaris, C., Theodosiou, A., Bak, M., Mehrjouy, M. M., Behjati, F., et al. (2017). Accurate Breakpoint Mapping in Apparently Balanced Translocation Families with Discordant Phenotypes Using Whole Genome Mate-Pair Sequencing. *PLoS One* 12 (1), e0169935. doi:10.1371/journal.pone.0169935

Beyazyurek, C., Ekmekci, C. G., Saglam, Y., Cinar, C., and Kahraman, S. (2010). Preimplantation Genetic Diagnosis (PGD) for Extremes-Ssuccessful Birth after PGD for a Consanguineous Couple Carrying an Identical Balanced Reciprocal Translocation. *Fertil. Steril.* 93 (7), 2413.e1. doi:10.1016/j.fertnstert.2009.12.032

Bonaglia, M. C., Bertuzzo, S., Ciaschini, A. M., Discepoli, G., Castiglia, L., Romaniello, R., et al. (2020). Targeted Next-Generation Sequencing Identifies the Disruption of the SHANK3 and RYR2 Genes in a Patient Carrying a De Novo t(1;22)(q43;q13.3) Associated with Signs of Phelan-McDermid Syndrome. *Mol. Cytogenet.* 13, 22. doi:10.1186/s13039-020-00490-6

Cheng, Y., Yu, Q., Ma, M., Wang, H., Tian, S., Zhang, W., et al. (2021). Variant Haplophasing by Long-Read Sequencing: a New Approach to Preimplantation Genetic Testing Workups. *Fertil. Steril.* 116 (3), 774–783. doi:10.1016/j.fertnstert.2021.04.012

Chow, J. F. C., Cheng, H. H. Y., Lau, E. Y. L., Yeung, W. S. B., and Ng, E. H. Y. (2020). Distinguishing between Carrier and Noncarrier Embryos with the Use of Long-Read Sequencing in Preimplantation Genetic Testing for Reciprocal Translocations. *Genomics* 112 (1), 494–500. doi:10.1016/j.ygeno.2019.04.001

Costa, D., Granada, I., Espinet, B., Collado, R., Ruiz-Xiville, N., Puiggros, A., et al. (2022). Balanced and Unbalanced Translocations in a Multicentric Series of 2843 Patients with Chronic Lymphocytic Leukemia. *Genes Chromosom. Cancer* 61 (1), 37–43. doi:10.1002/gcc.22994

Cretu Stancu, M., van Roosmalen, M. J., Renkens, I., Nieboer, M. M., Middelkamp, S., de Ligt, J., et al. (2017). Mapping and Phasing of Structural Variation in Patient Genomes Using Nanopore Sequencing. *Nat. Commun.* 8 (1), 1326. doi:10.1038/s41467-017-01343-4

De Gregori, M., Ciccone, R., Magini, P., Pramparo, T., Gimelli, S., Messa, J., et al. (2007). Cryptic Deletions Are a Common Finding in "balanced" Reciprocal and Complex Chromosome Rearrangements: a Study of 59 Patients. *J. Med. Genet.* 44 (12), 750–762. doi:10.1136/jmg.2007.052787

Dong, Z., Wang, H., Chen, H., Jiang, H., Yuan, J., Yang, Z., et al. (2018a). Identification of Balanced Chromosomal Rearrangements Previously Unknown Among Participants in the 1000 Genomes Project: Implications for Interpretation of Structural Variation in Genomes and the Future of Clinical Cytogenetics. *Genet. Med.* 20 (7), 697–707. doi:10.1038/gim.2017.170

Dong, Z., Yan, J., Xu, F., Yuan, J., Jiang, H., Wang, H., et al. (2019). Genome Sequencing Explores Complexity of Chromosomal Abnormalities in Recurrent Miscarriage. *Am. J. Hum. Genet.* 105 (6), 1102–1111. doi:10.1016/j.ajhg.2019.10.003

Dong, Z., Ye, L., Yang, Z., Chen, H., Yuan, J., Wang, H., et al. (2018b). Balanced Chromosomal Rearrangement Detection by Low-Pass Whole-Genome Sequencing. *Curr. Protoc. Hum. Genet.* 96, 8.18.1. doi:10.1002/cphg.51

Dutta, U. R., Rao, S. N., Pidugu, V. K., V, S. V., Bhattacherjee, A., Bhowmik, A. D., et al. (2019). Breakpoint Mapping of a Novel De Novo Translocation t(X;20)(q11.1;p13) by Positional Cloning and Long Read Sequencing. *Genomics* 111 (5), 1108–1114. doi:10.1016/j.ygeno.2018.07.005

Fiorentino, F., Kokkali, G., Biricik, A., Stavrou, D., Ismailoglu, B., De Palma, R., et al. (2010). Polymerase Chain Reaction-Based Detection of Chromosomal Imbalances on Embryos: the Evolution of Preimplantation Genetic Diagnosis for Chromosomal Translocations. *Fertil. Steril.* 94 (6), 2001–2011. doi:10.1016/j.fertnstert.2009.12.063

Guenzel, A. J., Smadbeck, J. B., Golden, C. L., Williamson, C. M., Benevides Demasi, J. C., Vasmatzis, G., et al. (2021). Clinical Utility of Next Generation Sequencing to Detect IGH/IL3 Rearrangements [t(5;14)(q31.1;q32.1)] in B-Lymphoblastic Leukemia/lymphoma. *Ann. Diagn. Pathol.* 53, 151761. doi:10.1016/j.anndiagpath.2021.151761

Howarth, K. D., Pole, J. C., Beavis, J. C., Batty, E. M., Newman, S., Bignell, G. R., et al. (2011). Large Duplications at Reciprocal Translocation Breakpoints that Might Be the Counterpart of Large Deletions and Could Arise from Stalled Replication Bubbles. *Genome Res.* 21 (4), 525–534. doi:10.1101/gr.114116.110

Hu, L., Cheng, D., Gong, F., Lu, C., Tan, Y., Luo, K., et al. (2016). Reciprocal Translocation Carrier Diagnosis in Preimplantation Human Embryos. *EBioMedicine* 14, 139–147. doi:10.1016/j.ebiom.2016.11.007

Hu, L., Liang, F., Cheng, D., Zhang, Z., Yu, G., Zha, J., et al. (2019). Location of Balanced Chromosome-Translocation Breakpoints by Long-Read Sequencing on the Oxford Nanopore Platform. *Front. Genet.* 10, 1313. doi:10.3389/fgene.2019.01313

Idowu, D., Merrion, K., Wemmer, N., Mash, J. G., Pettersen, B., Kijacic, D., et al. (2015). Pregnancy Outcomes Following 24-chromosome Preimplantation Genetic Diagnosis in Couples with Balanced Reciprocal or Robertsonian Translocations. *Fertil. Steril.* 103 (4), 1037–1042. doi:10.1016/j.fertnstert.2014.12.118

Jancuskova, T., Plachy, R., Stika, J., Zemankova, L., Hardekopf, D. W., Liehr, T., et al. (2013). A Method to Identify New Molecular Markers for Assessing Minimal Residual Disease in Acute Leukemia Patients. *Leuk. Res.* 37 (10), 1363–1373. doi:10.1016/j.leukres.2013.06.009

Li, G., Shi, W., Niu, W., Xu, J., Guo, Y., Su, Y., et al. (2020). The Influence of Balanced Complex Chromosomal Rearrangements on Preimplantation Embryonic Development Potential and Molecular Karyotype. *BMC Genomics* 21 (1), 326. doi:10.1186/s12864-020-6731-9

Li, H. (2018). Minimap2: Pairwise Alignment for Nucleotide Sequences. *Bioinformatics* 34 (18), 3094–3100. doi:10.1093/bioinformatics/bty191

Li, R., Wang, J., Gu, A., Xu, Y., Guo, J., Pan, J., et al. (2021). Feasibility Study of Using Unbalanced Embryos as a Reference to Distinguish Euploid Carrier from Noncarrier Embryos by Single Nucleotide Polymorphism Array for Reciprocal Translocations. *Prenat. Diagn.* 41 (6), 681–689. doi:10.1002/pd.5897

Liu, S., Wang, H., Leigh, D., Cram, D. S., Wang, L., and Yao, Y. (2021). Third-generation Sequencing: Any Future Opportunities for PGT. *J. Assist. Reprod. Genet.* 38 (2), 357–364. doi:10.1007/s10815-020-02009-9

Mackie Ogilvie, C., and Scriven, P. N. (2002). Meiotic Outcomes in Reciprocal Translocation Carriers Ascertained in 3-day Human Embryos. *Eur. J. Hum. Genet.* 10 (12), 801–806. doi:10.1038/sj.ejhg.5200895

Madjunkova, S., Sundaravadanam, Y., Antes, R., Abramov, R., Chen, S., Yin, Y., et al. (2020). Detection of Structural Rearrangements in Embryos. *N. Engl. J. Med.* 382 (25), 2472–2474. doi:10.1056/NEJMc1913370

Nattestad, M., Aboukhalil, R., Chin, C. S., and Schatz, M. C. (2021). Ribbon: Intuitive Visualization for Complex Genomic Variation. *Bioinformatics* 37 (3), 413–415. doi:10.1093/bioinformatics/btaa680

Pei, Z., Deng, K., Lei, C., Du, D., Yu, G., Sun, X., et al. (2021). Identifying Balanced Chromosomal Translocations in Human Embryos by Oxford Nanopore Sequencing and Breakpoints Region Analysis. *Front. Genet.* 12, 810900. doi:10.3389/fgene.2021.810900

Redin, C., Brand, H., Collins, R. L., Kammin, T., Mitchell, E., Hodge, J. C., et al. (2017). The Genomic Landscape of Balanced Cytogenetic Abnormalities Associated with Human Congenital Anomalies. *Nat. Genet.* 49 (1), 36–45. doi:10.1038/ng.3720

Schnause, A. C., Komlosi, K., Herr, B., Neesen, J., Dremsek, P., Schwarz, T., et al. (2021). Marfan Syndrome Caused by Disruption of the FBN1 Gene Due to A Reciprocal Chromosome Translocation. *Genes (Basel)* 12 (11), 1836. doi:10.3390/genes12111836

Sedlazeck, F. J., Rescheneder, P., Smolka, M., Fang, H., Nattestad, M., von Haeseler, A., et al. (2018). Accurate Detection of Complex Structural Variations Using Single-Molecule Sequencing. *Nat. Methods* 15 (6), 461–468. doi:10.1038/s41592-018-0001-7

Talkowski, M. E., Ordulu, Z., Pillalamarri, V., Benson, C. B., Blumenthal, I., Connolly, S., et al. (2012). Clinical Diagnosis by Whole-Genome Sequencing of a Prenatal Sample. *N. Engl. J. Med.* 367 (23), 2226–2232. doi:10.1056/NEJMoa1208594

Tan, Y. Q., Tan, Y. Q., and Cheng, D. H. (2020). Whole-genome Mate-Pair Sequencing of Apparently Balanced Chromosome Rearrangements Reveals Complex Structural Variations: Two Case Studies. *Mol. Cytogenet.* 13, 15. doi:10.1186/s13039-020-00487-1

Treff, N. R., Thompson, K., Rafizadeh, M., Chow, M., Morrison, L., Tao, X., et al. (2016). SNP Array-Based Analyses of Unbalanced Embryos as a Reference to Distinguish between Balanced Translocation Carrier and Normal Blastocysts. *J. Assist. Reprod. Genet.* 33 (8), 1115–1119. doi:10.1007/s10815-016-0734-0

Wang, H., Jia, Z., Mao, A., Xu, B., Wang, S., Wang, L., et al. (2020). Analysis of Balanced Reciprocal Translocations in Patients with Subfertility Using Single-Molecule Optical Mapping. *J. Assist. Reprod. Genet.* 37 (3), 509–516. doi:10.1007/s10815-020-01702-z

Wang, T., Mao, J., Liu, M. J., Choy, K. W., Li, H. B., Cram, D. S., et al. (2014). A Patient with Five Chromosomal Rearrangements and a 2q31.1 Microdeletion. *Clin. Chim. Acta.* 430, 129–133. doi:10.1016/j.cca.2014.01.002

Wang, Y., Tan, J., Wang, Y., Liu, A., Qiao, F., Huang, M., et al. (2021). Diagnosis of Shashi-Pena Syndrome Caused by Chromosomal Rearrangement Using Nanopore Sequencing. *Neurol. Genet.* 7 (6), e635. doi:10.1212/NXG.0000000000000635

Wapner, R. J., Martin, C. L., Levy, B., Ballif, B. C., Eng, C. M., Zachary, J. M., et al. (2012). Chromosomal Microarray versus Karyotyping for Prenatal Diagnosis. *N. Engl. J. Med.* 367 (23), 2175–2184. doi:10.1056/NEJMoa1203382

Wilch, E. S., and Morton, C. C. (2018). Historical and Clinical Perspectives on Chromosomal Translocations. *Adv. Exp. Med. Biol.* 1044, 1–14. doi:10.1007/978-981-13-0593-1_1

Xu, J., Zhang, Z., Niu, W., Yang, Q., Yao, G., Shi, S., et al. (2017). Mapping Allele with Resolved Carrier Status of Robertsonian and Reciprocal Translocation in Human Preimplantation Embryos. *Proc. Natl. Acad. Sci. U. S. A.* 114 (41), E8695–E8702. doi:10.1073/pnas.1715053114

Yao, G., Xu, J., Xin, Z., Niu, W., Shi, S., Jin, H., et al. (2016). Developmental Potential of Clinically Discarded Human Embryos and Associated Chromosomal Analysis. *Sci. Rep.* 6, 23995. doi:10.1038/srep23995

Zhang, S., Lei, C., Wu, J., Zhou, J., Sun, H., Fu, J., et al. (2017). The Establishment and Application of Preimplantation Genetic Haplotyping in Embryo Diagnosis for Reciprocal and Robertsonian Translocation Carriers. *BMC Med. Genomics* 10 (1), 60. doi:10.1186/s12920-017-0294-x

Conflict of Interest: The authors declare that the research was conducted in the absence of any commercial or financial relationships that could be construed as a potential conflict of interest.

Publisher's Note: All claims expressed in this article are solely those of the authors and do not necessarily represent those of their affiliated organizations, or those of the publisher, the editors and the reviewers. Any product that may be evaluated in this article, or claim that may be made by its manufacturer, is not guaranteed or endorsed by the publisher.

Copyright © 2022 Wang, Zhao, Fu, Li, Zhang and Kong. This is an open-access article distributed under the terms of the Creative Commons Attribution License (CC BY). The use, distribution or reproduction in other forums is permitted, provided the original author(s) and the copyright owner(s) are credited and that the original publication in this journal is cited, in accordance with accepted academic practice. No use, distribution or reproduction is permitted which does not comply with these terms.

frontiers | Frontiers in Genetics

TYPE Original Research
PUBLISHED 29 August 2022
DOI 10.3389/fgene.2022.932760

Check for updates

OPEN ACCESS

EDITED BY
Tieliu Shi,
Hunan University of Arts and Science, China

REVIEWED BY
Fengying Sun,
Second People's Hospital of Wuhu, China
Zahra Beyzaei,
Shiraz University of Medical Sciences, Iran

*CORRESPONDENCE
Zhongtao Gai,
gaizhongtao@sina.com
Yi Liu,
y_liu99@sina.com

†These authors have contributed equally to this work

SPECIALTY SECTION
This article was submitted to Genetics of Common and Rare Diseases, a section of the journal Frontiers in Genetics

RECEIVED 05 May 2022
ACCEPTED 25 July 2022
PUBLISHED 29 August 2022

CITATION
Dong R, Wei X, Zhang K, Song F, Lv Y, Gao M, Wang D, Ma J, Gai Z and Liu Y (2022), Genotypic and phenotypic characteristics of 12 chinese children with glycogen storage diseases. *Front. Genet.* 13:932760. doi: 10.3389/fgene.2022.932760

COPYRIGHT
© 2022 Dong, Wei, Zhang, Song, Lv, Gao, Wang, Ma, Gai and Liu. This is an open-access article distributed under the terms of the Creative Commons Attribution License (CC BY). The use, distribution or reproduction in other forums is permitted, provided the original author(s) and the copyright owner(s) are credited and that the original publication in this journal is cited, in accordance with accepted academic practice. No use, distribution or reproduction is permitted which does not comply with these terms.

Genotypic and phenotypic characteristics of 12 chinese children with glycogen storage diseases

Rui Dong[1,2†], Xuxia Wei[3,2†], Kaihui Zhang[1,2], Fengling Song[4,2], Yuqiang Lv[1,2], Min Gao[1,2], Dong Wang[1,2], Jian Ma[1,2], Zhongtao Gai[1,2*] and Yi Liu[1,2*]

[1]Pediatric Research Institute, Children's Hospital Affiliated to Shandong University (Jinan Children's Hospital), Jinan, China, [2]Shandong Provincial Clinical Research Center for Children's Health and Disease, Jinan, China, [3]Gastroenterology, Children's Hospital Affiliated to Shandong University (Jinan Children's Hospital), Jinan, China, [4]Children's Health Department, Children's Hospital Affiliated to Shandong University (Jinan Children's Hospital), Jinan, China

Background: Glycogen storage diseases (GSDs) are known as a group of disorders characterized by genetic errors leading to accumulation of glycogen in various tissues. Since different types of GSD can sometimes be clinically indistinguishable, next generation sequencing is becoming a powerful tool for clinical diagnosis.

Methods: 12 patients with suspected GSDs and their parents were enrolled in this study. The clinical and laboratory data of the patients were reviewed. Causative gene variants were identified in the patients using whole exome sequencing (WES) and verified by Sanger sequencing.

Results: Genetic testing and analysis showed that 7 patients were diagnosed with GSD II (Pompe disease), 2 patients with GSD III, 1 patient with GSD VI, and 2 patients with GSD IXα. A total number of 18 variants were identified in 12 patients including 11 variants in *GAA* gene, 3 variants in *AGL* gene, 2 variants in *PYGL* gene and 2 variants in *PHKA2* gene, of which 9 variants were reported and 9 variants were novel. SIFT, Polyphen-2, Mutation Taster, and REVEL predicted the novel variants (except *GAA* c.1052_1075 + 47del) to be disease-causing. The 3D structures of wild/mutant type GAA protein were predicted indicating that variants p. Trp621Gly, p. Pro541Leu, p. Ser800Ile and p. Gly293Trp might affect the proteins function via destroying hydrogen bonds or conformational constraints. Neither liver size nor laboratory findings allow for a differentiation among GSD III, GSD VI and GSD IXα.

Conclusion: Our study expanded the variation spectrum of genes associated with GSDs. WES, in combination with clinical, biochemical, and pathological hallmarks, could provide accurate results for diagnosing and sub-typing GSD and related diseases in clinical setting.

KEYWORDS

glycogen storage diseases, mutation, whole exome sequencing, GAA gene, AGL gene, PHKA2 gene, PYGL gene

Introduction

Glycogen storage diseases (GSDs) as the innate defects of carbohydrate metabolism are caused by enzyme deficiency in the glycogenolysis or gluconeogenesis (Liang et al., 2020). There are 19 types of GSD, named in Roman numerals from 0 to XV (GSD I was divided into 4 subtypes numbered a-d), classified by enzyme deficiency and affected tissue. In aggregate, GSDs are not considered rare diseases, but every subtype of the disorder are (Molares-Vila et al., 2021). The overall estimated GSD incidence is 1 case per 10,000 live births (Beyzaei et al., 2020). Like most metabolic diseases, the vast majority of GSDs are inherited in an autosomal recessive (AR) pattern, except for X-linked type IXα (Brown et al., 2015; Szymanska et al., 2021). In GSD II, the symptoms are caused by mutations in *GAA* gene and in GSD III, *AGL* gene. In GSD VI, the clinical manifestations are associated with mutations in *PYGL* gene and in GSD IXα, *PHKA1* and *PHKA2* gene (De Vito et al., 2019; Kim et al., 2020; Perveen et al., 2020; Grunert et al., 2021a).

GSDs are a group of clinically and genetically heterogenous diseases. The clinical manifestations of GSDs range from almost no symptoms to severe cardiac dysfunction, respiratory insufficiency, and sudden death (Molares-Vila et al., 2021). GSDs are divided into hepatic, muscle and mixed types according to glycogen accumulation in tissues (Lu et al., 2016; Zhao et al., 2019; Eghbali et al., 2020; Szymanska et al., 2021). The basic clinical symptoms of hepatic GSD are hypoglycemia and hepatomegaly. The characteristic feature of muscle GSD is progressive muscle pathology, including exercise-induced muscle weakness. In both types of GSD, there is also hypertransaminasemia. The different types of GSD are sometimes clinically indistinguishable, especially in hepatic GSDs (Choi et al., 2016). Early diagnosis and effective treatment of GSDs is necessary to prevent adverse outcomes. Clinical signs and symptoms and laboratory parameters such as hypoglycemia, hypertransaminasemia and increased triglycerides level are helpful in GSDs diagnosis. Liver biopsy is an invasive test to assess liver cell enzyme activity. Gene sequencing and genetic analysis, a technology that can provide precise diagnosis and procreation guidance and are more acceptable to patients, is increasingly used in the diagnosis of genetic diseases, including GSD (Shen and Shi, 2019; Fang et al., 2021; Huang et al., 2021; Li et al., 2021; Szymanska et al., 2021).

In this study, by clinical and next-generation sequencing analysis of 12 patients with suspected GSDs, we aimed to give them molecular diagnosis of GSD and determine the spectrum of genetic analysis specific to our cohort. As a result, we found 18 variants in *GAA*, *AGL*, *PHKA2* and *PYGL* gene related to GSD and the 12 patients were diagnosed with GSD types II, III, VI, and IXα respectively.

Materials and methods

Study cohort

A total of 12 hospitalized children (6 female, 6 male) in unrelated families with clinically suspected GSD were recruited for this study in Children's Hospital Affiliated to Shandong University (Jinan Children's Hospital) from November 2018 to October 2021. All patients from the Han Chinese population in Shandong Province, China were examined and diagnosed by experienced pediatric specialists from the Neurology or Gastroenterology Department. The clinical records of 12 patients with GSD were retrospectively reviewed.

Genetic analysis

Blood samples were obtained from the patients and their parents, and DNA was extracted form peripheral blood leukocytes using QIAamp DNA Blood Midi Kit (Qiagen, Shanghai, China). Mutation screening of the patients was applied by Whole exome sequencing (WES) with the Human Exome Probes P039Exome (MyGenostics, Beijing, China) on the Illumina NovaSeq5000 platform (Illumina, United States). The obtained mean exome coverage was more than 95% (>10X coverage; mean depth of over 100X). Paired-end alignment was performed with version GRCh37/hg19 of the human genome on Burrows-Wheeler Aligner software (BWA Version: 0.7.10). Variant frequencies were determined in thousands of genomes (1000 Genomes, http://www.1000genomes.org), ExAC (http://exac.broadinstitute.org/), Exome Variant Server (EVS, http://evs.gs.washington.edu/EVS) and in-house database to remove common variants (suballelic frequency >5%). Frameshift variants, missense variants, premature stop-gain, initiation codon loss, and typical splicing site changes were prioritized. Effect on protein function of variations were predicted by SIFT, PolyPhen-2, MutationTaster, and REVEL. Descriptions of variants in Human Gene Mutation Database (HGMD, http://www.hgmd.cf.ac.uk) and ClinVar (http://www.ncbi.nlm.nih.gov/clinvar) also were referenced. Swiss-Pdb Viewer 4.1 software was utilized to generate the 3D protein plots of wild-type and mutant type for novel missense variants. The variants identified in this study were classified according to the 2015 American College of Medical Genetics and Genomics (ACMG) guidelines (Richards et al., 2015).

Validation of gene mutations

The target variants screened from WES were verified by Sanger sequencing in parents and probands using ABI Prism 3700 automated sequencer (Applied Biosystems, Foster City, CA).

TABLE 1 | The clinical and laboratory features of the Chinese patients with GSD.

Patient	—	P1	P2	P3	P4	P5	P6	P7	P8	P9	P10	P11	P12
Diagnosis	—	GS II	GSD II	GSD II	GSD II	GSD II	GSD II	GSD II	GSD III	GSD III	GSD VI	GSD IXα	GSD IXα
Gender	—	F	F	M	F	F	F	M	F	M	M	M	M
Age	—	2m24d	7m9d	3y2m	2y1m	1y8m	13y3m	7m7d	1y	1y	2y8m	4y4m	4y2m
Age at the onset	—	Postnatal	Postnatal	2y	Postnatal	9m	12y9m	Postnatal	1y	11m	2y8m	3y2m	4y
Initial symptoms	—	HC	ET	MW	LB	MW	MW	HC	AD	AD	ET	ET	ET
Clinical symptoms	Motor development delay/ muscle weakness	+	+	+	+	+	+	+	–	–	–	–	–
	Hypertrophic cardiomyopathy	+	+	–	+	+	NA	+	–	–	–	NA	NA
	Hepatomegaly	NA	–	+	+	–	NA	–	+	+	+	+	+
	(mm below costal)	NA	NA	51	37	NA	NA	NA	72	83	53	68	70
	Short stature	–	–	+	+	–	NA	–	–	–	–	+	+
	Malnutrition	+	+	–	–	–	NA	–	–	–	–	–	–
Lab tests	Alanine aminotransferasea	119↑	161↑	148↑	150↑	305↑	NA	82↑	833↑	469↑	610↑	46↑	516↑
	Aspartate aminotransferasea	209↑	362↑	227↑	227↑	380↑	227↑	146↑	1131↑	636↑	999↑	78↑	516↑
	Lactate dehydrogenasea	586↑	964↑	667↑	599↑	817↑	589↑	1042↑	984↑	532↑	955↑	251↑	400↑
	Hydroxybutyrate dehydrogenasea	500↑	886↑	620↑	486↑	721↑	467↑	1015↑	456↑	301↑	468↑	207↑	251↑
	Glutamyl transpeptidasea	53.8↑	15.8	16	14.2	9.9	NA	15.2	100.6↑	201.2↑	66.2↑	28.7	243.3↑
	Ccreatine kinasea	624↑	538↑	717↑	815↑	820↑	2049↑	388↑	154	191	79	80	35
	Glycemiab	4.13	4.01	5.3	5.42	4.59	NA	6.5	1.09↓	0.86↓	3.3↓	3.53↓	2.64↓
	Lactic acidb	NA	2.1	NA	1.3	0.7	NA	1.1	1.5	2.8↑	3.9↑	NA	4.2↑
	Triglyceridesb	NA	2.00↑	NA	NA	0.86	NA	NA	3.36↑	8.36↑	NA	1.90↑	3.43↑
	Cholesterolb	3.20	4.20	7.59↑	7.48↑	4.63	NA	2.88	4.84	4.46	2.87	4.80	5.23

M, male; F, female; HC, Hypertrophic cardiomyopathy; ET, Hypertransaminase; MW, muscle weakness; LB, labored breathing; AD, abdomina distention. NA: not available; y, year(s); m, month(s); d, day(s); "+": Present; "-": Absent

Statistical analysis

Statistical analysis was performed on SPSS 24.0 software (SPSS Inc. Chicago IL, USA). The Median and Interquartile range (IQR) of onset age and diagnosis age was calculated. The Shapiro–Wilk test was used to test for normality of the data. For data with non-normal distribution, Kruskal-Wallis H test was used for multiple group comparisons and Mann-Whitney U test for two group. $P < 0.05$ (two-tailed) were considered statistically significant.

Results

Clinical manifestations and laboratory tests

Clinical details were available for 12 patients. The age, sex, physical examination and laboratory findings at the time of diagnosis were recorded and showed in Table 1. The average age of onset was 11.5 ± 36.5 months, and the age of diagnosis was 22.5 ± 38.5 months. The initial symptoms of patients in our cohort were hypertransaminases, motor retardation due to muscle weakness, hypertrophic cardiomyopathy, and abdominal distension. Patients 1-7 had elevated liver enzymes and muscle weakness and were classified to mixed GSD, while patients 8–12 had only a liver-related phenotype without muscle involvement and were classified to hepatic GSD.

Candidate variants

Compound heterozygous/homozygous variants in *GAA* gene (P1-P7), *AGL* gene (P8, P9), or *PYGL* gene (P10) were detected in our patients, respectively. Patients 11–12 were detected as heterozygotes for the PHKA2 gene variant. Totally 18 different variants in four GSD related genes were found (variants c.2662G>T, c.1798C>T, and c.1622C>T of *GAA* gene were detected twice), of which 9 variants were

TABLE 2 | Mutations analyzed by WES and classified according to the ACMG guidelines.

Patient	Gene	Het/ Hom	Mutation 1					Mutation 2				
			Location	DNA change	Protein change	Variant type	Pathogenic evaluation according to ACMG	Location	DNA change	Protein change	Variant type	Pathogenic evaluation according to ACMG
P1	**GAA**	**Chet**	**exon19**	**c.2662G>T**	**p.Glu888X**	**Nonsense**	**P**	**exon13**	**c.1861T>G**	**p.Trp621Gly**	**Missense**	**LP**
P2	GAA	Chet	exon14	c.1933G>A	p.Asp645Asn	Missense	P	exon13	c.1798C>T	p.Arg600Cys	Missense	P
P3	GAA	Chet	exon11	c.1622C>T	p.Pro541Leu	Missense	LP	exon17	c.2399G>T	p.Ser800Ile	Missense	LP
P4	GAA	Chet	exon6	c.1052_1075+47del	—	Splicing	P	exon11	c.1622C>T	p.Prp541Leu	Missense	LP
P5	GAA	Chet	exon13	c.1798C>T	p.Arg600Cys	Missense	P	exon11	c.1557G>A	p.Met519Ile	Missense	LP
P6	GAA	Chet	exon6	c.1004G>A	p.Giy335Glu	Missense	P	exon11	c.1634C>T	p.Pro545Leu	Missense	LP
P7	GAA	Chet	exon19	c.2662G>T	p.Glu888X	Nonsense	P	exon5	c.877G>T	p.Gly293Trp	Missense	LP
P8	AGL	Hom	intron30	c.4161+2T>G	—	Splicing	P	—	—	—	—	—
P9	AGL	Chet	exon30	c.4119delT	p.Cys1373Trpfs*11	Frame shift	P	exon32	c.4284T>G	p.Try1428X	Nonsense	P
P10	PYGL	Chet	intron12	c.1518+1G>A	—	Splicing	P	exon6	c.730C>T	p.Leu244Phe	Missense	LP
P11	PHKA2	Hemi	exon32	c.3507_3520del	p.Gln1169Hisfs*29	Frame shift	P	—	—	—	—	—
P12	PHKA2	Hemi	exon9	c.883C>G	p.Arg295Gly	Missense	LP	—	—	—	—	—

The variants are described using NM_000152 for GAA, NM_000642 for AGL, NM_002863 for PYGL and NM_000292 for PHKA2 transcript reference sequences. Chet, compound heterozygous; Hom, homozygous; Hemi, hemizygous; P, Pathogenic; LP, Likely Pathogenic; novel variants: Bold font.

10.3389/fgene.2022.932760

TABLE 3 | Chr positions of the variants in GAA, AGL, PHKA2 and PYGL gene.

Patient no.	Gene	Mutation 1		Mutation 2	
		Position	c.DNA	Position	c.DNA
1	GAA	chr17:78092467	c.2662G>T	chr17:78086483	c.1861T>G
2	GAA	chr17:78086719	c.1933G>A	chr17:78086420	c.1798C>T
3	GAA	chr17:78084810	c.1622C>T	chr17:78091466	c.2399G>T
4	GAA	chr17:78082185-78082256	c.1052_1075+47del	chr17:78084810	c.1622C>T
5	GAA	chr17:78086420	c.1798C>T	chr17:78084745	c.1557G>A
6	GAA	chr17:78082137	c.1004G>A	chr17:78084822	c.1634C>T
7	GAA	chr17:78092467	c.2662G>T	chr17:78081617	c.877G>T
8	AGL	chr1:100379296	c.4161+2T>G	—	—
9	AGL	chr1:100379251-100379252	c.4119delT	chr1:100381990	c.4284T>G
10	PYGL	chr14:51381418	c.1518+1G>A	chr14:51387716	c.730C>T
11	PHKA2	chrX:18912338- 18912352	c.3507_3520del	—	—
12	PHKA2	chrX:18958148	c.883C>G	—	—

TABLE 4 | Effect on protein function of the novel variations predicted by SIFT, PolyPhen-2, MutationTaster, and REVEL.

Patient	Gene	Variant	Variant type	1000 Genome	ExAc	gnomAD	SIFT		Polyphen-2		Mutation taster		REVEL	
							Score	P	Score	P	Score	P	Score	P
P1	GAA	p.Trp621Gly	Missense	—	—	—	0	D	1	PD	1	DC	0.777	D
P3	GAA	p.Pro541Leu	Missense	—	—	—	0.005	D	0.994	PD	1	DC	0.892	D
P3	GAA	p.Ser800Ile	Missense	—	—	—	0.009	D	0.989	PD	1	DC	0.769	D
P7	GAA	p.Gly293Trp	Missense	—	—	—	0	D	1	PD	1	DC	0.899	D
P12	PHKA2	p.Arg295Gly	Missense	—	—	—	0	D	0.998	PD	1	DC	0.992	D
P8	AGL	c.4161+2T>G	Splicing	—	—	—	NA	NA	NA	NA	1	DC	NA	NA
P10	PYGL	c.1518+1G>A	Splicing	—	—	—	NA	NA	NA	NA	1	DC	NA	NA
P11	PHKA2	c.3507_3520del	Frame shift	—	—	—	NA	NA	NA	NA	1	DC	NA	NA

P, Prediction; D, Damaging; PD, Probably_damaging; DC, Disease_causing; NA: not available.

reported and 9 variants were novel. The variants in the patients were inherited from their carrier parents, except for 2 male patients with *PHKA2* gene variant on the X chromosome were from their mother. GSD type, variation location, variation, amino acid variation, variant type, and mutation analysis results of the variations are given in Tables 2, 3.

The nine novel variants were determined after checked in all available databases and publications, including 1000 Genomes, ExAC, gnomAD, in-house databases and published articles. The scores of SIFT, Polyphen-2, Mutation Taster, and REVEL predicted that the novel variants (except c.1052_1075 + 47del) have a deleterious effect on the function of the protein (Table 4). No predictions of impact were available for variant c.1052_1075 + 47del by bioinformatics algorithms. In the novel variants, 3 splicing and 1 frameshift mutations was classified as pathogenic, 5 missense mutations as likely pathogenic according to the ACMG guidelines (Richards et al., 2015).

There were 4 mutations of *GAA* and 1 of *PHKA2* in the novel missense variants. The 3D protein structures of *GAA* with novel missense variants were predicted by Swiss-Pdb Viewer 4.1 indicating the variants might affect the proteins function via destroying hydrogen bonds, or conformational constraints which resulted in the proteins into disordered extended structures (Figure 1). The protein structure of *PHKA2* with p. Arg295Gly was not constructed because there was no suitable model in SWISS-MODEL database. Silico analysis showed that the p. Arg295 in *PHKA2* was highly conservative in different species of human, Macaque, canine, Cattle, et al. (Figure 2).

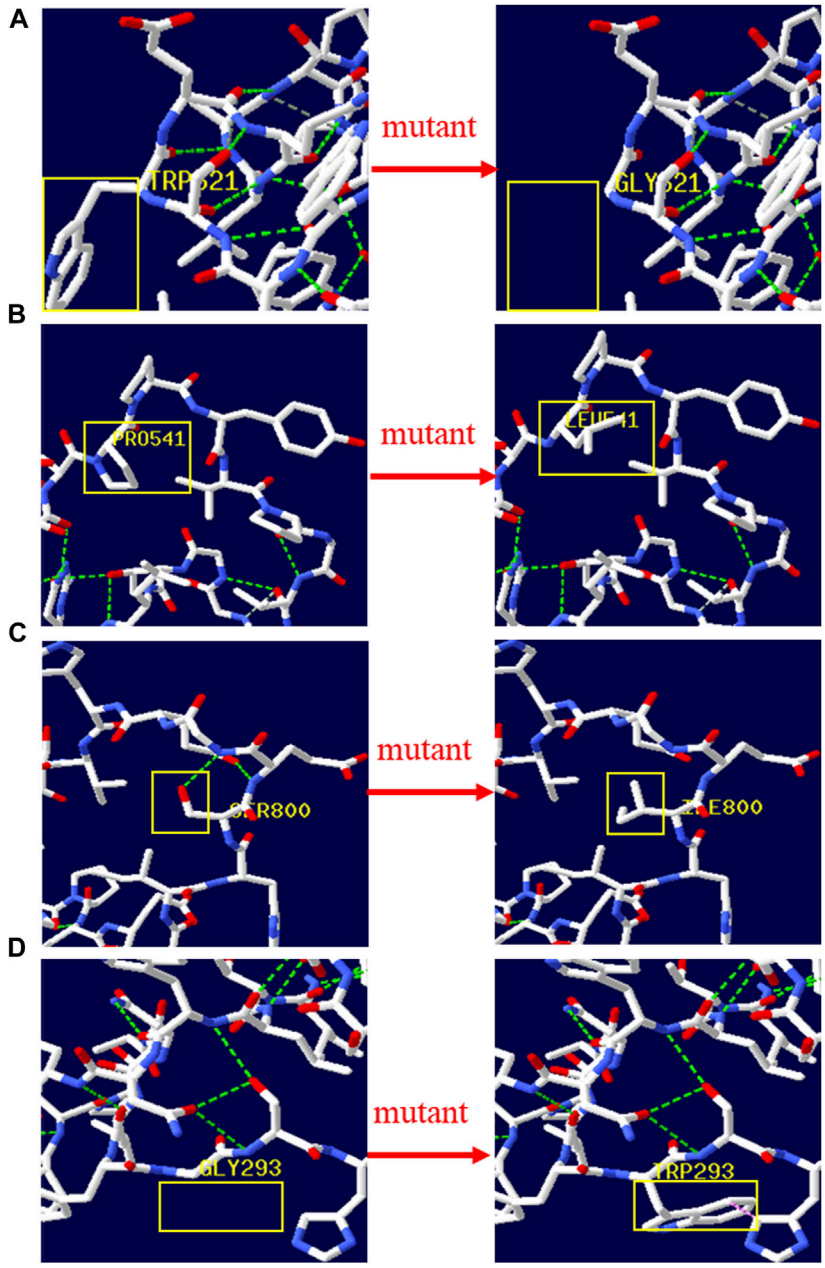


FIGURE 1
3D structure of wild type and mutant type of novel variants in GAA. The yellow boxes marked the sites of wild-type Gly293, Prp541, Trp621, Ser800 and mutated Gly621, Leu541, Ile800, Trp293. The 3D protein structures of novel variants in GAA gene were predicted by Swiss-Pdb Viewer 4.1 indicating the missense mutations might affect the proteins function via destroying hydrogen bonds, or conformational constraints which resulted in the proteins into disordered extended structures.

Genetic diagnosis and clinical analysis

Gene sequencing showed that 7 patients were diagnosed with GSD II, 2 patients with GSD III, 1 patient with GSD VI, and 2 patients with GSD IXα. In the study group, the most frequent subtype of GSD was type II with 58.3% (n = 7), followed by GSD III (n = 2) and IXα with 16.7% (n = 2).

Seven GSD II patients were divided into infantile-onset Pompe disease (IOPD) (P1, P2, P7) group and late-onset Pompe disease (LOPD) (P3-P6) group according to appearance cardiomyopathy within/out 12 months and age of onset (Molares-Vila et al., 2021). The initial symptoms of GSD II patients were Hypertrophic cardiomyopathy (66.6%) and Hypertransaminase (33.3%) in IOPD group, while

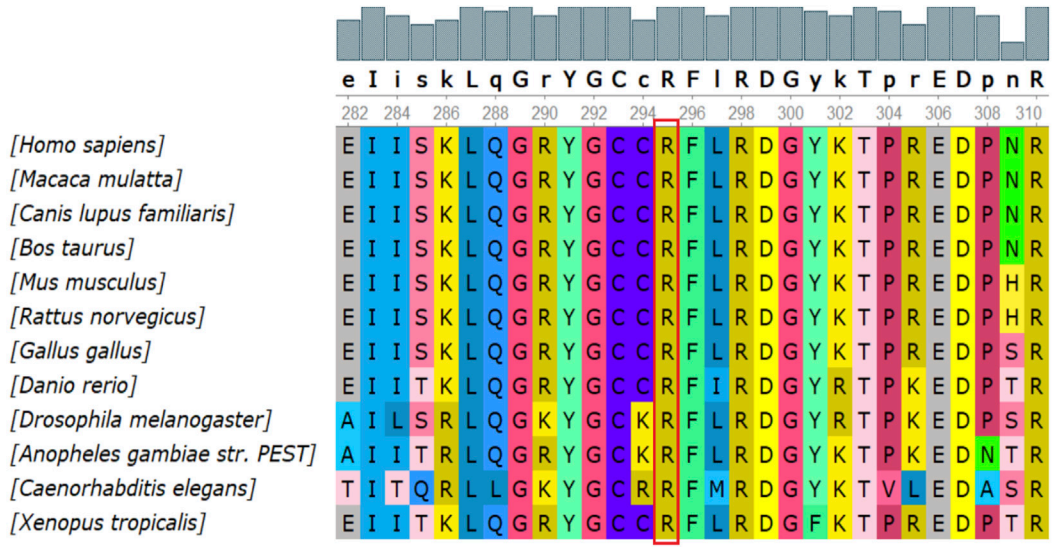


FIGURE 2
Conservation analysis of the p.Arg295Gly mutation in *PHKA2*. Silico analysis of p.Arg295 in *PHKA2* shows the site highly conservative in different species of human, Macaque, canine, Cattle, etc.

exercise-induced muscle weakness (75.0%) and labored breathing (25.0%) in LOPD group. In our study, laboratory findings of IOPD and LOPD were not significantly different except for CK values ($p > 0.05$).

There were 5 patients with hepatic GSD in our study, including 2 patients with GSD III, 1 patient with GSD VI, and 2 patients with GSD IXα. Hepatomegaly, hypoglycemia and hypertransaminase were observed in all patients, hypertriglyceridemia in 80% (4/5) patients and hyperlactate in 60% (3/5, 1 undetected) patients. The first and main symptom of patients (P8, P9) with GSD III was progressive abdominal distention (100%) due to enlarged liver. The main symptom observed in the patient (P10-P12) with GSD VI or IXα was hypertransaminasemia (100%) detected on laboratory examination accompanied by hepatomegaly. Neither liver size nor laboratory findings allow for a differentiation among GSD III, GSD VI and GSD IXα ($p > 0.05$). At diagnosis, both patients with GSD IX had a height shorter than -2 SDS, while growth retardation was not found in GSD III and GSD VI patients. Between GSD II group and the hepatic GSD group, significant differences in liver size and partial laboratory findings (glutamyl transpeptidasea, hydroxybutyrate dehydrogenasea, creatine kinasea, Glycemia, Lactic acid) were found.

Treatment and follow-up

Of seven GSD II patients, six received enzyme replacement therapy (ERT) (Myozyme®) injection, 4 of whom responded to treatment, 2 were discontinued due to death with severe myocardial hypertrophy and pulmonary hypertension and hypersensitivity, and 1 patient lost visit. Two patients with GSD III received oral raw cornstarch and increased dietary protein after diagnosis. During treatment, they occasionally experienced convulsions due to fasting hypoglycemia, and developed symptoms of short stature and delayed motor development. In patients with GSD VI and IXα, after receiving oral raw cornstarch, the clinical symptoms basically disappeared except for the hypertransaminases.

Discussion

Diagnosis and distribution of GSDs

The molecular mechanism of GSD is variation in genes encoding key enzymes in glycogenolysis or gluconeogenesis (Ying et al., 2020). With the development of gene sequencing technology, identification of variants by next-generation sequencing (NGS) has partially replaced traditional invasive examinations, such as liver biopsy, muscle biopsy, etc. As the accurate standard for diagnosis of GSD (Sperb-Ludwig et al., 2019; Beyzaei et al., 2020; Szymanska et al., 2021). In the present study, 18 different heterozygous candidate mutations (9 novel and 9 reported) were identified in 12 Chinese GSD families: 7 families carrying *GAA* mutations (7/12, 58.3%), 2 carrying *AGL* mutations (2/12, 16.7%), 1 carrying *PYGL* mutation (1/12, 8.3%), and

2 carrying *PHKA2* mutations (2/12, 16.7%). According to the ACMG guidelines (Richards et al., 2015), 4 of the 9 novel variants was classified as pathogenic, 5 classified as likely pathogenic, and all of them have not been reported in any human gene mutation databases or publications (Table 2). Early and accurate diagnosis of GSD is an important step in realizing personalized management, helping physicians to formulate the best treatment plan for patients and minimizing adverse outcomes (Retterer et al., 2016; Beyzaei et al., 2021; Unnisa et al., 2022). The median age of the 12 patients diagnosed in this study was 22 months (including 5 cases less than or equal to 1 year old), meaning that an earlier diagnosis and treatment is more conducive to reducing the risk of organ damage progression and death.

It has been known the geographical distribution of GSD subtypes and genotype was different. In a cohort of Iranian, GSD III (*AGL*), GSD IX (*PHKB* and *PHKG2*) was the major type of GSD (Beyzaei et al., 2021). In Turkish, the genetic analysis showed that the highest proportion of GSDs was type III with 39.5% (n = 15), followed by type I with 36.8% (n = 14) (Cakar et al., 2020). While in Spain, Vega et al. reported that more than three-quarters of patients with GSDs were type III or IXα (Vega et al., 2016). In our study cohort, more than half of the patients were diagnosed as GSD II which suggested that type II may be the most common subtype in the Chinese GSD population.

Patients with GSD II

GSD II (MIM# 232300), also known as Pompe disease, caused by deficiency of the enzyme acid α-glucosidase encoded by *GAA*, presents as a progressive myopathy due to accumulation of glycogen in lysosomes and cell destruction (van Capelle et al., 2016). GSD II presents as a broad clinical spectrum of phenotypes with considerable variation in age of onset, symptom/presenting sign, degree of severity, organ involvement, and nature history (Holzwarth et al., 2022). In our study, 7 patients were detected compound heterozygous mutations in *GAA* gene with an age ranging from birth to 12 years old. Three patients (P1, P2, P7) manifesting generalized myasthenia and hypertrophic cardiomyopathy within the first months of life were IOPD. Two of them also showed severe malnutrition. Four patients (P3-P6) who presented as progressive limb-girdle muscle weakness with hyperCKemia were LOPD. Noteworthily, although P4 developed dyspnea shortly after birth due to respiratory muscle involvement, but she had relatively mild myocardial damage and was classified as LOPD (Hout et al., 2003; Kishnani et al., 2006; Chawla et al., 2022).

Of the *GAA* variants reported worldwide, c.-32-13T>G is the most common, especially in Caucasian populations. In Asia Pacific, p. Asp645Glu, p. Trp746Cys, p. Gly576Ser, p. Glu888X were most reported (Bergsma et al., 2019; Reuser et al., 2019; Zhao et al., 2019). While in our study, p. Glu888X were detected in P1 and P7, and no other Asia-Pacific high-frequency variants were found. Previous genotype-phenotype correlation research have shown that variants p. Glu888X, p. Asp645Asn, and p. Arg600Cys were associated with IOPD (Reuser et al., 2019). The conclusion was confirmed in our study that 4 patients (P1, P2, P5, and P7) carried one or both of the above variants manifest as early-onset or severe symptom.

We identified 6 reported variants and 5 novel variants of *GAA* in seven patients with GSD II. Four of the new variants were missense variants and all of them located in the GAA protein domain: p. Gly293Trp maps to the N-terminal Beta Sheet domain, p. Prp541Leu and p. Trp621Gly maps to the catalytic GH31 domain, p. Ser800Ile Maps to the Proximal Beta Sheet field. The four variants were predicted to be disease-causing by SIFT, Mutation taster, REVEL and probably-damaging by Polyphen. The 3D protein structures of GAA protein were predicted and indicated that the novel missense mutations might affect the proteins function *via* destroying hydrogen bonds, or conformational constraints which resulted in the proteins into disordered extended structures (Figure 1). In addition, p. Gly293Arg, resulting in co-located but different amino acid changes with p. Gly293Trp, has been described in two LOPD patients and identified as pathogenic (Loscher et al., 2018). Another new variant was c.1052_1075 + 47del, a splice variant lacking 71 nucleotides spanning exon 6 and intron 6 that could theoretically affect normal mRNA splicing. However, bioinformatics algorithms were unable to predict the effect of this variant. According to ACMG criteria, four novel missense variants were classified as probable pathogenic variants and one novel splice variant was classified as pathogenic.

Patients with GSD III, VI and IXα

GSD III (*AGL*, MIM# 232400), VI (*PYGL*, MIM# 232700) and IXα (*PHKA2*, MIM# 306000) belong to hepatic GSD with basic features of hepatomegaly and hypoglycemia (Beyzaei et al., 2020). They share commonalities also in other clinical signs: metabolic abnormalities, short stature, and motor development delay/muscle weakness with aging, that lead to challenging to identify the subtypes of patients with hepatic GSD, especially between VI and IX (Qu et al., 2020; Szymanska et al., 2021). However, some subtypes have been found to have specific phenotypic features, for example growth delay is more common in GSD IX patients than in VI patients and hypoglycemia was more pronounced in GSD III than GSD VI and IX (Kishnani et al., 2019; Fernandes et al., 2020; Grunert et al., 2021b). In our study, there were 2 patients of GSD III, 1 patient of GSD VI and 2 patients of GSD IXα. Hepatomegaly, hypoglycemia

and hypertransaminase were observed in all patients, hypertriglyceridemia in 80% patients and hyperlactate in 60% patients. Neither liver size nor laboratory findings allow for a differentiation among GSD III, GSD VI and GSD IXα in our study, but only patients with GSD IXα had a height below -2 SDS, which was consistent with the findings of Grunert et al. (Grunert et al., 2021b). None of our patients had significant motor retardation when diagnosed. Interestingly, the initial symptom of two GSD III patients was abdominal distention due to hepatomegaly, whereas GSD VI and IX patients presented with elevated transaminases inadvertently during upper respiratory tract infection.

We identified 3 variants of *AGL* gene in patients with GSD III: p. Cys1373Trpfs*11 and p. Try1428X were detected compound heterozygous in patient 9 and already reported in Chinese population (Lu et al., 2016); c.4161 + 2T>G as a novel splicing variation was detected to be homozygous in P8 while her parents were from two unrelated families. c.4161 + 2T>G was predicted to affect normal splicing of mRNA and evaluated as disease-causing by Mutation taster. According to the standard of ACMG, c.4161 + 2T>G was classified as pathogenic mutation. Notably, the 3 variants were concentrated in the 30th intron or exon, and the 2 patients with them have similar phenotypes and onset times.

GSD VI is rare relative to other types of GSD, with an incidence of 1/60,000 to 1/85,000 (Zhan et al., 2021). As the only causative gene of GSD VI, *PYGL* gene has been recorded 80 types of mutations in the HGMD database (22 April 2022), among which missense/nonsense mutations are the most common. So far, 17 Chinese patients with GSD VI have been reported, and no *PYGL* hotspot variant has been found in this group (Lu et al., 2020; Luo et al., 2020; Zhan et al., 2021). For P10, we identified compound heterozygous point mutations in *PYGL* through WES, including a recurrent missense mutation p. Leu244Phe on exon 6 and a novel splicing mutation c.1518 + 1G>A on intron 12 (Lu et al., 2020). c.1518 + 1G>A was predicted to resulting in forming incorrect mRNA molecule and evluated as disease-causing by Mutation taster. Variant frequency was 0 in the database of 1000 Genomes, gnomAD and ExAC. According to the ACMG standard, c.1518 + 1G>A was classified as a pathogenic variant.

In liver form of GSD IXα, the disease is inherited in an X-linked recessive manner associated with *PHKA2* mutations (Fang et al., 2021; Mori et al., 2022). As of 22 April 2022, 166 *PHKA2* variants were recorded in the HGMD database, with missense/nonsense mutations (greater than 50%) being the most common, followed by small deletion variants. In this report, we detected two novel variants in *PHKA2*, c.3507_3520del (p.Gln1169Hisfs*29) and p. Arg295Gly. p. Gln1169Hisfs*29 lead to fourteen-nucleotide deletion within exon 32 of PHKA2, that seemed to result in a frameshift introducing a premature stop codon after 2602 bp of amino acid residue 1196 of 1235. The variant was predicted disease-causing by Mutation taster and evaluated as a pathogenic variant refer to ACMG guidelines. Notably, the *PHKA2* gene had a total of 33 exons, and one-fifth (34/166) of the reported variants were located in or spanned exons 30–33, suggesting that the C-terminus of the *PHKA2* was a variant-dense region. p. Arg295Gly is an unreported missense variant, but p. Arg295His (Fernandes et al., 2020) and p. Arg295Cys (Ban et al., 2003) had been described in GSD IXα patients and identified as pathogenic. Silico analysis of p. Arg295 in *PHKA2* shows the site highly conservative in different species of human, Macaque, canine, Cattle, et al. SIFT, Mutation taster and Polyphen predicted that p. Arg295Gly was damaging to protein function. Therefore, p. Arg295Gly was assessed as likely pathogenic according to ACMG criteria.

Conclusion

This study reported 12 Chinese patients with Glycogen storage disease and identified 18 gene variants of *GAA*, *AGL*, *PHKA2* and *PYGL* (9 novel and 9 reported) by whole-exome sequencing. Our study expanded the variation spectrum of gene associated with GSDs. Next-generation sequencing was considered the preferred diagnostic method for GSD because invasive liver biopsy can be avoided.

Data availability statement

The data presented in the study are deposited in the GenBank repository, accession number OP117444-OP117449.

Ethics statement

The studies involving human participants were reviewed and approved by Medical Ethics Committee of Children's Hospital Affiliated to Shandong University (Jinan Children's Hospital). Written informed consent to participate in this study was provided by the participants' legal guardian/next of kin.

Author contributions

ZG and YL conceived and designed this study. Experiments were conducted by RD, KZ, YL, MG, DW, and JM. Data were analyzed by RD, KZ, and YL. Clinical diagnosis of the patients was undertaken by FS, RD, and ZG. The paper was written by RD and XW. RD and XW contributed equally to this work.

Funding

This work was supported by the National Natural Science Foundation of China (81671362 and 32000075), the financial funding from Department of Science and Technology of Shandong Province (ZR2020QC066 and ZR2020QH102), the financial funding from Jinan Science and Technology Bureau (201907007).

Acknowledgments

We thank the patients and their families for their participation and contribution to the work.

Conflict of interest

The authors declare that the research was conducted in the absence of any commercial or financial relationships that could be construed as a potential conflict of interest.

Publisher's note

All claims expressed in this article are solely those of the authors and do not necessarily represent those of their affiliated organizations, or those of the publisher, the editors and the reviewers. Any product that may be evaluated in this article, or claim that may be made by its manufacturer, is not guaranteed or endorsed by the publisher.

References

Ban, K., Sugiyama, K., Goto, K., Mizutani, F., and Togari, H. (2003). Detection of PHKA2 gene mutation in four Japanese patients with hepatic phosphorylase kinase deficiency. *Tohoku J. Exp. Med.* 200, 47–53. doi:10.1620/tjem.200.47

Bergsma, A. J., In 't Groen, S. L. M., van den Dorpel, J. J. A., van den Hout, H., van der Beek, N., Schoser, B., et al. (2019). A genetic modifier of symptom onset in Pompe disease. *EBioMedicine* 43, 553–561. doi:10.1016/j.ebiom.2019.03.048

Beyzaei, Z., Ezgu, F., Geramizadeh, B., Imanieh, M. H., Haghighat, M., Dehghani, S. M., et al. (2021). Clinical and genetic spectrum of glycogen storage disease in Iranian population using targeted gene sequencing. *Sci. Rep.* 11 (1), 7040. doi:10.1038/s41598-021-86338-4

Beyzaei, Z., Geramizadeh, B., and Karimzadeh, S. (2020). Diagnosis of hepatic glycogen storage disease patients with overlapping clinical symptoms by massively parallel sequencing: a systematic review of literature. *Orphanet J. Rare Dis.* 15 (1), 286. doi:10.1186/s13023-020-01573-8

Brown, L. M., Corrado, M. M., van der Ende, R. M., Derks, T. G., Chen, M. A., Siegel, S., et al. (2015). Evaluation of glycogen storage disease as a cause of ketotic hypoglycemia in children. *J. Inherit. Metab. Dis.* 38 (3), 489–493. doi:10.1007/s10545-014-9744-1

Cakar, N. E., Gezdirici, A., Topuz, H. S., and Onal, H. (2020). Novel variants in Turkish patients with glycogen storage disease. *Pediatr. Int.* 62 (10), 1145–1150. doi:10.1111/ped.14286

Chawla, T., Preethish-Kumar, V., Polavarapu, K., Vengalil, S., Bardhan, M., Puri, R., et al. (2022). Late onset Pompe disease with novel mutations and atypical phenotypes. *J. Neuromuscul. Dis.* 9 (2), 261–273. doi:10.3233/JND-210728

Choi, R., Park, H. D., Kang, B., Choi, S. Y., Ki, C. S., Lee, S. Y., et al. (2016). PHKA2 mutation spectrum in Korean patients with glycogen storage disease type IX: Prevalence of deletion mutations. *BMC Med. Genet.* 17, 33. doi:10.1186/s12881-016-0295-1

De Vito, E. L., Arce, S. C., Monteiro, S. G., and Vaca Ruiz, G. A. (2019). Central drive and ventilatory failure in late-onset Pompe disease: At the gates of a new phenotype. *Neuromuscul. Disord.* 29 (6), 444–447. doi:10.1016/j.nmd.2019.03.008

Eghbali, M., Fatemi, K. S., Salehpour, S., Abiri, M., Saei, H., Talebi, S., et al. (2020). Whole-exome sequencing uncovers novel causative variants and additional findings in three patients affected by glycogen storage disease type VI and fanconi-bickel syndrome. *Front. Genet.* 11, 601566. doi:10.3389/fgene.2020.601566

Fang, Y., Yu, J., Lou, J., Peng, K., Zhao, H., and Chen, J. (2021). Clinical and genetic spectra of inherited liver disease in children in China. *Front. Pediatr.* 9, 631620. doi:10.3389/fped.2021.631620

Fernandes, S. A., Cooper, G. E., Gibson, R. A., and Kishnani, P. S. (2020). Benign or not benign? Deep phenotyping of liver glycogen storage disease IX. *Mol. Genet. Metab.* 131 (3), 299–305. doi:10.1016/j.ymgme.2020.10.004

Grunert, S. C., Hannibal, L., Schumann, A., Rosenbaum-Fabian, S., Beck-Wodl, S., Haack, T. B., et al. (2021a). Identification and characterization of a novel splice site mutation associated with glycogen storage disease type VI in two unrelated Turkish families. *Diagn. (Basel)* 11 (3), 500. doi:10.3390/diagnostics11030500

Grunert, S. C., Hannibal, L., and Spiekerkoetter, U. (2021b). The phenotypic and genetic spectrum of glycogen storage disease type VI. *Genes* 12 (8), 1205. doi:10.3390/genes12081205

Holzwarth, J., Minopoli, N., Pfrimmer, C., Smitka, M., Borrel, S., Kirschner, J., et al. (2022). Clinical and genetic aspects of juvenile onset Pompe disease. *Neuropediatrics* 53 (1), 39–45. doi:10.1055/s-0041-1735250

Hout, H. M. P. v. d., Hop, W., Diggelen, O. P. v., Smeitink, J. A. M., Smit, G. P. A., et al. (2003). The natural course of infantile pompe's disease: 20 original cases compared with 133 cases from the literature. *Pediatrics* 112 (2), 332–340. doi:10.1542/peds.112.2.332

Huang, W., Zhan, D., Li, Y., Zheng, N., Wei, X., Bai, B., et al. (2021). Proteomics provides individualized options of precision medicine for patients with gastric cancer. *Sci. China. Life Sci.* 64 (8), 1199–1211. doi:10.1007/s11427-021-1966-4

Kim, T. H., Kim, K. Y., Kim, M. J., Seong, M. W., Park, S. S., Moon, J. S., et al. (2020). Molecular diagnosis of glycogen storage disease type IX using a glycogen storage disease gene panel. *Eur. J. Med. Genet.* 63 (6), 103921. doi:10.1016/j.ejmg.2020.103921

Kishnani, P. S., Goldstein, J., Austin, S. L., Arn, P., Bachrach, B., Bali, D. S., et al. (2019). Diagnosis and management of glycogen storage diseases type VI and IX: a clinical practice resource of the American College of medical genetics and Genomics (ACMG). *Genet. Med.* 21 (4), 772–789. doi:10.1038/s41436-018-0364-2

Kishnani, P. S., Hwu, W. L., Mandel, H., Nicolino, M., Yong, F., Corzo, D., et al. (2006). A retrospective, multinational, multicenter study on the natural history of infantile-onset Pompe disease. *J. Pediatr.* 148 (5), 671–676. doi:10.1016/j.jpeds.2005.11.033

Li, Y., Chen, J., Xu, Q., Han, Z., Tan, F., Shi, T., et al. (2021). Single-cell transcriptomic analysis reveals dynamic alternative splicing and gene regulatory networks among pancreatic islets. *Sci. China. Life Sci.* 64 (1), 174–176. doi:10.1007/s11427-020-1711-x

Liang, Y., Du, C., Wei, H., Zhang, C., Zhang, M., Hu, M., et al. (2020). Genotypic and clinical analysis of 49 Chinese children with hepatic glycogen storage diseases. *Mol. Genet. Genomic Med.* 8 (10), e1444. doi:10.1002/mgg3.1444

Loscher, W. N., Huemer, M., Stulnig, T. M., Simschitz, P., Iglseder, S., Eggers, C., et al. (2018). Pompe disease in Austria: clinical, genetic and epidemiological aspects. *J. Neurol.* 265 (1), 159–164. doi:10.1007/s00415-017-8686-6

Lu, C., Qiu, Z., Sun, M., Wang, W., Wei, M., and Zhang, X. (2016). Spectrum of AGL mutations in Chinese patients with glycogen storage disease type III: identification of 31 novel mutations. *J. Hum. Genet.* 61 (7), 641–645. doi:10.1038/jhg.2016.24

Lu, S. Q., Feng, J. Y., Liu, J., Xie, X. B., Lu, Y., and Abuduxikuer, K. (2020). Glycogen storage disease type VI can progress to cirrhosis: ten Chinese patients with GSD VI and a literature review. *J. Pediatr. Endocrinol. Metab.* 33 (10), 1321–1333. doi:10.1515/jpem-2020-0173

Luo, X., Hu, J., Gao, X., Fan, Y., Sun, Y., Gu, X., et al. (2020). Novel PYGL mutations in Chinese children leading to glycogen storage disease type VI: two case reports. *BMC Med. Genet.* 21 (1), 74. doi:10.1186/s12881-020-01010-4

Molares-Vila, A., Corbalan-Rivas, A., Carnero-Gregorio, M., Gonzalez-Cespon, J. L., and Rodriguez-Cerdeira, C. (2021). Biomarkers in glycogen storage diseases: An update. *Int. J. Mol. Sci.* 22 (9), 4381. doi:10.3390/ijms22094381

Mori, T., Ishikawa, A., Shigetomi, H., Fukuda, T., and Sugie, H. (2022). A novel PHKA2 variant in a Japanese boy with glycogen storage diseases type IXa. *Pediatr. Int.* 64 (1), e14839. doi:10.1111/ped.14839

Perveen, S., Gupta, N., Kumar, M., Kaur, P., Chowdhury, M. R., and Kabra, M. (2020). Spectrum of amyloglucosidase mutations in Asian Indian patients with Glycogen storage disease type III. *Am. J. Med. Genet. A* 182 (5), 1190–1200. doi:10.1002/ajmg.a.61547

Qu, Q., Qian, Q., Shi, J., Liu, H., Zhang, Y., Cui, W., et al. (2020). The novel compound heterozygous mutations in the AGL gene in a Chinese family with adult late-onset glycogen storage disease type IIIa. *Front. Neurol.* 11, 554012. doi:10.3389/fneur.2020.554012

Retterer, K., Juusola, J., Cho, M. T., Vitazka, P., Millan, F., Gibellini, F., et al. (2016). Clinical application of whole-exome sequencing across clinical indications. *Genet. Med.* 18 (7), 696–704. doi:10.1038/gim.2015.148

Reuser, A. J. J., van der Ploeg, A. T., Chien, Y. H., Llerena, J., Jr., Abbott, M. A., Clemens, P. R., et al. (2019). GAA variants and phenotypes among 1, 079 patients with Pompe disease: Data from the Pompe Registry. *Hum. Mutat.* 40 (11), 2146–2164. doi:10.1002/humu.23878

Richards, S., Aziz, N., Bale, S., Bick, D., Das, S., Gastier-Foster, J., et al. (2015). Standards and guidelines for the interpretation of sequence variants: a joint consensus recommendation of the American College of medical genetics and Genomics and the association for molecular pathology. *Genet. Med.* 17 (5), 405–424. doi:10.1038/gim.2015.30

Shen, Y., and Shi, T. (2019). Innovation for better health of children. *Sci. China. Life Sci.* 62 (12), 1561–1562. doi:10.1007/s11427-019-1589-2

Sperb-Ludwig, F., Pinheiro, F. C., Bettio Soares, M., Nalin, T., Ribeiro, E. M., Steiner, C. E., et al. (2019). Glycogen storage diseases: Twenty-seven new variants in a cohort of 125 patients. *Mol. Genet. Genomic Med.* 7 (11), e877. doi:10.1002/mgg3.877

Szymanska, E., Jozwiak-Dziecielewska, D. A., Gronek, J., Niewczas, M., Czarny, W., Rokicki, D., et al. (2021). Hepatic glycogen storage diseases: Pathogenesis, clinical symptoms and therapeutic management. *Arch. Med. Sci.* 17 (2), 304–313. doi:10.5114/aoms.2019.83063

Unnisa, Z., Yoon, J. K., Schindler, J. W., Mason, C., and van Til, N. P. (2022). Gene therapy developments for Pompe disease. *Biomedicines* 10 (2), 302. doi:10.3390/biomedicines10020302

van Capelle, C. I., van der Meijden, J. C., van den Hout, J. M., Jaeken, J., Baethmann, M., Voit, T., et al. (2016). Childhood Pompe disease: clinical spectrum and genotype in 31 patients. *Orphanet J. Rare Dis.* 11 (1), 65. doi:10.1186/s13023-016-0442-y

Vega, A. I., Medrano, C., Navarrete, R., Desviat, L. R., Merinero, B., Rodriguez-Pombo, P., et al. (2016). Molecular diagnosis of glycogen storage disease and disorders with overlapping clinical symptoms by massive parallel sequencing. *Genet. Med.* 18 (10), 1037–1043. doi:10.1038/gim.2015.217

Ying, S., Zhihua, Z., Yucan, Z., Yu, J., Qian, L., Bixia, Z., et al. (2020). Molecular diagnosis of panel-based next-generation sequencing approach and clinical symptoms in patients with glycogen storage disease: A single center retrospective study. *Front. Pediatr.* 8, 600446. doi:10.3389/fped.2020.600446

Zhan, Q., Lv, Z., Tang, Q., Huang, L., Chen, X., Yang, M., et al. (2021). Glycogen storage disease type VI with a novel PYGL mutation: Two case reports and literature review. *Med. Baltim.* 100 (16), e25520. doi:10.1097/MD.0000000000025520

Zhao, Y., Wang, Z., Lu, J., Gu, X., Huang, Y., Qiu, Z., et al. (2019). Characteristics of Pompe disease in China: a report from the Pompe registry. *Orphanet J. Rare Dis.* 14 (1), 78. doi:10.1186/s13023-019-1054-0

frontiers | Frontiers in Genetics

TYPE Original Research
PUBLISHED 12 September 2022
DOI 10.3389/fgene.2022.990015

Check for updates

OPEN ACCESS

EDITED BY
Ruth Roberts,
ApconiX, United Kingdom

REVIEWED BY
Ngoc-Lan Nguyen,Vietnam Academy of Science and Technology, Vietnam
Fei Yin,
Xiangya hospital, Central South University, China
Muhammad Naeem,
Hebei Normal University, China

*CORRESPONDENCE
Murim Choi,
murimchoi@snu.ac.kr
Jong-Hee Chae,
chaeped1@snu.ac.kr

†These authors share senior authorship

SPECIALTY SECTION
This article was submitted to Genetics of Common and Rare Diseases, a section of the journal Frontiers in Genetics

RECEIVED 09 July 2022
ACCEPTED 23 August 2022
PUBLISHED 12 September 2022

CITATION
Park S, Jang SS, Lee S, Kim M, Sim H, Jeon H, Hong SE, Lee J, Lee J, Jeon EY, Lee J, Lee C-R, Kim SY, Kim MJ, Yoon JG, Lim BC, Kim WJ, Kim KJ, Ko JM, Cho A, Lee JS, Choi M and Chae J-H (2022), Systematic analysis of inheritance pattern determination in genes that cause rare neurodevelopmental diseases. *Front. Genet.* 13:990015. doi: 10.3389/fgene.2022.990015

COPYRIGHT
© 2022 Park, Jang, Lee, Kim, Sim, Jeon, Hong, Lee, Lee, Jeon, Lee, Lee, Kim, Kim, Yoon, Lim, Kim, Kim, Ko, Cho, Lee, Choi and Chae. This is an open-access article distributed under the terms of the Creative Commons Attribution License (CC BY). The use, distribution or reproduction in other forums is permitted, provided the original author(s) and the copyright owner(s) are credited and that the original publication in this journal is cited, in accordance with accepted academic practice. No use, distribution or reproduction is permitted which does not comply with these terms.

Systematic analysis of inheritance pattern determination in genes that cause rare neurodevelopmental diseases

Soojin Park[1], Se Song Jang[1], Seungbok Lee[1,2], Minsoo Kim[3], Hyungtai Sim[3], Hyeongseok Jeon[3], Sung Eun Hong[3], Jean Lee[3], Jeongeun Lee[3], Eun Young Jeon[3], Jeongha Lee[3], Cho-Rong Lee[3], Soo Yeon Kim[2], Man Jin Kim[2,4], Jihoon G. Yoon[2], Byung Chan Lim[1], Woo Joong Kim[1], Ki Joong Kim[1], Jung Min Ko[1], Anna Cho[5], Jin Sook Lee[6], Murim Choi[3*†] and Jong-Hee Chae[1,2*†]

[1]Department of Pediatrics, Seoul National University College of Medicine, Seoul National University Children's Hospital, Seoul, South Korea, [2]Department of Genomic Medicine, Seoul National University Hospital, Seoul, South Korea, [3]Department of Biomedical Sciences, Seoul National University College of Medicine, Seoul, South Korea, [4]Rare Disease Center, Seoul National University Hospital, Seoul, South Korea, [5]Department of Pediatrics, Seoul National University Bundang Hospital, Seongnam, South Korea, [6]Department of Pediatrics, Seoul National University Hospital Child Cancer and Rare Disease Administration, Seoul National University Children's Hospital, Seoul, South Korea

Despite recent advancements in our understanding of genetic etiology and its molecular and physiological consequences, it is not yet clear what genetic features determine the inheritance pattern of a disease. To address this issue, we conducted whole exome sequencing analysis to characterize genetic variants in 1,180 Korean patients with neurological symptoms. The diagnostic yield for definitive pathogenic variant findings was 50.8%, after including 33 cases (5.9%) additionally diagnosed by reanalysis. Of diagnosed patients, 33.4% carried inherited variants. At the genetic level, autosomal recessive-inherited genes were characterized by enrichments in metabolic process, muscle organization and metal ion homeostasis pathways. Transcriptome and interactome profiling analyses revealed less brain-centered expression and fewer protein-protein interactions for recessive genes. The majority of autosomal recessive genes were more tolerant of variation, and functional prediction scores of recessively-inherited variants tended to be lower than those of dominantly-inherited variants. Additionally, we were able to predict the rates of carriers for recessive variants. Our results showed that genes responsible for neurodevelopmental disorders harbor different molecular mechanisms and expression patterns according to their inheritance patterns. Also, calculated frequency rates for recessive variants could be utilized to pre-screen rare neurodevelopmental disorder carriers.

KEYWORDS

neurodevelopmental disorder, inheritance pattern, carrier prediction, whole exome sequencing, recessive disorders

Introduction

Genetic disorders are caused by various alterations in gene function. According to the Online Mendelian Inheritance in Men (OMIM) compendium, 4,617 genes and their variants are associated with human disease as of April 2022 (Amberger et al., 2015; Amberger and Hamosh, 2017). Broadly, disease-associated alterations can be categorized as resulting in either gain-of-function (GoF) or loss-of-function (LoF) of a gene. GoF is mostly associated with dominant inheritance, whereas LoF can appear in recessive form as well as dominant (as haploinsufficiency) (Jimenez-Sanchez et al., 2001; Schuster-Böckler and Bateman, 2008). Mendelian disorders with recessive inheritance patterns are primarily observed in ethnic groups with high rates of consanguineous marriages (Verma and Puri, 2015; Abouelhoda et al., 2016), whereas those with dominant and recessive inheritance patterns appear in comparable rates in other "outbred" ethnic groups (Baird et al., 1988). Despite recent efforts into patient genome sequencing, diagnosis, and the discovery of novel genes that cause rare Mendelian disorders, it is not yet clear what drives genes to carry variants that are inherited in dominant or recessive patterns. It seems intuitive to postulate that genes that cause diseases in recessive pattern are less critical and more tolerant in development and physiology as one has to carry defective variants in both alleles for a disease to manifest. Nevertheless, there is need to systematically evaluate whether other properties that may represent gene function, expression, and previous disease associations also play a role in the process.

The study of genes that cause recessive diseases is important because knowledge of such genes can be utilized to predict marriages between carriers and avoid the generation of new patients. This strategy has been already proven successful in a number of diseases, such as β-thalassaemia and Tay–Sachs disease (Kaback, 2001; Cao and Kan, 2013). However, those diseases are single gene disorders and display ethnic biases, making the process of variant curation and evaluation for pathogenicity and also the prediction of patients more efficient. Meanwhile, applying such an approach to diseases with heuristic symptoms requires considerably more effort because of the involvement of many genes and variants and the diverse clinical symptoms. Therefore, understanding the features of genetic variants that cause disease in a recessive inheritance pattern will provide a novel approach for avoiding generation of patients.

Complex structure and function of brain involve coordinated expression and function of many genes, and this is also reflected on a diverse array of rare Mendelian neurodevelopmental diseases (NDD) that we observe from patients. Such patients display abnormal brain function and/or structure which may affect motor function, learning ability, development, language, and other brain activities. Diagnosis of such diseases is a challenge because of the extreme genetic heterogeneity and rare occurrence, while whole exome sequencing (WES) has enhanced the yield of NDD diagnoses in clinical practice (Yang et al., 2013; Iglesias et al., 2014; Lee et al., 2014; Srivastava et al., 2014; Yang et al., 2014; Retterer et al., 2016; Trujillano et al., 2017).

Here we report analyses of the factors that confer effects on genes that cause diseases in dominant or recessive inheritance pattern. Based on a cohort of 1,180 Korean Neurodevelopmental Disorder (KND) patients and additional patient datasets from Deciphering Developmental Delay (DDD; n = 13,500) and the Simons Foundation Autism Research Initiative (SFARI; n = 34,868), we found that genes which follow a recessive inheritance pattern are more tolerant, harbor variants of lower functionality, interact with fewer other proteins, and are more enriched in metabolic and mitochondrial functional categories when compared to those that follow a dominant inheritance pattern. In addition, the ongoing accumulation of carrier information suggests possible future utility for carrier prediction as more NDD patient data become available.

Materials and methods

Patients and study criteria

Patients with NDD and their parents who visited the Seoul National University Children's Hospital (SNUCH) pediatric neurology clinic were recruited to this study. Informed consent and blood samples for genomic DNA were obtained under the approval of the Seoul National University Hospital (SNUH) internal review board (#1406-081-588). Patients with confirmed genetic variants identified through candidate gene sequencing, targeted gene sequencing panel, microarray, metabolic work-up, brain/spine MRI, or muscle biopsy were excluded. A total of 1,180 patients with complex neurological symptoms of suspected genetic origin were selected by the pediatric neurologists in SNUCH.

Whole exome sequencing

Genomic DNA was extracted from whole blood using the QIAamp DNA Blood Midi Kit according to the manufacturer's instructions (Qiagen, Valencia, CA). WES procedures including exome capturing and sequencing were performed at Theragen

Etex Bio Institute (Suwon, Korea). The data were analyzed as described previously (Lee et al., 2020). Briefly, Burrows-wheeler Aligner [v.0.7.15 (Li and Durbin 2010)] was used to align sequenced reads and the Picard software [v.2.8.0 (Broad Institute, 2019)], samtools [v.1.8 (Li et al., 2009)] and Genome Analysis Toolkit [GATK, v.4.1.4 (Mckenna et al., 2010)] were used for subsequent data processing steps such as removal of PCR duplicates, base recalibration, and variant quality control. ANNOVAR and SnpEff were used for variant annotation (Wang et al., 2010; Cingolani et al., 2012).

Gene expression analysis

The normalized transcript level (TPM) of each gene was extracted from the Genotype-Tissue Expression (GTEx) project [v8 (GTEx Consortium, 2020)]. The median TPM value across all brain regions for each gene was divided by the median value of all other regions to determine relative brain vs. body expression. These relative TPM values were then plotted to visualize the distribution of the gene set. RNA-seq data and exon microarray data from BrainSpan (http://www.brainspan.org) were used to analyze brain spatial and temporal gene expression in the brain (Kang et al., 2011). This dataset contains expression from 16 cortical and subcortical structures along the full course of human brain development.

Protein-protein interaction analysis

Protein correlation profiling of seven mouse tissues was used to explore tissue-specific PPI (Skinnider et al., 2021). The dataset contained more than 190,000 high-confidence PPIs identified with stable isotope labelling of tissues. We extracted for analysis those pairs that included proteins corresponding to the causal genes identified in the KND, DDD and SFARI cohorts.

Evaluation of pathogenic variants

The pathogenicity of variants in our dataset was assessed with reference to multiple databases as follows. Normal population database such as gnomAD, ExAC, 1000 Genomes, and KOVA were used to evaluate dominant variants that were never seen as heterozygous and recessive variants that were never seen as homozygous or hemizygous when filtered by allele frequency of 0.001 in heterozygous status. *In silico* prediction scores such as CADD (Rentzsch et al., 2019), SIFT (Ng and Henikoff, 2003), and phyloP (Siepel et al., 2005) were used to gain information regarding whether variants were evolutionarily well conserved at the amino acid level. Disease databases such as OMIM (Amberger et al., 2015; Amberger and Hamosh, 2017; Amberger et al., 2019), HGMD (Stenson et al., 2003), and ClinVar (Landrum et al., 2016) were used to find causative genes with consideration of genotype-phenotype associations. Then the variants were classified based on inheritance patterns such as *de novo*, compound heterozygous, homozygous, and hemizygous by comparing to genotypes in the parents. Copy number variation (CNV) analysis through WES was carried out by comparing the mean coverage depth of each captured interval to the mean coverage depth of parental samples as described previously (Lee et al., 2020).

Gene ontology analysis

To analyze disease associations and biological pathways that are enriched in a selected genes, a web-based analysis tool from Metascape (https://metascape.org/gp/index.html) was used. Conventional GO sources were used: biological process (BP), Cellular Component (CC) and Molecular Function (MF). Disease Gene Network (DisGeNET) was used for disease ontology. Results were collected and grouped into clusters for comparative analyses of biological process and disease association between gene groups.

Statistical evaluation

Wilcox test was used to determine the statistical significance of the observed differences in functional scores for genes with different inheritance modes. The statistical significance of the expression level in boxplots was measured by a two-sample t-test. Statistical analyses were performed with R version 3.6.2.

Results

Genetic analysis of 1,180 patients with neurodevelopmental disorders

Participants consisted of pediatric patients (mean age = 11.3 years, range 1–62) displaying one or more neurological symptoms including developmental delay, intellectual disability, intractable seizure, involuntary movements, or muscle weakness who visited SNUCH in 2014–2020 with idiopathic or undiagnosed symptoms. For genetic analysis, DNA from peripheral blood was subjected to WES. Among the 1,180 patients, parents of 707 patients were also sequenced. The resulting genome data were processed and pathogenic variants called with a standard process (Subjects and Methods). The pathogenic variants were identified in the 284 disease-causing genes in 1,180 KND patients (Supplementary Table S1). Overall, 41.9% of the patients carried known variants and 4.7% carried known variants but displayed symptoms different from those previously reported,

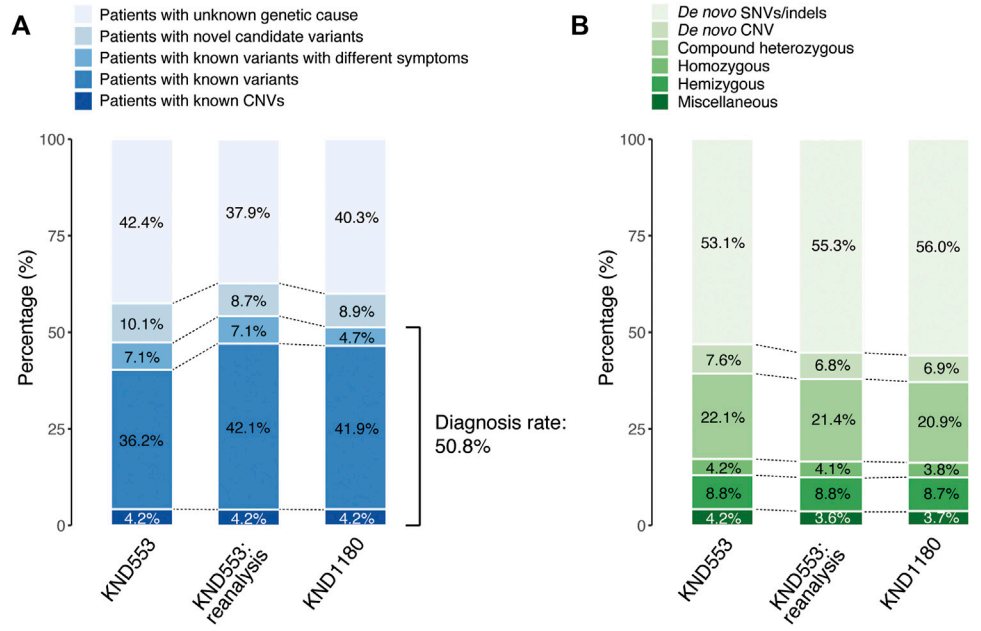


FIGURE 1
Genetic diagnosis of 1,180 KND patients (KND1180). **(A)** Diagnostic yields of the 553 KND patients in 2020 (KND553), reanalysis of KND553, and KND1180. **(B)** Breakdown of diagnosed patients by mode of inheritance.

possibly extending the disease spectra of these variants (Figure 1; Supplementary Table S2). Including the 4.2% of the patients with known CNVs (Supplementary Table S3), 50.8% of patients with pathogenic variants in known causal genes were definitively diagnosed by WES analysis (Figure 1A). This group with known variants was further divided according to variant inheritance pattern (Figure 1B). *De novo* variants were identified in more than half of diagnosed patients (62.9%) and recessive variants in about a quarter (24.7%). Lastly, 8.7% carried variants on the X chromosome with hemizygous status, making the proportion of inherited variants 33.4% (Figure 1B). This distribution of pathogenic variant inheritance is comparable to those reported in other studies using rare disease patients from outbred populations (Yang et al., 2013; Wright et al., 2015; Kuperberg et al., 2016; Marinakis et al., 2021).

Reanalysis improved diagnostic yield

Re-evaluation of patients previously determined to be without pathogenic variants often allows for the discovery of new variants due to accumulating understanding of gene-disease relationships and improved bioinformatic pipelines (Ewans et al., 2018; Epilepsy Genetics Initiative, 2019; Jalkh et al., 2019; Fung et al., 2020). Previous re-analysis studies have reported 5%–12% increases in diagnostic yield (Ewans et al., 2018; Epilepsy Genetics Initiative, 2019; Jalkh et al., 2019; Fung et al., 2020); here, we observed a 5.9% increase in diagnostic yield, discovering pathogenic variants in 33 patients among the 553 that were previously analyzed in 2020 (KND553; Figure 1A) (Lee et al., 2020). The variants implicated in these 33 cases can be broadly divided into two groups, 1) variants for which new entries in OMIM allowed defining them as pathogenic (n = 8; Table 1) and 2) pathogenic calls previously missed during the bioinformatic process (n = 25; Table 2).

Genetic characteristics of genes that follow a dominant or recessive pattern

NDDs display considerable clinical and biological heterogeneity. The innate function and expression pattern of a gene can impact both its inheritance mode and the phenotype when its function or expression is altered. Understanding their genetic properties associated with inheritance modes will help in gaining a more comprehensive view of NDD. To develop this understanding, we first analyzed functional enrichments of those pathogenic genes that follow a dominant or recessive pattern in KND, and compared them with corresponding gene sets from DDD or SFARI (Figure 2A). GO analysis revealed that KND genes are enriched in molecular function and biological process terms relating to brain developmental progression, such as regulation of membrane potential, chromatin organization, head development, and pyrophosphatase activity (Figure 2A).

TABLE 1 List of newly diagnosed cases due to new gene entry into OMIM.

Index	Gene	Inheritance	Variant type	Variant	Variant status	Phenotype[a]	OMIM entry number and date of creation
1	*GEMIN5*	Rec	Comp het	c.3857A>G; *p*.Tyr1286Cys	Novel	Progressive cerebellar atrophy with severe developmental arrest	#619333; 05/19/2021
				c.2510–2A>T	Novel		
2	*STAG2*	Dom	De novo het	c.3724C>T; *p*.Arg1242*	Novel	Holoprosencephaly	#301043; 04/07/2020
3	*MED12L*	Dom	De novo het	c.1895C>T; *p*.Ser632Leu	Novel	GDD with FD	#618872; 05/02/2020
4	*DHX16*	Dom	De novo het	c.2021C>T; *p*.Thr674Met	Reported	Congenital myopathy	#618733; 01/09/2020
5	*HK1*	Dom	De novo het	c.1475C>T; *p*.Thr492Met	Reported	Severe brain atrophy, deep cortex disruption	#618547; 08/20/2019
6	*ADH5*	Rec	Comp het	c.678delA; *p*.Asp227fs	Novel	GDD, myelodysplastic syndrome	#619151; 01/13/2021
				c.832G>C; *p*.Ala278Pro	Reported		
7	*SIAH1*	Dom	De novo het	c.613G>C; *p*.Gly205Arg	Reported	GDD and FD	#619314; 05/06/2021
8	*MN1*	Dom	De novo het	c.3850delC; *p*.His1284fs	Novel	CHARGE syndrome	#618774; 02/11/2020

[a]GDD, global developmental delay; FD, facial dysmorphism; CHARGE, coloboma, heart defects, atresia choanae, growth retardation, genital abnormalities, and ear abnormalities.

In addition, the published variants from DDD and SFARI shared biological mechanisms involved in brain development (Supplementary Figure S1). Interestingly, differential enrichments were observed between dominant and recessive genes, with remarkably little overlap between the two gene groups (Figure 2B; Supplementary Table S4). In particular, dominant genes were strongly enriched for synaptic functions, while recessive genes were characterized by metabolic process, mitochondrial function, and muscular disease terms. Remarkably, X-linked genes shared more terms with dominant genes than with recessive genes (Figure 2B). This is unexpected because the majority of X-linked genes follow a hemizygous pattern, where disease manifests when the only X-chromosome allele in a male patient is mutated, and may follow a recessive pattern.

Expression patterns of genes that follow dominant or recessive inheritance

Next, we used GTEx data to compare the expression profiles of KND genes in brain and other tissues to determine if expression profiles would also differ by inheritance pattern. The results showed that KND genes having brain-specific expression were more enriched in the dominant gene set compared to the recessive gene set ($p = 1.4 \times 10^{-7}$; Figure 2C). Interestingly, the relative brain expression of X-linked genes was more similar to dominant genes than to recessive genes. BrainSpan comprises a comprehensive survey of gene expression in the brain during development, and in the dataset, dominant genes displayed increased expression level relative to both recessive and X-linked genes (between dominant and recessive genes, $p = 1.4 \times 10^{-9}$ for the prenatal period and $p = 3.5 \times 10^{-6}$ for the postnatal period; Figure 2D). There was no substantial difference between prenatal and postnatal expression levels (Figure 2D). Therefore, our findings imply a clear distinction in function and expression level for genes of different inheritance modes.

Tissue-specific PPI networks

PPI information enables us to explore the biological function of a protein though its physical interactions with other proteins. A recent study provided data on protein pairs that interacted in seven mouse tissues, which we used to identify PPIs for KND genes in tissue-specific context (Skinnider et al., 2021). Focusing on brain tissue, we observed that the fraction of genes with PPIs was greater among dominant genes (59/163 = 36.2%) than for recessive genes (26/117 = 22.2%), and the mean number of interactions was also higher (7.2 for dominant genes vs. 4.5 for recessive genes) (Figure 2E). Among those recessive genes having PPIs at least one interaction in the brain, more than half also interacted

TABLE 2 List of newly diagnosed cases by data re-analysis.

Index	Gene	Inheritance	Variant type	Variant	Variant status	Phenotype[b]	Reason
1	*PMM2*	Rec	Comp het	c.194A>G; *p*.Asp65Gly	Novel	Progressive cerebellar atrophy	Not clear
				c.713G>C; *p*.Arg238Pro	Reported		
2	*PDHA1*	X-linked	De novo het	c.613G>A; *p*.Val205Met	Reported	Rett syndrome-like	Not clear
3	*ZEB2*	Dom	De novo het	c.2083C>T; *p*.Arg695*	Reported	Rett syndrome-like	Not clear
4	*KAT6B*	Dom	De novo het	c.3147G>A; *p*.Pro1049Pro	Reported	Rett syndrome-like	A synonymous variant; called during re-evaluation
5	*ACTB*	Dom	De novo het	c.547C>T; *p*.Arg183Trp	Reported	Severe dystonia, ID, and SNHL	Not clear
6	*CASK*	X-linked	Hemizygous	c.1667T>G; *p*.Leu556Arg	Novel	Autism spectrum disorder with FD	Not clear
7	*MAGEL2*	Dom	De novo het	c.2873G>A; *p*.Trp958*	Reported	ID with FD and multiple anomaly	Not clear
8	*NARS2*	Rec	Comp het	c.1163C>T; *p*.Thr388Met	Novel	EE	Not clear
				c.88G>C; *p*.Val30Leu	Novel		
9	*FOXG1*	Dom	pending	c.460dupG; *p*.Glu154fs	Reported	EE and microcephaly	Not clear
10	*DYRK1A*	Dom	De novo het	c.520G>T; *p*.Val174Leu	Reported	DD with microcephaly and FD	Not clear
				c.521T>A; *p*.Val174Glu	Novel		
11	*SLC16A2*	X-linked	Hemizygous	c.1265T>G; *p*.Leu422Arg	Novel	Neurodegenerative disorder	Not clear
12	*UGDH*	Rec	Comp het	c.1183G>A; *p*.Val395Met	Novel	EE with family history	Not clear
				c.1038–2A>G	Novel		
13	*PDHA1*	X-linked	Hemizygous	c.761T>C; *p*.Leu254Ser	Reported	Leigh Syndrome	Initially missed due to coverage depth <10
14	*TBR1*	Dom	De novo het	c.1588_1594dupGGCTGCA; *p*.Thr532fs	Reported	Rett syndrome-like	Initially missed due to coverage depth <10
15	*IQSEC2*	X-linked	De novo hemi	c.2139delC; *p*.Gly714fs	Novel	Rett syndrome-like	Initially missed due to coverage depth <10
16	*SMC1A*	X-linked	Possible *de novo* het[a]	c.2923C>T; *p*.Arg975*	Reported	Rett syndrome-like	Initially missed due to coverage depth <10
17	*AHDC1*	Dom	Possible *de novo* het[a]	c.2389G>T; *p*.Glu797*	Novel	Rett syndrome-like	Initially missed due to coverage depth <10
18	*IRF2BPL*	Dom	De novo het	c.562C>T; *p*.Arg188*	Reported	Neurodegenerative disease	Called during phenotype re-evaluation
19	*UBAP1*	Dom	De novo het	c.529dupA; *p*.Met177fs	Novel	Hereditary spastic paraplegia	Called during phenotype re-evaluation
20	*GABRB3*	Dom	Possible *de novo* het[a]	c.554C>T; *p*.Thr185Ile	Reported	Rett syndrome-like	Called during phenotype re-evaluation
21	*CDK13*	Dom	Possible *de novo* het[a]	c.2149G>A; *p*.Gly717Arg	Reported	Rett syndrome-like	Called during phenotype re-evaluation
22	*TRAPPC11*	Rec	Hom	c.302A>G; *p*.Tyr101Cys	Novel	Unknown muscular dystrophy, most likely calpainopathy	Called during phenotype re-evaluation
23	*SLC35A2*	X-linked	De novo hemi	c.1A>C; *p*.Met1?	Novel	Ullrich disease or Bethlem myopathy suspected	Called during phenotype re-evaluation
24	*DHDDS*	Dom	De novo het	c.110G>A; *p*.Arg37His	Reported	EE	Called during phenotype re-evaluation
25	*KMT2C*	Dom	De novo het	c.5716C>T; *p*.Arg 1906*	Novel	Female ID, microcephaly	Called during phenotype re-evaluation

[a]Variant is pathogenic in ClinVar, but parental samples were not available.
[b]ID, intellectual disability; DD, developmental delay; SNHL, sensorineural hearing loss; FD, facial dysmorphism; EE, epileptic encephalopathy.

with other proteins in all seven tissues (14/26 = 53.8%; Figure 2F), implying these genes to have a more ubiquitous functional pattern. PPIs from DDD and SFARI were also compared for validation (Supplementary Figure S2) and yielded similar patterns of brain-specific PPIs for dominant gene products and broader PPIs for recessive gene products.

Tolerance to pathogenic variants

The tolerance of a gene, indicating the degree to which a critical mutation in it may be detrimental to human development and physiology, is effectively represented by the probability of loss of function intolerance (pLI) and the observed/expected (O/E) constraint ratio scores in gnomAD (Lek et al., 2016). In KND, autosomal dominant genes tended to have pLI values close to 1, representing strong constraint, while autosomal recessive genes showed the opposite trend with pLI close to 0 (e.g., 75.0% of autosomal dominant genes are near 1, and 84.6% of autosomal recessive genes are near 0; Figure 3A). Consistent patterns were also observed for DDD and SFARI. Meanwhile, similar to the GO analysis findings, X-linked recessive genes exhibited patterns akin to dominant genes. These observations were recapitulated when using O/E values (Figure 3A). All told, these findings suggest that genes responsible for NDDs harbor different functions according to their inheritance patterns, and they share little in terms of the molecular pathways leading to disease phenotype.

Characteristics of variants that follow dominant or recessive inheritance

We next investigated whether the functionality of genetic variants would differ according to their inheritance pattern using functional prediction scores like CADD, SIFT, and PhyloP. Variants from DDD and SFARI were also compared for validation. This analysis revealed that functional prediction scores for recessive variants tend to be lower than those of dominant variants (between dominant and recessive variants, $p = 0.11$ for CADD, $p = 2.2 \times 10^{-4}$ for SIFT, $p = 9.6 \times 10^{-6}$ for PhyloP, and $p = 6.6 \times 10^{-7}$ for AA conservation; Figure 3B). This finding indicates that variants under recessive inheritance are less damaging and less critical in function, hence demonstrate little physiological effect on carriers.

Estimating carrier frequencies of variants that cause recessive neurodevelopmental disorders

In our previous study using 553 KND patients, we estimated that one in every 17 healthy individuals is a carrier for at least one pathogenic variant for a recessive genes represented in the KND cohort. This estimate remains unchanged using 1,180 patients (Lee et al., 2020), but with a patient set twice as large, we inferred that the power to predict carriers would substantially increase. We first collected a list of pathogenic LoF and missense variants from ClinVar and KND, and aggregated their population frequencies using the gnomAD East Asian and Korean Variant Archive [KOVA 2; 5,305 healthy Korean individual set (Lee et al., 2017)]. This provided us with an estimation of the number of carriers of recessive neurodevelopmental diseases in the general Korean population (Figure 4A; Supplementary Table S5). Among the 161 genes that carriers were found in KND1180 set, the estimation yields were variable by gene, ranging up to 1.2% of the general population for *VPS13B*, and no carriers were predicted for 23 genes (Figure 4A). Among the 138 genes that carriers were predicted, only 34 genes were previously found in KND553. On average, the estimation yield for KND1180 variants on the 34 overlapping genes were 1.9-fold higher than those determined for KND553 variants, implying that larger cohort size is critical for increased sensitivity (Figure 4B).

Discussion

NDDs show considerable variability at both phenotypic and genetic levels. We conducted WES analysis to reveal genetic etiology for 1,180 undiagnosed patients in the KND cohort. Previously reported diagnostic rates of WES vary substantially among studies, ranging from 25% to 56% (Yang et al., 2013; Iglesias et al., 2014; Lee et al., 2014; Yang et al., 2014; Wright et al., 2015; Retterer et al., 2016; Jalkh et al., 2019; Marinakis et al., 2021). Herein, we report that the diagnostic yield for definitive pathogenic variant findings in KND patients was 50.8%. Among the diagnosed patients, 33.4% carried inherited variants, demonstrating that a large portion of KND patients inherited pathogenic variants from healthy parents.

It is expected that exome reanalysis applying the latest versions of databases and using improved bioinformatic tools would increase diagnostic yield (Ewans et al., 2018; Epilepsy Genetics Initiative, 2019; Jalkh et al., 2019; Fung et al., 2020). We performed reanalysis of 291 patients from the KND553 set who remained without clear pathogenic variants. This reanalysis increased diagnostic yield from 47.5% to 53.4%, which can be attributed to a number of factors: newly discovered and deposited gene-disease associations in OMIM, increased coverage allowing identification of variants that may previously have been missed, filtering out in the initial analysis of synonymous variants affecting gene splicing of *KAT6B* (*p*.Pro1049=), and re-evaluation of previously analyzed variants (Figure 1; Tables 1, 2). Therefore, we also suggest that exome sequencing data should be periodically re-evaluated.

Since NDDs may variously be caused by alterations in genes with autosomal dominant, autosomal recessive, or X-linked inheritance modes, genotype-phenotype correlations are often difficult to establish. Also, we believe that studying the fundamental differences in genes that cause NDDs in recessive or dominant mode is crucial in understanding the mechanisms of NDD pathogenicity. As a first step, we analyzed the biological pathways of the KND genes to obtain systematic insights into the molecular mechanisms associated with different inheritance modes. The results revealed that dominant and recessive genes are

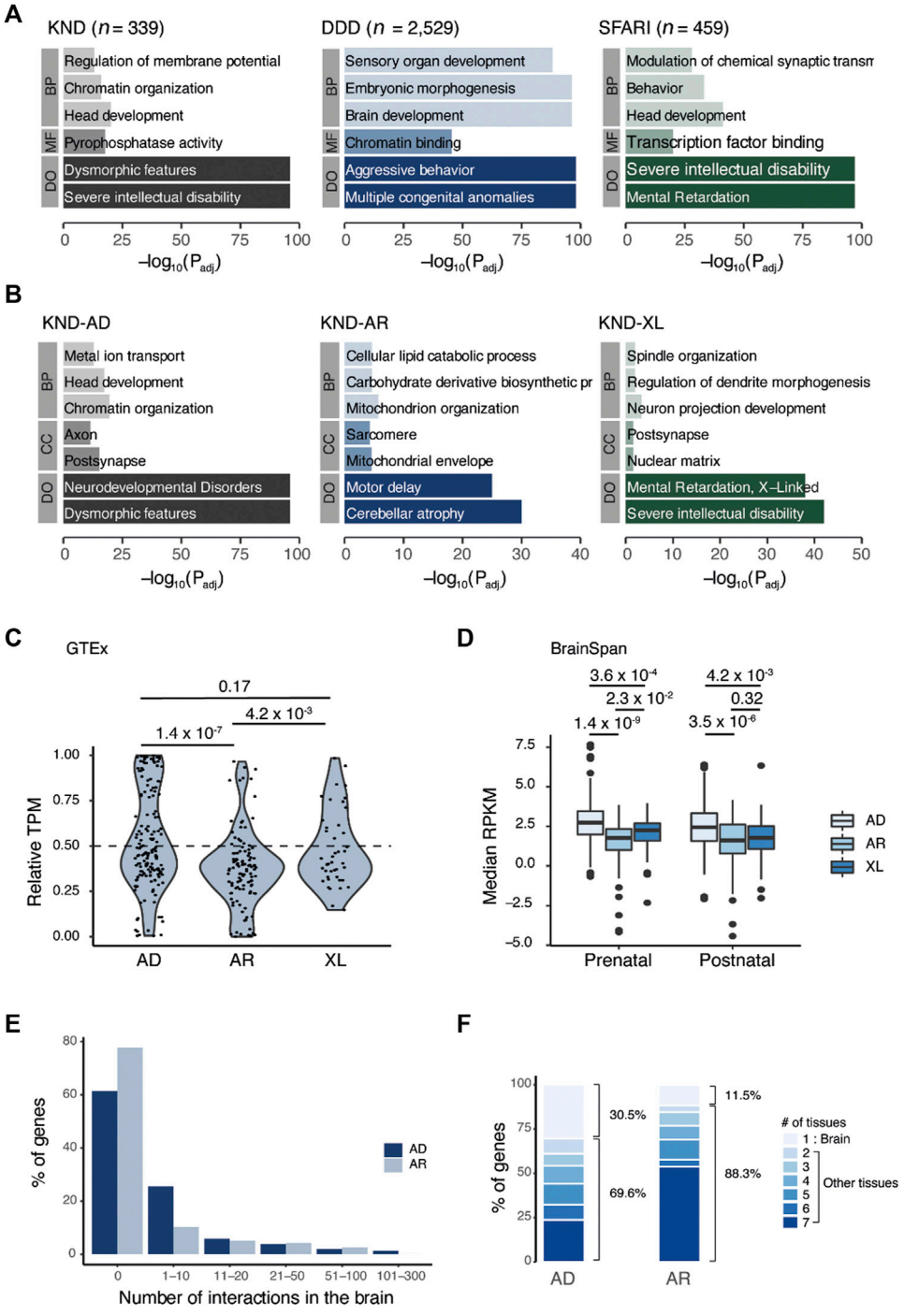


FIGURE 2
Comparative analysis of genes that cause neurodevelopmental disorders across inheritance patterns. **(A)** GO result of genes that led to the definitive diagnosis in KND, DDD, and SFARI. **(B)** Breakdown of KND genes by inheritance pattern. **(C)** Relative expression of genes in the brain vs. the body (brain/body median TPM). **(D)** Boxplot of median gene expression in the brain for two developmental periods. **(E)** Proportion of genes having the given number of PPI events in brain tissue. **(F)** Proportion of genes having the given number of PPI-positive tissues. Tissues that correspond to two to seven are heart, kidney, liver, lung, muscle, and thymus. BP, biological process; CC, cellular component; MF, molecular function; DO, disease ontology; AD, autosomal dominant; AR, autosomal recessive; XL, X-linked.

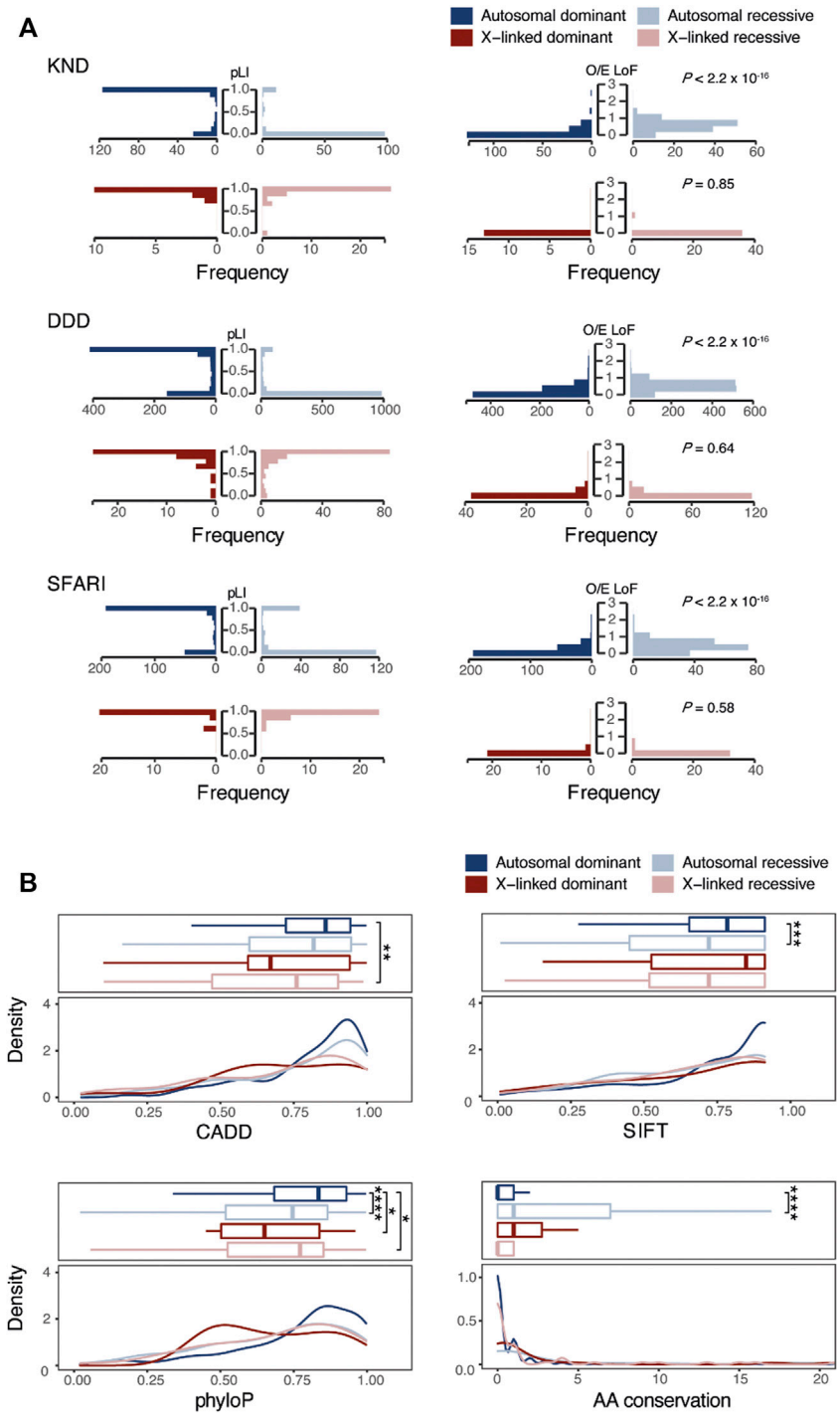


FIGURE 3
Comparison of genetic characteristics of genes and variants that follow dominant or recessive inheritance. **(A)** Comparison of pLI or O/E scores of NDD causal genes across inheritance patterns. **(B)** Comparison of functional (CADD, SIFT, and phyloP) and conservation scores among NDD causal variants according to inheritance patterns. "AA conservation" denotes the number of species with different amino acids in 99 human ortholog proteins. *, p-value < 0.1, **, p-value < 0.01, ***, p-value < 0.001. ****, p-value < 0.00001.

10.3389/fgene.2022.990015

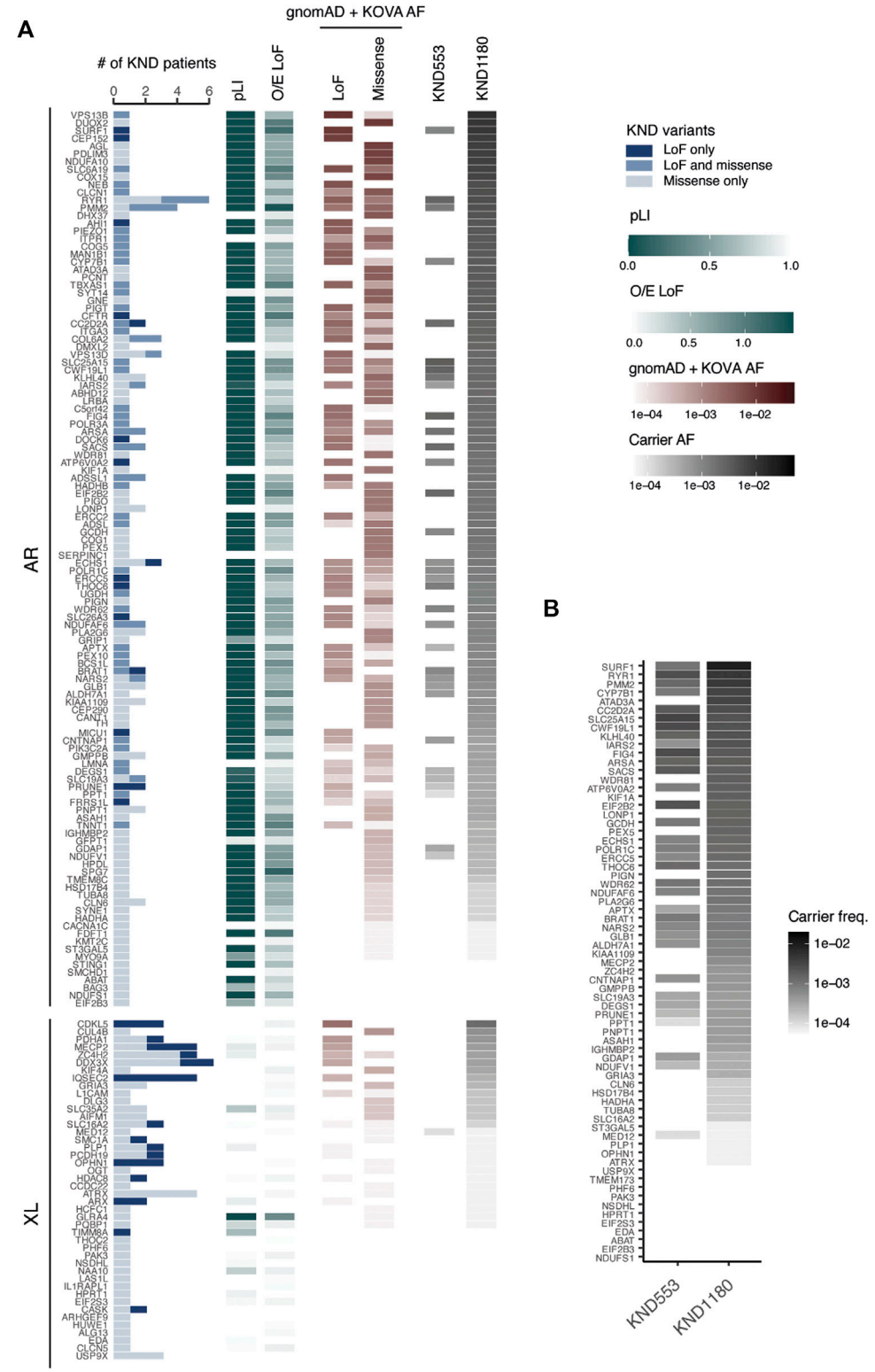


FIGURE 4
Ability to pre-determine NDD carrier status based on KND. **(A)** Heatmap displaying the number of KND patients carrying a causal variant, pathogenic variant frequency, and ability to predict carrier frequency on 161 genes. **(B)** Comparison of the ability to predict pathogenic variant carriers based on KND553 or KND1180 on the 34 overlapping genes.

most strongly associated with synaptic function and metabolic processes, respectively, implying that diseases can be caused through different molecular mechanisms according to their inheritance patterns. Moreover, we observed dominant and recessive gene sets to have opposite trends in pLI and O/E scores, which proved the differences in genetic architecture between these inheritance patterns. In addition, we found gene expression profiles to also reflected this fundamental difference. Profiling of brain expression patterns in GTEx and BrainSpan revealed the dominant gene sets to exhibit specific and increased expression in the brain compared to the recessive gene set, suggesting dominant genes to be more brain-specific. In addition to the GO and expression analyses, we investigated whether PPI data support an association of tissue-specific expression and function with inheritance mode. Tissue-specific PPI networks based on direct interactions have previously demonstrated biological relevance (Skinnider et al., 2021). Here, we observed that dominant genes to have more interactions specifically in brain tissue than recessive genes. In contrast, recessive genes tended to have interactions ubiquitous across all seven tissues. Therefore, combined biological studies including PPI networks, functional pathways and phenotype data may be effective in expanding our understanding of disease progression in NDD. We also investigated variant functional effects and found that variants with recessive pathogenic alleles were less deleterious than those having dominant alleles. This is well supported by the fact that parental carriers are mostly healthy, although recent large-scale analyses have revealed heterozygous carriers of rare diseases to harbor subtle effects in various aspects of individual health and reproductivity (Barton et al., 2021; Gardner et al., 2022).

The frequency of carriers varies among population groups and specific genetic conditions could be biased toward particular ethnic groups (Rozen et al., 1999; Lynch et al., 2004; Cao and Kan, 2013; Lazarin et al., 2013). Ethnic Koreans are an outbred population, and the culture has prohibited marriages between relatives and among members of family clans for more than 500 years (Deuchler, 1992). As a major tertiary clinical institution, SNUCH covers a large portion of rare NDD patients in the country. Therefore, this study provides an unprecedented opportunity to study the occurrence of recessive diseases in an outbred population. We estimated that 24.7% of patients in the KND1180 cohort were affected by recessive conditions, which allows us to use databases such as gnomAD East Asian and KOVA to calculate carrier frequencies for reported and predicted pathogenic variants in the general population. Our resulting carrier panel will have a sensitivity of 36.1%, which is not too much deviated from previous attempts on Chinese and Israeli populations (38.7% for well-defined recessive conditions and >30% for recessive retinal diseases, respectively) (Hanany et al., 2018; Chau et al., 2022).

As expected, the larger sample size of this cohort relative to the KND553 cohort resulted in a greater number of pathogenic genes and an increase in the reported disease-associated variants enrolled in ClinVar and OMIM. Although calculated carrier frequencies may differ from those observed in clinical practices, the findings from this study will provide genetic evidence for the utility of preconception carrier screening.

Conclusion

Recent efforts into genome-based diagnosis of rare Mendelian disorders have provided with many gene-disease relationships and understanding of disease pathophysiology. However, it has not been clearly elucidated whether there is any genetic feature that determine the modes of inheritance of sucj diseases. We took advantage of in-house as well as public patient genome data and found genetic features of recessive vs. dominant disorders. Furthermore, we demonstrate that we can utilize this understanding of recessive variants to carrier prediction to reduce future patients originated from rare recessive variants.

Data availability statement

The variant data presented in the study are deposited in the repository (https://www.sysbiolab.org/knd1180).

Ethics statement

The studies involving human participants were reviewed and approved by Seoul National University Hospital. Written informed consent to participate in this study was provided by the participants' legal guardian/next of kin.

Author contributions

J-HC and MC designed the project. SL, SYK, MJK, JGY, BCL, WJK, KJK, JMK, AC, JSL, and J-HC provided clinical examinations for the participants. SP, SSJ, SL, MK, HS, HJ, SEH, Jean L, Jeongeun L, Jeongha L, and C-RL collected and analyzed the data. SP, MC, and J-HC wrote the article. All authors read and approved the final manuscript.

Funding

The study was supported in part by the National Research Foundation (2020M3E5D7086836 and 2014M3C9A2064686),

the Korea Centers for Disease Control and Prevention (2021-ER0701-00 and 2017N-6901-00), and the Ministry of Health and Welfare (HI16C1986).

Acknowledgments

We thank the patients and families that participated in the study.

Conflict of interest

The authors declare that the research was conducted in the absence of any commercial or financial relationships that could be construed as a potential conflict of interest

Publisher's note

All claims expressed in this article are solely those of the authors and do not necessarily represent those of their affiliated organizations, or those of the publisher, the editors and the reviewers. Any product that may be evaluated in this article, or claim that may be made by its manufacturer, is not guaranteed or endorsed by the publisher.

Supplementary material

The Supplementary Material for this article can be found online at: https://www.frontiersin.org/articles/10.3389/fgene.2022.990015/full#supplementary-material

References

Abouelhoda, M., Sobahy, T., El-Kalioby, M., Patel, N., Shamseldin, H., Monies, D., et al. (2016). Clinical genomics can facilitate countrywide estimation of autosomal recessive disease burden. *Genet. Med.* 18, 1244–1249. doi:10.1038/gim.2016.37

Amberger, J. S., Bocchini, C. A., Schiettecatte, F., Scott, A. F., and Hamosh, A. (2015). OMIM.org: Online Mendelian Inheritance in Man (OMIM®), an online catalog of human genes and genetic disorders. *Nucleic Acids Res.* 43, D789–D798. doi:10.1093/nar/gku1205

Amberger, J. S., Bocchini, C. A., Scott, A. F., and Hamosh, A. (2019). OMIM.org: Leveraging knowledge across phenotype-gene relationships. *Nucleic Acids Res.* 47, D1038–D1043. doi:10.1093/nar/gky1151

Amberger, J. S., and Hamosh, A. (2017). Searching online mendelian inheritance in man (OMIM): A knowledgebase of human genes and genetic phenotypes. *Curr. Protoc. Bioinforma.* 58, 1–2. doi:10.1002/cpbi.27.1-1.2.12

Baird, P. A., Anderson, T. W., Newcombe, H. B., and Lowry, R. B. (1988). Genetic disorders in children and young adults: A population study. *Am. J. Hum. Genet.* 42, 677–693.

Barton, A. R., Hujoel, M. L. A., Mukamel, R. E., Sherman, M. A., and Loh, P.-R. (2021). *A spectrum of recessiveness among Mendelian disease variants in UK Biobank*. MedRxiv.

Broad Institute (2019). Picard toolkit [online]. Broad Institute, GitHub repository: Broad Institute. Available at: https://broadinstitute.github.io/picard/.

Cao, A., and Kan, Y. W. (2013). The prevention of thalassemia. *Cold Spring Harb. Perspect. Med.* 3, a011775. doi:10.1101/cshperspect.a011775

Chau, J. F. T., Yu, M. H. C., Chui, M. M. C., Yeung, C. C. W., Kwok, A. W. C., Zhuang, X., et al. (2022). Comprehensive analysis of recessive carrier status using exome and genome sequencing data in 1543 Southern Chinese. *NPJ Genom. Med.* 7, 23. doi:10.1038/s41525-022-00287-z

Cingolani, P., Patel, V. M., Coon, M., Nguyen, T., Land, S. J., Ruden, D. M., et al. (2012). Using *Drosophila melanogaster* as a model for genotoxic chemical mutational studies with a new program, SnpSift. *Front. Genet.* 3, 35. doi:10.3389/fgene.2012.00035

Deuchler, M. (1992). *The confucian transformation of Korea : A study of society and ideology*. Cambridge, Massachusetts: Harvard University Asia Center.

Epilepsy Genetics Initiative (2019). The Epilepsy Genetics Initiative: Systematic reanalysis of diagnostic exomes increases yield. *Epilepsia* 60, 797–806. doi:10.1111/epi.14698

Ewans, L. J., Schofield, D., Shrestha, R., Zhu, Y., Gayevskiy, V., Ying, K., et al. (2018). Whole-exome sequencing reanalysis at 12 months boosts diagnosis and is cost-effective when applied early in Mendelian disorders. *Genet. Med.* 20, 1564–1574. doi:10.1038/gim.2018.39

Fung, J. L. F., Yu, M. H. C., Huang, S., Chung, C. C. Y., Chan, M. C. Y., Pajusalu, S., et al. (2020). A three-year follow-up study evaluating clinical utility of exome sequencing and diagnostic potential of reanalysis. *NPJ Genom. Med.* 5, 37. doi:10.1038/s41525-020-00144-x

Gardner, E. J., Neville, M. D. C., Samocha, K. E., Barclay, K., Kolk, M., Niemi, M. E. K., et al. (2022). Reduced reproductive success is associated with selective constraint on human genes. *Nature* 603, 858–863. doi:10.1038/s41586-022-04549-9

GTEx Consortium (2020). The GTEx Consortium atlas of genetic regulatory effects across human tissues. *Science* 369, 1318–1330. doi:10.1126/science.aaz1776

Hanany, M., Allon, G., Kimchi, A., Blumenfeld, A., Newman, H., Pras, E., et al. (2018). Carrier frequency analysis of mutations causing autosomal-recessive-inherited retinal diseases in the Israeli population. *Eur. J. Hum. Genet.* 26, 1159–1166. doi:10.1038/s41431-018-0152-0

Iglesias, A., Anyane-Yeboa, K., Wynn, J., Wilson, A., Truitt Cho, M., Guzman, E., et al. (2014). The usefulness of whole-exome sequencing in routine clinical practice. *Genet. Med.* 16, 922–931. doi:10.1038/gim.2014.58

Jalkh, N., Corbani, S., Haidar, Z., Hamdan, N., Farah, E., Abou Ghoch, J., et al. (2019). The added value of WES reanalysis in the field of genetic diagnosis: Lessons learned from 200 exomes in the Lebanese population. *BMC Med. Genomics* 12, 11. doi:10.1186/s12920-019-0474-y

Jimenez-Sanchez, G., Childs, B., and Valle, D. (2001). Human disease genes. *Nature* 409, 853–855. doi:10.1038/35057050

Kaback, M. M. (2001). Screening and prevention in tay-sachs disease: Origins, update, and impact. *Adv. Genet.* 44, 253–265. doi:10.1016/s0065-2660(01)44084-3

Kang, H. J., Kawasawa, Y. I., Cheng, F., Zhu, Y., Xu, X., Li, M., et al. (2011). Spatio-temporal transcriptome of the human brain. *Nature* 478, 483–489. doi:10.1038/nature10523

Kuperberg, M., Lev, D., Blumkin, L., Zerem, A., Ginsberg, M., Linder, I., et al. (2016). Utility of whole exome sequencing for genetic diagnosis of previously undiagnosed pediatric neurology patients. *J. Child. Neurol.* 31, 1534–1539. doi:10.1177/0883073816664836

Landrum, M. J., Lee, J. M., Benson, M., Brown, G., Chao, C., Chitipiralla, S., et al. (2016). ClinVar: Public archive of interpretations of clinically relevant variants. *Nucleic Acids Res.* 44, D862–D868. doi:10.1093/nar/gkv1222

Lazarin, G. A., Haque, I. S., Nazareth, S., Iori, K., Patterson, A. S., Jacobson, J. L., et al. (2013). An empirical estimate of carrier frequencies for 400+ causal mendelian variants: Results from an ethnically diverse clinical sample of 23, 453 individuals. *Genet. Med.* 15, 178–186. doi:10.1038/gim.2012.114

Lee, H., Deignan, J. L., Dorrani, N., Strom, S. P., Kantarci, S., Quintero-Rivera, F., et al. (2014). Clinical exome sequencing for genetic identification of rare Mendelian disorders. *Jama* 312, 1880–1887. doi:10.1001/jama.2014.14604

Lee, S., Seo, J., Park, J., Nam, J. Y., Choi, A., Ignatius, J. S., et al. (2017). Korean variant archive (KOVA): A reference database of genetic variations in the Korean population. *Sci. Rep.* 7, 4287. doi:10.1038/s41598-017-04642-4

Lee, Y., Park, S., Lee, J. S., Kim, S. Y., Cho, J., Yoo, Y., et al. (2020). Genomic profiling of 553 uncharacterized neurodevelopment patients reveals a high proportion of recessive pathogenic variant carriers in an outbred population. *Sci. Rep.* 10, 1413. doi:10.1038/s41598-020-58101-8

Lek, M., Karczewski, K. J., Minikel, E. V., Samocha, K. E., Banks, E., Fennell, T., et al. (2016). Analysis of protein-coding genetic variation in 60, 706 humans. *Nature* 536, 285–291. doi:10.1038/nature19057

Li, H., and Durbin, R. (2010). Fast and accurate long-read alignment with Burrows-Wheeler transform. *Bioinformatics* 26, 589–595. doi:10.1093/bioinformatics/btp698

Li, H., Handsaker, B., Wysoker, A., Fennell, T., Ruan, J., Homer, N., et al. (2009). The sequence alignment/map format and SAMtools. *Bioinformatics* 25, 2078–2079. doi:10.1093/bioinformatics/btp352

Lynch, H. T., Rubinstein, W. S., and Locker, G. Y. (2004). Cancer in jews: Introduction and overview. *Fam. Cancer* 3, 177–192. doi:10.1007/s10689-004-9538-y

Marinakis, N. M., Svingou, M., Veltra, D., Kekou, K., Sofocleous, C., Tilemis, F. N., et al. (2021). Phenotype-driven variant filtration strategy in exome sequencing toward a high diagnostic yield and identification of 85 novel variants in 400 patients with rare Mendelian disorders. *Am. J. Med. Genet. A* 185, 2561–2571. doi:10.1002/ajmg.a.62338

Mckenna, A., Hanna, M., Banks, E., Sivachenko, A., Cibulskis, K., Kernytsky, A., et al. (2010). The genome analysis toolkit: A MapReduce framework for analyzing next-generation DNA sequencing data. *Genome Res.* 20, 1297–1303. doi:10.1101/gr.107524.110

Ng, P. C., and Henikoff, S. (2003). Sift: Predicting amino acid changes that affect protein function. *Nucleic Acids Res.* 31, 3812–3814. doi:10.1093/nar/gkg509

Rentzsch, P., Witten, D., Cooper, G. M., Shendure, J., and Kircher, M. (2019). Cadd: Predicting the deleteriousness of variants throughout the human genome. *Nucleic Acids Res.* 47, D886–D894. doi:10.1093/nar/gky1016

Retterer, K., Juusola, J., Cho, M. T., Vitazka, P., Millan, F., Gibellini, F., et al. (2016). Clinical application of whole-exome sequencing across clinical indications. *Genet. Med.* 18, 696–704. doi:10.1038/gim.2015.148

Rozen, P., Shomrat, R., Strul, H., Naiman, T., Karminsky, N., Legum, C., et al. (1999). Prevalence of the I1307K APC gene variant in Israeli Jews of differing ethnic origin and risk for colorectal cancer. *Gastroenterology* 116, 54–57. doi:10.1016/s0016-5085(99)70228-3

Schuster-Böckler, B., and Bateman, A. (2008). Protein interactions in human genetic diseases. *Genome Biol.* 9, R9. doi:10.1186/gb-2008-9-1-r9

Siepel, A., Bejerano, G., Pedersen, J. S., Hinrichs, A. S., Hou, M., Rosenbloom, K., et al. (2005). Evolutionarily conserved elements in vertebrate, insect, worm, and yeast genomes. *Genome Res.* 15, 1034–1050. doi:10.1101/gr.3715005

Skinnider, M. A., Scott, N. E., Prudova, A., Kerr, C. H., Stoynov, N., Stacey, R. G., et al. (2021). An atlas of protein-protein interactions across mouse tissues. *Cell* 184, 4073–4089.e17. e17. doi:10.1016/j.cell.2021.06.003

Srivastava, S., Cohen, J. S., Vernon, H., Barañano, K., Mcclellan, R., Jamal, L., Naidu, S., and Fatemi, A. (2014). Clinical whole exome sequencing in child neurology practice. *Ann. Neurol.* 76, 473–483. doi:10.1002/ana.24251

Stenson, P. D., Ball, E. V., Mort, M., Phillips, A. D., Shiel, J. A., Thomas, N. S., et al. (2003). Human gene mutation database (HGMD): 2003 update. *Hum. Mutat.* 21, 577–581. doi:10.1002/humu.10212

Trujillano, D., Bertoli-Avella, A. M., Kumar Kandaswamy, K., Weiss, M. E., Köster, J., Marais, A., et al. (2017). Clinical exome sequencing: Results from 2819 samples reflecting 1000 families. *Eur. J. Hum. Genet.* 25, 176–182. doi:10.1038/ejhg.2016.146

Verma, I. C., and Puri, R. D. (2015). Global burden of genetic disease and the role of genetic screening. *Semin. Fetal Neonatal Med.* 20, 354–363. doi:10.1016/j.siny.2015.07.002

Wang, K., Li, M., and Hakonarson, H. (2010). Annovar: Functional annotation of genetic variants from high-throughput sequencing data. *Nucleic Acids Res.* 38, e164. doi:10.1093/nar/gkq603

Wright, C. F., Fitzgerald, T. W., Jones, W. D., Clayton, S., Mcrae, J. F., Van Kogelenberg, M., et al. (2015). Genetic diagnosis of developmental disorders in the DDD study: A scalable analysis of genome-wide research data. *Lancet* 385, 1305–1314. doi:10.1016/S0140-6736(14)61705-0

Yang, Y., Muzny, D. M., Reid, J. G., Bainbridge, M. N., Willis, A., Ward, P. A., et al. (2013). Clinical whole-exome sequencing for the diagnosis of mendelian disorders. *N. Engl. J. Med.* 369, 1502–1511. doi:10.1056/NEJMoa1306555

Yang, Y., Muzny, D. M., Xia, F., Niu, Z., Person, R., Ding, Y., et al. (2014). Molecular findings among patients referred for clinical whole-exome sequencing. *Jama* 312, 1870–1879. doi:10.1001/jama.2014.14601

Glossary

OMIM the Online Mendelian Inheritance in Men
GoF gain-of-function
LoF loss-of-function
NDD neurodevelopmental diseases
WES whole exome sequencing
KND Korean Neurodevelopmental Disorder
DDD Deciphering Developmental Delay
SFARI Simons Foundation Autism Research Initiative
SNUH the Seoul National University Hospital
BWA Burrows-wheeler Aligner
GATK Genome Analysis Toolkit
TPM Transcripts Per Million
GTEx the Genotype-Tissue Expression
PPI Protein-protein interaction
CNV Copy number variation
GO Gene ontology
pLI the probability of loss of function intolerance
O/E the observed/expected
KOVA Korean Variant Archive
SNUCH the Seoul National University Children's Hospital
ID intellectual disability
GDD global developmental delay
CHARGE coloboma, heart defects, atresia choanae, growth retardation, genital abnormalities, and ear abnormalities
FD facial dysmorphism
EE epileptic encephalopathy
BP biological process
CC cellular component
MF molecular function
DO disease ontology
AD autosomal dominant
AR autosomal recessive
XL X-linked

frontiers | Frontiers in Genetics

TYPE Original Research
PUBLISHED 15 September 2022
DOI 10.3389/fgene.2022.934463

Check for updates

OPEN ACCESS

EDITED BY
Mike Mikailov,
United States Food and Drug Administration, United States

REVIEWED BY
Zhendi Wang,
Huazhong University of Science and Technology, China
Dongping Chen,
Shanghai University of Traditional Chinese Medicine, China

*CORRESPONDENCE
Fu Xiong,
xiongfu@smu.edu.cn
Yun Miao,
miaoyunecho@126.com

†These authors have contributed equally to this work and share first authorship

SPECIALTY SECTION
This article was submitted to Genetics of Common and Rare Diseases, a section of the journal Frontiers in Genetics

RECEIVED 02 May 2022
ACCEPTED 17 August 2022
PUBLISHED 15 September 2022

CITATION
Yan Z, Wang Y, Deng W, Zhou Y, Hu Y, Qi K, Liu D, Xia R, Liu R, Zeng W, Zhang W, Xu J, Xiong F and Miao Y (2022), A single-center analysis of genotype–phenotype characteristics of Chinese patients with autosomal dominant polycystic kidney disease by targeted exome sequencing. *Front. Genet.* 13:934463. doi: 10.3389/fgene.2022.934463

COPYRIGHT
© 2022 Yan, Wang, Deng, Zhou, Hu, Qi, Liu, Xia, Liu, Zeng, Zhang, Xu, Xiong and Miao. This is an open-access article distributed under the terms of the Creative Commons Attribution License (CC BY). The use, distribution or reproduction in other forums is permitted, provided the original author(s) and the copyright owner(s) are credited and that the original publication in this journal is cited, in accordance with accepted academic practice. No use, distribution or reproduction is permitted which does not comply with these terms.

A single-center analysis of genotype–phenotype characteristics of Chinese patients with autosomal dominant polycystic kidney disease by targeted exome sequencing

Ziyan Yan[1†], Yuchen Wang[1†], Wenfeng Deng[1†], Yi Zhou[1], Yangcheng Hu[1], Ka Qi[2], Ding Liu[3], Renfei Xia[1], Rumin Liu[1], Wenli Zeng[1], Wei Zhang[4], Jian Xu[1], Fu Xiong[5]* and Yun Miao[1]*

[1]Department of Transplantation, Nanfang Hospital, Southern Medical Univerisity, Guangzhou, China, [2]Hemodialysis Center, Qinhuangdao Charity Hospital, Qinhuangdao, China, [3]Division of Transplantation, Zhujiang Hospital, Southern Medical University, Guangzhou, China, [4]Guangzhou Jiajian Medical Testing Co Ltd, Guangzhou, China, [5]Department of Medical Genetics, School of Basic Medical Sciences, Southern Medical University, Guangzhou, China

Background: Autosomal dominant polycystic kidney disease (ADPKD) is mainly caused by *PKD1* and *PKD2* mutations. However, only a few studies have investigated the genotype and phenotype characteristics of Asian patients with ADPKD. This study aimed to investigate the relationship between the natural course of ADPKD genotype and phenotype.

Methods: Genetic studies of *PKD1/2* genes of Chinese patients with ADPKD in a single center were performed using targeted exome sequencing and next-generation sequencing on peripheral blood DNA.

Results: Among the 140 patients analyzed, 80.00% (n = 112) harbored *PKD1* mutations, 11.43% (n = 16) harbored *PKD2* mutations, and 8.57% (n = 12) harbored neither *PKD1* nor *PKD2* mutations. The average age at dialysis was 52.60 ± 11.36, 60.67 ± 5.64, and 52.11 ± 14.63 years, respectively. The renal survival rate of ADPKD patients with *PKD1* mutations (77/112) was significantly lower than that of those with *PKD2* mutations (9/16), leading to an earlier onset of end-stage renal disease (ESRD). Renal prognosis was poor for those with nonsense mutations, and they required earlier renal replacement therapy.

Conclusions: The genotype and phenotype characteristics of ADPKD patients potentially vary across ethnic groups. Our findings supplement the genetic profiles of Chinese ADPKD patients, could serve as a guide for therapy monitoring and prognosis assessment of ADPKD, and may improve the clinical diagnosis.

KEYWORDS
autosomal dominant polycystic kidney disease, PKD1, PKD2, mutation, TES using NGS

Introduction

Autosomal dominant polycystic kidney disease (ADPKD) is a common genetic renal disease, with an incidence of one per 1000 to 2500 individuals. It is characterized by progressive renal cyst enlargement, and approximately 50% of patients progress to end-stage renal disease (ESRD) by age 60 (Bergmann, 2015; Cornec-Le et al., 2019). ADPKD is a systemic disease that may cause various extrarenal complications, including hypertension, intracranial aneurysm, and heart valve disease (Lanktree and Chapman, 2017; Cornec-Le et al., 2019; Li et al., 2021).

ADPKD is mainly caused by mutations in *PKD1* (in approximately 80% of disease pedigrees) or *PKD2* (in approximately 15% of disease pedigrees). In the remaining 5–10%, rare or unknown mutations (e.g., *GANAB* and *HNF1B*) are involved (Besse et al., 2017; Cornec-Le et al., 2019). *PKD1* is located on chromosome 16 (16p13.3) and encodes polycystin-1 (PC1), the 11th transmembrane protein. In contrast, *PKD2* is located on chromosome 4 (4q21) and encodes polycystin-2 (PC2), a member of the transient receptor potential family of non-selective ion channels (Harris and Torres, 2009). Both PC1 and PC2 are located on the renal primary cilia, which is a dose-dependent mechano-sensor that regulates the differentiation and proliferation of renal tubular epithelial cells. Cystogenesis occurs when the concentration of PC1 or PC2 decreases below a certain threshold (Audrézet et al., 2016).

Previous studies have demonstrated the association of renal function with various genotypes and some mutation types. For example, patients with *PKD2* mutations reached ESRD 20 years later than those with *PKD1* mutations, and those with *PKD1* non-truncating (*PKD1*-NT) mutations progressed to ESRD 12 years later than those with truncating mutations (Cornec-Le et al., 2019). These findings indicate the significance of ADPKD genotypes in predicting renal prognosis.

However, thus far, the available studies on *PKD1*/*PKD2* mutations and clinical phenotypes have been mainly conducted in Western countries, and only a few studies have investigated the genotype and phenotype characteristics of Asian patients with ADPKD. Therefore, this study aimed to examine Chinese patients with ADPKD at a single center to explore the relationship between the natural course of ADPKD and genotype and phenotype. Our findings contribute new information on the genetic profiles of Chinese ADPKD populations.

Materials and methods

Patients

We retrospectively examined 140 ADPKD patients in the Nanfang Hospital (Guangzhou, China) between November 2013 and July 2018. ADPKD was diagnosed using the following criteria: presence of at least two renal cysts (unilateral or bilateral) in individuals aged <30 years; presence of at least two cysts in each kidney among those aged 30–59 years; and at least four cysts in each kidney among those aged ≥60 years (Ravine et al., 1994). Peripheral blood was collected from each patient, and baseline demographic characteristics (age and sex), age at ESRD, initiation of renal replacement therapy (RRT), and family history of ESRD/ADPKD were recorded.

Target gene enrichment, library construction, and capture sequencing

DNA was extracted from peripheral blood samples using a Solpure Blood DNA kit (Magen, Wuhan, China). The amplified DNA band was interrupted into small DNA fragments with a main band of less than 500 bp and a peak value of 350 bp for library preparation. Briefly, fragments were blunted, and an "A" was added to the 3′ end to connect to a special linker with a "T" base at the 5′ end. The library with adapters was amplified using pre-capture ligation-mediated PCR (LM-PCR). The fragment size of the library was determined by agarose gel electrophoresis, and the concentration of the library was determined by Qubit3.0 and real-time PCR. The library that passed the quality inspection was then diluted to the required concentration for testing, and sequencing analysis was carried out using the Illumina NextSeq 500 sequencing platform. Sequencing results were analyzed using bioinformatics and interpreted by a genetic counselor.

Analysis of next-generation sequencing (NGS) results

The annotation scope of the raw data included the variation in each exon and the variation in the 10 bp upstream and downstream introns of the exon. Variation types included frameshift, splicing, nonsense, missense, atypical, synonymous, and in-frame insertions/detection.

Quality control was conducted on the variant data. The ratio of the sequencing depth of each exon of the PKD1/2 gene is fixed for each sample (if there is no large fragment deletion or duplication). When the sequencing depth ratio of several consecutive exons (usually three or more) between PKD1 and PKD2 genes deviates from the baseline value, a large deletion will be considered, and further confirmation will be conducted by qRT-PCR accordingly. If not, we then compared the hg19 version human genome reference sequence of *PKD1* and *PKD2* gene sequences; searched the internal database (Guangzhou Jiajian medicine), dbSNP, esp6500, exac, and other population databases; and determined the insertion or deletion of small fragments (indel variation) and mononucleotide polymorphism. Variations with a minor allele frequency of <1% in gnomAD (low-frequency benign variation), artifacts, and variations in highly homologous regions were removed. Subsequently, SIFT and Polyphen2 were used to predict the conservation/pathogenicity/harmfulness of variants. The HGMD, PubMed, ClinVar, and other databases, as well as variant-related literature, were also searched. Variant classification was conducted according to the American Society for Medical Genetics and Genomics (ACMG) guidelines and reported as pathogenic, likely pathogenic, variant of unknown significance (VUS), likely benign, or benign.

Statistical analysis

Categorical variables are reported as numbers (percentages), whereas continuous variables are reported as median (range) or mean ± SD. Renal prognosis was evaluated using Kaplan–Meier survival analysis and single-variate analysis using the Cox proportional hazard model. Statistical analysis was performed using SPSS 26.0 software, and p-values < 0.05 were considered statistically significant.

Results

Demographic characteristics

Among the 140 patients, 79 (56.43%) were men and 61 (43.57%) were women. The average age of men at the visit was 57.22 ± 13.47 years, while that of women was 57.44 ± 11.94 years. A total of 90 (64.29%) patients reported a family history of ADPKD, comprising 36 patients (40.00%, 36/90) with single-parent history only, 21 (23.33%, 21/90) with sibling history only, and 33 with both parent and sibling history (36.67%, 33/90) (Table 1).

TABLE 1 Cohort information on ADPKD patients included in this study (n = 140).

Group	Proportion	Average age
Demographic information, age (mean ± SD)		
Male	79/140 (56.43%)	57.22 ± 13.47
Female	61/140 (43.57%)	57.44 ± 11.94
RRT distribution in different genotype, RRT age (mean ± SD)		
PKD1	77/112 (68.75%)	52.60 ± 11.36
PKD2	9/16 (56.25%)	60.67 ± 5.64
Others	9/12 (75.00%)	52.11 ± 14.63

[a]ADPKD: autosomal dominant polycystic kidney disease, RRT: renal replacement therapy.

Genotype distribution

Genetic analysis showed that 80.00% (n = 112) of the included patients harbored *PKD1* mutations and 11.43% (n = 16) harbored *PKD2* mutations, whereas no mutation was detected in the remaining 8.57% (n = 12). Among the 112 patients with *PKD1* mutations, 58.04% (n = 65) had truncating mutations (*PKD1*-T). In contrast, among the 16 patients with *PKD2* mutations, 93.75% (n = 15) had truncating mutations (*PKD2*-T). Furthermore, *PKD1*-missense, *PKD1*-frameshift, and *PKD1*-nonsense mutations were the most common mutations detected in this study, accounting for 25.78% (33/128), 24.22% (31/128), and 21.09% (27/128), respectively (Figure 1). The genotypes and mutation types of the study population are presented in Supplementary Table S1.

PKD1/PKD2 genotypes as renal prognostic indicators in ADPKD patients

As of July 2018, 67.86% (95/140) of patients progressed to ESRD and required RRT (i.e., hemodialysis, peritoneal dialysis, hemofiltration, hemodiafiltration, and kidney transplantation), including 77 patients with *PKD1* mutations, nine with *PKD2* mutations, and nine without *PKD1*/*PKD2* mutations. The average age of dialysis patients was 52.60 ± 11.36, 60.67 ± 5.64, and 52.11 ± 14.63 years, respectively. Among them, 61.05% (58/95) were men and 38.95% (37/95) were women, with an average age of 54.78 ± 12.05 and 51.03 ± 10.34 years, respectively.

Of the 77 patients with *PKD1* mutations, the average age of RRT initiation in 46 patients (59.74%) with *PKD1*-T mutations

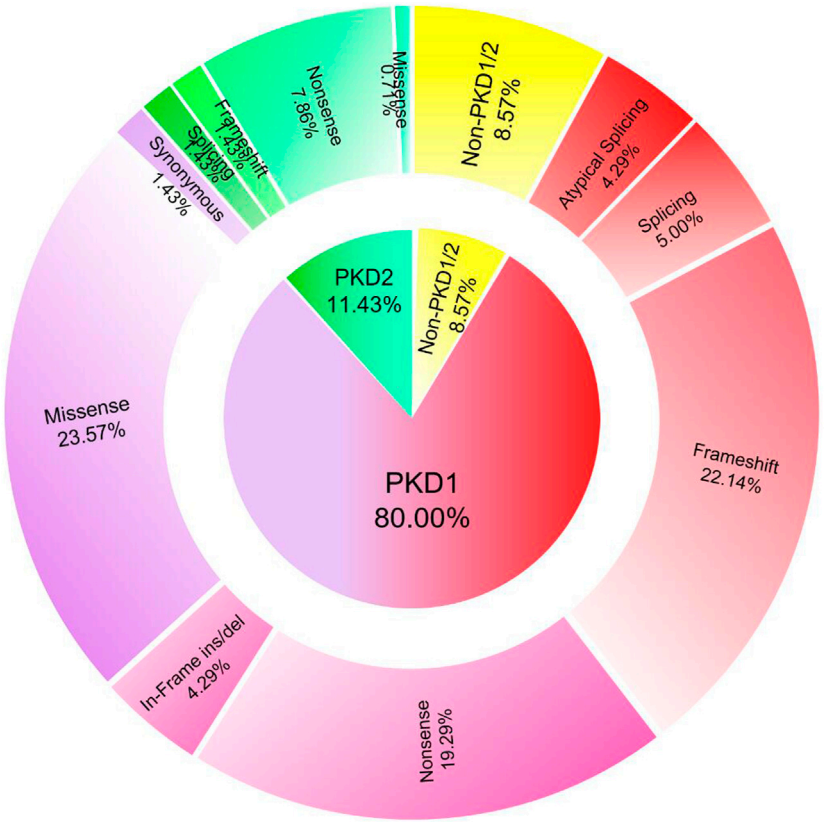


FIGURE 1
Distribution of genotypes and mutation types in ADPKD patients included in this study.

was 52.13 ± 8.29 years, while that in 31 patients (40.26%) with *PKD1*-NT mutations was 53.29 ± 14.76 years.

The results of univariate Cox regression analysis in patients with *PKD1* are shown in Table 2. Kaplan–Meier survival analysis revealed that renal survival is significantly worse in patients with *PKD1* mutations than in those with *PKD2* mutations, and patients with *PKD1* mutations reached ESRD earlier (Figure 2A, $p = 0.030$). In the *PKD1* cohort, the renal survival rate was significantly lower in patients with nonsense mutations than in those with other mutation types, thus requiring RRT earlier (Figure 2B, $p = 0.046$). However, other mutation types had no marked effect on renal prognosis. Meanwhile, sex or mutation position did not significantly affect the prognosis of ADPKD patients.

ACMG variants as renal prognostic indicators in ADPKD patients

According to the ACMG classification (Hampel et al., 2015), of the 128 mutations identified in the *PKD1/PKD2* cohort, 28.12% ($n = 36$) were pathogenic, 48.44% ($n = 62$) were likely pathogenic, and 23.44% ($n = 30$) were VUS (Figure 3). Among the 112 patients with *PKD1*, the median age of ESRD onset in those with pathogenic, likely pathogenic, and VUS mutations was 49.5 (20–67), 54 (20–84), and 56 (30–88) years, respectively. In the 16 patients with *PKD2*, only "pathogenic" ($n = 11$) and "likely pathogenic" mutations ($n = 5$) were detected.

Discussion

Stratifying the ADPKD population is a prerequisite for personalization of clinical therapy and patient care. Therefore, understanding the characteristics and clinical course of ADPKD patients is critical for selecting appropriate clinical interventions. The available genetic profiles of ADPKD patients available in the literature are mainly applicable to Western populations, and only a few studies have reported the genotype and phenotype characteristics of Asian patients (Sha et al., 2017). To uncover the genetic profiles of Asian ADPKD populations, we characterized the genotype, mutation type, and mutation

TABLE 2 Univariate analysis of risk factors related with RRT in the *PKD1* cohort.

Variable	Univariate analysis	
	Hazard ratio (95% CI)	*p*
Truncating	1.438 (0.896–2.308)	0.132
Mutation type		
Nonsense	1.646 (0.990–2.737)	0.055
Frameshift	1.062 (0.635–1.776)	0.820
Missense	0.704 (0.421–1.179)	0.182
In-frame insertions/deletions	0.688 (0.216–2.192)	0.527
Splicing	0.823 (0.332–2.043)	0.675
Synonymous	2.041 (0.498–8.374)	0.322
Atypical Splicing	0.795 (0.250–2.530)	0.698
Mutation Position		
PKD1 N-terminus domain	1.341 (0.808–2.225)	0.257
PKD domain	0.735 (0.337–1.603)	0.439
REJ domain	0.776 (0.426–1.414)	0.408
TM domain	1.126 (0.707–1.794)	0.617
PKD1 C-terminus domain	0.727 (0.228–2.315)	0.589

[a]RRT: renal replacement therapy, CI: confidence interval.

position based on targeted exome sequencing (TES) using NGS data and analyzed the prognostic differences in renal function among Chinese ADPKD populations.

The large size, complexity, and high GC content of *PKD1* increase the difficulty of mutation detection (Harris and Torres, 2009). *PKD1* contains 46 exons, and the duplication of its first 33 exons with six pseudogenes, which shares ~98% DNA sequence identity in the homology region, easily causes false-positive and false-negative results in genotype detection (Bogdanova et al., 2001; Song et al., 2017). In addition, as of October 2021, 1273 *PKD1*-related pathogenic mutations and 202 *PKD2*-related pathogenic mutations were recorded in the ADPKD database (PKDB, http://pkdb.mayo.edu). The high allelic heterogeneity between *PKD1* and *PKD2* creates challenges in the molecular diagnosis of ADPKD. Thus, a faster, more sensitive, and more economical assay for diagnosis and mutation screening of ADPKD is urgently required.

TES using NGS data is regarded as an effective method for investigating monogenic diseases. The coding regions of all target genes were first amplified by an LR-PCR-based method and then sequenced by an NGS platform, which can effectively avoid the interference of homologous sequences. In contrast, both whole-genome sequencing (WGS) and whole-exome sequencing (WES) sequencing failed to effectively avoid the interference of homologous sequences, and the cost of a single sequencing was higher. Due to the long sequence of the coding region of the target gene, one-generation sequencing is expensive and high throughput cannot be achieved. Therefore, with only a few genes and exons related to the disease being considered in TES (Ali et al., 2019), it allows automatic analysis of large amounts of data in a short period of time, as well as the mutation screening of various cystic diseases and potential modification genes. In this way, this method may revolutionize the genetic testing technology for ADPKD owing to its high accuracy and low cost.

Furthermore, 91.43% (128/140) of the mutations were detected in *PKD1*/*PKD2*, including 72 (56.25%) unreported mutations. We explain the 8.57% (12/140) cases of no mutations detected as follows. First, mutations in rare genes may be responsible for cystic diseases rather than *PKD1*/*PKD2* (i.e., *ALG8*, *ALG9*, *GANAB*, *PRKCSH*, *SEC6A*, and *SEC63*) (Besse et al., 2017; Besse et al., 2019). Second, somatic mosaicism, specifically variable involvement of affected cells, caused a low signal-to-noise ratio, thus making it difficult to detect mutations (Iliuta et al., 2017). Last, there might be omission of some deep intronic or pathogenic mutations in the regulatory region of *PKD1*/*PKD2*.

Currently, several international studies on genotype and phenotype characteristics have demonstrated the strong

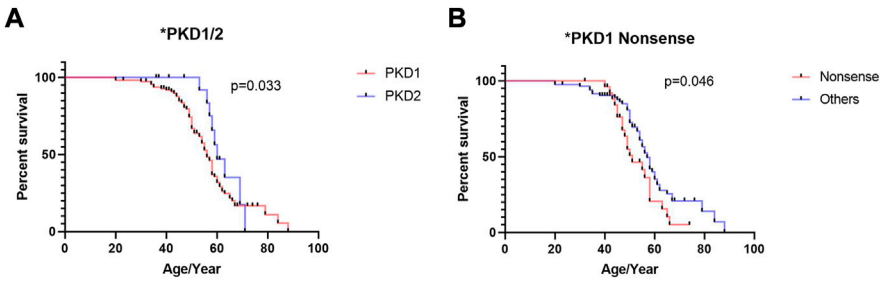


FIGURE 2
Kaplan–Meier survival analysis of ADPKD patients stratified by genotypes and mutation types. **(A)** Comparison of patients with PKD1 gene mutation and PKD2 gene mutation **(B)** Comparison of patients with PKD1 gene nonsense mutation and PKD1 gene other mutation. The end-point event was the start of regular renal replacement therapy.

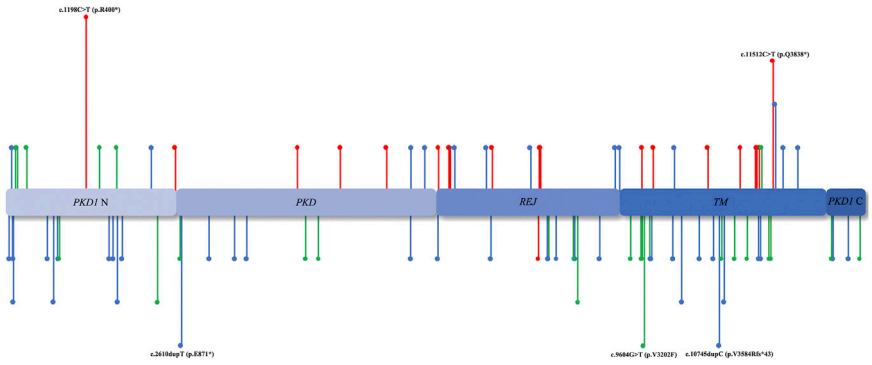


FIGURE 3
Mutation region. The distribution of *PKD1/PKD2* mutation sites in various domains. The unreported mutation sites are annotated below, whereas those reported previously are annotated above. The red lines represent ACMG I, the blue lines represent ACMG II, and the green lines represent ACMG III.

correlation of genotype and mutation type with the indicators used to assess the severity of renal diseases, including estimated glomerular filtration rate, height-adjusted total kidney volume, and the age of ESRD onset. For example, renal prognosis was worse in patients with *PKD1* than in those with *PKD2*, with a median age of ESRD onset of 58 and 79 years, respectively (Cornec-Le et al., 2019). Furthermore, the median age of patients with truncating mutations (i.e., splicing, frameshift, and nonsense) and non-truncating mutations (i.e., missense, in-frame insertions/detection, and atypical splicing) in *PKD1* was 55.6 and 67.9 years, respectively (Cornec-Le et al., 2019).

However, consistent with those of previous studies on the Asian ADPKD population (Dechao et al., 2018), our results also showed that the Chinese ADPKD study population reached ESRD earlier than international ADPKD populations. In this study, the median ages of *PKD1* and *PKD2* patients reaching ESRD were 54 and 58 years, respectively. Additionally, the renal survival rate of patients with *PKD1* nonsense mutations was significantly lower than that of patients with other *PKD1* mutations, whereas that of patients with other mutation types showed no significant difference. For example, we did not find a significant correlation between the occurrence of truncation mutations and renal prognosis in ADPKD patients, which was inconsistent with previous studies in the Asian population (Dechao et al., 2018). Hence, the genotype and phenotype characteristics of ADPKD patients vary across ethnic groups.

Moreover, modification effects have been demonstrated in ADPKD patients with the same mutation as the main effects (Cornec-Le et al., 2018). The ACMG has developed guidelines for explaining rare sequence variants, which are classified as "pathogenic," "likely pathogenic," "VUS," "likely benign," and "benign." However, some variants have been challenged because of the high cumulative incidence of "likely pathogenic" variants in *PKD1*/*PKD2*.

In this study, among the patients with *PKD1* mutations requiring RRT, the proportion of those with "pathogenic," "likely pathogenic," and "VUS" variants was 72.00% (18/25), 68.42% (39/57), and 66.67% (20/30), respectively, with corresponding median ages of ESRD onset of 49.5, 54, and 56 years, respectively. Despite their conformity with the classification of ACMG, the incidence of ADPKD and the proportion of RRT in those with "likely pathogenic" and "VUS" variants both exceeded the estimates reported by epidemiological studies (Cornec-Le et al., 2018). In addition, among the patients with *PKD2* mutations, the proportion of those with "pathogenic" and "likely pathogenic" variants requiring RRT was 45.45% (5/11) and 80.0% (4/5), respectively. Therefore, renal prognosis assessment of *PKD1*/*PKD2* mutation carriers or ADPKD patients based on the ACMG variant classification needs to be reconsidered.

Our findings indicate that the mutation position of *PKD1*/*PKD2* has no significant association with disease progression, which is consistent with the results of previous retrospective studies (Cornec-Le et al., 2013; Ali et al., 2019). According to the two-hit hypothesis, germline mutations inactivate the *PKD1* allele, regardless of the mutation position. Subsequently, a cyst developed in the absence of PC1 with a second inactivating mutation. In contrast, some hold opposing perspectives: the mutation location significantly influences the renal phenotype. Rossetti et al. suggested that the mutant gene might generate a functional product, explaining why patients with a 5′ mutant progressed to a more severe phenotype than those with a 3′ mutant (Hateboer et al., 2000; Rossetti et al., 2002).

In conclusion, we conducted a preliminary study on the genotype and phenotype characteristics of Chinese ADPKD patients based on TES using NGS data. Our findings provide new insights into the genetic profiles of Asian ADPKD populations. Our findings strongly suggest that TES using

NGS data could be the main method of ADPKD genetic investigation owing to its high precision, economic feasibility, and possibility of simultaneous mutation screening for various cystic diseases and potential modification genes. Hence, this method would contribute to the clinical diagnosis, treatment, and assessment of renal prognosis of ADPKD patients.

Data availability statement

The PKD1/2 genes-targeted exome sequencing data of patients are available at NCBI Sequence Read Archive with the BioProject accession number of PRJNA875618.

Ethics statement

The studies involving human participants were reviewed and approved by the Ethics Committee of the Nanfang Hospital, Southern Medical University (approval number: NFEC-2019-190). The patients/participants provided their written informed consent to participate in this study.

Funding

This study was funded by the National Natural Science Foundation of China (Grant No.82070770), the Natural Science Foundation of Guangdong Province (Grant No. 2020A1515010674), the President Funding of Nanfang Hospital (Grant Nos. 2018B009 and 2018C003), and the College Students' Innovative Entrepreneurial Training Plan Program (Grant Nos. X202012121239 and 202012121046).

Conflict of interest

Author WZ was employed by Guangzhou Jiajian Medical Testing Co., Ltd.

The remaining authors declare that the research was conducted in the absence of any commercial or financial relationships that could be construed as a potential conflict of interest.

Publisher's note

All claims expressed in this article are solely those of the authors and do not necessarily represent those of their affiliated organizations, or those of the publisher, the editors, and the reviewers. Any product that may be evaluated in this article, or claim that may be made by its manufacturer, is not guaranteed or endorsed by the publisher.

Supplementary material

The Supplementary Material for this article can be found online at: https://www.frontiersin.org/articles/10.3389/fgene.2022.934463/full#supplementary-material

References

Ali, H., Al-Mulla, F., Hussain, N., Naim, M., Asbeutah, A. M., AlSahow, A., et al. (2019). PKD1 duplicated regions limit clinical utility of whole exome sequencing for genetic diagnosis of autosomal dominant polycystic kidney disease. *Sci. Rep.* 9 (1), 4141. doi:10.1038/s41598-019-40761-w

Audrézet, M. P., Corbiere, C., Lebbah, S., Moriniere, V., Broux, F., Louillet, F., et al. (2016). Comprehensive PKD1 and PKD2 mutation analysis in prenatal autosomal dominant polycystic kidney disease. *J. Am. Soc. Nephrol.* 27 (3), 722–729. doi:10.1681/ASN.2014101051

Bergmann, C. (2015). ARPKD and early manifestations of ADPKD: the original polycystic kidney disease and phenocopies. *Pediatr. Nephrol.* 30 (1), 15–30. doi:10.1007/s00467-013-2706-2

Besse, W., Chang, A. R., Luo, J. Z., Triffo, W. J., Moore, B. S., Gulati, A., et al. (2019). ALG9 mutation carriers develop kidney and liver cysts. *J. Am. Soc. Nephrol.* 30 (11), 2091–2102. doi:10.1681/ASN.2019030298

Besse, W., Dong, K., Choi, J., Punia, S., Fedeles, S. V., Choi, M., et al. (2017). Isolated polycystic liver disease genes define effectors of polycystin-1 function. *J. Clin. Invest.* 127 (9), 1772–1785. doi:10.1172/JCI90129

Bogdanova, N., Markoff, A., Gerke, V., Horst, J., and Dworniczak, B. (2001). Homologues to the first gene for autosomal dominant polycystic kidney disease are pseudogenes. *Genomics* 74 (3), 333–341. doi:10.1006/geno.2001.6568

Cornec-Le, G. E., Alam, A., and Perrone, R. D. (2019). Autosomal dominant polycystic kidney disease. *Lancet* 393 (10174), 919–935. doi:10.1016/S0140-6736(18)32782-X

Cornec-Le, G. E., Audrézet, M. P., Chen, J. M., Hourmant, M., Morin, M. P., Perrichot, R., et al. (2013). Type of PKD1 mutation influences renal outcome in ADPKD. *J. Am. Soc. Nephrol.* 24 (6), 1006–1013. doi:10.1681/ASN.2012070650

Cornec-Le, G. E., Torres, V. E., and Harris, P. C. (2018). Genetic complexity of autosomal dominant polycystic kidney and liver diseases. *J. Am. Soc. Nephrol.* 29 (1), 13–23. doi:10.1681/ASN.2017050483

Dechao, X., Yiyi, M., Xiangchen, G., Bian, R., Lu, Y., Xing, X., et al. (2018). Novel mutations in the PKD1 and PKD2 genes of Chinese patients with autosomal dominant polycystic kidney disease. *Kidney Blood Press. Res.* 43 (2), 297–309. doi:10.1159/000487899

Hampel, H., Bennett, R. L., Buchanan, A., Pearlman, R., and Wiesner, G. L. (2015). A practice guideline from the American College of medical genetics and Genomics and the national society of genetic counselors: referral indications for cancer predisposition assessment. *Genet. Med.* 17 (1), 70–87. doi:10.1038/gim.2014.147

Harris, P. C., and Torres, V. E. (2009). Polycystic kidney disease. *Annu. Rev. Med.* 60, 321–337. doi:10.1146/annurev.med.60.101707.125712

Hateboer, N., Veldhuisen, B., Peters, D., Breuning, M. H., San-Millan, J. L., BogdaNovaN., et al. (2000). Location of mutations within the PKD2 gene influences clinical outcome. *Kidney Int.* 57 (4), 1444–1451. doi:10.1046/j.1523-1755.2000.00989.x

Iliuta, I. A., Kalatharan, V., Wang, K., Cornec-Le Gall, E., Conklin, J., Pourafkari, M., et al. (2017). Polycystic kidney disease without an apparent family history. *J. Am. Soc. Nephrol.* 28 (9), 2768–2776. doi:10.1681/ASN.2016090938

Lanktree, M. B., and Chapman, A. B. (2017). New treatment paradigms for ADPKD: moving towards precision medicine. *Nat. Rev. Nephrol.* 13 (12), 750–768. doi:10.1038/nrneph.2017.127

Li, Q., Wang, Y., Deng, W., Liu, Y., Geng, J., and Yan, Z. (2021). Heterogeneity of cell composition and origin identified by single-cell transcriptomics in renal cysts of patients with autosomal dominant polycystic kidney disease. *Theranostics* 11 (20), 10064–10073. doi:10.7150/thno.57220

Ravine, D., Gibson, R. N., Walker, R. G., Sheffield, L. J., Kincaid-Smith, P., and Danks, D. M. (1994). Evaluation of ultrasonographic diagnostic criteria for autosomal dominant polycystic kidney disease 1. *Lancet* 343 (8901), 824–827. doi:10.1016/s0140-6736(94)92026-5

Rossetti, S., Burton, S., Strmecki, L., Pond, G. R., San Millan, J. L., Zerres, K., et al. (2002). The position of the polycystic kidney disease 1 (PKD1) gene mutation correlates with the severity of renal disease. *J. Am. Soc. Nephrol.* 13 (5), 1230–1237. doi:10.1097/01.asn.0000013300.11876.37

Sha, Y. K., Sha, Y. W., Mei, L. B., Huang, X. J., Wang, X., Lin, S. B., et al. (2017). Use of targeted sequence capture and high-throughput sequencing identifies a novel PKD1 mutation involved in adult polycystic kidney disease. *Gene* 634, 1–4. doi:10.1016/j.gene.2017.08.040

Song, X., Haghighi, A., Iliuta, I. A., and Pei, Y. (2017). Molecular diagnosis of autosomal dominant polycystic kidney disease. *Expert Rev. Mol. diagn.* 17 (10), 885–895. doi:10.1080/14737159.2017.1358088

frontiers | Frontiers in Genetics

TYPE Original Research
PUBLISHED 12 October 2022
DOI 10.3389/fgene.2022.894080

Check for updates

OPEN ACCESS

EDITED BY
Ruth Roberts,
ApconiX, United Kingdom

REVIEWED BY
Kunqi Chen,
Fujian Medical University, China
Wan-Xin Peng,
Zhejiang University, China

*CORRESPONDENCE
Kai Wang,
wangkaimath@sina.com

SPECIALTY SECTION
This article was submitted to Genetics of Common and Rare Diseases, a section of the journal Frontiers in Genetics

RECEIVED 11 March 2022
ACCEPTED 12 September 2022
PUBLISHED 12 October 2022

CITATION
Li H, Lin D, Wang X, Feng Z, Zhang J and Wang K (2022), The development of a novel signature based on the m^{6}A RNA methylation regulator-related ceRNA network to predict prognosis and therapy response in sarcomas. *Front. Genet.* 13:894080. doi: 10.3389/fgene.2022.894080

COPYRIGHT
© 2022 Li, Lin, Wang, Feng, Zhang and Wang. This is an open-access article distributed under the terms of the Creative Commons Attribution License (CC BY). The use, distribution or reproduction in other forums is permitted, provided the original author(s) and the copyright owner(s) are credited and that the original publication in this journal is cited, in accordance with accepted academic practice. No use, distribution or reproduction is permitted which does not comply with these terms.

The development of a novel signature based on the m^{6}A RNA methylation regulator-related ceRNA network to predict prognosis and therapy response in sarcomas

Huling Li[1], Dandan Lin[1], Xiaoyan Wang[1], Zhiwei Feng[2], Jing Zhang[1] and Kai Wang[3]*

[1]School of Public Health, Xinjiang Medical University, Urumqi, China, [2]School of Continuing Education, Xinjiang Medical University, Urumqi, China, [3]Department of Medical Engineering and Technology, Xinjiang Medical University, Urumqi, China

Background: N^6 methyladenosine (m^{6}A)-related noncoding RNAs (including lncRNAs and miRNAs) are closely related to the development of cancer. However, the gene signature and prognostic value of m^{6}A regulators and m^{6}A-associated RNAs in regulating sarcoma (SARC) development and progression remain largely unexplored. Therefore, further research is required.

Methods: We obtained expression data for RNA sequencing (RNA-seq) and miRNAs of SARC from The Cancer Genome Atlas (TCGA) datasets. Correlation analysis and two target gene prediction databases (miRTarBase and LncBase v.2) were used to deduce m^{6}A-related miRNAs and lncRNAs, and Cytoscape software was used to construct ceRNA-regulating networks. Based on univariate Cox regression and least absolute shrinkage and selection operator (LASSO) Cox regression analyses, an m^{6}A-associated RNA risk signature (m6Ascore) model was established. Prognostic differences between subgroups were explored using Kaplan–Meier (KM) analysis. Risk score-related biological phenotypes were analyzed in terms of functional enrichment, tumor immune signature, and tumor mutation signature. Finally, potential immunotherapy features and drug sensitivity predictions for this model were also discussed.

Results: A total of 16 miRNAs, 104 lncRNAs, and 11 mRNAs were incorporated into the ceRNA network. The risk score was obtained based on RP11-283I3.6, hsa-miR-455-3p, and CBLL1. Patients were divided into two risk groups using the risk score, with patients in the low-risk group having longer overall survival (OS) than those in the high-risk group. The receiver operating characteristic (ROC) curves indicated that risk characteristic performed well in predicting the prognosis of patients with SARC. In addition, lower m6Ascore was also positively correlated with the abundance of immune cells such as monocytes and mast cells activated, and several immune checkpoint genes were highly expressed in the low-m6Ascore group. According to our analysis, lower m6Ascore may lead

to better immunotherapy response and OS outcomes. The risk signature was significantly associated with the chemosensitivity of SARC. Finally, a nomogram was constructed to predict the OS in patients with SARC. The concordance index (C-index) for the nomogram was 0.744 (95% CI: 0.707–0.784). The decision curve analysis (DCA), calibration plot, and ROC curve all showed that this nomogram had good predictive performance.

Conclusion: This m6Ascore risk model based on m^{6}A RNA methylation regulator-related RNAs may be promising for clinical prediction of prognosis and might contain potential biomarkers for treatment response prediction for SARC patients.

KEYWORDS

sarcomas, m^{6}A, risk score, prognosis, chemotherapy, immunotherapy

Introduction

Sarcomas (SARC) are comprised of an extensive, heterogeneous, and biologically diverse group of malignant tumors all of which are derived from mesenchymal cells (Hui, 2016). It has more than 100 different subtypes that can occur in any part of the body. Although there are more than 100 subtypes, sarcomas can be divided into two main types including soft-tissue sarcomas (STSs, accounting for 80%) and three major subtypes of bone sarcomas (BSs, including the osteosarcomas, chondrosarcomas, and Ewing's (EW) sarcomas) (Doyle, 2014; Hui, 2016; Alavi et al., 2018; Ferguson and Turner, 2018; Hatina et al., 2019). SARC are characterized by a low incidence rate (approximately 1% of all malignancies in adults and 10–15% of all malignancies in pediatric cancers) but a poor prognosis in most cases (Hui, 2016; Siegel et al., 2019). Despite advances in the treatment of STS and osteosarcoma, with comprehensive treatment strategies including surgery, chemotherapy, radiotherapy, and targeted therapy, the survival rate of patients with advanced STSs and BSs needs to be improved (Zhu et al., 2019a; Zhang et al., 2021a; Eaton et al., 2021). Although it is difficult to determine the survival for each subtype of sarcoma due to the heterogeneity of the disease, the 5-year survival rates for patients with STS and for patients with bone sarcomas are generally larger than (>) 80% and about 70%, respectively. However, 5-year survival rates of the patients developing advanced-stage STS or various bone sarcomas are less than (<) 20% and between 22% and 57%, respectively (Bone Cancer, 2021; SarcomasTissue, 2021; SEER, 2021). In addition, about 50% of STS patients and about 90% of BS patients end up with distant metastasis, which remains a major cause of death and a barrier to effective treatment (Bacci et al., 1998; Italiano et al., 2011). Sarcomas have a poor prognosis due to their aggressive growth and high risk of metastasis (Aung et al., 2019). Therefore, further investigations into the pathogenesis of sarcomas and identification of the novel prognostic biomarkers that facilitate the improvement of therapy and prognosis of sarcomas are urgently needed.

N^6-methyladenosine (m^{6}A) is the prevalent modification in eukaryotic mRNAs, whose reversible methylation may have a profound impact on gene expression regulation (Niu et al., 2013), and plays a critical role in RNA processing. m^{6}A RNA methylation is dynamically regulated by the corresponding m^{6}A regulators, which are well classified into three subtypes, namely, "methylases—writer," "demethylases—erasers," or "m^{6}A binding proteins—readers" depending on different functions (Yang et al., 2018; Chen et al., 2019a; Barbieri and Kouzarides, 2020). Increasing evidence has revealed the correlation between m^{6}A and human cancers, including ovarian cancer (Li et al., 2021a), hepatocellular carcinoma (Li et al., 2021b), and colorectal cancer (Ji et al., 2020). The literature has also indicated that m^{6}A-related genes might serve as novel prognostic biomarkers for different cancers, and that the m^{6}A-related risk score may assist in risk assessment and prognostic stratification (Li et al., 2021c; Xu et al., 2021). The m^{6}A regulators are also linked with the progression and prognosis of SARC. In recent years, there have been some studies on the role of m^{6}A methylation regulators in sarcomas. For instance, WTAP, which is highly expressed in osteosarcoma tissues and associated with the worse prognosis of osteosarcoma patients, was found to potentially promote osteosarcoma progression by inhibiting HMBOX1 in an m^{6}A-dependent manner *in vitro* and *in vivo* (Chen et al., 2020). Hou et al. (2020) evaluated the relationship between copy number variations (CNVs) and mutations of m^{6}A regulatory factors and the prognosis of patients with soft-tissue sarcomas by using The Cancer Genome Atlas (TCGA) database. Their analysis indicated that CNVs and mutations of KIAA1429, YTHDF3, and IGF2BP1 were independent risk factors predicting OS and DFS. Zhang et al. (2021a) constructed and validated a signature based on m^{6}A-related lncRNAs which could function as independent prognosis-specific predictors in STS, thereby providing novel insights into the roles of m^{6}A-related lncRNAs in STS. Noncoding RNAs (ncRNAs), such as long noncoding RNAs (lncRNAs) and microRNAs (miRNAs), function as key regulators of gene

expression, and the competitive endogenous RNA (ceRNA) network is a transcriptional regulatory network at the molecular level, consisting of lncRNA, miRNA, and mRNA (Salmena et al., 2011; Zhu et al., 2019b; Cava et al., 2019). More and more studies have shown that the competing endogenous RNAs (ceRNAs) have been suggested to be involved in essential biological processes and play crucial roles in the initiation and development of neoplasms, and they potentially serve as diagnostic and prognostic markers or therapeutic targets (Qi et al., 2015). At present, the mRNA–miRNA–lncRNA network is mostly studied in the ceRNA network. Recent studies have shown novel roles of the ceRNA network in thyroid cancer, colon adenocarcinoma, gastric cancer, hepatocellular carcinoma, and lung adenocarcinoma (Chang et al., 2020; Hu et al., 2020; Nie et al., 2020; Yang et al., 2020; Zhang et al., 2021b). In addition, a previous study has constructed a ceRNA network and predicted the prognosis of soft-tissue sarcoma recurrence (Huang et al., 2019). Gao et al. (2021) identified differentially expressed mRNAs (DEGs), lncRNAs (DELs), and miRNAs (DEMs) in sarcomas by comparing the gene expression profiles between sarcoma and normal muscle samples in Gene Expression Omnibus (GEO) datasets. Through target gene prediction, a lncRNA–miRNA–mRNA–ceRNA network that contained 113 mRNAs, 69 lncRNAs, and 29 miRNAs was constructed, which might provide insights into further research on the molecular mechanism and potential prognosis biomarkers. Yang et al. (2022) applied starBase and Cytoscape to construct a competing endogenous RNA (ceRNA) network based on m^{6}A-related prognostic lncRNA signature and revealed the prognostic role of m^{6}A-related lncRNAs in osteosarcoma and identified them as potential biomarkers for predicting the prognosis of patients with osteosarcoma. Although most studies have established prognostic models for patients with sarcoma based on the relationship between m^{6}A and noncoding RNA, the biomarkers included in the models are relatively single, and the starting point and perspective of each study are different. So far as we know, the m^{6}A-related ceRNA network and gene signature including three types of potential biomarkers of m^{6}A regulator- and m^{6}A-related noncoding RNAs (lncRNAs and miRNAs) in the regulation of soft-tissue sarcoma (STS) development and progression and prognostic values are largely unexplored. This study is based on the direction to launch a series of explorations on sarcoma.

In this study, based on transcript, somatic mutation, and clinical data obtained from The Cancer Genome Atlas (TCGA) and cBioPortal databases, we conducted extensive analysis. First, the correlation between the expression of 21 widely reported key m^{6}A RNA methylation regulators and the prognosis of SARC was analyzed. Second, a regulatory network of lncRNA (predicted by the LncBase v.2 database)–miRNA (predicted by miRTarBase)–m^{6}A regulators, including 16 miRNAs, 11 m^{6}A regulators, and 104 lncRNAs, was constructed. In addition, using LASSO Cox regression analysis, a risk score model based on miRNA and lncRNA and m^{6}A regulators in the ceRNA network was established to predict the prognosis, immune landscape, and chemosensitivity of SARC patients. Then, the risk score model was evaluated through the ROC curve. These may be potential biomarkers or therapeutic targets of SARC in the future. To further explore the potential relationship between m6Ascore and clinicopathological data, we developed a clinical m6Ascore nomogram to predict the prognosis of sarcoma patients.

Materials and methods

Acquisition of information of patients with SARC

All datasets used in this study were publicly available, and the detailed workflow for risk model construction and subsequent analyses is shown in Figure 1. The RNA sequencing (RNA-seq) transcriptome information (including mRNA, lncRNA, and miRNA expression data), patient clinical information, and somatic mutation status data were obtained from The Cancer Genome Atlas (TCGA)(query) (https://portal.gdc.cancer.gov/) and cBioPortal websites (http://www.cbioportal.org/). Patients with unclear survival time, survival status, and clinicopathological characteristics were excluded. Only patients with overall survival (OS) times of more than or equal to 30 days were included in the dataset.

Selection of m^{6}A genes and m^{6}A-related lncRNAs and miRNAs

According to other published studies, 21 m^{6}A genes were investigated in this study, including writers (*METTL3*, *METTL14*, *CBLL1*, *VIRMA [KIAA1429]*, *RBM15*, *RBM15B*, *ZC3H13*, and *WTAP*), readers (*YTHDC1*, *YTHDC2*, *YTHDF1*, *YTHDF2*, *YTHDF3*, *IGF2BP1*, *HNRNPA2B1*, *HNRNPC*, *FMR1*, *LRPPRC*, and *ELAVL1*), and erasers (*ALKBH5* and *FTO*). Using the STRING (version 11.0, http://string-db.org/) database, we retrieved the interactions of the 21 m^{6}A RNA methylation regulators and visualized the interactions. The Pearson correlation analysis was used to elucidate the correlation between different m^{6}A RNA methylation regulators. We downloaded the profiles of lncRNAs, miRNA, and m^{6}A genes from TCGA database. Thereafter, the Pearson correlation analysis was conducted to screen the m^{6}A gene-related lncRNAs and miRNAs in SARC samples. LncRNAs with correlation coefficients >0.4 and $p < 0.001$ were regarded as m^{6}A-related lncRNAs, while miRNAs with correlation coefficients <–0.15 and $p < 0.05$ were regarded as m^{6}A-related miRNAs.

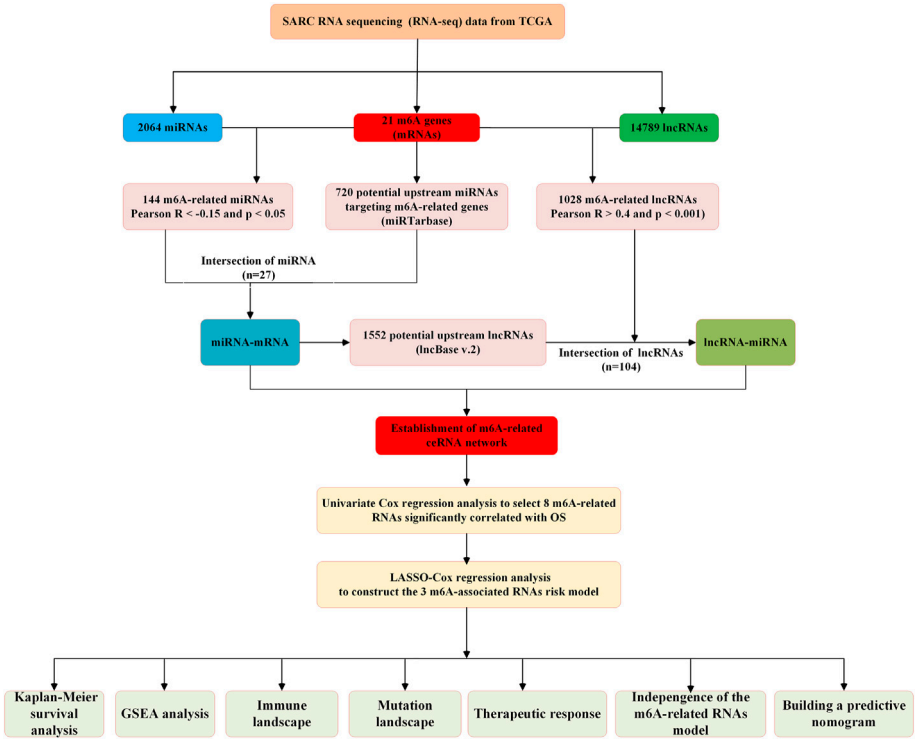


FIGURE 1
Flow chart of this study.

Construction of the m^{6}A-associated ceRNA network

All miRNAs that were negatively correlated with the 21 selected m^{6}A regulators (*METTL3*, *METTL14*, *CBLL1*, *VIRMA [KIAA1429]*, *RBM15*, *RBM15B*, *ZC3H13*, *WTAP*, *YTHDC1*, *YTHDC2*, *YTHDF1*, *YTHDF2*, *YTHDF3*, *IGF2BP1*, *HNRNPA2B1*, *HNRNPC*, *FMR1*, *LRPPRC*, *ELAVL1*, *ALKBH5*, and *FTO*) were obtained from TCGA-SARC dataset (Pearson correlation coefficient < −0.15 and $p < 0.05$). Then, the related miRNAs possessing potential binding sites with the 21 selected m^{6}A regulators were simultaneously predicted using the miRTarBase database (http://mirtarbase.cuhk.edu.cn/), and the intersection with the results from the analysis in the previous step was collected. Meanwhile, all lncRNAs were obtained from TCGA-SARC dataset and further screened according to their Pearson correlation coefficients (Pearson correlation coefficient >0.4, $p < 0.05$) with 21 selected m^{6}A regulators. Next, the related lncRNAs possessing potential binding sites with the interactive m^{6}A-related miRNAs were predicted using the LncBase v.2's experimental module (http://carolina.imis.athena-innovation.gr/), and the intersection with the results from the analysis in the previous step was obtained. Finally, the lncRNA–miRNA–m^{6}A regulator ceRNA network based on the foundation of the interactions between m^{6}A-related lncRNA and m^{6}A-related miRNA and between m^{6}A-related miRNA and m^{6}A regulators was created and visualized using the "ggalluvial" R package.

Establishment of the m^{6}A-associated risk model

First, by means of the "survival" package in R, univariate Cox regression analysis was utilized to explore the correlation between the genes in the ceRNA network and overall survival (OS) of SARC patients to determine the prognostic-related biomarkers. Then, we used the "glmnet" R package to perform LASSO regression analysis on the genes screened in the univariate Cox regression analysis. Finally, the genes that can be used as independent prognostic factors of OS were screened using multivariate Cox regression analysis, and their regression coefficients (β) were calculated. The following formula was used to calculate the prognostic risk score of each patient:

Risk score = β (mRNA1) * expr (mRNA1) + β (mRNA2) * expr (mRNA2) + … + β (mRNAn) * expr (mRNAn) + β (miRNA1) * expr (miRNA1) + β (miRNA2) * expr (miRNA2) + … + β (miRNAn) * expr (miRNAn) + β (lncRNA1) * expr

(lncRNA1) + β (lncRNA2) * expr (lncRNA2) + . . . + β (lncRNAn) * expr (lncRNAn).

At the same time, the cut-off point of risk score was picked using the "survminer" R package which divided patients into high- and low-risk groups. Subsequently, the Kaplan–Meier survival analysis and log-rank test were used to evaluate the difference in the overall survival (OS) between the risk score groups. Finally, to reflect the prediction ability of the risk score model, we generated the area under the curve (AUC) of the time-dependent receiver operating characteristic (tROC) curves ("riskRegression" package in R) and calculated the area under the curve (AUC) for 1-year, 3-year, and 5-year overall survival (OS).

Analysis of tumor immune signatures and function enrichment for m6Ascore

Tumor immune signatures were evaluated in two aspects: 1) immune checkpoints and 2) the levels of infiltrating immune and immune and stromal scores were calculated using CIBERSORT, TIMER, ssGSEA, and ESTIMATE algorithms. Parts of the results are available at the Genomic Data Commons (GDC, https://gdc.cancer.gov/) and Tumor IMmune Estimation Resource (TIMER2.0, http://timer.cistrome.org/). The gene set enrichment analysis (GSEA) was utilized to understand the biological processes involved in the high- and low-risk groups. Hallmarks in GSEA were used to identify predefined gene sets. A pathway with a |normalized enrichment score (NES)| >1.5, a p-value < 0.05, and a false discovery rate (FDR) < 0.05 was considered to be significant, as described in the *Results* section.

Analysis of the tumor mutation status in the low- and high-risk groups

The information of somatic mutations in TCGA samples was downloaded from cBioPortal database and TCGA database. The tumor mutational burden (TMB) is defined as the total number of gene mutations per million bases, including the total number of gene-coding errors, base substitutions, and gene insertions or deletions. The TMB value of each patient was calculated using the Perl programming language. Significantly mutated genes between the low- and high-m6Ascore groups and the interaction effect of gene mutations were analyzed using "maftools" R packages. The statistical test for the proportion of mutation was evaluated by the two-side Chi-squared test, and $p < 0.05$ was considered to be significant.

Prediction of therapeutic sensitivity in patients with different m6Ascore

We studied the predictive capacity of m6Ascore in responding immunotherapy and 138 drugs of chemotherapies/targeted therapies. Based on the public pharmacogenomics database, Genomics of Drug Sensitivity in Cancer (GDSC, https://www.cancerrxgene.org), the 50% inhibiting concentration (IC_{50}) values of the 138 drugs were calculated using the "pRRophetic" R packages. The potential response of patients to immunotherapy was inferred by the tumor immune dysfunction and exclusion (TIDE) algorithm. Generally, a lower TIDE score predicts a better response to immunotherapy. The results of TIDE module analysis of patients with SARC from TCGA dataset were downloaded from the TIDE website (http://tide.dfci.harvard.edu/).

Construction of a predictive nomogram

First, we developed univariate and multivariate Cox regression analyses of the m6Ascore risk signature and other clinicopathological characteristics to confirm the independence of the m6Ascore risk signature. Then, we used the aforementioned factors to establish a nomogram using the "rms" and "regplot" R packages to predict the prognosis of patients with sarcoma. Finally, ROC, C-index, calibration curve analysis, and DCA curves were used to determine whether our established nomogram was suitable for clinical use.

Statistical analysis

The continuous data are expressed as the mean (standard deviation, SD). The categorical data are expressed as frequency and percentage. The relativity between m6Ascore risk signature and immune checkpoint molecules, and TMB were analyzed using the Spearman or Pearson correlation analysis. The Chi-squared test was used to compare different proportions. The differences in proportions of the immune-infiltrating cells, immune checkpoint gene expression, TMB, IC_{50}, and TIDE-related signatures between high- and low-risk groups were compared using the Wilcoxon rank-sum test (Mann–Whitney U test). The Kaplan–Meier survival analysis and log-rank tests were used to analyze the differences in OS between different risk score groups. The univariate and multivariate Cox regression analyses were performed to screen the independent predictors for OS. In all statistical results, except for the special instructions, a two-tailed p-value less than 0.05 indicated statistical significance. All analyses were performed using R software (version 3.6.2, https://www.r-project.org/).

TABLE 1 Main clinicopathological characteristics of the 255 SARC patients.

Characteristic		Number of patients (N = 255)
Age		
Mean (SD)		60.7 (14.7)
Sex, n (%)		
	Female	138 (54.1%)
	Male	117 (45.9%)
Race, n (%)		
	Asian	6 (2.4%)
	Black or African American	18 (7.1%)
	White	223 (87.5%)
	Unknown	8 (3.1%)
Cancer status, n (%)		
	Tumor free	128 (50.2%)
	With tumor	98 (38.4%)
	Unknown	29 (11.4%)
Radiation therapy, n (%)		
	Yes	68 (26.7%)
	No	176 (69.0%)
	Unknown	11 (4.3%)
Cancer type, n (%)		
	Dedifferentiated liposarcoma	59 (23.1%)
	Desmoid/aggressive fibromatosis	2 (0.8%)
	Leiomyosarcoma	100 (39.2%)
	Malignant peripheral nerve sheath tumor	9 (3.5%)
	Myxofibrosarcoma	25 (9.8%)
	Synovial sarcoma	10 (3.9%)
	Undifferentiated pleomorphic sarcoma/malignant fibrous histiocytoma/high-grade spindle cell sarcoma	50 (19.6%)

Results

Prognostic analysis of m^{6}A-associated genes in SARC

A total of 255 patients with primary sarcoma had completed clinical data, including 117 (45.9%) males and 138 (54.1%) females, with the mean age being 60.7 ± 14.7. The detailed demographic and clinicopathological data of these SARC patients are shown in Table 1. With the STRING database used to understand the interaction between the 21 m^{6}A RNA methylation regulators, a PPI network was obtained (Figure 2A), which indicated that all enrolled 21 studied genes exhibited gene–gene interactions. In addition, we examined the relationship between 21 regulators through the Pearson correlation test and observed that all m^{6}A RNA methylation regulators were generally positively correlated (Figure 2B). *YTHDC1* showed a positive correlation with *ZC3H13* (correlation coefficient: 0.8) and *METTL14* (correlation coefficient: 0.8). *YTHDF3* showed a positive correlation with *KIAA1429* (correlation coefficient: 0.8). *HNRNPA2B1* showed a positive correlation with *ELAVL1* (correlation coefficient: 0.8). Next, according to the aforementioned criteria, we analyzed the prognostic role of the 21 m^{6}A-associated genes in SARC in a total of 245 patients with OS and RNA-seq data. We performed univariate and multivariate Cox regression analyses to explore whether these genes were associated with the prognosis of SARC patients. The results of univariate Cox regression revealed that *METTL3* (p = 0.032) and *CBLL1* (p = 0.048) were risk genes for SARC (Figure 3A). The multivariate Cox regression results revealed that both *CBLL1* (p = 0.033) and *RBM15* (p = 0.023) were risk factors for OS. It also revealed that *ALKBH5* (HR (hazard ratio) = 0.669, p = 0.021, and 95% CI (confidence interval) [0.475–0.942]) may be a protective gene for OS (Figure 3B).

Identification of key upstream miRNAs of 21 m^{6}A genes

The potential upstream miRNAs of 21 m^{6}A genes were predicted using the experimentally verified microRNA–target gene interaction database miRTarBase. Ultimately, it found that 720 miRNAs interacted with 20 m^{6}A genes (writers: *METTL3*, *METTL14*, *CBLL1*, *KIAA1429 [VIRMA]*, *RBM15B*, *ZC3H13*, and *WTAP*; readers: *YTHDC1*, *YTHDC2*, *YTHDF1*, *YTHDF2*, *YTHDF3*, *IGF2BP1*, *HNRNPA2B1*, *HNRNPC*, *FMR1*, *LRPPRC*, and *ELAVL*; and erasers: *ALKBH5* and *FTO*), while no upstream miRNA interacted with one m^{6}A gene (RBM15) in the database (Supplementary Table S1). Next, the matrix expressions of 21 m^{6}A genes and 2,064 miRNAs were abstracted from TCGA database. We defined the miRNAs that were significantly related to one of the 21 m^{6}A genes (Pearson R < -0.15 and p < 0.05) as m^{6}A-related miRNAs. Finally, 144 miRNAs were discerned as m^{6}A-related miRNAs (Supplementary Table S2). Also, the predicted miRNAs were then intersected with these m^{6}A-related miRNAs to select the 27 m^{6}A-related miRNAs (key miRNAs) that interacted with 12 m^{6}A genes. Cytoscape was used to construct an miRNA–mRNA regulatory network, including 30 miRNA–mRNA pairs (Figure 4).

Identification of upstream lncRNAs of key miRNAs in patients with SARC

Based on the ceRNA hypothesis that lncRNAs can compete with mRNAs for miRNA binding, thus playing a vital role in the process of tumor development and progression (Nie et al., 2020), this study further used the experimental module of LncBase

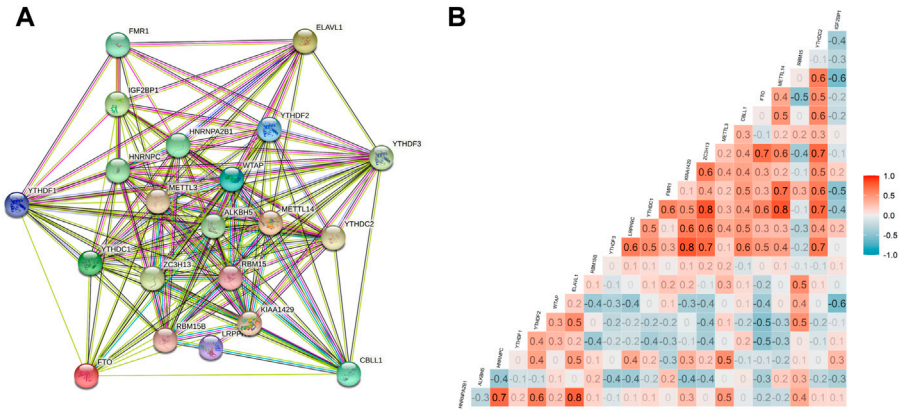


FIGURE 2
Interactions and correlations among m^{6}A RNA methylation regulators in SARC. **(A)** PPI network was constructed to evaluate the interactions among m^{6}A RNA methylation regulators; and **(B)** Pearson correlation analysis was used to analyze the correlations among m^{6}A RNA methylation regulators.

database (http://carolina.imis.athena-innovation.gr/diana_tools/web/index.php?r = *Lncbasev2%2Findex-experimental*), an online database, to predict the upstream lncRNAs that may interact with the 27 key miRNAs (hsa-miR-124-3p, hsa-miR-455-3p, hsa-miR-34a-5p, hsa-miR-214-5p, hsa-miR-124-5p, hsa-miR-302a-5p, hsa-miR-3202, hsa-miR-125a-3p, hsa-miR-224-3p, hsa-miR-4999-5p, hsa-miR-6766-5p, hsa-miR-6808-3p, hsa-miR-3133, hsa-miR-6885-3p, hsa-miR-1298-3p, hsa-miR-5692c, hsa-miR-378f, hsa-miR-378b, hsa-miR-5693, hsa-miR-3612, hsa-miR-6515-3p, hsa-miR-361-5p, hsa-miR-5008-3p, hsa-miR-6865-3p, hsa-miR-193b-3p, hsa-miR-23c, and hsa-miR-196b-5p), and a total of 1,552 lncRNAs were obtained (Supplementary Table S3). Then, the matrix expressions of 21 m^{6}A genes and 14,789 lncRNAs were abstracted from TCGA database. We defined the lncRNAs that were significantly related to one of the 21 m^{6}A genes (Pearson R > 0.4 and p < 0.001) as m^{6}A-related lncRNAs. Finally, 1,028 lncRNAs were discerned as the m^{6}A-related lncRNAs (Supplementary Table S4). Also, the predicted lncRNAs were then intersected with these m^{6}A-related lncRNAs to select the m^{6}A-related lncRNAs (n = 104) that interacted with 16 m^{6}A-related miRNAs. Cytoscape was used to construct an lncRNA–miRNA regulatory network, including 189 lncRNA–miRNA pairs (Figure 5).

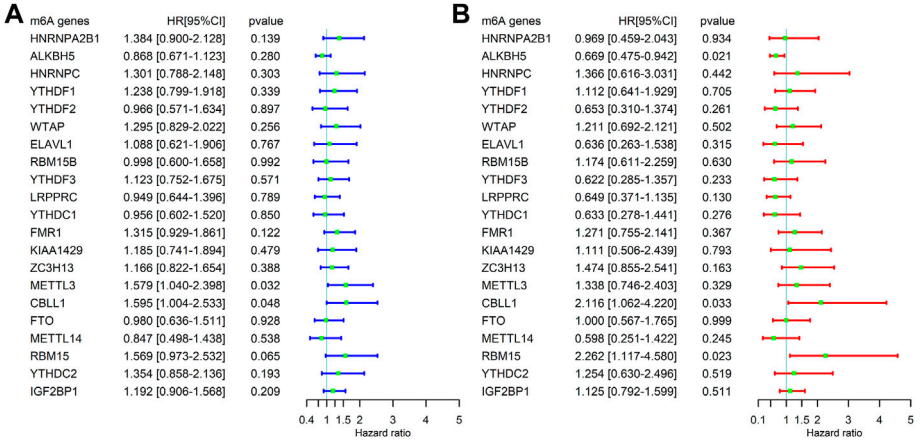


FIGURE 3
Correlation between the expression levels of m^{6}A-related genes and overall survival (OS) rates in SARC patients (N = 245). **(A)** Univariate analysis of m^{6}A-related genes associated with OS; **(B)** and multivariate analysis of m^{6}A-related genes associated with OS.

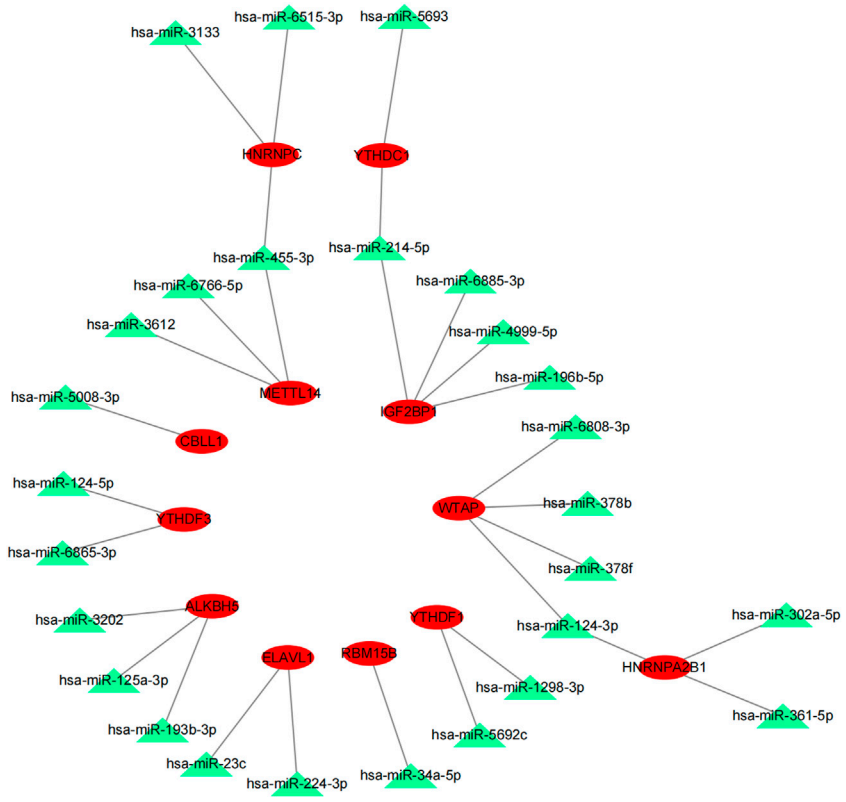


FIGURE 4
MiRNA–mRNA interaction network of m^{6}A genes.

Construction of an m^{6}A-related competing endogenous RNA (ceRNA) network

Based on the results mentioned previously, the miRNA–mRNA and lncRNA–miRNA were selected to establish an m^{6}A-associated ceRNA network that contained 104 lncRNAs, 16 miRNAs, and 11 mRNAs (Figure 6). We searched the lncRNAs and miRNAs in our study in the m6A-Atlas database (Tang et al., 2021), RMBase v2.0 (Xuan et al., 2018) and WHISTLE (Chen et al., 2019b) database, which were used to predict m^{6}A methylation sites in these RNAs. The search results (Supplementary Tables S6, S7) showed that most lncRNAs in this study had potential methylation sites. However, we did not retrieve the potential m^{6}A methylation sites of miRNAs in these libraries. Detailed information of the ceRNA network is listed in Supplementary Table S5.

Construction of a risk model according to m^{6}A-related RNAs in SARC patients

A total of 244 patient samples were included in the whole dataset. A total of 16 miRNAs, 104 lncRNAs, and 11 m^{6}A regulators (mRNAs) in the ceRNA network were selected as candidate biomarkers for the following step analysis. The result of univariate survival analysis showed that five m^{6}A-related lncRNAs (RP11-46C24.7, RP11-283I3.6, SLC25A21-AS1, RP11-81A1.6, and RP11-346C20.4), two m^{6}A-related miRNA (hsa-miR-455-3p and hsa-miR-124-3p), and one m^{6}A regulator (CBLL1) were associated with SARC prognosis ($p < 0.1$). Among these biomarkers, hsa-miR-455-3p (miRNA), hsa-miR-124-3p (miRNA), and CBLL1 (mRNA) were considered as risk biomarkers (HR > 1). Subsequently, to obtain the most useful predictive features, LASSO Cox regression analysis was performed on eight genes (Figures 7A,B). Based on the final Cox regression model results (Table 2), we selected 3 genes (*hsa-miR-455-3p*, *CBLL1*, and *RP11-283I3.6*) with $p < 0.1$ to construct the risk score model. Furthermore, we calculated the risk score (m6Ascore) of each sample based on the risk score model, and the formula was shown as follows:

Risk score = (0.09964) * hsa-miR-455-3p + (0.84723) * CBLL1 + (−0.35103) * RP11-283I3.6.

Patients with SARC were divided into the low-risk or high-risk groups with the optimal cutoff (2.492404) of the risk score. The Kaplan–Meier (KM) curve analysis result showed that the low-risk group had a better prognosis than the high-risk group

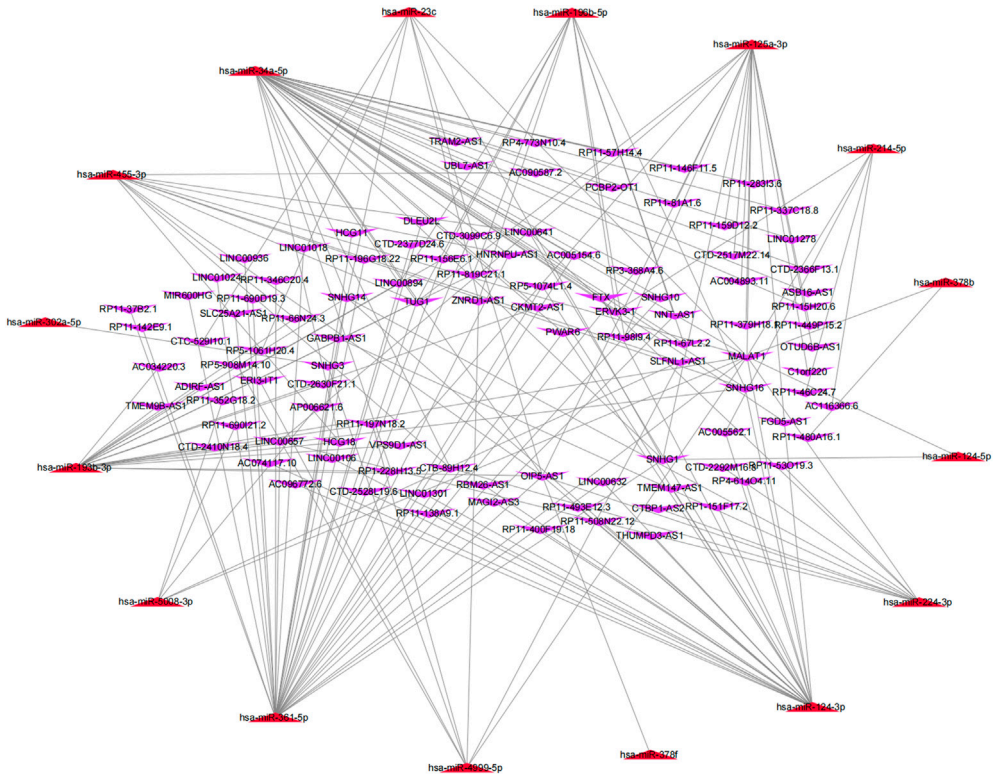


FIGURE 5
MiRNA–lncRNA regulatory network associated with m^{6}A genes in SARC.

(p = 0.00038) (Figure 7C). The distribution of risk score between low-risk and high-risk groups is depicted in Figure 7D, and a survival status map was plotted to demonstrate the status for each sample using TCGA sarcoma dataset values. A time-dependent ROC curve was performed to evaluate the sensitivity and specificity of the risk score. The m^{6}A-related signature's AUC values were 0.638 (0.515, 0.761), 0.663 (0.578, 0.749), and 0.679 (0.585, 0.773), respectively, for an OS of 1, 3, and 5 years (Figures 7E–G). This indicates that our risk score model could be used to predict SARC patient survival.

m6Ascore was associated with the SARC immune landscape

Our study explored the relationship between m6Ascore and the biological process of SARC, for which we conducted GSEA. GSEA using TCGA data of the hallmark gene sets indicated that in the two cohorts, DNA repair, E2F targets, G2M checkpoint, mitotic spindle, mTORC1 signaling, MYC targets v1, MYC targets v2, oxidative phosphorylation, protein secretion, and unfold protein response were significantly enriched in the high-risk group (the top ten pathways are shown in Figure 8A), while the angiogenesis was significantly enriched in the low-risk group (the one pathway is shown in Figure 8A; red line). This finding provided insights into the potential biological processes and signaling pathways modulated by m^{6}A-related RNAs in SARC.

The expression of immune checkpoints was used to predict immunotherapeutic benefits in multiple malignancies. Next, the study was aimed to explore whether m6Ascore could predict immunotherapeutic benefits in SARC patients. We analyzed the correlation between the high- and low-m6Ascore groups and 50 immune checkpoints. The expression of CD44 and VTCN1 was increased in the high-m6Ascore group, while the expression of TMIGD2, TNFRSF18, TNFRSF25, TNFRSF4, TNFRSF8, and NRP1 was increased in the low-m6Ascore group (Figure 8B). A chord chart was used to display the correlation between m6Ascore and immune checkpoint molecules. The results showed that m6Ascore was negatively correlated with the expression of TMIGD2, TNFRSF18, TNFRSF25, TNFRSF4, TNFRSF8, and NRP1 (Figure 8C), indicating that the poor prognosis of high-m6Ascore patients might be due to the tumor immunosuppressive microenvironment. We also investigated the differences in the distribution of infiltrating immune cells between the high-risk

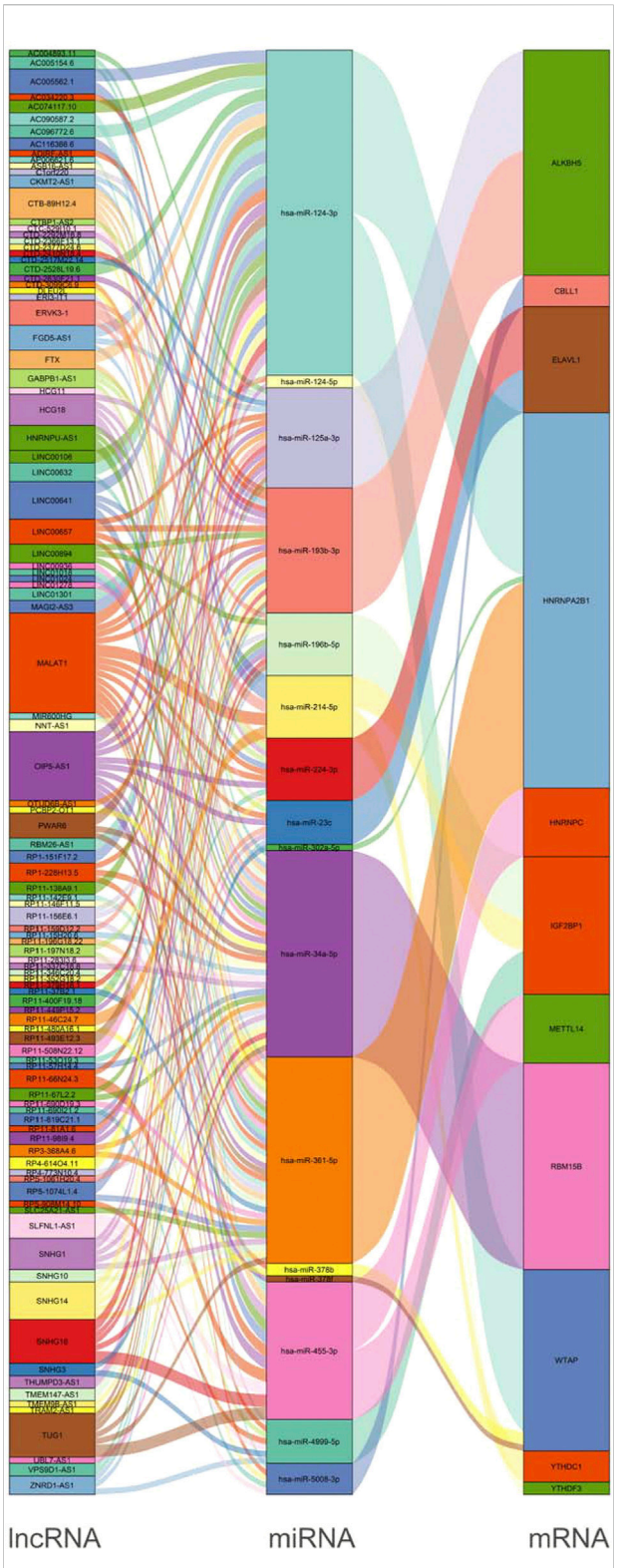


FIGURE 6
Construction of a network of lncRNA–miRNA–m^{6}A regulators.

and low-risk groups using CIBERSORT, ESTIMATE, ssGSEA, and TIMER algorithms. ESTIMATE score and immune cell types, which were differentially infiltrated between the low- and high-risk groups, are presented in Figure 8D. To analyze the composition of immune cells in different m6Ascore subgroups, we used the Wilcoxon rank-sum test to compare the distribution of immune cells in different m6Ascore subgroups. The results showed that only in CIBERSORT algorithm, the abundance of immune cells including macrophages M0 ($p < 0.05$) and T-cell CD4 memory activated ($p < 0.05$) was highly infiltrated in the high-m6Ascore subgroup, while monocytes ($p < 0.05$) and mast cells activated ($p < 0.05$) were more abundant in the low-m6Ascore subgroup (Figure 8E). Totally, these findings suggest that there are significant associations between m6Ascore and the tumor immune landscape in SARC.

Mutation status in SARC patients in the high- and low-m6Ascore groups

To investigate m6Ascore-related mechanisms in SARC, somatic mutations data were also analyzed. The frequency of mutations in top 20 genes between the two groups is shown in Figure 9A. A significant mutually exclusive phenomenon was observed among mutations of these genes (Figure 9B). Subsequently, differentially mutated genes between the two groups were detected, and the "maftools" package analysis result showed that CSMD1 was the only one significant differentially mutated gene detected between the high- and low-m6Ascore cohorts (Figure 9C). The CSMD1 mutation burden in the low-m6Ascore subtype was significantly higher than that in the high-m6Ascore subtype.

We further found that there was no significant correlation between m6Ascore and TMB (Figure 10A). Also, there was no significant difference in TMB between the patients with high m6Ascore and those with low m6Ascore (Figure 10B). However, we found that low TMB was associated with good OS (Figure 10C, log–rank test, $p = 0.0045$). Subsequently, we explored whether the combination of m6Ascore and TMB could be a more powerful predictive biomarker for prognosis. We integrated m6Ascore and TMB to stratify all the samples into the high-TMB/low-m6Ascore, low-TMB/low-m6Ascore, high-TMB/high-m6Ascore, and low-TMB/high-m6Ascore groups. As shown in Figure 10D, significant differences were found among all groups (log-rank test, $p < 0.0001$), and patients in the high-TMB/high-m6Ascore group exhibited poor OS. These results together strongly demonstrated that the risk score was positively correlated with tumor malignancy. Next, the "maftools" R package was used to analyze and summarize the mutation data. The top 20 driver genes with the highest alteration frequency between the aforementioned subgroups are shown in Figure 10E.

TABLE 2 Cox proportional hazard regression analysis and LASSO of eight genes.

Gene	Univariate Cox regression analysis			LASSO coefficient	Multivariate Cox regression analysis		
	HR	95% CI	P		HR	95% CI	P
hsa-miR-455-3p	1.13	1.03–1.23	0.013	0.09173461	1.11	1.00–1.22	0.040
RP11-46C24.7	0.64	0.45–0.91	0.014	−0.23437212	0.78	0.50–1.20	0.251
RP11-283I3.6	0.67	0.45–0.98	0.039	−0.31135641	0.70	0.47–1.06	0.091
SLC25A21-AS1	0.74	0.55–0.99	0.040	−0.10453847	0.89	0.60–1.33	0.575
CBLL1	1.60	1.00–2.54	0.048	0.75233906	2.33	1.43–3.81	0.001
RP11-81A1.6	0.75	0.56–1.01	0.057	−0.15084732	0.84	0.56–1.25	0.388
RP11-346C20.4	0.74	0.54–1.02	0.066	—			
hsa-miR-124-3p	1.21	0.98–1.50	0.075	0.06160625	1.08	0.86–1.36	0.531

HR, hazard ratio; CI, confidence interval.

m6Ascore prediction of response to chemotherapy and immunotherapy

To find the potency of m6Ascore as a biomarker for predicting the response of SARC patients to drugs (including chemotherapy, targeted therapy, and immunotherapy), we used the "pRRophetic" algorithm to estimate the therapeutic response based on the half-maximal inhibitory concentration (IC_{50}) available in the Genomics of Drug Sensitivity in Cancer (GDSC) database for each sample. We inferred the IC_{50} values of the 138 drugs in TCGA-SARC patients. Finally, we found that 69 compounds were screened out for significant differences in the estimated IC_{50} values between the two groups, and the high-risk group was more sensitive to these compounds including ATRA, cyclopamine, JNK inhibitor, PD173074, and QS11,while the low-risk group was more sensitive to the remaining compounds (Supplementary Figures S1–S3). Figures 11A-N display the top 14 compounds that might be used for further analysis in patients with SARC. In terms of response to immunotherapy, we used the TIDE algorithm to assess the potential clinical efficacy of immunotherapy in different m6Ascore subgroups. The TIDE algorithm assessed expression signatures of T-cell dysfunction and T-cell exclusion to assess tumor immune evasion and integrated them into the TIDE total score. In addition, the TIDE module was used to analyze multiple signatures to estimate tumor immune evasion, such as MDSC, M2 TAM, or CAF signatures. In our results (Figure 11O), the high-m6Ascore subgroup had a relatively higher T-cell exclusion score ($p < 0.05$), but there was no difference in the T-cell dysfunction scores between the two subgroups ($p > 0.05$). For other features produced by TIDE, although there was no significant difference in M2 TAM and CAF features between the two groups, the low-risk group had a relatively lower trend, and a lower proportion of MDSC was associated with the low-risk group ($p < 0.05$). These results suggest that SARC patients in the high-risk group may have a higher potential for the immunosuppressive TME status and be less responsive to ICI therapy. These findings identified the promising role of this risk signature as a predictor for chemotherapy and immunotherapy efficacy in the treatment of SARC patients.

Construction and evaluation of the nomogram predicting OS based on the m^{6}A-related signature

To confirm whether the m^{6}A-related signature for OS was an independent prognostic factor, univariate and multivariate Cox regression analyses were performed (Table 3). As the results showed, in the univariate Cox regression analysis, m6Ascore, age, and cancer status were significantly associated with the OS of sarcoma patients. Then, m6Ascore, age, and cancer status were identified as independent prognostic factors of sarcomas via multivariate Cox regression analysis. All these independent factors were combined to establish a nomogram for predicting the 1-, 3-, and 5-year OS (Figure 12A). As shown in Figure 12A, m6Ascore contributes more to the total score than other variables. The 1-, 3-, and 5-year OS rates of patients declined as the total score increased. The C-index of the nomogram model reached 0.744 (95% CI: 0.707–0.784). The calibration plots showed that the nomogram model predicted the overall survival of patients with SARC well (Figure 12B). We compared the clinical net benefit of the nomogram through DCA curves. The nomogram demonstrated a larger net benefit within most of the threshold probabilities (Figures 12C–E), indicating that the nomogram had high potential clinical utility for predicting prognosis in patients with SARC. Finally, Figures 12F–H show the predictive potential of the nomogram using time-dependent ROC curves. The area under the ROC curve (AUC) of the nomogram model for OS was 0.693 at 1 year, 0.772 at 3 years, and 0.834 at 5 years.

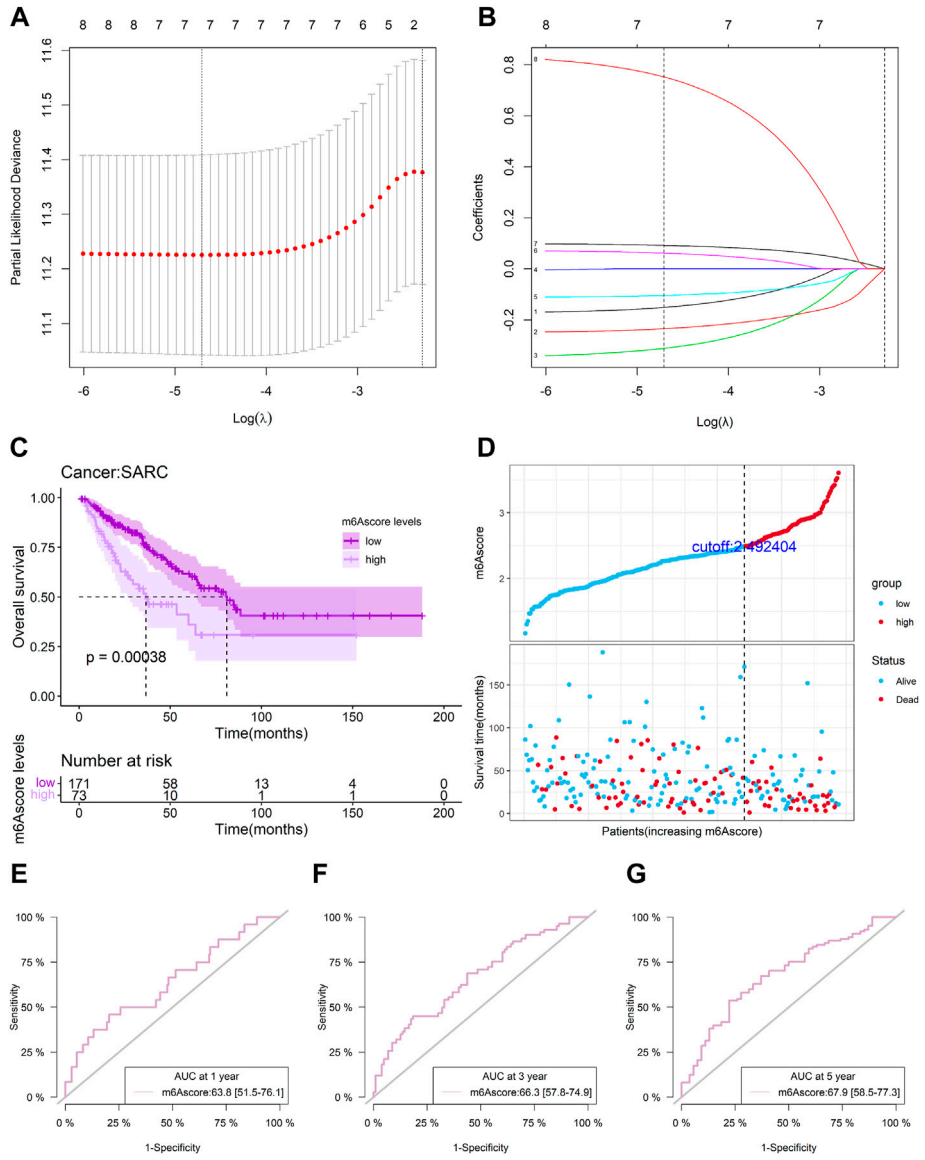


FIGURE 7
Risk model from m^{6}A-related genes. **(A-B)** LASSO Cox regression analysis of eight m^{6}A-related genes; **(C)** overall survival analysis for patients in high/low-risk groups; **(D)** distributions of risk score, different patterns of survival status, and survival time between the high- and low-risk groups; **(E-G)** and time-dependent ROC curves at 1, 3, and 5 years based on the m^{6}A-related gene signature.

Discussion

In the present study, the prognostic significance of 21 m^{6}A RNA methylation regulators in SARC was first explored. The study showed that only CBLL1 was found to be an independent risk factor for OS by univariate and multivariate Cox regression analyses. Numerous studies have shown that m^{6}A regulator-related signatures and m^{6}A regulator-related miRNA or lncRNA signatures may serve as prognostic biomarkers in patients with various types of cancer (Li et al., 2021c; Jin et al., 2021; Xu et al., 2021). However, the expression and functional roles of m^{6}A RNA methylation regulators and their associated regulatory networks in the occurrence and progression of SARC have not been widely discussed. Therefore, in this study, bioinformatics was used to analyze the existing sequencing datasets of integrated sarcoma, and miRNAs and lncRNAs related to m^{6}A regulators were obtained through correlation analysis, and the upstream miRNAs and lncRNAs of m^{6}A regulators were determined using miRTarBase and LncBase v.2 databases, respectively. The two parts of the results of miRNAs and lncRNAs were intersected to key miRNAs and lncRNAs, respectively. Finally, a lncRNA–miRNA–m^{6}A regulator ceRNA network was

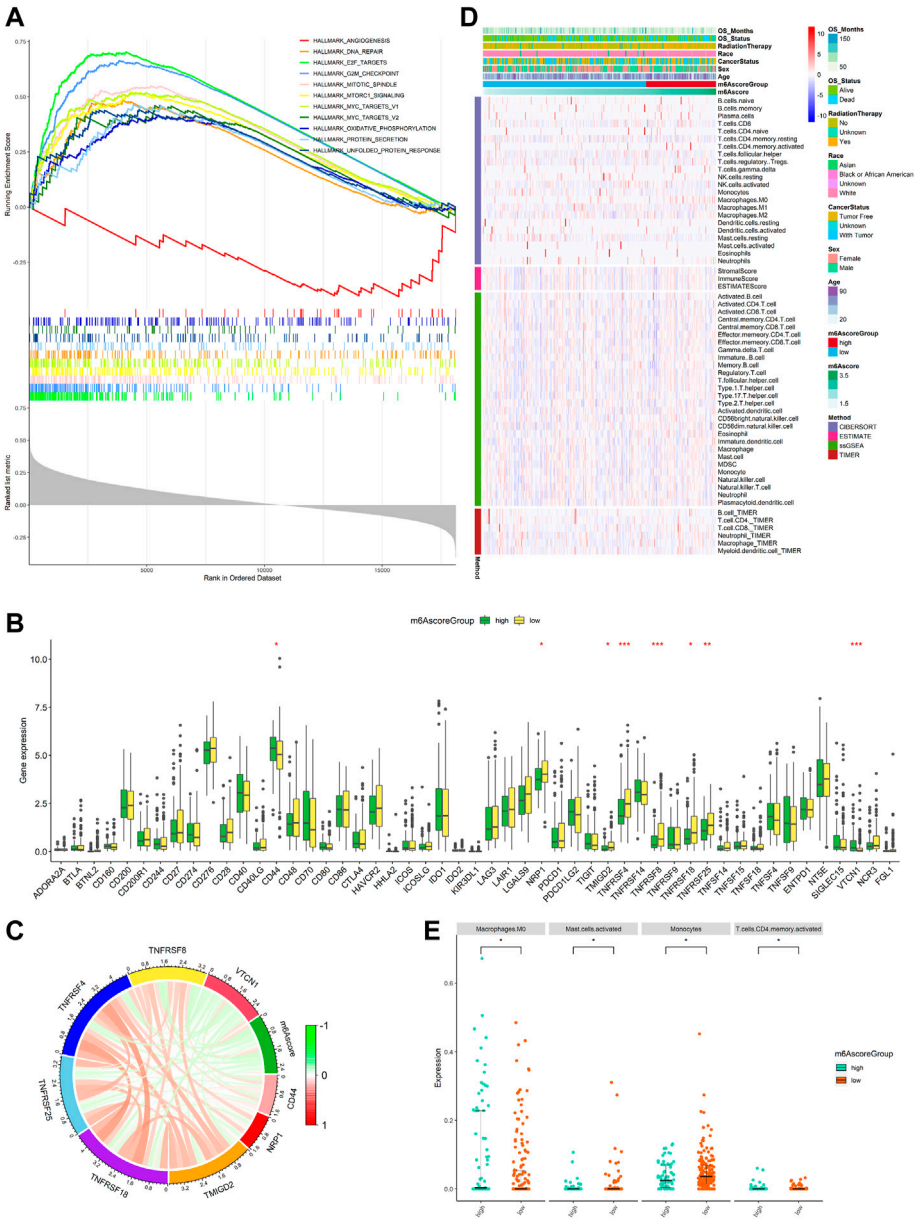


FIGURE 8
Function enrichment analysis for m6Ascore and immune landscape of different m6Ascore subgroups. **(A)** GSEA of samples with high or low m6Ascore. Top ten significant pathways associated with high m6Ascore ($p < 0.05$ and FDR-adjusted $q < 0.05$, NES > 1.5). Significant pathways in the red module are associated with low m6Ascore (nominal $p < 0.05$ and FDR adjusted $q < 0.05$, NES < 1.5); **(B)** comparison of immune checkpoint gene expression levels between the low-m6Ascore group and the high-m6Ascore group. *$p < 0.05$; **$p < 0.01$; ***$p < 0.001$; **(C)** correlation chord chart shows the mutual correlation between m6Ascore and several prominent immune-checkpoint-relevant genes (*CD44*, *VTCN1*, *TMIGD2*, *TNFRSF18*, *TNFRSF25*, *TNFRSF4*, *TNFRSF8*, and *VTCN1*); **(D)** heatmap for immune responses based on CIBERSORT, ESTIMATE, ssGSEA, and TIMER algorithms among the high- and low-risk group; and **(E)** beeswarm plot for infiltration levels of immune cells in high- and low-risk samples through the CIBERSORT. The statistical difference between the two groups was compared by the Wilcoxon rank-sum test. *$p < 0.05$; **$p < 0.01$; ***$p < 0.001$.

constructed, which contained 104 lncRNAs, 16 miRNAs, and 11 m^{6}A regulators. We should pay more attention to screening out key lncRNAs, miRNAs, and m^{6}A regulators that can predict OS. Therefore, considering all these genes in the ceRNA network, we performed univariate Cox regression analysis to identify genes associated with clinical prognosis in sarcoma patients. Eight genes were found to be significantly associated with clinical outcomes in sarcoma. Finally, LASSO regression analysis and multivariate Cox regression analysis were performed, and three genes (*RP11-283I3.6*, *hsa-miR-455-3p*, and *CBLL1*) were

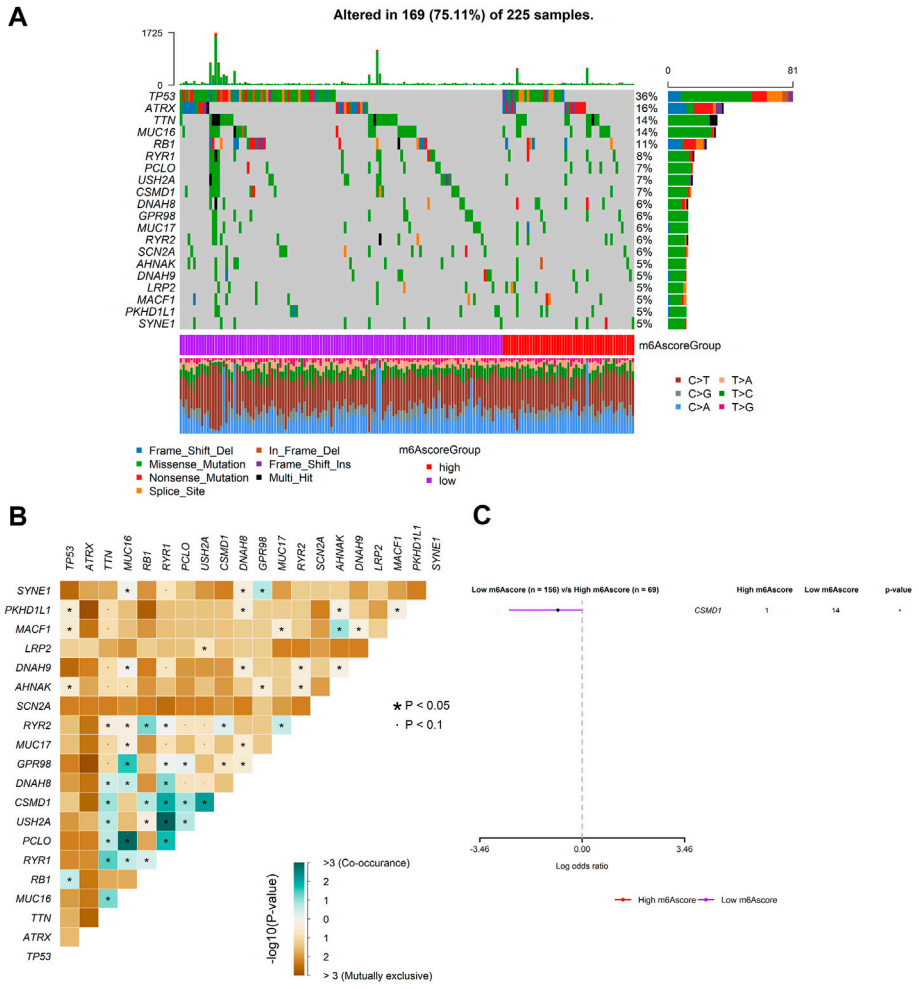


FIGURE 9
Mutation patterns of SARC patients. **(A)** Mutational patterns of 169 SARC patients in the low- and high-m6Ascore groups displayed by the oncoplot; **(B)** interaction effect of genes mutating differentially in patients in the low- and high-m6Ascore groups; and **(C)** forest plot of genes mutating differentially in patients of the low- and high-m6Ascore groups.

identified as prognostic biomarkers for SARC, and the three genes were included in the risk scoring model for predicting OS for SARC.

By searching for these genes in the PubMed database, it is found that the mechanisms of *hsa-miR-455-3p* and *CBLL1* in tumor progression or studies related to tumor progression have been reported. The aberrant expression of hsa-miR-455-3p and its prognostic value have been widely reported in various types of human cancers. In our study, hsa-miR-455-3p served as a risk biomarker for SARC, consistent with the results of bioinformatics analysis by Wang et al. (2019), which showed that the differential expression level of miR-455-3p was the most significant in gliomas. Subsequently, its expression in glioma patients was examined. Consistent with the results of bioinformatics analysis, the expression level of miR-455-3p was significantly upregulated in glioma tissues compared with normal tissues. Cox regression analysis further identified miR-455-3p as an independent prognostic indicator of overall survival in glioma patients. hsa-miR-455-3p is overexpressed in skin basal cell carcinoma (BCC) (Sand et al., 2012). However, the expression of miR-455-3p is obviously decreased in the tissues and cells of hepatocellular carcinoma (HCC). This miRNA can impair HCC cell malignancy via suppression of insulin growth factor receptor expression, thereby disrupting glycolysis (Hu et al., 2019; Jiang et al., 2019). Gao et al. (2018), Yang et al. (2017), and Shang et al. (2021) reported that low expression of miR-455-3p in non-small-cell lung cancer, esophageal squamous cell carcinoma (ESCC), and pancreatic cancer (PAAD) tissues was strongly associated with poor prognosis. miR-455-3p acts as a tumor suppressor in esophageal squamous cell carcinoma (ESCC) and inhibits cell proliferation and invasion by targeting FAM83F. miR-455-3p is involved in increasing the

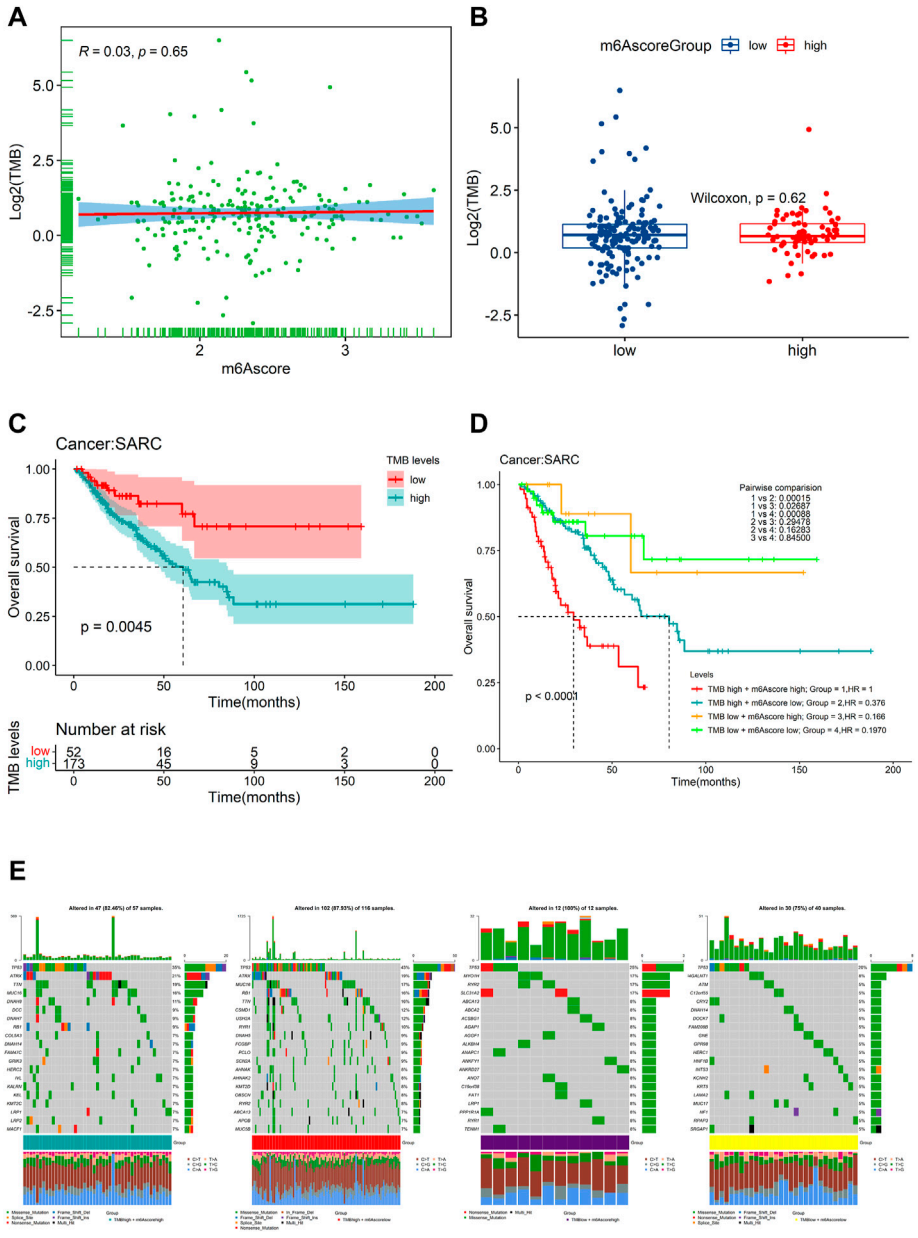


FIGURE 10
Relationship of the m6Ascore signature with TMB. **(A)** correlation between the m6Ascore signature and TMB depicted by scatter plots; **(B)** comparison of TMB between the high- and low-m6Ascore groups; **(C)** KM survival curves for the high- and low-TMB groups stratified at the optimal cutoff in TCGA-SARC cohorts (log-rank test, $p = 0.0045$); **(D)** Kaplan–Meier survival analysis for four groups stratified by combining the TMB and the m6Ascore signature in TCGA-SARC cohort; and **(E)** waterfall plot of tumor somatic mutation established by stratifying with m6Ascore and TMB. Each column represents an individual patient. Group1, high TMB /high m6Ascore, green; Group2, high TMB/low m6Ascore, red; Group3, low TMB/high m6Ascore, purple; and Group4, low TMB/low m6Ascore, yellow. The mutational types include frame shift del, frame shift ins, in-frame del, in-frame ins, missense mutation, multi-hit, nonsense mutation, and splice site.

expression of HOXC4, promoting transcriptional disorders in cancer. The miR-455-3p–HOXC4 axis is expected to be closely related to the metastasis and prognosis of human pancreatic cancer. Yi et al. (2020) and Sun et al. (2020) together showed that the expression of miR-455-3p was decreased in osteosarcoma tissues and cell lines. Patients with high miR-455-3p expression had satisfactory survival rates. miR-455-3p is a potential clinical therapeutic target and prognostic biomarker inhibiting proliferation, migration, and invasion and enhancing apoptosis. However, Hisaoka et al. (2011) showed that, compared to normal skeletal muscle, hsa-miR-455-3p was significantly

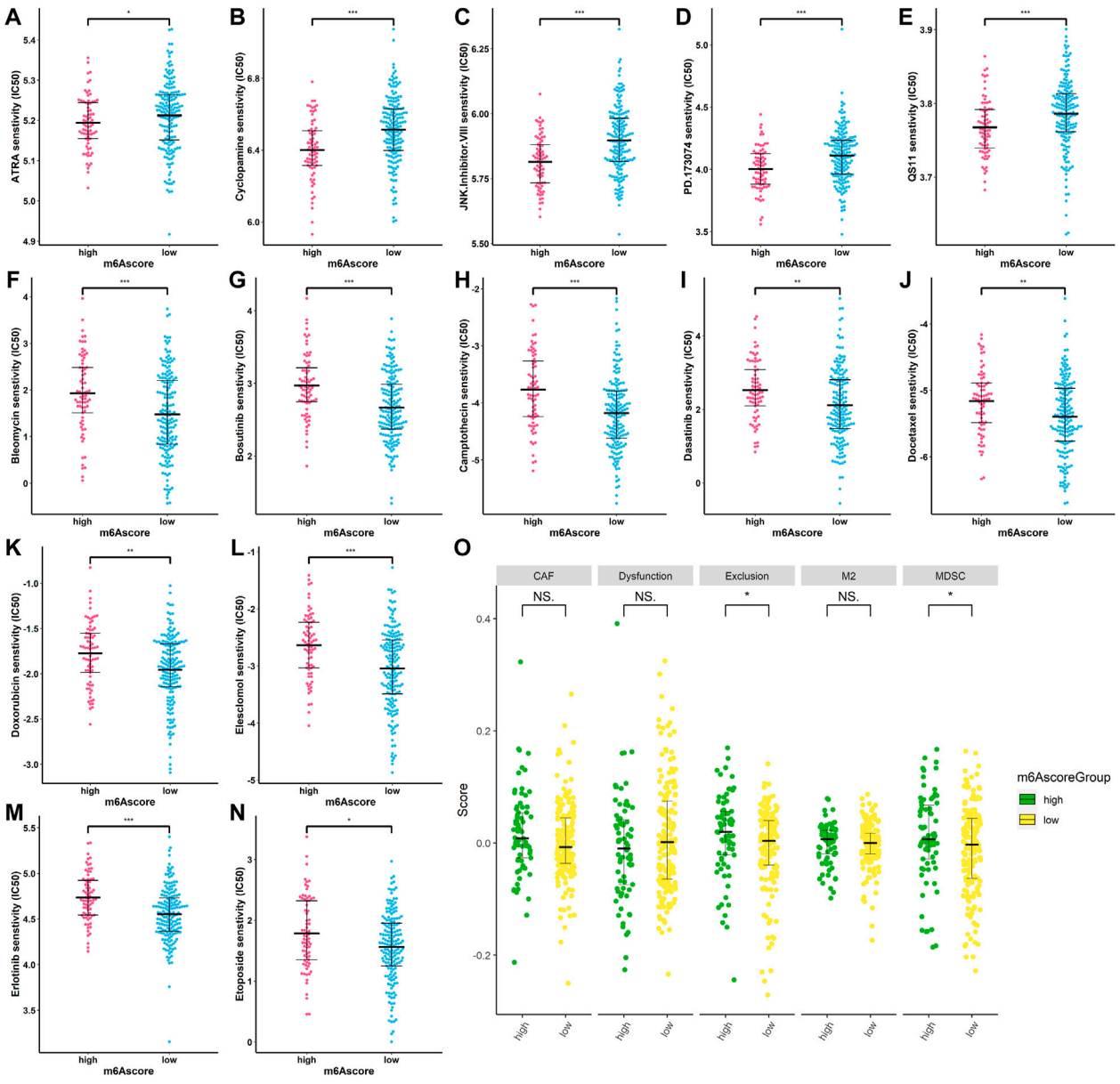


FIGURE 11
Correlation between m6Ascore and therapy. **(A–N)** IC_{50} of some chemotherapeutic drugs are in the high- and low-risk patients. *$p < 0.05$; **$p < 0.01$; ***$p < 0.001$; **(O)** TIDE prediction difference in the high- and low-risk patients. *$p < 0.05$; **$p < 0.01$; ***$p < 0.001$.

upregulated in synovial sarcomas, suggesting that the molecule has a potential oncogenic role, which calls for further investigation to develop a better understanding of the oncogenic mechanisms. Our finding is consistent with this study. *CBLL1* plays an important role in tumorigenesis. Hui et al. (2019) found that *CBLL1* was upregulated in non-small-cell lung cancer (NSCLC) tissues compared to the adjacent nontumor tissues, and the high expression of *CBLL1* was associated with the tumor size in NSCLC tissues. Their results confirmed that *CBLL1* promoted the proliferation by promoting G1/S cell cycle transition in NSCLC cells. Moreover, *CBLL1* knockdown inhibited cell invasion via increased E-cadherin protein expression and decreased expression of MMP2 and MMP9 in NSCLC cell lines. Previous studies found that *CBLL1*, an E3 ubiquitin ligase, inhibits ER pathway activity by binding to an ER co-activator and then further inhibits the proliferation and differentiation of BC cells (Makdissi et al., 2009). Zheng et al. (2021) confirmed that higher *CBLL1* expression was associated with a better prognosis in BC than lower *CBLL1* expression. Functional analysis showed that *CBLL1*

TABLE 3 Univariate and multivariate Cox regression analysis of the overall survival (OS) of patients with SARC.

Variable	Univariate analysis			Multivariate analysis		
	HR	95% CI	P	HR	95% CI	P
m6Ascore	2.58	1.62–4.11	<0.0001	3.08	1.84–5.17	<0.0001
Age	1.02	1.01–1.04	0.009	1.02	1.00–1.03	0.054
Sex						
Female	1					
Male	0.79	0.52–1.19	0.263			
Cancer status						
Tumor free	1			1		
With tumor	6.07	3.54–10.43	<0.0001	6.41	3.71–11.07	<0.0001
Unknown	3.33	1.61–6.89	0.001	3.68	1.75–7.76	0.001
Race						
Asian	1					
Black or African American	1.08	0.13–8.87	0.944			
White	0.79	0.11–5.75	0.813			
Unknown	3.41	0.35–32.9	0.288			
Radiation therapy						
No	1					
Yes	0.83	0.52–1.33	0.441			
Unknown	0.38	0.05–2.76	0.341			

HR, hazard ratio; CI, confidence interval.

was related to the ESR1-related pathway, apoptosis-related pathway, cell cycle pathway and immune-related pathway in BC. Although there is no report on the correlation between the expression of RP11-283I3.6 and CBLL1 and SARC progression, based on our results, we speculate that they may be potential biomarkers for sarcoma prognosis. The mechanism of action of these genes in sarcoma is unclear and requires further follow-up studies. Subsequently, based on this risk score feature, we divided all SARC patients into the high-risk and low-risk groups, and KM survival analysis showed that patients in the low-risk group had significantly higher OS than those in the high-risk group. The time-dependent AUC indicated that the risk scoring model had good predictive performance for OS.

The molecular heterogeneity features between high- and low-risk patients were further analyzed. GSEA showed that DNA repair, E2F targets, G2M checkpoint, mitotic spindle, mTORC1 signaling, MYC targets v1, MYC targets v2, oxidative phosphorylation, protein secretion, and unfold protein response were significantly enriched in the high-risk specimens. Meanwhile, activation of angiogenesis was detected in low-risk specimens. The tumor immune microenvironment comprising stromal cells and immune cells correlates with immunotherapy response (Zhou et al., 2020). Components of the immune microenvironment are key determinants of prognosis and response to immunotherapy (Das et al., 2020). Immunotherapy is an emerging new approach to treating a variety of cancers, including sarcomas. Exploring which patient can benefit from immunotherapy remains a great challenge. Here, the association between immune cell infiltration and this risk score was comprehensively analyzed using the CIBERSORT, ESTIMATE, ssGSEA, and TIMER algorithms in the present study. Compared with patients in the high-risk group, the low-risk patients had higher levels of monocytes and mast cells activated and decreased levels of macrophages M0 and T-cell CD4 memory activated infiltration. The infiltration of M0 macrophages is positively related to poor clinical outcomes in human malignancies, including STS, which is in accordance with the findings of our study (Zhu and Hou, 2020). Thus, the worse clinical outcomes of the high-risk group may be associated with infiltrating immune cellular populations. In addition, expression levels of several immune checkpoints, including TMIGD2, TNFRSF18, TNFRSF25, TNFRSF4, TNFRSF8, and NRP1, were also higher in the low-risk group. These data were indicative of this risk signature being closely related to immunotherapy. m6Ascore may be used as an indicator independent of TMB expression to predict the efficacy of ICB. Tumor mutational burden (TMB) has been identified as a biomarker of immunotherapy response (Hellmann et al., 2018a; Hellmann et al., 2018b), where higher TMB predicts higher benefits from immunotherapy (Hellmann et al., 2018a). However, the prognostic value of TMB varies across cancer types according to a pan-cancer study (Ding et al., 2018). In bladder urothelial carcinoma (BLCA), stomach adenocarcinoma (STAD), and uterine corpus endometrial carcinoma (UCEC), high TMB is associated with longer overall survival (OS). In HNSCC, kidney renal clear cell carcinoma (KIRC), and low-grade glioma (LGG), high TMB is associated with shorter OS. The Cox regression result of TMB in SARC patients showed that HR (95% CI) was 1.25 (0.63–2.49). In the

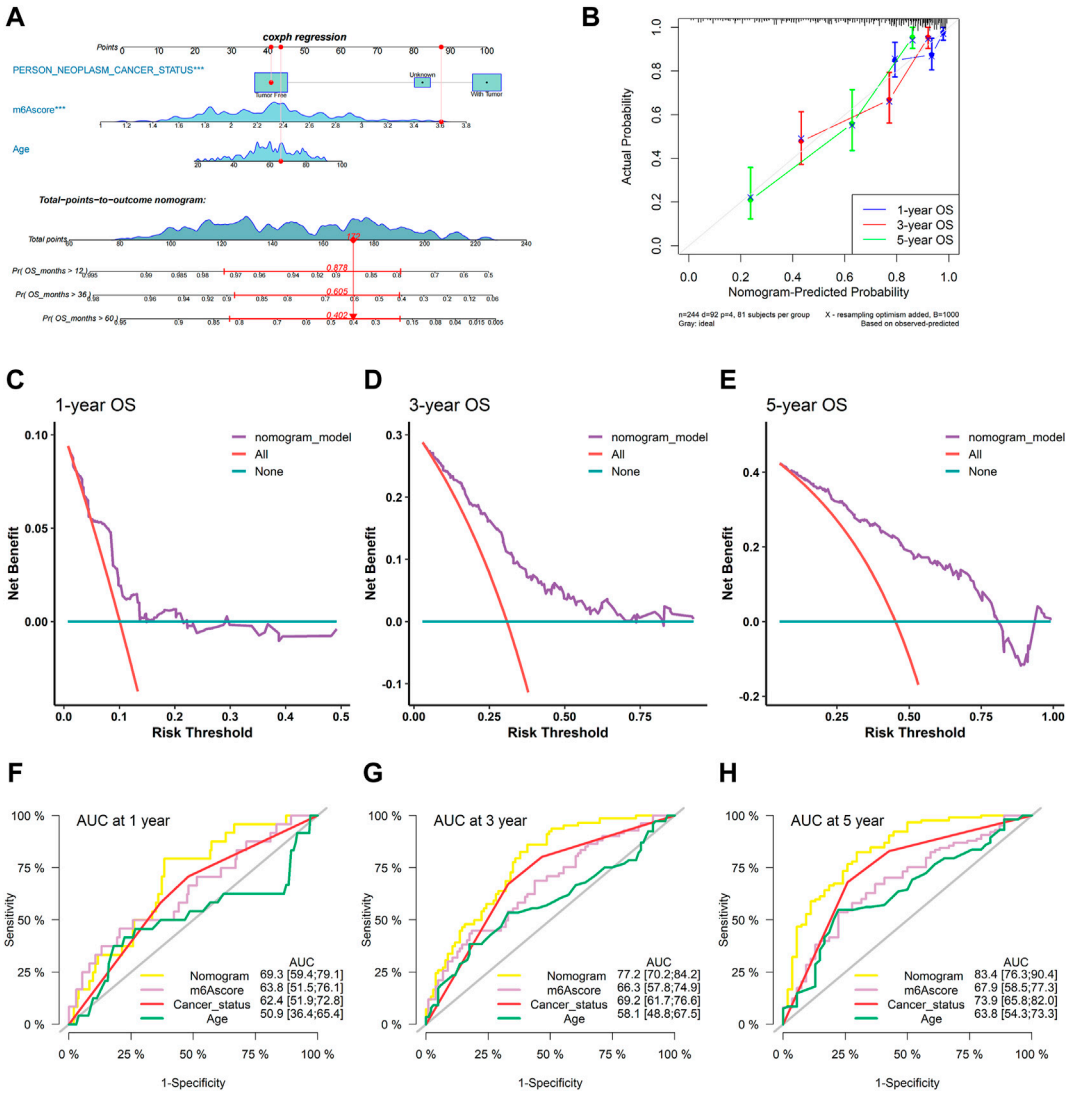


FIGURE 12
Construction and validation of the nomogram. **(A)** Nomogram based on the multivariate Cox regression model of SARC patients; **(B)** calibration plots for the internal validation of the current nomogram; the x-axis represents the nomogram-predicted overall survival, and the y-axis represents the actual overall survival of patients with SARC; **(C–E)** DCA of the nomogram based on m6Ascore for 1-, 3- and 5-year OS prediction; and **(F–H)** time-dependent ROC curves of nomogram, m6Ascore, cancer status, and age at 1, 3, and 5 years.

present study, patients with lower TMB had better prognosis than SARC patients with higher TMB, which is consistent with the trend of pan-cancer research. The significance of the results may be that the selected threshold is different. However, we did not observe a significant correlation between m6Ascore and TMB, nor did we observe a significant difference in the distribution of TMB between patients in the two different risk groups. The main reason is that with a threshold of $p < 0.05$, using Fisher's exact test, *CSMD1* was the only one significant differentially mutated gene detected between the high- and low-m6Ascore cohorts, and *CSMD1* was found to be mutating more in the low-m6Ascore group, which resulted in a similar gene mutation status in the two groups. These findings suggested that TMB and m6Ascore are independent biomarkers/indicators for predicting ICB response. Interestingly, the combination of TMB and the risk characteristic we constructed can more clearly and accurately stratify SARC patients. Compared with other subgroups, patients with high TMB/high m6Ascore have the worst prognosis, which also shows that the TMB status does not affect the prognostic value of m6Ascore. m6Ascore has the potential to predict immunotherapy responsiveness, which may be independent of TMB (Zhang et al., 2020; Guan et al., 2021; Lin et al., 2021; Sun et al., 2021; Wu et al., 2021). In addition, the TIDE results suggested that the patients in the low-risk group may respond better to immunotherapy. Based on estimated IC_{50} values, the patients in the low-risk group showed sensitive

chemotherapy responses to most drugs. Taken together, these findings suggest that this risk signature may play a role in the ICB treatment of SARC. Subsequent studies further confirmed that risk characteristic is independent prognostic factors in patients with sarcoma. Based on risk score and other clinically independent predictors, a nomogram for personalized clinical outcome prediction was established in the study, which was certified to perform well for predicting the 1-, 3-, and 5-year survival rates of SARC patients, showing a C-index of 0.744 (95% CI: 0.707–0.784).

Although potential biomarkers involved in tumorigenesis in a large number of samples were identified by the bioinformatics approach, it should be noted that this study also has some limitations as follows: 1) due to the lack of RNA-seq or microarray data in SARC patients, only TCGA data were included. Also, the SARC samples lacked some additional clinical follow-up information; therefore, factors such as the presence of other health conditions in patients to differentiate prognostic biomarkers were not included. 2) We internally verified the nomogram prediction model based on m6Ascore, and the findings of this study would be more meaningful if this model could be well validated externally with another real-world, independent, large-quantity, and high-quality cohort, and thus, a more diverse patient population could be extrapolated. However, the application of the prognostic prediction model based on m6Ascore required four types of data, namely, clinical data, RNA-seq (mRNAs and lncRNAs), and miRNA-seq, which involves high costs and is not easily feasible in practice. 3) Most importantly, experimental validation is needed to confirm these results and further explore the potential mechanism and role of these potential biomarkers in SARC. However, our findings showed that the nomogram model based on m6Ascore may be promising for clinical prediction of prognosis and might contain potential biomarkers for treatment response prediction for SARC patients, which remains an instructive and efficient way for predicting the accurate individual clinical outcomes of SARC patients.

Conclusion

In conclusion, in our study, a ceRNA network based on m^{6}A-related genes was successfully constructed through bioinformatics analysis of TCGA database. Candidate biomarkers in the ceRNA network were used to establish a risk profile of m^{6}A-related RNAs, which is significantly associated with the prognosis and immune microenvironment of SARC, and could effectively predict the prognosis and treatment efficacy of STSs. The results of this study suggest that these markers may play an important role in the therapeutic target and prognostic analysis of sarcoma patients.

Data availability statement

The original contributions presented in the study are included in the article/Supplementary Material, further inquiries can be directed to the corresponding author.

Author contributions

HL and KW designed the research. HL, DL, XW, and JZ conducted the data analysis. HL and DL wrote the manuscript. KW and ZF revised and completed the final manuscript. All authors have read and agreed to the published version of the manuscript.

Funding

This research was funded by the Tianshan Innovative Research Team of Xinjiang Uygur Autonomous Region, China (2020D14020).

Acknowledgments

The authors acknowledge the data support from databases such as TCGA, TIMER, cBioPortal, GDC, miRTarBase, and LncBase.

Conflict of interest

The authors declare that the research was conducted in the absence of any commercial or financial relationships that could be construed as a potential conflict of interest.

Publisher's note

All claims expressed in this article are solely those of the authors and do not necessarily represent those of their affiliated organizations, or those of the publisher, the editors, and the reviewers. Any product that may be evaluated in this article, or claim that may be made by its manufacturer, is not guaranteed or endorsed by the publisher.

Supplementary material

The Supplementary Material for this article can be found online at: https://www.frontiersin.org/articles/10.3389/fgene.2022.894080/full#supplementary-material

References

Alavi, S. N., Florou, V., Tinoco, G., Trent, J. C., and Wilky, B. A. (2018). A precision medicine approach in sarcoma: Identification of patients who may benefit from early use of pazopanib. *Discov. Med.* 25, 131–144.

Aung, T., Asam, C., and Haerteis, S. (2019). Ion channels in sarcoma: Pathophysiology and treatment options. *Pflugers Arch.* 471, 1163–1171. doi:10.1007/s00424-019-02299-8

Bacci, G., Ferrari, S., Mercuri, M., Bertoni, F., Picci, P., Manfrini, M., et al. (1998). Predictive factors for local recurrence in osteosarcoma: 540 patients with extremity tumors followed for minimum 2.5 years after neoadjuvant chemotherapy. *Acta Orthop. Scand.* 69, 230–236. doi:10.3109/17453679809000921

Barbieri, I., and Kouzarides, T. (2020). Role of RNA modifications in cancer. *Nat. Rev. Cancer* 20, 303–322. doi:10.1038/s41568-020-0253-2

Bone Cancer (2021). Bone cancer: Statistics, Available at:. https://www.cancer.net/cancer-types/bone-cancer-sarcoma-bone/statistics (Accessed September 25, 2021).

Cava, C., Bertoli, G., and Castiglioni, I. (2019). Portrait of tissue-specific coexpression networks of noncoding RNAs (miRNA and lncRNA) and mRNAs in normal tissues. *Comput. Math. Methods Med.* 2019, 9029351. doi:10.1155/2019/9029351

Chang, Z., Huang, R., Fu, W., Li, J., Ji, G., Huang, J., et al. (2020). The construction and analysis of ceRNA network and patterns of immune infiltration in Colon adenocarcinoma metastasis. *Front. Cell. Dev. Biol.* 8, 688. doi:10.3389/fcell.2020.00688

Chen, K., Wei, Z., Zhang, Q., Wu, X., Rong, R., Lu, Z., et al. (2019). Whistle: A high-accuracy map of the human N6-methyladenosine (m6A) epitranscriptome predicted using a machine learning approach. *Nucleic Acids Res.* 47, e41. doi:10.1093/nar/gkz074

Chen, S., Li, Y., Zhi, S., Ding, Z., Wang, W., Peng, Y., et al. (2020). WTAP promotes osteosarcoma tumorigenesis by repressing HMBOX1 expression in an m6A-dependent manner. *Cell. Death Dis.* 11, 659. doi:10.1038/s41419-020-02847-6

Chen, X. Y., Zhang, J., and Zhu, J. S. (2019). The role of m6A RNA methylation in human cancer. *Mol. Cancer* 18, 103. doi:10.1186/s12943-019-1033-z

Das, S., Camphausen, K., and Shankavaram, U. (2020). Cancer specific immune prognostic signature in solid tumors and its relation to immune checkpoint therapies. *Cancers* 12, 2476. doi:10.3390/cancers12092476

Ding, H., Zhao, J., Zhang, Y., Wang, G., Cai, S., and Qiu, F. (2018). Tumor mutational burden and prognosis across pan-cancers. *Ann. Oncol.* 29, viii16–viii17. viii16-viii17. doi:10.1093/annonc/mdy269.055

Doyle, L. A. (2014). Sarcoma classification: An update based on the 2013 world health organization classification of tumors of soft tissue and bone. *Cancer* 120, 1763–1774. doi:10.1002/cncr.28657

Eaton, B. R., Schwarz, R., Vatner, R., Yeh, B., Claude, L., Indelicato, D. J., et al. (2021). Osteosarcoma. *Pediatr. Blood Cancer* 68, e28352. doi:10.1002/pbc.28352

Ferguson, J. L., and Turner, S. P. (2018). Bone cancer: Diagnosis and treatment principles. *Am. Fam. Physician* 98, 205–213.

Gao, L., Zhao, Y., Ma, X., and Zhang, L. (2021). Integrated analysis of lncRNA-miRNA-mRNA ceRNA network and the potential prognosis indicators in sarcomas. *BMC Med. Genomics* 14, 67. doi:10.1186/s12920-021-00918-x

Gao, X., Zhao, H., Diao, C., Wang, X., Xie, Y., Liu, Y., et al. (2018). miR-455-3p serves as prognostic factor and regulates the proliferation and migration of non-small cell lung cancer through targeting HOXB5. *Biochem. Biophys. Res. Commun.* 495, 1074–1080. doi:10.1016/j.bbrc.2017.11.123

Guan, X., Xu, Z. Y., Chen, R., Qin, J. J., and Cheng, X. D. (2021). Identification of an immune gene-associated prognostic signature and its association with a poor prognosis in gastric cancer patients. *Front. Oncol.* 10, 629909. doi:10.3389/fonc.2020.629909

Hatina, J., Kripnerova, M., Houfkova, K., Pesta, M., Kuncova, J., Sana, J., et al. (2019). Sarcoma stem cell heterogeneity. *Adv. Exp. Med. Biol.* 1123, 95–118. doi:10.1007/978-3-030-11096-3_7

Hellmann, M. D., Callahan, M. K., Awad, M. M., Calvo, E., Ascierto, P. A., Atmaca, A., et al. (2018). Tumor mutational burden and efficacy of nivolumab monotherapy and in combination with ipilimumab in small-cell lung cancer. *Cancer Cell.* 33, 853–861. doi:10.1016/j.ccell.2018.04.001

Hellmann, M. D., Ciuleanu, T. E., Pluzanski, A., Lee, J. S., Otterson, G. A., Audigier-Valette, C., et al. (2018). Nivolumab plus Ipilimumab in lung cancer with a high tumor mutational burden. *N. Engl. J. Med.* 378, 2093–2104. doi:10.1056/NEJMoa1801946

Hisaoka, M., Matsuyama, A., Nagao, Y., Luan, L., Kuroda, T., Akiyama, H., et al. (2011). Identification of altered MicroRNA expression patterns in synovial sarcoma. *Genes. Chromosom. Cancer* 50, 137–145. doi:10.1002/gcc.20837

Hou, M., Guo, X., Chen, Y., Cong, L., and Pan, C. (2020). A prognostic molecular signature of N^6-Methyladenosine methylation regulators for soft-tissue sarcoma from the cancer Genome Atlas database. *Med. Sci. Monit.* 26, e928400. doi:10.12659/MSM.928400

Hu, H., Xu, H., Lu, F., Zhang, J., Xu, L., Xu, S., et al. (2020). Exploring the effect of differentially expressed long non-coding RNAs driven by copy number variation on competing endogenous RNA network by mining lung adenocarcinoma data. *Front. Cell. Dev. Biol.* 8, 627436. doi:10.3389/fcell.2020.627436

Hu, Y., Yang, Z., Bao, D., Ni, J. S., and Lou, J. (2019). miR-455-5p suppresses hepatocellular carcinoma cell growth and invasion via IGF-1R/AKT/GLUT1 pathway by targeting IGF-1R. *Pathol. Res. Pract.* 215, 152674. doi:10.1016/j.prp.2019.152674

Huang, R., Meng, T., Chen, R., Yan, P., Zhang, J., Hu, P., et al. (2019). The construction and analysis of tumor-infiltrating immune cell and ceRNA networks in recurrent soft tissue sarcoma. *Aging (Albany NY)* 11, 10116–10143. doi:10.18632/aging.102424

Hui, J. Y. (2016). Epidemiology and etiology of sarcomas. *Surg. Clin. North Am.* 96, 901–914. doi:10.1016/j.suc.2016.05.005

Hui, L., Zhang, S., Wudu, M., Ren, H., Xu, Y., Zhang, Q., et al. (2019). CBLL1 is highly expressed in non-small cell lung cancer and promotes cell proliferation and invasion. *Thorac. Cancer* 10, 1479–1488. doi:10.1111/1759-7714.13097

Italiano, A., Mathoulin-Pelissier, S., Cesne, A. L., Terrier, P., Bonvalot, S., Collin, F., et al. (2011). Trends in survival for patients with metastatic soft-tissue sarcoma. *Cancer* 117, 1049–1054. doi:10.1002/cncr.25538

Ji, L., Chen, S., Gu, L., and Zhang, X. (2020). Exploration of potential roles of m6A regulators in colorectal cancer prognosis. *Front. Oncol.* 10, 768. doi:10.3389/fonc.2020.00768

Jiang, W., Zhang, L., Guo, Q., Wang, H., Ma, M., Sun, J., et al. (2019). Identification of the pathogenic biomarkers for hepatocellular carcinoma based on RNA-seq analyses. *Pathol. Oncol. Res.* 25, 1207–1213. doi:10.1007/s12253-019-00596-2

Jin, Y., Wang, Z., He, D., Zhu, Y., Hu, X., Gong, L., et al. (2021). Analysis of m6A-related signatures in the tumor immune microenvironment and identification of clinical prognostic regulators in adrenocortical carcinoma. *Front. Immunol.* 12, 637933. doi:10.3389/fimmu.2021.637933

Li, L., Xie, R., and Wei, Q. (2021). Network analysis of miRNA targeting m6A-related genes in patients with esophageal cancer. *PeerJ* 9, e11893. doi:10.7717/peerj.11893

Li, Q., Ren, C. C., Chen, Y. N., Yang, L., Zhang, F., Wang, B. J., et al. (2021). A risk score model incorporating three m6A RNA methylation regulators and a related network of miRNAs-m6A regulators-m6A target genes to predict the prognosis of patients with ovarian cancer. *Front. Cell. Dev. Biol.* 9, 703969. doi:10.3389/fcell.2021.703969

Li, Y., Qi, D., Zhu, B., and Ye, X. (2021). Analysis of m6A RNA methylation-related genes in liver hepatocellular carcinoma and their correlation with survival. *Int. J. Mol. Sci.* 22, 1474. doi:10.3390/ijms22031474

Lin, Y., Pan, X., Zhao, L., Yang, C., Zhang, Z., Wang, B., et al. (2021). Immune cell infiltration signatures identified molecular subtypes and underlying mechanisms in gastric cancer. *NPJ Genom. Med.* 6, 83. doi:10.1038/s41525-021-00249-x

Makdissi, F. B., Machado, L. V., Oliveira, A. G., Benvenuti, T. T., Katayama, M. L., Brentani, M. M., et al. (2009). Expression of E-cadherin, snail and Hakai in epithelial cells isolated from the primary tumor and from peritumoral tissue of invasive ductal breast carcinomas. *Braz J. Med. Biol. Res.* 42, 1128–1137. doi:10.1590/s0100-879x2009001200002

Nie, K., Zheng, Z., Wen, Y., Pan, J., Liu, Y., Jiang, X., et al. (2020). A novel ceRNA axis involves in regulating immune infiltrates and macrophage polarization in gastric cancer. *Int. Immunopharmacol.* 87, 106845. doi:10.1016/j.intimp.2020.106845

Niu, Y., Zhao, X., Wu, Y. S., Li, M. M., Wang, X. J., and Yang, Y. G. (2013). N6-methyl-adenosine (m6A) in RNA: An old modification with a novel epigenetic function. *Genomics Proteomics Bioinforma.* 11, 8–17. doi:10.1016/j.gpb.2012.12.002

Qi, X., Zhang, D. H., Wu, N., Xiao, J. H., Wang, X., and Ma, W. (2015). ceRNA in cancer: possible functions and clinical implications. *J. Med. Genet.* 52, 710–718. doi:10.1136/jmedgenet-2015-103334

Salmena, L., Poliseno, L., Tay, Y., Kats, L., and Pandolfi, P. P. (2011). A ceRNA hypothesis: The rosetta stone of a hidden RNA language? *Cell.* 146, 353–358. doi:10.1016/j.cell.2011.07.014

Sand, M., Skrygan, M., Sand, D., Georgas, D., Hahn, S. A., Gambichler, T., et al. (2012). Expression of microRNAs in basal cell carcinoma. *Br. J. Dermatol.* 167, 847–855. doi:10.1111/j.1365-2133.2012.11022.x

Sarcomas Tissue, Soft (2021). Statistics. Available at: https://www.cancer.net/cancer-types/sarcoma-soft-tissue/statistics (Accessed September 25, 2021).

SEER (2021). Cancer statistics review, 1975-2017-SEER statistics, Available at:. https://seer.cancer.gov/csr/1975_2017/ (Accessed September 25, 2021).

Shang, X., Shi, L. E., Taule, D., and Zhu, Z. Z. (2021). A novel miRNA-mRNA Axis involves in regulating transcriptional disorders in pancreatic adenocarcinoma. *Cancer Manag. Res.* 13, 5989–6004. doi:10.2147/CMAR.S316935

Siegel, R. L., Miller, K. D., and Jemal, A. (2019). Cancer statistics, 2019. *Ca. Cancer J. Clin.* 69, 7–34. doi:10.3322/caac.21551

Sun, F., Yu, Z., Wu, B., Zhang, H., and Ruan, J. (2020). LINC00319 promotes osteosarcoma progression by regulating the miR-455-3p/NFIB axis. *J. Gene Med.* 22, e3248. doi:10.1002/jgm.3248

Sun, J., Shi, R., Zhang, X., Fang, D., Rauch, J., Lu, S., et al. (2021). Characterization of immune landscape in papillary thyroid cancer reveals distinct tumor immunogenicity and implications for immunotherapy. *Oncoimmunology* 10, e1964189. doi:10.1080/2162402X.2021.1964189

Tang, Y., Chen, K., Song, B., Ma, J., Wu, X., Xu, Q., et al. (2021). m6A-Atlas: a comprehensive knowledgebase for unraveling the N6-methyladenosine (m6A) epitranscriptome. *Nucleic Acids Res.* 49, D134–D143. doi:10.1093/nar/gkaa692

Wang, W., Mu, S., Zhao, Q., Xue, L., and Wang, S. (2019). Identification of differentially expressed microRNAs and the potential of microRNA-455-3p as a novel prognostic biomarker in glioma. *Oncol. Lett.* 18, 6150–6156. doi:10.3892/ol.2019.10927

Wu, J., Li, L., Zhang, H., Zhao, Y., Zhang, H., Wu, S., et al. (2021). A risk model developed based on tumor microenvironment predicts overall survival and associates with tumor immunity of patients with lung adenocarcinoma. *Oncogene* 40, 4413–4424. doi:10.1038/s41388-021-01853-y

Xu, F., Huang, X., Li, Y., Chen, Y., and Lin, L. (2021). m6A-related lncRNAs are potential biomarkers for predicting prognoses and immune responses in patients with LUAD. *Mol. Ther. Nucleic Acids* 24, 780–791. doi:10.1016/j.omtn.2021.04.003

Xuan, J. J., Sun, W. J., Lin, P. H., Zhou, K. R., Liu, S., Zheng, L. L., et al. (2018). RMBase v2.0: Deciphering the map of RNA modifications from epitranscriptome sequencing data. *Nucleic Acids Res.* 46, D327–D334. doi:10.1093/nar/gkx934

Yang, C., Wang, Y., Xue, W., Xie, Y., Dong, Q., and Zhu, C. (2020). Competing endogenous RNA (ceRNA) network analysis of autophagy-related genes in hepatocellular carcinoma. *Pharmgenomics. Pers. Med.* 13, 445–462. doi:10.2147/PGPM.S267563

Yang, H., Wei, Y. N., Zhou, J., Hao, T. T., and Liu, X. L. (2017). MiR-455-3p acts as a prognostic marker and inhibits the proliferation and invasion of esophageal squamous cell carcinoma by targeting FAM83F. *Eur. Rev. Med. Pharmacol. Sci.* 21, 3200–3206.

Yang, K., Wang, F., Li, K., Peng, G., Yang, H., Xu, H., et al. (2022). N6-methyladenosine modification-related long non-coding RNAs are potential biomarkers for predicting the prognosis of patients with osteosarcoma. *Technol. Cancer Res. Treat.* 21, 15330338221085354. doi:10.1177/15330338221085354

Yang, Y., Hsu, P. J., Chen, Y. S., and Yang, Y. G. (2018). Dynamic transcriptomic m6A decoration: Writers, erasers, readers and functions in RNA metabolism. *Cell. Res.* 28, 616–624. doi:10.1038/s41422-018-0040-8

Yi, X., Wang, Y., and Xu, S. (2020). MiR-455-3p downregulation facilitates cell proliferation and invasion and predicts poor prognosis of osteosarcoma. *J. Orthop. Surg. Res.* 15, 454. doi:10.1186/s13018-020-01967-1

Zhang, F., Yu, X., Lin, Z., Wang, X., Gao, T., Teng, D., et al. (2021). Using tumor-infiltrating immune cells and a ceRNA network model to construct a prognostic analysis model of thyroid carcinoma. *Front. Oncol.* 11, 658165. doi:10.3389/fonc.2021.658165

Zhang, L., Li, B., Peng, Y., Wu, F., Li, Q., Lin, Z., et al. (2020). The prognostic value of TMB and the relationship between TMB and immune infiltration in head and neck squamous cell carcinoma: A gene expression-based study. *Oral Oncol.* 110, 104943. doi:10.1016/j.oraloncology.2020.104943

Zhang, L., Tang, X. Z., Wan, J., Zhang, X., Zheng, T., Lin, Z., et al. (2021). Construction of a novel signature and prediction of the immune landscape in soft tissue sarcomas based on N6-methylandenosine-related LncRNAs. *Front. Mol. Biosci.* 8, 715764. doi:10.3389/fmolb.2021.715764

Zheng, F., Du, F., Qian, H., Zhao, J., Wang, X., Yue, J., et al. (2021). Expression and clinical prognostic value of m6A RNA methylation modification in breast cancer. *Biomark. Res.* 9, 28. doi:10.1186/s40364-021-00285-w

Zhou, Y. J., Zhu, G. Q., Lu, X. F., Zheng, K. I., Wang, Q. W., Chen, J. N., et al. (2020). Identification and validation of tumour microenvironment-based immune molecular subgroups for gastric cancer: Immunotherapeutic implications. *Cancer Immunol. Immunother.* 69, 1057–1069. doi:10.1007/s00262-020-02525-8

Zhu, K. P., Zhang, C. L., Ma, X. L., Hu, J. P., Cai, T., and Zhang, L. (2019). Analyzing the interactions of mRNAs and ncRNAs to predict competing endogenous RNA networks in osteosarcoma chemo-resistance. *Mol. Ther.* 27, 518–530. doi:10.1016/j.ymthe.2019.01.001

Zhu, N., and Hou, J. (2020). Assessing immune infiltration and the tumor microenvironment for the diagnosis and prognosis of sarcoma. *Cancer Cell. Int.* 20, 577. doi:10.1186/s12935-020-01672-3

Zhu, W., Zhu, L., Bao, Y., Zhong, X., Chen, Y., and Wu, Q. (2019). Clinical evaluation of neoadjuvant chemotherapy for osteosarcoma. *J. BUON* 24, 1181–1185.

frontiers | Frontiers in Pediatrics

TYPE Original Research
PUBLISHED 17 October 2022
DOI 10.3389/fped.2022.927885

Check for updates

OPEN ACCESS

EDITED BY
Matthew E. R. Butchbach,
Nemours Children's Health Delaware,
United States

REVIEWED BY
Mohsen Norouzinia,
Shahid Beheshti University of Medical Sciences,
Iran
Leila Jahangiri,
University of Cambridge, United Kingdom

*CORRESPONDENCE
Yunquan Li
LYQ20170926@163.com

†These authors have contributed equally to this work and share first authorship

SPECIALTY SECTION
This article was submitted to Genetics of Common and Rare Diseases, a section of the journal Frontiers in Pediatrics

RECEIVED 25 April 2022
ACCEPTED 20 September 2022
PUBLISHED 17 October 2022

CITATION
Li L, Chen S, Li J, Rong G, Yang J and Li Y (2022) Characterization of m6A-related lncRNA signature in neuroblastoma.
Front. Pediatr. 10:927885.
doi: 10.3389/fped.2022.927885

COPYRIGHT
© 2022 Li, Chen, Li, Rong, Yang and Li. This is an open-access article distributed under the terms of the Creative Commons Attribution License (CC BY). The use, distribution or reproduction in other forums is permitted, provided the original author(s) and the copyright owner(s) are credited and that the original publication in this journal is cited, in accordance with accepted academic practice. No use, distribution or reproduction is permitted which does not comply with these terms.

Characterization of m6A-related lncRNA signature in neuroblastoma

Liming Li†, Sisi Chen†, Jianhong Li, Guochou Rong, Juchao Yang and Yunquan Li*

Department of Pediatric Surgery, GuiPing People's Hospital, Guangxi, China

N6-methyladenosine (m6A) constitutes one of the most common modifications in mRNA, rRNA, tRNA, microRNA, and long-chain noncoding RNA. The influence of modifications of m6A on the stability of RNA depends upon the expression of methyltransferase ("writer") and demethylase ("eraser") and m6A binding protein ("reader"). In this study, we identified a set of m6A-related lncRNA expression profiles in neuroblastoma (NBL) based on the Therapeutically Applicable Research to Generate Effective Treatments (TARGET) program. Thereupon, we identified two subgroups of neuroblastoma (high-risk group and low-risk group) by applying consensus clustering to m6A RNA methylation regulators ("Readers,", "Writer," and "Erase"). Relative to the low-risk group, the high-risk group correlates with a poorer prognosis. Moreover, the present study also revealed that the high-risk group proves to be significantly positively enriched in the tumor-related signaling pathways, including the P53 signaling pathway, cell cycle, and DNA repair. This finding indicates that these molecular prognostic markers may also be potentially valuable in early diagnosis, which provides a new research direction for the study of molecular mechanisms underlying the development of NBL. In conclusion, this study constructed a new model of NBL prognosis based on m6a-associated lncRNAs. Ultimately, this model is helpful for stratification of prognosis and development of treatment strategies.

KEYWORDS
N6-methyladenosine, prognosis, risk score, neuroblastoma, lncRNAs

Introduction

Neuroblastoma (NBL) is a neuronal crest cell derived from the sympathetic nervous system, accounting for 6%–10% of childhood tumors (1). Most children with neuroblastoma exhibit metastatic and/or high-risk characteristics (2). It is moreover responsible for 12% of cancer-related deaths in children under the age of 15 (3). Neuroblastomas feature a wide range of tumor heterogeneity with different clinical manifestations and courses of disease in accordance with tumor biology (4, 5). Patients with medium- and low-risk conditions are mainly treated by operation, and additional chemotherapy can be included if necessary. Advances in the treatment of patients with high-risk diseases include intensive induction chemotherapy and myeloablative chemotherapy followed by differentiation therapy and immunotherapy for minimal residual conditions. These treatments can increase the 5-year overall

survival (OS) rate to 50% (6). Due to the fact that the initial symptoms of neuroblastoma are not typical, early accurate diagnosis remains a challenge. Risk stratification therapy helps reduce the intensity of treatment of children with low-and medium-risk conditions, and the establishment of prognostic models helps evaluate the treatment of high-risk children. Therefore, it is of great significance to determine the risk characteristics in the diagnostic stage for the purpose of evaluating the prognosis of children with neuroblastoma.

Epigenetics, involving changes in DNA or histones, has been widely studied in tumor progression (7). As a class of epigenetics, RNA modification has become a key regulator of RNA function and metabolism (8). N6-methyladenosine (m6A) constitutes one of the most common modifications in mRNA, rRNA, tRNA, microRNA, and long-chain noncoding RNA (9, 10). Dynamic m6A modification affects a variety of cellular processes, such as RNA stability, output, splicing, or translation (11). The effect of m6A on the stability of RNA depends on m6A readers, including YTHDF1, YTHDF2, YTHDF3, and YTHDC (12). In addition, m6A modification is regulated by two other enzymes: "Writer" (methyltransferase, including WTAP, KIAA1429, RBM15/15B, and METTL3/14/16) and "Erase" (demethylase, including ALKBH5 and FTO) (13). Increasing evidence proves that m6A-related lncRNAs can serve as a new potential target for prognosis and developing individualized therapies for a variety of cancers (14–16). However, the relationship between m6A methylation and NB remains unclear. Recently, a study reported that CoCl decreased the activity of demethylase and significantly changed the level of mA modification by affecting the expression of mA methyltransferase and demethylase in human neuroblastoma H4cells (17). In addition, it has been reported that miR-98/MYCN axis-mediated inhibition of neuroblastoma progression requires RNA mA modification (18). On top of that, the risk prediction model constructed by five m6A-related genes (*METT14*, *WTAP*, *HNRNPC*, *YTHDF1*, and *IGF2BP2*) is helpful in the clinical prognosis of NBL (19).

In this study, we identified a set of m6A-related genomic expression profiles in NB based on the *Therapeutically Applicable Research to Generate Effective Treatments* (TARGET: https://ocg.cancer.gov/programs/target) program. Subsequently, several lncRNAs related to m6A regulatory factors were identified as potential biomarkers. To evaluate the impact of m6A-related lncRNA on prognostic value, we eventually identified seven m6A-related lncRNAs that enabled us to construct a risk score, after which NB cases were divided into a high-risk group and a low-risk group based on the median risk score. Since then, we have analyzed the prognostic role of the risk score in NBL. Our results suggest that the risk score of m6A-related lncRNA may provide information for risk assessment and prognosis stratification. More importantly, the prognostic correlation of the risk marker was successfully verified in the internal subgroup analysis.

Data source and processing

The fragments per kilobase million (FPKM) data and the corresponding clinical information of NBL samples were downloaded from TARGET Data Matrix (https://ocg.cancer.gov/programs/ target/data-matrix). NBL samples without prognostic information were excluded. In our study, a total of 155 NBL patients with complete OS information were enrolled (**Supplementary file S1 and S2**). The data were annotated and collapsed into mRNAs and lncRNAs employing Ensembl (http://asia.ensembl.org) and using the Perl program. Finally, the lncRNA and mRNA expression profiles were extracted separately from the database. The flowchart of our work is shown in **Figure 1**.

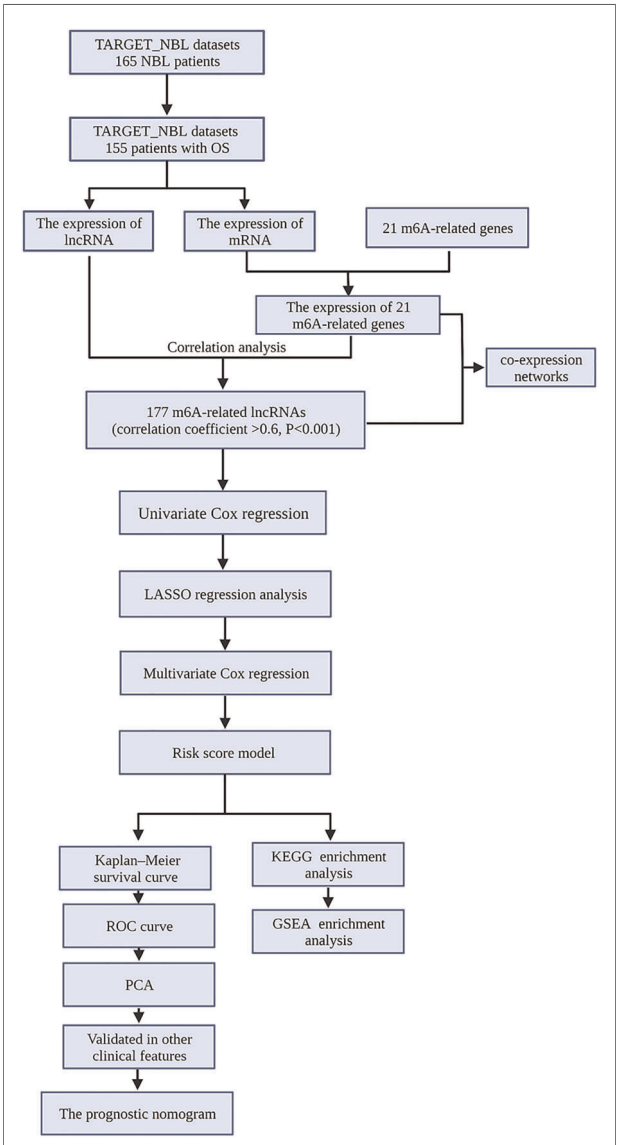


FIGURE 1
Analysis flow chart.

Identification of m6A methyltransferase-related lncRNAs

Twenty-one m6A-related genes were extracted based on previous studies including the Writers (*METTL3, METTL14, RBM15, RBM15B, WTAP, KIAA1429, CBLL1*, and *ZC3H13*), Erasers (*ALKBH5* and *FTO*), and Readers (*YTHDC1, YTHDC2, YTHDF1, YTHDF2, YTHDF3, GF2BP1, HNRNPA2B1, HNRNPC, FMR1, LRPPRC*, and *ELAVL1*) (20, 21). In addition, Pearson correlation analysis was performed in the statistical software R (version 4.0.3) to identify the potential lncRNA associated with m6A-related genes. A total of 177 m6A-related lncRNAs with Pearson correlation coefficients greater than 0.6 and $P < 0.01$ were included in subsequent studies, and subsequently, the coexpression networks between m6A genes and m6A-related lncRNAs were visualized using the Cytoscape software (v3.08).

Construction of the prognostic signature

By means of univariate Cox regression analysis, m6A-related lncRNAs that can be used to predict the prognosis of patients were screened. In addition, a forest plot was used to visualize the hazard ratio (HR) of these prognostic-related lncRNAs. Subsequently, the LASSO regression method was used to screen the best candidate, and a multifactor Cox regression analysis was carried out to establish the Cox risk assessment model by means of R packages ("survival" and "glmnet"). Afterward, the samples were divided into a high-risk group and a low-risk group based on median risk scores for both sets.

Evaluation of the risk score model

Based on the median value of the risk score, the heat map, risk curves, and scatter plots were plotted to show the differences in prognosis between the high-risk group and the low-risk group through the R packages ("pheatmap," "survival," and "survminer"). The Kaplan–Meier survival curve was used to compare the OS between the two groups. Furthermore, the receiver operating characteristic (ROC) curve and area under curve (AUC) were harnessed to evaluate the diagnostic and prognostic value of the risk score model and

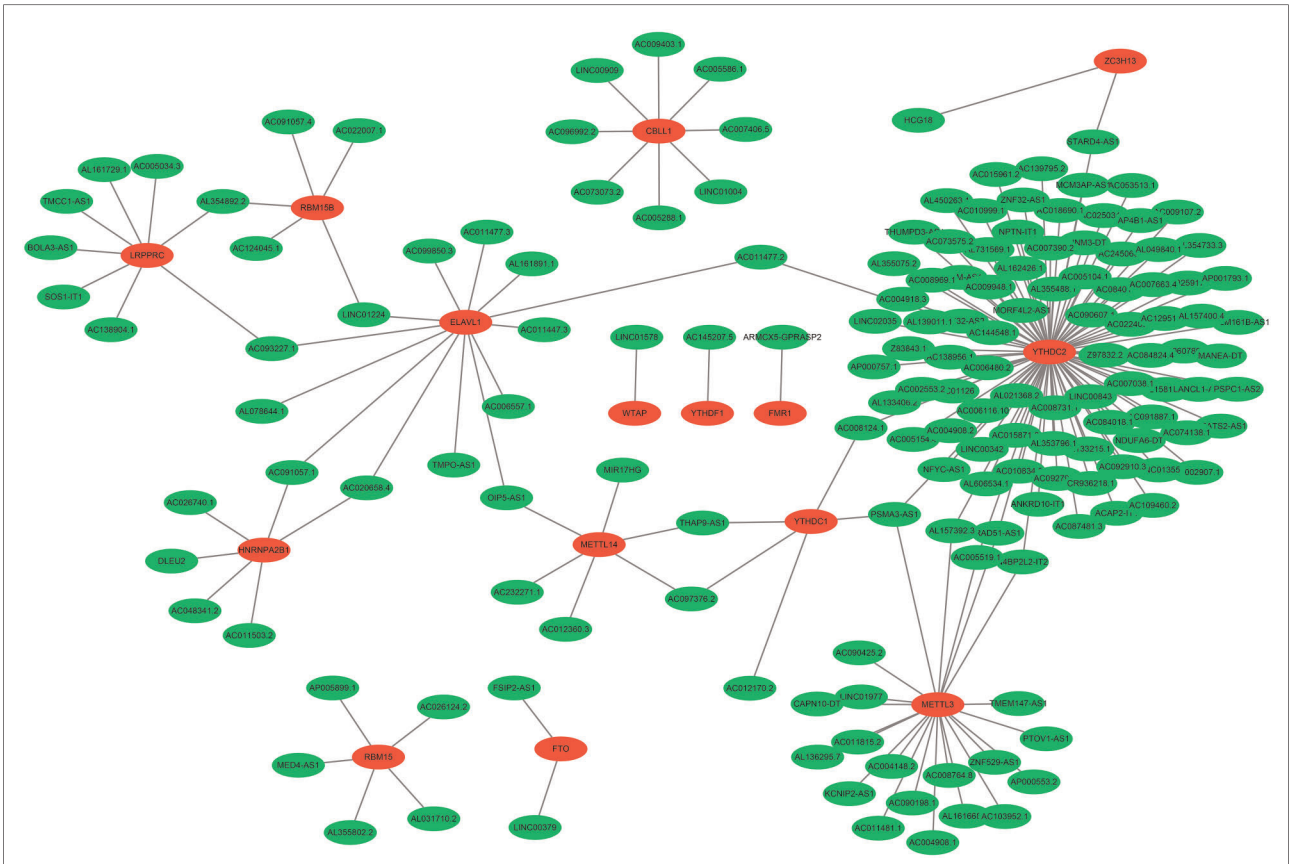


FIGURE 2
The coexpression networks between m6A genes and m6A-related lncRNAs. 177 lncRNAs co-expressed with m6A-related genes. The red nodes represent m6A genes and green nodes represent m6A-related lncRNAs.

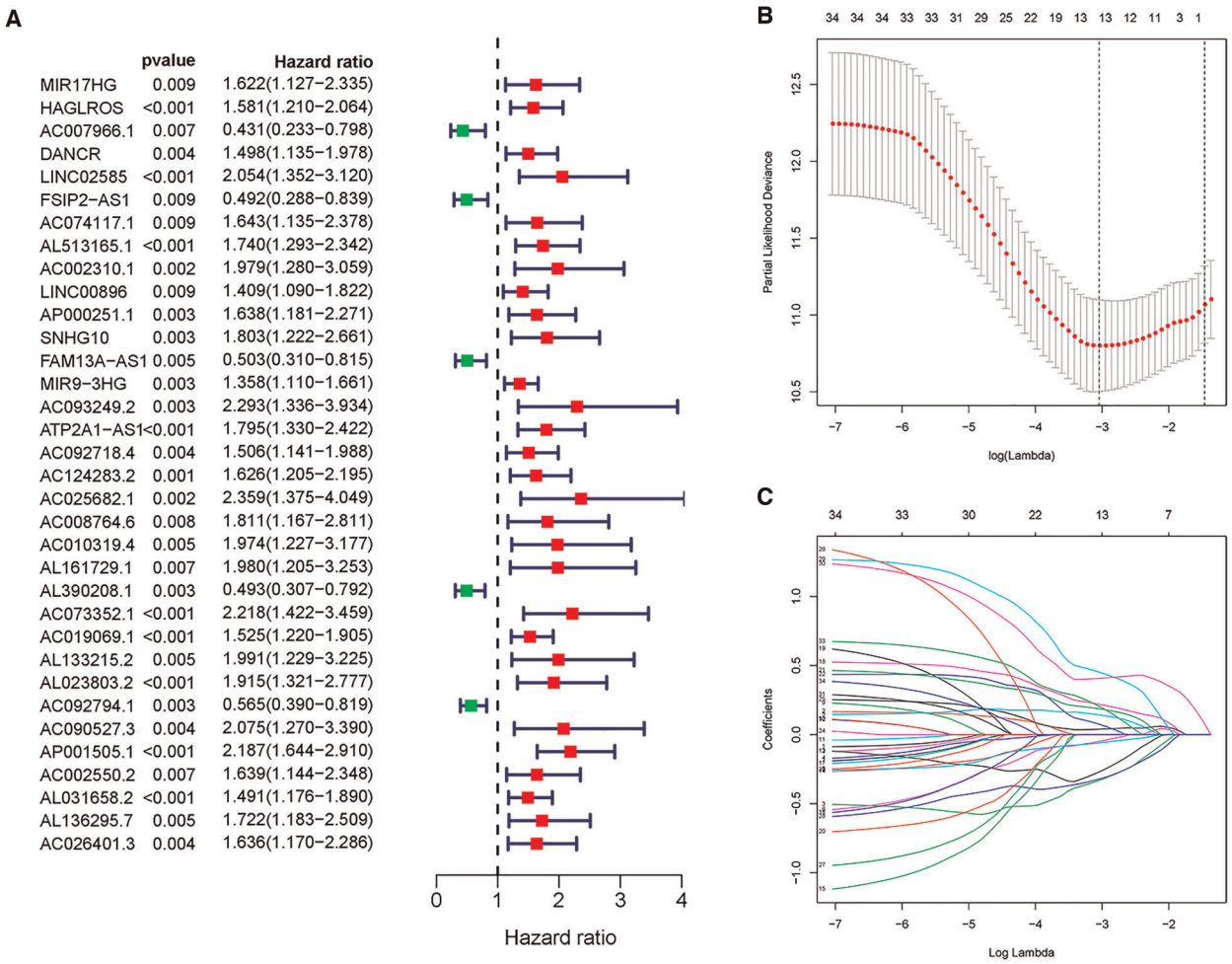


FIGURE 3
Univariate Cox regression analysis and LASSO regression analysis. (A) Forest plot of univariate Cox regression showed that 34 MRlncRNAs were prognostic factors of NBL. (B,C) LASSO regression was performed, calculating that the accuracy of the MRlncRNAs-related prediction model was the best when 13 MRlncRNAs were selected.

TABLE 1 Multivariate Cox regression analysis of the MRlncRNAs.

ID	Coef	HR	95% CI	*P* value
AC007966.1	−0.66867	0.512389	0.273306-0.960618	0.037046
AC124283.2	0.370511	1.448475	1.001015-2.095953	0.049374
AL161729.1	0.430911	1.538658	0.914183-2.58971	0.104763
AC092794.1	−0.66539	0.514072	0.322039-0.820616	0.005296
AC090527.3	0.705756	2.025378	1.143209-3.588281	0.015579
AP001505.1	0.507392	1.660954	1.151831-2.395117	0.006591
AL136295.7	0.442733	1.556957	0.952782-2.54425	0.077241

TABLE 2 The correlation between m6A-related genes and targeted lncRNAs.

ID	m6A-related genes	Correlation coefficent	*P* value	Regulation
AC124283.2	RBM15	0.549232	2.19×10^{-14}	Postive
AC092794.1	YTHDC2	0.606257	6.19×10^{-18}	Postive
AL161729.1	LRPPRC	0.641337	1.70×10^{-20}	Postive
AP001505.1	HNRNPC	0.522778	5.90×10^{-13}	Postive
AL136295.7	METTL3	0.618525	8.56×10^{-19}	Postive
AC007966.1	FTO	0.597777	2.32×10^{-17}	Postive
AC090527.3	METTL14	0.50319	5.65×10^{-12}	Postive

clinicopathological features. In turn, we combined the clinical data of patients and the risk model constructed in this study for univariate and multivariate Cox analyses and obtained the related forest plots using a survival R package. To further explore the impact of single-target lncRNA on NBL patients in the prognostic risk model, the Wilcoxon test was employed for a comparison of the relationship between the lncRNA expression level of each target and clinical parameters. Principal component analysis (PCA) was employed in order to perform effective dimension reduction, pattern recognition,

and exploratory visualization analysis on the expression profiles of the whole genome, m6A-related genes, m6A-related lncRNAs, and seven risk model lncRNAs.

Gene set enrichment analysis

Gene set enrichment analysis (GSEA) was performed in the NBL cohort to determine the underlying biological processes and cellular pathways of high-risk and low-risk subsets identified by m6A-associated lncRNA expression characteristics. A set of genes with a false discovery rate <0.25 and a standardized *P* value <0.05 were considered significant.

Establishment and validation of a prognostic nomogram

Based on risk score and prognostic clinical variables, we constructed a prognostic nomogram to quantitatively predict the prognosis of NBL patients. Subsequently, the concordance index (C-index) and calibration curves were employed to evaluate the reliability and accuracy of the prognostic nomogram. At this juncture, the "rms," "foreign," and "survival" packages were employed.

Statistical analysis

All statistical analyses were performed using R software (version 4.0.3). The programming language Perl (version 5.30.2) was implemented for data processing. The network was visualized using the Cytoscape software (v3.08).

Results

Identification of m6A-related lncRNA

The neuroblastoma-related RNA sequencing data were downloaded from the Target database, which included 155 neuroblastoma tissue samples featuring complete clinical

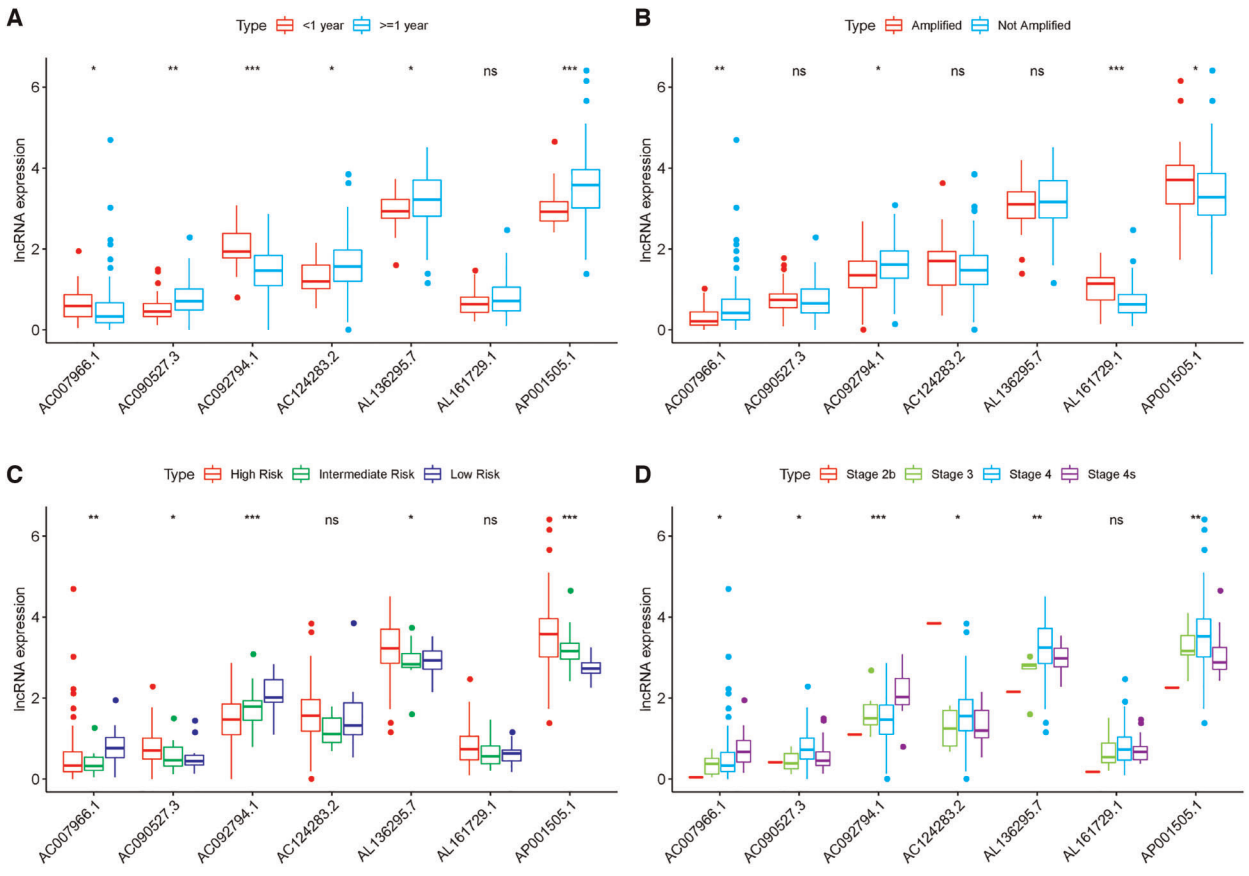


FIGURE 4
Correlation between the expression level of seven MRlncRNAs in the prediction model and clinical variables. (A–D) Most LncRNAs showed significantly different expressions between diverse groups in age (A), MYCN (B), risk score (C), and stage (D).

information. Subsequently, the expression profiles of m6A-related genes were obtained from the neuroblastoma-related RNA sequencing data. As a result, we discovered that 177 lncRNAs were significantly associated with M6A-related genes utilizing Pearson correlation analysis (correlation coefficient >0.6, $P < 0.001$), which was visualized by Cytoscape (**Figure 2**).

Construction of an MRlncRNA signature

Univariate Cox regression analysis is capable of providing clues for potential prognostic genes. Accordingly, we found that 34 MRlncRNAs (m6A-associated lncRNAs) had potential prognostic through the "Survival" package. As shown in **Figure 3A**, 5 MRlncRNAs had potentially prognostic value (HR > 1, $P < 0.05$), whereas 29 genes showed potential poor value (HR < 1, $P < 0.05$).

These lncRNAs were taken into consideration to build an MRlncRNA-related prediction model for the prognosis of NBL. To infinitely improve the accuracy of the prediction model, we carried out a LASSO regression analysis *via* the "GLMNet" package (**Figures 3B,C**). Results showed that the accuracy of the MRlncRNA-related prediction model was the best when 13 MRlncRNAs were selected. Simultaneously, we identified that 7 of 13 MRlncRNAs were independent predictors by multivariate Cox regression (**Table 1**). The correlation between these lncRNAs and m6A-related genes was further verified (**Table 2**). We initially established an MRlncRNA-related risk prediction model for NBL. Furthermore, we explored the correlation between these lncRNAs and clinicopathological features. The results showed that most of these lncRNAs, among different subgroups of age, risk score, stage, and amplification status, showed significant differences in expression, indicating that these lncRNAs were significantly correlated with the characteristics of clinical cases. As shown in **Figures 4A–D**, all lncRNAs except AL161729.1 showed significantly different expressions among diverse groups in age (≤1, >1) and stage subgroups (stage 2b, stage 3, stage 4, stage 4s). In the risk grouping (high risk, intermediate risk, low risk), these lncRNAs except AC0124283.2, and AL161729.1 showed significantly different expressions among diverse groups. Also, similar consequences were observed in the amplification status group (amplified, not amplified).

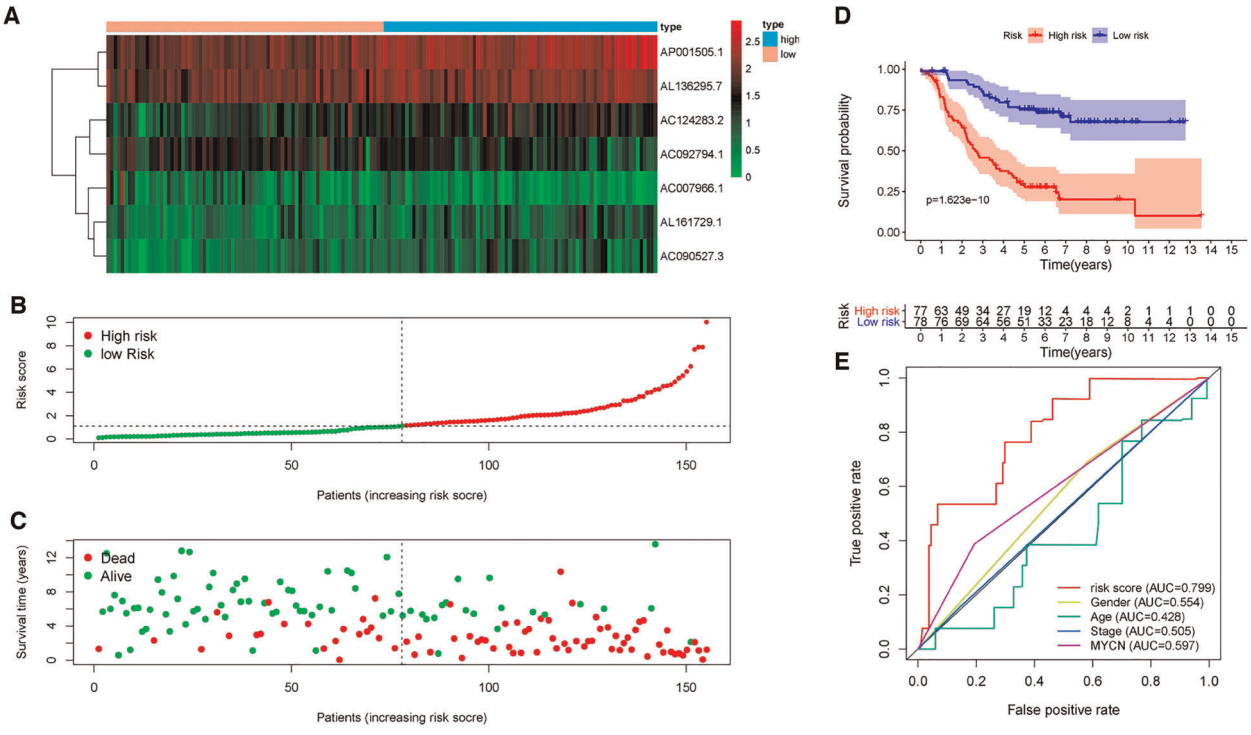


FIGURE 5
Prognostic value of risk models based on MRlncRNAs. (**A**) The heatmap of differential expression of seven lncRNAs in high- and low-risk groups. (**B**) Risk scores of NBL patients were sorted according to the risk model. (**C**) The scatter plot of the relationship between the risk scores and the survival time in NBL patients. (**D**) Kaplan–Meier overall survival curves showed that patients in the low-risk group exhibited better OS than those in the high-risk group. (**E**) ROC curve analysis showed that the risk score was the best diagnosis predictors compared with other clinicopathological characteristics.

The risk prediction model has great predicted performance

A risk score of each patient was calculated using the formula: risk score = $\sum$ I Coefficient (MRlncRNAsi) × Expression (MRlncRNAsi). We divided 155 neuroblastoma tissue samples into high- and low-risk groups based on the median value of the risk score. Accordingly, the heatmap hinted at the different expressions of these MRlncRNAs in a diverse risk group (**Figure 5A**); AC007966.1 and AC092794.1 were highly expressed in the low-risk group, whereas others were highly expressed in the high-risk group. Ranking the patients in the light of risk scores from low to high, we discovered that survival time decreased significantly (**Figures 5B,C**). Survival analysis using the Kaplan–Meier method based on the risk group showed that patients in the high-risk group had significantly lower survival rates than those in the low-risk group ($P < 0.001$) (**Figure 5D**). Following that, we explored the prediction accuracy of the risk model by calculating the AUC of the risk score and clinicopathologic features, such as age, gender, stage, and MYCN state, by the ROC curve analysis. The results demonstrated that, relative to other clinicopathological characteristics, the risk score proved to be the optimal diagnosis predictor (**Figure 5E**). Subsequently, PCA (**Figures 6A–D**) showed that the samples were notably divided into two risk clusters based on the expression of m6A-related genes (**Figure 6B**) or seven risk model lncRNAs (**Figure 6D**).

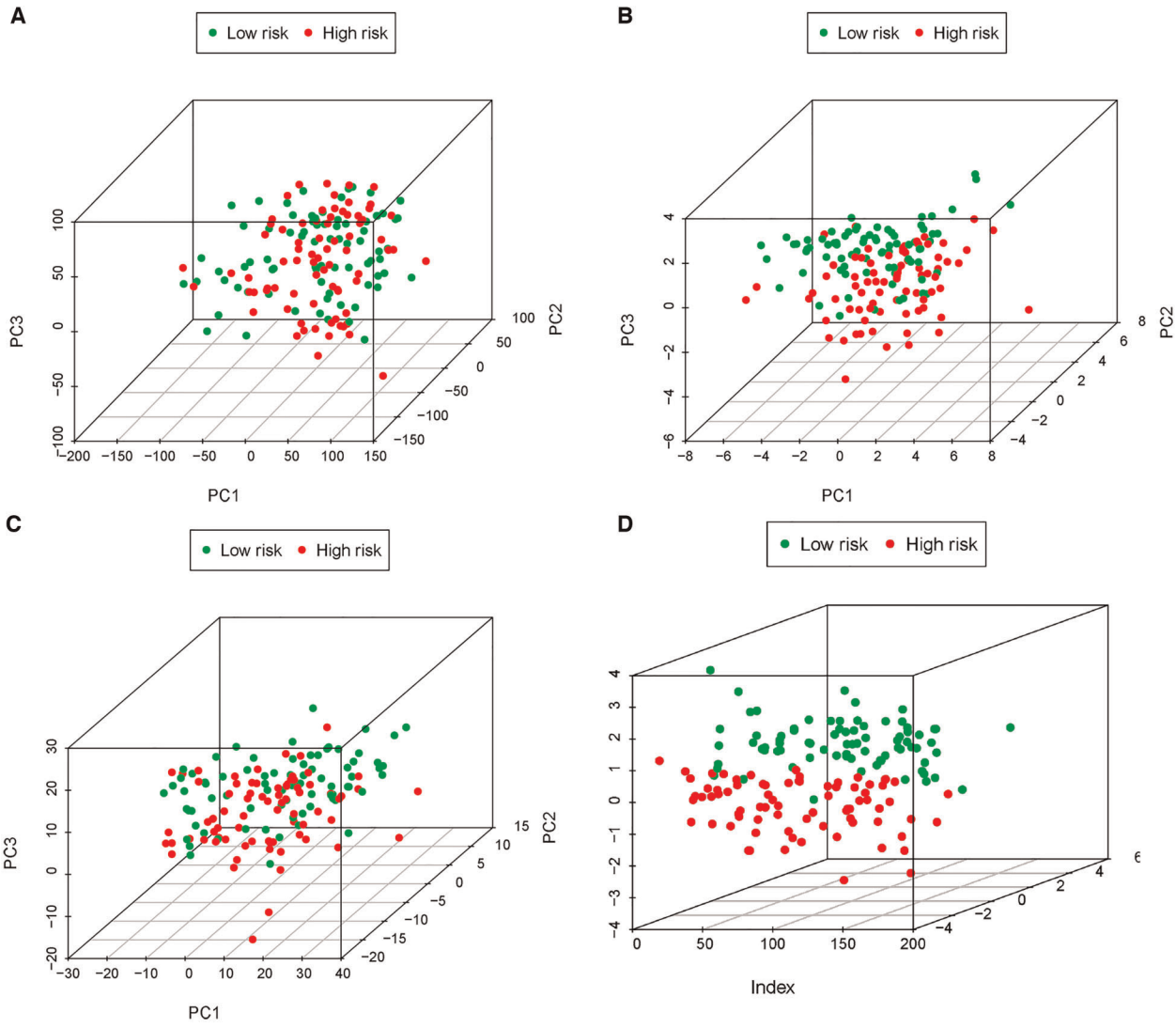


FIGURE 6
PCA of all expressed genes, m6A genes, 34 MRlncRNAs, and 7 MRlncRNAs in the prediction model. (**A**) Principal components analysis based on whole gene expression profiles. (**B**) Principal components analysis based on m6A-related genes. (**C**) Principal components analysis based on 34 MRlncRNAs. (**D**) Principal components analysis based on 7 MRlncRNAs in the prediction model.

The MRlncRNA signature was an independent prognostic indicator

Following considering the clinicopathological features, to determine the influence of clinicopathological features regarding the risk score based on the predictive model, univariate and multivariate regression analyses were used once more to assess the independence of predictive function concerning the risk score (**Figures 7A,B**). The results revealed that undergoing adjusting other clinicopathologic features, such as age, sex, stage, and MYCN amplification by multivariate Cox regression analysis, risk score remained an independent predictor [HR = 1.482, 95% CI (1.325–1.658); $P < 0.001$].

Furthermore, the nomogram showed that the risk score contributed the most to OS (**Figure 8A**). It was also discovered that the 3- and 5-year survival rates of patients were very low. Subsequently, we tested the prediction accuracy of the risk prediction model by the calibration curve, the results of which showed that the prediction accuracy of 1-year survival rates was relatively high (**Figure 8B**), while the prediction accuracy of 3- and 5-year survival rates were relatively poor (**Figures 8C,D**), which may be due to the small number of cases.

For conducting internal detection of the risk model, we classified patients according to their risk scores and tested the survival rates of different subgroups. As shown in **Figures 8E,F**, the survival rates of the high-risk group were significantly lower

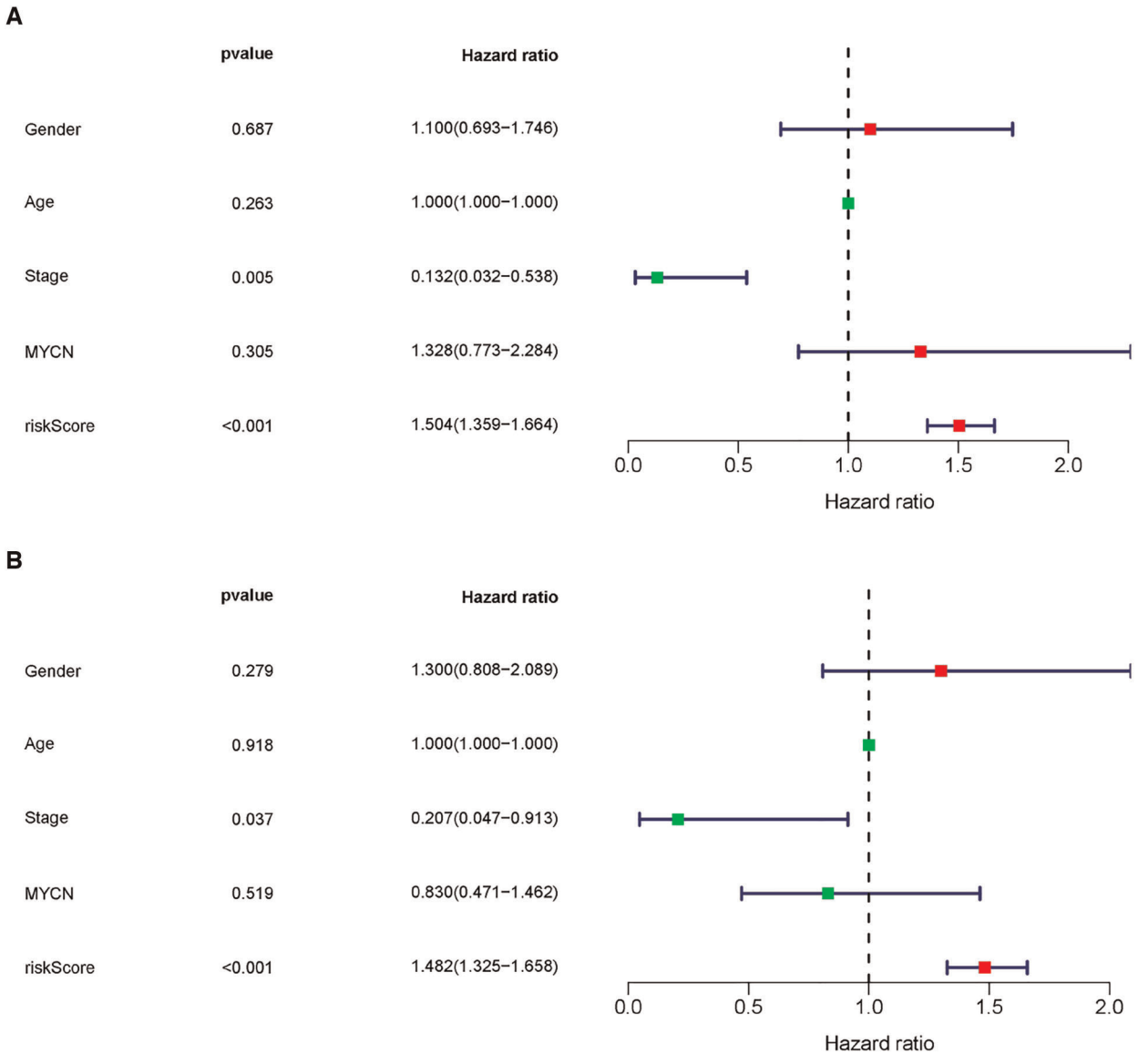


FIGURE 7
The MRlncRNAs signature was an independent prognostic indicator. Univariate (A) and multivariate (B) Cox regression analysis of the MRlncRNAs signature with clinicopathological features ($P < 0.05$).

10.3389/fped.2022.927885

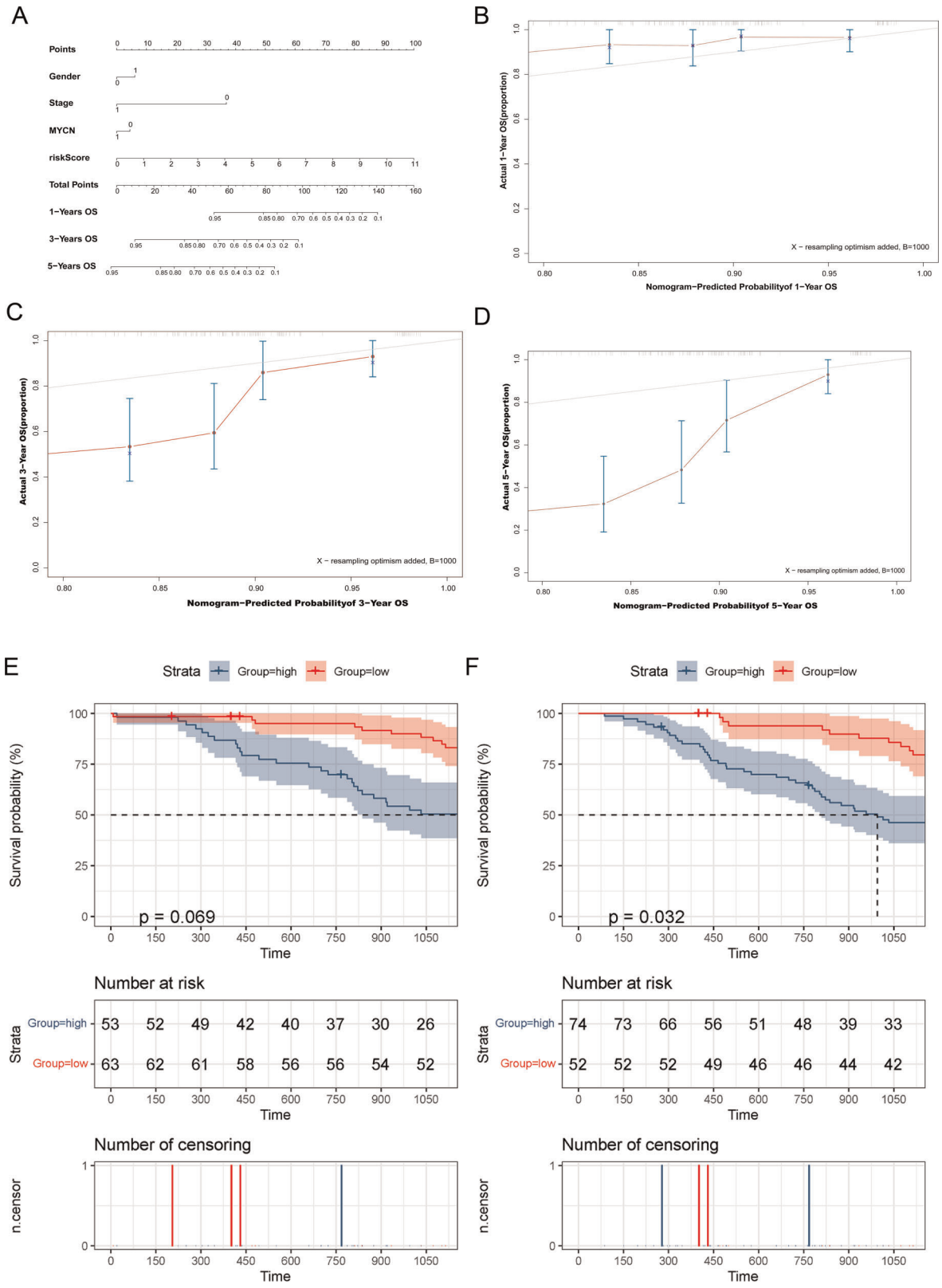


FIGURE 8
The MRlncRNAs possessed potential clinical value. (**A**) A nomogram of patients' clinical information, risk score, and OS. (**B**–**D**) Calibration plots for assessing agreement between the predicted and the actual OS at 1, 3, and 5 years. The survival curves of the MRlncRNAs signature stratified by the nonamplified MYCN group (**E**) and higher-age group (**F**).

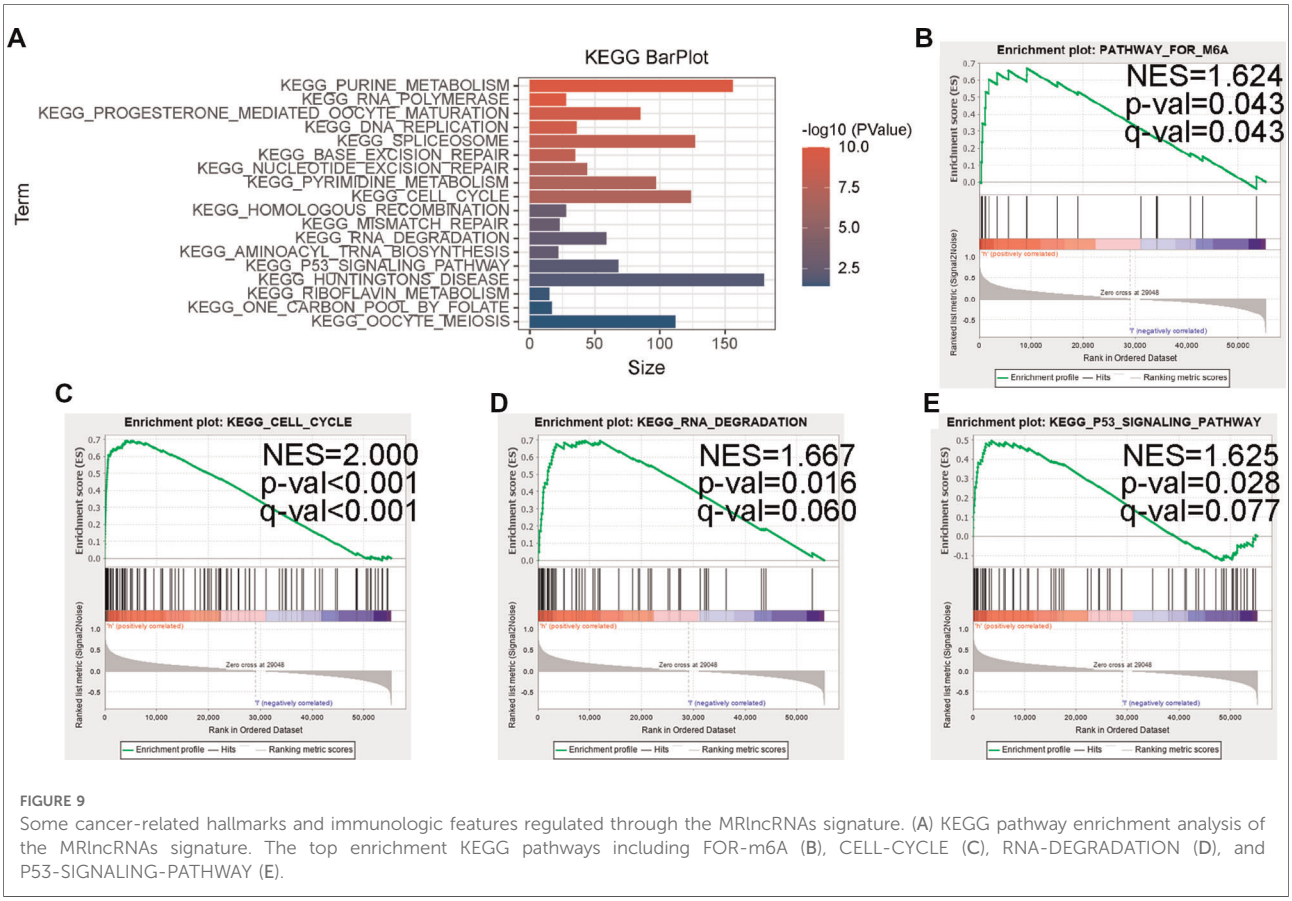


FIGURE 9
Some cancer-related hallmarks and immunologic features regulated through the MRlncRNAs signature. (**A**) KEGG pathway enrichment analysis of the MRlncRNAs signature. The top enrichment KEGG pathways including FOR-m6A (**B**), CELL-CYCLE (**C**), RNA-DEGRADATION (**D**), and P53-SIGNALING-PATHWAY (**E**).

than that of the low-risk group within the nonamplified MYCN group and higher-age group, whereas the significantly different surgical rates have not been observed in other subgroups, which may be due to the small number of patient cases. Subsequently, we performed a KEGG pathway enrichment analysis of prognosis-related MRlncRNAs. As shown in **Figures 9A–E**, the concentrations of pathway enrichment were mainly in "FOR_m6A," "CELL_CYCLE," "RNA_degradation," and "P53_signaling," indicating that this lncRNA was related to m6A and RNA_degradation, which was consistent with our study. Furthermore, these MRlncRNAs may also affect the progression of NBL by the cell cycle and P53 signal pathway.

Discussion

NBL is one of the most aggressive and poorly proposed solid tumors in children (22). As currently validated predictive tools, the International Neuroblastoma Staging System (INSS) stage, International Neuroblastoma Risk Group Staging System (INRGSS), and Children's Oncology Group (COG) risk stratification have been used to reflect and predict the progression and prognosis of NBL (23, 24). Currently, risk assessment systems for tumor patients are converging toward an integrated assessment of clinical, histopathological, and genetic prognostic markers (25–27). The COG pediatric NBL risk prediction model integrates clinical and histopathological factors while incorporating the MYCN gene. MYCN is the only biological marker for risk assessment. The results of clinical and molecular studies suggest that current risk assessment systems remain inadequate (28, 29), leading to over- or undertreatment of a small proportion of patients. In the clinical setting, new therapeutic prognostic markers are urgently required to improve the prognosis of NBL patients, design more effective treatments, and to better target the heterogeneity of NBL. In recent years, several studies have proposed that molecular markers, such as copy number alterations, gene expression classifiers, and somatic mutation patterns, can accurately reflect tumor biology. Furthermore, it has been shown that epigenetic alterations are closely associated with the development of NBL (30–33). Compounds targeting epigenetically modified proteins are increasingly evaluated as anticancer therapeutic agents, for m6A modifications involved in the development of NBL (34, 35). One study suggested that risk models constructed from m6A-related mRNAs may effectively predict the prognosis of children with NBL (34). Nonetheless, as of now, no study has reported on the association of m6A-related lncRNAs with NBL prognosis.

Through a systematic analysis of 21 widely reported m6A-related genes, lncRNA expression, and clinical features in 155 NBL tissues, m6A methylation regulators are the most

abundant form of methylation modification in lncRNAs and play an important role in the prognosis of NBL. Traditional stratified treatment strategies have made progress in improving the overall survival of NBL patients, while the result of patients with highly aggressive NBL remains unsatisfactory (29, 36). In the past few decades, there have been numerous in-depth studies on DNA and mRNA methylation, but few studies on lncRNA methylation. By analyzing transcriptomic data, differential expression of m6A-associated lncRNAs was found to be significantly associated with NBL malignancies. These seven genes constituted independent predictors of prognosis, and the predictive value of the risk model was verified in the independent dataset target. To further improve the prognostic accuracy, the inclusion of several gene expression-based risk estimation scores, integrating several prognostic determinants, such as age, tumor stage, and MYCN oncogene amplification, may be a useful addition to the INSS stage and COG risk stratification. As a new predictive method, molecular prognostic markers that can be quantified by standardized detection procedures change as the tumor progresses, thereby dynamically reflecting the prognosis of patients. Based on the model principal component analysis, the predictive model readily distinguishes between two major subgroups, including patients with good outcomes and those at high risk of dying from the disease. All seven genes included in the model were reported for the first time in NBL. These molecular prognostic markers may also be potentially valuable in early diagnosis, thus providing a new research direction to study the molecular mechanisms underlying the development of NBL. Nomogram is widely used in clinical oncology for evaluation due to the fact that it integrates molecular and clinicopathological parameters (37–40). The probability of each event can be relatively simply calculated and visualized. Nomogram combines the characteristics of seven genes and four clinicopathological parameters. The graphical scoring system is easy to understand and assists in personalized treatment and medical decisions.

In terms of molecular mechanism, we find that the high-risk group was closely associated with the characteristics of malignancy, including P53 signaling pathway, cell cycle, and DNA repair, by enrichment analysis of relevant lncRNA GSEA, which is in line with the current extensive findings on the regulation of lncRNA involvement in the cell cycle in NBL (41–43). Notably, the high-risk group was enriched in the m6A database.

However, the present study still bears several limitations. First, the conclusions are based on the analysis and summary of the TARGET database with fewer numbers; thus, due to the lack of a similar data set, it becomes difficult to verify the validity of this model. Second, the interaction between m6A regulators and prognostic lncRNAs needs future confirmation by assay data. Therefore, future studies with a larger sample size and basic experiments are needed to further confirm our conclusions.

In conclusion, the study constructed a new model of NBL prognosis based on m6A-associated lncRNAs. Accordingly, the prognostic genes identified in this model could serve as novel biomarkers of prognosis in NBL patients, enabling clinicians to adopt individualized treatment plans. In addition, these findings guide basic medical research on m6A methylation in neuroblastoma.

Data availability statement

The original contributions presented in the study are included in the article/**Supplementary Material**, further inquiries can be directed to the corresponding author.

Author contributions

LL, SC, and YL contributed to the study conception and design. Data collection and analysis were performed by JL, GR, and JY. The first draft of the manuscript was written by LL and all authors commented on previous versions of the manuscript. YL contributed to check this manuscript. All authors contributed to the article and approved the submitted version.

Acknowledgments

We acknowledge TARGET database for providing the original study data of PTC patients.

Conflict of interest

The authors declare that the research was conducted in the absence of any commercial or financial relationships that could be construed as a potential conflict of interest.

Publisher's note

All claims expressed in this article are solely those of the authors and do not necessarily represent those of their affiliated organizations, or those of the publisher, the editors and the reviewers. Any product that may be evaluated in this article, or claim that may be made by its manufacturer, is not guaranteed or endorsed by the publisher.

Supplementary material

The Supplementary Material for this article can be found online at: https://www.frontiersin.org/articles/10.3389/fped.2022.927885/full#supplementary-material.

References

1. Galenkamp K, Carriba P, Urresti J, Planells-Ferrer L, Coccia E, Lopez-Soriano J, et al. TNFα sensitizes neuroblastoma cells to FasL-, cisplatin- and etoposide-induced cell death by NF-κB-mediated expression of Fas. *Mol Cancer*. (2015) 14:62. doi: 10.1186/s12943-015-0329-x

2. Colletti M, Tomao L, Galardi A, Paolini A, Di Paolo V, De Stefanis C, et al. Neuroblastoma-secreted exosomes carrying miR-375 promote osteogenic differentiation of bone-marrow mesenchymal stromal cells. *J Extracell Vesicles*. (2020) 9:1774144. doi: 10.1080/20013078.2020.1774144

3. Park J, Bagatell R, Cohn S, Pearson A, Villablanca J, Berthold F, et al. Revisions to the international neuroblastoma response criteria: a consensus statement from the national cancer institute clinical trials planning meeting. *J Clin Oncol*. (2017) 35:2580–87. doi: 10.1200/jco.2016.72.0177

4. Pinto N, Applebaum M, Volchenboum S, Matthay K, London W, Ambros P, et al. Advances in risk classification and treatment strategies for neuroblastoma. *J Clin Oncol*. (2015) 33:3008–17. doi: 10.1200/jco.2014.59.4648

5. Vo K, Matthay K, Neuhaus J, London W, Hero B, Ambros P, et al. Clinical, biologic, and prognostic differences on the basis of primary tumor site in neuroblastoma: a report from the international neuroblastoma risk group project. *J Clin Oncol*. (2014) 32:3169–76. doi: 10.1200/jco.2014.56.1621

6. Matthay K, Maris J, Schleiermacher G, Nakagawara A, Mackall C, Diller L, et al. Neuroblastoma. *Na Rev. Dis Prim*. (2016) 2:16078. doi: 10.1038/nrdp.2016.78

7. Chang X, Lv Y, He J, Cao Y, Li C, Guo Q. Gene expression profile and prognostic value of m6A RNA methylation regulators in hepatocellular carcinoma. *J Hepatocell Carcinoma*. (2021) 8:85–101. doi: 10.2147/jhc.S296438

8. Doamekpor S, Grudzien-Nogalska E, Mlynarska-Cieslak A, Kowalska J, Kiledjian M, Tong L. DXO/Rai1 enzymes remove 5'-end FAD and dephospho-CoA caps on RNAs. *Nucleic Acids Res*. (2020) 48:6136–48. doi: 10.1093/nar/gkaa297

9. Jia R, Chai P, Wang S, Sun B, Xu Y, Yang Y, et al. m^6A modification suppresses ocular melanoma through modulating HINT2 mRNA translation. *Mol Cancer*. (2019) 18:161. doi: 10.1186/s12943-019-1088-x

10. Bushkin G, Pincus D, Morgan J, Richardson K, Lewis C, Chan S, et al. m^6A modification of a 3′UTR site reduces RME1 mRNA levels to promote meiosis. *Nat Commun*. (2019) 10:3414. doi: 10.1038/s41467-019-11232-7

11. Du Y, Hou G, Zhang H, Dou J, He J, Guo Y, et al. SUMOylation of the m^6A-RNA methyltransferase METTL3 modulates its function. *Nucleic Acids Res*. (2018) 46:5195–208. doi: 10.1093/nar/gky156

12. Gu C, Wang Z, Zhou N, Li G, Kou Y, Luo Y, et al. Mettl14 inhibits bladder TIC self-renewal and bladder tumorigenesis through N-methyladenosine of Notch1. *Mol Cancer*. (2019) 18:168. doi: 10.1186/s12943-019-1084-1

13. Lan Q, Liu P, Bell J, Wang J, Hüttelmaier S, Zhang X, et al. The emerging roles of RNA m^6A methylation and demethylation as critical regulators of tumorigenesis, drug sensitivity, and resistance. *Cancer Res*. (2021) 81:3431–40. doi: 10.1158/0008-5472.Can-20-4107

14. Wang H, Meng Q, Ma B. Characterization of the prognostic m6A-related lncRNA signature in gastric cancer. *Front Oncol*. (2021) 11:630260. doi: 10.3389/fonc.2021.630260

15. Chen Y, Lin Y, Shu Y, He J, Gao W. Interaction between N^6-methyladenosine (m^6A) modification and noncoding RNAs in cancer. *Mol Cancer*. (2020) 19:94. doi: 10.1186/s12943-020-01207-4

16. Zhou B, Yang H, Yang C, Bao Y, Yang S, Liu J, et al. Translation of noncoding RNAs and cancer. *Cancer Lett*. (2021) 497:89–99. doi: 10.1016/j.canlet.2020.10.002

17. Tang J, Zheng C, Zheng F, Li Y, Wang Y, Aschner M, et al. Global N6-methyladenosine profiling of cobalt-exposed cortex and human neuroblastoma H4 cells presents epitranscriptomics alterations in neurodegenerative disease-associated genes. *Environ Pollut*. (2020) 266:115326. doi: 10.1016/j.envpol.2020.115326

18. Cheng J, Xu L, Deng L, Xue L, Meng Q, Wei F, et al. RNA N-methyladenosine modification is required for miR-98/MYCN axis-mediated inhibition of neuroblastoma progression. *Sci Rep*. (2020) 10:13624. doi: 10.1038/s41598-020-64682-1

19. Li M, Wang J, Wang C, Xia L, Xu J, Xie X, et al. Microenvironment remodeled by tumor and stromal cells elevates fibroblast-derived COL1A1 and facilitates ovarian cancer metastasis. *Exp Cell Res*. (2020) 394:112153. doi: 10.1016/j.yexcr.2020.112153

20. Jin Y, Wang Z, He D, Zhu Y, Hu X, Gong L, et al. Analysis of m6A-related signatures in the tumor immune microenvironment and identification of clinical prognostic regulators in adrenocortical carcinoma. *Front Immunol*. (2021) 12:637933. doi: 10.3389/fimmu.2021.637933

21. Shi H, Wei J, He C. Where, when, and how: context-dependent functions of RNA methylation writers, readers, and erasers. *Mol Cell*. (2019) 74:640–50. doi: 10.1016/j.molcel.2019.04.025

22. Garaventa A, Poetschger U, Valteau-Couanet D, Luksch R, Castel V, Elliott M, et al. Randomized trial of two induction therapy regimens for high-risk neuroblastoma: HR-NBL1.5 International Society of Pediatric Oncology European Neuroblastoma Group Study. *J Clin Oncol*. (2021) 39:2552–63. doi: 10.1200/jco.20.03144

23. Sokol E, Desai A, Applebaum M, Valteau-Couanet D, Park J, Pearson A, et al. Age, diagnostic category, tumor grade, and mitosis-karyorrhexis index are independently prognostic in neuroblastoma: an INRG project. *J Clin Oncol*. (2020) 38:1906–18. doi: 10.1200/jco.19.03285

24. Pinto N, Naranjo A, Hibbitts E, Kreissman S, Granger M, Irwin M, et al. Predictors of differential response to induction therapy in high-risk neuroblastoma: a report from the Children's Oncology Group (COG). *Eur J Cancer*. (2019) 112:66–79. doi: 10.1016/j.ejca.2019.02.003

25. Giardiello D, Steyerberg E, Hauptmann M, Adank M, Akdeniz D, Blomqvist C, et al. Prediction and clinical utility of a contralateral breast cancer risk model. *Breast Cancer Res*. (2019) 21:144. doi: 10.1186/s13058-019-1221-1

26. Rosswog C, Schmidt R, Oberthuer A, Juraeva D, Brors B, Engesser A, et al. Molecular classification substitutes for the prognostic variables stage, age, and MYCN status in neuroblastoma risk assessment. *Neoplasia*. (2017) 19:982–90. doi: 10.1016/j.neo.2017.09.006

27. Ramos Elbal E, Galera Miñarro AM, Llinares Riestra ME, Bermúdez Cortés M, Fuster Soler JL. Neuroblastoma: validation of the INRG classification system in a small series. *Clin Transl Oncol*. (2019) 21:1776–80. doi: 10.1007/s12094-019-02099-7

28. Hero B, Simon T, Spitz R, Ernestus K, Gnekow A, Scheel-Walter H, et al. Localized infant neuroblastomas often show spontaneous regression: results of the prospective trials NB95-S and NB97. *J Clin Oncol*. (2008) 26:1504–10. doi: 10.1200/jco.2007.12.3349

29. Oberthuer A, Juraeva D, Hero B, Volland R, Sterz C, Schmidt R, et al. Revised risk estimation and treatment stratification of low- and intermediate-risk neuroblastoma patients by integrating clinical and molecular prognostic markers. *Clin Cancer Res*. (2015) 21:1904–15. doi: 10.1158/1078-0432.Ccr-14-0817

30. Almutairi B, Charlet J, Dallosso A, Szemes M, Etchevers H, Malik K, et al. Epigenetic deregulation of GATA3 in neuroblastoma is associated with increased GATA3 protein expression and with poor outcomes. *Sci Rep*. (2019) 9:18934. doi: 10.1038/s41598-019-55382-6

31. Domingo-Fernandez R, Watters K, Piskareva O, Stallings RL, Bray I. The role of genetic and epigenetic alterations in neuroblastoma disease pathogenesis. *Pediatr Surg Int*. (2013) 29:101–19. doi: 10.1007/s00383-012-3239-7

32. Durinck K, Speleman F. Epigenetic regulation of neuroblastoma development. *Cell Tissue Res*. (2018) 372:309–24. doi: 10.1007/s00441-017-2773-y

33. Parodi F, Carosio R, Ragusa M, Di Pietro C, Maugeri M, Barbagallo D, et al. Epigenetic dysregulation in neuroblastoma: a tale of miRNAs and DNA methylation. *Biochim Biophys Acta*. (2016) 1859:1502–14. doi: 10.1016/j.bbagrm.2016.10.006

34. Wang Z, Cheng H, Xu H, Yu X. Sui D. A five-gene signature derived from m6A regulators to improve prognosis prediction of neuroblastoma. *Cancer Biomark*. (2020) 28:275–84. doi: 10.3233/cbm-191196

35. Liu J, Cheng J, Li L, Li Y, Zhou H, Zhang J, et al. YTHDF1 gene polymorphisms and neuroblastoma susceptibility in Chinese children: an eight-center case-control study. *J Cancer*. (2021) 12:2465–71. doi: 10.7150/jca.54496

36. Oberthuer A, Hero B, Berthold F, Juraeva D, Faldum A, Kahlert Y, et al. Prognostic impact of gene expression-based classification for neuroblastoma. *J Clin Oncol*. (2010) 28:3506–15. doi: 10.1200/jco.2009.27.3367

37. Dong D, Tang L, Li Z, Fang M, Gao J, Shan X, et al. Development and validation of an individualized nomogram to identify occult peritoneal metastasis in patients with advanced gastric cancer. *Ann Oncol*. (2019) 30:431–38. doi: 10.1093/annonc/mdz001

38. Gandaglia G, Ploussard G, Valerio M, Mattei A, Fiori C, Fossati N, et al. A novel nomogram to identify candidates for extended pelvic lymph node dissection among patients with clinically localized prostate cancer diagnosed with magnetic resonance imaging-targeted and systematic biopsies. *Eur Urol*. (2019) 75:506–14. doi: 10.1016/j.eururo.2018.10.012

39. Dong D, Fang M, Tang L, Shan X, Gao J, Giganti F, et al. Deep learning radiomic nomogram can predict the number of lymph node metastasis in locally advanced gastric cancer: an international multicenter study. *Ann Oncol.* (2020) 31:912–20. doi: 10.1016/j.annonc.2020.04.003

40. Pietrantonio F, Miceli R, Rimassa L, Lonardi S, Aprile G, Mennitto A, et al. Estimating 12-week death probability in patients with refractory metastatic colorectal cancer: the Colon Life nomogram. *Ann Oncol.* (2017) 28:555–61. doi: 10.1093/annonc/mdw627

41. Yang H, Zhang X, Zhao Y, Sun G, Zhang J, Gao Y, et al. Downregulation of lncRNA XIST represses tumor growth and boosts radiosensitivity of neuroblastoma via modulation of the miR-375/L1CAM axis. *Neurochem Res.* (2020) 45:2679–90. doi: 10.1007/s11064-020-03117-9

42. Yu Y, Chen F, Yang Y, Jin Y, Shi J, Han S, et al. lncRNA SNHG16 is associated with proliferation and poor prognosis of pediatric neuroblastoma. *Int J Oncol.* (2019) 55:93–102. doi: 10.3892/ijo.2019.4813

43. Nie L, Li C, Zhao T, Wang Y, Liu J. LncRNA double homeobox A pseudogene 8 (DUXAP8) facilitates the progression of neuroblastoma and activates Wnt/β-catenin pathway via microRNA-29/nucleolar protein 4 like (NOL4L) axis. *Brain Res.* (2020) 1746:146947. doi: 10.1016/j.brainres.2020.146947

frontiers | Frontiers in Genetics

TYPE Original Research
PUBLISHED 25 October 2022
DOI 10.3389/fgene.2022.990098

Check for updates

OPEN ACCESS

EDITED BY
Ruth Roberts,
ApconiX, United Kingdom

REVIEWED BY
Sonal Rajiv Bakshi,
Nirma University, India
Rachel Michaelson,
Hebrew University of Jerusalem, Israel

*CORRESPONDENCE
Wenming Yang,
yangwm8810@126.com
Jiuxiang Wang,
wjxzx1218@163.com

SPECIALTY SECTION
This article was submitted to Genetics of Common and Rare Diseases, a section of the journal Frontiers in Genetics

RECEIVED 09 July 2022
ACCEPTED 22 September 2022
PUBLISHED 25 October 2022

CITATION
Zeng F, Yang Y, Xu Z, Wang Z, Ke H, Zhang J, Dong T, Yang W and Wang J (2022), Clinical manifestations and genetic analysis of a newborn with Arboleda–Tham syndrome. *Front. Genet.* 13:990098. doi: 10.3389/fgene.2022.990098

COPYRIGHT
© 2022 Zeng, Yang, Xu, Wang, Ke, Zhang, Dong, Yang and Wang. This is an open-access article distributed under the terms of the Creative Commons Attribution License (CC BY). The use, distribution or reproduction in other forums is permitted, provided the original author(s) and the copyright owner(s) are credited and that the original publication in this journal is cited, in accordance with accepted academic practice. No use, distribution or reproduction is permitted which does not comply with these terms.

Clinical manifestations and genetic analysis of a newborn with Arboleda–Tham syndrome

Feng Zeng[1], Yue Yang[2], Zhaohui Xu[3], Ziwen Wang[4], Huan Ke[5], Jianhong Zhang[1], Tongtong Dong[4], Wenming Yang[2]* and Jiuxiang Wang[6]*

[1]Department of Neonatology, Xuancheng Central Hospital, Xuancheng, Anhui, China, [2]Department of Neurology, The First Affiliated Hospital of Anhui University of Chinese Medicine, Hefei, Anhui, China, [3]Department of Paediatrics, The First Affiliated Hospital of Anhui University of Chinese Medicine, Hefei, Anhui, China, [4]Graduate School, Anhui University of Chinese Medicine, Hefei, Anhui, China, [5]Nursing Department, Xuancheng Central Hospital, Xuancheng, Anhui, China, [6]Experimental Center of Clinical Research, The First Affiliated Hospital of Anhui University of Chinese Medicine, Hefei, Anhui, China

Arboleda–Tham syndrome (ARTHS) is a rare disorder first characterized in 2015 and is caused by mutations in lysine (K) acetyltransferase 6A (KAT6A, a.k.a. MOZ, MYST3). Its clinical symptoms have rarely been reported in newborns from birth up to the first few months after birth. In this study, a newborn was diagnosed with ARTHS based on the clinical symptoms and a mutation c.3937G>A (p.Asp1313Asn) in KAT6A. The clinical manifestations, diagnosis, and treatment of the newborn with ARTHS were recorded during follow-up observations. The main symptoms of the proband at birth were asphyxia, involuntary breathing, low muscle tone, early feeding, movement difficulties, weak crying, weakened muscle tone of the limbs, and embrace reflex, and facial features were not obvious at birth. There was obvious developmental delay, as well as hypotonic and oro-intestinal problems in the first few months after birth. Mouse growth factor was used to nourish the brain nerves, and touching, kneading the back, passive movements of the limbs, and audio–visual stimulation were used for rehabilitation. We hope that this study expands the phenotypic spectrum of this syndrome to newborns and the library of KAT6A mutations that lead to ARTHS. Consequently, the data can be used as a basis for genetic counseling and in clinical and prenatal diagnosis for ARTHS prevention.

KEYWORDS

Arboleda–Tham syndrome, newborn, asphyxia, KAT6A, mouse growth factor

Introduction

Arboleda–Tham syndrome (MIM: 616268), also known as KAT6A syndrome, is a rare disorder mainly characterized by developmental delay, intellectual disability, and distinct facial features. It was first characterized in 2015, and initial descriptions included 10 affected cases (Tham et al., 2015). To date, about 90 patients have been reported, the youngest of which was diagnosed when 8 months old (Arboleda et al., 2015; Tham et al.,

2015; Bscch et al., 2019; Lin et al., 2020). Clinical symptoms have rarely been reported in newborns from birth up to the first few months after birth.

KAT6A protein is a lysine acetyltransferase belonging to the MYST family of acetyltransferases. It comprises 2,004 amino acids, a double PHD (plant homeodomain) zinc finger domain, a highly conserved MYST domain, a glutamate/aspartate-rich region, and a serine/methionine-rich region in the C-terminal region (Champagne et al., 1999; Champagne et al., 2001). The PHD zinc finger domains interact with histone H3 substrate and are required for the nuclear localization of chromatin (Ali et al., 2012; Dreveny et al., 2014). The MYST domain, which includes the acetyl-CoA-binding motif, enhances acetylation by binding to DNA through the zinc and helix-turn-helix motifs (Holbert et al., 2007). The glutamate/aspartate-rich region, also known as the NEMM (N-terminal part of Enok, MOZ, or MORF) domain, is conserved in *Drosophila* Enok and is important for the nuclear localization of KAT6A (Yang and Ullah, 2007). The serine/methionine-rich region possesses transcription activation activity (Kitabayashi et al., 2001).

KAT6A is an epigenetic modifier. It is a acetyltransferases acylate histone H3 and nonhistone proteins and is involved in numerous biological and developmental processes such as regulation of transcription, maintenance of hematopoietic and neural stem cells, hematopoietic cell differentiation, cell cycle, and mitosis. It interacts with BRPF1/2/3 (bromodomain–PHD finger protein), ING5 (inhibitor of growth 5), and MEAF6 (MYST/Esa1-associated factor 6) to form a tetrameric complex to acetylate lysine residues on histone H3 tails such as H3K9, H3K23, and H3K14 (Ullah et al., 2008; Qiu et al., 2012; Voss and Thomas, 2018). These histone modifications are associated with transcriptionally active genes *Tbx1*, *Tbx5T*, *Dlx5* locus, and *PI3K YAP* (Voss et al., 2012; Vanyai et al., 2019a; Vanyai et al., 2019b). *KAT6A* homozygous deletion mice ($KAT6A^{-/-}$ mice) have ventricular septal defects, and more than 50% of individuals with inactivating mutations in KAT6A or its paralog KAT6B present with ventricular septal defects and other congenital heart abnormalities (Vanyai et al., 2015; Bscch et al., 2019).

Currently, *KAT6A* is the only known ARTHS disease–causing gene, and more than 50 mutations have been identified in approximately 90 cases. This case report describes the clinical symptoms of a newborn with ARTHS from birth up to the first 17 weeks, and the treatment and genetic tests conducted.

Materials and methods

Case

This study was conducted according to the Declaration of Helsinki and was approved by the ethics committee of the Xuancheng Central Hospital (2021010). Written informed consent was obtained from the parents of the newborn. The newborn was born at the Xuancheng Central Hospital.

Exome capture, sequencing, and variation detection

Genomic DNA was isolated from the peripheral venous blood for WES to screen for the candidate causative mutation using IDT xGen Exome Research Panel and NovaSeq 6000 system (Illumina). The reads were mapped to the human reference genome (hg38) with BWA, SAMtools, and Picard software, obtaining 3.2 G bases mapped to the target exome regions with a mean depth of 183.99 times, and 99.71% of the exome was covered at least ten times. The GATK program was applied to perform base quality score recalibration, indel realignment, duplicate removal, SNP and INDEL discovery, and genotype scoring using the standard filtering parameters according to GATK. In total, 250,875 genetic variants were identified and annotated by ANNOVAR. The pathogenic variants were screened according to the ACMG classification guidelines and the clinical phenotype of the patients: 1) screening for variants and non-synonymous mutations in the exon region. 2) Screening for variants that are absent in the ExAC_EAS, ExAC_ALL, 1000 Genomes, and gnomAD databases, or minor allele frequency (MAF) < 0.01. 3) Evaluating the variants by reference to the dbSNP, OMIM, HGMD, ClinVar, and other databases. 4) Predicting the effect of variants on the protein function by SIFT, PolyPhen-2, LRT, MutationTaster, and FATHMM. Sanger sequencing was conducted to further confirm *KAT6A*. The control group comprised 100 DNA samples from healthy individuals.

Results

Clinical features of infant from birth to when 17 weeks old and treatment

The infant was born at 37 + 1 weeks by cesarean with Apgar scores of 5/7 at 1 and 5 min. He weighed 2.3 kg, was 47 cm long, and had a cranial circumference of 33 cm. The infant was asphyxiated for 31 min; he did not cry and had no suck, swallow, or gag reflex. His limbs had reduced muscle tone, undescended testicles, and a flat skull. His cardiac malformations showed an atrial septal defect of 3.0 mm, patent ductus arteriosus, and moderate pulmonary hypertension (Table 1).

After admission, he was mechanically ventilated, treated for mild hypothermia and infection, and provided with other symptomatic support. However, during the treatment, he had a poor response, low limb muscle strength, and weak sucking and swallowing function and needed nasal feeding. Due to weak spontaneous breathing, it was difficult to remove the machine. When 3 weeks old, he was changed to noninvasive auxiliary ventilation, and no seizures occurred.

At 4 weeks, the ventilator was withdrawn due to increased spontaneous breathing. His developmental delay remained

TABLE 1 Clinical characteristics of the case.

Age	1 day	4 weeks	10 weeks	17 weeks
Weight	2.3 kg	2.7 kg	4.2 kg	6 kg
Height	47 cm	50 cm	50 cm	62.5 cm
Head circumference	33 cm	34.5 cm	36.5 cm	40.5 cm
Developmental delay	Poor stimulation reaction and no crying	Dull face, poor response, no crying, and only grunts	Dull face and only a low roar	Dull face, no crying, no laugh, and a low roar
Motor dyspraxia	Hypertonicity in extremities (Grade I)	Hypertonicity in extremities and poor embrace reflex	Hypertonicity in upper extremities (Grade III), lower limbs (Grade II), and unable to raise the head	Unable to raise the head and reach unsupported sitting. Hypertonicity in extremities (upper limbs: Grade III; lower limbs: Grade II)
Oro-intestinal problems	No suck, swallow, and gag reflexes	Uncoordinated sucking and swallowing and most of the milk needs to be nasally fed	Feeding difficulties, constipation, and gastroesophageal reflux	Enhanced feeding capacity and improved coordinated sucking and swallowing. Voluntary voiding and defecation
Cardiac malformations	Atrial septal defect 3.0 mm, patent ductus arteriosus, and moderate pulmonary hypertension	Atrial septal defect 2.5 mm, patent ductus arteriosus, pulmonary hypertension, precardiac region, and ii/6 systolic murmurs	Atrial septal defect 3.2 mm and pulmonary hypertension (40 mmHg)	ND
Facial features	ND	Bilateral temporal stenosis, thin upper lip, and large low set posteriorly ears	Bilateral temporal stenosis, thin upper lip, tent-like mouth, and large low set posteriorly ears	Bilateral temporal stenosis, thin upper lip, and large low set posteriorly ears
Skull and brain abnormalities	Skull flat	Skull flat	Skull flat	Skull flat and anterior fontanelle 1 cm × 1 cm
Other clinical features and clinical guidelines	Undescended testicles	Hydrocele of tunica vaginalis	Obviously pale trunk and limbs skin, fairly white skin of hands and feet, slightly cool, and small bilateral testicles	Hospitalized pediatrics with pneumonia (recurrent respiratory infections)

ND, not defined.

evident. A head CT indicated neonatal hypoxic-ischemic encephalopathy, and the electroencephalogram presented bilateral asymmetric brain development and brain nerve cell damage. The subject had a dull face, bilateral temporal stenosis, thin upper lip, and large low set posteriorly ears and did not cry (Figure 1A). His muscle tone was in the extremities and his hug reflexes were poor. His sucking and swallowing were uncoordinated, and he received most of his milk *via* nasal feeding. The atrial septal defect was reduced to 2.5 mm with patent ductus arteriosus, pulmonary hypertension, precardiac region, and ii/6 systolic murmurs. Bilateral testicular B-ultrasound showed a left inguinal region; cryptorchidism was considered; and the right testicle was not detected (Table 1). Mouse growth factor was used to nourish the brain nerves with three courses of 30 μg by intramuscular injection once every other day (QOD) for 10 days. He also received rehabilitation such as touching, kneading the back, passive movement of limbs, audio–visual stimulation, and so on.

At 10 weeks, the infant only made a low roar, and feeding remained difficult with constipation and gastroesophageal reflux. He could not raise his head, and hypertonicity in the upper extremities was grade III and grade II in the lower limbs. His atrial septal defect was 3.2 mm, pulmonary hypertension was 40 mmHg, and hands and feet were obviously pale (Figures 1B–E). The baby also had small bilateral testicles.

At 17 weeks, he weighed 6.0 kg, measured 62.5 cm, and had a cranial circumference of 40.5 cm ($<P_3$). The infant did not cry or laugh and only made a low roar. He was still unable to raise his head and sit without support, and failed to reach for subjects. Hypertonicity in his upper limbs was grade III and grade II in the lower limbs. His feeding capacity was enhanced, and his coordination of sucking and swallowing had improved (Table 1). He could voluntarily void and defecate (Figures 1F–H). According to the clinical phenotypes of the proband, the patient may have ARTHS.

Clinical symptoms of other family members

The infant was the second child of his parents, and the first child (III:1) was a boy who died at about 3 months (Figure 2A). He was born at 37 + 2 weeks because of a decreased fetal heart rate. At birth, he weighed 3.250 g with normal amniotic fluid, low Apgar score, soft limbs, atrial septal defect (3 mm), and unexplained progressive aggravation of respiratory distress in the first hours after birth. He was assisted by mechanical ventilation through endotracheal intubation for 1 month and mainly fed by nasal feeding until 2 months old. After 2 months, he sounded a low roar; his upper limbs could move autonomously, but he could not move his legs; and his muscle strength was significantly reduced. At about



FIGURE 1
Clinical features of the infant from birth to when 17 weeks old. The newborn at 4 weeks **(A)**, 10 weeks **(B–E)**, and 17 weeks **(F–H)**. The infant shows characteristic features of Arboleda–Tham syndrome, e.g., broad nasal tip, thin upper lip, and tented mouth. A hemangioma was on the top of his head in the 10th week. Hands and feet skin color was fair and slightly cool in the 17th week.

3 months, he died of asphyxia due to milk reflux aspiration at night, so his DNA was unavailable. According to his parents, he presented with a dull face, cape mouth, and large ears.

II:1 was a 30-year-old female with slight cognitive impairment and expressive language disorder; nonverbal communication was better than verbal communication (Figure 3). II:3 was 26 years old, also with moderate cognitive impairment and expressive language disorder (Figure 2A). Their parents denied that either had other abnormalities other than intelligence. II:4 was a boy born over 30 years ago and had died 2 days after his birth without definitive pathogenesis; other growth and development defects were unclear. The grandparents of the infant presented no obvious clinical manifestations.

Mutation c.3937G > A (p.Asp1313Asn) in *KAT6A* causing Arboleda–Tham syndrome

There are few reports of newborns with ARTHS, so WES was performed to detect the pathogenic variant (Figure 2B). WES produced about 2.98 MB sequences, and 99.71% of the exome was covered at least 10 times. Filtering of common sequence changes resulted in 250,875 variants, of which 6 variants in *PHKA2*, *TTN*, *CACNA1S*, *KAT6A*, and *CUL7* were associated with the subject (Supplementary Table S1).

The *de novo* c.3937G>A variant of the *KAT6A* gene (NM_006766.5) is located in exon 17, which changes aspartic acid (Asp) to asparagine (Asn) at codon 1313 (Figures 4A,B). This variant was confirmed by Sanger sequencing (Supplementary Table S2) and was absent in 100 healthy individuals. Furthermore, Sanger studies showed that the newborn's mother carried this variant, but it was not detected in the father (Figure 2C). Evolutionary conservation analysis of the amino acid sequences of KAT6A proteins from different species shows that the impaired amino acid residue is highly evolutionarily conserved (Figure 4C), and SIFT (http://sift-dna.org) analysis showed that the variant was detrimental. The clinical features of the newborn were similar to ARTHS, so it was concluded that this *de novo* variant was the cause of this disease in the present family.

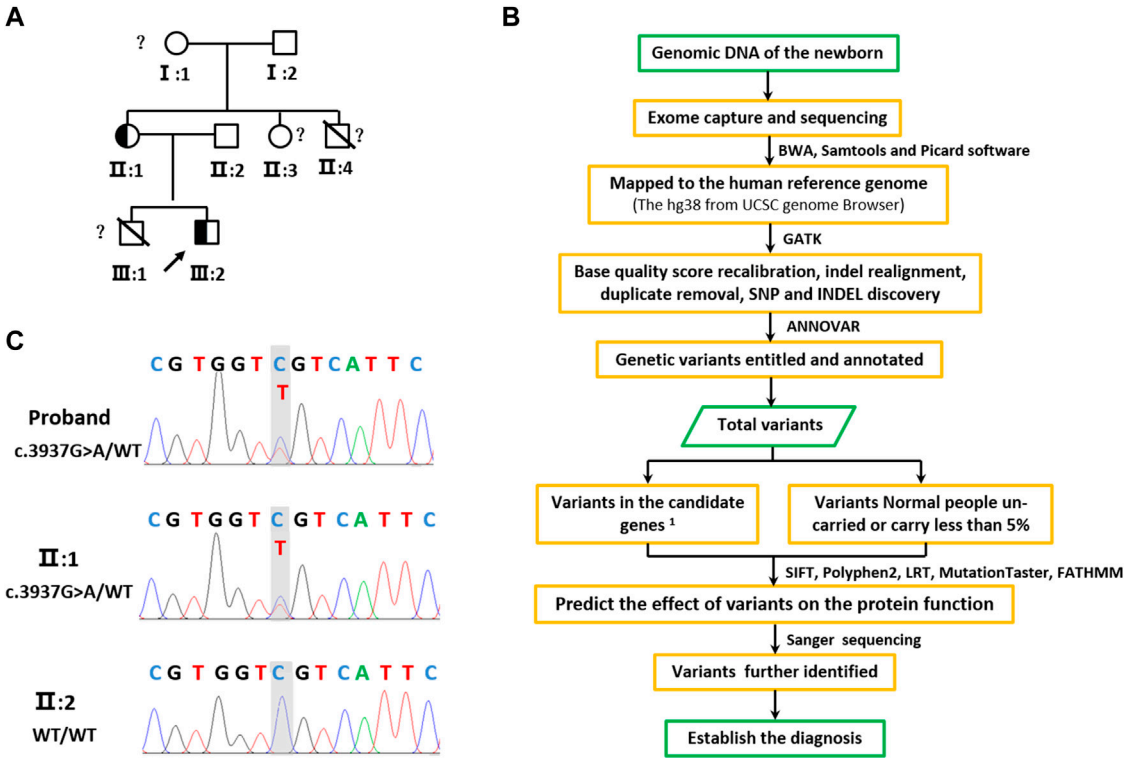


FIGURE 2
Pedigree tree and identified of KAT6A c.3937G>A variation. **(A)** Family pedigree. Black symbols indicate mutation carriers, while the other symbols indicate normal carriers. The arrow indicates the family proband. The peripheral blood genomic DNA of II:2 was used for WES. The peripheral blood genomic DNA of individuals II:1, II:2, and III:2 was used for Sanger sequencing. **(B)** Sequencing of the heterozygous variation c.3937G>A in the KAT6A gene of family members II:1, II:2, and the proband (III:1). Genome-wide exon sequencing and variants screening 1based on the disease and/or phenotypes and also 2based on the reports in OMIM, HGMD, and ClinVar.

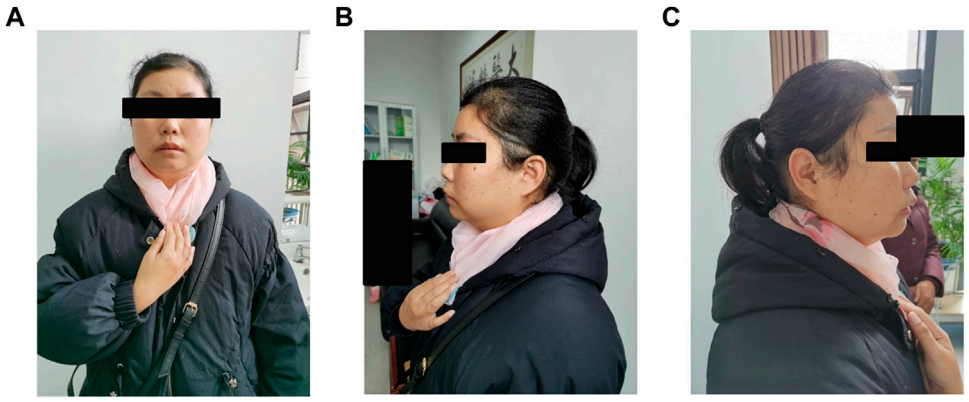


FIGURE 3
(A–C) Photos of the proband's mother. Physical characteristic features of this syndrome, such as bitemporal narrowing, broad nasal tip, low set ears, thin upper lip, micrognathia, and smooth philtrum are not observed.

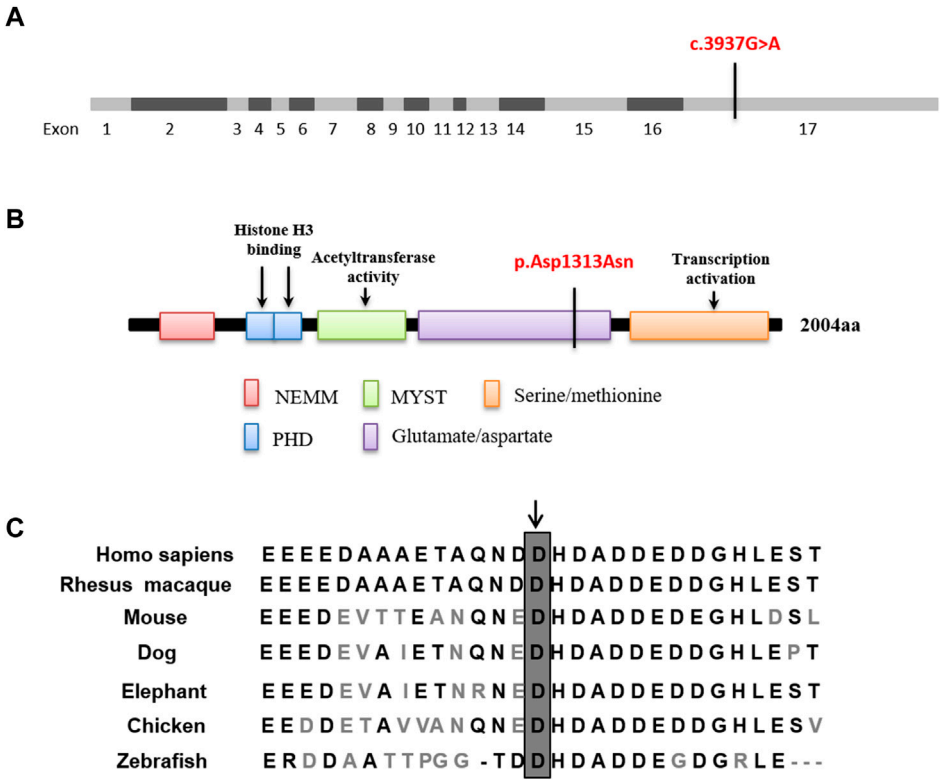


FIGURE 4
In silico analysis. **(A,B)** The *de novo* mutation c.3937G>A located in exon 17 which is predicted to lead to a missense mutation in the glutamate/aspartate domain. **(C)** Evolutionary conservation of the missense mutation. Sequence alignment of amino acids reveals that the amino acid at 1313 is highly conserved across different species.

Discussion

ARTHS manifests as a developmental delay, with about 90 patients being reported within 7 years. This case report describes the clinical features and treatment of one neonate with ARTHS from birth to when 17 weeks old. The main symptoms of ARTHS at birth were asphyxia, involuntary breathing, low muscle tone, early feeding, movement difficulties, weak crying, weakened muscle tone of the limbs, and embrace reflex. There was obvious developmental delay, as well as hypotonic and oro-intestinal problems in the first few months after birth (Table 1). Notably, the facial features were not obvious at birth.

Most neonatal genetic diseases have an early onset and progress rapidly with heterogeneous symptoms. Common manifestations include low muscle tone, feeding difficulty, respiratory failure, developmental delay, epilepsy, etc., therefore early diagnosis is difficult. The symptoms presented in this study will expand our understanding of the neonatal symptoms of ARTHS and provide a useful reference for clinical treatment.

At present, ARTHS cases are sporadic or inherited in autosomal dominant ways (Arboleda et al., 2015; Tham et al., 2015; Satoh et al., 2017; Bscch et al., 2019). In this study, the analysis of parental genotypes indicated that KAT6A c.3937G>A (p.Asp1313Asn) was transmitted by the newborn's mother, but the mother was only mildly retarded (Figure 2C). There were two boys in the family who had died within 3 months of their birth, but the cause of their death was unclear, and III:1 presented ARTHS facial symptoms (Figure 2A). They were considered ARTHS, but detecting their genotypes and confirming this diagnosis was impossible. However, these results suggest that ARTHS could be inherited through incomplete penetrance.

KAT6 catalyzes the acetylation of lysine residues on histones and nonhistone proteins, playing a key role in regulating gene expression *via* modification of histone lysine residues that modulate chromatin organization. As an epigenetic modifier, the effect of pathogenic KAT6 variants is probably affected by both the genetic background and different environmental conditions, such as the abundance of acyl-CoAs and the metabolic status of the cell (Johayra et al., 2017; Voss and Thomas, 2018). This may be why there are currently no typical ARTHS symptoms in this family. The phenotypic characteristics such as developmental delay and ID, facial dysmorphism, speech delay, hypotonia, and cardiac defects are

common in patients with ARTHS. There is also phenotypic variability between individual patients and rare features in a few patients affected by other variations apart from the KAT6A mutation. KAT6 deficiency or KAT6A harboring loss-of-function mutations regulates various developmental processes in mice and zebrafish. Homozygous deletion of the KAT6A gene in mice has resulted in high penetrance of ventricular septal defects. Ventricular septal defects and other congenital heart abnormalities are present in more than 50% of individuals with inactivating mutations in the KAT6A or KAT6B genes (Tham et al., 2015).

In summary, this is the first report to describe the clinical symptoms of a newborn with KAT6A mutation in the first months after birth and adds to the patient clinical data of ARTHS, especially symptoms in newborns. Also, the disease may be inherited through incomplete penetrance, so it should be considered cautiously.

Data availability statement

All datasets generated for this study are included in the article/supplementary material.

Ethics statement

The studies involving human participants were reviewed and approved by the Nursing Department, Xuancheng Central Hospital, Xuancheng, Anhui, 2021010. Written informed consent to participate in this study was provided by the participant's legal guardian/next of kin. Written informed consent was obtained from the individual(s) and minor(s)' legal guardian/next of kin for the publication of any potentially identifiable images or data included in this article.

Author contributions

FZ, JW, and WY conceived the project. YY and TD assisted in collecting the samples and patients' messages. FZ, WY, ZX, HK, and JZ participated in the clinical diagnosis. JW analyzed the data. YY and ZW performed the experiments. FZ drafted the manuscript. FZ, JW, and WY participated in reviewing, editing, and revising the manuscript. All the authors reviewed the manuscript and approved the submission.

Funding

The work was supported by the National Natural Science Foundation of China (Nos. 81703109 and 81803116), the Scientific Research Project of Anhui Higher Education Institution (KJ2021A0548), and the Natural Science Foundation of Anhui University of Chinese Medicine (2017zryb020).

Conflict of interest

The authors declare that the research was conducted in the absence of any commercial or financial relationships that could be construed as a potential conflict of interest.

Publisher's note

All claims expressed in this article are solely those of the authors and do not necessarily represent those of their affiliated organizations, or those of the publisher, editors, and reviewers. Any product that may be evaluated in this article, or claim that may be made by its manufacturer, is not guaranteed or endorsed by the publisher.

Supplementary material

The Supplementary Material for this article can be found online at: https://www.frontiersin.org/articles/10.3389/fgene.2022.990098/full#supplementary-material

References

Ali, M., Yan, K., Lalonde, M. E., Degerny, C., Rothbart, S. B., Strahl, B. D., et al. (2012). Kutateladze TG tandem PHD fingers of MORF/MOZ acetyltransferases display selectivity for acetylated histone H3 and are required for the association with chromatin. *J. Mol. Biol.* 424 (5), 328–338. doi:10.1016/j.jmb.2012.10.004

Arboleda, V. A., Lee, H., Dorrani, N., Zadeh, N., Willis, M., Macmurdo, C. F., et al. (2015). De novo nonsense mutations in KAT6A, a lysine acetyl-transferase gene, cause a syndrome including microcephaly and global developmental delay. *Am. J. Hum. Genet.* 96, 498–506. doi:10.1016/j.ajhg.2015.01.017

Bscch, J. K., Mbchb, D. G., Mbchb, E., Bchir, K., Med, S., Mckay, V., et al. (2019). KAT6A syndrome: Genotype–phenotype correlation in 76 patients with pathogenic KAT6A variants. *Genet. Med.* 21, 850–860. doi:10.1038/s41436-018-0259-2

Champagne, N., Bertos, N. R., Pelletier, N., Wang, A. H., Vezmar, M., Yang, Y., et al. (1999). Identification of a human histone acetyltransferase related to monocytic leukemia zinc finger protein. *J. Biol. Chem.* 274, 28528–28536. doi:10.1074/jbc.274.40.28528

Champagne, N., Pelletier, N., and Yang, X. (2001). The monocytic leukemia zinc finger protein MOZ is a histone acetyltransferase. *ONCOGENE* 20, 404–409. doi:10.1038/sj.onc.1204114

Dreveny, I., Deeves, S. E., Fulton, J., Yue, B., Messmer, M., Bhattacharya, A., et al. (2014). The double PHD finger domain of MOZ/MYST3 induces α-helical structure of the histone H3 tail to facilitate acetylation and methylation sampling and modification. *Nucleic Acids Res.* 42, 822–835. doi:10.1093/nar/gkt931

Holbert, M. A., Sikorski, T., Carten, J., Snowflack, D., Hodawadekar, S., and Marmorstein, R. (2007). The human monocytic leukemia zinc finger histone acetyltransferase domain contains DNA-binding activity implicated in chromatin targeting. *J. Biol. Chem.* 282, 36603–36613. doi:10.1074/jbc.M705812200

Johayra, S., Simone, S., Zuo-Fei, Y., Marie, C., Natarajan, V. B., Dylan, M. M., et al. (2017). Characterization of histone acylations links chromatin modifications with metabolism. *Nat. Commun.* 8 (1), 1141. doi:10.1038/s41467-017-01384-9

Kitabayashi, I., Aikawa, Y., Nguyen, L. A., and Al, E. (2001). Activation of AML1-mediated transcription by MOZ and inhibition by the MOZ-CBP fusion protein. *EMBO J.* 20, 7184–7196. doi:10.1093/emboj/20.24.7184

Lin, Y. F., Lin, T. C., Kirby, R., Weng, H. Y., Yang, C. F., Niu, D. M., et al. (2020). Diagnosis of Arboleda-Tham syndrome by whole genome sequencing in an Asian boy with severe developmental delay. *Mol. Genet. Metab. Rep.* 25, 100686. doi:10.1016/j.ymgmr.2020.100686

Qiu, Y., Liu, L., Chen, Z., Han, C., Shi, Y., Zhang, J., et al. (2012). Combinatorial readout of unmodified H3R2 and acetylated H3K14 by the tandem PHD finger of MOZ reveals a regulatory mechanism for HOXA9 transcription. *Genes Dev.* 26, 1376–1391. doi:10.1101/gad.188359.112

Satoh, C., Maekawa, R., Kinoshita, A., Mishima, H., Doi, M., Miyazaki, M., et al. (2017). Three brothers with a nonsense mutation in KAT6A caused by parental germline mosaicism. *Hum. Genome Var.* 4, 17045. doi:10.1038/hgv.2017.45

Tham, E., Lindstrand, A., Santani, A., Malmgren, H., Nesbitt, A., Dubbs, H. A., et al. (2015). Dominant mutations in KAT6A cause intellectual disability with recognizable syndromic features. *Am. J. Hum. Genet.* 96, 507–513. doi:10.1016/j.ajhg.2015.01.016

Ullah, M., Pelletier, N., Lin, X., Zhao, S. P., Wang, K., Degerny, C., et al. (2008). Molecular architecture of quartet MOZ/MORF histone acetyltransferase complexes. *Mol. Cell. Biol.* 28, 6828–6843. doi:10.1128/MCB.01297-08

Vanyai, H. K., Garnham, A., May, R. E., Mcrae, H. M., Voss, A. K., Wilcox, S., et al. (2019). MOZ directs the distal-less homeobox gene expression program during craniofacial development. *Development* 146, v175042. doi:10.1242/dev.175042

Vanyai, H. K., Garnham, A., May, R. E., Mcrae, H. M., Voss, A. K., Wilcox, S., et al. (2019). MOZ directs the distal-less homeobox gene expression program during craniofacial development. *DEVELOPMENT* 146, v175042. doi:10.1242/dev.175042

Vanyai, H. K., Thomas, T., and Voss, A. K. (2015). Mesodermal expression of Moz is necessary for cardiac septum development. *Dev. Biol.* 403, 22–29. doi:10.1016/j.ydbio.2015.04.011

Voss, A. K., and Thomas, T. (2018). Histone lysine and genomic targets of histone acetyltransferases in mammals. *BIOESSAYS* 40, 1800078. doi:10.1002/bies.201800078

Voss, A. K., Vanyai, H. K., Collin, C., Dixon, M. P., Mclennan, T. J., Sheikh, B. N., et al. (2012). MOZ regulates the Tbx1 locus, and moz mutation partially phenocopies DiGeorge syndrome. *Dev. Cell* 23, 652–663. doi:10.1016/j.devcel.2012.07.010

Yang, X. J., and Ullah, M. (2007). MOZ and MORF, two large MYSTic HATs in normal and cancer stem cells. *ONCOGENE* 26, 5408–5419. doi:10.1038/sj.onc.1210609

frontiers | Frontiers in Genetics

TYPE Case Report
PUBLISHED 01 November 2022
DOI 10.3389/fgene.2022.972598

Check for updates

OPEN ACCESS

EDITED BY
Tieliu Shi,
Hunan University of Arts and Science, China

REVIEWED BY
Sevgi Kalayoglu-Besisik,
Istanbul University, Turkey
Gaetano Isola,
University of Catania, Italy

*CORRESPONDENCE
Dingyu Duan,
dduan2016@163.com
Panpan Wang,
wangpp5@mail.sysu.edu.cn

†These authors have contributed equally to this work and share first authorship

SPECIALTY SECTION
This article was submitted to Genetics of Common and Rare Diseases, a section of the journal Frontiers in Genetics

RECEIVED 18 June 2022
ACCEPTED 10 October 2022
PUBLISHED 01 November 2022

CITATION
Lao Z, Fu J, Wu Z, Zhu L, Wu S, Lin Y, Hu C, Duan D and Wang P (2022), Case report: Five-year periodontal management of a patient with two novel mutation sites in ELANE-induced cyclic neutropenia.
Front. Genet. 13:972598.
doi: 10.3389/fgene.2022.972598

COPYRIGHT
© 2022 Lao, Fu, Wu, Zhu, Wu, Lin, Hu, Duan and Wang. This is an open-access article distributed under the terms of the Creative Commons Attribution License (CC BY). The use, distribution or reproduction in other forums is permitted, provided the original author(s) and the copyright owner(s) are credited and that the original publication in this journal is cited, in accordance with accepted academic practice. No use, distribution or reproduction is permitted which does not comply with these terms.

Case report: Five-year periodontal management of a patient with two novel mutation sites in *ELANE*-induced cyclic neutropenia

Zhentao Lao[1†], Jiarun Fu[1†], Zhiying Wu[2], Lihong Zhu[3], Shiwen Wu[1], Yongheng Lin[1], Chaoming Hu[4], Dingyu Duan[5]* and Panpan Wang[1,6]*

[1]Guangdong Provincial Key Laboratory of Stomatology, Guanghua School of Stomatology, Sun Yat-Sen University, Guangzhou, Guangdong, China, [2]Department of Microbiology, Key Laboratory for Tropical Diseases Control of the Ministry of Education, Zhongshan School of Medicine, Sun Yat-sen University, Guangzhou, Guangdong, China, [3]Department of Stomatology, The Second Clinical Hospital of Jinan University, Shenzhen People's Hospital, Shenzhen, China, [4]Institute of Stomatology, School and Hospital of Stomatology, Wenzhou Medical University, Wenzhou, China, [5]State Key Laboratory of Oral Diseases, Department of Periodontology, National Clinical Research Center for Oral Diseases, West China School and Hospital of Stomatology, Sichuan University, Chengdu, China, [6]Department of Periodontology, Guanghua School and Hospital of Stomatology, Sun Yat-sen University, Guangzhou, Guangdong, China

Cyclic neutropenia (CyN) is a rare, *ELANE*-related neutropenia. Oral manifestations are among the initial signs of CyN and an important reason that leads patients to seek professional help. This case report describes a 12-year-old girl with recurrent oral ulcers, severe chronic periodontitis, and pathological tooth migration as the initial and main clinical symptoms of CyN. Two novel mutations in *ELANE*, c.180T>G (p.I60M) and c.182C>G (p.A61G) associated with CyN were observed. Bioinformatics research indicated lower stability and impaired molecular linkages of the mutant neutrophil elastase (NE) encoded by *ELANE*. However, the enzyme affinity to the classic substrate Suc−Ala−Ala−Ala−pNA was not substantially changed, suggesting that the impaired integrity and stability of the mutant NE, rather than catalytic deficiency, might be the pathogenic mechanism of *ELANE* mutation-induced neutropenia. The patient was prescribed scaling and root planing (SRP) and monthly periodontal maintenance without systemic management. Although the routine periodontal treatment was occasionally interrupted by the 2019 coronavirus pandemic, her periodontal devastation remained well-remitted in the 5-year follow-up assessment. The results of this study confirmed the importance of plaque control and proper diagnosis in the periodontal management of such patients and provide better clinical references. In addition, the novel mutations identified in this study expand the spectrum of known *ELANE* mutations in CyN and further contribute to knowledge regarding its pathogenic mechanism.

KEYWORDS

cyclic neutropenia, *ELANE* gene, periodontitis, tooth displacement, oral manifestation, case report

Introduction

Cyclic neutropenia (CyN) is a rare hematological disease characterized by recurrent peripheral neutropenia involving cycles with 21-day intervals (Dale and Hammond, 1988; Dale et al., 2000). Associated symptoms such as fever, malaise, headaches, respiratory infections, and abdominal discomfort commonly accompany this condition (Lakshman and Finn, 2001). Each episode lasts for 3–6 days, and the affected individuals are generally normal between bouts. The predictable cyclicity is always used in differential diagnosis with severe congenital neutropenia (SCN), which manifests as more serious and sustained neutropenia (Horwitz et al., 2013; Skokowa et al., 2017). A total of 80–100% of CyN and 35–63% of SCN cases are caused by heterozygous mutations in *ELANE*, which maps to chromosome 19p13.3 and encodes neutrophil elastase (NE). Aberrant NE is thought to accelerate the apoptosis of maturing neutrophil precursors, subsequently decreasing the peripheral neutrophil count (Nanua et al., 2011; Walter and Ron, 2011; Borregaard, 2014; Rydzynska et al., 2021). The pathogenic genetic variants of CyN and SCN differ and the clinical presentations vary according to the mutations. In addition, age, hormones, and environmental factors may also contribute to the corresponding clinical manifestations.

Patients with CyN always exhibit oral manifestations, including recurrent aphthous ulcers (RAU), gingivitis, severe periodontitis, and the concomitant inflammatory mediator increases (Ródenas et al., 1992; Isola et al., 2020). Oral manifestations may be the first symptom in patients with CyN and may easily be misdiagnosed in dental clinics. In addition, these symptoms usually occur around early childhood and persist after adolescence, leading to a premature loss of permanent teeth and poor oral function. Therefore, early diagnosis and management of this complicated condition are challenging but essential. Herein, we report the case of a 12-year-old girl affected by CyN with oral manifestation (RAU and advanced periodontal destruction) as the first and sole symptom. This case presented two spontaneous mutations in exon2 of *ELANE*, c.180T>G (p.I60M) and c.182C>G (p.A61G), not previously reported in CyN. Scaling and root planing (SRP) along with monthly periodontal maintenance were performed. After 5 years of follow-up, the patient showed retardation of periodontal decline, with no tooth loss and little alveolar bone absorption. This case expands the spectrum of known mutations of congenital neutropenia, contributes new insights into the pathological mechanism of congenital neutropenia, verifies the importance of early diagnosis and plaque control, and summarizes our experiences.

Case report

A 12-year-old Chinese girl visited Shenzhen People's Hospital with a chief complaint of tooth displacement. Her parents had noticed tooth mobility and migration, red and swollen gums, and recurrent ulcers for the past 4 years.

This patient had had RAU since 4 years of age. After she reached menarche at 11 years, the RAU showed exacerbation during her menstrual period. Her general growth was adequate for her age, and she had a healthy mental and physical status, except for the oral symptoms. At 18 days of age, the patient developed hyperpyrexia and pneumonia after *Bacillus* Calmette-Guerin vaccination. Before 2 years of age, the patient had shown occasional skin pustulosis. She was diagnosed with hyper-IgE syndrome at 2 years of age and was administered thymopeptide for 6 months until her IgE levels returned to normal. During treatment, the doctors once noted a decrease in white blood cell counts but did not recommend further treatment. Similar symptoms were not observed in any of the three generations of her family. The patient's parents and younger sister were healthy and without immunological diseases. The patient brushed her teeth twice daily, 1–2 min each time, in a horizontal brushing motion, without using dentin floss or an interproximal brush, and had no bad habits.

The initial examination revealed that the marginal and attached gingiva was fiery red, swollen, and bled on contact (Figure 1A). The periodontal examination revealed general and deep periodontal pockets (6–9 mm). Teeth 16, 14, and 41 showed class III mobility, while teeth 21, 24, 25, 32, and 36 showed class II mobility. The patient also showed tooth migration and malocclusion, as well as poor oral hygiene. As the severe bone loss was not consistent with the dental plaque accumulation, further investigation for hematological disorders was initiated. A severe decrease in neutrophil count (280/μL), mildly decreased peripheral leukocyte count (3,340/μL), and mildly increased monocyte count (1,280/μL) were observed. The lymphocyte, eosinophil, and basophil counts were within normal limits (Supplementary Table S1). However, the peripheral smear results showed a severe decrease in segmented neutrocytes (2%), an increased monocyte proportion (41%), as well as mildly increased eosinophilic granulocytes (11%), basophilic granulocytes (2%), and lymphocytes (44%). The morphology and quantity of the erythrocytes and blood platelets were normal. Therefore, the patient was diagnosed with neutropenia. Combined with the early onset of symptoms and long course of recurring inflammation, the tentative diagnosis was congenital neutropenia. Antibody screening for anti-neutrophil cytoplasmic protease antibody PR3-ANCA (-), and anti-neutrophil cytoplasmic myeloperoxidase antibody (-) were performed to preclude autoimmune diseases (Supplementary Table S3). PCR screening for Epstein–Barr virus DNA (EBV-DNA) (-) and human cytomegalovirus DNA (HCMV-DNA) (-) was used to eliminate infectious diseases (Supplementary Table S3). The patient's lack of special drug use and toxic substance exposure further excluded other potential acquired neutropenia. Her phosphorus level was slightly elevated (1.7 mmol/L) and her serum potassium, sodium, chloride, and calcium levels were

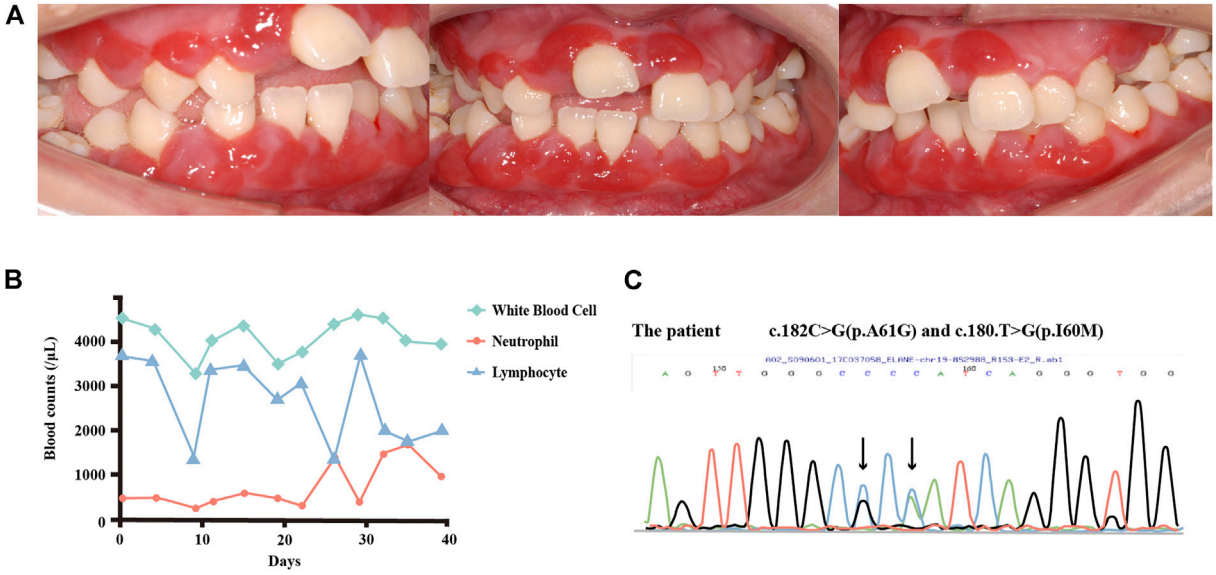


FIGURE 1
(A) Intraoral view of the patient in 2017. The marginal and attached gingiva were fiery red, with swelling and bleeding on contact. **(B)** Changes in the white blood cell, neutrophil, and lymphocyte counts over 6 weeks. The patient's neutrophil counts appeared to cycle between 200/μL and 1,500/μL, with the lymphocyte counts showing an inverse cycle pattern. **(C)** DNA sequence analysis of *ELANE*. The patient carries two spontaneous mutations. As both forward and reverse sequences can be used for verification in Sanger sequencing, the bases in the peak diagram may be the reverse complementary sequence of the detected bases. For instance, in c.180T > G, T > G is shown as A > C in the peak diagram.

within normal limits (Supplementary Table S2). Her $CD3^+CD4^+$(23.6%) and $CD4^+/CD8^+$Th/Ts (0.54%) levels were lower, while her IgG1 (17.40 g/L), IgG2 (7.85 g/L), and IgG3 (1.21 g/L) concentrations were above the normal limits (Supplementary Table S2). All other clinical findings are shown in Supplementary Table S4.

DNA sequencing was performed of samples from the patient and her parents to further confirm the diagnosis. No *ELANE* mutations were detected in the samples from her parents. Mutational analyses of the patient's sample revealed two substitutions in the 180th base (T to G), causing the amino acid substitution p.I60M, and in the 182nd base (C to G), causing the amino acid substitution p.A61G in exon2 (Figure 1C). These mutations were previously reported in patients with SCN (Xia et al., 2009) but had not yet been related to the cyclicity characteristics of CyN. The patient was then referred to Shenzhen Children's Hospital, where blood tests were conducted over 6 weeks. The evaluations of neutrophil count revealed a slight fluctuation between 200–500/μL during the first 3 weeks, which increased to 1,500/μL on the 25th day, before starting the following cycle with a greater amplitude (Figure 1B). An inverse trend in lymphocyte counts was observed, along with an oscillatory pattern in neutrophil count. A timeline with relevant examination, diagnosis, and treatment information is presented in Supplementary Figure S2.

After the final diagnosis of CyN, RAU, and periodontitis associated with systemic disease, the patient was referred to West China Hospital at Sichuan University for treatment. The periodontal examination revealed extensive and deep periodontal pockets, with depths reaching 6–10 mm around teeth 16, 14, 12, 11, 21, 24, 25, 31, 33, and 41–45. Severe gingival recessions of 4–7 mm were recorded at teeth 16, 14, 21, 25, and 46. Superficial dentin caries was observed on the occlusal surfaces of teeth 37 and 47 (Figures 2A,C). Panoramic radiography revealed generalized severe horizontal bone loss (Figure 2B). Obvious bone absorption was noted in the furcation areas of teeth 16 and 46. The recommended treatment plan was as follows:

1. Oral hygiene instructions (OHI),
2. Extraction of tooth 14,
3. SRP and local administration of minocycline ointment,
4. Resin filling restorations for teeth 37 and 47,
5. Periodontal maintenance before each menstruation,
6. Extraction of hopeless teeth at age 18 years,
8. Prosthetic rehabilitation.

The initial periodontal therapy included SRP, education, pharmacology, self-care, and occlusal adjustment. We performed careful periodontal maintenance every month before each menstruation. Minocycline ointment (Periocline; Sunstar Co., Japan) was applied to the periodontal pockets.

Since the patient was clinically well, without major systemic infections or complications, we did not recommend systemic

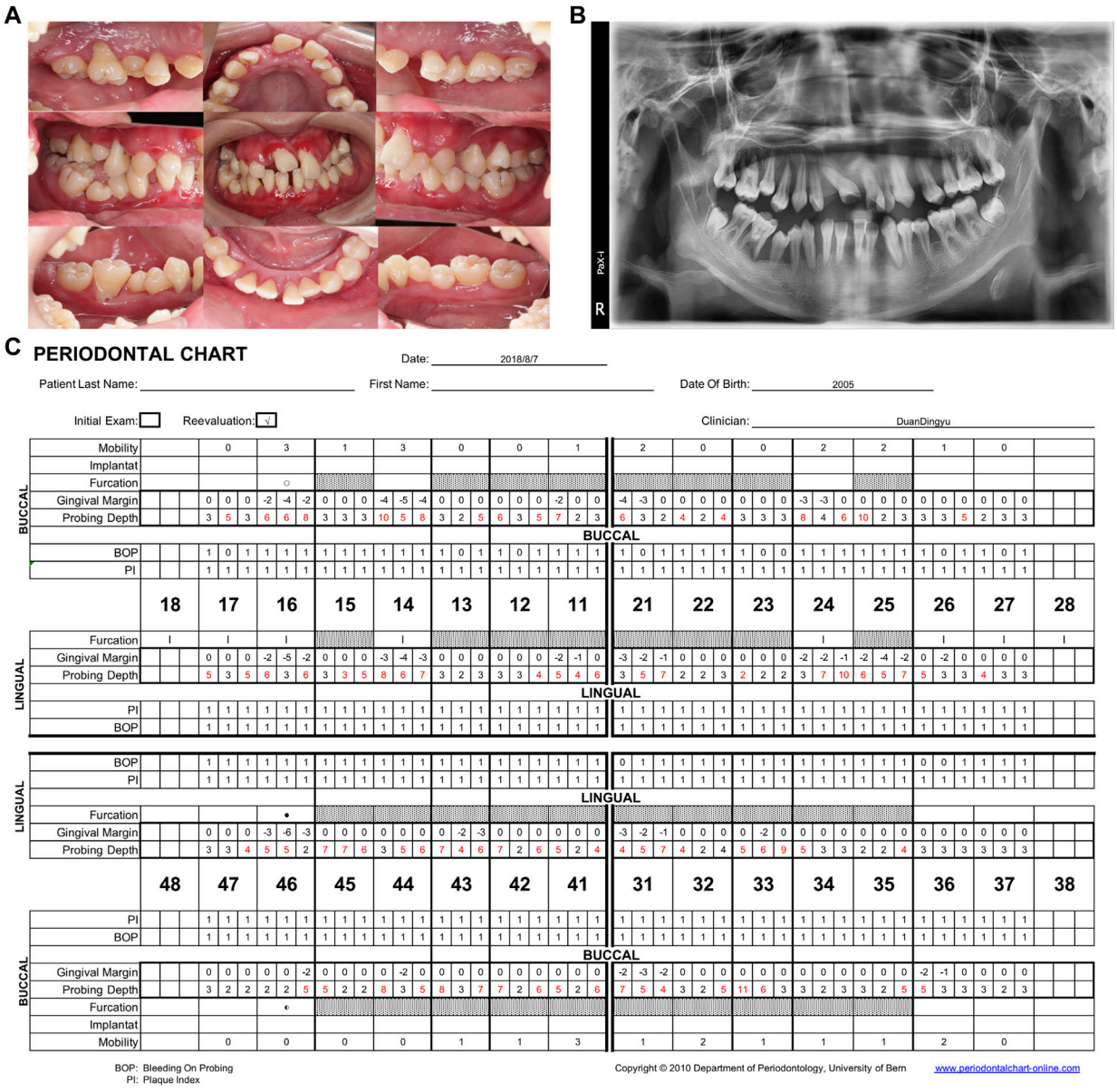


FIGURE 2
Follow-up examination in 2018. **(A)** Intraoral view showing redness, gingiva swelling and recession, irregular tooth alignment, and serious occlusion disorder. **(B)** Panoramic radiograph showing general disappearance of the lamina dura and complete horizontal absorption of the alveolar bone to 1/2–2/3 of the root length. The alveolar bone loss of 14, 16, 24, 25, and 46 involved the apical roots. **(C)** Periodontal chart. 93% bleeding on probing, mean PD: 4.2 mm. PD, probing depth.

administration following a comprehensive assessment of the risks and benefits. However, in January 2022, the patient developed a fever and was admitted to the hospital, where she received piperacillin–tazobactam, oseltamivir, and granulocyte colony-stimulating factor (G-CSF) therapy. As shown in Supplementary Figure S1, her neutrophil and WBC counts increased to normal after 3 days of G-CSF administration. The RAU was relieved after G-CSF therapy and antibiotic treatment.

After 5 years of periodontal follow-up, no extra teeth were lost, and the progression of periodontitis showed a degree of retardation. In contrast with the first visit in 2018, the bleeding on probing (50% in 2022 *versus* 93% in 2018) had decreased and the probing depth (mean PD: 3.9 mm in 2022 *versus* mean PD: 4.2 mm in 2018) had lessened considerably (Figure 3).

We then established a predictable tertiary structure of mutational neutrophil elastase through SWISS-MODEL

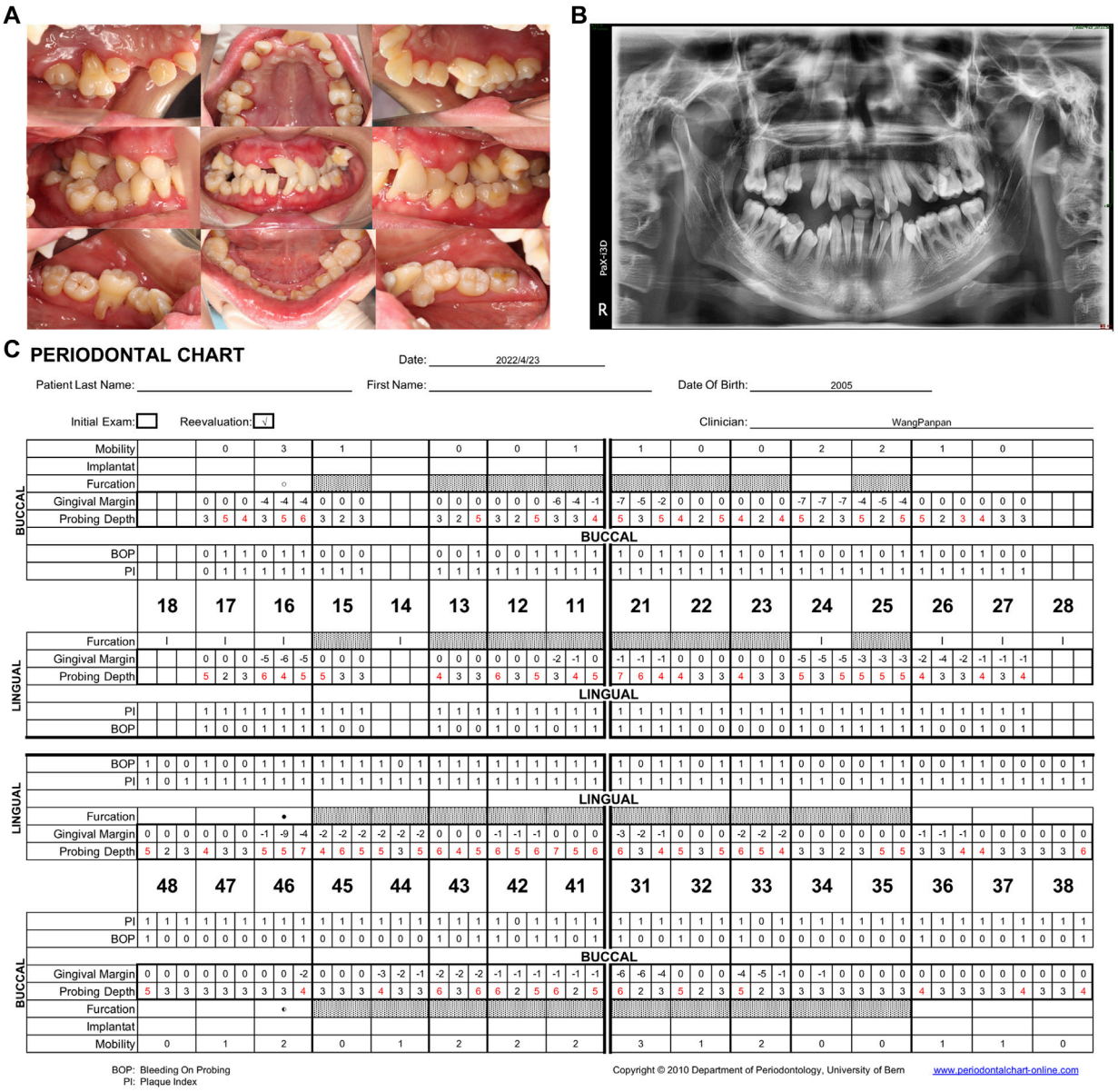


FIGURE 3
(A) Intraoral view in the Hospital of Stomatology, Sun-Yat sen University in 2022. After 5 years of follow-up, the gingival swelling and redness were reduced. **(B)** Panoramic radiograph showing general horizontal bone loss of 1/3–2/3 of the root length. **(C)** Periodontal chart. Specialized periodontal examination record of the patient after the 5-year follow-up. 50% bleeding on probing, mean PD: 3.9 mm. PD, probing depth.

homologous modeling (https://swissmodel.expasy.org/) and further characterized the NE modification using bioinformatics approaches. NE with the protein database bank ID 1b0f was used as the reference structure. The intra-molecular interactions around the mutant amino acids are depicted in Figure 4. As the ribbon diagram shows, the Ile60 and Ala61 residues are located at the beta-sheet and beta-turn areas, respectively. They are connected to Phe64 by three hydrogen bonds in wild-type NE. In the NE mutant, the three H-bonds between the 60th, 61st, and phe64 remained, but the bond lengths had increased, indicating weakened connections. Mutational energy calculations performed using the Discovery Studio server with a CHARMm force field revealed a dramatic reduction in stability of the double-mutated amino acid sequence, with a mutation energy of +4.18 kcal/mol. We also used Autodock Vina to predict the change in NE catalytic performance according to NE active pocket affinity with the classical substrate Suc–Ala–Ala–Ala–pNA. However, we

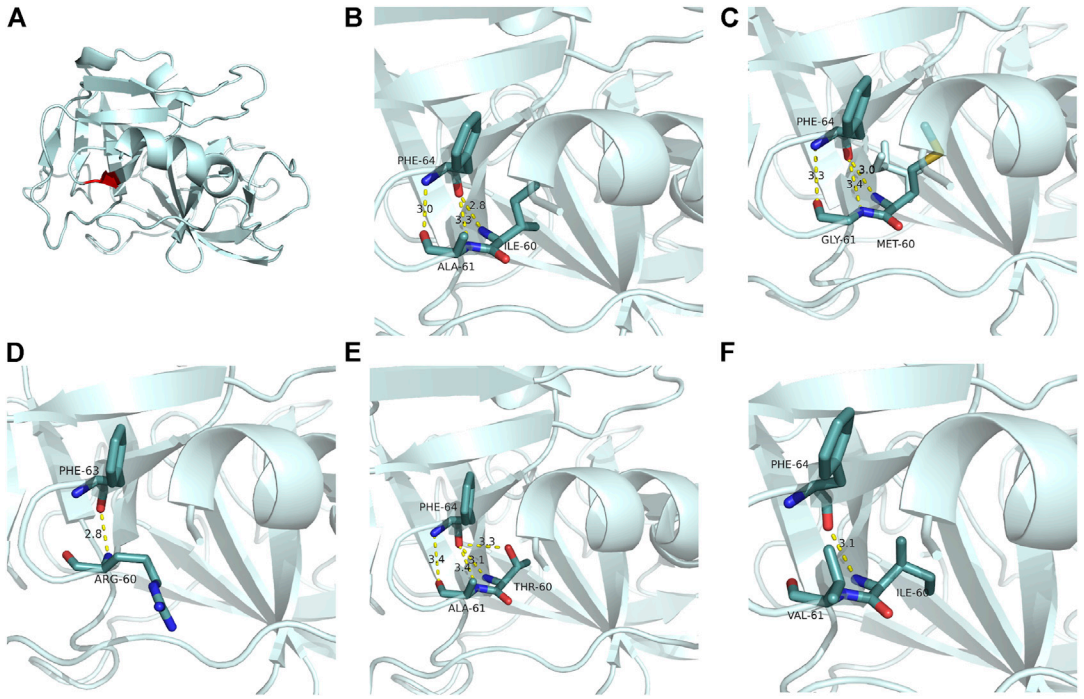


FIGURE 4
Ribbon diagrams of neutrophil elastase. **(A)** Position (red) of residues Ile60 and Ala61. **(B)** H-bonds between residues Ile60 and Ala61 and their substrate Phe64. **(C)** Changed H-bonds in NE mutant I60M, A61G (the present case). While three H-bonds remained between residues 60 and 61 and Phe64, the bond lengths increased, indicating weakened connections. **(D)** Phe64 lost two H-bonds with Arg60. (SCN, with a synchronous mutation of GFI1). **(E)** Phe64 obtained an additional H-bond with Thr60 (SCN). **(F)** Phe64 lost two H-bonds with Val60 (overlapping between SCN and CyN). Partial tertiary structures were deleted to show the variants and adjacent residues in the ribbon diagrams. The color codes for the molecules and bonds are as follows: carbon, pale cyan; oxygen, red; nitrogen, blue; sulfur, yellow; H-bond, yellow. PD, probing depth.

observed no significant difference between the wild-type and mutant NE.

Discussion

Timely and accurate diagnosis is important for CyN patients. Oral manifestations often occur as the first symptom of immunodeficiency diseases, and those patients are easily misdiagnosed as simple RAU or aggressive periodontitis without careful differentiation.

The patient in this case sought medical treatment with a chief complaint of tooth mobility and migration, red and swollen gums, and recurrent ulcers lasting for 4 years. The differential diagnosis was performed sequentially. First, we clarified whether the RAU lesion was caused by localized mucosal ulcerative diseases like erythema multiforme, or by infections or specific systemic diseases such as herpesvirus infection, HIV infection, Behcet's syndrome, Sweet's syndrome, and leukemias. Considering the unpredictable recurrence of oral ulcers and the accompanying systemic symptoms, the patient's RAU lesion was diagnosed as "aphthous-like ulcers with systemic disease". (Scully, 2006) Second, based on the discordance of the alveolar bone destruction and severity of dental plaque, we diagnosed the patient with "periodontitis associated with systemic disease" (Scully, 2006). Third, a significant reduction in neutrophil count (280/μL) was observed in the blood tests. The early onset of symptoms, long-term and recurring inflammation, lack of history of special drug use, lack of exposure to toxic and harmful substances, and negative results of specific antibody examinations and virus tests all pointed to congenital neutropenia. The 25-day oscillation in neutrophil counts in this case and lack of extra-hematopoietic manifestation suggested a diagnosis of CyN. DNA sequencing analysis further genetically confirmed the diagnosis.

Timely diagnosis and early treatment initiation are crucial to stop the disease progression at an early stage. CyN is a rare disease with an incidence of 0.5–1 case per million (Wright et al., 1981). However, the early diagnosis of CyN is difficult because of the need for serial differential blood count monitoring of absolute neutrophil count (2–3 times per week for 6–8 weeks) to determine the oscillatory pattern of neutrophil count. In children presenting with severe periodontitis, systemic problems should not be ruled out

without sufficient testing. Dentists should review the patient's medical status thoroughly, analyze differential diagnoses, and make appropriate referrals.

Understanding the interplay between *ELANE* mutations and clinical manifestations is important. A total of 80–100% of CyN and 35–63% of SCN cases present with *ELANE* mutations (Horwitz et al., 1999; Horwitz et al., 2007). Among reported *ELANE* mutations, 88% exist solely in CyN or SCN, while 12% exist in both diseases (overlapping mutations) (Horwitz et al., 1999). The patient in the present case showed two novel concurrent spontaneous *ELANE* mutations: c.180T>G (p.I60M) and c.182C>G (p.A61G). Both have been reported in SCN (Germeshausen et al., 2013) but not in CyN (in the gnomAD UCSC Genome Browser). These two extra overlapping mutations might cause both diseases. Determining the genotype-phenotype correlation is clinically significant. For instance, mutations only observed in CyN or overlapping mutations are more strongly associated with oral ulcers (96 of 99 patients, 97%) and are less likely to develop pneumonia (36 of 99 patients, 36%) compared to those unique to SCN (61 of 97 patients, 63%, both) (Makaryan et al., 2015). The clinical manifestations observed in the present case were consistent with this pattern.

The present case provided insights into the H-bonds among several mutant NEs and help explain the pathological mechanism of *ELANE*-related neutropenia. We found that I60M and A61G substitutions did not change the number of H-bonds but rather reduced their connections. This decreased energy due to the mutations also indicated a decreased stability of the mutant NE, consistent with the hypothesis that *ELANE* mutations result in the production of misfolded proteins to induce an unfolded protein response and apoptosis. Combined with the nearly identical NE affinities to the classical substrate before and after mutation, we suggest that protein integrity and stability instead of catalytic defects might be the mechanism by which *ELANE* mutations contribute to neutropenia.

However, the effect of changes in NE intramolecular interactions (such as H-bonds) on clinical phenotypes requires further investigation. Our analysis of four reported mutations in Ile60 or Ala61 showed that most mutations in SCN changed the number of H-bonds. For instance, the p.I60T mutation (Dale et al., 2000; Rydzynska et al., 2021) gained an additional H-bond with Thr60 (Figure 4E), while the p.A61V and p.I60_A61delinsR mutations lost two H-bonds (Figures 4D,F) (Horwitz et al., 1999; Dale et al., 2000; Germeshausen et al., 2013; Rydzynska et al., 2021). In the present case, the number of bonds remained the same (three), but they became weaker (Figure 4C). The two substituted amino acids, Met60 and Gly61, have basic properties very similar to those of the original amino acids, including size, side-chain structure, isoelectric point (I-M:6.02 to 5.74, A-G: 6.0 to 5.97), and polarity (all hydrophobic except for Gly, which had weak polarity). Therefore, the intra-molecular change in NE in the present case was so slight that the oral manifestation was the sole symptom.

Furthermore, there remains controversy regarding the mechanism of overlapping mutations and influencing factors. *ELANE* mutations seem to be a prerequisite for neutropenia, while the patient episodes, clinical features, and systemic symptoms are dependent on comprehensive complicated factors such as hormones and age, or other gene modifiers like GFI1 and LEF1 (Germeshausen et al., 2001; Xia et al., 2009; Newburger et al., 2010; Cho and Jeon, 2014; Aota et al., 2019; Mir et al., 2020). In the present case, the appearance of RAU and neutropenia was closely related to menstruation; however, the cause requires further investigation.

Considering the systemic factors involved, dental plaque management is essential. Most patients with CyN with chronic complications or infections experience tooth loss (Wright et al., 1981). A registry-based study of 45 patients in France under 30 years of age reported that, if plaque control was not emphasized, 18 and 17 showed partial and complete edentulism, respectively (Wright et al., 1981). In contrast, regular nonsurgical periodontal treatment has been proven to reduce dental plaques and improve clinical outcomes. (Gorlin and Chaudhry, 1960; Pernu et al., 1996; Hastürk et al., 1998; da Fonseca and Fontes, 2000; Goultschin et al., 2000; Block et al., 2015). Therefore, in cases with timely diagnosis, better periodontal outcomes were more likely in patients receiving regular periodontal and antibiotic treatments (Pernu et al., 1996; Hastürk et al., 1998; Goultschin et al., 2000). Patients who did not receive proper treatment showed worsened conditions, including tooth extraction and severe bone loss (Ródenas et al., 1992; Dale et al., 2000; Horwitz et al., 2007; Skokowa et al., 2017). Thus, professional prophylaxis and scaling should be performed monthly and even weekly when the neutrophil count starts to decline (Aota et al., 2019). The patient and her caregivers in the present case were educated regarding the importance of oral hygiene and trained to provide adequate home care, including correct brushing, flossing, and waterpik use, with chlorhexidine rinses as an adjunct (Lu and Meng, 2012). The use of fluoride rinse or gel could be additionally considered because of the high morbidity of caries.

The patient fully understood her state of illness and showed good medical compliance. Her supervisors also emphasized periodontal management, and both pushed through difficulties in adhering to monthly clinical visits. However, since the coronavirus disease outbreak in 2019, the patient's periodontal treatment has been interrupted occasionally. During the local epidemic, we had to turn to online guidance and supervision on the effects of oral hygiene control. Despite these difficulties, her high compliance and regular periodontal treatment led to a good outcome with no extraction.

This patient visited the dentist with severe tooth migration, which was aggravating every year. Specifically, tooth 31 presented

with severe mobility and had notable absorption of the mesial alveolar bone and broadening of the periodontal space owing to occlusal trauma. In such cases, further dental treatment is important, as tooth displacement can make oral hygiene practice difficult, thus promoting a pathologic environment conducive to more severe periodontitis. Progressive periodontitis might aggravate tooth migration, potentially leading to a vicious circle; thus, the necessity for earlier interventions to ameliorate this cycle warrants further discussion. A periodontal splint might have been considered earlier in this case, as it is easy to operate and the prognosis is relatively controllable, even though it cannot correct the deflection to normal. Although periodontal splinting fixation might have interfered with alveolar bone growth, it might have reduced occlusal trauma, with subsequent follow-up performed to determine whether to continue its use based on the findings.

Other multi-disciplinary treatment options for this patient were also discussed. Although the patient responded well to G-CSF, systemic therapy was not prescribed by her physician unless major systemic symptoms appeared. Combined with bone loss, orthodontic treatment should be avoided because there is an increased risk of accelerated periodontal breakdown. Periodontal flap surgery was not recommended because of the high potential for infection. We plan to extract hopeless teeth, such as 16, 15, 31, and 46, when the patient reaches maturity, at which time occlusal reconstruction with a periodontal splint will be recommended. Block et al. (2015) reported a case of eight implants in a 59-year-old patient with CyN, in which the 3-year follow-up revealed a stable alveolar bone level. Therefore, if the patient in the present case loses more teeth, a dental implant could be placed in the future.

In conclusion, we described a case of CyN with RAU and severe periodontitis as the main manifestations. Two novel spontaneous *ELANE* mutations were identified. First, this case demonstrated that *ELANE* mutations are a prerequisite for neutropenia and that the clinical features depend on comprehensive factors. Second, the manifestation of RAU and periodontitis could be early diagnostic signatures of systemic diseases such as CyN, which require a timely and accurate diagnosis for positive outcomes. Third, the proper management of dental plaques can effectively relieve gingival inflammation and slow alveolar bone loss.

Data availability statement

The datasets for this article are not publicly available due to concerns regarding participant/patient anonymity. Requests to access the datasets should be directed to the corresponding authors.

Ethics statement

Written informed consent was obtained from the individual (s), and minor (s)' legal guardian/next of kin, for the publication of any potentially identifiable images or data included in this article.

Author contributions

ZL and JF contributed to information collection, gene analysis, and drafting and final approval of the manuscript. DD and PW collected the clinical data, treated the patient, and wrote the manuscript. LZ was the initial dentist and contributed clinical data from the first visit. ZW interpreted and analyzed the gene results. SW, CH and YL assisted with the revision of the manuscript.

Funding

This study was supported by the National Natural Science Foundation of China (81500871, 81700984), the Natural Science Foundation of Guangdong Province, China (2016A030310214), and the Undergraduate Education Quality Program of Sun Yat-sen University [Academic Affairs (2022) No. 20].

Conflict of interest

The authors declare that the research was conducted in the absence of any commercial or financial relationships that could be construed as a potential conflict of interest.

Publisher's note

All claims expressed in this article are solely those of the authors and do not necessarily represent those of their affiliated organizations, or those of the publisher, the editors, and the reviewers. Any product that may be evaluated in this article, or claim that may be made by its manufacturer, is not guaranteed or endorsed by the publisher.

Supplementary material

The Supplementary Material for this article can be found online at: https://www.frontiersin.org/articles/10.3389/fgene.2022.972598/full#supplementary-material

References

Aota, K., Kani, K., Yamanoi, T., Momota, Y., Ninomiya, M., Yumoto, H., et al. (2019). Management of tooth extraction in a patient with ELANE gene mutation-induced cyclic neutropenia: A case report. *Medicine* 98 (39), e17372. doi:10.1097/MD.0000000000017372

Block, M. S., Brindis, M., Block, C. A., and Berron, J. M. (2015). Full-arch rehabilitation of a patient with cyclic neutropenia. *J. Oral Maxillofac. Surg.* 73 (9), e1–e101710. doi:10.1016/j.joms.2015.03.073

Borregaard, N. (2014). Severe congenital neutropenia: New lane for ELANE. *Blood* 123 (4), 462–463. doi:10.1182/blood-2013-11-537068

Cho, H.-K., and Jeon, I. S. (2014). Different clinical phenotypes in familial severe congenital neutropenia cases with same mutation of the ELANE gene. *J. Korean Med. Sci.* 29 (3), 452–455. doi:10.3346/jkms.2014.29.3.452

da Fonseca, M. A., and Fontes, F. (2000). Early tooth loss due to cyclic neutropenia: Long-term follow-up of one patient. *Special Care Dent.* 20 (5), 187–190. Official Publication of the American Association of Hospital Dentists, the Academy of Dentistry for the Handicapped, and the American Society for Geriatric Dentistry. doi:10.1111/j.1754-4505.2000.tb00017.x

Dale, D. C., and Hammond, W. P. (1988). Cyclic neutropenia: A clinical review. *Blood Rev.* 2 (3), 178–185. doi:10.1016/0268-960X(88)90023-9

Dale, D. C., Person, R. E., Bolyard, A. A., Aprikyan, A. G., Bos, C., Bonilla, M. A., et al. (2000). Mutations in the gene encoding neutrophil elastase in congenital and cyclic neutropenia. *Blood* 96 (7), 2317–2322. doi:10.1182/blood.V96.7.2317

Germeshausen, M., Deerberg, S., Peter, Y., Reimer, C., Kratz, C. P., and Ballmaier, M. (2013). The spectrum of ELANE mutations and their implications in severe congenital and cyclic neutropenia. *Hum. Mutat.* 34 (6), 905–914. doi:10.1002/humu.22308

Germeshausen, M., Schulze, H., Ballmaier, M., Zeidler, C., and Welte, K. (2001). Mutations in the gene encoding neutrophil elastase (ELA2) are not sufficient to cause the phenotype of congenital neutropenia. *Br. J. Haematol.* 115 (1), 222–224. doi:10.1046/j.1365-2141.2001.03069.x

Gorlin, R. J., and Chaudhry, A. P. (1960). The oral manifestations of cyclic (periodic) neutropenia. Does periadenitis mucosa necrotica recurrens (sutton) exist? A need for reevaluation. *Arch. Dermatol.* 82, 344–348. doi:10.1001/archderm.1960.01580030038004

Goultschin, J., Attal, U., Goldstein, M., Boyan, B. D., and Schwartz, Z. (2000). The relationship between peripheral levels of leukocytes and neutrophils and periodontal disease status in a patient with congenital neutropenia. *J. Periodontol.* 71 (9), 1499–1505. doi:10.1902/jop.2000.71.9.1499

Hastürk, H., Tezcan, I., Yel, L., Ersoy, F., Sanal, O., Yamalik, N., et al. (1998). A case of chronic severe neutropenia: Oral findings and consequences of short-term granulocyte colony-stimulating factor treatment. *Aust. Dent. J.* 43 (1), 9–13. doi:10.1111/j.1834-7819.1998.tb00144.x

Horwitz, M., Benson, K. F., Person, R. E., Aprikyan, A. G., and Dale, D. C. (1999). Mutations in ELA2, encoding neutrophil elastase, define a 21-day biological clock in cyclic haematopoiesis. *Nat. Genet.* 23 (4), 433–436. doi:10.1038/70544

Horwitz, M. S., Corey, S. J., Grimes, H. L., and Tidwell, T. (2013). ELANE mutations in cyclic and severe congenital neutropenia—genetics and pathophysiology. *Hematol. Oncol. Clin. North Am.* 27 (1), 19–41. doi:10.1016/j.hoc.2012.10.004

Horwitz, M. S., Duan, Z., Korkmaz, B., Lee, H. H., Mealiffe, M. E., and Salipante, S. J. (2007). Neutrophil elastase in cyclic and severe congenital neutropenia. *Blood* 109 (5), 1817–1824. doi:10.1182/blood-2006-08-019166

Isola, G., Polizzi, A., Alibrandi, A., Indelicato, F., and Ferlito, S. (2020). Analysis of endothelin-1 concentrations in individuals with periodontitis. *Sci. Rep.* 10 (1), 1652. doi:10.1038/s41598-020-58585-4

Lakshman, R., and Finn, A. (2001). Neutrophil disorders and their management. *J. Clin. Pathol.* 54 (1), 7–19. doi:10.1136/jcp.54.1.7

Lu, R. F., and Meng, H. X. (2012). Severe periodontitis in a patient with cyclic neutropenia: A case report of long-term follow-up. *Chin. J. Dent. Res.* 15 (2), 159–163.

Makaryan, V., Zeidler, C., Bolyard, A. A., Skokowa, J., Rodger, E., Kelley, M. L., et al. (2015). The diversity of mutations and clinical outcomes for ELANE-associated neutropenia. *Curr. Opin. Hematol.* 22 (1), 3–11. doi:10.1097/MOH.0000000000000105

Mir, P., Klimiankou, M., Findik, B., Hähnel, K., Mellor-Heineke, S., Zeidler, C., et al. (2020). New insights into the pathomechanism of cyclic neutropenia. *Ann. N. Y. Acad. Sci.* 1466 (1), 83–92. doi:10.1111/nyas.14309

Nanua, S., Murakami, M., Xia, J., Grenda, D. S., Woloszynek, J., Strand, M., et al. (2011). Activation of the unfolded protein response is associated with impaired granulopoiesis in transgenic mice expressing mutant Elane. *Blood* 117 (13), 3539–3547. doi:10.1182/blood-2010-10-311704

Newburger, P., Md, T., Zhu, Z., Bolyard, A., Aprikyan, A., Dale, D., et al. (2010). Cyclic neutropenia and severe congenital neutropenia in patients with a shared ELANE mutation and paternal haplotype: Evidence for phenotype determination by modifying genes. *Pediatr. Blood Cancer* 55, 314–317. doi:10.1002/pbc.22537

Pernu, H. E., Pajari, U. H., and Lanning, M. (1996). The importance of regular dental treatment in patients with cyclic neutropenia. Follow-up of 2 cases. *J. Periodontol.* 67 (4), 454–459. doi:10.1902/jop.1996.67.4.454

Ródenas, J. M., Ortego, N., Herranz, M. T., Tercedor, J., Pinar, A., and Quero, J. H. (1992). Cyclic neutropenia: A cause of recurrent aphthous stomatitis not to be missed. *Dermatol. (Basel, Switz.* 184 (3), 205–207. doi:10.1159/000247542

Rydzynska, Z., Pawlik, B., Krzyzanowski, D., Mlynarski, W., and Madzio, J. (2021). Neutrophil elastase defects in congenital neutropenia. *Front. Immunol.* 12, 653932. doi:10.3389/fimmu.2021.653932

Scully, C. (2006). Clinical practice. Aphthous ulceration. *N. Engl. J. Med.* 355 (2). doi:10.1056/NEJMcp054630

Skokowa, J., Dale, D. C., Touw, I. P., Zeidler, C., and Welte, K. (2017). Severe congenital neutropenias. *Nat. Rev. Dis. Prim.* 3, 17032. doi:10.1038/nrdp.2017.32

Walter, P., and Ron, D. (2011). The unfolded protein response: From stress pathway to homeostatic regulation. *Sci. (New York, N.Y.)* 334 (6059), 1081–1086. doi:10.1126/science.1209038

Wright, D. G., Dale, D. C., Fauci, A. S., and Wolff, S. M. (1981). Human cyclic neutropenia: Clinical review and long-term follow-up of patients. *Med. Baltim.* 60 (1), 1–13. doi:10.1097/00005792-198101000-00001

Xia, J., Bolyard, A. A., Rodger, E., Stein, S., Aprikyan, A. A., Dale, D. C., et al. (2009). Prevalence of mutations in ELANE, GFI1, HAX1, SBDS, WAS and G6PC3 in patients with severe congenital neutropenia. *Br. J. Haematol.* 147 (4), 535–542. doi:10.1111/j.1365-2141.2009.07888.x

frontiers | Frontiers in Pediatrics

TYPE Original Research
PUBLISHED 07 November 2022
DOI 10.3389/fped.2022.1029004

Check for updates

OPEN ACCESS

EDITED BY
Mike Mikailov,
United States Food and Drug Administration, United States

REVIEWED BY
Siqi Hu,
Seventh Medical Center of PLA General Hospital, China
Fuad Al Mutairi,
King Abdulaziz Medical City, Saudi Arabia

*CORRESPONDENCE
Jian Shen
hzsfybjyebk@163.com

SPECIALTY SECTION
This article was submitted to Genetics of Common and Rare Diseases, a section of the journal Frontiers in Pediatrics

RECEIVED 26 August 2022
ACCEPTED 17 October 2022
PUBLISHED 07 November 2022

CITATION
Li X and Shen J (2022) One potential hotspot *SLC25A20* gene variants in Chinese patients with carnitine-acylcarnitine translocase deficiency.
Front. Pediatr. 10:1029004.
doi: 10.3389/fped.2022.1029004

COPYRIGHT
© 2022 Li and Shen. This is an open-access article distributed under the terms of the Creative Commons Attribution License (CC BY). The use, distribution or reproduction in other forums is permitted, provided the original author(s) and the copyright owner(s) are credited and that the original publication in this journal is cited, in accordance with accepted academic practice. No use, distribution or reproduction is permitted which does not comply with these terms.

One potential hotspot *SLC25A20* gene variants in Chinese patients with carnitine-acylcarnitine translocase deficiency

Xiaoli Li and Jian Shen*

Department of Pediatrics, Affiliated Hangzhou First People's Hospital, Zhejiang University School of Medicine, Hangzhou, China

Background: Carnitine-acylcarnitine translocase deficiency (CACT deficiency) is a rare and life-threatening autosomal recessive disorder of mitochondrial fatty acid oxidation caused by variant of *SLC25A20* gene. The most prevalent missense variant in the *SLC25A20* gene in Asia was c.199–10T > G. Due to the c.199–10T > G variant, CACT deficiency is a severe phenotype.
Materials and Methods: Herein, we present a neonatal case with c.199–10T > G variant in China and analyze the clinical, biochemical, and genetic aspects of 78 patients previously identified with CACT deficiency.
Results: The patient presented with a series of severe metabolic crises that rapidly deteriorated and eventually died 3 days after delivery. The sequencing of the patient's genome indicated that he was homozygous for the c.199–10T > G variant. 30 patients were found to have the c.199–10T > G mutation, of which 23 were Chinese and 22 were afflicted by the c.199–10T > G splicing variation. In China, c.199–10T > G allele frequency was 82.6%.
Conclusion: In CACT deficiency, prompt recognition and treatment are critical. Our data suggested that c.199–10T > G may be a potential hotspot *SLC25A20* gene mutation in the Chinese population. Detection of single nucleotide polymorphism is possible for high-risk patients and parents in China.

KEYWORDS
CACT deficiency, *SLC25A20* gene, c.199–10T > G, hotspot mutation, single nucleotide polymorphism detection

Introduction

Carnitine-acylcarnitine translocase deficiency (CACT deficiency, OMIM # 212138) was first described by Stanley CA et al. in 1992 (1). It is a rare and life-threatening autosomal recessive disorder with an incidence of 1:60,000 in Hongkong and 1:1,017,593 in Zhejiang province China (2, 3). CACT deficiency, encoded by the *SLC25A20* gene on chromosome 3p21.31, is the cause of this condition (4). To shuttle long-chain fatty acids through the inner mitochondrial membrane and into the mitochondrial matrix, where mitochondrial β-oxidation takes place, CACT is an essential part of the carnitine cycle (5). Mitochondrial β-oxidation serves as the primary energy source for cardiac and skeletal muscles, while ketogenesis in the liver fuels brains tissue during prolonged fasting and exercise (1, 6, 7). CACT deficiency is characterized by a wide spectrum of clinical manifestations including hypoketotic

hypoglycemia, hyperammonemia, liver dysfunction, cardiomyopathy, severe neurologic impairment and progressive myopathy (8).

There are nine exons in the *SLC25A20* gene, which produces a 301-amino-acid protein (9). At least 42 pathogenic variants have been detected in mutation databases like the HGMD around the world (Human Gene Mutation Database, www.hgmd.org). There are 20 missenses, 10 small deletions, 2 small insertions, 1 small indel, 4 large deletions, and 5 splicing mutations in the mutation spectrum (10). *SLC25A20* gene missense variation c.199–10T > G was the most frequent in Asia. In our study, approximately 37.5% of pathogenic variants fall within this umbrella.

Though the spectrum of CACT deficiency is wide and continuous, there are two distinct clinical subtypes: a neonatal-onset severe form and an infancy-onset milder form (11). Severe classic presentation occurs at birth and has an extremely poor prognosis, with severe illness and debilitating symptoms. Moderate myopathy and hepatomegaly are seen in milder cases with more accessible residual transporter protein. Metabolic decompensation can be prevented and the prognosis improved with early detection and medicinal intervention (12).

In the present study, we described a patient with CACT deficiency which was failed to diagnosed and treated promptly and then leaded to rapid illness progression and eventual death. Furthermore, Patients previously diagnosed with CACT deficiency was reviewed systematically by describing the clinical, biochemical, and genetic characteristics and treatment to improve our understanding of this rare disorder.

Materials and methods

Case report

The patient was born at full term through a cesarean section. At 1 and 5 min, the baby's Apgar score was 10. The parents were healthy and had no history of consanguineous marriage. The mother's first child died at two days old from asphyxia, arrhythmia, and cardiac arrest. The baby seemed fine until he was 28 h old when he became very sleepy and showed no interest in breastfeeding. The patient was taken to the neonatal intensive care unit (NICU) for a checkup. During a physical exam, the baby's body temperature was 34.6°C, his blood pressure was 72/44 mmHg, and his SpO2 was 95%. **Table 1** gives detailed information about the patient's health. After a test for sepsis was done, he was given antibiotics, and a 6.5 mg/ka/minute glucose infusion was started. The patient had recurrent ventricular tachycardia, bradycardia, and complete right bundle branch block between the ages of 47 and 51 h. Lidocaine, epinephrine, and milrinone were used to treat the patient for several days after the attack. Several attempts to save her life failed, and she died 3 days after giving birth. At 48 h, a small spot of dried blood was taken as a sample. Acylcarnitine profile by MS/MS analysis showed C14-acylcanitine, 1.13 μM (0.07–0.4); C16-acylcanitine, 14.37 μM (0.49–6); C16:1-acylcanitine, 1.40 μM (0.02–0.49); C18-acylcanitine, 3.73 μM (0.24–1.90); C18:1-acylcanitine, 5.83 μM (0.38–2.92), which were identified to have CPT2 (carnitine palmitoyl-transferases 2) deficiency or CACT deficiency. The patient's genomic DNA was taken out. High-throughput sequencing found that the patient's *SLC25A20* gene had a homozygous c.199–10T > G splice site change (**Figure 1**). The child was diagnosed with CACT deficiency based on the signs and symptoms. Both parents were heterozygous carriers of the variation, but neither had any obvious symptoms.

Literature search

All patients previously genetically diagnosed with CACT deficiency were reviewed in the study. The literature search for "Carnitine-acylcarnitine translocase deficiency,"

TABLE 1 Summary of the patient with CACT deficiency biochemistry, ECG and Echo

Age at detection	28 h (at admission)	47 h	51 h
ALT (U/L)	20	26	–
AST (U/L)	74	74	87
HLD (U/L)	461	592	784
Lactate (mmol/L)	6.0	7.2	–
Ammonia (μmol/L)	128	355	433
CK (U/L)	384	418	596
CKMB (U/L)	66	136	168
Ca^{++} (mmol/L)	2.2	1.49	1.83
K^{+} (mmol/L)	5.98	6.52	6.59
TNI (μg/L)	–	0.03	–
Glucose (mmol/L)	1.9	1.49	1.3
ECG	–	VT/ CRBBB/ II-AVB	Bradycardia/VF/ Unusually broad and changing QRS wave complex
Echo	Left ventricular wall motion incoordination (EF55%)	–	Left ventricular wall motion incoordination (EF30%)

Cutoff value: ALT(alanine transaminase):9–50 U/L; AST(aspartate transaminase):15–40 U/L; HLD(lactate dehydrogenase):97–350 U/L; Lactate:1.5–2.5 mmol/L; Ammonia:18–72 μmol/L; CK(creatine kinase): 24–195 U/L; CK-MB(creatine kinase-MB):0–24 U/L; Ca^{++}2.0–2.6 mmol/L;

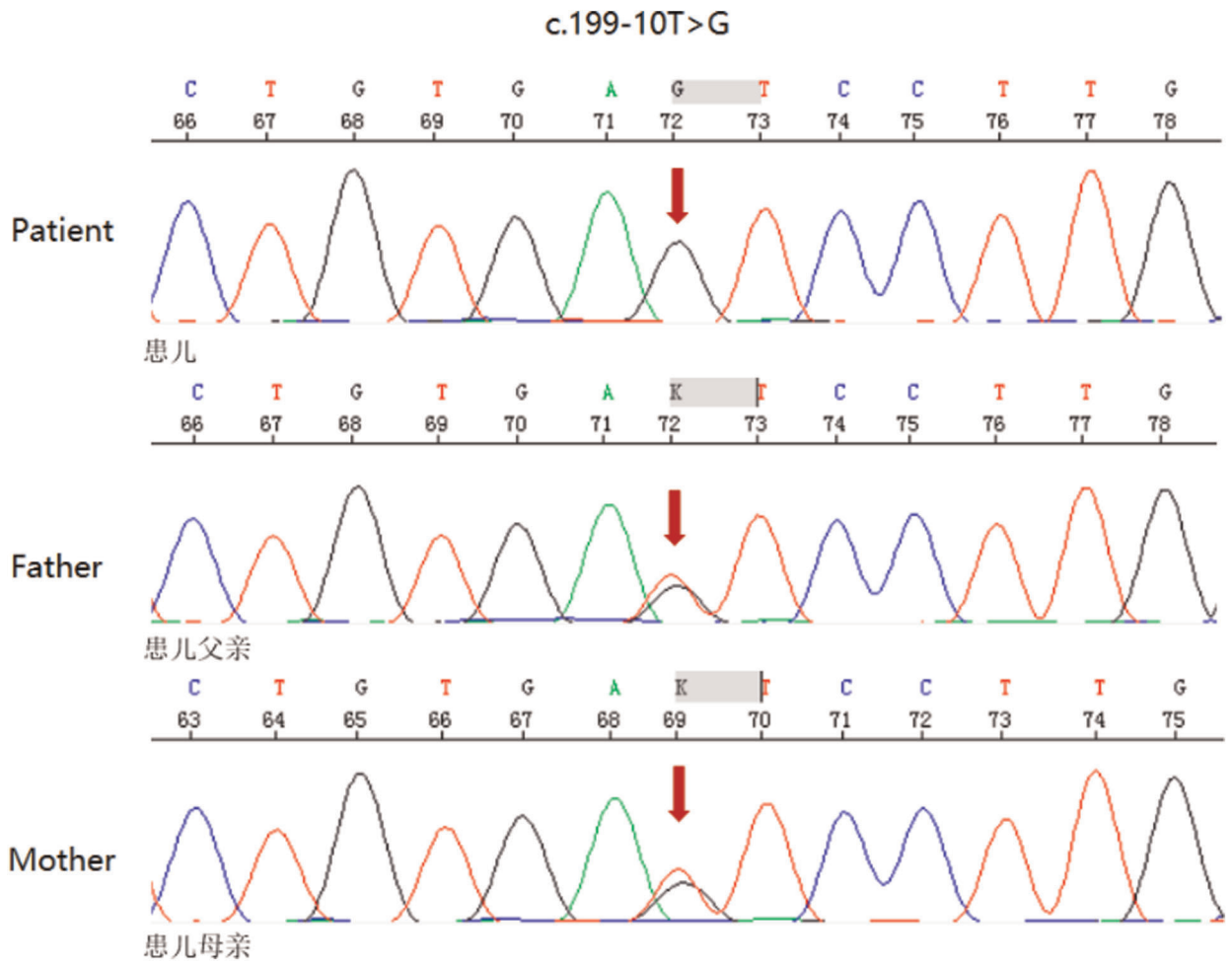


FIGURE 1
DNA sequence of SLC25A20 gene (a homozygous mutation of patient for maternally and paternally-inherited c.199–10 T > G variant. Parents were heterozygous carriers of the mutation. Mutation sites are indicated by red arrows)

"Carnitine-acylcarnitine translocase," "*SLC25A20* gene," "CACTD," as keywords on PubMed, Elsevier and Medline from 1992 to June 2022. (**Table 2**).

Results

Individual case reports are available for all cases as online.

Case for CACT deficiency

Over 30 years, 81 children with CACT deficiency were identified, 3 of which lacked genetic testing to determine the mutation sites. Therefore, in addition to the newly identified patient with CACT deficiency, we included 78 previously diagnosed patients in our sample.

Genetic findings

Patients harbored either homozygous or heterozygous *SLC25A20* mutations. 42 different variations have been discovered. The most prevalent splicing variant was homozygous c.199–10T > G (23/79). Heterozygous c.199–10T > G splicing variation (7/79) and homozygous c.82G > T splicing variation (7/79) were quite prevalent variations. Each of the forty remaining variants was detected one to three times. The c.199–10T > G variant was identified in thirty patients (38.0%), of whom 73.3% (22/30) were Chinese. 29.1% (23/79) of the patients were Chinese, and 95.7% (22/23) were affected by the

TABLE 2 Presenting features of patients with CDCT deficiency (1, 3, 5, 8–10, 13–32).

Patient ID	Ethnicity	Age at onset	Current age/age of death	Hypoglycemia	Hyperammonemia	CK	ALT	Arrhythmias	Cardiac hypertrophy	Cardiac arrest	Hepatomegaly	Seizures	Poor response/ Hypotonia	dyspnea	Other futures	SLC25A20 genotype
1	Malaysia	24 h	2.5 months	1	1	NA	NA	NA	NA	NA	NA	1	NA	NA	(C16 + C18:1)/ C2↑	Homozygous c.199–10T > G
2	Malaysia	24 h	5 day	1	1	NA	↑	AVB/VT/VF/ bradycardia	NA	NA	NA	NA	1	NA	(C16 + C18:1)/ C2↑	Homozygous c.199–10T > G
3	Chinese	24 h	3 year	1	1	↑	NA	RBBB/AVB	LV hypertrophy	1	NA	1	NA	NA	NA	Homozygous c.199–10T > G
4	Vietnamese	28 h	6 months	1	1	↑	NA	Broad complex VT	NA	NA	NA	NA	NA	NA	NA	Homozygous c.199–10T > G
5	Chinese	14.5 h	4 years lived	1	1	↑	NA	Bradycardia	cadiomyopathy with thickened LV/RV and septum	1	NA	1	NA	NA	C16, C18↑	Homozygous c.199–10T > G
6	Chinese	8 days	14 months lived	1	1	↑	↑	Bradycardia	Hypertrophic cardiomyopathy	NA	NA	NA	NA	1	Rhabdomyolysis C16, C18↑	Homozygous c.199–10T > G
7	Vietnamese	12 h	5 months lived	1	1	↑	NA	VT	NA	1	NA	1	NA	NA	C16, C18↑	Homozygous c.199–10T > G
8	Chinese	25 min	71 h	1	1	↑	NA	NA	NA	1	NA	1	NA	NA	(C16 + C18:1)/ C2↑	Homozygous c.199–10T > G
9	Chinese	24 h	48 h	1	1	↑	NA	AVB/VT	NA	NA	NA	1	1	1	C16, C18↑	Homozygous c.199–10T > G
10	Thailand	10 h	2 years and 8 months	1	1	↑	↑	NA	Hypertrophic cardiomyopathy	1	1	NA	NA	1	C16, C18↑	Homozygous c.199–10T > G
11	Thailand	48 h	4 months	1	1	↑	↑	NA	Hypertrophic cardiomyopathy	1	1	NA	1	NA	C16, C18↑	Homozygous c.199–10T > G
12	Chinese	Early Neonatal	2 months	1	NA	↑	NA	VT	Cardiac hypertrophy	1	NA	NA	1	1	C16, C18↑	Homozygous c.199–10T > G
13	Chinese	1 day	3 days	NA	NA	NA	NA	1	Cardiac hypertrophy	1	NA	NA	1	NA	C16, C18↑	Homozygous c.199–10T > G
14	Chinese	Treated from birth	19 months lived	NA	NA	NA	NA	VT	NA	NA	NA	NA	NA	NA	C16, C18↑	Homozygous c.199–10T > G
15	Chinese	2 days	2 days	1	1	NA	NA	1	Cardiac hypertrophy	1	NA	NA	NA	NA	C16, C18↑	Homozygous c.199–10T > G
16	Chinese	41 h	41 h	NA	NA	NA	NA	NA	NA	1	NA	NA	NA	NA	NA	Homozygous c.199–10T > G

(*continued*)

10.3389/fped.2022.1029004

TABLE 2 Continued

Patient ID	Ethnicity	Age at onset	Current age/age of death	Hypoglycemia	Hyperammonemia	CK	ALT	Arrhythmias	Cardiac hypertrophy	Cardiac arrest	Hepatomegaly	Seizures	Poor response/ Hypotonia	dyspnea	Other futures	SLC25A20 genotype
17	Chinese	32 h	32 months	1	1	NA	NA	NA	Hypertrophic cardiomyopathy	NA	NA	NA	NA	NA	NA	Homozygous c.199–10T > G
18	Chinese	28 h	38 h	NA	NA	NA	NA	VT/Bradycardia	NA	1	NA	NA	NA	NA	NA	Homozygous c.199–10T > G
19	Chinese	61 days	62 days	1	NA	↑	↑	NA	NA	NA	NA	NA	1	NA	NA	Homozygous c.199–10T > G
20	Chinese	In 7 days	In 7 days	1	1	NA	NA	NA	Hypertrophic cardiomyopathy	1	1	NA	NA	NA	C14↑, C16↑, C18↑, C16:1↑, C18:1↑	Homozygous c.199–10T > G
21	Chinese	In 7 days	In 7 days	1	1	NA	NA	NA	Hypertrophic cardiomyopathy	NA	1	NA	NA	NA	C14↑, C16↑, C18↑, C16:1↑, C18:1↑	Homozygous c.199–10T > G
22	–	1 day	4 years lived	1	1	NA	NA	symptomatic tachyarrhythmia	cardiac hypertrophy	NA	NA	NA	NA	NA	C16↑, C18↑	Homozygous c.199–10T > G
23	Chinese	2 days	3 days	1	1	↑	↑	VT/IRBBB Bradycardia	NA	1	NA	NA	1	NA	C14↑, C16↑, C18↑, C16:1↑, C18:1↑	Homozygous c.199–10T > G
24	Chinese	24 h	9 years lived	1	1	↑	↑	Broad complex tachyarrhythmia atrial flutter	biventricular hypertrophy	NA	NA	1	NA	NA	NA	c.109C > T c.199–10T > G
25	Chinese	24 h	71 h	1	1	↑	↑	1	NA	NA	NA	1	1	NA	C16↑, C18:1↑	c.199–10T > G c.1A > G
26	Chinese	24 h	6 days	1	1	↑	↑	NA	NA	NA	NA	NA	1	NA	C16, C18, (C16 + C18:1)/ C2↑	c.199–10T > G c.1A > G
27	Chinese	–	1 year and 3 months	1	1	↑	NA	NA	NA	NA	NA	NA	NA	NA	C14↑, C16↑, C18↑, C16:1↑, C18:1↑	c.199–10T > G c.1A > G
28	Japanese	48 h	2 years and 9 months	1	NA	NA	↑	NA	NA	NA	NA	NA	1	1	C14, C16, C18↑	c.199–10T > G c.576G > A
29	Chinese	2 days	3 days	1	1	↑	↑	1	cardiac hypertrophy	1	NA	NA	1	1	C16↑, C18↑	c.199–10T > G c.719-8_c.719-1dupCCCCACAG
30	Chinese	4 days	8 days	1	1	↑	↑	1	NA	NA	NA	1	1	1	C16↑, C18↑	c.199–10T > G c.719-8_c.719-1dupCCCCACAG
31	Pakistani descent	1 month	lived	NA	NA	NA	NA	NA	NA	NA	NA	NA	NA	NA	NA	Homozygous c.82G > T

(*continued*)

10.3389/fped.2022.1029004

TABLE 2 Continued

Patient ID	Ethnicity	Age at onset	Current age/age of death	Hypoglycemia	Hyperammonemia	CK	ALT	Arrhythmias	Cardiac hypertrophy	Cardiac arrest	Hepatomegaly	Seizures	Poor response/ Hypotonia	dyspnea	Other futures	SLC25A20 genotype
32	Pakistani descent	2 months	lived	1	NA	NA	NA	NA	LVH, Impaired contractility	NA	NA	NA	NA	NA	C16↑	Homozygous c.82G > T
33	Pakistani descent	–	lived	NA	NA	NA	NA	NA	NA	NA	NA	NA	NA	NA	NA	Homozygous c.82G > T
34	Pakistani descent	9 days	lived	1	NA	NA	NA	NA	NA	NA	NA	NA	NA	NA	C16↑	Homozygous c.82G > T
35	Pakistani descent	–	lived	NA	NA	NA	NA	NA	NA	NA	NA	NA	NA	NA	NA	Homozygous c.82G > T
36	Pakistani descent	1 month	lived	NA	NA	NA	NA	NA	NA	NA	NA	NA	NA	NA	NA	Homozygous c.82G > T
37	Pakistani descent	4 months	lived	1	NA	NA	NA	NA	Mild left ventricular hypertrabeculation	NA	NA	NA	NA	NA	NA	Homozygous c.82G > T
38	Malaysia	33 h	33 h	1	NA	NA	NA	NA	NA	1	1	NA	NA	NA	NA	c.109C > T c.706C > T
39	Indian	12 h	7 days	1	NA	NA	NA	Bradycardic arrest (rosc after 10 min)	NA	1	NA	1	NA	NA	NA	c.82G > T c.706C > T
40	Caucasian	10 h	3 days	1	1	NA	NA	VT	NA	1	NA	NA	NA	NA	NA	Homozygous c.646G > T
41	Iranian	24 h	11 years lived	1	1	↑	NA	SVT	NA	1	NA	1	NA	NA	NA	Homozygous c.67G > T
42	Guyana	15 h	3 years lived	1	1	NA	↑	NA	NA	NA	NA	1	NA	NA	NA	Homozygous c.110G > C
43	Caucasian	2 days	10 years lived	1	1	↑	NA	NA	NA	NA	NA	1	NA	NA	NA	c.50G > C c.326 + 1 delG
44	Iranian	Treated from birth	19 months lived	NA	1	NA	NA	AVT/VT	NA	NA	NA	NA	NA	NA	NA	Homozygous c.417 + 1G > A
45	Irish	32 h	16 months lived	1	1	↑	NA	AV	NA	1	NA	NA	NA	NA	Mild coagulation disorder	c.326 + 1delG (Splice donor); c.691G > C
46	New Zealanders	36 h	12 months lived	1	1	↑	NA	NA	echogenic myocadium	NA	NA	NA	NA	NA	NA	c.804delG
47	Iranian	5 months	–	1	NA	NA	NA	NA	Hypertrophic cardiomyopathy	NA	NA	NA	NA	NA	NA	Homozygous c.67G > T
48	Caucasian	2 months	–	1	NA	NA	↑	NA	NA	NA	NA	NA	NA	NA	Hypokalemia	c.397C > T deletion c.779_781delAAG

(*continued*)

10.3389/fped.2022.1029004

TABLE 2 Continued

Patient ID	Ethnicity	Age at onset	Current age/age of death	Hypoglycemia	Hyperammonemia	CK	ALT	Arrhythmias	Cardiac hypertrophy	Cardiac arrest	Hepatomegaly	Seizures	Poor response/ Hypotonia	dyspnea	Other futures	SLC25A20 genotype
49	Caucasian	20 days	–	1	1	NA	NA	NA	NA	NA	NA	NA	NA	NA	c.823C > T is nonsense mutation	large 26 kb deletion encompassing exons 5–9
50	Iranian	10 months	–	1	NA	↑	↑	NA	NA	NA	NA	1	NA	NA	NA	c.160_163del4ins4 and c.804delG
51	–	1 month	–	1	NA	NA	NA	1	NA	NA	NA	NA	NA	NA	NA	c.397C > T c.752_761del10
52	–	20 days	–	NA	NA	NA	NA	NA	NA	NA	NA	NA	NA	NA	NA	c.528delT c.496C > T
53	–	2 years	–	1	NA	NA	NA	NA	NA	NA	NA	NA	NA	NA	NA	c.168delT
54	Turkey	24 h	10 months	1	1	NA	↑	NA	NA	NA	NA	NA	NA	1	C16, C18, C18:1↑	Homozygous c.408C > A
55	Turkey	10 days	12 months	1	1	NA	↑	NA	NA	NA	NA	NA	1	1	C16↑	Homozygous c.270del
56	Turkey	24 h	52days	NA	1	NA	↑	NA	NA	NA	1	NA	NA	NA	C14, C16, C18, C18:1↑	Homozygous c.270del
57	Japanese	48 h	3 days	NA	NA	NA	NA	NA	NA	1	NA	NA	1	NA	C16, C18↑	c.576G > A c.106-2A > T
58	Dutch	Neonatal	9 years lived	1	NA	NA	NA	NA	NA	1	1	NA	NA	NA	NA	Insertion of a cytosine in bp 955–959
59	Dutch	36 h	24 months	1	NA	NA	NA	NA	Hypertrophic cardiomyopathy	NA	NA	NA	1	NA	NA	c.241G > A missense mutation
60	Dutch	24 h	12 years lived	1	NA	NA	↑	NA	Hypertrophic cardiomyopathy	1	1	NA	1	NA	NA	c.955insC mutation
61	Italian	1 month	6 months	1	1	NA	↑	1	NA	NA	NA	NA	1	1	C16, C18:1↑	c.718 + 1G > C c397C > T
62	Italian	2 days	8 months lived	1	NA	NA	NA	Bradycardia and tachycardia	Hypertrophic cardiomyopathy	NA	1	1	1	NA	C16, C18:1↑	c.843 + 4-843 + 50del
63	Spanish	NA	4.5years lived	NA	NA	NA	NA	NA	NA	NA	NA	NA	NA	NA	C16, C18:1↑	c.532C > T c.159dupT c163delA
64	Spanish	40 h	4 months	1	NA	↑	↑	NA	NA	NA	1	NA	NA	NA	NA	c.159dupT c163delA
65	Italian	72 h	3 years and 5 months lived	1	1	NA	↑	NA	Mild cardiomegaly	NA	NA	NA	1	NA	C16, C18:1↑	Homozygous c.842C > T
66	North American	18 h	2 years lived	1	1	↑	↑	NA	Hypertrophic cardiomyopathy	NA	NA	NA	1	NA	C12–C22↑	c.362delG c.691G > C

(*continued*)

10.3389/fped.2022.1029004

TABLE 2 Continued

Patient ID	Ethnicity	Age at onset	Current age/age of death	Hypoglycemia	Hyperammonemia	CK	ALT	Arrhythmias	Cardiac hypertrophy	Cardiac arrest	Hepatomegaly	Seizures	Poor response/ Hypotonia	dyspnea	Other futures	SLC25A20 genotype
67	Australian	27 h	After 27 h	1	NA	NA	NA	NA	NA	NA	1	NA	NA	NA	C14, C16 and C6-dicarboxylic (adipyl) acylcarnitines↑	c.326delG c.609-3C > G
68	Arabs	32 h	9 days	1	1	↑	↑	1	NA	1	NA	NA	NA	1	C6,C14,C16↑	Homozygous c.609-3C > G
69	South Africans	12 h	8 months	1	1	NA	NA	NA	Biventricular hypertrophy	NA	NA	NA	NA	NA	C12,C16,C18↑	Homozygous c59G > A
70	Spanish	8 months	4 years lived	1	NA	↑	↑	NA	NA	NA	1	1	1	NA	C14, C18↑	c.160_163del4ins4c.536A > G
71	Moroccan	33 h	12 months	1	NA	NA	NA	NA	NA	NA	NA	NA	NA	NA	NA	Homozygous c.536A > G
72	Spanish	Treated from birth	16 years lived	NA	NA	NA	NA	NA	NA	NA	NA	NA	NA	NA	NA	
73	American	5 days	3 years	1	1	NA	NA	LBBB/Prolonged QT interval	Hypertrophic cardiomyopathy	NA	NA	NA	NA	NA	NA	c.84delT a 506-kb deletion
74	Chinese	–	2 months	1	1	NA	↑	NA	Hypertrophic cardiomyopathy	NA	1	NA	NA	NA	C12, C14, C16, C18, C16:1, C18:1↑	c.270delC c.804delG
75	Italian	18 h	2 years lived	1	1	↑	↑	Tachycardia and acute arrhythmias	Biventricular hypertrophy	NA	1	NA	NA	NA	C2↓, C16:0, C18:1, C18:2↑	Homozygous c.713A > G
76	Japanese	2 days	5 years lived	NA	1	NA	NA	Bradycardia	NA	NA	1	NA	NA	1	C16, C14:C3, C16 + C18:1/C2↑	Homozygous c.824G > A
77	Japanese	2 days	26 months	1	1	NA	NA	VT	NA	1	NA	1	NA	NA	C16, C14:C3, C16 + C18:1/C2↑	Homozygous c.824G > A
78	Japanese	30 min	5 years lived	1	NA	NA	NA	NA	Biventricular hypertrophy	NA	NA	NA	NA	1	C16, C14:C3, C16 + C18:1/C2↑	Homozygous c.824G > A
79	American	2 days	lived	1	1	↑	NA	NA	Left ventricular septal hypertrophy	NA	NA	1	1	NA	C16, C18:1/C2↑	c.397C > T c.658G > A

1, existence; ↑, increase; VT, ventricular tachycardia; VF, ventricular fibrillation; LBBB, left bundle branch block; RBBB, right bundle branch block; AVB, Atrioventricular block.

10.3389/fped.2022.1029004

c.199–10T > G splicing mutation. The remaining sufferers were scattered in different nations. The frequency of the c.199–10T > G allele was 33.5% in all cases, whereas it was 82.6% in China.

Biochemical and clinical specifications

Twenty of the thirty individuals with the c.199–10T > G variant exhibited clinical symptoms within 48 h (66.7%). There were arrhythmias in 18 patients (60%), cardiomyopathy in 13 patients (43.3%), hepatomegaly in 4 patients (13.3%), seizures in 9 patients (30%), hyperammonemia in 22 patients (73.3%), increase of CKMB and ALT in 17 patients (56.7%) and 12 patients (40%) respectively. 23 of 30 individuals (76.7%) perished due to the variation c.199–10T > G, which is linked to a severe phenotype.

7/79 cases were attenuated, and homozygosity for variation c.82G > T was confirmed. All of these patients of Pakistani heritage survived. Three patients were diagnosed with cardiomyopathy, although only one had seizures. There were no other clinical signs noted in these patients.

42/79 individuals harbored additional *SLC25A20* mutations. 25 out of 42 participants exhibited clinical signs within 48 h (59.6%). These patients exhibited associated clinical manifestations: 14/42 (33.3%) had arrhythmias, 15/42 (35.7%) had bouts of cardiomyopathy, 11/42(26.2%) had hepatomegaly, and 7/42(16.7%) had seizures. Ammonia, CK and ALT levels were elevated in 22/42(52.3%), 11/42(26.2%) and 14/42(33.3%) patients, respectively.

Discussion

CACT deficiency appears to be very rare in the general population, except for a small number of ethnic subgroups. This study described the biochemical, clinical and genetic characteristics of patients with CACT deficiency, analyzed the distribution and ethnic specificity of the pathogenic genes, provided a theoretical basis of single nucleotide polymorphism detection, and thus contributed to the body of knowledge for early diagnosis and timely intervention in this rare disorder.

There is a wide variation in the prevalence of CACT deficiency among ethnic groups. About 30 cases of CTCT deficiency have been reported elsewhere, while there have been more than 50 reported in Asia. It is reported that the estimated incidence of CACT deficiency is 1/60,000 in Hongkong, 1/76,894 in Hunan, and at least 1/100,000 in Guangzhou China (2, 10, 15). Caucasian groups had a substantially lower incidence of CACT deficiency, which was reported to be 1:750,000–1:2,000,000. Indeed, the misleading clinical presentation, poor prognosis and the need to collect blood and urine specimens for metabolic investigation at an appropriate time in relation to the illness frequently limit the recognition of the disorder. For these reasons, the frequency of CACT deficient inborn defects is probably higher than recorded cases.

CACT deficiency is one of the most severe disorders of the carnitine transport system and mitochondrial fatty acid oxidation. The disorder results in deficient formation of energy-yielding substrates and toxicity of acylcarnitine accumulation which plays a pivotal role in the production of arrhythmias, and then presents a simultaneous dysfunction of the heart, liver, and skeletal muscle, associated with hypoketotic hypoglycemia (33). Severe classic manifestation, the most common, is accompanied by severe hypoketotic hypoglycemia, refractory hyperammonemia, elevated transaminase levels and CK, cardiomyopathy, and abrupt arrhythmias. The prognosis for those with the classic results is exceptionally dismal. Moderate myopathy and hepatomegaly are seen in milder cases, which are less common but do have more accessible residual transporter protein (11, 34, 35). Following an initial metabolic decompensation at birth, the neonate, in our case, developed hypoglycemia, hyperammonemia, and acute and severe arrhythmias before passing away. This may be related to the less residual enzyme activity and the increased accumulation of carnitine-acylcarnitine (33, 34). In our study, CACT deficiency due to the c.199–10T > G variation is a severe phenotype with a significantly higher mortality, arrhythmia, seizures, and hyperammonemia incidence than other variations, while CACT deficiency caused by the c.82G > T mutation is associated with milder phenotype (5). The most frequent mutation was a splicing site variation of c.199–10T > G.

Early recognition and timely treatment are crucial in CACT deficiency. NBS (Newborn screening) plays an important role in early detection of deficiency in enzymes of mitochondrial carnitine-acylcarnitinecycle. Most patients with CACT and CPT2 deficiency had a higher C12–C18:1 level than those without these (3). *SLC25A20* gene mutational analysis is required to identify CACT deficiency, but this can be done without CACT activity assessment. Once a CACT deficiency has been diagnosed, the proper treatment must be implemented. To begin, sufficient glucose must be provided to prevent lipolysis from being broken down. Fasting prevention with frequent meals, a diet rich in carbohydrate, restricting long-chain fatty acids, supplementing with medium chain triglycerides (MCT) and essential polyunsaturated fatty acids are recommended as long-term treatments for CACT deficiency. Administration of carnitine is controversial, on the one hand it exerts to prevent arrhythmias, and on the other hand it causes an increase of acylcarnitines, responsible of arrhythmias (26, 33, 35). Triheptanoin can ameliorate acute cardiomyopathy and increase survival in patients with severe long-chain fatty acid oxidation disorders (26). CACT deficiency can also be treated with skimmed breast milk (30).

There are nine exons in the *SLC25A20* gene, which spans more than 903 bp of genomic DNA on chromosome 3p21.31

(35). At least 42 pathogenic variants of *SLC25A20* have been discovered so far. In contrast to the majority of pathogenic variations, c.199–10T > G and c.82G > T were shown to be shared in Asian and Pakistani origins, respectively. The founder mutation c.82G > T was detected in people of Pakistani ancestry. Our study's Chinese patients were found to have a wide range of homology, with seven distinct variants. The most common variant, c.199–10T > G, suggests that c.199–10T > G may be a hotspot of *SLC25A20* gene mutation in the Chinese population. c.1A > G was detected only 3 times and was not yet found in other than Chinese populations, so it may be unique to the Chinese individuals. The remaining variant was detected only once or twice.

In conclusion, the biochemical, clinical, and genetic characteristics of Chinese patients with CACT deficiency identified in this investigation may aid early identification and intervention. In addition, it appeared from the data that the Chinese patients have a high degree of homozygosity. The c.199–10T > G variant, which is the most common one in this population, has the potential to be a hotspot *SLC25A20* gene mutation. As a result, economical and rapid single nucleotide polymorphism and the genotyping assay can be performed for high-risk patients and their parents in China. In addition, prenatal or presymptomatic diagnosis can be performed in siblings.

Data availability statement

All data, models, and code generated or used during the study appear in the submitted article.

Ethics statement

Written informed consent was obtained from the individual(s), and minor(s)' legal guardian/next of kin, for the publication of any potentially identifiable images or data included in this article.

Author contributions

JS: contributed significantly to analysis and manuscript preparation. XL: performed the data analyses and wrote the manuscript. All authors contributed to the article and approved the submitted version.

Funding

This work was supported by the Construction Fund of Hangzhou Medical Key Discipline (2020-2024) (Grant No.: OO20200448).

Conflict of interest

The authors declare that the research was conducted in the absence of any commercial or financial relationships that could be construed as a potential conflict of interest.

Publisher's note

All claims expressed in this article are solely those of the authors and do not necessarily represent those of their affiliated organizations, or those of the publisher, the editors and the reviewers. Any product that may be evaluated in this article, or claim that may be made by its manufacturer, is not guaranteed or endorsed by the publisher.

References

1. Stanley CA, Hale DE, Berry GT, Deleeuw S, Boxer J, Bonnefont JP. Brief report: a deficiency of carnitine-acylcarnitine translocase in the inner mitochondrial membrane. *N Engl J Med*. (1992) 327(1):19–23. doi: 10.1056/NEJM199207023270104

2. Hui J, Tang NL, Li CK, Law LK, To KF, Yau P, et al. Inherited metabolic diseases in the Southern Chinese population: spectrum of diseases and estimated incidence from recurrent mutations. *Pathology*. (2014) 46(5):375–82. doi: 10.1097/PAT.0000000000000140

3. Zhou D, Cheng Y, Yin X, Miao H, Hu Z, Yang J, et al. Newborn screening for mitochondrial carnitine-acylcarnitine cycle disorders in Zhejiang Province, China. *Front Genet*. (2022) 13:823687. doi: 10.3389/fgene.2022.823687

4. Rubio-Gozalbo ME, Bakker JA, Waterham HR, Wanders RJ. Carnitine-acylcarnitine translocase deficiency, clinical, biochemical and genetic aspects. *Mol Aspects Med*. (2004) 25(5–6):521–32. doi: 10.1016/j.mam.2004.06.007

5. Ryder B, Inbar-Feigenberg M, Glamuzina E, Halligan R, Vara R, Elliot A, et al. New insights into carnitine-acylcarnitine translocase deficiency from 23 cases: management challenges and potential therapeutic approaches. *J Inherit Metab Dis*. (2021) 44(4):903–15. doi: 10.1002/jimd.12371

6. Loft A, Schmidt SF, Caratti G, Stifel U, Havelund J, Sekar R, et al. A macrophage-hepatocyte glucocorticoid receptor axis coordinates fasting ketogenesis. *Cell Metab*. (2022) 34(3):473–86.e9. doi: 10.1016/j.cmet.2022.01.004

7. Stanley CA. Carnitine deficiency disorders in children. *Ann N Y Acad Sci*. (2004) 1033:42–51. doi: 10.1196/annals.1320.004

8. Li X, Zhao F, Zhao Z, Zhao X, Meng H, Zhang D, et al. Neonatal sudden death caused by a novel heterozygous mutation in SLC25A20 gene: a case report and brief literature review. *Leg Med*. (2022) 54:101990. doi: 10.1016/j.legalmed.2021.101990

9. Vatanavicharn N, Yamada K, Aoyama Y, Fukao T, Densupsoontorn N, Jirapinyo P, et al. Carnitine-acylcarnitine translocase deficiency: two neonatal cases with common splicing mutation and in vitro bezafibrate response. *Brain Dev*. (2015) 37(7):698–703. doi: 10.1016/j.braindev.2014.10.005

10. Tang C, Liu S, Wu M, Lin S, Lin Y, Su L, et al. Clinical and molecular characteristics of carnitine-acylcarnitine translocase deficiency: experience with six patients in Guangdong China. *Clin Chim Acta*. (2019) 495:476–80. doi: 10.1016/j.cca.2019.05.018

11. Palmieri F, Scarcia P, Monné M. Diseases caused by mutations in mitochondrial carrier genes SLC25: a review. *Biomolecules*. (2020) 10(4):655. doi: 10.3390/biom10040655

12. Maguolo A, Rodella G, Dianin A, Nurti R, Monge I, Rigotti E, et al. Diagnosis, genetic characterization and clinical follow up of mitochondrial fatty acid oxidation disorders in the new era of expanded newborn screening: a single centre experience. *Mol Genet Metab Rep*. (2020) 24:100632. doi: 10.1016/j.ymgmr.2020.100632

13. Habib A, Azize NAA, Rahman SA, Yakob Y, Suberamaniam V, Nazri MIBA, et al. Novel mutations associated with carnitine-acylcarnitine translocase and carnitine palmitoyl transferase 2 deficiencies in Malaysia. *Clin Biochem*. (2021) 98:48–53. doi: 10.1016/j.clinbiochem.2021.10.002

14. Wang GL, Wang J, Douglas G, Browning M, Hahn S, Ganesh J, et al. Expanded molecular features of carnitine acyl-carnitine translocase (CACT) deficiency by comprehensive molecular analysis. *Mol Genet Metab*. (2011) 103 (4):349–57. doi: 10.1016/j.ymgme.2011.05.001

15. Yan HM, Hu H, Ahmed A, Feng BB, Liu J, Jia ZJ, et al. Carnitine-acylcarnitine translocase deficiency with c.199–10 T > G and novel c.1A > G mutation: two case reports and brief literature review. *Medicine*. (2017) 96(45): e8549. doi: 10.1097/MD.0000000000008549

16. Gürbüz BB, Yılmaz DY, Özgül RK, Koşukcu C, Dursun A, Sivri HS, et al. Clinical and molecular characteristics of carnitineacylcarnitine translocase deficiency with c.270delC and a novel c.408C > A variant. *Turk J Pediatr*. (2021) 63(4):691–6. doi: 10.24953/turkjped.2021.04.017.

17. Fukushima T, Kaneoka H, Yasuno T, Sasaguri Y, Tokuyasu T, Tokoro K, et al. Three novel mutations in the carnitine-acylcarnitine translocase (CACT) gene in patients with CACT deficiency and in healthy individuals. *J Hum Genet*. (2013) 58(12):788–93. doi: 10.1038/jhg.2013.103

18. Pierre G, Macdonald A, Gray G, Hendriksz C, Preece MA, Chakrapani A. Prospective treatment in carnitine-acylcarnitine translocase deficiency. *J Inherit Metab Dis*. (2007) 30(5):815. doi: 10.1007/s10545-007-0518-x

19. Lee RS, Lam CW, Lai CK, Yuen YP, Chan KY, Shek CC, et al. Carnitine-acylcarnitine translocase deficiency in three neonates presenting with rapid deterioration and cardiac arrest. *Hong Kong Med J*. (2007) 13(1):66–8

20. Huizing M, Iacobazzi V, Ijlst L, Savelkoul P, Ruitenbeek W, van den Heuvel L, et al. Cloning of the human carnitine-acylcarnitine carrier cDNA and identification of the molecular defect in a patient. *Am J Hum Genet*. (1997) 61 (6):1239–45. doi: 10.1086/301628

21. IJlst L, van Roermund CW, Iacobazzi V, Oostheim W, Ruiter JP, Williams JC, et al. Functional analysis of mutant human carnitine acylcarnitine translocases in yeast. *Biochem Biophys Res Commun*. (2001) 280(3):700–6. doi: 10.1006/bbrc.2000.4178

22. Iacobazzi V, Invernizzi F, Baratta S, Pons R, Chung W, Garavaglia B, et al. Molecular and functional analysis of SLC25A20 mutations causing carnitine-acylcarnitine translocase deficiency. *Hum Mutat*. (2004) 24(4):312–20. doi: 10.1002/humu.20085

23. Korman SH, Pitt JJ, Boneh A, Dweikat I, Zater M, Meiner V, et al. A novel SLC25A20 splicing mutation in patients of different ethnic origin with neonatally lethal carnitine-acylcarnitine translocase (CACT) deficiency. *Mol Genet Metab*. (2006) 89(4):332–8. doi: 10.1016/j.ymgme.2006.06.009

24. Chen M, Cai Y, Li S, Xiong H, Liu M, Ma F, et al. Late-onset carnitine-acylcarnitine translocase deficiency with SLC25A2° c.199–10T > G variation: case report and pathologic analysis of liver biopsy. *Front Pediatr*. (2020) 8:585646. doi: 10.3389/fped.2020.585646

25. Vitoria I, Martín-Hernández E, Peña-Quintana L, Bueno M, Quijada-Fraile P, Dalmau J, et al. Carnitine-acylcarnitine translocase deficiency: experience with four cases in Spain and review of the literature. *JIMD Rep*. (2015) 20:11–20. doi: 10.1007/8904_2014_382

26. Mahapatra S, Ananth A, Baugh N, Damian M, Enns GM. Triheptanoin: a rescue therapy for cardiogenic shock in carnitine-acylcarnitine translocase deficiency. *JIMD Rep*. (2018) 39:19–23. doi: 10.1007/8904_2017_36

27. Norris MK, Scott AI, Sullivan S, Chang IJ, Lam C, Sun A, et al. Tutorial: triheptanoin and nutrition management for treatment of long-chain fatty acid oxidation disorders. *JPEN J Parenter Enteral Nutr*. (2021) 45(2):230–8. doi: 10.1002/jpen.2034

28. Iacobazzi V, Pasquali M, Singh R, Matern D, Rinaldo P, Amat di San Filippo C, et al. Response to therapy in carnitine/acylcarnitine translocase (CACT) deficiency due to a novel missense mutation. *Am J Med Genet A*. (2004) 126A (2):150–5. doi: 10.1002/ajmg.a.20573

29. Chinen Y, Yanagi K, Nakamura S, Nakayama N, Kamiya M, Nakayashiro M, et al. A novel homozygous missense SLC25A20 mutation in three CACT-deficient patients: clinical and autopsy data. *Hum Genome Var*. (2020) 7:11. doi: 10.1038/s41439-020-0098-y

30. Kritzer A, Tarrant S, Sussman-Karten K, Barbas K. Use of skimmed breast milk for an infant with a long-chain fatty acid oxidation disorder: a novel therapeutic intervention. *JIMD Rep*. (2020) 55(1):44–50. doi: 10.1002/jmd2.12152

31. Chong SC, Law LK, Hui J, Lai CY, Leung TY, Yuen YP. Expanded newborn metabolic screening programme in Hong Kong: a three-year journey. *Hong Kong Med J*. (2017) 23(5):489–96. doi: 10.12809/hkmj176274

32. Fan X, Xie BB, Zhang Q, Yi S, Geng GX, Yang Q, et al. Analysis of four carnitine-acylcarnitine translocase deficiency cases caused by homozygous mutation of SLC25A2° c.199–10T > G. *Zhonghua Er Ke Za Zhi*. (2018) 56 (7):545–9. doi: 10.3760/cma.j.issn.0578-1310.2018.07.014

33. Bonnet D, Martin D, De Lonlay P, Villain E, Jouvet P, Rabier D, et al. Arrhythmias and conduction defects as presenting symptoms of fatty acid oxidation disorders in children. *Circulation*. (1999) 100(22):2248–53. doi: 10.1161/01.cir.100.22.2248

34. Lopriore E, Gemke RJ, Verhoeven NM, Jakobs C, Wanders RJ, Roeleveld-Versteeg AB, et al. Carnitine-acylcarnitine translocase deficiency: phenotype, residual enzyme activity and outcome. *Eur J Pediatr*. (2001) 160(2):101–4. doi: 10.1007/s004310000644

35. Palmieri F. Mitochondrial transporters of the SLC25 family and associated diseases: a review. *J Inherit Metab Dis*. (2014) 37(4):565–75. doi: 10.1007/s10545-014-9708-5

frontiers | Frontiers in Pediatrics

TYPE Original Research
PUBLISHED 11 November 2022
DOI 10.3389/fped.2022.1010886

Check for updates

OPEN ACCESS

EDITED BY
Weida Tong,
National Center for Toxicological Research (FDA), United States

REVIEWED BY
Makoto Nabetani,
Yodogawa Christian Hospital, Japan
Jianxiang Liao,
Shenzhen Children's Hospital, China
Wei-De Lin,
China Medical University, Taiwan

*CORRESPONDENCE
Xinjie Liu
liuxinjie-ert@163.com

†These authors have contributed equally to this work

SPECIALTY SECTION
This article was submitted to Genetics of Common and Rare Diseases, a section of the journal Frontiers in Pediatrics

RECEIVED 03 August 2022
ACCEPTED 26 October 2022
PUBLISHED 11 November 2022

CITATION
Dong M, Zhang T, Hu R, Li M, Wang G and Liu X (2022) Genotype and phenotype spectrum of 10 children with *STXBP1* gene-related encephalopathy and epilepsy.
Front. Pediatr. 10:1010886.
doi: 10.3389/fped.2022.1010886

COPYRIGHT
© 2022 Dong, Zhang, Hu, Li, Wang and Liu. This is an open-access article distributed under the terms of the Creative Commons Attribution License (CC BY). The use, distribution or reproduction in other forums is permitted, provided the original author(s) and the copyright owner(s) are credited and that the original publication in this journal is cited, in accordance with accepted academic practice. No use, distribution or reproduction is permitted which does not comply with these terms.

Genotype and phenotype spectrum of 10 children with *STXBP1* gene-related encephalopathy and epilepsy

Meng Dong†, Tianyu Zhang†, Ruimei Hu, Meng Li, Guan Wang and Xinjie Liu*

Department of Pediatrics, Qilu Hospital, Shandong University, Jinan, China

Objective: *STXBP1* mutations are associated with early onset epileptic encephalopathy (EOEE). Our aim was to explore the phenotype spectrum, clinical treatment and prognosis of *STXBP1*-related encephalopathy (*STXBP1*-E).

Methods: Clinical and genetic data were collected from 10 patients with *STXBP1* mutations. These patients were examined and diagnosed from 2015 to 2021 at the Pediatric Department of Qilu Hospital. Blood samples were collected and sequenced by next generation sequencing and Candidate pathogenic variants were identified using Sanger sequencing in all family members.

Results: All of the patients showed severe epilepsy, varying degrees of intellectual disability and delayed motor. The patients developed multiple seizure types and abnormal electroencephalography (EEG) results at onset, and focal seizures were the most frequent seizure type. Among the patients, 2 were diagnosed with Ohtahara syndrome, 2 patient was diagnosed with West syndrome. The other 6 patients could not be diagnosed with any specifically recognized epilepsy syndrome. Five of the 10 patients had a history of fever with seizures, 4 of whom had eliminated intracranial infection according to the results of cerebrospinal fluid (CSF) examinations, and the other patient was diagnosed with anti-myelin oligodendrocyte glycoprotein (MOG) -associated encephalitis. We identified one patient with a complete deletion of *STXBP1* and 9 patients with *de novo* heterozygous mutations of *STXBP1*. Among those mutations, 4 were novel (c.56°C > T, c.1315A > T, c.751G > C, and c.554_559del), and 5 had been previously reported [c.364C > T, c.569G > A (2 cases), c.748C > T, and c.1651C > T]. For 8 of our patients, different combinations of anti-seizure medications (ASMs) led to seizure freedom. One patient with MOG antibodies in his serum obtained a poor therapeutic effect from the traditional ASMs treatment, so he had to achieve seizure-free status through vagus nerve stimulation (VNS), which had little effect on his psychomotor ability. Fortunately, in one case, patient psychomotor ability was improved through VNS.

Conclusion: Our study shows that *STXBP1* screening should be considered in patients with neonatal seizures with intellectual disability, and frequent seizures with fever should also be considered with the *STXBP1* mutation when intracranial infection is eliminated. VNS has expanded outcome measures to include behavioral and developmental function as well as seizure control.

KEYWORDS

STXBP1 mutations, early infantile epileptic encephalopathy, intellectual disability, phenotype spectrum treatment, prognosis

Introduction

Early-onset epileptic encephalopathy (EOEE) embodies the notion that continuous and repeated epileptic activity itself may contribute to severe neurological and cognitive impairment and prominent interictal epileptiform discharges during the neonatal or early infant period (1). After the initial identification of mutations for cryptogenic West syndrome and Ohtahara syndrome (2), in the genes *ARX, CDKL5, STXBP1, SLC25A22, SPTAN1, PLCb1, MAGI2, PNKP, SCN1A*, numerous other mutated genes for West syndrome, Dravet syndrome and various other types of childhood-onset epilepsy have been found, revealing that a significant proportion of cryptogenic EOEEs are single-gene disorders (3–5). West syndrome, also known as epileptic spasms or infantile spasms which belong to infantile epileptic spasms syndrome (IESS) (6). In 2008, the first mutation in the syntaxin binding protein 1 (*STXBP1*) gene was confirmed to be associated with EOEE (7). Since then, mutations in *STXBP1* have been described in different patient cohorts, the phenotypic spectrum of patients with *STXBP1* mutations has expanded, and an increasing number of studies have indicated that epilepsy and intellectual disease (ID) are 2 major features of *STXBP1* encephalopathy (*STXBP1-E*) (7, 8). However, Hamdan et al. reported a *STXBP1*-positive patient with mild nonsyndromic ID without epilepsy (9). Presently, *STXBP1-E* is considered a complex neurodevelopmental disorder rather than a primary epileptic encephalopathy (10). Previous studies have reported that vigabatrin, valproic acid (VPA), levetiracetam (LEV), adrenocorticotropic hormone and a ketogenic diet (KD) are effective at seizure control (11–15). However, the prognosis of the child is not good, so it is necessary to deeply understand this disease and improve the prognosis. Our study not only expands the phenotypic spectrum associated with *STXBP1-E* but also describes the role of VNS in controlling epilepsy and improving cognition.

Materials and methods

Clinical data and phenotypes groups

All the patients diagnosed EOEE were detected by next-generation sequencing from Jan 2015 to Jul 2021 at the Pediatric Department in Qilu Hospital and only ten previously unreported patients with a *STXBP1* mutation were enrolled in this study. Clinical data [classification in epileptic syndrome, epileptic spasms, ambulatory or video EEG monitoring, magnetic resonance imaging (MRI), history of status epilepticus, treatments, and follow-up until July 2021] were collected from their clinical cases. Approximately 2 ml of peripheral blood (plus EDTA anticoagulant) was obtained from the patient and their parents after receiving written informed consent.

We refer to the study from Wolking et al. (16), they discerned 4 different phenotypic groups and divided into four groups [developmental and epileptic encephalopathies, DEE; genetic epilepsies with febrile seizures (FS) plus, GEFS+; genetic generalized epilepsy, GGE; focal epilepsy] according to their clinical characters.

The investigation was performed with the approval of the ethics committee of Qilu Hospital.

Genetic analysis

Genomic DNA was extracted using a QIAamp Blood Midi Kit (QIAGEN, Valencia, CA). To identify disease-causing gene variants, a GenCap panel with 175 genes (including *STXBP1*, **Table 1**) associated with epilepsy was customized, and a capture strategy was performed using the GenCap custom enrichment kit (MyGenostics Inc, Beijing, China). An Illumina NextSeq 500 sequencer (Illumina, San Diego, CA, United States) was used with 150 bp paired-end reads. An ABI3730xl sequencer (Applied Biosystems, United States) was used to apply the Sanger sequencing method, and the results were compared to the capture sequencing results.

After sequencing, the raw data were saved in FASTQ format. Quality control (QC) filters were applied to remove reads with low quality. Then, the clean reads were assembled and spliced using the second-generation sequencing analysis platform provided by MyGenostics and the coverage and sequencing quality of the target region were evaluated. Finally, flash analysis platform was used to analyze the pathogenicity of variation, and the possible variation loci were determined. The pathogenicity of variation loci was also analyzed according to ACMG (American College of Medical Genetics and Genomics) genetic variation classification criteria and guidelines.

We performed a conservative analysis of the eight mutant amino acid sequences using Clustal Omega. Domains of *STXBP1* were identified based on the National Center for Biotechnology Information (NCBI) Conserved Domain Database. Multiple sequence alignment of *STXBP1* was

TABLE 1 Detected gene list.

PAH	L2HGDH	DHTKD1	CTH	ARX	MMACHC	ATP7B	GCSH
PTS	D2HGDH	GALK1	MTHFR	SLC6A8	MMAA	G6PD	CPS1
GCH1	IDH2	INPP5E	MTRR	GAMT	MMAB	ATP7A	OTC
QDPR	ETFA	LAMP2	MTR	GATM	ABCD4	PTPN11	ASS1
PCBD1	ETFB	MAOA	GNMT	ERCC8	GPHN	MVK	ASL
SPR	ETFDH	PNPLA2	AHCY	ERCC6	MCEE	ACSF3	ARG1
FAH	BCAT1	SLC2A1	SLC25A13	SLC46A1	MMADHC	OGDH	OAT
TAT	BCAT2	HSD17B10	SLC25A15	SLC19A1	HCFC1	FH	NAGS
HPD	SLC22A5	SLC2A2	GLUD1	FOLR1	LMBRD1	AASS	SLC7A7
HGD	CPT1A	SLC3A1	GLUL	FOLR2	GCDH	ABHD5	MAT1A
HAL	CPT2	SLC7A9	BCKDHA	DHFR	HMGCL	ACAT1	CBS
UROC1	SLC25A20	GLYCTK	BCKDHB	DDC	AUH	ADK	SUOX
FTCD	MLYCD	TYMP	DBT	PHGDH	TAZ	ALDH6A1	MOCS1
GLDC	ACADSB	TK2	DLD	PSAT1	OPA3	ASPA	MOCS2
AMT	ACADS	DGUOK	SARDH	ABAT	SERAC1	DBH	NR0B1
ACADM	POLG	PRODH	ALDH5A1	ALDH7A1	FBXL4	MCCC2	SOX9
ACADVL	SUCLA2	ALDH4A1	SRY	ALPL	KMT2D	PCCA	CYP21A2
HADHA	MPV17	SLC6A20	AR	PNPO	KDM6A	PCCB	CYP11B1
HADHB	C10orf2	SLC6A19	HSD17B3	ETHE1	SGSH	HLCS	HSD3B2
HADH	RRM2B	SLC36A2	SRD5A2	FOXG1	NAGLU	BTD	CYP17A1
ACAD8	SUCLG1	IVD	NR5A1	MECP2	HGSNAT	PC	StAR
TH	SLC25A4	MCCC1	WT1	CDKL5	GNS	MUT	

performed using the ClustalW program. Three-dimensional structural models of *STXBP1* were predicted with the Swiss-model web tool. Protein structure images were generated using the PDB file and PyMOL. Hydrogen bonds in the proteins were demonstrated using PyMOL to predict changes in mutant stability.

Results

STXBP1 molecular analysis

In total, we identified 9 *de novo* STXBP1 mutations in 10 patients by next generation sequencing to sequence all the *STXBP1* exons and splice junction boundaries from the genomic DNA. Upon searching in the HGMD (The Human Gene Mutation Database), 6 of them had been reported previously [c.364C > T, c.569G > A (2 cases), c.748C > T, c.1651C > T, c.56°C > T, one complete deletion], and the other 3 were novel mutations (c.1315A > T, c.751G > C, c.554_559del). Two unrelated patients (patient No. 2 and patient No. 8) had the same *STXBP1* nucleotide alteration (c.569G > A). The details of the *STXBP1* mutations are summarized in **Table 2** and **Figure 1**. According to ACMG (American College of Medical Genetics and Genomics) criteria, we have determined that the variants are Pathogenic variants (**Supplementary Figures S1, S2**).

Clinical characterization of *STXBP1*-positive of the 10 patients

The clinical features of this study with EOEE having *STXBP1* defects are summarized in **Table 3**. The median age of ascertainment was 14.5 months ($n = 10$, range = 1–35 months), with a median age of seizure onset of 8.5 months (range = 0–22 months), and most patients had intellectual disability prior to seizure onset (60%). At the last follow-up, all patients had development delay. Patient 1 and patient 2 were diagnosed with Ohtahara syndrome, and patient 1 developed into West syndrome at the age of 5 months. Two patients had West syndrome (patient 4, 9), and 6 patients were diagnosed with unclassified EOEEs (patients 2, 3, 5, 6, 7, and 8). Various seizure types presented during the course of the disease, including epileptic spasms, partial seizures, atonic seizures, absence seizures, myoclonic seizures, and tonic seizures. The initial seizure types of the patients were partial seizures in 4 cases (patients 3, 5, 6, and 7), tonic seizures in 1 case (patient 2), tonic-clonic seizures in 2 cases (patients 1 and 10) and spasms in 3 cases (patients 4, 8, and 9). One case (patient 3) had an average number of seizures a few times a month, and all were associated with high fever. Three cases (patients 2, 6, and 8) had an average number of seizures of ≤5 times per day, and 6 cases (patients 1, 4, 5, 7, 9, and 10) had an average number of 10–20 seizures per day. Five

10.3389/fped.2022.1010886

TABLE 2 Summary of the variants in the STXBP-1 mutations.

Patients	Exon	Nucleotide	Protein	Pathogenic analysis	Reference
1	exon6	c.364C > T	p. R122X	pathogenic	(17, 18)
2	exon7	c.569G > A	p. R190Q	pathogenic	(19)
3	exon7	c.56°C > T	p. P187l	uncertain	(20)
4	exon9	c.748C > T	p. Q250X	Pathogenic	(17)
5	exon15	c.1315A > T	p. I439F	uncertain	novel
6	exon18	c.1651C > T	p. R551C	Pathogenic	(21)
7	exon9	c.751G > C	p. A251P	Likely pathogenic	novel
8	exon7	c.569G > A	p. R190Q	Pathogenic	(19)
9	wholegene	c150928c02101	–	Pathogenic	(22)
10	exon7	c.554_559delinsTGTG	p. E185fs*28	uncertain	novel

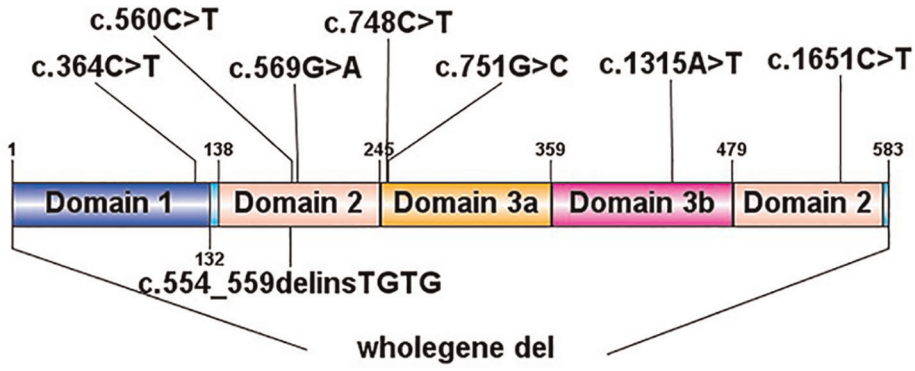


FIGURE 1
Pathogenic STXBP1 mutations.

patients (patients 2, 3, 6, 7, and 8) had a history of seizure with fever, and intracranial infection was eliminated in 4 patients (patients 2, 3, 7, and 8). In patient 6, cerebrospinal fluid examination showed positive MOG antibody. MRI showed abnormal signal near white matter in lateral ventricle triangle. There was still epileptic seizure after glucocorticoid and gamma globulin treatment, and the genetic examination showed *STXBP1* gene mutation.

Reviewing the above clinical characteristics of all patients, we could distinguish 3 different phenotypic groups. (1) Seven patients (patient 1, 2, 4, 5, 7, 9, 10) had intractable seizures, occurrence of developmental stagnation or regression after seizure onset, and additional neuropsychiatric deficits compatible with developmental and epileptic encephalopathy (DEE). (2) Patient 3 had an average number of seizures a few times a month, and all were associated with high fever. All the times, two seizure types presented during the course of the disease, focal seizures and tonic seizures, and had a relatively benign course, generally good drug response, normal development, and mild neuropsychiatric symptoms, corresponding to genetic epilepsies with febrile seizures plus (GEFS+). (3) The last 2 patients (patient 6, 8) with some form of focal epilepsy.

EEG abnormalities were observed in all patients, including burst suppression (patients 1 and 10), hypsarrhythmia (patient 9), multifocal epileptic activities (patients 2, 3, 7), focal epileptic activities (patients 4, 5, and 6), and slow background (patients 3, 5, 6, 8). The initial EEG of 7 patients with *STXBP1* mutations is shown in **Figure 2**. The other 3 patients had no initial EEG. At the last follow-up, EEG showed normalization after treatment in 3 cases (patients 3, 4, and 5). The initial brain MRI did not present any apparent structural abnormality. Of the nine patients included here, one patient had subdural effusion (patient 1), one had hypoxic-ischemic change (patient 4), and two had delayed myelination (patients 6 and 7). Blood biochemical examination showed no apparent abnormalities.

Treatment and prognosis

With regard to the treatment and prognosis, including the use of VNS, huge improvements in seizure activity were found in all of our cohorts. With ongoing brain maturation, patient 1, who did not become seizure-free during the first

TABLE 3 Clinical features of patients with STXBP-1 mutations.

Patient number	1	2	3	4	5	6	7	8	9	10
Age at study	2 years 11 months	1 year 2 months	1 year 5 months	3 months 17 days	1 year 10 months	9 months 10 days	8 months 20 days	1 year 1 month	2 years 7 months	1 month 11 days
Age at onset	1 month	1 year 1 month	1 year	2 months 23 days	10 months 25 days	9 months	8 months 14 days	1 year 1 month	1 month	9 days
sex	M	M	M	F	M	M	F	M	F	F
area	urban	urban	rural	rural	rural	rural	rural	rural	urban	rural
Seizure type (s)	tonic-clonic, spasms	tonic-clonic seizure, spasms, absence seizure	fever sensitivity, focal seizure, tonic	spasms, focal seizure	focal seizure, myoclonic	focal seizure	focal seizure	spasms, clonic, focal seizure, myoclonic	spasms, absencetonic-clonic, focal seizure	spasms, absencetonic-clonic, tonic-clonic, focal seizure
EEG at onset	burst suppression	multifocal epileptic activities	slow background, focal epileptic activities	focal epileptic activities, spasms	slow background, focal epileptic activities	slow background, focal epileptic activities	multifocal epileptic activities	slow background	Hypsarrhythmia	burst suppression
MRI	subdural effusion	nomal	nomal	Hypoxic ischemic change	nomal	delayed myelination	delayed myelination	nomal	nomal	nomal
evolution of treatment	PB, NZP + Pred, NZP + TPM	LEV	PB, VPA + CZP	LEV, LEV + TPM, VPA + TPM, VPA + TPM + LEV	OXC + CZP, OXC + CZP + VPA, VPA + LEV, VNS	PB, OXC + TPM, OXC + VPA + CZP + TPM, VNS	OXC, OXC + CZP, CZP + VPA, CZP + VPA + TPM	LEV	TPM, TPM + NZP	NZP + TPM, NZP + TPM + LEV, ACTH, ACTH + vigabatrin, TPM + LEV + vigabatrin
respond to therapy	sz free for near 8 years 8 months	sz free for more than 5 years	sz free for more than 3 years 5 months	sz free for more than 4 years 8 months	sz free for more than 2 years 6 months	sz free for more than 3 years 8 months	sz free for more han 3 years 3 months	sz free for more than 3 years 3 months	sz free for more than 6 years 4 months	no obvious seizures for 2 months
EEG follow up (age)	Hypsarrhythmia (4 months) multifocal and focal epileptic activities (2 years 11 months)	multifocal epileptic activities (4 years 3 months)	nomal (2 years 10 months)	nomal (5 months)	nomal (2 years 9 months)	slow background (2 years 5 months)	multifocal epileptic activities (1 year 10 months)	slow background (3 years 2 months)	Focal epileptic activities (2 years 7 months)	–
Current developmental or intellectual disability	no walk or speech, No social contact (9 years)	poor social contact (4 years 2 months)	nomal (3 years 9 months)	able to walk or speech, poor social contact (5 years)	able to say single syllables.No social contact (4 years)	nomal (4 years 7 months)	able to say single syllables (3 years)	able to say single syllables poor social contact (4 years 5 months)	able to say a few words,poor social contact (7 years)	No walk or speech, No social contact (1 year 6 months)
family history	no	mother	aunt (father's sister)	no	sister	no	no	no	no	No

(*continued*)

10.3389/fped.2022.1010886

10.3389/fped.2022.1010886

TABLE 3 Continued

Patient number	1	2	3	4	5	6	7	8	9	10
History of hypoxia	no	no	no	yes	no	no	no	no	no	no
Diagnosis	OS with evolution to IESS	EOEE	EOEE	IESS	EOEE	EOEE	EOEE	EOEE	IESS	OS
Clinical groups	DEE	DEE	GEFS+	DEE	DEE	Focal epilepsy	DEE	Focal epilepsy	DEE	DEE

F, female; M, male; sz, seizure; PB, phenobarbital; NZP, nitrazepam; Pred, prednison; TPM, topiramate; CZP, clonazepam; VPA, valproic acid; OXC, oxcarbazepine; LEV, Levetiracetam; VNS, vagus nerve stimulation; ID, intellectual disability; ACTH, adrenocorticotropic hormone; EEG, electroencephalograms; MRI, magnetic resonance imaging; IESS, Infantile epileptic spasms syndrome; OS, Ohtahara syndrome; EOEE, early-onset epileptic and encephalopathy; DEE, developmental and epileptic encephalopathies; GEFS+, genetic epilepsies with febrile seizures (FS) plus.

few months of life, developed epileptic spasms. Together with the observation that none of the patients with *STXBP1* mutations evolved to West syndrome later in life after controlling seizure. Four cases (patients 2, 4, 5, and 8) were free of seizures after treatment with LEV. Two patients received LEV monotherapy, they got seizures free when the dose of LEV got 40 mg/kg/d. Others received LEV combination therapy. Initially, patient 4 was treated with bolus doses of topiramate (TPM), nitrazepam (NZP) and VPA, but there was no significant improvement. Next, NZP was replaced with LEV, and the seizures were completely controlled. Patient 5 had failed with bolus doses of oxcarbazepine (OXC), clonazepam (CZP) and VPA. Next, CZP and OXC were replaced with LEV, and the seizures were completely controlled after treatment with LEV and VPA. To make things even better, he tried VNS after being seizure-free and improved his psychomotor ability. Patients 2 and 8 were free of seizures after treatment with LEV alone. Patient 6 had frequent convulsions after a two-day history of fever. The CSF analysis showed an elevated white count of 14 per cubic millimeter. Serum MOG antibodies were requested, and he was started on intravenous immunoglobulin, OXC, TPM, and glucocorticoid (GC). Two weeks later, although his repeat lumbar puncture (LP) was negative and the serum titer of MOG antibodies disappeared, his seizure status had not changed. Next, CZP and VPA were added successively; however, the seizures failed to respond to any medical treatment. Fortunately, he tried VNS, and his seizures promptly ceased after 20 days of VNS therapy. Although the effects of treatment on seizure frequency might be quantifiable, the effect on intellectual disability is not so easily assessed. The good news is that one case (patient 5) experienced improved psychomotor ability after VNS.

Discussion

STXBP1 is a member of the evolutionarily conserved Sec1/Munc-18 gene family that plays a central role in vesicular docking and fusion. Splicing mutations, a frameshift mutation, and nonsense mutations can lead to loss-of-function, which is a common mechanism underlying *STXBP1-E* (22). In this study, two novel recurrent missense mutations in *STXBP1* (c.1315A > T, c.751G > C) were detected in three patients with unclassified epileptic encephalopathy (patients 5 and 7). We found that all the patients with novel mutations had similar clinical symptoms: early onset seizures and intellectual disability.

Barcia et al. (15) and Wolking et al. (16) demonstrated that the clinical features in *STXBP1-E* are mostly shared with early onset seizures, a poor prognosis with severe intellectual disability and a high mortality rate and a frequent evolution to infantile spasms (IS). However, in our study, 10 patients

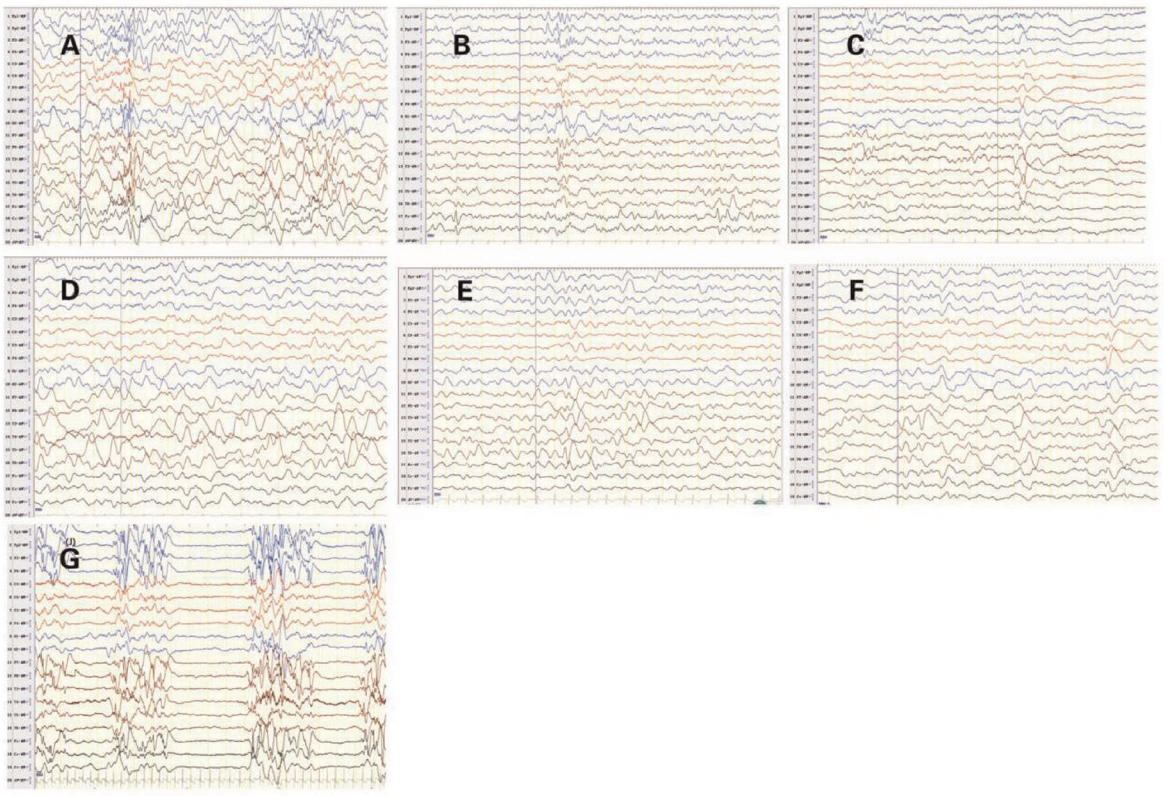


FIGURE 2
Initial electroencephalograms of patients with syntaxin-binding protein 1 (STXBP1) mutations. (**A**) Patient2 1year and 1months, Multifocal spikes and slow waves during sleep status. (**B**) Patient3 1year and 5months, slow background, multifocal slow waves. (**C**) Patient4 2 months and 29 days, spasms and focal epileptic activities originating from the left Anterior and middle temporal area. (**D**) Patient5 1 year and 2 months, slow background and Slow wave activity originating from the left middle and posterior temporal regions. (**E**) Patient6 9 months and 10days, sharp-slow waves originating from the right Posterior temporal area during sleep status on interictal EEG. (**F**) Patient7 8 months and 20 days, slow and spikes-slow waves originating from bilateral Parietal, Occipital, mid-posterior temporal areas during sleep status. (**G**) Patient10 1 months, burst suppression (BS).

eventually became seizure-free, three of the 10 patients were West syndrome and they were reducing the development of West syndrome. We consider this result to be related to prompt and early seizure control. If the notion is that seizures must be controlled as soon as possible to optimize prognosis, then optimal targeted therapies are needed to shorten exposure to repetitive seizures.

EOEE are characterized by recurrent clinical seizures and prominent interictal epileptiform discharges seen during the early infantile period. The underlying genetic cause often results in developmental delay in its own right, with the epileptic encephalopathy further adversely affecting development. Frequent epileptiform activity that impacts adversely on development, typically causing slowing or regression of developmental skills. Similar to the study from Wolking et al. (16), all the patients were also divided into four groups (DEE, GEFS+, GTCS and focal epilepsy) according to their clinical characters. In our study, we noted that developmental delay and epilepsy are characteristic features of *STXBP1*-E, in keeping with previous reports (7, 8). Although developmental delay can be seen at seizure onset, some degree of developmental delay is present prior to the onset of seizures in many patients (patients 1, 3, 4, 5, 6, and 10). Furthermore, in 2009, Hamdan et al. (8) reported *de novo* mutations, p. R388X and c.169 + 1G > A in 2 cases, with intellectual disability and nonsyndromic epilepsy. In 2011, Hamdan et al. (9) reported 1 case with a novel *de novo* truncating mutation, c.1206delT/p.402X, presenting with nonsyndromic intellectual disability deficit and no history of epilepsy. These findings suggest no correlation between seizures and intellectual disability, as described previously (23). *STXBP1* plays an important role in many aspects of neurodevelopment.

The initial EEG was abnormal in all patients. The main EEG finding was (multi)focal abnormality, while burst suppression or hypsarrhythmia was observed in three patients. This type of alteration is much less specific. At the last follow-up, the repeat EEG recordings of 3 cases (patients 3, 4, and 5) were

normal. Structural imaging with MRI was normal in most cases, although delayed myelination was present in two patients, subdural effusion was observed in one patient, and hypoxic-ischemic change was observed in one patient.

Treating *STXBP1-E* involves a multidisciplinary approach, including epilepsy control and neurological rehabilitation. Currently, there is no treatment for intellectual, motor or behavioral disturbances, which exert a significant impact on the quality of life of patients. Several studies have reported antiepileptic effects of LEV through modulating the synaptic vesicle release affected by *STXBP1* mutations (11, 24). LEV had a specific effect on the children with *STXBP1-E* in our study, and four patients presented a dramatic response to LEV with full epilepsy control. Among the various antiepileptic drugs, valproic acid and topiramate were partially effective in some patients. Serum MOG antibodies were found in patient 6, and he was given immunomodulation treatment. Although the study from Lopez et al. (25) have identified *STXBP1* as an important player in cytotoxic lymphocytes function, the immunomodulation treatment did not reduce seizure status in patient 6. Further studies are needed to clarify the correlation between *STXBP1-E* and autoimmune mechanism.

VNS has been used in the treatment of epilepsy in clinic, but the mechanism of its application is not completely clear, its mechanism may be: 1. VNS can increase the number of neurotransmitters, such as norepinephrine, 5-hydroxytryptamine and γ-aminobutyric acid (γ-aminobutyricacid) which can produce antiepileptic effect (26, 27). VNS treatment can cause the desynchronization of cortical electrical activity, and the number of spike waves and electrodes decreased significantly during the opening phase (28). The mechanism of VNS in the treatment of epilepsy might be the asynchrony of neural circuits in the hippocampus and thalamic cortex (29). At present, it is believed that the indications for the treatment of epilepsy with VNS include drug refractory epilepsy, unable to take other surgical treatment or poorly controlled epilepsy after other types of surgery. VNS is a relatively safe surgical method, which can be tolerated by most patients, it has low incidence of complications. Because the mechanism of this operation is not clear, ASMs is still the first choice for epileptic control. Fortunately, 1 patient showed improvement in cognitive function after VNS. This improvement may be a direct effect of VNS on behavior, concentration, and affect (30) and may be related to seizure reduction, reduced ASM load in association with successful antiepileptic treatment or putative effects of VNS on mood (26). The most favorable treatment regimens should note the improvement of the prognosis on both seizures and psychomotor ability. VNS may represent the patient's option for optimal seizure and cognitive outcomes. A recent study identified miR-218 and miR-424 as regulators of *STXBP1* expression. Inhibiting their interaction with *STXBP1* resulted in an increase in *STXBP1* protein levels (27). Guiberson et al. identified three chemical chaperones, trehalose, sorbitol, and 4-phenylbutyrate, which are able to restore *STXBP1* protein levels (28) and rescue synaptic deficits. A clinical pilot trial of 4-phenylbutyrate in a small group of *STXBP1* patients began in 2020, and it will be the first trial of a disease-modifying therapy in this patient population (27). Further studies are required to screen for and identify molecules that are effective for both wild-type and mutant *STXBP1*.

In conclusion, *STXBP1* analysis should be considered for infants with seizures and severe ID, and we have shown that the major clinical features of *STXBP1* mutations are frequent seizures from epilepsy, abnormal initial EEG, and intellectual disability. Frequent seizures with fever should also be considered with the *STXBP1* mutation when intracranial infection is eliminated. This study demonstrates better response to LEV in *STXBP1* disorder. Thus, we would suggest early consideration of the use of LEV in this population. VNS may be worthy of consideration as an option for treating *STXBP1*-E. Further studies are needed to determine the adequacy and ideal duration of VNS for optimal management.

Data availability statement

The raw data supporting the conclusions of this article will be made available by the authors, without undue reservation.

Ethics statement

The studies involving human participants were reviewed and approved by The ethics committee in Qilu Hospital of Shandong University. Written informed consent to participate in this study was provided by the participants' legal guardian/next of kin.

Author contributions

XL and RH: conceived and designed the study, and critical revision of manuscript for intellectual content. ML and GW: collected the patients' clinical data. MD and TZ: wrote the paper. All authors contributed to the article and approved the submitted version.

Acknowledgments

This work is supported by grants from the National Natural Science Foundation of China (82171352). We greatly thank the technical support from MyGenostics Co. Ltd. (Beijing) in the interpretation of gene results. We also thank the parents of the patient for signing the written consent for the publication of the cases.

Conflict of interest

The authors declare that the research was conducted in the absence of any commercial or financial relationships that could be construed as a potential conflict of interest.

Publisher's note

All claims expressed in this article are solely those of the authors and do not necessarily represent those of their affiliated organizations, or those of the publisher, the editors and the reviewers. Any product that may be evaluated in this article, or claim that may be made by its manufacturer, is not guaranteed or endorsed by the publisher.

Supplementary material

The Supplementary Material for this article can be found online at: https://www.frontiersin.org/articles/10.3389/fped.2022.1010886/full#supplementary-material.

References

1. Berg AT, Berkovic SF, Brodie MJ, Buchhalter J, Cross JH, van Emde Boas W, et al. Revised terminology and concepts for organization of seizures and epilepsies: report of the ILAE Commission on Classification and Terminology, 2005–2009. *Epilepsia*. (2010) 51(4):676–85. doi: 10.1111/j.1528-1167.2010.02522.x

2. Yamatogi Y, Ohtahara S. Age-dependent epileptic encephalopathy: a longitudinal study. *Folia Psychiatr Neurol Jpn*. (1981) 35(3):321–32. doi: 10.1111/j.1440-1819.1981.tb00233.x

3. Mastrangelo M, Leuzzi V. Genes of early-onset epileptic encephalopathies: from genotype to phenotype. *Pediatr Neurol*. (2012) 46(1):24–31. doi: 10.1016/j.pediatrneurol.2011.11.003

4. Carvill GL, Weckhuysen S, McMahon JM, Hartmann C, Møller RS, Hjalgrim H, et al. GABRA1 and *STXBP1*: novel genetic causes of Dravet syndrome. *Neurology*. (2014) 82(14):1245–53. doi: 10.1212/WNL.0000000000000291

5. Deprez L, Weckhuysen S, Holmgren P, Suls A, Dyck TV, Goossens D, et al. Clinical spectrum of early-onset epileptic encephalopathies associated with *STXBP1* mutations. *Neurology*. (2010) 75(13):1159–65. doi: 10.1212/WNL.0b013e3181f4d7bf

6. Zuberi SM, Wirrell E, Yozawitz E, Wilmshurst JM, Specchio N, Riney K, et al. Ilae classification and definition of epilepsy syndromes with onset in neonates and infants: position statement by the Ilae task force on nosology and definitions. *Epilepsia*. (2022) 63:1349–97. doi: 10.1111/epi.17239

7. Saitsu H, Kato M, Mizuguchi T, Hamada K, Osaka H, Tohyama J, et al. De novo mutations in the gene encoding *STXBP1* (MUNC18-1) cause early infantile epileptic encephalopathy. *Nat Genet*. (2008) 40(6):782–8. doi: 10.1038/ng.150

8. Hamdan FF, Piton A, Gauthier J, Lortie A, Dubeau F, Dobrzeniecka S, et al. De novo *STXBP1* mutations in mental retardation and nonsyndromic epilepsy. *Ann Neurol*. (2009) 65(6):748–53. doi: 10.1002/ana.21625

9. Hamdan FF, Gauthier J, Dobrzeniecka S, Lortie A, Mottron L, Vanasse M, et al. Intellectual disability without epilepsy associated with *STXBP1* disruption. *Eur J Hum Genet*. (2011) 19(5):607–9. doi: 10.1038/ejhg.2010.183

10. Gupta A. *STXBP1*-related EOEE - early onset epilepsy and encephalopathy, or is it early onset epileptic encephalopathy? *Epilepsy Curr*. (2016) 16(5):302–4. doi: 10.5698/1535-7511-16.5.302

11. Liu S, Wang L, Cai XT, Zhou H, Yu D, Wang Z. Therapeutic benefits of ACTH and levetiracetam in *STXBP1* encephalopathy with a de novo mutation: a case report and literature review. *Medicine*. (2018) 97(18):e0663. doi: 10.1097/MD.0000000000010663

12. Li T, Cheng M, Wang J, Hong S, Li M, Liao S, et al. De novo mutations of *STXBP1* in Chinese children with early onset epileptic encephalopathy. *Genes Brain Behav*. (2018) 17(8):e12492. doi: 10.1111/gbb.12492

13. Mignot C, Moutard ML, Trouillard O, Gourfinkel-An I, Jacquette A, Arveiler B, et al. *STXBP1*-related Encephalopathy presenting as infantile spasms and generalized tremor in three patients. *Epilepsia*. (2011) 52(10):1820–7. doi: 10.1111/j.1528-1167.2011.03163.x

14. Milh M, Villeneuve N, Chouchane M, Kaminska A, Laroche C, Barthez MA, et al. Epileptic and nonepileptic features in patients with early onset epileptic encephalopathy and *STXBP1* mutations. *Epilepsia*. (2011) 52(10):1828–34. doi: 10.1111/j.1528-1167.2011.03181.x

15. Barcia G, Chemaly N, Gobin S, Milh M, Bogaert PV, Barnerias C, et al. Early epileptic encephalopathies associated with *STXBP1* mutations: could we better delineate the phenotype? *Eur J Med Genet*. (2014) 57(1):15–20. doi: 10.1016/j.ejmg.2013.10.006

16. Wolking S, May P, Mei D, Møller RS, Balestrini S, Helbig KL, et al. Clinical spectrum of *STX1B*-related epileptic disorders. *Neurology*. (2019) 92(11):e1238–49. doi: 10.1212/WNL.0000000000007089

17. Liu J, Tong L, Song S, Niu Y, Li J, Wu X, et al. Novel and de novo mutations in pediatric refractory epilepsy. *Mol Brain*. (2018) 11(1):48. doi: 10.1186/s13041-018-0392-5

18. Butler KM, da Silva C, Alexander JJ, Hegde M, Escayg A. Diagnostic yield from 339 epilepsy patients screened on a clinical gene panel. *Pediatr Neurol*. (2017) 77:61–6. doi: 10.1016/j.pediatrneurol.2017.09.003

19. Retterer K, Juusola J, Cho MT, Vitazka P, Millan F, Gibellini F, et al. Clinical application of whole-exome sequencing across clinical indications. *Genet Med*. (2016) 18(7):696–704. doi: 10.1038/gim.2015.148

20. Weckhuysen S, Holmgren P, Hendrickx R, Jansen AC, Hasaerts D, Dielman C, et al. Reduction of seizure frequency after epilepsy surgery in a patient with *STXBP1* encephalopathy and clinical description of six novel mutation carriers. *Epilepsia*. (2013) 54(5):e74–80. doi: 10.1111/epi.12124

21. Yamamoto T, Shimojima K, Yano T, Ueda Y, Takayama R, Ikeda H, et al. Loss-of-function mutations of *STXBP1* in patients with epileptic encephalopathy. *Brain Dev*. (2016) 38(3):280–4. doi: 10.1016/j.braindev.2015.09.004

22. Stamberger H, Nikanorova M, Willemsen MH, Accorsi P, Angriman M, Baier H, et al. *STXBP1* Encephalopathy: a neurodevelopmental disorder including epilepsy. *Neurology*. (2016) 86(10):954–62. doi: 10.1212/WNL.0000000000002457

23. Dilena R, Striano P, Traverso M, Viri M, Cristofori G, Tadini L, et al. Dramatic effect of levetiracetam in early-onset epileptic encephalopathy due to *STXBP1* mutation. *Brain Dev*. (2016) 38(1):128–31. doi: 10.1016/j.braindev.2015.07.002

24. Hallböök T, Lundgren J, Stjernqvist K, Blennow G, Strömblad LG, Rosén I. Vagus nerve stimulation in 15 children with therapy resistant epilepsy; its impact on cognition, quality of life, behaviour and mood. *Seizure*. (2005) 14(7):504–13. doi: 10.1016/j.seizure.2005.08.007

25. Lopez J, Noori T, Minson M, Jovanoska LL, Thia K, Hildebrand MS, et al. Bi-Allelic mutations in *STXBP2* reveal a complementary role for *STXBP*1 in cytotoxic lymphocyte killing. *Front Immunol*. (2018) 9:529. doi: 10.3389/fimmu.2018.00529

26. Henry TR. Therapeutic mechanisms of Vagus nerve stimulation. *Neurology*. (2002) 59(6 Suppl 4):S3–14. doi: 10.1212/wnl.59.6_suppl_4.s3

27. DeGiorgio CM, Schachter SC, Handforth A, Salinsky M, Thompson J, Uthman B, et al. Prospective long-term study of Vagus nerve stimulation for

the treatment of refractory seizures. *Epilepsia*. (2000) 41(9):1195–200. doi: 10.1111/j.1528-1157.2000.tb00325.x

28. Yokoyama R, Akiyama Y, Enatsu R, Suzuki H, Suzuki Y, Kanno A, et al. The immediate effects of Vagus nerve stimulation in intractable epilepsy: an intra-operative electrocorticographic analysis. *Neurol Med Chir*. (2020) 60(5):244–51. doi: 10.2176/nmc.oa.2019-0221

29. Ilyas A, Toth E, Pizarro D, Riley KO, Pati S. Modulation of neural oscillations by Vagus nerve stimulation in posttraumatic multifocal epilepsy: case report. *J Neurosurg*. (2018):1–7. doi: 10.3171/2018.6.JNS18735

30. Manford M. Recent advances in epilepsy. *J Neurol*. (2017) 264(8):1811–24. doi: 10.1007/s00415-017-8394-2

frontiers | Frontiers in Pediatrics

TYPE Case Report
PUBLISHED 18 November 2022
DOI 10.3389/fped.2022.990230

Check for updates

OPEN ACCESS

EDITED BY
Ruth Roberts,
ApconiX, United Kingdom

REVIEWED BY
Robert Lebel,
Upstate Medical University, United States
Makoto Abe,
Osaka University, Japan
Chunyan Peng,
Hubei University of Medicine, China

*CORRESPONDENCE
Jiazhong Sun
sunjiazhong300@163.com
Junli Xue
l10045@yangtzeu.edu.cn

SPECIALTY SECTION
This article was submitted to Genetics of Common and Rare Diseases, a section of the journal Frontiers in Pediatrics

RECEIVED 09 July 2022
ACCEPTED 02 November 2022
PUBLISHED 18 November 2022

CITATION
Huang Q, Jiang C, Sun J, Xue J and Zhang VW (2022) Case report: A novel mutation in *TRPS*1 identified in a Chinese family with tricho-rhino-phalangeal syndrome I: A therapeutic challenge.
Front. Pediatr. 10:990230.
doi: 10.3389/fped.2022.990230

COPYRIGHT
© 2022 Huang, Jiang, Sun, Xue and Zhang. This is an open-access article distributed under the terms of the Creative Commons Attribution License (CC BY). The use, distribution or reproduction in other forums is permitted, provided the original author(s) and the copyright owner(s) are credited and that the original publication in this journal is cited, in accordance with accepted academic practice. No use, distribution or reproduction is permitted which does not comply with these terms.

Case report: A novel mutation in *TRPS*1 identified in a Chinese family with tricho-rhino-phalangeal syndrome I: A therapeutic challenge

Qi Huang[1], Cheng Jiang[2], Jiazhong Sun[1]*, Junli Xue[3]* and Victor Wei Zhang[4]

[1]Department of Endocrinology, Zhongnan Hospital of Wuhan University, Wuhan, China, [2]Emergency Center, Zhongnan Hospital of Wuhan University, Wuhan, China, [3]Department of Endocrinology, The Second Clinical Medical College, Yangtze University, Jingzhou, China, [4]Department of Clinical Genetics, AmCare Genomics Lab, Guangzhou, China

Tricho-rhino-phalangeal syndrome (TRPS) is a rare autosomal dominant malformation caused by mutations involving the *TRPS*1 gene. Patients with TRPS exhibit distinctive craniofacial and skeletal abnormalities. This report presents three intra-familial cases with *TRPS*1 gene mutations that showed the characteristic features of TRPS. A 13-year-old boy was admitted to Department of Endocrinology for the evaluation of short stature. Physical examination revealed that the boy had thin sparse hair, pear-shaped nose, protruding ears, small jaw and brachydactyly. A survey of his family history indicated that the boy's sister and mother shared the same clinical features. Radiological techniques demonstrated a different degree of skeletal abnormalities in these siblings. Next-generation sequencing and quantitative PCR were performed and showed a novel deletion mutation in exons 3–5 in the three familial cases, confirming the diagnosis of TRPS I. The healthy father did not carry the deletion mutation. Currently, there was no specific therapy for TRPS I; however, genetic consultation may be useful for family planning

KEYWORDS

tricho-Rhino-Phalangeal syndrome, *TRPS*1 gene, deletion mutation, short stature, sparse hair

Introduction

First reported by Giedion in 1966 (1), Tricho-rhino-phalangeal syndrome (TRPS) is a rare heritable congenital or sporadic disorder characterized by typical craniofacial features and noticeable skeletal abnormalities, especially of phalanges, metacarpals and metatarsal bones (2–4).

Based on clinical characteristics and genetic analysis, TRPS is distinguished into three subtypes: TRPS I (OMIM 190350), known as Giedion syndrome, have distinct clinical manifestations that often correspond to distinct mutations or haploinsufficiency in the *TRPS*1 gene (5). Moreover, TRPS II (OMIM 150230), also

named Langer-Giedion syndrome (LGS), is caused by a contiguous gene deletions involving both *TRPS*1 and *EXT*1 (6, 7). TRPS II differs from TRPS I by the presence of multiple exostoses and intellectual disability (6). TRPS III (OMIM 190351) is also associated with *TRPS*1 mutations. Besides typical TRPS feature, TRPS III cases have more severe skeletal malformations (7).

Herein, we describe a Chinese Han family with three TRPS I cases caused by a novel deletion mutation in the *TRPS*1 gene involving exons 3–5 (**Figure 1**).

Patients and clinical evaluation

Case 1

A 13-year-old boy, proband, was first admitted to our Endocrinology Department for evaluation of his short stature. He was born after a full term pregnancy and normal delivery, as the second child in non-consanguineous family. His parents reported that his birth weight and length was normal but gradually developed short stature upon birth. In addition, he often suffered from respiratory infections and his tonsils were removed. However, no intellectual impairment was observed.

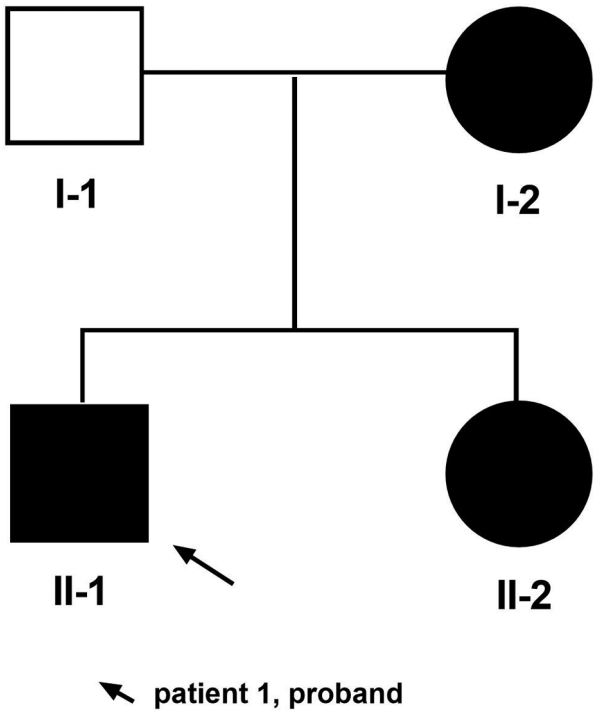


FIGURE 1
Pedigree of family. The arrow indicates patient 1 as the proband.

Upon admission, a routine examination revealed that the boy's weight was 81 kg (>97th percentile) and his standing height was 152.2 cm (3rd percentile). Pubertal development was normal. Another prominent dysmorphic feature included markedly thin and sparse scalp hair, protruding ears, a bulbous pear-shaped nose and a long philtrum with a thin upper lip [**Figure 2A(a)**].

Laboratory tests showed that serum levels of calcium, inorganic phosphate, alkaline phosphatase, free T4, TSH, PTH, corticosteroid and insulin-like growth factor 1 (IGF-1) were normal. The karyotype was 46, XY. Further extremity and radiological examinations showed brachydactyly of fingers and toes [**Figure 2B(a)**].

Case 2

The patient was a 23-year-old girl, the elder sister of patient 1. She showed similar features to her brother, with a height of 146 cm (<3rd percentile). She was almost bald and declined to take off her wig [**Figure 2A(b)**]. She showed a brachydactyly with obvious clinodactyly, a deviation of the forefinger, middle fingers and ring fingers bilaterally. Radiography revealed distortion of the proximal middle phalanges on the second, third and fourth fingers bilaterally. She also showed a skeletal malformation on second through fifth proximal phalanx on both feet [**Figure 2B(b)**].

Case 3

The mother of the siblings, with a height of 140 cm (<3rd percentile), presented with sparse scalp hair and a nose with a bulbous tip [**Figure 2A(c)**]. She also showed bone abnormalities on her hands [**Figure 2B(c)**], but she declined further laboratory tests and radiological examinations.

Molecular analysis

Genomic DNA from the proband and his family members was extracted from peripheral blood samples. A custom-designed Medical Exome Sequencing (MES, AmCare Genomic Lab), including target region capture of more than 5,000 phenotype-related genes contained in the Online Mendelian Inheritance in Man (OMIM), was applied and was followed by next-generation sequencing (NGS, PE 150) on the Illumina platform (Illumina, Inc.). Alignment of the sequence to the reference human genome (hg19) was performed by NextGen (Softgenetics, LLC). Trio analysis including both SNV annotation and exome-based CNV identification was done by an in-house pipeline. Synonymous as well as common SNPs (MAF > 0.1% in gnomAD) were filtered out subsequently. All

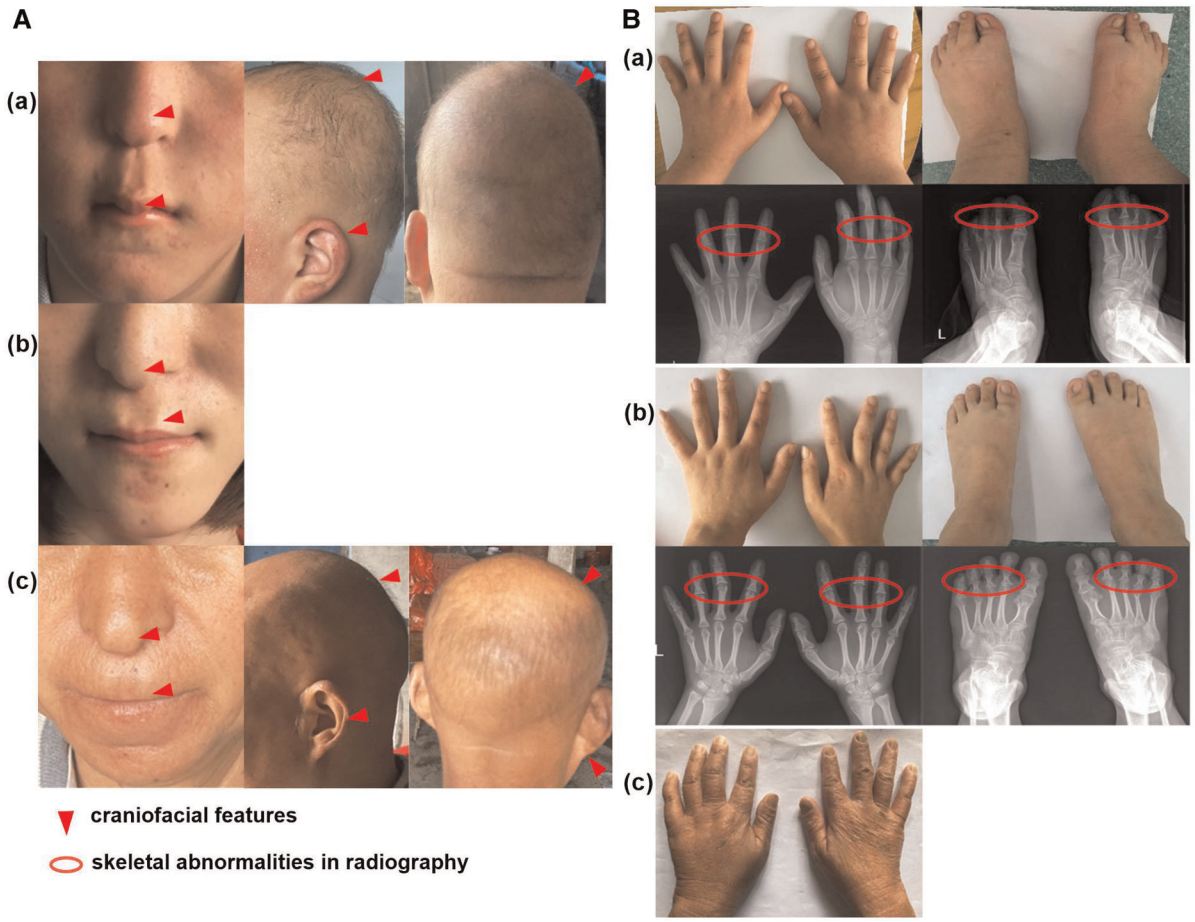


FIGURE 2
Clinical feature of the family cases. (A) The craniofacial feature of proband (a), his sister with wig (b) and mother (c); (B) The skeletal abnormalities of proband (a), his sister (b) and mother (c).

the candidate variants were further evaluated based on the ACMG guideline for SNV interpretation (8). A detailed protocol was described in a previous study (9).

The Candidate variant was validated by quantitative PCR (qPCR). Three pair primers of *TRPS*1 exon 3–5 were designed to amplify all exons of the deletion fragment as follows: TRPS1-EX3, 5′-TGAAACTGGGCTCAAACCTT-3′ (forward) and 5′-GGGG ACTCACTGGAGACAAA-3′ (reverse); TRPS1-EX4, 5′-CTGGTGGCCTCTGTACC ATT-3′ (forward) and 5′-ACAAAATA AAAGCTTCTCTCCCC-3′ (reverse); TRPS1-EX5, 5′- AGGAATCCCTTGGTTTCCAC -3′ (forward) and 5′-AGTCCGTCATACAC CCAAGC-3′ (reverse).

Molecular Findings

Based on the MES trio analysis and qPCR validation, a small heterozygous deletion c.38−? _2700+? del within the *TRPS*1 gene (NM_014112.5) was identified (**Figure 3A**). It is segregated in all the patients of this family (proband, his elder sister and mother), and the healthy father did not carry the deletion (**Figures 3B,C**). This novel small deletion includes exons 3 to 5, and is not present in gnomAD database, HGMD or any peer-reviewed publication. It is predicted to disrupt the reading frame and undergo nonsense-mediated decay (NMD) resulting in an amino acid change (p.Asn13Lysfs*3) because of the multiple exons deletion. According to the ACMG guideline, this variant is classified as likely pathogenic.

Discussion

*TRPS*1 was reported as the causal gene of TRPS I by Momeni et al. in 2000 (3). Haploinsufficiency is the known pathogenicity mechanism for the *TRPS*1 gene (7, 10). In a previous comprehensive study, deletion variants of *TRPS*1 have been reported in multiple cases, most of them are whole

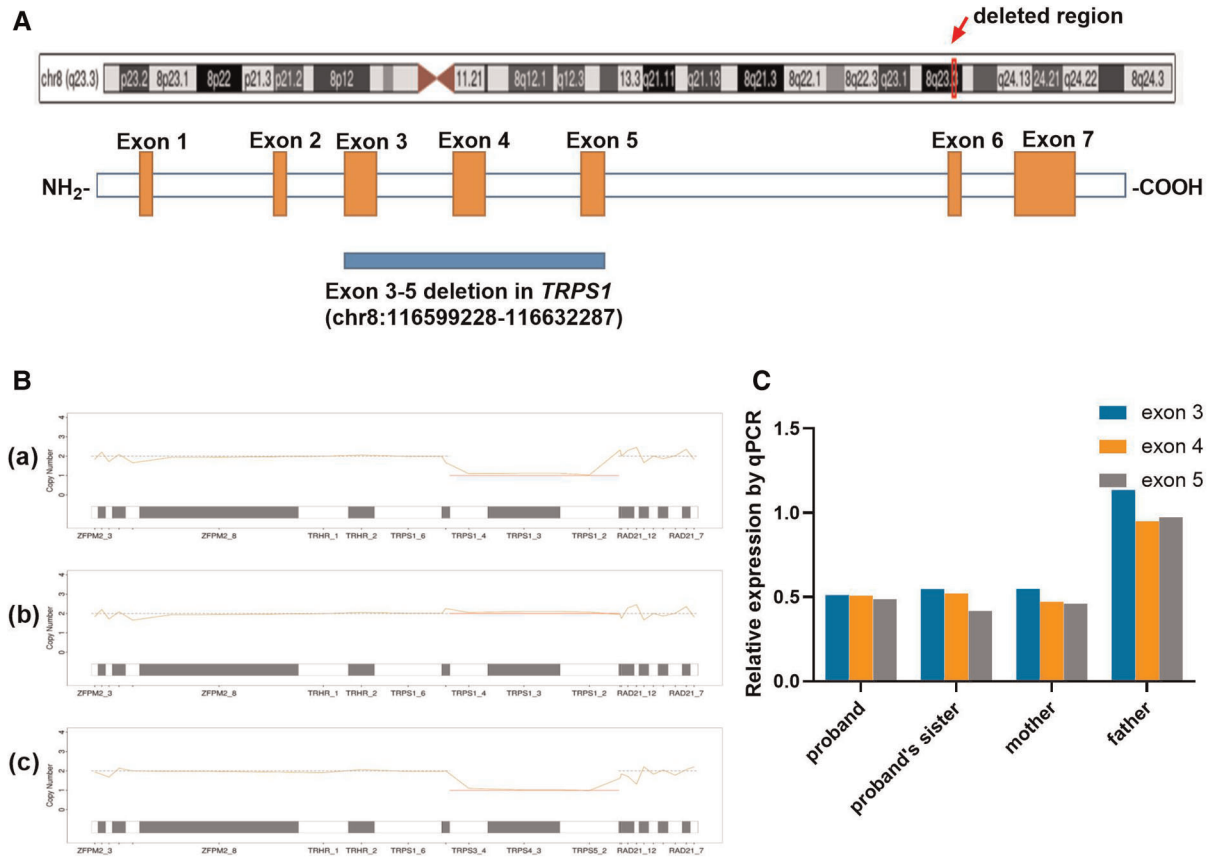


FIGURE 3
Genetic analysis. (**A**) Distribution of the muti-exon deletion in *TRPS*1 gene; (**B**) Copy number variation result of proband (a), his father (b) and mother (c) using NGS coverage depth data. The line charts present the copy number of 8q23 region for each family member, including *TRPS*1 and the gene's upstream and downstream locations. The proband and his mother were heterozygous for the deletion (×1) for exons 3–5 (CDS2-4), and his father was normal at this region. (**C**) qPCR results of all the family members. The proband, his sister and mother were carrying heterozygous deletion of exons 3–5 (×0.5), and his father was normal (×1).

gene deletions that include exons 1 to 7 or large fragments deletions. Only one patient carrying a smaller (exon 2–6) deletion within the gene has been reported (2). The recurrence of variable sizes of fragment deletion suggests the structure complexity in this region.

We are reporting the second family carrying a small 3-exon deletion within the *TRPS*1 gene, which is predicted to disrupt the functional GATA motif of TRPS1. A mouse model study has revealed that a heterozygous knockdown of the GATA motif leads to hair and facial anomalies that overlap with findings of TRPS (11).

Our study also provides further evidence that structure variation is a common cause of TRPS. In this study, we used an optimized pipeline that combined both the SNV identification and NGS coverage depth data for CNV (even the small deletion/duplications) calls within one dataset, which proved to be a sensitive and cost-effective genetic analysis for the suspected TRPS patients, as well as for the better understanding of the genetic etiology of TRPS.

Definitive diagnosis of the disease is essential to perform timely therapeutic procedures. Nevertheless some alternative approaches have been tried for therapy of a few TRPS cases with mixed results. Short stature is a frequent clinical finding in affected individuals. How to improve their short stature is what these patients and their parents are most interested in. K Stagi (12) and Sarafoglou (13) described their TRPS I cases with or without growth hormone (GH) deficiency, and a remarkable increase in growth was observed through GH therapy in four cases. However, Naselli (14) reported another two TRPS I cases with poor growth, and showed no improvement in linear growth after a 1-year GH replacement therapy. In our study, the evaluation of GH-IGF-1 axis revealed that the boy did not have GH deficiency. His bone age was 15-year assessed through RUS-CHN radiographic atlas method, therefore he had no indications for GH treatment.

Sparse scalp hair is another major feature of TRPS patients. Their diffuse alopecia varies from normal hair to complete baldness (15), and the treatment option for alopecia remains

unclear. Mi Soo Choi reported their experience in the medical treatment of a TRPS boy (15). In this case, neither topical minoxidil nor oral finasteride was effective in preventing the progression of alopecia or inducing hair growth. Finally, the patient's hairs started to re-grow at 4 months after hair transplantation operation. All of our three patients complained of hair loss and slow hair growth rate since their childhood. Compared to Mi Soo Choi's patient (15), whose occipital scalp hair had normal hair density and diameter, our patients' hair on the entire scalp was affected and tended to be thinner.

At present there is no special therapy for TRPS, even though alternative approaches were employed as GH replacement therapy for short stature and hair transplantation for baldness, the therapeutic results mixed. Therefore, genetic counseling may be useful for family planning.

Data availability statement

The datasets for this article are not publicly available due to concerns regarding participant/patient anonymity. Requests to access the datasets should be directed to the corresponding author.

Ethics statement

The studies involving human participants were reviewed and approved by Ethics committee of Zhongnan Hospital of Wuhan University. Written informed consent to participate in this study was provided by the participants' legal guardian/next of kin. Written informed consent was obtained from the individual(s), and minor(s)' legal guardian/next of kin, for the publication of any potentially identifiable images or data included in this article.

Author contributions

QH: conducted research. QH and CJ: wrote the paper. QH, JZS and JLX: conceived the research. VWZ: Writing-analyzed the data. All authors contributed to the article and approved the submitted version.

Funding

This work was supported by grants from the Natural Science Foundation of Hubei Province (2017CFB265) and National Natural Science Foundation of China (81800764).

Conflict of interest

The authors declare that the research was conducted in the absence of any commercial or financial relationships that could be construed as a potential conflict of interest.

Publisher's note

All claims expressed in this article are solely those of the authors and do not necessarily represent those of their affiliated organizations, or those of the publisher, the editors and the reviewers. Any product that may be evaluated in this article, or claim that may be made by its manufacturer, is not guaranteed or endorsed by the publisher.

References

1. Giedion A. Tricho-rhino-phalangeal syndrome. *Helv Paediatr Acta*. (1966) 21 (5):475–85. Das tricho-rhino-phalangeale Syndrom. ger.

2. Maas SM, Shaw AC, Bikker H, Lüdecke HJ, van der Tuin K, Badura-Stronka M, et al. Phenotype and genotype in 103 patients with tricho-rhino-phalangeal syndrome. *Eur J Med Genet*. (2015) 58(5):279–92. doi: 10.1016/j.ejmg.2015.03.002

3. Momeni P, Glöckner G, Schmidt O, von Holtum D, Albrecht B, Gillessen-Kaesbach G, et al. Mutations in a new gene, encoding a zinc-finger protein, cause tricho-rhino-phalangeal syndrome type I. *Nat Genet*. (2000) 24(1):71–4. doi: 10.1038/71717

4. Wang C, Xu Y, Qing Y, Yao R, Li N, Wang X, et al. TRPS1 Mutation detection in Chinese patients with tricho-rhino-phalangeal syndrome and identification of four novel mutations. *Mol Genet Genomic Med*. (2020) 8(10): e1417. doi: 10.1002/mgg3.1417

5. Kaiser FJ, Brega P, Raff ML, Byers PH, Gallati S, Kay TT, et al. Novel missense mutations in the TRPS1 transcription factor define the nuclear localization signal. *Eur J Hum Genet*. (2004) 12(2):121–6. doi: 10.1038/sj.ejhg.5201094

6. Shanske AL, Patel A, Saukam S, Levy B, Lüdecke HJ. Clinical and molecular characterization of a patient with langer-giedion syndrome and mosaic del(8) (q22.3q24.13). *Am J Med Genet, Part A*. (2008) 146a(24):3211–6. doi: 10.1002/ajmg.a.32615

7. Lüdecke HJ, Schaper J, Meinecke P, Momeni P, Gross S, von Holtum D, et al. Genotypic and phenotypic spectrum in tricho-rhino-phalangeal syndrome types I and III. *Am J Hum Genet*. (2001) 68(1):81–91. doi: 10.1086/316926

8. Richards S, Aziz N, Bale S, Bick D, Das S, Gastier-Foster J, et al. Standards and guidelines for the interpretation of sequence variants: a joint consensus recommendation of the American college of medical genetics and genomics and the association for molecular pathology. *Genet Med*. (2015) 17(5):405–24. doi: 10.1038/gim.2015.30

9. Wang Z, Lin J, Qiao K, Cai S, Zhang VW, Zhao C, et al. Novel mutations in HINT1 gene cause the autosomal recessive axonal neuropathy with neuromyotonia. *Eur J Med Genet*. (2019) 62(3):190–4. doi: 10.1016/j.ejmg.2018.07.009

10. Zepeda-Mendoza CJ, Cousin MA, Basu S, Jenkinson G, Oliver G, Pittock ST, et al. An intragenic duplication of TRPS1 leading to abnormal transcripts and causing trichorhinophalangeal syndrome type I. *Cold Spring Harbor Mol Case Stud*. (2019) 5(6):a004655. doi: 10.1101/mcs.a004655

11. Malik TH, Von Stechow D, Bronson RT, Shivdasani RA. Deletion of the GATA domain of TRPS1 causes an absence of facial hair and provides new insights into the bone disorder in inherited tricho-rhino-phalangeal syndromes. *Mol Cell Biol*. (2002) 22(24):8592–600. doi: 10.1128/MCB.22.24.8592-8600.2002

12. Stagi S, Bindi G, Galluzzi F, Lapi E, Salti R, Chiarelli F. Partial growth hormone deficiency and changed bone quality and mass in type I trichorhinophalangeal syndrome. *Am J Med Genet, Part A*. (2008) 146a (12):1598–604. doi: 10.1002/ajmg.a.32348

13. Sarafoglou K, Moassesfar S, Miller BS. Improved growth and bone mineral density in type I trichorhinophalangeal syndrome in response to growth hormone therapy. *Clin Genet*. (2010) 78(6):591–3. doi: 10.1111/j.1399-0004.2010.01434.x

14. Naselli A, Vignolo M, Di Battista E, Papale V, Aicardi G, Becchetti S, et al. Trichorhinophalangeal syndrome type I in monozygotic twins discordant for hip pathology. Report on the morphological evolution of cone-shaped epiphyses and the unusual pattern of skeletal maturation. *Pediatr Radiol*. (1998) 28(11):851–5. doi: 10.1007/s002470050481

15. Choi MS, Park MJ, Park M, Nam CH, Hong SP, Kim MH, et al. Treatment of hair loss in the trichorhinophalangeal syndrome. *Ann Dermatol*. (2018) 30 (3):382–3. doi: 10.5021/ad.2018.30.3.382

frontiers | Frontiers in Genetics

TYPE Original Research
PUBLISHED 24 November 2022
DOI 10.3389/fgene.2022.988047

Check for updates

OPEN ACCESS

EDITED BY
Ruth Roberts,
ApconiX, United Kingdom

REVIEWED BY
Yemin Zhang,
Wuhan University, China
Fei Yu,
Tongji University School of Medicine, China

*CORRESPONDENCE
Guoqun Luo,
2751096131@qq.com
Huan Li,
leywoom@163.com

†These authors have contributed equally to this work

SPECIALTY SECTION
This article was submitted to Genetics of Common and Rare Diseases, a section of the journal Frontiers in Genetics

RECEIVED 06 July 2022
ACCEPTED 01 November 2022
PUBLISHED 24 November 2022

CITATION
Zhong Y, Chen X, Zhao J, Deng H, Li X, Xie Z, Zhou B, Xian Z, Li X, Luo G and Li H (2022), Integrative analyses of potential biomarkers and pathways for non-obstructive azoospermia.
Front. Genet. 13:988047.
doi: 10.3389/fgene.2022.988047

COPYRIGHT
© 2022 Zhong, Chen, Zhao, Deng, Li, Xie, Zhou, Xian, Li, Luo and Li. This is an open-access article distributed under the terms of the Creative Commons Attribution License (CC BY). The use, distribution or reproduction in other forums is permitted, provided the original author(s) and the copyright owner(s) are credited and that the original publication in this journal is cited, in accordance with accepted academic practice. No use, distribution or reproduction is permitted which does not comply with these terms.

Integrative analyses of potential biomarkers and pathways for non-obstructive azoospermia

Yucheng Zhong[1†], Xiaoqing Chen[2†], Jun Zhao[1†], Hao Deng[1†], Xiaohang Li[1], Zhongju Xie[1], Bingyu Zhou[1], Zhuojie Xian[1], Xiaoqin Li[1], Guoqun Luo[1*] and Huan Li[1*]

[1]Assisted Reproductive Technology Center, Southern Medical University Affiliated Maternal & Child Health Hospital of Foshan, Foshan, China, [2]Department of Breast Surgical Oncology, Southern Medical University Affiliated Maternal & Child Health Hospital of Foshan, Foshan, China

Background: Non-obstructive azoospermia (NOA) is the most severe form of male infertility. Currently, the molecular mechanisms underlying NOA pathology have not yet been elucidated. Hence, elucidation of the mechanisms of NOA and exploration of potential biomarkers are essential for accurate diagnosis and treatment of this disease. In the present study, we aimed to screen for biomarkers and pathways involved in NOA and reveal their potential molecular mechanisms using integrated bioinformatics.

Methods: We downloaded two gene expression datasets from the Gene Expression Omnibus (GEO) database. Differentially expressed genes (DEGs) in NOA and matched the control group tissues were identified using the limma package in R software. Subsequently, Gene ontology (GO), Kyoto Encyclopedia of Genes and Genomes (KEGG), gene set enrichment analysis (GSEA), protein-protein interaction (PPI) network, gene-microRNAs network, and transcription factor (TF)-hub genes regulatory network analyses were performed to identify hub genes and associated pathways. Finally, we conducted immune infiltration analysis using CIBERSORT to evaluate the relationship between the hub genes and the NOA immune infiltration levels.

Results: We identified 698 common DEGs, including 87 commonly upregulated and 611 commonly downregulated genes in the two datasets. GO analysis indicated that the most significantly enriched gene was protein polyglycylation, and KEGG pathway analysis revealed that the DEGs were most significantly enriched in taste transduction and pancreatic secretion signaling pathways. GSEA showed that DEGs affected the biological functions of the ribosome, focaladhesion, and protein_expor. We further identified the top 31 hub genes from the PPI network, and friends analysis of hub genes in the PPI network showed that NR4A2 had the highest score. In addition, immune infiltration analysis found that $CD8^+$ T cells and plasma cells were significantly correlated with ODF3 expression, whereas naive B cells, plasma cells, monocytes, M2 macrophages, and resting mast cells showed significant variation in the NR4A2 gene expression group, and there were differences in T cell regulatory immune cell infiltration in the FOS gene expression groups.

Conclusion: The present study successfully constructed a regulatory network of DEGs between NOA and normal controls and screened three hub genes using integrative bioinformatics analysis. In addition, our results suggest that functional changes in several immune cells in the immune microenvironment may play an important role in spermatogenesis. Our results provide a novel understanding of the molecular mechanisms of NOA and offer potential biomarkers for its diagnosis and treatment.

KEYWORDS

non-obstructive azoospermia, differentially expressed genes, hub genes, bioinformatics, biomarker

1 Introduction

Over the past few decades, the incidence of infertility has rapidly increased every year. Infertility affects approximately 15% of couples of childbearing age. Azoospermia is the most severe phenotype of male infertility, with approximately 10–15% of infertile men seeking medical attention (Lotti et al., 2014; Tournaye et al., 2017). Some congenital or acquired causes can be found in the vast majority of cases of obstructive azoospermia (OA) (Krausz, 2011; Pan et al., 2018). Non-obstructive azoospermia (NOA), the most severe form of male factor infertility, is characterized by the lack of sperm in the ejaculate and affects about 5–10% of infertile men (Jarow et al., 1989; Lotti et al., 2014; Tournaye et al., 2017). OA is typically characterized by normal spermatogenesis, whereas NOA represents a heterogeneous condition in which spermatogenesis is impaired, including insufficient spermatogenesis and maturation arrest in Sertoli cell-only syndrome (Krausz, 2011; Lotti et al., 2014; Tournaye et al., 2017). Klinefelter syndrome and Y chromosome microdeletions are the most common congenital causes of NOA (Forti et al., 2010; Krausz, 2011; Corona et al., 2017). The etiology of acquired NOA includes torsion, mumps, orchitis, cryptorchidism, and iatrogenic problems (Krausz, 2011; Lotti et al., 2014; Tournaye et al., 2017). For nearly half of the patients with NOA, the etiology remains unknown (Poongothai et al., 2009). Previously, NOA was considered an untreatable condition that required fertilization with donor sperm. With the advent of microdissection testicular sperm extraction (mTESE) and intracytoplasmic sperm injection (ICSI), these techniques have become the first-line treatments for NOA patients (Krausz, 2011; Lotti et al., 2014; Tournaye et al., 2017). Unfortunately, the probability of retrieving sperm is only about 50% in men with NOA owing to partial and heterogeneous preserved focal spermatogenesis (Krausz, 2011; Lotti et al., 2014; Tournaye et al., 2017). Currently, the molecular mechanisms underlying NOA pathology remain unclear. However, this remains an important challenge to solve. Therefore, the identification of genetic abnormalities in patients with NOA is critical.

Several studies have identified potential biomarkers involved in NOA using microarray analysis, weighted gene co-expression network analysis (WGCNA), whole-exome sequencing, and single-cell transcriptome sequencing (scRNA-seq) (Wang et al., 2018; Zheng et al., 2019; Chen et al., 2020; Zhao et al., 2020). However, only a few of these biomarkers are currently used for the diagnosis of NOA. In addition, these studies did not integrate immune infiltration analysis, and the immune system plays an important role in testicular dysfunction and male infertility. Immune infiltration analysis can be used to study the infiltrated immune cells in the testes, to infer and discover the role of immune cells in NOA, and to develop diagnostic and therapeutic targets for the disease. This omission laid the foundation for the present study.

In the present study, we identified differentially expressed genes (DEGs) for NOA by analyzing two mRNA expression profiles downloaded from the Gene Expression Omnibus database (GEO, http://www.ncbi.nlm.nih.gov/geo/). Our results provide a novel understanding of the molecular mechanisms of NOA and offer potential biomarkers for its diagnosis and treatment.

2 Materials and methods

2.1 Microarray data

Two gene expression datasets (GSE45885 and GSE45887) (Zhao et al., 2021) related to male NOA were derived from GEO (GPL6244 [HuGene-1_0-st] Affymetrix Human Gene 1.0 ST Array [transcript (gene) version]) (Chicco, 2022) using the R package GEOquery (Hunt et al., 2022) of R software program. The data type was expression profiling by array, and the species was *Homo sapiens*. Twenty-seven NOA and four normal control samples were obtained from GSE45885, and GSE45887 contained 16 NOA and four normal control samples. The characteristics of GSE45885 and GSE45887 patients can be seen in Supplementary Tables S1, S2. The raw data from the GSE45885 and GSE45887 datasets were normalized using the limma package (Liu et al., 2021). The data analysis process can be seen in Figure 1.

2.2 Identification of differentially expressed genes (DEGs)

DEGs with the threshold criterion of $|\log2FC| > 1$ and $p < 0.05$ from NOA and normal control samples in GSE45885 and

GSE45887 datasets were screened with the limma package (Walker, 2009). Subsequently, heatmaps and volcano plots of DEGs from each dataset were plotted using the pheatmap package (Ning et al., 2022) and ggplot2 package (Gustavsson et al., 2022) in the R analysis platform.

2.3 Gene ontology (GO) and kyoto encyclopedia of genes and genomes (KEGG) enrichment analyses of DEGs

GO analysis is a common method for annotating and analyzing the biological processes of genes, including biological processes (BPs), molecular functions (MFs), and cellular components (CCs) (Ge et al., 2020). KEGG is a widely used database that stores information on genomes, biological pathways, diseases, and drugs (Kanehisa et al., 2021). We performed biological analyses using clusterProiler (Wu et al., 2021) in the R software statistical analysis platform (significant at $p < 0.05$) to visualize the GO terms and KEGG pathway enrichment analysis of DEGs from NOA and normal control samples.

2.4 Gene set enrichment analysis (GSEA)

GSEA determines whether a set of predefined genes shows statistically significant, concordant differences between related phenotypes to screen for significant differential biological functions (Nguyen et al., 2021). We obtained the "C2. kegg.v7.4. symbols" gene set from MSigDB (Liberzon et al., 2015) for GSEA of the two datasets. Furthermore, GSEA was automatically completed and visualized using clusterProiler (Wu et al., 2021) in R software, and statistical significance was set at $p < 0.05$.

2.5 Construction of protein-protein interaction (PPI) network

PPI (Das and Mitra, 2021) networks are composed of individual proteins that interact with each other, and are involved in various aspects of biological signal transmission, gene expression regulation, energy and substance metabolism, and cell cycle regulation. Systematic analysis of functional interactions between proteins is of great significance for comprehending the principle of proteins in biological systems, the reaction mechanism of biological signals, and the mechanisms of generation or development of diseases under special physiological states, as well as the functional relationships between proteins.

The STRING (Szklarczyk et al., 2021) database currently covers 9.6 million proteins and 13.8 million protein-protein interactions from 5,090 organisms and contains known and predicted protein-protein interactions. The results of the STRING database were derived from experimental data, PubMed abstract texts, other database data, and bioinformatics methods. In this study, a PPI network of DEGs of NOA was constructed using the STRING database and visualized using the Cytoscape (Puig et al., 2020) software.

2.6 Construction of miRNA-hub gene and transcription factor-hub gene regulatory networks

Hub genes were identified using GOSemSim (Kamran and Naveed, 2022) in R software. In addition, the functional similarity between proteins was evaluated using the geometric mean of semantic acquaintance in CCs and MF using GOSemSim in R software. We also analyzed hub genes using the NetworkAnalyst database (https://www.networkanalyst.ca/NetworkAnalyst/home.xhtml) and constructed miRNA-hub gene interaction and transcription factor-hub gene networks.

2.7 Immune infiltration analysis by CIBERSORT

CIBERSORT (Le et al., 2021) is a deconvolution algorithm for the expression matrix of immune cell subtypes based on linear support vector regression to estimate the abundance of immune cell infiltration in a mixed-cell population using RNA-seq data. We analyzed immune cell infiltration and the proportion of NOA tissue using CIBERSORT and conducted a correlation analysis of related immune cells by obtaining the hub gene to evaluate the relationship between the hub gene and NOA immune infiltration levels.

2.8 Statistical analysis

R version 4.0.2 software (https://cran.r-project.org/) was used to conduct the statistical analyses. For the comparison of the two groups of continuous variables, the statistical significance of the normally distributed variables was estimated using the independent Student's t-test, and the differences between the non-normally distributed variables were analyzed using the Mann-Whitney U test. All statistical p-values were bilateral, and a p-value of <0.05 was considered statistically significant.

3 Results

3.1 Identification of DEGs in NOA

First, we obtained the corresponding data using the R package GEOquery package and standardized the original

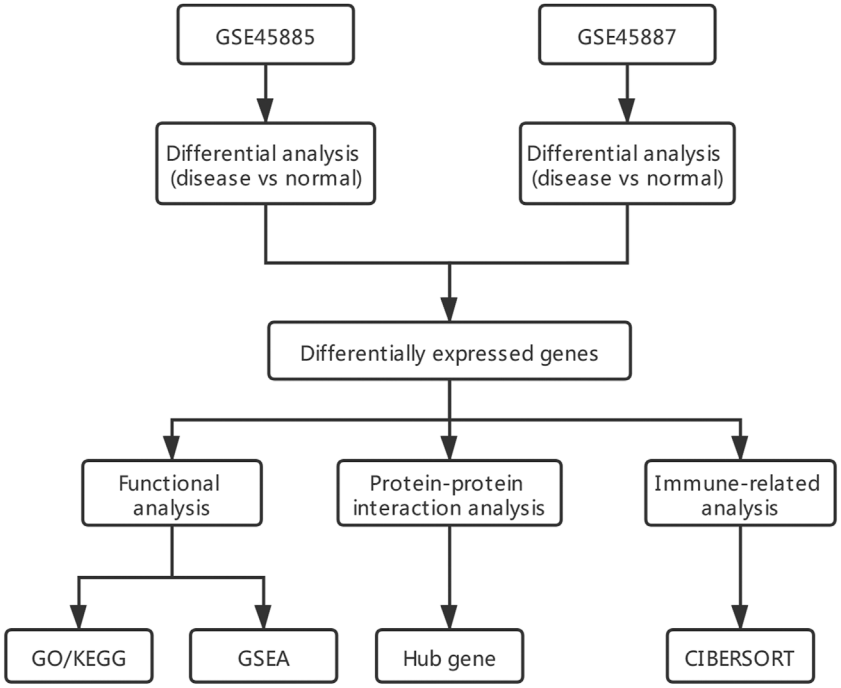


FIGURE 1
Analysis flow chart. GO/KEGG: Gene ontology (GO) and Kyoto encyclopedia of genes and genomes (KEGG); GSEA: gene set enrichment analysis.

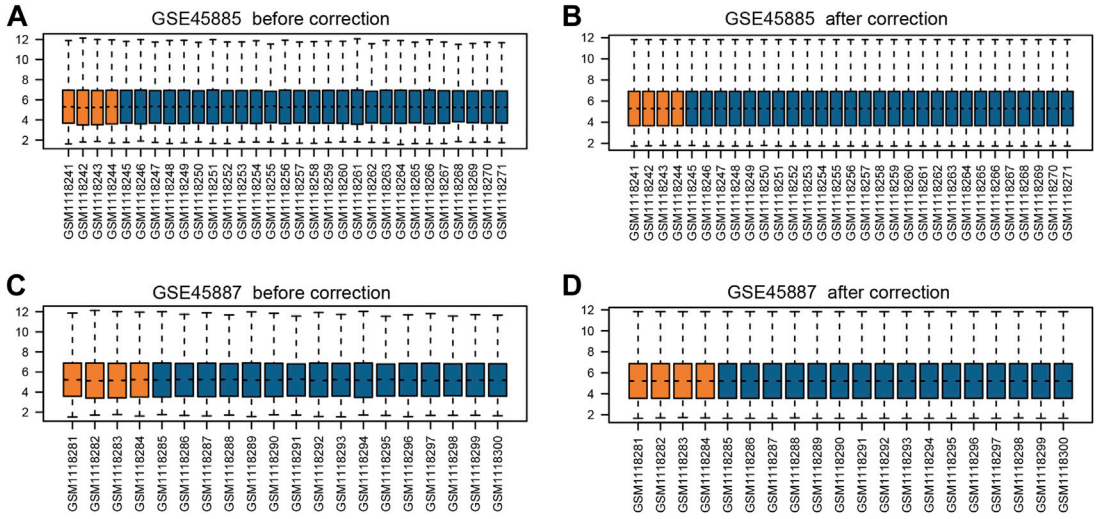


FIGURE 2
Box plots of gene expression data before and after normalization. **(A)** GSE45885 before correction, **(B)** GSE45885 after correction, **(C)** GSE45887 before correction, **(D)** GSE45887 after correction. The x-axis label represents the sample symbol and the y-axis label represents the gene expression values. The orange bar represents the data of normal control samples and the blue bar represents the data of NOA samples.

datasets using the limma package (Figures 2A–D). In order to further judge whether the data set samples have obvious overall differences in expression profiles, we performed PCA analysis and found that the disease group and control group samples had obvious overall differences (Figures 3A,B).

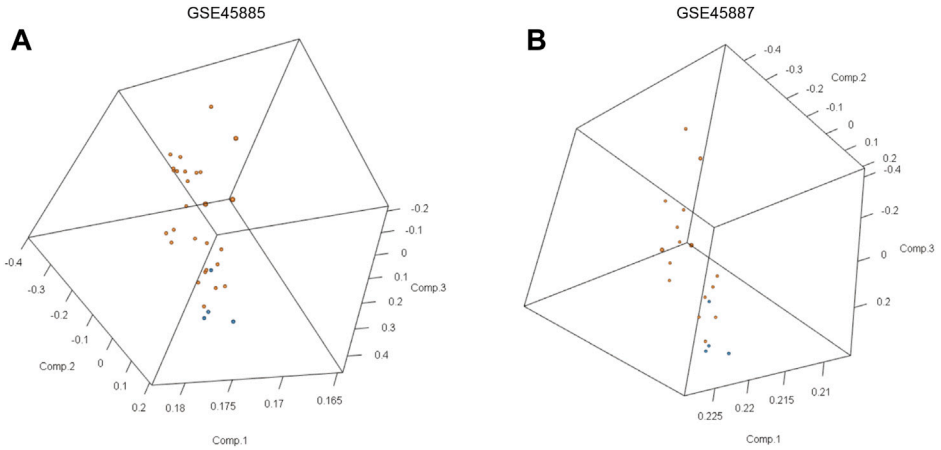


FIGURE 3
Principal component analyses (PCA) of gene expression between the NOA group and control group in GSE45885 and GSE45887. **(A)** 3D-PCA data distribution of GSE45885, **(B)** 3D-PCA data distribution of GSE45887. The orange point represents the data of normal control samples and the blue point represents the data of NOA samples.

Next, we used the limma package to perform differential analysis, and the results are as follows: the combined GEO dataset (Combined Datasets) has a total of 698 differentially expressed genes (DEGs) that satisfy the threshold of |logFC| > 0 and adj.p < 0.05, under this threshold, 70 up-regulated genes (logFC >0 and adj. p < 0.05) and 507 down-regulated genes (logFC <0 and adj. p < 0.05) in the GSE45885 dataset (Figure 4A), and utilized the top 40 differentially expressed genes A classification heat map was drawn (Figure 4B); there were 17 up-regulated genes (logFC >0 and adj. p < 0.05) and 104 down-regulated genes (logFC <0 and adj. p < 0.05) in the GSE45887 dataset. The 40 differentially expressed genes were classified as heatmaps (Figure 4D). The top 40 differential genes obtained are: PRM1, PRM2, GTSF1L, TNP1, FSCN3, C19orf62, ACTL7A, AKAP4, ABHD1, GAPDHS, LELP1, FNDC8, BANF2, FAM205A, ACSBG2, ODF1, BPIFA3, GSG1, UBQLN3, SMCP, RN7SL648P, MGC24103, RN7SL751P, MIR145, MIR30E, MIR27B, MIR99A, MIR32, MIRLET7G, MIRLET7A2, MIR199A2, MT-TT, MT-TW, MT-TD, MIR509-1, RNU1-59P, MT-TK, MT-TL2, MT -TS2, MT-TH (Figures 4C,D).

3.2 PPI network construction and hub gene identification

We intersected the differentially expressed genes from the analysis of the two datasets and visualized them using a Venn diagram, resulting in 119 differentially expressed genes (Figure 5A). Then, we conducted PPI (Protein-Protein Interaction Networks, PPI) analysis on 119 differential genes through the STRING database, and imported the protein interaction results into Cytoscape for visualization and drawing, and found that 31 genes have strong similarities of biological functions (Figure 5B), are: TEKT4, ODF3, ACTN3, DOT1L, MUC1, CCDC116, RSPH4A, ELL, GLT6D1, HSF1, SPATA31E1, NSUN4, TBL3, FAM187B, NR4A2, DUS1L, CCDC96, SNX2, FER1L5, DOC2A, FER1L6, STAC3, CLPB, FAM163A, SLFNL1, FOS, PLCD4, DUSP1, INPP1, CATSPER4, DNAH1.

Then, the networkAnalyst database was used to analyze these 119 genes, and jointly used the JASPAR database (Zheng et al., 2019) and miRTarBase v8.0 (Chen et al., 2020) to analyze the transcription factors of differential genes and their possible binding miRNAs. The results of the analysis were then imported into Cytoscape for visualization, displaying the transcription factor-differential gene network (Figure 5C) and the differential gene-miRNA network (Figure 5D). Figure 5E shows the friends analysis results of the hub gene. The top 8 genes with scores are NR4A2, FOS, COF3, MUC1, ELL, DUSP1, STAC3, TEKT4, among which NR4A2 has the highest score, which may play an important role in the occurrence of NOA effect.

3.3 KEGG and GO enrichment analyses

To investigate the relationship between the DEGs of NOA and BCs, MFs, CCs, biological pathways, and diseases, functional and pathway enrichment analyses were performed. Regarding BPs of GO analysis, DEGs of NOA were significantly enriched in protein polyglycylation, negative regulation of cytokine-mediated signaling pathways, and negative regulation of

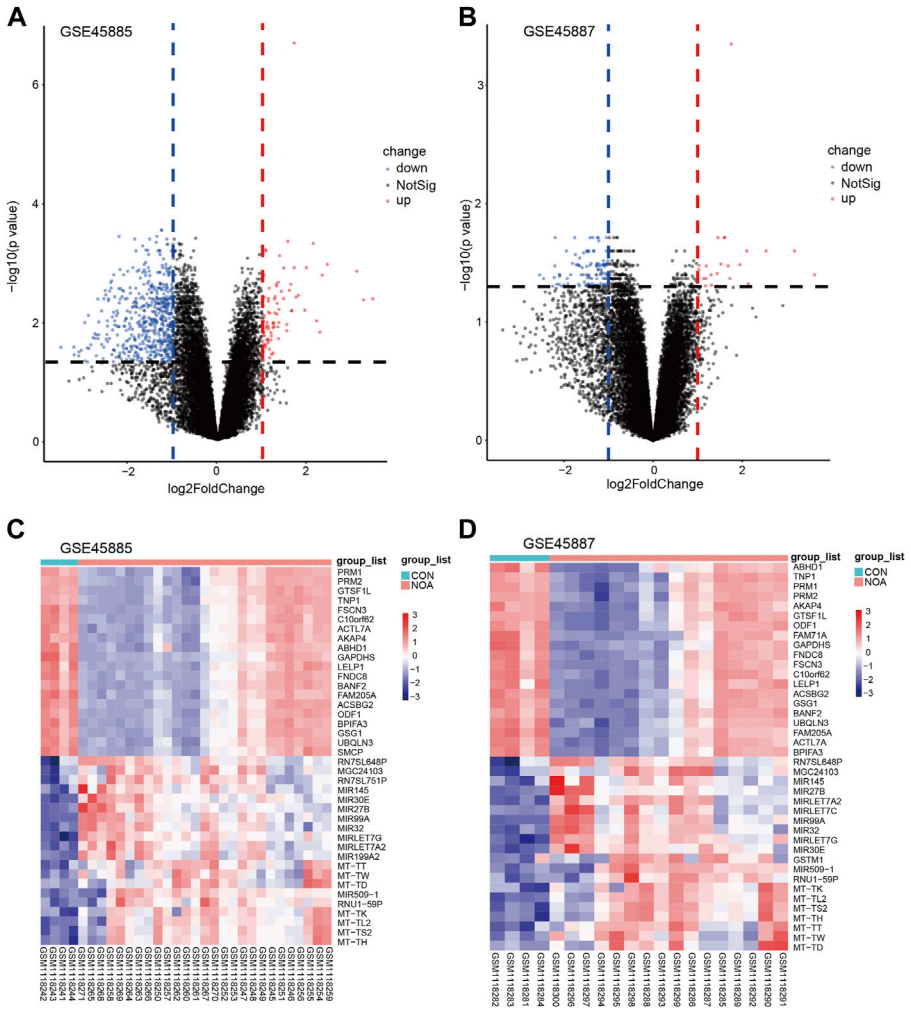


FIGURE 4
Volcano plots and heatmap of DEGs. **(A)** Volcano plots of GSE45885, **(B)** volcano plots of GSE45887. The x-axis label represents log2FoldChange and the y-axis label represents−log10 (adjusted *p*-value). Data points in red represent upregulated, and green represent downregulated genes. No significantly changed genes are marked as gray points. Heatmap of the top 40 DEGs screened by limma package in R software. **(C)** Heatmap of GSE45885, **(D)** heatmap of GSE45887. Red areas represent highly expressed genes and blue areas represent lowly expressed genes in NOA. Darker color indicates the higher multiple of DEGs. DEGs: differentially expressed genes; NOA: non-obstructive azoospermia.

response to cytokine stimulus. For CCs, DEGs of NOA were significantly enriched in sperm flagellum, 9 + 2 motile cilium, axoneme, ciliary plasm, and motile cilium. Changes in MFs of hub genes were mainly enriched in RNA binding involved in posttranscriptional gene silencing, mRNA binding involved in posttranscriptional gene silencing, protein-glycine ligase activity, and protein-glycine ligase activity. Additionally, using the logFC value of genes, we visualized the changes in gene expression and the relationship between functions using GOplot software (Figure 6B). KEGG pathway enrichment demonstrates that the DEGs of NOA were primarily enriched in the taste transduction and pancreatic secretion signaling pathway Supplementary Table S3, and the most significant enrichment signaling pathway, hSA04742: Taste transduction, is shown in Figure 6C.

3.4 GSEA and gene set variation analysis (GSVA)

GSEA was performed to determine the effect of gene expression on NOA, and the results show that the DEGs affected the biological functions of the ribosome, focaladhesion, and protein_expor (Figures 7A,B). To evaluate the enrichment of different metabolic pathways in different samples, we analyzed the expression levels of genes

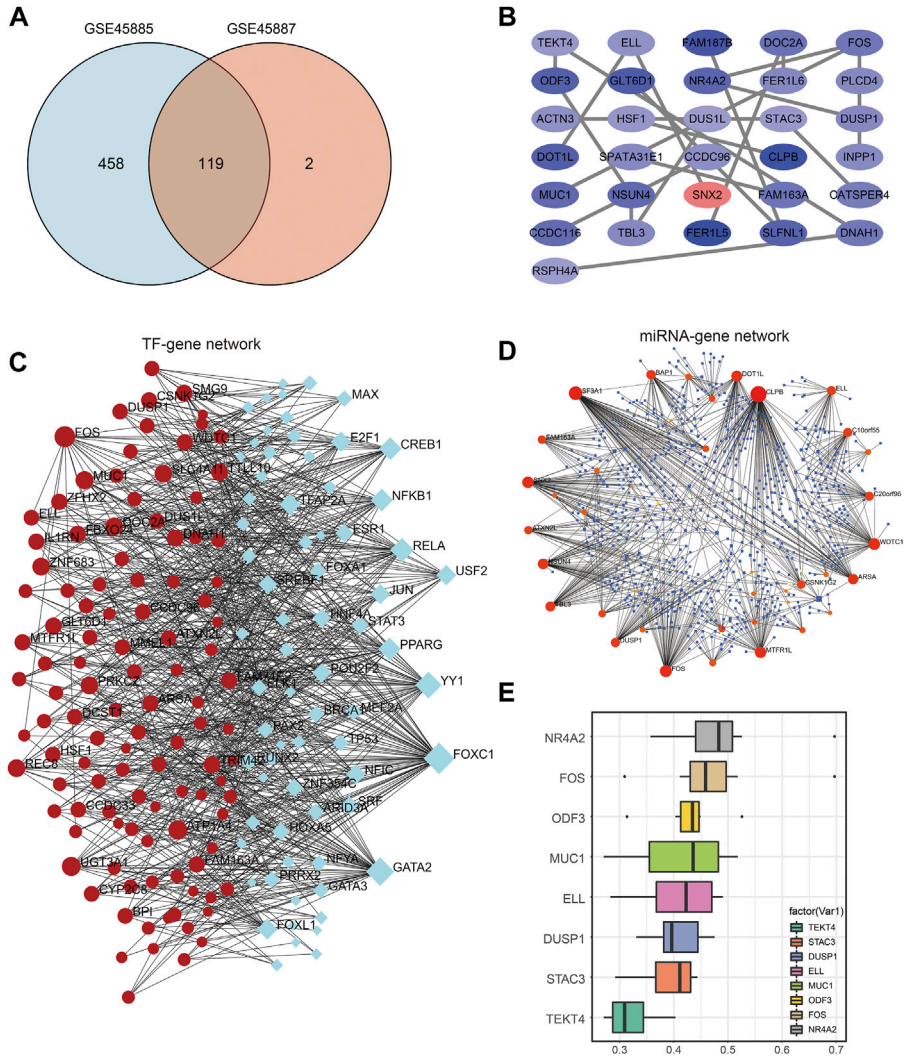


FIGURE 5
PPI network construction and hub gene regulatory network. **(A)** Venn diagram of co-expressed DEGs from GSE45885and GSE45887. **(B)** DEG-related PPI networks of NOA. Red nodes represent highly expressed genes and blue nodes represent lowly expressed genes in NOA. **(C)** DEG-related TF-mRNA networks of NOA. **(D)** DEG-related miRNA-mRNA networks of NOA. **(E)** Friend analysis of hub gene in PPI network. DEGs: differentially expressed genes; NOA: non-obstructive azoospermia; PPI: protein-protein interaction.

in different samples that converted them into gene sets in different samples using GSVA, and the enrichment was visualized using the pheatmap package (Figure 7C). We found that sample grouping could distinguish the results of the GSEA.

3.5 Immune infiltration analysis

To assess the level of immune infiltration in male non-obstructive azoospermia tissue, we used the CIBERSORT algorithm to calculate the degree of infiltration of 22 types of immune cells in the tissue.

Using the wilcox.test algorithm to analyze and filter out immune cells with low expression abundance, a total of 15 immune cells were included, including B cells naive, B cells memory, Plasma cells, T cells CD8, T cells CD4 memory resting, T cells follicular helper, T cells regulatory (Tregs), NK cells resting, NK cells activated, Monocytes, Macrophages M0, Macrophages M2, Dendritic cells activated, Mast cells resting, Mast cells activated, and draw a panorama of immune cell entry in NOA (Figure 8A). Next, the correlation between individual immune cells in both datasets was assessed (Figure 8B). To assess the functional correlation between key genes and immune cells in male non-obstructive azoospermia, we selected the top three hub genes for analysis.

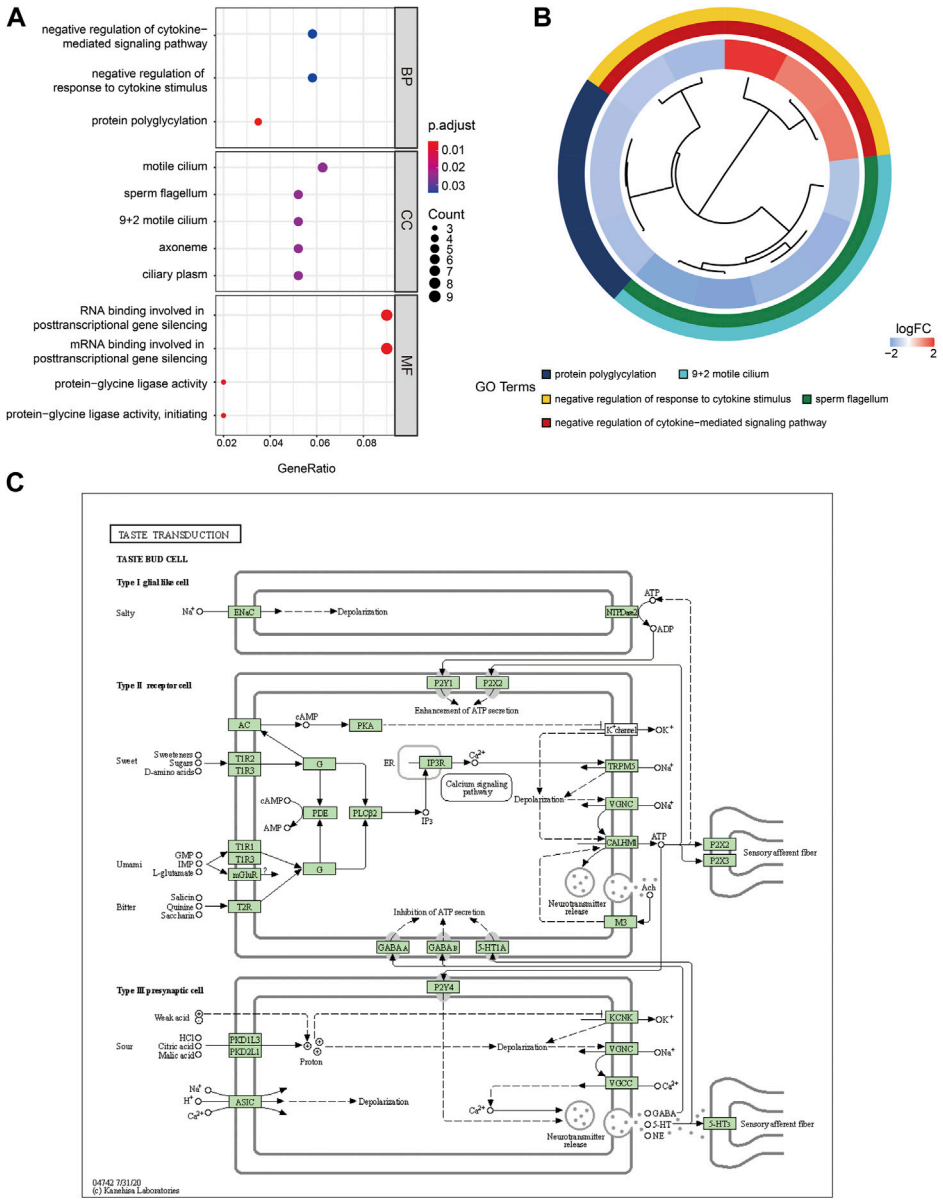


FIGURE 6
GO enrichment and KEGG pathway analysis of DEGs. **(A)** GO enrichment result of DEGs. The x-axis label represents gene ratio and y-axis label represents GO terms. The color indicates GO terms, red indicates activated and blue indicates inhibited. The size of circle represents gene count. Different colors of circles represent different adjusted *p* values. **(B)** GOplot results combined with gene expression logFC. **(C)** The most significant enrichment signaling pathway was hSA04742: taste transduction. GO: Gene ontology; KEGG: Kyoto Encyclopedia of Genes and Genomes; MF: molecular function; BP: biological processes; CC: cell composition.

According to the expression value of the hub gene, the samples were divided into high expression group and low expression group, and calculated the difference of immune cell infiltration levels between the high and low expression groups. As shown in Figures 8C–E, in the disease group and the ODF3 high and low expression group, there were differences in the immune cell infiltration of B cells naïve, plasma cells, Macrophages M2, Dendritic cells activated, and Mast cells resting, among which Macrophages M2 and Mast cells resting were low. Expression genes, plasma cells, B cells naïve, and Dendritic cells activated are highly expressed genes; however, in the high and low expression groups of NR4A2 gene, there are differences in the immune cell infiltration of B cells naive, Plasma cells, Monocytes,

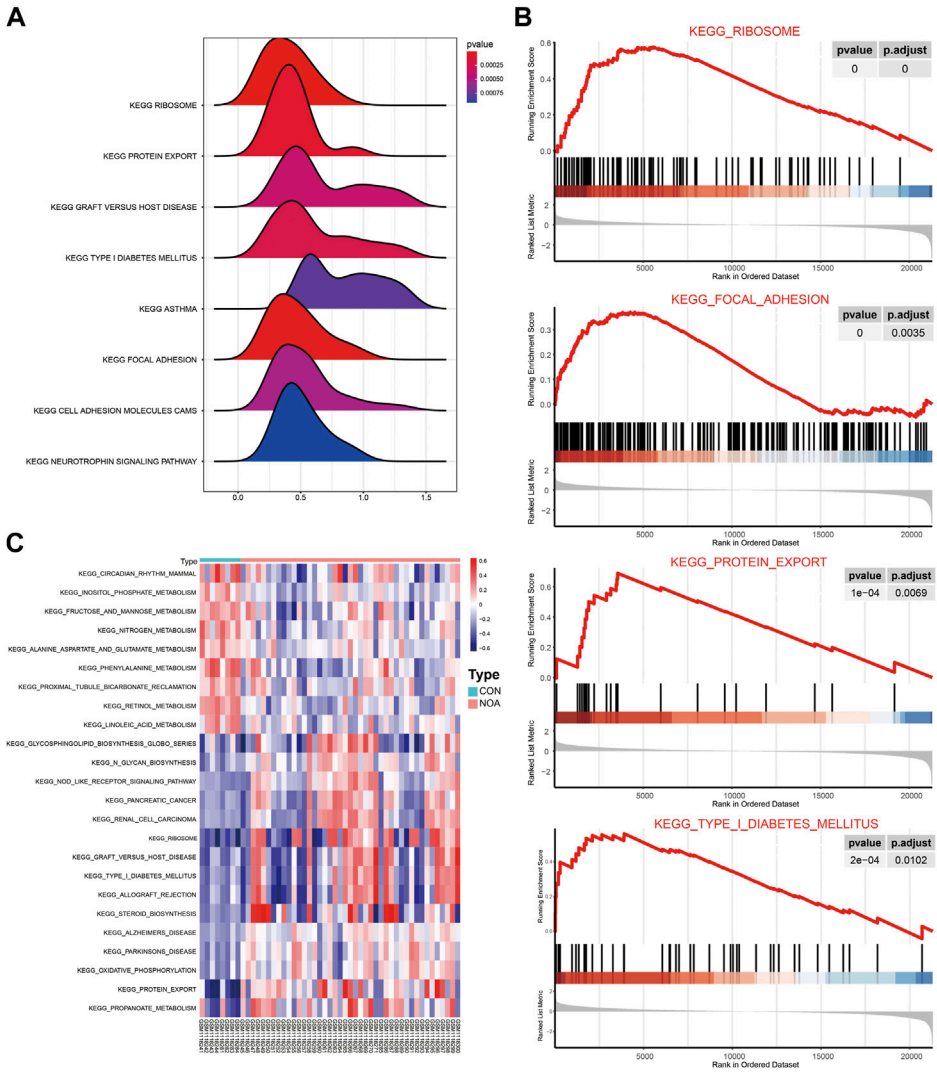


FIGURE 7
GSEA and GSVA. **(A)** Results of GSEA are presented by ridge maps. The x-axis label represents gene ratio and y-axis label represents KEGG pathway. **(B)** Top four most significant enriched gene sets in NOA: ribosome signaling pathway; focal adhesion signaling pathway; protein expor signaling pathway; type I diabetes mellitus signaling pathway. **(C)** Results of GSVA were visualized with heatmaps. Red indicates activated and blue indicates inhibited. GSEA: Gene Set Enrichment Analysis; GSVA: Gene Set Variation Analysis.

Macrophages M2, and Mast cells resting. The expressed genes are B cells naïve, Plasma cells, and the low-expressed genes are Monocytes, Macrophages M2, Mast cells resting, and there are differences in the infiltration of T cells regulatory (Tregs) immune cells in the high and low expression groups of FOS genes, which are low-expressed genes. It was statistically significant ($p < 0.05$, statistically significant; $p < 0.01$, highly statistically significant; $p < 0.001$, extremely statistically significant). The above results indicate that the functional changes of several immune cells may play an important role in the immune microenvironment of NOA patients.

4 Discussion

Spermatogenesis is a complex and subtle process characterized by three specific functional phases: mitotic proliferation and expansion, meiosis, and spermiogenesis (Neto et al., 2016). Genetic mutations play an important role in NOA (Peña et al., 2020). Compared to that of OA, the pathogenesis of NOA is more complex and difficult to understand. However, there are currently no specific therapeutic targets for NOA. Thus, it is of great significance to construct a molecular regulatory network of NOA to search for therapeutic targets. In this study, we integrated the

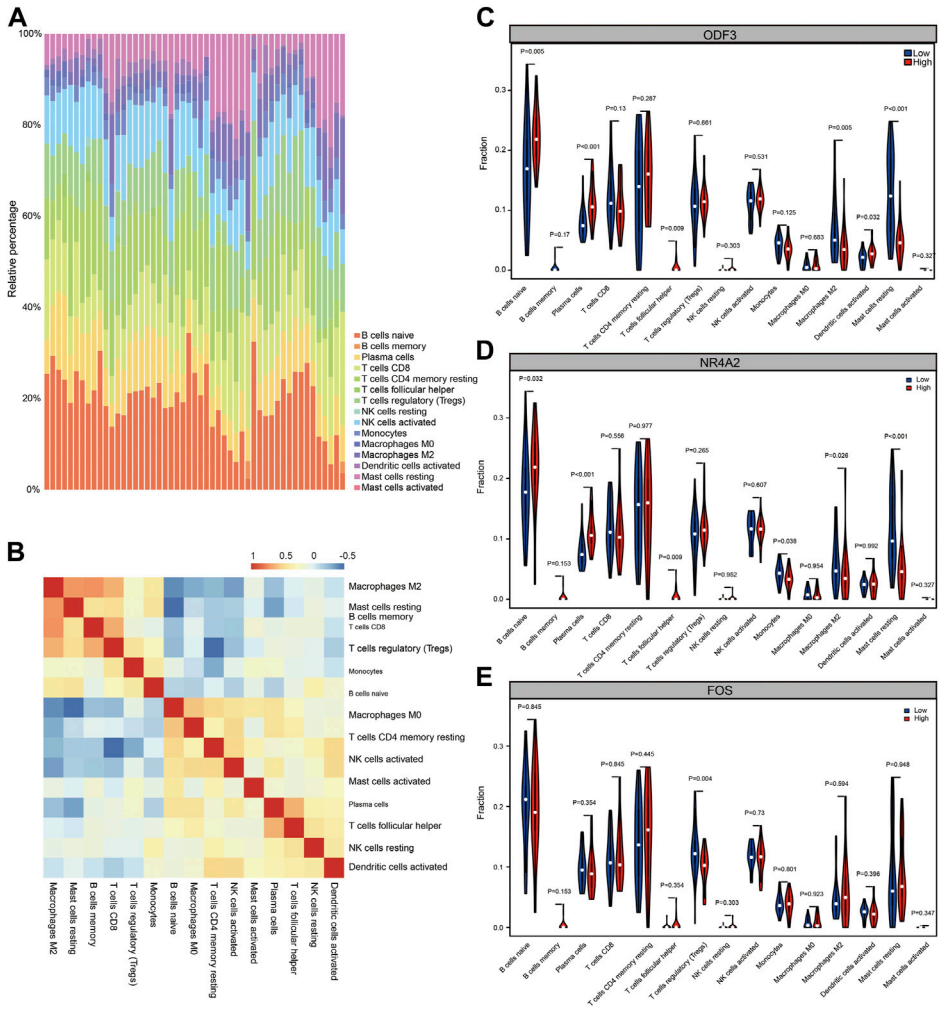


FIGURE 8
Immune infiltration analysis. **(A)** CIBERSORT algorithm analysis of immune cell infiltration panorama. Different colors represent different immune cell subsets. **(B)** CIBERSORT algorithm analysis of immune cell infiltration panorama correlation heat map. Red represents positive correlation and blue represents negative correlation. **(C)** Functional correlation between ODF3 expression in NOA and immune cells. **(D)** Functional correlation between NR4A2 expression in NOA and immune cells. **(E)** Functional correlation between FOS expression in NOA and immune cells.

GSE45885 and GSE45887 datasets and identified 527 and 121 common DEGs, respectively, using bioinformatics methods, among which 119 DEGs were at the intersection of the two datasets and 31 genes had similar biological functions. To further investigate the molecular mechanism of the pathogenesis of NOA, we analyzed the transcription factors of 119 DEGs and their possible binding miRNAs and successfully identified three hub genes (NR4A2, FOS, and ODF3). KEGG and GO enrichment analyses of DEGs showed that the DEGs of NOA were mainly enriched in taste transduction and pancreatic secretion signaling pathways. Moreover, the three most important hub genes (NR4A2, FOS, and ODF3) were analyzed for immune cell infiltration in NOA testicular tissue, suggesting that changes in the function of several immune cells in the immune microenvironment may play an important role in spermatogenesis. These results suggest that NR4A2, FOS, and ODF3 are potential biomarkers for the diagnosis and treatment of NOA.

NR4A2 belongs to the nuclear receptor superfamily and is involved in multiple BPs including proliferation, metabolism, immunity, cellular stress, apoptosis, and DNA repair (Safe et al., 2016). In addition to Nr4a proteins, which are known transcription factors, they are also important receptors of hormones (Ke et al., 2004). Testosterone and dihydrotestosterone secreted from Leydig cells are crucial for the initiation and maintenance of spermatogenesis (Walker, 2009). Dysfunction of Leydig cells contributes to testicular spermatogenesis disorders in OA patients (Walker, 2009). A

previous study reported that NR4A2 plays an essential role in Leydig cells, and can regulate the transcription of steroidogenic acute regulatory protein (StAR) or 3β-hydroxysteroid dehydrogenase (3β-HSD) in Leydig cells (Martin and Tremblay, 2010; Hu et al., 2018). Dai et al. (2021), (Martin et al., 2008) investigated the expression patterns, distribution, and functions of NR4A2 in male Tianzhu white yaks and found that NR4A2 is involved in the regulation of male yak reproduction, especially steroid hormones and androgen metabolism. Our study further indicates that NR4A2 might play an essential role in spermatogenesis, and the detailed regulatory mechanism of NR4A2 in the spermatogenesis of patients with NOA needs to be further studied. FOS, also known as the c-fos gene, is a transcription factor. One study showed that the expression of c-fos mRNA is appreciably lower and ERβ mRNA is higher in the testes of men with NOA than in those with OA, which suggests that c-fos transcriptional activity is associated with spermatogenesis. However, few studies have focused on c-Fos transcriptional activity during spermatogenesis, and the detailed mechanisms are unclear. The outer dense fiber (ODF) protein is a keratin that includes ODF1, ODF2, and ODF3 (Araújo et al., 2009). The tail is an important structure for proper sperm function. Studies have demonstrated that ODF proteins are the main cytoskeletal structures of the sperm tail and are preferentially expressed during mammalian spermiogenesis (Kierszenbaum, 2002; Petersen et al., 2002). Among them, ODF3 is transcribed in the testes, more specifically in spermatids, and is involved in sperm tail formation (Petersen et al., 2002; Sarkar et al., 2022). Unfortunately, there is little evidence that ODF3 is an important trigger for the pathophysiological process of NOA.

We conducted KEGG and GO enrichment analyses of DEGs and found that the DEGs of NOA were mainly enriched in taste transduction and pancreatic secretion signaling pathways. A recent study showed that olfactory receptor 2 is present in vascular macrophages (Orecchioni et al., 2022). However, no studies have reported the involvement of these pathways in spermatogenesis. Whether these pathways are involved in spermatogenesis needs to be verified using larger sample sequencing and experiments.

A previous study has confirmed that inflammation in the reproductive tract contributes to testicular dysfunction and male infertility (Hedger, 2011). Therefore, we performed immune infiltration analysis and found that immune cells are involved in the pathophysiological process of NOA. One study reported that T cell subsets are essential for intact spermatogenesis and may be targets for the treatment of chronic orchitis and immune infertility (Gong et al., 2020). Suppressor T cells predominate in patients with obstructive azoospermia, whereas T cells of the helper phenotype predominate in patients with unilateral testicular obstruction (el-Demiry et al., 1987), but T cells and their subset distribution in the testis of NOA are unknown. In addition, several studies have suggested that B cells and macrophages contribute to spermatogenesis (Cabas et al., 2011; de Oliveira et al., 2021), similar to our results. Dong et al. (2021) also found that macrophages are the most important immune cells in NOA by immune infiltration analysis. All these studies showed that immune cells play an important role in NOA, and the mechanism by which immune cells impact spermatogenesis should be further studied.

Although we obtained several key findings in the present study, there are still some limitations. First, although we analyzed two datasets with 51 patients, the effects of race and region on the findings were not observed. We look forward to verifying our results using a larger, real-world sample size. Second, our analysis was based on data from a public database and we did not conduct experiments to verify our results. Third, the hub genes, pathway enrichment, and results of immune infiltration analysis were not validated by external datasets or clinical samples. Fourth, we must admit that WGCNA is a better analytical method, while DEGs is the more common method to screen for differential genes. We believe that the analysis method combining WGCNA and DEGs will make the results more rigorous and credible, which is what we need to work on in the future. Finally, owing to the lack of patient prognosis information in the dataset, genes related to patient prognosis were not screened out.

In conclusion, the present study successfully constructed a regulatory network of DEGs between NOA and normal controls and screened three hub genes using integrative bioinformatics analysis. In addition, our results suggest that functional changes in several immune cells in the immune microenvironment may play an important role in spermatogenesis. Our results provide a novel understanding of the molecular mechanisms of NOA and offer potential biomarkers for its diagnosis and treatment.

Data availability statement

Publicly available datasets were analyzed in this study. The names of the repository/repositories and accession number(s) can be found in the article/Supplementary Material.

Author contributions

All authors listed have made substantial, direct, and intellectual contribution to the work and approved it for publication.

Funding

This study was supported by funding from Innovation Project of Women and Children medical research center affiliated to Foshan Institute of Fetal Medicine (FEYJZX-2020-008 and FEYJZX-2020-006) and Research Funds from Foshan Municipal Science and Technology Project (2020001005568). We thank all support.

Conflict of interest

The authors declare that the research was conducted in the absence of any commercial or financial relationships that could be construed as a potential conflict of interest.

Publisher's note

All claims expressed in this article are solely those of the authors and do not necessarily represent those of their affiliated organizations, or those of the publisher, the editors and the reviewers. Any product that may be evaluated in this article, or claim that may be made by its manufacturer, is not guaranteed or endorsed by the publisher.

Supplementary material

The Supplementary Material for this article can be found online at: https://www.frontiersin.org/articles/10.3389/fgene.2022.988047/full#supplementary-material

References

Araújo, F. C., Oliveira, C. A., Reis, A. B., Del Puerto, H. L., Martins, A. S., and Reis, F. M. (2009). Expression of the proto-oncogene c-fos and the immunolocalization of c-fos, phosphorylated c-fos and estrogen receptor beta in the human testis. *Histol. Histopathol.* 24, 1515–1522. PMID: 19795350. doi:10.14670/HH-24.1515

Cabas, I., Chaves-Pozo, E., Alcázar, A. G., Meseguer, J., Mulero, V., and García-Ayala, A. (2011). Dietary intake of 17α-ethinylestradiol promotes leukocytes infiltration in the gonad of the hermaphrodite gilthead seabream. *Mol. Immunol.* 48, 2079–2086. doi:10.1016/j.molimm.2011.07.001

Chen, S., Wang, G., Zheng, X., Ge, S., Dai, Y., Ping, P., et al. (2020). Whole-exome sequencing of a large Chinese azoospermia and severe oligospermia cohort identifies novel infertility causative variants and genes. *Hum. Mol. Genet.* 29, 2451–2459. doi:10.1093/hmg/ddaa101

Chicco, D. (2022). geneExpressionFromGEO: An R package to facilitate data reading from gene expression Omnibus (GEO). *Methods Mol. Biol.* 2401, 187–194. doi:10.1007/978-1-0716-1839-4_12

Corona, G., Pizzocaro, A., Lanfranco, F., Garolla, A., Pelliccione, F., Vignozzi, L., et al. (2017). Sperm recovery and ICSI outcomes in klinefelter syndrome: A systematic review and meta-analysis. *Hum. Reprod. Update* 23, 265–275. doi:10.1093/humupd/dmx008

Dai, L., Zhang, Q., Shi, J., Bai, X., An, X., Zhang, B., et al. (2021). The distribution, expression patterns and functional analysis of NR1D1 and NR4A2 in the reproductive axis tissues of the male Tianzhu White Yak. *Animals.* 11, 3117. doi:10.3390/ani11113117

Das, B., and Mitra, P. (2021). Protein interaction network-based deep learning framework for identifying disease-associated human proteins. *J. Mol. Biol.* 433 (19), 167149. doi:10.1016/j.jmb.2021.167149

de Oliveira, S. A., Cerri, P. S., and Sasso-Cerri, E. (2021). Impaired macrophages and failure of steroidogenesis and spermatogenesis in rat testes with cytokines deficiency induced by diacerein. *Histochem. Cell Biol.* 156, 561–581. doi:10.1007/s00418-021-02023-7

Dong, M., Li, H., Zhang, X., and Tan, J. (2021). Weighted correlation gene network analysis reveals new potential mechanisms and biomarkers in non-obstructive azoospermia. *Front. Genet.* 12, 617133. doi:10.3389/fgene.2021.617133

el-Demiry, M. I., Hargreave, T. B., Busuttil, A., Elton, R., James, K., and Chisholm, G. D. (1987). Immunocompetent cells in human testis in health and disease. *Fertil. Steril.* 48, 470–479. doi:10.1016/s0015-0282(16)59421-7

Forti, G., Corona, G., Vignozzi, L., Krausz, C., and Maggi, M. (2010). Klinefelter's syndrome: A clinical and therapeutical update. *Sex. Dev.* 4, 249–258. doi:10.1159/000316604

Ge, S. X., Jung, D., and Yao, R. (2020). ShinyGO: A graphical gene-set enrichment tool for animals and plants. *Bioinformatics* 36 (8), 2628–2629. doi:10.1093/bioinformatics/btz931

Gong, J., Zeng, Q., Yu, D., and Duan, Y. G. (2020). T lymphocytes and testicular immunity: A new insight into immune regulation in testes. *Int. J. Mol. Sci.* 22, 57. doi:10.3390/ijms22010057

Gustavsson, E. K., Zhang, D., Reynolds, R. H., Garcia-Ruiz, S., and Ryten, M. (2022). ggtranscript: an R package for the visualization and interpretation of transcript isoforms using ggplot2. *Bioinformatics* 38 (15), 3844–3846. doi:10.1093/bioinformatics/btac409

Hedger, M. P. (2011). Toll-like receptors and signalling in spermatogenesis and testicular responses to inflammation--a perspective. *J. Reprod. Immunol.* 88, 130–141. doi:10.1016/j.jri.2011.01.010

Hu, X., Ding, Z., Hong, Z., Zou, Z., Feng, Y., Zhu, R., et al. (2018). Spermatogenesis improved by suppressing the high level of endogenous gonadotropins in idiopathic non-obstructive azoospermia: A case control pilot study. *Reprod. Biol. Endocrinol.* 16, 91. doi:10.1186/s12958-018-0401-7

Hunt, G. P., Grassi, L., Henkin, R., Smeraldi, F., Spargo, T. P., Kabiljo, R., et al. (2022). GEOexplorer: A webserver for gene expression analysis and visualisation. *Nucleic Acids Res.* 50 (W1), W367–W374. doi:10.1093/nar/gkac364

Jarow, J. P., Espeland, M. A., and Lipshultz, L. I. (1989). Evaluation of the azoospermic patient. *J. Urol.* 142, 62–65. doi:10.1016/s0022-5347(17)38662-7

Kamran, A. B., and Naveed, H. (2022). GOntoSim: A semantic similarity measure based on LCA and common descendants. *Sci. Rep.* 2 (1), 3818. doi:10.1038/s41598-022-07624-3

Kanehisa, M., Furumichi, M., Sato, Y., Ishiguro-Watanabe, M., and Tanabe, M. (2021). Kegg: Integrating viruses and cellular organisms. *Nucleic Acids Res.* 49 (D1), D545–D551. doi:10.1093/nar/gkaa970

Ke, N., Claassen, G., Yu, D. H., Albers, A., Fan, W., Tan, P., et al. (2004). Nuclear hormone receptor NR4A2 is involved in cell transformation and apoptosis. *Cancer Res.* 64, 8208–8212. doi:10.1158/0008-5472.CAN-04-2134

Kierszenbaum, A. L. (2002). Keratins: Unraveling the coordinated construction of scaffolds in spermatogenic cells. *Mol. Reprod. Dev.* 61, 1–2. doi:10.1002/mrd.1124

Krausz, C. (2011). Male infertility: Pathogenesis and clinical diagnosis. *Best. Pract. Res. Clin. Endocrinol. Metab.* 25, 271–285. doi:10.1016/j.beem.2010.08.006

Le, T., Aronow, R. A., Kirshtein, A., and Shahriyari, L. (2021). A review of digital cytometry methods: Estimating the relative abundance of cell types in a bulk of cells. *Brief. Bioinform.* 22 (4), bbaa219. doi:10.1093/bib/bbaa219

Liberzon, A., Birger, C., Thorvaldsdóttir, H., Ghandi, M., Mesirov, J. P., and Tamayo, P. (2015). The Molecular Signatures Database (MSigDB) hallmark gene set collection. *Cell Syst.* 1, 417–425. PMID: 26771021; PMCID: PMC4707969. doi:10.1016/j.cels.2015.12.004

Liu, S., Wang, Z., Zhu, R., Wang, F., Cheng, Y., and Liu, Y. (2021). Three differential expression analysis methods for RNA sequencing: Limma, EdgeR, DESeq2. *J. Vis. Exp.* 2021, 175. doi:10.3791/62528

Lotti, F., Corona, G., Mondaini, N., Maseroli, E., Rossi, M., Filimberti, E., et al. (2014). Seminal, clinical and colour-Doppler ultrasound correlations of prostatitis-like symptoms in males of infertile couples. *Andrology* 2, 30–41. doi:10.1111/j.2047-2927.2013.00156.x

Martin, L. J., Boucher, N., Brousseau, C., and Tremblay, J. J. (2008). The orphan nuclear receptor NUR77 regulates hormone-induced StAR transcription in Leydig cells through cooperation with Ca2+/calmodulin-dependent protein kinase I. *Mol. Endocrinol.* 22, 2021–2037. doi:10.1210/me.2007-0370

Martin, L. J., and Tremblay, J. J. (2010). Nuclear receptors in Leydig cell gene expression and function. *Biol. Reprod.* 83, 3–14. doi:10.1095/biolreprod.110.083824

Neto, F. T., Bach, P. V., Najari, B. B., Li, P. S., and Goldstein, M. (2016). Spermatogenesis in humans and its affecting factors. *Semin. Cell Dev. Biol.* 59, 10–26. doi:10.1016/j.semcdb.2016.04.009

Nguyen, T. M., Bharti, S., Yue, Z., Willey, C. D., and Chen, J. Y. (2021). Statistical enrichment analysis of samples: A general-purpose tool to annotate metadata neighborhoods of biological samples. *Front. Big Data* 4, 725276. doi:10.3389/fdata.2021.725276

Ning, W., Wei, Y., Gao, L., Han, C., Gou, Y., Fu, S., et al. (2022). HemI 2.0: An online service for heatmap illustration. *Nucleic Acids Res.* 50 (W1), W405–W411. doi:10.1093/nar/gkac480

Orecchioni, M., Kobiyama, K., Winkels, H., Ghosheh, Y., McArdle, S., Mikulski, Z., et al. (2022). Olfactory receptor 2 in vascular macrophages drives atherosclerosis by NLRP3-dependent IL-1 production. *Science* 375, 214–221. doi:10.1126/science.abg3067

Pan, M. M., Hockenberry, M. S., Kirby, E. W., and Lipshultz, L. I. (2018). Male infertility diagnosis and treatment in the era of *in vitro* fertilization and intracytoplasmic sperm injection. *Med. Clin. North Am.* 102, 337–347. doi:10.1016/j.mcna.2017.10.008

Peña, V. N., Kohn, T. P., and Herati, A. S. (2020). Genetic mutations contributing to non-obstructive azoospermia. *Best. Pract. Res. Clin. Endocrinol. Metab.* 34, 101479. doi:10.1016/j.beem.2020.101479

Petersen, C., Aumüller, G., Bahrami, M., and Hoyer-Fender, S. (2002). Molecular cloning of Odf3 encoding a novel coiled-coil protein of sperm tail outer dense fibers. *Mol. Reprod. Dev.* 61, 102–112. doi:10.1002/mrd.1136

Poongothai, J., Gopenath, T. S., and Manonayaki, S. (2009). Genetics of human male infertility. *Singap. Med. J.* 50, 336–347.

Puig, R. R., Holmås, S., Mironov, V., and Kuiper, M. (2020). Network building with the Cytoscape BioGateway app explained in five use cases. *Curr. Protoc. Bioinforma.* 72 (1), e106. doi:10.1002/cpbi.106

Safe, S., Jin, U. H., Morpurgo, B., Abudayyeh, A., Singh, M., and Tjalkens, R. B. (2016). Nuclear receptor 4A (NR4A) family - orphans no more. *J. Steroid Biochem. Mol. Biol.* 157, 48–60. doi:10.1016/j.jsbmb.2015.04.016

Sarkar, S., Yadav, S., Mehta, P., Gupta, G., and Rajender, S. (2022). Histone methylation regulates gene expression in the round spermatids to set the RNA payloads of sperm. *Reprod. Sci.* 29, 857–882. doi:10.1007/s43032-021-00837-3

Szklarczyk, D., Gable, A. L., Nastou, K. C., Lyon, D., Kirsch, R., Pyysalo, S., et al. (2021). The STRING database in 2021: Customizable protein-protein networks, and functional characterization of user-uploaded gene/measurement sets. *Nucleic Acids Res.* 49 (D1), D605–D612. doi:10.1093/nar/gkaa1074

Tournaye, H., Krausz, C., and Oates, R. D. (2017). Concepts in diagnosis and therapy for male reproductive impairment. *Lancet. Diabetes Endocrinol.* 5, 554–564. doi:10.1016/S2213-8587(16)30043-2

Walker, W. H. (2009). Molecular mechanisms of testosterone action in spermatogenesis. *Steroids* 74, 602–607. doi:10.1016/j.steroids.2008.11.017

Wang, M., Liu, X., Chang, G., Chen, Y., An, G., Yan, L., et al. (2018). Single-cell RNA sequencing analysis reveals sequential cell fate transition during human spermatogenesis. *Cell Stem Cell* 23, 599–614. e4. doi:10.1016/j.stem.2018.08.007

Wu, T., Hu, E., Xu, S., Chen, M., Guo, P., Dai, Z., et al. (2021). clusterProfiler 4.0: A universal enrichment tool for interpreting omics data. *Innovation*. 2 (3), 100141. doi:10.1016/j.xinn.2021.100141

Zhao, L., Yao, C., Xing, X., Jing, T., Li, P., Zhu, Z., et al. (2020). Single-cell analysis of developing and azoospermia human testicles reveals central role of Sertoli cells. *Nat. Commun.* 11, 5683. doi:10.1038/s41467-020-19414-4

Zhao, M., Liu, Y., Ding, G., Qu, D., and Qu, H. (2021). Online database for brain cancer-implicated genes: Exploring the subtype-specific mechanisms of brain cancer. *BMC Genomics* 22 (1), 458. doi:10.1186/s12864-021-07793-x

Zheng, W., Zou, Z., Lin, S., Chen, X., Wang, F., Li, X., et al. (2019). Identification and functional analysis of spermatogenesis-associated gene modules in azoospermia by weighted gene coexpression network analysis. *J. Cell. Biochem.* 120, 3934–3944. doi:10.1002/jcb.27677

frontiers | Frontiers in Pediatrics

TYPE Case Report
PUBLISHED 07 December 2022
DOI 10.3389/fped.2022.1041080

Check for updates

OPEN ACCESS

EDITED BY
Tieliu Shi,
Hunan University of Arts and Science, China

REVIEWED BY
Siqi Hu,
Seventh Medical Center of PLA General Hospital, China
Cheng Jiang,
Wuhan University, China

*CORRESPONDENCE
Dongmei Chen
271675951@qq.com

SPECIALTY SECTION
This article was submitted to Genetics of Common and Rare Diseases, a section of the journal Frontiers in Pediatrics

RECEIVED 10 September 2022
ACCEPTED 15 November 2022
PUBLISHED 07 December 2022

CITATION
Zhu Y and Chen D (2022) Two novel mutations in *VPS33B* gene cause a milder ARC syndrome with prolonged survival in a 12-year-old patient: Case report.
Front. Pediatr. 10:1041080.
doi: 10.3389/fped.2022.1041080

COPYRIGHT
© 2022 Zhu and Chen. This is an open-access article distributed under the terms of the Creative Commons Attribution License (CC BY). The use, distribution or reproduction in other forums is permitted, provided the original author(s) and the copyright owner(s) are credited and that the original publication in this journal is cited, in accordance with accepted academic practice. No use, distribution or reproduction is permitted which does not comply with these terms.

Two novel mutations in *VPS33B* gene cause a milder ARC syndrome with prolonged survival in a 12-year-old patient: Case report

Yingjie Zhu and Dongmei Chen*

Department of Emergency/Critical Care Medicine, Children's Hospital of Nanjing Medical University, Nanjing, China

Arthrogryposis–renal dysfunction–cholestasis (ARC) syndrome is a rare autosomal recessive disease caused by *VPS33B* and *VIPAR* gene mutations. The main clinical manifestations are congenital joint contracture, renal dysfunction mainly characterized by distal renal tubular dysfunction, and low glutamyltransferase cholestasis. Most patients with ARC die within 2 years of birth. Here, we report the case of a 12-year-old girl with an ARC phenotype who experienced long-term survival with only mild clinical symptoms. We detected two new heterozygous mutation sites of the *VPS33B* gene in this child, c.1081C > T (*p*.GLN361X, 257) and c.244T > C (*p*.Cys82Arg), through the gene detection technique; the tertiary structure of the protein was predicted by using the SWISS-model. We further reviewed the literature and summarized the clinical manifestations and gene loci of 19 ARC syndrome patients with long-term survival reported so far.

KEYWORDS

ARC syndrome, VPS33B, genetics, novel mutation, prolonged survival

Introduction

Arthrogryposis–renal dysfunction–cholestasis (ARC) syndrome (OMIM No. 208085) is a rare autosomal recessive inheritance disease, which was first reported in a child born from a consanguineous marriage. ARC syndrome is mainly concentrated in Arab countries where consanguineous marriages are common. Sporadic cases can also be seen in North Africa, European countries such as Spain, Italy, and Portugal, and Asian countries such as Japan and China. With the continuous popularization of genetic testing technology, the number of case reports of ARC syndrome has gradually increased, but its incidence is still unknown. ARC syndrome is a multisystem disease with three main characteristic symptoms, namely, congenital arthrogryposis, renal dysfunction dominated by distal tubular dysfunction, and low glutamyl transferase cholestasis. Other clinical features include dysplasia, ichthyosis and hyperkeratosis, hearing loss, platelet dysfunction, bleeding tendency, recurrent infection, and hypothyroidism. ARC syndrome is caused by mutations in vacuolar sorting–associated protein 33B (*VPS33B*) or *VIPAS39* (also known as VPS33B-interacting protein or apical–basolateral polarity regulator) (1). *VPS33B* gene is

located on chromosome 15q26.1, with a length of 23.9 kb and 23 exons. The encoded *VPS33B* protein is mainly involved in intracellular protein transport. *VPS33B* gene is expressed in the fetal and adult bone, kidneys, liver, and skin. Therefore, ARC syndrome patients have impaired structure and function of motor units, renal tubules, hepatic lobules, and epithelial cells. As a result, joint contracture, amino aciduria, glycosuria, cholestasis, ichthyosis, and other multisystem manifestations can occur. Due to recurrent infection, acidosis, or severe bleeding, most ARC syndrome patients do not reach their second year of life (2, 3). However, recently, reports of children with long-term survival have been increasing (4). Here, we report a patient who was admitted to our hospital with a complaint of yellow skin staining along with icteric sclera, contracture of finger and toe joints, dry skin, and signs of ichthyosis. Further examination revealed hyperbilirubinemia and low GGT cholestasis, which could not be reduced during the patient's 10-day stay at the hospital. Whole exon gene sequencing revealed that the patient had late-onset ARC. Unlike typical cases, the patient showed no indications of ARC at birth or infancy. We inferred that, unlike typical cases, the patient had mild symptoms and prolonged survival due to two new *VPS33B* gene mutations.

Case description

The patient was a 12.9-year-old girl from Mainland China, who presented with yellow skin staining that she had for 5 days. she was the only child to the parents, who were not consanguineous. Furthermore, the patient's mother had a full-term normal pregnancy and was not diagnosed with any abnormalities. The patient's birth weight was 3.5 kg. Apart from mild joint contracture, no abnormalities were detected after birth, and she experienced normal growth and development. Her first hospital visit was at the age of 5 when she was diagnosed with ichthyosis because of repeated dry and itchy skin with desquamation. There was no significant improvement in this condition even after she was administered external and oral drugs.

In this second hospital visit, the patient was brought with a complaint of yellow skin staining, accompanied by obvious hunger. Physical examination showed yellowing all over the body, accompanied by icteric sclera, contracture of the finger and toe joints, dry skin all over the body accompanied by incessant itching, and hand and foot desquamation, which is a manifestation of ichthyosis, as shown in **Figure 1**.

The outpatient examination showed 230.2 μmol/L TBil, 26.7 μmol/L IBil, 32.9 g/L albumin, 31 U/L AST, 32 U/L ALT, 16 U/L GGT, and 173 μmol/L bile acid. Her renal and coagulation functions were normal; routine urine tests showed high urine bilirubin, moderate levels of urine protein, and normal urine sugar. Cranial MRI showed a slightly higher signal in the bilateral basal ganglia on T1WI. Abdominal B-ultrasound showed mild liver enlargement and abdominal CT showed full shadows in the liver and pancreas and small flaky high-density shadows in the bilateral kidneys. MRCP was normal, ruling out any organic disease of the biliary tract.

The patient was admitted after these tests. In addition to all the other symptoms, at the time of admission, we observed that the child was irritable and had a speech disorder. We speculated that this might be related to bilirubin encephalopathy. As part of

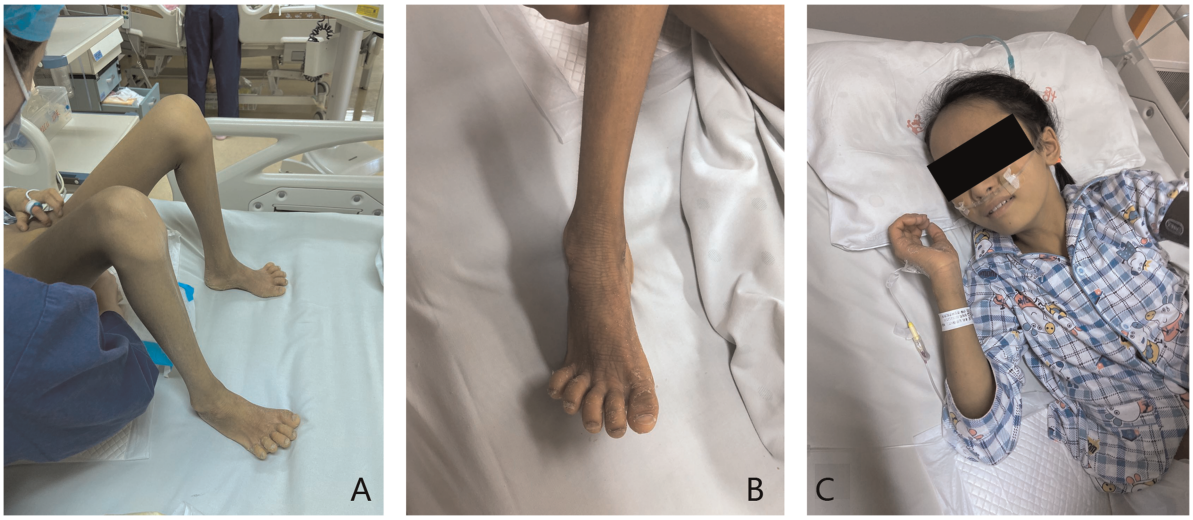


FIGURE 1
Clinical symptoms. (**A**) Joint contracture can be seen in the finger and toe joints of the patient. (**B**) The patient has dry skin and hand and foot desquamation, which is the manifestation of ichthyosis. (**C**) The patient has a yellow skin stain all over the body, accompanied by icteric sclera.

the treatment process post-admission, the patient was given ursodeoxycholic acid, ornithine aspartate injection, lactulose, probiotics, atomolan, compound glycyrrhizic anhydride, fresh frozen plasma, and a non-protein diet, but there was no significant improvement in her hyperbilirubinemia and low GGT cholestasis. This finally led us to conduct a whole exon gene sequencing to shed light on this unexplained juvenile cholestasis. While awaiting the sequencing results, we started eight plasma transfusions on the 3rd day of her admission, but the bilirubin and bile acid of the patient decreased only slightly and increased again after the plasma exchange stopped (Table 1).

On the 10th day after admission, the child developed a fever and was given anti-infection treatment. Because plasma exchange could not reduce the bilirubin level, we suggested liver transplantation. However, her parents rejected this suggestion and chose to leave our hospital; the patient then underwent a liver puncture examination at another hospital; the pathological results showed intrahepatic bile duct stenosis. We later followed up with the patient and learned that her bilirubin and bile acid levels had gradually decreased upon treatment with oral ursodeoxycholic acid; our most recent follow-up revealed that the patient's bilirubin and bile acid levels were normal, but the skin symptoms did not improve.

Finally, the whole exon gene sequencing of the patient revealed that she had two heterozygous mutations in the *VPSS33B* gene. The first was c.1081(exon14) C > T, NM_018668, *p*.Q361X,257. Following ACMG guidelines, the mutation was determined to be pathogenic (PVS1 + PM2 + PP3), which was inherited from her mother. The second was c.244(exon4) T > C, NM_018668, *p*.C82R, which, based on ACMG guidelines, was determined to be a likely pathogenic mutation (PVS1 + PM2 + PM3 + PP3), inherited from her father (Figure 2). These two newly discovered gene mutations may be related to the mild ARC syndrome reported previously.

Discussion and conclusions

Unlike typical ARC that occurs immediately after birth, clinical manifestations in our patient occurred at different stages of life. Joint contracture occurred after birth, ichthyosis occurred at the age of 5, and cholestasis, elevated bilirubin, and mild proteinuria occurred at the age of 12. Such differences in manifestation may be linked to new, previously unknown gene mutations. At present, 75% of patients with ARC syndrome have the *VPS33B* gene mutation. The gene is located at chromosome 15q26.1 and encodes a VPS33B protein consisting of 617 amino acids (1). We found two related gene mutations by the whole exon gene sequencing of this patient, which have not been reported so far. The first is c.1081C > T (*p*.Q361X,257), a heterozygous mutation located in the 14th exon of the *VPS33B* gene, inherited from her mother. This mutation indicates that cytosine at position 1,081 of the *VPS33B* gene coding region is replaced by thymine, resulting in the termination of amino acid translation at position 361 of VPS33B protein, the loss of 257 amino acids, and the protein being truncated (Figure 3B shows the wild-type *VPS33B* gene; Figure 3C shows the mutation). The second, c.244T > C (*p*.C82R), is also a heterozygous mutation, located in the fourth exon of the *VPS33B* gene, originating from the patient's father; this indicates that the thymine at position 244 of the *VPS33B* gene coding region has been replaced by cytosine, resulting in cysteine residue at position 82 of the tertiary structure of the VPS33B protein replaced by arginine (*p*.C82R). We used a

TABLE 1 Changes of transaminase, bile acid, and bilirubin in the patient.

Hospital days	ALT (U/L) [7–30]	AST (U/L) [14–44]	TBiL (μmol/L) [3.4–17.1]	DBiL (μmol/L) [0–6.8]	IBiL (μmol/L) [1.7–13.7]	GGT (U/L) [5–19]	TP (g/L) [61–79]	Bile acid (μmol/L) [<10]
0	31	32	230.2	126.7	103.5	16	32.9	–
2	19	23	355.73	285.19	70.54	16	28.1	173.0
4	10	17	377.64	297.61	80.03	20	35.0	–
6	7	13	339.82	273.81	66.01	19	32.7	–
7	8	16	373.77	296.2	77.57	19	33.9	151.1
9	4	9	275.98	223.42	52.56	14	29.9	–
11	10	12	193.88	160.79	33.09	15	33	170.1
13	15	15	189.48	156.4	33.08	17	34.8	–
15	18	16	238.82	193.5	48.06	21	38.2	188.9
17	18	18	258.82	210.76	45.32	24	40.2	–
19	14	14	240.99	199.89	41.1	20	36.2	239.9
21	20	16	255.57	211.96	43.61	21	35.7	–
22	25	21	265.97	218.53	47.44	20	36.4	264.6

ALT, alanine transaminase; AST, aspartate transaminase; TBiL, total bilirubin; DBiL, direct bilirubin; IBiL, indirect bilirubin; GGT, G-glutamyltransferase; TP, total protein.

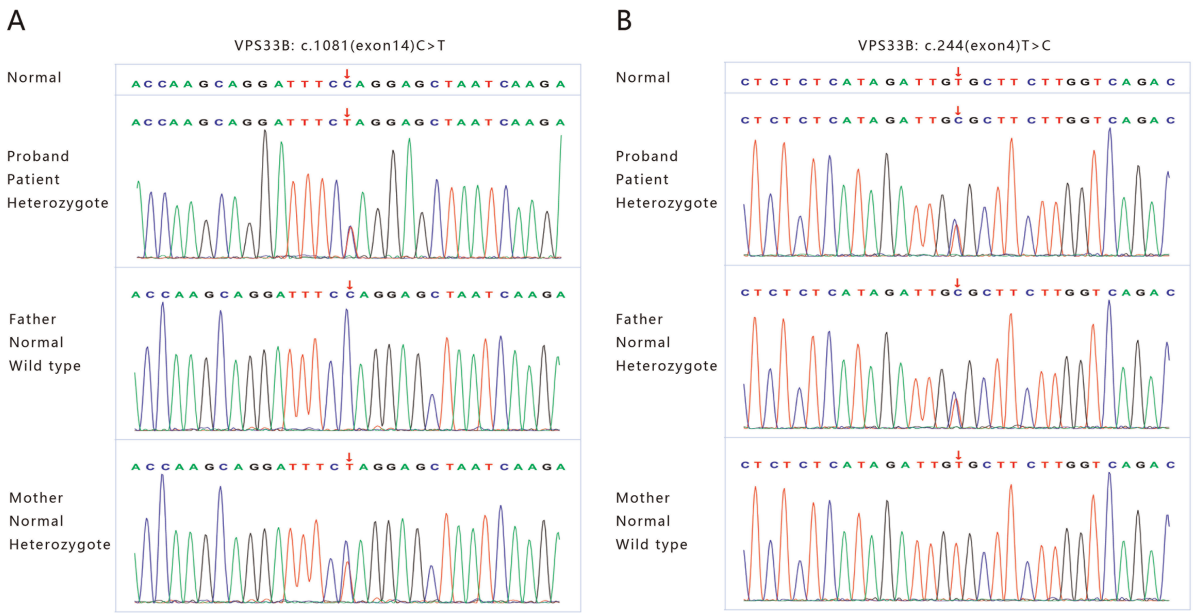


FIGURE 2
The whole exon gene sequencing showing two novel heterozygous mutations in *VPSS33B* gene. (A) The first mutation is c1081(exon14)C > T, NM_018668, *p*.Q361X,257, which originated from the patient's mother. (B) The second mutation is c.244(exon4)T > C, NM_018668, *p*.C82R, which originated from the patient's father.

SWISS-Model (swissmodel.expasy.org) to predict the tertiary structure of the protein. The results showed that c.1081C > T caused the early termination of amino acid coding, resulting in significant changes in the protein structure. c.244T > C makes Arg82, which replaces Cys82, forming a hydrogen bond with Leu29, Leu30, Asp38, and Phe40, respectively, while Cys82 forms a hydrogen bond only with Leu29 and Leu30 in the wild type. Compared with the wild type, the number of hydrogen bonds increased and the protein conformation changed, as shown in **Figures 3D,E**. Using software, we also identified that Gln361 and Cys82 were located in the highly conserved amino acid region, and the conserved amino acid mutation was likely to damage the protein function, as shown in **Figure 3F**.

VPS33B is homologous with yeast Sec-1/Munc18 family protein VPS33P. The secondary structure analysis of the VPS33B protein in this patient shows that *p*.Q361X,257 and *p*.C82R are indeed located in the Sec1 protein domain (**Figure 3A**). Sec-1/Munc18 protein (SM protein) regulates vesicle trafficking and fusion by binding to the T-SNARE of the Syntaxin family in a variety of modes, and SM protein plays an important role in membrane protein trafficking and maintenance of cell polarity (5, 6). This protein binds and modulates the conformation of SNARE protein, which is homologous to neuronal synaptic membrane protein syntaxin and is critical for neurotransmitter release and other secretory events (7). It is possible that our patient's irritability is related to mutations in this region. Current studies have found that both *VPS33B* and *VIPAR* interact with the HOPS complex protein VPS18. *VIPAR* may interact with VPS18 only in the absence of *VPS33B*, so the *VPS33B-VIPAR* complex is unlikely to participate in the HOPS interaction (8). However, *VIPAR* may interact with VPS18 in mutant *VPS33B* cells, implying that this interaction may be involved in the pathogenesis of ARC syndrome. The *VPS33B* gene is expressed in the bone, kidneys, liver, and skin; thus, the clinical manifestations show multisystem involvement (9).

Hanley et al. used a VPS33Bfl/fl-AlfpCre mouse model and found that VPS33B is crucial for maintaining the structure and function of mammalian hepatocytes. Patients with ARC syndrome with *VPS33B* mutation have cholestasis, high plasma ALP activity, and high bile acid level, while transaminase activity and GGT levels remain normal. This is because of an incorrect localization of apical membrane proteins, such as ARE, in hepatocytes but a normal localization of basolateral membrane proteins in hepatocytes (10). The study also found that VPS33B affects bile acid homeostasis and lipid metabolism in mice and contributes to the progress of liver cholestasis. VPS33B affects the progress of liver metabolism in both bile acid circulation and lipid metabolism, while VPS33B deficiency plays a key role in aggravating cholestasis and liver injury (7, 11).

We summarized the histories of patients with mostly mild and partial clinical manifestations of ARC syndrome, who were reported to have achieved long-term survival thus far, as shown in **Table 2**. Surprisingly, in the acute phase, we could

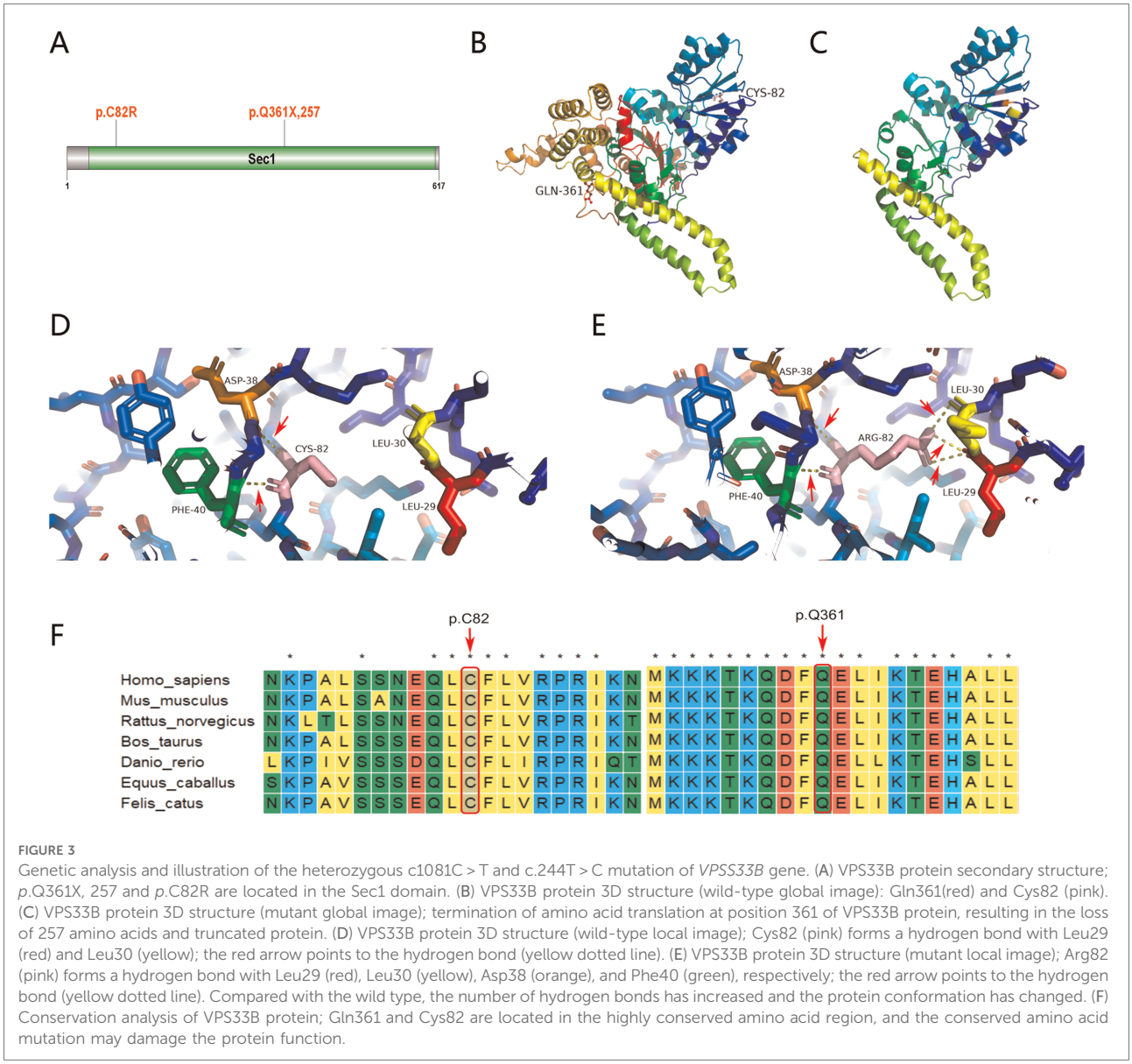


FIGURE 3
Genetic analysis and illustration of the heterozygous c1081C > T and c.244T > C mutation of *VPS33B* gene. (**A**) VPS33B protein secondary structure; *p*.Q361X, 257 and *p*.C82R are located in the Sec1 domain. (**B**) VPS33B protein 3D structure (wild-type global image): Gln361(red) and Cys82 (pink). (**C**) VPS33B protein 3D structure (mutant global image); termination of amino acid translation at position 361 of VPS33B protein, resulting in the loss of 257 amino acids and truncated protein. (**D**) VPS33B protein 3D structure (wild-type local image); Cys82 (pink) forms a hydrogen bond with Leu29 (red) and Leu30 (yellow); the red arrow points to the hydrogen bond (yellow dotted line). (**E**) VPS33B protein 3D structure (mutant local image); Arg82 (pink) forms a hydrogen bond with Leu29 (red), Leu30 (yellow), Asp38 (orange), and Phe40 (green), respectively; the red arrow points to the hydrogen bond (yellow dotted line). Compared with the wild type, the number of hydrogen bonds has increased and the protein conformation has changed. (**F**) Conservation analysis of VPS33B protein; Gln361 and Cys82 are located in the highly conserved amino acid region, and the conserved amino acid mutation may damage the protein function.

not alleviate low GGT cholestasis and hyperbilirubinemia through plasma exchange in our patient, but the child's bilirubin and bile acid indices returned to normal with just oral drug treatment after discharge, suggesting that hyperbilirubinemia and cholestasis may have been paroxysmal. Similar histories were reported in other cases. For instance, patient number 7, whose history is summarized in **Table 2**, presented with a spontaneous resolution of hyperbilirubinemia. To understand why such a phenotype exists, it may be necessary to further study the upstream and downstream regulation of relevant genes.

At present, among the gene mutations that are related to prolonged survival of patients with ARC, five were found to have c.1225 + 5G > C gene mutations (**Table 3**). Previously, it was also reported that c.1225 + 5G > C mutations are related to mild ARC syndrome. *VPS33B* c.1225 + 5G > C mutation produces a truncated VPS33B protein (residue 1,420) that is still partially co-domain with VIPAR. At the same time, cell experiments show that the c.1225 + 5G > C mutant still retains a part of the ability to interact with VIPAR, but the mutant affects the ability of the complex to co-locate on tubular vesicular circulating membrane, which at least partially impairs their cell function (8). Two gene mutation sites in our patient, c.1081C > T and c.244T, caused the deletion of C-terminal amino acids of the protein, but the N-terminal coding was not affected. c.244T > C also increased the number of hydrogen bonds in the tertiary structure of the protein and did not change the overall structure of the protein, which may

TABLE 2 Clinical manifestations of ARC syndrome in patients with prolonged survival.

Patient	Consanguineous mating	Ethnic	Gender	Arthrogryposis	Renal dysfunction	Cholestasis	Include ichthyosis/ hyperkeratosis	Platelet dysfunction	Sensorineural deafness	Agenesis of the corpus callosum	Severe failure to thrive	Recurrent infection	survival
1 (12)	+	Spanish	M	+	–	+	–	–	+	–	+	–	alive at 3y
2 (4)	+	Arab	F	+	+	+	–	N	–	+	+	–	alive at 7.7y
3 (4)	+	Arab	M	+	+	+	–	N	–	+	+	–	alive at 3.3y
4 (13)	–	Mexico	F	–	+	–	–	+	–	–	+	+	died at 8.5y
5 (14)	–	Spanish	F	+	+	+	+	+	–	+	+	+	alive at 6y
6 (15)	+	Brazil	M	+	–	+	+	–	–	+	+	–	alive at 17y
7 (15)	+	Brazil	F	–	–	+	+	–	–	–	+	–	alive at 10y
8 (15)	–	Brazil	M	–	–	+	+	+	+	–	+	–	alive at 11y
9 (16)	–	Japan	M	–	Proteinuria	–	–	–	+	–	+	–	alive at 6y
10 (16)	–	Japan	M	–	+	+	–	–	+	–	–	–	alive at 24y
11 (17)	–	Spanish	F	+	+	–	+	–	+	–	–	–	alive at 12y
12 (18)	+	Austria	M	–	Proteinuria	–	+	–	+	–	–	–	alive at 13y
13 (18)	–	Austria	F	+	–	–	+	–	+	–	+	–	alive at 35y
14 (18)	–	Austria	M	+	–	–	+	–	+	–	+	–	alive at 59y
15 (8)	–	Peru/ Puerto Rico	M	+	+	+	–	+	+	–	+	–	alive at 5.5y
16 (8)	N	Puerto Rico/ Mexico	F	+	+	+	+	–	+	+	+	–	alive at 3.5y
17 (19)	+	China	M	–	Proteinuria	+	–	–	–	–	–	–	alive at 7y
18 (19)	–	China	M	–	Proteinuria	+	–	–	–	–	–	–	alive at 4y
19 (19)	–	China	F	–	Proteinuria	+	–	–	–	–	–	–	alive at 9y

10.3389/fped.2022.1041080

TABLE 3 Currently known *VPS33B* gene mutation sites associated with prolonged survival in ARC syndrome.

Patient	Gene	Mutation sites	Hom/Het	Amino acid
1 (12)	*VPS33B*	c.1225 + 5G > C c.1246C > T	 hom	 p.R416X
2 (4)	*VPS33B*	c.1157A > C	hom	p.His386Pro
3 (4)				
4 (13)	*VPS33B*	c.1609_1657 + 9del c.1225 + 5G > C		
5 (14)	*VPS33B*	c.1225 + 5G > C c.440_499del	het het	 Pro147Argfs*4
6 (15)	*VPS33B*	c.1148T > A	hom	p.(Ile383Asn)
7 (15)	*VPS33B*	c.1148T > A	hom	p.(Ile383Asn)
8 (15)	*VPS33B*	c.1148T > A c.940-2A > G	het het	p.(Ile383Asn)
9 (16)	*VPS33B*	c.403 + 2T > A c.1582-9C > G	het het	
10 (16)	*VIPAS39*	c.339del c.1035C > G	het het	p.(Phe113Leufs*60)] p.(Tyr345*)
11 (17)	*VPS33B*	c1225 + 5G > C		
12 (18)	*VPS33B*	c.[390G > A;392G > A]	hom	p.Gly131Glu
13 (18)	*VPS33B*	c.[390G > A;392G > A]	hom	p.Gly131Glu
14 (18)	*VPS33B*	c.[390G > A;392G > A] c.240-1G > C	het het	p.Gly131Glu
15 (8)	*VPS33B*	c.240–577_290-156del c.1225 + 5G > C.	het	p.Gln421Valfs∗8
16 (8)	*VPS33B*	c.1261_1262delCA c.1225 + 5G > C	het	p.Gln421Valfs∗8
17 (19)	*VPS33B*	c.1726T > C	hom	p.Cys576Arg
18 (19)	*VPS33B*	c.1726T > C	het	p.Cys576Arg
19 (19)	*VPS33B*	c.1726T > C	het	p.Cys576Arg

have helped preserve the function of VPS33B protein, resulting in a mild phenotype of ARC and prolonged survival in the patient.

Our discovery of two new gene mutation sites in an ARC patient with prolonged survival further suggests that other unexplained cholestasis in older children may be linked to ARC gene mutation. Furthermore, missense mutations were common in other ARC syndrome patients who had prolonged survival (**Table 3**).

At present, there is no clear and effective treatment for ARC syndrome. Most such patients are given supportive treatments such as fluid supplementation, anti-infection, and enteral nutrition to relieve acidosis, hyperbilirubinemia, and recurrent infection in order to stabilize their condition and improve their quality of life. Although there is no effective gene therapy for ARC syndrome at present, it is believed that with the deepening of molecular genetics research and the development of clinical diagnosis and treatment technology, gene therapy will bring new hope to the prevention and treatment of ARC syndrome. We hope our findings can support developments in gene therapy for patients with mild ARC.

Data availability statement

The datasets presented in this study can be found in online repositories. The names of the repository/repositories and accession number(s) can be found in the article/Supplementary Material.

Ethics statement

Written informed consent was obtained from the individual(s) and minor(s)' legal guardian/next of kin for the publication of any potentially identifiable images or data included in this article.

Author contributions

YZ provided clinical information and wrote the manuscript. DC undertook critical discussion and supervised the study. All

authors contributed to the article and approved the submitted version.

Funding

Publication charges for this article have been funded by the General Project of Science and Technology Development Fund of Nanjing Medical University (grant no. NMUB20210070).

Acknowledgments

We thank the patient and her family members and all the medical staff involved in the care of this patient.

Conflict of interest

The authors declare that the research was conducted in the absence of any commercial or financial relationships that could be construed as a potential conflict of interest.

Publisher's note

All claims expressed in this article are solely those of the authors and do not necessarily represent those of their affiliated organizations, or those of the publisher, the editors and the reviewers. Any product that may be evaluated in this article, or claim that may be made by its manufacturer, is not guaranteed or endorsed by the publisher.

References

1. Gissen P, Tee L, Johnson CA, Genin E, Caliebe A, Chitayat D, et al. Clinical and molecular genetic features of ARC syndrome. *Hum Genet*. (2006) 120:396–409. doi: 10.1007/s00439-006-0232-z

2. Zhou Y, Zhang J. Arthrogryposis-renal dysfunction-cholestasis (ARC) syndrome: from molecular genetics to clinical features. *Ital J Pediatr*. (2014) 40:77. doi: 10.1186/s13052-014-0077-3

3. Jang WY, Cho TJ, Bae JY, Jung HW, Ko JS, Park MS, et al. Orthopaedic manifestations of arthrogryposis-renal dysfunction-cholestasis syndrome. *J Pediatr Orthop*. (2011) 31:107–12. doi: 10.1097/BPO.0b013e3182032c83

4. Rodrigo DBC, Squires JE, McKiernan PJ. VPS33BA Novel mutation in gene causing a milder ARC syndrome phenotype with prolonged survival. *JIMD Rep*. (2019) 47:4–8. doi: 10.1002/jmd2.12027

5. Gerien KS, Zhang S, Russell AC, Zhu YH, Purde V, Wu JQ. Roles of Mso1 and the SM protein Sec1 in efficient vesicle fusion during fission yeast cytokinesis. *Mol Biol Cell*. (2020) 31:1570–83. doi: 10.1091/mbc.E20-01-0067

6. Akbar MA, Ray S, Krämer H. The SM protein car/Vps33A regulates SNARE-mediated trafficking to lysosomes and lysosome-related organelles. *Mol Biol Cell*. (2009) 20(6):1705–14. doi: 10.1091/mbc.e08-03-0282

7. Fu K, Wang C, Gao Y, Fan S, Zhang H, Sun J, et al. Metabolomics and lipidomics reveal the effect of hepatic Vps33b deficiency on bile acids and lipids metabolism. *Front Pharmacol*. (2019) 10:276. doi: 10.3389/fphar.2019.00276

8. Smith H, Galmes R, Gogolina E, Straatman-Iwanowska A, Reay K, Banushi B, et al. Associations among genotype, clinical phenotype, and intracellular localization of trafficking proteins in ARC syndrome. *Hum Mutat*. (2012) 33 (12):1656–64. doi: 10.1002/humu.22155

9. Huizing M, Didier A, Walenta J, Anikster Y, Gahl WA, Krämer H. Molecular cloning and characterization of human VPS18, VPS 11, VPS16, and VPS33. *Gene*. (2001) 264(2):241–7. doi: 10.1016/S0378-1119(01)00333-X

10. Hanley J, Dhar DK, Mazzacuva F, Fiadeiro R, Burden JJ, Lyne AM, et al. Vps33b is crucial for structural and functional hepatocyte polarity. *J Hepatol*. (2017) 66:1001–11. doi: 10.1016/j.jhep.2017.01.001

11. Fu KL, Chen P, Zhou YY, Jiang YM, Gao Y, Zhang HZ, et al. Hepatic Vps33b deficiency aggravates cholic acid-induced cholestatic liver injury in male mice. *Acta Pharmacol Sin*. (2022) 43:933–40. doi: 10.1038/s41401-021-00723-3

12. Agawu A, Sheppard S, Lin HC. A novel VPS33B mutation causing a mild phenotype of arthrogryposis, renal dysfunction, and cholestasis syndrome. *J Pediatr Gastroenterol Nutr*. (2019) 69(2):e55–6. doi: 10.1097/MPG.0000000000002306

13. Weyand AC, Lombel RM, Pipe SW, Shavit JA. The role of platelets and ϵ-aminocaproic acid in Arthrogryposis, Renal Dysfunction, and Cholestasis (ARC) syndrome associated hemorrhage. *Pediatr Blood Cancer*. (2016) 63(3):561–3. doi: 10.1002/pbc.25814

14. Rosales A, Mhibik M, Gissen P, Segarra O, Redecillas S, Ariceta G. Severe renal fanconi and management strategies in arthrogryposis-renal dysfunction-cholestasis syndrome: a case report. *BMC Nephrol*. (2018) 19(1):1–5. doi: 10.1186/s12882-018-0926-1

15. Linhares ND, Fagundes ED, Ferreira AR, Queiroz TC, da Silva LR, Pena SD. Mild phenotype of arthrogryposis, renal dysfunction, and cholestasis syndrome 1 caused by a novel VPS33B variant. *Front Genet*. (2022) 13:1–8. doi: 10.3389/fgene.2022.796759

16. Satomura Y, Bessho K, Nawa N, Kondo H, Ito S, Togawa T, et al. Novel gene mutations in three Japanese patients with ARC syndrome associated mild phenotypes: a case series. *J Med Case Rep*. (2022) 16(1):1–6. doi: 10.1186/s13256-022-03279-w

17. Duong MD, Rose CM, Reidy KJ, Del Rio M. An uncommon case of Arthrogryposis, Renal Dysfunction, and Cholestasis (ARC) syndrome and review of the renal involvement: questions. *Pediatr Nephrol*. (2020) 35(2):247–8. doi: 10.1007/s00467-019-04336-1

18. Gruber R, Rogerson C, Windpassinger C, Banushi B, Straatman-Iwanowska A, Hanley J, et al. Autosomal Recessive Keratoderma-Ichthyosis-Deafness (ARKID) syndrome is caused by VPS33B mutations affecting rab protein interaction and collagen modification. *J Invest Dermatol*. (2017) 137(4):845–54. doi: 10.1016/j.jid.2016.12.010

19. Qiu YL, Liu T, Abuduxikuer K, Hao CZ, Gong JY, Zhang MH, et al. Novel missense mutation in VPS33B is associated with isolated low gamma-glutamyltransferase cholestasis: attenuated, incomplete phenotype of arthrogryposis, renal dysfunction, and cholestasis syndrome. *Hum Mutat*. (2019) 40(12):2247–57. doi: 10.1002/humu.23770

frontiers | Frontiers in Genetics

TYPE Original Research
PUBLISHED 13 December 2022
DOI 10.3389/fgene.2022.957915

Check for updates

OPEN ACCESS

EDITED BY
Tieliu Shi,
Hunan University of Arts and Science, China

REVIEWED BY
Alessio Di Fonzo,
IRCCS Ca'Granda Foundation Maggiore Policlinico Hospital, Italy
Yaqiong Jin,
Beijing Children's Hospital, Capital Medical University, China

*CORRESPONDENCE
Yi Liu,
y_liu99@sina.com
Zhongtao Gai,
gaizhongtao@sina.com

†These authors have contributed equally to this work

SPECIALTY SECTION
This article was submitted to Genetics of Common and Rare Diseases, a section of the journal Frontiers in Genetics

RECEIVED 17 June 2022
ACCEPTED 09 November 2022
PUBLISHED 13 December 2022

CITATION
Wang Y, Lv Y, Li Z, Gao M, Yang X, Li Y, Shi J, Gao Z, Liu Y and Gai Z (2022), Phenotype and genotype analyses of Chinese patients with autosomal dominant mental retardation type 5 caused by *SYNGAP1* gene mutations. *Front. Genet.* 13:957915. doi: 10.3389/fgene.2022.957915

COPYRIGHT
© 2022 Wang, Lv, Li, Gao, Yang, Li, Shi, Gao, Liu and Gai. This is an open-access article distributed under the terms of the Creative Commons Attribution License (CC BY). The use, distribution or reproduction in other forums is permitted, provided the original author(s) and the copyright owner(s) are credited and that the original publication in this journal is cited, in accordance with accepted academic practice. No use, distribution or reproduction is permitted which does not comply with these terms.

Phenotype and genotype analyses of Chinese patients with autosomal dominant mental retardation type 5 caused by *SYNGAP1* gene mutations

Yanxin Wang[1†], Yuqiang Lv[2,3†], Zilong Li[2,3], Min Gao[2,3], Xiaomeng Yang[2,3], Yue Li[2,3], Jianguo Shi[4,3], Zaifen Gao[4,3], Yi Liu[2,3]* and Zhongtao Gai[2,4,3]*

[1]Department of Pediatrics, Children's Hospital Affiliated to Shandong University, Ji'nan, China, [2]Pediatric Research Institute, Children's Hospital Affiliated to Shandong University, Ji'nan, China, [3]Shandong Provincial Clinical Research Center for Children's Health and Disease, Ji'nan, China, [4]Epilepsy Center, Children's Hospital Affiliated to Shandong University, Ji'nan, China

Background: Autosomal dominant mental retardation type 5 (MRD5), a rare neurodevelopmental disorder (NDD) characterized by intellectual disability (ID), developmental delay (DD), and epilepsy predominantly, is caused by a heterozygous mutation in the *SYNGAP1* gene. *SYNGAP1* mutations have been rarely reported in the Chinese population. Here, we present an investigation of *SYNGAP1* mutations in a clinical cohort with ID and DD in Shandong, a northern province in China, to further explore the genotype and phenotype correlations.

Methods: A retrospective study was conducted on 10 children with *SYNGAP1* mutations presenting ID, DD, and epilepsy who were diagnosed between January 2014 and May 2022. Clinical data and genetic tests were collected. Treatment and regular follow-ups were carried out to pay close attention to the prognosis of the patients.

Results: We described 10 unrelated affected individuals with *SYNGAP1* mutations, displaying ID, DD, epilepsy, or seizures. All mutations of *SYNGAP1* in the 10 patients were *de novo*, except patient 3 whose father was unavailable, including five nonsense mutations, two frameshift mutations, two splicing mutations, and one codon deletion. Among these mutations, five were novel and the other five were previously reported. Significantly, all patients with epilepsy were sensitive to anti-seizure drugs, especially sodium valproate. Furthermore, rehabilitation training seemed to exert a more improved effect on motor development than language development for the patients.

Conclusion The 10 patients carrying *SYNGAP1* mutations were diagnosed as MRD5. Five novel genetic mutations were found, which expanded the mutational spectrum of the *SYNGAP1* gene. The identification of these mutations in this study helps explore the relationship between genotypes

and phenotypes and contributes to genetic counseling and therapeutic intervention for patients with MRD5.

KEYWORDS

autosomal dominant mental retardation type 5, mutation, *SYNGAP1*, intellectual disability, developmental delay, next-generation sequencing, epilepsy

Introduction

Autosomal dominant mental retardation type 5 (MRD5; OMIM #612621), a recently described single-gene disorder, is defined as a rare neurodevelopmental disorder characterized by moderate to severe intellectual disability (ID) and psychomotor developmental delay (DD) in the first year of life, with a high frequency of comorbid epilepsy and autism spectrum disorder (ASD) (Deciphering Developmental Disorders Study, 2015; Agarwal et al., 2019; Verma et al., 2020). With the rapid development of molecular diagnostic techniques, the heterozygous loss-of-function mutations of the synaptic Ras GTPase-activating protein 1 (*SYNGAP1*) gene (OMIM #603384) have been deemed the genetic etiology of MRD5 in an autosomal dominant manner (Parker et al., 2015; Weldon et al., 2018). Reportedly, the estimated incidence of *SYNGAP1* mutations accounts for ~0.75% of patients with neurodevelopmental disorders (NDDs) (Berryer et al., 2013; Deciphering Developmental Disorders Study, 2015; Mignot et al., 2016; Weldon et al., 2018; Zhang et al., 2021). As merely more than 200 cases of MDR5 are reported worldwide, the definite incidence has not been established to date (Gamache et al., 2020; Zhang H et al., 2020).

The *SYNGAP1* gene is on chromosome 6p21.3 and consists of 19 exons encoding synaptic RAS-GTPase-activating protein (SynGAP), which is localized to dendritic spines in the postsynaptic density (PSD) of excitatory glutamatergic neurons and primarily expressed in the developing brain, particularly the forebrain and the hippocampus. By alternative splicing, SynGAP could produce distinct functional protein isoforms and perform different functions, such as regulation of neural excitability, development of dendritic arborization, maturation of the dendritic spine, and plasticity of synapses (Araki et al., 2015; Meili et al., 2021; Kilinc et al., 2022). There are various predicted functional domains in SynGAP, including the pleckstrin homology (PH) domain (pos. 150–251) in the N-terminus; C2 domain (pos. 263–362) and RasGAP domain (pos. 392–729) in the core region; and the SH3 domain (pos. 785–815), the coiled-coil (CC) domain (pos. 1,189–1,262), and other C-terminal domains that resulted from alternative splicing such as QTRV for isoform α1, TADH for isoform α2, PRGH for isoform β, and LLIR for isoform γ, although their exact functions and molecular mechanisms remain unclear (Berryer et al., 2013; Gamache et al., 2020; Kilinc et al., 2022). Loss-of-function mutations in *SYNGAP1* resulting in SynGAP haploinsufficiency contribute to a constellation of symptoms of ID, DD, and seizures, which have recently been termed a neurodevelopmental disorder—MRD5 (Agarwal et al., 2019; Kilinc et al., 2022).

To date, reported cases regarding MRD5 have been predominantly from Europe, whereas only a few cases have been elucidated previously in China (Pei et al., 2018; Lu et al., 2019; Gao et al., 2020; Zhang et al., 2021). In the study, we present the clinical and mutational characteristics of additional 10 Chinese patients with MRD5 identified by next-generation sequencing (NGS) from a clinical cohort of 1,986 cases with NDDs manifesting ID, DD, epilepsy, and ASD between January 2014 and May 2022 in Shandong Province of China, and five novel mutations in the *SYNGAP1* gene were discovered.

Materials and methods

Patients

Five male and five female patients from unrelated families were identified and diagnosed as having MRD5 from a clinical cohort of 1,986 cases with NDDs between January 2014 and May 2022 at Children's Hospital affiliated to Shandong University. All patients from the Han Chinese population in Shandong Province in China were examined and clinically diagnosed by experienced pediatric neurologists of the hospital according to the DMS-5 criteria. All clinical data were gathered, including family history, clinical features, laboratory tests, magnetic resonance imaging (MRI) of the brain, and electroencephalogram (EEG).

Exome sequencing

Peripheral blood samples were obtained from all patients and their parents except patient 3, whose father was unavailable. Genomic DNA was extracted from blood samples with the TIANamp Blood DNA Kit (Tiangen, China) in accordance with the standard protocol. The whole exome sequencing (WES) with the SeqCap EZ Choice XL Library (Roche NimbleGen) was used to capture the exon regions and adjacent intron regions (50 bp) (Illumina, America). The mean sequencing depth of the targeted areas was 134.09X, of which 97.71% of the target sequences were more than 20X.

Sequencing data were compared with the UCSC hg19 human reference genome sequence using NextGene V2.3.4 software to identify genetic mutations. At the same time, mutations were

further annotated by NextGene V2.3.4 and associated with multiple databases, such as 1000 Genomes, ExAC, dbSNP, HGMD, ClinVar, ESP6500, OMIM, and Inhouse databases. Then, pathogenicity was predicted by PolyPhen-2, SIFT, MutationTaster, and REVEL. When all the aforementioned analyses were finished, the obtained mutations eventually were the candidates for pathogenic mutations. Thereafter, the pathogenicity assessment of genetic mutations was carried out, which was based on the 2015 American College of Medical Genetics and Genomics (ACMG) guidelines (Richards et al., 2015).

Validation of genetic mutations

Sanger sequencing was applied to validate the mutations detected by exome sequencing in the patients and their parents. Primer sets were designed by Primer Premier v5.0 software. Furthermore, AmpliTaq Gold® 360 DNA Polymerase (Applied Biosystems) was used for PCR amplification. PCR products were then purified and sequenced on an ABI Prism 3700 automated sequencer (Applied Biosystems, CA, United States).

Statistical analysis

Statistical analysis was performed with SPSS 19.0 software. Chi-squared tests were used to test the significance of mutations in different groups, and results were regarded as statistically significant when the p-value was <0.05.

Results

Clinical findings

Five male and five female children were recruited into our study with a mean diagnostic age of 41.6 months (ranging from 14 months to 89 months). Intellectual disability and global developmental delay of varying levels were observed in all the patients, of whom five (P4, P5, P6, P7, and P10) had seizures, four (P2, P4, P9, and P10) showed ataxia or gait abnormalities, and six (P2, P4, P5, P6, P9, and P10) were observed to have behavioral problems, while one patient (P5) was clinically diagnosed with ASD. In addition, one patient P3 manifested hypotonia of four limbs, especially the upper ones, and one patient P9 had internal strabismus of the eyes. All the patients had impaired speaking ability, particularly three patients P4, P6, and P7 who remain verbally disabled.

The age of seizure onset for the five affected individuals (P4, P5, P6, P7, and P10) varied from 18 months to 60 months (mean age 37.8 months). The types of seizures monitored by EEGs consisted of atypical absence (4/5), eyelid myoclonia (1/5), atypical absence with myoclonus (1/5), myoclonic seizure (1/5), atonic seizure (1/5), myoclonus with atonic seizure (1/5), and unclassified fall attack (1/5). Additionally, the EEG of a patient (P3) was abnormal with multifocal waves and spikes without a predominant rhythm, while seizure onset was not observed. As for the five patients with seizures, generalized seizures with diffuse slow wave backgrounds occurred in four individuals (P4, P6, P7, and P10), but the focal seizure was only noticed in one patient P5, and no trigger of seizures was identified.

Furthermore, a normal or non-specific presentation was observed in brain MRI, while patient 3 displayed a slightly widened extracerebral lacuna in the left temporal pole and two patients (P8 and P9) showed the possibility of the terminal band in the bodies of the lateral ventricles. Additionally, no abnormality in karyotypes, metabolic screening, and the function of the thyroid glands was observed. However, the levels of growth hormone were obviously below normal, which remained to be explored further. Clinical data are shown in detail in Table 1.

Genetic findings and analysis of novel mutations

Among the 10 individuals, nine distinctive mutations were identified; two patients (P7 and P10) shared the same mutation of c.2059C>T (p.R687X), five mutations were novel, and the remaining five were reported (Table 2). All mutations were validated as *de novo* with the exception of patient 3 as his father was unavailable. The 10 mutations consisted of nonsense (5, 50%), frameshift (2, 20%), splicing (2, 20%), and codon deletion (1, 10%). The mutation sites were distributed in exons 4, 5, 8, 12, and 15 and introns 6 and 10 (Figure 1A) and were located on the domains of SynGAP from PH to RasGAP domains, with two on the PH domain, one on the C2 domain, three on the RasGAP domain, and two on the C-terminal unknown domain (Figure 1B). According to the American College of Medical Genetics and Genomics (ACMG) guidelines, eight mutations in nine patients were determined as pathogenic, and one mutation (c.917_925del/p.V306_W308del) was likely pathogenic (Table 2). The five novel mutations, including two splicing, one codon deletion, one frameshift, and one nonsense, were predicted to disrupt the function of the protein.

Treatment and medical follow-up

During the mean follow-up period of 33.2 months, all affected individuals were subjected to rehabilitation training for more than one year. Preliminary improvement in motor development could be seen with varying degrees. Almost all patients except patient 3 were equipped with the ability to walk

TABLE 1 Clinical information of 10 Chinese patients.

Clinical information	P1	P2	P3	P4	P5	P6	P7	P8	P9	P10
Gender	Female	Female	Male	Male	Female	Male	Male	Female	Female	Male
Age	30 m	89 m	14 m	58 m	31 m	24 m	30 m	34 m	43 m	63 m
ID	+	+	+	+	+	+	+	+	+	+
IQ	–	44	N/A	43	–	–	–	–	43	–
Language delay	+	+	+	+	+	+	+	+	+	+
Age of speaking	N/A	N/A	N/A	–	N/A	–	–	18 m	N/A	N/A
Current speech ability	Two–three words	Simple sentences	Two–three words	Verbal disability	Two words	Verbal disability	Verbal disability	Several words	Four words	A few words
Motor delay	+	+	+	+	+	+	+	+	+	+
Age of walking	N/A	16 m	Unable to walk	18 m	18 m	20 m	27 m	18 m	N/A	N/A
Impairment of motor	Mild	Moderate	Severe	Moderate	Moderate	Moderate	Moderate	Mild	Moderate	Severe
Hypomyotonia	–	–	+	–	–	–	–	–	–	–
Ataxia	–	+	N/A	+	–	–	–	–	+	+
ASD	–	–	–	–	+	–	–	–	-	–
Behavioral problems	–	+	N/A	+	+	+	–	–	+	+
Malformations	–	–	–	–	–	–	–	–	Internal strabismus	–
Seizures	–	–	–	+	+	+	+	–	–	+
Age of seizure onset	–	–	–	55 m	27 m	18 m	29 m	–	–	60 m
Onset type of seizures	–	–	–	FA	AAb	AAb with or without M; At; M; M with At	AAb	–	–	EMA; AAb
Effect of ASMs	–	–	–	Sensitive	Sensitive	Sensitive	Sensitive	–	–	Sensitive
EEG	N/A	N/A	Abnormal	Abnormal	Abnormal	Abnormal	Abnormal	N/A	N/A	Abnormal
MRI	N/A	Normal	Nonspecific	N/A	Normal	Normal	Normal	Nonspecific	Nonspecific	Normal
Karyotype	46, XX	46, XX	46, XY	46, XY	46, XX	46, XY	46, XY	46, XX	46, XX	46, XY
Metabolic screening	N/A	N/A	N/A	Normal	Normal	Normal	N/A	N/A	Normal	N/A
Functions of the thyroid gland	Normal	Normal	N/A	Normal	Normal	N/A	N/A	N/A	N/A	N/A
Growth hormone (≧10 ug/L)	0.23	N/A	N/A	7.73	3.92	N/A	N/A	N/A	N/A	N/A

+, present; –, absent; N/A, not available; y, year(s); m, month(s); FA, fall attack; AAb, atypical absence; M, myoclonia; At, atonia; EMA, eyelid myoclonia; ASM, anti-seizure medication.

unaided despite the existence of an unsteady gait in three children (P5, P9, and P10). Patient 3 was able to sit unaided for approximately 30 min but had difficulty in standing independently, even though his electromyogram was normal. In contrast to motor development, there was no significant improvement in the language development of the patients, particularly three patients (P4, P6, and P7) who still had verbal disability, whereas the other seven children could only speak few words.

Anti-seizure drugs sodium valproate and lamotrigine were administered to the five patients with epilepsy, demonstrating significant improvement. Patient 4 initially did not take medications under medical supervision until the identical type of seizure occurred once. After sodium valproate was prescribed, seizure was under control eventually. Up to now, patient 4 has been free from seizures for 11 months. Patient 5 was prescribed a medication combination of sodium valproate and lamotrigine and remained seizure-free for 1 year. Patient 6 was administered with sodium valproate and has been seizure-free for more than 3 years. Similarly, patient 7 was also sensitive to valproate, although his EEGs are still abnormal. Sodium valproate also worked for patient 10 but was discontinued for a month, during which the patient experienced seizure recurrence twice. Until sodium valproate was taken again, his seizure was controlled, and this stable status has lasted for 11 months.

TABLE 2 Genetic information of 10 patients in our study.

Patient	Mutation site	cDNA change	Mutation type	Amino acid change	Source of mutation	Status	ACMG	Pathogenicity
P1	Exon 4	c.333delA	Frameshift	p.K114Sfs*20	*De novo*	Reported in Carvill et al. (2013)	PVS1+PS1+PS2	Pathogenic
P2	Intron 6	c.664–2A>G	Splicing	—	*De novo*	Novel	PVS1+PS2+PM2	Pathogenic
P3	Intron 10	c.1677-1G>C	Splicing	—	Father: not available. Mother: no mutation	Novel	PVS1+PM2+PP3	Pathogenic
P4	Exon 8	c.917_925del	Codon deletion	p.V306_W308del	*De novo*	Novel	PS2+PM2	Likely pathogenic
P5	Exon 15	c.2764C>T	Nonsense	p.R922X	*De novo*	Reported in Parker et al. (2015)	PVS + PS1+PS2+PM2	Pathogenic
P6	Exon 8	c.1176delG	Frameshift	p.G393Afs*9	*De novo*	Novel	PVS + PS2+PM2	Pathogenic
P7	Exon 12	c.2059C>T	Nonsense	p.R687X	*De novo*	Reported in Gao et al. (2018)	PVS + PS2+PM2	Pathogenic
P8	Exon 5	c.427C>T	Nonsense	p.R143X	*De novo*	Reported in Carvill et al. (2013)	PVS1+PS2+PS4+PM2	Pathogenic
P9	Exon 15	c.2620C>T	Nonsense	p.Q874X	*De novo*	Novel	PVS1+PS2+PM2	Pathogenic
P10	Exon 12	c.2059C>T	Nonsense	p.R687X	*De novo*	Reported in Gao et al. (2018)	PVS1+PS2+PM2	Pathogenic

All variants were described by NM_006772.2 for *SYNGAP1* transcript reference sequences using the version of GRCh37/hg19.

Genotype–phenotype correlation

To elucidate the genotype–phenotype correlation of Chinese patients, we searched all publications regarding *SYNGAP1* mutations in the Chinese population in PubMed and all available Chinese databases, such as Wanfang and China National Knowledge Infrastructure. Thus, data on a total of 23 patients with *SYNGAP1* mutations were summarized, and the patients were divided into four different groups according to their mutation type (nonsense, splicing, frameshift, and missense) in the *SYNGAP1* gene (Pei et al., 2018; Lu et al., 2019; Gao et al., 2020; Zhang et al., 2021). All 23 patients presented ID and DD, of which only three patients with nonsense, frameshift, and splicing mutations were diagnosed as ASD, while the numbers of patients with seizures varied in the four groups. Among them, there were seven (7/10, 70%) patients with seizures in the nonsense group, six (6/7, 85.7%) in the frameshift group, two (2/5, 40%) in the splicing group, and one (1/1, 100%) in the missense group. Statistically, the results exhibited no significant difference among the four groups (Table 3). In terms of the correlation between the phenotypes and the locations of the mutations in the *SYNGAP1* gene, our patients with mutations in exons 4 and 5 displayed milder developmental delay and no comorbid epilepsy, whereas those with mutations in exons 8–15 had moderate to severe clinical manifestations (Figure 1A). However, there was no association between the various manifestations and different mutation domains (Figure 1B).

Discussion

The genetic basis of MRD5 has been attributed to the loss-of-function mutation of the *SYNGAP1* gene, which is ranked the fourth most common NDD-related gene among a large spectrum of genes sharing overlapping phenotypes, accounting for ~0.75% of all NDD patients (Berryer et al., 2013; Deciphering Developmental Disorders Study, 2015; Kilinc et al., 2022). To date, more than 200 patients with *SYNGAP1* mutations associated with various phenotypes, such as ID, DD, epilepsy, ASD, and schizophrenia, have been reported in the Human Gene Mutation Database (HGMD) (Jimenez-Gomez et al., 2019; Gamache et al., 2020; Zhang H et al., 2020). Nevertheless, there has been no established diagnostic criterion for MRD5 until now. Here, we additionally identified 10 affected individuals harboring heterozygous mutations of the *SYNGAP1* gene (five novel and five reported) to further clarify the clinical and genetic characteristics.

The 10 patients in this study were identified from a clinical cohort of 1,986 cases with NDDs. Thus, the incidence of *SYNGAP1* mutation is approximately 0.5% in our NDD cohort, which is a little less than the previous reports (Berryer

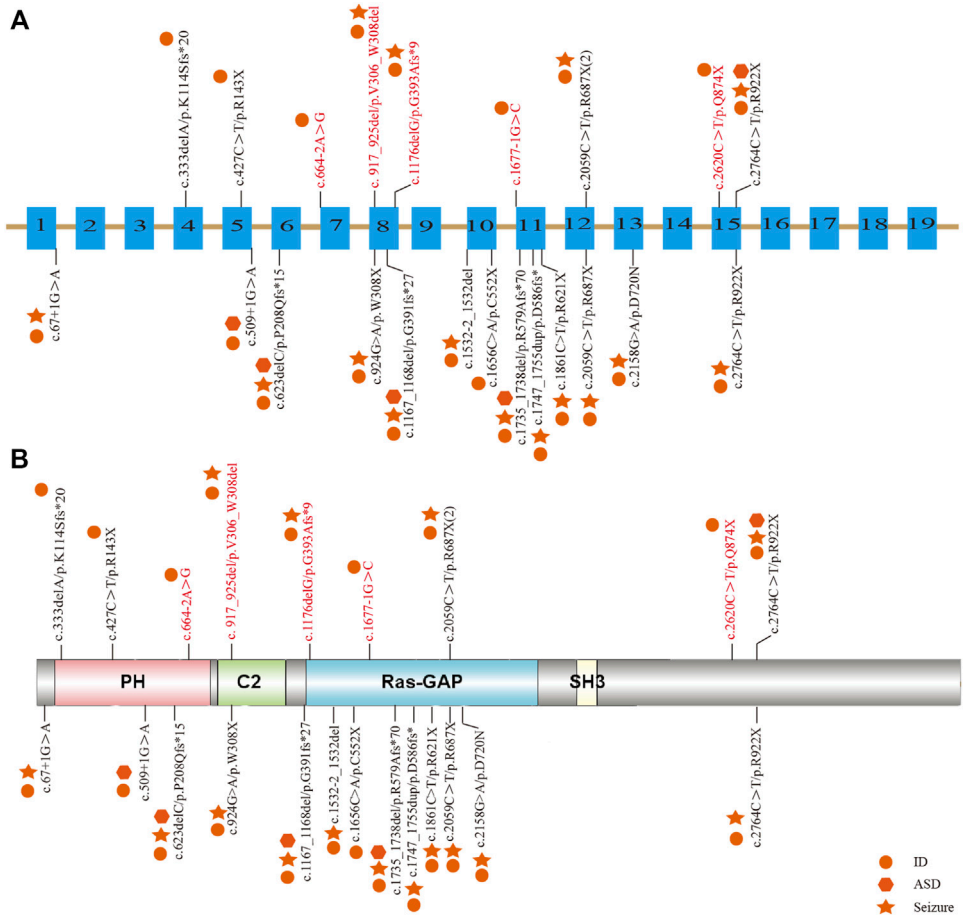


FIGURE 1
Distribution of mutations in Chinese patients among different exons and domains. The mutations in our study are listed prior to the exons or domains, in which five novel mutations are marked in red. The other mutations from previous studies in China are listed beneath the exons or domains. The various shapes represent different phenotypes, in which the circle means ID/DD, the star means seizure, and the hexagon means ASD. **(A)** Distribution of mutations in the exons of the SYNGAP1 gene. **(B)** Distribution of mutations in the domains of SynGAP.

TABLE 3 Comparison of cardinal features in 23 Chinese patients.

	Nonsense	Frameshift	Splicing	Missense
Number	10	7	5	1
Male/female	4/6	5/2	4/1	0/1
Mean age	45.5 m	57.6 m	50.2 m	9 m
ID	10	7	5	1
DD	10	7	5	1
ASD	1	1	1	0
Seizure	7	6	2	1

m, month(s).

et al., 2013; Kilinc et al., 2022). The main phenotypes of the 10 patients include ID (10/10, 100%), DD (10/10, 100%), epilepsy (5/10, 50%), and ASD (1/10, 10%). Consistent with previous literature, all patients manifested DD and ID during their first year of life, while impaired global development was the most remarkable feature in their early stages, of which the majority were moderately to severely affected. Compared with motor retardation, language development was impaired more badly with three individuals (P4, P6, and P7) who still appeared speechless in the last follow-up visit (Agarwal et al., 2019; Jimenez-Gomez et al., 2019; Zhang et al., 2021). In addition, the dynamic detection of GH and assessments of physical development also deserved more attention, which had not been reported in the previous literature. In terms of epilepsy, only five (50%) patients in the study were diagnosed, but they were all sensitive to anti-epilepsy drugs, especially sodium valproate, which is different from the previous Chinese study (Zhang et al., 2021). However, the pharmacoresistant rate among

all Chinese patients was similar to that of reported foreign patients (Mignot et al., 2016; Agarwal et al., 2019).

Significantly, rehabilitation training exerted a more positive effect on motor development than language development, which is consistent with the previous report (Zhang et al., 2021), but long-term prognosis could not be predicted due to the short follow-up time window, demonstrating that a standardized lifelong follow-up will be needed. In contrast to most studies regarding much younger patients, Prchalova et al. (2017) described an adult female patient with similar phenotypes as other patients carrying a *de novo* splicing mutation (c.1676 + 5G>A) in the *SYNGAP1* gene. Retrospecting her medical history, they noticed that a few of the phenotypes such as growth delay, microcephaly, and seizures could be alleviated or well-controlled with age, whereas several phenotypes such as facial features, unsteady gait, and cognitive and language performance showed a tendency to deteriorate, indicating a specific dynamic of the *SYNGAP1*-related phenotypes from a young age to adulthood. Whether early training and drug interventions could exert an underlying influence on disorder prognosis remains to be observed in the long-term clinical follow-up.

The *SYNGAP1* gene is rather complex and can be expressed in multiple isoforms with different distributions and regulatory functions. Numerous isoforms including three N-terminal (A, B, and C) and four C-terminal (α1, α2, β, and γ) variations were generated using distinct promoters and alternative splicing, each of which performed its own functions in a distinct subcellular location (Agarwal et al., 2019; Araki et al., 2020; Kilinc et al., 2022). Reportedly, α1 and β isoforms are highly enriched in forebrain neurons; while the former mainly focuses on excitatory synapses, the latter spreads over both excitatory and inhibitory synapses (Gou et al., 2020; Araki et al., 2020; Kilinc et al., 2022). Additionally, both SynGAP α1 and α2, two C-terminal isomers , also present opposing effects in the regulation of synaptic strength under the underlying control of the N-terminal sequence (McMahon et al., 2012). However, the unique role of each one or the association among numerous isoforms has not been completely understood. To our knowledge, reported mutations in the *SYNGAP1* gene were involved in different domains from PH, RasGAP to C-terminal unknown domains, but no clear relationship associated with phenotypes was found. Genetically, the priority of mutation types was nonsense, frameshift, splicing, and codon deletion, in turn, in which nonsense mutations were the most common. In our study, five novel mutations were identified, including two splicing mutations (c.664–2A>G and c.1677-1G>C), one frameshift mutation (c.1176delG), one codon deletion (c.917_925del), and one nonsense mutation (c.2620C>T) in five patients, respectively. Nonsense and frameshift mutations are also known as truncated mutations, which are related to truncated proteins and loss of functions directly. The two splicing mutations that occurred in introns disrupt the acceptor sites and, thus, result in errors during the splicing process, causing alterations of the open reading frame and the protein (Anna and Monika, 2018). Codon deletion with deletion of nine bases is an in-flame mutation that could shorten the length of the DNA strand and thus change the structure of the protein, which further results in conformational defects. As a result, the underlying effect of the 10 *de novo* heterozygous mutations is associated with *SYNGAP1* haploinsufficiency, further declaring that the *SYNGAP1* gene indeed acts as a significant component in neurodevelopment. In addition, SynGAP consists of various domains (Figure 1B): the PH domain refers to membrane localization of proteins; the C2 domain is involved in Ca^{2+} binding; the RasGAP domain contains many phosphorylation sites for kinases such as calmodulin-dependent protein kinase II (CaMKII) and participates in the activation of downstream molecules such as Ras and Rap; the SH3 domain mediates protein–protein interactions such as between NMDAR and PSD-95; and the coiled-coil domain is responsible for the multimerization among SynGAP isoforms (Agarwal et al., 2019; Gamache et al., 2020). All mutations in our study are involved in different domains, mainly from PH to RasGAP, and are considered deleterious for damaging the corresponding functional domains of proteins.

Together with 13 other Chinese patients reported previously, no remarkable alteration in mutation types and pathogenicity was observed. Meanwhile, those patients also shared a spectrum of clinical features. With respect to seizure types, eyelid myoclonia and absence appeared to be the most frequent ones. The existence of differences between our retrospective studies and previous reports (Pei et al., 2018; Lu et al., 2019; Gao et al., 2020; Zhang et al., 2021) verified the necessity of a large multicenter prospective cohort study. Additionally, six abnormal EEGs were observed without any seizure onset, and whether anti-seizure medication should be prescribed for them is still unknown due to the absence of established guidelines regarding medication regime and prognosis management at present. Moreover, we analyzed the clinical and genetic features among different mutation types in Chinese patients, but no clue regarding the phenotype–genotype correlation was identified. Vlaskamp et al. (2019) identified the correlation between the phenotypes and mutation locations; that is, milder phenotypes were often relevant to mutations in exons 1–4, whereas more severe phenotypes frequently occurred in exons 8–15. In line with the aforementioned findings, our patients with mutations in exons 4 and 5 displayed milder developmental delay and no comorbid epilepsy, whereas those with mutations in exons 8–15 had moderate to severe clinical manifestations. The exact pathogenic mechanisms have not been fully understood and remain to be explored further.

SynGAP has been considered to play an important role in synaptic plasticity and the development of neurons. The gross structure of an intact synapse consists of a presynaptic membrane, postsynaptic membrane, and synaptic cleft, facilitating information transmission from biochemical neurotransmitters to electrophysiological signals and further

activating downstream signaling cascades of the NMDAR-mediated Ras signaling pathways (Araki et al., 2020; Meili et al., 2021). In this pathway, NMDAR is activated by glutamate neurotransmitters released from the presynaptic membrane, resulting in a Ca^{2+} influx into the postsynaptic neuron. Subsequently, calmodulin-dependent protein kinase II (CaMKII) is triggered, and then SynGAP is phosphorylated, further negatively regulating Ras-mediated ERK/MAPK signaling cascades and restraining AMPAR insertion at the postsynaptic membrane (Jeyabalan and Clement, 2016; Meili et al., 2021). Structurally, SynGAP competes for binding to the PDZ domain of scaffolding protein PSD-95 with transmembrane AMPAR regulatory proteins (TARPs), which also facilitates AMPAR trafficking to PSD (Walkup et al., 2016). Thus, *SYNGAP1* haploinsufficiency results in decreased enzymatic activity on Ras and number of binding sites for PSD-95, which further leads to increased AMPAR levels at baseline (Gamache et al., 2020). Aberrant alterations greatly affect neural development, including increased excitability, excitation/inhibition imbalance, and loss of experience-dependent plasticity, which are responsible for cognition, learning, memory, and motor defects (Aceti et al., 2015; Uzunova et al., 2016; Zhang Y et al., 2020; Ni and Li, 2021). In addition, the Ras substrate and other members in the small GTPase-activating protein (GAP) superfamily, such as Rap and Rac, are also regulated by *SYNGAP1*. However, the ability to regulate Rap is even more powerful than that of Ras, although the relevant mechanisms are rarely involved (Agarwal et al., 2019).

Pathogenic processes have not been fully understood on the basis of molecular studies. Thus, animal models are generated for further exploration. Given that *SYNGAP1* is highly conserved across species (Kilinc et al., 2018), animal models provide us with unique insights into the pathogenesis of genetic haploinsufficiency. To date, *SYNGAP1*$^{-/+}$ mice have been extensively utilized, whereas homozygous *SYNGAP1* knockout mice fail to survive for more than a week, indicating the vital role of SynGAP in postnatal development (Berryer et al., 2013). Using mouse models, Aceti et al. (2015) showed that the deletion of SynGAP exerted a negative effect on the critical development period of cortical synaptogenesis after birth and accelerated dendrite elongation and spine morphogenesis in cortical pyramidal neurons, thus hampering synaptic plasticity relevant to the reorganization of brain circuits depending on experience. With alternative detection of structural abnormalities in the neurons of mutant mice, some progress has been achieved from behavioral studies of mouse models. In line with previous reports (Ozkan et al., 2014; Berryer et al., 2016), Nakajima et al. found that heterozygous knockout mice exhibit increased locomotor activity, decreased prepulse inhibition, and impaired working and reference spatial memory, which was determined by a series of comprehensive behavioral tests (Nakajima et al., 2019). These findings recapitulate phenotypes in patients with *SYNGAP1* mutations and can be combined with phenotypes at the molecular level, realizing the effect of mutual complementation.

Conclusion

Collectively, our study demonstrated the clinical characteristics of 10 Chinese individuals with MRD5 caused by *SYNGAP1* mutations, and half of these mutations were novel, which contributed to expanding the mutational spectrum of the *SYNGAP1* gene. Furthermore, nonsense mutations remained the most frequent mutation type. The identification of these mutations in this study is helpful in exploring the relationship between genotypes and phenotypes. More importantly, it is likely that several underlying phenotypes have not yet emerged because all the probands are in the early stage of growth and development, implying that a long-term follow-up is essential.

Data availability statement

The data presented in this study are deposited in the GenBank repository (https://www.ncbi.nlm.nih.gov/Genbank), accession number ON996974 to ON996976, and OP161168 to OP161171.

Ethics statement

The study involving human participants was reviewed and approved by the Medical Ethics Committee of Children's Hospital affiliated to Shandong University. Written informed consent was obtained from the participants' legal guardians for the publication of any potentially identifiable images or data included in this article.

Author contributions

ZGai and YLiu conceived and designed this study. Experiments were conducted by YW, YLv, MG, XY, YLi, and ZL. Data were analyzed by YW and YLv. Clinical diagnosis of the patients was undertaken by JS and ZGao. The paper was written by YW and YLv.

Funding

This study was supported by the Natural Science Foundation of Shandong Province (ZR2020QC066).

Acknowledgments

We thank the patients and their families for their participation and contribution to this work.

Conflict of Interest

The authors declare that the research was conducted in the absence of any commercial or financial relationships that could be construed as a potential conflict of interest.

Publisher's note

All claims expressed in this article are solely those of the authors and do not necessarily represent those of their affiliated organizations, or those of the publisher, the editors, and the reviewers. Any product that may be evaluated in this article, or claim that may be made by its manufacturer, is not guaranteed or endorsed by the publisher.

Supplementary material

The Supplementary Material for this article can be found online at: https://www.frontiersin.org/articles/10.3389/fgene.2022.957915/full#supplementary-material

References

Aceti, M., Creson, T. K., Vaissiere, T., Rojas, C., Huang, W. C., Wang, Y. X., et al. (2015). Syngap1 haploinsufficiency damages a postnatal critical period of pyramidal cell structural maturation linked to cortical circuit assembly. *Biol. Psychiatry* 77, 805–815. doi:10.1016/j.biopsych.2014.08.001

Agarwal, M., Johnston, M. V., and Stafstrom, C. E. (2019). SYNGAP1 mutations: Clinical, genetic, and pathophysiological features. *Int. J. Dev. Neurosci.* 78, 65–76. doi:10.1016/j.ijdevneu.2019.08.003

Anna, A., and Monika, G. (2018). Splicing mutations in human genetic disorders: examples, detection, and confirmation. *J. Appl. Genet.* 59, 253–268. doi:10.1007/s13353-018-0444-7

Araki, Y., Zeng, M., Zhang, M., and Huganir, R. L. (2015). Rapid dispersion of SynGAP from synaptic spines triggers AMPA receptor insertion and spine enlargement during LTP. *Neuron* 85, 173–189. doi:10.1016/j.neuron.2014.12.023

Araki, Y., Hong, I., Gamache, T. R., Ju, S., Collado-Torres, L., Shin, J. H., et al. (2020). SynGAP isoforms differentially regulate synaptic plasticity and dendritic development. *Elife* 9, e56273. doi:10.7554/eLife.56273

Berryer, M. H., Hamdan, F. F., Klitten, L. L., Moller, R. S., Carmant, L., Schwartzentruber, J., et al. (2013). Mutations in SYNGAP1 cause intellectual disability, autism, and a specific form of epilepsy by inducing haploinsufficiency. *Hum. Mutat.* 34, 385–394. doi:10.1002/humu.22248

Berryer, M. H., Chattopadhyaya, B., Xing, P., Riebe, I., Bosoi, C., Sanon, N., et al. (2016). Decrease of SYNGAP1 in GABAergic cells impairs inhibitory synapse connectivity, synaptic inhibition and cognitive function. *Nat. Commun.* 7, 13340. doi:10.1038/ncomms13340

Carvill, G. L., Heavin, S. B., Yendle, S. C., Mcmahon, J. M., O'roak, B. J., Cook, J., et al. (2013). Targeted resequencing in epileptic encephalopathies identifies de novo mutations in CHD2 and SYNGAP1. *Nat. Genet.* 45, 825–830. doi:10.1038/ng.2646

Deciphering Developmental Disorders Study (2015). Large-scale discovery of novel genetic causes of developmental disorders. *Nature* 519, 223–228. doi:10.1038/nature14135

Gamache, T. R., Araki, Y., and Huganir, R. L. (2020). Twenty years of SynGAP research: From synapses to cognition. *J. Neurosci.* 40, 1596–1605. doi:10.1523/JNEUROSCI.0420-19.2020

Gao, Z. J., Jiang, Q., Chen, X. L., Chen, Q., Ji, X. N., Mao, Y. Y., et al. (2018). Study of de novo point mutations in known genes among patients with unexplained intellectual disability or developmental delay. *Zhonghua Yi Xue Za Zhi* 98, 3426–3432. doi:10.3760/cma.j.issn.0376-2491.2018.42.010

Gao, Z., Lyu, Y., Zhang, K., Gao, M., Ma, J., Wang, D., et al. (2020). A case with autosomal dominant mental retardation type 5 due to de novo SYNGAP1 variant. *Zhonghua Yi Xue Yi Chuan Xue Za Zhi* 37, 661–664. doi:10.3760/cma.j.issn.1003-9406.2020.06.016

Gou, G., Roca-Fernandez, A., Kilinc, M., Serrano, E., Reig-Viader, R., Araki, Y., et al. (2020). SynGAP splice variants display heterogeneous spatio-temporal expression and subcellular distribution in the developing mammalian brain. *J. Neurochem.* 154, 618–634. doi:10.1111/jnc.14988

Jeyabalan, N., and Clement, J. P. (2016). SYNGAP1: mind the gap. *Front. Cell. Neurosci.* 10, 32. doi:10.3389/fncel.2016.00032

Jimenez-Gomez, A., Niu, S., Andujar-Perez, F., McQuade, E. A., Balasa, A., Huss, D., et al. (2019). Phenotypic characterization of individuals with SYNGAP1 pathogenic variants reveals a potential correlation between posterior dominant rhythm and developmental progression. *J. Neurodev. Disord.* 11, 18. doi:10.1186/s11689-019-9276-y

Kilinc, M., Creson, T., Rojas, C., Aceti, M., Ellegood, J., Vaissiere, T., et al. (2018). Species-conserved SYNGAP1 phenotypes associated with neurodevelopmental disorders. *Mol. Cell. Neurosci.* 91, 140–150. doi:10.1016/j.mcn.2018.03.008

Kilinc, M., Arora, V., Creson, T. K., Rojas, C., Le, A. A., Lauterborn, J., et al. (2022). Endogenous Syngap1 alpha splice forms promote cognitive function and seizure protection. *Elife* 11, e75707. doi:10.7554/eLife.75707

Lu, J., Zhang, Y., Han, C., Zhu, J., Wang, J., and Yao, R. (2019). Identification of a novel SYNGAP1 mutation in a child with intellectual disability. *Zhonghua Yi Xue Yi Chuan Xue Za Zhi* 36, 716–719. doi:10.3760/cma.j.issn.1003-9406.2019.07.015

Mcmahon, A. C., Barnett, M. W., O'leary, T. S., Stoney, P. N., Collins, M. O., Papadia, S., et al. (2012). SynGAP isoforms exert opposing effects on synaptic strength. *Nat. Commun.* 3, 900.

Meili, F., Wei, W. J., Sin, W. C., Meyers, W. M., Dascalu, I., Callaghan, D. B., et al. (2021). Multi-parametric analysis of 57 SYNGAP1 variants reveal impacts on GTPase signaling, localization, and protein stability. *Am. J. Hum. Genet.* 108, 148–162. doi:10.1016/j.ajhg.2020.11.011

Mignot, C., von Stulpnagel, C., Nava, C., Ville, D., Sanlaville, D., Lesca, G., et al. (2016). Genetic and neurodevelopmental spectrum of SYNGAP1-associated intellectual disability and epilepsy. *J. Med. Genet.* 53, 511–522. doi:10.1136/jmedgenet-2015-103451

Nakajima, R., Takao, K., Hattori, S., Shoji, H., Komiyama, N. H., Grant, S. G. N., et al. (2019). Comprehensive behavioral analysis of heterozygous Syngap1 knockout mice. *Neuropsychopharmacol. Rep.* 39, 223–237. doi:10.1002/npr2.12073

Ni, Y., and Li, J. (2021). Neural mechanisms of social learning and decision-making. *Sci. China. Life Sci.* 64, 897–910. doi:10.1007/s11427-020-1833-8

Ozkan, E. D., Creson, T. K., Kramar, E. A., Rojas, C., Seese, R. R., Babyan, A. H., et al. (2014). Reduced cognition in Syngap1 mutants is caused by isolated damage within developing forebrain excitatory neurons. *Neuron* 82, 1317–1333. doi:10.1016/j.neuron.2014.05.015

Parker, M. J., Fryer, A. E., Shears, D. J., Lachlan, K. L., Mckee, S. A., Magee, A. C., et al. (2015). De novo, heterozygous, loss-of-function mutations in SYNGAP1 cause a syndromic form of intellectual disability. *Am. J. Med. Genet. A* 167A, 2231–2237. doi:10.1002/ajmg.a.37189

Pei, Y., Li, W., Du, L., and Wei, F. (2018). Novel mutation of SYNGAP1 associated with autosomal dominant mental retardation 5 in a Chinese patient. *Fetal Pediatr. Pathol.* 37, 400–403. doi:10.1080/15513815.2018.1497113

Prchalova, D., Havlovicova, M., Sterbova, K., Stranecky, V., Hancarova, M., and Sedlacek, Z. (2017). Analysis of 31-year-old patient with SYNGAP1 gene defect points to importance of variants in broader splice regions and reveals developmental trajectory of SYNGAP1-associated phenotype: case report. *BMC Med. Genet.* 18, 62. doi:10.1186/s12881-017-0425-4

Richards, S., Aziz, N., Bale, S., Bick, D., Das, S., Gastier-Foster, J., et al. (2015). Standards and guidelines for the interpretation of sequence variants: a joint consensus recommendation of the American College of medical genetics and Genomics and the association for molecular pathology. *Genet. Med.* 17, 405–424. doi:10.1038/gim.2015.30

Uzunova, G., Pallanti, S., and Hollander, E. (2016). Excitatory/inhibitory imbalance in autism spectrum disorders: Implications for interventions and therapeutics. *World J. Biol. Psychiatry* 17, 174–186. doi:10.3109/15622975.2015.1085597

Verma, V., Mandora, A., Botre, A., and Clement, J. P. (2020). Identification of an individual with a SYGNAP1 pathogenic mutation in India. *Mol. Biol. Rep.* 47, 9225–9234. doi:10.1007/s11033-020-05915-4

Vlaskamp, D. R. M., Shaw, B. J., Burgess, R., Mei, D., Montomoli, M., Xie, H., et al. (2019). SYNGAP1 encephalopathy: A distinctive generalized developmental and epileptic encephalopathy. *Neurology* 92, e96–e107. doi:10.1212/WNL.0000000000006729

Walkup, W. G., Mastro, T. L., Schenker, L. T., Vielmetter, J., Hu, R., Iancu, A., et al. (2016). A model for regulation by SynGAP-α1 of binding of synaptic proteins to PDZ-domain 'Slots' in the postsynaptic density. *Elife* 5, e16813. doi:10.7554/eLife.16813

Weldon, M., Kilinc, M., Lloyd Holder, J., Jr., and Rumbaugh, G. (2018). The first international conference on SYNGAP1-related brain disorders: a stakeholder meeting of families, researchers, clinicians, and regulators. *J. Neurodev. Disord.* 10, 6. doi:10.1186/s11689-018-9225-1

Zhang, H., Yang, L., Duan, J., Zeng, Q., Chen, L., Fang, Y., et al. (2021). Phenotypes in children with SYNGAP1 encephalopathy in China. *Front. Neurosci.* 15, 761473. doi:10.3389/fnins.2021.761473

Zhang, H., Ji, X., Li, P., Liu, C., Lou, J., Wang, Z., et al. (2020). Liquid-liquid phase separation in biology: mechanisms, physiological functions and human diseases. *Sci. China. Life Sci.* 63, 953–985. doi:10.1007/s11427-020-1702-x

Zhang, Y., Zhang, Y. Y., and Fang, F. (2020). Neural mechanisms of feature binding. *Sci. China. Life Sci.* 63, 926–928. doi:10.1007/s11427-019-1615-4

frontiers | Frontiers in Genetics

TYPE Review
PUBLISHED 04 January 2023
DOI 10.3389/fgene.2022.1051153

Check for updates

OPEN ACCESS

EDITED BY
Tieliu Shi,
Hunan University of Arts and Science, China

REVIEWED BY
Siqi Hu,
Seventh Medical Center of PLA General Hospital, China
Yu Leng Phua,
Mount Sinai Genomics, Inc., United States

*CORRESPONDENCE
Yukun Pan,
panyukun@barbelltx.com
Jinzhong Chen,
kingbellchen@fudan.edu.cn

SPECIALTY SECTION
This article was submitted to Genetics of Common and Rare Diseases, a section of the journal Frontiers in Genetics

RECEIVED 22 September 2022
ACCEPTED 06 December 2022
PUBLISHED 04 January 2023

CITATION
Chen A, Pan Y and Chen J (2023), Clinical, genetic, and experimental research of hyperphenylalaninemia. *Front. Genet.* 13:1051153. doi: 10.3389/fgene.2022.1051153

COPYRIGHT
© 2023 Chen, Pan and Chen. This is an open-access article distributed under the terms of the Creative Commons Attribution License (CC BY). The use, distribution or reproduction in other forums is permitted, provided the original author(s) and the copyright owner(s) are credited and that the original publication in this journal is cited, in accordance with accepted academic practice. No use, distribution or reproduction is permitted which does not comply with these terms.

Clinical, genetic, and experimental research of hyperphenylalaninemia

Anqi Chen[1], Yukun Pan[2]* and Jinzhong Chen[3]*

[1]Department of Forensic Medicine, School of Basic Medical Sciences, Shanghai Medical College, Fudan University, Shanghai, China, [2]Barbell Therapeutics Co. Ltd., Shanghai, China, [3]State Key Laboratory of Genetic Engineering, Institute of Genetics, School of Life Sciences, Fudan University, Shanghai, China

Hyperphenylalaninemia (HPA) is the most common amino acid metabolism defect in humans. It is an autosomal-recessive disorder of the phenylalanine (Phe) metabolism, in which high Phe concentrations and low tyrosine (Tyr) concentrations in the blood cause phenylketonuria (PKU), brain dysfunction, light pigmentation and musty odor. Newborn screening data of HPA have revealed that the prevalence varies worldwide, with an average of 1:10,000. Most cases of HPA result from phenylalanine hydroxylase (PAH) deficiency, while a small number of HPA are caused by defects in the tetrahydrobiopterin (BH4) metabolism and DnaJ heat shock protein family (Hsp40) member C12 (DNAJC12) deficiency. Currently, the molecular pathophysiology of the neuropathology associated with HPA remains incompletely understood. Dietary restriction of Phe has been highly successful, although outcomes are still suboptimal and patients find it difficult to adhere to the treatment. Pharmacological treatments, such as BH4 and phenylalanine ammonia lyase, are available. Gene therapy for HPA is still in development.

KEYWORDS

phenylalanine (Phe), hyperphenylalaninemia (HPA), phenylketonuria (PKU), phenylalanine hydroxylase (PAH), tetrahydrobiopterin (BH4), DnaJ heat shock protein family (Hsp40) member C12 (DNAJC12), dietary restriction, gene therapy

Introduction

Phenylketonuria (PKU), the severe form of hyperphenylalaninemia (HPA), has been reported for near 90 years (Fölling. 1934; Grisch-Chan et al., 2019). It is the most common metabolic disorder of amino acid metabolism in humans, which is recognized by accumulated phenylalanine (Phe) in blood with an average incidence of 1:10,000 of the populations (Hillert et al., 2020). Although extensive works have been carried out to elucidate the pathological mechanism, the approach to HPA treatment has been rarely updated. Since the 1950s, a Phe-restricted diet has been the standard treatment for control the high blood Phe levels found in HPA (Sarkissian et al., 1999). Dietary management as a therapy remains a reliable and effective approach for preventing the manifestations of HPA for many (MacDonald et al., 2020). Recently, two drugs have been approved and used successfully for the correction of HPA (Keil et al., 2013; Burton et al., 2020). Several genetic diseases have been relieved using gene therapies

(Welch et al., 2007; Sun, Zheng, and Simeonov 2017; Pogue et al., 2018), but the complete non-dietary treatment for HPA stays at very early-stage. This review aims to summarize the current understanding of HPA from the aspects of history, dietary treatments, pharmacological approaches, as well as the ongoing experimental gene therapies.

Milestones in PKU

In 1934, doctor Fölling (Fölling, 1934) studied two siblings with an intellectual disability and a musty odor and identified phenylpyruvic acid in their urine. The disease was named Følling's disease and described as the inheritance of phenylpyruvic amentia (phenylketonuria, PKU) (Penrose 1935). PKU was the result of impaired Phe to Tyr conversion (Jervis 1947). Twenty years after Følling's report, the first description of a Pherestricted diet began a new era of PKU therapy (Bickel, Gerrard, and Hickmans 1953). In 1963, the Guthrie bacterial inhibition assay (Scriver 1998) was established for detecting PKU in newborns. In 1971, the catalytic characteristics of the PAH system were determined (Kaufman 1971). A second cause of HPA, a defect in the tetrahydrobiopterin (BH4) metabolism, was identified in 1974 (Bartholome 1974). The third cause of HPA, a DnaJ heat shock protein family (Hsp40) member C12 (DNAJC12) variant, was identified in 2017 (Anikster et al., 2017). Regarding pharmacological treatment, BH4, as an adjunct treatment, decreases blood Phe concentrations in some cases (Kure et al., 1999) and phenylalanine ammonia lyase (PAL) provides an alternate treatment option (Longo et al., 2014).

Epidemiology

More than 50 years ago, measurement of the blood Phe concentrations in newborns was developed. Since then, this approach has been widely used worldwide (Guthrie and Susi 1963). Normal Phe concentrations are below 120 μmol/L, and Phe/Tyr is below 1.5. The prevalence of HPA varies worldwide (van Spronsen et al., 2021). In Europe, the prevalence ranges from 1:2,700 live births in Italy to <1:100,000 live births in Finland (Hillert et al., 2020). HPA prevalence is the lowest in Asian populations, such as Thailand, where it is 1:212,535 (Sutivijit, Banpavichit, and Wiwanitkit 2011). In China, the prevalence is 1:159,24 live births and ranges from 1:349,63 (Gansu Province) to 1: 666,667 (Guangxi Municipality) live births (Xiang et al., 2019).

Phe hydroxylation pathway and HPA

PAH, chaperone DNAJC12, and the BH4 system are necessary for metabolizing Phe to Tyr. Pathogenetic mutations in the genes synthesizing these enzymes are the potential causes of HPA, accumulating phenylpyruvate and hypotyrosinemia. The side way product phenylpyruvate is rapidly excreted in urine, but the tissue concentrations are probably too low to be of any clinical consequences (Jervis 1952). Hypotyrosinemia might be present in PKU cases and related to light pigmentation. However, there might be enough Tyr in food to support the Tyr-related neurotransmitter. Actually, supplementing the diet with Tyr does not prevent severe cognitive disability in individuals with PKU (Batshaw, Valle, and Bessman 1981). Restriction of Phe intake can prevent the major manifestations of PKU, which suggests HPA itself as the primary neurotoxin in PKU (van Vliet et al., 2018).

Cerebral effects of HPA

The most severe manifestations in PKU patients are intellectual disability and epilepsy. Similar to other aromatic amino acids and other large neutral amino acids (LNAAs), Phe is transferred to the brain by the large neutral amino acid transporter 1 (LAT1) on the blood–brain barrier (BBB) (Kanai et al., 1998). High levels of Phe mediate competition for binding to LAT1 with other LNAAs, leading to their deficiency in the brain (de Groot et al., 2010). These deficiencies are probably responsible for the impaired cerebral protein synthesis in PKU (Hoeksma et al., 2009) and contribute to brain monoamine neurotransmitter deficiencies (van Vliet et al., 2015). High Phe levels in the brain can inhibit Tyr hydroxylase (TH) and tryptophan hydroxylase 2 (TPH2), the rate-limiting steps in dopamine and serotonin synthesis, which result in disturbances of the monoamine neurotransmitters implicated as contributors to the neuropsychiatric symptoms (de Groot et al., 2010). Supplementation of LNAAs without Phe has been promoted as a treatment approach to PKU, by competitive inhibition of Phe across the BBB (van Vliet et al., 2016) (Figure 1).

In vitro experiments with both cultured neurons and animal models, HPA caused disturbances of neuronal dendritic growth and synaptic connectivity (Hartwig et al., 2006; Hörster et al., 2006). HPA can impair the cholesterol or other brain lipids synthesis and thereby interfere with myelin-related structures (Shefer et al., 2000). HPA has also resulted in the forming of amyloid-like fibrils, a pathological structure similar to the amyloid plaques associated with Alzheimer's disease (Adler-Abramovich et al., 2012).

The cerebral energy metabolism was abnormal in a PKU animal model. Glucose metabolism is reduced in the frontal cortex of hyperphenylalaninaemic Pah^{enu2} mice, which might be related to behavioral abnormalities (Qin and Smith 2007; Winn et al., 2016). HPA can inhibit pyruvate kinase or other enzymes involved in glycolysis or oxidative phosphorylation (Miller,

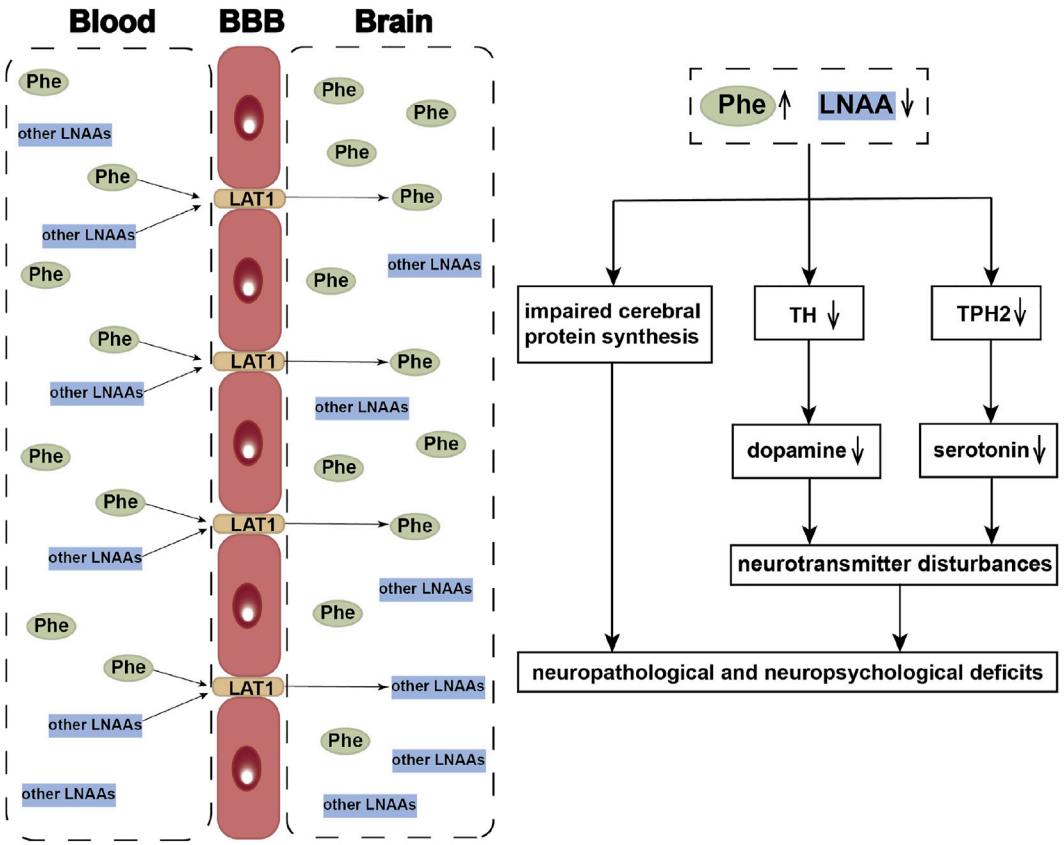


FIGURE 1
Neuropathological and neuropsychological deficits of HPA. LAT1 functions as a transporter mediating uptake of large neutral amino acids (LNAAs), such as phenylalanine (Phe), tyrosine (Tyr), and tryptophan *etc.*, across the blood-brain barrier (BBB). When phenylalanine hydroxylase is defective, the elevated blood Phe concentrations competitively inhibit the other LNAAs transporting into the brain. The reduced LNAAs concentrations contribute to the impaired cerebral protein synthesis and neurotransmitter deficiency, which further resulted in the occurrence of neuropathological and neuropsychological deficits. LNAAs, large neutral amino acids; Phe, phenylalanine; Tyr, tyrosine; TH, Tyr hydroxylase; TPH2, tryptophan hydroxylase 2.

TABLE 1 The genes associated with hyperphenylalaninemia (HPA).

Deficiency	Gene	Inheritance	Location	Genomic coordinates (GRCh38)	MIM number
PAH deficiency	PAH	autosomal recessive	12q23.2	12:102,836,889–102,958,441	261600
BH4 deficiency	PTS	autosomal recessive	11q23.1	11:112,226,428–112,233,973	261640
	GCH1	autosomal recessive	14q22.2	14:54,842,017–54,902,826	233910
	QDPR	autosomal recessive	4p15.32	4:17,486,395–17,512,090	261630
	PCBD1	autosomal recessive	10q22.1	10:70,882,280–70,888,565	264070
DNAJC12 deficiency	DNAJC12	autosomal recessive	10q21.3	10:67,796,669–67,838,188	617384

PAH, phenylalanine hydroxylase; BH4, tetrahydrobiopterin; DNAJC12: DnaJ heat shock protein family (Hsp40) member C12; PTS: 6-pyruvoyltetrahydropterin synthase; GCH1: GTP, cyclohydrolase 1; QDPR: quinoid dihydropteridine reductase; PCBD1: pterin-4, alpha-carbinolamine dehydratase 1.

Hawkins, and Veech 1973). Recently, several reports have suggested that HPA alters the methylation pattern and increases oxidative stress (Dobrowolski et al., 2016; van der Goot et al., 2019).

Diagnosis and screening

The genotypes of patients with HPA are considered deficient in PAH, BH4 and DNAJC12 (Table 1). Most cases of HPA are

caused by pathogenetic mutations of the PAH gene located on human chromosome 12 (Woo et al., 1983). More than 1000 PAH pathogenetic mutations have been reported where patients might be compound heterozygous for two different PAH variants, and more than 2000 genotypes resulted in the HPA phenotype (Hillert et al., 2020).

PAH pathogenetic mutations are inherited in an autosomal-recessive manner and result in expressing mutant protein with low/no catalytic activity, or even the absence of PAH protein expression (Garbade et al., 2019). BH4 deficiency due to inherited defects was found in the biopterin system, which consists of GTP cyclohydrolase 1 (GTPCH), 6-pyruvoyl-tetrahydropterin synthase (PTPS), dihydropteridine reductase (DHPR) or pterin-4a-carbinolamine dehydratase (PCD). PAH is disrupted in the absence of the chaperone DNAJC12, and this is described as an additional cause of inherited HPA (van Spronsen et al., 2017).

The Guthrie filter paper based newborn screening test for HPA has resulted in diagnoses in the neonatal period worldwide. To screen for PKU, the bacterial inhibition assay (BIA) and fluorimetric microassay (FMA) are employed to quantify Phe levels. A better method, tandem mass spectrometry (TMS) allows Phe and Tyr to be measured simultaneously. The PKU-positive screening result is determined by a cut-off of Phe concentrations ranging from 120 to 240 μmol/L in combination with a Phe to Tyr ratio >1.5–2 (van Wegberg et al., 2017).

Once HPA has been determined, it is necessary to distinguish PAH deficiency, disorders of the BH4 metabolism, and DNAJC12 defects. A panel comprising all genes known to cause HPA (possibly a larger panel with more than HPA-related genes) can provide final diagnostic confirmation and predict the metabolic phenotype in PAH deficiency. This is valuable for HPA diagnosis and treatment, especial for autosomal-recessive guanosine triphosphate cyclohydrolase (GTPCH) or serine racemase (SR) deficiency, which might present with normal blood Phe in the neonatal screening (van Wegberg et al., 2017). Thanks to the improvement of genotyping, most BH4 loading tests are covered for BH4 deficiencies, even in all HPA cases (Blau et al., 2014).

Dietary management

HPA screening aims for early diagnosis and prevention of intellectual disability by dietary management. Since the intellectual disability caused by PKU is irreversible, the prevention is more important than treatment. The dietary management of PKU should be initiated as soon as possible to prevent the cognitive and neurologic deficits (Evers et al., 2020). Unlike patients who experienced the neurocognitive consequences of late diagnosis and treatment, patients diagnosed and treated as infants may experience improved growth and development (Knox 1960). For late-diagnosed PKU patients, dietary management is also recommended, because behavior and epilepsy can be improved after dietary control (Koch et al., 1999).

Phe is an essential amino acid that cannot be produced by the body, and the blood Phe level is highly dependent on Phe intake. For this reason, dietary management should be successful. However, there is still a higher incidence of attention-deficit–hyperactivity disorder and specific learning disabilities in PKU, even with good dietary control (Arnold et al., 2004). Dietary management is comprised of limited natural protein intake, supplementation with a Phe-free amino acid mixture, and consumption of low-protein food products (MacDonald et al., 2020). Although the dietary treatment must be individualized and monitored, the protein and Phe deficiency can also cause adverse effects such as growth restriction, anorexia, alopecia, lethargy, and eczematous eruptions (Hanley et al., 1970). The basis of dietary treatment has changed little since 1953. Despite substantial efforts to improve quality, taste, and consumption methods of Phe-free amino acid mixtures, acceptance can be poor (Daly et al., 2021). Phe control during childhood is particularly important. The children themselves, as well as their family members, should understand the importance of Phe control, and sometimes it is necessary to hold the method of Phe test (Bilginsoy et al., 2005). Higher blood Phe concentrations are not always associated with poorer neurocognitive outcomes (Leuzzi et al., 2020), and the need to decrease blood Phe levels in adult PKU patients is unsure (Burlina et al., 2019). These adult patients might consider stopping dietary treatment. Consequently, they may not resume normal natural protein intake and be at risk of deficiency for some micronutrients (Lammardo et al., 2013). Regarding maternal PKU, the risk of fetal developmental abnormalities is increased if the maternal blood Phe concentrations exceed 360 μmol/L. For optimal metabolic control, the American College of Medical Genetics (ACMG) recommends lifelong maintenance of Phe concentrations within the range of 120–360 μmol/L (van Wegberg et al., 2017).

Pharmacological treatments

Sapropterin (Kuvan®, BioMarin) is a BH4 synthetic analog, an oral drug approved by FDA in 2008. Sapropterin is an exogenous synthetic BH4, and it is given as an effective replacement for endogenous BH4. The rationale for Sapropterin administration is to restore the Phe metabolism by enhancing the activity of the defective PAH. Since BH4 is a cofactor of PAH, the excess cofactor would help stimulate residual PAH to process Phe, and thereby decrease the blood Phe concentrations (Battaglia-Hsu and Feillet, 2010; Dubois and Cohen 2010). Sapropterin can increase dietary Phe tolerance (Keil et al., 2013) in some patients, thus enabling them to liberalize dietary restrictions. However, this drug does not

response to all patients with PKU or BH4 deficiency (Dubois and Cohen 2010). Ten years later, a pegylated Phe ammonia lyase (pPAL, Palynziq®, BioMarin), was approved by FDA. The rationale for Palynziq® to reduce blood Phe concentrations through converting Phe to ammonia and transcinnamic acid (Thomas et al., 2018). The drug also changed the lives of PKU patients (Burton et al., 2020). Based on clinical experience and knowledge of adverse immunological events, the guidelines for pegvaliase treatment induction and maintenance in PKU patients have been proposed (Longo et al., 2019). Of all patients, 60.7% were able to achieve blood Phe concentrations less than 360 μmol/L without restricting dietary protein intake (Thomas et al., 2018). The pPAL injection for treatment of PKU patients has proved effective (Thomas et al., 2018). As a foreign protein, the immune-mediated responses remain the most important safety issue for this drug (Gupta et al., 2018).

Experimental therapies

The lifelong restricted diet supplemented with Phe-free protein substitutes has been the gold standard treatment for PKU patients (Burlina et al., 2020). However, the patient adherence to this therapy trends to be difficult after childhood, owing to the substantial time, cost and lifestyle burdens (Rose et al., 2019). Consequently, an effective, non-pathological, and long-term non-dietary restriction treatment is urgently needed. Gene therapy has been applied to cure genetic diseases such as spinal muscular atrophy (SMA) (Mendell et al., 2017; Waldrop et al., 2020) and hemophilia B (Lu et al., 2016; George et al., 2017). New approaches using gene therapy for PKU are considered promising because of the results from established PKU murine and mouse models (Isabella et al., 2018; Li et al., 2021). US and European authorities have approved injectable pegvaliase for PKU, at the same time, they have also incited other approaches to improve enzyme-based therapies to decrease the frequency and severity of this adverse effect (Hydery and Coppenrath 2019).

Rubius Therapeutics evaluated the safety and tolerability of RTX-134, the allogeneic human red blood cells (RBCs) expressing the AvPAL (which consists an Anabaena variabilis phenylalanine ammonia lyase gene inside the cell); unfortunately, this clinical trial failed to provide the expected signals of efficacy. Although the clinical trial using liver cell transplantation is in the recruiting process, the potential for transplant rejection will be unavoidable. Therefore, all participants must be treated with life-long immune suppression medications (NCT01465100), which will expose the patients to higher risks of an immune-mediated adverse reaction. Compared to the transplantation of enzyme-loaded RBCs, the enzyme substitution therapy with phenylalanine ammonialyase (PAL) appears more promising for decreasing Phe concentrations. CDX-6114 (Codexis Inc. And Nestlé) is a PAL-like enzyme that can remove Phe during digestion. To date, the results from three clinical trials (NCT03577886, NCT03797664, and NCT04085666) showed that the drug was well tolerated at different dose levels without any serious adverse events or GI-related symptoms. Unfortunately, further investigation was stopped because of the altered compositions. Other orally administered enzymes are SYNB 1618 and SYNB 1943 (Synlogic Biotic), which are engineered bacterial therapeutic drugs for oral delivery. SYNB 1618 and SYNB 1943 are expected to control Phe levels in patients with PKU. The strong positive results with these two drugs will undoubtedly initiate a phase 3 clinical trial in the near future. It has been reported that more than 10% catalytic activity is necessary for correcting PHA to below 700 μmol/L Phe (Hamman et al., 2005). However, the results observed from several PKU-related gene therapies were far from satisfactory, which suggested the treatments were still in an early stage.

For genetic disorders, genome editing using recombinant adeno-associated virus (rAAV) vectors is one of the most popular gene therapy strategies (Wang, Tai, and Gao 2019). The open read frame (ORF) of PAH is relatively small, which makes it fit well to the AAV vector. Furthermore, the native expression and residence of PAH is in liver cells, where the protein expression is easy and intracellular proteins would not be exposed to the immune system (Wang, Tai, and Gao 2019). The benefits mentioned above have laid the foundations for AAV-based gene therapy for PKU.

Since PKU is a genetic disorder owing to the mutation in the PAH gene, genome editing-based gene therapies have been developed to modify the genes. AAV-based CRISPR-Cas base editors provided more than 20% PAH activity in Pah^{enu2} mice and restored physiological blood Phe concentrations (Villiger et al., 2018; Richards et al., 2020). By using a dual AAV-based editing system, Zhou et al. (Zhou et al., 2022) achieved efficient correction of PKU-related mutations *in vitro* and *in vivo*. Co-delivery of SaCas9/sgRNA/donor templates with AAV receptor (AAVR) *via* AAV8 vectors also corrected the single mutation (PahR408W), and dramatically increased the editing efficiency *in vivo* (Yin et al., 2022). The advantage of this method is that the modified cells were maintained throughout the hepatocyte proliferation. Although effective in mice, no human clinical trials are reported. In addition, AAV-based gene therapies with AAV2/5-PAH were not successful; they could not correct the PAH deficiency without a high dosage of AAV (1014 vg/mouse) that might result in liver damage (Mochizuki et al., 2004; Oh et al., 2004). Alternatively, vectors pseudotyped with capsids from AAV serotype 8 were generated to explore a long-term non-dietary restriction treatment. The rAAV serotype 8 vectors exerted neither hepatic toxicity nor immunogenicity in the treated mice, and the blood Phe decreased to normal levels independent of the gender differences (Ding, Georgiev, and Thöny 2006; Rebuffat et al., 2010; Tao et al., 2020). At the same

TABLE 2 Summary of the clinical trials and AAV-based experimental gene therapies.

Clinical trials								
Study title	Interventions	Delivery	Phase	ClinicalTrials.gov identifier	Sponsor and principal investigator	Start date	Completion date (estimated)	Ages eligible for study
AAV Gene Therapy Study for Subjects With PKU	BMN 307: AAV2/8 gene therapy infusion	Systemic delivery	Phase 1/2 Active, not recruiting	NCT04480567	BioMarin Pharmaceutical	24 September 2020	December 2027	15 Years and older
Gene Therapy Clinical Study in Adult PKU (pheNIX)	HMI-102: AAVHSC15 vector expressing human PAH (HMI-102)	Systemic delivery	Phase 1/2: Recruiting	NCT03952156	Homology Medicines, Inc.	10 June 2019	September 2023	18 Years–55 Years
Safety and Efficacy of HMI-103, a Gene Editing Development Candidate in Adults with Classical PKU Due to PAH Deficiency	HMI-103: an AAVHSC15 vector HMI-103 Phe EDIT	Systemic delivery	Phase 1: Recruiting	NCT05222178	Homology Medicines, Inc.	3 June 2022	June 2028	18 Years–55 Years
Liver Cell Transplant for Phenylketonuria	Hepatocyte transplantation	Transplantation	Phase 1/2: Recruiting	NCT01465100	Ira Fox	15 December 2022	December 2023	14 Years–55 Years
Safety and Tolerability of RTX-134 in Adults with Phenylketonuria	RTX-134 RBC	Systemic delivery	Phase I: failure	NCT04110496	Rubius	29 January 2020	March 2035	18 Years and older
Safety and Tolerability of CDX-6114 in Healthy Volunteers	CDX-6114	Oral delivery	Phase 1: completed	NCT03577886	Codexis Inc	4 July 2018	4 September 2018	18 Years–55 Years
A Study of the Safety and Tolerability of CDX-6114 in Healthy Volunteers			Phase 1: completed	NCT03797664	Codexis Inc	14 December 2018	12 April 2019	18 Years–55 Years
Pharmacodynamics, Safety, Tolerability and Pharmacokinetics of CDX-6114 in Patients with Phenylketonuria (PKU)			Phase 1: completed	NCT04085666	Nestlé	1 June 2019	30 August 2020	18 Years–55 Years
Safety, Tolerability, Pharmacodynamics and Pharmacokinetics of CDX 6114 in PKU Patients			Withdrawn (study product composition to move from liquid to solid)	NCT04256655	Nestlé	1 December 2020	30 December 2021	18 Years–65 Years
Safety and Tolerability of SYNB1618 in Healthy Adult Volunteers and Adult Subjects With Phenylketonuria (PKU)	SYNB1618: engineered bacterial drug overexpressing PAL to metabolize phenylalanine in the gut	Oral delivery	Phase 1/2a: completed	NCT03516487	Synlogic	17 April 2018	21 June 2019	18 Years–64 Years

(Continued on following page)

10.3389/fgene.2022.1051153

TABLE 2 (*Continued*) Summary of the clinical trials and AAV-based experimental gene therapies.

Clinical trials								
Study title	Interventions	Delivery	Phase	ClinicalTrials.gov identifier	Sponsor and principal investigator	Start date	Completion date (estimated)	Ages eligible for study
Safety and Tolerability of SYNB1934 in Healthy Adult Volunteers	SYNB1618 and 1943: engineered bacterial drug overexpressing PAL to metabolize phenylalanine in the gut		Phase 1: completed	NCT04984525		2 July 2021	10 December 2021	18 Years–64 Years
Efficacy and Safety of SYNB1618 and SYNB1934 in Adult Patients With Phenylketonuria (SynPheny-1)			Phase 2: recruiting	NCT04534842		25 August 2020	August 2022	18 Years and older

Experimental therapies					
Vectors	Treatment	Delivery	Insightful Conclusions	Investigator	References
liver-tropic rAAV2/ 8 vectors	A liver-tropic rAAV2/8 vectors + Vanillin Treatment	Systemic delivery	• Lifelong and permanent correction of the Pah^{enu2} allele in a portion of treated hepatocytes • Partial restoration of liver PAH activity • Substantial reduction of blood Phe • Prevention of maternal PKU effects during breeding	Department of Molecular and Medical Genetics, Oregon Health & Science	Mol Ther Methods Clin Dev. 2019 December 24; 17:234–245
AAV-base editor systems (CRISPR-Cas-associated base editors)	An rAAV vectors CRISPR-Cas-associated base editors	Systemic delivery	• Restored physiological Phe blood levels • Up to 63% mRNA correction rates • Restoration of 65% PAH enzyme activity • Reversion of hypopigmented phenotype	Department Biology, Institute for Molecular Health Sciences, ETH Zürich	Nat Med. 2018 October; 24 (10):1519–1525
AAV-Anc80	The synthetic AAV vector Anc80 *via* systemic administration to deliver a functional copy of a codon-optimized human PAH	Systemic delivery	• A safely and durably PKU curation • The significant and durable reduction of circulating Phe (nearly decreased to control levels in males) • Reversion of hypopigmented phenotype	Children's Hospitals and Clinics of Minnesota, Minneapolis, Minnesota, United States.	J Inherit Metab Dis. 2021 November; 44 (6): 1369–1381
AAV8-PAL	An rAAV8 viral vector expressing the humanized PAL under the control of human antitrypsin (hAAT) promoter	Systemic delivery	• Long-term HPA correction in both genders	State Key Laboratory of Biotherapy and Cancer Center, West China Hospital, Sichuan University, Chengdu, Sichuan 610041, China	Mol Ther Methods Clin Dev. 2020 January 13; 19: 507–517

(Continued on following page)

10.3389/fgene.2022.1051153

TABLE 2 (*Continued*) Summary of the clinical trials and AAV-based experimental gene therapies.

Experimental therapies					
Vectors	Treatment	Delivery	Insightful Conclusions	Investigator	References
AAV2-PKU-5 and rAAV2-PKU-5/8	An rAAV vector containing the murine PAH cDNA	Systemic delivery	• Complete correction of HPA in both males and females with a rAAV8 vector • Reversion of hypopigmented phenotype	Division of Clinical Chemistry and Biochemistry, University Children's Hospital Zürich	Gene Ther. 2006 April; 13 (7):587–93
ssAAV8/CAG-mPAH and scAAV/LP1-mPAH	An AAV8-pseudotyped vector constructed with a self-complementary AAV (scAAV) genome	Systemic delivery	• Long duration of the treatment • Reduction of blood Phe to normal or near-normal levels for more than 1 year in both genders	Division of Genetic Therapeutics, Center for Molecular Medicine, Jichi Medical University, Shimotsuke, Japan	J Gene Med. 2011 February; 13 (2): 114–22
AAV8-AAVR and the SaCas9 system	Co-delivery of SaCas9/sgRNA/donor templates with AAVR *via* AAV8 vectors	Systemic delivery	• Dramatically increased AAV transduction efficiency *in vitro* and *in vivo* • Increased indel rate over 2-fold and homologous recombination rate over 15-fold for the correction of the single mutation in PahR408W mice • Significantly decreased Phe level and ameliorated PKU symptom	Shanghai Key Laboratory of Regulatory Biology, Institute of Biomedical Sciences and School of Life Sciences, East China Normal University, Shanghai, 200241, China	Sci China Life Sci. 2022 April; 65 (4):718–730
rAAV2/8-hPAH	A pseudotyped recombinant AAV2/8-hPAH vector and infused it into female PKU mice through the hepatic portal vein or tail vein	Systemic delivery	• Increased PAH activity (female: 65–70%; male: 90%) • Plasma Phe concentration in female decreased to the normal value • The offspring of the treated female PKU mice can rescue from the harmful effect of maternal HPA • Reversion of hypopigmented phenotype	Department of Biochemistry, School of Medicine, Ewha Womans University, Seoul, Korea	J Korean Med Sci. 2008 October; 23 (5): 877–83
rAAV2/1-PAH-GTPCH-PTPS	A rAAV2 pseudotype 1 vector expressing PAH along with GTPCH and 6-pyruvoyltetrahydrobiopterin synthase (PTPS)	Gastrocnemius muscles injection	• The stable and long-term reduction of blood Phe • Reversal of PKU-associated coat hypopigmentation	Division of Clinical Chemistry and Biochemistry, Department of Pediatrics, University of Zürich	Mol Ther. 2008 April; 16 (4):673–81

(Continued on following page)

10.3389/fgene.2022.1051153

TABLE 2 (*Continued*) Summary of the clinical trials and AAV-based experimental gene therapies.

Experimental therapies					
Vectors	Treatment	Delivery	Insightful Conclusions	Investigator	References
AAV2/1-PKU5, AAV2/2-PKU5, and AAV2/8-PKU5	Three different recombinant AAV2 genomes packaged with either serotype 1, 2, or 8 capsid were generated to express the PAH gene	Gastrocnemius muscles injection	• Restored liver PAH activity and Phe clearance (long-term clearance: AAV2/1-PKU5 and AAV2/8-PKU5 only) • Therapeutic correction in both genders (more effectively in males) • Subsequent supplementation with synthetic tetrahydrobiopterin resulted in a transient decrease in blood phenylalanine in female after rAAV2/8 injection	Division of Clinical Chemistry and Biochemistry, Department of Pediatrics, University of Zürich, CH-8032 Zürich, Switzerland	Hum Gene Ther. 2010 April; 21 (4):463–77
AAV5/CAG-mPAH.	A recombinant adeno-associated virus (AAV) vector carrying the murine PAH cDNA	Systemic delivery	• Completely normalized pf PHA phenotype • Substantial blood Phe reduction in male • Long-term correction of HPA • Transduction ameliorated the PKU phenotype (reversed central nervous system dysfunctions and correction of hypopigmentation)	Division of Genetic Therapeutics, Center for Molecular Medicine, Jichi Medical School, Tochigi, Japan	Gene Ther. 2004 July; 11 (13):1081–6
rAAV-mPAH-WPRE	A rAAV-mouse phenylalanine hydroxylase-woodchuck hepatitis virus post-transcriptional response element (rAAV-mPAH-WPRE) vector	Systemic delivery	• Rapid reduction of serum Phe levels • Reversed neuropathologic phenotypes	Department of Biochemistry and Molecular Biology, PO Box 100245, College of Medicine, University of Florida, Gainesville, FL 32610, United States.	Brain Res. 2007 January 5; 1127 (1):136–50
AAV8-miniSaCBE-PLUS-PKU	A dual AAV strategy for *in vivo* delivery of base editors, in which deaminases were linked to Cas9 through the interaction of GCN4 peptide and its single chain variable fragment (scFv) antibody	Systemic delivery	• Up to 27.7% correction *in vitro* • Significantly rescued Phe metabolism and reduced urine phenyl ketone • Rescue of hyperphenylalaninemia-associated syndromes *in vivo* (e.g. growth retardation, hypopigmentation, and behaviors)	Laboratory of Biotherapy, National Key Laboratory of Biotherapy, Cancer Center, West China Hospital, Sichuan University, Renmin Nanlu 17, Chengdu 610041, Sichuan, China	Mol Ther Methods Clin Dev. 2022 Jan 7; 24: 230–240
AAVHSC15-PAH	AAVHSC15: a clade F AAV isolated from human $CD34^+$ hematopoietic stem cells (HSCs) AAVHSC15-PAH: The AAVHSC15 vector containing a codon-optimized form of the human phenylalanine hydroxylase cDNA	Systemic delivery	• Sustained reduction of serum Phe • Sustained reduction in serum Phe and normalized tyrosine levels for the lifespan of Pah^{enu2} mice • Restored brain levels of Phe and the downstream serotonin metabolite 5-hydroxyindoleacetic acid • Reversal of PKU-associated coat hypopigmentation	Research and Development, Homology Medicines, Patriots Park, Bedford, MA 01730, United States.	Mol Ther Methods Clin Dev. 2020 March 13; 17: 568–580

10.3389/fgene.2022.1051153

time, therapeutic ranges of Phe reverted the hair from brown to black in PAH-deficient mice. The better results came from AAV2/8-PAH (Rebuffat et al., 2010) and AAVHSC15 (Ahmed et al., 2020), which obtained a long-lasting correction of PAH activity in Pah^{enu2} mice. Similar observations were made using either the recombinant triplecistronic AAV2 pseudotype 1 vector (Ding et al., 2008) or the pseudotyped rAAV2/8-hPAH vector (Jung et al., 2008). Remarkably, the offspring of the treated mice were rescued from the pathologic effect (Jung et al., 2008). In a comparative study, both the rAAV2 pseudotype 1 (rAAV2/1) and rAAV2/8 vectors showed the long-term phenylalanine clearance. Although an elevated phenylalanine level was detected in female mice after 8–10 months of rAAV2/8 injection, it was corrected by either administering synthetic tetrahydrobiopterin supplementation or injecting a different AAV pseudotype vector (Rebuffat et al., 2010). Overall, the rAAV8 vectors not only corrected hyperphenylalaninemia in both males and females, but, more importantly, they exerted neither hepatic toxicity nor immunogenicity in Phe-deficient mice.

The effective outcomes and the feasibility of a single intravenous injection have paved the way to develop the clinical gene therapy procedure for PKU patients. At present, two activated clinical trials are ongoing with AAVHSC15 (NCT03952156 and NCT05222178), and one with AAV2/8 (NCT04480567). HMI-102 and HMI-103 exerted therapeutic effects by using an AAVHSC15 vector containing a functional copy of the human PAH gene. Both of them were the *in vivo* treatments that delivered functioning PAH genes to the liver by one-time I.V. administration. The difference is in the way the drugs work in the body. HMI-102 is designed to deliver the functional gene in the form of episomes, and HMI-103 creates the functional PAH protein by the integrated PAH gene and unintegrated PAH episomes (Table 2).

An ideal strategy for gene therapy is expected to be non-pathogenic, transduction efficient, as well as sustained long-term expressed. PAH-deficient mice achieved nearly complete restoration of liver PAH activity and reversed symptoms without dietary supervision using AAV-mediated gene therapy. Despite the conventional AAV-pseudotype vectors, a series of newly developed AAV vectors also achieved the satisfactory results. Harmful changes in the brains of Pah^{enu2} mice were reversed after the portal vein delivery of an rAAV-mouse PAH-woodchuck hepatitis virus post-transcriptional response element (rAAV-mPAH-WPRE) vector (Embury et al., 2007). Kaiser et al. (2021) synthesized the AAV vector Anc80, a synthetic serotype using *in silico* techniques, to deliver a functional copy of a codon-optimized human PAH gene to the Pah^{enu2} mice. They observed the circulating Phe was reduced nearly to the control levels in males, but the clinic curative effect still needs to be proved in human trials.

Conclusion

PKU results from the severe form of HPA, a syndrome recognized by high concentrations of blood Phe. Consequently, blood Phe levels is the most important marker for diagnosis and treatment. Over the past 50 years, the classical lifelong dietary treatment has been regarded as the most effective approach to prevent disease consequences. Recently, the pharmaceutical therapies have provided alternative options for treatment. Several studies have suggested that AAV-based gene therapy might be another promising approach for HPA curation using only one-time administration without dietary restriction, while its security and efficacy await the results of ongoing clinical trials. Considering the uncertainties around the capacity and long-term durability of gene therapy, more optimizations are needed in the near future.

Author contributions

Conceptualization, JC and YP; writing—original draft preparation, AC; writing—review and editing, AC; supervision, JC and YP; project administration, JC and YP; funding acquisition, JC and YP. All authors have read and agreed to the published version of the manuscript.

Funding

This research was funded by National Key Research and Development Project of China (grant number: 2021YFC2301500) and Shanghai Pujiang Program (grant number: No. 2020PJD019).

Conflict of interest

Author YP is employed by Barbell Therapeutics Co. Ltd.

The remaining authors declare that the research was conducted in the absence of any commercial or financial relationships that could be construed as a potential conflict of interest.

Publisher's note

All claims expressed in this article are solely those of the authors and do not necessarily represent those of their affiliated organizations, or those of the publisher, the editors and the reviewers. Any product that may be evaluated in this article, or claim that may be made by its manufacturer, is not guaranteed or endorsed by the publisher.

References

Adler-Abramovich, L., Vaks, L., Carny, O., Trudler, D., Magno, A., Caflisch, A., et al. (2012). 'Phenylalanine assembly into toxic fibrils suggests amyloid etiology in phenylketonuria. *Nat. Chem. Biol.* 8, 701–706. doi:10.1038/nchembio.1002

Ahmed, S. S., Rubin, H., Wang, M., Faulkner, D., Sengooba, A., Dollive, S. N., et al. (2020). 'Sustained correction of a murine model of phenylketonuria following a single intravenous administration of AAVHSC15-PAH. *Mol. Ther. Methods Clin. Dev.* 17, 568–580. doi:10.1016/j.omtm.2020.03.009

Anikster, Y., Haack, T. B., Vilboux, T., Pode-Shakked, B., Thöny, B., Shen, N., et al. (2017). 'Biallelic mutations in DNAJC12 cause hyperphenylalaninemia, dystonia, and intellectual disability. *Am. J. Hum. Genet.* 100, 257–266. doi:10.1016/j.ajhg.2017.01.002

Arnold, G. L., Vladutiu, C. J., Orlowski, C. C., Blakely, E. M., and DeLuca, J. (2004). 'Prevalence of stimulant use for attentional dysfunction in children with phenylketonuria. *J. Inherit. Metab. Dis.* 27, 137–143. doi:10.1023/B:BOLI.0000028725.37345.62

Bartholome, K. (1974). 'Letter: A new molecular defect in phenylketonuria. *Lancet* 2, 1580. doi:10.1016/s0140-6736(74)90337-7

Batshaw, M. L., Valle, D., and Bessman, S. P. (1981). 'Unsuccessful treatment of phenylketonuria with tyrosine. *J. Pediatr.* 99, 159–160. doi:10.1016/s0022-3476(81)80985-7

Battaglia-Hsu, S. F., and Feillet, F. (2010). Sapropterin in the treatment of phenylketonuria. *Clin. Med. Insights Ther.* 2, CMT.S2721–31. doi:10.4137/cmt.s2721

Bickel, H., Gerrard, J., and Hickmans, E. M. (1953). 'Influence of phenylalanine intake on phenylketonuria. *Lancet* 265, 812–813. doi:10.1016/s0140-6736(53)90473-5

Bilginsoy, C., Waitzman, N., Leonard, C. O., and Ernst, S. L. (2005). 'Living with phenylketonuria: Perspectives of patients and their families. *J. Inherit. Metab. Dis.* 28, 639–649. doi:10.1007/s10545-005-4478-8

Blau, N., Duran, M., Gibson, K. M., and Dionisi, C. V. (2014). 'Physician's guide to the diagnosis, treatment, and follow-up of inherited metabolic diseases. *Congenital Disorders of Glycosylation*. Switzerland: Springer Nature.

Burlina, A. P., Cazzorla, C., Massa, P., Loro, C., Gueraldi, D., and Burlina, A. B. (2020). The impact of a slow-release large neutral amino acids supplement on treatment adherence in adult patients with phenylketonuria. *Nutrients* 12, 2078. doi:10.3390/nu12072078

Burlina, A. P., Lachmann, R. H., Manara, R., Cazzorla, C., Celato, A., van Spronsen, F. J., et al. (2019). 'The neurological and psychological phenotype of adult patients with early-treated phenylketonuria: A systematic review. *J. Inherit. Metab. Dis.* 42, 209–219. doi:10.1002/jimd.12065

Burton, B. K., Longo, N., Vockley, J., Grange, D. K., Harding, C. O., Decker, C., et al. (2020). 'Pegvaliase for the treatment of phenylketonuria: Results of the phase 2 dose-finding studies with long-term follow-up. *Mol. Genet. Metab.* 130, 239–246. doi:10.1016/j.ymgme.2020.06.006

Daly, A., Evans, S., Pinto, A., Ashmore, C., and MacDonald, A. (2021). Protein substitutes in PKU; their historical evolution. *Nutrients* 13, 484. doi:10.3390/nu13020484

de Groot, M. J., Hoeksma, M., Blau, N., Reijngoud, D. J., and van Spronsen, F. J. (2010). 'Pathogenesis of cognitive dysfunction in phenylketonuria: Review of hypotheses. *Mol. Genet. Metab.* 99, S86–S89. doi:10.1016/j.ymgme.2009.10.016

Ding, Z., Georgiev, P., and Thöny, B. (2006). 'Administration-route and gender-independent long-term therapeutic correction of phenylketonuria (PKU) in a mouse model by recombinant adeno-associated virus 8 pseudotyped vector-mediated gene transfer. *Gene Ther.* 13, 587–593. doi:10.1038/sj.gt.3302684

Ding, Z., Harding, C. O., Rebuffat, A., Elzaouk, L., Wolff, J. A., and Thöny, B. (2008). 'Correction of murine PKU following AAV-mediated intramuscular expression of a complete phenylalanine hydroxylating system. *Mol. Ther.* 16, 673–681. doi:10.1038/mt.2008.17

Dobrowolski, S. F., Lyons-Weiler, J., Spridik, K., Vockley, J., Skvorak, K., and Biery, A. (2016). 'DNA methylation in the pathophysiology of hyperphenylalaninemia in the PAH(enu2) mouse model of phenylketonuria. *Mol. Genet. Metab.* 119, 1–7. doi:10.1016/j.ymgme.2016.01.001

Dubois, E. A., and Cohen, A. F. (2010). Sapropterin. *Br. J. Clin. Pharmacol.* 69, 576–577. doi:10.1111/j.1365-2125.2010.03643.x

Embury, J. E., Charron, C. E., Martynyuk, A., Zori, A. G., Liu, B., Ali, S. F., et al. (2007). 'PKU is a reversible neurodegenerative process within the nigrostriatum that begins as early as 4 weeks of age in Pah(enu2) mice. *Brain Res.* 1127, 136–150. doi:10.1016/j.brainres.2006.09.101

Evers, R. A. F., van Wegberg, A. M. J., Anjema, K., Lubout, C. M. A., van Dam, E., van Vliet, D., et al. (2020). 'The first European guidelines on phenylketonuria: Usefulness and implications for BH(4) responsiveness testing. *J. Inherit. Metab. Dis.* 43, 244–250. doi:10.1002/jimd.12173

Fölling, A. (1934). 'Über Ausscheidung von Phenylbrenztraubensäure in den Harn als Stoffwechselanomalie in Verbindung mit Imbezillität. *Hoppe-Seyler´s. Z. fur Physiol. Chem.* 227, 169–181. doi:10.1515/bchm2.1934.227.1-4.169

Garbade, S. F., Shen, N., Himmelreich, N., Haas, D., Trefz, F. K., Hoffmann, G. F., et al. (2019). 'Allelic phenotype values: A model for genotype-based phenotype prediction in phenylketonuria. *Genet. Med.* 21, 580–590. doi:10.1038/s41436-018-0081-x

George, L. A., Sullivan, S. K., Giermasz, A., Rasko, J. E. J., Samelson-Jones, B. J., Ducore, J., et al. (2017). 'Hemophilia B gene therapy with a high-specific-activity factor IX variant. *N. Engl. J. Med.* 377, 2215–2227. doi:10.1056/NEJMoa1708538

Grisch-Chan, H. M., Schwank, G., Harding, C. O., and Thöny, B. (2019). 'State-of-the-Art 2019 on gene therapy for phenylketonuria. *Hum. Gene Ther.* 30, 1274–1283. doi:10.1089/hum.2019.111

Gupta, S., Lau, K., Harding, C. O., Shepherd, G., Boyer, R., Atkinson, J. P., et al. (2018). 'Association of immune response with efficacy and safety outcomes in adults with phenylketonuria administered pegvaliase in phase 3 clinical trials. *EBioMedicine* 37, 366–373. doi:10.1016/j.ebiom.2018.10.038

Guthrie, R., and Susi, A. (1963). A simple phenylalanine method for detecting phenylketonuria in large populations of newborn infants. *Pediatrics* 32, 338–343. doi:10.1542/peds.32.3.338

Hamman, K., Clark, H., Montini, E., Al-Dhalimy, M., Grompe, M., Finegold, M., et al. (2005). 'Low therapeutic threshold for hepatocyte replacement in murine phenylketonuria. *Mol. Ther.* 12, 337–344. doi:10.1016/j.ymthe.2005.03.025

Hanley, W. B., Linsao, L., Davidson, W., and Moes, C. A. (1970). 'Malnutrition with early treatment of phenylketonuria. *Pediatr. Res.* 4, 318–327. doi:10.1203/00006450-197007000-00002

Hartwig, C., Gal, A., Santer, R., Ullrich, K., Finckh, U., and Kreienkamp, H. J. (2006). 'Elevated phenylalanine levels interfere with neurite outgrowth stimulated by the neuronal cell adhesion molecule L1 *in vitro*. *FEBS Lett.* 580, 3489–3492. doi:10.1016/j.febslet.2006.05.026

Hillert, A., Anikster, Y., Belanger-Quintana, A., Burlina, A., Burton, B. K., Carducci, C., et al. (2020). 'The genetic landscape and epidemiology of phenylketonuria. *Am. J. Hum. Genet.* 107, 234–250. doi:10.1016/j.ajhg.2020.06.006

Hoeksma, M., Reijngoud, D. J., Pruim, J., de Valk, H. W., Paans, A. M., and van Spronsen, F. J. (2009). 'Phenylketonuria: High plasma phenylalanine decreases cerebral protein synthesis. *Mol. Genet. Metab.* 96, 177–182. doi:10.1016/j.ymgme.2008.12.019

Hörster, F., Schwab, M. A., Sauer, S. W., Pietz, J., Hoffmann, G. F., Okun, J. G., et al. (2006). 'Phenylalanine reduces synaptic density in mixed cortical cultures from mice. *Pediatr. Res.* 59, 544–548. doi:10.1203/01.pdr.0000203091.45988.8d

Hydery, T., and Coppenrath, V. A. (2019). A comprehensive review of pegvaliase, an enzyme substitution therapy for the treatment of phenylketonuria. *Drug Target Insights* 13, 1177392819857089. doi:10.1177/1177392819857089

Isabella, V. M., Ha, B. N., Castillo, M. J., Lubkowicz, D. J., Rowe, S. E., Millet, Y. A., et al. (2018). 'Development of a synthetic live bacterial therapeutic for the human metabolic disease phenylketonuria. *Nat. Biotechnol.* 36, 857–864. doi:10.1038/nbt.4222

Jervis, G. A. (1952). Studies on phenylpyruvic oligophrenia; phenylpyruvic acid content on blood. *Proc. Soc. Exp. Biol. Med.* 81, 715–720. doi:10.3181/00379727-81-19998

Jervis, G. A. (1947). 'Studies on phenylpyruvic oligophrenia; the position of the metabolic error. *J. Biol. Chem.* 169, 651–656. doi:10.1016/s0021-9258(17)30882-7

Jung, S. C., Park, J. W., Oh, H. J., Choi, J. O., Seo, K. I., Park, E. S., et al. (2008). 'Protective effect of recombinant adeno-associated virus 2/8-mediated gene therapy from the maternal hyperphenylalaninemia in offsprings of a mouse model of phenylketonuria. *J. Korean Med. Sci.* 23, 877–883. doi:10.3346/jkms.2008.23.5.877

Kaiser, R. A., Weber, N. D., Trigueros-Motos, L., Allen, K. L., Martinez, M., Cao, W., et al. (2021). 'Use of an adeno-associated virus serotype Anc80 to provide durable cure of phenylketonuria in a mouse model. *J. Inherit. Metab. Dis.* 44, 1369–1381. doi:10.1002/jimd.12392

Kanai, Y., Segawa, H., Miyamoto, K. I., Uchino, H., Takeda, E., and Endou, H. (1998). Expression cloning and characterization of a transporter for large neutral amino acids activated by the heavy chain of 4F2 antigen (CD98). *J. Biol. Chem.* 273, 23629–23632. doi:10.1074/jbc.273.37.23629

Kaufman, S. (1971). 'The phenylalanine hydroxylating system from mammalian liver. *Adv. Enzymol. Relat. Areas Mol. Biol.* 35, 245–319. doi:10.1002/9780470122808.ch6

Keil, S., Anjema, K., van Spronsen, F. J., Lambruschini, N., Burlina, A., Bélanger-Quintana, A., et al. (2013). 'Long-term follow-up and outcome of phenylketonuria patients on sapropterin: A retrospective study. *Pediatrics* 131, e1881–e1888. doi:10.1542/peds.2012-3291

Knox, W. E. (1960). An evaluation of the treatment of phenylketonuria with diets low in phenylalanine. *Pediatrics* 26, 1–11. doi:10.1542/peds.26.1.1

Koch, R., Moseley, K., Ning, J., Romstad, A., Guldberg, P., and Guttler, F. (1999). 'Long-term beneficial effects of the phenylalanine-restricted diet in late-diagnosed individuals with phenylketonuria. *Mol. Genet. Metab.* 67, 148–155. doi:10.1006/mgme.1999.2863

Kure, S., Hou, D. C., Ohura, T., Iwamoto, H., Suzuki, S., Sugiyama, N., et al. (1999). 'Tetrahydrobiopterin-responsive phenylalanine hydroxylase deficiency. *J. Pediatr.* 135, 375–378. doi:10.1016/s0022-3476(99)70138-1

Lammardo, A. M., Robert, M., Rocha, J. C., van Rijn, M., Ahring, K., Bélanger-Quintana, A., et al. (2013). 'Main issues in micronutrient supplementation in phenylketonuria. *Mol. Genet. Metab.* 110, S1–S5. doi:10.1016/j.ymgme.2013.08.008

Leuzzi, V., Chiarotti, F., Nardecchia, F., van Vliet, D., and van Spronsen, F. J. (2020). 'Predictability and inconsistencies of cognitive outcome in patients with phenylketonuria and personalised therapy: The challenge for the future guidelines. *J. Med. Genet.* 57, 145–150. doi:10.1136/jmedgenet-2019-106278

Li, Y., Tan, Z., Zhang, Y., Zhang, Z., Hu, Q., Liang, K., et al. (2021). 'A noncoding RNA modulator potentiates phenylalanine metabolism in mice. *Science* 373, 662–673. doi:10.1126/science.aba4991

Longo, N., Dimmock, D., Levy, H., Viau, K., Bausell, H., Bilder, D. A., et al. (2019). 'Evidence- and consensus-based recommendations for the use of pegvaliase in adults with phenylketonuria. *Genet. Med.* 21, 1851–1867. doi:10.1038/s41436-018-0403-z

Longo, N., Harding, C. O., Burton, B. K., Grange, D. K., Vockley, J., Wasserstein, M., et al. (2014). 'Single-dose, subcutaneous recombinant phenylalanine ammonia lyase conjugated with polyethylene glycol in adult patients with phenylketonuria: An open-label, multicentre, phase 1 dose-escalation trial. *Lancet* 384, 37–44. doi:10.1016/S0140-6736(13)61841-3

Lu, W., Zhou, Q., Yang, H., Wang, H., Gu, Y., Shen, Q., et al. (2016). 'Gene therapy for hemophilia B mice with scAAV8-LP1-hFIX. *Front. Med.* 10, 212–218. doi:10.1007/s11684-016-0438-y

MacDonald, A., van Wegberg, A. M. J., Ahring, K., Beblo, S., Bélanger-Quintana, A., Burlina, A., et al. (2020). 'PKU dietary handbook to accompany PKU guidelines. *Orphanet J. Rare Dis.* 15, 171. doi:10.1186/s13023-020-01391-y

Mendell, J. R., Al-Zaidy, S., Shell, R., Arnold, W. D., Rodino-Klapac, L. R., Prior, T. W., et al. (2017). 'Single-Dose gene-replacement therapy for spinal muscular atrophy. *N. Engl. J. Med.* 377, 1713–1722. doi:10.1056/NEJMoa1706198

Miller, A. L., Hawkins, R. A., and Veech, R. L. (1973). 'Phenylketonuria: Phenylalanine inhibits brain pyruvate kinase *in vivo*. *Science* 179, 904–906. doi:10.1126/science.179.4076.904

Mochizuki, S., Mizukami, H., Ogura, T., Kure, S., Ichinohe, A., Kojima, K., et al. (2004). 'Long-term correction of hyperphenylalaninemia by AAV-mediated gene transfer leads to behavioral recovery in phenylketonuria mice. *Gene Ther.* 11, 1081–1086. doi:10.1038/sj.gt.3302262

Oh, H. J., Park, E. S., Kang, S., Jo, I., and Jung, S. C. (2004). 'Long-term enzymatic and phenotypic correction in the phenylketonuria mouse model by adeno-associated virus vector-mediated gene transfer. *Pediatr. Res.* 56, 278–284. doi:10.1203/01.PDR.0000132837.29067.0E

Penrose, L. S. (1935). Inheritance of phenylpyruvic amentia (phenylketonuria). *Lancet* 226, 192–194. doi:10.1016/s0140-6736(01)04897-8

Pogue, R. E., Cavalcanti, D. P., Shanker, S., Andrade, R. V., Aguiar, L. R., de Carvalho, J. L., et al. (2018). 'Rare genetic diseases: Update on diagnosis, treatment and online resources. *Drug Discov. Today* 23, 187–195. doi:10.1016/j.drudis.2017.11.002

Qin, M., and Smith, C. B. (2007). 'Regionally selective decreases in cerebral glucose metabolism in a mouse model of phenylketonuria. *J. Inherit. Metab. Dis.* 30, 318–325. doi:10.1007/s10545-007-0583-1

Rebuffat, A., Harding, C. O., Ding, Z., and Thöny, B. (2010). 'Comparison of adeno-associated virus pseudotype 1, 2, and 8 vectors administered by intramuscular injection in the treatment of murine phenylketonuria. *Hum. Gene Ther.* 21, 463–477. doi:10.1089/hum.2009.127

Richards, D. Y., Winn, S. R., Dudley, S., Nygaard, S., Mighell, T. L., Grompe, M., et al. (2020). 'AAV-Mediated CRISPR/Cas9 gene editing in murine phenylketonuria. *Mol. Ther. Methods Clin. Dev.* 17, 234–245. doi:10.1016/j.omtm.2019.12.004

Rose, A. M., Grosse, S. D., Garcia, S. P., Bach, J., Kleyn, M., Simon, N. E., et al. (2019). The financial and time burden associated with phenylketonuria treatment in the United States. *Mol. Genet. Metab. Rep.* 21, 100523. doi:10.1016/j.ymgmr.2019.100523

Sarkissian, C. N., Shao, Z., Blain, F., Peevers, R., Su, H., Heft, R., et al. (1999). 'A different approach to treatment of phenylketonuria: Phenylalanine degradation with recombinant phenylalanine ammonia lyase. *Proc. Natl. Acad. Sci. U. S. A.* 96, 2339–2344. doi:10.1073/pnas.96.5.2339

Scriver, C. C. (1998). A simple phenylalanine method for detecting phenylketonuria in large populations of newborn infants, by Robert Guthrie and Ada Susi, Pediatrics. *Pediatrics* 32, 318–343. doi:10.1542/peds.102.s1.236

Shefer, S., Tint, G. S., Jean-Guillaume, D., Daikhin, E., Kendler, A., Nguyen, L. B., et al. (2000). Is there a relationship between 3-hydroxy-3-methylglutaryl coenzyme a reductase activity and forebrain pathology in the PKU mouse? *J. Neurosci. Res.* 61, 549–563. doi:10.1002/1097-4547(20000901)61:5<549:AID-JNR10>3.0.CO;2-0

Sun, W., Zheng, W., and Simeonov, A. (2017). 'Drug discovery and development for rare genetic disorders. *Am. J. Med. Genet. A* 173, 2307–2322. doi:10.1002/ajmg.a.38326

Sutivijit, Y., Banpavichit, A., and Wiwanitkit, V. (2011). 'Prevalence of neonatal hypothyroidism and phenylketonuria in southern Thailand: A 10-year report. *Indian J. Endocrinol. Metab.* 15, 115–117. doi:10.4103/2230-8210.81941

Tao, R., Xiao, L., Zhou, L., Zheng, Z., Long, J., Zhou, L., et al. (2020). 'Long-Term metabolic correction of phenylketonuria by AAV-delivered phenylalanine amino lyase. *Mol. Ther. Methods Clin. Dev.* 19, 507–517. doi:10.1016/j.omtm.2019.12.014

Thomas, J., Levy, H., Amato, S., Vockley, J., Zori, R., Dimmock, D., et al. (2018). 'Pegvaliase for the treatment of phenylketonuria: Results of a long-term phase 3 clinical trial program (PRISM). *Mol. Genet. Metab.* 124, 27–38. doi:10.1016/j.ymgme.2018.03.006

van der Goot, E., Bruinenberg, V. M., Hormann, F. M., Eisel, U. L. M., van Spronsen, F. J., and Van der Zee, E. A. (2019). 'Hippocampal microglia modifications in C57Bl/6 Pah(enu2) and BTBR Pah(enu2) phenylketonuria (PKU) mice depend on the genetic background, irrespective of disturbed sleep patterns. *Neurobiol. Learn. Mem.* 160, 139–143. doi:10.1016/j.nlm.2018.05.002

van Spronsen, F. J., Blau, N., Harding, C., Burlina, A., Longo, N., and Bosch, A. M. (2021). Phenylketonuria. *Nat. Rev. Dis. Prim.* 7, 36. doi:10.1038/s41572-021-00267-0

van Spronsen, F. J., Himmelreich, N., Rüfenacht, V., Shen, N., Vliet, D. V., Al-Owain, M., et al. (2017). 'Heterogeneous clinical spectrum of DNAJC12-deficient hyperphenylalaninemia: From attention deficit to severe dystonia and intellectual disability. *J. Med. Genet.* 55, 249–253. doi:10.1136/jmedgenet-2017-104875

van Vliet, D., Bruinenberg, V. M., Mazzola, P. N., van Faassen, M. H., de Blaauw, P., Kema, I. P., et al. (2015). 'Large neutral amino acid supplementation exerts its effect through three synergistic mechanisms: Proof of principle in phenylketonuria mice. *PLoS One* 10, e0143833. doi:10.1371/journal.pone.0143833

van Vliet, D., Bruinenberg, V. M., Mazzola, P. N., van Faassen, M. H., de Blaauw, P., Pascucci, T., et al. (2016). 'Therapeutic brain modulation with targeted large neutral amino acid supplements in the Pah-enu2 phenylketonuria mouse model. *Am. J. Clin. Nutr.* 104, 1292–1300. doi:10.3945/ajcn.116.135996

van Vliet, D., van Wegberg, A. M. J., Ahring, K., Bik-Multanowski, M., Blau, N., Bulut, F. D., et al. (2018). 'Can untreated PKU patients escape from intellectual disability? A systematic review. *Orphanet J. Rare Dis.* 13, 149. doi:10.1186/s13023-018-0890-7

van Wegberg, A. M. J., MacDonald, A., Ahring, K., Bélanger-Quintana, A., Blau, N., Bosch, A. M., et al. (2017). 'The complete European guidelines on phenylketonuria: Diagnosis and treatment. *Orphanet J. Rare Dis.* 12, 162. doi:10.1186/s13023-017-0685-2

Villiger, L., Grisch-Chan, H. M., Lindsay, H., Ringnalda, F., Pogliano, C. B., Allegri, G., et al. (2018). 'Treatment of a metabolic liver disease by *in vivo* genome base editing in adult mice. *Nat. Med.* 24, 1519–1525. doi:10.1038/s41591-018-0209-1

Waldrop, M. A., Karingada, C., Storey, M. A., Powers, B., Iammarino, M. A., Miller, N. F., et al. (2020). 'Gene therapy for spinal muscular atrophy: Safety and early outcomes. *Pediatrics* 146, e20200729. doi:10.1542/peds.2020-0729

Wang, D., Tai, P. W. L., and Gao, G. (2019). 'Adeno-associated virus vector as a platform for gene therapy delivery. *Nat. Rev. Drug Discov.* 18, 358–378. doi:10.1038/s41573-019-0012-9

Welch, E. M., Barton, E. R., Zhuo, J., Tomizawa, Y., Friesen, W. J., Trifillis, P., et al. (2007). 'PTC124 targets genetic disorders caused by nonsense mutations. *Nature* 447, 87–91. doi:10.1038/nature05756

Winn, S. R., Scherer, T., Thöny, B., and Harding, C. O. (2016). 'High dose sapropterin dihydrochloride therapy improves monoamine neurotransmitter turnover in murine phenylketonuria (PKU). *Mol. Genet. Metab.* 117, 5–11. doi:10.1016/j.ymgme.2015.11.012

Woo, S. L., Lidsky, A. S., Güttler, F., Chandra, T., and Robson, K. J. (1983). 'Cloned human phenylalanine hydroxylase gene allows prenatal diagnosis and carrier detection of classical phenylketonuria. *Nature* 306, 151–155. doi:10.1038/306151a0

Xiang, L., Tao, J., Deng, K., Li, X., Li, Q., Yuan, X., et al. (2019). 'Phenylketonuria incidence in China between 2013 and 2017 based on data from the Chinese newborn screening information system: A descriptive study. *BMJ Open* 9, e031474. doi:10.1136/bmjopen-2019-031474

Yin, S., Ma, L., Shao, T., Zhang, M., Guan, Y., Wang, L., et al. (2022). 'Enhanced genome editing to ameliorate a genetic metabolic liver disease through co-delivery of adeno-associated virus receptor. *Sci. China. Life Sci.* 65, 718–730. doi:10.1007/s11427-020-1744-6

Zhou, L., Su, J., Long, J., Tao, R., Tang, W., Qin, F., et al. (2022). 'A universal strategy for AAV delivery of base editors to correct genetic point mutations in neonatal PKU mice. *Mol. Ther. Methods Clin. Dev.* 24, 230–240. doi:10.1016/j.omtm.2022.01.001

frontiers | Frontiers in Genetics

TYPE Original Research
PUBLISHED 04 January 2023
DOI 10.3389/fgene.2022.989215

Check for updates

OPEN ACCESS

EDITED BY
Ruth Roberts,
ApconiX, United Kingdom

REVIEWED BY
Ihtisham Bukhari,
Fifth Affiliated Hospital of Zhengzhou University, China
Andrzej Kochański,
Mossakowski Medical Research Institute, Polish Academy of Sciences, Poland

*CORRESPONDENCE
Fang Liu,
liufanglafy@126.com

†These authors have contributed equally to this work and share first authorship

SPECIALTY SECTION
This article was submitted to Genetics of Common and Rare Diseases, a section of the journal Frontiers in Genetics

RECEIVED 08 July 2022
ACCEPTED 01 December 2022
PUBLISHED 04 January 2023

CITATION
Liu F, Dai L, Li Z and Yin's X (2023), Novel variants of *NEK9* associated with neonatal arthrogryposis: Two case reports and a literature review. *Front. Genet.* 13:989215. doi: 10.3389/fgene.2022.989215

COPYRIGHT
© 2023 Liu, Dai, Li and Yin's. This is an open-access article distributed under the terms of the Creative Commons Attribution License (CC BY). The use, distribution or reproduction in other forums is permitted, provided the original author(s) and the copyright owner(s) are credited and that the original publication in this journal is cited, in accordance with accepted academic practice. No use, distribution or reproduction is permitted which does not comply with these terms.

Novel variants of *NEK9* associated with neonatal arthrogryposis: Two case reports and a literature review

Fang Liu[1†]*, Liying Dai[2†], Zhi Li[1] and Xiaowei Yin's[1]

[1]Department of Pediatrics, NICU, the 980th Hospital of the People's Liberation Army Joint Service Support Force, Bethune International Peace Hospital, Shijiazhuang, China, [2]Department of Neonatology, Anhui Children's Hospital, Hefei, China

Objective: Pathogenic variants in *NEK9* (MIM: 609798) have been identified in patients with lethal congenital contracture syndrome 10 (OMIM: 617022) and arthrogryposis, Perthes disease, and upward gaze palsy (APUG and OMIM: 614262). The shared core phenotype is multiple joint contractures or arthrogryposis. In the present study, three novel variants of *NEK9* associated with neonatal arthrogryposis were reported.

Methods: The clinical data of two premature infants and their parents were collected. The genomic DNA was extracted from their peripheral blood samples and subjected to trio-whole-exome sequencing (trio-WES) and copy number variation analysis.

Results: Using trio-WES, a total of three novel pathogenic variants of *NEK9* were detected in the two families. Patient 1 carried compound heterozygous variations of c.717C > A (p. C239*741) and c.2824delA (p.M942Cfs*21), which were inherited from his father and mother, respectively. Patient 2 also carried compound heterozygous variations of c.61G > T (p. E21*959) and c. 2824delA (p. M942Cfs*21), which were inherited from his father and mother, respectively. These variants have not been previously reported in the ClinVar, HGMD, or gnomAD databases.

Conclusion: This is the first report about *NEK9*-related arthrogryposis in neonatal patients. The findings from this study suggest that different types of mutations in *NEK9* lead to different phenotypes. Our study expanded the clinical phenotype spectrum and gene spectrum of *NEK9*-associated arthrogryposis.

KEYWORDS

NIMA-related kinase 9 (NEK9), arthrogryposis, recessive, mutation, clinical

1 Introduction

Arthrogryposis is frequently used to describe multiple congenital contractures that impact more than two areas of the body. Arthrogryposis is not a specific diagnosis but instead a clinical finding, and it is a feature of more than 300 different disorders. The prevalence of arthrogryposis is 1 in 3,000 live births (Bamshad et al., 2009; Kowalczyk et al., 2016; Fahy and Hall, 1990). Arthrogryposis is further a group of clinical mitotic control from scattered single gene mutations, chromosomal disorders, and mitochondrial disorders (Bamshad et al., 2009).

NEK9 encodes a member of the NIMA family of serine/threonine protein kinases, which is triggered in mitosis and, in turn, triggers other family members during mitosis (O'Connell et al., 2003). The functions of *NEK9* in the spindle assembly and centrosome separation (Kaneta and Ullrich, 2013) are essential in the regulation of mitosis. Dysfunction of *NEK9* leads to multiple system impairments, including ocular, skeletal, and central nervous system anomalies and various tumors (Sheppard et al., 2020; Panchal and Evan Prince, 2022). Pathogenic variants in *NEK9* were identified in the fetus with lethal congenital contracture syndrome 10 (OMIM: 617022) and in children with arthrogryposis, Perthes disease, and upward gaze palsy (APUG and OMIM: 614262). To our knowledge, only eight cases have been fully reported (Alkuraya, 2010; Shaheen et al., 2015; Casey Jillian et al., 2016; Stals Karen et al., 2018; Deden et al., 2020).

In this study, we reported two unrelated neonates from non-consanguineous families with healthy parents. The patient presented with arthrogryposis (HP: 0012453), pyloric stenosis (HP: 0002021), atrial septal defect (HP: 0001631), and pulmonary stenosis (HP: 0001642). Using trio-WES, we identified two novel compound heterozygotic variants of *NEK9* (c.717 C > A, p. C239*741 and c.2824delA, p.M942Cfs*21; c.61 G > T, p. E21*959 and c.2824delA, p.M942Cfs*21). Our findings expand the clinical phenotype spectrum and the gene spectrum of *NEK9*-associated arthrogryposis.

2 Subjects and methods

2.1 Subjects

2.1.1 Patient 1

Patient 1 was a boy, who was delivered by cesarean section with maternal placental abruption. Gestational age was only 32^{+2} weeks, birth weight: 1680 g (< 3rd), length: 40 cm (< 3rd), and head circumference: 30 cm (< 3rd). His mother was 31 years old, and the pregnancy was uneventful. His father was 35 years old. The parents were unrelated and in good health; there was no family history of congenital malformations or hypertension. After birth, the premature baby was hospitalized in the NICU of the local maternal and child health hospital. He was transferred to our hospital on the second day after birth due to respiratory distress and pulmonary hypertension. He was treated with exogenous pulmonary surfactant, blood plasma, and mechanical ventilation for 7 days and then was extubated to CPAP for another 14 days. Five weeks later, his saturation could reach more than 90% in room air. Cranial ultrasound was performed routinely on days 3 and 7 after admission, and he was detected as having severe intraventricular hemorrhage (grade III) with ventricular dilatation (10 mm–15 mm). The hemorrhage was absorbed after three weeks with the bilateral ventricle mild dilatation. Other clinical manifestations included normal scrotal pigmentation, normal penis size, and bilateral testicular descent. Echocardiography revealed patent foramen ovale, mild pulmonary stenosis, and mild-to-moderate pulmonary hypertension. Liver, kidney, and thyroid functions were normal. Serum lipid and myocardial enzyme levels were in the normal range. Routine blood, urine, and stool test results were normal. Normal plasma amino acid and urinary orotic acid levels were demonstrated.

Special appearance: from the beginning of admission, doctors noticed that the boy's neck was stiff; the pediatrician and the physical therapist also confirmed the presence of a moderate form of arthrogryposis involving the elbows and knees, and his bilateral third, fourth, and fifth fingers were camptodactyly (Figure 1). After tube feeding, he presented with abdominal distension, vomiting, and larger gastric retention. Abdominal X-ray showed a huge stomach bubble, and pyloric stenosis was suspected in gastrointestinal angiography and abdominal ultrasonography. On the 32nd day after birth, the patient underwent pyloric hypertrophy resection surgery. He was given tube feeding 4 days after the operation, until complete enteral feeding.

2.1.2 Patient 2

Patient 2 was a boy, delivered by cesarean section with maternal polyhydramnios. Gestational age was only 34^{+2} weeks, birth weight: 2,700 g (50th–90th), length: 43 cm (10th), and head circumference: 33 cm (50th–90th). The parents were unrelated and in good health; there was no family history of congenital malformations or hypertension. After birth, the premature baby was hospitalized in the NICU of the local hospital and was diagnosed with sepsis at 6 days of age, and he received regular antibiotic treatment. Echocardiography showed atrial septal defect and pulmonary artery stenosis. Brain magnetic resonance imaging showed that the T2WT signal in the white matter of the bilateral cerebral hemispheres was high, and the EEG was normal. After birth, the pediatrician noticed that the child's muscle tone was significantly increased, his neck was stiff, and the passive extension of his elbows, hips, and knees was limited. The patient was discharged after 2 months of birth, and he was still unable to suck and required tube feeding.



FIGURE 1
Patient I: sparse eyebrows and hair, prominent forehead, wide eye distance, wide nose bridge, and prominent antihelix stem. His bilateral third, fourth, and fifth fingers were camptodactyly. Mild deformity of the left toe was also present.

3 Method

3.1 Sample collection

The study was approved by the Ethics Committee of Bethune International Peace Hospital and Anhui Provincial Children's Hospital. The parents of the boys gave written informed consent for clinical examination, genetic analysis, and data publication. A peripheral blood sample was collected from the two boys and their parents. Genomic DNA of the two boys and their parents were obtained from the peripheral blood leukocytes using the Blood Genome Column Medium Extraction Kit (Kangweishiji, China) for trio-whole-exome sequencing (trio-WES) and copy number variation (CNV) analysis.

3.2 Genetic analysis

Genomic DNA of the two boys and their parents were obtained from the peripheral blood leukocytes using the Blood Genome Column Medium Extraction Kit (Kangweishiji, China) for trio-whole-exome sequencing (trio-WES) and copy number variation (CNV) analysis. DNA pieces were hybridized and exome enrichment was captured using xGen Exome Research Panel v1.0 (IDT, Iowa, United States) which contains 429,826 probes, targets 39 Mb protein-coding region, and overlaps 51 Mb of end-to-end tiled probe space. Illumina NovaSeq 6000 series sequencer (PE150) was operated, and more than 99% of the target sequence was sequenced. Sequencing raw data were processed by FASTQ for removing adapters and filtering low-quality reads. The paired-end reads were aligned to the Ensemble GRCh37/hg19 reference genome using Burrows–Wheeler aligner (BWA). Base quality score recorrecting and variant calling were conducted using GATK. SNPs and indels were screened in accordance with the sequencing depth and variant quality. Variant annotation and pathogenicity prediction were processed based on the databases for minor allele frequencies (1000 Genomes, dbSNP, ESP, ExAC, and gnomAD), and the pathogenicity of genetic variants was predicted by bioinformatics tools such as PolyPhen, MutationTaster, REVEL, and CADD. Finally, variants were classified according to the American College of Medical Genetics and Genomics (ACMG) guideline (Richardset al., 2015).

Detection of CNV: raw image files were processed by applying Bcl To FASTQ (Illumina) for raw data generation. The reads were then mapped to the GRCh37/hg19 human reference genome using BWA software. Variant calling for CNVs of 100 KB and above in length was detected using Chigene independently developed software packages for CNV detection, and the candidate CNVs were filtered and detected using public CNV databases (Decipher, ClinVar, OMIM, DGV, and ClinGen). The biological harm and related phenotypes of CNVs were assessed by annotated information and frequency databases depending on ACMG practice guidelines and CNV diagnostic guidelines (Richards et al., 2015; Riggs et al., 2022).

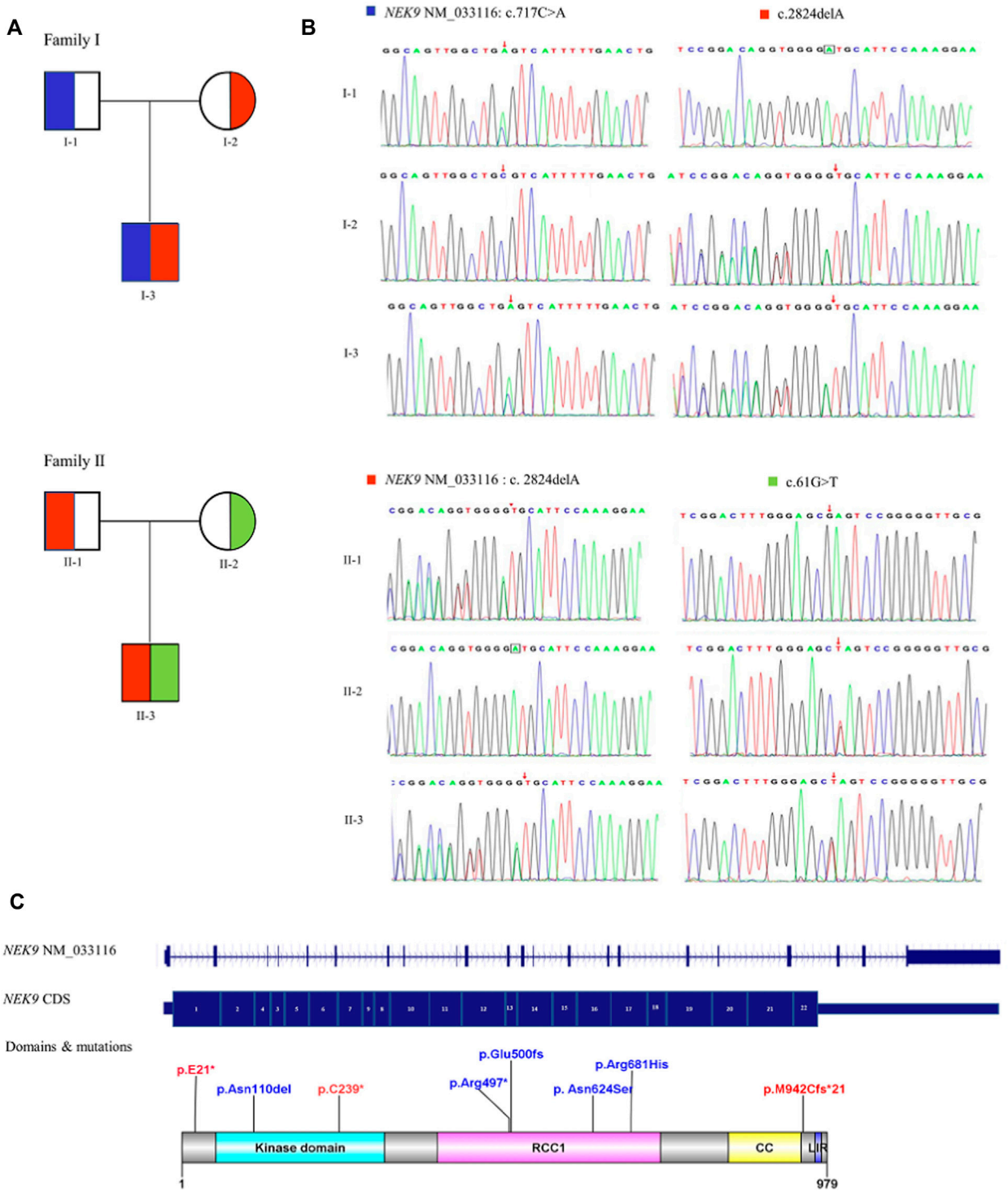


FIGURE 2
Diagram of *NEK9* mutations and gene structure. **(A)** Pedigree diagrams of two families with *NEK9* mutations. Each color corresponds to a novel variant of *NEK9*. **(B)** Sanger sequencing results of the diagnostic variants in the two families. **(C)** Distribution diagram of domains and mutations associated with lethal congenital contracture syndrome 10 (LCCS10, OMIMZ# 617022) and arthrogryposis, Perthes disease, and upward gaze palsy (APUG,OMIMZ# 6142622) in serine/threonine-protein kinase *NEK9*. RCC1, RCC1-repeats; CC, coiled-coil domain; and LIR, LC3-interacting region.

TABLE 1 Summary of phenotypic features of all reported patients.

Origin	Patient	GA weeks	Sex	Developmental index	SGA	Age	Clinical I manifestation	PMID
Consanguineous Irish Traveller family A	1	28^{+4} dead	M	BW: 892 (< 3rd) HC: 25 (9th) L: NA	+	—	Shortening of all four limbs, contractures of all major joints, micrognathia, short neck with reduced flexion, long overlapping fingers, adducted thumbs, and narrow hips with right-sided hydrocele	26908619
	2	21^{+1} TOP	M	BW: 260.85 g HC: 17.5 cm L: NA	+	—	Shortening of all four limbs, contractures of all major joints, long narrow head, long philtrum, high arched palate, micrognathia, neck short and stiff, overlapping fingers, adducted thumbs, hips and shoulders internally rotated, and appearance of pterygia secondary to severe contractures	
Consanguineous Irish Traveller family B	3	26^{+2} SB	F	BW: 630 g OFC: 23.3 (< 3rd) L:NA	+	—	Shortening of all four limbs, contractures of all major joints, small eyes, low-set ears, long philtrum, small chin, narrow palate, short neck with right torticollis, thoracic scoliosis, lateral deviation of fingers, and abnormal palmar creases	
	4	31 SB	F	BW: 890 g HC: 25.5 cm (< 3rd) L: NA	+	—	Shortening of all four limbs;, contractures of all major joints, beaked nose with a saddle bridge, long philtrum, macroglossia, sunken and downward-slanting eyes, and large omphalocele	
Consanguineous	5	Fetus		NA	NA	NA	Arthrogryposis multiplex congenita and fetal akinesia sequence	29096039
Consanguineous Saudi family	6 siblings	Term	F	BW: 3480 g (75th), HC: 35 cm (75–90th), L: 50 cm (50th)	-	12 years	Newborn examination showed limited hip abduction; later orthopedics confirmed multiple joint contractures involving the hands, elbows, hips, and knees; mild camptodactyly most pronounced in the left middle finger; mild atrial septal defect and mild pulmonary stenosis; uncontrolled bronchial asthma; severe atopic dermatitis in infancy; bilateral Perthes disease (avascular necrosis of the femoral head); upward gaze palsy; and normal cognitive development and normal growth parameters at 12 years old	21271645
	7 siblings	35	F	NA	—	15 years	Premature delivery at 35 weeks; newborn examination showed pulmonic stenosis and ventricular septal defect, pyloric stenosis (at 4 weeks of age); later in infancy, evaluation by pediatric orthopedics confirmed the presence of mild form of arthrogryposis involving the hands, elbows, hips, knees, and ankles; severe flexion deformity of the fingers; avascular necrosis of the right femoral head (at 2 years old); upward gaze palsy; uncontrolled bronchial asthma (since early childhood); obstructive sleep apnea (at 11 years old); IQ 85; and height 146 cm (< 3rd centile).	

(Continued on following page)

TABLE 1 (*Continued*) Summary of phenotypic features of all reported patients.

Origin	Patient	GA weeks	Sex	Developmental index	SGA	Age	Clinical l manifestation	PMID
Cousin of the two sisters	8	40	F	NA	—	7.5 years	Newborn examination showed pyloric stenosis and widespread limited mobility of joints; limited extension of elbows and knees, markedly reduced rotation and range of both hips; overriding toes; upward gaze palsy; subtle facial dysmorphism; two femoral heads and echocardiography was normal; normal cognitive development and normal growth parameters at 7.5 years old; and repeated episodes of bronchial asthma	
NA	9	Fetus	NA	NA		NA	Short long bones, bowed femur, clubfeet, deviation of hand, scoliosis, micrognathia, and abnormal filling stomach	32333414
Chinese Han	10	32^{+2}	M	BW: 1680 g (< 3rd), HC: 30 cm (< 3rd), L: 40 cm (< 3rd)	+	2.5 months discharge	32^{+2} weeks, premature boy, IUGR; ventilator treatment after birth due to respiratory distress and pulmonary hemorrhage; newborn examination showed neck stiff, mild-moderate form of arthrogryposis involving the hands, elbows, and hips; his bilateral third, fourth, and fifth finger were camptodactyly; mild deformity of left toe; subtle facial dysmorphism; patent foramen ovale, mild pulmonary stenosis, mild-moderate pulmonary hypertension; and pyloric stenosis	This study
Chinese Han	11	34^{+4}	M	BW: 2700 g (50–90th), HC: 33 cm (50–90th), L: 43 cm (10th)	_	2 months discharge	Newborn examination showed marked increase in muscle tone; atrial septal defect and mild pulmonary stenosis; moderate form of arthrogryposis involving the hands, elbows, hips, and knees; and tube feeding due to not sucking	This study

*GA, gestational age; SB, stillbirth; TOP, termination of pregnancy; BW, birth weight; L, length; HC, head circumference; SGA, small for GA; NA, not available.

4 Results

4.1 Results of genetic analysis

By trio-WES, a total of three novel pathogenic variants of *NEK9* were detected from the two families. Patient 1 carried compound heterozygous variations: c.717 C > A (p. C239*741) and c.2824delA (p. M942Cfs*21), which were inherited from his father and mother, respectively. These variants have not been reported in the ClinVar, HGMD, and public databases (gnomAD v2.1.1, http://gnomad.broadinstitute.org/ and the 1000 Genomes Project, http://www.internationalgenome.org). According to ACMG guidelines, we confirmed the two variants to be likely pathogenic (PVS1+PM2 and PVS1-Strong + PM2+PM3) (Richards et al., 2015; Harrison et al., 2019). Patient 2 also carried compound heterozygous variations, which were c. 61 G > T (p. E21*959) and c.2824delA (p.M942Cfs*21) that were inherited from his father and mother, respectively. This variant of c.61 G > T has also not been reported in the ClinVar, HGMD, and public databases (gnomAD v2.1.1, http://gnomad.broadinstitute.org/ and the 1000 Genomes Project, http://www.internationalgenome.org). According to ACMG guidelines, we confirmed the variant to be pathogenic (PS2+PM1+PM2+PP2+PP3) (Richards et al., 2015; Harrison et al., 2019).

Moreover, we did not detect pathogenic or likely pathogenic variants in genes known to be associated with the clinical features of probands using trio-WES.

Sanger sequencing results of the two families and the diagram of domains and mutations in *NEK9* associated with skeletal dysplasia are present in Figure 2. A summary of phenotypic and genotype features of all reported patients involving the *NEK9* gene is shown in Tables 1, 2.

4.2 Literature review

Keywords related to "*NEK9*" and "skeletal dysplasia," "arthrogryposis," "recessive," "lethal congenital contracture syndrome 10," and "arthrogryposis, Perthes disease, and upward gaze palsy" were used during the search in the Wanfang Data Knowledge Service Platform and Weipu Database (Chinese Journal Full-text Database covering time to August 2022), and no relative case was reported. The same keywords were used in PubMed (covering time to August 2022), and three publications were found containing eight cases of skeletal dysplasia; only six cases have been identified with pathogenic mutations in the *NEK9* gene, and genetic analysis was not carried out in another two cases. From HGMD (covering time to August 2022), we have found other two articles about skeletal dysplasia associated with *NEK9*.

In 2016, Casey et al. studied two Irish Traveller families with recessive lethal skeletal dysplasia. In the first family, there were two offspring with fetal akinesia, multiple contractures, shortening of upper and lower limbs, short broad ribs, narrow chest and thorax, pulmonary hypoplasia, and protruding abdomen. In the second family, three offspring had the same features, and one of them also exhibited bowed femurs. None of the affected babies survived: one baby died 1 h after birth, two babies were stillborn, one baby died *in utero*, and a fetus was induced by abortion. WES identified a novel homozygous stop-gain mutation in *NEK9* (c.1489C > T; p. Arg497*) in four affected fetuses (DNA was not available from the third fetus in the second family) (Casey Jillian et al., 2016).

In 2011, Alkuraya described a consanguineal Saudi family in which two sisters and one female cousin had almost the same disease, characterized by arthrogryposis, Perthes disease (avascular necrosis of the hip), and upward gaze palsy (APUG). They had multiple joint contractures including the elbows, hips, knees, and hands. Two had camptodactyly of the fingers, and one had overriding toes. At about 3 years, two children were diagnosed with avascular necrosis of the hip, and the third child had a mild collapse of the medial aspect of both femoral heads. Upward gaze palsy was apparent in childhood. All girls had bronchial asthma, and one had atopic dermatitis. Other features included pyloric stenosis in two girls, pulmonic stenosis in two girls, and a ventricular septal defect and small atrial septal defect in each one. Development was basically normal (Alkuraya et al., 2010). In 31 multiplex consanguineous families that appeared to have novel dysmorphology syndromes, including the Saudi family originally described by Alkuraya (2011), Shaheen et al. (2016) performed autozygome analysis followed by whole-exome and whole-genome sequencing. In the Saudi family with APUG, they identified a homozygous pathogenic missense mutation in *NEK9* (c.2042G > A, p. Arg681His) (Shaheen et al., 2015).

In 2018 and 2020, by parental exome sequencing in pregnancies, Stals and Deden (Stals et al., 2018; Deden et al., 2020) identified three mutations (c.1498delG and p.Glu500fs, associated with LCCS10 and c.1871A > G, p. Asn624Ser; c.329_331delACA, p. Asn110del associated with APUG) in *NEK9* in fetuses with congenital anomalies detected by ultrasound imaging. c.1498delG was identified as a pathogenic variant, and the other two were tentatively considered by the author to be of unknown significance.

5 Discussion

5.1 Humans have eleven different NEK (NIMA-related kinases) genes, named *NEK1* to *NEK11*

The NEK genes encode serine/threonine kinases, which play important roles in the regulation of the cell cycle and are involved in several cellular activities, such as centrosome separation, spindle assembly, chromatin condensation, nuclear envelope breakdown, spindle assembly checkpoint signaling, cytokinesis, cilia formation, and DNA damage response. The NEK9 gene (*location:* 14q24.3) contains 22 exons and encodes a member of the NIMA family of serine/threonine protein kinases NEK9 (NIMA-related protein kinase 9 with 979 amino acids). NEK9 is composed of an N-terminal protein kinase domain (residues 52–308), the central auto-inhibitory regulator of chromosome condensation 1 (RCC1)-repeats (residues 388–726), a C-terminal coiled-coil (CC) domain (residues 892–939), and a predicted LC3-interacting region (LIR) motif (residues 965–970) (Kalvari et al., 2014; Cullati et al., 2017; Yamamoto et al., 2021).

The conserved kinase domain is responsible for phosphorylating different substrates including histones, myelin basic protein, beta-casein, and BICD2. Phosphorylation of histone H3 on serine and threonine residues and beta-casein on serine residues is important for G1/S transition and S phase progression. *NEK6* and *NEK7* can be activated by *NEK9* phosphorylation (Belham et al., 2003; TanChin-Ming and Lee, 2003; Richards Mark et al., 2009), which is crucial in spindle formation and mitosis regulation. The C-terminal regions of the NEKs are highly divergent but have one relatively common feature that promotes autophosphorylation and activation (Fry et al., 2012). *NEK8* and *NEK9* can autophosphorylate in the non-catalytic C-terminal region to regulate their localization and/or activation (Bertran et al., 2011; Zalli et al., 2012).

Diseases associated with *NEK9* include nevus comedonicus (OMIMZ# 617025) (Levinsohn et al., 2016); lethal congenital contracture syndrome 10 (LCCS10, OMIMZ# 617022) (Casey Jillian et al., 2016); and arthrogryposis, Perthes disease, and upward gaze palsy (APUG, OMIMZ# 6142622 (Alkuraya et al., 2010). Reports related to *NEK9* gene variants are very limited. To date, five pathogenic mutations have been reported on the HGMD® home page (cf.ac.uk) (Figure 2), including two

TABLE 2 Summary of genotype features of all reported patients involved in the NEK9 gene.

Patient nos.	Gene	Inheritance	Diagnosis	Omimid	Mu type	HGVS DESCR	NM	Year	PMID
1	NEK9	AR	Lethal congenital contracture syndrome 10	#617022	Homozygous non-sense	c.1489C>T; p. Arg497* pathogenic	NM_033116.4	2016	26908619
2									
3									
4									
5	NEK9	AR	Lethal congenital contracture syndrome 10	#617022	Homozygous frameshift	c.1498delG; p.Glu500fs pathogenic	NM_033116.5	2018	29096039
6	NEK9	AR	Arthrogryposis, Perthes disease, and upward gaze palsy	#614262	Homozygous	c.2042G >A, p.Arg681 His	NM_033116.4	2015	26633546
7					Missense	Pathogenic			
9	NEK9	AR	Arthrogryposis, Perthes disease, and upward gaze palsy	#614262	Missense	c.1871A > G p. Asn624Ser pathogenic?	NM_033116.5	2020	32333414
					Frameshift	c.329_331delACA, p. Asn110del pathogenic?			
10	NEK9	AR	Arthrogryposis, Perthes disease, and upward gaze palsy	#614262	Non-sense	c.717 C > A, p.C239*741 likely pathogenic	NM_033116	2022	Novel, this study
					frameshift	c.2824delA, p.M942Cfs*21 likely pathogenic			
11	NEK9	AR	Arthrogryposis, Perthes disease, and upward gaze palsy	#614262	Non-sense	c.61 G > T p.E21* 959 pathogenic	NM_033116	2019	Novel, this study
					Frameshift	c.2824delA, p.M942Cfs*21 likely pathogenic			

cases of prenatal diagnosis, four cases of stillbirth, and two cases of children. Diagnosis names include LCCS10 and APUG.

LCCS10 is an autosomal recessive disorder characterized by degeneration of anterior horn neurons, extreme skeletal muscle atrophy, and congenital non-progressive joint contractures. The contractures can involve the upper or lower limbs and/or the vertebral column, resulting in varying degrees of flexion or extension limitations that are evident at birth (Casey Jillian et al., 2016). APUG is an autosomal recessive, syndromic form of arthrogryposis, a disease characterized by persistent joint flexure, upward gaze palsy, and avascular necrosis of the hip (Alkuraya et al., 2010; Shaheen et al., 2015).

In this study, patient 1 presented a mild-moderate form of arthrogryposis involving the hands, elbows, hips, and knees; stiff neck; camptodactyly of the fingers; and subtle facial dysmorphism, atrial septal defect, patent ductus arteriosus, and pyloric stenosis. Genetic analysis identified the compound heterozygous variation in NEK9: c.717 C > A (p.C239*741) and c.2824delA, p.M942Cfs*21. The c.717 C > A (p. C239*741) resulted in premature termination of protein translation and elimination of the final 741 amino acids. The mutation of c.2824delA located before the last domain of the peptide chain (LIR, Figure 2), is presumed to have some effects on the stability of protein structure. These two variants are consistent with disease co-segregation in families. Patient 2 presented with a mild-moderate form of arthrogryposis involving the elbows, hips, and knees, and he had an atrial septal defect and mild pulmonary stenosis. Genetic analysis revealed that he carried a compound heterozygous variation in *NEK9*, where one variation was the same as that of patient 1 (c.2824delA and p.M942Cfs*21) and the other was c.61 G > T, p. E21*959; this mutation causes premature translation termination, thereby affecting their function.

The two Chinese Han neonates' clinical presentation was almost consistent with APUG; however, the patient is still young, and other manifestations such as Perthes disease and upward gaze palsy need further observation. It is worth noting that

moderate persistent pulmonary hypertension was observed in patient 1. We speculated that the cause of pulmonary hypertension was pulmonary stenosis. This is a new feature that has not been reported before. Patient 1 can be bottle-fed on his own currently, and with the help of a physical therapist, his joint contracture has been relieved. It is a pity that patient 2 in Anhui Province was lost to follow-up after being discharged.

According to the aforementioned literature, variants in *NEK9*, which are associated with LCCS10, were homozygous nonsense and frameshift, and variants associated with APUG are either homozygous missense mutations or compound heterozygous mutants, such as the two cases in this study. In other words, different types of mutations in the same gene lead to different phenotypes. Patients with homozygous nonsense mutations or frameshift mutations will have severe phenotypes, while patients with homozygous missense mutations or compound heterozygous mutations may have mild symptoms.

What is the mechanism of the aforementioned diseases caused by *NEK9* gene mutation? Some researchers have suggested that it could be related to ciliary disorders. Casey (2016) not only found patients with lethal skeletal dysplasia fibroblasts that displayed a significant reduction in cilia number and length, but also provided evidence of the *NEK9* ortholog in C. elegans, nekl-1, which was almost exclusively expressed in a subset of ciliated cells, a strong indicator of cilia-related functions. Casey suggested that the lethal skeletal dysplasia caused by *NEK9* mutation may represent a novel ciliopathy (Casey Jillian et al., 2016). The LIR motif on *NEK9* C-terminal is conserved in land-living vertebrates and functions in primary cilia formation by mediating the *NEK9*–GABARAP interaction and *MYH9* degradation (Yamamoto et al., 2021). Dysfunctions in non-motile cilia are characterized as renal anomalies, skeletal anomalies, brain malformations, hepatic disease, hearing loss, anosmia, retinal dystrophy, central obesity, and facial anomalies (Reiter and Leroux, 2017). Critically, all the truncated mutant proteins in reported patients lack LIR motif, which may partly explain the complex and changeable clinical symptoms caused by *NEK9* mutations.

In summary, we identified the *HEK9* pathogenic variant in two Chinese neonatal infants with arthrogryposis. By comparative analysis of literature reports, we propose different types of mutations in *NEK9*, which will lead to different phenotypes. Patients with homozygous non-sense mutations or homozygous frameshift mutations in *NEK9* will have severe phenotypes (LCCS10), while patients with homozygous missense mutations or compound heterozygous mutations may have mild symptoms (APUG). With more and more case reports, the *NEK9* gene could be better understood. Our findings expand the genotype–phenotype knowledge of *NEK9*-associated arthrogryposis and provide evidence for further genetic counseling.

Data availability statement

The datasets presented in this study can be found in online repositories. The names of the repository/repositories and accession number(s) can be found in the article/Supplementary Material.

Ethics statement

This study was approved by the Ethics Committee of Bethune International Peace Hospital. Participating centers were obliged to inform parents about the scientific use of the anonymized data at the time of data collection.

Author contributions

FL: data collection, analysis, interpretation, literature search, and manuscript writing. Remaining authors: data collection and proofreading of the manuscript. All authors agreed to the final version of the manuscript.

Funding

This study was supported by the Key R & D Program Project of Hebei Province—Special Project on Health and Biomedicine (No. 182777128D).

Acknowledgments

We appreciate the patients and their family members for their participation. We thank the Beijing Chigene Translational Medicine Research Center Co., Ltd., for NGS sequencing.

Conflict of interest

The authors declare that the research was conducted in the absence of any commercial or financial relationships that could be construed as a potential conflict of interest.

Publisher's note

All claims expressed in this article are solely those of the authors and do not necessarily represent those of their affiliated organizations, or those of the publisher, the editors, and the reviewers. Any product that may be evaluated in this article, or claim that may be made by its manufacturer, is not guaranteed or endorsed by the publisher.

References

Alkuraya, F. S. (2010). Arthrogryposis, perthes disease, and upward gaze palsy: A novel autosomal recessive syndromic form of arthrogryposis. *Am. J. Med. Genet. A* 155A (2), 297–300. doi:10.1002/ajmg.a.33794

Bamshad, M., Van Heest, A. E., and Pleasure, D. A. (2009). Arthrogryposis: A review and update. *J. Bone Jt. Surg. Am.* 91 (4), 40–46. doi:10.2106/JBJS.I.00281

Bartłomiej, K., and Feluś, J. (2016). Arthrogryposis: An update on clinical aspects, etiology, and treatment strategies. *Arch. Med. Sci.* 12 (1), 10–24. doi:10.5114/aoms.2016.57578

Bertran, M. T., Sdelci, S., Regue´, L., Avruch, J., and Cand Roig, J. (2011). Nek9 is a Plk1-activated kinase that controls early centrosome separation throughNek6/7 and Eg5. *EMBO J.* 30, 2634–2647. doi:10.1038/emboj.2011.179

Casey Jillian, P., Brennan, K., Scheidel, N, McGettigan, P., Lavin, P. T., Carter, S., et al. (2016). Recessive NEK9 mutation causes a lethal skeletal dysplasia with evidence of cell cycle and ciliary defects. *Hum. Mol. Genet.* 25 (9), 1824–1835. doi:10.1093/hmg/ddw054

Christopher, B., Roig, J., Caldwell Jennifer, A., Aoyama, Y., Kemp, B. E., Comb, M., et al. (2003). A mitotic cascade of NIMA family kinases. Nercc1/Nek9 activates the Nek6 and Nek7 kinases. *J. Biol. Chem.* 278 (37), 34897–34909. doi:10.1074/jbc.M303663200

Cullati, S. N., Kabeche, L., Kettenbach, A. N., and Gerber, S. A. (2017). A bifurcated signaling cascade of NIMA-related kinases controls distinct kinesins in anaphase. *J. Cell Biol.* 216 (8), 2339–2354. doi:10.1083/jcb.201512055

Deden, C., Neveling, K., Zafeiropopoulou, D., Gilissen, C., Pfundt, R., Rinne, T., et al. (2020). Rapid whole exome sequencing in pregnancies to identify the underlying genetic cause in fetuses with congenital anomalies detected by ultrasound imaging. *Prenat. Diagn.* 40 (8), 972–983. doi:10.1002/pd.5717

Fahy, M. J., and Hall, J. G. (1990). A retrospective study of pregnancy complications among 828cases of arthrogryposis. *Genet. Couns.* 1, 3–11.

Fry, A. M., O'Regan, L., Sabir, S. R., and Bayliss, R. (2012). Cell cycle regulation by the NEK family of protein kinases. *J. Cell Sci.* 125 (19), 4423–4433. doi:10.1242/jcs.111195

Kalvari, T. S., Mulakkal, N. C., Osgood, R., Johansen, T., Nezis, I. P., Promponas, V. J., et al. (2014). iLIR: A web resource for prediction of Atg8-family interacting proteins. *Autophagy* 10 (5), 913–925. doi:10.4161/auto.28260

Kaneta, Y., and Ullrich, A. (2013). NEK9 depletion induces catastrophic mitosis by impairment of mitotic checkpoint control and spindle dynamics. *Biochem. Biophys. Res. Commun.* 442 (3-4), 139–146. doi:10.1016/j.bbrc.2013.04.105

Levinsohn, J. L., Sugarman, J. L., McNiff, J. M., Antaya, R. J., and Choate, K. A. (2016). Somatic mutations in NEK9 cause nevus comedonicus. *Am. J. Hum. Genet.* 98 (5), 1030–1037. doi:10.1016/j.ajhg.2016.03.019

O'Connell, M. J., Krien, M. J., and Hunter, T. (2003). Never say never. The NIMA-related protein kinases in mitotic control. *Trends Cell Biol.* 13 (5), 221–228. doi:10.1016/s0962-8924(03)00056-4

Panchal, N. K., and Evan Prince, S. (2022). The NEK family of serine/threonine kinases as a biomarker for cancer. *Clin. Exp. Med.* 17. doi:10.1007/s10238-021-00782-0

Reiter, J. F., and Leroux, M. R. (2017). Genes and molecular pathways underpinning ciliopathies. *Nat. Rev. Mol. Cell Biol.* 18 (9), 533–547. doi:10.1038/nrm.2017.60

Richards Mark, W., Laura, O'R., Corine, M-D., Blot, J. M. Y., Cheung, J., Hoelder, S., et al. (2009). An autoinhibitory tyrosine motif in the cell-cycle-regulated Nek7 kinase is released through binding of Nek9. *Mol. Cell* 36 (4), 560–570. doi:10.1016/j.molcel.2009.09.038

Richards, S., Aziz, N., Bale, S., Bick, D., Das, S., Gastier-Foster, J., et al. (2015). Standards and guidelines for the interpretation of sequence variants: A joint consensus recommendation of the American College of medical genetics and genomics and the association for molecular pathology. *Genet. Med.* 17 (5), 405–424. doi:10.1038/gim.2015.30

Riggs, E. R., Andersen Erica, F., Cherry Athena, M., Kantarci, S., Kearney, H., Patel, A., et al. (2022). Technical standards for the interpretation and reporting of constitutional copy-number variants: A joint consensus recommendation of the American College of medical genetics and genomics (ACMG) and the clinical genome resource (ClinGen). *Genet. Med.* 23 (11), 245–257. doi:10.1038/s41436-019-0686-8

Shaheen, R., Patel, N., Shamseldin, H., Alzahrani, F., Al-Yamany, R., Almoisheer, A., et al. (2015). Accelerating matchmaking of novel dysmorphology syndromes through clinical and genomic characterization of a large cohort. *Genet. Med.* 18 (7), 686–695. doi:10.1038/gim.2015.147

Sheppard, S. E., Smith, A., Grand, K., Pogoriler, J., Rubin, A. I., Schindewolf, E., et al. (2020). Further delineation of the phenotypic spectrum of nevus comedonicus syndrome to include congenital pulmonary airway malformation of the lung and aneurysm. *Am. J. Med. Genet. A* 182 (4), 746–754. doi:10.1002/ajmg.a.61490

Stals Karen, L., Matthew, W., Júlia, B., Caswell, R., Parrish, A., Rankin, J., et al. (2018). Diagnosis of lethal or prenatal-onset autosomal recessive disorders by parental exome sequencing. *Prenat. Diagn.* 38 (1), 33–43. doi:10.1002/pd.5175

TanChin-Ming, B., and Lee, S-C. (2003). Nek9, a novel FACT-associated protein, modulates interphase progression. *J. Biol. Chem.* 279 (10), 9321–9330. doi:10.1074/jbc.M311477200

Yamamoto, Y., Chino, H., Tsukamoto, S., Ode, K. L., Ueda, H. R., and Mizushima, N. (2021). NEK9 regulates primary cilia formation by acting as a selective autophagy adaptor for MYH9/myosin IIA. *Nat. Commun.* 12 (1), 3292. doi:10.1038/s41467-021-23599-7

Zalli, D., Bayliss, R., and Fry, A. M. (2012). The Nek8 protein kinase, mutated in thehuman cystic kidney disease nephronophthisis, is both activated and degraded duringciliogenesis. *Hum. Mol. Genet.* 21, 1155–1171. doi:10.1093/hmg/ddr544

frontiers | Frontiers in Pediatrics

TYPE Case Report
PUBLISHED 06 January 2023
DOI 10.3389/fped.2022.990729

Check for updates

OPEN ACCESS

EDITED BY
Ruth Roberts,
ApconiX, United Kingdom

REVIEWED BY
Antonio Condino-Neto,
University of São Paulo, Brazil
Stephanie Boisson-Dupuis,
The Rockefeller University, United States
Ruben Martinez-Barricarte,
Vanderbilt University Medical Center,
United States

*CORRESPONDENCE
Sainan Shu
✉ shusainan@163.com

SPECIALTY SECTION
This article was submitted to Genetics of Common and Rare Diseases a section of the journal Frontiers in Pediatrics

RECEIVED 10 July 2022
ACCEPTED 13 December 2022
PUBLISHED 06 January 2023

CITATION
Liu L, Huang Y, Liao Y and Shu S (2023) Autosomal dominant chronic mucocutaneous candidiasis with STAT1 mutation can be associated with chronic active hepatitis: A case report.
Front. Pediatr. 10:990729.
doi: 10.3389/fped.2022.990729

COPYRIGHT
© 2023 Liu, Huang, Liao and Shu. This is an open-access article distributed under the terms of the Creative Commons Attribution License (CC BY). The use, distribution or reproduction in other forums is permitted, provided the original author(s) and the copyright owner(s) are credited and that the original publication in this journal is cited, in accordance with accepted academic practice. No use, distribution or reproduction is permitted which does not comply with these terms.

Autosomal dominant chronic mucocutaneous candidiasis with STAT1 mutation can be associated with chronic active hepatitis: A case report

Lingling Liu, Yuan Huang, Yi Liao and Sainan Shu*

Department of Pediatrics, Tongji Hospital, Tongji Medical College, Huazhong University of Science and Technology, Wuhan, China

Background: Chronic mucocutaneous candidiasis (CMC) is a heterogeneous primary immunodeficiency disease characterized by chronic or recurrent *Candida* infections of the skin, nails, and mucosa and is mostly associated with STAT1 gain-of-function (GOF) mutation (GOF-STAT1 mutation).
Case presentation: A two-year-old girl was presented with recurrent liver dysfunction, oral candidiasis, acute bronchial pneumonia, and cytomegalovirus infection. Even after a series of treatments, including antifungal voriconazole, nystatin treatment for oral *Candida*, antibiotics against bacterial infection, and bicyclol to protect the liver, the child still exhibited signs of splenomegaly. Although we performed relevant etiological tests on the child and conducted histopathology and electron microscopic examination of the liver, we could not explain the clinical symptoms. So, a genetic test was conducted to clarify the diagnosis. Since the child suffered recurrent fungal infections, we speculated that she had combined immunodeficiency. Therefore we performed high-precision clinical display PLUS detection and found that the transcription factor STAT1 had a heterozygous GOF mutation (*p*. R274W) in its coiled-coil domain.
Conclusion: The clinical manifestations of chronic mucocutaneous candidiasis caused by GOF-STAT1 mutations are complex and range from mild local fungal infections to severe systemic diseases and are sometimes fatal. Clinicians need to be aware of the possibility of this disease in children with recurrent fungal infections for early diagnosis and treatment.

KEYWORDS

chronic mucocutaneous candidiasis, GOF-STAT1 mutation, liver dysfunction, fungal infections, pediatric

Introduction

Chronic mucocutaneous candidiasis (CMC) is a heterogeneous primary immunodeficiency disease which is characterized by recurrent or chronic infections affecting the skin, nails, and oral and genital mucosae caused by Candida species (1). CMC disease (CMCD) refers to primary immunodeficiency without any obvious clinical signs. CMC can be classified as CMC syndrome or CMC disease based on its

clinical manifestations and the mutations involved. This definition, however, is not exact. On the other hand, patients with syndromic CMC have various clinical and infectious symptoms in addition to CMC. Syndromic CMC involves hyper-IgE syndrome (HIES), autoimmune polyendocrinopathy-candidiasis-ectodermal dystrophy (APECED), and caspase recruitment domain-containing protein 9 (CARD9), IL-12Rβ1 and IL-12p40 deficiency, RORγT deficiency, STAT1 gain-of-function (2, 3). CMC's most common genetic cause is gain-of-function mutations in the STAT1 gene (STAT1-GOF); These mutations can lead to defective responses in Type 1 and Type 17 helper T cells (Th1 and Th17) (1). Besides being associated with fungal infections, GOF-STAT1 mutations are linked with autoimmune disorders such as vitiligo, thyroid disease, type I diabetes, psoriasis, and autoimmune hepatitis (AIH). Furthermore, CMC patients are more likely to develop aneurysms and malignancies. Patients with STAT1 functional mutations have a higher incidence of cerebral aneurysms than the healthy population, and CMC may be associated with the clinical manifestation of several primary immunodeficiency diseases (1, 2, 4, 5). As a result, AD STAT1 GOF is now categorized as syndromic CMC.

Here, we presented a CMC patient with liver dysfunction, oral candidiasis, acute bronchial pneumonia, and cytomegalovirus infection. It was a case of AD CMC with STAT1 mutation, and chronic active hepatitis may be related to this special situation.

Case presentation

A two-year-old girl was hospitalized for "hepatic dysfunction and recurring oral candidiasis for more than ten months." She was hospitalized at a local hospital with "bronchitis" at the age of one year and one month, where she was found to have liver dysfunction with ALT and AST levels of 624 U/l and 644 U/l, respectively. Her condition improved after one week of treatment with glutathione and bicyclol. After continuing glutathione and bicyclol for more than one week, the liver enzyme levels returned to normal. At the age of one year and five months, she was treated at a local clinic for approximately three days due to oral candidiasis and poor appetite, and her ALT and AST levels were 1,019 U/L and 898 U/L respectively. She was admitted to the hospital. A liver, gallbladder, pancreas, and spleen ultrasound indicated gallbladder wall edema and splenomegaly. The child was then given anti-infective ceftezole and ganciclovir antiviral therapy. The treatment, however, proved ineffective, and the patient was moved to our hospital. Laboratory tests were performed during hospitalization with the following results: LDH 638 U/L (120–300 U/L), AST 1539 U/L (≤40 U/L), ALT 607 U/L (≤41 U/L), γ-GT 109 U/L (10–71 U/L), total cholesterol 2.52 mmol/L (<5.18), and total bile acid 58.3 μmol/L. There was no obvious coagulation abnormality. Screening for antibodies against hepatitis C virus (HCV), HAV, HEV, HIV, PVB, *Treponema pallidum* (TP), and hepatitis B virus (HBV) were negative; The concentration of Immunoglobulin A was 0.15 g/L (0.11–1.45 g/L), Immunoglobulin G was 8.8 g/L (3.3–12.3 g/L), Immunoglobulin M was 0.79 g/L (0.33–1.75 g/L), Complement C3 was 0.81 g/L (0.65–1.39 g/L), and Complement C4 was 0.23 g/L (0.16–0.38 g/L). The levels of blood ammonia (57 μmol/L) and ceruloplasmin (0.498 g/L), and the results of the lymphocyte subset analysis [T cells, B cells, and natural killer (NK) cells] indicated no significant abnormalities (**Supplementary material Table S1**). The level of anti-CMV-IgM and anti-CMV-IgG was 2.85 AU/ml and 89.74 AU/ml, respectively. IgG antibody against Epstein-Barr virus early antigen and nuclear antigen was <5.0 U/ml and 140.0 U/ml, respectively. The levels of IgG and IgM antibodies against Epstein-Barr virus capsid antigen were 39.2 U/ml and <10.0 U/ml, respectively. The Epstein-Barr virus DNA assay showed 9.08E + 002 copy/ml (0–500 copy/mL). *Mycobacterium tuberculosis* was not cultured either in a solid or liquid medium. The analysis of autoantibodies revealed cytoplasmic antinuclear antibodies as granule 1:100 and anti-liver cytosol-1 antibody (ALC-1) as suspicious, whereas screening for anti-GP210 antibody was weakly positive (**Supplementary material Table S2**). Retest The child was diagnosed with liver dysfunction, oral candidiasis, acute bronchial pneumonia, and cytomegalovirus infection. Liver protection was provided by administering enzyme-lowering (glutathione, bicyclol, magnesium isoglycyrrhizinate) and anti-infective (cefoperazone and sulbactam sodium, voriconazole) substances. Then the child was discharged and was orally administered bicyclol and glutathione tablets to reinforce treatment. For the next four months, liver function was measured in conventional outpatient clinics and was high (ALT: 50 U U/L, AST: 137 U/L). Since the cause for this elevated liver function remained unclear, the child was readmitted to the hospital. Liver biopsy and high-precision clinical display PLUS detection were conducted with the consent of the guardians. Liver perfusion analysis revealed incomplete lobular structure, partial hydrolysis of some hepatocytes, infiltration of a few lymphocytes into the portal area, and mild hyperplasia of the fibers. These observations were consistent with the pathological changes observed in G1S1 chronic hepatitis (**Figure 1**). A liver biopsy under an electron microscope showed that the liver tissue was slightly swollen with a reduced endoplasmic reticulum, slight hyperplasia, expansion of the smooth endoplasmic reticulum, and blurred mitochondrial structures. Most of the hepatocytes showed a slight increase in the number of small lipid droplets in their cytoplasm, with few showing depositions of not many cholestatic pigment particles. The gaps between hepatocyte surfaces were slightly wider, and a few capillary bile ducts were somewhat dilated and cholestatic. Hepatic stellate cells

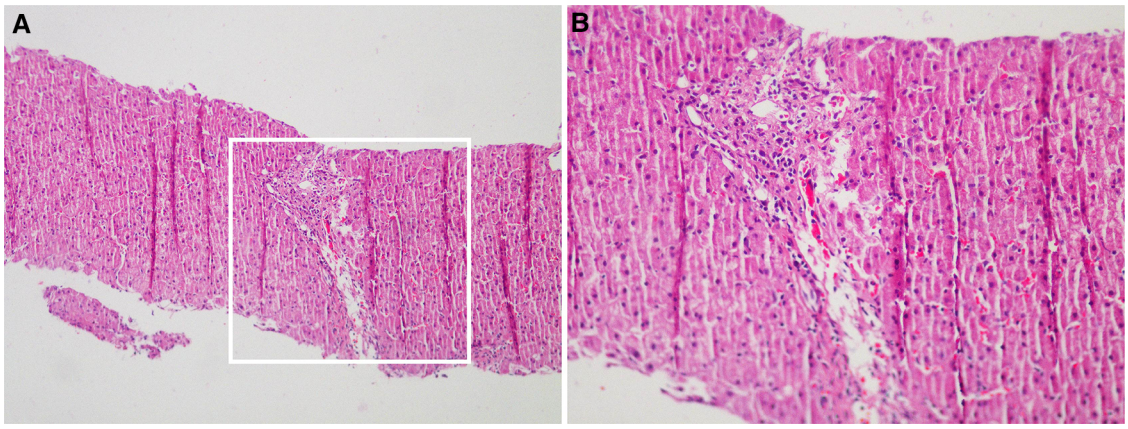


FIGURE 1
Liver perfusion analysis revealed incomplete lobular structure, partial hydrolysis of some hepatocytes, infiltration of a few lymphocytes into the portal area, and mild hyperplasia of the fibers. These observations were consistent with the pathological changes observed in G1S1 chronic hepatitis (**A**): Original magnification: 100×; (**B**): Original magnification: 200×).

were prominent in the Disse cavity, and focal bundles of collagen fibers were deposited. Kupffer cells were observed in the hepatic sinusoids with no portal area (**Figure 2**). High-precision clinical display PLUS detection revealed a heterozygous GOF mutation (*p*.R274W) in the coiled-coil (CC) domain of the transcription factor STAT1 (**Figure 3**). The legal guardian provided written informed consent to participate in this study.

We monitored the clinical progress of this child for more than three years. After multiple treatments (antifungal voriconazole, nystatin treatment for oral Candida, antibiotics against bacterial infection, and liver protection with bicyclol and glutathione), the child still exhibited splenomegaly. Serial radiological investigations of the chest were conducted (**Figure 4**). We intermittently gave the child glutathione, bicyclol treatment, and oral antifungal therapy during this period. The child's family members were very cooperative with the doctor's treatment and brought her to the hospital regularly for re-examination to evaluate her liver function. Fortunately, the child's condition is stable, with no further clinical progress.

Discussion

STAT1 gene mutation has been linked to several diseases. Inborn errors of human STAT1 immunity underlie 4 distinct disorders: autosomal recessive (AR) complete STAT1 deficiency, AR partial STAT1 deficiency, autosomal dominant (AD) STAT1 deficiency, and AD STAT1 gain-of-function. Each disease has its own set of clinical manifestations (6). STAT1 immunodeficiency type 31B with mycobacteria and viral infection is autosomal recessive, whereas the others are autosomal dominant. The STAT1 GOF phenotype is listed as Immunodeficiency 31C in the Online Mendelian Inheritance in Man and displays an autosomal-dominant inheritance pattern. These disorder clinical manifestations include primarily respiratory infections, immunodeficiency, and recurring infections with bacteria and other pathogens (5, 7, 8). STAT1 is the target of hereditary loss-of-function (LOF) or GOF mutations producing different clinical phenotypes. Patients with autosomal dominant STAT1- LOF mutations are infected with mycobacteria, whereas those with autosomal recessive STAT1 LOF mutations are prone to mycobacterial and viral infections, although the susceptibility to viral infection is not high. These mutations reflect the failure of interferon (IFN)-γ and IFN-α/βmediated immunity (4, 6, 9).

GOF-STAT1 mutations are associated with CMC, as reported by Liu et al. (4). STAT1 mutations strongly influence the pathogenesis of immunodeficiency diseases. Depner et al. (10) showed that GOF-STAT1 mutation attenuates the dephosphorylation of active STAT1 protein, leading to the accumulation of phosphorylated STAT1 in the nucleus. Sustained activation of STAT1 can alter the function of STAT1-dependent interleukin (IL)-17 inhibitors and inhibit the STAT3-induced differentiation of IL-17 T cells. GOF-STAT1 mutations lead to defects in the differentiation of Th17 T cells, which is characterized by decreased production of IL-17 and IL-22 (11). Since IL-17 and IL-22 play important antifungal roles in the skin and mucosa, GOF-STAT1 mutations might increase the susceptibility of CMC patients to fungal infection (12).

Using high-precision clinical display PLUS detection, genetic testing of the child revealed a heterozygous variation in the STAT1 gene: c.820C > T (*p*.R274W). Sequencing of the patient's mother and father simultaneously showed that this

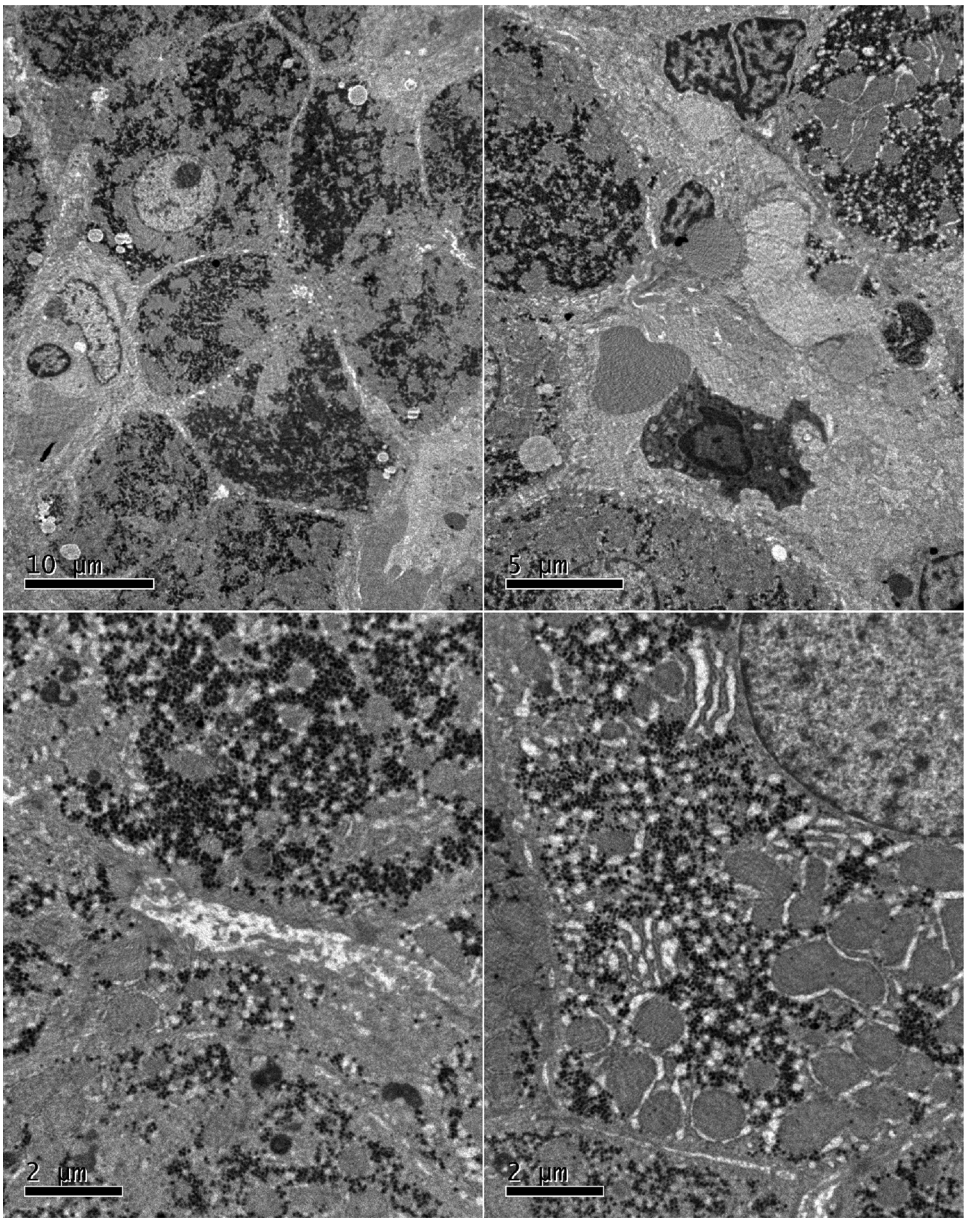


FIGURE 2
A liver biopsy under an electron microscope showed that the liver tissue was slightly swollen with a reduced endoplasmic reticulum, slight hyperplasia, expansion of the smooth endoplasmic reticulum, and blurred mitochondrial structures. Most of the hepatocytes showed a slight increase in the number of small lipid droplets in their cytoplasm, with few showing depositions of not many cholestatic pigment particles. The gaps between hepatocyte surfaces were slightly wider, and a few capillary bile ducts were somewhat dilated and cholestatic. Hepatic stellate cells were prominent in the Disse cavity, and focal bundles of collagen fibers were deposited. Kupffer cells were observed in the hepatic sinusoids with no portal area.

variation was inherited from the mother. The mutations affect the coiled-coil domain and impair the nuclear dephosphorylation that activates STAT1, which is related to their functional gain and advantage (4, 13, 14). Other harmful mutations at the same amino acid location (*p*.R274G, *p*.R274Q) have been reported in related clinical cases (5, 15). This mutation is not found in any population genetic database. The mutation-containing region of STAT1 is a key component whose amino acid sequence is highly conserved across species. According to the computer-aided study, this mutation most likely affects protein structure/function. The reports on the patient's clinical symptoms, the sequence analysis of her family, and the American College of Medical Genetics and Genomics (ACMG) published standards and

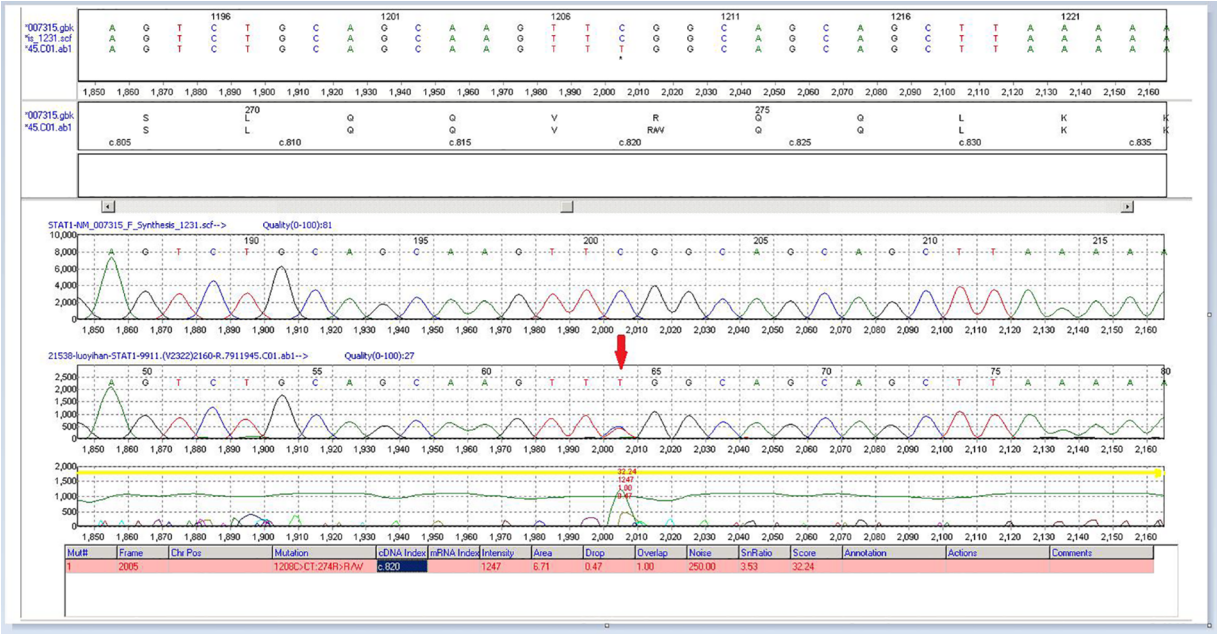


FIGURE 3
High-precision clinical display PLUS detection revealed a heterozygous GOF mutation (*p*.R274W) in the CC domain of the transcription factor STAT1.

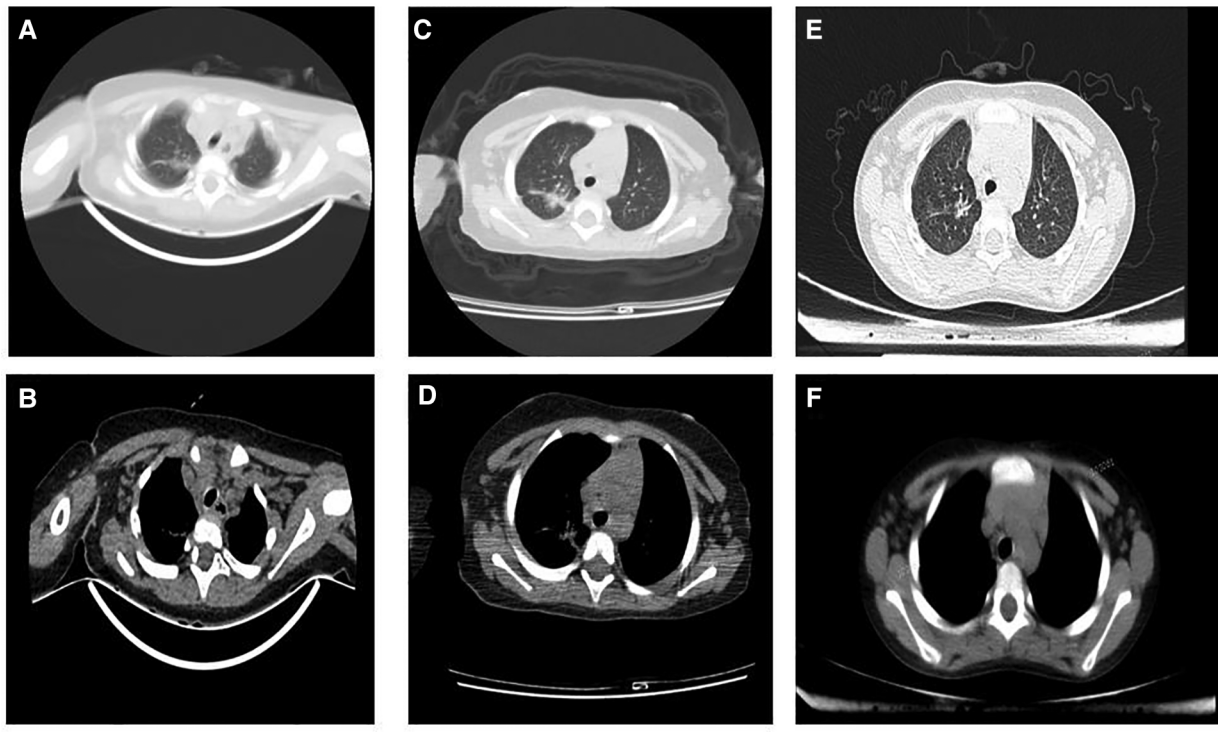


FIGURE 4
Serial radiologic investigations of the chest. (**A and B**): 2018.08.16 Infection in the upper middle lobe of the right lung, increased bilateral axillary lymph nodes. (**C** and **D**): 2019.01.17 Infection in the upper lobe of the right lung and lower lobe of both lungs, the lesions in the upper lobe of the right lung were slightly larger than before (2018-08-16); bilateral axillary lymph nodes increased. (**E** and **F**): 2021.08.16 The transparency of both lungs is uneven, considering the possibility of bronchiolitis, please combine the clinical; Mediastinal lymph node enlargement.

guidelines for interpreting sequence variants (16) suggested that this variant was the cause of the disease. Besides developing chronic fungal infections, children can also develop chronic active hepatitis. Chronic active hepatitis is a rare complication with unknown pathogenesis. It might be related to viral infection, increased inflammatory cytokines and/or mutations (15–17). Clinical hepatitis caused by HCMV is relatively rare in immunocompromised populations; however, hepatitis is a well-known manifestation of HCMV infection in immunocompromised hosts, especially in liver transplant patients. The exact mechanism by which HCMV induces hepatitis is not fully established. People think that an inflammatory response with sustained cytokines (i.e., IL-17, IFN-γ, and TNF) release appear to be the dominant liver mechanism (17). Mutations in GOF-STAT1 lead to enhanced IFN-γ-induced gene expression but also impair the IFN-γ restimulation response (8). IFN-γ was higher in patients with various forms of fulminant hepatic failure. IFN-γ- strongly induces IL-18BP, which can buffer IL-18 activity in the liver through negative feedback. Excessive IL-18 immunity may be the pathogenic mechanism of fulminant liver failure (18, 19). Therefore, we speculate that viral infection and GOF-STAT1 gene mutation are involved in the pathogenesis of chronic hepatitis in children. In a study by Hori et al. a patient with chronic hepatitis also had a mutation in the same amino acid residue as that observed in our patient (*p*.R274Q) (16), indicating the contribution of specific STAT1 gene mutations (e.g., *p*.R274Q or *p*.R274W) to disease pathogenesis.

The clinical manifestations of CMC caused by GOF-STAT1 mutations are complex and range from mild local fungal infections to severe systemic diseases. Since CMC is an immunodeficiency disease, it is mainly treated with bone marrow transplantation, which allows the patients to develop cellular immunity against fungal infections, thus alleviating the clinical symptoms. Although bone marrow transplantation is not a routine treatment for CMC, it is effective, with successful cases reported in some studies (16, 20). However, bone marrow transplantation is limited by immune rejection. Additionally, since the relationship between genotype and clinical manifestation is not clear, determining the indications and best treatment options for bone marrow transplantation might be challenging. However, bone marrow transplantation might be the last resort for CMC patients receiving antifungal drugs with a poor prognosis, but further studies are needed to determine its effectiveness.

Data availability statement

The datasets presented in this study can be found in online repositories. The names of the repository/repositories and accession number(s) can be found in the article/ **Supplementary Material**.

Ethics statement

Written informed consent was obtained from the minor(s)' legal guardian/next of kin for the publication of any potentially identifiable images or data included in this article.

Author contributions

Analyzed and interpreted the data: LLL, YH, YL, SNS. Wrote the paper: LLL, SNS. All authors contributed to the article and approved the submitted version.

Acknowledgments

Thanks to editeg for editing and proofreading this manuscript.

Conflict of interest

The authors declare that the research was conducted in the absence of any commercial or financial relationships that could be construed as a potential conflict of interest.

Publisher's note

All claims expressed in this article are solely those of the authors and do not necessarily represent those of their affiliated organizations, or those of the publisher, the editors and the reviewers. Any product that may be evaluated in this article, or claim that may be made by its manufacturer, is not guaranteed or endorsed by the publisher.

Supplementary material

The Supplementary Material for this article can be found online at: https://www.frontiersin.org/articles/10.3389/fped.2022.990729/full#supplementary-material.

References

1. Carey B, Lambourne J, Porter S, Hodgson T. Chronic mucocutaneous candidiasis due to gain-of-function mutation in STAT1. *Oral Dis*. (2019) 25 (3):684–92. doi: 10.1111/odi.12881

2. Okada S, Puel A, Casanova J, Kobayashi M. Chronic mucocutaneous candidiasis disease associated with inborn errors of IL-17 immunity. *Clin Transl Immunology*. (2016) 5(12):e114. doi: 10.1038/cti.2016.71

3. Humbert L, Cornu M, Proust-Lemoine E, Bayry J, Jean-Louis W, Vantyghem MC, et al. Chronic mucocutaneous candidiasis in autoimmune polyendocrine syndrome type 1. *Front Immunol*. (2018) 9:2570. doi: 10.3389/fimmu.2018.02570

4. Liu L, Okada S, Kong X, Kreins A, Cypowyj S, Abhyankar A, et al. Gain-of-function human STAT1 mutations impair IL-17 immunity and underlie chronic mucocutaneous candidiasis. *J Exp Med*. (2011) 208(8):1635–48. doi: 10.1084/jem.20110958

5. Sampaio EP, Hsu AP, Pechacek J, Bax HI, Dias DL, Paulson ML, et al. Signal transducer and activator of transcription 1 (STAT1) gain-of-function mutations and disseminated coccidioidomycosis and histoplasmosis. *J Allergy Clin Immunol*. (2013) 131(6):1624–34. doi: 10.1016/j.jaci.2013.01.052

6. Mizoguchi Y, Okada S. Inborn errors of STAT1 immunity. *Curr Opin Immunol*. (2021) 72:59–64. doi: 10.1016/j.coi.2021.02.009

7. Okada S, Asano T, Moriya K, Boisson-Dupuis S, Kobayashi M, Casanova J, et al. Human STAT1 gain-of-function heterozygous mutations: chronic mucocutaneous candidiasis and type I interferonopathy. *J Clin Immunol*. (2020) 40(8):1065–81. doi: 10.1007/s10875-020-00847-x

8. Consonni F, Dotta L, Todaro F, Vairo D, Badolato R, et al. Signal transducer and activator of transcription gain-of-function primary immunodeficiency/immunodysregulation disorders. *Curr Opin Pediatr*. (2017) 29(6):711–7. doi: 10.1097/MOP.0000000000000551

9. Boisson-Dupuis S, Kong XF, Okada S, Cypowyj S, Puel A, Abel L, et al. Inborn errors of human STAT1: allelic heterogeneity governs the diversity of immunological and infectious phenotypes. *Curr Opin Immunol*. (2012) 24 (4):364–78. doi: 10.1016/j.coi.2012.04.011

10. Depner M, Fuchs S, Raabe J, Frede N, Glocker C, Doffinger R, et al. The extended clinical phenotype of 26 patients with chronic mucocutaneous candidiasis due to gain-of-function mutations in STAT1. *J Clin Immunol*. (2016) 36(1):73–84. doi: 10.1007/s10875-015-0214-9

11. Puel A, Cypowyj S, Bustamante J, Wright JF, Liu LY, Lim HK, et al. Chronic mucocutaneous candidiasis in humans with inborn errors of interleukin-17 immunity. *Science*. (2011) 332(6025):65–8. doi: 10.1126/science.1200439

12. McDonald DR. TH17 Deficiency in human disease. *J Allergy Clin Immunol*. (2012) 129(6):1429–35.; quiz 1436-7. doi: 10.1016/j.jaci.2012.03.034

13. van de Veerdonk FL, Plantinga TS, Hoischen A, Smeekens SP, Joosten L, Gilissen C, et al. STAT1 Mutations in autosomal dominant chronic mucocutaneous candidiasis. *N Engl J Med*. (2011) 365(1):54–61. doi: 10.1056/NEJMoa1100102

14. Zheng J, van de Veerdonk FL, Crossland K, Smeekens S, Chan CM, Shehri TA, et al. Gain-of-function STAT1 mutations impair STAT3 activity in patients with chronic mucocutaneous candidiasis (CMC). *Eur J Immunol*. (2015) 45 (10):2834–46. doi: 10.1002/eji.201445344

15. Manns MP, Manns MP, Czaja AJ, Gorham JD, Krawitt EL, Mieli-Vergani G, et al. Diagnosis and management of autoimmune hepatitis. *Hepatol*. (2010) 51 (6):2193–213. doi: 10.1002/hep.23584

16. Hori T, Ohnishi H, Teramoto T, Tsubouchi K, Naiki T, Hirose Y, et al. Autosomal-dominant chronic mucocutaneous candidiasis with STAT1-mutation can be complicated with chronic active hepatitis and hypothyroidism. *J Clin Immunol*. (2012) 32(6):1213–20. doi: 10.1007/s10875-012-9744-6

17. Da Cunha T, Wu GY. Cytomegalovirus hepatitis in immunocompetent and immunocompromised hosts. *J Clin Transl Hepatol*. (2021) 9(1):106–15.

18. Belkaya S, Michailidis E, Korol CB, Kabbani M, Cobat A, Bastard P, et al. Inherited IL-18BP deficiency in human fulminant viral hepatitis. *J Exp Med*. (2019) 216(8):1777–90. doi: 10.1084/jem.20190669

19. Jouanguy E. Human genetic basis of fulminant viral hepatitis. *Hum Genet*. (2020) 139(6-7):877–84. doi: 10.1007/s00439-020-02166-y

20. Aldave JC, Cachay E, Núñe L, Chunga A, Murillo S, Cypowyj S, et al. A 1-year-old girl with a gain-of-function STAT1 mutation treated with hematopoietic stem cell transplantation. *J Clin Immunol*. (2013) 33(8):1273–5. doi: 10.1007/s10875-013-9947-5

frontiers | Frontiers in Genetics

TYPE Case Report
PUBLISHED 13 January 2023
DOI 10.3389/fgene.2022.970204

Check for updates

OPEN ACCESS

EDITED BY
Ruth Roberts,
ApconiX, United Kingdom

REVIEWED BY
Joshi Stephen,
Human Genome Sequencing Center,
United States
Giuseppe Fiorentino,
Azienda Ospedaliera dei Colli, Italy

*CORRESPONDENCE
Liangliang Jiang,
1025229485@qq.com

SPECIALTY SECTION
This article was submitted to Genetics of Common and Rare Diseases, a section of the journal Frontiers in Genetics

RECEIVED 15 June 2022
ACCEPTED 28 December 2022
PUBLISHED 13 January 2023

CITATION
Bi S, Dai L, Jiang L, Wang L, Teng M, Liu G and Teng R-J (2023), Chronic granulomatous disease associated with Duchenne muscular dystrophy caused by Xp21.1 contiguous gene deletion syndrome: Case report and literature review.
Front. Genet. 13:970204.
doi: 10.3389/fgene.2022.970204

COPYRIGHT
© 2023 Bi, Dai, Jiang, Wang, Teng, Liu and Teng. This is an open-access article distributed under the terms of the Creative Commons Attribution License (CC BY). The use, distribution or reproduction in other forums is permitted, provided the original author(s) and the copyright owner(s) are credited and that the original publication in this journal is cited, in accordance with accepted academic practice. No use, distribution or reproduction is permitted which does not comply with these terms.

Chronic granulomatous disease associated with Duchenne muscular dystrophy caused by Xp21.1 contiguous gene deletion syndrome: Case report and literature review

Shaohua Bi[1], Liying Dai[1], Liangliang Jiang[2]*, Lili Wang[3], Mia Teng[4], Guanghui Liu[1] and Ru-Jeng Teng[4]

[1]Division of Neonatology, Anhui Provincial Children's Hospital, Hefei, Anhui, China, [2]Department of Pediatrics, Anhui Provincial Children's Hospital, Hefei, Anhui, China, [3]First Affiliated Hospital of Anhui Medical University, Hefei, Anhui, China, [4]Department of Pediatrics, Medical College of Wisconsin, Milwaukee, WI, United States

Chronic granulomatous disease (CGD) and Duchenne muscular dystrophy (DMD) are X-linked recessive disorders whose genes are 4.47 Mb apart within Xp21.1. A combination of both diseases is rare with only five cases reported in the literature where it is known as Xp21.1 "contiguous gene deletion syndrome". We describe a male neonate who presented with sepsis at 19 days of age. The diagnosis of CGD with DMD was established through copy number variation sequencing (CNV-seq) with an extensive 7.5 Mb deletion of Xp21.2-Xp11.4 of the proband. One of his elder sisters and his mother are carriers. The deletion includes six known genes: glycerol kinase (*GK*), dystrophin (*DMD*), cilia- and flagella-associated protein 47 (*CFAP47*), gp91 (*CYBB*), Kell antigen (*XK*), and retinitis pigmentosa GTPase regulator (*RPGR*). Laboratory assays revealed an increased creatine kinase (CK) level, decreased gp91 expression, and a positive nitroblue tetrazolium test. Due to the extensive gene deletion and the poor prognosis, the family determined to pursue conservative management without further laboratory workup. The patient passed away from a fulminant infection at the age of three-month at a local medical facility. To the best of our knowledge, this case of Xp21.1 contiguous gene deletion syndrome represents the most extensive deletion of genes in this region ever reported. A literature review of similar cases is presented.

KEYWORDS

chronic granulomatous disease, Duchenne muscular dystrophy, contiguous gene deletion syndrome, neonatal sepsis, hypertriglyceridemia

Introduction

Chronic granulomatous disease (CGD) is a rare primary immune deficiency caused by a defective nicotinamide adenine dinucleotide phosphate (NADPH) oxidase complex. NADPH oxidase is composed of five subunits (gp91phox, p22phox, p47phox, p67phox, p40phox) and the absence of any one subunit can cause the disease (Chiriaco et al., 2016). CGD patients suffer from repeated bacterial and fungal infections due to their phagocytes' inability to generate superoxide through respiratory burst (Warren and Shimada, 2018). CGD's most common genetic defect is a point mutation in the CYBB gene. Most reported CGD cases had either a base

mutation or an intragenic gene deletion (Roos et al., 2021). However, results from sequencing determinations of copy number variations (CNVs) uncovered a few cases identified as having Xp21.1 contiguous deletion syndrome. The clinical manifestations of patients with the Xp21 deletion spectrum can be quite variable. McLeod syndrome (MLS) may coexist if the deletion involves the *XK* gene due to its proximity. MLS patients have XK antigen deficiency, spinous erythrocytosis, and a specific nervous system phenotype (Roulis et al., 2018). Although the *DMD* gene is far from the *CYBB* gene, DMD may also be part of the spectrum if the deletion is extensive enough.

Duchenne muscular dystrophy/Becker muscular dystrophy (DMD/BMD) is one of the most common X-linked recessive genetic muscular diseases, and it also has a poor prognosis. DMD was named for the French neurologist, Guillaume Duchenne (Duchenne, 1867), and it is quite rare with an incidence of about 1 in 3,500 live male births. Typical clinical features of DMD include progressive muscular atrophy, pseudohypertrophy of the gastrocnemius muscle, and a highly elevated blood level of creatine kinase (CK), 50-300 times the normal levels in the early stage of the disease and slowly decreasing with age (Kim et al., 2017). Classical DMD affects mainly adolescent males, who generally lose the ability to stand and walk before their teens. DMD patients often die by their 20s from either heart failure or respiratory failure. This disease is rarely diagnosed in neonates without a targeted genetic test.

Here, we report a neonatal case of CGD combined with DMD diagnosed through a genetic workup. The neonate was transferred to our facility with a severe infection. Flow cytometry showed decreased gp91phox expression. Low-depth whole-genome sequencing of copy number variations (CNV-Seq) showed a ~7.5 Mb deletion in the loci between 21.1 and 11.4 on the short-arm of the X chromosome (Xp). The genetic data established the diagnosis of DMD before the typical increase in the muscle enzyme in the blood and the various disorders that only manifest later in life.

Case presentation

The 19-day-old male neonate was born to a G5P3023 mother via cesarean section due to macrosomia at a gestation of 41^{+1} weeks with a birth weight of 4250 g. Apgar scores were 10 for both 1 and 5 min. After 3 days of broad-spectrum antibiotic treatment, the neonate was transferred to our hospital under the impression of neonatal sepsis without improvement. The blood culture from the referring hospital did not identify the pathogen. Physical examination upon admission showed a rectal temperature of 38.1°C, but the patient appropriately responded to stimulation. He had a soft and flat anterior fontanelle, mild tachypnea with clear air entry, a heart rate of 145 beats/min, no hepatosplenomegaly, full range of motion of all four limbs, and normoactive bowel sound. A laboratory test showed a white blood cell count of 33.24×10^9/L with 71% neutrophils, a hemoglobin of 143 g/L, platelet count of 322×10^9/L, and C-reactive protein (CRP) of 133.84 mg/L. Biochemical assays showed an alanine aminotransferase (ALT) of 124.2 U/L, aspartate aminotransferase (AST) of 137.5 U/L, and an abnormally high triglyceride level of 8.66 mmol/L (0.68–1.69 mmol/L). The blood culture upon admission was also negative, probably due to antibiotic treatment before the transfer. The creatine kinase (CK) level was 1115 IU/L (0–210 IU/L) which was high, but typical for DMD patients, who usually have a CK above 2,000 IU/L. Abdominal ultrasound demonstrated several hypoechoic areas within the liver compatible with liver abscess. The two large foci were measured as 2.5 cm × 2.5 cm x 2.0 cm at 3.5 cm below the rib and 1.4 cm × 1.3 cm x 1.2 cm at 3.8 cm below the xiphoid process (Figure 1A). Chest CT showed multiple nodules in both lung fields with cavity formation compatible with lung abscess (Figure 1B). The neutrophil respiratory burst test and the quantitative $gp91^{phox}$ protein flow cytometry confirmed the diagnosis of CGD (Figure 1C). No abnormality was found in echocardiography or eye examination.

Informed consent for genetic testing was obtained from both parents, and the study was conducted according to the declaration of Helsinki and approved by the medical ethics committee of Anhui Children's Hospital. CNV-seq was used for its faster turnaround time, availability, and reasonable cost in our region. Blood was obtained from the proband and his family through venipuncture. Genomic DNA was extracted from mononuclear white cells using a human genomic DNA extraction kit (Qiagen, Hilden, Germany). DNA was extracted from K_2-EDTA-treated venous blood using the TIANamp blood DNA kit (#DP348-03). The integrity of the extracted DNA was evaluated by electrophoresis on 2% agarose. DNA specimens with OD 260/280 between 1.8 and 2.0, concentrations above 20 ng/μL, and amounts >500 ng were used to prepare the DNA library with a Hieff NGS® OnePot DNA Library Prep Kit for Illumina® (#12205ES24, Yeasen Biotechnology, Shanghai, PRC), according to the provided protocol. Magnetic beads were used to purify the amplified PCR products before Nextseq500 sequencing using the SE150 mode. The readouts in FASTQ format that passed the quality assurance test were then compared to reference data and aligned using Bowtie 2 into BAM files. The Picard tools were employed to obtain the mapping ratio to remove the repeated sequences generated by PCR. The processed sequences were used for analysis by the CNV kit with the pipeline for the BAM files according to the predetermined bin size. Gene fragments with normal chromosome number and size less than 100 KB were used to compare against available databases. The total sequencing data amounted to 1.03 Gb, with 7,815,225 reads, and an average genome sequencing depth of about 0.3x. Mutations were identified by comparison with available databases (dbSNP at www.ncbi.nlm.nih.gov/snp/; ExAC at www.exac.broadinstitute.org/; 1000 genomes at www.1000genomes.org/) and performing a hazard prediction analysis on the reliable variation spectrum by filtering out invalid mutations (SIFT at https://sift.bii.a-star.edu.sg/; PolyPhen-2 at http://genetics.bwh.harvard.edu/pph2/; MutationTaster at www.mutationtaster.org/). The mutations were rated according to the ACMG pathogenicity criteria (Richards et al., 2015). The software detected the off-line data, analyzed the genes contained in the CNV interval, judged the microdeletions/duplications in the sample data, and associated them with the DECIPHER database (www.decipher.sanger.ac.uk/), dbVar database (www.bigd.big.ac.cn/databasecommons), DGV database (http://dgv.tcag.ca/dgv/app/home), ClinGen (https://www.clinicalgenome.org/), OMIM database (www.omim.org), and other public databases.

The genetic analysis showed the deletion of a 7.5 Mb fragment of chromosome Xp21 between p21.2 and p11.4 (Chr X: 30577566-38080045, SEQ [grch37] del Xp21.2-p11.4) in the proband (Figure 2). One of his older sisters and his mother were heterozygous for the same deletion (Figure 3). The DECIPHER database contains many pathogenic CNVs within this region of the X-chromosome, including six OMIM disease entities such as the *GK* gene that is associated with glycerol kinase deficiency (*GKD*, OMIM

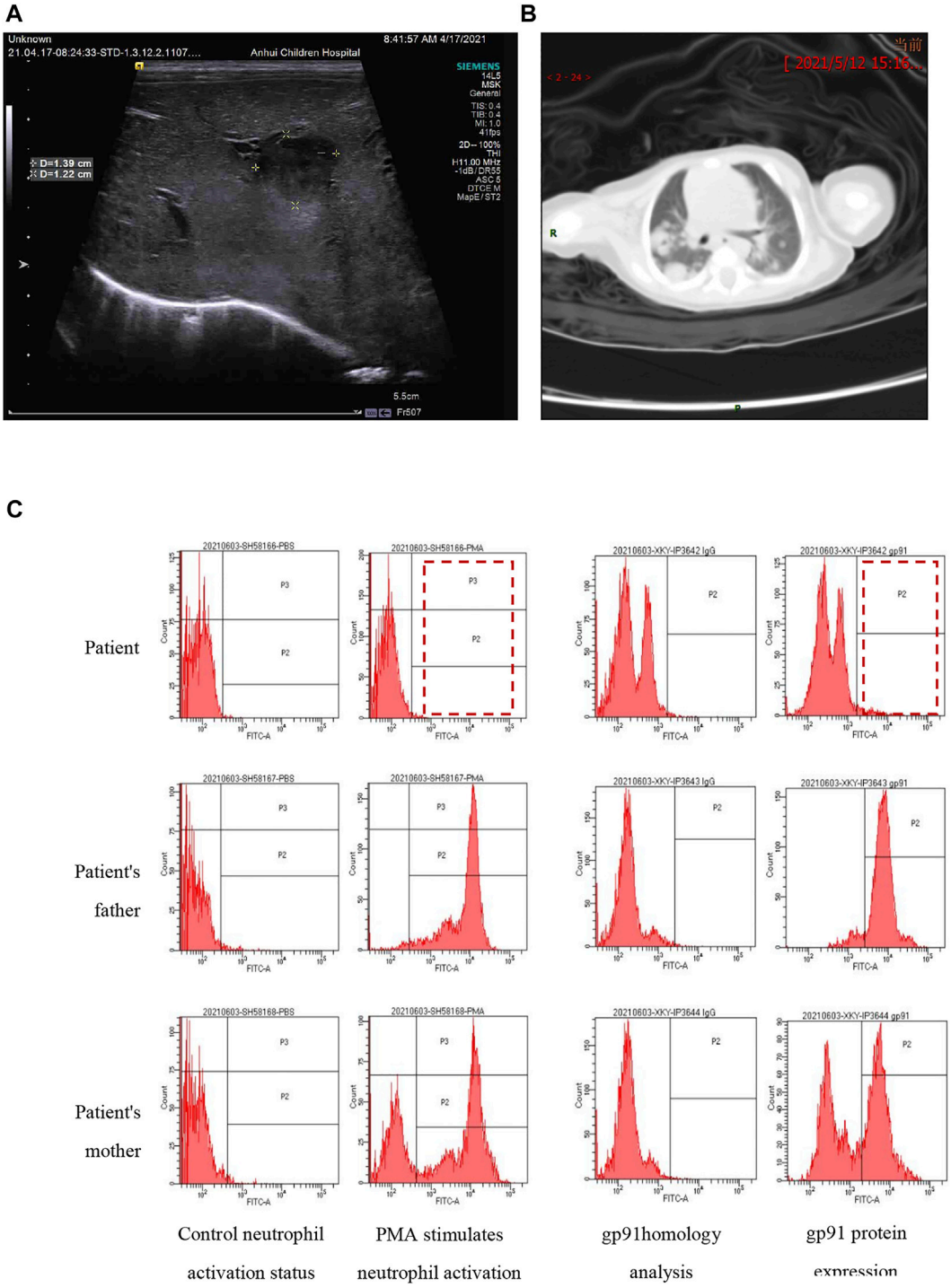


FIGURE 1
The images show suspected liver abscesses **(A)** and lung abscesses **(B)**. The neutrophil respiratory burst test **(C)** was performed by flow cytometry. The left panel shows neutrophil activation by phorbol 12-myristate 13-acetate (PMA). The father had normal activation with a single peak in zone P2 and P3 (>90% activation), while the proband had no activation (1.5%), and the mother had two activation peaks (62.7%). The right panel shows gp91phox expression: 4.6% in the proband, 51.7% in the mother, and >90% in the father. The results indicate that the proband is a case of CGD while his mother is a carrier.

#307030); the *DMD* gene that is associated with DMD (*DMD*, OMIM #310200); the *CFAP47* gene that is associated with X-linked spermatogenic failure (*SPGFX3*, OMIM#301059); the *XK* gene that is associated with McLeod syndrome with or without CGD (*MLS*, OMIM #300842); the *CYBB* gene that is associated with X-linked CGD (*CGDX*, OMIM #306400); and the *RPGR* gene that is associated with retinitis pigmentosa (RP3, OMIM#312610).

After admission, the neonate was treated empirically with broad-spectrum antibiotics. His body temperature stabilized after 1 day of treatment, and the blood assay results and CRP gradually normalized.

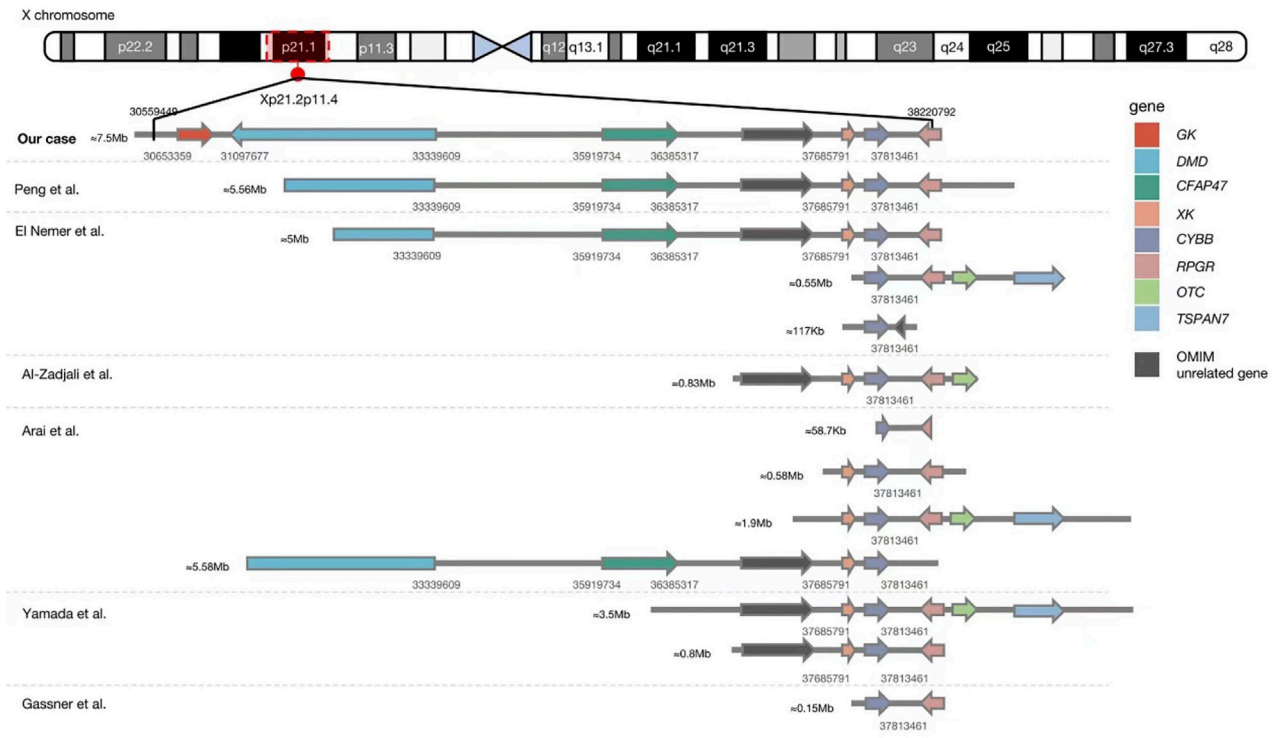


FIGURE 2
Comparison between our case and previously reported Xp21.1 contiguous gene deletion syndrome with known deletion sites. The detailed genetic data of eight cases in one case series reported by Lhomme et al. (Lhomme et al., 2020) (8/8 with McLeod phenotype, 2/8 with DMD, and 1/4 with retinitis pigmentosa) are unavailable, so they cannot be aligned in this figure. Our patient had the most extensive gene deletion of ~7.5 Mb involving six genes with known phenotypes and a gene of unknown significance.

The liver abscess resolved after two weeks of antibiotics based on ultrasound imaging. Chest CT revealed that the multiple nodules in both lungs associated with lung abscesses were also decreased in size after antibiotics. The infant was discharged home two months later. After an extensive multidisciplinary care conference with the family, the decision was made to pursue conservative medical management due to the anticipated poor long-term outcome. The family refused further workup to confirm the other disorders associated with the extensively deleted chromosome. Unfortunately, the infant passed away 1 month after discharge at a local medical facility.

Discussion

We report a rare case of Xp21.1 contiguous gene deletion syndrome (Chr X: 30577566-38080045; SEQ [grch37] del Xp21.2-p11.4), confirmed by CNV-seq, presenting as a neonatal infection involving both liver and lungs. The mother and one of the older sisters are heterozygous for the same deletion. The 7.5 Mb deletion is the most extensive compared to the reported cases (Table 1). A positive respiratory burst test, a reduced gp91^{phox} expression, and genetic sequencing confirmed the diagnosis of CGD. The atypical elevation in serum CK level in a genetically confirmed case of DMD can be explained by the limited muscle damage early in life and indicates that the borderline CK level is not a useful biomarker during early infancy to diagnose DMD.

CGD is a rare immune deficiency disorder caused by an inability to generate superoxide anion due to defective NADPH oxidase activity (NOX2). CGD patients are prone to repeated bacterial infections with typical pathogens, including *Staphylococcus aureus*, *Burkholderia cepacia*, *Aspergillus* spp, and *Serratia marcescens* (Segal et al., 2000; Winkelstein et al., 2000; Dekkers et al., 2008). Most CGD patients are diagnosed after 1 year (Hou et al., 2019). The main clinical manifestations are repeated and severe organ infections, including lungs, lymph nodes, liver, and skin. Occasionally CGD can present as a cardiac abscess or phlebitis, complicating the diagnosis, especially in neonates (Song et al., 2014). The most common type of CGD (~66%) is caused by a mutation on Xp21 involving the *CYBB* gene. According to the literature, the pathology in less than 1% of CGD patients is caused by the contiguous gene deletion syndrome (Roos et al., 2021). The database of our region is not available for comparison.

Compared with simple CGD, the deletion of larger fragments around the *CYBB* gene can lead to a more complex phenotype. DMD is a neuromuscular disease caused by the deletion or mutation of the *DMD* gene on Xp21 (Maggio et al., 2016) and usually presents after childhood with patients developing respiratory failure or heart failure by the age of 20. There is no clear clinical manifestation in DMD neonates, so the diagnosis is rarely established during this period. Although the CPK level was abnormally high in our case, it was not typical for DMD, in which the CPK level is usually above 2,000 at diagnosis. The lack of muscle damage can explain the lack of clinical manifestation of DMD early in life and why the CPK level was not in

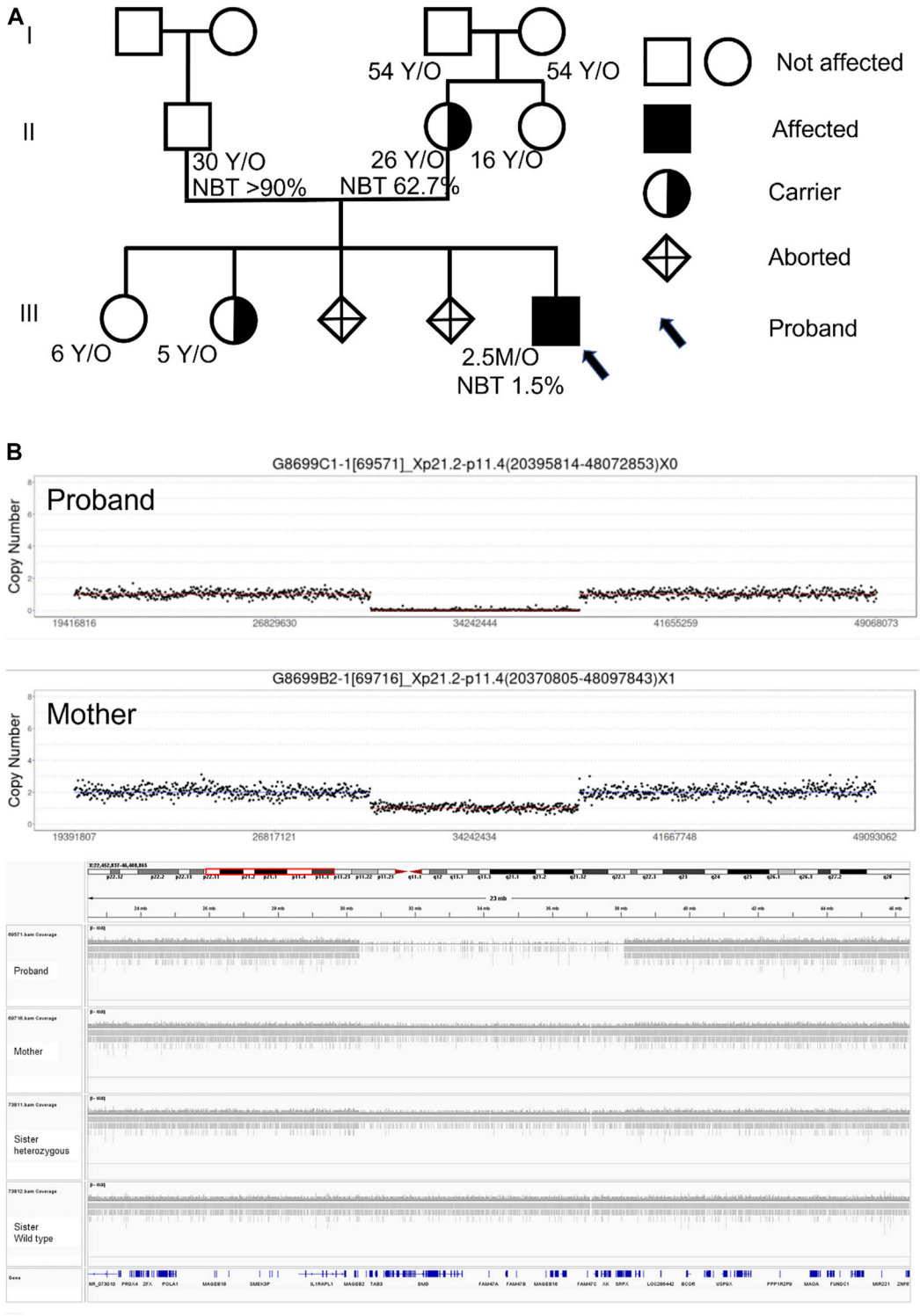


FIGURE 3
(A) Pedigree, nitroblue tetrazolium test (NBT), and genetic test results of family members. All four grandparents and the father have no Xp21.2-11.4 deletion, but the mother and one older sibling are carriers. **(B)** CNV-seq results of the proband and his mother.

the DMD range in our case. We could not confirm the diagnosis of DMD without performing the genetic test.

Our case had four other known genes deleted. The most commonly associated *XK* gene deletion in males may lead to MLS presenting as a slowly progressive disorder that primarily involves the central/peripheral nervous system, heart, and immune system, mimicking symptoms of Huntington's disease, accompanied by cognitive decline and mental disorders. The average age of onset of the MLS is between 30 and 40 years (Jung et al., 2007; Gassner et al., 2017). The *XK* gene encodes a complex Kell blood group on the

TABLE 1 Age of onset, initial clinical manifestation, and genetic information of reported cases.

Reported	Age of onset	Initial clinical manifestations	Inheritance	Genes involved in the report	Deletion site	Deletion size	References
Our case	19 D/O	Neonatal infection, liver and lung abscess	Inherited	GK, **DMD**, CFAP47, XK, CYBB, RPGR	Xp21.2-Xp11.4	~7.5 Mb	-
Gassner et al	10Y/O	pulmonary aspergillosis	*De novo*	CYBB, RPGR	N/A	~0.15 Mb	15
Lhomme et al	1.2 Y/O	Pneumonia	*De novo*	XK, CYBB	Xp21.1-Xp21.4	210 Kb	17
	3.9 Y/O	Pneumonia	Inherited	XK, CYBB	N/A	N/A	
	1 M/O	Adenitis	*De novo*	XK, CYBB	N/A	N/A	
	6 M/O	Adenitis	Inherited	**DMD**, XK, CYBB	Xp21, complete	5.5 Mb	
	1.2 Y/O	Liver abscess	*De novo*	XK, CYBB	N/A	3.75 Mb	
	2 M/O	Adenitis	Inherited	XK, CYBB	N/A	N/A	
	2.6 Y/O	Adenitis	Inherited	XK, CYBB	N/A	N/A	
	1.5 Y/O	Osteomyelitis	Inherited	XK, CYBB	N/A	1.3 Mb	
Peng et al	4M/O	Skin infection	Inherited	**DMD**, CFAP47, XK, CYBB, RPGR	N/A	~5.56 Mb	22
El Nemer et al	N/A	N/A	N/A	**DMD**, CFAP47, XK, CYBB, RPGR	N/A	~5 Mb	23
	N/A	N/A	N/A	CYBB, RPGR, OTC, TSPAN7	N/A	~0.55 Mb	
	N/A	N/A	N/A	CYBB	N/A	117 Kb	
Al-Zadjali et al	10Y/O	Pyoderma, chest infections, gluteal abscess, bowel granuloma	Inherited	XK, CYBB, RPGR, OTC	N/A	~0.83 Mb	24
Arai et al	N/A	N/A	N/A	CYBB, RPGR	N/A	58.7 Kb	25
	N/A	N/A	N/A	XK, CYBB, RPGR	N/A	~0.59 Mb	
	N/A	N/A	N/A	XK, CYBB, RPGR, OTC, TSPAN7	N/A	~1.94 Mb	
	N/A	N/A	N/A	**DMD**, CFAP47, XK, CYBB	N/A	~5.71 Mb	
Yamada et al	3Y/O	Perianal abscesses, lymphadenitis	*De novo*	XK, CYBB, RPGR, OTC, TSPAN7	N/A	~3.5 Mb	26
	20Y/O	Perianal abscesses	Inherited	XK, CYBB, RPGR	N/A	0.8 Mb	

N/A: not described in the reports.

10.3389/fgene.2022.970204

erythrocyte membrane resulting in echinocytosis and hemolysis (Yu et al., 2001; Lhomme et al., 2020). Due to the proximity of genes, some MLS patients can present with CGD, chronic hemolysis, or neuromuscular symptoms after infancy (Roulis et al., 2018; Lhomme et al., 2020).

Pseudo-hypertriglyceridemia secondary to high glycerol blood levels has been described in *GK* deletion (Zaffanello et al., 2004). One of the manifestations of *GK* deletion is a high glycerol level in urine which may help establish the diagnosis (Wikiera et al., 2021). Cryptorchidism and strabismus are two of the most common clinical signs of *GK* deletion, which were not seen in our case. Our case had hypertriglyceridemia, but we did not have the opportunity to verify whether it was due to high glycerol levels in the blood.

The *RPGR* deletion has been reported as one type of retinitis pigmentosa (Cehajic-Kapetanovic et al., 2020). The proximity of the *RPGR* genes and the *CYBB* gene makes it a common co-existing disorder (11/16) (El Nemer et al., 2000; Peng et al., 2007; Yamada et al., 2010; Arai et al., 2012; Al-Zadjali et al., 2015; Gassner et al., 2017; Lhomme et al., 2020). In our case, X-linked retinitis pigmentosa, cone-rod dystrophy, and primary ciliary dyskinesia secondary to the *RPGR* gene mutation may manifest later in life. The *CFAP47* deletion can cause male infertility (Liu et al., 2021). Although these problems will not be present during infancy, they are critical for genetic counseling.

Our literature search has identified only seven reports of Xp21.1 contiguous gene deletion syndrome, including twenty patients with a deletion involving the *CYBB* gene (El Nemer et al., 2000; Peng et al., 2007; Yamada et al., 2010; Arai et al., 2012; Al-Zadjali et al., 2015; Gassner et al., 2017; Lhomme et al., 2020). The age of clinical presentation, initial clinical manifestation, and genetic information of the reported cases are summarized in Table 1. The lack of proper molecular technology prevented us from identifying cases before the year 2000. The range of chromosome deletion was between 58.7 Kb and 5.56Mb, with an average of 2.22 Mb (Figure 2). It is worth noting that the distance between the *CYBB* and *XK* genes is only 47 Kb which explains why 80% of reported patients (16/20) had both *CYBB* and *XK* gene deletions. Although some patients did not show neurological problems, almost all had hematological changes due to erythrocyte Kell blood group antigen reduction. The distance between *CYBB* and *DMD* genes is about 4.47Mb, so only six cases (including ours) had both manifestations. Without the genetic test, we would not have been able to detect the co-existence of DMD in our CGD patient, who was brought to us during his early infancy.

It is crucial to pursue an extensive genetic analysis, if possible, to detect other gene deletions in the Xp21 segment in neonatal patients with CGD (Lhomme et al., 2020). This is especially critical because the future male offspring have a 50% chance of being affected, while 50% of the female offspring will be carriers with variable degrees of presentation. The whole family genetic screening showed that the mother was the one with the *de novo* mutation, and one of the older sisters was identified as a carrier (Figure 3). The neighboring genes cover many complex phenotypes that will not manifest early in life. However, their involvement can be challenging for long-term management and genetic counseling. Other than the initial presentation as CGD, knowledge of the associated problems like muscular dystrophy, hemolytic risk, hypertriglyceridemia, blindness, and long-term neurological morbidities is essential for the family to make the appropriate decisions. Although bone marrow transplantation is a promising treatment for CGD (Lhomme et al., 2020), the extensive gene deletion in our case painted a grim picture for the family and influenced the decision whether or not to pursue aggressive management.

In conclusion, we reported a newborn patient with CGD complicated with multiple disorders due to an extensive deletion involving Xp21.2-Xp11.4. The ~7.5 MB fragment deletion is the most extensive ever reported. The co-existence of CGD and glycerol kinase deficiency has not been reported in the literature. We understand the limitation of using CNV-seq to identify the genetic changes in our index case, but the availability and the short turnaround time led us to adopt this method. The death of the baby in early infancy prevented us from observing other clinical manifestations, and this case report emphasizes the importance of genetic analysis in patients with early onset CGD.

Data availability statement

The datasets for this article are not publicly available due to concerns regarding participant/patient anonymity. Requests to access the datasets should be directed to the corresponding author.

Ethics statement

Written informed consent was obtained from the (individual(s) AND/OR minor(s)' legal guardian/next of kin) for the publication of any potentially identifiable images or data included in this article.

Author contributions

SB, LJ, and R-JT drafted the manuscript. SB and MT reviewed the medical records. LD, LW, GL, and R-JT revised the manuscript. SB, LJ, and R-JT finalized the manuscript.

Funding

The support came from Anhui Provincial children's Hospital, and the Internal Support of Department of Pediatrics, Medical College of Wisconsin.

Conflict of interest

The authors declare that the research was conducted in the absence of any commercial or financial relationships that could be construed as a potential conflict of interest.

Publisher's note

All claims expressed in this article are solely those of the authors and do not necessarily represent those of their affiliated organizations, or those of the publisher, the editors, and the reviewers. Any product that may be evaluated in this article, or claim that may be made by its manufacturer, is not guaranteed or endorsed by the publisher.

References

Al-Zadjali, S., Al-Tamemi, S., Elnour, I., AlKindi, S., Lapoumeroulie, C., Al-Maamari, S., et al. (2015). Clinical and molecular findings of chronic granulomatous disease in Oman: Family studies. *Clin. Genet.* 87 (2), 185–189. doi:10.1111/cge.12351

Arai, T., Oh-ishi, T., Yamamoto, H., Nunoi, H., Kamizono, J., Uehara, M., et al. (2012). Copy number variations due to large genomic deletion in X-linked chronic granulomatous disease. *PLoS One* 7 (2), e27782. doi:10.1371/journal.pone.0027782

Cehajic-Kapetanovic, J., Xue, K., Martinez-Fernandez de la Camara, C., Nanda, A., Davies, A., Wood, L. J., et al. (2020). Initial results from a first-in-human gene therapy trial on X-linked retinitis pigmentosa caused by mutations in RPGR. *Nat. Med.* 26 (3), 354–359. doi:10.1038/s41591-020-0763-1

Chiriaco, M., Salfa, I., Di Matteo, G., Rossi, P., and Finocchi, A. (2016). Chronic granulomatous disease: Clinical, molecular, and therapeutic aspects. *Pediatr. Allergy Immunol.* 27 (3), 242–253. doi:10.1111/pai.12527

Dekkers, R., Verweij, P. E., Weemaes, C. M., Severijnen, R. S., Van Krieken, J. H., and Warris, A. (2008). Gastrointestinal zygomycosis due to Rhizopus microsporus var. rhizopodiformis as a manifestation of chronic granulomatous disease. *Med. Mycol.* 46 (5), 491–494. doi:10.1080/13693780801946577

Duchenne, G. B. A. (1867). The pathology of paralysis with muscular degeneration (paralysie myosclerotique), or paralysis with apparent hypertrophy. *Br. Med. J.* 2 (363), 541–542. doi:10.1136/bmj.2.363.541

El Nemer, W., Colin, Y., Collec, E., Gane, P., Cartron, J. P., and Kim, C. L. (2000). Analysis of deletions in three McLeod patients: Exclusion of the XS locus from the xp21.1-xp21.2 region. *Eur. J. Immunogenet* 27 (1), 29–33. doi:10.1046/j.1365-2370.2000.00188.x

Gassner, C., Brönnimann, C., Merki, Y., Mattle-Greminger, M. P., Sigurdardottir, S., Meyer, E., et al. (2017). Stepwise partitioning of Xp21: A profiling method for XK deletions causative of the McLeod syndrome. *Transfusion* 57 (9), 2125–2135. doi:10.1111/trf.14172

Hou, L., Niu, W. T., Ji, H. Y., Hu, X. F., Fang, F., and Ying, Y. Q. (2019). Serum biomarkers for early diagnosis of Chinese X-CGD children: Case reports and a literature review. *Curr. Med. Sci.* 39 (2), 343–348. doi:10.1007/s11596-019-2041-3

Jung, H. H., Danek, A., and Frey, B. M. (2007). McLeod syndrome: A neurohaematological disorder. *Vox Sang.* 93 (2), 112–121. doi:10.1111/j.1423-0410.2007.00949.x

Kim, E. Y., Lee, J. W., Suh, M. R., Choi, W. A., Kang, S. W., and Oh, H. J. (2017). Correlation of serum creatine kinase level with pulmonary function in Duchenne muscular dystrophy. *Ann. Rehabil. Med.* 41 (2), 306–312. doi:10.5535/arm.2017.41.2.306

Lhomme, F., Peyrard, T., Babinet, J., Abou-Chahla, W., Durieu, I., Moshous, D., et al. (2020). Chronic granulomatous disease with the McLeod phenotype: A French national retrospective case series. *J. Clin. Immunol.* 40 (5), 752–762. doi:10.1007/s10875-020-00791-w

Liu, C., Tu, C., Wang, L., Wu, H., Houston, B. J., Mastrorosa, F. K., et al. (2021). Deleterious variants in X-linked CFAP47 induce asthenoteratozoospermia and primary male infertility. *Am. J. Hum. Genet.* 108 (2), 309–323. doi:10.1016/j.ajhg.2021.01.002

Maggio, I., Chen, X., and Gonçalves, M. A. (2016). The emerging role of viral vectors as vehicles for DMD gene editing. *Genome Med.* 8 (1), 59. doi:10.1186/s13073-016-0316-x

Peng, J., Redman, C. M., Wu, X., Song, X., Walker, R. H., Westhoff, C. M., et al. (2007). Insights into extensive deletions around the XK locus associated with McLeod phenotype and characterization of two novel cases. *Gene* 392 (1-2), 142–150. doi:10.1016/j.gene.2006.11.023

Richards, S., Aziz, N., Bale, S., Bick, D., Das, S., Gastier-Foster, J., et al. (2015). Standards and guidelines for the interpretation of sequence variants: A joint consensus recommendation of the American College of medical genetics and genomics and the association for molecular pathology. *Genet. Med.* 17 (5), 405–424. doi:10.1038/gim.2015.30

Roos, D., van Leeuwen, K., Hsu, A. P., Priel, D. L., Begtrup, A., Brandon, R., et al. (2021). Hematologically important mutations: X-Linked chronic granulomatous disease (fourth update). *Blood Cells Mol. Dis.* 90, 102587. doi:10.1016/j.bcmd.2021.102587

Roulis, E., Hyland, C., Flower, R., Gassner, C., Jung, H. H., and Frey, B. M. (2018). Molecular basis and clinical overview of McLeod syndrome compared with other neuroacanthocytosis syndromes: A review. *JAMA Neurol.* 75 (12), 1554–1562. doi:10.1001/jamaneurol.2018.2166

Segal, B. H., Leto, T. L., Gallin, J. I., Malech, H. L., and Holland, S. M. (2000). Genetic, biochemical, and clinical features of chronic granulomatous disease. *Med. Baltim.* 79 (3), 170–200. doi:10.1097/00005792-200005000-00004

Song, S. M., Park, M. R., Kim, D. S., Kim, J., Kim, Y. J., Ki, C. S., et al. (2014). Identification of a novel mutation in the CYBB gene, p.Asp378Gly, in a patient with X-linked chronic granulomatous disease. *Allergy Asthma Immunol. Res.* 6 (4), 366–369. doi:10.4168/aair.2014.6.4.366

Warren, M., and Shimada, H. (2018). Cytologic and ultrastructural findings of bronchoalveolar lavage in patients with chronic granulomatous disease. *Pediatr. Dev. Pathology Official J. Soc. Pediatr. Pathology Paediatr. Pathology Soc.* 21 (4), 347–354. doi:10.1177/1093526617736188

Wikiera, B., Jakubiak, A., Łaczmanska, I., Noczyńska, A., and Śmigiel, R. (2021). Complex glycerol kinase deficiency - long-term follow-up of two patients. *Pediatr. Endocrinol. Diabetes Metab.* 27 (3), 227–231. doi:10.5114/pedm.2021.109681

Winkelstein, J. A., Marino, M. C., Johnston, R. B., Jr, Boyle, J., Curnutte, J., Gallin, J. I., et al. (2000). Chronic granulomatous disease. Report on a national registry of 368 patients. *Med. Baltim.* 79 (3), 155–169. doi:10.1097/00005792-200005000-00003

Yamada, M., Arai, T., Oishi, T., Hatano, N., Kobayashi, I., Kubota, M., et al. (2010). Determination of the deletion breakpoints in two patients with contiguous gene syndrome encompassing CYBB gene. *Eur. J. Med. Genet.* 53 (6), 383–388. doi:10.1016/j.ejmg.2010.08.003

Yu, L. C., Twu, Y. C., Chang, C. Y., and Lin, M. (2001). Molecular basis of the kell-null phenotype: A mutation at the splice site of human KEL gene abolishes the expression of Kell blood group antigens. *J. Biol. Chem.* 276 (13), 10247–10252. doi:10.1074/jbc.M009879200

Zaffanello, M., Zamboni, G., Tonin, P., Solero, G. P., and Tatò, L. (2004). Complex glycerol kinase deficiency leads to psychomotor and body-growth failure. *J. Paediatr. Child. Health* 40 (4), 237–240. doi:10.1111/j.1440-1754.2004.00346.x

frontiers | Frontiers in Pediatrics

TYPE Case Report
PUBLISHED 16 January 2023
DOI 10.3389/fped.2022.993165

Check for updates

OPEN ACCESS

EDITED BY
Ruth Roberts,
ApconiX, United Kingdom

REVIEWED BY
Jakub Piotr Fichna,
Mossakowski Medical Research Institute, Poland
George Papadimas,
National and Kapodistrian University of Athens, Greece
Jianxiang Liao,
Shenzhen Children's Hospital, China

*CORRESPONDENCE
Qian-Ye Zhao
✉ 18705130535@163.com

SPECIALTY SECTION
This article was submitted to Genetics of Common and Rare Diseases, a section of the journal Frontiers in Pediatrics

RECEIVED 13 July 2022
ACCEPTED 09 December 2022
PUBLISHED 16 January 2023

CITATION
Zhang S-s, Gu L-n, Zhang T, Xu L, Wei X, Chen S-h, Shi S-j, Sun D-q, Zhou S-h and Zhao Q-y (2023) Case report: Fatal infantile hypertonic myofibrillar myopathy with compound heterozygous mutations in the *CRYAB* gene.
Front. Pediatr. 10:993165.
doi: 10.3389/fped.2022.993165

COPYRIGHT
© 2023 Zhang, Gu, Zhang, Xu, Wei, Chen, Shi, Sun, Zhou and Zhao. This is an open-access article distributed under the terms of the Creative Commons Attribution License (CC BY). The use, distribution or reproduction in other forums is permitted, provided the original author(s) and the copyright owner(s) are credited and that the original publication in this journal is cited, in accordance with accepted academic practice. No use, distribution or reproduction is permitted which does not comply with these terms.

Case report: Fatal infantile hypertonic myofibrillar myopathy with compound heterozygous mutations in the *CRYAB* gene

Shan-shan Zhang[1], Li-niu Gu[2], Teng Zhang[3], Lu Xu[4], Xiang Wei[1], Su-hong Chen[1], Su-jie Shi[1], Da-quan Sun[1], Shao-hong Zhou[1] and Qian-ye Zhao[1]*

[1]Pediatric Respiratory Ward I, Lianyungang Maternal and Children's Hospital, Lianyungang, China, [2]Department of Immunization Planning, Lianyungang Center for Disease Control and revention, Lianyungang, China, [3]Department of Science & Education, Lianyungang Maternal and Children's Hospital, Lianyungang, China, [4]Department of Neonatology, Lianyungang Maternal and Children's Hospital, Lianyungang, China

Background: Fatal infantile hypertonic myofibrillar myopathy (FIHMM) is an autosomal recessive hereditary disease characterized by amyotrophy, progressive flexion contracture and ankylosis of the trunk and limb muscles, apnea and respiratory failure, and increased creatine phosphate levels. It is caused by mutations in the *CRYAB* gene, and only around 18 cases including genetic mutations have been reported worldwide. All patients with FIHMM develop respiratory distress, progressive stiffness of the limbs, and have a poor prognosis. However, no effective treatment for *CRYAB*-associated respiratory failure has been reported. Here, we report a case of FIHMM with a novel heterozygous missense mutation.

Case Presentation: A 2-year-old female developed scoliosis of the lumbar spine and restrictive ventilatory dysfunction in infancy. She was admitted to the hospital with labored breathing on the third day after the second injection of inactivated poliomyelitis vaccine. Acute respiratory failure, pneumothorax, and cardiac arrest arose in the patient during hospitalization, and progressive stiffness of the trunk and limb muscles appeared, accompanied by obvious abdominal distension and an increase in phosphocreatine kinase levels. Screenings for genetic metabolic diseases in the blood and urine were normal. Electromyography revealed mild myogenic damage. A muscle biopsy indicated the accumulation of desmin, α-crystallin, and myotilin in the musculus biceps brachii, and dense granules were observed in muscle fibers using electron microscopy. Mutation analysis of *CRYAB* revealed a novel heterozygous missense mutation in the proband, *c.302A > C* (*p.His101Pro*) and *c.3G > A* (*p.Met1Ile*), which inherited from her asymptomatic, heterozygous carrier parents, respectively. The proband was finally diagnosed as FIHMM. One month after the FIHMM diagnosis, the child died of respiratory failure.

Conclusion: We report a case of FIHMM with a novel heterozygous missense mutation of *CRYAB*. This finding might improve our understanding of FIHMM and highlight a novel mutation in the Chinese population.

KEYWORDS

CRYAB, fatal infantile hypertonic myofibrillar myopathy, gene, mutation, whole exome sequencing

Introduction

Fatal infantile hypertonic myofibrillar myopathy (FIHMM) is an autosomal recessive hereditary disease caused by mutations in the *CRYAB* gene. Symptoms such as weak crying, sleep apnea, recurrent respiratory tract infection, and progressive stiffness of the trunk, abdomen, and limbs are observed during the neonatal period or in early infancy (1–4). All patients suffer from respiratory failure; thus, the disease has a poor prognosis. To date, no effective treatment has been reported for FIHMM. Here, we describe a case of FIHMM in which a novel compound heterozygous missense mutation of *CRYAB* was found.

Case presentation

Ethical compliance

The proband's parents provided written informed consent to participate in this study in compliance with the Declaration of Helsinki, and the Institutional Review Board at Lianyungang Maternal and Child Health Hospital approved this study (project no. LYG-MEP2021004).

A 2-year-old female was hospitalized for respiratory distress on the third day after the second injection of inactivated poliomyelitis vaccine. Oxygen saturation fluctuated from 68% to 92% in ambient air. The child showed no fever, no coughing and wheezing, no vomiting and diarrhea at early onset. She had been admitted to our hospital previously for premature delivery (gestational age: 29 weeks and 4 days), neonatal shock, intrahepatic cholestasis, bronchopulmonary dysplasia, and extrauterine growth retardation for more than 70 days, and she had suffered from severe bronchopneumonia, pneumothorax (twice), scoliosis of the lumbar spine, and restrictive ventilatory dysfunction at 1 year old. She was G_3P_1 and delivered with a birth weight of 1.2 kg. Her mother had aborted twice previously for embryo arrested development. Her parents are both healthy, and there was no family history of similar symptoms.

Admission Physical Exam: T.37 °C, P.160/min, RR.50/min, Wt.10 kg, BP.90/60 mmHg, SaO_2.70%. The patient was malnourished, looked mentally fatigued, and suffered from dyspnea. The pharynx was slightly congested, and the neck was soft. Inspiratory three-concave signs were positive. Bilateral respiratory motion and tactile fremitus were symmetric bilaterally. There were some rough and middle moist rales predominantly in the pulmonary bilateral middle-inferior field according to chest auscultation, but no wheezing or pleural friction sounds were heard. Her heart rate was 160 beats per minute, and her cardiac rhythm was regular. In the precordial area, a 2/6 systolic blowing cardiac murmur was detected. The abdomen was distended. No hepatosplenomegaly was found. There was serious kyphosis of the lumbar spine. The four limbs could be moved freely. No abnormalities were found in a nervous system examination.

Auxiliary Examinations: No abnormalities were found in all tests, including routine blood, high-sensitivity C-reactive protein, and routine urine and stool tests. The results of PCR tests for nine respiratory viruses, EB virus, thirteen respiratory bacteria, *Mycoplasma pneumoniae*, and *Chlamydia pneumoniae* were all negative. Five items of coagulation, renal function, troponin, and hematuria tandem mass spectra were all in the normal range. Procalcitonin levels fluctuated from 1.651 to 7.480 ng/ml. Creatine phosphate kinase levels kept increasing. Arterial blood gas analysis showed an increase in $PaCO_2$ under the support of a ventilator. Bronchoalveolar lavage fluid and sputum cultures indicated the presence of *Candida tropicalis*, *Burkholderia cepacia*, and *Acinetobacter baumannii*. Cardiac color Doppler ultrasound showed the presence of the foramen ovale, aortic regurgitation (mild to moderate), slight thickening of the ventricular septum and left ventricular posterior wall, and normal cardiac function. A chest and abdominal CT scan indicated the presence of bilateral pneumonia (**Figure 1**) and pleural effusion, enlarged liver volume, a small effusion around the liver, a strip-shaped high-density focus in the gallbladder (nature to be determined), thickened bilateral abdominal wall muscle tissue, and atrophic bilateral erector spinal muscles. A spinal CT scan showed scoliosis of the lumbar spine and no bone destruction in each vertebral body. There were no spontaneous potentials in acupuncture electromyogram of anterior tibialis, medial peroneal muscles, vastus medialis, medial femoral, the first dorsal interossei, musculus biceps brachii and musculus triceps brachii. The conductive velocity and amplitude of sensory and motor nerve were at the normal range, and consequently, mild myogenic damage was deduced. Histochemical staining (H&E, Gomori Trichrome, ORO and PAS), enzyme histochemistry and special staining (NADH-TR, SDH, COX, SDH / COX, ATPase, ACP, AMP, NSE, phosphorylase and PFK), immunohistochemistry staining (Alexa Fluor or FITC labelled Desmin, α-Crystallin, Myotilin, titin, dystrophin, α, β, γ, δ-Sarcoglycan, Dysferlin, Lamininα2), and monoclonal antibody staining of Collagen VI were conducted in muscle biopsy. The Pathological results showed the accumulation of desmin, α-crystallin, and myotilin in the musculus biceps brachii, and dense granules were observed in muscle fibers using electron microscopy, which demonstrated myogenic fibromyopathy (**Figure 2**).

Diagnostic assessment

Based on the above-described clinical findings, we inferred a possible diagnosis of hereditary myopathy. To confirm this diagnosis, whole exome sequencing (WES), conducted at the

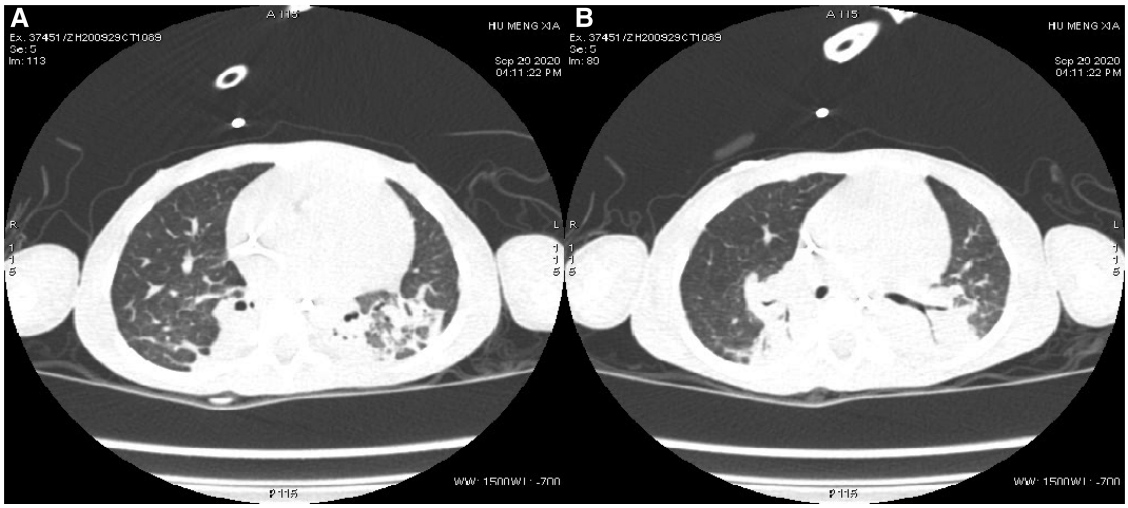


FIGURE 1
Changes in pulmonary imaging. (**A**) Consolidation of the bilateral lower lobe; (**B**) atelectasis of the posterior basal segment of the right lung.

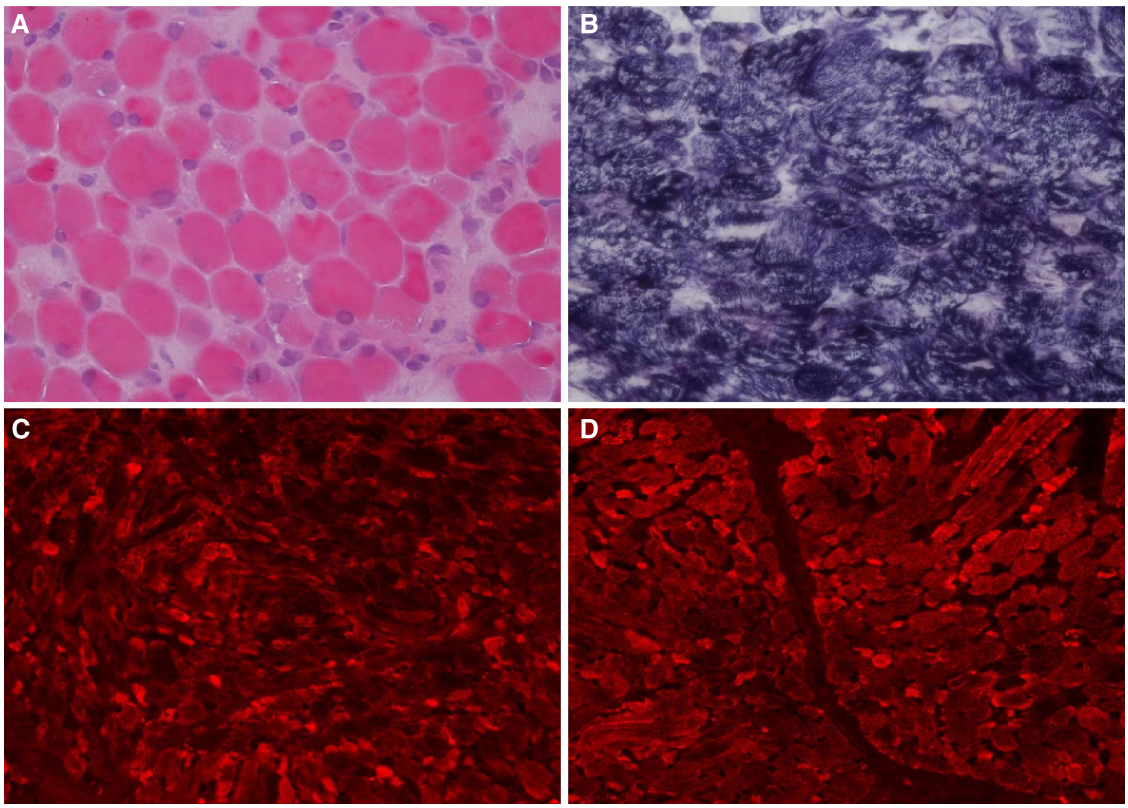


FIGURE 2
Histochemical and immunohistochemical staining of muscle biopsies (×200). Following HE staining (**A**), different sizes of muscle fibers were observed, and degeneration, necrosis, and regeneration of the muscle fibers was evident as well as the deposition of amorphous materials. Some muscle fiber staining was significantly darker than the surrounding myofibrils according to modified Gömöri trichrome staining (**B**). Fluorescence antibody staining of desmin, α-crystallin (**C**), and myotilin (**D**) revealed high expression levels of these proteins in the sediment.

Wuhan Kangshengda Medical Research Institute, was used by a high-throughput analysis technique. The data were filtered to generate "clean reads" by removing adapters and low-quality reads (Q20). Sequencing reads were mapped to the reference human genome version hg19 (2009–02 release, http://genome.ucsc.edu/). Nucleotide changes observed in the aligned reads were called and reviewed using NextGENe software (SoftGenetics, State College, PA). In addition to the detection of deleterious mutations and novel single-nucleotide variants, sequence variants were annotated using population and literature databases including dbSNP, TGP, Clinvar, and HGMD. All variants were elucidated according to ACMG standards and categorized as pathogenic, likely pathogenic, uncertain significant,, likely benign and benign (5). Possible pathogenicity was predicted according to the online tools of PolyPhen-2, and MutationTaster. Moreover, reanalysis of the WES results were conducted on the patient and her parents.

CRYAB gene complex with heterozygous mutations was found in the proband (GeneBank reference sequence: NM_001885). The variant, *CRYAB* (NM_001885): *c.302A > C* (*p.His101Pro*), was located in the region of exon 3 of *CRYAB*, in which the NO.302 nucleotide was mutated from adenine to cytosine (*c.302A > C*), leading to a mutation of the NO.101 amino acid from histidine to proline (**Figure 3A**), which was inherited from currently asymptomatic, heterozygous carrier mother. According to *ACMG Standard and Guidelines for the Interpretation of Sequence Variants*, the mutation is uncertain significance with two moderate evidence of pathogenicity (PM1 and PM2), and a supporting evidences of pathogenicity (PP3). The variant was predicted to be "probably damaging" by PolyPhen2 with a score of 0.995 (sensitivity: 0.04, specificity: 0.98) (6) and "disease causing" by MutationTaster with a score of 1. The Swiss-Model computer model was used to predict the influence of this identified mutation on protein structure, with the analysis conducted by Hangzhou Waylan Biotechnology Co. The *CRYAB c.302A > C* (*p.His101Pro*) mutation affected the formation of a hydrogen bond (**Figure 4**), which influenced the three-dimensional structure of the CRYAB protein severely and caused functional defects, indicating the disease causing mutation.

The other variant, *CRYAB* (NM_001885): *c.3G > A* (*p.Met1Ile*) (provided in Data S.), inherited from her unaffected heterozygous carrier father, was located in the region of exon 2 of *CRYAB* (**Figure 3B**), in which the NO.3 nucleotide was mutated from guanine to adenine (*c.3G > A*), resulting in a mutation of the NO.1 amino acid from methionine to isoleucine. The mutation is clearly pathogenic with a very strong evidence of pathogenicity (PVS1) and a moderate evidence of pathogenicity (PM2) (detailed in Data S). According to the N-terminal rule (7), the *CRYAB c.3G > A* (*p.Met1Ile*) mutation shortens the half-life of the CRYAB protein, thereby decreasing its stability. Result showed the variant is probably damaging with a score of 0.999 (sensitivity: 0.14, specificity: 0.99) using PolyPhen-2 tool, and "disease causing" by MutationTaster with a score of 1, which suggests that there is a high probability that the *CRYAB c.3G > A* (*p.Met1Ile*) mutation may be the cause of FIHMM. The list of the variants left after final filtering step are provided in the Data S. However, it was not clear whether the two intrauterine fetal deaths suffered by the proband's mother were related to gene abnormality because WES screening was not performed on that occasion.

Discussion

FIHMM was first reported among mid-western Canadian aboriginals in 1994 (2, 8) identified *CRYAB* as the gene responsible for this disease. *CRYAB* is located in chromosomal region 11q22.3∼q23, is composed of three exons and 175 nucleotides (9), and encodes αB-crystallin (10), also known as HSPB5, which is a member of the small heat-shock protein family and a molecular chaperone that interacts with desmin in the assembly of intermediate filaments. These act as chaperones to prevent protein aggregation (11), stabilize myofibrils, maintain muscle fiber elasticity, allow remodeling after repeated contraction (2, 12), inhibit the aggregation and precipitation of denatured proteins, and prevent loss of function under stress conditions (13). Due to the high expression of αB-crystallin in human type-I myofibers, *CRYAB* variants often cause selective muscle fibrosis atrophy of the trunk, spine, and limbs, such as in myofibrillar myopathy type II (14–16), dilated cardiomyopathy 1 type II (9), FIHMM (8), and multitype cataracts (17, 18). Among these diseases, FIHMM is an autosomal recessive hereditary disease that generally arises in the early period as a serious muscular atrophy condition (2, 4, 14), with clinical manifestations including progressive stiffness of the trunk and limb muscles, flexion contracture (19), ankylosis, faint crying, dysphagia and dyspnea. Immunohistochemistry staining of muscle biopsies showed accumulations of desmin, and dense granules in the myocytes using electron microscopy.

To date, *CRYAB*-related fatal infantile hypertonic MFM (OMIM 613869), that is FIHMM, was induced primarily by homozygous mutations in *CRYAB* gene. Two sporadic cases included *CRYAB c.3G > A (p.Met1Ile)* (3) and *CRYAB c.343delT (p.Ser115ProfsX14)* (19) mutations, respectively. Among the Canadian aboriginal population, the variant, *CRYAB c.60delC* (*p.Ser21AlafsX24*) homozygous mutation was described in 12 cases with FIHMM (2). Lu et al. (4) reported four Chinese cases with the homozygous mutation gene in *CRYAB c.3G > A* (*p.Met1Ile*), that results in the loss of methionine initiation and the absence of a protein, which was different with our report, a heterozygous missense mutation in *CRYAB gene, c.302A > C* (*p.His101Pro*) and *c.3G > A* (*p.Met1Ile*).

In our report, the heterozygous missense mutations in the *CRYAB* gene of the proband were inherited from her

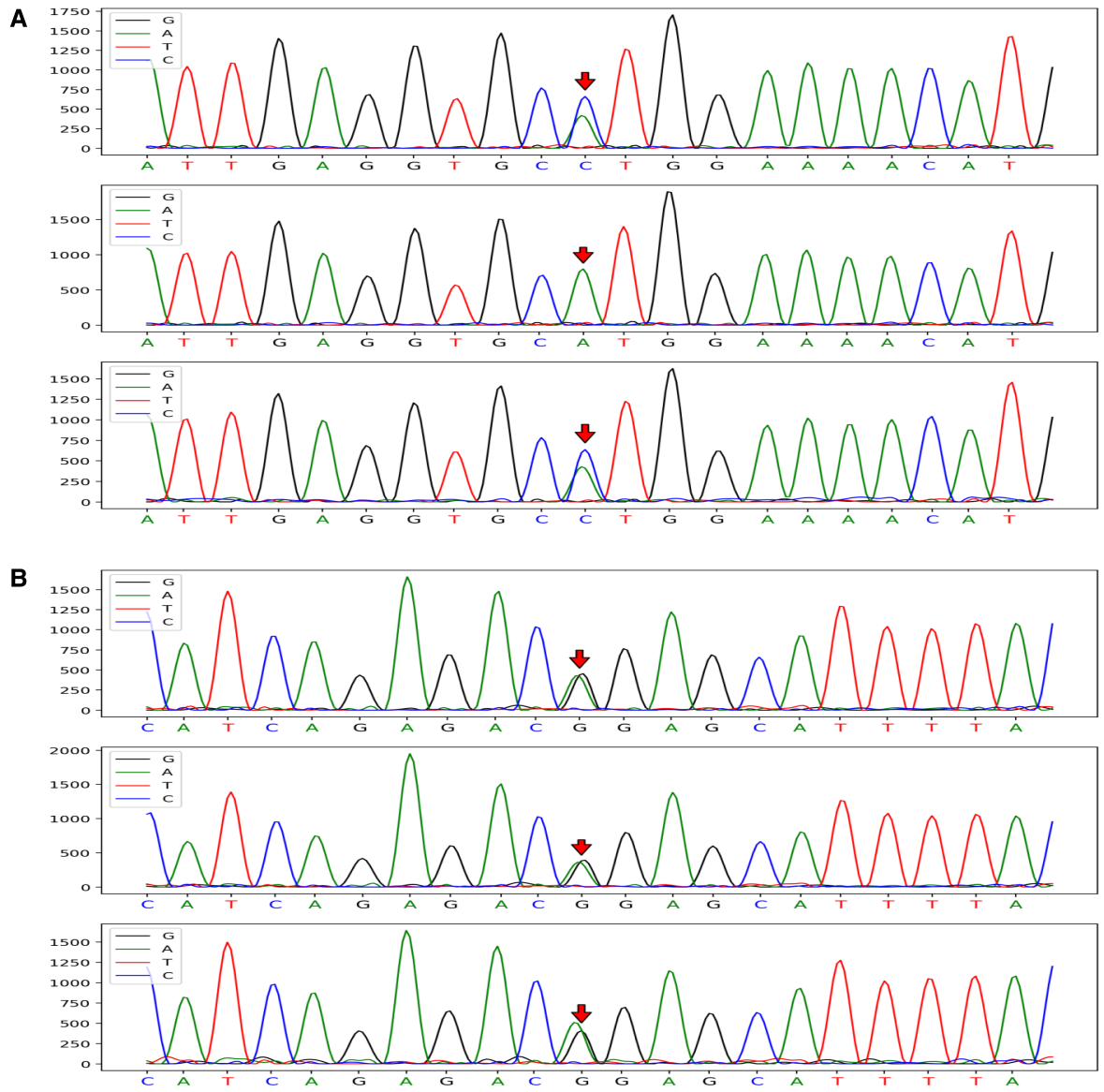


FIGURE 3
CRYAB gene sequences of the proband and her parents (mutation sites are marked with arrows). The *CRYAB* c.302A > C (p.H101P) mutation was located in the region of exon 3 of chromosome 11 and resulted in the mutation of the NO. 302 nucleotide from adenine to cytosine (**A**). The proband with FIHMM and her mother carried the same gene mutation; however, her father's gene locus was normal. The *CRYAB* 3G > A (p.M1I) mutation was located in the region of exon 2 of chromosome 11 and caused the mutation of a synthetic amino acid from methionine to isoleucine (**B**). The mutation carried by the proband was inherited from her unaffected father, whereas her mother's gene locus was normal.

currently asymptomatic parents. The proband showed recurrent respiratory tract infection in infancy, and gradually developed the symptoms of erector spinae muscle atrophy and lumbar kyphosis deformity without bone destruction in the vertebra lumbalis after the age of 1 year. As the illness progressed, the proband presented with a stiffness of the trunk and limb muscles, abdominal distension, uncorrectable respiratory failure (type II), and increasing creatine phosphate kinase levels. Finally, the child died after artificial respiration support was ended. The clinical feature of this case was in accordance with *CRYAB c.3G > A* (*p.Met1Ile*) homozygous mutation related FIHMM phenotype reported in the literature (2, 8). Electromyography results of the proband were consistent with myogenic damage, and the muscle biopsy showed the accumulation of desmin, α-crystallin, myotilin and dense granules in the musculus biceps brachii. Meanwhile, immunohistochemistry staining of titin, dystrophin, α, β, γ, δ-Sarcoglycan, Dysferlin and Laminα2 were all negative in muscle biceps. Except for *CRYAB*, Fifteen mutation genes associated with Myofibrillar myopathy (MFM) phenotype, including five classic

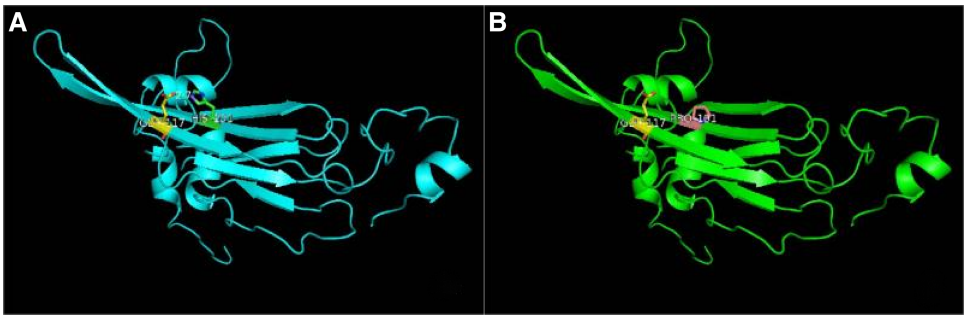


FIGURE 4
Effect of the *CRYAB* c.302A > C (p.H101P) mutation on the three-dimensional structure of the protein predicted by functional model software. (**A**) Wide type and (**B**) mutant type. A hydrogen bond was absent in the mutation site of αB-crystallin.

genes *DES*, *ZASP*, *FLNC*, *BAG3*, *MYOT*, and other genes *FHL1*, *TTN*, *DNAJB6*, *PLEC*, *LMNA*, *ACTA1*, *HSPB8*, *KY*, *PYROXD1*, and *SQSTM + TIA1* (digenic) were not found in the results (20, 21). Meanwhile, FIHMM as a atypical MFM, manifest a progressive stiffness of the trunk and limb muscles. The mutation in DMPK associated with tonic muscular dystrophy was not identified. Therefore, according to the clincal phenotype, relevant pathological results, and combined with gene mutations in *CRYAB:c.302A > G* (*p.His101Pro*) and *c.3G > A* (*p.Met1Ile*), the proband was finally diagnosed as FIHMM, which conformed to the law of recessive inheritance. The two variants were not the same allele. We speculate that there is a possible involvement of complex genetic background. It is hard to pinpoint. *CRYAB c.302A > G* (*p.His101Pro*) as a variant of minor pathogenicity might help the other variant with very strong pathogenicity, *CRYAB c.3G > A* (*p.Met1Ile*), produce pathogenic results. The relevant mechanism still needs further research.

In conclusion, this article reports one infant with FIHMM with a novel heterozygous variant in *CRYAB*. The report broadened genetic spectrum of the *CRYAB* mutations related FIHMM. This study may aid in diagnosis, carrier detection, and genetic counsel of *CRYAB*-related neonatal onset MFM.

Data availability statement

The original contributions presented in the study are included in the article/Supplementary Material, further inquiries can be directed to the corresponding author/s.

Ethics statement

The studies involving human participants were reviewed and approved by the Institutional Review Board at Lianyungang Maternal and Child Health Hospital. Written informed consent to participate in this study was provided by the participants' legal guardian/next of kin.

Author contributions

S-sZ wrote the manuscript. L-nG and Q-yZ took part in the treatment and wrote the manuscript. TZ, LX, and XW took part in the treatment, performed the genetic analysis, and wrote the manuscript. S-hC, S-jS, D-qS, and S-hZ took part in the treatment. All authors contributed to the article and approved the submitted version.

Acknowledgment

We thank director WL for his help in information collection.

Conflict of interest

The authors declare that the research was conducted in the absence of any commercial or financial relationships that could be construed as a potential conflict of interest.

Publisher's note

All claims expressed in this article are solely those of the authors and do not necessarily represent those of their affiliated organizations, or those of the publisher, the editors and the reviewers. Any product that may be evaluated in this article, or claim that may be made by its manufacturer, is not guaranteed or endorsed by the publisher.

References

1. Del Bigio MR, Chudley AE, Sarnat HB, Campbell C, Goobie S, Chodirker BN, et al. Infantile muscular dystrophy in Canadian aboriginals is an αB-crystallinopathy. *Ann Neurol*. (2011) 69:866–71. doi: 10.1002/ana.22331

2. Forrest KM, Al-sarraj S, Sewry C, Buk S, Tan SV, Pitt M, et al. Infantile onset myofibrillar myopathy due to recessive CRYAB mutations. *Neuromuscul Disord*. (2011) 21:37–40. doi: 10.1016/j.nmd.2010.11.003

3. Ma K, Luo D, Tian T, Li N, He X, Rao C, et al. A novel homozygous initiation codon variant associated with infantile alpha-bcrystallinopathy in a Chinese family. *Mol Genet Genomic Med*. (2019) 7:e825. doi: 10.1002/mgg3.825

4. Lu XG, Yu U, Han CX, Mai JH, Liao JX, Hou YQ. C.3G>A mutation in the CRYAB gene that causes fatal infantile hypertonic myofibrillar myopathy in the Chinese population. *J Integr Neurosci*. (2021) 20:143–51. doi: 10.31083/j.jin.2021.01.267

5. Richards S, Aziz N, Bale S, Bick D, Das S, Gastier-Foster J, et al. Standards and guidelines for the interpretation of sequence variants: a joint consensus recommendation of the American college of medical genetics and genomics and the association for molecular pathology. *Genet Med*. (2015) 17:405–24. doi: 10.1038/gim.2015.30

6. Adzhubei IA, Schmidt S, Peshkin L, Ramensky VE, Gerasimova A, Bork P, et al. A method and server for predicting damaging missense mutations. *Nat Methods*. (2010) 7:248–9. doi: 10.1038/nmeth0410-248

7. Tasaki T, Sriram SM, Park KS, Kwon YT. The N-end rule pathway. *Annu Rev Biochem*. (2012) 81:261–89. doi: 10.1146/annurev-biochem-051710-093308

8. Lacson AG, Seshia SS, Sarnat HB, Anderson J, Degroot WR, Chudley A, et al. Autosomal recessive, fatal infantile hypertonic muscular dystrophy among Canadian natives. *Can J Neurol Sci*. (1994) 21:203–12. doi: 10.1017/S0317167100041172

9. Inagaki N, Hayashi T, Arimura T, Koga Y, Takahashi M, Shibata H, et al. Alpha B-crystallin mutation in dilated cardiomyopathy. *Biochem Biophys Res Commun*. (2006) 342:379–86. doi: 10.1016/j.bbrc.2006.01.154

10. Palmio J, Udd B. Myofibrillar and distal myopathies. *Rev Neurol*. (2016) 172:587–93. doi: 10.1016/j.neurol.2016.07.019

11. Chebotareva NA, Roman SG, Borzova VA, Eronina TB, Mikhaylova VV, Kurganov BI. Chaperone-like activity of HSPB5: the effects of quaternary structure dynamics and crowding. *Int J Mol Sci*. (2020) 21:4940. doi: 10.3390/ijms21144940

12. Arbustini E, Pasotti M, Pilotto A, Pellegrini C, Grasso M, Previtali S, et al. Desmin accumulation restrictive cardiomyopathy and atrioventricular block associated with desmin gene defects. *Eur J Heart Fail*. (2006) 8:477–83. doi: 10.1016/j.ejheart.2005.11.003

13. Markossian KA, Yudin IK, Kurganov BI. Mechanism of suppression of protein aggregation by α-crystallin. *Int J Mol Sci*. (2009) 10:1314–45. doi: 10.3390/ijms10031314

14. Golenhofen N, Perng MD, Quinlan RA, Drenckhahn D. Comparison of the small heat shock proteins alphaB-crystallin, MKBP, HSP25, HSP20, and cvHSP in heart and skeletal muscle. *Histochem Cell Biol*. (2004) 122:415–25. doi: 10.1007/s00418-004-0711-z

15. Fichna JP, Potulska-Chromik A, Miszta P, Redowicz MJ, Kaminska AM, Zekanowski C, et al. A novel dominant D109A CRYAB mutation in a family with myofibrillar myopathy affects αB-crystallin structure. *BBA Clin*. (2017) 7:1–7. doi: 10.1016/j.bbacli.2016.11.004

16. Fichna JP, Maruszak A, Żekanowski C. Myofibrillar myopathy in the genomic context. *J Appl Genet*. (2018) 59:431–9. doi: 10.1007/s13353-018-0463-4

17. Berry V, Francis P, Reddy MA, Collyer D, Vithana E, Mackay I, et al. Alpha-B crystallin gene (CRYAB) mutation causes dominant congenital posterior polar cataract in humans. *Am J Hum Genet*. (2001) 69:1141–5. doi: 10.1086/324158

18. Zhuang J, Cao Z, Zhu Y, Liu L, Tong Y, Chen X, et al. Mutation screening of crystallin genes in Chinese families with congenital cataracts. *Mol Vis*. (2019) 25:427–37. PMID: 31523120

19. Brady JP, Garland DL, Green DE, Tamm ER, Giblin FJ, Wawrousek EF. AlphaB-crystallin in lens development and muscle integrity: a gene knockout approach. *Invest Ophthalmol Vis Sci*. (2001) 42:2924–34. PMID: 11687538

20. Fichna JP, Karolczak J, Potulska-Chromik A, Misza P, Berdynski M, Sikirska A, et al. Two desmin gene mutations associated with myofibrillar myopathies in Polish families. *PLoS One*. (2014) 9:e115470. doi: 10.1371/journal.pone.0115470

21. Sacconi S, Feasson L, Antoine JC, Pecheux C, Bernard R, Cobo AM, et al. A novel CRYAB mutation resulting in multisystemic disease. *Neuromuscul Disord*. (2012) 22:66–72. doi: 10.1016/j.nmd.2011.07.004

frontiers | Frontiers in Genetics

TYPE Case Report
PUBLISHED 17 January 2023
DOI 10.3389/fgene.2023.1005624

Check for updates

OPEN ACCESS

EDITED BY
Tieliu Shi,
Hunan University of Arts and Science, China

REVIEWED BY
Hanan Elfadil Shamseldin,
King Faisal Specialist Hospital and Research Centre, Saudi Arabia
Yaqiong Jin,
Beijing Children's Hospital, Capital Medical University, China

*CORRESPONDENCE
Jin Han,
hanjin1123@163.com

SPECIALTY SECTION
This article was submitted to Genetics of Common and Rare Diseases, a section of the journal Frontiers in Genetics

RECEIVED 28 July 2022
ACCEPTED 03 January 2023
PUBLISHED 17 January 2023

CITATION
Chen C, Han J, Xue J, Li R, Chen G, Yang X, Tang J, Li F and Li D (2023), Case Report: Early diagnosis of lethal multiple pterygium syndrome with micrognathia: Two novel mutations in the *CHRND* gene. *Front. Genet.* 14:1005624. doi: 10.3389/fgene.2023.1005624

COPYRIGHT
© 2023 Chen, Han, Xue, Li, Chen, Yang, Tang, Li and Li. This is an open-access article distributed under the terms of the Creative Commons Attribution License (CC BY). The use, distribution or reproduction in other forums is permitted, provided the original author(s) and the copyright owner(s) are credited and that the original publication in this journal is cited, in accordance with accepted academic practice. No use, distribution or reproduction is permitted which does not comply with these terms.

Case Report: Early diagnosis of lethal multiple pterygium syndrome with micrognathia: Two novel mutations in the *CHRND* gene

Caiyuan Chen[1], Jin Han[1]*, Jiaxin Xue[1], Ru Li[1], Guilan Chen[1], Xin Yang[1], Jiajie Tang[1,2], Fucheng Li[1] and Dongzhi Li[1]

[1]Prenatal Diagnosis Center, Guangzhou Women and Children's Medical Center, Guangzhou Medical University, Guangzhou, China, [2]School of Information Management, Wuhan University, Wuhan, China

Lethal multiple pterygium syndrome (LMPS) is a rare disease with genetic and phenotypic heterogeneity and is inherited in an autosomal recessive (AR) pattern. Here, we have presented clinically significant results describing two novel mutations of *CHRND* gene: NM_000751.2: c.1006C>T p.(Arg336Ter) and NM_000751.2:c.973_975delGTG p.(Val325del), and measurement of the facial angle for determining micrognathia by prenatal diagnosis in the first trimester of pregnancy for a Lethal multiple pterygium syndrome case. In conclusion, this report complements the spectrum of genetic variants and phenotype of Lethal multiple pterygium syndrome and provides reliable recommendation for the counseling of future pregnancies in families with the disease.

KEYWORDS

lethal multiple pterygium syndrome, CHRND gene, micrognathia, prenatal diagnosis, first trimester

Introduction

Lethal multiple pterygium syndrome (MIM 253290), a rare disorder, was first reported by Gillen and Pryse-Davis. And it is one of the types of multiple pterygium syndrome (MPS) (Brink et al., 2003; Morgan et al., 2006), with an incidence of <1/100000, which has not been assessed concretely (Orpha, 2019). Either autosomal or X-linked recessive inheritance has been suggested, and the latter is rarely reported (Tolmie et al., 1987; Hertzberg et al., 2000). LMPS is distinguished by multiple pterygium, arthrogryposis and akinesia, nuchal cystic hygroma, hydrops fetalis, intrauterine growth retardation, and death (de Die-Smulders et al., 1990b). Furthermore, other detailed manifestations such as micrognathia, low-set ears, and cleft lip and palate have also been noted (Meizner et al., 1993). Three clinical subtypes of LMPS have been reported thus far. First: early type, characterized by fetal edema and/or cystic hygroma and lethality in the second trimester; second: late type, characterized by absence of fetal edema and survival into the third trimester; third: Finnish type, characterized by hydrops fetalis from second trimester and beyond (de Die-Smulders et al., 1990a).

The pathogenesis of LMPS is closely related to AChR which comprises four different subunits that are controlled by their own genes. For example, the *CHRND* (MIM 100720) gene, which can cause four main types of congenital myasthenic syndrome (CMS): LMPS (MIM 253290), slow-channel CMS (MIM 616321), fast-channel CMS (MIM 616322), and AChR deficiency CMS (MIM 616323), is encoded by the δ subunit (Mishina et al., 1986; Engel et al.,

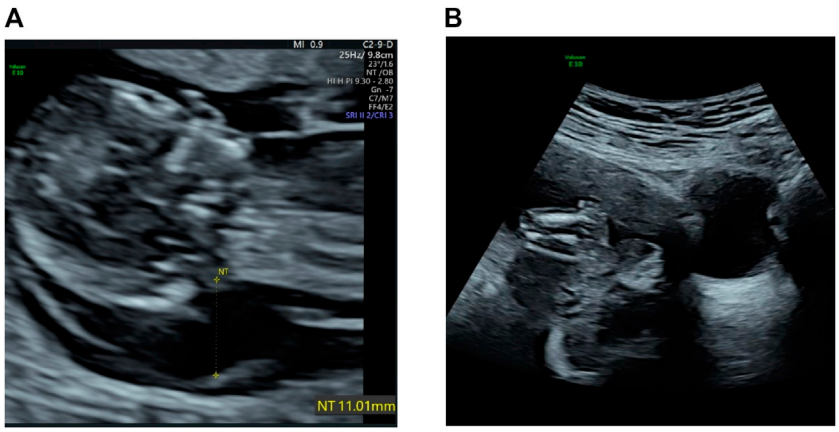


FIGURE 1
(A) Transabdominal ultrasound at 12 weeks shows a large cystic hygroma. **(B)** Flexion contracture of lower limb and edema.

2015). At the same time, to date, the genes *RAPSN* (MIM 601592), *nebulin* (*NEB*; MIM 161650), *CHRNA1* (MIM 100690), and *CHRNG* (MIM 100730) also cause varying pathogeneses in LMPS, with *CHRNG* mutations been observed in 30% of the cases (Morgan et al., 2006; Abdalla et al., 2017; Mohtisham et al., 2019). In adddition, previous studies have reported that LMPS can also be caused by uniparental disomy (UPD) of chromosome two carrying the pathogenic variant of *CHRND* (NM_000751.2) (Shen et al., 2018).

In view of the characteristic and non-specific nature of LMPS, this report aims to further study its etiology, clinical features, and the significance of prenatal examination in order to lay a solid foundation for early identification of LMPS in the future, which is helpful for prenatal diagnosis and counseling.

Case report

A 34-year-old woman was admitted to the Prenatal Diagnosis Center of Guangzhou Women and Children's Medical Center due to fetal nuchal cystic hygroma at 12 weeks of gestation. The pregnant woman denied alcohol, illicit drug, and tobacco usage. And that she had an adverse pregnancy in which the embryo had stopped developing without further detailed examination of the fetus. This fetus is the second child of the parents who are both healthy, safe and non-consanguineous. In addition, there was also no family history of hereditary disease.

Prenatal ultrasound findings

Abdominal two-dimensional (2D) ultrasound (US) revealed a single fetus at an estimated gestational age of 12 weeks 5 days on the basis of crown–rump length (CRL) of 64 mm. The fetus had a markedly increased nuchal translucency (NT) of 11 mm and absence of nasal bone (NB) (Figure 1A), edema and bilateral fixed flexion deformities of the knees and elbows (Figure 1B), vertical wrists, and a cyst in the right choroid plexus. Absence of limb motion was noted during the 20-min examination. In particular, micrognathia was observed, and we measured the mandibulomaxillary facial (MMF) angle as 62.02° by three-dimensional (3D) US and clearly observed contracture of upper limb (Figure 2). However, thickness of the placenta, cardiac structure, and middle cerebral artery peak systolic velocity (MCA-PSV) were normal.

Phenotype of postpartum fetus

As the prognostic impact of the condition is lethal, termination of the pregnancy with prostaglandin induction was proposed to the parents after consultation. Postartum fetus was noted to have multiple dysmorphic features (Figure 3), viz., nuchal cystic hygroma, contractures of the extremities, bilateral fetal talipes, subscalp hemorrhage, and short neck as well as spina bifida.

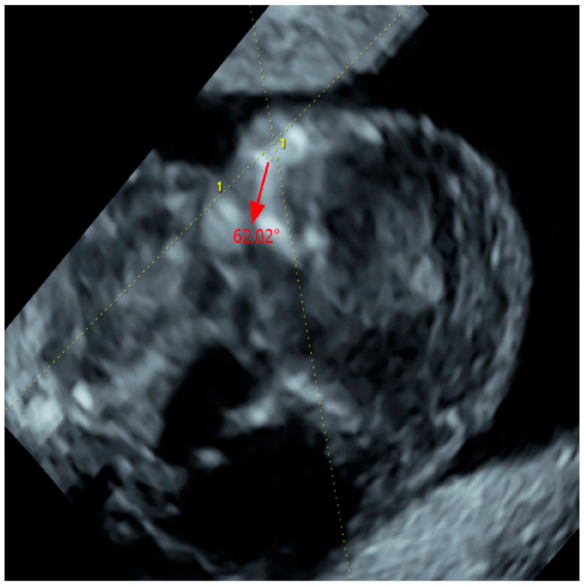


FIGURE 2
The measurement of Maxilla-nasion-mandible angle (MMF, 62.02°) (red arrow).

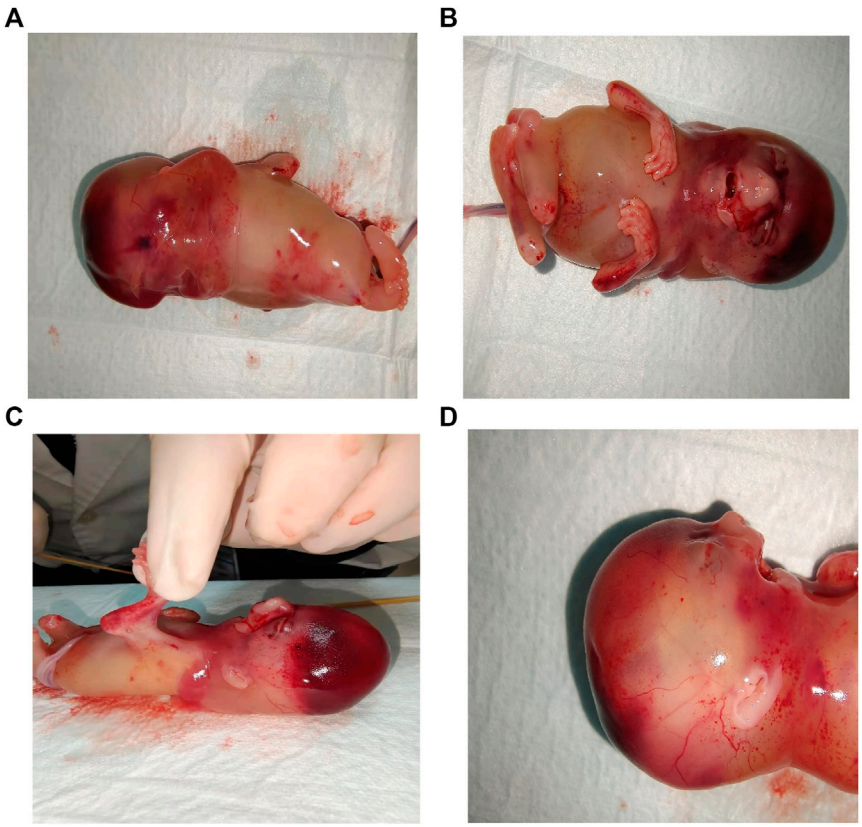


FIGURE 3
Stillbirth phenotypes: **(A)** Nuchal cystic hygroma. **(B)** Contractures of the extremities and vertical wrist. **(C)** Pterygium of antecubital and popliteal regions. **(D)** Side view: Pterygia of neck, low-set ears, micrognathia and gaping mouth.

Multiple pterygia were predominantly striking at the neck, antecubital, and popliteal regions. Facial abnormalities observed were micrognathia, low-set ears, cleft palate, and gaping mouth. Genitalia were that of a normal male.

Whole-exome sequencing

Quantitative fluorescent-PCR (QF-PCR) and chromosomal microarray analysis (CMA) of the fetus were performed. And the couple were also advised to undergo whole-exome sequencing (WES) to further identify the etiology by prenatal consultation. Genomic DNA was randomly fragmented and purified using the magnetic particle method. WES was performed on an IIIumina HiSeq 2,500 sequencer (Illumina, San Diego, CA, United States) for a minimal of 10.14 Gb read-depth per case. Sequencing reads after quality control were aligned to the human reference genome by BWA (hg19). Nucleotide changes in the aligned reads were reviewed using NextGENe software (Version 2.4.1.2; SoftGenetics, State College, PA, United States). Novel variants were filtered against the 1,000 Genomes (http://www.1000genomes.org/), dbSNP (http://www.ncbi.nlm.nih.gov/snp), and Genome Aggregation databases (http://gnomad.broadinstitute.org/). Databases of ClinVar (version #372716), OMIM (version #602063.0005), ClinGen (version #CA5788214), as well as Human Gene Mutation were referred to in the analyses. Furthermore, the software Mutation Taster and PROVEAN were used to predict the impact of non-sense variant. For the in-frame deletion variants, the prediction tool was NNSplice. Common variants (population frequency <1% in gnomAD) were considered. Finally, PCR was performed to amplify the affected fragment of *CHRND* gene (NM_000751.2) using specific primers, and the purified PCR products were applied to Sanger sequencing to affirm the variant(s).

Results

The results of QF-PCR and CMA were normal. And the minor allele frequency of c.1006C>T was 0.00002387 in gnomAD, which is also described in database dbSNP (rs754087173) and ClinVar (SCV002022550.1) but not recorded in the 1,000 Genomes databases. Moreover, the protein was truncated due to a non-sense variant, which caused a shift in the location of termination codon. And the in-frame deletion variant c.973_975delGTG resulted in protein length changes, which is not recorded in the gnomAD, dbSNP, and 1,000 Genomes databases. Based on the above mentioned outcomes and ACMG standards, one of the variants [NM_000751.2:c.1006C>T p.(Arg336Ter)] of *CHRND* gene, as maternal, was defined as likely pathogenic (LP:PVS1 + PM2) and the other [NM_000751.2:c.973_975delGTG p.(Val325del)], as paternal, was a variant of uncertain significance (VUS:PM2 + PM3 + PM4). Sanger sequencing of the fetus and parents further confirmed these results that parents were asymptomatic carriers of one variant (Figure 4).

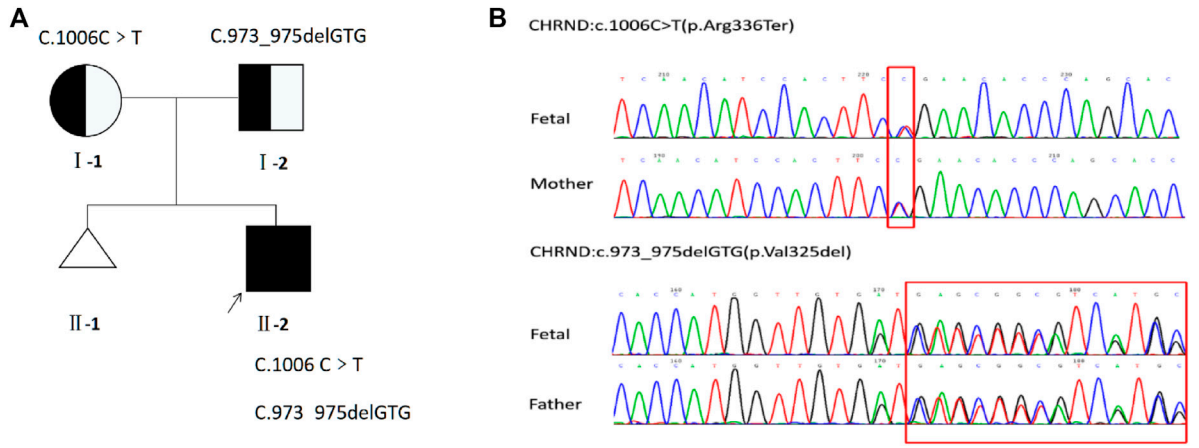


FIGURE 4
(A) Pedigree of the family. **(B)** Sequencing of *CHRND* gene (reference cDNA sequence, NM_000751.2) revealed two heterozygous variations, resulting in C to T substitution at nucleotide position 1006 [c.1006C>T p.(Arg336Ter)] and GTG deletion at nucleotide position 973 to 975 [c.973_975delGTG p.(Val325del)].

Previous cases

In the available literature, a total of four cases of LMPS caused by *CHRND* gene confirmed by US and genetic testing were reported from 2008 to 2018 (Table 1). Assuming that the information without mentioning sufficient in the articles were ruled out, it was revealed that only one case was found during early pregnancy which had four times of adverse pregnancy history, three of them may be LMPS by comprehensive analysis. And one showed micrognathia on the US but in the second trimester. Clinical details are summarized in Table 1.

Discussion

LMPS is a rare disease and is fatal before birth or in the early neonatal period (HALL, 1984), and until the advent of prenatal diagnosis for causative genes, fetal abnormalities observed on US and autopsy had remained the only method to diagnose the disorder (Lockwood et al., 1988). As far as previous reports are concerned, nearly 22 LMPS cases (born or unborn) had increased during the decade before 2000 (Moerman et al., 1990; Meyer-Cohen et al., 1999). However, the data lacked reliability and comparability due to the absence of diagnostic results. Therefore, few cases of LMPS had been definitively diagnosed antenatally. WES gradually became a vital prenatal diagnostic technique for this kind of diseases (Todd et al., 2015), and the variants of the proband not reported before were then newly observed.

LMPS is caused by primary defects at any point in the motor system, mainly due to abnormalities in AChR, which are crucial for signaling between nerve cells and muscle cells (Hall, 1997; Morgan et al., 2006). During the fetal development, muscle-specific AChR is critical for signal transmission between nerve and muscle cells, and composes of four different subunits, two α subunits, one β, one δ and one γ/ε subunit, decided by *CHRNA1*(MIM 100690), *CHRNB1* (MIM 100710), *CHRND* (MIM 100720) and *CHRNG* (MIM 100730)/*CHRNE* (MIM 100725), respectively. And the ε subunit will replace the γ after around 33 weeks gestation (Mishina et al., 1986). The process of AChR formation, including assembly, clustering, anchoring, activation, and linking, must be rigorous to ensure that all subunits are functional during signaling. At the same time, this process requires the participation of many functional proteins, Such as musculoskeletal tyrosine kinase [MUSK (MIM 601296)], the muscle-intrinsic activator of MUSK named downstream of tyrosine kinase 7 [DOK7 (MIM 610285)], and the receptor-associated protein, *RAPSN* (MIM 601592) et al. (Sanes and Lichtman, 2001). In conclusion, abnormalities in any of the steps will cause the corresponding disease. For the report, the non-sense variant (c.1006C>T) causing a shift in the location of termination codon resulted in protein truncation, and the in-frame deletion variant (c.973_975delGTG) made the number of amino acids reduced, thus shortening the protein length. According to the InterPro database, both sites are Neurotransmitter-gatedion-channel transmembrane regions and conserved regions. The above results may affect *CHRND* gene, which in turn affects δ subunit, further affects AChR, and finally leads to LMPS. However, the above analysis needs to be further confirmed by more experiments.

In this case, LMPS caused by *CHRND* gene mutation in the fetus is a fatal disease and an AR disorder, which comes from the parents in the carrier state (Orpha, 2019). The pregnant woman had a history of missed abortion in the past, and although no further relevant diagnostic examinations were performed, it could not be ruled out that it was caused by this gene mutation. Eight phenotypes of the fetus reported in this report were consistent with the OMIM database (Omim, 2017), including the classic phenotypes of pterygium, nuchal cystic hygroma, edema, limb flexion and absence of limb motion, and others such as micrognathia, low-set ears and cleft palate. However, other unrecognized phenotypes may be limited by the small gestational week of the fetus, of the fetus, limited mobility, and the absence of further autopsy and/or imaging after labor induction. In general, the genotype and phenotype analysis are basically consistent, which is consistent with the diagnostic results. The mutation caused by this gene should be paid attention to and detailed examination should be performed.

A total of three families have previously been reported to have affected fetuses. In a Turkish family reported in 2008, the first

TABLE 1 Summary of clinical manifestations in the current patients with *CHRND* gene variants.

Year	Michalk et al. (2008)			Shen et al. (2018)	Current case (2022)
Case	F1	F2		F3[f]	F4
Variant	NM_000751.2: c.234G>A(p.Trp57Ter)	NM_000751.2:c.1390C>T (p.Phe74Leu), NM_000751.2:c.283T>C (p.Arg443Ter)		NM_000751.2:c.236T>A (p. Ile79Lys), NM_000751.2:c.340G>C (p.Val114Leu)	NM_000751.2: c.973_975delGTG(p.Val325del), NM_000751.2:c.1006C>T(p.Arg336Ter)
Variant type	Homozygous non-sense	Compound non-sense-missense		Homozygous missense	Compound nonsense-in-frame deletion
Gender	M	M		M	M
Ethnicity	Turkish	German		NM	Chinese
Consanguinity	+	–		–	–
GA(week)	15[a]	13[a]	19[a]	31.5[b]	12[c]
Outcome	TOP	TOP	TOP	Death[d]	TOP
MA(yr)	NM	NM		NM	34
GPA	G3P1A1[e]	G5P0A4[e]	G6P0A5[e]	NM	G2P0A1[e]
Prenatal ultrasound findings					
Growth retardation	+	+	+	NM	–
Decreased movements	+	+	NM	NM	NM
Pterygia	NM	NM	NM	NM	–
Contracture	+	+	+	+	+
Polyhydramnios	NM	NM	NM	+	–
Edema/cystic hygroma	+/+	NM/+	+/+	NM	+/+
Absence of nassal bone	NM	NM	NM	NM	+
Cleft palate	NM	NM	NM	NM	-
Micrognathia	NM	NM	NM	NM	+
Low-set ears	NM	NM	NM	NM	–
Others features	NM	NM	NM	Absence of stomach bubble	Choroid plexus cyst
Phenotype of postpartum fetus					
Pterygia	+	+	+	+	+
Contracture	+	+	+	+	+
Edema/cystic hygroma	NM/NM	NM/NM	NM/NM	NM/NM	–/+
Cleft palate	NM	NM	NM	NM	+
Micrognathia	NM	+	+	+	+
Low-set ears	NM	+	+	NM	+
Scoliosis	+	NM	NM	NM	NM
Others features	Pectus excavatum;broad ribs, claviculae and os metatarsale; reduced muscle bulk/hypoplasia	NM	Facio cranial dysmorphism; down-slanting palpebral fissures; hypertelorism; a depressed nasal bridge	Small chest	Subscalp hemorrhage; short neck; bilateral fetal talipes; spina bifida

+, present; -, not present; GA, gestation age; TOP, termination of pregnancy; MA, maternal age; GPA, gravida para abortus; NM, not mentioned.
[a]GW, of TOP.
[b]GW, of amniocentesis.
[c]GW, at US, diagnosis.
[d]The fetus was delivered preterm and died shortly after birth.
[e]adverse pregnancy history.
[f]The variants originated from uniparental disomy (UPD) and the variants of c.340G>C (p.Val114Leu) was non-pathogenic.

pathogenic child did not receive further prenatal diagnosis, and the proband was the second child with LMPS, and the results showed that the *CHRND* gene suggested the first reported homozygous non-sense mutation. And in the German family, the genetic diagnosis of the fifth child was initiated, which indicated compound heterozygous mutation of *CHRND*, and the pregnancy was terminated in the first trimester, but the mother had already had two miscarriages and two pathogenic fetuses. The subsequent sixth abnormal fetus was identical to the fifth.

The pregnant women chose to terminate the above pregnancies (Michalk et al., 2008). This family may not receive genetic counseling and diagnosis in time, which may result in multiple adverse pregnancy history, and cause great trauma to the pregnant woman and her family. Therefore, further counseling and examination should be performed after fetal abnormalities are found. Additionally, the genetic mutation of *CHRND* in the fourth case reported in 2018 occurred in UPD on chromosome 2 (Shen et al., 2018), which further complemented the pathogenesis of LMPS. The fifth case of *CHRND* gene (NM_000751.2) with novel variant causing LMPS was presented in this report, but there were some differences. LMPS can be diagnosed prenatally in the first trimester without pregnancy history of LMPS. Micrognathia and absence of NB were observed in the US at early pregnancy and cleft palate was noted in the postpartum fetus, which the other cases were not reported in detail. In addition, the typical phenotypes of the fetus, such as nuchal cystic hygroma and contracture of the limbs, were highly consistent between prenatal super and induced labor. Generalized analysis, the fetus was classified to the "early" form of LMPS, and new clinical features were observed that could aid in early identification and diagnosis. Howerer, the typical sign of pterygium was not found by prenatal US in all the above cases, which may be due to the fact that the limbs of the fetus are often flexed and the movement of the fetus is limited and the cystic hygroma in the neck. We need to further improve the level of US technology and knowledge of doctors, which is conducive to the early detection of fetal abnormalities.

This may be the first case of LMPS, thus far, in which the facial angle was measured by 3D US to identify micrognathia during early pregnancy. Maxilla–nasion–mandible angle (MNM), inferior facial angle (IFA), and frontal nasomental angle (FNM) were excluded due to the absence of NB, and MMF was selected. Compared with the critical value of previous statistical results in the first trimester, the value was less than normal [MMF 103.1°–114.5° (Borenstein et al., 2007)], which provides an objective reference index for micrognathia. In addition, the various modes of 3D US compensate for the defects in 2D US so that the fetal structure is clear and easy to observe (Platt et al., 2006). This facilitates the early detection of more abnormal phenotypes in the fetus to attain a definitive diagnosis and determine the next management measures.

It has been demonstrated that the autopsy results are vital for further analysis of the genetics and phenotype of prenatal VUS and LP. Based on the comprehensive analyses of prenatal and postnatal phenotypes, one of the mutations (c.1006C>T) was defined as pathogenic (P: PVS1 + PM2 + PP4) and the other (c.973_975del) was LP (PM2 + PM3 + PM4 + PP4), which reversely confirmed the prenatal phenotype and disease outcome corresponding to *CHRND* gene (NM_000751.2). In addition, the parents are made aware that the risk of the offspring developing the disease is 25% after prenatal consultation. They should also be offered preventive measures. As the primary prevention strategy, the couple should consider undergoing adjuvant reproductive technology (ART). As the secondary prevention strategy, routine examination (consultation, ultrasound, and molecular diagnosis) would be indispensable for pregnant women with abnormal fetuses, and then timely intervention to choose the best course of treatment.

In conclusion, we have reported compound heterozygous variants apart from the variation spectrum of the *CHRND* (NM_000751.2) gene and a new diagnosis method for the early recognition of micrognathia, which is vital to provide appropriate genetic counseling to the parents. And micrognathia and nuchal cystic hygroma can be identified in the first trimester, which should be focused on, and clinical intervention should be performed as soon as possible.

Data availability statement

The datasets for this article are not publicly available due to concerns regarding participant/patient anonymity. Requests to access the datasets should be directed to the corresponding author.

Ethics statement

Written informed consent was obtained from the individual(s) for the publication of any potentially identifiable images or data included in this article.

Author contributions

All authors listed have made a substantial, direct, and intellectual contribution to the work and approved it for publication.

Funding

This study was supported (or partially supported) by the two foundations: GuangDong Basic and Applied Basic Research Foundation (2021A1515220070), and Guangzhou Women and Children's Medical Center (GWCMC2020-6-007).

Acknowledgments

The authors would like to thank the family members for their participation and staff members at the Prenatal diagnosis center of Guangzhou Women and Children's Medical Center, Guangdong Province, China, for their cooperation. The authors would also like to thank two foundations [GuangDong Basic and Applied Basic Research Foundation (2021A1515220070), and Guangzhou Women and Children's Medical Center (GWCMC2020-6-007)] and the Genome Aggregation database (gnomAD) for providing genome variant data.

Conflict of interest

The authors declare that the research was conducted in the absence of any commercial or financial relationships that could be construed as a potential conflict of interest.

Publisher's note

All claims expressed in this article are solely those of the authors and do not necessarily represent those of their affiliated organizations, or those of the publisher, the editors and the reviewers. Any product that may be evaluated in this article, or claim that may be made by its manufacturer, is not guaranteed or endorsed by the publisher.

References

Abdalla, E., Ravenscroft, G., Zayed, L., Beecroft, S. J., and Laing, N. G. (2017). Lethal multiple pterygium syndrome: A severe phenotype associated with a novel mutation in the nebulin gene. *Neuromuscul. Disord.* 27 (6), 537–541. doi:10.1016/j.nmd.2017.01.013

Borenstein, M., Persico, N., Strobl, I., Sonek, J., and Nicolaides, K. H. (2007). Frontomaxillary and mandibulomaxillary facial angles at 11 + 0 to 13 + 6 weeks in fetuses with trisomy 18. *Ultrasound Obstet. Gynecol.* 30 (7), 928–933. doi:10.1002/uog.5188

Brink, D. S., Luisiri, A., and Grange, D. K. (2003). Case report: Lethal multiple pterygium syndrome. *Pediatr. Pathol. Mol. Med.* 22 (6), 461–470. doi:10.1080/pdp.22.6.461.470

de Die-Smulders, C. E., Schrander-Stumpel, C. T., and Fryns, J. P. (1990a). The lethal multiple pterygium syndrome: A nosological approach. *Genet. Couns. (Geneva, Switzerland).* 1 (1), 13–23.

de Die-Smulders, C. E., Vonsée, H. J., Zandvoort, J. A., and Fryns, J. P. (1990b). The lethal multiple pterygium syndrome: Prenatal ultrasonographic and postmortem findings; a case report. *Eur. J. Obstet. Gynecol. Reprod. Biol.* 35 (2-3), 283–289. doi:10.1016/0028-2243(90)90175-z

Engel, A. G., Shen, X. M., Selcen, D., and Sine, S. M. (2015). Congenital myasthenic syndromes: Pathogenesis, diagnosis, and treatment. *Lancet Neurol.* 14 (4), 461–34. doi:10.1016/S1474-4422(15)00010-1

Hall, J. G. (1997). Arthrogryposis multiplex congenita: Etiology, genetics, classification, diagnostic approach, and general aspects. *J. Pediatr. Orthop. B* 6 (3), 159–166. doi:10.1097/01202412-199707000-00002

Hall, J. G. (1984). Editorial comment: The lethal multiple pterygium syndromes. *Am. J. Med. Genet.* 17 (4), 803–807. doi:10.1002/ajmg.1320170410

Hertzberg, B. S., Kliewer, M. A., and Paulyson-Nunez, K. (2000). Lethal multiple pterygium syndrome: Antenatal ultrasonographic diagnosis. *J. Ultrasound Med.* 19 (9), 657–660. doi:10.7863/jum.2000.19.9.657

Lockwood, C., Irons, M., Troiani, J., Kawada, C., ChAudhury, A., and Cetrulo, C. (1988). The prenatal sonographic diagnosis of lethal multiple pterygium syndrome: A heritable cause of recurrent abortion. *Am. J. Obstet. Gynecol.* 159 (2), 474–476. doi:10.1016/s0002-9378(88)80112-1

Meizner, I., Hershkovitz, R., CaRmi, R., and KatzM. (1993). Prenatal ultrasound diagnosis of a rare occurrence of lethal multiple pterygium syndrome in two siblings. *Ultrasound Obstet. Gynecol.* 3 (6), 432–436. doi:10.1046/j.1469-0705.1993.03060432.x

Meyer-Cohen, J., Dillon, A., and Conradi, S. (1999). Lethal multiple pterygium syndrome in four male fetuses in a family: Evidence for an X-linked recessive subtype? *Am. J. Med. Genet.* 82 (1), 97–99. doi:10.1002/(sici)1096-8628(19990101)82:1<97::aid-ajmg22>3.0.co;2-g

Michalk, A., Stricker, S., Becker, J., Rupps, R., Pantzar, T., Miertus, J., et al. (2008). Acetylcholine receptor pathway mutations explain various fetal akinesia deformation sequence disorders. *Am. J. Hum. Genet.* 82 (2), 464–476. doi:10.1016/j.ajhg.2007.11.006

Mishina, M., Takai, T., Imoto, K., NodaM.Takahashi, T., Numa, S., et al. (1986). Molecular distinction between fetal and adult forms of muscle acetylcholine receptor. *Nature* 321 (6068), 406–411. doi:10.1038/321406a0

Moerman, P., Fryns, J. P., Cornelis, A., BerGmans, G., Vandenberghe, K., and Lauweryns, J. M. (1990). Pathogenesis of the lethal multiple pterygium syndrome. *Am. J. Med. Genet.* 35 (3), 415–421. doi:10.1002/ajmg.1320350319

Mohtisham, F. S., Sallam, A., and Shawli, A. (2019). Lethal multiple pterygium syndrome. *BMJ Case Rep.* 12 (5), e229045. doi:10.1136/bcr-2018-229045

Morgan, N. V., Brueton, L. A., Cox, P., Greally, M. T., Tolmie, J., Pasha, S., et al. (2006). Mutations in the embryonal subunit of the acetylcholine receptor (CHRNG) cause lethal and Escobar variants of multiple pterygium syndrome. *Am. J. Hum. Genet.* 79 (2), 390–395. doi:10.1086/506256

Omim (2017). Gene-phenotype relationships. Available at: https://www.omim.org/entry/100720?search=CHRND&highlight=chrnd#geneMap.

Orpha (2019). Orpha.net. Available at:https://www.orpha.net/consor/cgi-bin/OC_Exp.php?lng=en&Expert=33108.2019.

Platt, L. D., Devore, G. R., and Pretorius, D. H. (2006). Improving cleft palate/cleft lip antenatal diagnosis by 3-dimensional sonography: The "flipped face" view. *J. Ultrasound Med.* 25 (11), 1423–1430. doi:10.7863/jum.2006.25.11.1423

Sanes, J. R., and Lichtman, J. W. (2001). Induction, assembly, maturation and maintenance of a postsynaptic apparatus. *Nat. Rev. Neurosci.* 2 (11), 791–805. doi:10.1038/35097557

Shen, W., Young, B. A., BosworthM.Wright, K. E., Lamb, A. N., and Ji, Y. (2018). Prenatal detection of uniparental disomy of chromosome 2 carrying a CHRND pathogenic variant that causes lethal multiple pterygium syndrome. *Clin. Genet.* 93 (6), 1248–1249. doi:10.1111/cge.13164

Todd, E. J., Yau, K. S., Ong, R., Slee, J., McGillivray, G., Barnett, C. P., et al. (2015). Next generation sequencing in a large cohort of patients presenting with neuromuscular disease before or at birth. *Orphanet J. Rare Dis.* 10, 148. doi:10.1186/s13023-015-0364-0

Tolmie, J. L., Patrick, A., and Yates, J. R. (1987). A lethal multiple pterygium syndrome with apparent X-linked recessive inheritance. *Am. J. Med. Genet.* 27 (4), 913–919. doi:10.1002/ajmg.1320270418

frontiers | Frontiers in Genetics

TYPE Case Report
PUBLISHED 26 January 2023
DOI 10.3389/fgene.2023.1062326

Check for updates

OPEN ACCESS

EDITED BY
Mike Mikailov,
United States Food and Drug Administration, United States

REVIEWED BY
Manish Kumar Sinha,
National Dairy Research Institute (ICAR), India
Pradeep Nag,
University of Missouri System, United States

*CORRESPONDENCE
Alice Luddi,
luddi@unisi.it

†These authors have contributed equally to this work and share last authorship

‡These authors have contributed equally to this work and share first authorship

SPECIALTY SECTION
This article was submitted to Genetics of Common and Rare Diseases, a section of the journal Frontiers in Genetics

RECEIVED 05 October 2022
ACCEPTED 06 January 2023
PUBLISHED 26 January 2023

CITATION
Luongo FP, Luddi A, Ponchia R, Ferrante R, Di Rado S, Paccagnini E, Gentile M, Lupetti P, Guazzo R, Orrico A, Stuppia L and Piomboni P (2023), Case report: The CCDC103 variant causes ultrastructural sperm axonemal defects and total sperm immotility in a professional athlete without primary ciliary diskinesia.
Front. Genet. 14:1062326.
doi: 10.3389/fgene.2023.1062326

COPYRIGHT
© 2023 Luongo, Luddi, Ponchia, Ferrante, Di Rado, Paccagnini, Gentile, Lupetti, Guazzo, Orrico, Stuppia and Piomboni. This is an open-access article distributed under the terms of the Creative Commons Attribution License (CC BY). The use, distribution or reproduction in other forums is permitted, provided the original author(s) and the copyright owner(s) are credited and that the original publication in this journal is cited, in accordance with accepted academic practice. No use, distribution or reproduction is permitted which does not comply with these terms.

Case report: The CCDC103 variant causes ultrastructural sperm axonemal defects and total sperm immotility in a professional athlete without primary ciliary diskinesia

Francesca Paola Luongo[1‡], Alice Luddi[1‡*], Rosetta Ponchia[1], Rossella Ferrante[2], Sara Di Rado[2], Eugenio Paccagnini[3], Mariangela Gentile[3], Pietro Lupetti[3], Raffaella Guazzo[4], Alfredo Orrico[1], Liborio Stuppia[2†] and Paola Piomboni[1,5†]

[1]Department of Molecular and Developmental Medicine, University of Siena, Siena, Italy, [2]Department of Psychological Sciences, Health and Territory, University of Chieti-Pescara, Chieti, Italy, [3]Department of Life Sciences, University of Siena, Siena, Italy, [4]Pathology Unit, Siena University Hospital, Siena, Italy, [5]Assisted Reproductive Unit, Siena University Hospital, Siena, Italy

Primary ciliary dyskinesia (PCD) is an inherited autosomal-recessive disorder characterized by abnormal ciliary motion, due to a defect in ciliary structure and/or function. This genetic condition leads to recurrent upper and lower respiratory infections, bronchiectasis, laterality defect, and subfertility. Male infertility is often associated with PCD, since the ultrastructure of the axoneme in the sperm tail is similar to that of the motile cilia of respiratory cells. We present the first reported case of a male patient from a non-consanguineous Italian family who exhibited a severe form of asthenozoospermia factor infertility but no situs inversus and absolutely no signs of the clinical respiratory phenotype, the proband being a professional basketball player. Whole-exome sequencing (WES) has identified a homozygote mutation (CCDC103 c.461 A>C, p.His154Pro) in the proband, while his brother was a heterozygous carrier for this mutation. Morphological and ultrastructural analyses of the axoneme in the sperm flagellum demonstrated the complete loss of both the inner and outer dynein arms (IDA and ODA, respectively). Moreover, immunofluorescence of DNAH1, which is used to check the assembly of IDA, and DNAH5, which labels ODA, demonstrated that these complexes are absent along the full length of the flagella in the spermatozoa from the proband, which was consistent with the IDA and ODA defects observed. Noteworthy, TEM analysis of the axoneme from respiratory cilia showed that dynein arms, although either IDAs and/or ODAs seldom missing on some doublets, are still partly present in each observed section. This case reports the total sperm immotility associated with the CCDC103 p.His154Pro mutation in a man with a normal respiratory phenotype and enriches the variant spectrum of ccdc103 variants and the associated clinical phenotypes in PCD, thus improving counseling of patients about their fertility and possible targeted treatments.

KEYWORDS

sperm immotility, axoneme, ccdc103, nasal cilia, dynein arms, infertility

Introduction

The movement of sperm cells is due to the axonemal complex, where the motile activity is generated by two series of adenosine triphosphate (ATP)-dependent dynein arms, that generates a sliding force that is transformed into a wave throughout the whole sperm tail by accessory cytoskeletal structures. According to the number of heavy-chain motors within each dynein complex, different group of dyneins may be distinguished; usually, heavy chains are considerable proteins composed of about 4500 residues. Apart from dyneins, additional components are required for the assembly of the final motor complexes as well as for the regulation of their movement. Indeed, the axoneme assembly is a very complex process, and the mechanism of the correct arrangement of all the dynein arms on the doublet microtubules is still a key question (King, 2016). As regard to the outer arms to interact with the doublet microtubules, several docking complexes including coiled-coil proteins (DC1 and DC2) and a calmodulin homolog (DC3) are needed (Takada and Kamiya, 1994). More recently, an additional protein, namely, coiled-coil domain containing-103 (ccdc103), has been demonstrated to be essential for outer arm insertion into the microtubule structure (texture) (Panizzi et al., 2012). ccdc103 has very important biophysical properties (e.g., a very high melting temperature) as well as the ability to form highly stable dimers and/or oligomers. Due to these peculiar properties, it has been supposed that ccdc103 polymerization during axonemal growth may provide, along the outer doublets, a high-affinity road with which the heterotrimeric outer arms/docking complex (ODA/DC) can then associate (Takada and Kamiya, 1994; Owa et al., 2014). Mutations in ccdc103 have been detected in primary ciliary dyskinesia (PCD, MIM 244400) patients with situs inversus totalis and absence of dynein arms in the sperm (Shoemark et al., 2018; Pereira et al., 2019). PCD, whose estimated global prevalence is about 1:10000 live-born children (Afzelius and Stenram, 2006; Hannah et al., 2022), is a heterogeneous autosomal recessive disease characterized by abnormal ciliary motion, due to a defect in ciliary structure and/or function. This genetic condition leads to recurrent upper and lower respiratory tract infections, bronchiectasis, laterality defect, and subfertility (Mirra et al., 2017). Male infertility is often associated with PCD, since the ultrastructure of the axoneme in the sperm tail is similar to that of motile cilia of respiratory cells (Sironen et al., 2020). Indeed, numerous mutations in more than 40 genes have been so far identified causing asthenozoospermia in PCD patients (Olm et al., 2015; Boaretto et al., 2016). Motility defects, indeed, have been identified in men bearing mutations in CFAP300 and in DNAF2 that show complete absence of dynein arms; the lack of inner dynein arms is a feature of sperm bearing mutations in DNAH1 and DNAH2, while mutations of CCDC40 induce axonemal disorganization and complete asthenozoospermia. Likewise, mutations of proteins forming the radial spokes (CFAP251) and the central pairs (e.g., AK7 and ARMC2) cause total sperm immotility (Sironen et al., 2020).

A high heterogeneity has been reported associated to the missense mutation p.His154pro (rs145457535) in ccdc103, with patients showing different degrees of axonemal defects, ranging from normal ultrastructure to partial or complete ODA/IDA defects (Casey et al., 2015; Shoemark et al., 2018).

The availability of multiple algorithms for diagnosis (Shoemark et al., 2019) and the presence of PCD phenotype heterogeneity still make the PCD confirmation a challenge. Therefore, a better knowledge of the pathogenic effect of mutation in PCD-related genes is advised.

Patients and methods

The patient, a 40-year-old man from a non-consanguineous family, underwent spermatological and genetic analyses during an infertility evaluation for the search of a pregnancy at the ART Centre of the Siena University Hospital, Italy. The most recurrent causes for male infertility (including hormone levels, chromosomal defects, and Y-chromosome microdeletion) were excluded. The medical history of the subject was recovered, and respiratory complaints were excluded. Moreover, chest X-ray revealed normal left/right body symmetry. Ejaculated sperm, nasal cilia, and peripheral blood samples were collected from the patient; peripheral blood sample was also collected from the patient's brother. All the participants provided written informed consent for the use of their samples and data. This study was approved by the University of Siena's ethics committee (CEAVSE, protocol number 18370, 2/10/2020). All experiments were performed in accordance with the relevant guidelines and regulations.

Genomic DNA preparation and whole-exome sequencing

Exome sequencing was performed on the patient by extracting DNA from the blood and ejaculated sperm using QIAamp DNA Blood Kits (Qiagen, Hilden, Germany) following the manufacturer's instructions. Whole-exome sequencing (WES) was performed using the Ion Torrent S5 system (Thermofisher, Applied Biosystem; Foster City, CA, United States) after library preparation using Ion AmpliSeq™ Exome RDY Kit 4 × 2 (Thermofisher, Applied Biosystem; Foster City, CA, United States), consisting of fragmentation and adapter ligation onto the PCR products and clonal amplification. The sequencing step was carried out with Ion Torrent specific equipment and reagents according to the protocols. The prepared samples of ion sphere particles (ISPs) were loaded onto an Ion 550™ chip with the Ion Chef (Thermofisher, Applied Biosystem; Foster City, CA, United States), and sequencing was performed using the Ion S5™ sequencing reagents (Thermofisher, Applied Biosystem; Foster City, CA, United States). NGS data analysis was performed using Ion Reporter 5.14 software (Thermofisher; Foster City, CA, United States), which performs alignment between the obtained data and the Hg19 Human reference genome. Specifically, 34 genes related to PCD/Kartagener syndrome were selected and analyzed (gene table, Supplementary File S3). The sequencing analysis produced a total of 293,903 amplicons. The uniformity of base coverage was over 98% in all batches, and the base coverage was over 20 X at all target regions. Sanger sequencing was used for the confirmation of the gene variant detected by WES.

Transmission electron microscopy

Samples of nasal mucosa and ejaculated sperm were fixed in 2.5% glutaraldehyde diluted in 0.1 M sodium cacodylate buffer, pH 7.2 for 1 h, washed in cacodylate buffer overnight, and postfixed in 1% osmium tetroxide for 1 h at 4°C. The samples were dehydrated

with a graded series of ethanol and embedded in epoxy resin. In order to improve microtubule's visualization, a rate of ejaculated sperm was fixed in a mixture of 2% glutaraldehyde and 1% tannic acid in 0.1 M phosphate buffer. The sample was left in the fixative for a week and then washed 10 times for 5 min in distilled water; after that, the sample was stained for 2 h in 1% uranyl acetate in distilled water (Afzelius et al., 1995). The sample was dehydrated and embedded as previously described. Ultrathin sections of 70 nm were collected on copper grids, stained with uranyl acetate and lead citrate, and observed with an FEI Tecnai G2 Spirit transmission electron microscope (Hillsboro, OR, United States) equipped with a TVIPS CMOS camera TemCam F-216 (Gauting, Germany).

Immunofluorescence analysis

Immunofluorescence on the spermatozoa was performed after fixation with 4% PFA for 25 min as previously described (Luddi et al., 2022). Once resuspended, the samples were smeared into glass slides and left to dry. The slides were incubated in a blocking solution containing 5% goat normal serum in 1% PBS/BSA (bovine serum albumin) and then incubated overnight at 4°C with DNAH1, DNAH5, and anti-β-tubulin primary antibodies (RRID: AB_10670849, AB_10672791, and AB_1844090, respectively) used according to the manufacturer's instructions. The slides were washed three times in PBS and incubated with FITC-labeled anti-rabbit and TRITC-labeled anti-mouse secondary antibodies (Supplementary Table S1). After washing in PBS, the slides were stained with 4′,6-diamidino-2-phenylindole (DAPI) (LifeTechnologies, Carlsbad, CA, United States) to counterstain the nuclei, mounted with DABCO, and then, observed with a Leica DM6000 microscope (Leica Mycrosistem, Wetzlar, Germany). Images were captured with a CFTR6500 digital camera (Leica Mycrosistem, Wetzlar, Germany). The specificity of immunostaining was confirmed by using pre-immune sera instead of the primary antibody, followed by incubation with the secondary antibody.

Bioinformatics

The PubMed (https://pubmed.ncbi.nlm.nih.gov/), OMIM (https://secure.jhu.edu/form/OMIM), HGMD (https://www.hgmd.cf.ac.uk/ac/index.php), ClinVar (https://www.ncbi.nlm.nih.gov/clinvar/), and gnomAD v2.1.1 (https://gnomad.broadinstitute.org/) databases and the professional version of the Human Splicing Finder system (HSF_Pro) were used to evaluate the pathogenicity of the variants. Variant annotation was carried out through TVC- Torrent Variant Caller and Ion Reporter 5.14. The mutated protein was predicted by MutPred2 and Polyphen2 and analyzed by DynaMut software (Rodrigues et al., 2018). CCDC103 protein Q8IW40.pdb and the point amino acid mutation H154P were analyzed by DynaMut software. The impact of amino acid changes in any given protein is predicted based on the positive or negative changes in Gibbs free energy ($\Delta\Delta G^{\circ}$) between unfolded *versus* folded states in that protein. It is well known that a protein $\Delta\Delta G^{\circ}$ can represent its stability as a value. STRING analysis was performed by using STRING network building tool software (https://string-db.org) by the "multiple protein" option. *Homo sapiens* was selected as the preferred "organism." In the "settings" section, "molecular action" was selected as the preferred interaction among proteins to be visualized. Textmining, experiments, databases, and co-expression were selected as active interaction sources. The minimum required interaction score was 0.700, which was considered high confident. No more than five interactors were permitted to be added. The network view summarizes the predicted associations for a particular group of proteins. The nodes represent proteins, while the edges represent the predicted functional associations.

Results

Semen analysis and ultrastructural evaluation of the axoneme structure

The patient, a 40-year-old man from a non-consanguineous family, underwent spermatologic and genetic analyses during an infertility evaluation for the search of a pregnancy at the ART Centre of the University Hospital, at Siena, Italy. The most recurrent causes for male infertility (including hormone levels, chromosomal defects, and Y-chromosome microdeletions) were excluded, and semen analyses at light microscopy according to the WHO (WHO laboratory manual for the examination and processing of human semen, 2022) were repeated four times during a period of 2 years showing sperm parameters over the 5th percentile, except for the progressive motility, which resulted in all sample being completely absent (0%) (Supplementary Table S2). To further characterize the gamete ultrastructure, we carried out transmission electron microscopy (TEM) of the ejaculated sperm. TEM of sperm tails sections conducted at different sectioning levels revealed the complete absence in all the examined cells of both the inner and outer dynein arms (IDA and ODA, respectively), the microtubule-associated molecular motors with ATPase activity which, by promoting the reciprocal sliding of doublets, enable flagellar beating (Figures 1A–C). The same scenario was also confirmed in a rate of ejaculated sperm treated with tannic acid. In particular, in this sample, it was possible to evidence that the doublets have a canonical A- and B-tubule protofilament pattern (Figures 1D, E). No structural alterations of other axonemal components, such as nexin bridges, connecting adjacent microtubular doublet or radial spokes were identified.

In order to confirm the absence of the dynein arm protein along the sperm flagellum, we carried out immunofluorescence of DNAH1 (Figure 1F, upper panel), which is used to check the assembly of IDA and DNAH5 (Figure 1F, lower panel), which labels ODA, in sperm from the proband and unmutated individuals. In the normal spermatozoa, immunostaining of the proteins was located along the whole sperm tail, whereas DNAH1 and DNAH5 immunostaining was absent along the full length of the flagella in the sperm from the proband, which was consistent with the IDA and ODA absence observed at the TEM level (Figures 1A–C); nor the proteins were delocalized in other cellular compartments, such as cytoplasmic residues. The defect affecting the sperm axoneme is, therefore, compatible with PCD, which is clinically considered a severe risk factor for infertility. In order to confirm the diagnosis of PCD, nasal cilia samples were evaluated at the ultrastructural level. Our observations revealed that the dynein arms were not uniformly distributed along microtubular doublets with either IDAs and/or ODAs seldom missing on some doublets in the observed sections. Other detectable modifications of cytoskeletal axonemal components were not found (Figures 1G–L). The ultrastructural feature of the nasal ciliary axoneme is coherent with the absence of respiratory problems in the patient, despite the total sperm immotility.

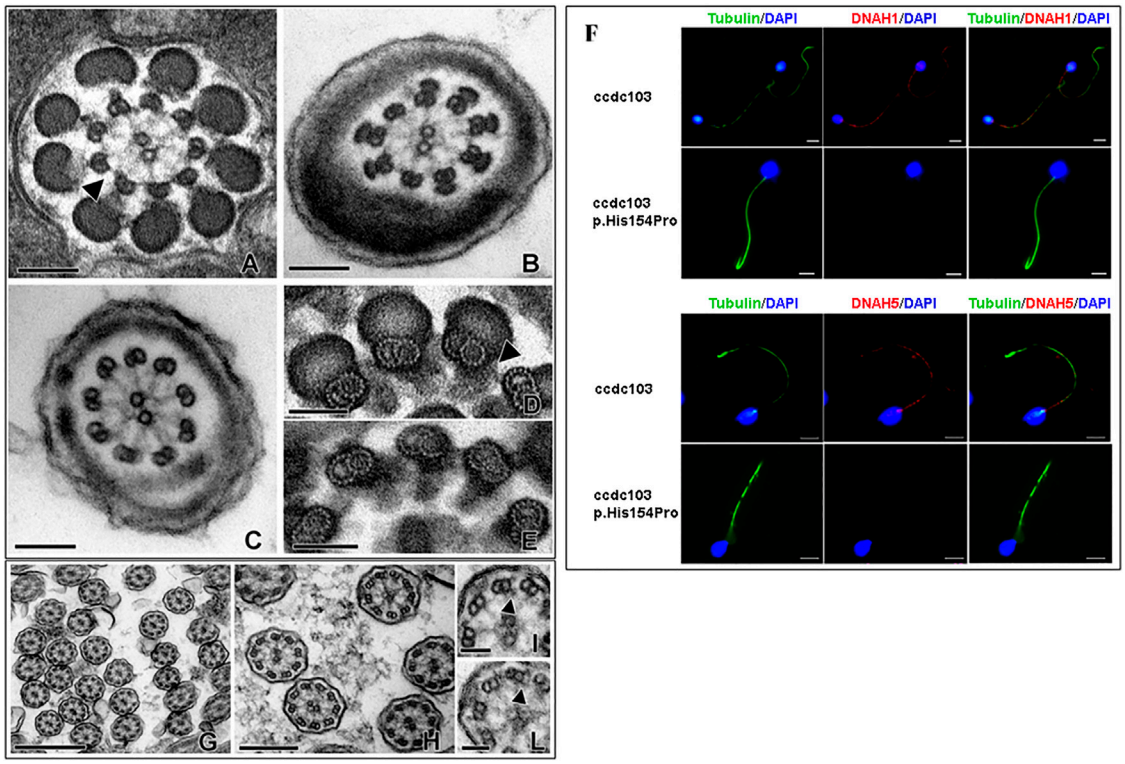


FIGURE 1
Electron microscopy micrographs of different section levels of the spermatozoa flagellum with a focus on IDA and ODA **(A–C)**, spermatozoa samples treated with tannic acid **(D, E),** and nasal mucosa samples **(G–L)**. Scale bar for A-B-C 100 nm, D-E-H-I 50 nm, F 500 nm, and G 200 nm. Immunofluorescence **(F)** of the ejaculated sperm revealed the absence of both DNAH1 and DNAH5 in the patient (red) compared to the normal control. An anti-tubulin antibody was used to mark the sperm axoneme (green), and DAPI was used to label the nuclei (blue).

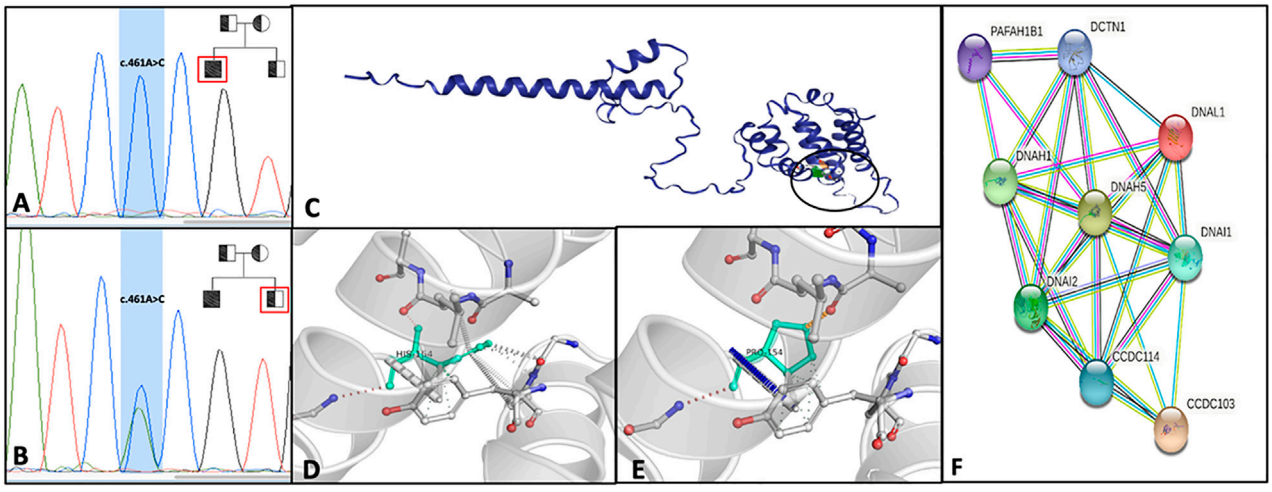


FIGURE 2
Electropherograms of the patients with ccdc103 c.461 A>C mutation in homozygous **(A)** and his heterozygote brother **(B)**; in the right corner of Images A and B, the family pedigree is shown. Squares and circles represent, respectively, males and females. Filled symbol represents the affected member, and slashed symbols represent deceased members. **(C)** DynaMut prediction of interactomic interaction of CCDC103. Wild-type **(D)** and mutant H154P **(E)** residues are colored in light green and represented as sticks alongside the surrounding residues involved in any interactions. **(F)** STRING analysis summarizing functional information about ccdc103 with respect to the biological process, gene ontology category and predicting possible associations among them. STRING networks consist of nodes (spheres) representing proteins, while edges represent the predicted mode of action among proteins.

Identification of a homozygous mutation p.His154Pro in CCDC103

We performed WES in the DNA extracted from the ejaculated sperm of the patient, and we found the homozygous variant c.461 A>C. This mutation results in the nucleotide substitution A>C in position 461 in exon 4 of the *CCDC103* gene and causes the substitution of the amino acid histidine with prolin in position 154 of the coded protein (p.His154Pro). Sanger sequencing confirmed the presence of this variant in the genomic DNA isolated from peripheral lymphocytes of the proband (Figure 2A), thus excluding a *de novo* germinal mutation. The genetic investigation of the brother, a fertile man without PCD symptoms, revealed the same variant in heterozygosis, definitively demonstrating their parents are obligate carriers of this mutation (Figure 2B).

This CCDC103 mutation has been previously reported with variable phenotypes (Casey et al., 2015; Pereira et al., 2019; Shoemark et al., 2019); to better understand its pathogenicity at the molecular level, we performed *in silico* analysis using DynaMut2 software. The prediction of the change in stability upon point mutations in proteins has many applications in protein analysis and engineering. The stability of the abovementioned single amino acid variants was analyzed by normal mode analysis (NMA) using DynaMut. The total predicted change in stability ΔΔG (kcal/mol) for CCDC103 amino acid point substitution p.His154Pro is .549 with a confidence estimation of .802. ΔΔGpred <.0 indicates a stabilizing estimation, confidence estimation given as a value between .0 (not reliable) and 1.0 (highly reliable) (Figures 2C–E).

The STRING analysis (http://string-db.org/) of the interactors of CCDC103 pointed to a number of related proteins, most notably, DNAH1, DNAH5, DNAI1, and DNAI2 (Figure 2F). Proteins reported in the net are involved in outer and inner dynein arms assembly and regulation of cilium movement biological processes. Moreover, among diseases–genes associations are highlighted *situs inversus* and PCD, and among GO, dynein intermediate chain binding (GO:0045505), ATP-dependent microtubule motor activity, minus-end-directed (GO:0008569), and dynein light intermediate chain binding (GO:0051010) were identified.

Discussion

This study simultaneously evaluated the effect of the CCDC103 p.His154Pro gene mutation on the ultrastructure of the axoneme in both respiratory cilia and sperm flagellum. CCDC103 p.His154Pro was previously reported as a high prevalence mutation causing PCD (Casey et al., 2015; Shoemark et al., 2018; Zubair et al., 2022). Anyway, the men carrying this homozygote mutation showed a fully immotile sperm but no *situs inversus* and absolutely no signs of clinical respiratory problems, the proband being a professional basketball player.

CCDC103 is an oligomeric coiled-coil domain protein that specifically binds and stabilizes polymerized microtubules, thus playing a critical role in the dynein arms assembly (King and Patel-King, 2015). Several studies demonstrated that the p.His154Pro variant in CCDC103 affected indistinctly both the cilia and the sperm flagellum, therefore hypothesizing that this mutation may act in a shared pathway of dynein arms formation in both cell types. This case reports evidence of different degrees of ultrastructural abnormalities in the axoneme of respiratory cells, with only a partial ODA and/or IDA lacking in analyzed axonemes. At the same time, we report the complete absence of both IDA and ODA arms in all sperm flagella. This significant pleiotropic effect may justify the total absence of respiratory problems in the patient, despite the complete sperm immotility.

A previous study reported this mutation affecting the axoneme of both cilia and sperm, thus suggesting that this variant in CCDC103 acts in a shared pathway of dynein arms formation in both cell types (Zubair et al., 2022). Anyway, some differences are known in the pathways regulating the axoneme structure of cilia and sperm, with NOTCH signaling required to activate the centriole amplification genes in cilia development, whereas WNT signaling playing a critical role in sperm flagellum formation (Choksi et al., 2014).

Our data are also supported by a recently published study demonstrating the tissue specific activity of this CCDC103. Indeed, CCDC103 forms dimers and higher order oligomers whose sizes appear tissue-specific (Pereira et al., 2019). Moreover, CCDC103 is expressed at a very high level in the sperm, while its expression in nasal cells is very low (Pereira et al., 2019). These data further confirm that CCDC103 may have a special role in sperm function and corroborate our findings showing a different spectrum of alteration in nasal *versus* sperm axoneme, where all IDA and ODA were missing.

In silico analysis classified with high confidence scores as deleterious this variation; the much reduced frequency of p.His154Pro in population databases further supports a presumed pathogenic role of this sequence variant.

In conclusion, we report the total sperm immotility associated with the CCDC103 p.His154Pro mutation in a man with a normal respiratory phenotype. Major limitation of this study is that we cannot exclude the fact that this proband is an unusual outlier, displaying a complete IDA and ODA loss phenotype exclusively in the sperm. Anyway, this case report, enriching the variant spectrum of CCDC103 variants and the associated clinical phenotypes in PCD, will improve the counseling for infertile patients with severe sperm motility problems suggesting a revision of the fertility guidelines that must include an accurate ultrastructural analysis of the ejaculated sperm. Moreover, the identification of this mutation has directed the diagnostic process toward the CCDC103 gene sequencing also in his partner; this allows offering a correct genetic counseling about the inheritance of this trait to the offspring. Transmission electron microscopy represents the gold standard to diagnose these genetic-based sperm defects (Baccetti et al., 2001) and should be offered to this type of patients, given the pleiotropic expression of CCDC103 we demonstrated, in accordance with the scientific literature.

Data availability statement

The original contributions presented in the study are publicly available. This data can be found here: https://www.ncbi.nlm.nih.gov/sra/PRJNA924559.

Ethics statement

The studies involving human participants were reviewed and approved by CEAVSE University Hospital. The patients/participants provided their written informed consent to participate in this study.

Author contributions

PP and LS conceived and designed the study; AO, PP, and LS provided patient clinical data and samples; AL, FPL, and MG prepared the draft of the manuscript; AL, FPL, EP, RP, RG, MG, SD, and RF performed the bioinformatics analysis and experiments; and PP, LS, AL, PL, and LS reviewed and edited the manuscript. All authors revised the manuscript critically, approved the final manuscript as submitted, and agreed to be accountable for all aspects of the work.

Funding

This study was supported by the University of Siena's and University of Chieti's internal funds.

Acknowledgments

The authors are grateful to the patients and family members for their participation in this study.

Conflict of interest

The authors declare that the research was conducted in the absence of any commercial or financial relationships that could be construed as a potential conflict of interest.

Publisher's note

All claims expressed in this article are solely those of the authors and do not necessarily represent those of their affiliated organizations, or those of the publisher, the editors, and the reviewers. Any product that may be evaluated in this article, or claim that may be made by its manufacturer, is not guaranteed or endorsed by the publisher.

Supplementary material

The Supplementary Material for this article can be found online at: https://www.frontiersin.org/articles/10.3389/fgene.2023.1062326/full#supplementary-material

References

Afzelius, B. A., Dallai, R., Lanzavecchia, S., and Bellon, P. L. (1995). Flagellar structure in normal human spermatozoa and in spermatozoa that lack dynein arms. *Tissue Cell* 27, 241–247. doi:10.1016/s0040-8166(95)80044-1

Afzelius, B. A., and Stenram, U. (2006). Prevalence and genetics of immotile-cilia syndrome and left-handedness. *Int. J. Dev. Biol.* 50, 571–573. doi:10.1387/ijdb.052132ba

Baccetti, B., Capitani, S., Collodel, G., Di Cairano, G., Gambera, L., Moretti, E., et al. (2001). Genetic sperm defects and consanguinity. *Hum. Reprod.* 16, 1365–1371. doi:10.1093/humrep/16.7.1365

Boaretto, F., Snijders, D., Salvoro, C., Spalletta, A., Mostacciuolo, M. L., Collura, M., et al. (2016). Diagnosis of primary ciliary dyskinesia by a targeted next-generation sequencing panel: Molecular and clinical findings in Italian patients. *J. Mol. Diagn* 18, 912–922. doi:10.1016/j.jmoldx.2016.07.002

Casey, J. P., Goggin, P., McDaid, J., White, M., Ennis, S., Betts, D. R., et al. (2015). A case report of primary ciliary dyskinesia, laterality defects and developmental delay caused by the co-existence of a single gene and chromosome disorder. *BMC Med. Genet.* 16, 45. doi:10.1186/s12881-015-0192-z

Choksi, S. P., Lauter, G., Swoboda, P., and Roy, S. (2014). Switching on cilia: Transcriptional networks regulating ciliogenesis. *Development* 141, 1427–1441. doi:10.1242/dev.074666

Hannah, W. B., Seifert, B. A., Truty, R., Zariwala, M. A., Ameel, K., Zhao, Y., et al. (2022). The global prevalence and ethnic heterogeneity of primary ciliary dyskinesia gene variants: A genetic database analysis. *Lancet Respir. Med.* 10, 459–468. doi:10.1016/S2213-2600(21)00453-7

King, S. M. (2016). Axonemal dynein arms. *Cold Spring Harb. Perspect. Biol.* 8, a028100. doi:10.1101/cshperspect.a028100

King, S. M., and Patel-King, R. S. (2015). The oligomeric outer dynein arm assembly factor CCDC103 is tightly integrated within the ciliary axoneme and exhibits periodic binding to microtubules. *J. Biol. Chem.* 290, 7388–7401. doi:10.1074/jbc.M114.616425

Luddi, A., Luongo, F. P., Dragoni, F., Fiaschi, L., Vicenti, I., Lupetti, P., et al. (2022). Cellular and molecular mechanisms of *in vivo* and *in vitro* SARS-CoV-2 infection: A lesson from human sperm. *Cells* 11, 2631. doi:10.3390/cells11172631

Mirra, V., Werner, C., and Santamaria, F. (2017). Primary ciliary dyskinesia: An update on clinical aspects, genetics, diagnosis, and future treatment strategies. *Front. Pediatr.* 5, 135. doi:10.3389/fped.2017.00135

Olm, M. A. K., Caldini, E. G., and Mauad, T. (2015). Diagnosis of primary ciliary dyskinesia. *J. Bras. Pneumol.* 41, 251–263. doi:10.1590/S1806-37132015000004447

Owa, M., Furuta, A., Usukura, J., Arisaka, F., King, S. M., Witman, G. B., et al. (2014). Cooperative binding of the outer arm-docking complex underlies the regular arrangement of outer arm dynein in the axoneme. *Proc. Natl. Acad. Sci.* 111, 9461–9466. doi:10.1073/pnas.1403101111

Panizzi, J. R., Becker-Heck, A., Castleman, V. H., Al-Mutairi, D. A., Liu, Y., Loges, N. T., et al. (2012). CCDC103 mutations cause primary ciliary dyskinesia by disrupting assembly of ciliary dynein arms. *Nat. Genet.* 44, 714–719. doi:10.1038/ng.2277

Pereira, R., Oliveira, M. E., Santos, R., Oliveira, E., Barbosa, T., Santos, T., et al. (2019). Characterization of CCDC103 expression profiles: Further insights in primary ciliary dyskinesia and in human reproduction. *J. Assist. Reprod. Genet.* 36, 1683–1700. doi:10.1007/s10815-019-01509-7

Rodrigues, C. H., Pires, D. E., and Ascher, D. B. (2018). DynaMut: Predicting the impact of mutations on protein conformation, flexibility and stability. *Nucleic Acids Res.* 46, W350–W355. doi:10.1093/nar/gky300

Shoemark, A., Dell, S., Shapiro, A., and Lucas, J. S. (2019). ERS and ATS diagnostic guidelines for primary ciliary dyskinesia: Similarities and differences in approach to diagnosis. *Eur. Respir. J.* 54, 1901066. doi:10.1183/13993003.01066-2019

Shoemark, A., Moya, E., Hirst, R. A., Patel, M. P., Robson, E. A., Hayward, J., et al. (2018). High prevalence of CCDC103 p.His154Pro mutation causing primary ciliary dyskinesia disrupts protein oligomerisation and is associated with normal diagnostic investigations. *Thorax* 73, 157–166. doi:10.1136/thoraxjnl-2017-209999

Sironen, A., Shoemark, A., Patel, M., Loebinger, M. R., and Mitchison, H. M. (2020). Sperm defects in primary ciliary dyskinesia and related causes of male infertility. *Cell. Mol. Life Sci.* 77, 2029–2048. doi:10.1007/s00018-019-03389-7

Takada, S., and Kamiya, R. (1994). Functional reconstitution of chlamydomonas outer dynein arms from alpha-beta and gamma subunits: Requirement of a third factor. *J. Cell Biol.* 126, 737–745. doi:10.1083/jcb.126.3.737

WHO laboratory manual for the examination and processing of human semen (2022). Available at:https://www.who.int/publications-detail-redirect/9789240030787 (Accessed October 4, 2022).

Zubair, M., Khan, R., Ma, A., Hameed, U., Khan, M., Abbas, T., et al. (2022). A recurrent homozygous missense mutation in CCDC103 causes asthenoteratozoospermia due to disorganized dynein arms. *Asian J. Androl.* 24, 255–259. doi:10.4103/aja2021122

frontiers | Frontiers in Pediatrics

TYPE Case Report
PUBLISHED 03 February 2023
DOI 10.3389/fped.2023.1068718

Check for updates

OPEN ACCESS

EDITED BY
Tieliu Shi,
Hunan University of Arts and Science, China

REVIEWED BY
Siqi Hu,
Seventh Medical Center of PLA General Hospital, China
Andre Travessa,
Santa Maria Hospital, Portugal

*CORRESPONDENCE
Ying Liu
✉ rbly250@163.com
Jin Wu
✉ 18980861822@163.com

SPECIALTY SECTION
This article was submitted to Genetics of Common and Rare Diseases, a section of the journal Frontiers in Pediatrics

RECEIVED 13 October 2022
ACCEPTED 12 January 2023
PUBLISHED 03 February 2023

CITATION
Chen C, Wu J and Liu Y (2023) Case Report: Recombinant human growth hormone therapy in a patient with spondyloepiphyseal dysplasia, Kondo-Fu type.
Front. Pediatr. 11:1068718.
doi: 10.3389/fped.2023.1068718

COPYRIGHT
© 2023 Chen, Wu and Liu. This is an open-access article distributed under the terms of the Creative Commons Attribution License (CC BY). The use, distribution or reproduction in other forums is permitted, provided the original author(s) and the copyright owner(s) are credited and that the original publication in this journal is cited, in accordance with accepted academic practice. No use, distribution or reproduction is permitted which does not comply with these terms.

Case Report: Recombinant human growth hormone therapy in a patient with spondyloepiphyseal dysplasia, Kondo-Fu type

Congli Chen[1,2], Jin Wu[1,2]* and Ying Liu[1,2]*

[1]Department of Pediatrics, West China Second Hospital, Sichuan University, Chengdu, China, [2]Key Laboratory of Birth Defects and Related Diseases of Women and Children (Sichuan University), Ministry of Education, Chengdu, China

Background: Variants in membrane-bound transcription factor peptidase, site 1 (MBTPS1) gene, can result in clinically rare spondyloepiphyseal dysplasia of Kondo-fu type (OMIM #618392, SEDKF), Silver–Russell syndrome, and CAOP (cataract, alopecia, oral mucosal disorder, and psoriasis-like) syndrome.
Case presentation: A 6-year-old Chinese male child diagnosed with SEDKF underwent 3 years of growth hormone therapy. A genetic examination revealed two new nonsense variants in the MBTPS1 gene on chromosome 16q23-q24 with compound heterozygotes c.1589(exon12)A > G and c.163(exon2)G > A.
Conclusion: The MBTPS1 gene c.1589(exon12)A > G and c.163(exon2)G > A on chromosome 16q23-q24 is associated with SEDKF. Growth hormone therapy can repair growth retardation in patients with spondyloepiphyseal dysplasia, Kondo-Fu type; however, more evidence of such patient cases is required to support this hypothesis.

KEYWORDS
spondyloepiphyseal dysplasia, Kondo-Fu type, MBTPS1, genotype, phenotype, rhGH therapy

Background

Site-1 protease (S1P) encoded by the MBTPS1 (membrane-bound transcription factor peptidase, site 1) gene regulates cholesterol and lipid homeostasis *via* cleavage of substrates at non-basic residues, endoplasmic reticulum function, and lysosome biogenesis in mice and cultivated cells (1–4). MBTPS1 is also essential for the transcription of bone matrix and mineralization, expressing proteins including type XI collagen, Phex, Dmp1, fibronectin, and fibrillin in bone osteoblasts and osteocytes (5).

Variants in MBTPS1 may be associated with lysosomal dysfunction (6, 7), reportedly resulting in a variety of phenotypes. Spondyloepiphyseal dysplasia, Kondo-fu type (OMIM #618392, SEDKF), was reported in 2018 (6) and 2020 (8) and was characterized by severely retarded growth, skeletal anomalies, dysmorphic features, epilepsy, craniosynostosis, and elevated levels of blood lysosomal enzymes. In 2020, Meyer et al. (9) reported a patient with variants in MBTPS1 presenting Silver–Russell syndrome, characterized by a heterogeneous congenital growth retardation syndrome. In 2022, Chen et al. (10) illustrated two unrelated patients with CAOP (cataract, alopecia, oral mucosal disorder, and psoriasis-like) syndrome caused by variants in MBTPS1. In addition, hyperCKemia and focal myoedema were found to be related to variants in MBTPS1. The number of human diseases with site-1 protease

Abbreviations
MBTPS1, membrane-bound transcription factor peptidase, site 1; S1P, site-1 protease; SEDKF, spondyloepiphyseal dysplasia, Kondo-fu type; CAOP, cataract, alopecia, oral mucosal disorder, and psoriasis-like; rhGH, recombinant human growth hormone; WES, whole exome sequencing; MRI, magnetic resonance imaging.

deficiency is extremely rare, and totally, only two cases of SEDKF, one case of Silver–Russell syndrome, two cases of CAOP syndrome, and one patient presenting with hyperCKemia and focal myoedema have been reported (6, 8–11). In addition, the precise effect of recombinant human growth hormone (rhGH) therapy on the height of patients with growth retardation with MBTPS1 variants remains unclear.

Herein, we report a case of a 6-year-old Chinese boy with an analogous SEDKF phenotype, including skeletal dysplasia, distinctive facies, and decreased body weight with a novel homozygous nonsense variant in MBTPS1, and who received rhGH therapy for 3 years. To the best of our knowledge, he is the third individual with SEDKF. Therefore, the existence of this rarely diagnosed disease with variants in MBTPS1 and the exact influence of rhGH therapy on the height of patients need to be elucidated further.

Case presentation

The patient was born as the first child of unrelated and healthy parents. His mother was 28 years old and the father was 34 years old when the child was delivered. He was a term baby through spontaneous vaginal delivery in the year 2016 after an uneventful pregnancy, except for a successful rescue of meconium aspiration syndrome, and had no family history of the disease. He received artificial feeding after birth with 600–700 ml of milk per day, and supplementary food was added at the age of 5 months. At 4 months of age, he presented with motor retardation with poor head-up ability and low muscular tension but no other abnormal signs of hearing, expressive language, and intelligence development.

At the age of 11 months, he presented with poor appetite and slow growth in height and weight but had no manifestation of emesis, diarrhea, or jaundice. A food intolerance test revealed that he was positive (++) for milk protein. At the age of 35 months, he underwent surgical lens removal for a congenital lamellar cataract.

The proband's born weight (BW) was 2,680 g (−1.59SD, P5.5), and birth length was 49 cm (−0.78SD, P21.7). At the age of 14 months, he presented with a short stature and a slightly sloping shank; his height was 63.80 cm (−5.3SD, ≤P0.1), and his weight was 6.00 kg (−3.8SD, ≤P0.1). At the age of 35 months, his height was 78.2 cm (−4.86SD, ≤P0.1), weight was 9 kg (−3.33SD, ≤P0.1), and BMI was 14.72 (−0.62SD, P26.7). The growth standards of Chinese children were developed on the basis of a study of their physical development in nine provinces and cities in the year 2005 and published in the 7th issue of the *Chinese Journal of Pediatrics* in 2009, and since then, our physical measurements have been assessed using these standards (**Figure 1A**).

The boy showed distinctive facies with macrotia, retromicrognathia, sternal malformation, protruding abdomen, and kyphoscoliosis (**Figure 2A**).

A growth hormone stimulation test showed that under the stimulation of arginine and levodopa, the growth hormone level peaked at 60 min: 6.7 ng/ml (**Figure 2B**). Alkaline phosphatase was slightly above the reference limit (321 U/L, 161.9–296.4). No abnormality was detected in the liver and kidney function, electrolytes, blood gas analysis, parathyroid hormone, and thyroid function tests; also, IGF-1 levels were normal.

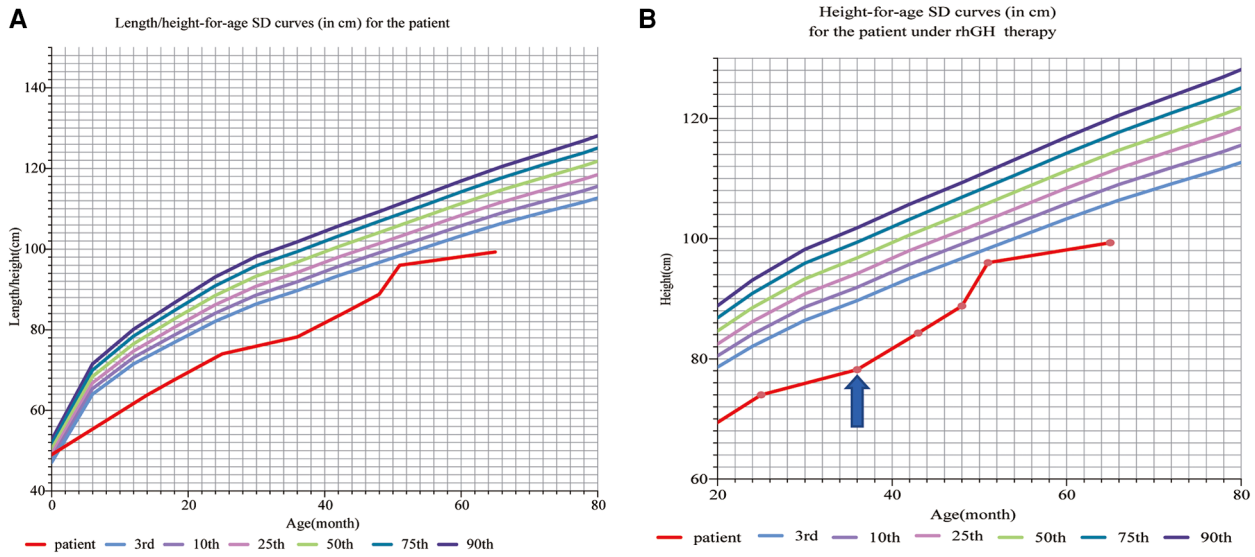


FIGURE 1
(A) Length/height-for-age SD curves (in cm) for a patient before rhGH therapy: according to the Chinese children's growth standards, the proband's born weight (BW) is 2,680 g (−1.59SD, P5.5), and birth length is 49 cm (0.78SD, P21.7). At the age of 14 months, the patient presented with a short stature and a slightly sloping shank, his height was 63.80 cm (−5.3SD, ≤P0.1), and his weight was 6.00 kg (−3.8SD, ≤P0.1). At the age of 36 months, his height was 78.2 cm (−4.84SD, ≤P0.1), weight was 9 kg (−3.33SD, ≤P0.1), and BMI was 14.72 (−0.62SD, P26.7). (B) Height-for-age SD curves (in cm) for the patient under rhGH therapy. The patient received rhGH therapy at a dosage of 0.15–0.2 IU/kg/d ih at the age of 36 months (the arrow points to). At the age of 36 months, his height was 78.2 cm (−4.84SD, ≤P0.1), weight was 9 kg (−3.33SD, ≤P0.1), and BMI was 14.72 (−0.62SD, P26.7). After 3 years of rhGH therapy, the patient showed rapid growth, following which his height was 99 cm (−3.96SD, ≤P0.1) and weight was 12.80 kg (−2.84SD, ≤P0.1) at the age of 65 months. rhGH, recombinant human growth hormone.

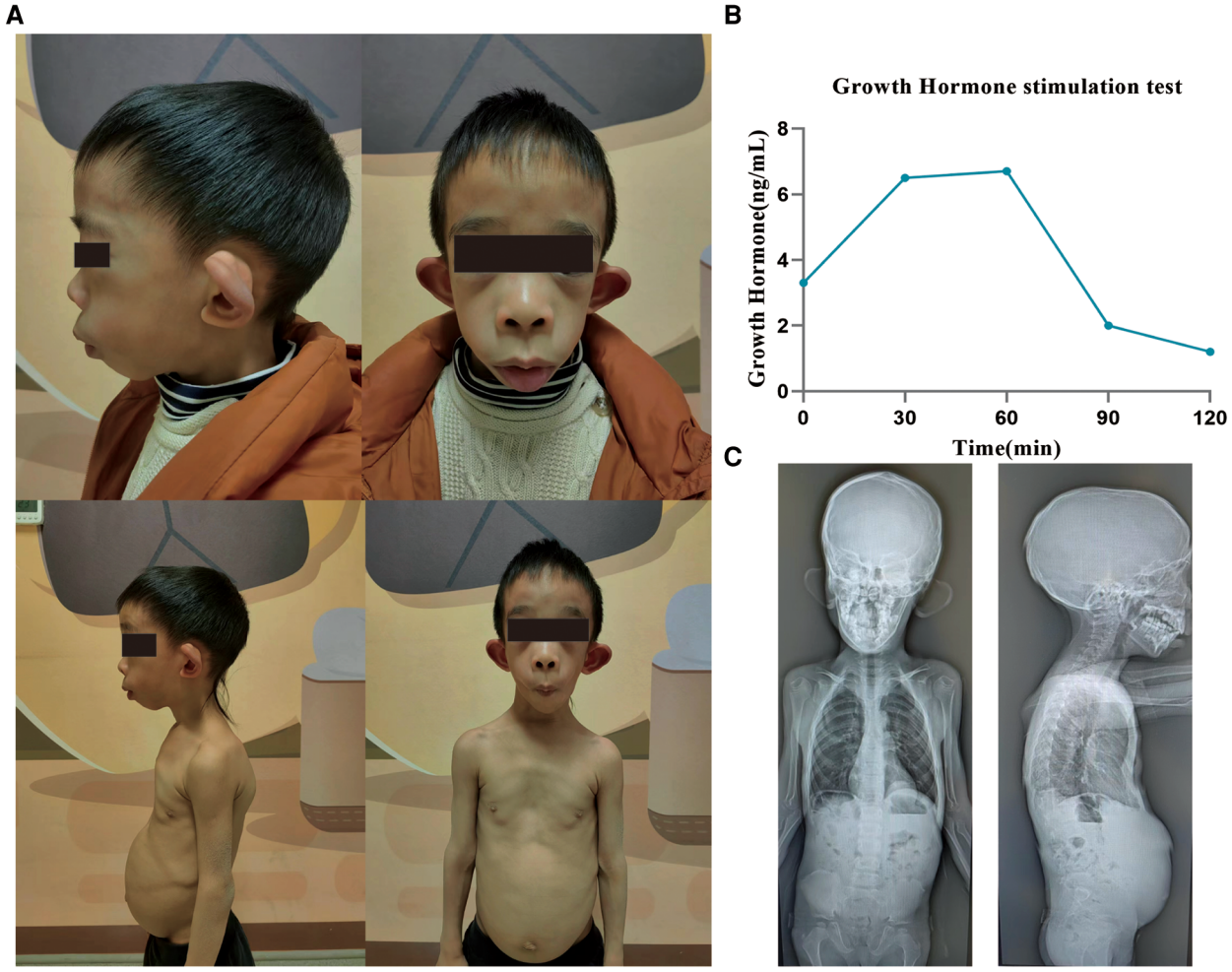


FIGURE 2
Clinical characteristics of a patient with the variant in MBTPS1. (A) The patient shows distinctive facies with macrotia, retromicrognathia, sternal malformation, protruding abdomen, and kyphoscoliosis. (B) The growth hormone stimulation test shows that under the stimulation of arginine and levodopa, the growth hormone level peaks at 60 min: 6.7 ng/ml (peak >10 indicates normal levels, 5–10 indicates part deficiency, and <5 indicates deficiency). (C) Radiographs at the age of 6 years. A notable straightened physiological curvature of the cervical, thoracic, and lumbar spine, irregular morphology of cones, reduced bone density of the cones, C2–C3 and C3–C4 intervertebral disc space narrowing, and bilateral shallow acetabulum. MBTPS1, membrane-bound transcription factor peptidase, site 1.

Radiographs taken at the age of 6 years revealed a straightened physiological curvature of the cervical, thoracic and lumbar spine, irregular morphology of cones, reduced bone density of the cones, C2–C3 and C3–C4 intervertebral disc space narrowing, and bilateral shallow acetabulum (**Figure 2C**).

Brain magnetic resonance imaging (MRI), echocardiography, and renal ultrasonography were unremarkable.

A chromosome examination showed that the karyotype was 46, XY, containing benign copy number variations. By whole exome sequencing (WES), c.1589(exon12)A > G in chr16:84108206 and c.163(exon2)G > A in chr16:84135226 were detected in the patient. The heterozygous variant of c.1589(exon12)A > G was found in his father, whereas his mother had the wild type (**Figure 3A**). The other heterozygous variant c.163(exon2)G > A was found in his mother, whereas his father had the wild type (**Figure 3B**). Both variants' minor allele frequencies were <0.05% and were not listed in the ClinVar (https://clinicalgenome.org) and Genome AD databases. Bioinformatics protein function prediction software SIFT, PolyPhen_HDIV, PolyPhen2_HVAR, PROVEAN, MutationTaster, and GERP were used to predict the protein function. The result of c.1589(exon12)A > G was pathogenic moderate (PM2), and the results of c.163(exon2)G > A were PM2 and pathogenic supporting (PP3). According to ACMG guidelines (12), both c.1589(exon12)A > G and c.163(exon2)G > A were classified to be of uncertain significance, respectively.

With the analogous SEDKF phenotype, including skeletal dysplasia, distinctive facies, decreased body weight, and growth retardation and WES genetic test revealing c.1589(exon12)A > G and c.163(exon2)G > A variant in MBTPS1, the proband was diagnosed with SEDKF.

The patient received rhGH therapy at a dosage of 0.15–0.2 IU/kg/d ih at the age of 3 years, in addition to basic therapies administering calcium, vitamin A, and vitamin D.

After 3 years of rhGH therapy, the patient showed rapid growth, following which his height was 99 cm (−3.96SD, ≤P0.1) and weight 12.80 kg (−2.84SD, ≤P0.1) (**Figure 1B**), and his upper segment was 54 cm. Strikingly, the IGF-1 levels and thyroid function were normal.

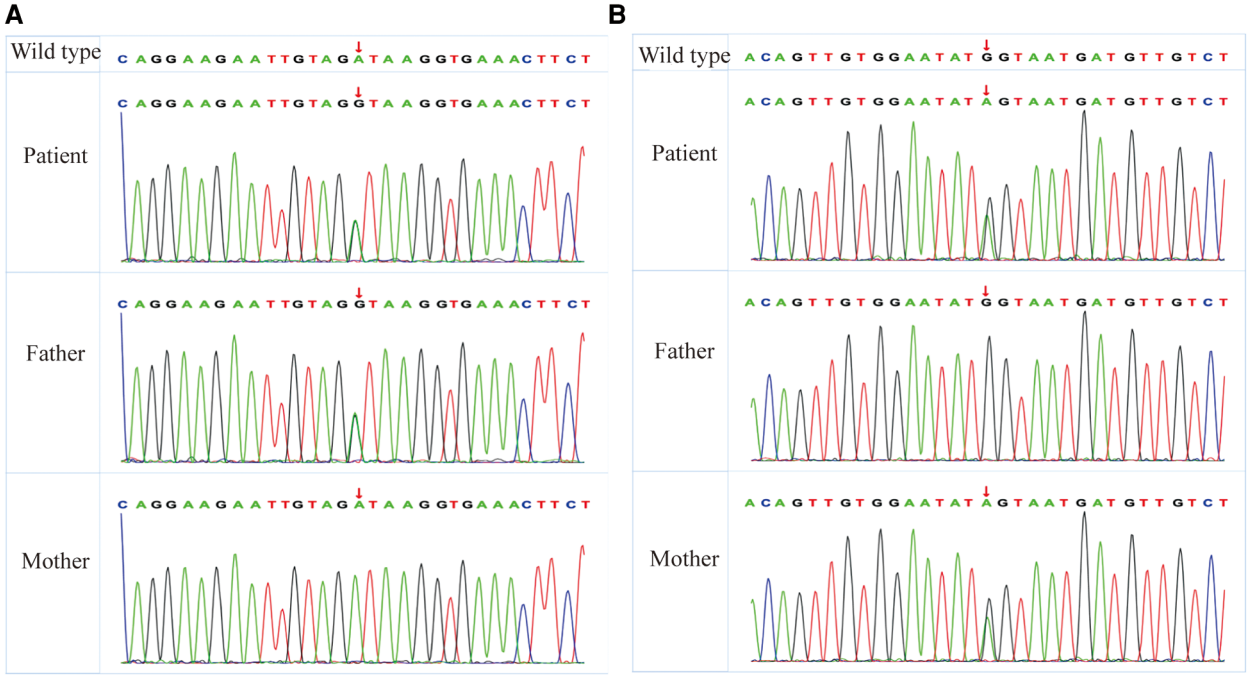


FIGURE 3
WES reveals heterozygous MBTPS1 p.Asp530Gly (exon12; c.1589A > G) and p.Glu55Lys (exon2; c.163T > C) variants in the patient. (A) The heterozygous variant of p.Asp530Gly (exon12; c.1589A > G) was found in his father, whereas his mother had the wild type. (B) The other heterozygous variant of p.Glu55Lys (exon2; c.163T > C) was found in his mother, whereas his father had the wild type. WES, whole exome sequencing; MBTPS1, membrane-bound transcription factor peptidase, site 1.

Discussion and conclusion

MBTPS1 encodes a member of the subtilisin-like proprotein convertase family (2), which includes proteases that process protein and peptide precursors trafficking through regulated or constitutive branches of the secretory pathway (7). S1P (encoded by MBTPS1) deficiency causes a partial impairment of mannose-6-phosphate-dependent Golgi-to-lysosome transport of lysosomal enzymes and may be associated with lysosomal dysfunction (7).

Two patients with SEDKF, one patient with Silver–Russell syndrome, two patients with CAOP syndrome, and one patient with hyperCKemia and focal myoedema presented with variants in MBTPS1. Patients with SEDKF showed severe retarded growth, skeletal anomalies, dysmorphic features, epilepsy, craniosynostosis, and elevated levels of blood lysosomal enzymes (6, 8). Kondo et al. discovered shortened tubular bones and delayed ossification of epiphyses and carpal bones, while Carvalho et al. uncovered diffuse osteoporosis, ovoid lumbar vertebrae bodies, irregular cervical vertebrae bodies, long bones with irregular metaphysis and epiphyses, mildly enlarged metaphysis, small tubular epiphyses, and copper beaten skulls. The patient with Silver–Russell syndrome presented with a heterogeneous congenital growth retardation, including a triangular face, large ears, funnel chest, kyphosis, pes valgus, sandal grooves, cataract, unilateral inguinal hernia, and motor milestone delay (9). The two unrelated patients presented with CAOP syndrome (10).

In addition, the proband had something in common with the other patients with variants in MBTPS1. He was featured as small for gestational age, short stature with growth drop-off at 14 months, poor bodyweight gain, characteristic facies such as a prominent forehead and posteriorly rotated ears, delayed ossification of carpal bones, and cataract and surgical lens removal for congenital lamellar cataract (**Table 1**).

Being the first reported case of SEDKF in China, this patient was found to harbor a compound heterozygous variant in the MBTPS1 gene (OMIM #603355) on chromosome 16q23-q24 through genetic testing. Because the child was young, there was no obvious spinal change. Also, food intolerance with diarrhea after ingestion of milk was noted. Unlike other children, there was no apparent carpal retardation in this child.

The patient with SEDKF, reported by Kondo et al. in 2018, received growth hormone replacement therapy for 1 year but discontinued it as a result of limited response. Silver–Russell syndrome can also be treated with growth hormone therapy, but it is not easy to achieve normal height after treatment. Due to the proband's short stature and growth retardation, a growth hormone stimulation test was conducted on this patient, and the results suggested a dysfunction of growth hormone secretion, but the child's IGF-1 level was normal. Although he received rhGH therapy for 3 years, its efficacy might be limited due to an underlying genetic defect in the IGF-1 function. However, after treatment, the child's height increased from −4.86SD to −3.96SD, indicating that the growth hormone had specific benefits in increasing the height of such patients.

However, due to a lack of experimental examinations, a comparison of the increasing levels of lysosomal enzyme with other cases is not possible.

TABLE 1 Characteristics of patients with MBTPS1 gene variants in the literature.

Reference	Kondo et al. (2018)	Schweitzer et al. (2019)	Meyer et al. (2020)	Carvalho et al. (2020)	Chen et al. (2022)	Chen et al. (2022)	Present study
Patient number	1	2	3	4	5	6	7
Skeletal dysplasia	+	–	+	+	–	–	+
Sternal malformation	+	NA	+	+	–	–	+
Short stature	+	NA	+	+	–	–	+
Kyphoscoliosis	+	NA	NA	–	–	–	+
Retromicrognathia	+	NA	+	+	–	–	+
Large ears	+	NA	+	+	–	–	+
Cataract	NA	NA	+	+	+	+	+
Protruding abdomen	NA	NA	NA	+	–	–	+
Elevated blood lysosomal enzymes	+	NA	+	+	–	ND	ND
Elevated hepatic transaminase	–	+	–	+	NA	NA	–
HyperCKemia	–	+	NA	–	–	ND	–
Focal myoedema	NA	+	NA	NA	–	ND	–
Cutaneous lesions	–	NA	NA	NA	+	+	–
Mucosal lesions	–	NA	NA	NA	+	ND	–
Associated variation	Exon 3; c.285dupT/ exon 9; c.1094A > G	Exon 23; c.3007C > T	c.1094A > G homozygosity	Exon 22; c.2948G > A	c.1064T > G/ c.3157T > C	c.3159A > T/ c.2072-2A > T	Exon12; c. 1589A > G/exon2; c.163G > A

MBTPS1, membrane-bound transcription factor peptidase, site 1; ND, not detected; NA, not available.

Here, we reported the case of a patient with variants in the MBTPS1 gene, c.1589(exon12)A > G and c.163(exon2)G > A, associated with SEDKF. As the patient showed a relatively significant height increase with growth hormone treatment, it can be assumed that growth hormone therapy can repair growth retardation in patients with spondyloepiphyseal dysplasia, Kondo-Fu type; however, more evidence of such patient cases is required to support this hypothesis.

Data availability statement

The original contributions presented in the study are included in the article/Supplementary Material, further inquiries can be directed to the corresponding authors.

Ethics statement

Written informed consent was obtained from the minor(s)' legal guardian/next of kin for the publication of any potentially identifiable images or data included in this article.

Author contributions

CC gave the background details of the manuscript, described the clinical case, and carried out research in the medical literature. YL collected the images of the clinical case, analyzed the genetic data of the patients, and reviewed the clinical presentation. YL and JW reviewed the manuscript. All authors contributed to the article and approved the submitted version.

Acknowledgments

The authors thank the family members of the patients for giving their permission to publish the clinical data and images.

Conflict of interest

The authors declare that the research was conducted in the absence of any commercial or financial relationships that could be construed as a potential conflict of interest.

Publisher's note

All claims expressed in this article are solely those of the authors and do not necessarily represent those of their affiliated organizations, or those of the publisher, the editors and the reviewers. Any product that may be evaluated in this article, or claim that may be made by its manufacturer, is not guaranteed or endorsed by the publisher.

References

1. Fagerberg L, Hallstrom BM, Oksvold P, Kampf C, Djureinovic D, Odeberg J, et al. Analysis of the human tissue-specific expression by genome-wide integration of transcriptomics and antibody-based proteomics. *Mol Cell Proteomics*. (2014) 13 (2):397–406. doi: 10.1074/mcp.M113.035600

2. Brown MS, Goldstein JL. The SREBP pathway: regulation of cholesterol metabolism by proteolysis of a membrane-bound transcription factor. *Cell*. (1997) 89(3):331–40. doi: 10.1016/S0092-8674(00)80213-5

3. Walker AK, Jacobs RL, Watts JL, Rottiers V, Jiang K, Finnegan DM, et al. A conserved SREBP-1/phosphatidylcholine feedback circuit regulates lipogenesis in metazoans. *Cell*. (2011) 147(4):840–52. doi: 10.1016/j.cell.2011.09.045

4. Baranski TJ, Faust PL, Kornfeld S. Generation of a lysosomal enzyme targeting signal in the secretory protein pepsinogen. *Cell*. (1990) 63(2):281–91. doi: 10.1016/0092-8674(90)90161-7

5. Gorski JP, Huffman NT, Vallejo J, Brotto L, Chittur SV, Breggia A, et al. Deletion of Mbtps1 (Pcsk8, S1p, ski-1) gene in osteocytes stimulates soleus muscle regeneration and increased size and contractile force with age. *J Biol Chem*. (2016) 291(9):4308–22. doi: 10.1074/jbc.M115.686626

6. Kondo Y, Fu J, Wang H, Hoover C, McDaniel JM, Steet R, et al. Site-1 protease deficiency causes human skeletal dysplasia due to defective inter-organelle protein trafficking. *JCI Insight*. (2018) 3(14):e121596. doi: 10.1172/jci.insight.121596

7. Achilleos A, Huffman NT, Marcinkiewicyz E, Seidah NG, Chen Q, Dallas SL, et al. MBTPS1/SKI-1/S1P proprotein convertase is required for ECM signaling and axial elongation during somitogenesis and vertebral development. *Hum Mol Genet*. (2015) 24(10):2884–98. doi: 10.1093/hmg/ddv050

8. Carvalho DR, Speck-Martins CE, Brum JM, Ferreira CR, Sobreira NLM. Spondyloepimetaphyseal dysplasia with elevated plasma lysosomal enzymes caused by homozygous variant in MBTPS1. *Am J Med Genet A*. (2020) 182(7):1796–800. doi: 10.1002/ajmg.a.61614

9. Meyer R, Elbracht M, Opladen T, Eggermann T. Patient with an autosomal-recessive MBTPS1-linked phenotype and clinical features of Silver-Russell syndrome. *Am J Med Genet A*. (2020) 182(11):2727–30. doi: 10.1002/ajmg.a.61833

10. Chen F, Ni C, Wang X, Cheng R, Pan C, Wang Y, et al. S1p defects cause a new entity of cataract, alopecia, oral mucosal disorder, and psoriasis-like syndrome. *EMBO Mol Med*. (2022) 14(5):e14904. doi: 10.15252/emmm.202114904

11. Schweitzer GG, Gan C, Bucelli RC, Wegner D, Schmidt RE, Shinawi M, et al. A mutation in site-1 protease is associated with a complex phenotype that includes episodic hyperCKemia and focal myoedema. *Mol Genet Genomic Med*. (2019) 7(7):e00733. doi: 10.1002/mgg3.733

12. Richards S, Aziz N, Bale S, Bick D, Das S, Gastier-Foster J, et al. Standards and guidelines for the interpretation of sequence variants: a joint consensus recommendation of the American college of medical genetics and genomics and the association for molecular pathology. *Genet Med*. (2015) 17(5):405–24. doi: 10.1038/gim.2015.30

frontiers | Frontiers in Genetics

TYPE Case Report
PUBLISHED 01 March 2023
DOI 10.3389/fgene.2023.1063202

Check for updates

OPEN ACCESS

EDITED BY
Tieliu Shi,
Hunan University of Arts and Science, China

REVIEWED BY
Elena Guzzolino,
Meyer Children's Hospital, Italy
Cathy J. Hatcher,
Philadelphia College of Osteopathic Medicine (PCOM), United States

*CORRESPONDENCE
Tong Li,
litong3zx@sina.com

†These authors have contributed equally to this work and share first authorship

SPECIALTY SECTION
This article was submitted to Genetics of Common and Rare Diseases, a section of the journal Frontiers in Genetics

RECEIVED 06 October 2022
ACCEPTED 10 February 2023
PUBLISHED 01 March 2023

CITATION
Lang Y, Zheng Y, Qi B, Zheng W, Zhao C, Zhai H, Wang G, Luo Z and Li T (2023), Case report: Novel TBX5-related pathogenic mechanism of Holt–Oram syndrome.
Front. Genet. 14:1063202.
doi: 10.3389/fgene.2023.1063202

COPYRIGHT
© 2023 Lang, Zheng, Qi, Zheng, Zhao, Zhai, Wang, Luo and Li. This is an open-access article distributed under the terms of the Creative Commons Attribution License (CC BY). The use, distribution or reproduction in other forums is permitted, provided the original author(s) and the copyright owner(s) are credited and that the original publication in this journal is cited, in accordance with accepted academic practice. No use, distribution or reproduction is permitted which does not comply with these terms.

Case report: Novel TBX5-related pathogenic mechanism of Holt–Oram syndrome

Yuheng Lang[1,2,3,4,5†], Yue Zheng[1,2,3,4,5†], Bingcai Qi[1,3,4,5†], Weifeng Zheng[1,3,4,5], Chengxiu Zhao[6], Hu Zhai[1,3,4,5], Gang Wang[1,3,4,5], Zhiqiang Luo[1,3,4,5] and Tong Li[1,2,3,4,5*]

[1]Department of Heart Center, Tianjin Third Central Hospital, Tianjin, China, [2]School of Medicine, Nankai University, Tianjin, China, [3]Tianjin Key Laboratory of Extracorporeal Life Support for Critical Diseases, Tianjin, China, [4]Artificial Cell Engineering Technology Research Center, Tianjin, China, [5]Tianjin Institute of Hepatobiliary Disease, Tianjin, China, [6]Department of Anesthesiology, Handan First Hospital, Handan, China

Introduction: Holt–Oram syndrome (HOS) is a rare genetic disorder characterized by upper limb abnormalities, congenital heart defects, and/or conduction abnormalities. Sequence alteration of T-box transcription factor 5 (TBX5) is correlated with the incidence of HOS.

Case description: We present the case of a 24-year-old female with upper limb alterations (congenital dysplasia in the wrist and elbow joints) and an anomalous left main trunk arising from the right coronary sinus. The patient inherited a base T (reference C) at rs883079 from her mother and base C (reference T) at rs10850326 from her father, both of which belong to the 3′-untranslated region (UTR) of the TBX5 gene; no alterations in TBX5 expression or single-nucleotide polymorphisms (SNPs) in other exon areas were found. We explored the effects of TBX5 on cardiomyocytes using the HL-1 cell line and TBX5-knockdown cells.

Discussion: Quantitative polymerase chain reaction analysis demonstrated that TEKT2, TEKT4, and SPTB expression decreased after TBX5 knockdown, while chromatin immunoprecipitation analysis further revealed that TBX5 binds to the TEKT2, TEKT4, and SPTB promoter regions to promote gene transcription. Our findings support a novel TBX5-related pathogenic mechanism in HOS.

KEYWORDS

Holt–Oram syndrome, Tbx5, ChIP, case report, SNP

1 Introduction

Holt–Oram syndrome (HOS; MIM 142900) is a rare genetic disorder characterized by upper limb abnormalities, congenital heart defects, and/or conduction abnormalities (Barisic et al., 2014). The uncommon subtypes of HOS are Tabatznik syndrome (type II; arrhythmias and brachytelephalangy), a Spanish variant (type III; arrhythmia and brachydactyly type C), and a potential Slovenian type (type IV; arrhythmia, dilated cardiomyopathy, and brachydactyly) (Zaragoza et al., 2017; Spiridon et al., 2018).

Abbreviations: HOS, Holt–Oram syndrome; miRNA, microRNA; SNP, single-nucleotide polymorphism; UTR, untranslated region.

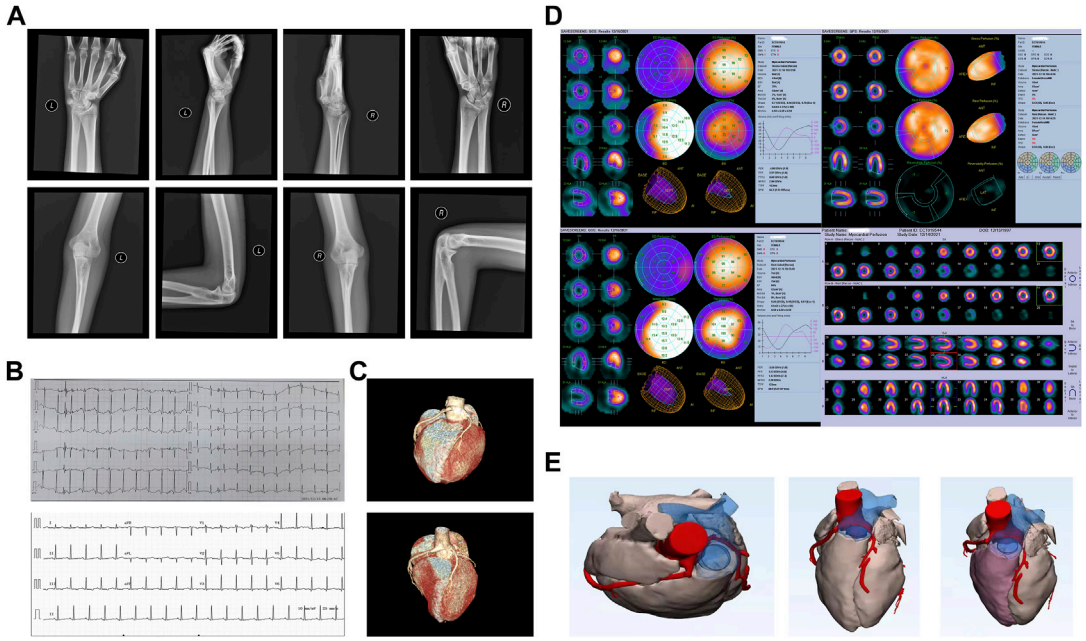


FIGURE 1
Patient's clinical characteristics. **(A)** Bilateral elbow wrist joint examination, demonstrating a partial fusion of bones at the proximal end of both the ulna and radius, widening of the radial ulnar joint at the distal end, and poor alignment. **(B)** Electrocardiography before (top) and after surgery (bottom). **(C)** Computed tomography angiography of the cardiac structure before (top) and after surgery (bottom). **(D)** Resting and adenosine load-gated myocardial perfusion imaging demonstrated that there was no typical reversible abnormal perfusion in the left ventricular myocardium, and the left ventricular cardiac function index was normal. **(E)** Three-dimensionally printed heart model used to determine the surgical approach.

HOS is caused by a mutation in the T-box transcription factor 5 (TBX5) gene (located on chromosome 12q24.1), a protein-coding gene consisting of nine coding exons and belonging to the T-box domain (Spiridon et al., 2018). The Nkx2.5/GATA4/TBX5 axis controls heart and limb development, and the abnormal expression of TBX5 induces abnormalities by altering the expression of some critical genes, such as ANF and KLF13 (Darwich et al., 2017; Russell et al., 2018). Mutations in TBX5 were identified in more than 70% of HOS cases. Pathogenic TBX5 variants include missense or non-sense substitutions, large deletions of multiple exons, frameshift mutations, and intragenic duplications (Spiridon et al., 2018).

Because of its rare occurrence and consistent phenotypes and symptoms, only a few studies have been conducted on HOS development and little is known of the functions of its molecular components. In this study, we aimed to describe a novel TBX5-related pathogenic mechanism of HOS in which there was no mutation in TBX5 or single-nucleotide polymorphisms (SNPs) in other exon areas except the 3′-untranslated region (UTR). Our study findings could promote the development of more effective prognostic and treatment tools and enable early identification of individuals at risk of transferring the disease.

2 Case description

In December 2021, a 24-year-old female was admitted to the hospital because of intermittent chest tightness and suffocation for 6 years, followed by 3 months with no medical history. The results of the medical examination were as follows: temperature 36.8°C, pulse 72 times/min, respiratory rate 16 times/min, and blood pressure 113/76 mmHg. More results included clear, stable breathing, coarse breath sounds in both lungs, no rale or wet rale, no uplift in the precardiac area, strong heart sound, consistent heart rhythm (HR 72 beats/min), no murmur in the auscultation area of each valve, flat and soft abdomen, no tenderness, internal rotation malformation of both upper limbs, no external rotation, and no edema in either of the lower limbs.

A bilateral elbow wrist joint examination demonstrated the partial fusion of the bones at the proximal end of both the ulna and radius, widening of the radial ulnar joint at the distal end, and poor alignment, suggesting congenital dysplasia in the wrist and elbow joints (Figure 1A). Cardiac color ultrasonography showed no abnormalities in the cardiac structure or function in the resting state (left ventricular ejection fraction = 65%). Outpatient coronary computed tomography angiography and angiography after admission revealed that her left coronary artery originated from the right coronary sinus and the slender left coronary artery was contorted between the aorta and the pulmonary artery (Figures 1B, C). In the cardiac systolic movement, severe stenosis appeared in the left coronary artery opening; however, no obvious stenosis was observed in the right coronary artery, left descending artery, or left circumflex artery. Resting and adenosine load-gated myocardial perfusion imaging revealed no typical reversible abnormal perfusion in the left ventricular myocardium and showed that the left ventricular cardiac function index was normal (Figure 1D).

The transient heart rate increased and chest tightness appeared after admission. An electrocardiogram examination suggested a high

TABLE 1 TBX5 SNPs among the Holt–Oram syndrome patient, her father, and her mother.

	CHROM	POS	dbSNP ID	REF	ALT	Func	Subcellular_location
Patient	12	114793240	rs883079	C	T	UTR3	Nucleus but not nucleoli
Patient	12	114793297	rs10850326	T	C	UTR3	Nucleus but not nucleoli
Patient	12	114832510	rs2236017	C	A	Intronic	Nucleus but not nucleoli
Father	12	114793297	rs10850326	T	C	UTR3	Nucleus but not nucleoli
Father	12	114794057	rs2113433	T	G	Intronic	Nucleus but not nucleoli
Father	12	114823098	rs77090182	C	T	Intronic	Nucleus but not nucleoli
Father	12	114832510	rs2236017	C	A	Intronic	Nucleus but not nucleoli
Mother	12	114793240	rs883079	C	T	UTR3	Nucleus but not nucleoli
Mother	12	114794057	rs2113433	T	G	Intronic	Nucleus but not nucleoli
Mother	12	114823089	rs17731453	G	A	Intronic	Nucleus but not nucleoli
Mother	12	114823098	rs77090182	C	T	Intronic	Nucleus but not nucleoli
Mother	12	114832510	rs2236017	C	A	Intronic	Nucleus but not nucleoli
Mother	12	114832727	rs181002410	A	G	Intronic	Nucleus but not nucleoli

Red, the TBX5 SNP inherited from her mother; blue, the TBX5 SNP inherited from her father.

sinus heart rate, HR 123 beats/min, and ST segment depression. A three-dimensional printed model was used to determine the appropriate surgical approach (Figure 1E). Midline thoracotomy was performed by cardiopulmonary bypass. We found that the left main trunk was deformed between the ascending aorta and the main pulmonary artery and arose from the right coronary sinus; therefore, correction surgery for coronary artery malformation was performed to reconstruct the left main trunk. On the first day after surgery, the patient had a heart rate of 130 beats/min and no other symptoms, such as chest tightness, appeared. A coronary computed tomography angiographic examination was performed again after surgery, which demonstrated that the left main trunk had returned to a normal shape.

To investigate the genetic etiology, we performed mutation and SNP analyses of the patient's family using SAMtools and ANNOVAR (Novogene, Beijing, China). The screened mutations and SNPs were correlated using ClinVar (https://ncbi.nlm.nih.gov/clinvar/), which indicated that the patient inherited a base T (reference C) at dbSNP ID rs883079 from her mother and base C (reference T) at dbSNP ID rs10850326 from her father, both of which belong to the 3′-UTR of the TBX5 gene (Table 1). However, no alterations in TBX5 expression or SNPs in other exons were found. The patient also inherited a SALL4 SNP in the exon area from both her father and mother. We identified 578 exons, 498 3′-UTRs, and 346 5′-UTR mutations in the patient, including the female urogenital genes PKD1, SON, and BMPR1B, as well as the reproduction-related genes TEKT2, TEKT4, COL11A1, ANKRD11, LEMD3, and SPTB (Supplementary Materials: Raw Data).

We explored the effects of TBX5 on the HL-1 cell line with TBX5 knockdown *via* transfection of small interfering RNAs (Ubigene, Guangzhou, China; Figure 2A). Quantitative polymerase chain reaction analysis demonstrated that the expression of TEKT2, TEKT4, and SPTB decreased after TBX5 knockdown (Figure 2B), and chromatin immunoprecipitation analysis further revealed that TBX5 binds to TEKT2, TEKT4, and SPTB promoter regions to promote gene transcription (Figures 2C, D; Table 2). We performed sequence alignment between the TBX5 3′-UTR regions, including rs883079 and rs10850326, and microRNAs (miRNA), including hsa-miR-98-5p, hsa-miR-10a, hsa-miR-10b, and hsa-miR-182-5p. All four miRNAs could bind to the TBX5 3′-UTR that included rs883079, while only hsa-miR-10a and hsa-miR-182-5p could bind to the region that included rs10850326, demonstrating that the increased binding of miRNAs and TBX5 3′-UTR in HOS further decreased TBX5 expression (Figure 2E). These SNPs and familial mutations may be associated with the differential expression of TBX5 (Figure 2F).

3 Discussion

TBX5 is located in the long arm of chromosome 12 (12q24.1) and it plays a fundamental role in tissue and organ formation during embryonic development and in maintaining the normal development of the upper limbs and heart (structure and electric system) through the activation of different genes (Stennard and Harvey, 2005; Ríos-Serna et al., 2018). Variants of this gene include pathogenic, non-pathogenic, and others of uncertain significance. Pathogenic TBX5 variants promote the development of pathogenic changes and diseases through missense or non-sense substitutions, large deletions of multiple exons, frameshift mutations, and intragenic duplications (Spiridon et al., 2018). This pathology is conserved in vertebrates and exists in the mouse HOS and zebrafish heartstring model. Even a slight deviation in TBX5 expression can alter the severity of the disease phenotype, which partially explains why the same mutation can have different outcomes.

Hand deformities sometimes lead to a diagnosis of congenital heart disease; however, a genetic investigation is more appropriate to diagnose and prevent complications in subsequent generations. TBX5 variants, such as those with non-sense, splicing, and missense mutations, were detected in two previous studies of 78 HOS patients and their family members as well as three other families (Jhang et al., 2015; Vanlerberghe et al., 2019). TBX5 variants in eight individuals from four unrelated families were also correlated with familial dilated cardiomyopathy and atrial septal aneurysm along with tricuspid atresia and pulmonary stenosis, which represented a novel phenotype that may have other underlying mechanisms (Shankar et al., 2017; Patterson et al., 2020). This finding supports the diverse roles of TBX5 in cardiovascular

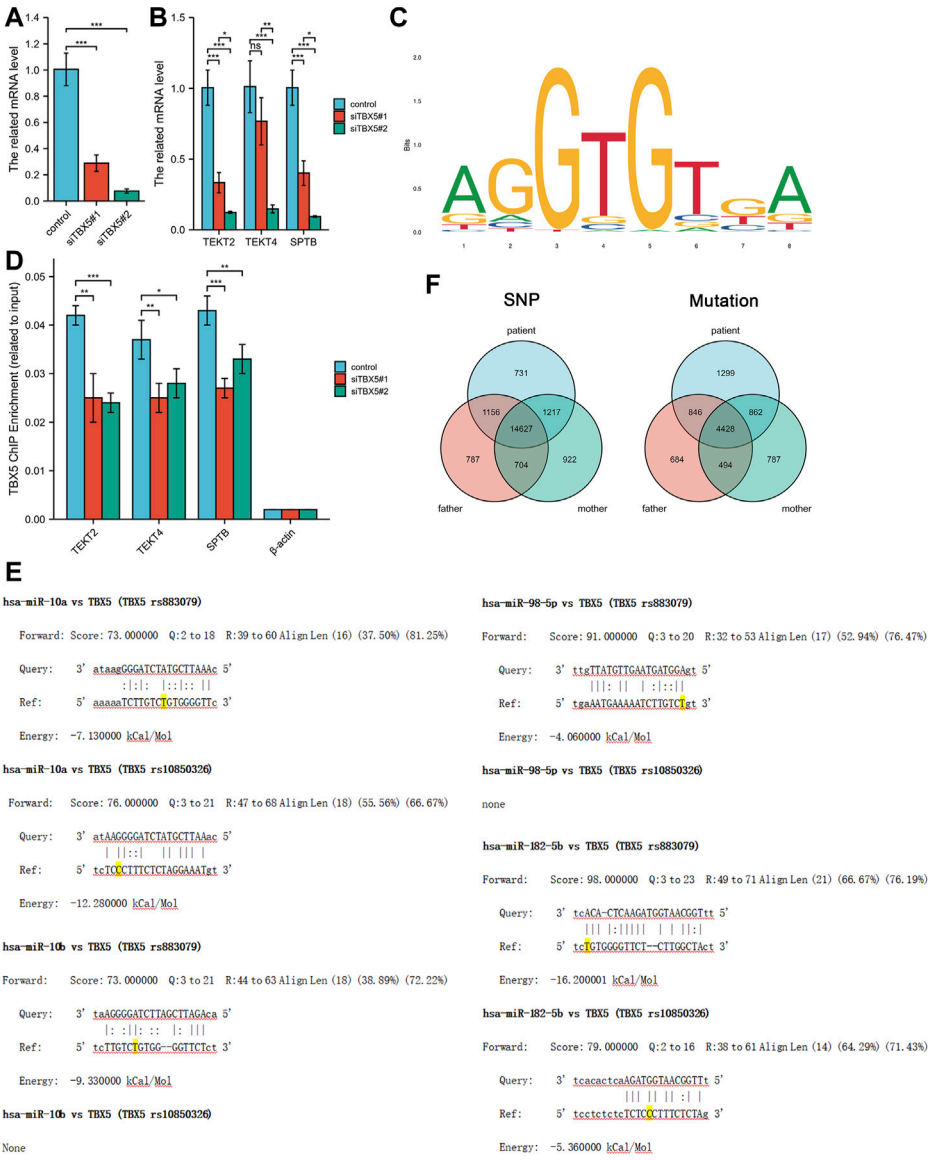


FIGURE 2
Effects of TBX5 expression on cardiomyocytes. **(A)** TBX5 expression after TBX5 knockdown in the HL-1 cell line by transfection of small interfering RNAs. **(B)** Expression of TEKT2, TEKT4, and SPTB decreased after TBX5 knockdown, indicating that they are downstream of TBX5. **(C)** Chromatin immunoprecipitation analysis showed that binding of TEKT2, TEKT4, and SPTB DNA fragments to TBX5 decreased after TBX5 knockdown, demonstrating that TBX5 promoted TEKT2, TEKT4, and SPTB transcription by binding to the promoters. β-Actin was used as the internal control. **(D)** Motif of binding sites between TBX5 protein and the promoters of the DNA fragments. **(E)** Sequence alignment between TBX5 3′-UTRs, including rs883079 and rs10850326, and microRNAs (miRNA), including hsa-miR-98-5p, hsa-miR-10a, hsa-miR-10b, and hsa-miR-182-5p. The bases on the rs883079 and rs10850326 are labeled yellow. **(F)** Venn diagram of single-nucleotide polymorphisms and mutations in the HOS patient's family determined using whole-exome sequencing. *$p < 0.05$, **$p < 0.01$, and ***$p < 0.001$; ns, not significant.

development and function and confirms the importance of long-term cardiac surveillance for individuals affected by HOS (Patterson et al., 2020). In the current case, the patient inherited the base T (reference C) at POS114793240 from her mother and base C (reference T) at POS114793297 from her father, both of which belong to the 3′-UTR of the TBX5 gene. The two dbSNP IDs were benign based on the ClinVar analysis. HOS is caused by a mutation in TBX5, which has been identified in more than 70% of cases (Spiridon et al., 2018). The patient's symptoms were not as severe as those of other HOS patients with mutations and SNPs at TBX5 exon sites. Therefore, we hypothesized that the two dbSNP IDs and their interactions with miRNAs may be the cause of her morbidity.

miR-98-5p regulated the myocardial differentiation of mesenchymal stem cells by targeting TBX5 in rat bone marrow samples, and miR-10a and miR-10b targeted the 3′-UTR of TBX5 to repress its expression in human embryonic kidney 293T cells (Wang et al., 2014; Sun et al., 2018). miR-182-5p exerted an evolutionarily conserved role as a TBX5 effector in the onset of cardiac propensity for arrhythmia in zebrafish, thereby mediating the relationship between TBX5, arrhythmia, and heart development (Guzzolino

TABLE 2 Specific primers used for quantitative real-time PCR.

Name	F	R
TEKT2	ATGGCGACACTAAGTTTCAAGC	TGGCGGATTTGGTGGGAAG
TEKT4	GGCCCCACAGTCAATAGATGT	GGGCATAAGAGTTCTGAAACCA
SPTB	GCTCCCACGACATTGTAGATG	GTGTTTCACGACCTTCCTGAG
TEKT2 promoter	CGAGAACATGGAAAACGGGTG	CTCTTAAAATGTGTTTCCTGC
TEKT4 promoter	TGAGACAGAGGAGCAGGGCAA	TTGTTGGAAACAGAATCGACA
SPTB promoter	GCTGGTAGCAAGGCTGGGACA	CTGTTTTTGAGCAGGCCAGTC
β-Actin	GGCTGTATTCCCCTCCATCG	CCAGTTGGTAACAATGCCATGT

et al., 2020). A marked sensitivity in the developing heart of TBX5 gene-edited mice to Tbx5 dosage demonstrated the "rheostatic" control of Tbx5, which elucidates the disrupted transcriptional and cellular mechanisms in congenital heart defects (Mori et al., 2006). In this study, we conducted sequence alignment between the TBX5 3′-UTR regions, including rs883079 and rs10850326, and relevant miRNAs, including has-miR-98-5p, has-miR-10a, has-miR-10b, and has-miR-182-5p, and found that the binding of miRNAs and TBX5 3′-UTRs was promoted in HOS to further decrease TBX5 expression, thus inducing the transcription of HOS-promoting genes.

The mechanisms mediated by miRNAs and TBX5 may be spatiotemporally regulated, which may explain why the patient's father and mother had SNPs and mutations but not HOS. The patient also inherited the SALL4 SNP in the exon area from both her father and mother. In zebrafish, SALL4 acts downstream of TBX5 and is required for pectoral fin outgrowth; mutations at the SALL4 locus on chromosome 20 resulted in a range of clinically overlapping phenotypes, including Okihiro syndrome, HOS, acro-renal-ocular syndrome, and thalidomide embryopathy (Harvey and Logan, 2006). Koshiba-Takeuchi et al. (2006) demonstrated that TBX5 regulated SALL4 expression in the developing mouse forelimb and heart, and mice heterozygous for the gene trap allele of SALL4 showed limb and heart defects that mirrored the human disease. TBX5 and SALL4 interact both positively and negatively to regulate the patterning and morphogenesis of the forelimb and heart. Thus, a positive and negative feed-forward circuit between TBX5 and SALL4 may potentially regulate the patterning of the embryonic limb and heart and represent a unifying mechanism for HOS. However, the exact consequences and mechanisms of the variants in SALL4 are unknown and require further research.

We identified 578 exons, along with 498 3′-UTRs and 346 5′-UTR mutations, in the patient using whole-exome sequencing, including the female urogenital genes PKD1, SON, and BMPR1B, as well as the reproduction-related genes TEK, COL11A1, ANKRD11, LEMD3, and SPTB, which was consistent with the findings of Tian et al. (2022).

This study had some limitations. To further explore the effects of TBX5 on cardiomyocytes, the HL-1 cell line was used with TBX5 knockdown. Quantitative polymerase chain reaction and chromatin immunoprecipitation analyses revealed that TBX5 binds to the TEKT2, TEKT4, and SPTB promoter regions to promote gene transcription. Further studies on mouse models and human cohorts are required. In addition, we only carried out sequence alignments between the TBX5 3′-UTR regions and previously reported miRNAs, and further validation is still needed. The effects of other genes on HOS formation and progression still need to be investigated.

We provide a novel gene signature of HOS, including TBX5 3′-UTR and downstream genes, such as SALL4 SNP, which may be a potential therapeutic target. Our findings support a novel TBX5-related pathogenic mechanism in HOS, though further experimental validation is needed. If this mechanism is correct, novel approaches can be devised for gene expression correction using pharmacological agents.

Data availability statement

The datasets for this article are not publicly available due to concerns regarding participant/patient anonymity. Requests to access the datasets should be directed to the corresponding author.

Ethics statement

The studies involving human participants were reviewed and approved by Tianjin Third Central Hospital. The human ethic approval has been submitted. Written informed consent to participate in this study was provided by the participants' legal guardian/next of kin. Written informed consent was obtained from the minor(s)' legal guardian/next of kin for the publication of any potentially identifiable images or data included in this article.

Author contributions

Conceptualization, YL and YZ; funding acquisition, TL; patient's family data collection and analysis, YZ, WZ, CZ, HZ, GW, ZL, and YL; cell experiments, YZ and BQ; visualization, YZ; writing—original draft, YZ; writing—review and editing, YL, YZ, and TL.

Funding

This work was funded by the Tianjin Key Medical Discipline (Specialty) Construction Project (TJYXZDXK-035A), Tianjin

"Project + Team" Key Training Special Project (no. XC202040), Tianjin "131" Innovative Talent Team Project (no. 201939), Key Project of Tianjin Natural Science Foundation (no. 21JCZDJC00240), Tianjin Municipal Health and Health Committee Science and Technology Project (no. ZD20001), Tianjin Health Committee Traditional Chinese Medicine and Integrated Traditional Chinese and Western Medicine Project (no. 2021139), Hebei Provincial Health Committee Project (no. 20220676), Hebei Provincial Health and Family Planning Committee Key Medical Science Research Project (no. 20171087), and Tianjin Municipal Health and Health Committee Science and Technology Talent Cultivation Project (no. KJ20008).

Acknowledgments

The authors would like to express their gratitude to all those who helped them in the writing of this manuscript. The authors thank all the peer reviewers for their opinions and suggestions. The authors would like to thank Tianjin Xinwei Technology Development Co., Ltd., for providing the 3D-printed heart model.

Conflict of interest

The authors declare that the research was conducted in the absence of any commercial or financial relationships that could be construed as a potential conflict of interest.

Publisher's note

All claims expressed in this article are solely those of the authors and do not necessarily represent those of their affiliated organizations, or those of the publisher, the editors, and the reviewers. Any product that may be evaluated in this article, or claim that may be made by its manufacturer, is not guaranteed or endorsed by the publisher.

References

Barisic, I., Boban, L., Greenlees, R., Garne, E., Wellesley, D., Calzolari, E., et al. (2014). Holt oram syndrome: A registry-based study in europe. *Orphanet J. Rare Dis.* 9, 156.

Darwich, R., Li, W., Yamak, A., Komati, H., Andelfinger, G., Sun, K., et al. (2017). KLF13 is a genetic modifier of the Holt-Oram syndrome gene TBX5. *Hum. Mol. Genet.* 26 (5), 942–954. doi:10.1093/hmg/ddx009

Guzzolino, E., Pellegrino, M., Ahuja, N., Garrity, D., D'Aurizio, R., Groth, M., et al. (2020). miR-182-5p is an evolutionarily conserved Tbx5 effector that impacts cardiac development and electrical activity in zebrafish. *Cell Mol. Life Sci.* 77 (16), 3215–3229. doi:10.1007/s00018-019-03343-7

Harvey, S. A., and Logan, M. P. (2006). sall4 acts downstream of tbx5 and is required for pectoral fin outgrowth. *Development* 133 (6), 1165–1173. doi:10.1242/dev.02259

Jhang, W. K., Lee, B. H., Kim, G. H., Lee, J. O., and Yoo, H. W. (2015). Clinical and molecular characterisation of Holt-Oram syndrome focusing on cardiac manifestations. *Cardiol. Young* 25 (6), 1093–1098. doi:10.1017/S1047951114001656

Koshiba-Takeuchi, K., Takeuchi, J. K., Arruda, E. P., Kathiriya, I. S., Mo, R., Hui, C. C., et al. (2006). Cooperative and antagonistic interactions between Sall4 and Tbx5 pattern the mouse limb and heart. *Nat. Genet.* 38 (2), 175–183. doi:10.1038/ng1707

Mori, A. D., Zhu, Y., Vahora, I., Nieman, B., Koshiba-Takeuchi, K., Davidson, L., et al. (2006). Tbx5-dependent rheostatic control of cardiac gene expression and morphogenesis. *Dev. Biol.* 297 (2), 566–586. doi:10.1016/j.ydbio.2006.05.023

Patterson, J., Coats, C., and McGowan, R. (2020). Familial dilated cardiomyopathy associated with pathogenic TBX5 variants: Expanding the cardiac phenotype associated with Holt-Oram syndrome. *Am. J. Med. Genet. A* 182 (7), 1725–1734. doi:10.1002/ajmg.a.61635

Ríos-Serna, L. J., Díaz-Ordoñez, L., Candelo, E., and Pachajoa, H. (2018). A novel de novo TBX5 mutation in a patient with Holt-Oram syndrome. *Appl. Clin. Genet.* 11, 157–162. doi:10.2147/TACG.S183418

Russell, M. W., Chung, W. K., Kaltman, J. R., and Miller, T. A. (2018). Advances in the understanding of the genetic determinants of congenital heart disease and their impact on clinical outcomes. *J. Am. Heart Assoc.* 7 (6), e006906. doi:10.1161/JAHA.117.006906

Shankar, B., Bhutia, E., Kumar, D., Kishore, S., and Das, S. P. (2017). Holt-oram syndrome: A rare variant. *Iran. J. Med. Sci.* 42 (4), 416–419.

Spiridon, M. R., Petris, A. O., Gorduza, E. V., Petras, A. S., Popescu, R., and Caba, L. (2018). Holt-oram syndrome with multiple cardiac abnormalities. *Cardiol. Res.* 9 (5), 324–329. doi:10.14740/cr767w

Stennard, F. A., and Harvey, R. P. (2005). T-box transcription factors and their roles in regulatory hierarchies in the developing heart. *Development* 132 (22), 4897–4910. doi:10.1242/dev.02099

Sun, H. H., Sun, P. F., and Liu, W. Y. (2018). MiR-98-5p regulates myocardial differentiation of mesenchymal stem cells by targeting TBX5. *Eur. Rev. Med. Pharmacol. Sci.* 22 (22), 7841–7848. doi:10.26355/eurrev_201811_16409

Tian, W., Chen, N., Ye, Y., Ma, C., Qin, C., Niu, Y., et al. (2022). A genotype-first analysis in a cohort of Mullerian anomaly. *J. Hum. Genet.* 67, 347–352. Online ahead of print. doi:10.1038/s10038-021-00996-w

Vanlerberghe, C., Jourdain, A. S., Ghoumid, J., Frenois, F., Mezel, A., Vaksmann, G., et al. (2019). Holt-oram syndrome: Clinical and molecular description of 78 patients with TBX5 variants. *Eur. J. Hum. Genet.* 27 (3), 360–368. doi:10.1038/s41431-018-0303-3

Wang, F., Yang, X. Y., Zhao, J. Y., Yu, L. W., Zhang, P., Duan, W. Y., et al. (2014). miR-10a and miR-10b target the 3'-untranslated region of TBX5 to repress its expression. *Pediatr. Cardiol.* 35 (6), 1072–1079. doi:10.1007/s00246-014-0901-y

Zaragoza, M. V., Hakim, S. A., Hoang, V., and Elliott, A. M. (2017). Hearthand syndrome IV: A second family with LMNA-related cardiomyopathy and brachydactyly. *Clin. Genet.* 91 (3), 499–500.

frontiers | Frontiers in Pediatrics

TYPE Case Report
PUBLISHED 02 March 2023
DOI 10.3389/fped.2023.1001222

Check for updates

OPEN ACCESS

EDITED BY
Zhichao Liu,
Boehringer Ingelheim, United States

REVIEWED BY
Sarah Ducamp,
Harvard Medical School, United States
Ilaria Maccora,
University of Florence, Italy

*CORRESPONDENCE
Huasong Zeng
✉ huasongxuqing@163.com

SPECIALTY SECTION
This article was submitted to Genetics of Common and Rare Diseases, a section of the journal Frontiers in Pediatrics

RECEIVED 23 July 2022
ACCEPTED 20 January 2023
PUBLISHED 02 March 2023

CITATION
Chen X, Fu F, Mo X, Cheng S and Zeng H (2023) Case report: Sideroblastic anemia with B-cell immunodeficiency, periodic fevers, and developmental delay: Three cases and a literature review.
Front. Pediatr. 11:1001222.
doi: 10.3389/fped.2023.1001222

COPYRIGHT
© 2023 Chen, Fu, Mo, Cheng and Zeng. This is an open-access article distributed under the terms of the Creative Commons Attribution License (CC BY). The use, distribution or reproduction in other forums is permitted, provided the original author(s) and the copyright owner(s) are credited and that the original publication in this journal is cited, in accordance with accepted academic practice. No use, distribution or reproduction is permitted which does not comply with these terms.

Case report: Sideroblastic anemia with B-cell immunodeficiency, periodic fevers, and developmental delay: Three cases and a literature review

Xiangyuan Chen[1], Fang Fu[2], Xiaolan Mo[3], Suyun Cheng[1] and Huasong Zeng[1]*

[1]Department of Allergy, Immunology and Rheumatology, Guangzhou Women and Children's Medical Center, Guangdong Provincial Clinical Research Center for Child Health, Guangzhou Medical University, Guangzhou, China, [2]Department Institute of Birth Health and Perinatal Medicine, Guangzhou Women and Children's Medical Center, Guangdong Provincial Clinical Research Center for Child Health, Guangzhou Medical University, Guangzhou, China, [3]Department of Pharmacy, Guangzhou Women and Children's Medical Center, Guangdong Provincial Clinical Research Center for Child Health, Guangzhou Medical University, Guangzhou, China

Sideroblastic anemia with B-cell immunodeficiency, periodic fevers, and developmental delay (SIFD) is a serious autosomal recessive syndrome caused by biallelic mutations in cytosine–cytosine–adenosine tRNA nucleotidyltransferase 1 (*TRNT1*). The main clinical features of SIFD are periodic fevers, developmental delay, sideroblastic or microcytic anemia, and immunodeficiency. Herein, we report three cases of SIFD with compound heterozygous variants of *TRNT1*. Patients 1 and 2 were siblings; they presented with periodic fevers, arthritis, low immunoglobulin A, bilateral cataracts, anemia, and neurodevelopmental and developmental delay. Patient 3 had severed clinical features with recurrent fever and infections. She was treated with infliximab and symptomatic treatments but without therapeutic effect. She received a stem cell transplantation of umbilical cord blood but died of posttransplant infection and posttransplant graft-vs.-host disease 17 days after transplantation. Finally, a literature review revealed that *TRNT1* variants differed among SIFD patients. Our cases and literature review further expand existing knowledge on the phenotype and *TRNT1* variations of SIFD and suggest that the early genomic diagnosis of *TRNT1* is valuable to promptly assess bone marrow transplantation and tumor necrosis factor inhibitor treatments, which might be effective for the immunodeficiency and inflammation caused by SIFD.

KEYWORDS

SIFD, TRNT1, immunodeficiency, periodic fever, developmental delay

Introduction

Sideroblastic anemia with B-cell immunodeficiency, periodic fevers, and developmental delay (SIFD) is an autosomal recessive syndrome characterized by severe sideroblastic anemia in the neonatal period or infancy that was first reported in 2013 (1). Next-generation sequencing enables the determination of mutations in the gene nucleotidyltransferase (*TRNT*)-1 (2). *TRNT1* encodes the nucleotidyltransferase tRNA (tRNA-NT) enzyme that catalyzes the addition of the cytosine–cytosine–adenosine (CCA) terminus to the 3′ end of tRNA precursors, which is essential for aminoacylated tRNAs to participate in protein biosynthesis (3, 4). Biallelic *TRNT1* variants impair neuronal cell development and heme synthesis, resulting in SIFD (5), which includes some common clinical features such as

sideroblastic anemia, immune deficiency, and periodic fevers. In many individuals with TRNT1 deficiency, the immunoglobulin level is low (hypogammaglobulinemia) (3). To date, only 60 confirmed SIFD cases with *TRNT1* mutations have been described worldwide (3, 5–29). In this study, we report three cases of SIFD resulting from *TRNT1* mutations, including one family with two cases. From these two cases, we identified novel mutations in *TRNT1* (c.1056 + 1G > A and c.1246A > G). In addition, we identified an affected child with severe clinical features. **Table 1** shows the clinical features, biochemical detection indices, and genetic analyses of the SIFD patients in this study. Through a systematic review of cases from published articles, we provide new insights for clinicians toward diagnosing SIFD by connecting clinical features and *TRNT1* mutations.

Case report

Patient 1 (P1), born to non-consanguineous parents, presented with persistent low-grade fever (37.4–38°C) since 8 months of age. The inflammatory markers were elevated every 1–2 months without infective factors, but she recovered following symptomatic treatment. At 16 months of age, she had pain and swelling of her right knee joint with flexion contracture. She could bend her knee and briefly stand but could not walk without hypotonia. At 19 months of age, she was diagnosed with bilateral cataracts. At 7 years of age, cranial magnetic resonance imaging (MRI) showed mild atrophy-like changes in the bilateral cerebral hemispheres and underdeveloped bilateral frontal lobes, suggesting neurodevelopmental delay. The patient had some hearing problems. She could hear louder voice, but no specific hearing test was carried out. She presented with fever several times as an outpatient. She had mild microcytic hypochromic anemia. Sideroblastic anemia could not be determined as her parents did not consent to having her undergo bone marrow aspiration for further examination. Immunoglobulin tests showed a low level of immunoglobulin A (IgA) (<0.07 g/L, range 0.13–0.35 g/L), while immunoglobulin G (IgG), M (IgM), and E (IgE), and complement C3 and C4 were normal. The lymphocyte counting test showed that the ratios and amounts of B- and T-lymphocytes were normal. At this time, she was 16 years old, 12 kg (< −3 SD) in weight, 102 cm (< −3 SD) in height, and had a 48 cm head circumference (**Figure 1A**). Unfortunately, she did not undergo follow-up visits due to family reasons.

Patient 2 (P2) was the younger male sibling of P1. Similar to his sister, he had unspecified periodic fevers, low levels of IgA, arthritis, and developmental delay; however, he had normal hearing. He was examined routinely at our hospital in the first 3 months after birth. The patient was diagnosed with mild microcytic hypochromic anemia with low levels of IgA (<0.07 g/L, range 0.13–0.35 g/L), whereas neutrophil phagocytosis, B- and T-lymphocyte rates and counts, and IgG were normal. Using ultrasound diagnosis, we found that he had hydrocephalus. At 4 months of age, the patient had diarrhea for the first time for undefined reasons. He was hospitalized at 8 months old with bronchopneumonia and diarrhea. He was diagnosed with a respiratory syncytial virus infection through a pharyngeal swab trial. Thereafter, he experienced febrile episodes every 3–4 weeks, lasting 3–7 days each time. At 19 months of age, he had pain and swelling of the bilateral knee joints and refused to walk on foot. Ultrasonography detection revealed effusions in his knee joints. At 2 years of age, he was diagnosed with bilateral cataracts. Immunological examination showed a slight decrease in IgA, while IgG, IgM, IgE, and B-lymphocyte counts were normal. Afterward, he received intravenous immunoglobulin (IVIG) 400 mg/kg treatment irregularly, resulting in fewer fevers. At 37 months of age, he was hospitalized again due to fever and diarrhea. At 5 years of age, he contracted bronchopneumonia and a type A influenza virus infection. Nevertheless, there were no abnormalities in cardiac and urological ultrasound and cranial MRI detection results. In the same year, his vision was restored after extracapsular cataract extraction with intraocular lens implantation at our hospital. At this point, he was 8 years old, 11 kg (<−3 SD) in weight, 98 cm (<−3 SD) in height, had a 49-cm head circumference (**Figure 1B**), and could speak simple and short sentences with three to seven words, but the pronunciation was not clear. He stumbled by himself, and fever episodes recurred every 2–3 months.

P1 and her younger brother P2 were treated in our department since May 2016. With the approval of the hospital ethics committee (approval number: 2016021645), peripheral blood was collected from them and their parents for whole-genome sequencing at the Institute of Eugenics and Perinatology at our hospital. The parents had heterozygous mutations in the *TRNT1* gene. Their father had a mutation at c.1246A > G (p.K416E), which has been reported previously (6, 7, 20), whereas their mother had an unreported mutation at c.1056 + 1G > A. The biallelic heterozygous variants of *TRNT1* [c.1056 + 1G > A and c.1246A > G (p.K416E)] were determined in P1 and P2. The c.1056 + 1G > A variant is located at the mRNA splice region in a highly conserved sequence representing functional domains, indicating that the variant may have a structural alteration of the TRNT1 protein, affecting its function. Nevertheless, it has been considered a pathogenic variant with low frequency based on the assessment of the American College of Medical Genetics and Genomics and the Association for Molecular Pathology (ACMG-AMP) (30).

Patient 3 (P3), a Chinese girl, was born from a pair of non-consanguineous Chinese individuals through normal pregnancy (**Figure 1C**). The mother has a thalassemia trait, but the father is normal. **Figures 1D,E** show the pedigrees of the two families in this study. Patient 3 presented with a febrile illness and swelling of the skin and soft tissues in the right clavicular region at 3 months of age. The patient was hospitalized to undergo right chest wall debridement and drainage due to bronchopneumonia and necrotic fasciitis. She was hospitalized again at 5 months of age for an abscess in the buttocks and at 6 months of age for bronchopneumonia, perforated sigmoid colon, abdominal adhesions, acute diffuse peritonitis, sepsis, fungal infection, acute suppurative pharyngitis, acute bronchitis, and fat liquefaction in a postoperative wound. Therefore, she underwent a sigmoid colostomy by partially resectioning her colon to repair the perforation. One month later, she was hospitalized again for sepsis, pneumonia, and necrotizing fasciitis in her left big toe. Again, she underwent right chest wall debridement and drainage at 8 months of age when she presented with a fever and cough. Thereafter, she received IVIG treatment every 4 weeks to reduce infection. The

10.3389/fped.2023.1001222

TABLE 1 Clinical features, biochemical detection index, and genetic analysis of SIFD patients ($n = 3$).

Clinical features	Patient 1	Patient 2	Patient 3	
Country of birth	China	China	China	
Gender	Female	Male	Female	
Ethnicity	Han	Han	Han	
Consanguinity	No	No	No	
Age at onset (months)	8	4	3	
Age at diagnosis (months)	116	24	10	
Clinical diagnosis	Recurrent fevers Microcytic anemia Respiratory infection Developmental delay Cerebral atrophy Mild hearing impairment Amyotrophy Microcephaly Cataract Arthritis	Recurrent fevers Microcytic anemia Respiratory infection Diarrhea Developmental delay Amyotrophy Microcephaly Cataract Arthritis	Recurrent fevers Microcytic anemia Respiratory infection Peritonitis Skin soft tissue infection	
Biochemical detection index				Normal reference value
Hb (g/dl)	100 ↓	94 ↓	77↓	110–140
MCV (fl)	67.6 ↓	60.6 ↓	76.7↓	82–100
MCH (pg)	21 ↓	19.1↓	24.6↓	27–34
MCHC (g/L)	311 ↓	315 ↓	321.00	316–354
CRP (mg/L)	33.6 ↑	30.6 ↑	215.0↑	0–8
ESR (mm/h)	24.00	35	NA	0–15
IL-6 (pg/ml0	NA	9.70	21.6↑	0–16.6
TNF-α (pg/ml)	NA	2.10	6.3↑	0–5.2
IgG (g/L)	6.5	8.84	9.73 (after IVIG)	5–10.6
IgA (g/L)	<0.07 ↓	<0.07 ↓	<0.07 ↓	0.13–0.35
IgM (g/L)	0.73	0.56	0.22↓	0.4–1.28
IgE (g/L)	10	12	<5	0–60
C3	0.85	0.97	0.63↓	0.8–1.5
C4	0.19	0.22	0.15	0.12–0.4
Lymphocyte subsets				
WBC (10^9/L)	5.80	8.6	50.5↑	5–12
CD3+	65%	72% ↑	96.99% ↑	39–70%
CD3 + CD4+	43% ↑	53% ↑	67.80% ↑	15–37%
CD3 + CD8+	21%	17%	27.82%	14–39%
CD3-CD19+	19%	17%	0.09% ↓	11–28%
CD3-CD16+/CD56+	12%	9%	2.92% ↓	8–34%
Therapy				
Antibiotics	Yes	Yes	Yes	
IVIG	No	Yes	Yes	
TNF-α inhibitor	No	No	Yes	
Stem cell transplantation	No	No	Yes	
Alive/dead	Living	Living	Dead	

(*continued*)

10.3389/fped.2023.1001222

TABLE 1 Continued

Clinical features	Patient 1	Patient 2	Patient 3	
Genetic analysis of TRNT1 mutations	c.1056 + 1G > A/c.1246A > G (p.K416E)	c.1056 + 1G > A/c.1246A > G (p.K416E)	c.574C > T (p.Q192*/c.464T > C (p.I155T)	

SIFD, sideroblastic anemia with B-cell immunodeficiency, periodic fevers, and developmental delay; CRP, C-reactive protein; TNF, tumor necrosis factor; IgG, immunoglobulin G; IgA, immunoglobulin A; IgM, immunoglobulin M; IgE, immunoglobulin E; IVIG, intravenous immunoglobulin.
The table shows the statistically significant differences between measurement results and normal range. ↑ The values are higher than normal range. ↓ The values are lower than normal range.

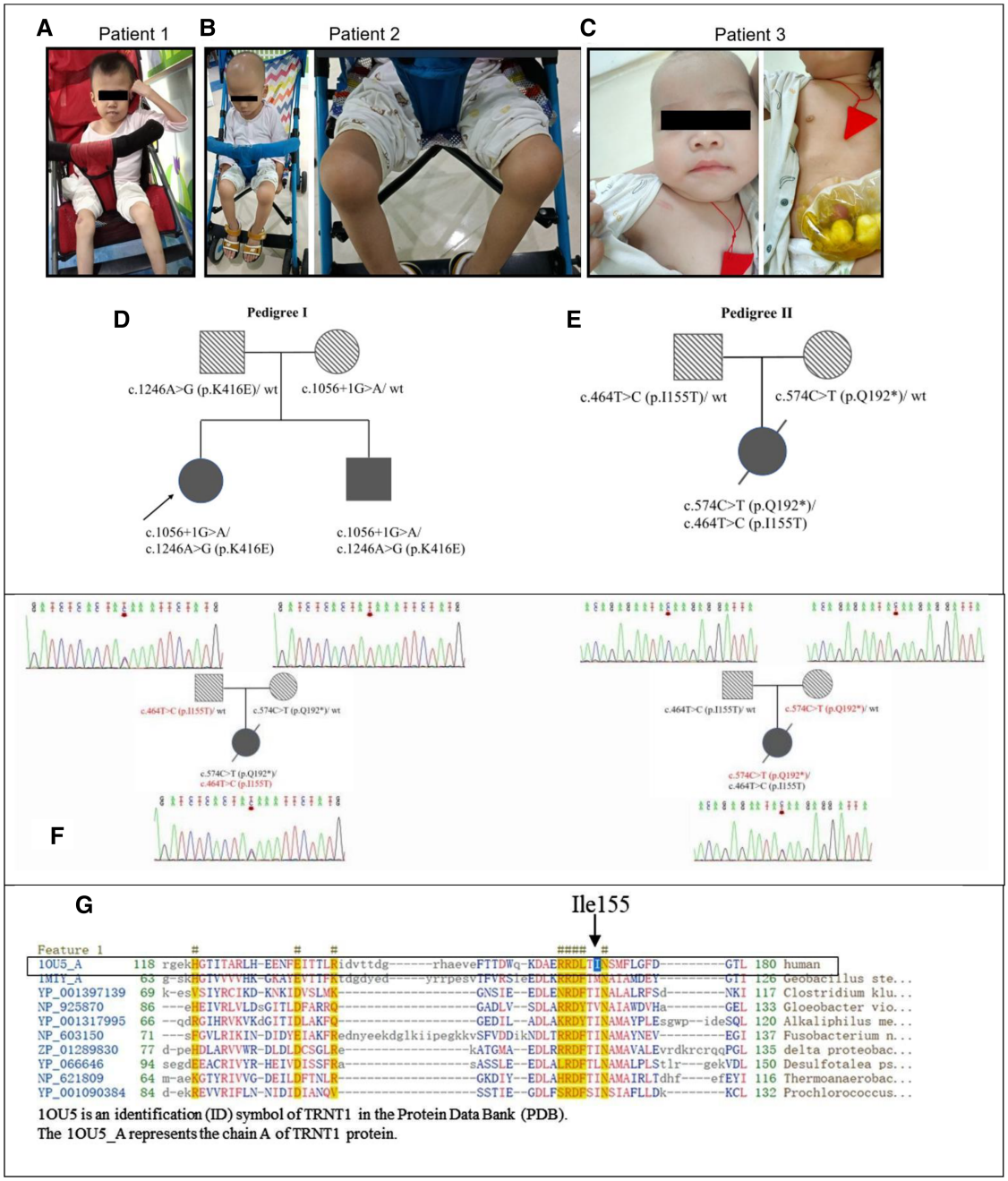


FIGURE 1
The genetic and clinical characteristics of SIFD patients. (A) Patient 1 at the age of 14 years presented with hypotrophic muscle and arthritis. (B). Patient 2 at the age of 7 years presented with hypotrophic muscle and arthritis. (C) Patient 3 at the age of 11 months. (D) The pedigree of siblings in the first family with patient 1 and patient 2. (E) The pedigree of patient 3. (F) The Sanger sequencing chromatograms of *TRNT1* gene compound heterozygous variations of the family with patient 3. The mutation c.574C > T (p.Q192*) inherited from her mother and c.464T > C (p.I155T) inherited from her father. (G) The conserved amino acid sequence in protein TRNT1. The black arrow points a conservative amino acid (Ile155) of protein *TRNT1* in human. SIFD, sideroblastic anemia with B-cell immunodeficiency, periodic fevers, and developmental delay.

compound heterozygous *TRNT1* variant with two functional mutations at c.574C > T (p.Q192*) (inherited from her mother) and c.464T > C (p.I155T) (inherited from her father) was identified through whole-exome sequencing (**Figure 1F**). No thalassemia gene mutation was found. At 9 months of age, the patient was diagnosed with primary immune deficiency disorders (PID), IgG deficiency, skin and soft tissue infection, iron deficiency anemia, enterocolitis, arthritis, eczema, thrombocytosis, and oral candidiasis. She received IVIG combined with ibuprofen, methylprednisolone, and infliximab to combat inflammation, combined with cephalosporin, vancomycin, meropenem, and fluconazole for anti-infection at another hospital. However, the treatment was ineffective. At 15 months of age, she was hospitalized in the intensive care unit for critical illness. Laboratory tests showed that her white blood cell count was 50.5×10^9/L, neutrophils accounted for 91%, of which band form neutrophilic granulocyte accounted for 47%. No smears were performed at this point; however, the high-sensitivity C-reactive protein (hsCRP) abundance was up to 215 mg/L. *Staphylococcus* infection was detected using a blood culture test. Lymphocyte counts showed B-lymphocyte deficiency and serum immunoglobulin deficiency. A cardiac ultrasound examination showed normal myocardial and intracardiac structure and function. Next, patient 3 was treated with linezolid for bacterial infections. Ring sideroblasts could not be determined without bone marrow aspiration. At 17 months of age, patient 3 underwent umbilical cord blood (UCB) stem cell transplantation. After 5 days of treatment, she had a fever, rash, and mucus discharge from the colostomy. In addition, her inflammatory marker and liver enzyme levels were increased. The results of a blood culture test indicated the patient had a *Stenotrophomonas maltophilia* infection. Taken together, the patient was diagnosed with a posttransplant infection, a posttransplant graft-vs.-host disease, pancytopenia, and metabolic acidosis. Seventeen days after transplantation, the patient died due to severe sepsis and multiorgan failure.

Discussion

SIFD is a heritable, autosomal recessive disorder with severe multiorgan damage and often results in death during the first decade of life (6). Using whole-exome sequencing, a direct link between *TRNT1* and SIFD was first reported in 2014 (6). *TRNT1* is a nuclear gene encoding the tRNA-NT enzyme, which plays a role in the posttranscriptional modification of tRNAs by adding the CCA trinucleotide to the 3′-end of newly synthesized tRNAs (3, 4). Sasarman et al. suggested that *TRNT1* mutations would impair mitochondrial translation, resulting from defective CCA addition to mitochondrial $tRNA^{Ser(AGY)}$, resulting in an increase in mitochondrial reactive oxygen species that persistently trigger NLRP3 inflammasome activation (12). Recent research suggests that except for previously reported mitochondrial tRNAs, *TRNT1* mutations severely affect the expression of mature cytosolic tRNAs (7). The *TRNT1* mutant cells fail to upregulate protein clearance pathways and perturbations in proteostasis activation in the innate immune system, which results in the overexpression of interleukin-1 (IL-1) and tumor necrosis factor (TNF) (7), suggesting that *TRNT1* mutations are indeed one of the causes of SIFD disease.

TNF inhibitors are typical anti-inflammatory medications used to treat autoimmune diseases such as rheumatoid, juvenile, and psoriatic arthritis, plaque psoriasis, ankylosing spondylitis, ulcerative colitis, and Crohn's disease (31, 32). TNF inhibitors, which could inhibit proinflammatory cytokines in tissues and blood to reduce fever, blood transfusion demand, and chronic anemia, were first reported to treat SIFD patients in 2019 (7). Giannelou et al. described that three patients received etanercept, and one received infliximab treatment and was followed up from 2 to 12 years (7). It was suggested that TNF inhibitor therapy could effectively suppress fevers and restore inflammatory factors to normal in these patients. In the current study, patient 3 also received the infliximab treatment for anti-inflammation. Unfortunately, the treatment was ineffective. Considering the various clinical features in patients with various *TRNT1* variants, more clinical data are needed to assess the therapeutic effect of TNF inhibitors.

Bone marrow transplants are the only reported effective option (4). Three patients have been reported as having received bone marrow transplants. One patient was transplanted with matched bone marrow from his sibling at 5 months of age. However, this patient died following significant neurological complications 38 weeks posttransplant (10). Another patient underwent a myeloablative allogeneic bone marrow transplantation at 9 months of age, remaining healthy over 3 years posttransplantation, except for pigmentary retinitis that occurred 32 months posttransplantation (1). The last patient showed no systemic symptoms 3 years posttransplantation but had moderate hearing loss and retinopathy (4). In the present report, patient 3 underwent UCB stem cell transplantation. However, the patient died due to *S. maltophilia* infection and transplantation-related complications.

To date, 60 SIFD patients with *TRNT1* variants have been reported in previous publications (3, 5–29). In **Table 2**, we have summarized all the *TRNT1* variants including the three new cases. Through this work, the summarized *TRNT1* mutations can be used by other researchers or clinicians to further investigate their functions in SIFD disease. Patients with the c.1246A > G mutation in *TRNT1* exhibited typical clinical features such as periodic fevers, sideroblastic anemia, developmental delay, diarrhea, bilateral hearing loss, bilateral cataracts, recurrent swelling of digits in hands and knees, and hypotrophic muscle (6, 7, 20). In the present study, the siblings with newly reported *TRNT1* mutations (c.1246A > G and c.1056 + 1G > A) had similar clinical features, including periodic fevers, mild anemia, developmental delay, bilateral cataracts, recurrent swelling of knees, and hypotrophic muscle. Considering the unreported *TRNT1* mutation (c.1056 + 1G > A) is located in the mRNA splice region within a highly conserved sequence, this variant might have more impact and requires more studies in the future.

Patient 3 with *TRNT1* mutations [c.574C > T (p.Q192*/c.464T > C (p.I155T)] had severe clinical features, including recurrent fevers, immune deficiency disorders, and developmental delay. The resolved human protein structure of TRNT1 with its Protein Data Bank (PDB) identification (ID) is shown in **Figure 2A**. The c.464T > C (p.I155T) mutation in *TRNT1* affects the conservative amino

10.3389/fped.2023.1001222

TABLE 2 Reported pathogenetic variants in *TRNT1*.

Reference	No	Single-nucleotide Variant 1	Protein variant 1	Type of mutation	Single-nucleotide Variant 2	Protein variant 2	Type of mutation
(3)	1	c.668T > C	p.I223T	Missense	c.342 + 5G > T	NA	Splicing
	2	c.668T > C	p.I223T	Missense	c.342 + 5G > T	NA	Splicing
(5)	3	c.525delT	p.L176*	Nonsense	c.938T > C	p.L313S	Missense
(6)	4	c.569G > T	p.R190I	Missense	c.569G > T	p.R190I	Missense
	5	c.569G > T	p.R190I	Missense	c.569G > T	p.R190I	Missense
	6	c.569G > T	p.R190I	Missense	c.569G > T	p.R190I	Missense
	7	c.668T > C	p.I223T	Missense	c.668T > C	p.I223T	Missense
	8	c.668T > C	p.I223T	Missense	c.1057-7C > G	NA	Splicing
	9	c.668T > C	p.I223T	Missense	c.1057-7C > G	NA	Splicing
	10	c.668T > C	p.I223T	Missense	c.1057-7C > G	NA	Splicing
	11	c.668T > C	p.I223T	Missense	c.218_219ins22	NA	Frameshift
	12	c.668T > C	p.I223T	Missense	c.1142insATGT	p.W381fs	Frameshift
	13	c.668T > C	p.I223T	Missense	c.1252_1253insA	p.S418fs	Frameshift
	14	c.668T > C	p.I223T	Missense	No mutation detected	NA	NA
	15	c.1246A > G	p.K416E	Missense	c. del1054_1056 + 10	NA	Splicing
	16	c.1246A > G	p.K416E	Missense	c. del1054_1056 + 10	NA	Splicing
	17	c.608 + 1 G > T	NA	Splicing	c.461C > T	p.T154I	Missense
	18	c.977T > C	p.I326T	Missense	c.472A > G	p.M158V	Missense
	19	c.497T > C	p.L166S	Missense	c.461C > T	p.T154I	Missense
(7)	20	c.644A > G	p.H215R	Missense	c.644A > G	p.H215R	Missense
	21	c.644A > G	p.H215R	Missense	c.644A > G	p.H215R	Missense
	22	c.295C > T	p.R99W	Missense	c.488A > T	p.D163V	Missense
	23	c.295C > T	p.R99W	Missense	c.488A > T	p.D163V	Missense
	24	c.329C > T	p.T110I	Missense	c.383A > G	p.D128G	Missense
	25	c.329C > T	p.T110I	Missense	c.383A > G	p.D128G	Missense
	26	c.488A > T	p.D163V	Missense	c.668T > C	p.I223T	Missense
	27	c.1246A > G	p.K416E	Missense	c.1245_1246insA	p.S418Kfs*9	Frameshift
	28	c.668T > C	p.I223T	Missense	c.1245_1246insA	p.S418Kfs*9	Frameshift
(8)	29	c.295C > T	p.R99W	Missense	c.295C > T	p.R99W	Missense
	30	c.295C > T	p.R99W	Missense	c.295C > T	p.R99W	Missense
	31	c.295C > T	p.R99W	Missense	c.295C > T	p.R99W	Missense
(9)	32	c.1246A	p.S418fs	Frameshift	c.609-26 T > C	NA	Splicing
	33	c.1246A	p.S418fs	Frameshift	c.609-26 T > C	NA	Splicing
	34	c.1246A	p.S418fs	Frameshift	c.126_128delAGA	p.E43del	Frameshift
(10)	35	c.608 + 1 G > T	NA	Splicing	c.668T > C	p.I223T	Missense
	36	c.608 + 1 G > T	NA	Splicing	c.668T > C	p.I223T	Missense
(11)	37	c.218_219ins22	p.I223T	Frameshift	c.218_219ins22	p.I223T	Frameshift
	38	c.977T > C	p.I326T	Missense	c.977T > C	p.I326T	Missense
(12)	39	c.443C > T	p.A148V	Missense	c.443C > T	p.A148V	Missense
	40	c.383A > G	p.D128G	Missense	c.518A > T	p.Y173F	Missense

(*continued*)

TABLE 2 Continued

Reference	No	Single-nucleotide Variant 1	Protein variant 1	Type of mutation	Single-nucleotide Variant 2	Protein variant 2	Type of mutation
(13)	41	c.295C > T	p.R99W	Missense	c.295C > T	p.R99W	Missense
(14)	42	c.295C > T	p.R99W	Missense	c.1234C > T	p.R412*	Nonsense
(15)	43	c.498_501delATTT	p.F167fs	Nonsense	c.947C > T	p.A316V	Missense
(16)	44	NA	NA		NA	NA	
(17)	45	c.565T > C	p.I155T	Missense	c.608G > A	p.R203K	Missense
(18)	46	c.1213G > A	p.G405R	Missense	c.1057-7C > G	NA	Splicing
(19)	47	c.977T > C	p.I326T	Missense	c.977T > C	p.I326T	Missense
	48	c.1213G > A	p.G405R	Missense	c.1057-7C > G	NA	Splicing
(20)	49	c.938delT	p.L313fs	Frameshift	c.1246A > G	p.K416E	Missense
	50	c.608G > A	p.R203K	Missense	c.1246A > G	p.K416E	Missense
(21)	51	c.1057-7C > G	NA	Splicing	c.1092A > T	p.E364D	Missense
	52	c.1057-7C > G	NA	Splicing	c.1092A > T	p.E364D	Missense
(22)	53	c.668T > C	p.I223T	Missense	c.1057-7C > G	NA	Splicing
(23)	54	c.914A > T	p.D305V	Missense	c.914A > T	p.D305V	Missense
(24)	55	c.361 G > A	p.E121K	Missense	c.407 C > G	p.A136G	Missense
(25)	56	c.495_498del	p.F167Tfs*9	Frameshift	c.1246A > G	p.K416E	Missense
(26)	57	c.88A > G	p.M30V	Missense	c.363G > T	p.E121D	Missense
	58	c.302 T > C	p.I101T	Missense	c.1234C > T	p.R412*	Nonsense
(27)	59	c.383A > G	p.D128G	Missense	c.1168G > A	p.G390S	Missense
(28)	60	c.948-949delAAinsGG	p.K317E	Missense	c.948-949delAAinsGG	p.K317E	Missense
This study	61	c.1246A > G	p.K416E	Missense	c.1056 + 1G > A	NA	Splicing
	62	c.1246A > G	p.K416E	Missense	c.1056 + 1G > A	NA	Splicing
	63	c.574C > T	p.Q192*	Nonsense	c.464T > C	p.I155T	Missense

NA, not available.

acid sequence of this protein, which may contribute to protein dysfunction (**Figures 1G**, **2C**). Most importantly, the novel c.574C > T (p.Q192*) mutation causes protein truncation (**Figure 2B**), which may contribute to the dysfunction of TRNT1. Though we have no evidence to prove the function of truncated TRNT1 in mitochondrial, combined with the biallelic mutations, the dysfunctional TRNT1 protein may have finally led patient 3 to acquire SIFD. Therefore, alteration of TRNT1 protein structure by c.574C > T (p.Q192*) and c.464T > C (p.I155T) mutations may indicate a poor prognosis for patients with SIFD. In the present study, the c.574C > T mutation is reported for the first time. Other studies on this mutation could not be found. Therefore, its function in SIFD deserves to be further explored in the future. Besides the two aforementioned *TRNT1* mutations, the previously reported c.1246A > G (p.K416E) mutation could also produce dysfunctional proteins in patients 1–2 (**Figure 2D**) (6). Therefore, future studies should consider more effective treatments to correct this mutation, such as gene editing and repair.

The literature review and this study found 63 SIFD patients with *TRNT1* mutations (3, 5–29). However, clinical characteristics were not reported in 16 cases (6). Therefore, we summarized the clinical features of 47 patients in **Table 3**. These patients have a very varied phenotypic appearance. Developmental delay (66%) and recurrent fevers (68%) are the most common clinical features in SIFD patients with *TRNT1* mutations. The majority of patients have sideroblastic anemia (55%). Cataracts are found in 30% of patients, hearing loss in 21%, diarrhea in 34%, skin and subcutaneous diseases in 26%, and poor balance in 17%. Some SIFD patients also exhibit several features like ataxia, hypotonia, splenomegaly, retinitis pigmentosa, seizures, and cardiomyopathy (3, 5–29).

Conclusion

Due to the close association between *TRNT1* variants and SIFD disease, the early detection of *TRNT1* mutations in patients with SIFD would help them get timely treatment. In the present study, we reported three SIFD cases with newly discovered mutations (c.1056 + 1G > A and c.574C > T) in *TRNT1*. Bone marrow

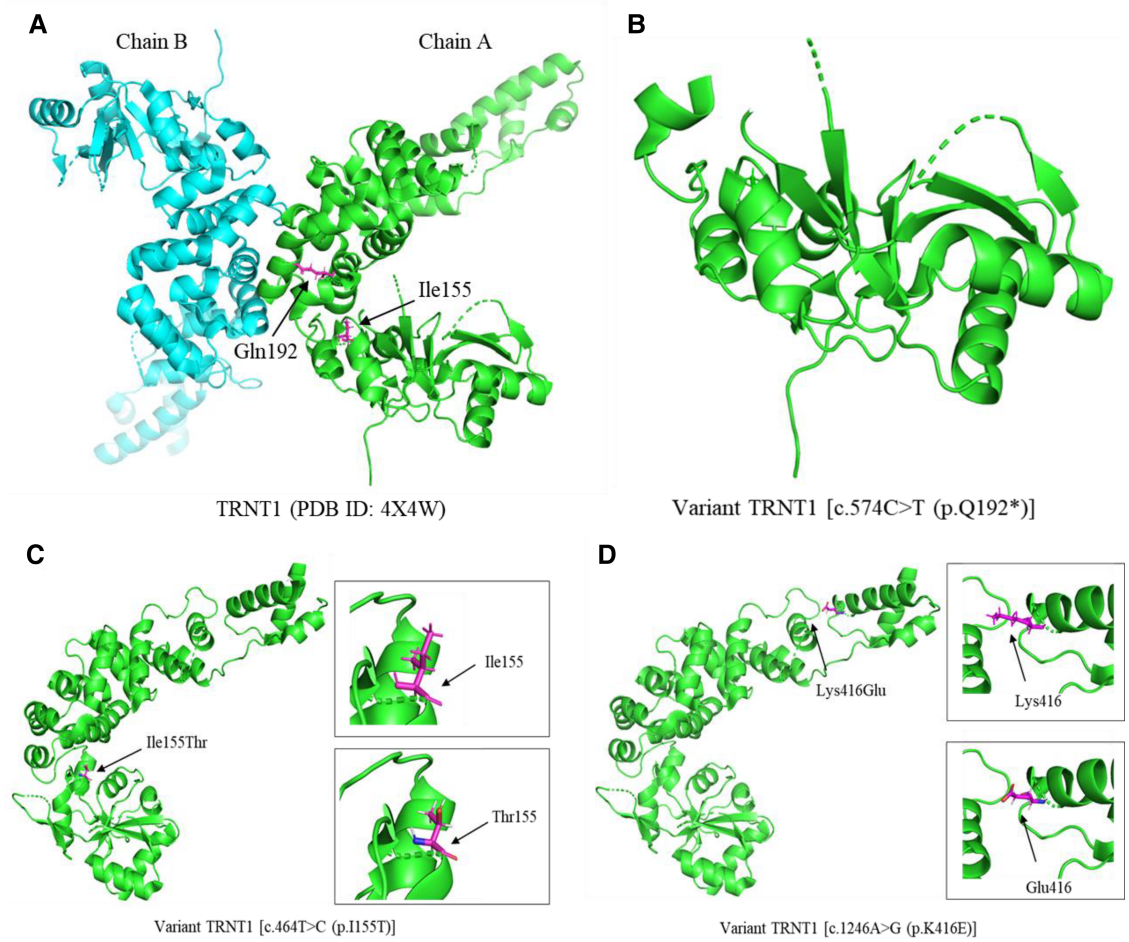


FIGURE 2
The cartoon diagram of 3D protein structure of TRNT1 and its variants. (**A**) The resolved human protein structure of TRNT1 with its PDB identification (ID). (**B**) The protein structure of variant TRNT1 [c.574C > T (p.Q192*)]. (**C**) The protein structure of variant TRNT1 [c.464T > C (p.I155T)]. The black arrows point the amino acids isoleucine (Ile) and threonine (Thr) at the site of 155. (**D**) The protein structure of variant TRNT1 [c.1246A > G (p.K416E)]. The black arrows point the amino acids lysine (Lys) and glutamate (Glu) at the site of 416. PDB, Protein Data Bank; ID, identification.

TABLE 3 Clinical features in patients with *TRNT1* mutations.

Clinical features	% of 47 patients	% of 14 deaths
Developmental delay	66% (31/47)	36% (5/14)
Recurrent fevers	68% (32/47)	71% (10/14)
Sideroblastic anemia	55% (26/47)	86% (12/14)
Cataracts	30% (14/47)	7% (1/14)
Hearing loss	21% (10/47)	14% (2/14)
Diarrhea	34% (16/47)	7% (1/14)
Skin and subcutaneous diseases	26% (12/47)	29% (4/14)
Poor balance	17% (8/47)	0% (0/14)
Total mortality rate	29.8% (14/47)	

transplantation and TNF inhibitor therapy for patients with SIFD may greatly relieve disease symptoms and meet clinical demands.

The inadequacies of this article are that the laboratory testings were not comprehensive for some reasons. The siblings of patients 1 and 2 failed to return to the hospital for further consultation due to family reasons, which led to lose effective treatment measures, and could not evaluate the prognosis appropriately. Also, maybe we need try more measures such as etanercept, colchicine, and anakinra when infliximab treatment failed before stem cell transplantation in patient 3. In addition, we did not carry out the functional study of the new mutations in *TRNT1*, hoping that subsequent studies can clarify the relationship between molecular mechanisms and clinical phenotypes in the future.

Data availability statement

The original contributions presented in the study are included in the article/**Supplementary Material**, further inquiries can be directed to the corresponding author.

Ethics statement

The studies involving human participants were reviewed and approved by hospital ethics committee (approval number:

2016021645) of Guangzhou Women and Children's Medical Center. Written informed consent to participate in this study was provided by the participants' legal guardian/next of kin. Written informed consent was obtained from the individual(s), and minor(s)' legal guardian/next of kin, for the publication of any potentially identifiable images or data included in this article.

Author contributions

XC, XM, and HZ contributed to conception and design of the study. FF and SC organized the database. XC wrote the first draft of the manuscript. All authors contributed to the article and approved the submitted version.

Funding

This study was supported by the Guangzhou Municipal Health Commission (award number 20211A011024).

Conflict of interest

The authors declare that the research was conducted in the absence of any commercial or financial relationships that could be construed as a potential conflict of interest.

Publisher's note

All claims expressed in this article are solely those of the authors and do not necessarily represent those of their affiliated organizations, or those of the publisher, the editors and the reviewers. Any product that may be evaluated in this article, or claim that may be made by its manufacturer, is not guaranteed or endorsed by the publisher.

Supplementary material

The Supplementary Material for this article can be found online at: https://www.frontiersin.org/articles/10.3389/fped.2023.1001222/full#supplementary-material.

References

1. Wiseman DH, May A, Jolles S, Connor P, Powell C, Heeney MM, et al. A novel syndrome of congenital sideroblastic anemia, B-cell immunodeficiency, periodic fevers, and developmental delay (SIFD). *Blood*. (2013) 122(1):112–23. doi: 10.1182/blood-2012-08-439083

2. Yohe S, Thyagarajan B. Review of clinical next-generation sequencing. *Arch Pathol Lab Med*. (2017) 141(11):1544–57. doi: 10.5858/arpa

3. Wedatilake Y, Niazi R, Fassone E, Powell CA, Pearce S, Plagnol V, et al. TRNT1 deficiency: clinical, biochemical and molecular genetic features. *Orphanet J Rare Dis*. (2016) 11(1):90. doi: 10.1186/s13023-016-0477-0

4. Hou YM. CCA Addition to tRNA: implications for tRNA quality control. *IUBMB Life*. (2010) 62(4):251–60. doi: 10.1002/iub.301

5. Yang L, Xue X, Zeng T, Chen X, Zhao Q, Tang X, et al. Novel biallelic TRNT1 mutations lead to atypical SIFD and multiple immune defects. *Genes Dis*. (2020) 7 (1):128–37. doi: 10.1016/j.gendis.2020.01.005

6. Chakraborty PK, Schmitz-Abe K, Kennedy EK, Mamady H, Naas T, Durie D, et al. Mutations in TRNT1 cause congenital sideroblastic anemia with immunodeficiency, fevers, and developmental delay (SIFD). *Blood*. (2014) 124(18):2867–71. doi: 10.1182/blood-2014-08-591370

7. Giannelou A, Wang H, Zhou Q, Park YH, Abu-Asab MS, Ylaya K, et al. Aberrant tRNA processing causes an autoinflammatory syndrome responsive to TNF inhibitors. *Ann Rheum Dis*. (2018) 77(4):612–9. doi: 10.1136/annrheumdis-2017-212401

8. Hull S, Malik AN, Arno G, Mackay DS, Plagnol V, Michaelides M, et al. Expanding the phenotype of TRNT1-related immunodeficiency to include childhood cataract and inner retinal dysfunction. *JAMA Ophthalmol*. (2016) 134(9):1049–53. doi: 10.1001/jamaophthalmol.2015.5833

9. DeLuca AP, Whitmore SS, Barnes J, Sharma TP, Westfall TA, Scott CA, et al. Hypomorphic mutations in TRNT1 cause retinitis pigmentosa with erythrocytic microcytosis. *Hum Mol Genet*. (2016) 25(1):44–56. doi: 10.1093/hmg/ddv446

10. Barton C, Kausar S, Kerr D, Bitetti S, Wynn R. SIFD As a novel cause of severe fetal hydrops and neonatal anaemia with iron loading and marked extramedullary haemopoiesis. *J Clin Pathol*. (2018) 71(3):275–8. doi: 10.1136/jclinpath-2017-204698

11. Fouquet C, Le Rouzic MA, Leblanc T, Fouyssac F, Leverger G, Hessissen L, et al. Genotype/phenotype correlations of childhood-onset congenital sideroblastic anaemia in a European cohort. *Br J Haematol*. (2019) 187(4):530–42. doi: 10.1111/bjh.16100

12. Sasarman F, Thiffault I, Weraarpachai W, Salomon S, Maftei C, Gauthier J, et al. The 3' addition of CCA to mitochondrial tRNASer(AGY) is specifically impaired in patients with mutations in the tRNA nucleotidyl transferase TRNT1. *Hum Mol Genet*. (2015) 24(10):2841–7. doi: 10.1093/hmg/ddv044

13. Frans G, Moens L, Schaballie H, Wuyts G, Liston A, Poesen K, et al. Homozygous N-terminal missense mutation in TRNT1 leads to progressive B-cell immunodeficiency in adulthood. *J Allergy Clin Immunol*. (2017) 139(1):360–363.e6. doi: 10.1016/j.jaci.2016.06.050

14. Kumaki E, Tanaka K, Imai K, Aoki-Nogami Y, Ishiguro A, Okada S, et al. Atypical SIFD with novel TRNT1 mutations: a case study on the pathogenesis of B-cell deficiency. *Int J Hematol*. (2019) 109(4):382–9. doi: 10.1007/s12185-019-02614-0

15. Rigante D, Stellacci E, Leoni C, Onesimo R, Radio FC, Pizzi S, et al. Biallelic TRNT1 variants in a child with B cell immunodeficiency, periodic fever and developmental delay without sideroblastic anemia (SIFD variant). *Immunol Lett*. (2020) 225:64–5. doi: 10.1016/j.imlet.2020.06.012

16. Hoang TK, Albert DA. Novel presentations of periodic fever syndromes: discrepancies between genetic and clinical diagnoses. *Eur J Rheumatol*. (2019) 6 (1):12–8. doi: 10.5152/eurjrheum.2018.18023

17. Lougaris V, Chou J, Baronio M, Gazzurelli L, Lorenzini T, Soresina A, et al. Novel biallelic TRNT1 mutations resulting in sideroblastic anemia, combined B and T cell defects, hypogammaglobulinemia, recurrent infections, hypertrophic cardiomyopathy and developmental delay. *Clin Immunol*. (2018) 188:20–2. doi: 10.1016/j.clim.2017.11.008

18. Bader-Meunier B, Rieux-Laucat F, Touzot F, Frémond ML, André-Schmutz I, Fraitag S, et al. Inherited immunodeficiency: a new association with early-onset childhood panniculitis. *Pediatrics*. (2018) 141(Suppl 5):S496–500. doi: 10.1542/peds.2017-0213

19. Frémond ML, Melki I, Kracker S, Bondet V, Duffy D, Rice GI, et al. Comment on: 'aberrant tRNA processing causes an autoinflammatory syndrome responsive to TNF inhibitors' by Giannelou et al: mutations in TRNT1 result in a constitutive activation of type I interferon signalling. *Ann Rheum Dis*. (2019) 78(8):e86. doi: 10.1136/annrheumdis-2018-213745

20. Orlando F, Naddei R, Stellacci E, Gallinoro CM, Melis D, Tartaglia M, et al. Etanercept as a successful therapy in autoinflammatory syndrome related to TRNT1 mutations: a case-based review. *Clin Rheumatol*. (2021) 40(10):4341–8. doi: 10.1007/s10067-021-05653-3

21. Odom J, Amin H, Gijavanekar C, Elsea SH, Kralik S, Chinen J, et al. A phenotypic expansion of TRNT1 associated sideroblastic anemia with immunodeficiency, fevers, and developmental delay. *Am J Med Genet A*. (2022) 188(1):259–68. doi: 10.1002/ajmg.a.62482

22. Jfri A, El-Helou T, Watters KA, Bélisle A, Litvinov IV, Netchiporouk E. Congenital sideroblastic anemia associated with B cell immunodeficiency, periodic fevers, and developmental delay: a case report and review of mucocutaneous features. *SAGE Open Med Case Rep*. (2019) 7:2050313X19876710. doi: 10.1177/2050313X19876710

23. Topyildiz E, Edeer Karaca N, Bas I, Aykut A, Durmaz A, Guven Bilgin RB, et al. A novel homozygous TRNT1 mutation in a child with an early diagnosis of common variable immunodeficiency leading to mild hypogammaglobulinemia and hemolytic anemia. *J Pediatr Hematol Oncol*. (2021) 43(6):e780–4. doi: 10.1097/MPH.0000000000002101

24. Mendonca LO, Prado AI, Costa IMC, Bandeira M, Dyer R, Barros SF, et al. Case report: expanding clinical, immunological and genetic findings in sideroblastic anemia with immunodeficiency, fevers and development delay (SIFD) syndrome. *Front Immunol*. (2021) 12:586320. doi: 10.3389/fimmu.2021.586320

25. Bardou MLD, Rivitti-Machado MC, Michalany NS, de Jesus AA, Goldbach-Mansky R, Barros JCR, et al. Neutrophilic dermatosis: a new skin manifestation and novel pathogenic variant in a rare autoinflammatory disease. *Australas J Dermatol*. (2021) 62(2):e276–9. doi: 10.1111/ajd.13527

26. Wang J, Deng Q, He X, Chen D, Hang S, Gao Y, et al. Two cases of sideroblastic anemia with B-cell immunodeficiency, periodic fevers, and developmental delay (SIFD) syndrome in Chinese Han children caused by novel compound heterozygous variants of the TRNT1 gene. *Clin Chim Acta*. (2021) 521:244–50. doi: 10.1016/j.cca.2021.07.019

27. Maccora I, Ramanan AV, Vergnano S, Roderick MR. Sideroblastic anaemia, immunodeficiency, periodic fevers and developmental delay (SIFD) presenting as systemic inflammation with arthritis. *Rheumatology (Oxford)*. (2021) 60(7):e234–6. doi: 10.1093/rheumatology/keab010.31

28. Kisla Ekinci RM, Zararsiz A, Demir GU, Anlas O. A rare autoinflammatory disorder in a pediatric patient with favorable response to etanercept: sideroblastic anemia with B cell immunodeficiency, periodic fevers, and developmental delay syndrome. *Pediatr Allergy Immunol Pulmonol*. (2022) 35(3):129–32. doi: 10.1089/ped.2022.0090

29. Maccora I, Ramanan AV, Wiseman D, Marrani E, Mastrolia MV, Simonini G. Clinical and therapeutic aspects of sideroblastic anaemia with B-cell immunodeficiency, periodic fever and developmental delay (SIFD) syndrome: a systematic review. *J Clin Immunol*. (2023) 43(1):1–30. doi: 10.1007/s10875-022-01343-0

30. Richards S, Aziz N, Bale S, Bick D, Das S, Gastier-Foster J, et al. Standards and guidelines for the interpretation of sequence variants: a joint consensus recommendation of the American College of Medical Genetics and Genomics and the Association for Molecular Pathology. *Genet Med*. (2015) 17(5):405–24. doi: 10.1038/gim.2015.30

31. Willrich MA, Murray DL, Snyder MR. Tumor necrosis factor inhibitors: clinical utility in autoimmune diseases. *Transl Res*. (2015) 165(2):270–82. doi: 10.1016/j.trsl.2014.09.006

32. Jang DI, Lee AH, Shin HY, Song HR, Park JH, Kang TB, et al. The role of tumor necrosis factor alpha (TNF-α) in autoimmune disease and current TNF-α inhibitors in therapeutics. *Int J Mol Sci*. (2021) 22(5):2719. doi: 10.3390/ijms22052719

frontiers | Frontiers in Genetics

TYPE Original Research
PUBLISHED 24 March 2023
DOI 10.3389/fgene.2023.1055372

Check for updates

OPEN ACCESS

EDITED BY
Tieliu Shi,
Hunan University of Arts and Science, China

REVIEWED BY
Alejandra Cervera,
National Institute of Genomic Medicine (INMEGEN), Mexico
Sean Michael Wilson,
Loma Linda University, United States

*CORRESPONDENCE
Xiaobing Shen,
xb.shen@seu.edu.cn

SPECIALTY SECTION
This article was submitted to Genetics of Common and Rare Diseases, a section of the journal Frontiers in Genetics

RECEIVED 27 September 2022
ACCEPTED 15 March 2023
PUBLISHED 24 March 2023

CITATION
Li Q, Xu Z, Fang F, Shen Y, Lei H and Shen X (2023), Identification of key pathways, genes and immune cell infiltration in hypoxia of high-altitude acclimatization *via* meta-analysis and integrated bioinformatics analysis. *Front. Genet.* 14:1055372. doi: 10.3389/fgene.2023.1055372

COPYRIGHT
© 2023 Li, Xu, Fang, Shen, Lei and Shen. This is an open-access article distributed under the terms of the Creative Commons Attribution License (CC BY). The use, distribution or reproduction in other forums is permitted, provided the original author(s) and the copyright owner(s) are credited and that the original publication in this journal is cited, in accordance with accepted academic practice. No use, distribution or reproduction is permitted which does not comply with these terms.

Identification of key pathways, genes and immune cell infiltration in hypoxia of high-altitude acclimatization *via* meta-analysis and integrated bioinformatics analysis

Qiong Li[1,2], Zhichao Xu[1,2], Fujin Fang[1,2], Yan Shen[1,2], Huan Lei[1,2] and Xiaobing Shen[1,2]*

[1]Key Laboratory of Environmental Medicine Engineering, Ministry of Education, School of Public Health, Southeast University, Nanjing, Jiangsu, China, [2]Department of Epidemiology and Health Statistics, School of Public Health, Southeast University, Nanjing, Jiangsu, China

Background: For individuals acutely exposed to high-altitude regions, environmental hypobaric hypoxia induces several physiological or pathological responses, especially immune dysfunction. Therefore, hypoxia is a potentially life-threatening factor, which has closely related to high-altitude acclimatization. However, its specific molecular mechanism is still unclear.

Methods: The four expression profiles about hypoxia and high altitude were downloaded from the Gene Expression Omnibus database in this study. Meta-analysis of GEO datasets was performed by NetworkAnalyst online tool. Kyoto Encyclopedia of Genes and Genomes (KEGG), Gene ontology (GO) enrichment analysis, and visualization were performed using R (version 4.1.3) software, respectively. The CIBERSORT analysis was conducted on GSE46480 to examine immune cell infiltration. In addition, we experimentally verified the bioinformatics analysis with qRT-PCR.

Results: The meta-analysis identified 358 differentially expressed genes (DEGs), with 209 upregulated and 149 downregulated. DEGs were mostly enriched in biological processes and pathways associated with hypoxia acclimatization at high altitudes, according to both GO and KEGG enrichment analyses. ERH, VBP1, BINP3L, TOMM5, PSMA4, and POLR2K were identified by taking intersections of the DEGs between meta-analysis and GSE46480 and verified by qRT-PCR experiments, which were inextricably linked to hypoxia. Immune infiltration analysis showed significant differences in immune cells between samples at sea level and high altitudes.

Conclusion: Identifying the DEGs and pathways will improve our understanding of immune function during high-altitude hypoxia at a molecular level. Targeting hypoxia-sensitive pathways in immune cells is interesting in treating high-altitude sickness. This study provides support for further research on high-altitude acclimatization.

KEYWORDS

high-altitude acclimatization, meta-analysis, bioinformatics analysis, immune infiltration, hypoxia

1 Introduction

The change in immune function caused by hypoxia is of mounting medical and public concern worldwide. The supply of oxygen, which varies in different tissues, has been demonstrated to be vital for the correct functioning of all organs and systems in the human body. Hypoxia occurs due to the restriction of oxygen supply, leading to significant changes in oxygen-dependent physiological processes (Knox et al., 2017). Severe hypoxia has been associated with disease outbreaks and has also long been known to impact immune function (Taylor and Colgan, 2017).

One study has shown that hypoxia affects immune cell survival, while immune cells also have important roles in hypoxia homeostasis (Monaci et al., 2020). Hypoxia drives cell maturation in immunologic niches, accompanying inflammation in peripheral tissues (Norris et al., 2019). And it was confirmed that hypoxia is often correlated with macrophage content, neovessel count, and the expression of the hypoxia-inducible transcription factor 1α (HIF-1α) (Mateo et al., 2014). Furthermore, activation of HIFs and the HIF-1 pathway are critical in regulating early high-altitude acclimatization and participating in the pathogenesis of un-acclimatization (Schweizer et al., 2019).

High-altitude acclimatization can be defined as a physiological process in our body upon exposure to hypobaric hypoxia. It comprises a series of responses in different body systems, including restoring, transporting, and utilizing oxygen (O^2) (Liu et al., 2016). Acute exposure to high altitude is associated with a spectrum of disorders encompassing acute mountain sickness (AMS), high altitude pulmonary edema (HAPE), and high altitude cerebral edema (HACE) in un-acclimatized individuals (Duan et al., 2020). Additionally, high-altitude hypoxia can also interfere with a variety of physiological functions, including immune function (Mei et al., 2020). Thus, studying high-altitude acclimatization is important to protect the health of people traveling and working at high altitudes. Here, we aim to access the molecular mechanism of the effect of high-altitude acclimatization on immune function. But, *in vivo* data on immunomodulatory effects of hypoxia or hypoxia mimetics in animal models are conflicting (Kiers et al., 2018). Meta-analysis of gene expression data sets was performed to help identify potential molecular signatures and gain insights into underlying biological processes based on gene expression datasets. The combination of meta-analysis and bioinformatics analyses may help to resolve existing inconsistencies and contradictions. We wanted to investigate whether there are common key genes that play important roles in multiple types of cells and influence immune function. To verify this hypothesis, we performed a systematic review of transcriptomics datasets from different cells in hypoxia and normoxia in the Gene Expression Omnibus (GEO), followed by consistent processing of meta-analysis, pathway enrichment, and overlap analyses. Then we download GSE46480 as the validation dataset for meta-analysis and immune infiltration analysis. At last, we experimentally verified the bioinformatics analysis with quantitative reverse-transcription polymerase chain reaction (qRT-PCR). This study aimed to demonstrate a systematic workflow for evidence synthesis of transcriptomic studies using meta-analysis and bioinformatics methods to identify potential biomarkers and pathogenic factors during high-altitude acclimatization. Here, we present a workflow of this study, as shown in Figure 1.

2 Materials and methods

2.1 Database search and datasets selection

We inquired about the two databases on 1 March 2022, for meta-analysis: GEO from the National Center for Biotechnology Information (NCBI) (Barrett et al., 2013) and ArrayExpress from the European Bioinformatics Institute (EMBL-EBI) (Athar et al., 2019). The search strategy is shown in Supplementary File S1 and the keywords used in the search were hypoxia and immune. Eligible datasets were those meeting all inclusion criteria and none of the exclusion criteria (Figure 2). The datasets were excluded if they were: 1) A tumor-related study; 2) A non-expression profiling study; 3) Not human cells; 4) A study design other than hypoxia/control; 5) Not cell culture. Finally, GSE145935, GSE116660, and GSE60729 were selected for meta-analysis, which included 12 normoxia samples and 12 hypoxia samples. Then, we choose GSE46480 as the validation dataset for immune infiltration analysis, which compares healthy volunteers at sea level with those exposed to altitude acutely. The details of the four GEO datasets are shown in Supplementary File S2.

2.2 Data normalization, meta-analysis and identification of DEGs

The online tool, NetworkAnalyst (http://www.networkanalyst.ca) (Zhou et al., 2019), performs a meta-analysis on three GEO datasets to normalize the data and determine the differentially expressed genes (DEGs). The merged data of NetworkAnalyst was shown in Supplementary File S3.

As a result of the batch-effect adjustment, a random-effects model (REM) was used in Combining Effect Sizes for the meta-analysis. The effect size is defined as the difference between two group means divided by standard deviation, considered combinable and comparable across different studies. The REM model can also incorporate unknown cross-study heterogeneities through a random effect. We selected REM based on statistical heterogeneity estimated using Cochran's Q test (Figure 3A). Cochran's Q test is calculated as the weighted sum of squared differences between individual study effects and the pooled effect across studies. It suggests that fixed-effects models (FEMs) should be assumed when the estimated Q values have an approximately chi-squared distribution. The use of REM is usually recommended if the distribution deviates significantly from a chi-squared distribution.

The GEO2R online tool (http://www.ncbi.nlm.nih.gov/geo/geo2r/) provided by the NCBI GEO database enabled comparisons between healthy participants at sea level and those exposed to altitude for the GSE46480 dataset.

All of the differential expression analysis is based on the "limma" method. Benjamini–Hochberg's False Discovery Rate (FDR) is used

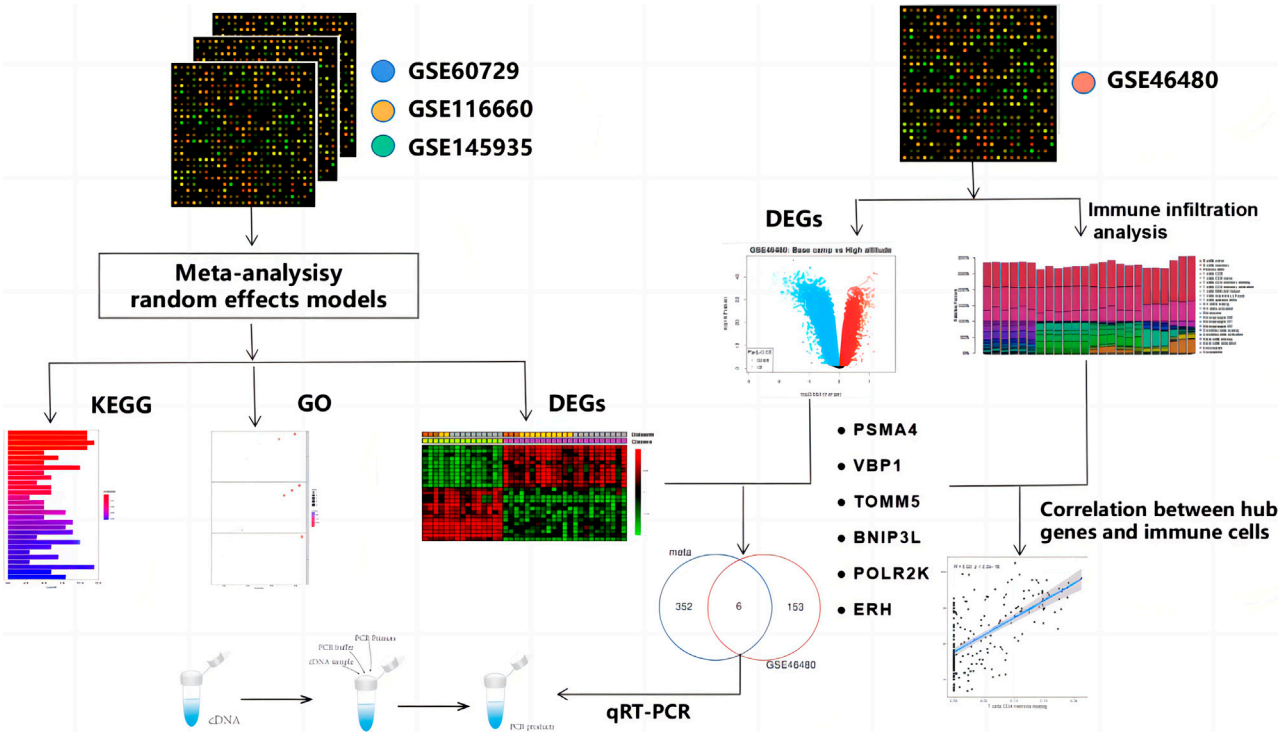


FIGURE 1
Workflow of this study.

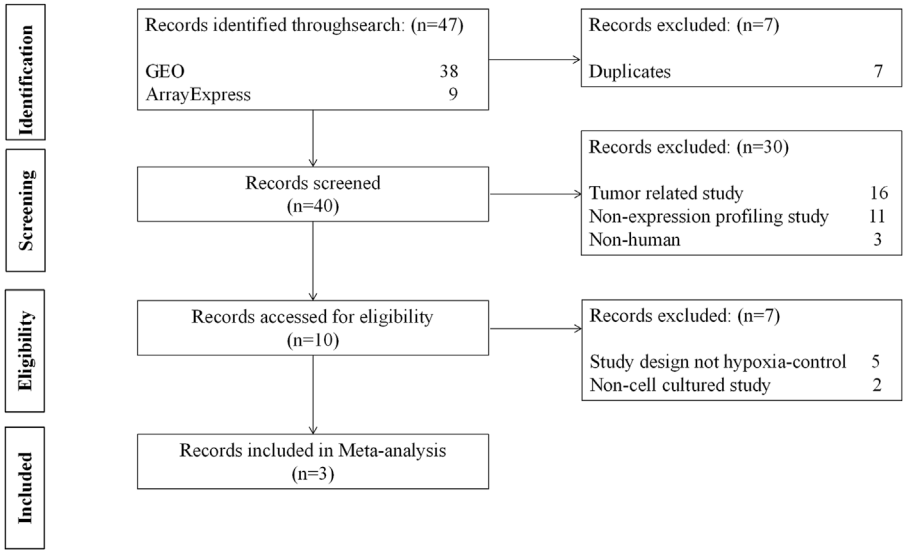


FIGURE 2
The flow diagram of datasets selection, including identification, screening, eligibility and inclusion stage.

to adjust the cut-off *p*-values. The genes were considered DEGs between normoxia and hypoxia samples when they had an FDR < 0.05 and a log (|FC|) > 1. To better visualize these DEGs, we made heatmaps and volcano plots by using NetworkAnalyst software and GEO2R.

2.3 Biological enrichment analysis

After the meta-analysis, a biological enrichment analysis was conducted on the statistically significant DEGs. Kyoto Encyclopedia of Genes and Genomes (KEGG), Gene Ontology (GO) enrichment

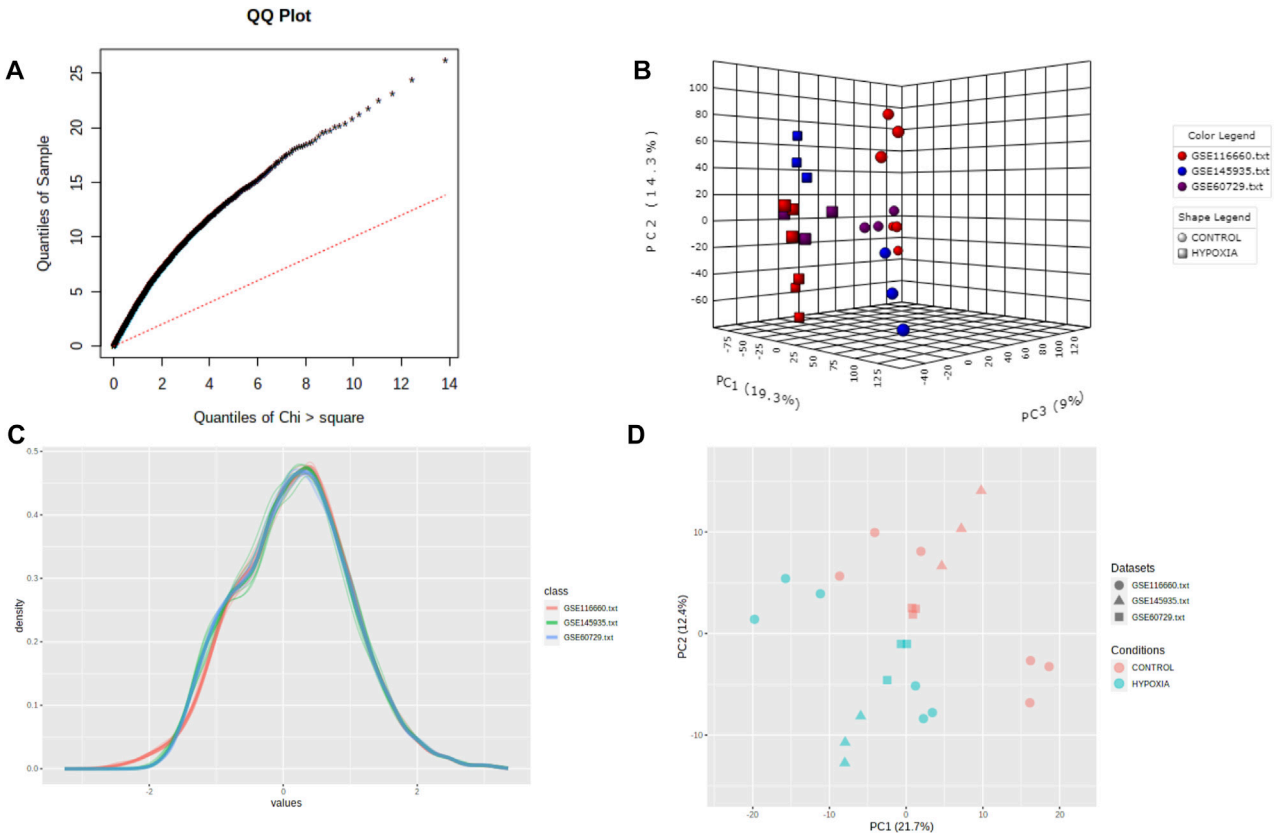


FIGURE 3
Quality control of meta-analysis. **(A)** The QQ-plot of Cochran's Q test. **(B)** The three-dimensional plot of PCA score. **(C)** The density plot of the datasets. **(D)** The plane figure of PCA.

analysis and visualization were performed using the packages: "colorspace", "stringi", "DOSE", "clusterProfiler", "digest", "GOplot", "ggplot2" of R software (version 4.1.3). Our analysis focused on the terms associated with the three main GO categories: biological processes, molecular functions, and cellular components. Q < 0.05 was used to select the significantly enriched functions and pathways. Q is the adjusted *p*-value.

2.4 Immune infiltration by CIBERSORT analysis

We performed the relative percent and content of 22 immune cell subsets by using CIBERSORT analytical tool (Newman et al., 2019). Using the "corrplot" package, we calculated the percentage of immune cells in the gene expression matrix and the relationship between genes and immune cells. After that, "vioplot" package was used to visualize CIBERSORT results.

2.5 Quantitative reverse-transcription polymerase chain reaction (qRT-PCR)

We used a lung epithelial cell line (BEAS-2B cells) and a human monocytic leukemia cell line (THP 1 cells) in culture media [RPMI medium 1,640 supplemented with 10% fetal bovine serum (Invitrogen)] for the validation of the mRNA expression between control and hypoxia groups. Cells in control groups were cultured 24 h under 5% CO_2, 21% O_2, and atmospheric pressure, while cells in hypoxia groups were cultured 24 h under 5% CO_2, 1% O_2, and 65 kPa for air pressure. Total RNA was extracted from the BEAS-2B cells and THP 1 cells by using RNA-easy Isolation Reagent (Vazyme, Nanjing, China). RNA was reverse-transcribed into complementary DNA (cDNA) using StarScript III All-in-one RT Mix with gDNA Remover (GenStar, Beijing, China). qRT-PCR was performed by 2 × RealStar Green Fast Mixture with ROX (GenStar, Beijing, China). The primers were synthesized by The Beijing Genomics Institute (BGI) (Beijing, China), as described in Supplementary File S4. The fold change in relative mRNA expression was calculated using the $2^{-\Delta\Delta Ct}$ method.

2.6 Statistics analysis

The R software (4.1.3 version) was used to conduct statistical analyses. The Student's t-test and Kruskal–Wallis test were used to compare the differences between the two groups. As a result, $p < 0.05$ (*), $p < 0.01$ (**), $p < 0.001$ (***), and $p < 0.0001$ (****) were considered significant.

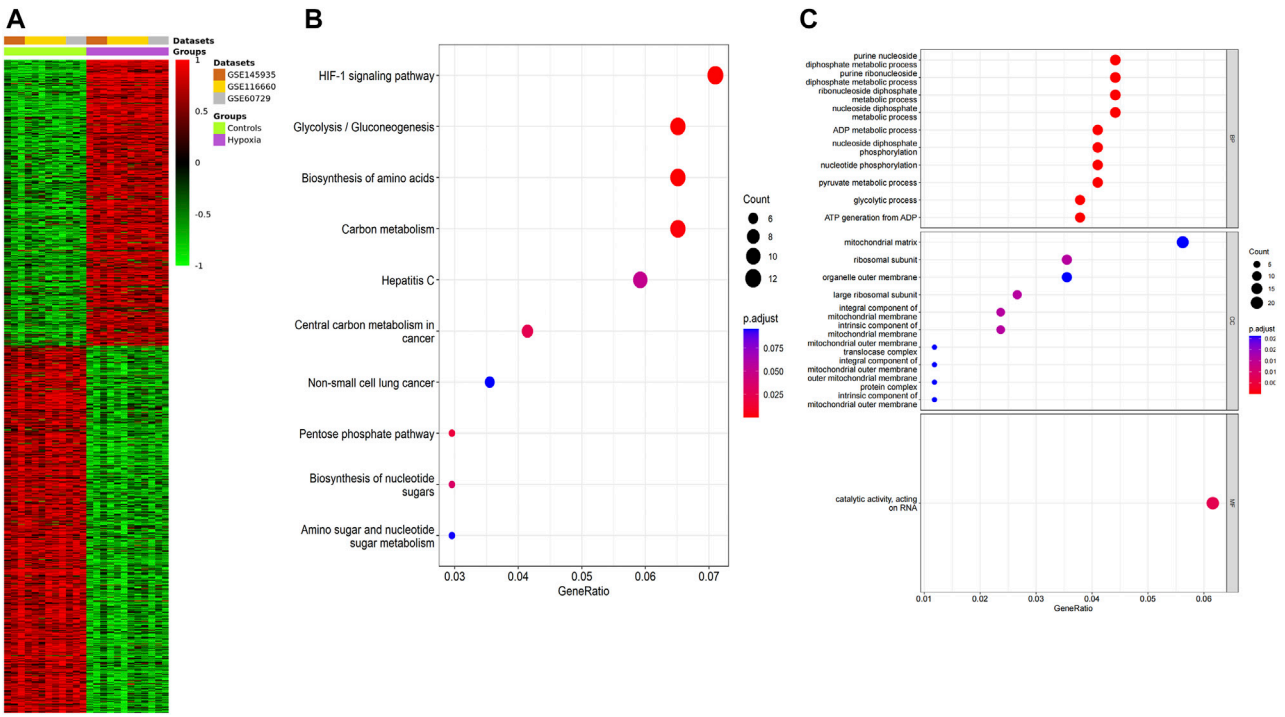


FIGURE 4
Function annotation of meta-analysis results. **(A)** The heatmap of the DEGs according to the adjusted *p*-value and logFC. Red indicates higher gene expression, and green shows lower gene expression. **(B)** KEGG terms in the enrichment analysis of the DEGs. **(C)** GO terms in the enrichment analysis of the DEGs.

TABLE 1 KEGG pathways of meta-analysis results.

ID	Description	Gene ratio	Bg ratio	p.adjust
hsa04066	HIF-1 signaling pathway	12/169	109/8,115	<0.001
hsa00010	Glycolysis/Gluconeogenesis	11/169	67/8,115	<0.001
hsa01230	Biosynthesis of amino acids	11/169	75/8,115	<0.001
hsa01200	Carbon metabolism	11/169	115/8,115	0.0016
hsa05230	Central carbon metabolism in cancer	7/169	70/8,115	0.025
hsa00030	Pentose phosphate pathway	5/169	30/8,115	0.018
hsa01250	Biosynthesis of nucleotide sugars	5/169	37/8,115	0.034

3 Results

3.1 Identification of DEGs based on meta-analysis

We performed a quality assessment of the three datasets for meta-analysis by drawing PCA plots and a density plot (Figures 3B–D). After quality control, the result of the meta-analysis shows 358 significant genes (209 genes upregulated, 149 genes downregulated) (Supplementary File S5). Next, a heatmap was used to visualize these DEGs, shown in Figure 4A.

3.2 Enrichment analysis

GO analysis and KEGG pathway analysis were carried out using the R software. The top 8 biological processes were selected based on P. adjust < 0.05 (Table 1) and were drawn in a bubble plot (Figure 4B). KEGG pathway enrichment analysis showed that DEGs were enriched in the HIF-1 signaling pathway, Glycolysis/Gluconeogenesis, Biosynthesis of amino acids, and Carbon metabolism. GO enriched in enrichment analyses showed that DEGs were mainly enriched in these biological processes: ncRNA metabolic process, nucleotide metabolic process, ATP metabolic process, response to oxygen levels, glycolytic process, cellular

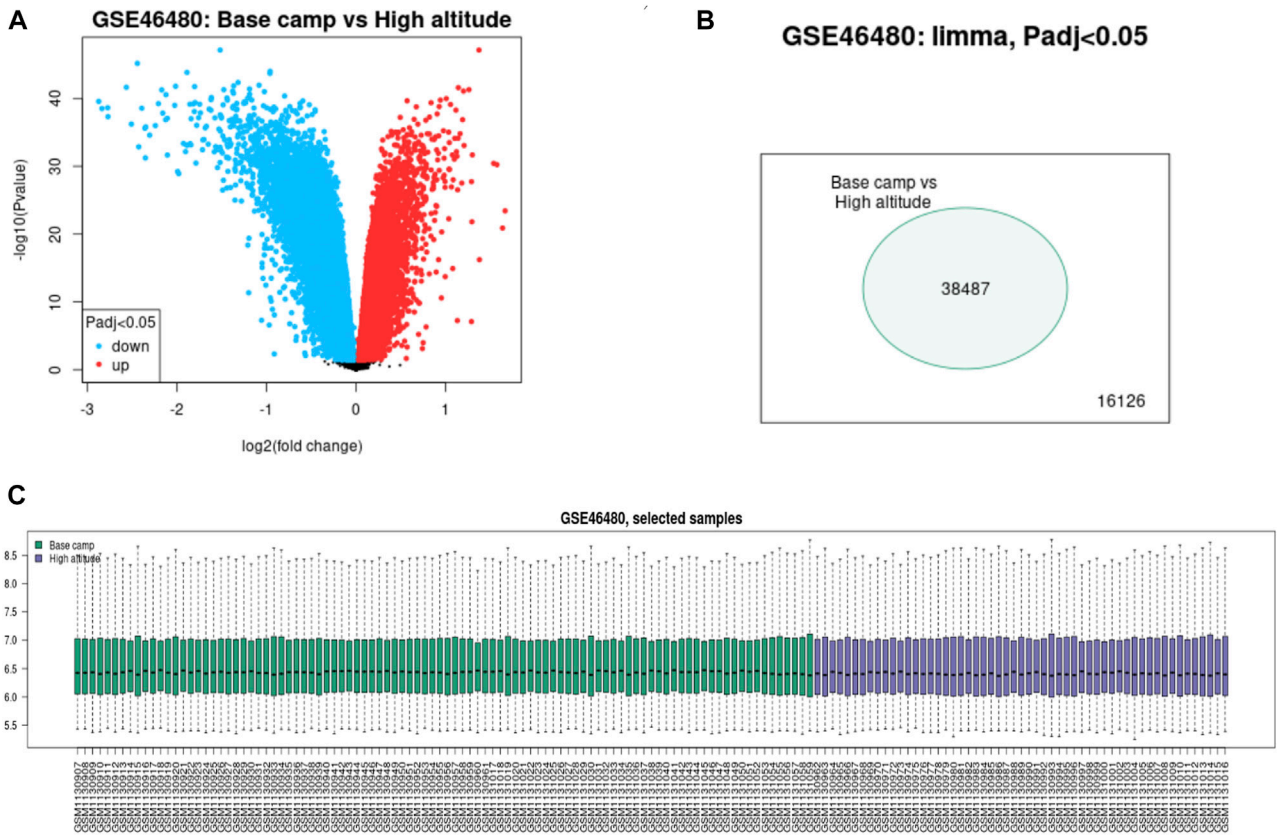


FIGURE 5
Difference expression of genes analysis of the samples from base camp to high altitude in GSE46480. **(A)** Volcano plot of the DEGs. Blue points represent downregulated genes. Red points represent the upregulated genes. **(B)** Venn diagram of the differentially expressed probe in GSE46480. **(C)** Quality control of the samples of GSE46480.

response to hypoxia, et al. (Supplementary File S6; Figure 4C). Accordingly, GO and KEGG enrichment analyses both showed that DEGs were mainly enriched in these biological processes and pathways which are closely related to hypoxia acclimatization at high altitudes.

3.3 Common DEGs of meta-analysis and GSE46480

We download GSE46480 in the GEO database to verify whether the DEGs of the meta-analysis are statistically significant in the process of high-altitude acclimatization and find the relationship between them. 173 DEGs (172 genes downregulated, one gene upregulated) were found between healthy samples at sea level and after acute exposure to altitude in GSE46480 (Supplementary File S7, Figures 5A, B). The data went through rigorous quality control and standardization (Figure 5C). Taking intersections of the DEGs between meta-analysis and GSE46480, we identified six genes associated with high-altitude hypoxia, ERH, VBP1, BINP3L, TOMM5, PSMA4, POLR2K, shown in Figure 6; Supplementary File S8. Except that BINP3L was upregulation, the other five genes showed downregulation in response to hypoxia. And we found that the six genes were all downregulation in GSE46480, which has common trends in gene expression except for BINP3L (Table 2).

3.4 Immune infiltration analyses

To explore whether these six genes are involved in immune regulation in hypoxia acclimatization at high altitudes, we analyzed the role of immune infiltrates between healthy samples at sea level and after acute exposure to altitude in GSE46480. A CIBERSORT analysis can reveal innate and adaptive immune responses during high-altitude acclimatization. Nineteen types of immune cells were detected in at least one sample among 22 types (Figure 7A; Supplementary File S9). The correlation heatmap result showed that T cells CD8 and T cells CD4 memory activated had a negative correlation (p-value = −0.60), NK cells resting and T cells gamma delta had a negative correlation, too (p-value = −0.62), T cells gamma delta and T cells CD4 memory resting had a positive correlation (p-value = 0.57), shown in Figure 7B; Supplementary File S10. The heatmap showed the relative percent of the 22 immune cells (Supplementary File S11). Moreover, the violin plot of the immune cell showed that B cells naive, T cells CD8, T cells CD4 memory naive, T cells regulatory (Tregs), NK cells resting, Macrophages

10.3389/fgene.2023.1055372

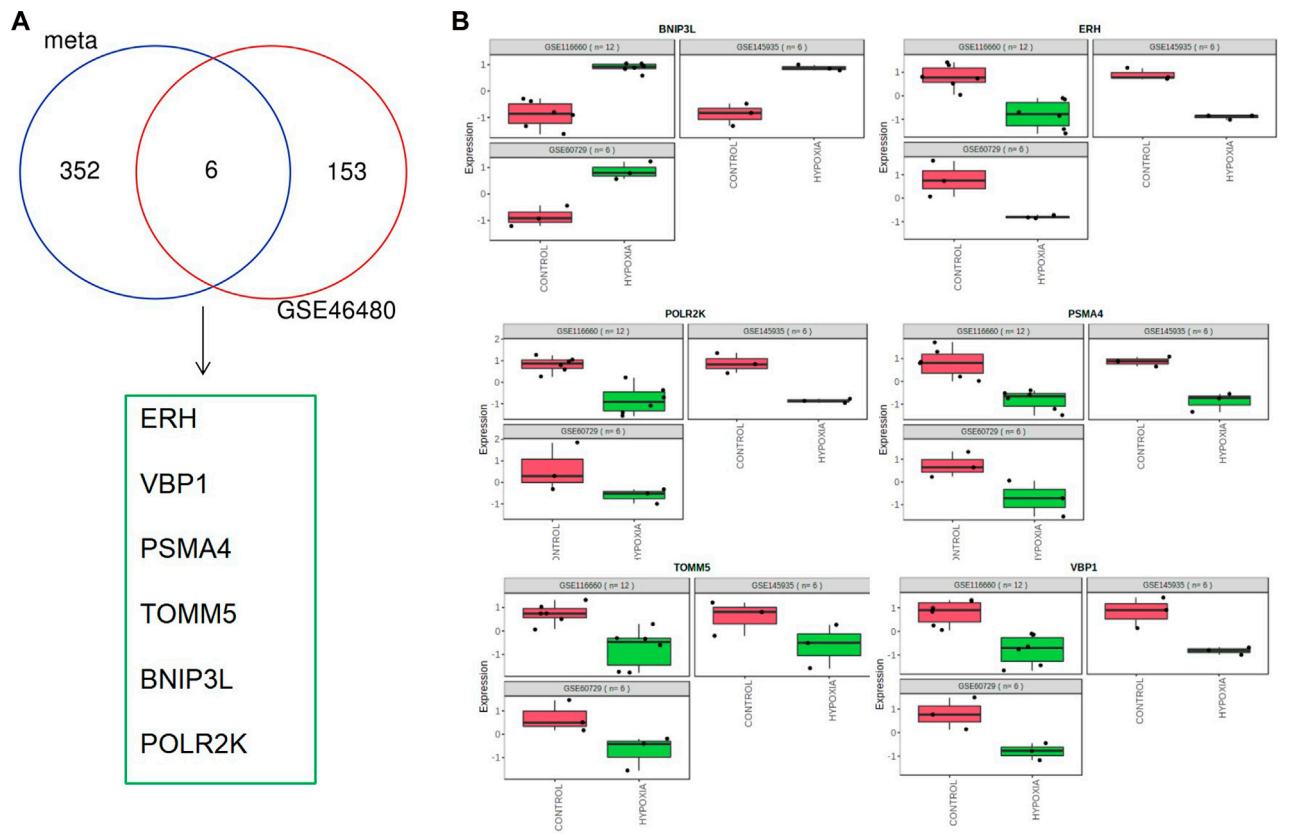


FIGURE 6
Common differentially expressed genes in meta-analysis and GSE46480. **(A)** Venn diagram of differentially expressed genes identified from the meta-analysis and GSE46480. **(B)** Scatter plots of common differentially expressed genes in the three GEO datasets for meta-analysis.

TABLE 2 Validation of the six differentially expressed genes in GSE46480.

Gene	adj.P.Val	t	logFC	Gene.title
ERH	2.76E-40	−18.01	−1.15	enhancer of rudimentary homolog (*Drosophila*)
VBP1	1.01E-35	−16.24	−1.12	VHL binding protein 1
PSMA4	2.41E-33	−15.39	−1.32	proteasome subunit alpha 4
TOMM5	1.20E-37	−16.94	−1.04	translocase of outer mitochondrial membrane 5
BNIP3L	1.67E-32	−15.09	−1.27	BCL2 interacting protein 3 like
POLR2K	2.83E-38	−17.19	−1.25	RNA polymerase II subunit K

M0, Neutrophils were statistically more in samples in the baseline. T cells CD4 memory resting, T cells gamma delta, Dendritic cells activated, and Mast cells resting statistically more in high-altitude samples ($p < 0.05$), shown in Figure 7C.

In the present study, we sought to determine whether the six genes we identified play a role in immune cells. Therefore, scatter plots were performed to survey the correlation between the six hub genes and immune cells. The results showed that except for BNIP3L, all the other five genes have positive correlations with T cells gamma delta and T cells CD4 memory resting according to the screening criteria ($R > 0.6$, $p < 0.05$), shown in Figure 8.

3.5 Verification of the mRNA expression of six hub genes

qRT-PCR was performed to examine the statistical difference in the mRNA expression of hub genes under two different culture conditions in BEAS-2B cells and THP 1 cells. The two experimental results showed that BINP3L was upregulated, and the other five genes were all downregulated in hypoxia groups, which was consistent with the results from the meta-analysis by bioinformatics methods as shown in Figure 9. Although the expression of PSMA4 in THP1 cells was not statistically different in the two groups, the *p*-value was 0.0513. The experimental results

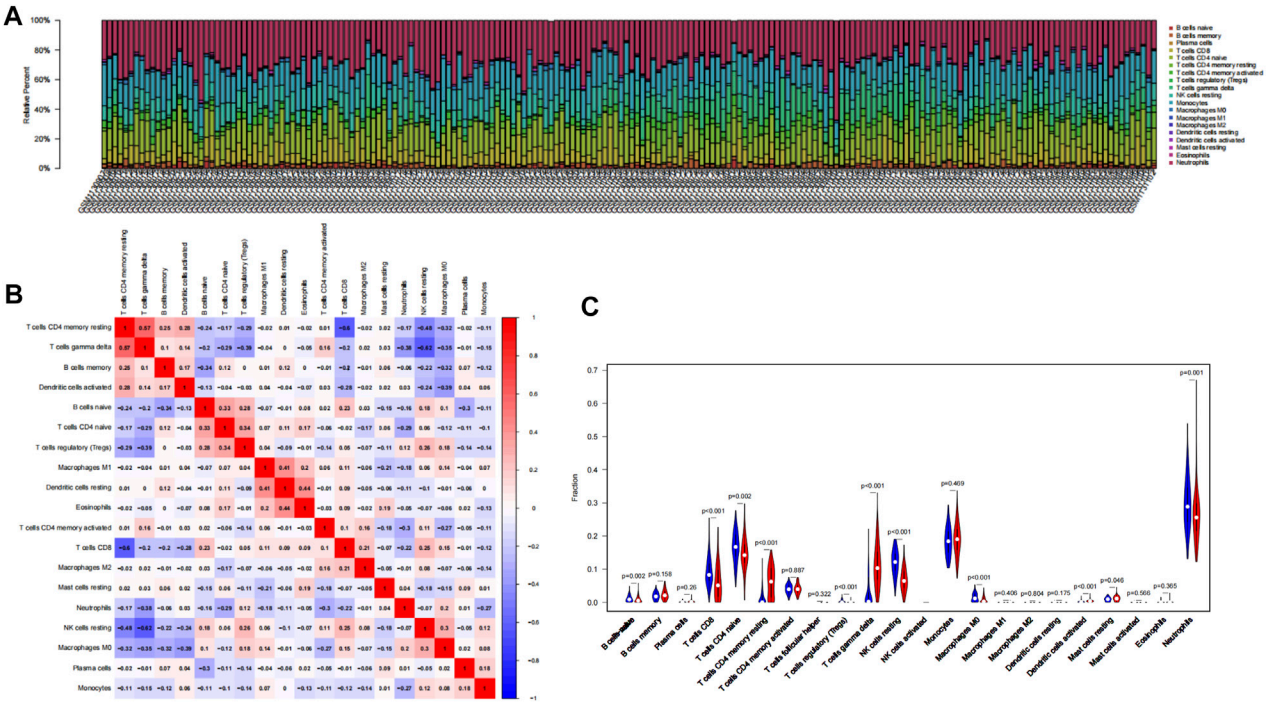


FIGURE 7
Results of CIBERSORT analysis of GSE46480. **(A)** Landscape of immune cell infiltration. **(B)** Correlation matrix of infiltration degree of immune cells in samples at high altitude. Red indicates trends consistent with the positive correlation, and blue indicates trends consistent with the negative correlation between two immune cells. The bigger the statistics of the number data, the more positive or negative correlation. **(C)** Violin diagram of immune cell proportions in two groups. The blue fusiform fractions on the left represent the basecamp group, and the red fusiform fractions on the right represent the high-altitude group.

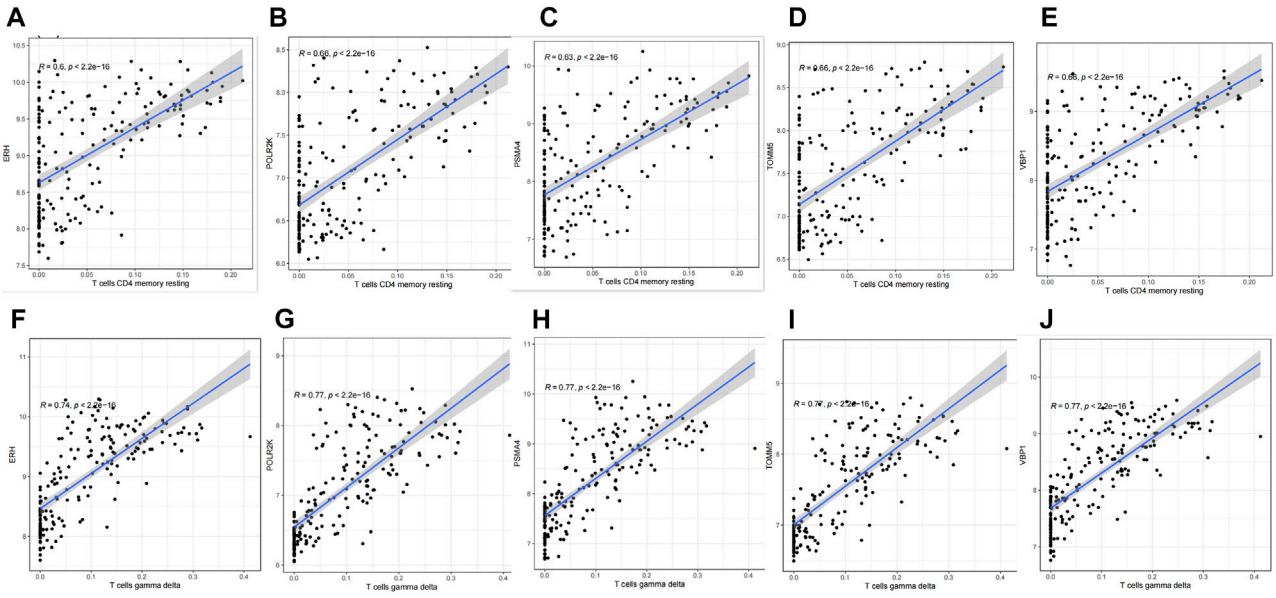


FIGURE 8
Correlation between hub genes and immune cells infiltration. **(A)** ERH & T cell CD4 memory resting. **(B)** POLR2K & T cell CD4 memory resting. **(C)** PSMA4 & T cell CD4 memory resting. **(D)** TOMM5 & T cell CD4 memory resting. **(E)** VBP1 & T cell CD4 memory resting. **(F)** ERH & T cell gamma delta. **(G)** POLR2K & T cell gamma delta. **(H)** PSMA4 & T cell gamma delta. **(I)** TOMM5 & T cell gamma delta. **(J)** VBP1 & T cell gamma delta.

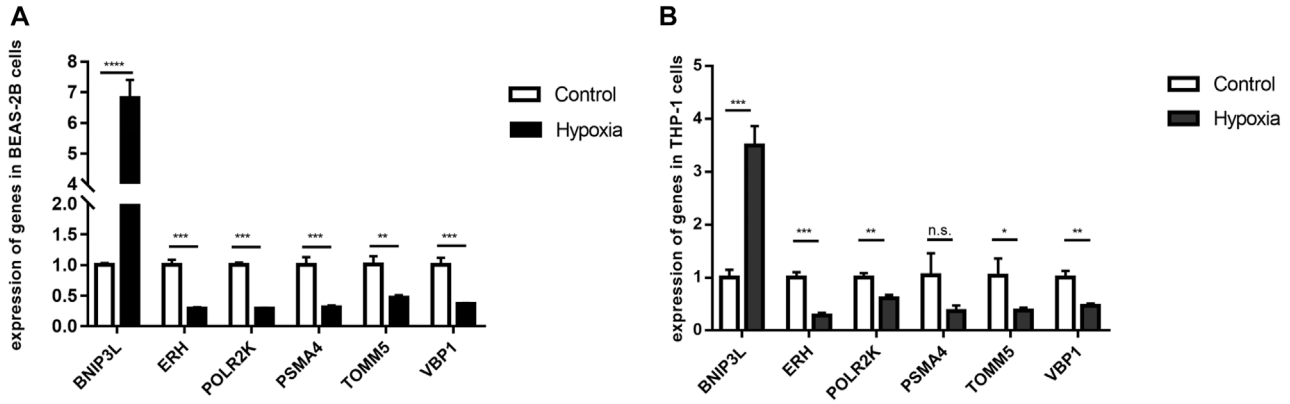


FIGURE 9
mRNA levels of six hub genes were different in control and hypoxia groups by verified by qRT-PCR results. $p < 0.05$ (*), $p < 0.01$ (**), $p < 0.001$ (***) and $p < 0.0001$ (****) were considered significant. **(A)** BEAS-2B cells. **(B)** THP 1 cells.

further showed that our meta-analysis is of great significance and has practical value.

4 Discussion

Hypoxia affects the development and function of the immune system (Yang et al., 2009). In particular, acute hypoxia-mediated impairment of immune function has been widely described and associated with increased susceptibility to disease (Yi et al., 2020). High-altitude hypoxia could cause an alteration in immunity in individuals with poor acclimatization (Khanna et al., 2018). A large population resides permanently in high-altitude regions like the Tibetan plateau, and every year thousands of people visit the Tibetan plateau for its beauty, therefore, the potential harm of the plateau environment on human health cannot be neglected. Hence, as stated in the introduction, research on the plasticity mechanism of immune function and clarifying their respective roles regarding altitude acclimatization is of great significance. Our study explored common genes and pathways differentially expressed in multiple cell types under hypoxia in an attempt to find the impact of key genes on immune function at high altitudes.

4.1 The pathways obtained by meta-analysis are consistent with that in high-altitude acclimatization

GSE145935, GSE116660, and GSE60729 were selected for meta-analysis in this study. What they have in common is that they are all cultured *in vitro* on human cells under hypoxic and normoxic conditions and sequenced to analyze the effect of transcriptome differences on immune function. The difference is that the cell type used in GSE145935 is astrocytes, GSE116660 is NK cells and GSE60729 is DC cells. The 358 DEGs in the meta-analysis confirmed that they had been specifically involved in the HIF-1 signaling pathway, Glycolysis/Gluconeogenesis, Biosynthesis of amino acids, Carbon metabolism, Central carbon metabolism in cancer, Pentose phosphate pathway, Biosynthesis of nucleotide sugars. Interestingly, these signaling pathways are important topics in high-altitude medicine, especially the HIF-1 signaling pathway, Glycolysis/Gluconeogenesis, and Biosynthesis of amino acids and Carbon metabolism. According to the research results, we justified the design of the meta-analysis on the datasets of hypoxia and immune, which could determine important features, patterns, functions, and connections, thus leading to the generation of new biological hypotheses.

The HIF-1 signaling pathway mediated a variety of important processes in hypoxia adaptation, which included Extracellular oxygen sensing (Tanaka et al., 2017), angiogenesis (Fu et al., 2018), and cell proliferation (Yoo et al., 2011), glucose metabolism (He et al., 2018). The HIF protein consists of a constitutively expressed beta subunit and an oxygen-sensitive alpha subunit (Biddlestone et al., 2015). The HIF complex can regulate several hundred genes by binding to hypoxia response elements in gene promoters to increase oxygen supply to hypoxic tissues (Semenza, 2009).

Moreover, HIF-1α is one of the most important regulators of glucose metabolism and has under its control the majority of pathways that can be fueled by glucose, including glycolysis, pentose phosphate pathway, serine synthesis, nucleotide synthesis, and one-carbon metabolism (He et al., 2018). These findings are surprisingly consistent with our KEGG analysis results, which indicates that our analysis is correct and meaningful. Glycolysis/gluconeogenesis is an important biological process in energy metabolism. It has been reported that Tibetans living at high altitudes may be prone to glucose tolerance (Okumiya et al., 2016). The levels of blood insulin and glucose in the Tibetan high-altitude population are lower (Murray, 2016). In addition, glucose uptake increased after insulin stimulation, and skeletal muscle underwent morphological changes due to hypoxia acclimation at high altitudes (Hennis et al., 2015). The glycolysis/gluconeogenesis signaling pathway may play an important role in the high-altitude adaptation of Tibetans living at high altitudes and protect them from the disease.

It has previously been reported that severe environmental hypoxia inhibits insulin/mTOR signaling and amino acid

transport in primary human trophoblast cells (Nelson et al., 2003) and in the placenta of pregnant mice *in vivo* (Higgins et al., 2016). Inhibition of amino acid synthesis will reduce the availability of amino acids and may also affect the rate of protein synthesis (Yang et al., 2018). Hypoxia and ER stress generally prevents the Biosynthesis of amino acids (Vaughan et al., 2020), and therefore, it may be an important pathway of high-altitude acclimation.

Under hypoxia physiological conditions, the body will also generate a broad range of biological processes, particularly participation in stress and defense responses, carbon metabolism, protein synthesis, and various metabolic processes. Carbon metabolism supports multiple physiological processes, including redox defense, amino acid homeostasis, Biosynthesis (purines and thymidine), and epigenetic maintenance (Ducker and Rabinowitz, 2017).

Central carbon metabolism (CCM) traditionally includes the glycolysis pathway (EMP), pentose phosphate pathway (PPP), and tricarboxylic acid cycle (TCA). Aside from providing energy, central carbon metabolism also provides precursors to other metabolisms in the body (Bayram et al., 2020). A pentose phosphate pathway initiates the oxidative decomposition of glucose through direct oxidation and can be oxidized and decomposed separately. In addition, it is the main pathway for the metabolism of pentose. In this way, it can enhance the body's adaptability by complementing and cooperating with EMP and TCA (Minamoto et al., 2015). A redox reaction is one of the main chemical reactions, and oxidoreductase is the enzyme responsible for catalyzing these reactions. Oxidoreductase plays a key role in metabolic pathways such as the tricarboxylic acid cycle and pentose phosphate pathway. Glucose is the most important energy material. It plays the physiological functions of oxidative energy supply (main part), providing a carbon source for synthesizing lipids and proteins and forming glycolipids. Its decomposition pathway in organisms is mainly central carbon metabolism (Ju et al., 2017). When glucose metabolism is abnormal in hypoxic conditions in high-altitude areas, it can cause various body diseases.

Nucleotide sugars are very important for organisms. They are a key link to the Biosynthesis of carbohydrates and their conjugates (Mikkola, 2020). Nucleotide sugar is a glycosyl donor in glycan synthesis, which participates in the correct function and survival of organisms. Glycans mediate the communication and interactions of cells, and defects in glycosylation can cause severe disease, which can lead to fatal outcomes (Endo, 2019).

Hence, hypoxia has wide-ranging effects, causing various biological processes, as we mentioned above. The results of DEGs enrichment analysis of meta-analysis showed that these signaling pathways were closely associated with high-altitude acclimatization. It further shows that it is reasonable to use meta-analysis to find the candidate genes and pathways related to altitude acclimatization.

4.2 The six hub genes are closely related to high-altitude acclimatization

The main objective of our study is to identify key genes that have an impact on immune function during altitude hypoxia. Therefore, we selected the dataset GSE46480, which is most relevant to high-altitude disease, for further analysis. The GSE46480 dataset included 98 subjects with acute mountain sickness who participated in the United States Antarctic Program. Sixty-five men and thirty-three women, ranging in age from 26 to 50, were transported from sea level to an altitude of 3,200 m in less than 4 hours. Blood samples were collected from subjects 3 days after arrival at high altitude and peripheral blood mononuclear cells were isolated for sequencing. The 196 samples in the GSE46480 dataset are blood samples collected from 98 subjects at two time points. Moreover, 98 subjects were chosen from healthy volunteers who were diagnosed with acute mountain sickness. Hence, the selection of GSE46480 and the combination of its data helped us to further explore whether the results of the meta-analysis had a meaningful impact on the development of high-altitude disease. We intersected 173 differential genes from GSE46480 with 358 genes from the meta-analysis and finally identified 6 key genes, ERH, VBP1, BINP3L, TOMM5, PSMA4, and POLR2K. As far as we know, little research has investigated the association between these genes and high-altitude hypoxia. Next, we will discuss the role of these genes in the process of high-altitude acclimatization.

ERH (mRNA splicing and mitosis factor) encodes a highly conserved homodimeric protein found in unicellular eukaryotes, plants, and metazoan (Weng and Luo, 2013). A wide range of cellular processes may be affected by eukaryotic ERH proteins, including cell cycle progression, mRNA transcription, and splicing, as well as DNA replication and repair (Tsubota and Phillips, 2016). DNA replication is impaired without ERH, resulting in lower restart rates from a replication stress challenge and sustained DNA damage (Kavanaugh et al., 2015). Also, the ERH gene was continuously regulated during erythropoiesis, and its expression increased during differentiation (da Cunha et al., 2010). When the oxygen partial pressure of tissue decreases and the mucopolysaccharide in the matrix tends to become acidic, it is not conducive to the differentiation of erythroid cells (Thornton et al., 2020). Therefore, the expression of the ERH gene was inhibited during hypoxia at high altitudes.

VBP1 (Von Hippel-Lindau-binding protein 1) physically interacts with von Hippel-Lindau protein (pVHL), which is crucial for the regulation of HIF-1α in the presence of oxygen (Kim et al., 2018). A study revealed that VBP1 could enhance the stability of the pVHL and act as an adaptor molecule in VHL-promoted ubiquitination and the proteasomal degradation of HIF-1α under normoxic physiological conditions (Xu and Her, 2013). In addition to pVHL, HIF-1α is the most important degrading target. Nevertheless, the hydroxylation of HIF-1α occurs less during hypoxia, which leads to HIF-1α accumulation. The accumulated HIF-1α activated the transcription of HIF-1α downstream factors, triggering a continuous transcription of hypoxia response genes (Cockman et al., 2000). Consequently, we can speculate that VBP1 may affect the pVHL-mediated degradation of HIF-1α in high-altitude acclimatization.

BNIP3L (BCL2 interacting protein 3-like)protein localized on the mitochondrial outer membrane is a specific receptor for mitophagy recognition during red blood cell maturation, hypoxia, and metabolic stress (Brennan et al., 2018). Under hypoxic conditions, BNIP3L is critical for hypoxia-induced autophagy and cell survival. BNIP3L may be an important mitochondrial sensor for various stress stimuli, and it promotes mitochondria removal during

reticulocyte differentiation (Di Rita et al., 2018). In addition, hypoxia-induced autophagy *via* BNIP3 (BCL2 interacting protein 3) or BNIP3L was shown to be protective against cell death, and the expression of BNIP3 is strongly activated by hypoxia, which is the direct transcriptional target for HIF-1α and inhibits the proliferation of alveolar epithelial cells and promotes their apoptosis (Vara-Perez et al., 2021). Therefore, our meta-analysis showed that the expression of BNIP3L was upregulated in the hypoxia groups in all three studies, which was verified with qRT-PCR.

The TOMM5 subunit is one of three smaller components of TOMM40, which is part of the TOMM complex, translocase of the outer mitochondrial membrane. The protein translocase is located in the mitochondrial outer membrane that transports mitochondrial pre-proteins into mitochondria. There is evidence that TOMM5 helps maintain the structural integrity of the TOMM complex (Kato and Mihara, 2008). Through its association with the TOMM40 precursor, TOMM5 also contributes to the final assembly and placement of the mature TOMM40 in the mitochondrial membrane (Becker et al., 2010). Mice lacking the outer mitochondrial membrane homolog 5 [Tomm5 (−/−)] exhibited an unexpected lung-specific phenotype characterized by extensive intra-alveolar fibrosis, indicating that TOMM5 activity is particularly significant for mitochondrial function in the unique environment of the lung (Vogel et al., 2013). According to their findings in this mouse model, defective TOMM5 alleles could contribute to an increased susceptibility to certain lung diseases in humans and animals (Vogel et al., 2013). Therefore, we supposed that severe hypoxia causes alveolar injury, and the expression of TOMM5 is downregulated in the hypoxic environment presented by high altitude, which is consistent with the results of this study.

PSMA4 (proteasome 20S subunit alpha 4) encodes a subunit of the proteasome (O'Brien et al., 2018). And PSMA4 plays a role in promoting cancer cell proliferation, including proliferation and apoptosis (Zhao et al., 2017). Compared to normal lung tissues, lung tumors have higher PSMA4 mRNA levels, and downregulation of PSMA4 expression reduces proteasome activity and induces apoptosis in lung cancer cells (Deshpande et al., 2013). *In vitro*, PSMA4 knockdown reduces proteasome activity and causes ubiquitinated protein accumulation. The proteasome regulates many cellular processes, including transcription, cell cycle progression, and apoptosis (Wang et al., 2015). One study also found that PSMA family genes were positively correlated with the cell cycle, ubiquinone metabolism, oxidative stress, and immune response signaling. PSMA4 gene is rarely reported in the research of high-altitude medicine. Still, according to the above description, we speculate that it plays an important role in the process of high-altitude acclimatization.

POLR2K (RNA polymerase II, I, and III subunit K) encodes one of the smallest subunits of RNA polymerase II, the polymerase responsible for synthesizing messenger RNA in eukaryotes. Two other DNA-directed RNA polymerases share this subunit (Lin et al., 2012). POLR2K contributes to the Pol III preinitiation complex assembly as an important gene in the RNA processing machinery. Upregulation of POLR2K may facilitate Pol III assembly, which is required for protein synthesis, contributing to cell proliferation and cancer development. Upregulation of POLR2K may facilitate Pol III assembly, contributing to cell proliferation and cancer development (Gutierrez-Arcelus et al., 2019). In a previous study investigating the pathogenesis of pneumonia, POLR2K was found to encode crucial proteins in the PPI network (Huang et al., 2017). However, no studies have been performed to investigate the association between POLR2K and high-altitude acclimatization. In the present study, POLR2K was downregulated in the meta-analysis and the samples at the high altitude of GSE46480.

4.3 Immune infiltration analysis shows significant differences in samples at sea level and after acute exposure to altitude

Many diseases are immune-related, including hypoimmune, hyperimmune, or immune dysfunction. Hypoxia induces angiogenesis, reshapes cell metabolism, and regulates the expression of several immunoregulatory molecules. Our question is whether and how the immune function will change when people are exposed to hypoxia at high altitudes. Therefore, we used CIBERSORT analysis to explore the immune cell infiltration in the organism and the relationship between immune cells and 6 key genes during hypoxia at high altitudes. The result showed that the infiltration of several immune cells (T cells CD4 memory resting, T cells gamma delta, Dendritic cells activated, Mast cells resting) was significantly increased, and the infiltration of several immune cells (B cells naive, T cells CD8, T cells CD4 memory naive, T cells regulatory (Tregs), NK cells resting, Macrophages M0, Neutrophils) were significantly decreased in the samples in high-altitude compared to the samples in sea-level. In the correlation analysis of the infiltration degree of immune cells, T cells CD8 and T cells CD4 memory activated, NK cells resting and T cells gamma delta had a negative correlation, while T cells gamma delta and T cells CD4 memory resting had a positive correlation. A hypoxic environment increases inflammation to expedite pathogen clearance by modulating the immune response (Dominguez-Gutierrez et al., 2014). Angiogenesis, metabolism rewiring, and immunomodulatory molecules are all activated by hypoxia (Lin et al., 2020). Considering that the subjects in the GSE46480 dataset developed acute high altitude sickness after arrival at high altitude, and immune infiltration analysis showed significant differences, we think that the oxygen-deprived environment at high altitudes will, therefore, alter the functionality of infiltrated immune cell populations. The infiltrating immune cells may be exerting their deleterious effects in the body after exposure to high altitude; alternatively, infiltration of immune cells into systemic blood vessels or other organs may mediate the deleterious effects of immune cells in high-altitude sickness. Meanwhile, several immune-related genes have been shown to correlate with disease susceptibility. Compared with sojourners from the lowlands, the Tibetan population has evolved distinct high-altitude adaptive features in their long-term habitation in the Tibetan Plateau, particularly the superior resistance to hypoxia. However, the mechanisms of high-altitude adaptation in different human populations are distinct and complex. All subjects in GSE46480 were of high-altitude non-adapted ancestry and they suffered from acute mountain sickness during their initial visit to high altitudes. The inhibition of these genes may contribute to immune cells exhaustion or death, impair immune function, and increase susceptibility to high-altitude sickness. The hub genes in

this study strongly correlate with immune infiltrating cells, so they may play an important role in regulating the function of immune cells of lowlanders going to high altitudes for the first time.

In general, ERH, VBP1, PSMA4, TOMM5, BNIP3L, and POLR2K have been identified as the key genes that were associated with immune cells in high-altitude hypoxia. HIF-1 signaling pathway, Glycolysis/Gluconeogenesis, and Biosynthesis of amino acids and Carbon metabolism were important signaling pathways that occur in cells to adapt to hypoxic environments. We apply a meta-analysis to harmonize a deliberately varied selection of gene expression datasets of different cell types. Our findings are consistent with the three datasets included in the meta-analysis in demonstrating that hypoxia affects the immune function of the body and that key genes play an important role in the hypoxic process. Furthermore, our study identified six key genes that are strongly associated with hypoxia at high altitudes and verified that they play important roles in multiple types of cells and influence immune function. These results may provide a new perspective for the study of high-altitude acclimatization. However, this study still has some limitations. First, the results of this study were only validated with qRT-PCR experiments, and in-depth experiments will be conducted in future studies. Second, our meta-analysis had small sample sizes, and thus the results ought to be interpreted with caution.

5 Conclusion

The 6 hub genes, pathways, and immune infiltration analysis we identified may be involved in high-altitude acclimatization. These findings will help us to enhance our general understanding of the molecular mechanism of immune function during high-altitude hypoxia. Targeting hypoxia-sensitive pathways in immune cells is of interest in treating high-altitude sickness. They are involved in processes that are targets for drug development, which will guide precision medicine treatment. This study provides support for further research on high-altitude acclimatization.

Data availability statement

Publicly available datasets were analyzed in this study. This data can be found here: https://www.ncbi.nlm.nih.gov/.

Author contributions

QL: conceptualization, methodology, software, writing original draft. ZX: data acquisition, analysis. FF: review and editing. YS: collect the data. HL: resources, interpretation of data. XS: guided and supervised this study. All authors critically read the manuscript and gave final approval for publication.

Conflict of interest

The authors declare that the research was conducted in the absence of any commercial or financial relationships that could be construed as a potential conflict of interest.

Publisher's note

All claims expressed in this article are solely those of the authors and do not necessarily represent those of their affiliated organizations, or those of the publisher, the editors and the reviewers. Any product that may be evaluated in this article, or claim that may be made by its manufacturer, is not guaranteed or endorsed by the publisher.

Supplementary material

The Supplementary Material for this article can be found online at: https://www.frontiersin.org/articles/10.3389/fgene.2023.1055372/full#supplementary-material

References

Athar, A., Fullgrabe, A., George, N., Iqbal, H., Huerta, L., Ali, A., et al. (2019). ArrayExpress update - from bulk to single-cell expression data. *Nucleic Acids Res.* 47, D711–D715. doi:10.1093/nar/gky964

Barrett, T., Wilhite, S. E., Ledoux, P., Evangelista, C., Kim, I. F., Tomashevsky, M., et al. (2013). NCBI GEO: Archive for functional genomics data sets-update. *Nucleic Acids Res.* 41, D991–D995. doi:10.1093/nar/gks1193,

Bayram, S., Furst, S., Forbes, M., and Kempa, S. (2020). Analysing central metabolism in ultra-high resolution: At the crossroads of carbon and nitrogen. *Mol. Metab.* 33, 38–47. doi:10.1016/j.molmet.2019.12.002

Becker, T., Guiard, B., Thornton, N., Zufall, N., Stroud, D. A., Wiedemann, N., et al. (2010). Assembly of the mitochondrial protein import channel: Role of Tom5 in two-stage interaction of Tom40 with the SAM complex. *Mol. Biol. Cell* 21, 3106–3113. doi:10.1091/mbc.E10-06-0518

Biddlestone, J., Bandarra, D., and Rocha, S. (2015). The role of hypoxia in inflammatory disease (review). *Int. J. Mol. Med.* 35, 859–869. doi:10.3892/ijmm.2015.2079

Brennan, L. A., McGreal-Estrada, R., Logan, C. M., Cvekl, A., Menko, A. S., and Kantorow, M. (2018). BNIP3L/NIX is required for elimination of mitochondria, endoplasmic reticulum and Golgi apparatus during eye lens organelle-free zone formation. *Exp. Eye Res.* 174, 173–184. doi:10.1016/j.exer.2018.06.003

Cockman, M. E., Masson, N., Mole, D. R., Jaakkola, P., Chang, G. W., Clifford, S. C., et al. (2000). Hypoxia inducible factor-alpha binding and ubiquitylation by the von Hippel-Lindau tumor suppressor protein. *J. Biol. Chem.* 275, 25733–25741. doi:10.1074/jbc.M002740200

da Cunha, A. F., Brugnerotto, A. F., Duarte, A. S., Lanaro, C., Costa, G. G., Saad, S. T., et al. (2010). Global gene expression reveals a set of new genes involved in the modification of cells during erythroid differentiation. *Cell Prolif.* 43, 297–309. doi:10.1111/j.1365-2184.2010.00679.x

Deshpande, R., Asiedu, M. K., Klebig, M., Sutor, S., Kuzmin, E., Nelson, J., et al. (2013). A comparative genomic approach for identifying synthetic lethal interactions in human cancer. *Cancer Res.* 73, 6128–6136. doi:10.1158/0008-5472.CAN-12-3956

Di Rita, A., Peschiaroli, A., Strobbe, D., Hu, Z., Gruber, J., Nygaard, M., et al. (2018). HUWE1 E3 ligase promotes PINK1/PARKIN-independent mitophagy by regulating AMBRA1 activation via IKKα. *Nat. Commun.* 9, 3755. doi:10.1038/s41467-018-05722-3

Dominguez-Gutierrez, P. R., Ceribelli, A., Satoh, M., Sobel, E. S., Reeves, W. H., and Chan, E. K. (2014). Positive correlation of STAT1 and miR-146a with anemia in patients with systemic lupus erythematosus. *J. Clin. Immunol.* 34, 171–180. doi:10.1007/s10875-013-9973-3

Duan, Y. B., Zhu, J. B., Yang, J. X., Liu, G. Q., Bai, X., Qu, N., et al. (2020). Regulation of high-altitude hypoxia on the transcription of CYP450 and UGT1A1 mediated by PXR and CAR. *Front. Pharmacol.* 11, 574176. doi:10.3389/fphar.2020.574176

Ducker, G. S., and Rabinowitz, J. D. (2017). One-carbon metabolism in health and disease. *Cell Metab.* 25, 27–42. doi:10.1016/j.cmet.2016.08.009

Endo, T. (2019). Mammalian O-mannosyl glycans: Biochemistry and glycopathology. *Proc. Jpn. Acad. Ser. B Phys. Biol. Sci.* 95, 39–51. doi:10.2183/pjab.95.004

Fu, C., Tyagi, R., Chin, A. C., Rojas, T., Li, R. J., Guha, P., et al. (2018). Inositol polyphosphate multikinase inhibits angiogenesis via inositol pentakisphosphate-induced HIF-1α degradation. *Circ. Res.* 122, 457–472. doi:10.1161/CIRCRESAHA.117.311983

Gutierrez-Arcelus, M., Teslovich, N., Mola, A. R., Polidoro, R. B., Nathan, A., Kim, H., et al. (2019). Lymphocyte innateness defined by transcriptional states reflects a balance between proliferation and effector functions. *Nat. Commun.* 10, 687. doi:10.1038/s41467-019-08604-4

He, L., Gomes, A. P., Wang, X., Yoon, S. O., Lee, G., Nagiec, M. J., et al. (2018). mTORC1 promotes metabolic reprogramming by the suppression of GSK3-dependent Foxk1 phosphorylation. *Mol. Cell* 70, 949–960.e4. doi:10.1016/j.molcel.2018.04.024

Hennis, P. J., O'Doherty, A. F., Levett, D. Z., Grocott, M. P., and Montgomery, H. M. (2015). Genetic factors associated with exercise performance in atmospheric hypoxia. *Sports Med.* 45, 745–761. doi:10.1007/s40279-015-0309-8

Higgins, J. S., Vaughan, O. R., Fernandez de Liger, E., Fowden, A. L., and Sferruzzi-Perri, A. N. (2016). Placental phenotype and resource allocation to fetal growth are modified by the timing and degree of hypoxia during mouse pregnancy. *J. Physiol.* 594, 1341–1356. doi:10.1113/JP271057

Huang, S., Feng, C., Zhai, Y. Z., Zhou, X., Li, B., Wang, L. L., et al. (2017). Identification of miRNA biomarkers of pneumonia using RNA-sequencing and bioinformatics analysis. *Exp. Ther. Med.* 13, 1235–1244. doi:10.3892/etm.2017.4151

Ju, H. Q., Ying, H., Tian, T., Ling, J., Fu, J., Lu, Y., et al. (2017). Mutant Kras- and p16-regulated NOX4 activation overcomes metabolic checkpoints in development of pancreatic ductal adenocarcinoma. *Nat. Commun.* 8, 14437. doi:10.1038/ncomms14437

Kato, H., and Mihara, K. (2008). Identification of Tom5 and Tom6 in the preprotein translocase complex of human mitochondrial outer membrane. *Biochem. Biophys. Res. Commun.* 369, 958–963. doi:10.1016/j.bbrc.2008.02.150

Kavanaugh, G., Zhao, R., Guo, Y., Mohni, K. N., Glick, G., Lacy, M. E., et al. (2015). Enhancer of rudimentary homolog affects the replication stress response through regulation of RNA processing. *Mol. Cell Biol.* 35, 2979–2990. doi:10.1128/MCB.01276-14

Khanna, K., Mishra, K. P., Ganju, L., Kumar, B., and Singh, S. B. (2018). High-altitude-induced alterations in gut-immune Axis: A review. *Int. Rev. Immunol.* 37, 119–126. doi:10.1080/08830185.2017.1407763

Kiers, D., Wielockx, B., Peters, E., van Eijk, L. T., Gerretsen, J., John, A., et al. (2018). Short-term hypoxia dampens inflammation *in vivo* via enhanced adenosine release and adenosine 2B receptor stimulation. *EBioMedicine* 33, 144–156. doi:10.1016/j.ebiom.2018.06.021

Kim, J. A., Choi, D. K., Min, J. S., Kang, I., Kim, J. C., Kim, S., et al. (2018). VBP1 represses cancer metastasis by enhancing HIF-1α degradation induced by pVHL. *FEBS J.* 285, 115–126. doi:10.1111/febs.14322

Knox, H. J., Hedhli, J., Kim, T. W., Khalili, K., Dobrucki, L. W., and Chan, J. (2017). A bioreducible N-oxide-based probe for photoacoustic imaging of hypoxia. *Nat. Commun.* 8, 1794. doi:10.1038/s41467-017-01951-0

Lin, P., Wen, D. Y., Chen, G., Dang, Y. W., He, Y., and Yang, H. (2020). Predictive value of hypoxia, metabolism and immune factors for prognosis in hepatocellular carcinoma: A retrospective analysis and multicenter validation study. *J. Cancer* 11, 4145–4156. doi:10.7150/jca.41983

Lin, Y., Li, Z., Ozsolak, F., Kim, S. W., Arango-Argoty, G., Liu, T. T., et al. (2012). An in-depth map of polyadenylation sites in cancer. *Nucleic Acids Res.* 40, 8460–8471. doi:10.1093/nar/gks637

Liu, B., Huang, H., Wang, S. X., Wu, G., Xu, G., Sun, B. D., et al. (2016). Physiological adjustments and circulating MicroRNA reprogramming are involved in early acclimatization to high altitude in Chinese han males. *Front. Physiol.* 7, 601. doi:10.3389/fphys.2016.00601

Mateo, J., Izquierdo-Garcia, D., Badimon, J. J., Fayad, Z. A., and Fuster, V. (2014). Noninvasive assessment of hypoxia in rabbit advanced atherosclerosis using ^{18}F-fluoromisonidazole positron emission tomographic imaging. *Circ. Cardiovasc Imaging* 7, 312–320. doi:10.1161/CIRCIMAGING.113.001084

Mei, L., Zheng, Y. M., Song, T., Yadav, V. R., Joseph, L. C., Truong, L., et al. (2020). Rieske iron-sulfur protein induces FKBP12.6/RyR2 complex remodeling and subsequent pulmonary hypertension through NF-κB/cyclin D1 pathway. *Nat. Commun.* 11, 3527. doi:10.1038/s41467-020-17314-1

Mikkola, S. (2020). Nucleotide sugars in chemistry and biology. *Molecules* 25, 5755. doi:10.3390/molecules25235755

Minamoto, Y., Otoni, C. C., Steelman, S. M., Buyukleblebici, O., Steiner, J. M., Jergens, A. E., et al. (2015). Alteration of the fecal microbiota and serum metabolite profiles in dogs with idiopathic inflammatory bowel disease. *Gut Microbes* 6, 33–47. doi:10.1080/19490976.2014.997612

Monaci, S., Aldinucci, C., Rossi, D., Giuntini, G., Filippi, I., Ulivieri, C., et al. (2020). Hypoxia shapes autophagy in LPS-activated dendritic cells. *Front. Immunol.* 11, 573646. doi:10.3389/fimmu.2020.573646

Murray, A. J. (2016). Energy metabolism and the high-altitude environment. *Exp. Physiol.* 101, 23–27. doi:10.1113/EP085317

Nelson, D. M., Smith, S. D., Furesz, T. C., Sadovsky, Y., Ganapathy, V., Parvin, C. A., et al. (2003). Hypoxia reduces expression and function of system A amino acid transporters in cultured term human trophoblasts. *Am. J. Physiol. Cell Physiol.* 284, C310–C315. doi:10.1152/ajpcell.00253.2002

Newman, A. M., Steen, C. B., Liu, C. L., Gentles, A. J., Chaudhuri, A. A., Scherer, F., et al. (2019). Determining cell type abundance and expression from bulk tissues with digital cytometry. *Nat. Biotechnol.* 37, 773–782. doi:10.1038/s41587-019-0114-2

Norris, P. C., Libreros, S., and Serhan, C. N. (2019). Resolution metabolomes activated by hypoxic environment. *Sci. Adv.* 5, eaax4895. doi:10.1126/sciadv.aax4895

O'Brien, T. D., Jia, P., Caporaso, N. E., Landi, M. T., and Zhao, Z. (2018). Weak sharing of genetic association signals in three lung cancer subtypes: Evidence at the SNP, gene, regulation, and pathway levels. *Genome Med.* 10, 16. doi:10.1186/s13073-018-0522-9

Okumiya, K., Sakamoto, R., Ishimoto, Y., Kimura, Y., Fukutomi, E., Ishikawa, M., et al. (2016). Glucose intolerance associated with hypoxia in people living at high altitudes in the Tibetan highland. *BMJ Open* 6, e009728. doi:10.1136/bmjopen-2015-009728

Schweizer, R. M., Velotta, J. P., Ivy, C. M., Jones, M. R., Muir, S. M., Bradburd, G. S., et al. (2019). Physiological and genomic evidence that selection on the transcription factor Epas1 has altered cardiovascular function in high-altitude deer mice. *PLoS Genet.* 15, e1008420. doi:10.1371/journal.pgen.1008420

Semenza, G. L. (2009). Regulation of oxygen homeostasis by hypoxia-inducible factor 1. *Physiol. (Bethesda)* 24, 97–106. doi:10.1152/physiol.00045.2008

Szklarczyk, D., Gable, A. L., Lyon, D., Junge, A., Wyder, S., Huerta-Cepas, J., et al. (2019). STRING v11: Protein-protein association networks with increased coverage, supporting functional discovery in genome-wide experimental datasets. *Nucleic Acids Res.* 47, D607–D613. doi:10.1093/nar/gky1131

Tanaka, Y., Hosoyama, T., Mikamo, A., Kurazumi, H., Nishimoto, A., Ueno, K., et al. (2017). Hypoxic preconditioning of human cardiosphere-derived cell sheets enhances cellular functions via activation of the PI3K/Akt/mTOR/HIF-1α pathway. *Am. J. Transl. Res.* 9, 664–673.

Taylor, C. T., and Colgan, S. P. (2017). Regulation of immunity and inflammation by hypoxia in immunological niches. *Nat. Rev. Immunol.* 17, 774–785. doi:10.1038/nri.2017.103

Thornton, N., Karamatic Crew, V., Tilley, L., Green, C. A., Tay, C. L., Griffiths, R. E., et al. (2020). Disruption of the tumour-associated EMP3 enhances erythroid proliferation and causes the MAM-negative phenotype. *Nat. Commun.* 11, 3569. doi:10.1038/s41467-020-17060-4

Tsubota, S. I., and Phillips, A. C. (2016). Drosophila enhancer of rudimentary homolog, ERH, is a binding partner of RPS3, RPL19, and DDIT4, suggesting a mechanism for the nuclear localization of ERH. *Mol. Biol. Int.* 2016, 8371819. doi:10.1155/2016/8371819

Vara-Perez, M., Rossi, M., Van den Haute, C., Maes, H., Sassano, M. L., Venkataramani, V., et al. (2021). BNIP3 promotes HIF-1α-driven melanoma growth by curbing intracellular iron homeostasis. *EMBO J.* 40, e106214. doi:10.15252/embj.2020106214

Vaughan, O. R., Thompson, F., Lorca, R. A., Julian, C. G., Powell, T. L., Moore, L. G., et al. (2020). Effect of high altitude on human placental amino acid transport. *J. Appl. Physiol.* 128, 127–133. doi:10.1152/japplphysiol.00691.2019

Vogel, P., Read, R. W., Rehg, J. E., and Hansen, G. M. (2013). Cryptogenic organizing pneumonia in Tomm5(-/-) mice. *Vet. Pathol.* 50, 65–75. doi:10.1177/0300985812450723

Wang, T., Chen, T., Thakur, A., Liang, Y., Gao, L., Zhang, S., et al. (2015). Association of PSMA4 polymorphisms with lung cancer susceptibility and response to cisplatin-based chemotherapy in a Chinese Han population. *Clin. Transl. Oncol.* 17, 564–569. doi:10.1007/s12094-015-1279-x

Weng, M. T., and Luo, J. (2013). The enigmatic ERH protein: Its role in cell cycle, RNA splicing and cancer. *Protein Cell* 4, 807–812. doi:10.1007/s13238-013-3056-3

Xu, Y., and Her, C. (2013). VBP1 facilitates proteasome and autophagy-mediated degradation of MutS homologue hMSH4. *FASEB J.* 27, 4799–4810. doi:10.1096/fj.13-235127

Yang, M., Ma, C., Liu, S., Sun, J., Shao, Q., Gao, W., et al. (2009). Hypoxia skews dendritic cells to a T helper type 2-stimulating phenotype and promotes tumour cell migration by dendritic cell-derived osteopontin. *Immunology* 128, e237–e249. doi:10.1111/j.1365-2567.2008.02954.x

Yang, X., Xia, R., Yue, C., Zhai, W., Du, W., Yang, Q., et al. (2018). ATF4 regulates CD4(+) T cell immune responses through metabolic reprogramming. *Cell Rep.* 23, 1754–1766. doi:10.1016/j.celrep.2018.04.032

Yi, X., Xu, C., Huang, P., Zhang, L., Qing, T., Li, J., et al. (2020). 1-Trifluoromethoxyphenyl-3-(1-Propionylpiperidin-4-yl) urea protects the blood-brain barrier against ischemic injury by upregulating tight junction protein expression, mitigating apoptosis and inflammation *in vivo* and *in vitro* model. *Front. Pharmacol.* 11, 1197. doi:10.3389/fphar.2020.01197

Yoo, Y. G., Christensen, J., and Huang, L. E. (2011). HIF-1α confers aggressive malignant traits on human tumor cells independent of its canonical transcriptional function. *Cancer Res.* 71, 1244–1252. doi:10.1158/0008-5472.CAN-10-2360

Zhao, X., Dong, X., Luo, X., Pan, J., Ju, W., Zhang, M., et al. (2017). Ubiquitin-proteasome-collagen (CUP) pathway in preterm premature rupture of fetal membranes. *Front. Pharmacol.* 8, 310. doi:10.3389/fphar.2017.00310

Zhou, G., Soufan, O., Ewald, J., Hancock, R. E. W., Basu, N., and Xia, J. (2019). NetworkAnalyst 3.0: A visual analytics platform for comprehensive gene expression profiling and meta-analysis. *Nucleic Acids Res.* 47, W234–W241. doi:10.1093/nar/gkz240

frontiers | Frontiers in Genetics

TYPE Case Report
PUBLISHED 12 June 2023
DOI 10.3389/fgene.2023.1067242

Check for updates

OPEN ACCESS

EDITED BY
Ruth Roberts,
ApconiX, United Kingdom

REVIEWED BY
Chih-Chien Sung,
Tri-Service General Hospital, Taiwan
Lisa Gianesello,
University of Padua, Italy

*CORRESPONDENCE
Heng Li,
hengli75@hotmail.com
Jianghua Chen,
chenjianghua@zju.edu.cn

RECEIVED 11 October 2022
ACCEPTED 04 May 2023
PUBLISHED 12 June 2023

CITATION
Chen W, Zhou Q, Chen H, Li H and Chen J (2023), Novel compound heterozygous variants of *SLC12A3* gene in a Chinese patient with Gitelman syndrome: a case report.
Front. Genet. 14:1067242.
doi: 10.3389/fgene.2023.1067242

COPYRIGHT
© 2023 Chen, Zhou, Chen, Li and Chen. This is an open-access article distributed under the terms of the Creative Commons Attribution License (CC BY). The use, distribution or reproduction in other forums is permitted, provided the original author(s) and the copyright owner(s) are credited and that the original publication in this journal is cited, in accordance with accepted academic practice. No use, distribution or reproduction is permitted which does not comply with these terms.

Novel compound heterozygous variants of *SLC12A3* gene in a Chinese patient with Gitelman syndrome: a case report

Wenqing Chen[1,2,3,4], Qin Zhou[1,2,3,4], Hongjun Chen[1,2,3,4], Heng Li[1,2,3,4]* and Jianghua Chen[1,2,3,4]*

[1]Kidney Disease Center, The First Affiliated Hospital, College of Medicine, Zhejiang University, Hangzhou, China, [2]Key Laboratory of Kidney Disease Prevention and Control Technology, Hangzhou, Zhejiang, China, [3]Institute of Nephropathy, Zhejiang University, Hangzhou, China, [4]Zhejiang Clinical Research Center of Kidney and Urinary System Disease, Hangzhou, China

Background: The Gitelman syndrome (GS) is an autosomal recessive disorder of renal tubular salt handling. Gitelman syndrome is characterized by hypokalemia, metabolic alkalosis, hypomagnesemia, hypocalciuria, and renin-angiotensin-aldosterone system (RAAS) activation, and is caused by variants in the *SLC12A3* gene. Gitelman syndrome has a heterogeneous phenotype, which may or may not include a range of clinical signs, posing certain difficulties for clinical diagnosis.

Case presentation: A 49-year-old man was admitted to our hospital due to muscular weakness. The patient's history revealed previous recurrent muscular weakness events associated with hypokalemia, featured by a minimum serum potassium value of 2.3 mmol/L. The reported male patient had persistent hypokalemia, hypocalciuria and normal blood pressure, without presenting obvious metabolic alkalosis, growth retardation, hypomagnesemia, hypochloremia or RAAS activation. We performed whole-exome sequencing and identified a novel compound heterozygous variant in the *SLC12A3* gene, c.965-1_976delGCGGACATTTTTGinsACCGAAAATTTT in exon8 and c.1112T>C in exon9 in the proband.

Conclusion: This is a study to report a heterogeneous phenotype Gitelman syndrome with a novel pathogenic compound heterozygous variant in the *SLC12A3* gene. This genetic study expands the variants spectrum, and improve the diagnostic accuracy of Gitelman syndrome. Meanwhile, further functional studies are required to investigate the pathophysiological mechanisms of Gitelman syndrome.

KEYWORDS

Gitelman syndrome, clinical characteristics, *SLC12A3* gene, whole-exome sequencing, gene mutation

Introduction

Gitelman syndrome (GS) (OMIM 263800) is an inherited autosomal recessive salt-losing tubulopathy caused by biallelic inactivating variants in the *SLC12A3* gene encoding a thiazide-sensitive sodium-chloride cotransporter (NCC), which is exclusively expressed in the apical membrane of cells lining the distal convoluted tubule (DCT) (Reyes and Medina, 2022). With a prevalence of approximately 1–10 per 40,000 cases, which is

potentially higher in Asia. GS is an autosomal recessive disorder, but homozygous variants are found in only 18% of patients (Hsu et al., 2009; Blanchard et al., 2017; Wang et al., 2020). More than 45% of GS cases featured compound heterozygous variants, 30% had single heterozygous variants, and 7% exhibited three or more variants (Lee et al., 2016; Blanchard et al., 2017). The gender effect on phenotype in GS has been reported, with male patients carrying compound heterozygous variants leading to splicing defects and intrinsic functional alterations in NCC exhibiting severe phenotypes (Riveira-Munoz et al., 2007). Several variants in *SLC12A3* and *CLCNKB* were identified in patients, and associated with clinical phenotypes in patients with GS and Gitelman-like syndrome (Lee et al., 2016; Kong et al., 2019). Here, we report a male patient with GS, characterized by a novel compound heterozygous variant of the *SLC12A3* gene.

Materials and methods

Whole exome sequencing

Genomic DNA (gDNA) of patient was extracted from the peripheral blood using MagPure Buffy Coat DNA Midi KF Kit (Magen, China). Then, gDNA was broken into 100–500 bp fragments using enzyme kit (BGI, China), 280–320 bp fragments were collected by magnetic beads. Agilent 2100 bioanalyzer and BMG were used to estimate the enrichment degree, and qualified products were collected to make DNA nanoballs and quantified according to different library quantities. DNA nanoballs were sequenced with PE100 + 100 on MGISEQ-2000. The average sequencing depth of the target region is ≥ 200×, more than 96% of the locus have a coverage depth of >20×.

Case presentation

Clinical history and laboratory data

A 49-year-old male was presented to our hospital with the major complaints of fatigue, polydipsia, polyuria, and repeated muscle weakness, but without a history of salt craving, constipation, physical, and intellectual disability over a 30-year period. Due to the diagnosis of renal tubular acidosis 25 years earlier, the patient had token potassium sodium hydrogen citrate granules orally for a long time to maintain the blood potassium at 2.0–2.5 mmol/L. Two months earlier, the patient was admitted to the endocrinology department due to fatigue and developed hypokalemia. The patient was supplied with potassium chloride sustained release tablets. During the follow-up, serum potassium levels were maintained between 2.3 and 2.55 mmol/L. He was hospitalized in our department due to recurrent fatigue.

The patient had a height of 169 cm, weight of 69 kg, and a heart rate of 78 beats per minute with no growth retardation. His respiratory rate was 18 breaths per minute, temperature was 37.0°C, and 24-h urine volume was 1.9–2.4 L. We monitored the blood pressure of this patient twice a day, with the systolic blood pressure in the range of 95–123 mmHg, and the diastolic blood pressure in the range of 60–76 mmHg. The laboratory investigation revealed hypokalemia, hypocalciuria and normal blood pressure, without obvious metabolic alkalosis, hypomagnesemia, hypochloremia or RAAS activation (Table 1). The fractional excretion rate of potassium (FEK%) was significantly increased to 30.25% (normal range, 8%–12%) and spot potassium-creatinine ratio elevated to 7.33, suggesting that hypokalemia resulted from renal potassium loss (Table 1). Urinalysis showed microalbuminuria, normal urinary immunoglobulin IgG, elevated β2-microglobulinuria, and elevated urinary retinol binding protein, which indicated proximal tubular injury. Other possible causes of hypokalemia, such as thyrotoxic periodic paralysis, renal tubular

TABLE 1 Biochemical characteristics of the proband.

Variable	Test value	Reference range
Blood tests		
Potassium (mmol/L)	2.09	3.50–5.30
Sodium (mmol/L)	148	137–147
Chloride (mmol/L)	105	99–110
Calcium (mmol/L)	2.00	2.11–2.52
Phosphate (mmol/L)	0.46	0.85–1.51
Magnesium (mmol/L)	0.97	0.75–1.02
Urea nitrogen (mmol/L)	3.38	3.1–8.00
Creatinine (μmol/L)	102	57–97
Fasting blood glucose (mmol/L)	4.45	3.90–6.10
Uric acid (μmol/L)	302	208–428
PTH(pg/mL)	9.6	15–65
ACTH (8AM) (pg/mL)	30	0.00–46.00
Renin–angiotensin–aldosterone system		
Renin (upright) (μIU/mL)	42.1	4.4–46.1
Aldosterone (upright (pg/L)	147	30–353.0
ARR	3.49	
Renin (supine) (μIU/mL)	17.3	2.8–39.9
Aldosterone (supine) (pg/L)	115	30–236.0
Arterial blood gas analysis		
PH	7.408	7.35–7.45
pCO_2	39.7	35–45
Bicarbonate (mmol/L)	26.9	22–27
Urine tests		
PH	8.0	4.5–8.0
Urine protein (g/L)	±(0.15)	-
MAU (g/mol.Cr)	0.890	0.000–3.000
Urinal β2 microglobulin (g/mol.Cr)	2.478	0.000–0.045
URBP(g/mol.Cr)	1.305	0.000–0.105
UACR (g/g)	0.23	0–0.20
Urinary aldosterone (μg/24 h)	5.442	1.0–8.0
urinary free cortisol (μg/24 h)	260.4	20.9–292.3
Calcium (mmol/24 h)	1.9	2.5–7.5
Potassium (mmol/24 h)	80	25–100
Magnesium (mmol/24 h)	5.52	2.50–8.50
Sodium (mmol/24 h)	365	130–260
Chloride (mmol/24 h)	327	170–250
Phosphate (μmol/24 h)	11.8	12.9–42.0
spot potassium-creatinine ratio	7.33	>2.0 mmol/mmol
spot calcium-creatinine ratio	0.16	<0.2 mmol/mmol
FEMg%	4.64%	>4%
FECL%	6.79%	>0.5%

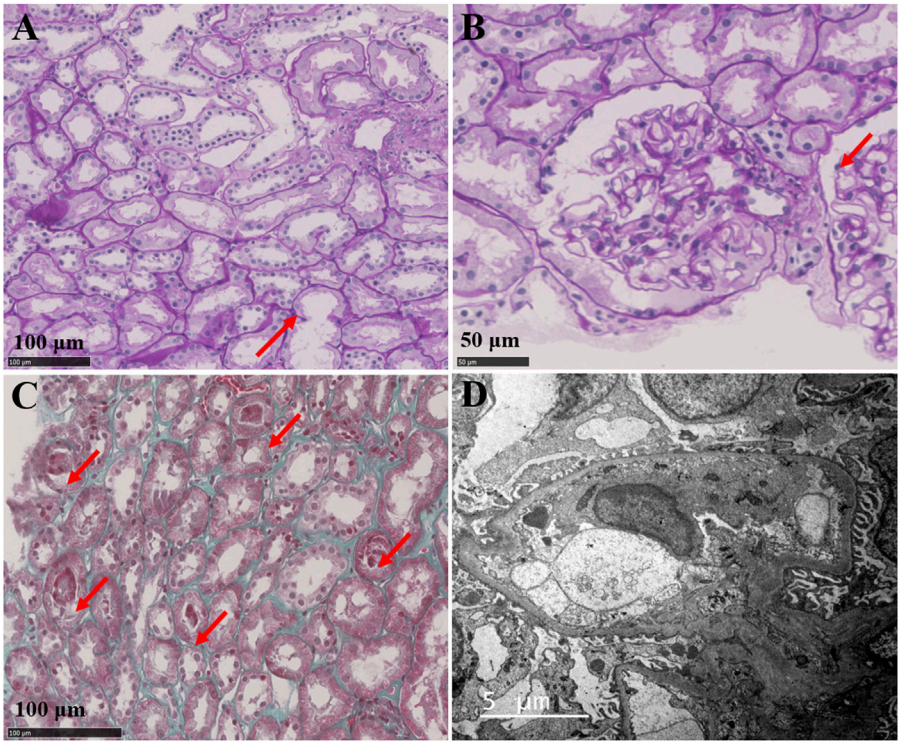


FIGURE 1
Renal pathology **(A)** Light microscope observations of PAS staining showing the focal granular and vacuolar degeneration of tubular epithelial cells; the brush border of some renal tubules fell off and the lumen expanded (arrow), and no special lesions were found in renal interstitium **(B)** Light microscope observations of PAS staining showing that the juxtaglomerular apparatus proliferation was not obvious (arrow) **(C)** Light microscope observations of MASSON staining showing exfoliated tubular epithelial cells and protein tubular formation in some kidney tubules (arrow) **(D)** Electron microscopy showing no obvious abnormalities, electron dense deposits or significant GBM thickening (280–450 nm).

acidosis, and hypercortisolism, were excluded. The enhanced computed tomography of adrenal gland showed possible right adrenal myelolipoma and left adrenal outer limb nodular protrusion, and hyperplasia was also considered (Supplementary Figure S1). Nevertheless, the renin-angiotensin-aldosterone system was normal, hence primary aldosteronism was excluded.

The electrocardiogram (ECG) showed normal sinus rhythm, abnormality of T-waves but no prolongation of the QT interval. The urinary ultrasound showed kidneys with normal size and without obvious abnormality in the ureters (Supplementary Figure S2). The pure tone audiometry of the patient was normal. The ophthalmology examination indicated that sclerochoroidal calcifications could be excluded. A renal biopsy was performed, and the renal pathology revealed a mild injury of the renal tubular epithelium (Figure 1). The light microscope showed focal granular degeneration, cell swelling, brush edge falling off, and without tubular atrophy and tubulitis. Vacuolar degeneration of the renal tubular epithelial cells was observed, and no special lesions were found in the renal interstitium.

Diagnosis and treatment

The patient was diagnosed with GS based upon clinical features and biochemical parameters according to the criteria (Blanchard et al., 2017), whereas the confirmation of clinically suspected GS rested on genetic testing. The blood potassium was maintained at 3.3–3.5 mmol/L by clinical follow-up, with the addition of 3 g potassium chloride tablets in three divided doses and 40 mg spironolactone in two divided doses. Subsequently, the patient's symptoms dramatically improved.

Whole exome sequence results

For a precise diagnosis, we performed whole-exome sequencing and identified a novel compound heterozygous variant in the *SLC12A3* gene. One of the variants, *SLC12A3* (NM_001126108.1, c.965-1_976delGCGGACATTTTTGinsACCGAAAATTTT) is caused by the deletion of 13 nucleotides GCGGACATTTTTG, and the insertion of 12 nucleotides ACCGAAAATTTT at nucleotide positions 965-976 of the coding sequence. Another variant *SLC12A3* (NM_001126108.1, c.1112T>C, p.Ile371Thr) is caused by the substitution of nucleotide T with C. Sanger sequence were used to verify the mutations (Figures 2A, B).

Meanwhile, the sister of the proband had normal manifestations, no variants were found. Notably, a heterozygous variant (NM_001126108.1, c.965-1_976delGCGGACATTTTTGinsACCGAAAATTTT) was identified in the *SLC12A3* gene in the proband's daughter. The daughter is 24-year-old, appeared healthy, was found to have normal plasma

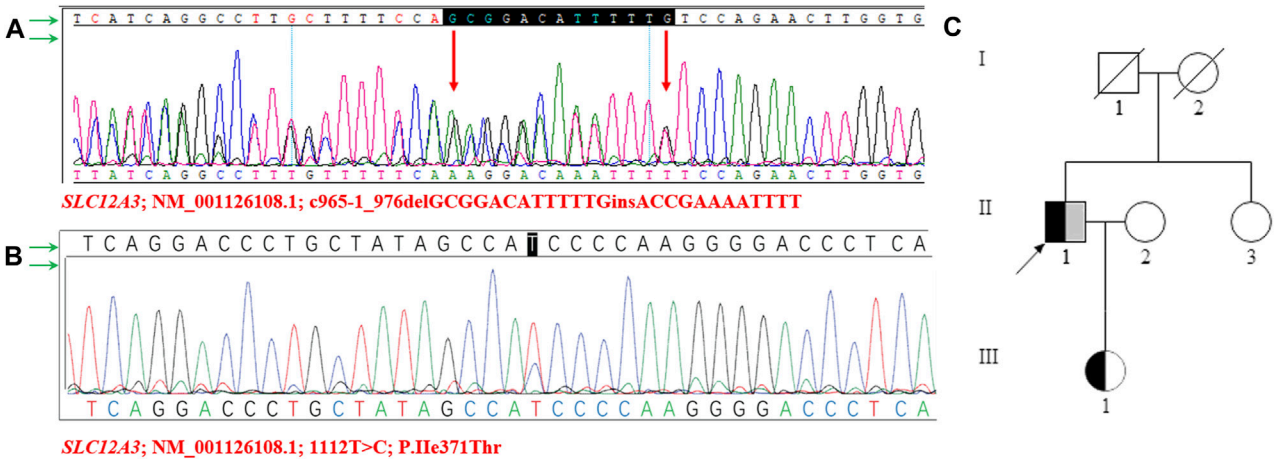


FIGURE 2
Sanger sequencing diagram of *SLC12A3* gene and pedigree of the family structure **(A–B)** The proband's NGS revealed two heterozygous variants in the *SLC12A3* gene (c.1112T>C and c.965-1_976delGCGGACATTTTTGinsACCGAAAATTTT), which were confirmed by sanger sequencing **(C)** The pedigree of the family structure. The marked symbols show patients who carried compound heterozygous variants of *SLC12A3*. The variants of c.1112T>C were presented in black, and c.965-1_976delGCGGACATTTTTGinsACCGAAAATTTT was shown in grey. Circles present females, and squares present males. The arrow shows proband. The deceased parents of proband and II-1 showed normal phenotypes, without any features of Gitelman syndrome.

potassium (4.2 mmol/L) and normal serum creatinine (67 μmol/L) levels. The serum potassium, sodium, chloride, calcium, and magnesium levels of the family members were unremarkable. The pedigree structure of the family was drawn according to the clinical manifestations and the sequencing results (Figure 2C).

Functional changes predictive of c.1112T>C variants

Variants were located in the intracellular and extracellular carboxyterminal domain of the NCC protein (Figure 3A). The variant (NM_001126108.1, c.965-1_976delGCGGACATTTTTGinsACCGAAAATTTT) in the *SLC12A3* gene is a known GS associated variant (Shao et al., 2008; Wang et al., 2021). However, the variant *SLC12A3* (NM_001126108.1, c.1112T>C, p.Ile371Thr) is not included in the databases (HGMD Professional and ClinVar). According to the American College of Medical Genetics and Genomics (ACMG) guidelines, the variation was judged to be of undetermined significance. The web-based software Variant Taster predicted that this variant was disease causing and capable of triggering amino acid sequence changes, frameshift, and splice site changes (Figure 3B). Two pathogenic in-trans variants in a single gene can produce the phenotype of this disease. Since the daughter of the proband carries only one of the two *SLC12A3* variants, we can assume that these two variants are in-trans in the proband. In addition, we used CADD to predict the variant *SLC12A3* (NM_001126108.1, c.1112T>C, p.Ile371Thr). The CADD-phred score is 26.8. We used mutation taster online website to predict and find that the variant is disease causing, and the prob is 0.999999999971332 (Figure 3B). Thus, the two variants may support the GS phenotype.

Three-dimensional structure prediction of SLC12A3 protein

Sequence alignment of SLC12A3 protein revealed that the isoleucine of p.371 was conserved among different species (Figure 3C). We used bioinformatics techniques to perform protein function prediction and secondary structure simulation (Supplementary Table S1). We used the SWISS-MODEL workspace (http://swissmodel.expasy.org) to characterize the effects of the novel variants, *SLC12A3* (NM_001126108.1, c.965-1_976delGCGGACATTTTTGinsACCGAAAATTTT) and (NM_001126108.1, c.1112T>C, p.Ile371Thr) on the protein structure of NCC, which demonstrated that the alterations caused by the variants modified the protein structure, and might even affected the function in terms of NCC physiology. The variant *SLC12A3* (NM_001126108.1, c.1112T>C, p.Ile371Thr) is only a point variant, with no significant change in the protein structure compared to wild type (Figures 3D, E). *SLC12A3* (NM_001126108.1, c.965-1_976delGCGGACATTTTTGinsACCGAAAATTTT) cause protein structure changes into a smaller structure, may affect SLC12A3 protein function (Figure 3F).

Discussion

GS is characterized by hypokalemic metabolic alkalosis, hyperreninemia and hyperaldosteronemia. An adult patient subject to our case study was found with hypokalemia due to fatigue, and had been misdiagnosed as renal tubular acidosis for a long period. The long-term use of potassium sodium hydrogen citrate granules was insufficient for treatment. Based on the patient's medical history and laboratory tests, the condition was conjectured to be GS with a heterogeneous phenotype.

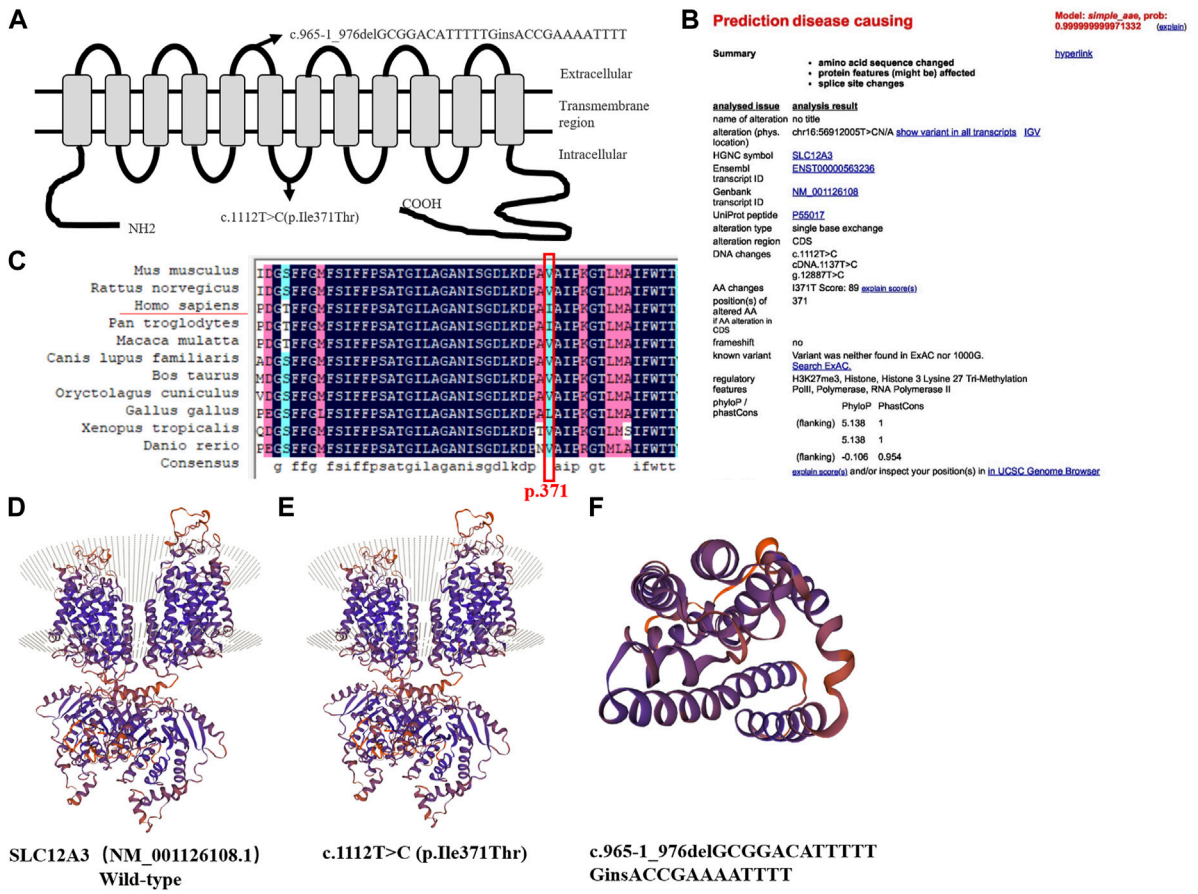


FIGURE 3
Predicted topological localization of NCC variants and effect of *SLC12A3* variants on the modeled structure of NCC protein, evaluation of the pathogenic potential of c.1112T>C variant in *SLC12A3* **(A)** Schematic diagram of NCC protein with the intercellular N- and C-terminal domains and transmembrane segments. The sites of detected variants are denoted by arrows in our study **(B)** The web-based software Variant Taster showed that this variant was disease causing, and the variant at this position was reported **(C)** Analysis of amino acid conservation based on the NCBI database. Evolutionary conservation of Ile371Thr using the ClustalX program. The black frame marks the Ile371Thr site **(D–E)** Compared to the wild-type, c.1112T>C (p.Ile371Thr) is only a point variant, with no significant change in the protein sequence **(F)** c.965-1_976delGCGGACATTTTT causes nonsense mediated mRNA degradation (NMD), because the protein sequence becomes shorter due to the early appearance of the stop codon, hence the structure is smaller.

Patients with GS with homozygous or compound heterozygous variants in *CLCNKB* and *SLC12A3* were reported in many studies, and variants in *CLCNKB* in particular seem to be responsible for a mixed Bartter-Gitelman phenotype or at least are involved in a switch in the clinical phenotype (Zelikovic et al., 2003). Thus far, there has been no report of GS associated with compound heterozygous variants in *SLC12A3*. With a compound heterozygous variant in *SLC12A3*, our patient's clinical manifestations were consistent with a heterogeneous phenotype GS in this study.

Features in an individual GS patient may vary. Patients are often asymptomatic or present with symptoms such as muscle weakness, fatigue, salt craving, thirst, nocturia, constipation, cramps, carpopedal spasms, or tetanic episodes triggered by hypomagnesemia (Blanchard et al., 2017). The presence of both hypocalciuria and hypomagnesemia is highly predictive of the clinical diagnosis of GS, although hypocalciuria is extremely variable and hypomagnesemia may be absent (Tseng et al., 2012). Some previous studies reported normomagnesemia in GS patients (Liu et al., 2016; Ma et al., 2016; Wang et al., 2017), which indicates that patients with normal magnesium exhibit milder clinical manifestations than hypomagnesemic patients (Jiang et al., 2014). Our patient's blood magnesium levels were normal and without RAAS activation. Low to normal plasma aldosterone concentration in male patients may reflect the suppressive effect of aldosterone by more severe hypokalemia (Tseng et al., 2012). It has been confirmed in the phenotype analysis that male patients had more severe hypokalemia and associated neuromuscular symptoms than females (Riveira-Munoz et al., 2007; Tseng et al., 2012).

Research suggests that GS may be associated with proteinuria, and chronic kidney disease might develop in GS patients due to either chronic hypokalemia, which is associated with tubulointerstitial nephritis, tubule vacuolization and cystic changes, or volume depletion and increased reninangiotensin-aldosterone, which may contribute to renal damage and fibrosis (Blanchard et al., 2017). Our patient presented a low level of proteinuria, which included elevated β2-microglobulinuria and urinary retinol binding protein, indicating proximal tubular

injury. Moreover, the renal biopsy showed tubulointerstitial injury, without obvious parabulbar organ hyperplasia.

In conclusion, this paper presented a case of novel compound heterozygous variants in the *SLC12A3* gene (c.1112T>C and c.965-1_976delGCGGACATTTTTGinsACCGAAAATTTT) in a 49-year-old Chinese male with persistent hypokalemia, hypocalciuria, metabolic alkalosis and normal blood pressure, but without obvious metabolic alkalosis, hypomagnesemia, hypochloremia, or RAAS activation. The GS phenotype was complicated; accordingly, symptoms of GS are usually nonspecific and variable. This case expands the variants spectrum, and improve the diagnostic accuracy of GS. Thus far, the molecular basis of the phenotype variability in GS remains unknown, and it is not clear whether it has a critical role in managing patients and predicting their prognosis, hence further studies are needed to clarify the underlying mechanism.

Data availability statement

The original contributions presented in the study are included in the article's Supplementary Material, further inquiries can be directed to the corresponding authors.

Ethics statement

All procedures performed in studies involving human participants were in accordance with the ethical standards of the Zhejiang University College of Medicine, the First Affiliated Hospital, and all pedigree members provided their written informed consent to participate. Written informed consent was obtained from the patient for publication of this study and any accompanying images.

Author contributions

WC and QZ participated in the experiments and wrote this article. HC was responsible for the sample and information collection. HL and JC guided the entire essay. All authors listed have made a substantial, direct, and intellectual contribution to the work and approved it for publication.

Funding

This work was supported by the Zhejiang Provincial Natural Science Foundation of China (LQ19H050004 to WC).

Acknowledgments

We are grateful to all the staff at the Kidney Disease Center of the First Affiliated Hospital of Zhejiang University for their sincere support.

Conflict of interest

The authors declare that the research was conducted in the absence of any commercial or financial relationships that could be construed as a potential conflict of interest.

Publisher's note

All claims expressed in this article are solely those of the authors and do not necessarily represent those of their affiliated organizations, or those of the publisher, the editors and the reviewers. Any product that may be evaluated in this article, or claim that may be made by its manufacturer, is not guaranteed or endorsed by the publisher.

Supplementary material

The Supplementary Material for this article can be found online at: https://www.frontiersin.org/articles/10.3389/fgene.2023.1067242/full#supplementary-material

References

Blanchard, A., Bockenhauer, D., Bolignano, D., Calò, L. A., Cosyns, E., Devuyst, O., et al. (2017). Gitelman syndrome: Consensus and guidance from a kidney disease: Improving global outcomes (KDIGO) controversies conference. *Kidney Int.* 91 (1), 24–33. doi:10.1016/j.kint.2016.09.046

Hsu, Y. J., Yang, S. S., Chu, N. F., Sytwu, H. K., Cheng, C. J., and Lin, S. H. (2009). Heterozygous variants of the sodium chloride cotransporter in Chinese children: Prevalence and association with blood pressure. *Nephrol. Dial. Transplant.* 24 (4), 1170–1175. official publication of the European Dialysis and Transplant Association - European Renal Association. doi:10.1093/ndt/gfn619

Jiang, L., Chen, C., Yuan, T., Qin, Y., Hu, M., Li, X., et al. (2014). Clinical severity of Gitelman syndrome determined by serum magnesium. *Am. J. Nephrol.* 39 (4), 357–366. doi:10.1159/000360773

Kong, Y., Xu, K., Yuan, K., Zhu, J., Gu, W., Liang, L., et al. (2019). Digenetic inheritance of SLC12A3 and CLCNKB genes in a Chinese girl with Gitelman syndrome. *BMC Pediatr.* 19 (1), 114. doi:10.1186/s12887-019-1498-3

Laghmani, K., Beck, B. B., Yang, S. S., Seaayfan, E., Wenzel, A., Reusch, B., et al. (2016). Polyhydramnios, transient antenatal bartter's syndrome, and MAGED2 mutations. *N. Engl. J. Med.* 374 (19), 1853–1863. doi:10.1056/NEJMoa1507629

Lee, J. W., Lee, J., Heo, N. J., Cheong, H. I., and Han, J. S. (2016). Mutations in SLC12A3 and CLCNKB and their correlation with clinical phenotype in patients with gitelman and gitelman-like syndrome. *J. Korean Med. Sci.* 31 (1), 47–54. doi:10.3346/jkms.2016.31.1.47

Liu, T., Wang, C., Lu, J., Zhao, X., Lang, Y., and Shao, L. (2016). Genotype/phenotype analysis in 67 Chinese patients with gitelman's syndrome. *Am. J. Nephrol.* 44 (2), 159–168. doi:10.1159/000448694

Ma, J., Ren, H., Lin, L., Zhang, C., Wang, Z., Xie, J., et al. (2016). Genetic features of Chinese patients with gitelman syndrome: Sixteen novel SLC12A3 mutations identified in a new cohort. *Am. J. Nephrol.* 44 (2), 113–121. doi:10.1159/000447366

Reyes, J. V., and Medina, P. (2022). Renal calcium and magnesium handling in Gitelman syndrome. *Am. J. Transl. Res.* 14 (1), 1–19.

Riveira-Munoz, E., Chang, Q., Godefroid, N., Hoenderop, J. G., Bindels, R. J., Dahan, K., et al. (2007). Transcriptional and functional analyses of SLC12A3 mutations: New clues for the pathogenesis of gitelman syndrome. *J. Am. Soc. Nephrol. JASN* 18 (4), 1271–1283. doi:10.1681/ASN.2006101095

Shao, L., Liu, L., Miao, Z., Ren, H., Wang, W., Lang, Y., et al. (2008). A novel SLC12A3 splicing mutation skipping of two exons and preliminary screening for alternative splice variants in human kidney. *Am. J. Nephrol.* 28 (6), 900–907. doi:10.1159/000141932

Tseng, M. H., Yang, S. S., Hsu, Y. J., Fang, Y. W., Wu, C. J., Tsai, J. D., et al. (2012). Genotype, phenotype, and follow-up in Taiwanese patients with salt-losing tubulopathy associated with SLC12A3 mutation. *J. Clin. Endocrinol. metabolism* 97 (8), E1478–E1482. doi:10.1210/jc.2012-1707

Wang, F., Shi, C., Cui, Y., Li, C., and Tong, A. (2017). Mutation profile and treatment of Gitelman syndrome in Chinese patients. *Clin. Exp. Nephrol.* 21 (2), 293–299. doi:10.1007/s10157-016-1284-6

Wang, J., Xiang, J., Chen, L., Luo, H., Xu, X., Li, N., et al. (2021). Molecular diagnosis of non-syndromic hearing loss patients using a stepwise approach. *Sci. Rep.* 11 (1), 4036. doi:10.1038/s41598-021-83493-6

Wang, X., Ding, Y., Liu, Q., and Yang, G. (2020). A novel compound heterozygous mutation of SLC12A3 gene in a Chinese pedigree with Gitelman syndrome. *Endocrine* 67 (3), 673–677. doi:10.1007/s12020-019-02152-z

Zelikovic, I., Szargel, R., Hawash, A., Labay, V., Hatib, I., Cohen, N., et al. (2003). A novel mutation in the chloride channel gene, CLCNKB, as a cause of Gitelman and Bartter syndromes. *Kidney Int.* 63 (1), 24–32. doi:10.1046/j.1523-1755.2003.00730.x

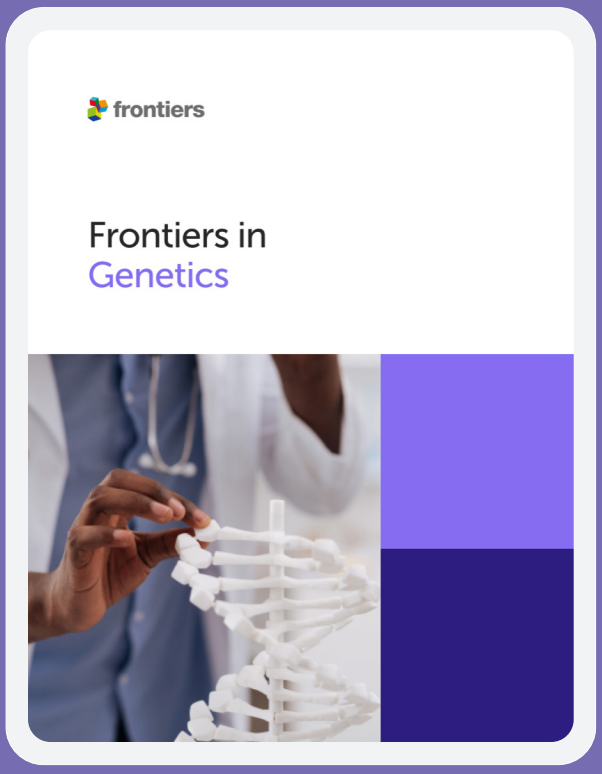
Frontiers in Genetics

Highlights genetic and genomic inquiry relating to all domains of life

The most cited genetics and heredity journal, which advances our understanding of genes from humans to plants and other model organisms. It highlights developments in the function and variability of the genome, and the use of genomic tools.

Discover the latest Research Topics

See more →



Frontiers

Avenue du Tribunal-Fédéral 34
1005 Lausanne, Switzerland
frontiersin.org

Contact us

+41 (0)21 510 17 00
frontiersin.org/about/contact